Artificial Molecular Machines

A thesis submitted to The University of Manchester for the degree of
Doctor of Philosophy
in the Faculty of Science and Engineering

2020

Burkhard J. Groh

Department of Chemistry

Blank page

List of Contents

Blank page

1. List of Abbreviations

2-aldrithiol	2,2′-dipyridyl disulfide
24C8	24-crown-8
27C9	27-crown-9
aa-tRNA	aminoacyl-transfer RNA
ABC	ATP-binding cassette
ADMP	azido-1,3-dimethylimidazolinium hexafluorophosphate
AMT	active metal template
ATRP	atom transfer radical polymerization
BDP	binding protein dependent
BEMP	2-tert-butylimino-2-diethylamino-1,3-dimethyl-perhydro-1,3,2-diaza-phosphorine
Boc	*t*-butyl carbamate
Bz	benzoyl
CBS	Corey-Bakshi-Shibata
CD	cyclodextrin
CPL	circularly polarised light
CuAAC	copper-catalysed azide-alkyne cycloaddition
DB24C8	dibenzo-24-crown-8
DB30C10	dibenzo-30-crown-10
dba	dibenzylideneacetone
DBA	dibenzyl ammonium
DCE	1,2-dichloroethylene
DIPEA	*N*,*N*-diisopropylethylamine
DMAP	4-(dimethylamino)pyridine
DMF	*N*,*N*-dimethylformamide
DMSO	dimethylsulfoxide
DNMR	dynamic NMR
dNTP	deoxynucleoside triphosphate
dpp	2,9-diphenyl-1,10-phenanthroline
EDCI	1-ethyl-3-(3-dimethylaminopropyl)carbodiimide
EDTA	ethylenediaminetetraacetic acid
EF-G	elongation factor G
ET	electron transfer
Fmoc	9-fluorenylmethoxycarbonyl
IF	initiation factor
IRC	internal reaction coordinate
MBA	monobenzyl ammonium
MBP	maltose-binding protein
MeCN	acetonitrile
MOM	methoxymethyl
mRNA	messenger RNA

Ms	methanesulfonyl
NBD	nucleotide-binding domains
NBS	*N*-bromosuccinimide
NCL	native chemical ligation
NMP	nitroxide-mediated radical polymerization
NMR	nuclear magnetic resonance
NOE	nuclear Overhauser effect
NOESY	nuclear Overhauser effect spectroscopy
PCy	tricyclohexylphosphine
PES	potential energy surface
PET	photoinduced electron transfer
PMB	*p*-methoxybenzyl ether
PPTS	*p*-toluenesulfonic acid pyridine salt
PRE	pre-translocational (ribosome)
PSS	photostationary state
PTLC	preparatory thin layer chromatography
PTZ	phenothiazine
RAFT	reversible addition-fragmentation chain transfer
ROESY	rotating frame nuclear Overhauser effect spectroscopy
RPS	ribosomal peptide synthesis
rt	room temperature
STAB	sodium triacetoxyborohydride
TBAF	tetra-*n*-butylammonium fluoride
TBAI	tetra-*n*-butylammonium iodide
TBDMS	*t*-butyldimethylsilyl
TBDPS	*t*-butyldiphenylsilyl
TBTA	tris(benzyltriazolylmethyl)amine
TCA	trichloroacetic acid
Tf	triflate/trifluoromethanesulfonate
TFA	trifluoroacetic acid
THF	tetrahydrofuran
THI	thermal helix inversion
TIPS	triisopropylsilyl
TLC	thin layer chromatography
tpy	2,2′:6′,2″-terpyridine
Tr	trityl
Ts	tosyl
TSAF	tris(dimethylamino)sulfonium difluorotrimethylsilicate

2. Abstract

During this degree two main projects have been investigated related to the design and operation of rotaxane-based synthetic molecular machines.

The first system explored aims to mimic ribosomal peptide synthesis as a paragon of an ideal molecular assembler. It relies on the concept of constructing molecules by translating a given piece of information encoded as a sequence of reactive barriers installed on the machine's track into a predetermined product (Figure 2.1). The basis of the translation chosen uses Wittig chemistry to construct stilbene sequences under basic operation conditions from an aldehyde macrocycle and several bifunctional aldehyde phosphonium units through a succession of carbon-carbon bond forming reactions.

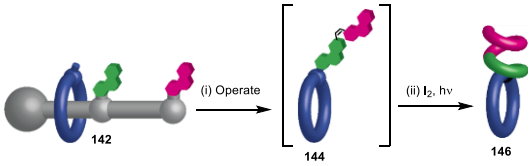

Figure 2.1. Helicene synthesis by a rotaxane-based molecular machine. The operation affords stilbene sequences that can be converted to helicenes via oxidative photocyclization.

During this study we have been able to show that when applying a phenanthrene motive, stilbenes obtained from the operation of the machine can subsequently be transformed into helicenes with the aid of light and an oxidant. We showed that applying this concept the two-step operation of a one- and two-barrier machine successfully yields [5]- and [9]helicenes, respectively, which could be isolated and characterised. It was noticed that in contrast to the absence of selectivity for the *E*–*Z* ratio of standards, the corresponding stilbene products from the operation are formed preferentially in one of the possible configurations.

As a second project, we have been working on a system that relies on the group's design of a rotary and linear motor system (Figure 2.2). It is based on the successive uptake, pH-induced shuttling between two different stations (blue to orange) and final release of a macrocycle (red) from and back into bulk solution. And it controls the direction of the macrocycle's translation with a pair of barriers that become labile under orthogonal conditions for hydrazone (yellow) and disulfide exchange (purple). It is combined with dissipative pulses of a chemical fuel to give an autonomous molecular pump. To complement the analysis and further corroborate the translation process we developed a design that includes a fluorophore unit. We anticipated that with the aid of a switchable intramolecular fluorescence quenching process an indication of the macrocycle's position and its motion during the operation can be inferred. We postulated that in our example, the intermediate binding of a crown-ether macrocycle to a methyl triazolium unit could modulate the fluorescence of a proximal fluorophore. The design has the potential to allow measuring the kinetics of the dethreading and importantly, it has the capacity to directly visualise each pump cycle.

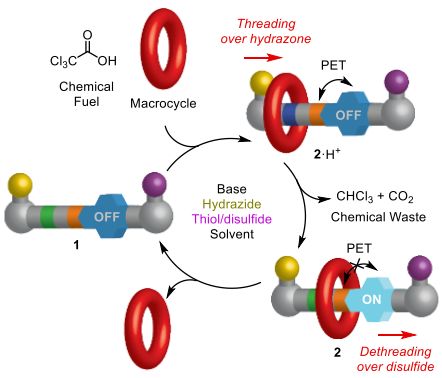

Figure 2.2. Chemically fuelled unidirectional linear transport of 27C9 with pyrene-based rotaxane pump **2**/**2**·H⁺ indicating the position of the macrocycle with a fluorescence read out.

At the current stage of investigations, a series of improved designs were developed, a working bistable pump synthesised, and its operation attempted. We were able to establish a procedure that allows isolation of intermediate hydrazone (pseudo)[2]rotaxanes. This allowed testing their switching properties with NMR and fluorescence spectroscopy and we were able to successfully show reversible threading and shuttling. Furthermore, we were able to single out an optimal size for the pump's macrocycle and improve the conditions for its operation. Besides this, a system of two fluorophores (anthracene and pyrene) was identified that could be applied as a potential pair of orthogonal fluorescence indicators for the simultaneous monitoring of two machines. Future work will involve optimising the last dethreading step of the operation with the final pump design and examining the kinetics with fluorescence spectroscopy.

3. Declaration

No portion of the work referred to in the thesis has been submitted in support of an application for another degree or qualification of this or any other university or other institute of learning.

4. Copyright Statement

5. Dedications and Acknowledgement

I would like to thank Prof David Leigh for the generous opportunity to become part of his fantastic group and to contribute to the exciting research that is taking place in the field of molecular machines.

I would also like thank all past and present members of the Leigh group that I was given the chance to meet and work with over the past four years. I am much obliged for the open, hospitable, and engaging environment that has been created. I am grateful for all the time I spent with all of you!







Finally, I would like to thank my parents and siblings whose continuous support and encouragement has been invaluable source of motivation and inspiration for my life and this work.

Blank page

6. Molecular Machines – An Introduction

6.1. Finding Inspiration in Nature

From every point of view, universality of life and diversity that has been attained by expanding a common finite biochemical framework into every place conceivable is beyond example ranging from large macroscopic multicellular life forms such as whales to tiny, microscopic organisms such as unicellular diatoms. What is more, life constitutes our own existence; it affects our perception and also stimulates imagination as manifested for example in its wide-ranging influence on art[1] and science.[2] Importantly, understanding its fundamental principles has brought significant advances in medical diagnosis and treatment as demonstrated by several Nobel Laureates in Physiology or Medicine such as W. G. Kaelin, P. J. Ratcliffe, G. L. Semenza who have been honoured in 2019 for their contributions of identifying the complex metabolic and physiological functions that allow organisms to adapt to varying levels of oxygen.[3]

As it has been shown, the very basis of life can be primarily attributed to the appearance of a complex heterogeneous unit of dynamic molecular systems embedded in an integrated anisotropic confinement known as the cell (Figure 6.1).[4] This structural and functional arrangement enabled by self-assembly processes has been found responsible for executing all inherent chemical processes of life in a dynamic, self-regulated, self-sustained and self-generated manner. This is made possible by successfully integrating functions for replication, metabolism, and compartmentalization through organisation of complex chemical reactions.[5] Moreover, both on its own or in larger heterogenous assemblies, cells form the minimal repeating element for the successful emergence and omnipresence of life

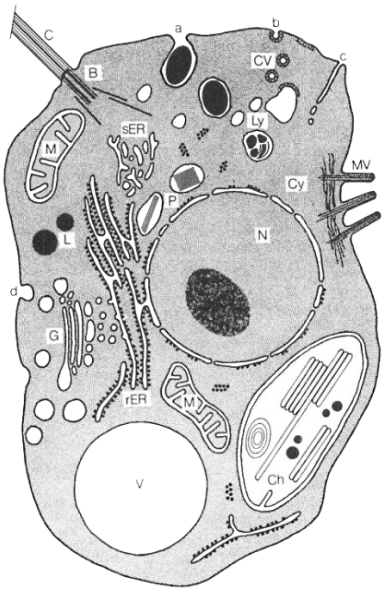

Figure 6.1. Compartmentation in a eukaryotic cell. N, nucleus, and nucleolus; Cy, cytoplasm with free polysomes; Ch, chloroplast with thylacoids, starch and lipid droplets; M, mitochondria; sER, smooth endoplasmic reticulum; rER, rough endoplasmic reticulum; G, Golgi apparatus (dictyosome); V, vacuole; Ly, lysosomes; CV, coat vesicles; P, peroxisomes with protein crystals; L, lyosomes; C, cilia or flagellum; B, basal body; MV, microvilli; a, b, c, types of endocytosis; d, exocytosis. Reprinted by permission from John Wiley and Sons: reference 6, Copyright 2008.

To date, many important aspects of life and its working are known; It has been established early on that independent of the individual life form and its behaviour that emerges the basis of every cell is the effect of an evolution of a universal set of biochemical constituents that allow to control each and every action on the molecular level (Figure 6.2).[4] Every single participating component on its own takes on a specialised function emanating from its molecular structure. Combining different components and coupling their functions together then gives control over a wide range of different reactions beyond thermodynamic equilibrium.[7] This includes, for example, the (bidirectional) material transport or sensing at the cell's interface or the general assembly, metabolism, and information processing within the inside of a cell separate from the influences of the environment.[8] Eventually, it is the exceptional ability of this diverse collection of structural and functional units to act in conjunction not only to achieve local control of biochemical reactions and ensuing cellular

dynamics but also on a whole, to coordinate tasks between cells. Altogether, this organisation lays the foundation for life with an increasing complexity.[7,8]

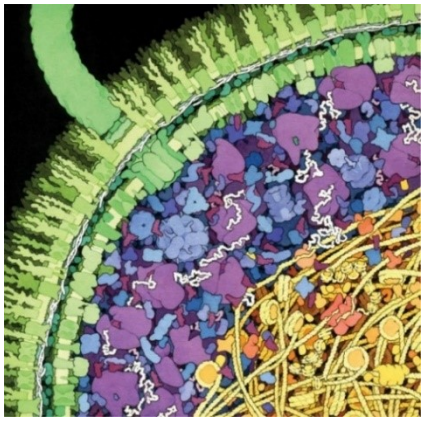

Figure 6.2. Cross-section of a bacterial cell. The composition of macromolecules is depicted to scale, with an effort to show the impact of native concentrations of macromolecules on the environment: For example, ribosomes are in purple, white strands are mRNA, enzymes are in blue and membrane components including the lipid bilayer and membrane proteins are stained in green. Reprinted by permission from Springer Nature: reference 9, Copyright 2009.

From a principal point of view, the cause for this phenomena can first and foremost be referred to the (inter)actions of the collection of biological components termed biomolecules:[4] Operating on the cellular level this group of molecules can further be divided into four main classes comprising proteins, carbohydrates, lipids, and nucleic acids. The assignment is based on the observation that larger constituents of the biological library are overwhelmingly built from predetermined sequences of different chemical precursors termed monomers. When joined these monomers form larger macroscopically sized assemblies in the form of polymers.[10] Complemented with self-assembly processes this basic concept has proven successful for continuously adapting to changing environmental conditions.

Historically, each biomolecule is recognised primarily as a type of a structure that because of its chemical constitution entails a specific intrinsic property that allows to promote a particular function on the molecular level.[4] This perception finds its expression in the observation that unique tasks on the cellular level are related to specific biochemical classes. Examples of this include the processing low-molecular-weight molecules that is metabolites. This function is achieved by proteins composed of about twenty different amino acids in linear sequence to provide final catalytic properties. In contrast, (genetical) information and its regulation is kept primarily in the form of DNA as a double-stranded sequence of four complementary nucleotides. Furthermore, carbohydrates can serve as a source of energy and structural framework for cellular organisation but also a means for intercell communication and intracellular protein regulation. They comprise a whole range of different largely polar components including monosaccharides, such as glyceraldehyde, mannose, or glucose that when connected give higher order oligomers. Besides this, lipid components serve as basis for the formation of cell membranes owing to their largely hydrophobic properties that drive the self-assembly process.

Ranging between a few up to hundreds of nanometres in size and consisting of up to several thousand covalently linked atoms on average activities of biomolecules are also determined by their extrinsic properties.[8,11] This can be rationalised by the large number of molecular degrees of freedom that arise with an increasing molecular size, particularly, in the case of proteins. They make their appearance, for instance, in the form of conformational isomerism, and it is known that due to the ensuing dynamics this can allow adaption of various shapes in dynamic exchange on account of localised bond and collective domain motions (Figure 6.3).[12] And in many cases, only when correctly folded and stabilised in their native form biomolecules exhibit the desired activity.[4] In fact, active measures are put in place on the cellular level to modulate those characteristic attributes. For example, alteration of the intertwined topology of chromosomes is applied as

means for regulating the expression of the genetical information encoded in the underlying DNA sequence during replication and transcription.

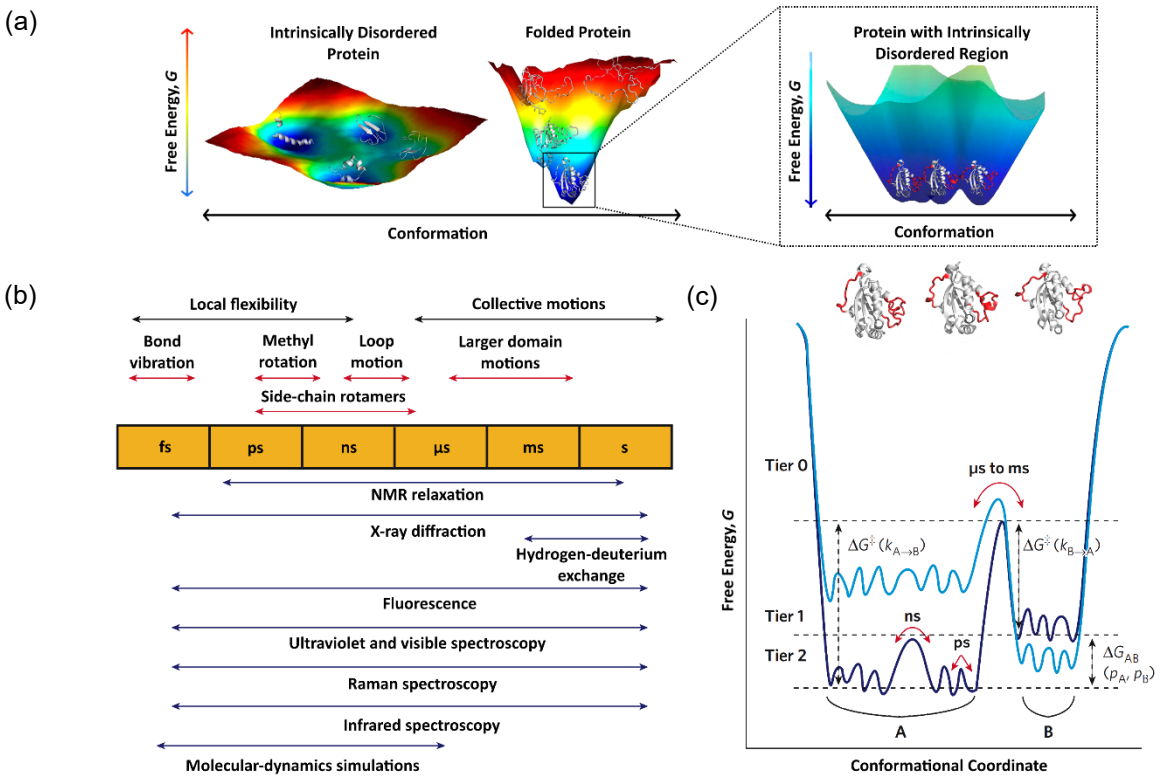

Figure 6.3. Implication of conformational isomerism for the structure and dynamics of proteins. (a) Schematic energy profile for an intrinsically disordered peptide (CcdA C-terminal, PDB ID: 3tcj) and a folded protein (human nucleoside diphosphate kinase, PDB ID: 1nsk);[12b] close-up of the minimal free energy well where intrinsically disordered regions are shown in red and ordered parts are shown in white below. Adapted by permission from MDPI: reference 12b, Creative Commons CC BY 2014. The energy landscape that define the amplitude and timescale of protein motions.[12c] (b) Timescale of dynamic processes in proteins and the experimental methods that can detect fluctuations on each timescale. (c) One-dimensional cross-section through the high dimensional energy landscape of a protein showing the hierarchy of protein dynamics and the energy barriers. Adapted by permission from Springer Nature: reference 12c, Copyright 2007.

Importantly, it has become evident that to escape the convergent dynamic equilibrium, certain proteins have evolved which show the capacity to elevate from the "thermodynamic sink"[7] and upset the balance by actively biasing molecular dynamics towards a single direction.[13] They overcome the limitation of the perpetual randomizing effect of thermal motion by using a chemical transformation as a specific driving force for a concomitant mechanical action that translates into unidirectional molecular movement. Harnessing the free energy released along a predetermined reaction path these actions can result in distinctly controlled conformational changes that when taken together delineate rotary or and translational motion. In particular proteins' action of moving from one state to another has shown to iconically resemble the actions of classical macroscopic machine-like devices such as pumps or rotors (Figure 6.4).[14] For instance, examining F1-ATPase (Figure 6.4 (b)) decorated with a fluorescent actin filament spectroscopically, Noji and co-workers concluded[15] that this membrane-bound protein assembly "acts as a rotary motor, the smallest known." To emphasis this aspect, the protein-based machinery is often referred to as nanomachines, or molecular machines not only to give an indication of their size but also to highlight their ascribed machine-like working.[16]

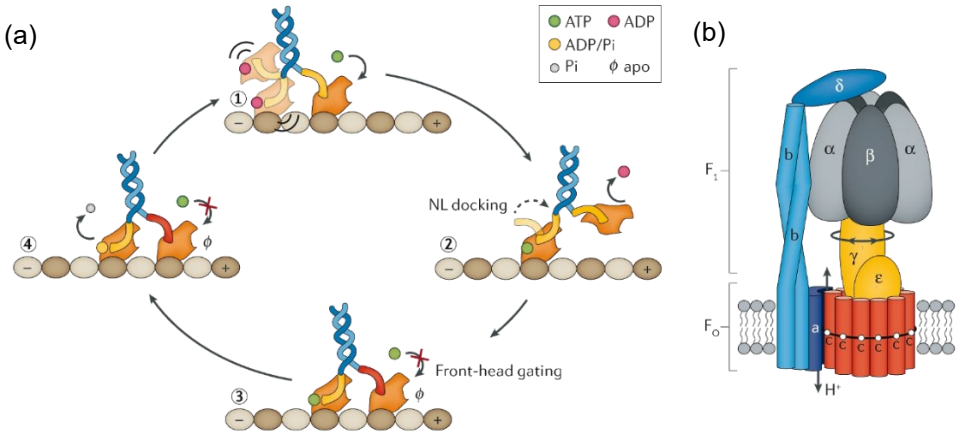

Figure 6.4. Biological examples of chemo-mechanical molecular movement processes of proteins. (a) Schematic illustration of the bipedal walking process of kinesin dimer along microtubules and (b) structural overview of the membrane-bound F-type ATP synthase assembly that can act as a rotatory motor for the formation of ATP from ADP and monomeric phosphate Pi driven by a transmembrane proton gradient. Adapted by permission from Springer Nature: reference 17, Copyright 2019.

As of this writing, several representative members of the biological machinery have been identified and studied in detail.[4a,18] Certain representatives whose function is primarily characterised by mechanical motion, are further termed motor proteins or (bio)molecular motors;[13] Relying on a chemical process such ATP hydrolysis or a chemical potential these machines specifically utilise chemo-mechanical coupling to drive unidirectional linear or (oscillatory) rotary processes.[19,20]

For instance, studying the linear movement of molecular motors proteins that proceed along a given track, it has been concluded that the series of actions can be vividly described by a “walking” procedure. Representatives for this unique biomolecular behaviour are e.g. bipedal members of the (super)family of myosin proteins (Figure 6.5).[21] Machines of this group perform conveyance of cellular vesicles from one place to another along a single direction pointed out by the polar structure of an actin filament; They are able to selectively “walk” either towards (Figure 6.5 (a)) or away (Figure 6.5 (b)) of the plus end of the polar actin track. When coupled together synchronous activity can also lead to macroscopic muscle contraction (Figure 6.5 (c)). Similarly, kinesin[22] and dynein[23] proteins have been found to allow for complementary cargo transport between the different ends of microtubules.

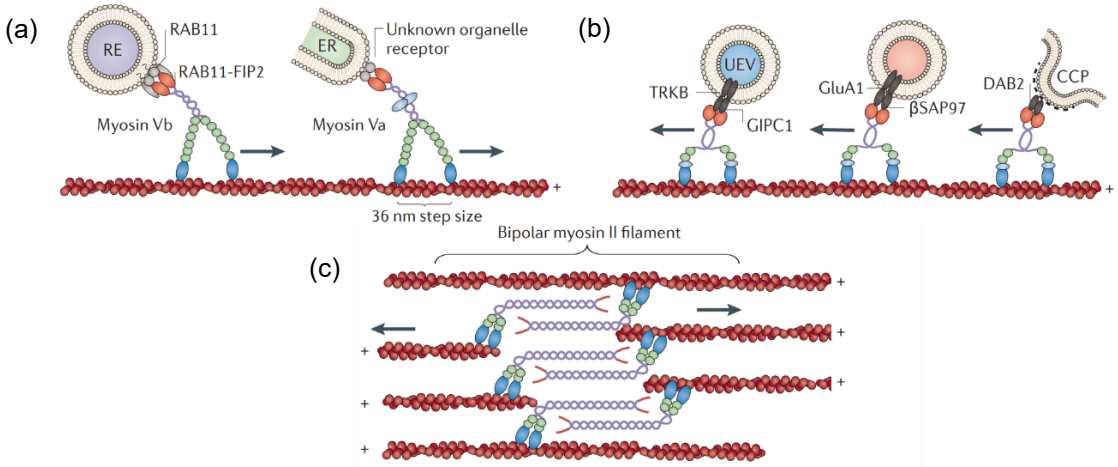

Figure 6.5. Mechanisms of function of synaptic myosins. (a) Myosin V organelle tethering and transport. Myosin V can associate with different organelles and move towards the barbed end of an actin filament

(indicated by the arrow). (b) Myosin VI organelle anchoring and motility, actin filament organization. Myosin VI dimerizes upon binding of cargo adaptors to its cargo-binding domain (red). Parts of the proximal tail (purple) might contribute to heavy chain dimerization. Dimerized myosin VI walks processively towards the pointed minus end of actin. (c) Myosin II actin filament contraction and crosslinking. Myosin II molecules associate in an antiparallel fashion to form bipolar 'thick filaments' (sarcomeric myosin II) or 'minifilaments' (non-muscle myosin II). Translocation (indicated by arrows) of the myosins in bipolar assemblies towards the barbed plus ends of antiparallel actin filaments leads to contraction of the actin filament array. Adapted by permission from Springer Nature: reference 21b, Copyright 2013.

Actively harnessing the proton gradient across a membrane between different compartments enzyme ATP synthase drives the thermodynamically unfavourable reaction of ATP from ADP and monomeric phosphate by rotatory motion (F-type, see for example Figure 6.4 (b)).[24] Alternatively, members of the vacuolar ATPases (V-type) use ATP as a fuel to enable the reverse action and regulate the intramolecular pH by actively transporting protons across the membrane. Taking a different approach, assemblies of helical flagellum and protein flagellin consume ATP as a fuel to impart (bi)directional cellular propulsion actuated by the rotary movement of the flagellum's anchor.[25] In this case, rotary motion is transduced into oscillatory movement of the flagellum's filament that acts as propelling force for bacterial movement.

In contrast to this, different types of DNA polymerases[26] (Figure 6.6) but also ribosomes[27] copy or translate information, respectively, by linearly processing a given sequence. In each case taking a primary strand of information i.e., a single strand of DNA or RNA, a secondary strand of complementary information is assembled from matching pairs of monomeric units. As a result, a copy or translation of either DNA or protein sequence is achieved, respectively. Overall, those machines are in many respect nature's paragon of an ideal assembly line.[162] And in both cases the action of DNA replication and protein translation resembles the mechanism of a zipper. During the unidirectional linear motion along the primary line of information the asymmetric shape introduced by the channel of a moving slider unit (the protein) ensures the correct assembly a secondary row carrying the encoded information. Taking the example of DNA polymerase, the duplication of DNA can be compared with the action of combining, figuratively speaking, the shape of one row of protruding teeth with another complementary line that is assembled just-in-time. Unlike the macroscopic example, the connection is established not by mechanical but via non-covalent interactions.

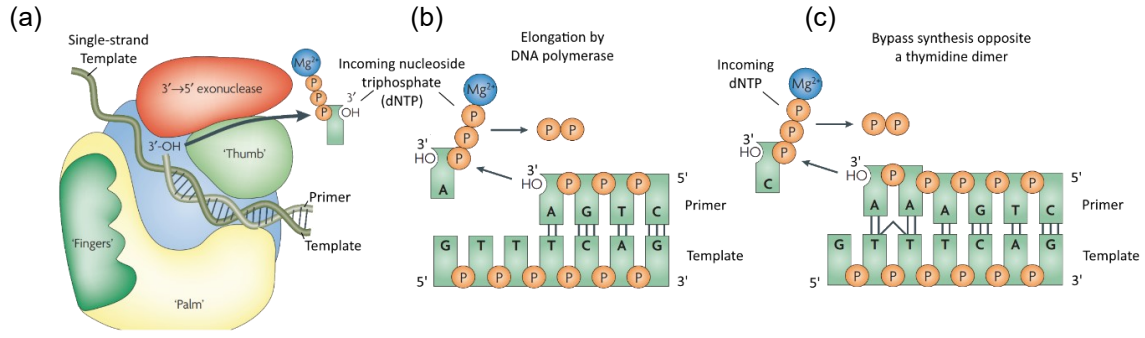

Figure 6.6. DNA polymerase catalysis and structure.[26b] (a) Model of a prototypical DNA polymerase with an associated 3′-5′ exonuclease domain that preferentially removes non-complementary nucleotides immediately after incorporation. (b) Elongation of the primer terminus proceeds by sequential addition of 5′ deoxynucleoside monophosphates, derived from 5′ deoxynucleoside triphosphates (dNTPs), with accompanying release of pyrophosphate. A divalent cation (presumably Mg^{2+} in cells) is coordinated with the phosphate groups on the incoming dNTP, and the reaction proceeds by nucleophilic attack of the 3′-OH primer termini on the α-phosphorus. (c) Bypass synthesis of thymine dimers by Y-family DNA polymerases. Adapted by permission from Springer Nature: reference 26b, Copyright 2008.

Associated to this process, the family of DNA topoisomerases have been found to regulate the complexity of intertwined double-helical DNA strands by reducing local topology prior to DNA replication, transcription, and repair.[28] The resulting action requires local exposure of the information encoded in entangled DNA through a procedure that can be illustrated as a conceptual cutting, reorganisation, and reconnection activity. At each turn, two units of a single strand are processed when advancing the strand of DNA during replication.

In summary, considering not only those examples described above but the collection of molecular machines in its entirety biology demonstrates a fine example of controlling every principal aspect of each contributing molecular component. It accomplishes this task with a variety of different techniques by successfully implementing mechanisms to actively guide movement on the molecular level in response to environmental changes. This has shown effective, for example, to replicate the underlying compartmentalised structure of the cell both with high fidelity and frequency and allowed it to become persistent.[7] And by doing so, nature has laid out a library of powerful concepts that sets a high standard for chemistry and at the same, provides a reference on which alternative synthetic systems can be modelled and utilised for potential tasks of traditional mechanical applications.

6.2. Aims of the Investigations

With this in mind and catalysed by the introduction of supramolecular concepts and methods[29] several attempts have been made to investigate synthetic molecular systems that resemble the working of biological machines.[30,31] Taking the cue from nature without exclusively confining to the original biochemical framework it has been anticipated that alternative systems can be created that form the basis for so-called (artificial) molecular machines.[30] It is the fundamental premise of those investigations that by learning how to create functionally and interactant systems and finding out methods to control and integrate them into complex assemblies, progressively more and more sophisticated functions can be established – perhaps, comparable to nature's example.[32] Understanding their working would provide the required first insight into controlling motion on the molecular level.[33] Additionally, those lessons acquired from the actuation of molecular machines may allow mechanical tasks to be performed more efficiently and learning about molecular machines could also shed light on the principles of life.[34]

Thus, development of molecular machines and their prospective applications in current technology have been described as of general importance.[35] This position has been emphasised by the decision of the Nobel Committee to award the Nobel Prize in Chemistry 2016 to J.-P. Sauvage,[35b] J. F. Stoddart,[35c] and B. L. Feringa.[35d] In the view of the progress achieved towards "designing and synthesising molecular machines" the committee[36] noted that "in a sense, we are at the dawn of a new industrial revolution of the twenty-first century and the future will show how molecular machinery can become an integral part of our lives."

From a historic perspective, it was physicist R. Feynman who in a discourse on "There's Plenty of Room at the Bottom" in 1959 created the first notion that prompted studies of building artificial molecular-sized machines.[35a,37] Under the title "an invitation to enter a new field of physics" R. Feynman outlined the possible advantages that may come along with increased miniaturisation from a general point of view. He pointed out that if small not only information storage and computation density would increase but also new types of

machinery might be possible when operated on the atomic level. Once attained, he noticed[37] that resulting technology “would have an enormous number of technical applications.”

Yet, pursuing this abstract goal of an atom-based machinery has turned out to be a complex evolving problem. Several basic issues have arisen since its first original intimation by Feynman, and several different strategies have been adapted to approach them both with synthetic[20,31,38] and theoretical methods[39] but also, for example, by examination of biological systems.[13] The basic cause for the complexity of this task can be attributed to a lack of a common agreement on the direction of principal studies: Neither a potential starting point nor an approach had been identified by Feynman for the initial investigations.[40]

6.3. Forming of a Definition

This has manifested itself for example in the several distinct definitions of “molecular machines” that have been reported in the literature: Well ahead of the beginnings of the field and also the early discoveries in biochemistry G. W. Leibnitz[41] already pointed out in 1714 that “machines of nature, namely living organisms, are still machines even in their smallest parts, *ad infinitum.*” He added that “a machine made by human artifice is not a machine in each of its parts.” Along with the advances in biochemistry this has led to the intermediate conclusion[14] that biological machines are “devices that can produce useful work through the interaction of individual molecules at the molecular scale of length.”

In contrast to this, following the talk of Feynman physicist K. E. Drexler initially argued that except of the physical size and methods for actualisation, there is no obvious distinction between the concepts and working of classical macroscopic and artificial molecular machines.[42a] In line with this statement, he found that the existing definition of machines as “any system, usually of rigid bodies, formed and connected to alter, transmit, and direct applied forces in a predetermined manner to accomplish a specific objective, such as the performance of useful work” can be applied to molecular machines, too. This particular attitude[42] has however been reconsidered in light of ensuing discussions.[43]

It has arrived at the currently established formulation of Balzani and Stoddart[36,44] who have described artificial machines as “an assembly of a distinct number of molecular components that are designed to perform machinelike movements (output) as a result of an appropriate external stimulation (input).” In a similar way, Credi et. al.[45] concluded that molecular machines are “a type of molecular device in which the components can be set in motion relative to one another in a controlled manner, resulting in the potential ability to carry out a function.” The term “molecule device” in turn refers to “an assembly of a discrete number of molecular components designed to execute a predetermined task.” Refining this definition, Leigh and colleagues[31] proposed that machines form “a system in which a stimulus triggers the controlled motion of one molecular or submolecular component relative to another, potentially resulting in a net task being performed.” Finally, it has been emphasised by Steed and Atwood[29f] that members of the molecular machinery are “a functioning entity composed of a number of interacting components that collectively carry out a predefined task for (presumably) beneficial result. [That is] a machine, or device, differs from a chemical substance in that it is useful for what it does, rather than for what it is.”

6.4. Development of Molecular Machines

6.4.1. Correlating Molecular Movement Through Nonbonded Interactions

The progressive change of the perception of molecular machines becomes particularly apparent when looking at the development of actual examples. At the start, investigations were mainly influenced by general physical and engineering concepts; Summarised as “hard matter” or techno mimetic approach building premises of nano-sized machines were directly inspired by classical mechanics and machines[33,40] and thus scientists have first and foremost tried to understand how molecular motion can be transmitted, for example, by different types of transmission as depicted in Figure 6.7.

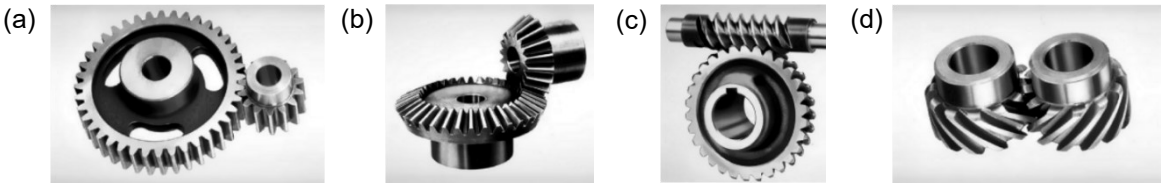

Figure 6.7. Macroscopic gearing systems. (a) Spur, (b) bevel, (c) worm (d) and helical gears. Adapted with permission from 46. Copyright 2005 American Chemical Society.

The rationale behind this approach originated in the idea that fundamental physical laws and mechanical working principles retain their validity during the miniaturisation process.[42b-c] It has been anticipated that by creating suitable mechanical elements with molecular structures, once established within a biological or chemical context, would enable the development of artificial machine components; And combining those components according to known engineering concepts enables assembly of first nanomachines.

With this notion in mind, a large number of molecular systems have been investigated whose structures resemble macroscopic objects.[46] This has allowed studying the fundamental molecular dynamics of different chemical motives with analytical techniques such as NMR, in particular, lineshape analysis.[47] One of the earliest experimental studies in this regard was reported by Christie and co-workers on 6,6′-dinitro-2,2′-diphenic acid **3**. They have shown that this biaryl system exists in two kinetically stable enantiomeric forms at room temperature, the *P*- (right-handed, positive) and *M*-conformer (left-handed, minus) (Scheme 6.1), and that those two stereoisomers can be successfully separated by fractional crystallisation with brucine.[48]

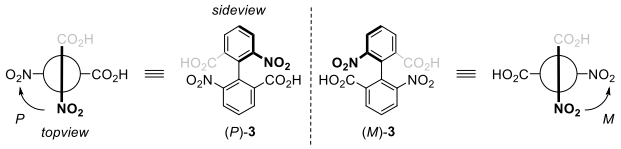

Scheme 6.1. Isolated atropisomers of diphenic acid **3** by Christie and co-workers.[48]

Similar observations have been made on related sterically hindered biaryl system such as biphenyl, anilines and styrenes.[46] The effect has been termed atropisomerism and attributed to the restricted rotation around the single bond as a result of the steric interactions and concomitant energy barrier for the interconversion between different isomers.[49] Accordingly, ^{19}F NMR experiments performed by Schuster and colleagues on triaryl carbonium cations e.g. 3,3',3"-trifluorotriphenylcarbonium ion **4** (Scheme 6.2 (a)) have demonstrated that the steric interactions between neighbouring aryl substituents can result in adoption of a discrete “propeller” like conformation (Scheme 6.2 (d)).[50] And in analogy to its mechanical counterpart this rotator can interconvert between isomers via a “flip” mechanism.

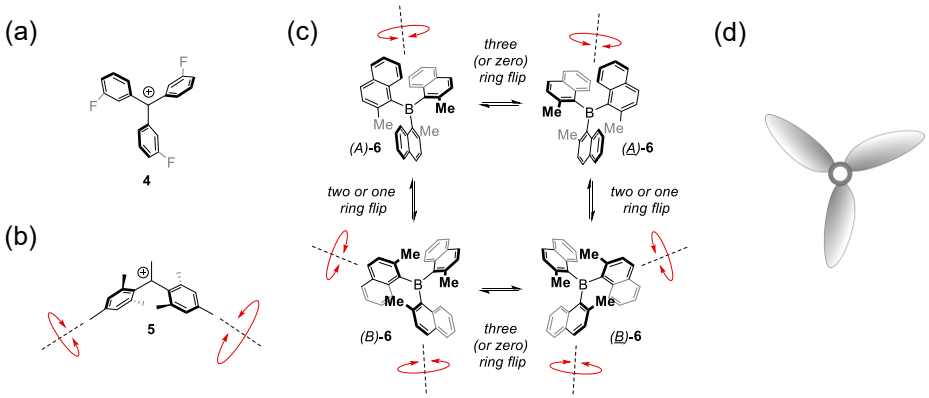

Scheme 6.2. Correlated motion in molecular propeller systems. (a) Hindered rotation around the central axes of 3,3',3"-trifluorotriphenylcarbonium ion **4**.[50] (b) Correlated rotation in dimesitylcarbonium ion **5**.[51] (c) Concerted rotation in tris-1-(2-methylnaphthyl)borane **6** via a three- and a two-/one-flip mechanism between diastereomers (*A*)-**6**, (*A*)-**6**, (*B*)-**6** and (*B*)-**6**.[52] (d) Illustration of a three-bladed propeller.

Moreover, studying the hindered rotation of a range of dimesitylcarbonium ions Kwart et. al. noted that the high frequency of the interconversion between possible enantiomers of systems such as **5** (Scheme 6.2 (b)) can only be explained if there is a mechanism that corresponds to an almost unrestricted rotation.[51] They concluded that the rotation of the mesityl rings is correlated and that the observed dynamics can be related to a "cogwheel effect." This basic concept was also shown to be applicable to describe the dynamics of other chemical systems such biaryl ethers, corresponding disulfides, ketones, etc.[46] This includes the work of K. Mislow and co-workers who have taken a closer look at the dynamics of D_3 symmetric triaryl borane systems such as methyl substituted tris(1-naphthyl)borane **6** as shown in Scheme 6.2 (c) above.[52b] Based on theoretical studies in conjunction with experimental ^{1}H NMR lineshape analysis they summarised that interconversion between isomers of the system can only explained if there exists a process that allows rotation of two or more components in synchrony.[52]

Correspondingly, Oki et. al. have proposed that attaching a large group such as a triptycene unit to one side of a hindered single bond could similarly influence the rotation of an opposite group due to the size of the sterically demanding bicyclic unit.[53] Changing the substitution pattern of an ether or methylene moiety, they have shown for systems such as **7a-d** that this allows isolation of discrete isomers which depending on the size of each group exhibit different rates of interconversion between conformers. At the same time, Mislow and Iwamura have made similar observations for bistriptycene rotors **8a-b** (Scheme 6.3).[54]

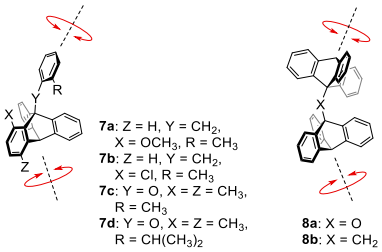

Scheme 6.3. Triptycene based molecular rotors **7a-d** reported by Oki[53] and **8a-b** by Iwamura and Mislow.[54]

Replacing the methylene or ether connection with the coordination geometry of transition metal platinum(II) Shionoya and co-workers have unveiled that reversible *cis-trans* isomerisation of the quadratic planar complex $PtCl_2$**10**$_2$ can in addition enable switching between states of mechanically correlated motion and uncoupled rotations of two rotators (Figure 6.8).[55]

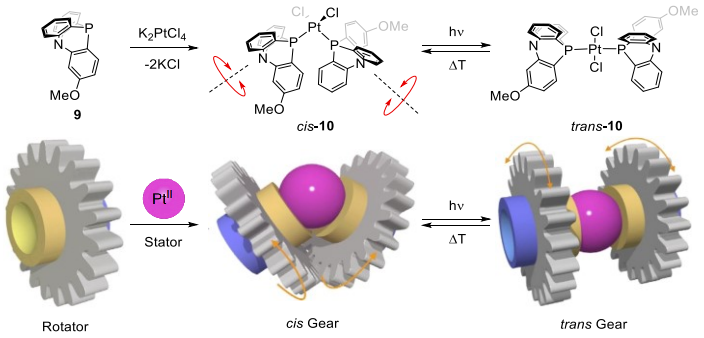

Figure 6.8. Schematic representation of a Pt^{II}-centred molecular gear $PtCl_2$**10**$_2$.[55] Adapted by permission from Springer Nature: reference 55, Creative Commons CC BY 2017.

As an alternative, the same authors have adopted the linear coordination of silver with triazole and pyridine and developed several examples of double[56] and multiple-decker sandwich systems[57] such as Ag_3**11**$_2$ (Figure 6.9).[56b] They showed that likewise, those silver complexes display mechanical coupling between two rotational degrees of motion and thus, they concluded that those complexes mimic molecular ball bearings.

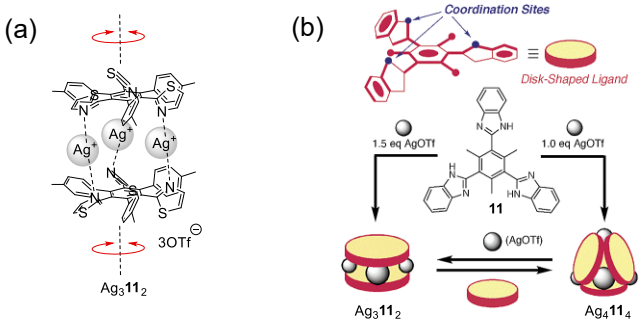

Figure 6.9. Complexation of disks **11** using silver ions into superstructures Ag_3**11**$_2$ and Ag_4**11**$_4$ reminiscent of ball bearings.[56b] (a) Structure of the complex and (b) scheme of the complexation. Adapted with permission from 56b. Copyright 2002 American Chemical Society.

In view of these results, Shionoya and co-workers have then developed a rotaxane-based system Ag_3**12**$_2$ that similar to the mechanisms of a crank allows conversion of rotational into translation motion with the help of a linear axle (Scheme 6.4).[58] Using a short phenylene acetylene track that functions as the crank axel the authors were able to achieve correlation with the rotation of the sandwich complex by the aid of a crown ether macrocycle that acts as a crank case. They illustrated that the crown ether can further function as a means of regulation. They showed that if the position of the macrocycle is fixed through formation of the ammonium complex “the rate of rotation becomes extremely slow.”

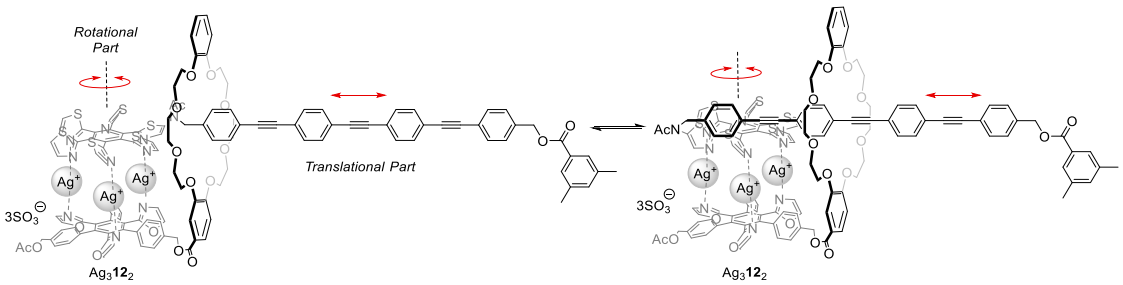

Scheme 6.4. Design and mechanism of a molecular crank system Ag_3**12**$_2$ using a rotaxane-based architecture to affect translation of rotational into linear motion.[58]

Aside from this, several examples of exploring other types of rotational motion have been reported that for instance, mimic a classical turnstile. They are based either on the triptycene group,[59] crown ether derived macrocycles[60] or other architectures.[61] A notable example of this endeavour is the bistable reversible switch **13**/**13**·Ag^+ created by the Hosseini group whose intramolecular rotation can be controlled by reversible addition of silver ions via linear intramolecular coordination between the two pyridine units (Scheme 6.5).[60f]

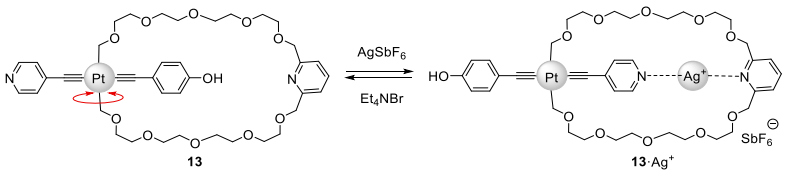

Scheme 6.5. Molecular design of a reversible bistable switch **13**/**13**·Ag^+ that functions as a molecular analogue to a classical turnstile.[60f] It becomes fixed by the coordination of silver in between opposite pyridinium units. Removal of the silver ions via precipitation with a bromide salt restores the free rotation.

Taking those but also other examples into account it has been found[62] that the principal approach of studying basic and coupled movement between different molecular degrees of freedom provides a first step towards understanding the dynamics under thermodynamic control and that those systems are of significant interest in view of the "intellectual challenge" and "their potential application in nanotechnology." However, it has been concluded[40] that those potential systems "must fight against the physics and chemistry intrinsic to their length scale." In practice, none of the concepts proposed has allowed operation of a molecular machine that displays unidirectional motion and in turn, to perform work.[46] In general, thermally-driven movement occurs in either direction and with equal probability.[63] And, neither the momentum nor the direction of motion can be controlled directly with those systems due to the symmetry of their designs.[30] Thus, on average, those system remain in place despite the actual steady dynamics on the molecular level.

6.4.2. Controlling Molecular Movement with External Stimuli

Consequently, simultaneous with the exploration of mechanically coupled motion, first attempts have been made to also attain active control over fundamental molecular degrees of freedom such as the rotation around the single[64] and double bond[65] but also the translationary motion encountered in mechanically interlocked architectures[66] (Figure 6.10).[31,67] It was anticipated that by learning from nature and its mechanisms of operation similarly unidirectional processes can be affected that would allow overcoming the "randomizing effect of Brownian motion".[13a] And that, taking e.g., ATP synthase as a reference, machines can be created that allow conversion of chemical energy into mechanical force.

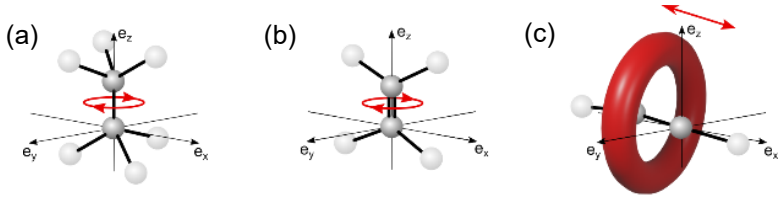

Figure 6.10. Principles molecular degrees of freedom investigated for controlling motion in (artificial) molecular motor systems.[31,67] Rotation around (a) the single and (b) double bond. (c) Translation within an interlocked architecture such as rotaxanes.

Controlling the Rotation around Single Bonds

One of the first examples of actively controlling the rotation around single bond with an external chemical stimulus was reported by Kelly and colleagues (Scheme 6.6).[68]

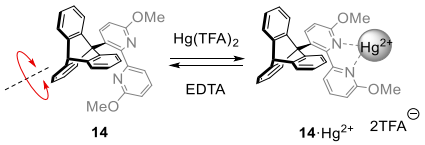

Scheme 6.6. Kelly's reversible bistable molecular brake **14** constructed from a triptycene unit and a 2,2'-bipyridine unit.[68a] Switching from a state of free to reduced rotation is achieved by complexation to mercury.

The system **14** explored was constructed from a triptycene unit attached to the 6 position of a 2,2'-bipyridine motif through a central carbon-carbon axis. When analysing the created system with ^{1}H DNMR at lower temperatures characteristic broadening of peaks was observed which suggested free molecular rotation around the single bond down to −80 °C. Once treated with a Hg^{2+} salt, however, ensuing binding of the transition metal to the bipyridine unit significantly reduced the rotation. This chemically-induced breaking effect made its appearance in the preservation of two sets of sharp proton peaks by NMR for temperatures up to −30 °C. Kelly et. al. explained this finding by the adoption of a planar bipyridine geometry and the steric interactions between the pyridine and triptycene protons lead to an increase of the energy barrier for the rotation around the central carbon-carbon bond. Further to this, they showed that upon removal of the metal salt with EDTA the original dynamic behaviour can be restored.

Building on this result other molecular brake systems have been created, for example, based on the restricted rotation of an isoindolinone system via reversible oxidation/reduction of a sulfide/sulfoxide unit,[69] but also, on the basis of reversible protonation of a biaryl system containing a quinoline motive as reported by Shimizu and co-workers.[70] The latter has also served as the basis for another design that uses a urea based receptor to prevent the rotation of an *N*-aryl succinimide framework by the addition of tetra-*n*-butylammonium acetate.[71] In like manner, electrochemical switching between the two conformers of paracyclophane macrocycles[72] and a bipyridylene-bridged bisporphyrin system[73] has allowed to control the momentum of the rotation around a single bond. Likewise, Feringa et. al. have used pseudorotaxane formation as means to modulate the rotation of an alkene-based motor system.[74]

Beyond achieving basic switching of the rotation in system **14** Kelly et. al. have also investigated whether the rotation around the crowded single bond can become asymmetric and thus, directional, when linking the triptycene unit to an intrinsically helically-shaped moiety instead (Scheme 6.7).[62]

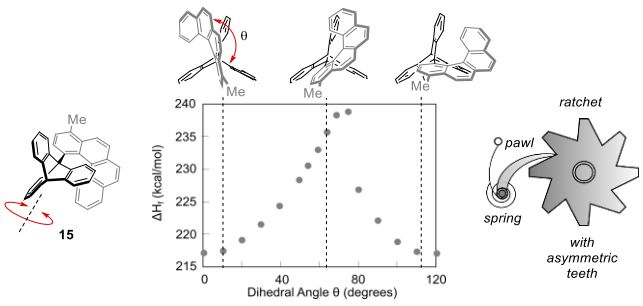

Scheme 6.7. Kelly's molecular analogue of Feynman's ratchet and pawl model **15** and its predicted energy profile for the rotation around the hindered alkyl bond.[62]

Specifically, they investigated the possibility to replace the bistable bipyridine motive of the original brake system **14** with a chiral [4]helicene moiety. They hoped that the curvature of the helical unit in compound **15** would conduce to differences in the steric interactions between alternate faces of the distorted aromatic π-system and the triptycene unit and hence, to an asymmetric rotation profile. The authors were assuming that molecule **15** can act as direct correspondent to Feynman's classical ratchet-and-pawl concept and allow validation of its design principles on the molecular level.[62,75,76] But, despite the intuitive assumption that the asymmetric energy profile for the rotation would favour the rotation over one side and disfavour the reverse process experimental results with ^{1}H NMR spin polarisation experiments[62] have unequivocally proven that ratchet **15** "rotates equally in both directions". This finding supported the prediction[30] that "the rate of rotation depends solely on transition state energy and temperature, and not on the shape of the barrier to rotation."

To overcome this limitation, Kelly and colleagues have then explored the application of urethane bond formation as means to lock an intermediate conformation in a kinetically stable position and at the same time restrict the rotation in one direction over one side.[77] They were able to demonstrate that using an amine functionalised triptycene system **16** its conversion to a reactive isocyanide **17** can be exploited in conjunction with a thermally induced isomerisation to achieve unidirectional rotation by 120° (Scheme 6.8 (a)).

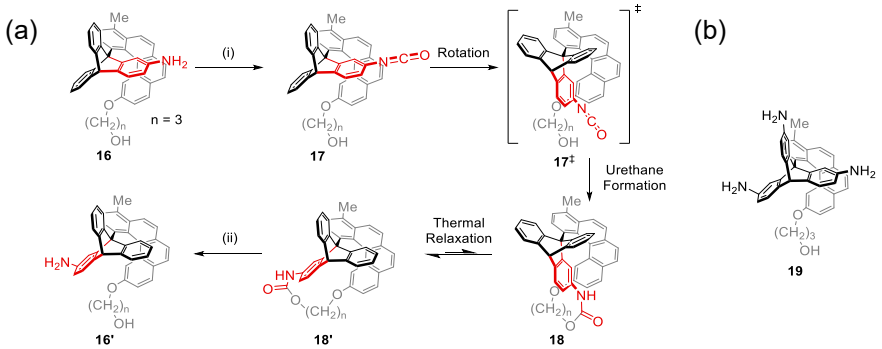

Scheme 6.8. Chemically-induced unidirectional rotation (120°) around a triptycene–helicene single bond.[77] (a) Reaction sequence for the 120° rotation of **16** to **16'** via relaxation of **18** and (b) proposed system **19** for a 360° rotation. Reaction and conditions: (i) $COCl_2$, Et_3N, $CDCl_3$, rt, 10 h, then (ii) $NaBH_4$, EtOH, 0 °C, 8 h.

In detail, beginning with amine **16** initial acylation with phosgene and concomitant elimination of hydrogen chloride with triethyl amine affords isocyanide derivative **17**. As an effect of the asymmetric design, spontaneous motion of the triptycene motive by thermal motion occurs clockwise towards the propyl alcohol ether chain where it triggers the urethane formation and thus, traps conformation **17‡** in nonequilibrium state **18**. This high energy intermediate state is kinetically unstable and thus, when allowed to relax predominately yields the lower energy conformation **18'**. In this case, the alternative pathway that would restore the original conformation **16** is prevented by the covalent connection. It is this key strain mediated discrimination between the forward and backwards rotation via relaxation under thermodynamic control – the balance breaking step[30,78] – that leads to the desired unidirectional motion. Kelly and co-workers subsequently also hydrolysed the urethane bond to unlock the system and form the rotated amine **16'**.

In following studies, the authors have investigated the effect of shortening the alcohol tether (n = 2 in Scheme 6.8 (a)).[64,77b] They have found that this reduces the rate-limiting thermal relaxation from about 6 h (n = 3) to few minutes (n = 2) and restrains the rate of rotation to the isocyanide formation.

The authors hoped that addition of two supplementary amine units on the triptycene would then allow completing the remaining 240° of rotation all around the axis with a molecule such as **19** by a sequence of two extra fuel pulses (Scheme 6.8 (b)).[64] To ensure regioselective isocyanide formation the Kelly group has further decided to include a 4-(dimethylamino)pyridine (DMAP) unit to "selectively deliver the phosgene equivalent to the proximal amino group" (Scheme 6.9).[79] Yet, despite success in realising initial DMAP-containing compound **20**;[80] preliminary operations with the phosgene fuel indicated the formation of bi- and triurethane species among the desired monoacylated species **21'**. To prevent this overreaction and restrain the isocyanide formation to the correct amine group several other acylation methods were trialled. However, the intramolecular isocyanide formation has proven elusive even with the initial acylation taking place as expected. Unfortunately, this has prevented the ultimate operation of Kelly's rotator **20**.

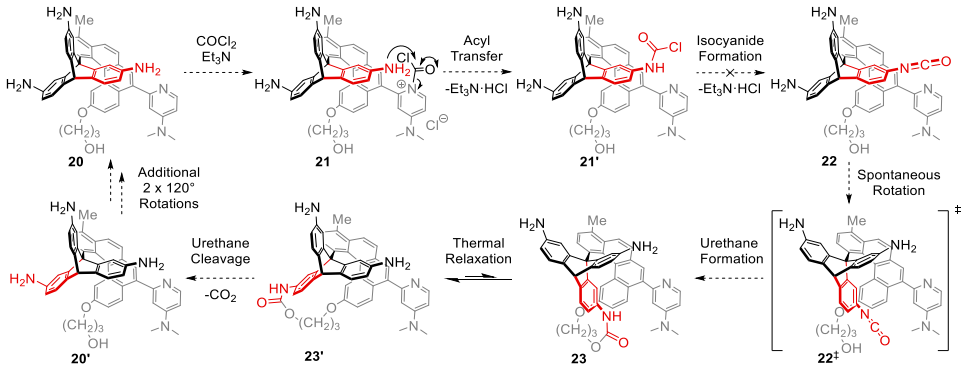

Scheme 6.9. Attempted operations of triptycene-helicene based motor system **20** for the phosphene induced 360° unidirectional rotation.[80] To achieve regioselective monoacylation the motor system has been extended by a DMAP unit.[80a] Final operation has been averted by the inherent lack of reactivity of acylated state **21'**.

Separate to this, attempts were made to also effect rotation around the axis of sterically hindered biaryl systems.[31] Relying on the steric influence of ortho substituents it was anticipated that modifying the energy barrier for the interconversion between different atropisomers can ultimately create distinct kinetically stable states. And, by taking advantage of reported diastereoselective reactions and coordinating the transformation between atropisomers in correct order, similarly, unidirectional rotation can be attained.[81]

With this intention, Branchaud and colleagues have investigated a series of biaryl-based lactone systems such as **24** (Scheme 6.10).[82] They contemplated that once lactone **25** has been formed the ring-opening to **26** with suitable nucleophiles could twist the top part of a biaryl motif around one direction of the central axis.

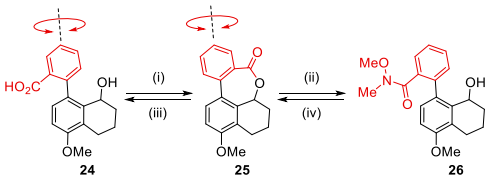

Scheme 6.10. Sequential transformation of lactone **25** reported by Branchaud and peers for achieving rotation around the central axis of a biaryl system by a sequential lactonization and ring opening under Weinreb conditions.[82a] Reaction and conditions: (i) 5% HCl. (ii) *N,O*-dimethyl hydroxylamine hydrochloride, ^{i}PrMgCl, THF, then 5% HCl. (iii) LiOH, THF:H_2O, reflux, then oxalic acid. (iv) TFA, neat.

The basic operation devised (Scheme 6.10) starts from biphenylene carboxylic acid **24** by forming the intramolecular seven-membered lactone ring between the upper and lower rotator parts under acidic conditions.[82a] Following ring-opening of **25** under Weinreb conditions with *N,O*-dimethyl hydroxylamine and

isopropyl magnesium chloride affords *N*-methoxy amide **26**. It has been shown by Branchaud et. al. that the amide can then be hydrolysed back to lactone **25** under acidic conditions and subsequently converted to the starting carboxylic acid **24** with lithium hydroxide. In this case no directionality is achieved, but successive studies on biaryl systems **27** and **30** have shown that by using a chiral nucleophile such as lithio(*S*)-1-phenylethanamine or instead employing a chiral alcohol unit, this issue can be resolved (Scheme 6.11).[82b-c]

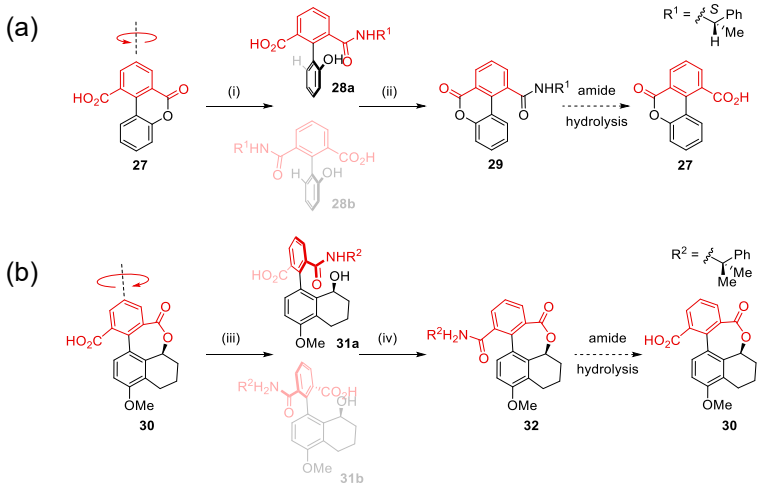

Scheme 6.11. Biaryl based motor systems (a) **27**[82b] and (b) **30**[82c] reported by Branchaud and colleagues for achieving a 180° unidirectional rotation by sequential lactonization and diastereoselective ring opening under Weinreb conditions. Reaction and conditions: (i) lithio (*S*)-1-phenylethanamine, THF, rt, then (ii) 2 N HCl, 58% over two steps. (iii) $PhC(CH_3)_2NH_2$, $AlMe_3$, CH_2Cl_2, reflux. (iv) DCC, DMAP, DMAP·HCl, $CHCl_3$, reflux.

It was expected that due to the stereoselectivity of the transformation the ensuing rotation around the central carbon-carbon bond mainly proceeds via a single pathway because of the difference in the energy barriers for different ring-opening reactions. In fact, Branchaud and peers were able to prove this assumption by successfully monitoring intermediates **28a** and **28b** as well as **31a** and **31b** and measuring ratios between these configurations. In the case of biaryl system **28** (Scheme 6.11 (a)) an *e.e.* value of up to 50% was obtained whereas in the case of **31** (Scheme 6.11(b)) the lactone was selectively opened to **32** via **31a** with an *e.e.* value greater than 99%. The second step, the selective amide hydrolysis in the presence of the lactone, has however proven difficult and therefore rendered originally envisaged 360° rotation impossible.[31]

Yet, reinvestigating the methodology Feringa et. al. were able to successfully design an alternative reaction for system **33** that completes a full 360° rotation around the central carbon-carbon bond (Figure 6.11).[83]

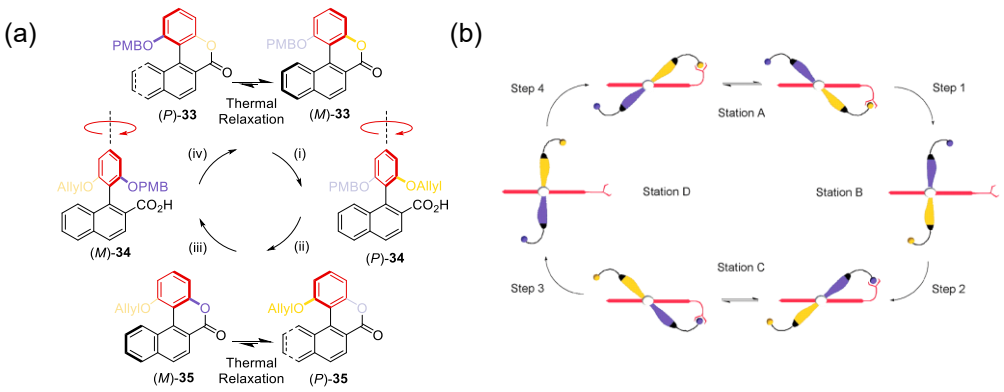

Figure 6.11. Reversible, unidirectional rotation (360°) of biaryl motor **33** by chemical energy.[83] (a) Operation scheme. (b) Schematic illustration for the operation of unidirectional molecular motor **33**. From reference 83.

Reprinted with permission from AAAS. Reaction and conditions: (i) (*S*)-2-methyl-CBS oxazaborolidine, BH_3·THF, THF, 0 °C, 25 min, 92%, then allyl bromide, K_2CO_3, DMF, rt, 20 h, then CrO_3·H_2SO_4·H_2O, Me_2CO, rt, 2 h, then $NaClO_2$, 2-methyl-2-butene, AcOH:H_2O:THF, rt, 1 h, 76% over three steps. (ii) $Ce(OTf)_3$, $MeNO_2$, 1,3-dimethoxybenzene, 60 °C, 25 min, 76%. (iii) (*S*)-2-methyl-CBS oxazaborolidine, BH_3·THF, THF:PhMe, 0 °C, 7 min, 56%, then *p*-methoxybenzyl chloride, K_2CO_3, NaI, Me_2CO, reflux, 30 h, 87%, then MnO_2, CH_2Cl_2, rt, 48 h, then $NaClO_2$, 2-methyl-2-butene, AcOH:H_2O:THF, rt, 1 h, 82% over two steps. (iv) $Pd(PPh_3)_4$, HCO_2H, THF, reflux, 24 h, then DCC, rt, 15 min, 99% over two steps.

They have found that instead of successive diastereoselective amide formation and hydrolysis, alternating protection and deprotection of two phenolic alcohols under orthogonal conditions can successfully affect the transformation between discrete equilibrium states in a unidirectional manner. In practice, they have shown that the selective ring opening of lactone (*M*)-**33** (Station A) with (*S*)-2-methyl-oxazaborolidine i.e., the Corey-Bakshi-Shibata (CBS) reagent[289] selectively furnishes one of the alcohol atropisomers that can be subsequently protected with allyl carbonate (Allyl) group to give (*P*)-**34** (Station B). Following removal of the *p*-methoxybenzyl ether (PMB) protecting group under orthogonal conditions frees one of phenolic alcohol groups (purple) which can then be reacted with the opposite carboxylic acid motive to give intermediate lactone (*P*)-**35** (Station C) by rotation around the central axis. Being configurationally unstable, however, the strained lactone (*P*)-**35** relaxes towards low energy conformer (*M*)-**35** via helix inversion under thermodynamic control. This completes the first 180° of rotation. Theron, a sequence of another ring opening reaction with (*S*)-CBS reagent, PMB formation and further oxidation of the generated benzyl alcohol yields atropisomer (*M*)-**34** (Station D). Accordingly, selective removal of the allyl group then enables lactone formation to (*P*)-**33** and after a second helix inversion restores the original lactone in state (*M*)-**33**. Altogether, a reaction sequence of ten steps is performed to complete one full 360° rotation in an overall yield of 21%. Due to high enantioselectivity of the key CBS reduction the full reaction cycle results in a highly directional process that additionally, is reversible by the choice of reagents.

Building on a palladium based redox cycle, Feringa and colleges have then extended this idea and outlined a scheme to perform a 360° unidirectional rotation in an alternative sulfoxide containing biaryl motor system (*S,M*)-**36**/(*S,P*)-**36** (Scheme 6.12).[84]

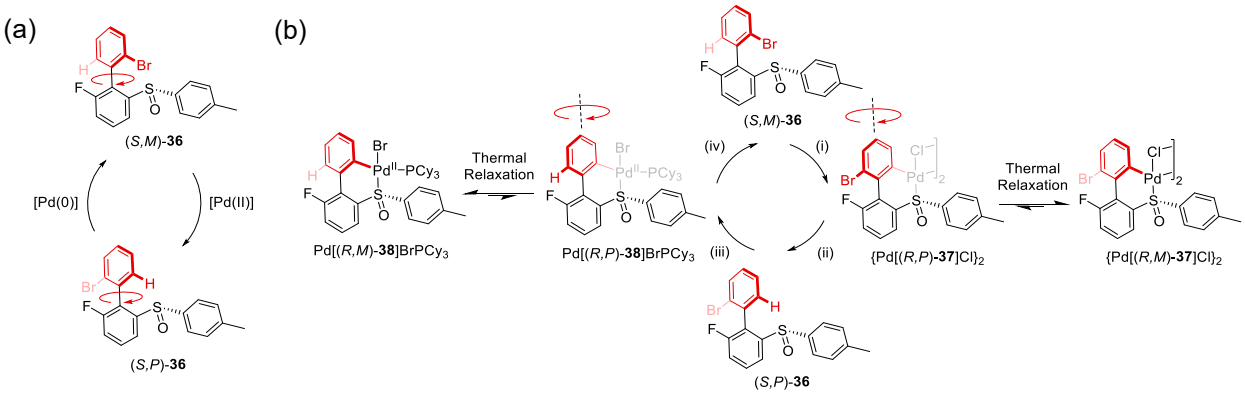

Scheme 6.12. Palladium-mediated 360° unidirectional rotation of biaryl motor system (*S,M*)-**36**/(*S,P*)-**36**.[84] (a) Proposed concept of unidirectional rotation via combination of axial and central chirality by shuttling between Pd(0) and Pd(II) redox states. (b) Operation scheme. Reaction and conditions: (i) $Pd(OAc)_2$, TFA, 1,2-DCE, 80 °C, 22 h, then LiCl, Me_2CO, rt, 4 h. (ii) *dba*, 1,2-DCE, rt, 15 min, then $NaBH(OAc)_3$, rt, 20 min. (iii) PCy_3, THF, 40 °C, 20 h. (iv) NBS, CH_2Cl_2, rt, 24 h, 45% over four steps, yielding 1.00:1.32 mixture of (*S,M*)-**36** and (*S,P*)-**36** and representing a 19% overall yield obtained for the performed 360° rotational cycle.

It is based on the difference in reactivity between palladium(0) and palladium(II) complexes towards the selective oxidative insertion into an aromatic C-Br bond and sulfoxide directed C-H bond activation. Feringa and colleagues have shown that by selectively switching between the different palladium oxidation states this can guide the transition between four distinct conformers over 360°. At the outset, it was hoped that once finding suitable methods for successfully modulating oxidation states the operation of motor **36** will become autonomously (Scheme 6.12 (a)). As of currently, however, the operation is conducted by the following four step reaction sequence in an overall yield of 19% for the 360° rotation cycle.

First, starting from atropisomer (*S,M*)-**36** (Scheme 6.12 (b)) palladium(II) acetate and trifluoroacetic acid (TFA) were added to affect the regioselective sulfoxide-directed C-H insertion. This gave high energy palladacycle {Pd[(*R,P*)-**37**]Cl}$_2$ which spontaneously relaxed to its low energy counterpart {Pd[(*R,M*)-**37**]Cl}$_2$ via helix inversion. Next, reductive elimination of the organopalladium(II) hydrido complex H–Pd[(*R,M*)-**37**]Cl was performed with reducing agent sodium triacetoxyborohydride (STAB). Completing this step recovered the original aromatic C-H bond and at the same time, concluded the first 180° rotation to atropisomer (*S,P*)-**36**. The remaining 180° rotation was affected by treating the reaction mixture with tricyclohexylphosphine (PCy) in addition to dialkene ligand dibenzylideneacetone (dba) to induce selective oxidative insertion of the generated palladium(0) into the C-Br. This resulted in the formation of Pd[(*R,P*)-**38**]BrPCy$_3$ as an intermediate and ultimately, when completing the second helix inversion, conformer Pd[(*R,M*)-**38**]BrPCy$_3$. Final bromination with *N*-bromo succinimide (NBS) then restored machine (*S,M*)-**36** in its original state.

Revisiting the previous concept of the biaryl motor **33** (see Figure 6.11) Feringa and coworkers have recently also demonstrated the working of an alternative design that, likewise its predecessor, undergoes a full 360° unidirectional rotation but relies on a six step stereoselective esterification and lactone hydrolysis protocol to mediate the interconversion between atropisomers (Scheme 6.13).[291]

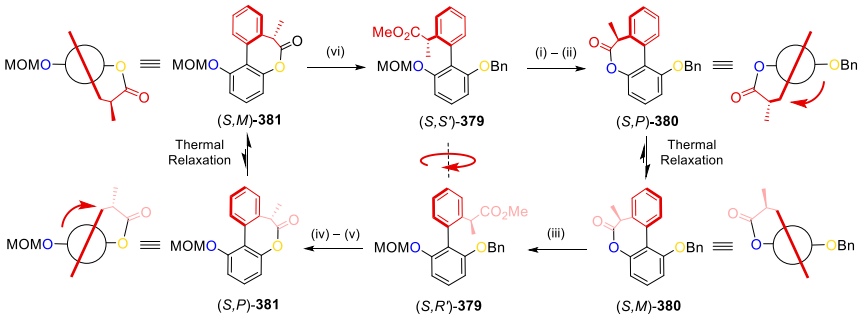

Scheme 6.13. Chemically driven 360° unidirectional rotation of biaryl motor system (*S,S'*)-**379**/(*S,R'*)-**379**.[291] The stereochemistry of each equilibrium structure of the six step reaction cycle has been confirmed by single-crystal X-ray diffraction. Reaction and conditions: (i) HCl, MeOH, rt, overnight, then NaOH aq., 15 h, 95%. (ii) 1-ethyl-3-(3-dimethylaminopropyl)carbodiimide (EDCI), Et_3N, CH_2Cl_2, 26 °C, 16 h, 97%. (iii) MeONa, MeOH:THF, 0 °C, 10 h, then NaH, MOM-Cl, DMF, 0 °C, 5 h, 82%. (iv) Pd/C, H_2, and then NaOH aq. 15 h, 92. (v) EDCI, Et_3N, CH_2Cl_2, 26 °C, 16 h, 94%. (vi) MeONa, 10 h, then BnBr, DMF, rt, 12 h, 87%.

The design relies on the incorporation of a stereogenic centre at the upper rotor in **379** which serves as a steric bias that steers the rotation of the biaryl motor along a single direction at each lactonization step (Scheme 6.13, step (ii) and (v)). In conjunction with the orthogonal phenolic protecting groups methoxymethyl (MOM) and Bn the authors are able to sequentially perform a full rotational cycle and in addition, characterise each intermittent atropisomer in detail via NMR, UV-vis, CD, and single-crystal X-ray diffraction.

Controlling the Rotation around Double Bonds

Separate to these studies, the Feringa group has also explored the unidirectional rotation around overcrowded alkene systems via photochemical isomerisation. This approach ensues from earlier studies on chiroptical switches.[85] They have built on the observation that switching between opposite handedness of (*P*)- and (*M*)-configurations of helices such as **39** or **40** can be used as means of storing information in the form of chirality that can be read-out with circularly polarised light (CPL) (Scheme 6.14).[85e] Moreover, this behaviour can be used to interconvert between the different chiral states of a cholesteric liquid crystalline phase when using switchable helical shaped molecules such as **39** as a dopant.

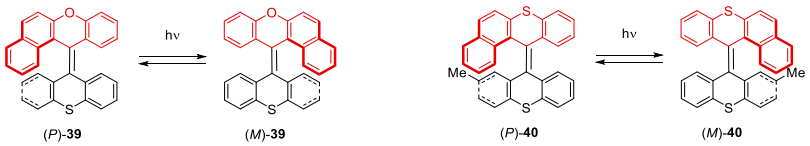

Scheme 6.14. Examples of chiroptical switches based on the photochemical isomerisation of helicenes. Photochemical interconversion of (*P*)- and (*M*)-helices of **39** and **40** upon irradiation with left or right circularly polarised light.[85e]

Importantly, in an effort to find a solution for controlling the direction of photochemical isomerisation Feringa and colleagues have synthesised alkene **41** (Scheme 6.15).[86] Exploring its dynamics under irradiation with light they have noticed that the incorporation of two additional chiral centres opposite to the helicene moieties can lead to a unidirectional rotary behaviour when carefully adjusting the conditions both for the isomerisation of the double bond and the following helix inversion; And that when alternating the isomerisation, a four step reaction sequence can give a full 360° rotation around the central carbon-carbon double bond.

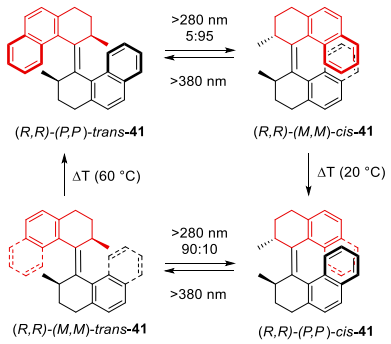

Scheme 6.15. First molecular motor design **41** capable of a unidirectional 360° rotation via a twofold photochemical isomerisation and thermally induced helix inversion.[86]

In detail, using a wavelength above λ ≥ 280 nm the authors observed that conformer (*R,R*)-(*P,P*)-*trans*-**41** undergoes selective *trans*-*cis* isomerisation to (*R,R*)-(*M,M*)-*cis*-**41** at the photostationary state (PSS). This intermediate can relax spontaneously to its lower energy state (*R,R*)-(*P,P*)-*cis*-**41** via thermal helix inversion (THI)[31] in irreversible manner if raising the temperature to 20 °C. This rotates the top over one side by 180°. To drive the rotary cycle another step forward, light at longer wavelength λ ≥ 380 nm was used to induce the reverse *cis*-*trans* isomerisation to kinetically stable intermediate (*R,R*)-(*M,M*)-*trans*-**41**. The remaining part of the cycle was concluded by promoting the irreversible helix inversion at a temperature of 60 °C. This study pointed out the opportunity of using a photochemical reaction to selectively alter the conditions for transformation between states to perform a controlled rotary cycle around a double bond.[87a]

Demonstrating the feasibility of the concept the author proceeded by changing different components of the molecular motor design.[87] They predicted that by changing the chemical substituents but retaining the alkene framework could improve photochemical and thermal relaxation properties of the original motor system **41** and thus enhance its rotation characteristics, in particular, its rotational frequency[88] and ultimately allow operation at room temperature.[31] As a first step, the differences in activation energies for the isomerisation between different helix conformations were addressed. By replacing the original symmetric design **41** for a system that builds on two separate upper and lower units Feringa and co-workers developed a second iteration of the molecular motor design that builds on a bis(thianyl) motif.[89] With this updated concept in hand Feringa et. al. created several systems such as molecular motor **42** (Scheme 6.16) that show the unique ability to continuously operate at a single wavelength – in this example at a wavelength of λ = 365 nm – and also do away with one of the chiral centres but retain unidirectional rotatory behaviour.

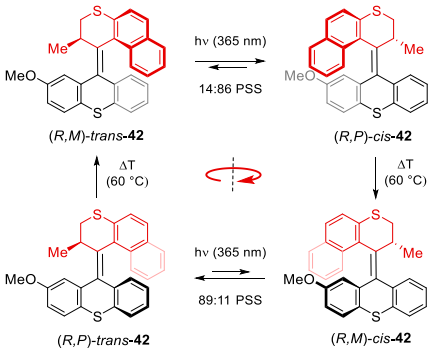

Scheme 6.16. Second molecular motor design **42** capable of a unidirectional 360° rotation under constant irradiation with light via a single stereogenic centre.[89]

Concomitant with the continuing optimisation of the optimisation of the motor design, Feringa and colleagues have also questioned whether the direction of the motor can be reversed with for instance epimerization of an attached stereogenic centre.[90] The system **43** investigated for this purpose includes a stereo centre at the β position of the upper motor part in form of an *N,N*-dimethyl amide substituent (Scheme 6.17).

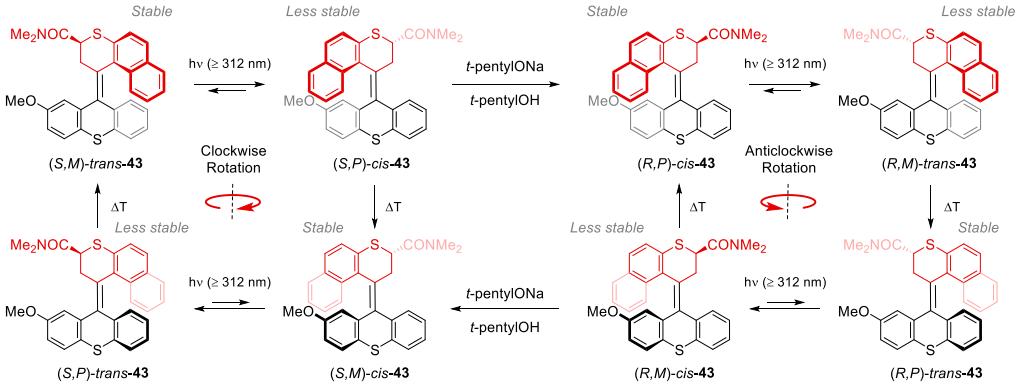

Scheme 6.17. Reversing the direction in a light-driven rotary molecular motor **43** via base-catalysed epimerization of a stereogenic centre.[90]

The authors have shown that steric interactions in the remote β position can similarly influence direction of the rotation by controlling the equilibrium distribution the THI, albeit less efficiently. Importantly, they were able to successfully develop conditions for the central epimerisation step using sodium *t*-pentoxide/*t*-pentanol to induce the inversion from (*S*,*P*)-*cis*-**43** to (*R*,*P*)-*cis*-**43**. Feringa et. al. have demonstrated that both the

starting (*S*,*P*)-*cis*-**43** and newly formed diastereomer (*R*,*P*)-*cis*-**43** are capable of undergoing unidirectional rotation via two photoisomerization and THI reactions but in opposite directions.

Controlling the Translation in Mechanically Interlocked Systems

Besides efforts to affect one-dimensional rotation around covalent bonds several groups worked on guiding the translationary motion in mechanically interlocked architectures.[31] Stimulated by the studies of Sauvage and peers on the construction of molecular machines based on a rotaxane and catenane architecture[91] several systems have been synthesised that can be switch reversibly between different equilibrium states.[92] This includes the original work of the Sauvage group who have studied the electrochemical properties of [2]catenane system **44** consisting of two separate, mechanically interlocked macrocycles comprising 2,9-diphenyl-1,10-phenanthroline (*dpp*) and (2,2′:6′,2″-terpyridine (*tpy*) ligand motifs (Scheme 6.18).[93]

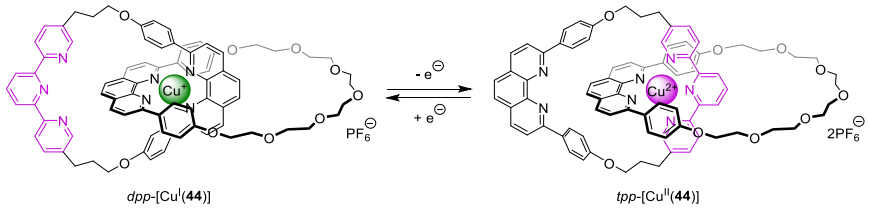

Scheme 6.18. Electrochemical switching of [2]catenane *dpp*-[Cu^{I}(**44**)]/*tpy*-[Cu^{II}(**44**)].[93]

They have demonstrated that the two ligands selectively coordinate to the two oxidation states of Cu(I)/Cu(II) in an alternate fashion and thus, reversible transformation between the different [2]catenane complexes – *dpp*-[Cu^{II}(**44**)] and *tpy*-[Cu^{II}(**44**)] – can be achieved via cycles of reductions and oxidation.

The first example reported to achieve distinctly controlled transport of a macrocycle in a [2]catenane system with more than two stations was reported by the Leigh group (Figure 6.12).[94]

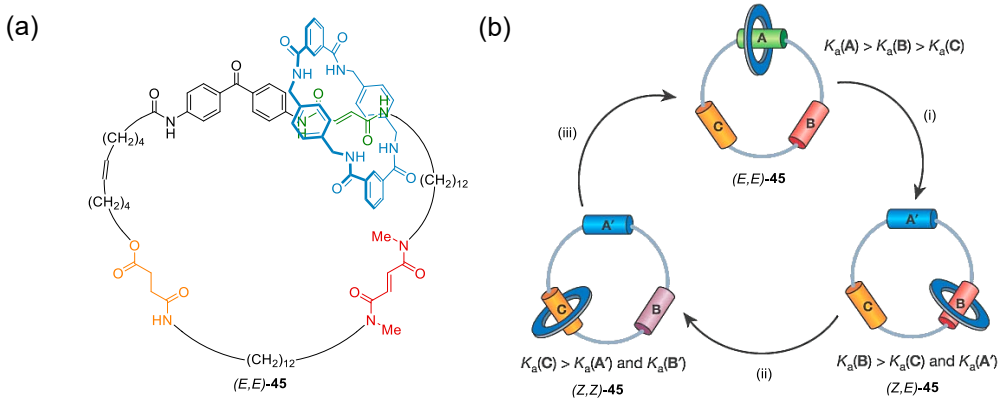

Figure 6.12. Bidirectional sequential movement between three different binding sites in a [2]catenane motor (*E,E*)-**45**.[94] (a) Structure and (b) corresponding operation scheme. Adapted by permission from Springer Nature: reference 94, Copyright 2003. Reaction and conditions: (i) 350 nm, CH_2Cl_2, 5 min, 65– 67%. (ii) 254 nm, CH_2Cl_2, 20 min, 48–51%. (iii) 100 °C, $C_2H_2Cl_4$, 24 h, ≤100% or ethylene diamine, 50 °C, 48 h, 50–74%.

The basic design of their [2]catenane motor (*E,E*)-**45** relies on incorporating three different binding motives in the form of a fumaramide (A, green), a tertiary fumaramide (B, red) and a succinamide (C, orange) unit along the track of a large macrocycle. Combined with a smaller benzylic amide macrocycle that wraps around the track those motives serve as (binding) stations for the rotary motion of catenane system (*E,E*)-**45** with

an affinity in an order as listed above. To a lesser extent also the amide connection has shown to engage with the macrocycle via weak hydrogen bonding. Leigh et. al. further included a benzophenone unit in the main track that acts as a selective photosensitizer for the isomerisation of the adjacent fumaramide station.

The operation of **45** proceeds through a series of light-induced isomerisation reactions. It begins with the irradiation of (*E,E*)-**45** with light at a wavelength of λ = 350 nm which selectively induces *trans-cis* isomerisation of the fumaramide group (A, green) to its maleamide analogue (A', blue). The station in is latter configuration A' has a lower binding affinity towards the macrocycle and thus, the macrocycle moves to the tertiary fumaramide (B, red) to give (*Z,E*)-**45**. Following second irradiation at a shorter wavelength λ = 254 nm also switches tertiary fumaramide station B (red) from the *E* to the *Z* configuration. This biases the macrocycle one step further towards the weak succinamide station C (orange) to give catenane (*Z,Z*)-**45**. Final *cis-trans* isomerisation either by a thermal or ethylene diamine catalysed process then restores the original catenane (*E,E*)-**45**. Over the course of the reaction the intermediate shuttling of the macrocycle between the stations describe a full periodic cycle but because the system can shuttle in both directions at each step no net unidirectional rotation is affected. In many ways, this confirms the observation Kelly has made with molecular ratchet **14** highlighting that direction of the shuttling is independent of the transition state profile and the path taken between equilibrium states under thermodynamic control.

Yet, in the same report Leigh and colleagues have also shown that the formation of a corresponding [3]catenane (*E,E*)-**46** provides the opportunity to overcome this limitation (Figure 6.13).[94] They demonstrated that in the case of the [3]catenane system **46** the two smaller benzylic amide macrocycles (blue and red) occupy both the strong fumaramide (A, green) and weaker tertiary fumaramide station B (red). They realised that upon light-induced isomerisation, the presence of the leading red macrocycle at station B effectively blocks the path for the trailing blue macrocycle to proceed from the maleamide station A' (blue) to the tertiary fumaramide motive (B, red). As result, it is forced to move to the succinamide station C (orange). This, however, can only occur in only one of the possible directions by the very presence of the other macrocycle.

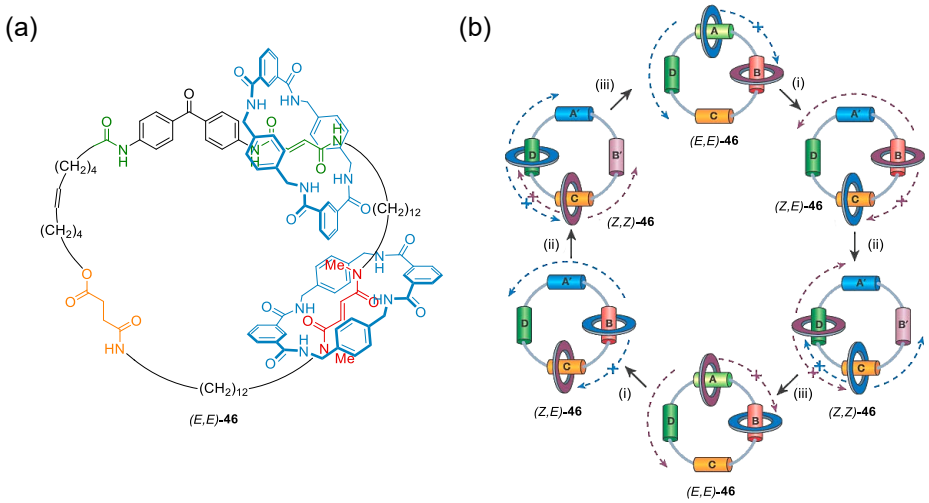

Figure 6.13. Stimuli-induced unidirectional rotation in a four-station [3]catenane motor (*E,E*)-**46**.[94] (a) Structure and (b) corresponding operation scheme. Adapted by permission from Springer Nature: reference 94, Copyright 2003. Reaction and conditions: (i) 350 nm, CH_2Cl_2, 5 min, 67%. (ii) 254 nm, CH_2Cl_2, 20 min, 50%. (iii) 100 °C, $C_2H_2Cl_4$, 24 h, ≤100%, cat. ethylenediamine, 50 °C, 48 h, 65%, or cat. Br_2, 400–670 nm, CH_2Cl_2, −78 °C, 10 min, ≤100%.

This effect, succinctly termed 'follow-the-leader' process,[31] ensures that overall, not only the translocation from (*E,E*)-**46** to (*Z,E*)-**46** but also following steps takes place in a unidirectional manner. When repeating the remaining operation scheme as described in the previous section for [2]catenane (*E,E*)-**45** this yields a complete rotary cycle in six steps and shows that successive translation of macrocycles in an alternating direction can also successfully delineate unidirectional motion. The motion is solely guided by the steric between the two macrocyclic components and their interactions with different binding stations on the track.

On the whole, the previous series of examples demonstrate the gradual shift in the design and understanding of molecular machines from the initial creation of geometrical shapes and study of their correlated motion to the investigation of principal chemical motives whose conformation can be controlled with suitable chemical methods.[33,40] It highlights the underlying complexity of creating and successfully designing molecular machines. And, along with the previous studies an attempt has been made to develop a generalized theory that could help developing a rational approach of how to control movement on the molecular with chemical methods.

6.5. Fundamental Concepts for Controlling Molecular Motion

6.5.1. Molecular Switches

It is known that at ambient temperature thermal motion gives rise to steady motion on the molecular level in the form of e.g., translational, rotational, or oscillatory movement and random thermal fluctuations known as Brownian motion. But particles driven by thermal energy first and foremost move in *every* direction with *equal* probability.[63] In other words, due to this inherent symmetry the average of thermal motion or "thermal noise" will always be zero over time.[39] This implies[63] that under thermodynamic control particles do not undergo spontaneous "concerted, ordered motion" in the form of directional movement and therefore, thermal motion can neither be harnessed nor act as a stimulus to perform "useful" work with molecular machines.[31,38f]

In fact, studies of "thought-machines" such as Maxwell's demon, Szilard's engine or Smoluchowski's trapdoor have proven theoretically that work cannot be extracted from isolated systems when resting in thermal equilibrium.[38f,78] This finding is also expressed in the Kelvin statement of the Second Law of Thermodynamics:[63] "No process is possible in which the sole result is the absorption of heat from a reservoir and its complete conversion into work." Notably, it has been R. Feynman who by analysis of a so-called miniature ratchet and pawl device showed that random thermal motion in the form of Brownian motion cannot be convert into (mechanical) work with a molecular-sized machine unless applying an (external) thermal gradient.[39] Additionally, violation of Heisenberg's uncertainty relationship breaks the results of the second law of thermodynamic, too.[95] That is the inherent uncertainty related to the quantum mechanical description of the molecular system already seems to imply that work cannot be extracted from equilibrium systems which further confirms the preceding analysis.

It has been highlighted by Leigh et. al.[31] that "the challenge of designing molecular motors lies not with producing motion at the molecular level, but in controlling the directionality of movement." Insofar it has been a significant advancement in the field of molecular machines when Stoddart and co-workers[96] introduced the basic concept of using discrete binding motifs so-called "stations" to control the position of a movable part termed "shuttle." Applying this idea to a rotaxane architecture they have demonstrated that when

incorporating multiple different stations into a linear thread, those components can function as reversible switchable binding motives for a mechanically interlocked macrocycle. Provided that the stations and the shuttle can interact, the resulting equilibrium distribution is then determined by the relative difference in binding affinity of the ring towards the track at individual locations (Scheme 6.19).[96,97]

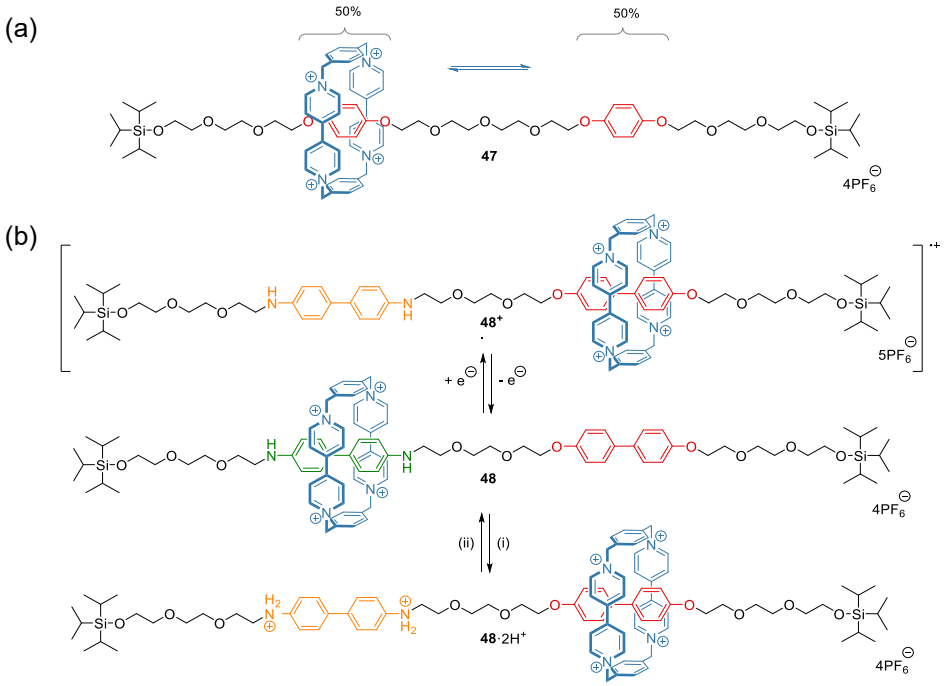

Scheme 6.19. A chemically and electrochemically switchable molecular shuttle **48**.[96,97] (a) Symmetrical **47** and (b) nonsymmetric [2]rotaxane **48**. Reaction and conditions: (i) TFA-d_1, CD_3CN. (ii) pyridine-d_5, CD_3CN.

They concluded that this concept of "molecular shuttles" can provide "the [first] prototype for the construction of more intricate molecular assemblies where the components will be designed to receive, store, transfer, and transmit information in a highly controllable manner." As a first example, they have shown that in the symmetrical case i.e. [2]rotaxane **47** (Scheme 6.19 (a)) shuttling of the tetracationic bipyridine-based macrocycle between two hydroquinone units gives rise to equal populations of the two (identical) complexes that are in constant exchange under thermodynamic control. Crucially, turning their attention towards the corresponding nonsymmetric [2]rotaxane **48** comprising a bisphenol (red) and benzidine unit (orange/green) (Scheme 6.19 (b)) Stoddart et. al. realised that applying external stimuli could allow switching of the position of the macrocycle between two distinct equilibrium positions. Investigating the effect of protonation, they have observed that the macrocycle changes its position from the benzidine to the bisphenol station upon addition of a strong acid. And after neutralisation with base the original equilibrium position is recovered. Alternatively, reducing the benzidine group had a similar effect showing that lowering the binding affinity towards the macrocycle can induce reversible shuttling towards the bisphenol motive.

This and many other examples have laid the foundation for the field of molecular switches and several concepts have been developed that allowed switching the position of macrocycles under various conditions both in rotaxanes but also, for instance, catenanes and other mechanically interlocked architectures.[30,92] Furthermore, several applications have been devised that take advantage of distinct properties between different stations to achieve, for instance, catalysis[98,99] or material applications in solution or solid phase.[100]

6.5.2. Molecular Ratchets

While changing the degree of interactions between the two different binding motifs with external stimuli allowed changing the equilibrium positions it was also evident that this does not give control over the direction of the translation process.[78] Additionally, once reversing the conditions for the molecular switches created, the progress of translation is entirely undone. In fact, nature has shown that to bias the direction of a moving component and perform work under thermodynamic control an additional component is required to construct functioning molecular machines.[101]

Molecular Energy Ratchets

Based on these considerations Leigh et. al. have concluded that by incorporating a second irreversible step in-between the transformation of molecular switches that prevents relaxation back to their equilibrium position, systems can be progressively driven "energetically uphill" similar to a classic ratchet. They have exemplified this idea based on the results of preceding studies on a [2]rotaxane systems **49a-c** (Scheme 6.20) where they had shown that the equilibrium distribution of a benzyl amide macrocycle can be switched reversibly from a fumaramide to a succinamide unit via photochemical isomerisation to a maleamide.[102] They had determined that switching the position of the macrocycle between the two compartments of the axle can be achieved in yields of up 70% at the PSS with the help of external photosensitizer benzophenone. This process had been found to be completely reversible when promoting the opposite *cis-trans* isomerisation with heat or catalytic amounts of ethylene diamine.

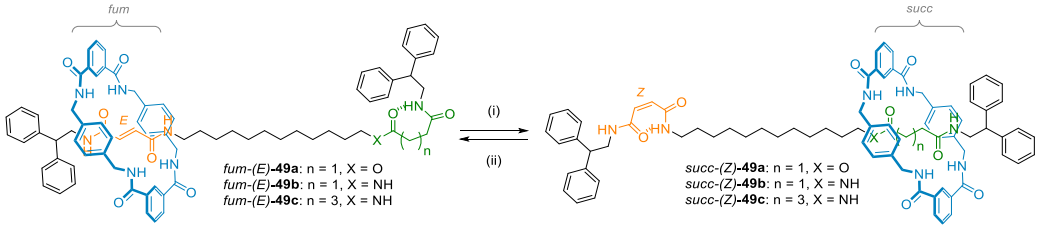

Scheme 6.20. Light- and heat-switchable molecular shuttles **49a-c**.[102] Reaction and conditions: (i) 254 nm, 30 min, CH_2Cl_2, 54% for (*Z*)-**49a,** 48% for (*Z*)-**49b**, 39% for (*Z*)-**49c**; or 350 nm, 5 min, benzophenone, CH_2Cl_2, 65% for (*Z*)-**49a,** 65% for (*Z*)-**49b**, 60% for (*Z*)-**49c**. (ii) $C_2H_2Cl_4$ at 120 °C, 7 d, 80% for (*E*)-**49a,** 80% for (*E*)-**49b**, 95% for (*E*)-**49c**, 1 d.

Building upon these results, Leigh and colleagues have investigated the possibility of transforming the basic molecular shuttle into a corresponding ratchet analogue by introducing an intermediate alcohol functionality in between the two sites on the track of the basic rotaxane system (Scheme 6.21).[78] They reasoned that this group can be reversible (de)protected with, for instance, a *t*-butyldimethylsilyl (TBDMS) group whose steric bulk, once installed on the alcohol, prevents the macrocycle from relaxing to its equilibrium position and effectively act as a stopper unit that "unlinks the two compartments".[31] Once removed, the connection between the two sites is restored and the macrocycle can freely move from one station to another. Altogether, by performing the isomerisation and (de)protection in a suitable order this successively shifts and lock the position of the macrocycle in a state of higher energy – like the working of classical ratchet.

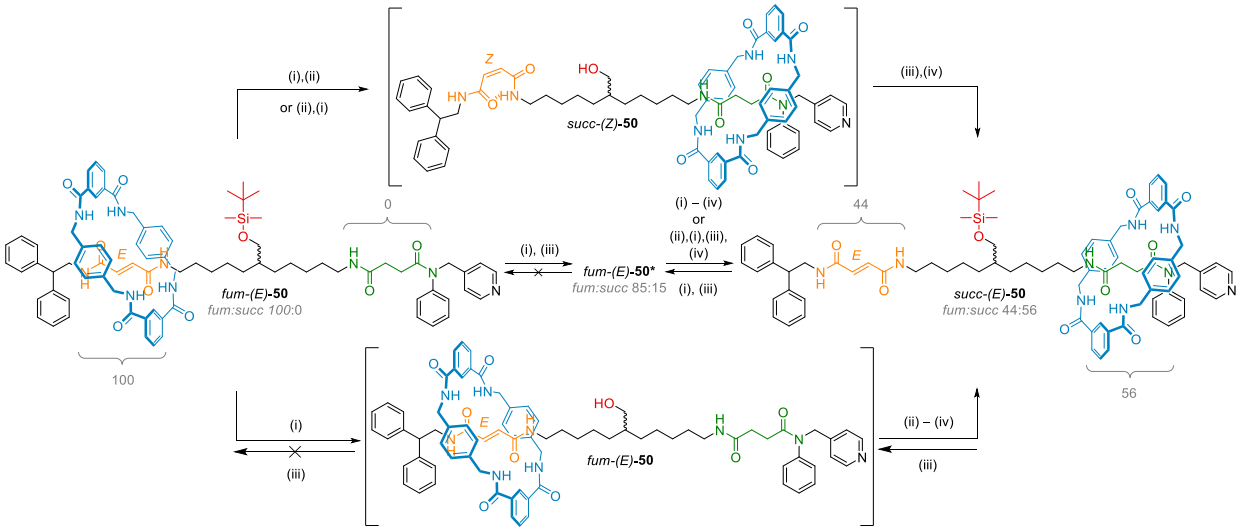

Scheme 6.21. Operation of molecular ratchet **50** via selective (de)protection of a primary alcohol.[78] Reaction and conditions: (i) HAc, 60 °C, 1 h. (ii) 312 nm, 5 × 5 min, CH_2Cl_2, rt. (iii) TBDMS-Cl, imidazole, DMAP, CH_2Cl_2, rt, 1 h. (iv) Piperidine, CH_2Cl_2, rt, 12 h, quantitative.

The operation developed for this purpose begins from initial state *fum*-(*E*)-**50** where the macrocycle rests exclusively on the fumaramide station in a ratio of 100:0 for the occupancy between the fumaramide (orange) and succinamide station (green). First, studying the removal of the stopper unit under acidic conditions and reinstalling it afterwards, they obtained a new equilibrium state *fum*-(*E*)-**50*** (centre) whose ratio of occupancy between the fumaramide (orange) and succinamide (green) has decreased to a value of 85:15. Allowing the system to relax, this value represents the true equilibrium distribution of the macrocycle between the two stations in absence of the additional stopper and formed the starting point for the ratcheting operation. To actively increase the occupancy of the macrocycle on the weaker succinamide binding side (green) the author performed the *trans-cis* isomerisation of the fumaramide unit with light at 312 nm in between the (de)protection steps. The maleamide moiety formed at the PSS has a lower binding affinity towards the macrocycle and thus in the absence of the TBDMS group the macrocycle shuttled towards the succinamide station. After reinstallation of the stopper, a final ratio of occupancy of 44:56 was obtained for state *succ*-(*Z*)-**50**. Furthermore, even when recovering the fumaramide in its *E*-form with the silyl stopper still installed, the equilibrium distribution of the macrocycle remained intact and kinetically stable towards relaxation to lower energy state *fum*-(*E*)-**50***. This result confirmed the working of the anticipated ratcheting mechanism and showed that work has been performed on the system. Leigh et. al. also demonstrated that the energy stored in *succ*-(*E*)-**50** can be released by resetting the system with an additional (de)protection step.

In fact, it has been concluded that the molecular system **50** showcases all main aspects of an energy ratchet mechanism.[31] This class of molecular ratchets has been found to represent one of the possible categories of molecular machines that allow to perform unidirectional processes by temporarily modulating the potential energy surface (PES) of the underlying system with external means. As a general rule the workings of an energy ratchet can be described by a sequence of four distinct steps that when combined lead to concerted thermal motion between five different states (Figure 6.14).[101]

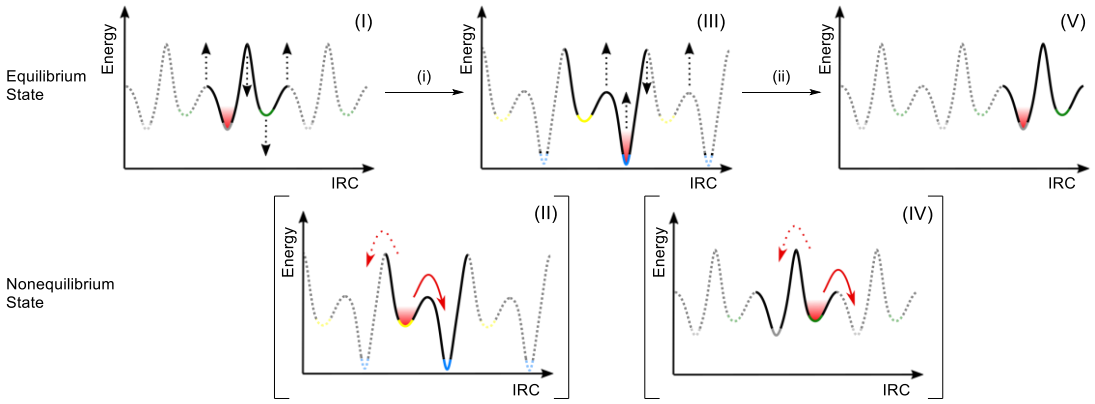

Figure 6.14. Principle working of a flashing/energy ratchet mechanism.[31] By successively modulating relative heights of energy maxima (barriers) and minima of equilibrium states (I) and (III) with external stimuli (i) and (ii) relaxation of nonequilibrium states (II) and (IV). This can lead to highly directional transport of populations under thermodynamic control if the reaction in direction of the IRC is kinetically favoured over its reverse.

In a generalised form the process begins with altering the initial state (I) at the internal reaction coordinate (IRC) of the system's PES with an external stimulus such as with addition of a chemical reactant. In the context of the molecular ratchet shown in Scheme 6.21 this corresponds to either removing/reinstating the silyl protecting group (i.e., lowering/increasing the energy barrier, respectively) or switching the fumaramide station from the *E*- to *Z*-configuration. (i.e., increasing the energy of the equilibrium population while concomitantly lowering the energy minima/wells) If performed in suitable order the new nonequilibrium state (II) created can then relax selectively to the new equilibrium state (III) under thermodynamic control if this reaction is kinetically favoured. To put it differently, the overall process becomes directional if the alternative reaction paths are unfavourable. In the example of the [2]rotaxane ratchet system **50** relaxation of the system occurred via shuttling of the macrocycle from one compartment to another through thermal motion. It is effectively controlled by the bulk and stability of the covalently linked silyl protecting group and guided by the relative binding affinity of the stations. Importantly, the ratio of the equilibrium adopted is solely governed by the difference in free energy between sperate states and does not depend on the actual profile of the transition state. It is determined by the difference in free energies at the IRC before and after the reaction. Performing another external stimulus, the system can further return to its original state (I) through thermal relaxation from state (IV) in case of a periodic PES or otherwise, driven towards a new state (V). In the previous example Leigh and co-workers have shown that the second step can simply be used to release the energy stored in state *succ*-(*E*)-**50** by successive deprotection and reprotection of the alcohol stopper unit. Overall, due to external modulation the ratcheting process occurs in a highly concerted fashion that is dictated predominately by the diffusion constant of reactants.[39b]

With this fundamental knowledge established, also the unidirectional translation in a [2]catenane systems was achieved. With reference to the molecular ratchet **50** Leigh and co-workers created [2]catenane *succ*-(*Z*)-**51** (Scheme 6.22).[103] Similar to the previous [2]/[3]catenane systems **45** and **46** as depicted in Figure 6.12 and Figure 6.13, [2]catenane *succ*-(*Z*)-**51** was based on the reversible light-induced switching of a fumaramide/maleamide station. In combination with a succinamide unit as part of the main track these two units directed the position of a smaller benzyl amide macrocycle (blue) under thermodynamic control. However, in line with the energy ratchet concept, supplementary to this, two additional orthogonal barriers were introduced that block the path of the moving macrocycle. The groups chosen for the design, the TBDMS

and a trityl (Trt) units, that can be selectively removed under orthogonal conditions via a suitable choice of reagents. Altogether, this framework included all the components for operating the energy ratchet mechanism in a cyclic manner. Leigh and co-workers showed that at each step of the reaction sequence the position of the smaller macrocycle and its direction under nonequilibrium conditions can be controlled by a suitable order of reactions that modulates the underlying potential energy surface of the main track.

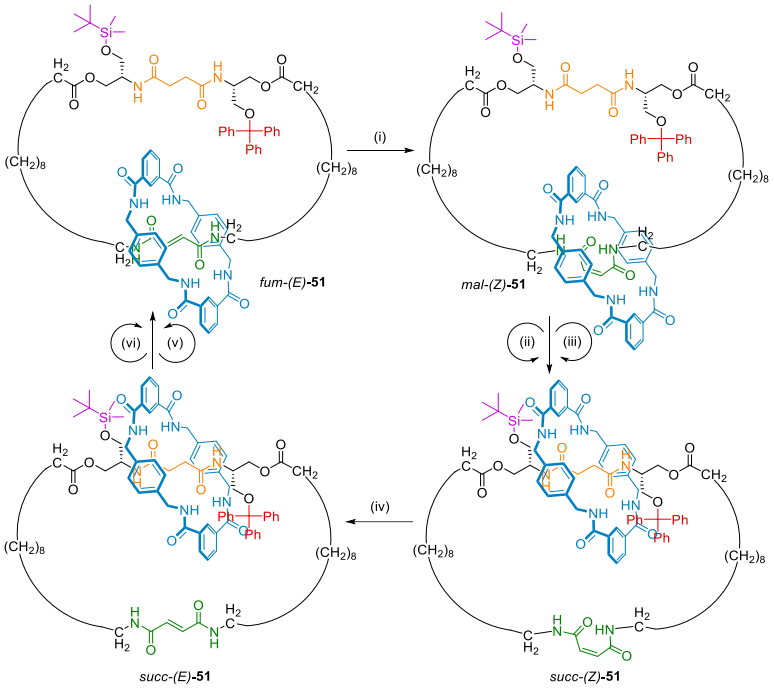

Scheme 6.22. Reversible 360° rotation in sequentially operated [2]catenane (*E*)-**51**/(*Z*)-**51**.[103] Reaction and conditions: (i) 254 nm, CH_2Cl_2, rt, 5 min, 50%. (ii) TBAF, CH_2Cl_2, rt, 20 min, then 2,4,6-collidine, TBDMSOTf, 1 h, –78 °C, 61% over two steps. (iii) $Me_2S{\cdot}BCl_3$, CH_2Cl_2, –10 °C, 15 min, then 2,4,6-collidine, TrtOTf, 5 h, –78 °C, 63% over two steps. (iv) piperidine, CH_2Cl_2, rt, 1h, ≤100%. (v) $Me_2S{\cdot}BCl_3$, CH_2Cl_2, –10 °C, 10 min, then TrtCl, Bu_4NClO_4 2,4,6-collidine, 16 h, –10 °C, 74% over two steps. (vi) TBAF, CH_2Cl_2, rt, 20 min, then 2,4,6-collidine, TBDMSOTf, 40 min, –10 °C, 76% over two steps.

Starting from *fum*-(*E*)-**51** *trans-cis* isomerisation of the fumaramide station to its corresponding maleamide form *mal*-(*Z*)-**51** reduces the binding towards the macrocycle. Once removing either the TBDMS group or the trityl ether the macrocycle therefore shuttles to the succinamide station to afforded *succ*-(*Z*)-**51** in a clockwise or anticlockwise manner, respectively, depending on the reaction conditions. Locked in this state after reconstitution of the protecting groups reverse *cis-trans* isomerisation recovers the original fumaramide station *succ*-(*E*)-**51**. Likewise, depending on the following deprotection/protection the macrocycle can then return to the original state *succ*-(*Z*)-**51** in either a clockwise or anticlockwise direction. Coordinating the sequence of reactions in appropriate order, Leigh and peers were able to achieve a full 360° rotation. They highlighted the importance of understanding the principles that control dynamics on the molecular level.

Molecular Information Ratchets

Separate to this, an information ratchet mechanism can be employed to transfer the population of a system in a unidirectional manner (Figure 6.15).[31,104] In this case, the location of the population (red, the information) has a direct influence on the underlying PES and as an effect, can give rise to either an increase or decrease

of the transition state energy of a particular pathway along the IRC. Effectively, an information ratchet therefore acts as a position dependent catalyst that displays net directional motion on the basis of the difference between the transition state energies $\Delta G_1^{\ddagger}$ and $\Delta G_2^{\ddagger}$ of two (or more) alternate reaction pathways.

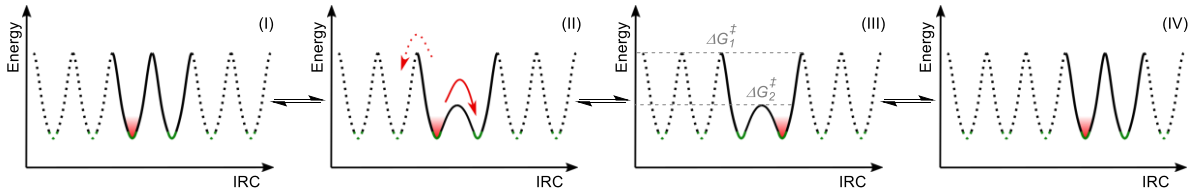

Figure 6.15. Principle working of an information ratchet mechanism.[31] The position of the population selectively lowers transition energies of the reaction along the IRC from $\Delta G_1^{\ddagger}$ to $\Delta G_2^{\ddagger}$ such that ensuing relaxation under thermodynamic control leads to a net directional motion.

The first example specifically employing an information ratchet mechanism was reported by the Leigh group in 2007 (Scheme 6.23).[105] The design of molecular ratchet **52** was based on the reversible shutting of a DB24C8 macrocycle between a dibenzyl (DBA) and monobenzyl ammonium (MBA) station and took advantage of the photoisomerization of a stilbene unit in the presence of a pair of external and internal photosensitizers. As shown by the authors and others,[106] the stilbene can act as gate for the advancing macrocycle. Its basic working relied on the difference in photosensitization of the stilbene unit between the internal benzophenone-functionalised macrocycle and an external benzil additive **53** at the PSS.[107]

Mechanistically, beginning from *DBA*-(*Z*)-**52** the stilbene gate is initially closed, but (local) electron transfer (ET) from the adjacent macrocycle can allow isomerisation to *DBA*-(*E*)-**52**. In this form the stilbene gate is open, and the macrocycle undergoes free shuttling between the DBA and the MBA station under thermodynamic control. Once relocated, however, when residing on the MBA station intramolecular ET from the distant macrocycle becomes inefficient and intermolecular ET from benzil **53** dominates.

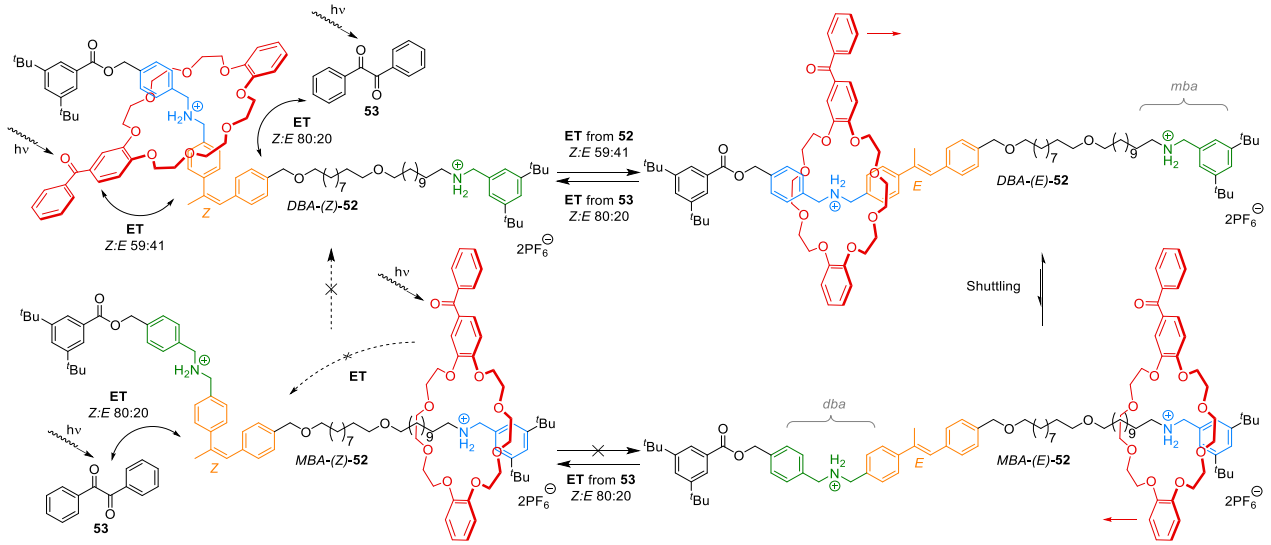

Scheme 6.23. Operation of a light-based molecular information ratchet **52** in the presence of photosensitizer benzil **53**.[105] Reaction and conditions: benzil **53**, 350 nm, CD_3OD, 298K.

As a result, once relocated the macrocycle is retained in its position with the stilbene gate remaining closed. The role of the benzophenone sensitizer attached to the macrocycle is to act as a position-dependent gate-opener that competes with the position-independent gate-closing mechanism of benzil **53**. By following the isomerisation of the stilbene unit in its open state (*E*)-**52** and comparing the results with the ratio between

occupied DBA and MBA stations with ^{1}H NMR Leigh et. al. were able to monitor a continuous drop of the DBA occupation – which confirmed the working of the ratchet. Moreover, while without the external photosensitiser the macrocycle distribution remains constant it continues to change upon addition of benzil.

The same group also reported the operation of a chemically driven information ratchet **57** (Scheme 6.24).[108]

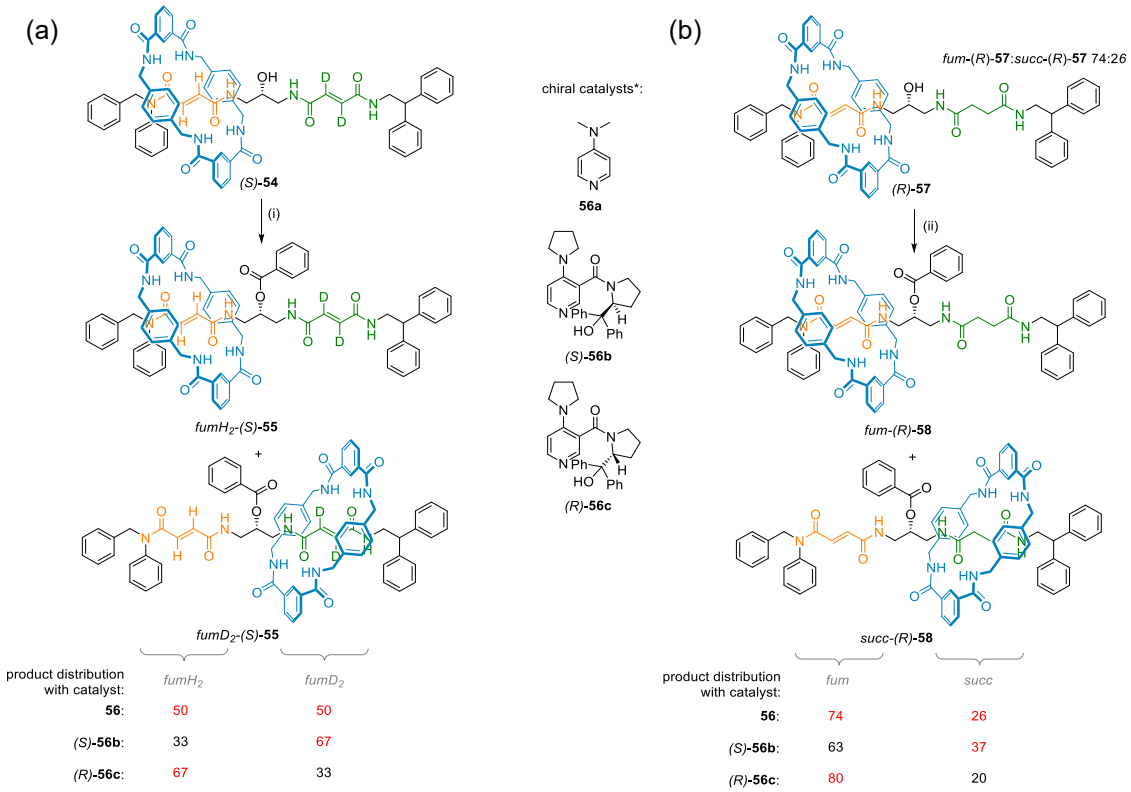

product distribution with catalyst:	$fumH_2$	$fumD_2$
56:	50	50
(*S*)-**56b**:	33	67
(*R*)-**56c**:	67	33

product distribution with catalyst:	*fum*	*succ*
56:	74	26
(*S*)-**56b**:	63	37
(*R*)-**56c**:	80	20

Scheme 6.24. A chemically driven molecular information ratchet **57** using catalyst DMAP **56a** and chiral proline-based derivatives (*S*)-**56b** and (*R*)-**56c** for the operation.[108] Operation of (a) the symmetrical (*S*)-**54** and (b) the nonsymmetric machine (*R*)-**57**. Reaction and conditions: (i) Bz_2O, Et_3N, DMAP **56a**, (*S*)-**56b** or (*R*)-**56c**, CH_2Cl_2, rt, 8 h. (ii) Bz_2O, Et_3N, DMAP **56a**, (*S*)-**56b** or (*R*)-**56c**, CH_2Cl_2, rt, 8 h.

Rather than using a position-dependent electronic interaction between the macrocycle and the track in the excited state as a means to control the isomerisation of a stilbene gate, Leigh and co-workers anticipated that the bulk of the macrocycle can alone suffice to discriminate between the two sides of a reactive centre and enable selective addition of a stopper with a chiral catalyst. They were able to show that depending on the location of the macrocycle next to the chiral secondary alcohol on the track, the difference in steric interactions between different shuttling states and a chiral DMAP-based catalyst can be exploited to trap the macrocycle in a single state. Relying on the shuttling of a benzyl amide macrocycle between different fumaramide and succinamide stations, they demonstrated that the formation of a benzoyl (Bz) ester with benzoic anhydride and triethylamine yields a thermodynamically stable stopper group that depending on the handedness of chiral pyridine-based nucleophilic catalysts drives the macrocycle preferentially over to one side of a rotaxane. By applying this method, the authors were able to obtain a (permanent) snapshot of the shuttling process under the influence of different external catalytic factors. It has provided an example for enantiomeric resolution of an enantiotopic co-conformational rotaxane substrate[109] and due to the reversibility of the shuttling the system also meets the criteria for dynamic kinetic resolution.[110]

Starting with the symmetrical system (*S*)-**54** (Scheme 6.24 (a)) Leigh et. al. have initially shown that in the case of using chiral proline-based catalysts (*S*)-**56b** and (*R*)-**56c** for the benzylation reaction opposite ratios of the trapped rotaxane *fumD*$_2$-(*S*)-**55** and *fumH*$_2$-(*S*)-**55** can be obtained, respectively (for detailed results, see Scheme 6.24). And the corresponding control experiment with using DMAP as a catalyst has confirmed that the ratio is an effect of the chirality of the catalyst and not inherently biased by the deuteration. They proceeded to explore the effect of chirality transfer in the nonsymmetric case (Scheme 6.24 (b)). The machine chosen for the experiment was [2]rotaxane system (*R*)-**57** that includes a fumaramide (orange) and a succinamide station (green). In equilibrium, the macrocycle resides preferentially on the former station and therefore, when using DMAP as catalyst, a higher ratio of the *fum*-(*R*)-**58** product was obtained. Importantly, when changing to a chiral catalyst, they have found that ratio can be selectively increased or decreased depending on the choice of the pyridine-based catalysts (*S*)-**56b** and (*R*)-**56c**, respectively. In either case, distributions between *fum*-(*R*)-**58** and *fum*-(*S*)-**58** achieved with the chiral catalysts deviate from the control experiment with DMAP. And because these ratios are different to the outcome of the reaction when using an achiral catalyst, Leigh et. al. have proved that the chirality of the system can successfully be transferred into a kinetically stable, nonequilibrium state. And this confirmed the working of the ratchet mechanism.

In a later study, the Leigh group has then included a third stations to explore the possibility of unidirectional transport with this chemically driven information ratchet mechanism (Scheme 6.25).[111]

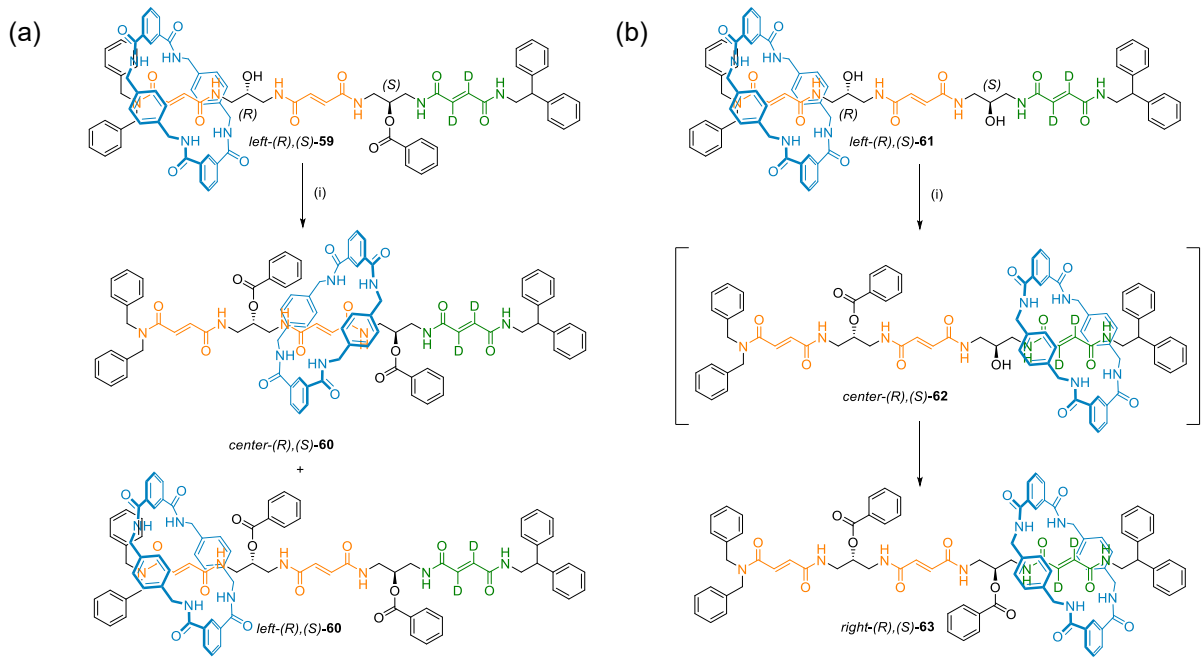

product distribution with catalyst:	*left*	*center*
56a:	64	36
(S)-**56b**:	13	87
(R)-**56c**:	96	4
(S)-**56b**:*(R)*-**56c** 50:50:	45	55

product distribution with catalyst:	*left*	*center*	*right*
56a:	39	18	43
(S)-**56b**:	-	21	79
(R)-**56c**:	75	25	-
(S)-**56b**:*(R)*-**56c** 50:50:	10	77	13

Scheme 6.25. Three-compartment chemically driven molecular information ratchets **59** and **61**.[111] Operation of (a) with two (left-(*R*)-(*S*)-**59)** and (b) three stations (left-(*R*)-(*S*)-**61**). Reaction and conditions: (i) BzCl, Et_3N, DMAP **56a**, (*S*)-**56b**, (*R*)-**65c**, or (*S*)-**56b**:(*R*)-**56c** (50:50) CH_2Cl_2, rt, 2 h. (ii) BzCl, Et_3N, DMAP **56a**, (*S*)-**56b**, (*R*)-**56c**, or (*S*)-**56b**:(*R*)-**56c** (50:50) CH_2Cl_2, rt, 2 h.

The first system *left*-(*R*)-(*S*)-**59** described in their report consisted of a sequence of two fumaramide stations separated by a secondary alcohol and a third deuterated fumaramide unit which due the preformed benzyl

ester cannot be accessed by the macrocycle (Scheme 6.25 (a)). Repeating the previous operation conditions with the similar reagents and DMAP **56a** and proline-based derivatives (*S*)-**56b** and (*R*)-**56c** Leigh and co-workers were first and foremost able to reproduce the results of the previous system (*R*)-**57** (Scheme 6.25 (b)). Either an increase or decrease of the product distribution between *center*-(*R*)-(*S*)-**60** and *left*-(*R*)-(*S*)-**60** products was found when using chiral catalyst (*S*)-**56b** and (*R*)-**56c** when comparing the results with the DMAP-catalysed operation. Interestingly, when adding a mixture of the two chiral catalysts to the reaction, a near equal product distribution between the left and centre compartments was obtained which suggests that under influence of the combined catalytic system, the intermediate rotaxane *center*-(*R*)-(*S*)-**59** (not-shown) reacts faster with the substrate than in the corresponding *left*-(*R*)-(*S*)-**59** form.

The operation of *left*-(*R*)-(*S*)-**61** (Scheme 6.25 (**b**)) has further shown that in absence of the initial benzoyl ester the system developed can also be used to perform directional transport over three stations. Leigh et. al. showed that they can guide the position of the macrocycle and selectively direct it to one of the three stations with different catalysts.[111] First and foremost, they noticed that in the case of using DMAP **56a** as a catalyst the dynamic kinetic resolution afforded a product distribution with most of the macrocycle being trapped on the left and right fumaramide stations. In contrast, using either proline-based catalyst (*S*)-**56b** or (*R*)-**56c** resulted into the selective formation of the *right*-(*R*)-(*S*)-**63** and *left*-(*R*)-(*S*)-**63** form, respectively. Finally, when repeating the operation with the mixture of (*S*)-**56b** and (*R*)-**56c** a preference for the formation of the *center*-(*R*)-(*S*)-**63** form was seen. Considering the overall level of control achieved with this reaction, Leigh et. al. summarised that the concept "should prove useful in designing systems in which macrocycles can be transported directionally and progressively through an increasing number of compartments.

This anticipation was confirmed by the later realisation of a chemically fuelled [2]catenane rotary motor that retains the previous basic chemical framework but substitutes the stable benzoyl motif with a corresponding labile 9-fluorenylmethoxycarbonyl (Fmoc) connection which is both simultaneously formed and (slowly) cleaved under the operation (Figure 6.16 (a)).[112]

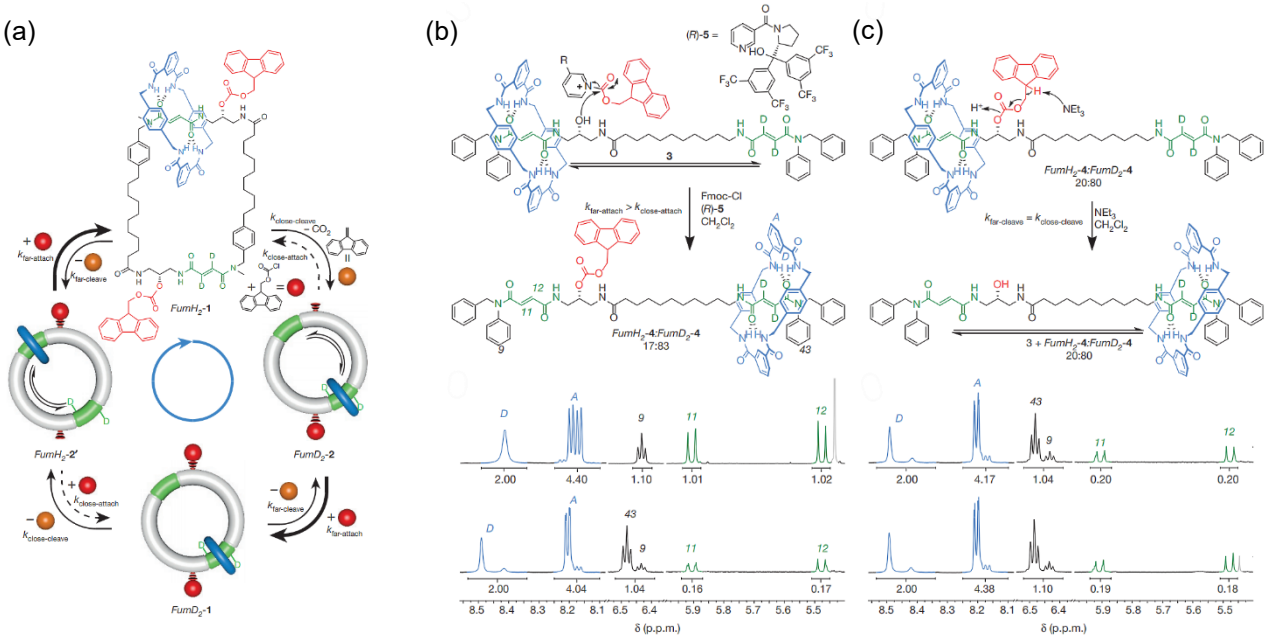

Figure 6.16. Directional chemically fuelled transport of a macrocycle. (a) Operation of a chemically fuelled [2]catenane rotary motor. [2]Rotaxane model systems that demonstrate (b) directional bias for Fmoc addition

and (c) position independent Fmoc cleavage. Reprinted by permission from Springer Nature: reference 112, Copyright 2016.

As with the previous chemically-based information ratchet systems, Leigh and co-workers have found that in a model [2]rotaxane system initial Fmoc protection of a chiral secondary alcohol with the aid of a bulky chiral pyridine catalyst favours the formation of a single positional isomer where the macrocycle is located further away from the reactive centre (Figure 6.16 (b)). In effect, they were able to drive the macrocycle from one fumaramide station, located in direct proximity to the alcohol, to another that is further away from the reaction centre leading to a net directional transport of the macrocycle. However, Fmoc deprotection also occurs under the same reaction conditions and therefore, once all Fmoc-Cl had been consumed Leigh et. al. also observed the recovery of the free alcohol with additional triethylamine. They noticed that the base-catalysed removal takes place with equal rate for both positional isomers; At every interval, the deprotection when monitored with ^{1}H NMR retained the original ratio between starting positional isomers (Figure 6.16 (c)). Hence, the authors have concluded that when applied to a cyclic system such as the [2]catenane depicted in Figure 6.16 (a) accumulation of several random protection/deprotection steps, in total, can result into a net directional shuttling of the macrocycle between an identical pair of fumaramide and secondary alcohol units when sequentially connected at opposite ends.

Facilitated by the incorporation of deuterium labelling, Leigh and colleagues demonstrated that when operating the initial doubly-protected [2]catenane motor stepwise occupancy of the fumaramide station can be periodically reversed between alternate stations when starting from a single positional isomer.[112] They further inferred from the equilibration of the ^{1}H proton signals seen in following autonomous operation in the presence of Fmoc-Cl fuel that maintaining a steady state where only one of the Fmoc groups is in place potentially gives rise to unidirectional movement of the macrocycle (Figure 6.17).

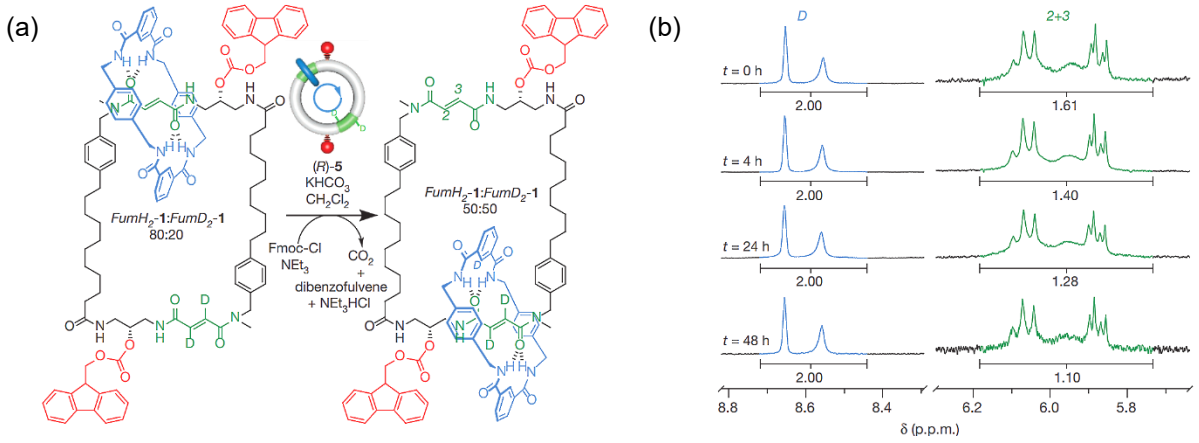

Figure 6.17. Directional transport of a chemically fuelled [2]catenane rotary motor. (a) Reaction conditions: (*R*)-**5** (5 equivalents), $KHCO_3$ (20 equivalents), CH_2Cl_2, room temperature, Fmoc-Cl, CH_2Cl_2, added via syringe pump at 2.4 equivalents per hour, then NEt_3 (1.5 equivalents) after 1 h of Fmoc-Cl addition. (b) Partial ^{1}H NMR spectra (500MHz, CD_2Cl_2:CD_3OD 1:1, 300K) of 80:20 $FumH_2$-**1**:$FumD_2$-**1** and after operation for 4 h, 24 h and 48 h. The region 5.7–6.3 ppm is scaled vertically six times compared to region 8.3–8.8 ppm. The two macrocycle positional isomers of catenane **1** each exist as four tertiary amide rotamers. Reprinted by permission from Springer Nature: reference 112, Copyright 2016.

Though its exact mechanistic aspects still remain subject to extensive theoretical investigations[39e] Leigh and co-workers have showcased the generality of this information ratchet mechanism and the system developed is one of the first examples of an autonomously operating chemically fuelled molecular motor system.

All in all, these efforts have shown how the understanding of basic chemical transformations can be combined and applied to create working examples of artificial molecular machines with a molecular ratchet design.[31] Even more, advancements in the field have created the opportunity to create more and more complex systems that are able to perform controlled (unidirectional) movement in a progressive manner. Eventually, it is hoped that continuing to learn how to apply the and regulate these mechanisms will allow converting motion into a useful function that extend current synthetic possibilities.[32b] In every case, taking inspiration from nature and studying its underlying concepts remains to be an insightful resource for improving the molecular machine design and to ultimately realise Feynman's original goal.

Given the plethora of unexplored and existing biological examples and the growing number of chemical transformations reported several opportunities exist to explore nature's fundamental processes and transfer it into a chemical design that mimics its function. Stimulated by this opportunity and based on earlier studies two basic unidirectional translationary processes have been studied with artificial rotaxane-based molecular machines whose results will be presented in the following: First the linear synthesis of small molecules with predefined sequences borrowing from the working of ribosomal peptide synthesis. Second, the translation process of a molecular pump system that has the potential to directly illuminate a unidirectional molecular transport process with fluorescence spectroscopy.

7. Helicene Synthesis by a Rotaxane-Based Molecular Machine

The following work as summarised in Figure 7.1 has been conducted together with the help of Justin T. J. Spence and Daniel J. Tetlow. The synthesis and analysis of the operation were performed by B. Groh and J. T. J. Spence. It is based on the idea proposed by D. J. Tetlow and the project was supervised by J. T. J. Spence and D. J. Tetlow.

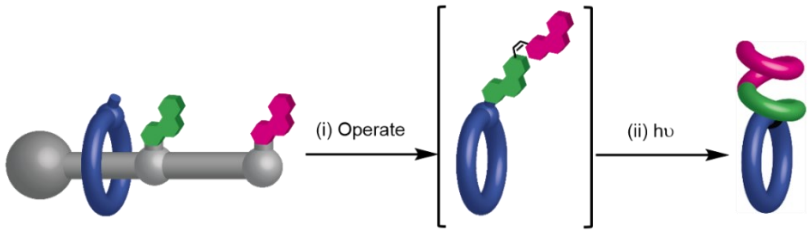

Figure 7.1. Principal concept of helicene synthesis by a rotaxane-based molecular machine. The operation affords a stilbene sequences that can be subsequentially converted to corresponding helicenes via oxidative photocyclization.

7.1. Background

One of the central aspects of all living organisms constitutes the efficient, perpetual synthesis of a wide variety of complex molecules such as proteins or DNA with high sequence fidelity from a pool of similar reactive substrates.[4] In light of this biological precedent, it has been anticipated that comparable catalytic systems may be established, too, facilitated by the advances that have been made towards controlling molecular motion with molecular machines.[98,162] It has been pointed out that in consideration of the significance of catalytic processes in chemical manufacturing, several potential advantages over its traditional spatially separate and stepwise preparation methods (Figure 7.2 (a)) can emerge when performing reactions in an autonomous manner and in parallel by analogy with, for example, ribosomal peptide synthesis (RPS, Figure 7.2 (b)).[113] During the past, several strategies have been developed that learning from the inherent examples of biological processes such as RPS and understanding translation mechanisms have allowed conflating acquired concepts into an artificial molecular machine design. This includes the synthesis of general sequence-specific products with rotaxane-based[98] or DNA-templated methods (Figure 7.2 (c)).[113]

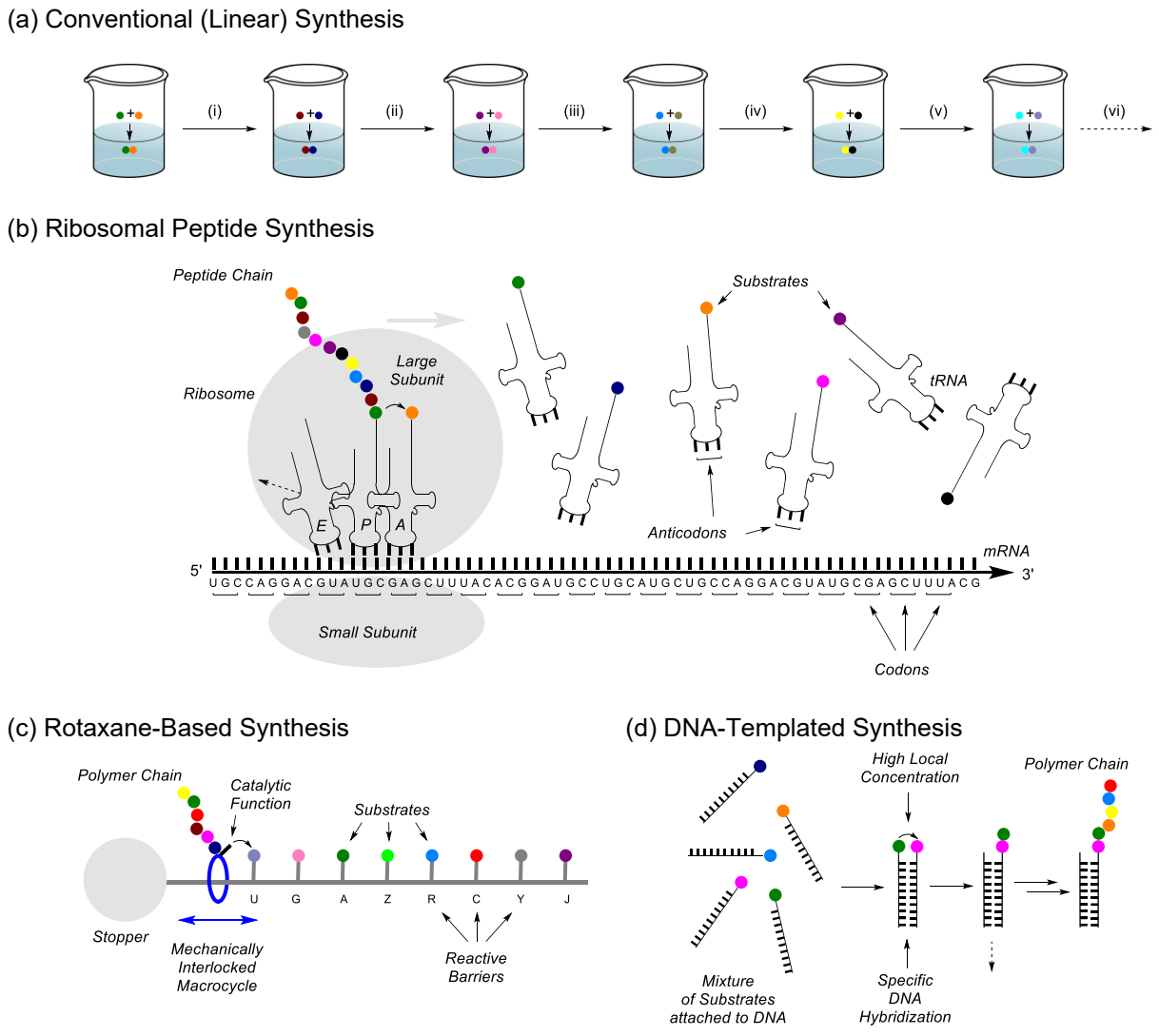

Figure 7.2. Illustration of chemical synthesis strategies.[113] (a) The conventional (linear) synthesis approach mandates spatial separation for a succession of reactions and requires isolation and transfer of reactive substrates in between reactions. (b) Biological machines such as the ribosomes perform sequence-specific synthesis in parallel and in presence of reactants by relying on self-assembly processes such as

hybridization between anticodon-codon pairs to control the proximity of reactive substrates and enable their linkage in a catalytic manner.[27] (c) Rotaxane-based machines similarly control linkage of reactive substrates trough the restricted, free linear movement of a macrocycle within a mechanically interlocked architecture. With this concept substrates are linked in order via a series of (preinstalled) reactive barriers that dictate the order of assembly.[114] (d) DNA-templated synthesis relies on sequence-specific nucleic acid hybridization. The sequence is defined by the DNA template and only when in proximity two given substrates can react.[113]

7.1.1. Ribosomal Peptide Synthesis

RPS is a central and universal aspect of life; Independent of the organism it is making its appearance in form of the ribosome as a ribonucleoprotein assembly. The ribosome is responsible for the continuous (re)synthesis of polypeptide sequences from templating messenger RNA, (mRNA) peptide fragment containing aminoacyl-transfer RNA (aa-tRNA) and initiation factors (IFs).[27] Due to its universal role as starting point for synthesis of proteinic structures analysis of the ribosome has drawn much attention and with increased knowledge, has revealed several aspects of its principal constitution (Figure 7.3) and functioning (Figure 7.5). The importance of these studies is underlined by awarding the Nobel Prize in Chemistry 2009 to V. Ramakrishnan, T. A. Steitz and A. E. Yonath whose individual contributions have led to a detailed understanding of the ribosomal behaviour on the molecular level.[115]

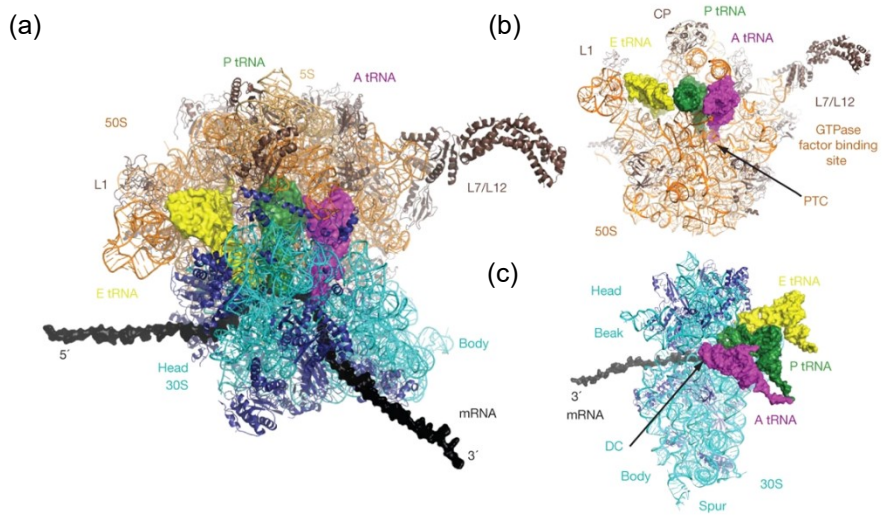

Figure 7.3. Structure of the bacterial ribosome. (a), 'Top' view of the 70S ribosome with mRNA and A- (magenta) P- (green) and E-site (yellow) tRNAs. Exploded view of (b) the 30S subunit (cyan) and (c) the 50S subunit (orange). The structure of the L7/L12 arm was fit onto the 70S ribosome, with mRNA elongated by modelling. Adapted by permission from Springer Nature: reference 27a, Copyright 2009.

In common to all organisms, the ribosome is first and foremost described by a dynamic globular assembly consisting of a small and large subunit. In case of the bacterial ribosome (70S) a 50S and a 30S subunit is found (Figure 7.3),[27a] whereas its eukaryotic analogue (80S) comprise a large 60S and small 40S subunit. In general, each subunit in turn is composed of several different RNA and protein components that only when combined yield the two distinct quaternary structures. Taken together with the target information in form of mRNA released from the nucleus after DNA transcription and additional IFs this enables the formation of the active ribosome assembly via a series of coordinated steps. As shown in Figure 7.3, they allow bringing together the two ribonucleoprotein halves and lock them in the correct position over the encompassing linear mRNA thread. As a result of this arrangement, three separate compartments located at the inside of the

central cavity are established exposing a series of active binding sites termed A- (aminoacyl), P- (peptidyl), and E-site (exit) for substrate-containing tRNA units, respectively. Then, starting from a purine-rich initiator region known as the Shine-Dalgarno sequence coming immediately after the leading 5' end of the mRNA,[4] pairing of the initiator region displaying the AUG codon with the corresponding anticodon of an initiator tRNA marks the beginning of the elongation cycle.

At the onset, tRNA components with different aminoacyl residues continuously enter the central cavity from the A-site but are only able to remain in place if the ternary recognition site on the tRNA (the anticodon loop) successfully matches with a complementary ternary fragment (the codon) on the opposite mRNA sequence. The discrimination achieved at this step forms the basis for the subsequent peptide-bond formation between adjacent aa-tRNA components occupying the A- and P- site: At each step of the synthesis the aminoacyl end of the nascent peptide chain attached to the tRNA unit **64$_P$** at the P-site is transferred onto the terminal amino group of the tRNA unit **65$_A$** at the A-site (Scheme 7.1).

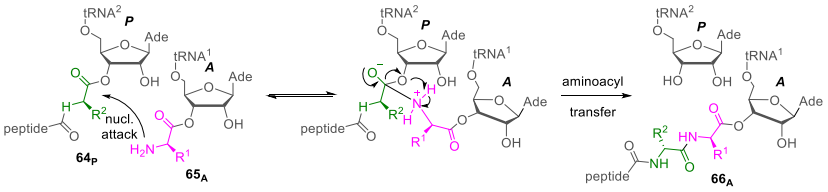

Scheme 7.1. Schematic mechanism of the aminoacyl transfer step during the ribosomal peptide translation. Transfer off the nascent peptide chain takes place from the P- to the A-site.

To proceed, the deacylated tRNA at the P-site is moved to the E-site and in the following, replaced by the new aa-tRNA unit holding the elongated peptide sequence **66$_A$**. To facilitate this process the ribosome adapts a ratcheting step that gives rise to rotational movement of the two subunits relative to each other as illustrated in the transition from state (a) and (b) to (c) in Figure 7.4.[116]

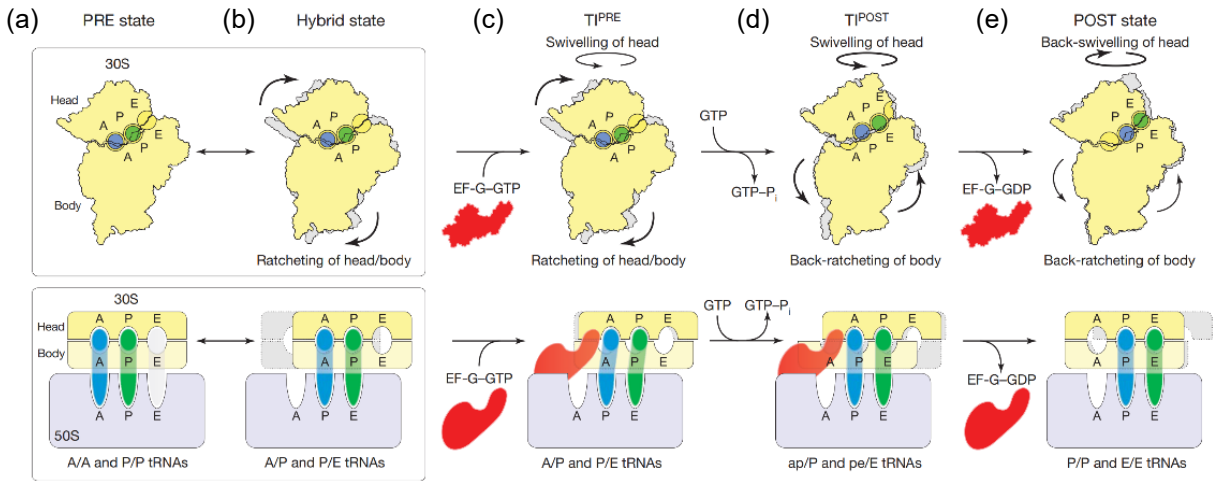

Figure 7.4. Illustration of the ribosomal translocation ratchet mechanism.[116a] The pre-translocational (PRE) ribosome exists in (a) a dynamic equilibrium between base states with classical A/A and P/P tRNAs and (b) rotated states with hybrid A/P and P/E tRNAs. (c) Binding of EF-G–GTP to (a) PRE state (b) or hybrid state stabilizes the ratcheted state. (d) Fast GTP hydrolysis by EF-G accelerates translocation. Domain IV of EF-G uncouples back-ratcheting from the reverse movement of the A/P and P/E tRNAs back into classical states. Through a head swivelling and back-ratcheting motion, the tRNAs move from aa/P and pp/E into the 30S intra-subunit ap/P and pe/E hybrid states. (e) Complete back-ratcheting of the 30S subunit leads to the POST-state 70S–EF-G complex. Back-swivelling of the 30S head re-establishes tRNAs in the classical

(pp/P) P and E (ee/E) states. Translocation is completed by the dissociation of EF-G–GDP. Reprinted by permission from Springer Nature: reference 116a, Copyright 2010.

Evidence suggests that this action is stabilised by the binding of an elongation factor G (EF-G).[27a] Concurrent to this process mRNA shifts by one unit and expresses the following codon unit at the freed A-site. The release of bound EF-G along with deacylated tRNA then concludes a single elongation cycle allowing further peptide bond formation reactions to occur.

Over the course of translation, the growing peptide chain progressively diverts out of the active space of the ribosomal cavity through a dedicated channel of the large subunit into solution where individual peptide units can be subject to various post-translational modifications such as methylation,[117] prenylation[118] or, acetylation[119] to give the final protein. The entire process of ribosomal translation cycle can be differentiated between the initial formation of the active ribosome assembly, the active elongation period, and the disassembly and final release of the formed nascent protein sequence into the solution (Figure 7.5).[27a]

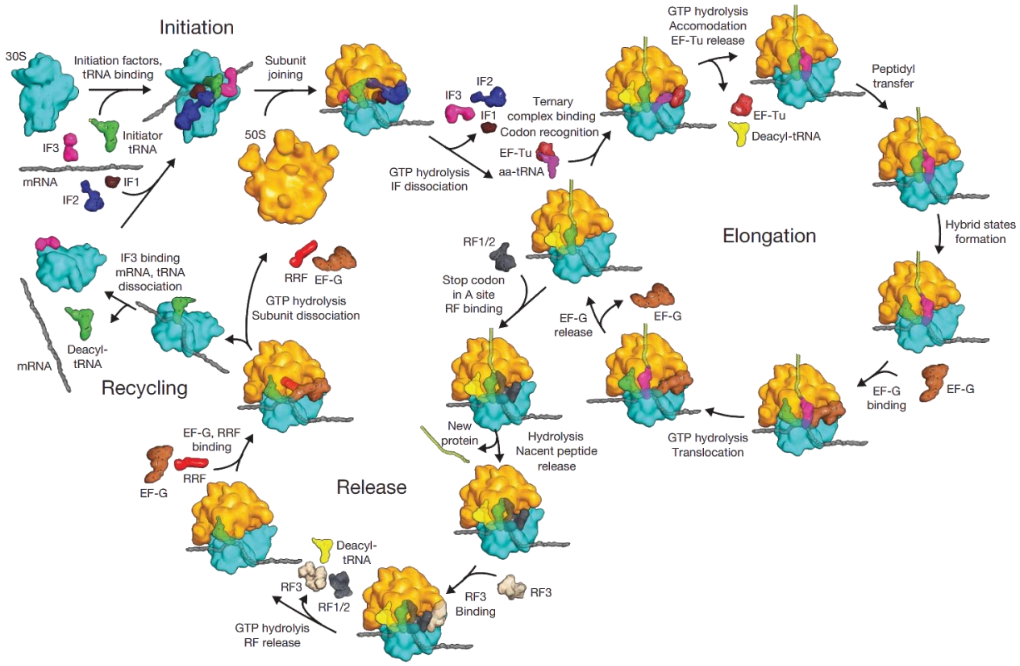

Figure 7.5. Overview of the bacterial translation cycle. For simplicity, not all intermediate steps are shown. aa-tRNA, aminoacyl-tRNA; EF elongation factor; IF, initiation factor; RF, release factor. Reprinted by permission from Springer Nature: reference 27a, Copyright 2009.

It has been highlighted[4a] that applying these complex steps the ribosome is capable of processing approx. three to eighteen amino acids per second[120] with an observed error frequency below 10^{-4}.

7.1.2. Synthesis via [2]Rotaxane-Based Molecular Machines

Taking inspiration of the reminiscent shape and translation mechanism, the ribosome has also been subject to investigations for mimicking the basic working with an artificial molecular machine.[98] Specifically, an attempt has been made to replicate the linear directional behaviour of RPS by modelling the underlying sequence-specific peptide translation with the help of a rotaxane-based architecture.[114] The principal design is based on a preassembled [2]rotaxane and utilises a macrocycle bearing a catalytic unit as a structural analogue for the dynamic protein assembly during the elongation cycle (Figure 7.6).

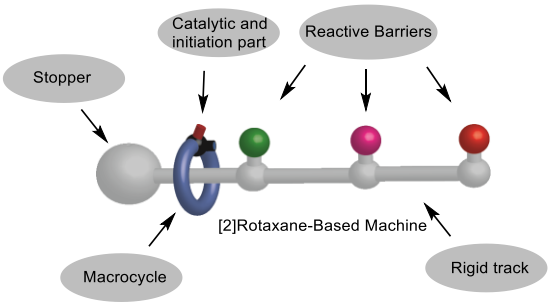

Figure 7.6. Illustration of the principal design of a [2]rotaxane-based molecular assembler.[114]

In correspondence to the biological operation processing of a piece of sequence information is affected through free (i.e., uncontrolled) linear movement of the mechanically interlocked macrocycle. Facilitated by Brownian motion the path of the macrocycle along the rigid track then determines the sequence of the formed peptide. To attain directionality for the molecular degree of freedom in absence of an active ratcheting mechanism the rotaxane system is enclosed on one side with a bulky stopper. On the other side it is closed off by an elongated track that carries a succession of reactive barriers that blocks the path of an advancing macrocycle prior to operation.

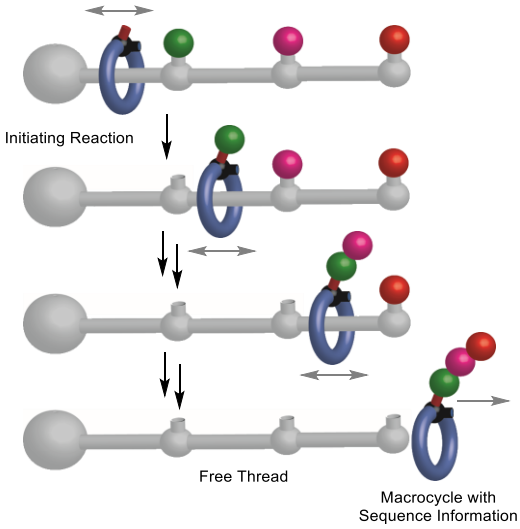

Figure 7.7. Proposed mechanism of the operation of [2]rotaxane-based molecular assembler.[114]

It has been envisioned that once the catalytic function of the macrocycle becomes active, linear movement of the macrocycle within the [2]rotaxane system then allows carrying along a series of predetermined, consecutive reactions (Figure 7.7). Ensuing from the reaction between a reactive arm and the first barrier in line, at each step the catalytic unit is taking up a fragment from a barrier and connecting it with a growing intermediate on the macrocycle. If successfully taking away a barrier the path then becomes clear for subsequent reactions and, over the course of the translation, leads to the assembly of sequence-specific product. Once the final barrier has been collected, the macrocycle slips off the thread into the bulk medium and this concludes the operation of the molecular machine.

Applying this concept, a series of molecular synthesiser machines have been developed and Leigh and co-workers have shown that when operated, machines **67** and **70** are able to successfully perform the sequence-specific synthesis of α-peptides (Scheme 7.2 (a)),[114] and β-peptides (Scheme 7.2 (b)),[121] respectively, with the aid of native chemical ligation (NCL) as catalytic function.[122]

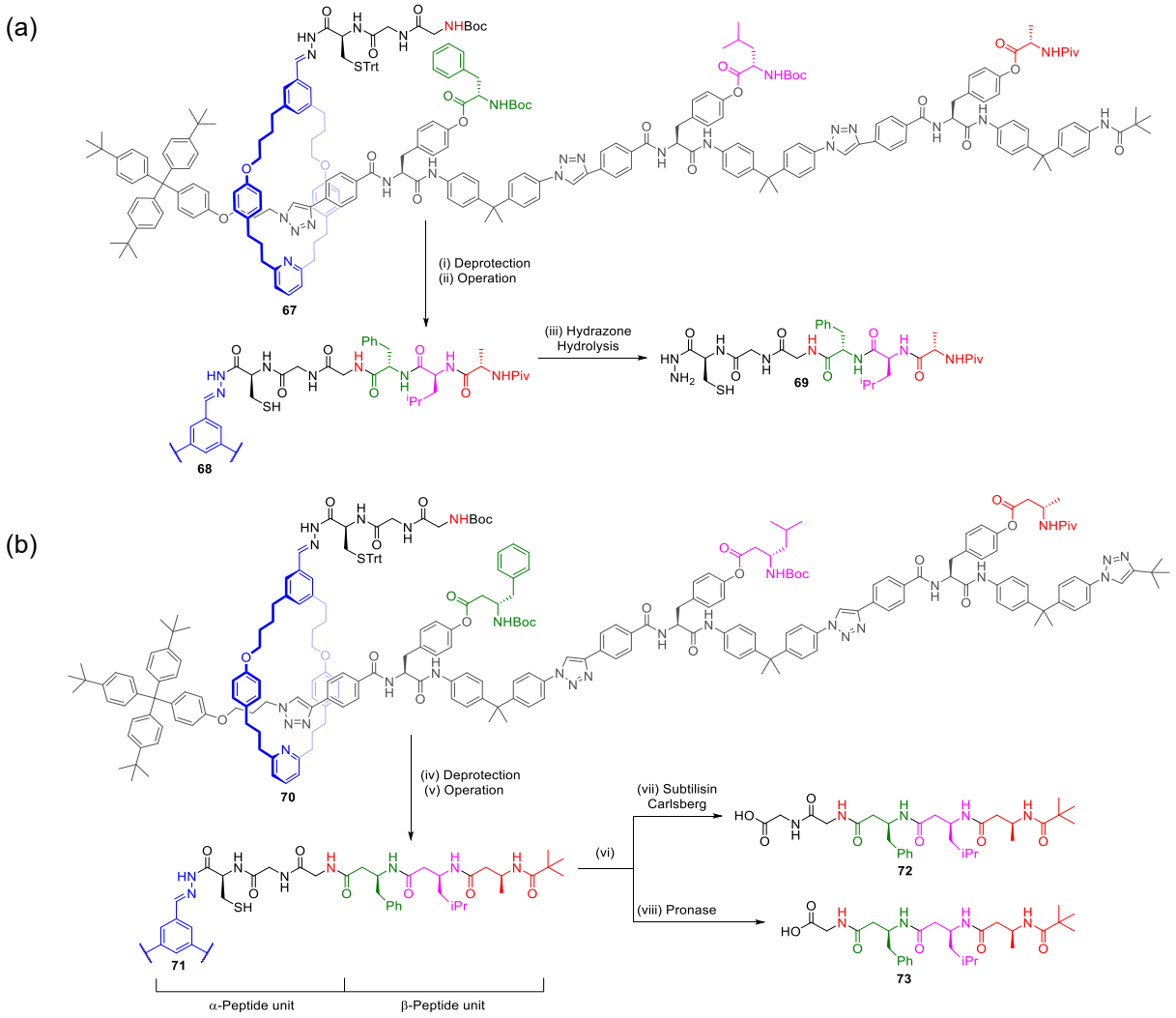

Scheme 7.2. Sequence-specific peptide synthesis via [2]rotaxane-based molecular machines. (a) The first machine **67** developed affords the α-peptide sequence **68** that can be further hydrolysed to give a macrocycle-free product **69**.[114a] (b) Further modification of the design has enabled the sequence-specific β-peptide synthesis with machine **70**.[121] Upon operation it yields a combined α- and β-peptide containing product **71** that has been transformed to two different final compounds, **72** and **73**. Reaction conditions: (i) 20% CF_3CO_2H, CH_2Cl_2, rt, 2 h, 100%. (ii) DIPEA, TCEP, CH_3CN:DMF, 60 °C, 36 h. (iii) 30% CF_3CO_2H, CH_2Cl_2:H_2O, rt, 18 h. (iv) CF_3CO_2H, TIPSH, CH_2Cl_2, rt, 1 h. (v) Et_3N, PPh_3, DMF, 60 °C, 7 d, 29% over two steps (58% based on macrocycle). (vi) V-044, TCEP·HCl, NEt_3, ^{t}BuSH, DMF:H_2O, rt, 65 h, 64%. Methoxyamine·HCl, $CHCl_3$:MeOH, reflux, 1 h, 75%. (vii) Subtilisin Carlsberg (1 mg/mL), phosphate buffer (pH 8, 0.1 M), 50 °C, 5 d. (viii) Pronase (1 mg/mL), H_2O, 37 °C, 4 d.

In both cases, initial rotaxane systems have been constructed from macrocycle **75** including a pyridine and aldehyde unit, an azide-functionalised stopper **74** and respective tracks **76a-b** bearing terminal alkyne units via an active metal template (AMT) approach (Figure 7.8 (a) and (b)).[123]

Addition of the reactive catalytic unit to the machine precursors have been performed in a second step by hydrazone formation. Using a suitable hydrazide derivative, the attached small peptide chain simultaneously functions as catalytic unit and initiation element for the operation. In both examples, (Scheme 7.2 (a) and (b)) catalytic functioning via NCL of **67** and **70** is provided by a cysteine fragment bearing a thiol group.

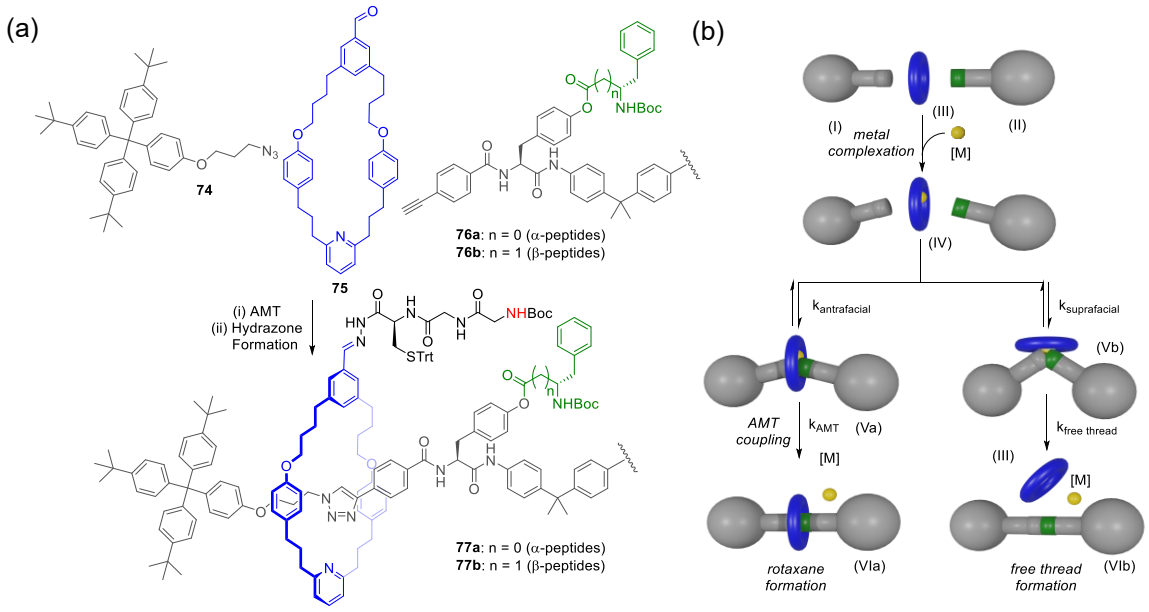

Figure 7.8. Active metal template synthesis of rotaxanes. (a) Reported preparation of synthons **77a** and **77b** from azide stopper **74**, aldehyde macrocycle **75** and terminal alkynes **76a** or **76b**.[114,121] Reaction conditions: (i) **76a**, $Cu(CH_3CN)_4PF_6$ in CH_2Cl_2:*t*BuOH, rt, 4 d, 30%. **76b**, $Cu(CH_3CN)_4PF_6$ in CH_2Cl_2:*t*BuOH, rt, 16 h, 40%. (ii) aniline, BocGlyGlyCys(*S*-Trt)NHN=CHC$_6$H$_4$OCH$_3$, DMSO:2-(*N*-morpholino)ethanesulfonic acid buffer (aq., pH 6.0), 60 °C, 2 d, 90%. (**77a** and **77b**) T (b) Schematic illustration of the AMT mechanism.[123] Addition of metal ion [M] to azide-alkyne substrates (I) and (II) and macrocycle (III) leads to the initial formation of a macrocycle-metal complex (IV). If catalysing the cycloaddition of (I) and (II) from the same side (suprafacial) of the macrocycle intermediate (Vb) free thread (VIb) is obtained. If compounds (I) and (II) instead are approaching from alternative faces (antrafacial) the reaction results into a mechanically interlocked product (VIa) through intermediate (Va). The outcome of the reaction is determined by the difference in kinetics between k_{AMT} and $k_{free\ thread}$ of the final step.

After deprotection of the amine and thiol protecting groups operation of the furnished [2]rotaxane machines can be actuated with base (Scheme 7.3). When in proximity to a barrier nucleophilic attack of the free thiol onto the peptide fragment at the phenol ester then first and foremost leads to the formation of an intermediary thiol ester between the catalytic cysteine arm and the cleaved peptide fragment. Subsequent intramolecular *S,N* acyl shift to the terminal amine affords the thermodynamically favourable amide connection in a second step and at the same time restores the thiol arm for another series of reactions with following barriers. With each iteration, a peptide fragment is appended to the growing peptide chain on the macrocycle. Once the final barrier has been processed the final macrocyclic product dethreads into solution. It has been shown that in a second step the macrocycle component can be further removed from the product by final cleavage of the hydrazone bond[114a] and converted via an enzyme-catalysed reaction.[121]

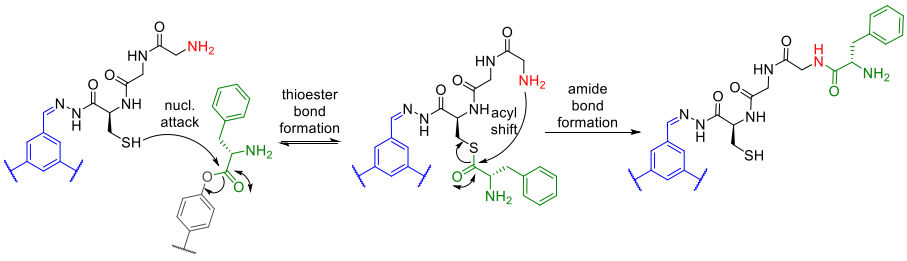

Scheme 7.3. Proposed general mechanism for the elongation of growing peptide chain via native chemical ligation during the operation of a peptide-forming artificial molecular machine.[114a]

In a similar way, by substituting the original track with a polymeric styrene analogue incorporating a narrow-range statistical distribution of leucine esters operation of alternative machine **78** has provided corresponding polyleucine amide sequence **79** (Scheme 7.4).[124] After removal of the thiol functionality via reductive desulfurization oligoleucine foldamer **80** was isolated. Adopting a helical structure this compound was shown to catalyse the reaction of chalcone substrate **81** to epoxide **82** in high yield and stereoselectivity.

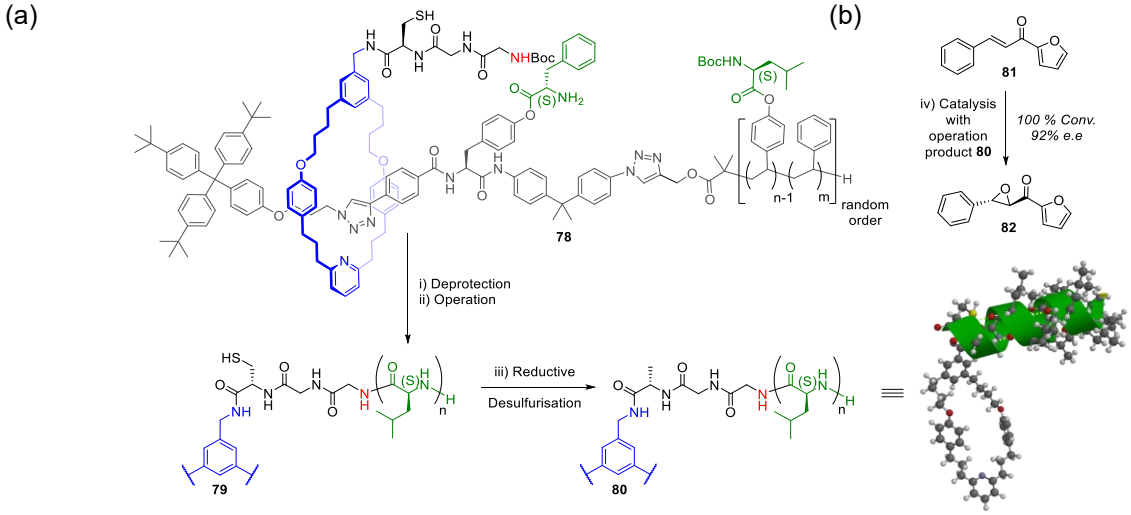

Scheme 7.4. Synthesis of an asymmetric catalyst with the aid of a [2]rotaxane-based molecular machine **78**.[124] (a) Operation of **78** yields polyleucine product **79**.After deprotection, the furnished foldamer adopts a helical structure **80** that functions as a catalyst for (b) the reaction of chalcone **81** to epoxide **82**. Reaction conditions: (i) $^{i}Pr_3SiH$ in CH_2Cl_2:CF_3CO_2H, rt, 2 h, quantitative. (ii) Et_3N, Ph_3P, DMF-d_7, 65 °C, 96 h, 50%. (iii) V-50, ^{t}BuSH, Et_3N, TCEP·HCl, DMF, rt, 22 h, 77%. (iv) **80** (15 mol%), urea·H_2O_2, DBU, THF, rt, 4 d, 100%.

Motivated by these results, another rotaxane-based system was developed that performs sequential carbon-carbon bond forming reactions (Scheme 7.5).[125] The molecular machines **83** and **85** use Wittig type reactions[126] to construct stilbene sequences through the reaction of an aldehyde macrocycle and a series of bifunctional barrier units comprising an aldehyde and a phosphonium group. The latter is functioning as a reactive anchor point to link barriers with the track. Furthermore, the series of building blocks are separated by rigid triphenylene spacer units and linked together at the tetrasubstituted phosphorous centres via copper-catalysed azide-alkyne cycloaddition (CuAAC).[127] The proposed operation takes place with the addition of non-nucleophilic neutral phosphazene base 2-tert-butylimino-2-diethylamino-1,3-dimethyl-perhydro-1,3,2-diazaphosphorine (BEMP)[128] via formation of intermediate non-stabilised phosphonium ylides. Under thermodynamic equilibrium the steric bulk of the covalently attached phosphonium ylide prevents the macrocycle passing over the barrier unit unless it has reacted with the proximal phosphonium ylide. Only the less sterically demanding, phosphine oxide allows the macrocycle to proceed. And once passed, with each intramolecular carbon-carbon forming reaction completed the sequence information encoded in the track is translated from the phosphonium ylide to the terminal aldehyde end on the macrocycle. Eventually, once the macrocycle has reached the end of the track final dethreading then affords the operation product.

In practise, this has allowed successful operation of both preliminary 2-barrier machine **83** (Scheme 7.5 (a)) and final 4-barrier machine **85** (Scheme 7.5 (b)). In the latter case, the desired tetrastilbene product **86** has been isolated in a yield of up to 21% and separated from the remaining track (69%) demonstrating the principal working of the proposed machine concept.

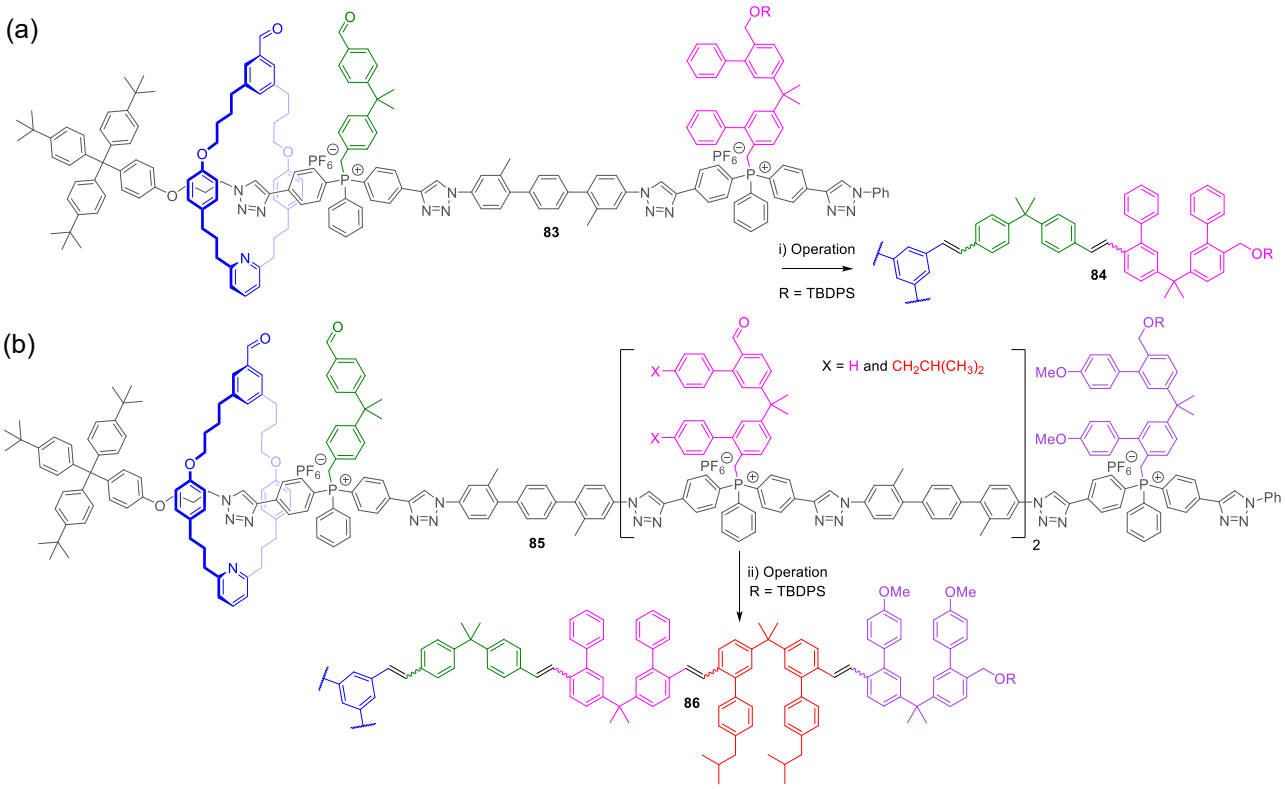

Scheme 7.5. Iterative sequence-specific carbon-carbon bond formation with [2]rotaxane-based molecular machines **83** and **85**.[125] Operation of (a) 2-barrier **83** and (b) 4-barrier machine **85**. Reaction conditions: (i) BEMP, CH_2Cl_2, –78 °C to rt, 18 h, 53%. (ii) BEMP, CH_2Cl_2, –78 °C to rt, 5 d, 21%.

In addition to this, the authors also studied the effect of the interlocked-architecture on the stereochemistry resulting from the non-stabilised phosphor ylide with a model 1-barrier machine **87**. By comparing the results with the individual non-interlocked components **75** and **89** they noticed an increase in *E*-selectivity when using LDA as a base in THF (Scheme 7.6).[129] Performing the reaction with the separate reactants **75** and **89** an *E*–*Z* ratio of 41:59 was observed by ^{1}H NMR. The ratio increased to 88:12 for the product isolated (55%) from the operation of rotaxane machine **87**. This finding has been ascribed to potentially unfavourable conditions for the formation of (*Z*)-isomers during the stereo determining oxaphosphetane step.

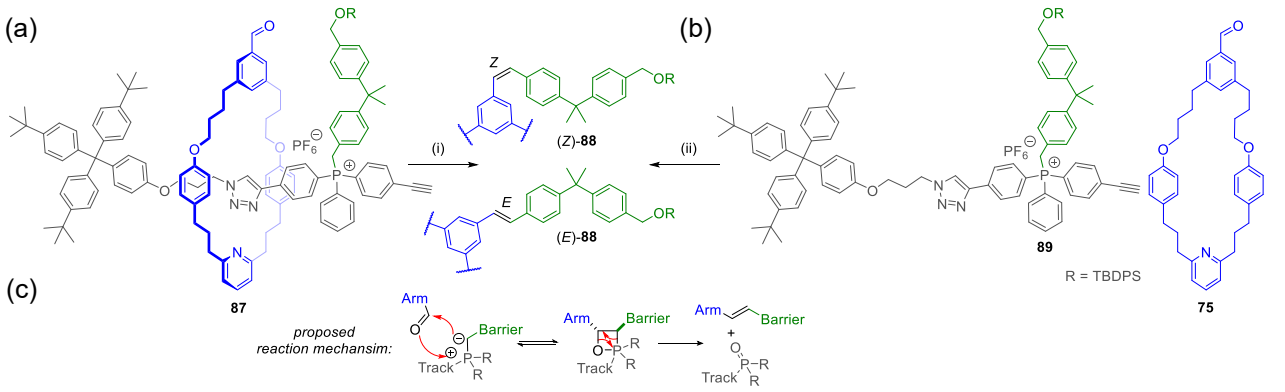

Scheme 7.6. Analysing the stereoselectivity of different Wittig reactions. Results for the operation of (a) 1-barrier machine **87** and (b) separate, non-interlocked components **75** and **89**. (c) Proposed reaction mechanism for the Wittig reaction in a [2]rotaxane-based architecture.[129] Reaction conditions: (i) LDA, THF, –78 °C to reflux, 18 h, 55%. (ii) LDA, THF, –78 °C to reflux, 18 h, no yield reported.

7.1.3. Processive Catalysis with Rotaxane-Based Molecular Machines

Beyond RPS and the construction of sequence-specific small-molecule products also the behaviour of an alternative class of active biological systems has been studied with rotaxane-based machines.[98] The biomimetic machines developed resemble the working of so-called processive enzymes that are able to catalyse an onward reaction with a linear polymeric substrate at the inside of their hollow structure (Figure 7.9).[130] Representative for such an operation are, for example, toroidal λ-exonuclease (Figure 7.9 (a))[131] or clamp-DNA polymerase (Figure 7.9 (b)-(d)).[132] Examining their working has pointed out an alternative concept for performing catalysis with rotaxane-based machines.[98,130]

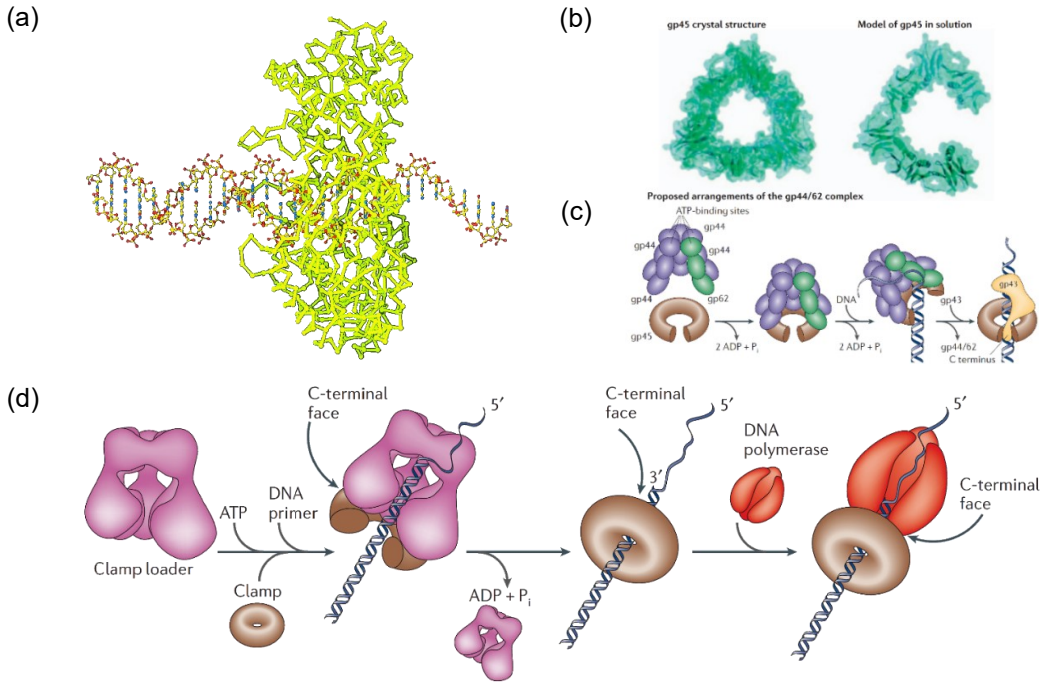

Figure 7.9. Processive catalytic biological machines. (a) Proposed model for the interaction of λ-exonuclease with DNA. The long axis of the DNA coincides or approximately coincides with the threefold axis of the protein trimer. The tapered channel within the toroidal structure of the protein is wide enough to accommodate double-stranded DNA at one end but only single-stranded DNA at the other. Shown are the gp45 clamp and the gp44/62 clamp loader of bacteriophage T4. From reference 131a. Reprinted with permission from AAAS. Copyright 1997. (b) Ribbon and surface diagrams of gp45. The crystal structure of gp45 (left) is a closed clamp. On the right is a model of the solution structure of gp45 in the open form. (c) The clamp-loading mechanism of bacteriophage T4. The gp44/62 clamp loader (comprising four gp44 subunits (purple) and one gp62 subunit (green)) hydrolyses two molecules of ATP to bind and stabilize the open gp45 clamp. DNA binding to the gp44/62–gp45 complex results in further ATP hydrolysis, which is followed by the departure of the clamp loader and the association of the C-terminal tail of the gp43 DNA polymerase that is 'jammed' into the middle of one gp45-clamp interface. (d) Clamp loading and the use of sliding clamps in processive DNA synthesis. Adapted by permission from Springer Nature: reference 132b, Copyright 2006.

One of the first attempts to explore the effect of an interlocked architecture on the behaviour of a reaction taking place at the inner cavity of a macrocycle has been reported by Nolte et. al. Applying a manganese porphyrin complex, they postulated that the catalyst would allow intramolecular oxidation of a polybutadiene track (Scheme 7.7).[133] To avoid intermolecular reactions and limit oxidation to the inside of the cavity, the top side of the active macrocyclic manganese complex was concealed with a bulky terminal pyridine ligand. When analysing the outcome of the reaction with ^{1}H NMR and integrating signals for different products of

starting *E*–*Z* isomers of polybutadiene substrates **92a** and **92b**, the authors noted differences both in turnover and selectivity by changing from an interlocked to a non-interlocked architecture. In the case of using catalyst **90** epoxidation predominately occurred with (*E*)-alkenes showing an *E*:*Z* ratio of 4.0 (**93a**) and 1.7 (**93b**) whereas porphyrin model catalyst **91** preferentially yields opposite (*Z*)-isomer derivatives in an *E*:*Z* ratio of 0.3 (**93a**) and 0.7. (**93b**) In the same way, a decrease in turnover number has been observed when operating machine **94** (140 h) in comparison to catalyst **91** (310 h).

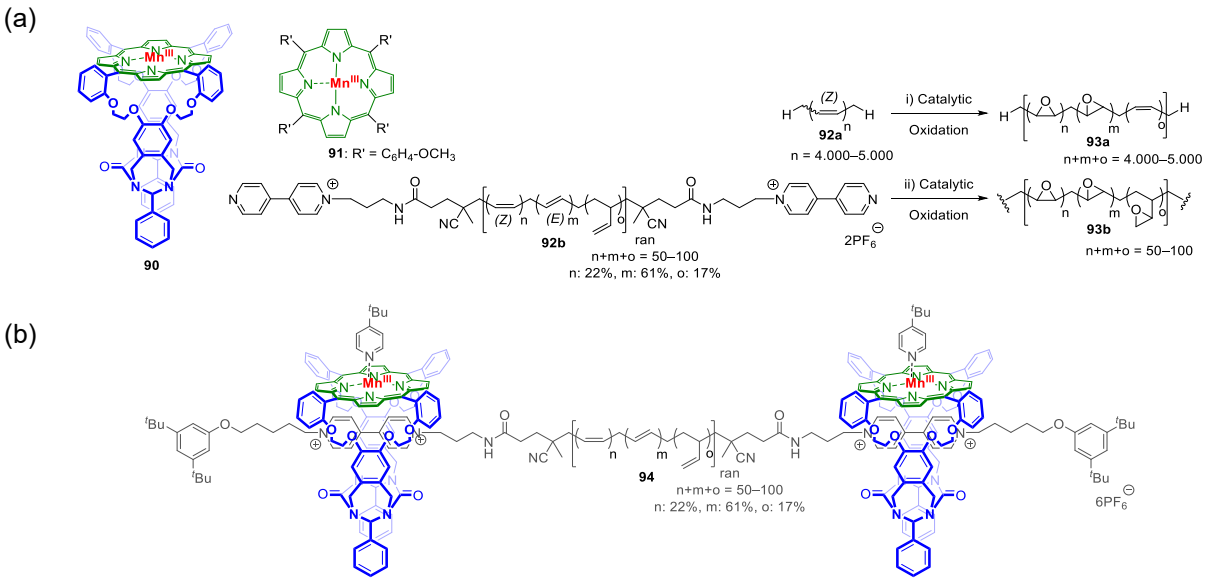

Scheme 7.7. Epoxidation of polybutadiene substrates by a rotaxane-based molecular machine **94** using a porphyrin-manganese based catalyst.[133] (a) For both epoxidations of polymeric substrates **92a** and **92b** observed activity and selectivity by ^{1}H NMR differs between the non-interlocked **91** and interlocked catalyst **90** when capping the manganese(III) system on one side with 4-*t*-butylpyridine. Reaction conditions: (i) and (ii) catalyst **90** or **91**, PhIO, 4-*t*-butylpyridine in $CHCl_3$. (b) Rotaxane-based molecular machine **94** obtained by complexation of **90** to polybutadiene track **92b** and capping the pseudorotaxane with alkyl stoppers.

When pre-isolating the proposed intermediate pseudorotaxane of **90** and polymeric track **92b** and capping it on either side with appropriate stopper units to give rotaxane **94** similar results have been obtained for the operation. This has led the authors conclude that the catalytic activity is an effect of the interlocked architecture and therefore, successfully mimics the working of DNA polymerases. However, they stated that is has been unclear ”whether the catalytic process is sequentially processive or random, that is, whether the catalyst moves step by step along the chain or hops randomly.”[133] Further kinetic studies with related systems have revealed that, in general, activity of the macrocyclic catalyst is further affected by the different mechanisms of the initial threading in open pseudorotaxane systems.[134]

In addition to this, Nolte and co-workers have also operated biohybrid pseudo[2]rotaxane system **99**.[135] Attaching three units of manganese-porphyrin catalyst **96** to the same side of trimeric ring-shaped bacteriophage clamp protein gp45 and threading the catalyst onto DNA biohybrid **99** was obtained. This machine as illustrated in Figure 7.10 selectively oxidised supercoiled DNA sequences at AAA-sites. This furnished free aldehyde moieties which upon treatment with biotin derivative **98** yielded conjugated DNA plasmids. Following labelling of the biotinylated positions with streptavidin has then allowed monitoring the operation with AFM. Using this protocol, the authors were able to introduce the expected globular features into the underlying DNA. If the association of the catalyst with DNA was prevented by closing the gp45 clamp

with an octapeptide sequence **97** prior to operation, the appearance of these features became random. All in all, this has led the authors to conclude that the operation of **99** is processive indeed.

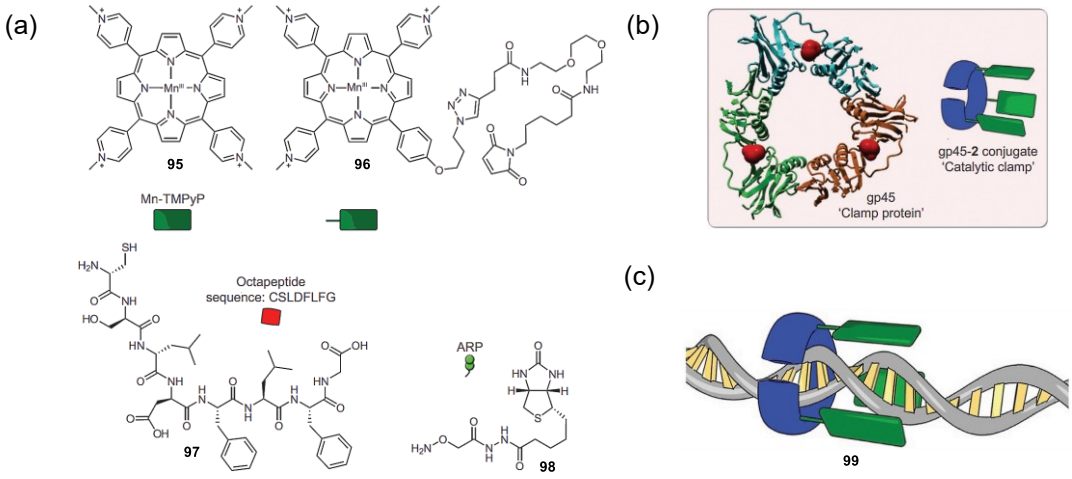

Figure 7.10. Linear processive clamp-like biohybrid catalyst for DNA oxidation of a circular DNA plasmid substrate. (a) Structures and shape representations of reaction components. (b) Protein clamp gp45 and its catalytic protein clamp conjugate. The E212C mutant of gp45 is shown, and its cysteine residues are emphasized in red. Its structure is based on PDB-file 1CZD with the E212C mutation performed in silico. (c) The concept for a clamp-shaped biohybrid catalyst is based on synthetic catalyst **95**, which with aid of a maleimide unit in **96** can be conjugated to the gp45 clamp protein to form a catalytic clamp. This biohybrid catalyst can associate with DNA and slide along it, which confers processivity to the catalytic behaviour of **99**. Adapted by permission from Springer Nature: reference 135, Copyright 2013.

Beyond this, the group of Takata and colleagues have studied the effect of a [2]rotaxane architecture on the intramolecular palladium-catalysed hydroamination reaction of allyl- and propargyl-urethane units to corresponding oxazolidinone derivatives (Scheme 7.8).[136]

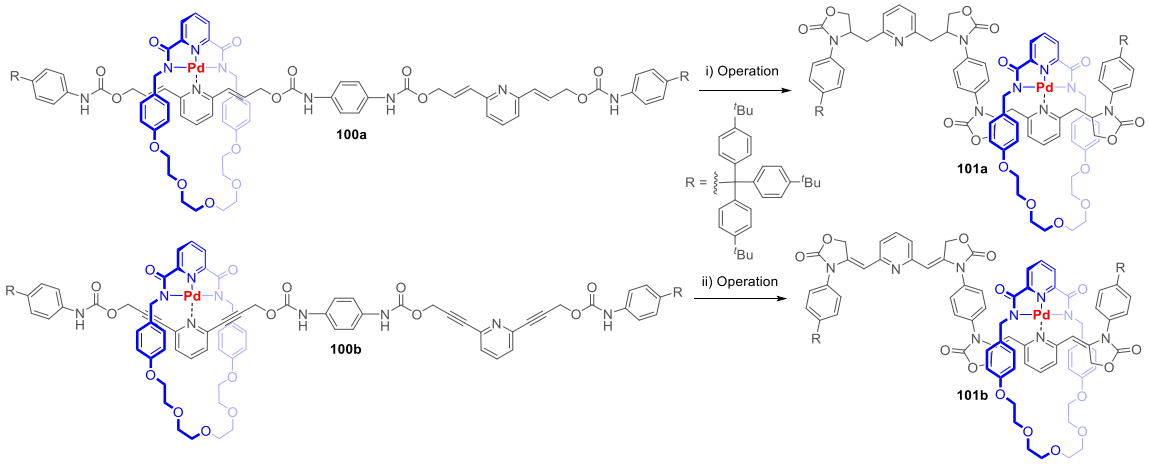

Scheme 7.8. Successive intramolecular palladium-catalysed hydroamination reaction of allyl- and propargyl-urethane containing [2]rotaxanes **100a** and **100b**.[136] Reaction conditions: $Mg(OMe)_2$ in MeOH:THF, reflux, (i) 1 min, 16%. and (ii) 90 min, 99%.

The systems **100a** and **100b** are capped by bulky stoppers to prevent dethreading and include pyridine units in the track to allow for threading with macrocycle **102** (see Scheme 7.9 below). Adjacent to the binding sites of the palladium bound macrocycle are allyl- and propargyl-urethane moieties that have been observed to cyclise in the presence of the macrocycle and additional $Mg(OMe)_2$. This gives rise to a racemic mixture of

syn- and *anti*-stereoisomers of oxazolidinone products under reflux. The proposed intramolecular mechanism for the reaction was confirmed by comparing the reaction between macrocycle **102** and threads **103a** or **103b** (Scheme 7.9).[137] Only in the case of the latter the anticipated cyclisation product **104b** was formed whereas repeating the reaction with the former thread **103a** containing large bulky stopper units was entirely prevented. This finding is further supported by separate studies exploring the effect of the macrocycle's ring size on the reaction with thread **103b** revealing that only when binding a macrocycle of suitable size subsequent cyclisation reaction takes place.

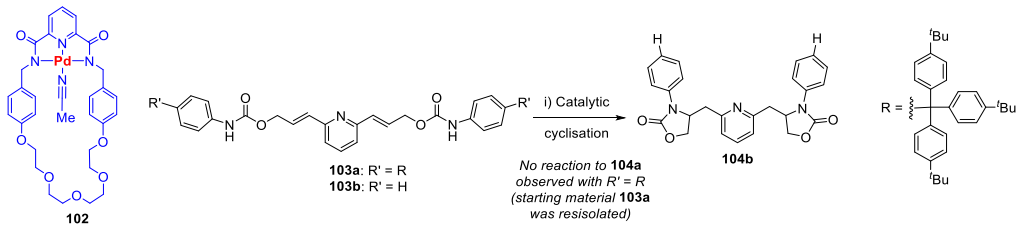

Scheme 7.9. Intramolecular hydroamination reaction of allyl-urethane substrates **103b** (R' = H) and **103a** (R' = R, see Scheme 7.8) catalysed by palladium macrocycle **102**. Differences in reactivity between the two substrates suggest that can only occur in the intermediate pseudorotaxane system.[137] Reaction conditions: (i) **103a**, $Mg(OMe)_2$ in MeOH:THF, 30 °C, 30 h, 99%. **103b**, $Mg(OMe)_2$ in MeOH:THF, 30 °C, 30 h, no reaction observed, starting material **103b** recovered.

Borrowing from the synthetic function of biological polymerase machines Harada and co-workers have developed a series of cyclodextrin (CD) dimer systems (Figure 7.11).[138] They showed that using a variety of systems of covalently linked face to face dimers of CD such as a combination of α- and β-CD a suitable catalytic environment is created for the ring-opening polymerisation of δ-valerolactone. They noticed that when subjected to the monomer at elevated temperature this catalyst yielded significantly higher polymerisation activity than individual CD components and the molecular weight obtained was further influenced both by the length of the linker and the combination of cyclodextrin parts. In view of the difference in polymerisation activity between pre-functionalised dethreaded and threaded dimers they concluded that in all those cases one CD unit of dimer catalyst effectively serves as "clamp" for the polymerisation catalysed by the opposing cavity of another CD unit – in analogy of the biological sliding DNA clamp loader complex.[139]

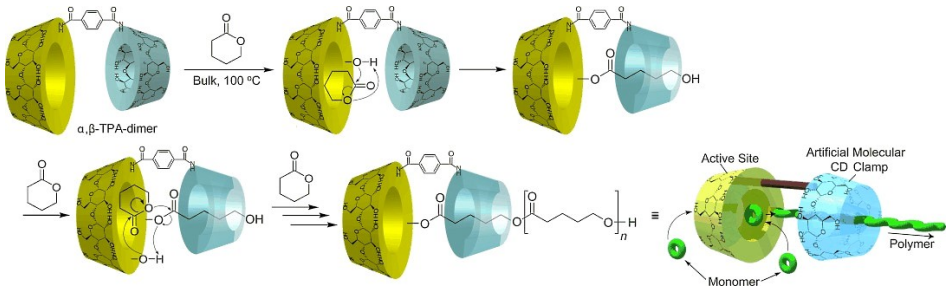

Figure 7.11. Molecular clamp reported for the ring-opening polymerisation of δ-valerolactone. (VL) Proposed mechanism for the polymerization of δ-VL initiated by a terephthalamide (TPA) linked CD dimer. Typical reaction conditions for the polymerisation initiated with α,β-TPA-dimer: α,β-TPA-dimer, δ-VL, 100 °C, 120 h, 74%. Reprinted by permission from John Wiley and Sons: reference 138, Copyright 2011.

7.1.4. Synthesis via DNA-Templated Molecular Machines

Returning back to modelling the synthetic behaviour of the ribosome, it has been concluded that applying DNA hybridization offers another possibility to control reaction sequences.[113,140] Instead of combining substrates in order within a preassembled rotaxane architecture the DNA-Template Synthesis (DTS) approach takes advantage of designing suitable DNA-based labels that function as mutually complementary templates and therefore, can encode information about the order of reaction between reactive substrates. When arranged in a suitable manner self-assembly of DNA components then allows combining reactive substrates at different positions, such as ends of a helix, junctions or, cross nicks where they can engage with one another to form predetermined connections. This strategy is the result of the several advances that have been made towards the synthesis and modification of DNA[17,141] and in direct relation to the work on DNA nanomachines[142] and technology.[143]

The first autonomous examples described in the literature to resemble the working of the ribosome employs an artificial DNA-based walker unit **W** and large region-encoding single-stranded DNA template **T** and as the basis for a multicomponent machine (Figure 7.12).[140]

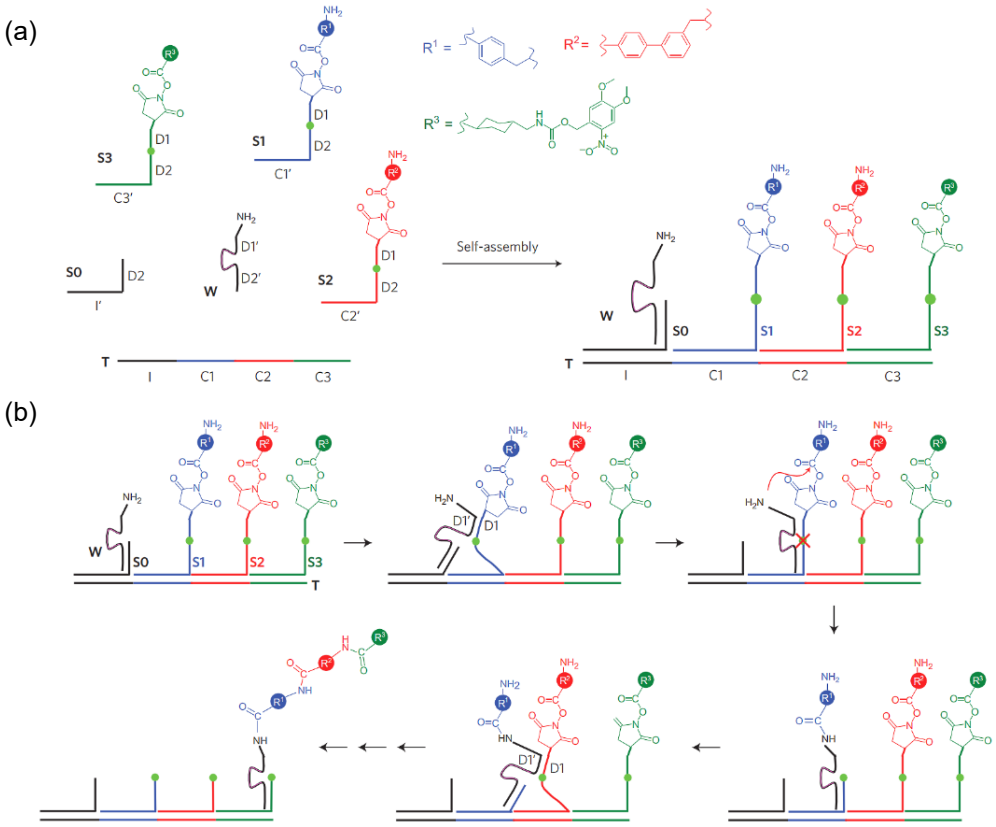

Figure 7.12. Autonomous multistep organic synthesis in a single isothermal solution mediated by a DNA walker.[140] (a) The system comprises six DNA or DNA-linked molecules. Three substrates **S1**-**S3** and an initiator **S0** can hybridize on a single-stranded DNA track **T**. Each substrate has an amino acid NHS ester at its 5′ end and two ribonucleotides (green dot) in the middle of its DNA sequence. The DNA walker **W** contains a 3′ amine group and an RNA-cleaving DNAzyme (purple line) that can cleave the ribonucleotides in the substrates. (b) DNA-mediated multistep synthesis of a tripeptide. All steps take place in a single solution under one set of reaction conditions without external intervention. Reprinted by permission from Springer Nature: reference 140, Copyright 2010.

Combined with a set of complementary nucleotides functionalised with non-natural amino acids **S1**-**S3** as well as a nonfunctionalized initiator codon **S0** the linear system formed provides a route for a defined sequence of aminolysis reactions of activated peptide esters. Like the working of the previous rotaxane-based systems[114] the unidirectional movement of the DNA walker along the base template **T** once attached to the initiator codon **S0** acts as a mean to sequentially join following substrates. With this design Liu and college have been able to make a variety of tripeptide sequences by "relying entirely on effective molarity increases brought about by DNA hybridization." Furthermore, it has been noted that unlike the ribosome the artificial system created is not limited by specificity to certain proteinogenic substrates allowing creation of general peptide sequences.[144]

In the following, O'Reilly and co-workers have described a framework that relies on partially self-complementary strands of DNA (hairpins) as a means to combine reactive substrates in a sequence specific manner with the help of hybridization chain reactions as an alternative to a walker unit (Figure 7.13).[145]

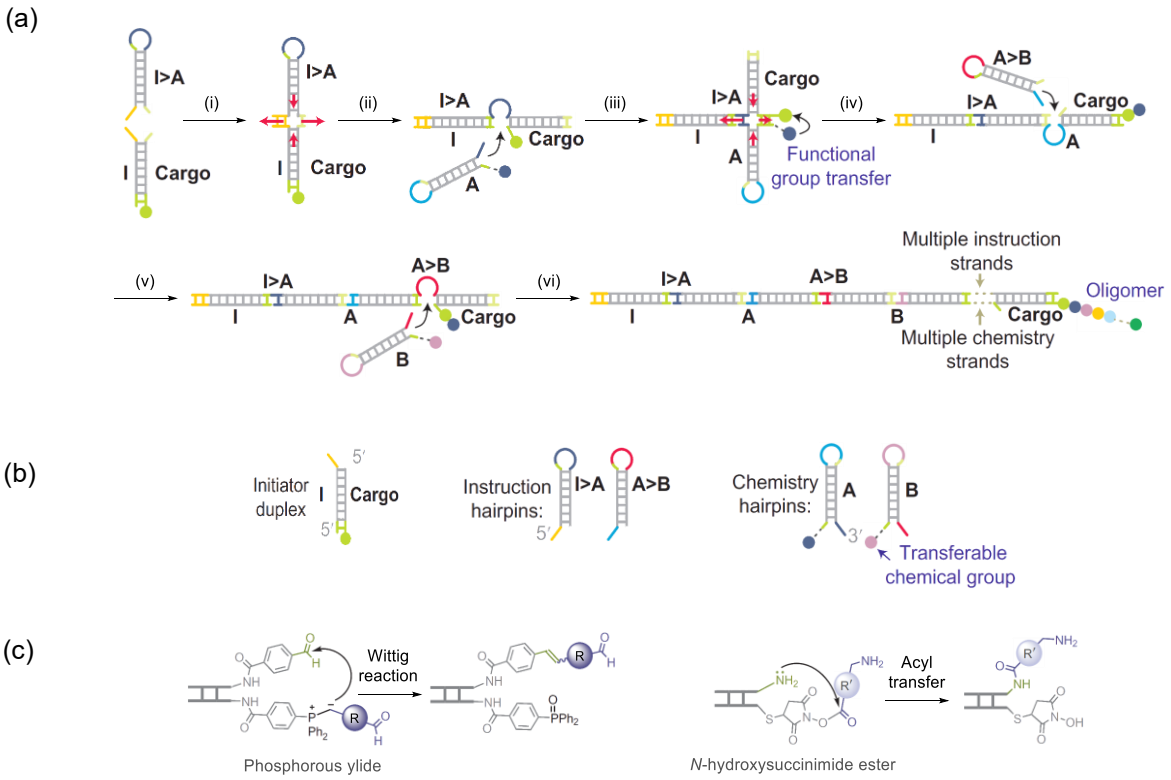

Figure 7.13. Operation of a DNA-based molecular assembler.[145] (a) Proposed assembler mechanism: (i) Hybridization of the initiating duplex **I:Cargo** to the matching toeholds of the first instruction **I>A** creates a Holliday junction whose (ii) migration (indicated by red arrows) leads to the opening of the loop domain of the hairpin. Loop opening activates the sequestered toehold domain (blue) that specifies that the chemistry hairpin **A** is to be added next. (iii) **A** is recruited to the chain by hybridization of its external toehold to this newly exposed domain. (iv) Junction migration completes insertion and reveals a sequestered toehold that is recognized by and (v) triggers insertion of instruction **A>B**. (vi) Chain extension proceeds by alternate addition of instruction and chemistry hairpins. As each chemistry hairpin is added to the chain, its building block is held in close proximity to the growing oligomer attached to **Cargo**, enhancing the rate of transfer of the incoming building block from its DNA adapter to the oligomer. (b) Assembler components. **Cargo** starts in the initiating duplex, which carries an identifying toehold on strand **I** (yellow). 'Chemistry' hairpins (for example, **A** and **B**) carry building blocks for DTS. 'Instruction' hairpins (for example, **I>A** and **A>B**) program the assembly sequence. Each hairpin carries external and internal address toeholds (coloured) and one of two generic external toeholds (green). (c) Chemistries used for oligomer propagation. Adapted by permission from Springer Nature: reference 145, Copyright 2016.

At the start of the developed autonomous process as shown in Figure 7.13, initially, the substrate carrying duplex **I** is allowed to combine with instructive hairpin **I>A** to give a staggered assembly. Next, upon spontaneous re-hybridization of partially unmatched DNA sequences the fully self-complementary linear DNA strand is formed. The obtained linear structure, however, exposes a junction site and this discontinuity in the double-stranded DNA motive provides a template for the addition of another unit, in this case, a so-called (chemistry) hairpin. Once a substrate-carrying hairpin **A** becomes associated with the junction site this yields a second staggered assembly and as a result, allows combining the two substrates of **I** and **A**. Following the rearrangement after transfer of the substrate from site **I** to **A** this in turn reveals another junction site for assembly with a new instruction unit **I>B**. Again, this implies the addition of fragment **B** to the growing oligomer chain. And overall, provided enough complementary units exist, this process can be repeated over and over. And by devising a suitable sequence of alternate combinations of substrate and instruction hairpins and supressing intermachine reactions at high dilution this allowed the synthesis of several sequence-specific products. Furthermore, the authors were able use two different types of reactive substrates and produce a series of composite oligomers via a succession of Wittig and acyl transfer reactions.

7.2. Motivation

In many ways, developing synthetic methods for controlling the sequence of synthetic oligomer and polymers remains an attractive goal.[10] Despite unprecedent advances, current synthetic polymers hardly match the superior material and adaptive properties of their natural counterparts composed of amino acids, nucleotides, terpenes, and many other components and stabilised mainly by weak non-covalent interactions. Importantly, when comparing the sophisticated biological methods to control the formation and to convey information with the generated polymers no correspondent artificial system does exist. As such, significant attention has been devoted to learning from nature and creating the first library of dynamic polymers that would equally be enabled by secondary interactions.[10,146,147] For example, understanding the composition and generation of natural polymers such as a spider's web[148] or terpenoids[149] keeps being part of active research due to potential applications. Similarly, while methods for preparation of peptide series both by in vivo[150] and ex vivo[151] have already been devised, corresponding examples for the synthesis of arbitrary sequence-specific polymers via e.g., carbon-carbon bond formation[152] or other types of reactions[153] are rare.[154]

In most cases, general methods for formation carbon-carbon bonds are limited to generation of sequence-controlled block polymers or copolymers with variable sequences of comonomers. Notable examples in this regard are controlled living radical polymerisation methods such as reversible addition-fragmentation chain transfer (RAFT),[155] nitroxide-mediated radical polymerization (NMP),[156] atom transfer radical polymerization (ATRP)[157] or photoinduced electron transfer (PET) reactions.[158] In one of the examples reported in the literature it was shown that when performing ATRP in an iterative fashion this enables the synthesis of a well-defined decablock copolymer.[159] However, even with those advanced protocols in hand – loosely speaking – broad molecular distributions of polymers are obtained when compared to the immediate stringent control during transcription and the exceptional sequence accuracy maintained during the replication of an average human genome with up to 109 base pairs.[4a] Yet, it was hoped[10] that eventually, generation of synthetic oligomers and polymers with sequence control will "provide major improvements for

atom economy, molecular precision, adjustment of physicochemical properties, and device miniaturization." Feasibility of this approach has been shown by a number of peptide-based examples[160] for instance by using short strands of oligonucleotides which when polymerised by CuAAC self-assemble into β-sheets and then form higher order tertiary structures.[161] Developing a rotaxane-based molecular machine with the ability to create an arbitrary sequence-controlled polymer thus constitutes an attractive goal not only from a fundamental theoretical but also from a practical and economic point of view.

7.3. Aims

From this perspective an attempt has been made to expand on the first generation of carbon-carbon bond forming molecular machines[125] and explore the formation of alternative stilbene substrates. It has been hoped that further transformation in analogy to the post-translational modification of peptides can allow the construction of distinct secondary structures similar to the examples found for proteins[163] and DNA.[4] In this regard, it has been noted that oxidative cyclodehydrogenation of assembled stilbene sequences could afford different length helical structures. The helicenes formed would potentially give rise to interesting catalytic, synthetic, and material applications due to their unique chiroptical properties.[164] Notably, it has been realised that for the preparation of large helicenes several protocols have been reported in the literature that already combine a series of multiple Wittig-type reactions with the photoinduced cyclodehydrogenation of stilbene precursors[164a,165] to give, for example, [11] **106**, [12] **108** and [14]helicenes **110** as shown in Scheme 7.10.[164b]

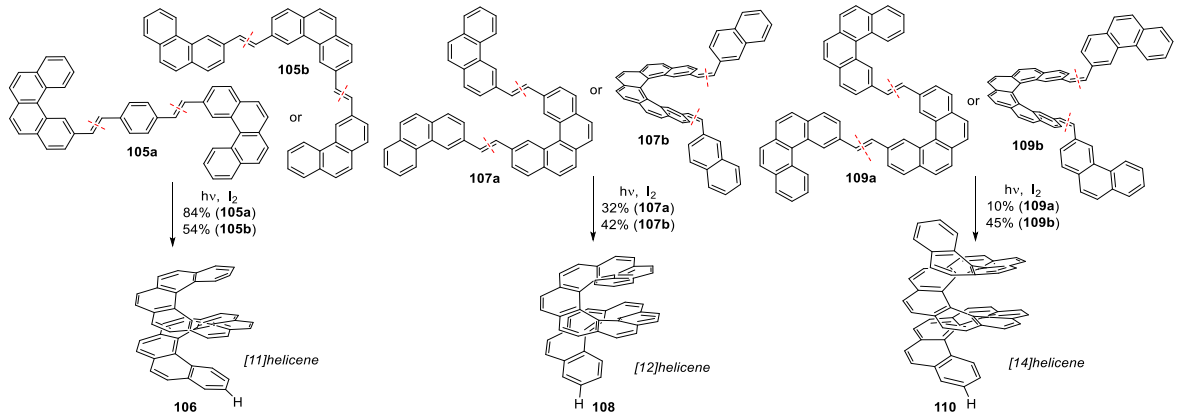

Scheme 7.10. Photosynthesis of a [11]- **106**, [12]- **108** and [14]-helicene **110** by photoinduced double cyclodehydrogenations of a bis(arylvinyl)arens precursors.[164b] Red lines mark the disconnection of carbon-carbon double bonds where substrates have been joined by a Wittig type reaction.

The current state-of-the-art in carbon-based helicene synthesis was recently reported by Fujita and collaborators.[166] Relying on an extended linear synthesis based on three Wittig-type reactions (Scheme 7.11) Fujita and co-workers were able to obtain a highly conjugated hexavinylene precursor **118** which they ultimately transformed into the corresponding [16]helicene **119** via a sextuple photocyclization reaction. Moreover, they were able to demonstrate that after subsequent removal of triisopropylsilyl (TIPS) protecting groups and palladium catalysed deoxygenation under Heck conditions with reductant formic acid hydrocarbon helicene **120** can be isolated which was characterised with NMR spectroscopy.

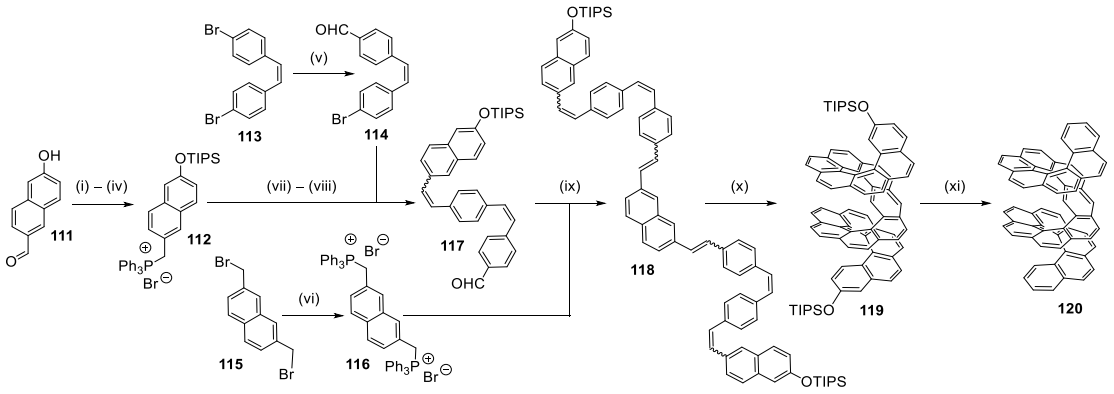

Scheme 7.11. Linear synthesis of [16]helicene **120** by Fujita and co-workers.[166] Reaction conditions: (i) TIPSCl, imidazole, CH_2Cl_2. (ii) $NaBH_4$, EtOH, 86% in 2 steps. (iii) CBr_4, PPh_3, CH_2Cl_2. (iv) PPh_3, PhMe, 78% in 2 steps. (v) ^{n}BuLi, THF then DMF, 67%. (vi) [18]-crown-6, KOH, CH_2Cl_2, 77%. (vii) ^{n}BuLi, THF then DMF, 79%. (viii) PPh_3, $CHCl_3$. (ix) [18]-crown-6, KOH, CH_2Cl_2, 85% in 2 steps. (x) hv, I_2, PhMe, 7%. (xi) TBAF, THF, then TF_2O, pyridine, CH_2Cl_2, then PPh_3, $Pd(OAc)_2$, Et_3N, HCO_2H, DMF, 11% in 3 steps.

The aim of this project is to adapt the design of the developed carbon-carbon bond forming molecular machines[125] and explore the possibility of including principal helicene precursors such as phenanthrene building blocks into a new machine design **121** via a synthetic procedure as outlined in Scheme 7.12. The basic design reuses previous building blocks such as the azide stopper **74** as well as aldehyde macrocycle **75**[114a] and diazide linker **123**[125] to connect a series of bifunctional phenanthrene phosphonium barriers **124a** and 124**b** via CuAAC or copper-catalysed AMT synthesis to afford [2]rotaxane machine **121**.

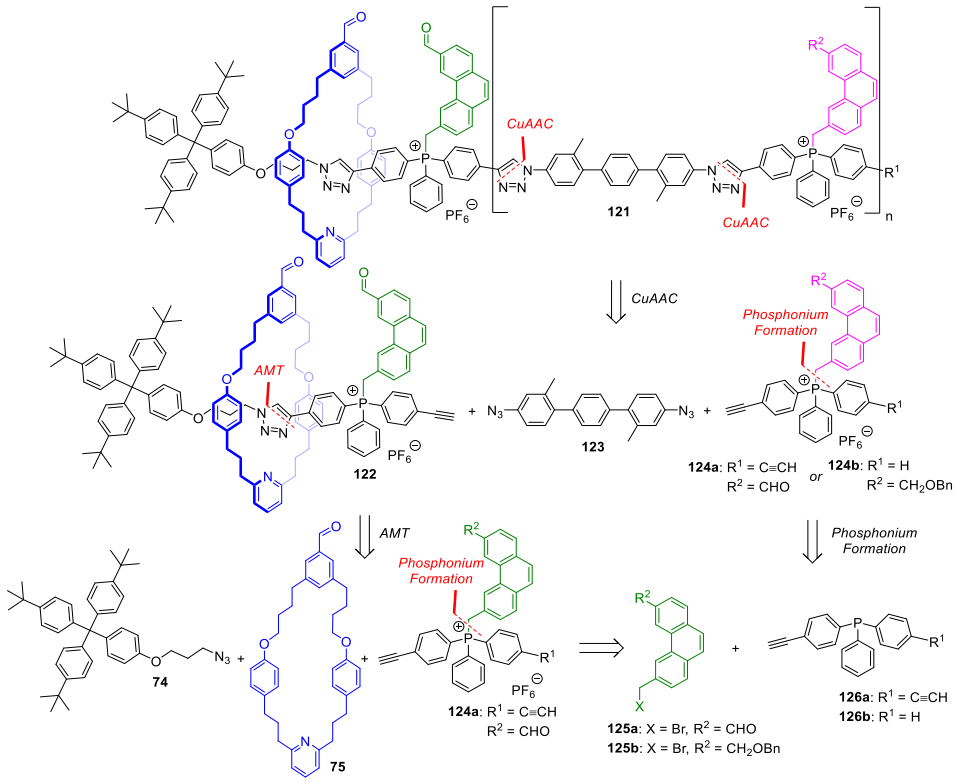

Scheme 7.12. Proposed retrosynthesis of a [2]rotaxane-based molecular machine **121** capable of forming (oligo)stilbene sequences via a succession of Wittig type reactions between bifunctional phenanthrene aldehyde phosphonium ylides and an aldehyde macrocycle based on previous design.[125] Azide stopper **74** as well aldehyde macrocycle **75**[114a] and azide linker **123**[125] will be reused from earlier machine designs.

Once an initial barrier has been synthesised and its stability within the rotaxane architecture confirmed the 1-barrier operation will be studied. If successful, optimisation for the cyclisation conditions will be performed and subsequently tested as a one-pot operation cyclisation procedure (Figure 7.14). With each successive Wittig reaction, the macrocycle is intended to remove a phenanthrene barrier and with each cleavage event the macrocycle can move further along the length of the rotaxane axle and access the next barrier. When performed under high dilution, reaction with barriers out of sequence is prevented by the compartmentalisation of the macrocycle and the rigidity of the thread, which holds reactive non-proximal barriers out of reach of the aldehyde macrocycle. Following the transfer of all the phenanthrene groups from the track to the macrocycle, it dethreads from the end of the track into the bulk medium. In a next step, irradiation with light will induce photoisomerization of the stilbene to dihydrophenanthrenes that can be oxidised in presence of an oxidant to give helicenes. Potentially, an extension of the concept will then allow synthesis of longer stilbene sequences and in turn give rise to larger helicene products.

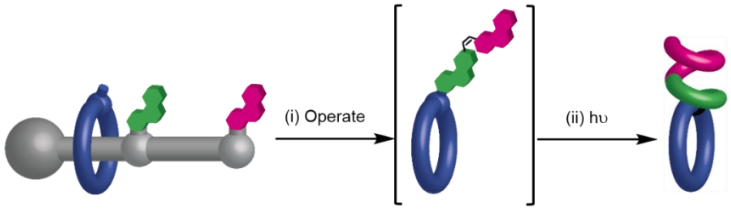

Figure 7.14. Concept of helicene synthesis by a [2]rotaxane-based molecular machine through iterative carbon-carbon bond formation and subsequent oxidative cyclisation with light.

7.4. Results and Discussion

Based on the literature reports for the preparation of tri- and disubstituted phosphines via condensation of chlorophosphine and aryl lithium compounds,[167] the initial established strategy of making triaryl phosphines involved going through oxide intermediates (Scheme 7.13)[178] and therefore, required a final reduction with either trichlorosilane and triethylamine[125] or a combination of oxalyl chloride and lithium aluminium hydride.[168]

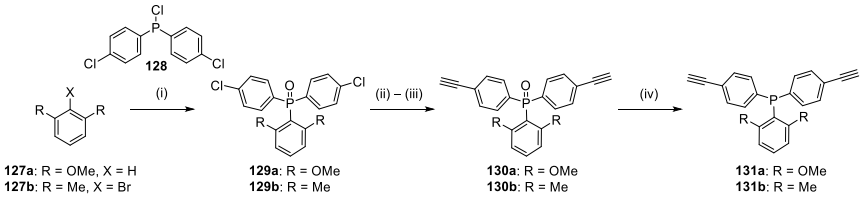

Scheme 7.13. Exemplary conventional synthesis of trisubstituted phosphines **131a** (R = OMe) and **131b** (R = Me).[178] Reaction conditions: (i) *t*BuLi, Et_2O, −78 °C to rt, 2 h, then chlorophosphine **128**, −78 °C to rt, 20 h, then H_2O_2, PhMe, rt, 6 h, 69% (**129a**, R = OMe) and 75% (**129b**, R = Me). (ii) $[Pd(CH_3CN)_2]Cl_2$, X-Phos, Cs_2CO_3, (triisopropylsilyl)acetylene, CH_3CN, 90 °C, 20 h, h, 99% (R = OMe) and 98% (R = Me). (iii) TBAF, THF, rt, 1 h, 98% (**130a**, R = OMe) and 91% (**130b**, R = Me). (iv) $(COCl)_2$, PhMe, rt, 10 min, then $LiAlH_4$. rt, 30 min, 69% (**131a**, R = OMe) and 65% (**131b**, R = Me).

To simplify this process, an alternative method has been established; It was concluded that the extra methoxy and methyl substituents in **131a** and **131b**, as originally considered, do not hold any advantage for the operation and thus, can be omitted.[178] This has reduced the synthesis to the preparation of 1**26a** (two terminal ethynyl units) and **126b** (one terminal ethynyl unit) which, after optimisation, we were able to prepare in one step (Scheme 7.14). The procedure developed starts with the lithium-bromide exchange of

commercially available compound **132** and reacts the generated aryl lithium species with either dichloro-phenyl- or chlorobis(phenyl)phosphine. In a last step, the TMS protecting groups are removed with sodium methoxide *in-situ*. Overall, this method afforded phosphines in reliable yields of 99% (**126a**) and 75% (**126b**).

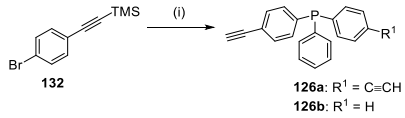

Scheme 7.14. One-step synthesis of a terminal **126a** and an internal phosphine **126b**. Reaction conditions: (i) ^{n}BuLi, Et_2O, −78 °C to −10 °C, 15 min, then PPh_2Cl, −78 °C to rt, 16 h, then NaOMe, rt, 6 h, 99%. ^{n}BuLi, Et_2O, −78 °C to −10 °C, 15 min, then $PPhCl_2$, −78 °C to rt, 5 h, then NaOMe, rt, 16 h, 75%.

In addition, we were able to achieve the synthesis of the two benzyl bromides **125a** and **125b** (Scheme 7.15); Starting from 4,4'-stilbenedicarboxylic acid **133** oxidative photocyclization of the intermediary formed ethyl diester led to the corresponding phenanthrene diester[169] which after reduction with lithium aluminium hydride[170] gave root phenanthrene diol **134**. Following desymmetrisation was then conducted via two pathways to synthesise both benzyl bromides **125b** and **125a**. First, phenanthrene diol **134** was mono protected as benzyl ether (**135b**), and the free benzylic alcohol moiety was then converted to the bromide **125b** by an Appel type reaction. Second, phenanthrene diol **134** was desymmetrised via oxidation with Dess-Martin periodinane to provide mono-aldehyde **135a**. The desired aldehyde bromide **125a** was then prepared by another Appel type reaction in excellent yield.

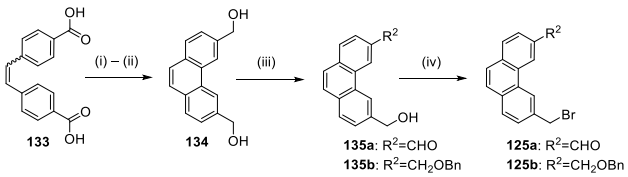

Scheme 7.15. Preparation of phenanthrene precursors **125a** and **125b**. Reaction conditions: (i) $SOCl_2$, 65 °C, 16 h, EtOH, 78°C, 5 h, 82% over two steps. (ii) hv, I_2, air, PhMe, rt, 16 h, $LiAlH_4$, THF, 0 °C to rt, 1 h, 70% over two steps. (iii) DMP, $CHCl_3$:CH_3CN, 0 °C to rt, 2 h, 52% (**135a**); BnBr, NaH, TBAI, DMF, 0 °C to rt, 2 h, 42% (**135b**). (iv) CBr_4, PPh_3, CH_2Cl_2, 0 °C, 15 min, 97% (**125a**); CBr_4, PPh_3, CH_2Cl_2, 0 °C, 15 min, 99% (**125b**).

With benzyl bromides **125b** in hand the phosphonium salt with triphenylphosphine has been prepared via condensation and subsequent salt-exchange with an excess of potassium hexafluorophosphate to aid solubility (Scheme 7.16). This allowed testing the proposed one-pot Wittig and cyclisation reaction by first combining phosphonium salt **136** with aldehyde macrocycle **75** under basic conditions and then cyclising the product with light from a narrowband LED at a wavelength of 365 nm and using iodine as an oxidant[165a].

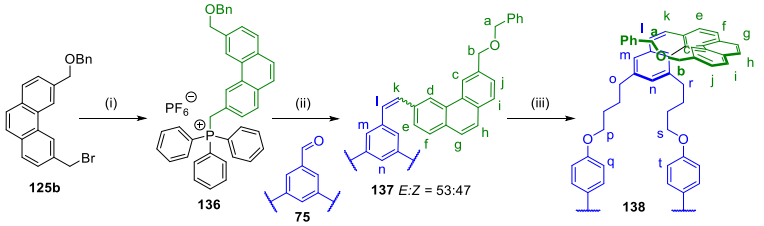

Scheme 7.16. Model Wittig reaction for the operation and cyclisation of a 1-barrier machine. Reaction conditions: (i) PPh_3, PhMe, 110 °C, 16 h, then KPF_6, THF, rt, 30 min, 97% over two steps. (ii) BEMP, CH_2Cl_2, –78 °C to rt, 6 h, 72%. (iii) hv, I_2 (1.1 equiv.), propylene oxide (50.0 equiv.), PhMe, rt, 11 h, 48%.

Analysing the obtained stilbene product **127** with ^{1}H NMR in the first place, it was noticed that the carbon-carbon bond had been formed in an *E*−*Z* ratio of 47:53 (Figure 7.15). We assumed that the lack of stereoselectivity at this point may be the result of generating a semi-stabilised benzyl ylide and using a bulky aldehyde macrocycle **75**. A survey of the literature suggested that this finding can also be an effect of the salt-free conditions which at modest concentration are known to favour the formation of (*Z*)-alkenes over thermodynamically more stable (*E*)-alkenes.[171]

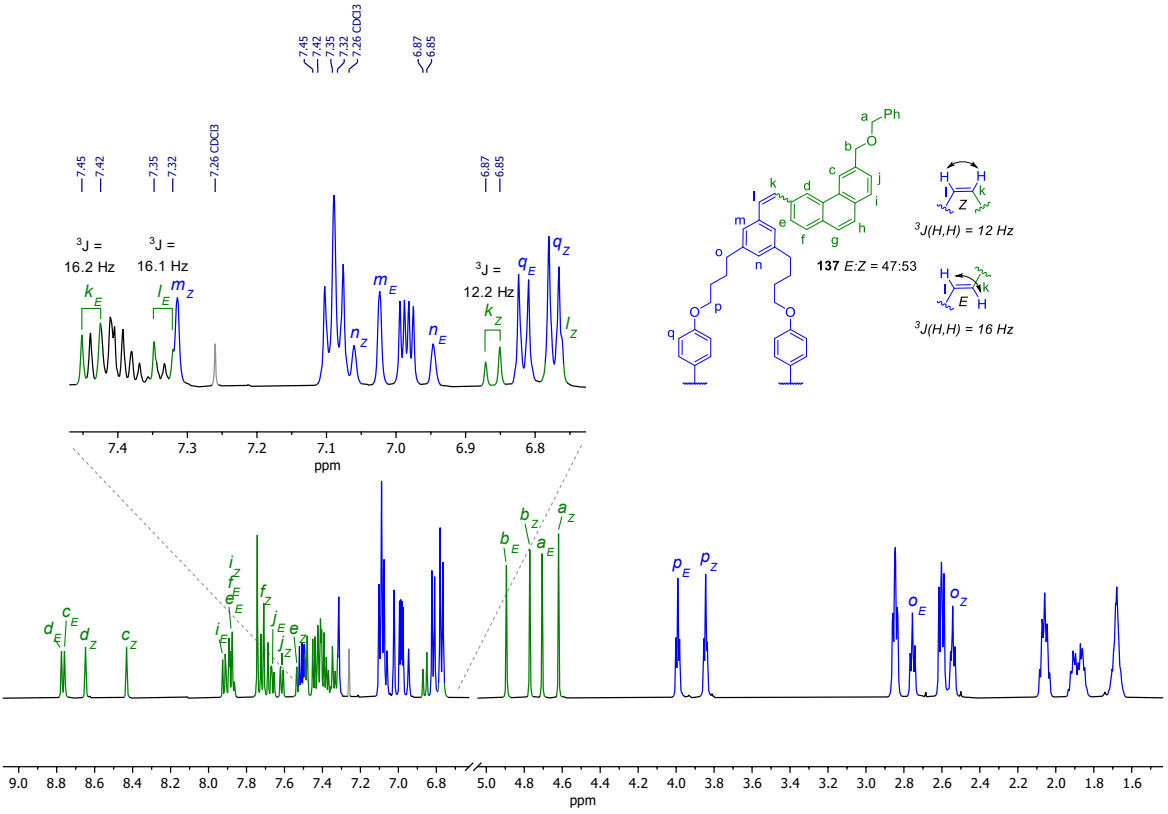

Figure 7.15. Partial ^{1}H NMR spectra (600 MHz, $CDCl_3$, 298 K) of isolated stilbene product **137** (E:Z = 47:53) from the Wittig reaction between aldehyde macrocycle **75** and phosphonium salt **136** showing relevant peaks for the assignment of the E−Z ratio correspond to labelling in Scheme 7.16. Determined vicinal couplings for the constituting alkene bond of $^{3}J_Z$(H,H) = 12 Hz and $^{3}J_E$(H,H) = 16 Hz are in line with expectations.[172]

With the desired Wittig reactivity initially confirmed, we have then prepared the phosphonium barriers **124a** and **124b** by heating corresponding benzyl bromides **125a** or **125b** and phosphines **126a** or **126b** in toluene overnight under argon. This yielded the two barriers in yields of 67% and 87%, respectively (Scheme 7.17).

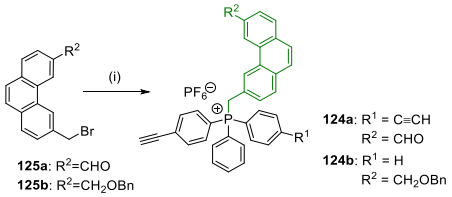

Scheme 7.17. Synthesis of preparation of phenanthrene barriers **124a** and **124b**. Reaction conditions: (i) **125a**, **126a**, PhMe, 120 °C, 16 h, then KPF_6, THF, rt, 30 min, 67% (**124a**) over two steps; **125b**, **126b**, PhMe, 120 °C, 16 h, then KPF_6, THF, rt, 30 min, 87% (**124b**) over two steps.

7.4.1. One-Barrier Operation and Cyclisation

Next, synthesis of the 1-barrier rotaxane was attempted using previously reported conditions for the copper-catalysed AMT synthesis.[123-125] Upon iterative size exclusion significant amounts of 1-barrier rotaxanes **122a** and **122b** were afforded alongside accompanying free threads **139a** and **139b** (Scheme 7.18).

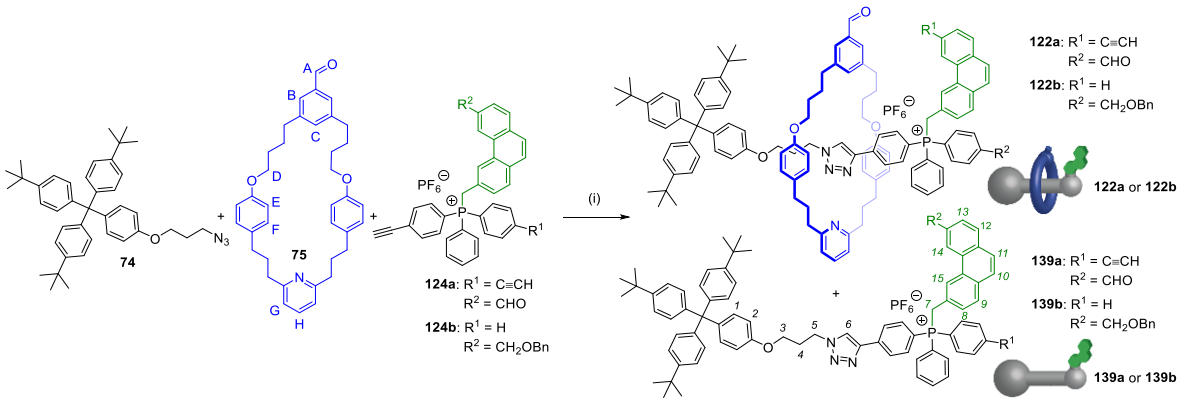

Scheme 7.18. Synthesis of rotaxane synthon **122a**, 1-barrier machine **122b**, and corresponding free threads **139a** and **139b**. Reaction conditions: (i) **74**, **75**, **124a**, $[Cu(CH_3CN)_4]PF_6$, CH_2Cl_2:^{t}BuOH, rt, 16 h, 24% (rotaxane **122a**) and 40% (free thread **139a**); **74**, **75**, **124b**, $[Cu(CH_3CN)_4]PF_6$, CH_2Cl_2:^{t}BuOH, rt, 40 h, 29% (rotaxane **122b**) and 16% (free thread **139b**).

The anticipated mechanically interlocked structures of obtained compounds **122a** and **122b** were confirmed by high-resolution mass spectrometry and analysis with ^{1}H NMR spectroscopy (Figure 7.16). Comparison between aldehyde macrocycle **75** (i), rotaxane **122a** (ii) and free thread **139a** (iii) shows a characteristic shielding effect for the macrocycle as indicated by a low-field shift of proton signals of phenol H_E-H_F and alkyl ether groups H_D but also for the aldehyde signal H_A and other identified signals H_B, H_C, H_G and H_H. Similarly, positions on the axle H_1-H_6 experience a shielding effect in surrounding of the proposed location of the macrocycle. All in all, these indications suggested formation of 1-barrier rotaxane synthons **122a** and **122b**.

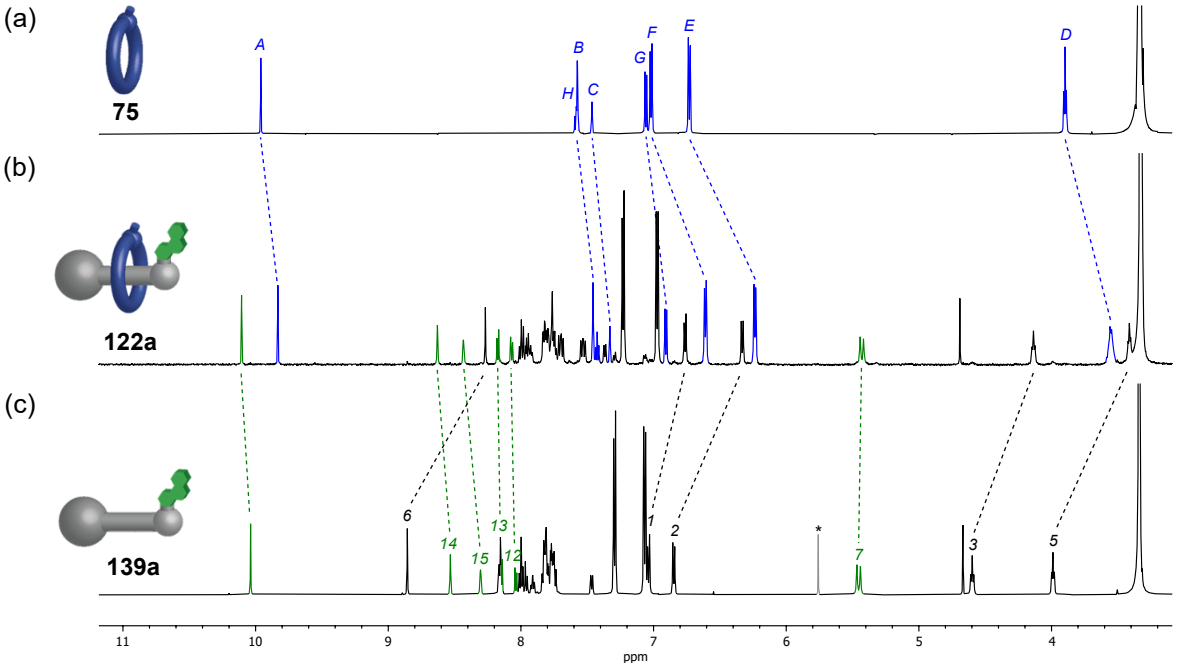

Figure 7.16. Partial ^{1}H NMR spectra (600 MHz, DMSO-d_6, 298 K) of (a) macrocycle **75**, (b) rotaxane **122a** and (c) free thread **139a**. Peak assignments correspond to labelling in Scheme 7.18.

Moreover, isolated rotaxanes **122a** and **122b**, do not display signs of dethreading or decomposition upon storage over multiple weeks at room-temperature, even in concentrated solutions. This observation has led us to conclude that the phenanthrene motive indeed suffice to serve as a kinetically and thermodynamically stable barrier and allowed proceeding to testing the operation of 1-barrier machine **122b** (Scheme 7.19).

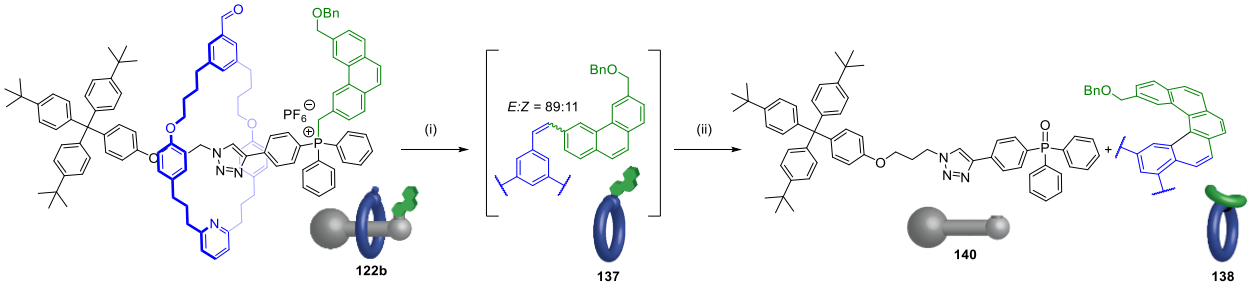

Scheme 7.19. One-pot operation and cyclisation of 1-barrier machine **122b**. Reaction conditions: (i) BEMP (10 equiv.), CH_2Cl_2, –78 °C to rt, 16 h. (ii) hv, I_2 (2.2 equiv.), propylene oxide (100.0 equiv.), PhMe-d_8, rt, 16 h, 56% ([5]helicene **138**) and 71% (free thread **140**).

And to our delight, upon addition of resin bound BEMP to 1-barrier machine **122b** at lower temperatures and subsequently warming the reaction to room-temperature we have been able to successfully detect the desired olefin **137** as indicated by results obtained with mass spectrometry (Figure 7.17 and Figure 7.18 (a)).

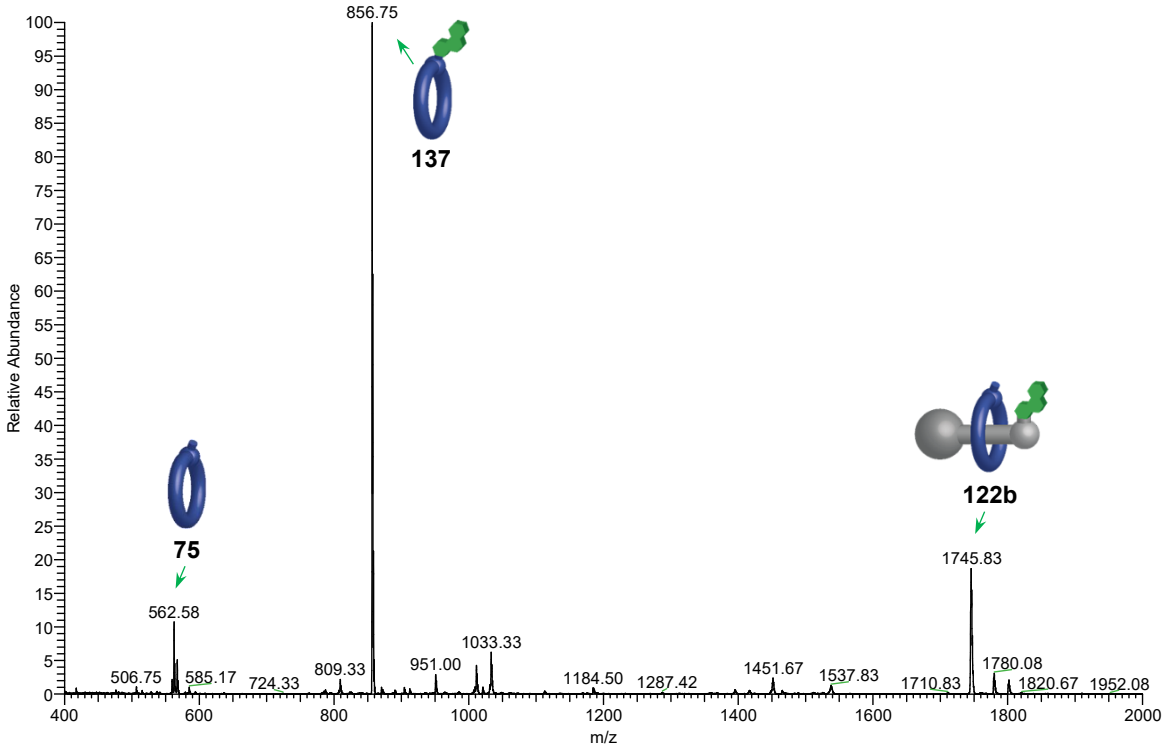

Figure 7.17. One-pot operation and cyclisation of 1-barrier machine **122b**. Observed crude operation products by LR(ESI)-(+)-MS indicating formation of 1-barrier machine **122b**. Major peaks correspond to $[M+H]^+$ and $[M]^+$ ions; The peak at m/z 856 correlates to [**137**+H]$^+$, m/z 562 to unreacted macrocycle [**75**+H]$^+$ as a result of barrier hydrolysis during operation and m/z 1745 correlates to unreacted machine [**122b**-PF_6]$^+$.

To further promote the cyclisation, the solvent was changed *in-situ* from dichloromethane to toluene before irradiating the crude reaction mixture at 365 nm with an LED in the presence of additional I_2 and propylene oxide. And repeating the analysis we were able to confirm the final generation of [5]helicene **138** (Figure *7.18* (b)), which could be isolated in a 56% yield from the operation.

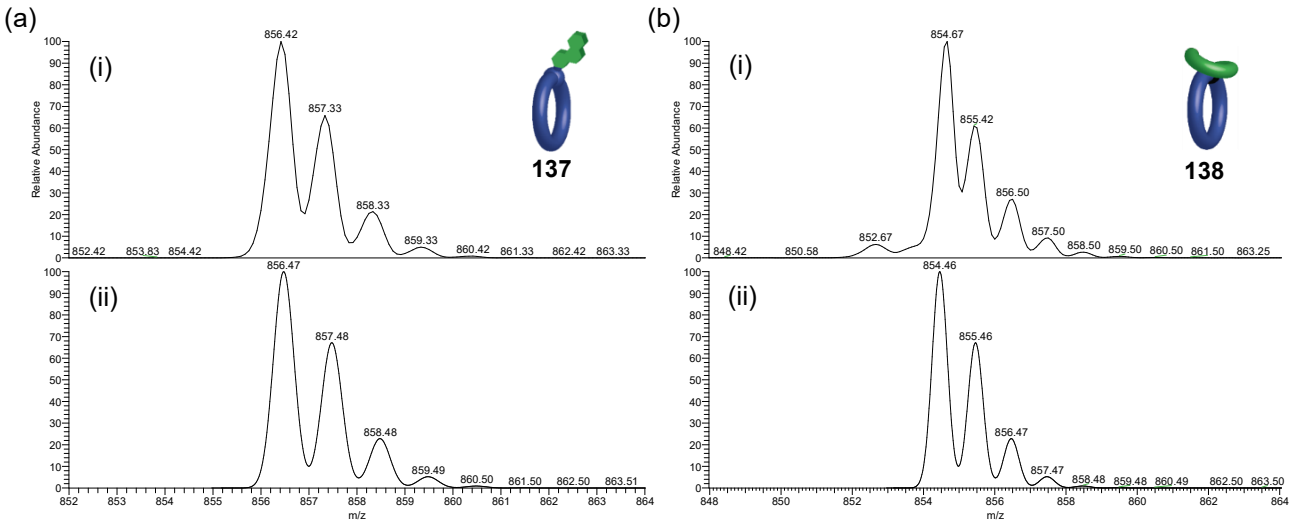

Figure 7.18. Analysis of the operation of 1-barrier machine **122b**. (a) (i) Observed and (ii) predicted product **137** recorded from the crude operation mixture. The predicted isotope pattern is for $[C_{61}H_{61}NO_3H]^+$ corresponding to [**137**+H]$^+$. (b) (i) Observed and (ii) predicted product of cyclisation **138** recorded from the crude operation mixture. The predicted isotope pattern is for $[C_{61}H_{59}NO_3H]^+$ corresponding to [**138**+H]$^+$.

In contrast to the reaction performed by conventional means (see Scheme 7.16, isolated as *E:Z* 47:53 mixture) the stilbene intermediate **137** formed during the operation predominately gave the (*E*)-isomer **137** in an *E*−*Z* ratio of 89:11 as determined by ^{1}H NMR spectroscopy (Figure 7.19). This finding confirmed previous observations for the stereoselectivity obtained with another stilbene-forming 1-barrier machine **87** when using LDA as a base in THF (Scheme 7.6).[129] This result supports the postulated mechanism via an interlocked architecture. Furthermore, despite the difference in the phenanthrene rotaxane architecture even when performing the reaction at room-temperature with BEMP, the (*E*)-isomer continues to be performed preferentially, possibly, due to kinetic reasons. Efforts to use protecting group TBDPS instead of benzyl ether resulted in desilylation during the acidic conditions of the cyclisation conditions.[179]

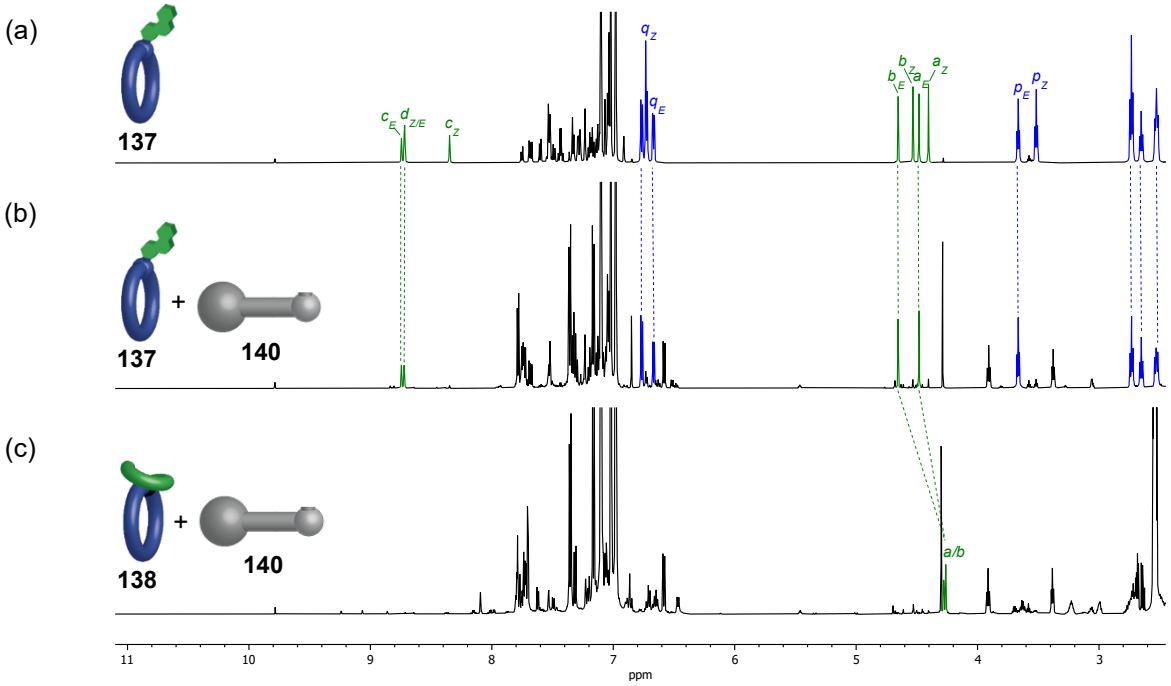

Figure 7.19. Comparison of partial ^{1}H NMR spectra (600 MHz, toluene-d_8, 298 K) of (a) 1-barrier authentic standard **137** vs (b) crude 1-barrier operation of **122b** after solvent exchange. (c) Crude 1-barrier cyclisation after addition of propylene oxide and iodine and subsequent irradiation.

Overall, the results of the initial study of the operation and cyclisation with 1-barrier machine **122b** have suggested the working of the underlying concept. They successfully enabled the preparation and isolation of [5]helicene **138** and allowed inspecting the furnished structure with ^{1}H NMR (Figure 7.20). It was found that helicene **138** displayed significant shielding and diastereotopic splitting for proton signals of the upper part of the macrocycle such as H_p and H_o. This may be the result of the interactions between the macrocycle and the adjacent extended aromatic helical system; however, this could not be confirmed with supplementary 2D NOESY experiments, ($CDCl_3$, mixing time t_8 = 400 ms) but corresponds well similar diastereotopic protons reported in literature for other helicene derivatives.[173] Unfortunately, attempts to further characterise the structure of [5]helicene **138** via single-crystal X-ray diffraction have remained unsuccessful.

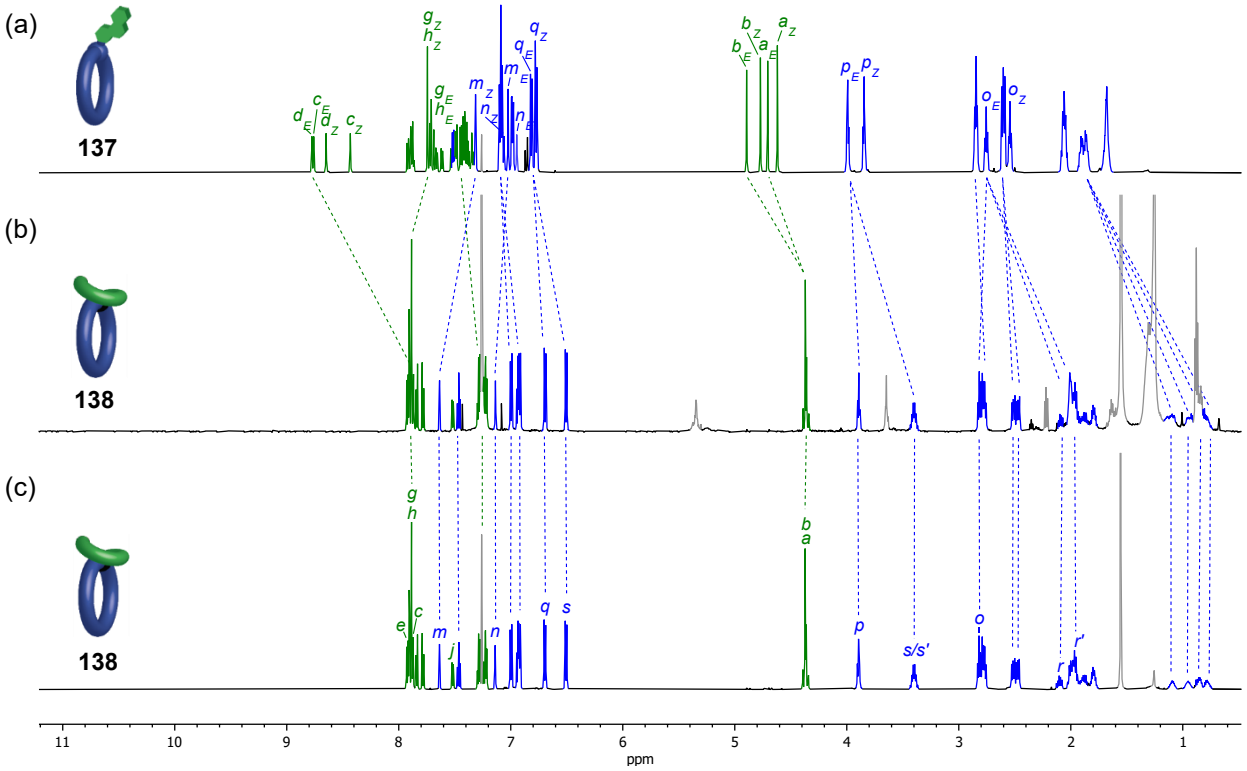

Figure 7.20. Comparison of ^{1}H NMR spectra (600 MHz, $CDCl_3$, 298 K) of (i) authentic standard **137** synthesised by conventional means as a mixture of E–Z isomers in a ratio of 47:53, (ii) isolated [5]helicene **138** from operation of 1-barrier machine **122b** and (iii) 1-barrier authentic standard of [5]helicene **138**. The assignments correspond to the lettering shown in Scheme 7.16.

7.4.2. Two-Barrier Operation and Cyclisation

Nevertheless, with those positive results for the operation in hand, the synthesis of 2-barrier machine **142** has been attempted. Starting from diazide linker **123** the terminal barrier **124b** was introduced via desymmetrisation with copper-mediated click chemistry in the presence of a large excess of diazide linker **123** (4 equivalens) to supress the competing twofold CuAAC reaction. Employing these conditions has led to the formation of the elongated track **141** in a yield of 68%. The obtained tailpiece fragment was subsequently connected with 1-barrier rotaxane synthon **122a** to afford final 2-barrier machine **142** in 84% (Scheme 7.20).

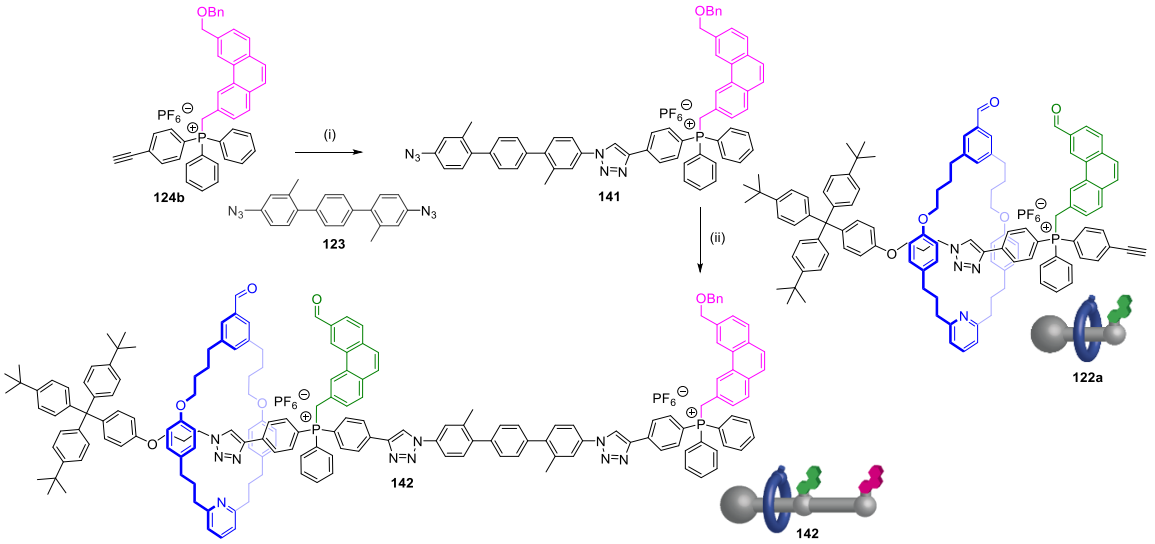

Scheme 7.20. Synthesis of 2-barrier machine **142** via elongation of terminal barrier **124b** with diazide linker **123**. Reaction conditions: (i) TBTA, $[Cu(CH_3CN)_4]PF_6$, CH_2Cl_2:^{t}BuOH, rt, 16 h, 68%. (ii) rotaxane synthon **122a**, TBTA, $[Cu(CH_3CN)_4]PF_6$, CH_2Cl_2:^{t}BuOH, rt, 16 h, 84%.

Machine **142** was then operated with resin bound BEMP according to the conditions described in Scheme 7.21. Initially, in the case where the reaction was performed at high concentration (>50 μM) the incorporation of multiple phenanthrene units has been observed giving rise to a polymeric distribution without retention of the predefined sequence. At higher dilution, however, *inter machina* cross over products diminished and became negligible when re-performing the operation at a final concentration of 2.5 μM (Figure 7.21).

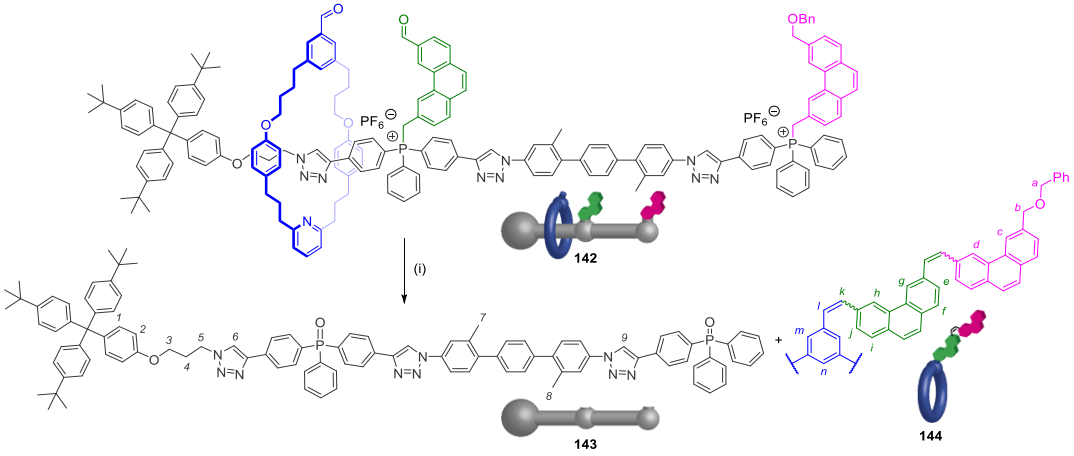

Scheme 7.21. Operation of 2-barrier machine **142**. Reaction conditions: (i) BEMP (40.0 equiv.), CH_2Cl_2, –78 °C to rt, 16 h, 24% (stilbene product **144**) and 66% (free thread **143**).

And fortunately, when analysing the reaction mixture from the operation with mass spectrometry the desired 2-barrier product **144** has been observed (Figure 7.21 (a)). In addition, however, major peaks related to first, the loss of the first barrier due to hydrolysis prior to the reaction with aldehyde macrocycle (m/z 856) and second, pick up of only the first barrier and then slipping of the machine due to hydrolysis of the second barrier (m/z 764) as well as unreacted aldehyde macrocycle **75** (m/z 562) were noted.

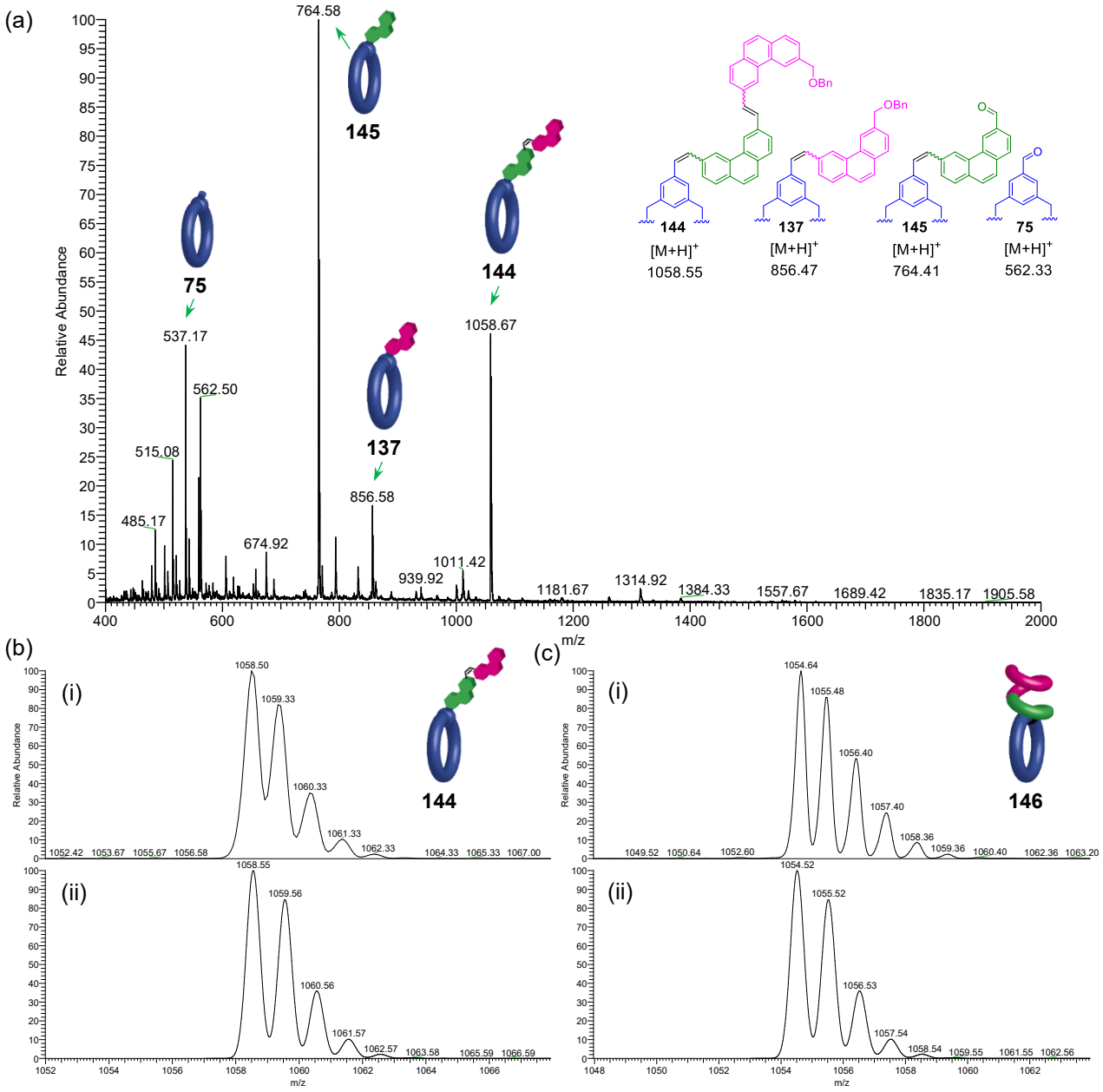

Figure 7.21. Operation of 2-barrier machine **142** and cyclisation of product **144**. (a) Observed crude operation products **75**, **137**, **144** and **145** by LR(ESI)-(+)-MS from the operation of 2-barriermachine **142**. The peak at m/z 1058 correlates to [**144**+H]$^+$; The most intense peak (m/z 764, [**145**+H]$^+$) corresponds to pick up of only the first barrier and the minor peak at m/z 856 ([**137**+H]$^+$) corresponds to the loss of the first barrier. The peak at m/z 562 correlates to macrocycle [**75**+H]$^+$. (b) (i) Observed and (ii) predicted (bottom) LR(ESI)-(+)-MS of product of operation **144** recorded from the crude operation mixture. The predicted isotope pattern is for $[C_{77}H_{71}NO_3H]^+$ corresponding to [**144**+H]$^+$. (c) (i) Observed and (ii) predicted (bottom) LR(ESI)-(+)-MS of product of cyclisation **146** recorded from the crude operation mixture. The predicted isotope pattern is for $[C_{77}H_{67}NO_3H]^+$ corresponding to [**146**+H]$^+$.

Based on this result it was concluded that the desired 2-barrier barrier product **144** was formed. A more detailed analysis of the crude reaction with ^{1}H NMR spectroscopy and quantification of separate components by integration has shown that it is generated as one of the major products of operation. As shown in Figure 7.22 aldehyde side-products **145** (iv; for its structure, see Figure 7.21 (d)) and macrocycle **75** (v) stemming from loss of the first and second barrier due to hydrolysis are minor compared to the actual 2-barrier product **144** (i) from the operation. Determining the relative value by integration a ratio of 64:26:9:1 for the free thread

143, isolated product (*Z,Z)*-**144**, aldehyde stilbene **145** and aldehyde macrocycle **75** has been found. This finding also corresponds well with the obtained isolated yields for the free thread **143** (66%) and isolated product (*Z,Z)*-**144**. (24%) Unfortunately, the immediate comparison does not include 1-barrier product **137** due to lack of a well-separated diagnostic peak in the crude reaction with ^{1}H NMR.

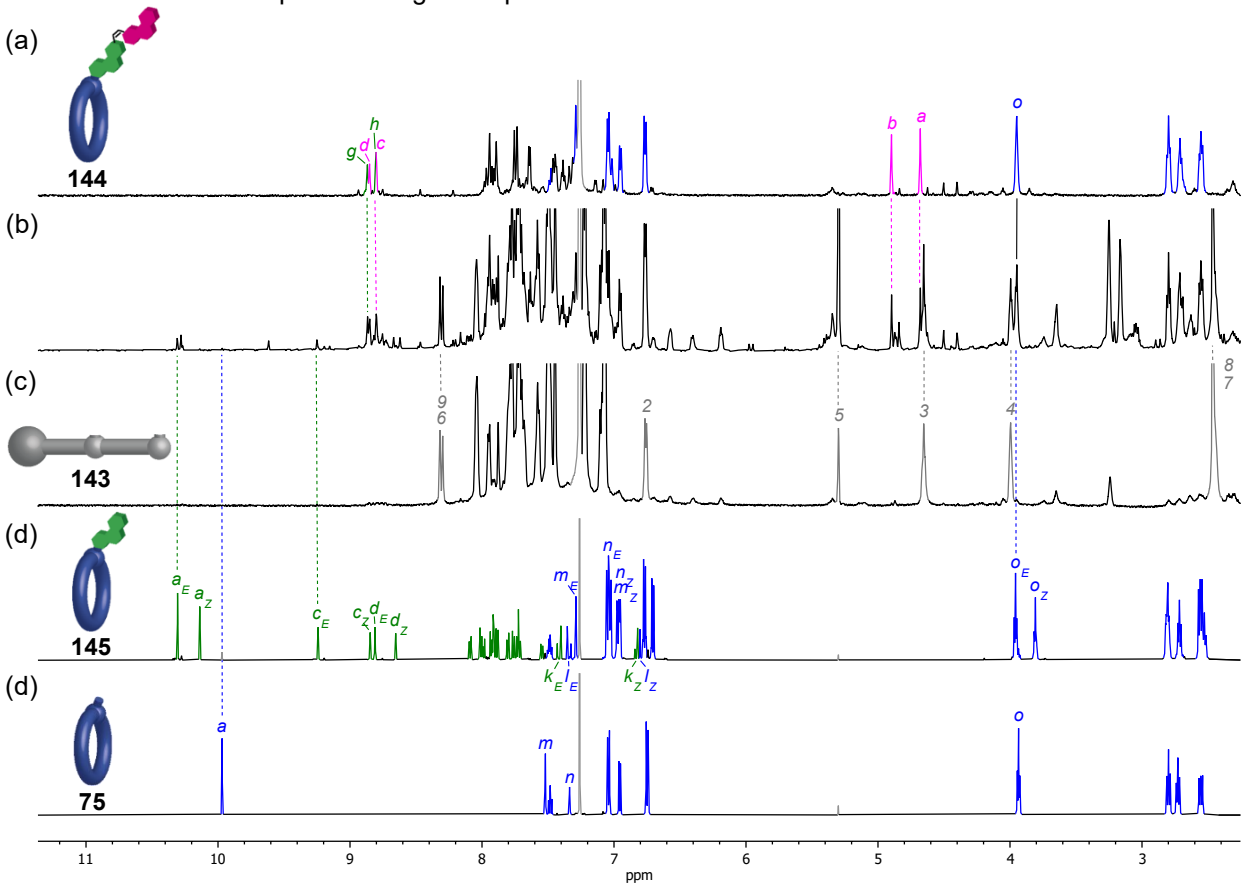

Figure 7.22. Partial ^{1}H NMR spectra (600 MHz, $CDCl_3$, 298 K) of (a) the product of 2-barrier operation (*Z,Z*)-**144** after isolation, (b) crude reaction mixture after 48 h, (c) Isolated thread **143**, (d) aldehyde stilbene **145** prepared by conventional methods as a mixture of *E*–*Z* isomers in a ratio of 55:45 and (e) aldehyde macrocycle **75**. In the crude reaction, the free thread **143** ($H_{6,9}$) isolated product (Z,Z)-**145**, (H_b) aldehyde stilbene **145** (H_{aE}) and aldehyde macrocycle **75** (H_a) approx. take a ratio of 64:26:9:1 as determined by weighted integration of characteristic peaks in brackets. The assignments correspond to the lettering shown in Scheme 7.18 and Scheme 7.21.

Furthermore, in contrast to the originally reported system[125] where the high stereoselectivity is only observed for the reaction with the first barrier, then drops to a ratio of *E:Z* = 55:45 for subsequent iterations; a reverse in stereoselectivity was conferred into the product for the reaction with two barriers, with the major product observed as an 80:20 mixture of two isomers. The identity of the major isomer was ascertained by comparison to a standard prepared by conventional means (Scheme 7.22). The standard **144** was itself isolated as an approximately equal mixture of four isomers, which upon irradiation with light, photoisomerised to the *cis-cis* configuration (see Figure 7.22 (i) and (ii)).[287]

Comparison of this product to the compound isolated from the operation, confirmed that machine **142** produced stilbene **144** as an enriched (*Z,Z)*-isomer. This difference in selectivity between 1- and 2-barrier machine operation has been attributed to the rigidity of the highly conjugated oligomer (compared to the bisphenol A oligomer previously reported)[125] translating the stereoselectivity afforded by the mechanical bond. While the reaction at the first barrier preferentially yields an *E*-isomer the reaction at the second barrier

in 2-barrier machine **142** appears to confer the opposite handedness. Furthermore, presence of the *E*-isomer of aldehyde stilbene intermediate **145** as detected by ^{1}H NMR spectroscopy (Figure 7.22 (ii)) suggests that the Wittig reaction at the second barrier becomes slow if initially the *E*-isomer of the aldehyde intermediate **145** is formed and thus is taken over by hydrolysis of the second barrier. Taken these two observations together it seems that only if the two sequential Wittig reactions are *cis*-selective the desired 2-barrier product **144** can successfully be obtained when competing with hydrolysis of ylide barriers. Isolation of a second isomer from the operation of machine **142** of unknown stereoselectivity in small quantities further supports this argument and maybe seen as a measure of residual moisture or other nucleophiles present during the reaction at high dilution.[174] The obtained yield of 26% for the two isomers of **144** from the operation of 2-barrier machine **142** also agrees well the expected statistical value for the distribution of four possible isomers when under first approximation stereoisomers form in equal ratio.

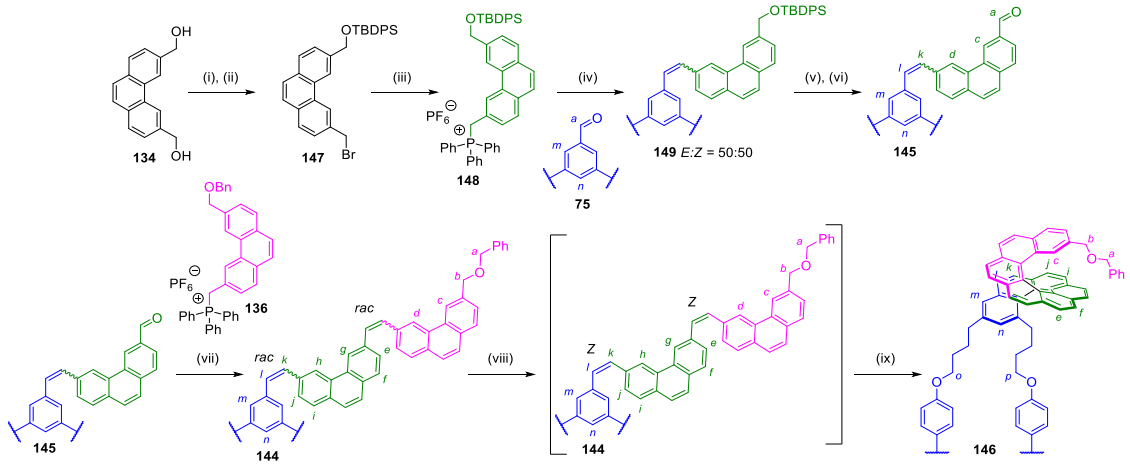

Scheme 7.22. Synthesis of 2-barrier operation standards for stilbene **144** and [9]helicene **146** by conventional methods. Reaction conditions: (i) TBDPSCl, ^{i}Pr$_2$Net, DMF, rt, 16 h, 54%. (ii) CBr$_4$, PPh$_3$, CH$_2$Cl$_2$, 0 °C, 30 min, 62%. (iii) PPh$_3$, PhMe, 120 °C, 16 h, then KPF$_6$, THF, rt, 30 min, 65% over two steps. (iv) macrocycle **75**, BEMP, CH$_2$Cl$_2$, –78 °C to rt, 6 h, 94%. (v) TBAF, THF, rt, 50 min, 91%. (vi) DMP, CH$_2$Cl$_2$, 0 °C, 80 min, 97%. (vii) phosphonium salt **136**, BEMP, CH$_2$Cl$_2$, –78 °C to rt, 3 h, 83%. (viii) hv (365 nm), CD$_2$Cl$_2$, rt, 15 min, 51%. (iv) hv (365 nm), I$_2$ (2.2 equiv.), propylene oxide (50.0 equiv.), PhMe, rt, 182 h, 10%.

Continuing with the helicene transformation, the isolated stilbene oligomer **144** was submitted to the same photocyclization conditions as initially developed for 1-barrier machine **122b**. After irradiation at 365 nm for 182 h, [9]helicene **146** was isolated in 10% yield after repeated purification by a combination of preparatory TLC and size exclusion chromatography. As it has turned out, the main limitation for the output of the reaction represents the low solubility of intermediate cyclisation species under acidic conditions: Collecting the reoccurring precipitate during the reaction, dissolving the material in deuterated DMSO and analysing the product with ^{1}H NMR it was suggested that protonation of the pyridine group was most likely the cause for the undesired precipitation of intermediates. Although this undesirable effect has considerably reduced the amount of helicene product, nevertheless it was possible to obtain enough material to confirm its identity and characterise the generated structure in detail with ^{1}H NMR and mass spectrometry.

Like the [5]helicene product **138** substantial desymmetrisation and diastereotopic splitting have been observed for [9]helicene. The majority of the protons of the upper part of the macrocycle, in particular those protons, that sit directly above and below the aromatic system of the helicene, experience significant shielding whose shifts exceed those measured for the smaller system **138**. For example, protons H$_p$

experience an even more significant upfield shift of approximately 0.7 ppm in relation to H_o; likewise, protons H_b split into a diastereotopic pair that are separated by about 0.5 ppm due to the high chiral expression imposed by the helicene.

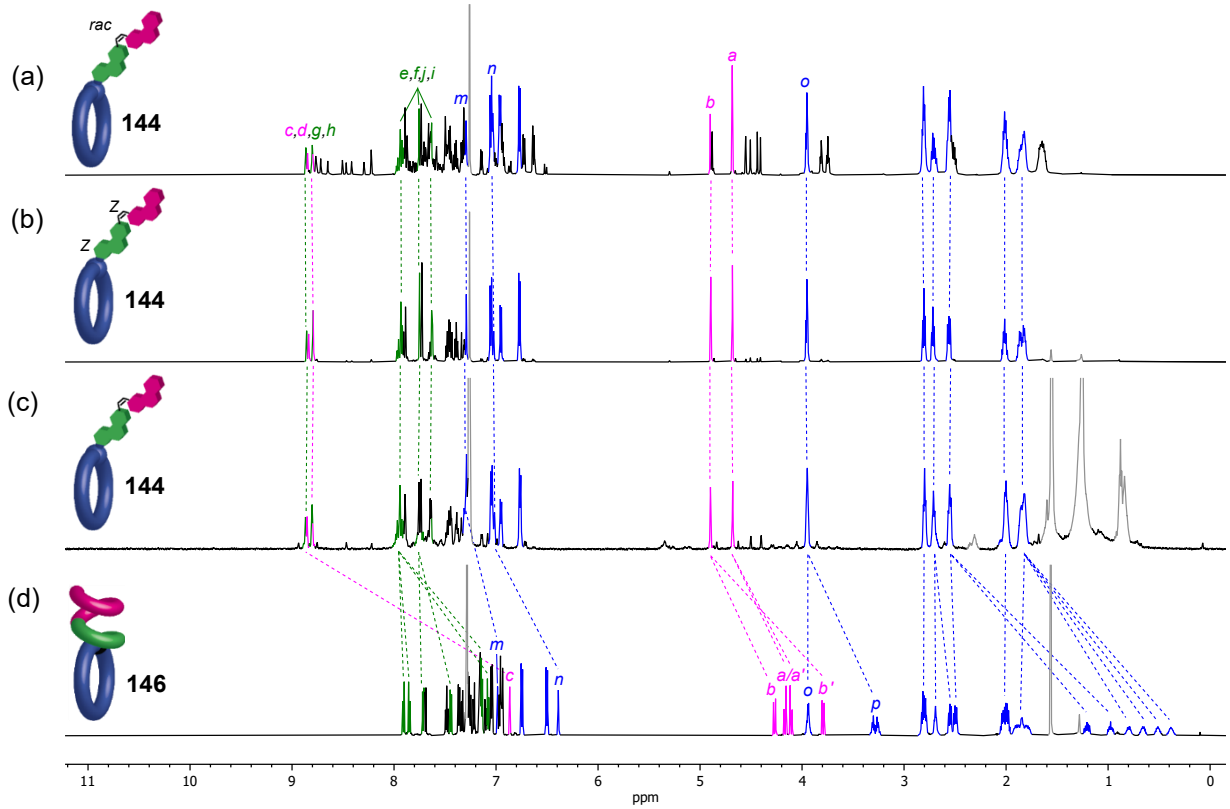

Figure 7.23. ^{1}H NMR spectra (600 MHz, $CDCl_3$, 298 K) of (a) **144** synthesised by sequentially as a mixture of four isomers, (b) above after irradiation at 365 nm for 15 minutes, (c) **144** isolated from operation of 2-barrier machine **142** and (d) [9]helicene **146**. The assignments correspond to the lettering in Scheme 7.22.

The one-pot operation of 2-barrier machine **142** was also attempted, where the intermediate stilbene **144** was submitted to the same conditions as for **137** in toluene with additional iodine and propylene oxide. Unfortunately, the photoisomerization of the crude mixture was unsuccessful; No conversion to desired helicene **146** was seen even after prolonged exposure and using different wavelengths (365, 320, 280, 265 nm or using a xenon-lamp, with and without air present) and despite the absence of a significant absorption of conjugated phosphine oxide track **143** in the spectroscopic region. (Figure 7.24) Any attempts to characterise the structure of [9]helicene **146** via single-crystal X-ray diffraction have remained unsuccessful.

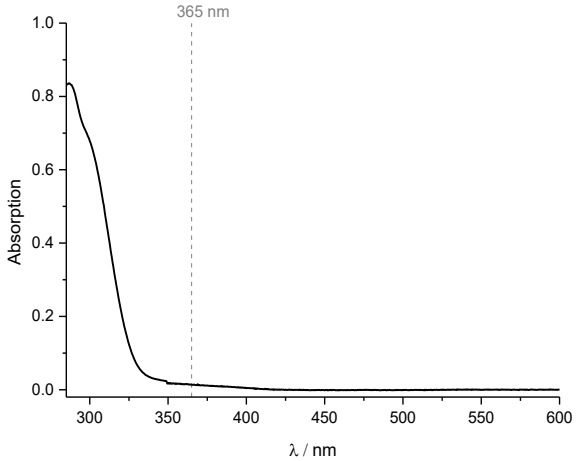

Figure 7.24. UV-vis absorption spectra (toluene, rt) of isolated 2-barrier thread **143** with an absorption value of 0.014 at 365 nm.

7.5. Conclusion and Outlook

In summary, with these investigations both the synthesis and operation of a 1- and 2-barrier machine have been demonstrated successfully. Furthermore, conversion of the isolated stilbene product via subsequent cyclisation has allowed the isolation and characterisation of [5]- and [9]helicene products **138** and **146** (see for example, Figure 7.25). In the former case, an operation procedure was established that has enabled to perform the two consecutive reactions in a single step. The additional functional behaviour represents an improvement over previous operation of a molecular machine capable of forming stilbene sequences[125] and mimics the pathway of nature to synthesise for example proteinogenic structures with a well-defined shape that in a sophisticated way can give rise for complex catalytic opportunities.

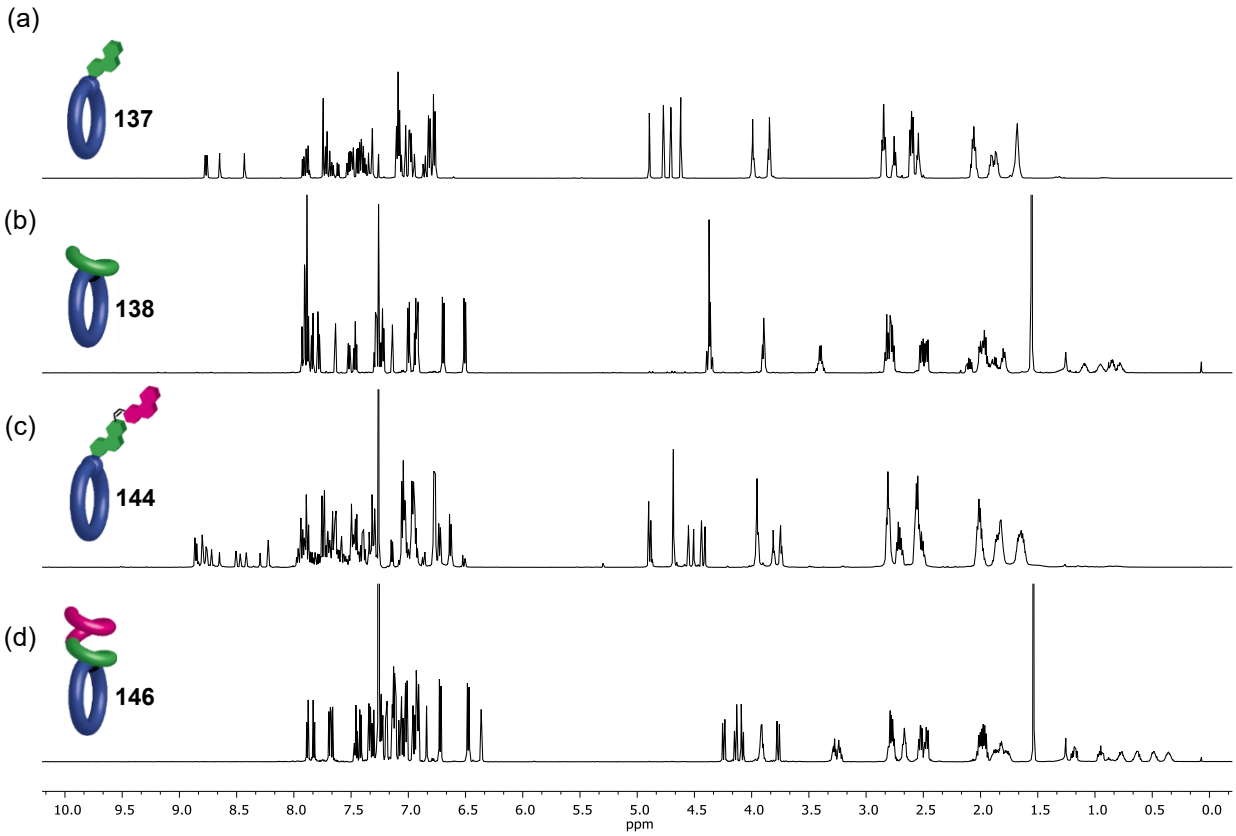

Figure 7.25. ^{1}H NMR (600 MHz, $CDCl_3$) stack plot comparison of (a) 1-barrier operation standard **137** (E/Z mixture), (b) [5]helicene **138**, (c) 2-barrier operation standard **144** (mixture of four isomers) and (d) [9]helicene **146**.

The unique stereo control noticed for the formation of 1- and 2-barrier stilbene sequences provides a first hint at the reaction mechanisms during the operation of the presented molecular machines. Based on the observations it appears that the mechanical bond strongly influences the reactivity with different intermediate alkene isomers presumably as a result from rigidity of the phenanthrene motive to such an extent that it favours a single diastereomer. While this gives rise to interesting synthetic behaviour, specifically, a reverse selectivity from predominately (*E*)- to (*Z,Z*)-isomer accompanied with the transition from a 1-barrier to a 2-barrier machine, concomitantly formed unfavourable intermediate isomers are lost when competing with observed hydrolysis of reactive phosphor ylide barriers during operation.

This effect has proofed to be a major limitation for extending the presented operation concept beyond the operation of a 2-barrier machine. Results from preliminary operations of 3-barrier machine suggested that

the substitution of the phenanthrene motive with this machine design has an inherently minor effect on the potential outcome of the operation.[178-179] Due to the positive results obtained from operating a 4-barrier machine with the original design using a bisphenol A motive[125] it seems that the reduced flexibility introduced with the polyaromatic substrate may act as a hinderance for obtaining a high-yielding reaction. An improved design such as **150** depicted in Scheme 7.23 may therefore incorporate a preformed stilbene, just a naphthalene motive or, alternatively, a more flexible chemical spacer unit or macrocycle to promote the reaction with intermediate barriers, likely, at the expense of stereo control. Furthermore, susceptibility of the barriers towards hydrolysis may be reduced by stabilisation of intermediate phosphorous ylide with a suitable substitution of the phosphonium track. (for example, with an electron-withdrawing CF_3 group at position R^1 marked in Scheme 7.23). All in all, this clearly demonstrates the exceptional balance that nature has achieved with ribosomal peptide translation allowing the formation of large polymeric sequences efficiently and with unmatched error rate. It highlights that ultimate sequence control can be achieved if the machine is adapted towards a defined set of substrates.[144]

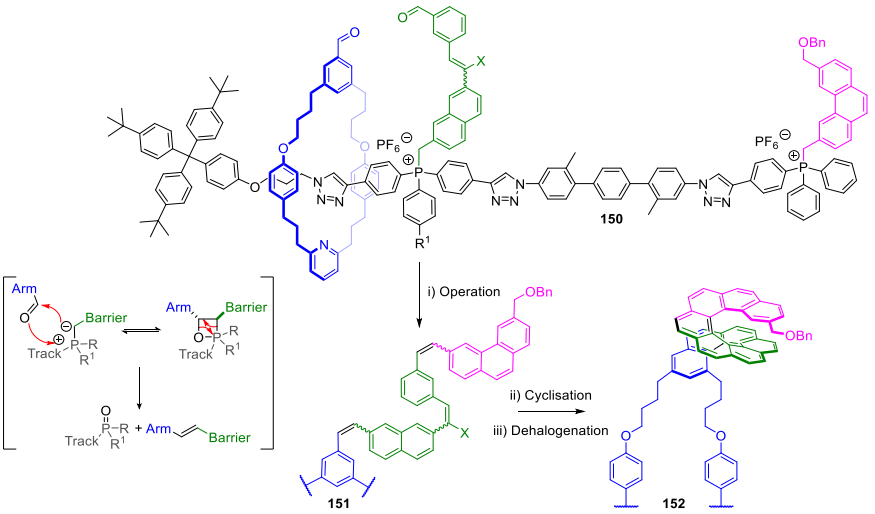

Scheme 7.23. Proposed operation of an improved 2-barrier molecular machine **150** anticipated furnishing final helicene product **152** through cyclisation of stilbene sequence **151**.

With regards to the second transformation step it also remains interesting to ask whether an alternative substitution pattern of the phenanthrene motive or the use of, for example, a suitable "bromine auxiliary"[164f,175] (at position X = Br in Scheme 7.23) may further increase the yield for the helicene formation. Solubility issues experienced with the pyridine containing macrocycle under the acidic conditions of the cyclisation may be avoided either by using alternative reported conditions for the helicene formation[176] or for example methylation of the pyridine functionality prior to the photoisomerization. Careful control over the conditions of the performed Mallory photocyclization may be further beneficial for the formation of helicenes, as well.[177] In light of the published examples application of the helicene product for a catalytic transformation appears possible, too.[164e]

Overall, the results from this study may provide an additional stimulus to continue to take inspiration form nature and to develop a better understanding of what can be achieved by small molecule synthesising molecular machines. The current example has confirmed their potential to construct molecules in sequence-controlled manner via iterative carbon-carbon bond formation with Wittig type chemistry.

8. Unidirectional Linear Transport with a Fluorescence Read Out

The following work as summarised in Figure 8.1 was performed together with the help of Marcel Dommaschk, Salma Kassem, and Daniel J. Tetlow. The synthesis and analysis of the operation were performed by B. Groh. This was complemented by the provison of substances for an initial machine design synthesised by M. Dommaschk and S. Kassem and highlighted at relevant parts in the following. Optical studies were conducted by B. Groh and M. Dommaschk. It is based on the idea developed by D. A. Leigh, D. J. Tetlow and B. Groh. The project was supervised by M. Dommaschk and D. J. Tetlow.

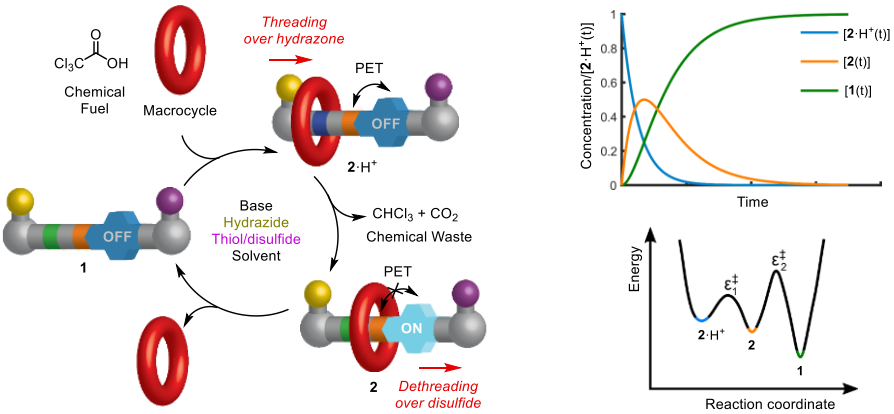

Figure 8.1. Proposed pyrene-based rotaxane pump **2**/**2**·**H**$^+$ and its operation with 27C9.

8.1. Background

8.1.1. Unidirectional Molecular Transport by Membrane Proteins

Because of the compartmentalised structure of life selective material transport across the cell membrane constitutes an indispensable activity for all biological organisms.[8] It takes on a critical role for enabling, sustaining, and protecting the key structural and functional organisation of cells and gives rise to a rich framework of substrate, energy, and information handling mechanisms.[180] It provides the foundation for powering all mechanical or chemical tasks via dissipative nonequilibrium processes.[5,8] This is achieved by maintaining and balancing a range of chemical and redox gradients across membrane by actively pumping components from one side of the cell's boundary to the other against the thermodynamic equilibrium.[180]

This critical task is performed by the actions of macromolecular assemblies in form of large, specialised transmembrane proteins.[8] Located at the periphery and bridging the lipid bilayer barrier between two compartments these proteins can act as gate keepers that upon a suitable stimuli, actively control the movement and/or direction of a specific type of particles (Figure 8.2). Members of this class of machines have shown to accomplish, for example, selective and directional ion[181] and substrate transport[192d] but also advanced signalling processes[284] e.g., in form of G protein-coupled receptor kinases.[285]

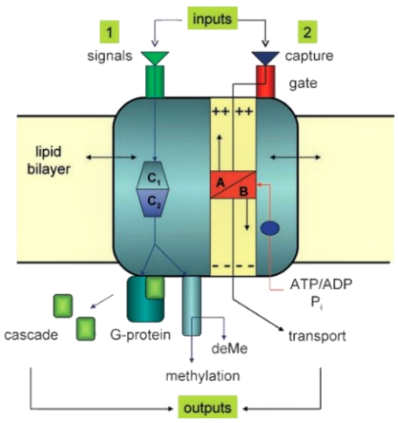

Figure 8.2. General scheme depicting the operation of integral membrane proteins in cellular cognition. (1) Receptor-mediated information flow (signal transduction cascades). Extracellular binding of hormones and chemo sensors produces conformational rearrangements (C1, C2) in the receptor that result in activation of intracellular processes. (2) Transport-mediated information flow. Selected ions and molecules are bound close to the extracellular side depending on charge, size, and polarity, and transmission is activated by gated responses determined by proton gradients, electrochemical potentials, auxiliary ligand binding, or photoinduced conformational changes. Reprinted by permission from John Wiley and Sons: reference 8, Copyright 2008.

Ion Transport

One of the central aspects for biochemical transport processes is mediating and regulating the flux of ions across the membrane. In fact, this represents one of the essential tasks of the biological machinery.[181a] To first and foremost overcome the physical separation and facilitate movement of charged entities across non-polar lipid bilayers, Nature has evolved different classes of ion transporter proteins that make their appearance as globular objects at the cell boundary (Figure 8.3).[8,181a] First, ion channels that employ a single gate mechanism function. They were found to act as passive, ion-specific bidirectional transporter authorities. When actuated with an appropriate stimulus, this group of proteins can either permit or prevent collective movement of ions in direction of an existing electrochemical gradient through a well-defined membrane aperture (Figure 8.3 (a)).[181b] It has been concluded that ion channels effectively catalyse the removal of a gradient in response to a molecular signal on the cellular level at a "very high conduction rate" close to diffusion limit.[181a] Notable examples of this machinery are highly selective and widely preserved structures of potassium channels[182] or different types of CLC chloride channels.[183]

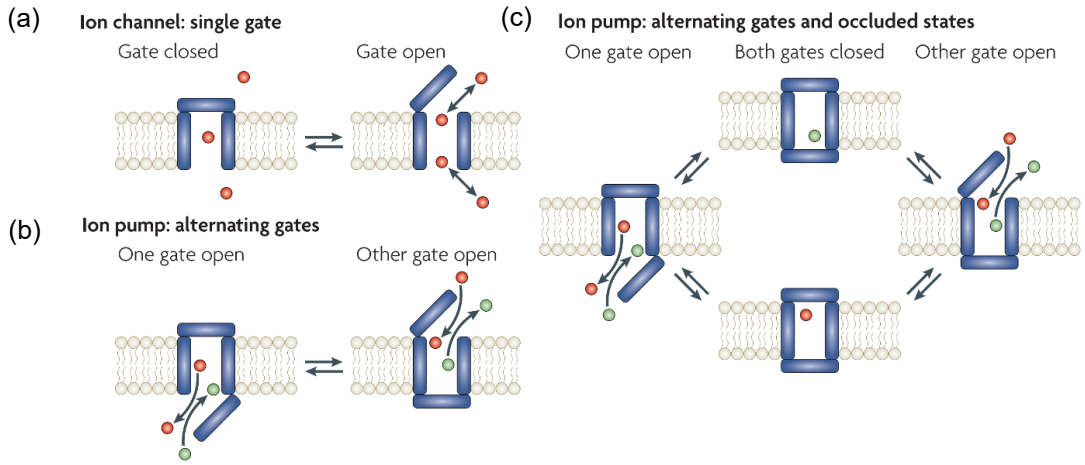

Figure 8.3. Ion channels versus ion pumps, in principle. (a) Schematic representation of an ion channel as a membrane-spanning pore through which ion (red spheres) movement is controlled by a single gate, represented by a hinged door. (b) Ion pump as a membrane-spanning pore with two gates that open and close alternately. Coupling of an energy source to switch the relative binding affinity for red versus green ions between the left- and right-hand states enables active exchange of red for green ions across the membrane. (c) Occluded states, with both gates closed around bound ions, preclude inadvertent opening of the second gate before closure of the first gate, which would allow ions to flow down their electrochemical potential gradient several orders of magnitude faster than the pump can move them against that gradient. Pumped ion movement is rate limited by the gating reactions, rather than by electro diffusion. Adapted by permission from Springer Nature: reference 181b, Copyright 2009.

Secondly, transporter proteins termed molecular pumps that are driven by a dissipative process such as ATP hydrolysis. Those proteins actively transport cargos in a unidirectional manner against a present gradient from side to another.[181b] They coordinate the energetic uphill transport via alternate opening and closing of two separate gates that vividly, can be described as either a pump or an exchange activity (Figure 8.3 (b) and (c)). To further differentiate between the energy form applied members of this class of proteins are further distinguished between primary or secondary transporters. In the former case, the chemical fuel ATP is harnessed to establish an increase or decrease in intracellular ion concentration, whereas in the latter case, an already established (ion) gradient is utilised as a potential to carry out another transport process either in the same (Sym-) or opposite (Antiporter) direction.[184] For instance, in the case of excitatory neurotransmission, a sodium gradient acts as intermediary for the thermodynamically unfavourable transmembrane glutamate intake and maintaining this imbalance is critical for the communication between cells.[187] Other examples of common ions involved in the operation of secondary pumps, are abundant alkali metal potassium ions, alkaline earth metal calcium ions or anionic chloride atoms.[181a] Similar to the operation of a classical pump, it is the overall rate of the mutually exclusive gate opening and closing events that determines the efficacy of a pump and its ability to generate an effective ion current. In many cases molecular pumps exhibit around hundred “gating reactions” per second, which is less than a comparable passive transport through ion channels but sufficient to maintain a vitally important nonequilibrium state.[181b]

ATPases

Members of the ATPase family are multiprotein assemblies that are involved in the active transport of protons H^+ across the membrane.[24b] On part of this group, so-called F-type ATP synthases, are able to harness an existing H^+ gradient for the synthesis of ATP from ADP and inorganic phosphate P_i, whereas other members,

so-called vacuolar (V-type) ATPases operate in reverse and allow regulating the intramolecular pH by actively maintaining a H^+ gradient with available ATP. Bacterial F-type and V-type ATPases are known or at least suspected to operate both pathways in a bifunctional manner depending on the conditions. Regardless of the function, ATPases share the same principal design that links the rotary motion of an intracellular V_1/F_1 domain with the movement of an integral V_0/F_0 domain translated through a central connecting axis D/γ and several peripheral stalks (Figure 8.4). In every case, the rotary domain V_1/F_1 comprises three ATP binding sites whereas membrane bound V_0/F_0 domain functions as translocation part for the proton transport.

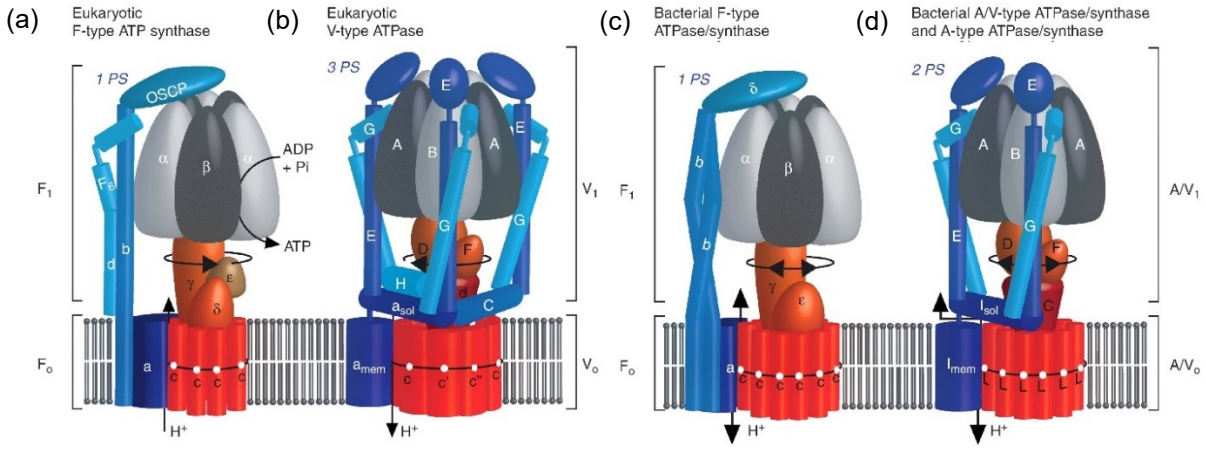

Figure 8.4. Schematic diagrams of rotary ATPase subtypes and their major subunits. (a) Eukaryotic mitochondrial F-type ATP synthase (containing one peripheral stalk, PS) synthesizes ATP using energy derived from a transmembrane proton gradient generated by respiration. (b) Eukaryotic V-type ATPases (containing three PS) are situated in intracellular membranes using energy from ATP hydrolysis to pump protons across membranes. (c) Bacterial F-type ATPases/synthases (containing one PS) synthesize ATP but can revert and act as proton pumps if ATP levels are high. (d) Bacterial V-type and archaeal A-type ATPases share the same architecture and contain two peripheral stalks. Like bacterial F-type ATPases they are believed to be bi-functional. Nucleotide binding subunits are shown in greys, other stator subunits in blues, rotor subunits in reds and protons as white spheres. Reprinted from reference 24b, Copyright 2014, with permission from Elsevier.

While the number and structure of individual components differs depending on the cell type, the primary function and gives rise to distinct specialised subtypes (Figure 8.4), the basic working principles of ATPases are preserved (Figure 8.5).[24b] Mechanistically, it has been found that the root cause of directional rotary motion can be attributed to the unidirectional flow of protons either to the inside (F-type), outside (V-type) or in alternate directions (A/V-type) through two offset ports of a membrane bound stator subunit a (see Figure 8.4).[188] On the interface of these ports sits a membrane bound cylindric proteolipid assembly of subunits *c* that on the peripheral carries negatively charged carboxy groups of glutamate residues (Figure 8.5 (a)).[24b,189] Once protonated at the entry position, this allows the proteolipid unit to move one segment further towards the inside of the lipid bilayer and reveals another free (charged) carboxy group (Figure 8.5 (b-c)). When reaching the exit port, conveyed protons can dissociate from the holding carboxylate arm to the opposite site of the lumen facilitated by additional interactions arginine residues (Figure 8.5 (d)). The resultant rotation achieved with this general conveyor belt-like mechanism, in turn, is transferred to the moving of the top V_1/F_1 domain which in case of ATP synthase applies the torque to affect the thermodynamically unfavourable synthesis of ATP from ADP through mechanochemical coupling.[24a,188,190] In contrast, catalytic hydrolysis of ATP with V-type ATPases generates a torque which is conferred into the movement of the proteolipid unit and thereby permits the opposite translocation of protons against a present gradient.[191]

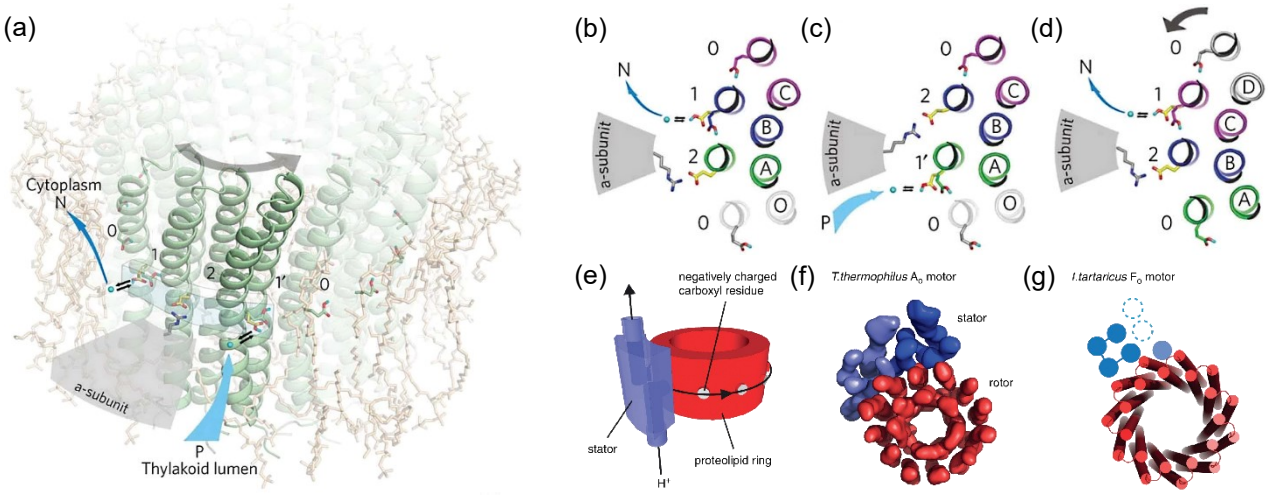

Figure 8.5. Illustration of proton translocation and coupled rotation in the F_o complex from S. platensis. (a) Schematic picture of the different states taken by the binding sites (0-1-2-1′-0), as the c-subunits (green) face the lipid membrane or the hydrated interface (blue) of the a-subunit (gray). The view of the interface is tilted from the membrane plane 20° toward the reader. (b-d) Specific sequence of steps in the proposed mechanism; these are (b) opening and deprotonation; (c) rearrangement of Glu-Arg ion pair and re-protonation; (d) rotation. The c-subunits are shown from the cytoplasmic side at the level of the ion-binding sites. Subunit a is depicted as gray sector, highlighting the conserved arginine. The direction of the rotation in the figure is that in the ATP synthesis mode, but the model is evidently reversible. Adapted by permission from Springer Nature: reference 189, Copyright 2010. The R_0 motor and models for the generation of rotation, with the proteolipid ring in red and the R_0 stator subunit in blue. (e) Schematic model of the 'two half-channels' hypothesis. (f) A_0 portion of the T. thermophilus bacterial A/V-type ATPase/synthase, with the R_0 stator subunit four helix bundles shown in light and dark blue. (g) Schematic model of the F_0 motor 2D EM density. Adapted from reference 24b, Copyright 2014, with permission from Elsevier.

ATP-Binding Cassette Transporters

Further to ion transport, an alternative example for actively moving general substrates across the cell boundary instead is given by the superfamily of ATP-binding cassette (ABC) transporter proteins.[192] ABC proteins generally comprise a pair of transmembrane domains (TMDs) whose conformation is controlled by the binding of ATP to attached intracellular peripheral nucleotide-binding domains (NBD).[192d] They facilitate unidirectional transport of specific cargo(s) either to the outside or inside through the adaption of an alternating inward- and outward-facing conformation (Figure 8.6).[193] Distinct members of the family can be categorised into different classes of subfamilies depending on the structure and related mechanisms, the substrate involved and, its transport direction (importers and exporters), but also in respect of their evolutionary origin.[193-194] In most cases, the working of ABC transporters further depends on separate extracellular substrate-specific binding proteins (BPs) that "bind their substrate with high affinity, in the range of 0.01 to 1 μM" and preliminary binding protein dependent (BDP). The wrapping of the substrate has shown critical for initiation the active transport process.[192b] For example, type I ABC transporters are known to promote taking in small molecules such as organic and inorganic ions, carbohydrates and amino acids and their oligomers (Figure 8.6 (a)).[192] In the case of maltose transport by bacteria, this necessitates the presence of a periplasmic maltose-binding protein (MBP).[195] In addition, type II analogues allow importing larger hydrophobic targets such as iron containing siderophores, haem or vitamin B_{12}[196] via an additional contraction step in the sequence of conformational changes to enable substrate transport (Figure 8.6 (b)).[192d]

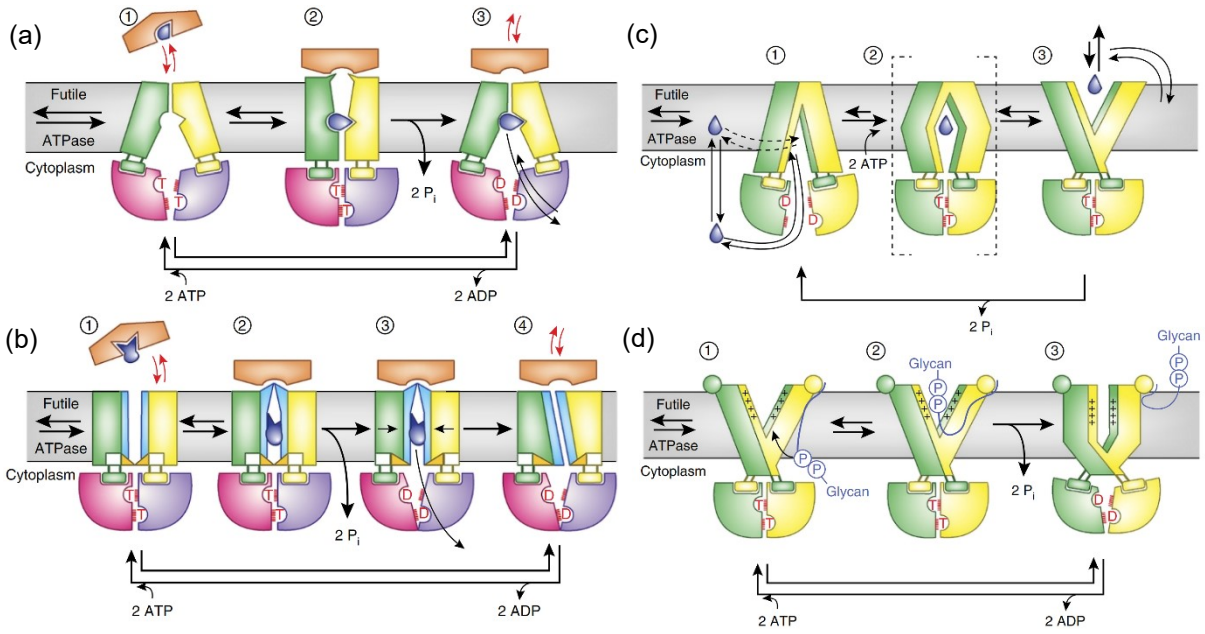

Figure 8.6. Illustration of the different types of ATP-binding cassette transport mechanisms. (Left side) Distinct mechanisms of type I and type II ABC importers. Green and yellow, TMDs; pink and purple, NBDs; orange, binding proteins; dark blue, substrates; T, ATP; D, ADP. Dashed red lines in the NBDs depict the ABC signature motifs. Circled numbers denote states. (a) Schematic of a type I importer mechanism. (b) Schematic of a type II importer containing three distinct gates. The blue lines in the TMDs represent TM5, which forms cyto gate 1, and the peri gate. The orange triangles represent cyto gate 2, which is formed by the loop between TM2 and TM3. Small arrows in the TMDs of state 3 indicate forces acting on the translocation pathway and entrapped substrate. (Right side) Distinct mechanisms of B-family ABC exporters. Green and yellow, half-transporters; T, ATP; D, ADP. Dotted red lines in the NBDs depict the ABC signature motifs. Circled numbers denote states. In outward-open conformations, the TMDs of the transporters form two wings toward the external side of the membrane. Each wing contains two TM helices from one TMD and four TM helices from the other. (c) Alternating access proposed for multidrug or peptide transporters. (d) Outward-only mechanism with substrate loading directly into the outward-facing cavity, as proposed for the LLO flippase PglK. P_i, inorganic phosphate. Adapted by permission from Springer Nature: reference 192d, Copyright 2016.

Separate to this, BP-independent ABC transporters (B-type) facilitate direct translocation of substrates in response to substrate binding promoted by the hydrolysis of ATP (Figure 8.6 (c) and (d)). While their principal mechanisms remain subject to continuing research[192d] several representatives have been identified that for instance, enable translation of phosphorylated membrane lipids,[197] the export of peptide sequences in connecting with antigen processing,[198] heavy metals, such as mercury[199] and other substrates,[200] and the vital import of nickel and cobalt.[201]

8.1.2. Rotaxane-Based Unidirectional Linear Molecular Transport

Ensuing from the increasing knowledge of biological systems, simultaneously, several attempts have been made to imitate the natural membrane transport behaviour with synthetic methods.[202-203] On the one hand, examples of the bidirectional passive transport of cells' ion channels have provided a stimulus for the design of a plethora of artificial supramolecular systems[202] that in a simplified form control the release of cargos with suitable stimuli.[204] One the other hand, the active unidirectional linear transport as displayed by molecular pumps[18] has provided a source of inspiration for the creation of artificial counterparts.[31,38e,205] It has been

recognised that in particular mechanically interlocked structures in the form of rotaxanes and catenanes[92,206] lend themselves as a suitable target for the proof-of-principle studies.[38e] Based on the concepts of switchable molecular shuttles[92,207] as a framework for creating molecular ratchets[40,78,105] (for an example of an energy ratchet mechanism, see Figure 8.7) a variety of systems have been proposed that featured unidirectional linear transport of macrocyclic substrates.

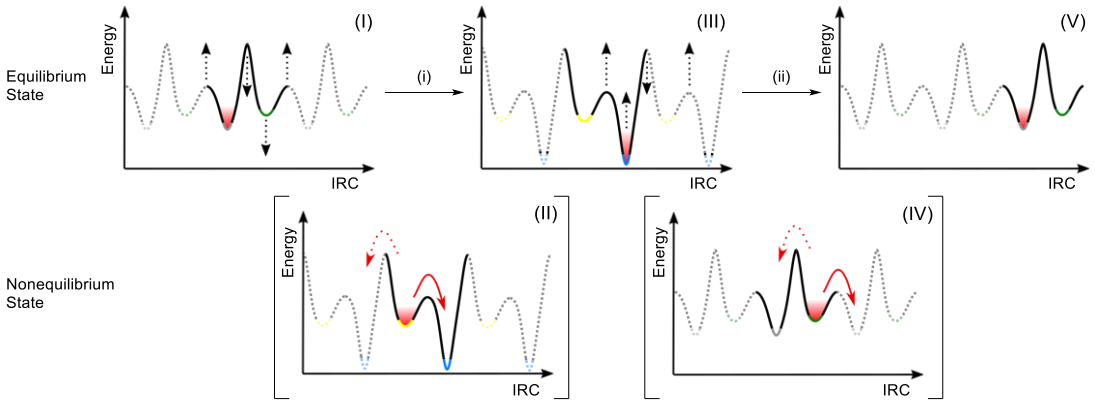

Figure 8.7. Illustration of an energy ratchet mechanism for the unidirectional transport of a population i.e., a particle (red) from one state (**A**) to another (**A'**) through intermediate **B** via temporal modulation of the underlying potential energy surface (PES). PESs and concentration profiles for the transport. (i) Raising the energy minima while lowering the adjacent maxima and minima of state **A** (grey) at t_0 creates nonequilibrium state **A*** (yellow, t_1) which (ii) after thermal relaxation results in the formation of intermediate **B** (blue) at t_2. Following (iii) second modulation of the PES then triggers (iv) the movement of the population from disturbed state **B*** (green, t_3) to final equilibrium state **A'** (grey) at t_4. By continuously actively varying the relative heights of the energy barriers and minima of the energy wells, populations can be transported directionally. Their motion may be monitored through measuring equilibrium states **A**/**A'** and **B** with suitable methods.

To date, several principal chemical frameworks have been developed that have demonstrated molecular transport processes in the form of macrocycle movement across the linear axle of rotaxanes in a repetitive, progressive[208-210] but also dissipative manner.[211-213]

Conceptually, those molecular systems rely either on, for example, replicating the biological gating reaction[181b] by actively controlling the threading, shuttling and dethreading of a macrocycle with alternative energy ratchet mechanisms (Figure 8.7).[31, 40,214] Through modulation of a set of energy barriers with chemical and optical methods under nonequilibrium conditions these systems have achieved molecular transport phenomena in direct correspondence to the working of living organisms.[215] Or, at the same time, by adapting the differences in kinetics between distinct faces of a macrocycle; pre-positioning of a series of barriers in a suitable order can similarly result in unidirectional translation of a macrocycle under thermal equilibrium.[216-219] Representative examples for both approaches will be presented in the following beginning with the first systems that exhibited unidirectional threading and dethreading behaviour as a result of using a nonsymmetric macrocycle such as cyclodextrin (CD).

Unidirectional Linear Threading and Dethreading of Rotaxane-Based Systems

Early investigations on cyclodextrin-based molecular machines[220] (in particular studies from Kaifer and co-workers), on rotaxane based systems have shown that using alkyl motifs **154** (n =1) or **155** (n = 5) subsequent threading with nonsymmetric α-cyclodextrin (α-CD) **153** and final caping with 5-amino-2-naphthalenesulfonate **156** can lead to the observation of two different isomers **157a** and **157b** (n = 1) as well as **158a** and **158b** (n = 5) via ^{1}H NMR spectroscopy (Scheme 8.1).[221a]

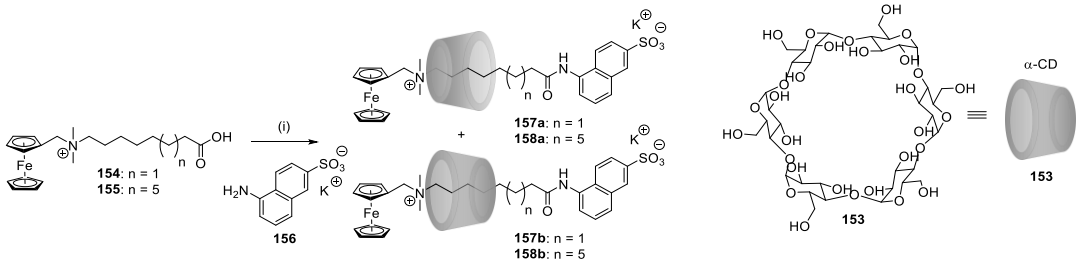

Scheme 8.1. Synthesis of [2]rotaxanes **157** and **158** and study of their isomers obtained from the threading of α-cyclodextrin **153** onto nonsymmetric thread **154** and **155** reported by Kaifer et. al.[221] Reaction conditions: (i) α-CD **153**, EDC, potassium 5-amino-2-naphthalene sulfonate **156**, H_2O, rt, 1 d, no reported yield.

In a following evaluation the authors noted that depending on the length of the alkylic chain opposite ratios for the two enantiomers can be observed.[221b] In the case of reacting short chain **154** with α-CD a ratio of **157a**:**157b** = 6:4 was determined whereas in the case of the longer derivative **155** the proportion changes to **158a**:**158b** = 4:6. Interestingly, when isolating and further separating individual isomers of **157** and **158** the authors have seen slow dethreading of isomers **157a** and **158a** in contrast to isomers **157b** and **158b** which remained stable under similar conditions. They attribute this finding to the asymmetry of the thread which when modelling with CPK in the case of **157a** and **158a** has suggested that the macrocycle can pass over the naphthalene sulfonate group whereas for **157b** and **158b** this pathway appeared disfavoured. Therefore, this system can be seen as the first example of "orientational" isomers which give rise two distinct unidirectional dethreading behaviour[218-219] and distinct fluorescence properties.[222] Related to those studies, similar observations have been made for the synthesis of other open pseudo[2]- and [3]rotaxane systems.[223]

In particular, when comparing between an open pseudo[2]rotaxane **162** and a closed [2]rotaxane system **160**, Park and colleagues have shown that a mixture of open viologen systems **161** and α-CD **153** can afford a single isomer of pseudo[2]rotaxane **162** via preferential "unidirectional movement" (Scheme 8.2).[224]

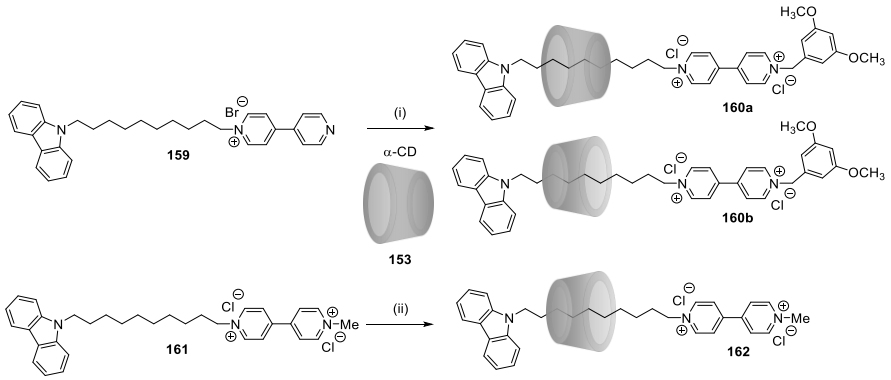

Scheme 8.2. Isomeric [2]rotaxanes **160a** and **160b** and unidirectional threading of [2]pseudorotaxane **162** composed of α-cyclodextrin and aliphatic chain-linked carbazole-viologen thread **159** and its methylated

analogue **161**.[224] Reaction conditions: (i) α-CD **153**, DMF, rt, 1 d, then 3,5-dimethoxybenzylbromide, rt, 6 d, 27% (isolated as a mixture of isomers **160a** and **160b** with ratio 7:9). (ii) α-CD **162**, DMF, rt, 1 d.

The authors reasoned that the cause for this phenomenon lies in the subtle differences in threading and dethreading kinetics between opposite orientations of the macrocycle as a result of the distinct topologies of the two faces α-CD in an aqueous solution. Based on this and earlier experimental results by Matsuo and co-workers,[223a] it has been concluded that an orientation with the wider opening facing the open end of [2]pseudorotaxane is favoured, leading to preferential formation of **162**. In the above example this is also supported by the apparent excess of corresponding isomer **160b** in the mixture of isolated [2]rotaxanes **160a** and **160b** from thread **159** when capping with 3,5-dimethoxybenzylbromide as judged by both ^{1}H NMR and circular dichroism spectroscopy.[218,224] Likewise, Anderson and collaborators have made similar observations with a short length diazo naphthalene sulfonate derivative.[225] Encapsulating the diazo compound with methyl ether protected α-CD as a means to enhance its dye stability and capping the formed intermediary pseudo[2]rotaxane with trichloro triazine and linking the [2]rotaxane to cellulose they have seen a preference for the formation of a single isomer. This finding has then acted as a stimulus to create a light-driven molecular shuttle when replacing the azobenzene motive with a stilbene unit (Figure 8.8).[226]

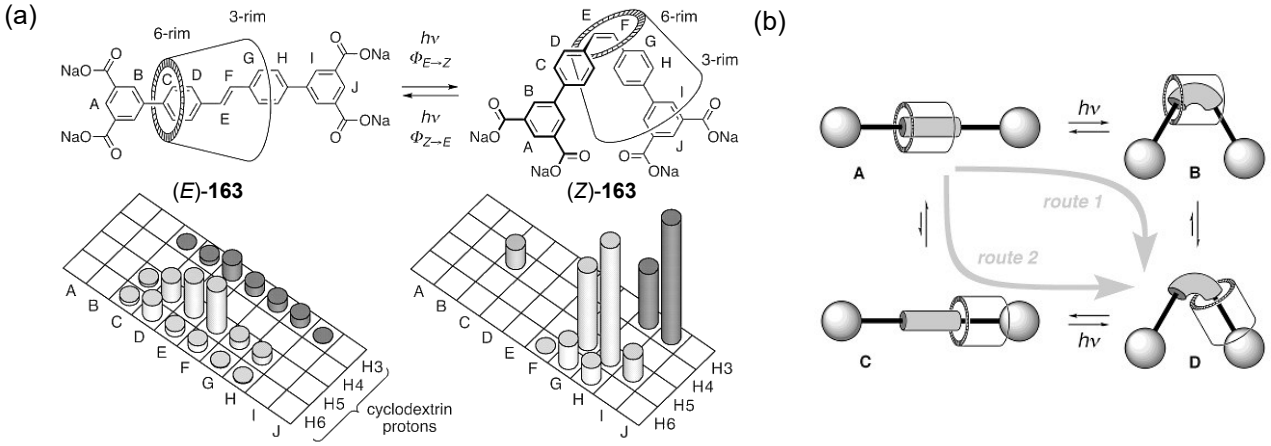

Figure 8.8. Unidirectional photoinduced shuttling in [2]rotaxane **163** with a symmetric stilbene track and α-CD.[226] (a) Photoisomerization of molecular machine (E)-**163** to isomer (Z)-**163**, and key NOEs observed in these two isomers between H_A–H_J of the track and H3–H6 of the cyclodextrin; H3 and H5 are internal protons near the wide and narrow rim, respectively, H4 is on the external surface and H6 is on the narrow rim. The height of each column indicates the strength of the NOE (determined from the integrated NOE intensities). (b) Proposed mechanisms for the photoinduced isomerization of rotaxane **163**. Reprinted by permission from John Wiley and Sons: reference 226, Copyright 2002.

Due to the unique structure of the mechanically interlocked compound **163** two mechanism were discussed to explain the observation of a single isomer upon photoinduced *E*–*Z* isomerisation (Figure 8.8 (b)). In consideration of the reduced quantum yield of the stilbene *E*–*Z* isomerisation process and the absence of a similar behaviour in sterically more demanding analogues it has been concluded that these indications manifest unidirectional movement of the macrocycle prior to the conversion of the stilbene unit to the *cis* isomer. (via route 2 in Figure 8.8) This is in line with experimental observations from Nakashima et. al.[227]

The light-driven shuttling effect has also aroused the interest of Tian and colleagues and lead to the design of other unidirectional shuttling [2]rotaxane systems.[228] Likewise, a rotaxane is obtained as a single isomer from first, threading α-CD onto an isophthalate terminated stilbene-containing axle and second capping with a disulfonic-1,8-naphthalimide derivative via palladium-catalysed Suzuki-coupling. As an extension of their

investigations Tian et. al. have further described the selective formation of opposite regioisomers and compared their optical response upon shuttling via induced circular dichroism.[229]

Contrary to this, Harada and colleagues have examined in which way the substitution pattern of a terminal pyridinium group affects the pseudo[2]rotaxane formation between α-CD and a nonsymmetric thread (Scheme 8.3 (a)).[230] They have postulated that due to the distinct faces of α-CD the rate of association would differ between the two orientations of the macrocycle relative to the thread. And in fact, introducing a methyl group at the 2-position of a terminal pyridinium group two pseudo[2]rotaxane isomers are formed at noticeably different rates when analysing the reaction mixture with ^{1}H NMR longitudinal relaxation and further ^{1}H^{1}H correlation experiments. A similar kinetic behaviour is observed when incorporating an additional viologen unit that can give rise to the formation of pseudo[2]- and [3]rotaxanes respectively.[231] Moreover, the authors highlighted that independent of the rotaxane architecture, the initial unequal ratio of isomers can be brought to align when heating the reaction at higher temperature.[230-231]

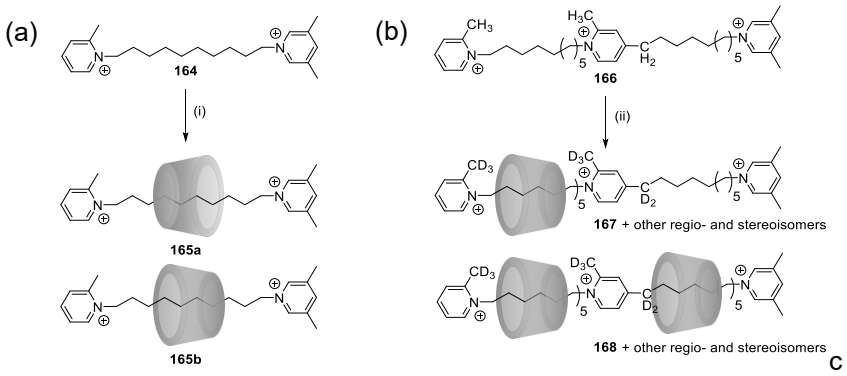

Scheme 8.3. Kinetically controlled face-selective threading of α-CD onto asymmetric axles **164** and **166**. (a) Formation of kinetically favoured **165a** and disfavoured orientation **165b** of pseudo[2]rotaxane. Threading conditions: (i) α-CD **153**, D_2O, 30 °C, 70 d, degree of complex formation: ~80% after 9 d and **165a**:**165b** 5:1 after 10 h.[230] (b) Kinetically studies of the face-selective formation of a collection of pseudo[2]- **167** and [3]rotaxanes **168** regio- and stereoisomers.[232] Threading conditions: (ii) α-CD **153**, D_2O, 70 °C, 7 d.

With the aim of further shedding light on the kinetics of the threading, translation, and dissociation processes in those systems, in a separate study Harada et. al. have deduced the rate constants for the formation of a complex mixture of pseudo[2]rotaxane[233] and pseudo[3]rotaxane isomers (Scheme 8.3 (b)).[232] In the latter studies, deuteration of the acidic terminal 2-methyl substituents and the methylene unit at the 4-position of the internal pyridinium group was noticed.[232] Further investigation on this effect for a range of different cyclodextrin-based macrocycles have shown that this reaction is unique for α-CD. They summarise that with the understanding developed and when combined with “appropriate energy barriers and an enthalpically-driven coupled reaction” in the form of an energy ratchet mechanism, controlled unidirectional linear movement of a cyclodextrin macrocycle may become feasible.

Separate to this, Arduini and co-workers have reported two attempts to effect unidirectional threading with nonsymmetric tris(phenyl ureate) calix[6]arene **169** onto a nonsymmetric viologen motive capped on side with a diphenyl acetate ester.[234] By changing the order of stopper addition, they were also able to prepare the two different stereoisomers of [2]rotaxane viologen system **172** selectively (Scheme 8.4).[235] Starting from desymmetrised thread precursors **170** or **171** and using calix[6]arene macrocycle **159** the corresponding [2]rotaxanes isomers **172a** and **172b** were isolated in 25% and 18% yield, respectively.

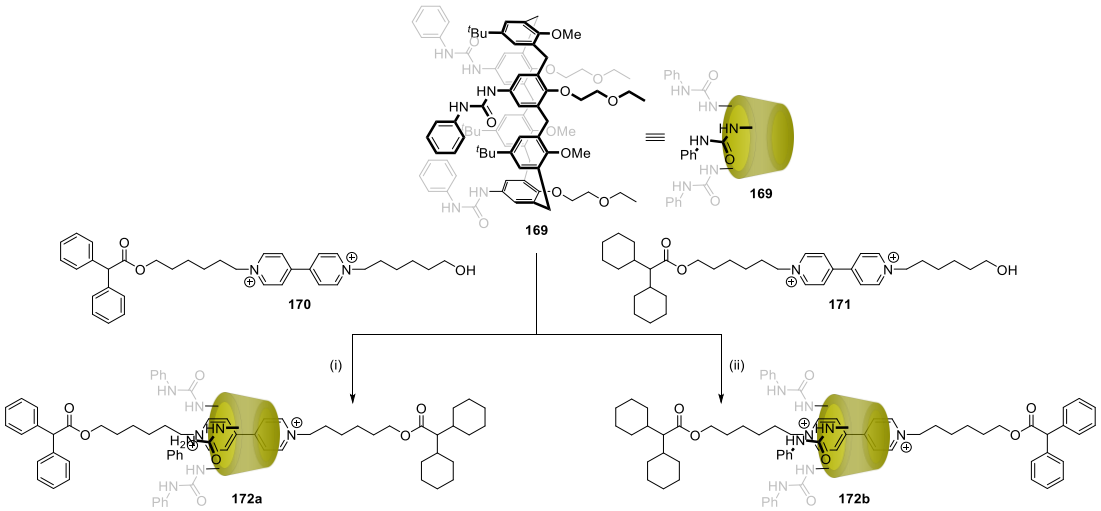

Scheme 8.4. Selective synthesis of two constitutionally isomeric oriented calix[6]arene-based rotaxanes **172a** and **172b**.[235] Reaction conditions: (i) axle **170**, PhMe, reflux, 1 h, then dicyclohexylacetyl chloride, reflux, 12 h, 25%. (ii) axle **171**, PhMe, reflux, 1 h, then diphenyl acetyl chloride, reflux, 12 h, 25%.

In addition to those previous experimental results several authors have constituted that, the unidirectional threading and dethreading behaviour as a result of the difference in kinetics between opposite orientations could ultimately provide useful beyond the formation of single orientational isomers.[217,236] For example, Arduini et. al. concluded that understanding how to achieve control of the random unidirectional movement process in conjunction with an (active) ratchet mechanism could open up new possibilities "for the construction of processive linear motors based on rotaxanes and, at least as a perspective, for rotary motors based on catenanes."[236b]

Unidirectional Linear Transport with Ratchet-Based Mechanisms

In fact, turning the attention to molecular motors and consideration of their working principles has shown a general approach for achieving directional (linear) translation that does not prerequisite an inherent difference in kinetics between distinct orientations of transported components. Emanating from the early ideas of Feynman[37,237] several concepts have been formulated that are suitable for the unidirectional movement of a particle along a predefined direction beyond thermodynamic control.[78] And with an increased understanding of those active transport processes a number of unique chemical ratchet systems have been developed.[31] Operating those system has successfully allowed performing translational motion in a processive, directional, repetitive, and increasingly autonomous manner by taking advantage of the well-defined correlation between different mechanically linked components.

Some principal examples have been described that outline a general scheme for effecting unidirectional linear transport in rotaxane-based systems either with energy or information ratchet mechanisms. In view of the existing, increasing number of work reported, in the following, a few relevant examples shall be discussed to highlight the differences between the main design principles needed to perform unidirectional transport of a macrocycle with an open pseudorotaxane machine.

Light-Based Unidirectional Linear Molecular Transport

Encouraged by the reported designs of light-switchable rotaxanes[92,238,239] and based on the photoisomerism of stilbenes with different sensitizers[107] applied as a function for the realization of an information ratchet,[105] Tokunaga and collaborators have reinvestigated the idea of converting an intermediary pseudo[2]rotaxanes into kinetically stable [2]rotaxanes via isomerisation with light (Scheme 8.5 (a)).[106a]

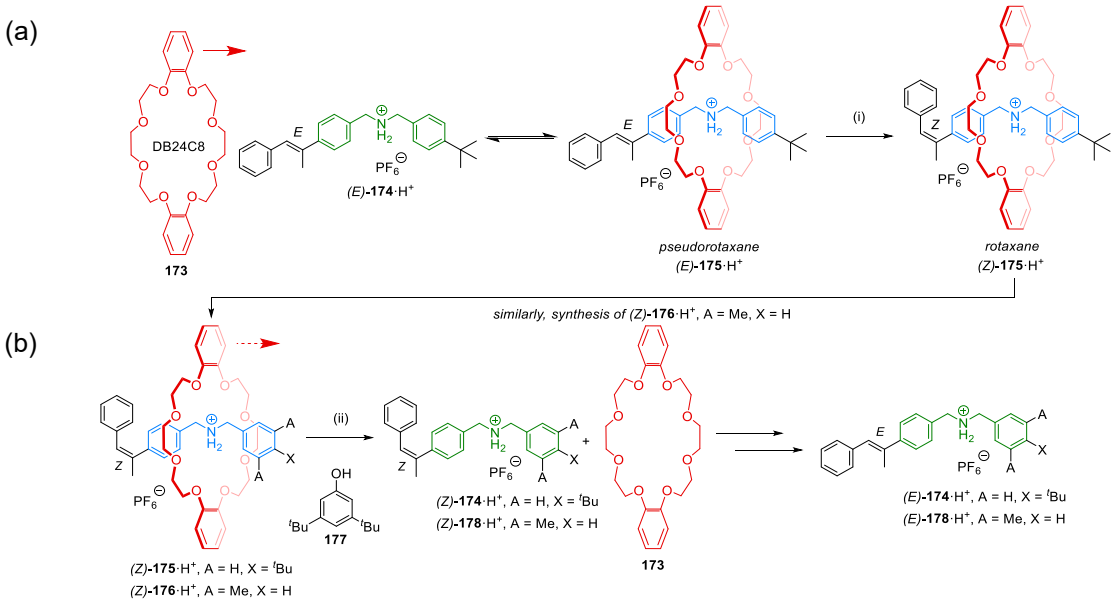

Scheme 8.5. (a) Photochemical synthesis and (b) thermally assisted dethreading of [2]rotaxane (*Z*)-**175**·H$^+$ (A = H, X = *t*Bu) and (*Z*)-**176**·H$^+$ (A = Me, X = H).[106] Compounds were prepared from corresponding (*E*)-isomers via photoinduced *E*–*Z* isomerisation of terminal α-methyl stilbene unit in the presence of sensitizers benzil, 9-fluorenone, duroquinone and pyrene. Reaction conditions: (i) hv (Hg-lamp), $CDCl_3$:CD_3CN, 0 °C, 10 min, 73% [87%] (benzil), 54% [79%] (9-fluorenone), 71% [79%] (duroquinone) and 58% [77%] (pyrene). Reported NMR yields are added in square brackets. (ii) 3,5-bis(*t*-butyl)phenol **177**, DMSO-d_6, 80-110 °C.

Threading dibenzo-24-crown-8 (DB24C8) onto a dibenzyl ammonium motif enclosed on side with a bulky stopper, they have demonstrated that when subsequently switching the stilbene this approach allows isolation of [2]rotaxanes such as (*Z*)-**175**·H$^+$ (A = H, X = *t*Bu). In addition, they showed that compounds obtained this way can also be disassembled back into starting materials by dethreading in reverse induced by isomerization with light or alternatively, in the opposite direction with a thermally assisted kinetic process (Scheme 8.5 (b)).[106b] Moreover, they were able to determine the influence of using different sensitizers such benzil or pyrene on the yield for isolated rotaxanes. Importantly, monitoring the reaction with ^{1}H NMR the authors were able to investigate the subsequent dethreading kinetics in the case of [2]rotaxanes (*Z*)-**175**·H$^+$ and (*Z*)-**176**·H$^+$ in detail which permitted the quantification of the thermal process yielding the free enthalpy $\Delta H^{\ddagger}$, entropy $\Delta S^{\ddagger}$ and energy $\Delta G^{\ddagger}$ for the transition state.[241]

Further to this, Credi and co-workers have explored the photoinduced switching and (de)threading of a linear system (*Z,Z*)-**179**·H$^+$/(*E,E*)-**179**·H$^+$ composed of two azobenzene units attached to opposite ends of a protonated dibenzyl ammonium binding site. By the same token, this has enabled determining rate and equilibrium constants of the pseudo[2]rotaxane (*E,E*)-**180**·H$^+$ and corresponding [2]rotaxane (*Z,Z*)-**180**·H$^+$ formation with DB24C8 via UV-vis absorption and ^{1}H NMR spectroscopy (Scheme 8.6).[242]

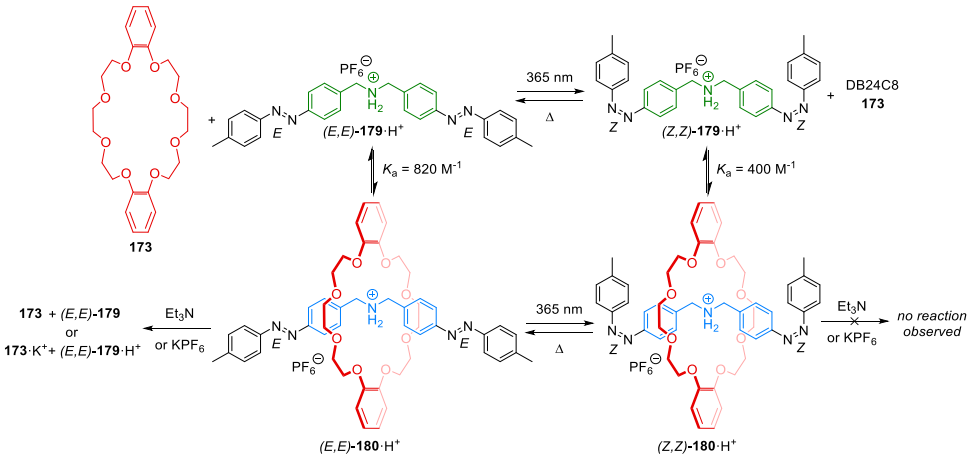

Scheme 8.6. Reversible photo switching from pseudo[2]rotaxane (*E,E*)-**180**·H$^+$ to [2]rotaxane (*Z,Z*)-**180**·H$^+$ and measurement of their equilibrium constants with axle (*Z,Z*)-**179**·H$^+$ and (*E,E*)-**179**·H$^+$ and macrocycle **173** components.[242] General threading and switching conditions: CD_3CN, 298 K. Thermal *Z*–*E* isomerization was performed at 293 K in the dark.

In this particular example, it was found that the dethreading between the open (*E,E*)-**180** and closed form (*Z,Z*)-**180** differs by four orders of magnitude when performing the light-mediated *E*–*Z* isomerisation. Moreover, when deprotonated with triethylamine the generated [2]rotaxane (*Z,Z*)-**180** remains stable but in the (*E,E*)-**180** form the containing macrocycle dethreads quickly. Similar observations have been reported when effecting dethreading with a competitive guest in the form of potassium ions.[242]

With these results in hand and taking advantage of other dethreading studies published earlier on substituted dibenzyl ammonium systems,[243] the authors were poised to create the first example of a unidirectional linear molecular transporter based on the isomerisation of an azobenzene system that conveys a crown ether macrocycle along the axis of asymmetric thread **181**·H$^+$ with a five step reaction sequence (Scheme 8.7).[208]

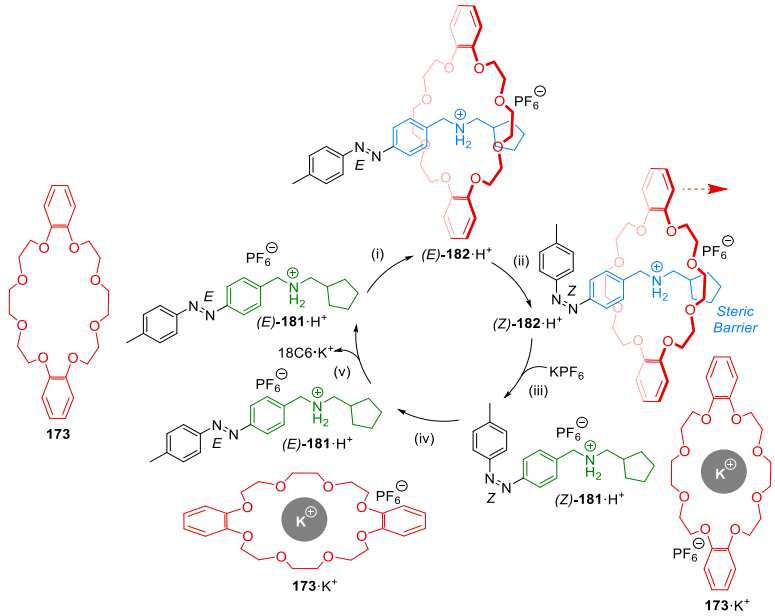

Scheme 8.7. Photoactivated controlled linear directional transport of macrocycle DB24C8 **173** along the axis of nonsymmetric compound **181**·H$^+$.[208] Reaction conditions: (i) DB24C8 **173**, CD_3CN, rt. (ii) 365 nm, rt, 15 min. (iii) KPF_6, rt, 7 h. (iv) 71 °C, 2 h, alternatively, rt, 8 d. (v) [18]crown-6.

The operation reported begins with threading DB24C8 onto protonated axle (*E*)-**181**·H$^+$, to give intermediary pseudo[2]rotaxane (*E*)-**182**·H$^+$, which under irradiation with light allows conversion to (*Z*)-**182**·H$^+$ with a reported yield greater than 95%. As seen before, judging by the kinetic measurements of the association constants and threading rates of dicyclopentyl ammonium complex with DB24C8,[243] the pseudo[2]rotaxane (*Z*)-**182**·H$^+$ gives rise to slow dethreading of the macrocycle over the steric barrier of the cyclopentyl moiety. This process can be accelerated by the addition of potassium ions.[242] Due to the short reaction observed for this step in comparison to symmetric rotaxane (*Z,Z*)-**180**·H$^+$, it has been reasoned that dethreading indeed takes place preferentially over the cyclopentyl and not over the azobenzene group. The liberated axle (*Z*)-**181**·H$^+$ is subsequently reconverted to the *E*-form by thermal dethreading. Lastly, the macrocycle **173**·K$^+$ is freed from the potassium ion by an excess of [18]crown-6 to reset the system to the starting point.

The authors were able to operate the same machine (*E*)-**181**·H$^+$ in an autonomous fashion (Scheme 8.8).[211] The principal differences between the previous and the updated operation of the system are the replacement of the original macrocycle DB24C8 by a dinaphthyl analogue **182** and the use of dichloromethane as a solvent for the operation in place of acetonitrile. With these two changes, both an increase in the association constant between the dinaphthyl macrocycle **192** and axle (*E*)-**181**·H$^+$ and a decrease of the binding affinity in the closed state (*Z*)-**181**·H$^+$ were established.[38e] As an effect, the separate steps of addition and removal of potassium ions as a chemical stimulus to promote dethreading were no longer required for the operation. Additionally, depending on whether an irradiation wavelength above 400 nm or below at 365 or 287 nm was employed, the operation has continued to take place via the anticipated energy ratchet mechanism or by alternative information ratchet contribution, respectively.[38e,211]

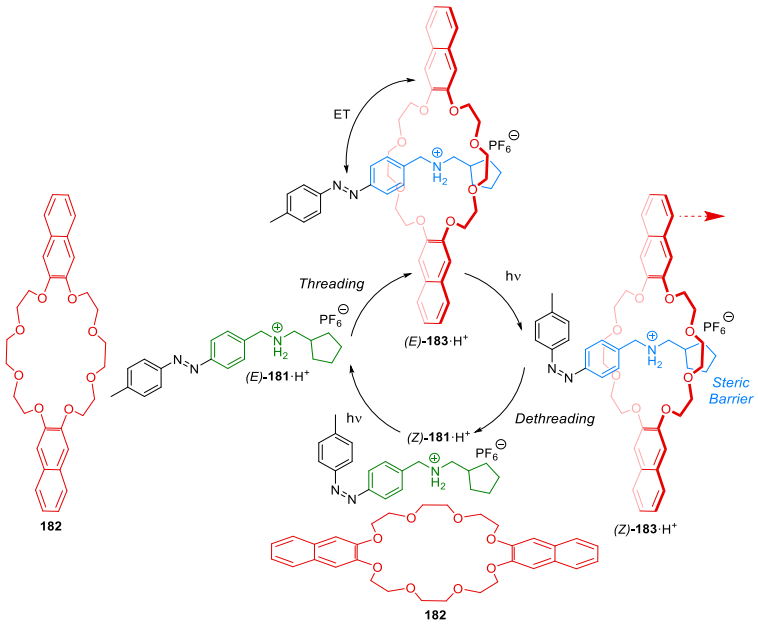

Scheme 8.8. Light-powered autonomous and directional molecular transport of a dissipative self-assembling rotaxane-based system (*E*)-**183**·H$^+$/(*Z*)-**183**·H$^+$ with dinaphthalene macrocycle **182**.[211] Operation conditions: 365 nm, CH_2Cl_2, 20 °C.

The cause for these two distinctive modes of operation have been inferred from the UV-vis absorption spectra of separate macrocycle **182** and (*E*)-**181**·H$^+$ and the combined mixture upon formation of pseudo[2]rotaxane (*E*)-**183**·H$^+$.[244] For the mixture a local absorption maximum at 345 nm was seen which

depletes upon threading and shifts to longer wavelengths to approx. 440 nm. As consequence, when using an irradiation wavelength above 400 nm the *E*–*Z* isomerisation only becomes possible once the pseudorotaxane is formed. In this case the operation occurs via an energy ratchet mechanism. On the contrary, when performing the isomerisation at 365 or 287 nm, the authors have argued that due to an electron transfer process from naphthalene chromophores of the macrocycle **182** to the azobenzene unit the ensuing position-dependent sensitization forms an information ratchet mechanism. Moreover, it has been demonstrated that the continuous operation molecular pump (*E*)-**181**·H^+ leads to a decrease of free macrocycle that is determined by the kinetics of the dethreading over the cyclopentyl moiety. This assertion was substantiated when following the operation of molecular pump (*E*)-**181**·H^+ in comparison to an unprotonated sample (*E*)-**181** under continuous irradiation. The authors concluded that the monitored drop of fluorescence intensity related to free macrocycle **182** upon irradiation of the mixture provided sufficient evidence for the proposed working of the pump system.

Redox-Based Unidirectional Linear Molecular Transport

Different to this, Stoddart and cohorts have constructed a molecular pump system **185**$^+$ that uses the electrochemical switchable[245] binding interaction between tetracationic cyclobis-(paraquat-*p*-phenylene) [246] macrocycle[246] **184**$^{4+}$ and a dioxynaphthalene motive[247] to effect unidirectional linear transport through a cycle of reduction and oxidation steps (Scheme 8.9).[212] In the given example, due to electrostatic repulsive interactions between the macrocycle **184**$^{4+}$ and the 3,5-dimethylpyridinium unit, threading occurred preferentially over the isopropyl phenolate group. Once threaded, the following dethreading was affected by reduction with zinc powder to give the reduced macrocycle **184**$^{2(\bullet(+))}$. In this state, repulsion between the macrocycle and the pyridinium barrier is diminished and thus, by a kinetic argument, leads to dethreading over the smaller and sterically less demanding 3,5-dimethylpyridinium group when compared to the alternate 2-isopropyl phenolate barrier for the majority of macrocycles. Upon re-oxidation in air the original state of the pump system was restored allowing further cycles to take place.

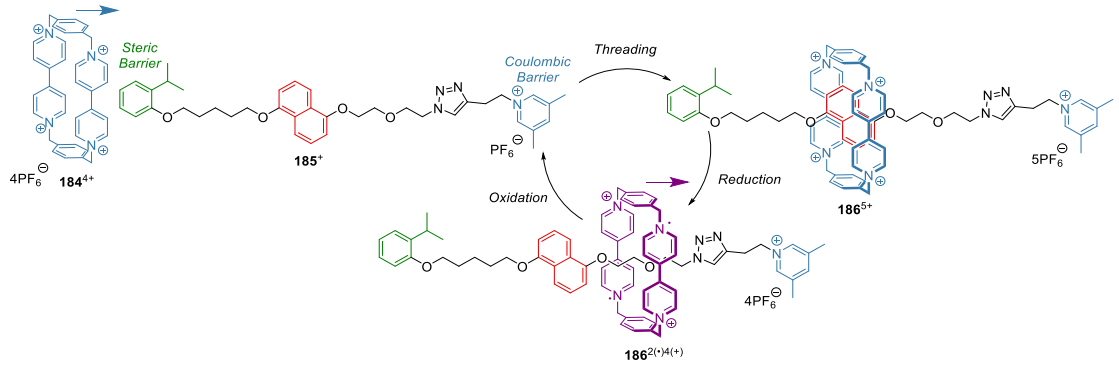

Scheme 8.9. Unidirectional translation of macrocycle **184**$^{4+}$ along the axis of dioxynaphthalene containing thread **185**$^+$. The operation was performed via successive reduction and oxidization cycles achieved by heterogenous reduction with Zn dust and subsequent oxidation by exposure to air.[212]

In addition, taking advantage of previous studies[248] and combining the pump system **185**$^+$ with $Ru(bpy)_3Cl_2$ and phenothiazine (PTZ) **170**, photoinduced electron transfer from the excited state of the ruthenium photo sensitizer to the threaded macrocycle under irradiation with light at 450 nm has led to a similar operation as

with the two step chemically-induced reaction sequence (Scheme 8.10). First, upon charge transfer the reduced macrocycle dethreads and second, the original pseudo[2]rotaxane is reformed via charge recombination with oxidised PTZ, that allows the oxidised macrocycle to rethread back onto the axle over the 2-isopropyl phenolate barrier. Using this strategy, the authors were able to demonstrate the dissipative, light-based autonomous operation of machine **185**$^{+}$, by monitoring the reaction with UV-vis spectroscopy.

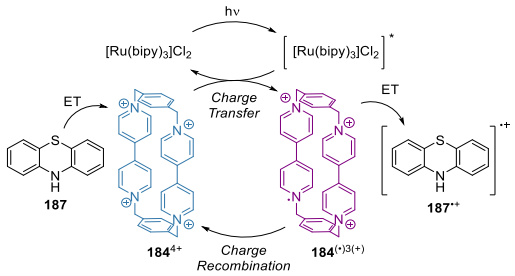

Scheme 8.10. Proposed continuous light-based dissipative catalytic cycle for the operation of machine **185**$^{+}$ with $Ru(bpy)_3^{2+}$ sensitizer and phenothiazine **170**$^{\bullet+}$.[212]

Building onto previous investigations,[249] on the redox properties of viologen derivatives and their application as guest in the reduced form as radical cation **184**$^{\bullet+}$ for cationic macrocycle **184**$^{2(\bullet+)}$, Stoddart and colleagues have also explored the stepwise operation of a molecular switch **184**$^{3+}$(Scheme 8.11).[250]

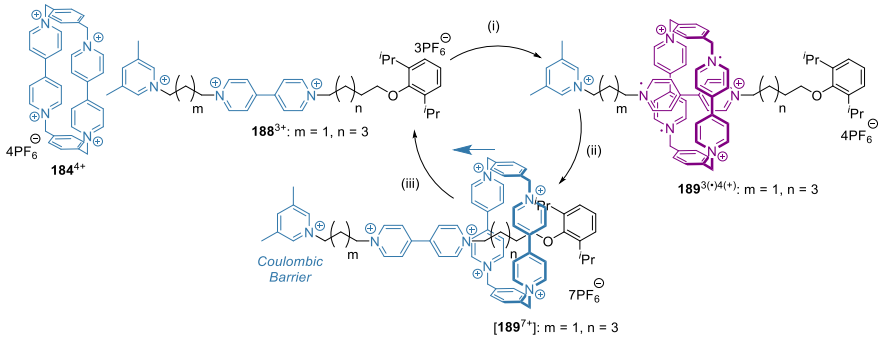

Scheme 8.11. Switchable threading and dethreading in reverse of macrocycle **184**$^{4+}$ onto axle **188**$^{3+}$ by cycles of reduction and oxidation steps.[250] Typical conditions for the operation: (i) Zn, CD_3CN, rt, 5 min, then (ii) tris(4-bromophenyl)ammoniumyl hexachloroantimonate, 0 °C. (iii) rt, 30 min.

With this system, the authors were able to observe both the threading of macrocycle **184**$^{2(\bullet+)}$ from one side of the nonsymmetric axle **188**$^{\bullet2(+)}$ over the pyridinium barrier (after reduction with zinc dust) and the dethreading in reverse upon oxidation. Relying on NMR and UV-vis spectroscopy they were able follow the initial formation of pseudo[2]rotaxane **189**$^{3(\bullet)4(+)}$, the transition to nonequilibrium state [**189**]$^{7+}$ and its subsequent deferred decay through slow release of the macrocycle back into solution. They constituted that, as before,[212] the 3,5-dimethylpyridinium unit acts as a coulombic barrier and consequently, threading of the reduced macrocycle cation **184**$^{2(\bullet+)}$ is faster than dethreading once the macrocycle exists as tetra cation **184**$^{4+}$ on account of the increased repulsive electrostatic interactions between the macrocycle and the pyridinium end group. Furthermore, due to a high activation energy barrier for the dethreading the reverse reaction could be followed in detail separately by ^{1}H NMR. Repeating this operation for a range of threads with a different connection between the pyridinium barrier and the viologen binding station (parameter *m*, Scheme 8.11), a direct influence on the kinetic barrier was observed. This pointed out a relationship between the dissociation barrier energy and the length of the alkylic connection. In one instance (m = 0, n = 5) this has allowed isolation of a stable [2]rotaxane. Building on these results, a more recent (re)investigation of this

basic redox-activated concept has yielded a daisy chain polymer. Similar to the example shown in Scheme 8.11 the location of the macrocyclic when incorporated into the track can be controlled via redox cycles which further confirmed the generality of this concept.[251]

With those two results in hand, a series of energy ratchet systems have been synthesised with the aim of using the 2-isopropyl phenolate unit as a kinetic barrier for accumulation of macrocycles (Scheme 8.12).[209]

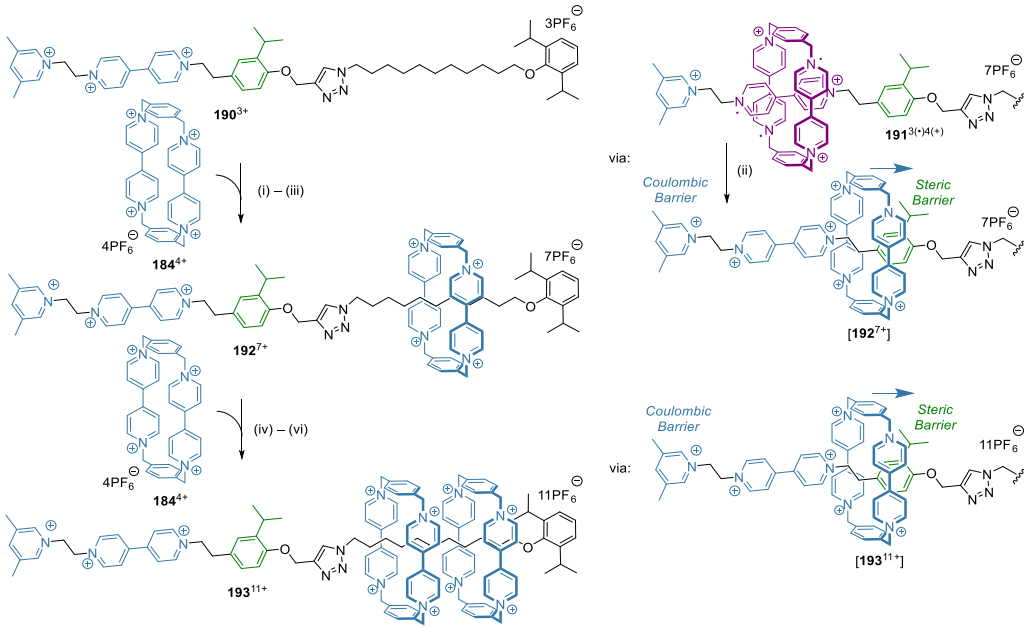

Scheme 8.12. An energy ratchet system **190**$^{3+}$ that allows capturing of two tetracationic macrocycles **184**$^{4+}$ onto an oligomeric collection domain via a sequence of two subsequent reduction and oxidation cycles.[209] Operation procedure: (i) Zn, CH_3CN, rt, 10 min, then (ii) $NOPF_6$, 30% [95%] over two steps. (iii) 42 °C, 3 h. (iv) Zn, CH_3CN, rt, 10 min, then (v) $NOPF_6$, 15% [85%] over two steps. (vi) 42 °C, 3 h. NMR reported yields are given in square brackets.

The design established by Stoddart et. al. relies on the redox-switchable binding interaction between reduced cyclobis-(paraquat-*p*-phenylene) macrocycle and a viologen unit, in conjunction with a pair of 3,5-dimethylpyridinium and 2-isopropyl phenolate barriers to form an energy ratchet mechanism. The operation has been conducted via reaction with zinc and subsequent oxidation with e.g., air or alternatively, with nitrosyl salts. In a similar manner, the pyridinium unit has shown to act as a coulombic barrier and thus, thermally assisted relaxation favours onward shuttling of the macrocycle over the steric 2-isopropyl moiety to the collection domain, instead of the reverse dethreading. Optimising the chemical framework, Stoddart and co-workers have arrived at the final design **190**$^{3+}$ that includes a triazole unit as additional binding motive after the steric 2-isopropyl unit to promote the capture of a second macrocycle. Using NMR spectroscopy, they were able to provide evidence for the formation of an intermediary nonequilibrium states [**192**$^{7+}$] and [**193**$^{11+}$] where the macrocycle is entrapped between the pyridinium and 2-isopropyl phenolate barriers. Moreover, noticing that both, kinetically stable intermediates [**192**$^{7+}$] and [**193**$^{11+}$] can be pushed forward to **192**$^{7+}$ and **193**$^{11+}$ by heating the sample at 42 °C, they were able to determine the activation energies for the relaxation via ^{1}H NMR. They highlighted that this form of ratchet mechanism transfers macrocycles from solution onto a thread and subsequently kinetically entraps those particles in the collection region in a state of “reduced translational freedom (lower entropy)”.[252] Thus, they concluded, that this concept sketches out on an

alternative direction to progressively perform active unidirectional linear transport. Similar to the biology, work is performed "uphill" of a proverbial energy landscape[78] against a electrochemical gradient.

Further optimisations of the underlying structure have led to the creation of a second generation design that allows for operating molecular machine **194**$^{8+}$ at room temperature by reducing the length between the viologen and 2-isopropyl moiety (Scheme 8.13).[253]

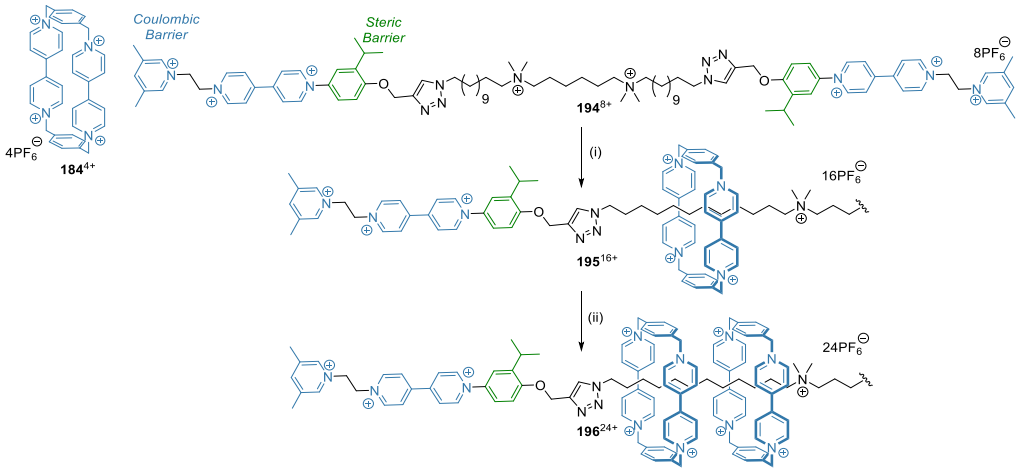

Scheme 8.13. Operation of second generation energy ratchet system **194**$^{8+}$ via cycles of electrochemical reduction and oxidation reactions.[253] Isolated [3]- **195**$^{16+}$ and [5]rotaxanes **196**$^{24+}$. Operation conditions: CH_3CN, 40 °C. (i) –0.7 V, 10 min, then +1.4 V, 10 min, **194**$^{8+}$:**195**$^{16+}$ = 22:78. (ii) –0.7 V, 10 min, then 20 min resting period, then +1.4 V, 10 min then 10 min resting period, **195**$^{16+}$: **196**$^{24+}$ = 53:47.

Additional heating was no longer necessary to effect relaxation of intermediates. Alike, capturing of free macrocycle was observed when performing operation machine **194** electrochemically. By repeating reduction and oxidation cycles, this has allowed isolation of symmetric [3]- **195** and [5]rotaxanes **196** with a final product distribution of 53:47 for **195**:**196**.[254]

Taking a step forward, Stoddart and collaborators have in the following also extended this energy ratchet design[209,253] and created a second molecular pump. Replacing the basic collection domain with a second viologen station preceded by another, second pyridinium barrier they obtained **197**$^{6+}$ (Scheme 8.14).[210]

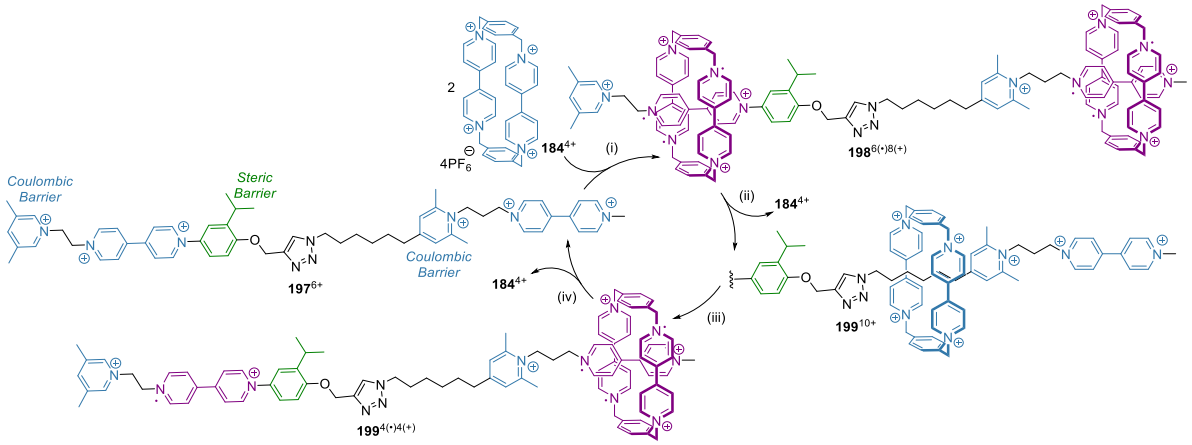

Scheme 8.14. Operation of molecular pump **197**$^{6+}$ via two cycles of electrochemical or chemical reduction and oxidation reactions with zinc dust and $NOPF_6$.[210] Isolated [2]rotaxane **199**$^{10+}$. Operation conditions: CH_3CN, 40 °C. (i) –0.7 V, 40 min, then 20 min resting period. (ii) +1.4 V, 40 min, then 20 min resting period, 45% over two steps. (iii) –0.7 V, 10 min, then 20 min resting period. (ii) +1.4 V, 10 min, then 10 min resting period, 89% over two steps.

With this adaption, they were able to successfully take up tetracationic macrocycle **184**$^{4+}$ from solution yielding [2]rotaxane **198**$^{10+}$ with the first electrochemical or chemical reduction and oxidation cycle with zinc and nitrosonium salt. Performing a second cycle, this allowed the macrocycle shuttle over the coulombic 3,5-dimethylpyridinium barrier to the reduced radical viologen binding station to give intermediate **199**$^{4(\bullet)4(+)}$ from where it dethreads into solution upon oxidation. To confirm this, the [2]rotaxane **199**$^{10+}$ resulting from the operation of the first redox cycle with **197**$^{6+}$ and macrocycle **184**$^{4+}$ was isolated and characterised prior to submitting **199**$^{10+}$ back again to a new, second redox cycle. And when looking at the ^{1}H NMR Stoddart and co-workers were indeed able to monitor the reappearance of the proton signals for the original tetracationic macrocycle **184**$^{4+}$. Integration of the signals has further suggested a high operation efficiency.

While writing these lines, the same authors have reported another (third) attempt to further improve the basic pump design (Scheme 8.15).[290]

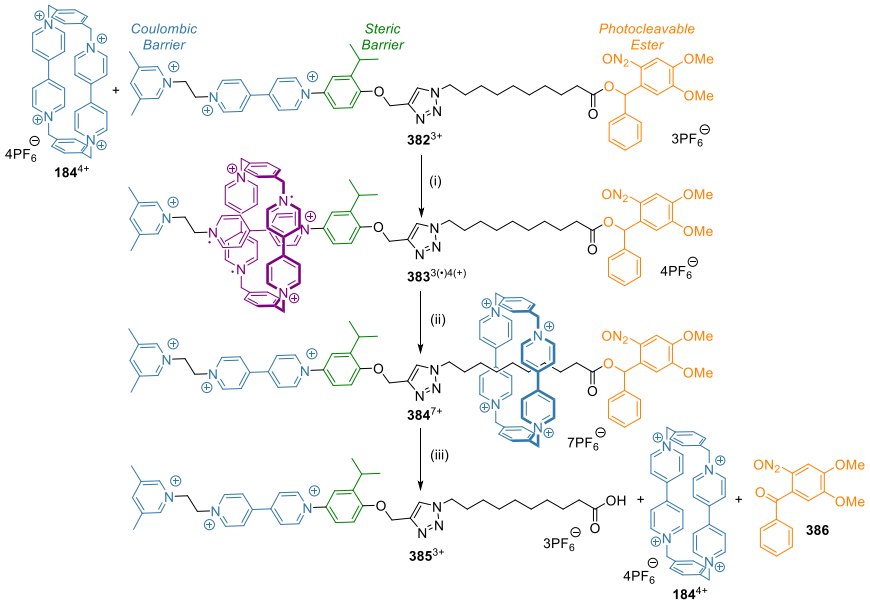

Scheme 8.15. Operation of molecular pump **382**$^{3+}$ via combined electrochemical reduction and oxidation cycles and cleavage of photolabile nitro benzhydryl ester with light.[290] Isolated free thread **385**$^{3+}$, macrocycle **184**$^{4+}$ and ketone **386**. Operation conditions: $TBAPF_6$, CH_3CN, rt. (i) –0.7 V, 20 min, then 20 min resting period. (ii) +0.7 V, 20 min, then 10 min resting period, 54% over two steps. (iii) 365 nm, 25 min, quantitative.

They showed that by including a photolabile stopper the selective, irreversible light-induced cleavage of a terminal *O*-nitro benzhydryl ester provides spatiotemporal control over the final release of the macrocycle.

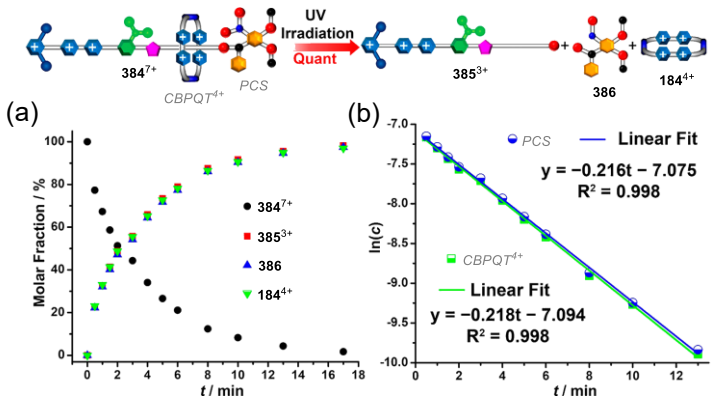

Figure 8.9. Kinetic analysis of molecular pump **382**$^{3+}$ as monitored by ^{1}H NMR spectroscopy. (a) Plots of molar fractions of **384**$^{7+}$, **385**$^{3+}$, **386**, and **184**$^{4+}$ and (b) logarithmic plots of threaded macrocycle **184**$^{4+}$

(*CBPQT*$^{4+}$, green squares) and *O*-nitrobenzhydryl ester (*PCS*, blue circles) during photocleavage. Adapted with permission from reference 290. Copyright 2020 American Chemical Society.

They demonstrated that this still, can give unidirectional transport of the tetracationic macrocycles **184**$^{4+}$ along an asymmetric thread through an intermediary [2]rotaxane via a three step reaction sequence comprising electrochemical reduction, oxidation, and final UV irradiation (365 nm).

Chemical Fuel-based Unidirectional Linear Molecular Transport

Distinct to this, Leigh and co-workers have explored the possibility of guiding the unidirectional molecular transport of a crown ether macrocycle with a dissipative, chemically fuelled energy ratchet mechanism.[213] They were able to perform the operation of a cyclic [2]catenane motor system **200**/**200**·**H**$^+$ (Scheme 8.16).

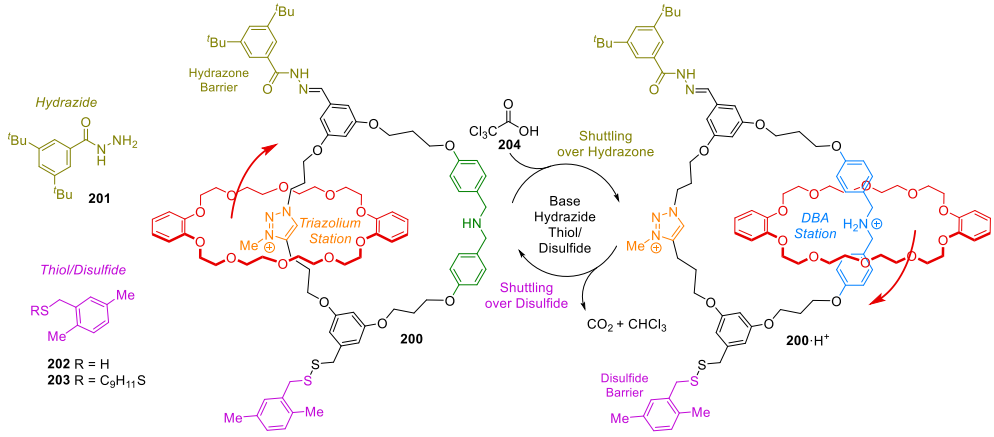

Scheme 8.16. Operation of cyclic [2]catenane motor **200**/**200**·H$^+$ using pulses of a chemical fuel trichloroacetic acid **204**.[213] Operation conditions: Et_3N (base), thiol **202**, disulfide **203**, hydrazide **201**, 2-methyl-2-butene, CD_3CN, rt. Each pulse of fuel contained 80 equivalents of acid. The first cycle is completed within 17 h and in total four translation cycles have been performed.

The system's design is based on the pH-dependent shuttling of macrocycle dibenzo-30-crown-10 (DB30C10) between the dibenzyl ammonium and methyl triazolium station.[255] It relies on reversibly switching the macrocycle's position from the protonated dibenzyl ammonium to triazolium station by deprotonating the secondary ammonium salt with base and restoring the initial state with acid. Leigh and colleagues showed that the direction of the macrocycle's translation can be successfully controlled with an alternate pair of hydrazone and disulfide barriers which become labile under acidic and basic conditions, respectively. Importantly, when combined with the application of dissipative chemical fuel trichloroacetic acid (TCA) **204** (Scheme 8.17), which leads to a temporal lowering of the pH, they were able to achieve the complete operation cycle as shown in Scheme 8.16 in a single step.

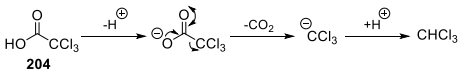

Scheme 8.17. Base-catalysed decarboxylation of chemical fuel trichloroacetic acid 204.

This has allowed them to drive the system's operation several times with a series of chemical pulses without any intermediate purification. Moreover, the same concept has allowed to take up macrocycles from solution and pump them against thermodynamic equilibrium onto a holding area with linear pump **206**. (Scheme 8.18)

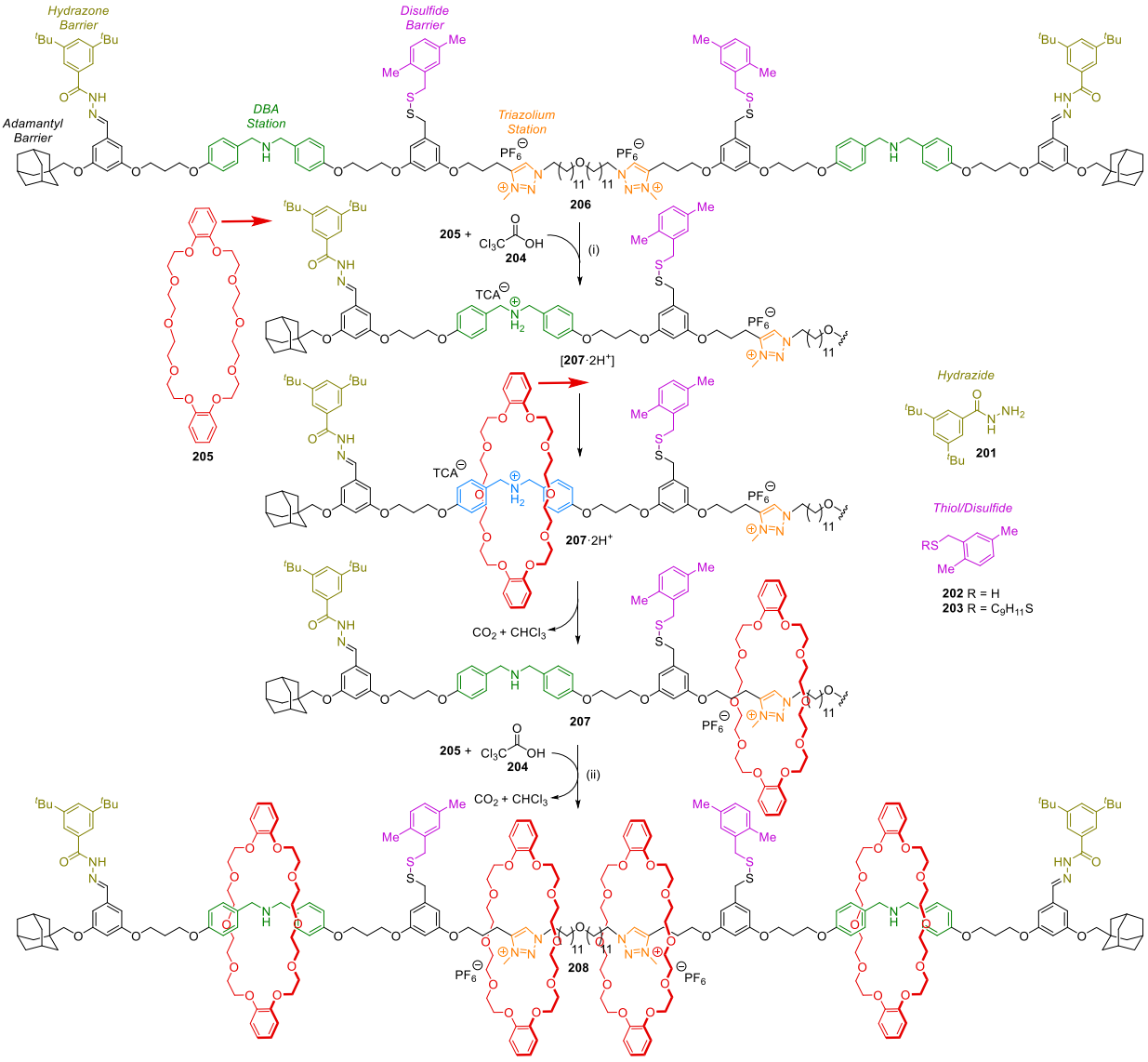

Scheme 8.18. Operation of molecular pump **206** with several pulses of chemical fuel **204**.[213] Reagents and conditions: DB30C10 **205**, thiol **202**, disulfide **203**, Et_3N, hydrazide **201**, CD_2Cl_2:CD_3CN 9:1. After addition of the (i) first pulse and (ii) a series of another three pulses of chemical trichloroacetic acid. (200 equivalents) First cycle (i) yields an average pump occupancy of 1.9 and (ii) subsequent succession of cycles a final pump occupancy of 3.7 as determined by integration via ^1H NMR. This corresponds to the formation of [3]- **207** and [5]rotaxane **208**, respectively.

The design for the linear pump similarly relies on the protonation of a dibenzyl amine unit and the promotion of hydrazone exchange under intermediate acidic conditions immediately after addition of acid **104**. Associated with this, movement of the macrocycle is induced and effects the translation from nonequilibrium state [**207**·H^+] to **207**·H^+ over the hydrazone barrier. Meanwhile, in presence of additional base delayed decomposition of chemical fuel **204** generates $CHCl_3$ and CO_2 which can escape the reaction and slowly resets the operation system back to its original basic conditions. Accompanying the increase of pH, deprotonation of the dibenzyl ammonium binding station occurs and yields nonequilibrium state [**207**]. While the simultaneous reduction of the hydrazone exchange rate prevents the relaxation of the macrocycle in reverse, the onset of free-thiol **202** enabled disulfide exchange leads to the contrary movement to the triazole station over the disulfide barrier and yields final state **207**. By combining those elements and connecting two ratchet units in an opposing inwards direction in form of an open system with adamantyl groups, the authors

were able successfully take up a pair of macrocycles **206** from solution onto thread **206** to give [3]rotaxane **207** by a single pulse of TCA. With additional pulses, the occupancy could be increased to yield the [5]rotaxane **208**.

8.2. Motivation

In common to the transport processes of molecular machines proposed in preceding examples is that the movement of the macrocycle has in general been established on the basis of observing a series of well-defined equilibrium states either via NMR or UV-vis spectroscopy: When taking together, they described the overall anticipated linear molecular motion. This applies, for instance, to Leigh's chemically fuelled pump **208**,[231] Stoddart's first pump design **185**$^{+}$ operated either with light or by redox cycles[212] or his second pump prototype **197**$^{6+}$.[210] Furthermore, in the case where there was no immediate method for monitoring discrete states, evidence has been provided on account of kinetic arguments for the principal translation process. The lack of information was resolved by separate or comparing analysis of operation components. This approach has been utilised e.g., by Credi and co-workers for analysing the operation of light based molecular pump **181**·H^{+} when operated either sequentially[208] or autonomously.[211] This strategy also underlies the unidirectional threading and dethreading studies conducted by Arduini,[236b-c] Harada[230-233] and Park.[219,236a]

Notably, in the case of Stoddart's molecular switch **188**$^{3+}$[250] and energy ratchet **190**$^{3+}$[209] an additional direct indication for the proposed unidirectional linear transport was given by the detection of kinetically stable nonequilibrium states [**192**$^{7+}$] and [**193**$^{11+}$] (see Scheme 8.12). The detection of those species is the direct result of the large energy barriers $\Delta G_2^{\ddagger}$ = 23.0 kcal mol^{-1} (transition of [**192**$^{7+}$] to **192**$^{7+}$) and $\Delta G_2^{\ddagger}$ = 23.1 kcal mol^{-1} (transition of [**193**$^{11+}$] to **193**$^{11+}$)[209] that are assoicated with respective second steps of those consecutive reactions (see Figure 8.10 for further explanation).[256] Given the thermal energy available to the system at room temperature (kT = 0.592 kcal mol^{-1})[63] and the general kinetics of a consecutive reaction this has provided a unique first opportunity to study molecular translation beyond analysis of equilibrium states but incurred an (undesired) additional heating step for the operation of machine **190**$^{3+}$.[209,253]

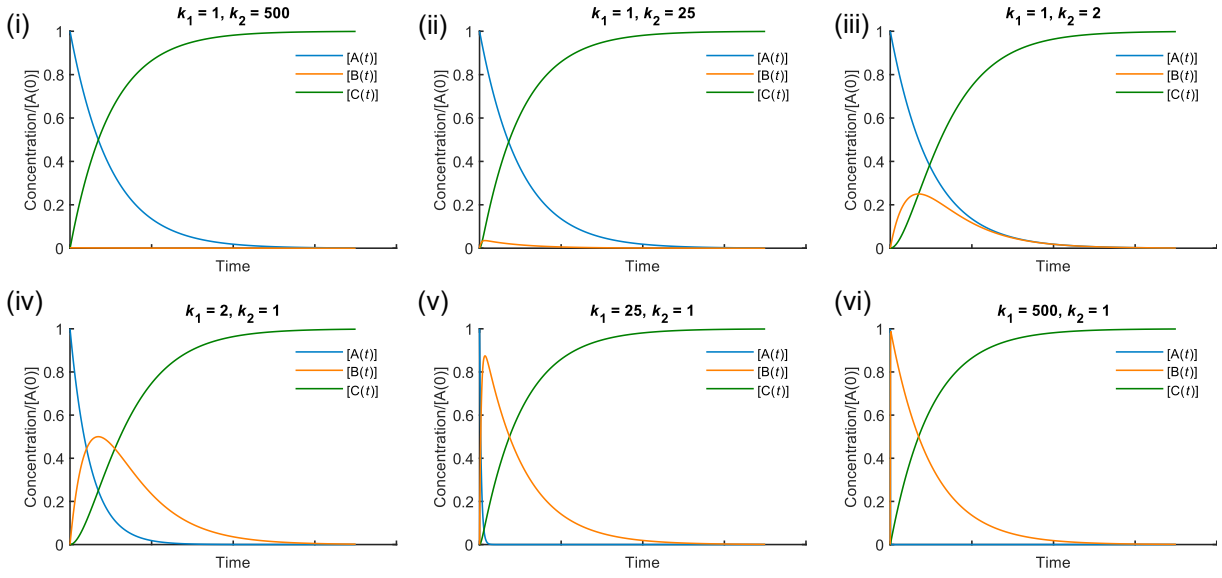

Figure 8.10. Plots of the (normalised) concentration as a function of time for (i) – (vi) a series of distinct consecutive reactions $A \xrightarrow{k_1} B$; $B \xrightarrow{k_2} C$ where A denotes the starting compound, (blue) B an intermediate, (red)

C the final outcome of the reaction (yellow). Label k_1, k_2 correspond to the rate constants of the sequence of first order processes. Analytical terms for the solution of the differential equation have been derived from the literature[256] and reveal the differences in the proportion of intermediate B during the reaction. (i) – (ii) When B is consumed faster than it is formed in the first place B does not appear in significant quantities whereas on the contrary (v) – (vi) when conversion to C from B becomes slow the decay of the intermediate can be approximated by a first order reaction after an initial induction period. For (iii) – (iv) intermediate cases the ratio of k_1 and k_2 can also be determined via monitoring intermediate B.

Turning to the study of related biological systems, similar complication arise when attempting to delineate the complex working of the nature's sophisticated molecular machinery.[31] In many cases, it is impossible to understand the full implications of subtle conformational changes that go along with each mechanical task performed by proteins. It has been concluded that despite progress, investigations of systems such as ABC transporters remain a challenging subject even with current analytical techniques.[192d,257] Though different experimental[258,260] and theoretical methods[259] have allowed developing a conception for their principle working mechanisms at the cell boundary and increasingly, in their native environment, attaining knowledge and further experimental evidence of the complete actions constitutes an ongoing research subject.[38b]

8.3. Aims

From this perspective, it appeared promising to ask whether, ensuing from the chemically fuelled molecular motor **200**/**200**·H⁺ and pump **206**/**206**·H⁺ concept,[213] the aspect of unidirectional motion could be visualised by the virtue of an additional optical technique. Based on the evidence for fluorescence switching via chemically-induced shuttling of rotaxane based-systems in the literature,[262] it appeared likely that an intramolecular quenching process, such as photoinduced electron transfer (PET)[261] (see Figure 8.11 for an illustration of its mechanism) from a methyl triazolium unit to an anthracene fluorophore,[262c] may be applied to detect the position of a macrocycle in a nonequilibrium state **B** as an intermediate between discrete equilibrium states **A** and **C** (see Figure 8.10).

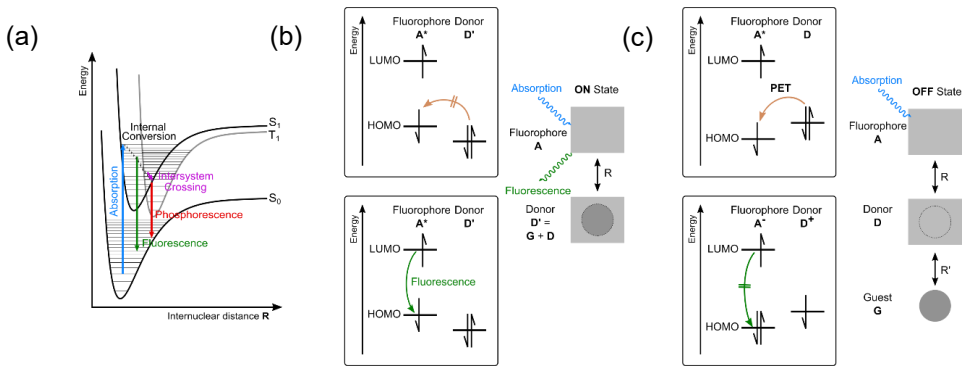

Figure 8.11. Schematic illustration of an intramolecular fluorescence quenching process as a result of photoinduced electron transfer.[261] (a) Isolated or (b) in absence of a suitable (electron) donor **D** with matching redox potential E^0_{red} (**D**⁺/**D**) excited fluorophore **A*** can undergo relaxation from an electronically excited state (S_1) to the ground state (S_0) by fluorescence with corresponding signal intensity I_0 (bottom). (c) If in proximity to a suitable donor **D** and redox potentials of both **A*** and **D** are complementary formation of a transient excited fluorophore–donor pair **A***–**D** can permit a bimolecular electron-transfer reaction. (PET, top) The charge transfer to (**A**⁻–**D**⁺)* or **A**⁻$_{solv}$ and **D**⁺$_{solv}$, prevents original fluorescence (bottom) and, therefore, leads to a decrease of the measured fluorescence intensity I over unaffected systems with intensity I_0. The fluorescence quenching is affected both by the intramolecular distance R between donor **D** and fluorophore **A** and if donor constitutes a supramolecular host **D** also the intermolecular distance R' to a suitable guest **G**.

It was anticipated that if the fluorescence signal of an intermediate **B** in a consecutive reaction can be modulated successfully in this way this, in turn, will substantiate the working of the unidirectional pump transport process and also complement the analysis of the operation with ^{1}H NMR. It was hoped that if the fluorescence signal corresponds with the expected profile for an intermediate of a consecutive reaction, this immediately gives a “visual” indicator of the postulated transport mechanism (Figure 8.12).

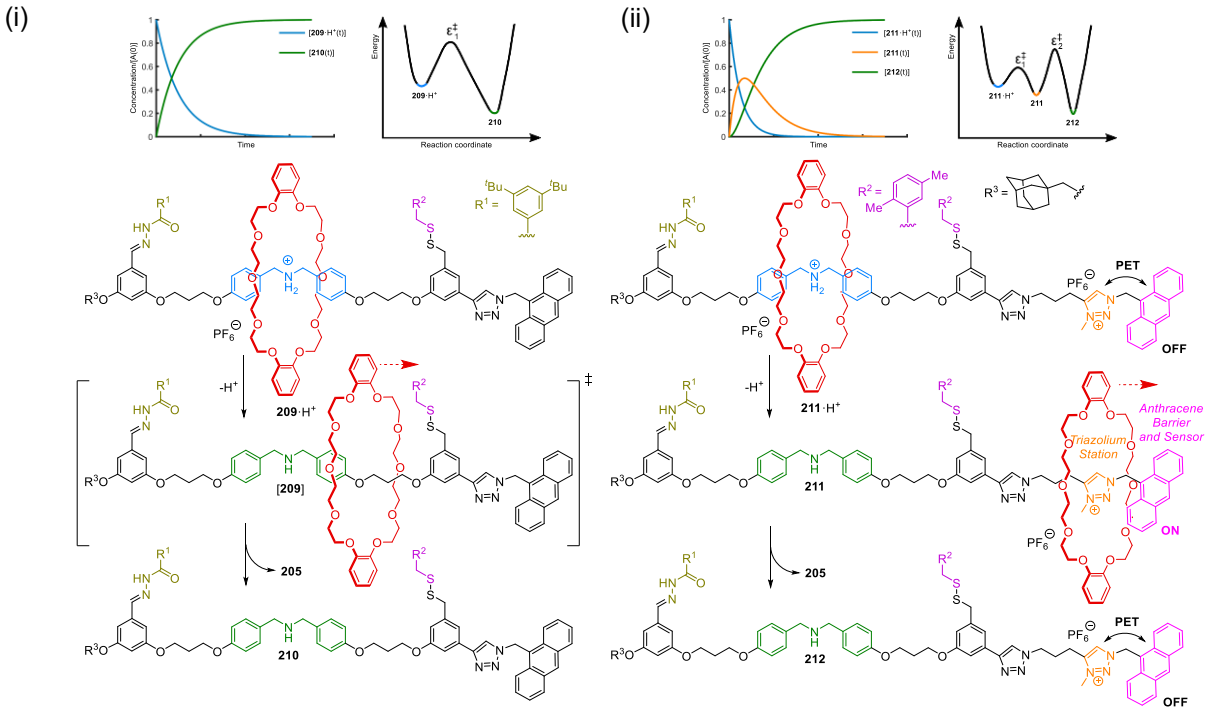

Figure 8.12. Schematic illustration of using the switchable fluorescence of an anthracene residue in proximity to an intermediate triazolium binding station as means to illuminate unidirectional transport of a molecular pump **211**/**211**·H$^+$. It is anticipated that in comparison to (i) a first-order dethreading reaction from **209** to **210** (ii) the addition of a methyl triazolium unit will give rise to a consecutive reaction with intermediate **211** which based on previous observation[262c] is suggested to exhibit an increased fluorescence with macrocycle **205**.

Looking at the proposed system depicted in Figure 8.12 (ii), as described in the original motor publication,[213] it is expected that by the initial addition of a chemical fuel **204**, acidification would lead to the threading of DB30C10 **205** onto the dibenzyl ammonium (DBA) station of hydrazone thread **212** (facilitated by dynamic hydrazone exchange of the barrier) to give [2]rotaxane **211**·H$^+$. As the decomposition of acid **204** in the presence of base takes place, relocation of the macrocycle **205** occurs from the DBA station over the disulfide barrier (facilitated by dynamic hydrazone exchange) to the triazolium station, resulting into the formation of intermediate **211**. In this state, the previous intramolecular quenching effect via PET from the triazolium donor to anthracene in its excited state is known to subside and as a consequence, the fluorescence supposed to be enhanced (ON state, see Figure 8.11). Slow dethreading of the macrocycle **205** is then anticipated to restore the original PET process and decrease the measured fluorescence signal back on a lower level (OFF state, see Figure 8.11). In comparison, dethreading in the absence of a triazolium unit will not influence the fluorescence. Altogether, it has been hoped that with every new pulse of chemical fuel another reaction cycle will be affected and directly correspond with the rise of fluorescence from the anthracene unit. Ideally, the dethreading would occur slowly so that the kinetics of this process can be observed by combination of fluorescence and ^{1}H NMR spectroscopy. Additionally, it has been realised that carrying on this idea with a supplementary fluorescence sensor such as alternative pyrene fluorophore[262d] this also opens up the possibility for construction of more complex systems (Scheme 8.19).

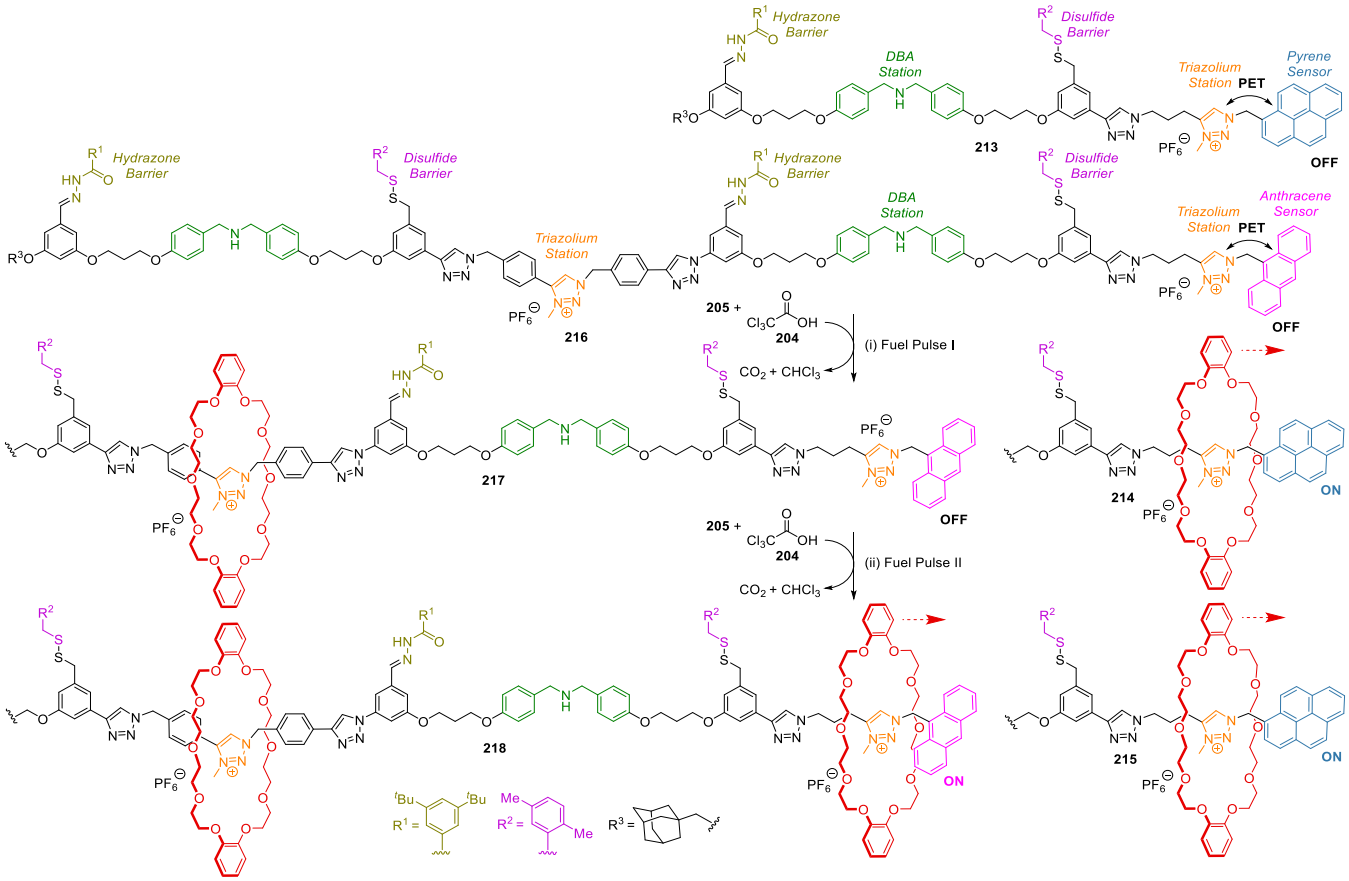

Scheme 8.19. Proposed simultaneous operation of an exemplary two component molecular pump system **213** and **216**. (i) Upon addition of chemical fuel pulse I and II, fluorescence of the pyrene pump **213** is transiently turned on in states **214** and **215** and complement by an additional temporary fluorescence signal of anthracene functionalised pump **218** (ii) upon addition of second pulse II.

Monitoring two component molecular pump system **213** and **216** with ^{1}H NMR would be averted by the pure number and limited separation of individual characteristic proton signals and most certainly, severely complicated by homonuclear couplings. Relying on an optical read out instead, it has been envisaged that the framework developed could ultimately enable operation and successfully monitoring of a multiple component system, i.e., a set of different molecular pumps. This could allow to explore more complex functional behaviour: If, for instance, two molecular pumps can be constructed that incorporate a different number of energy ratchet units their combined operation with a series of fuel pulses will give a unique fluorescence response that depends on the translation path of the macrocycle in different machines. In the case of the potential example depicted in Scheme 8.19 the application of the first chemical fuel pulse I leads to a temporal increase of fluorescence for machine **213** only, whereas for the second fuel pulse II both fluorescence sensors in **213** and **215** become active.

With this second target in mind the first goal of this project was to explore the formation of new anthracene stopper **219** and study its fluorescence properties in comparison to the literature (Scheme 8.20).[262b-c]

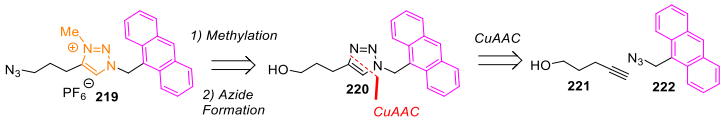

Scheme 8.20. Proposed retrosynthesis of an anthracene-functionalised stopper **219** with a triazolium station.

With regards to the synthesis, it has been suggested that the basic methyl triazolium motive may be constructed by alkylation with Meerwein's salt starting from the corresponding triazole, which itself may be formed by the CuAAC of 9-(azidomethyl)anthracene **222** to commercially available compound 4-pentyn-1-ol **221**. The required anthracene azide **222** in turn is reported to be synthesised through halide formation and following substitution with sodium azide[263] from commercially available 9-hydroxymethylanthracene or can be made by the reaction with azido-1,3-dimethylimidazolinium hexafluorophosphate (ADMP).[264] If applicable, this would allow proceeding to trial the construction of a 2-barrier pump **223** as outlined in Scheme 8.21.

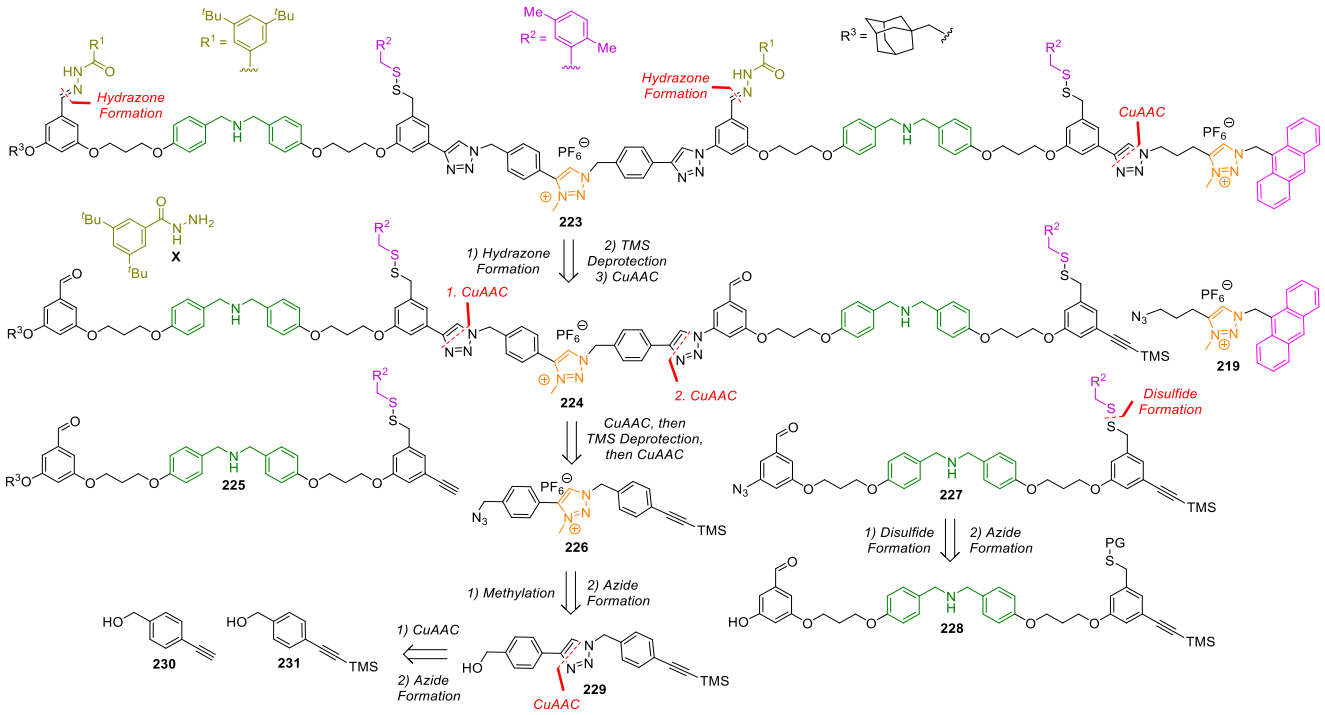

Scheme 8.21. Targeted retrosynthesis of 2-barrier molecular pump **223**.

The proposed principal framework is based on the original chemical building blocks of the molecular motor **200** and pump **206** concept[213] and their synthesis is used as a guideline to shape energy ratchet fragments **225** (left part) and **227** (right part). Furthermore, a bifunctional triazolium unit **226** (middle part) is introduced whose preparation is envisaged to mirror those described for the anthracene stopper **219** to connect the two components **225** and **227** by means of a successive twofold CuAAC reaction via intermediate deprotection of an alkyne:[265] First, connecting the left energy ratchet unit **225** with the middle unit **226** by CuAAC and second, removing the TMS-protecting group in order to subsequently enable the addition of the terminal alkyne to the right ratchet unit **227** by another CuAAC reaction. As a last step, the anthracene stopper **219** will be introduced via second TMS deprotection followed by another CuAAC. Once successfully assembled the operation of targeted 2-barrier pump will be investigated with ^{1}H NMR. In addition to this, the influence of different macrocycles such as DB30C10 **205** on the fluorescence of the anthracene unit will be explored. Optionally, in combination with another orthogonal fluorophore successful results would then potentially allow for proposed combined operation of a 1- and 2-barrier pump system.

8.4. Results and Discussion

8.4.1. UV-vis and Fluorescence Studies of an Anthracene Stopper

Addressing the synthesis of terminating anthracene stopper **219**, as a first step, 9-(azidomethyl)anthracene **222** was prepared starting from commercially available 9-anthracenemethanol **232** (Scheme 8.22). The treatment with ADMP reagent[264] was conducted at lower temperatures to avoid the decomposition of the product under basic reaction conditions The obtained azide was then used to form the corresponding triazole **220** with 4-pentyn-1-ol via CuAAC, which when treated a second time with ADMP afforded primary azide **233** in very good yields. Last, methylation with Meerwein's salt provided the triazolium stopper **219** as the either the $PF6^-$ or TFA^- salt in an overall yield of 29% or 28% over four steps, respectively.

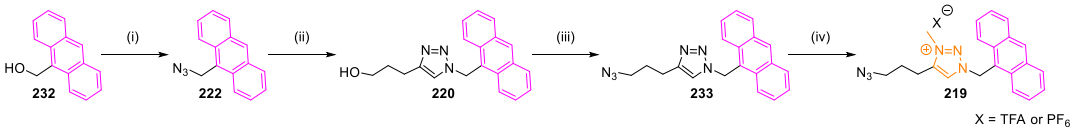

Scheme 8.22. Synthesis of anthracene stopper **219**. Reagents and conditions: (i) ADMP, DBU, THF, –10 °C, 85 min, 49%. (ii) 4-pentyn-1-ol, $[Cu(CH_3CN)_4]BF_4$, CH_2Cl_2:^{t}BuOH, rt, 15 h, 93%. (iii) ADMP, DBU, THF, 0 °C, 145 min, 88%. (iv) Me_3OBF_4, CH_2Cl_2, 0 °C, 1 h, then KPF_6, THF, rt, 15 min or anion-exchange (amberlyst A26/TFA^-, CH_3CN), 73% (X = PF_6) or 70% (X = TFA).

With a series of anthracene fluorophores in hand, the study of their optical properties was performed to establish the basis for monitoring operations with fluorescence spectroscopy (Figure 8.13). Taking 9-anthracenemethanol **232** as a reference, it has been found that despite similar absorption properties, introduction of the methyl triazolium motive in **219** significantly reduces the fluorescence intensity by a factor of approximately 25, if measuring solutions at equal absorption levels. In contrast to this, the non-methylated triazole derivative **220** shows about a threefold increase in fluorescence over reference 9-anthracene-methanol **232** both at near identical concentration and absorption level. This demonstrated that the fluorescence signal of the anthracene fluorophore with a main absorption maximum at λ = 254 nm and observed three fluorescence peaks at λ_{max} = 388, 411 and 435 nm is highly sensitive to the chemical environment of the triazole/triazolium motive. Based on this observation, it seemed likely that binding of a crown ether macrocycle to this unit would also have an effect on the fluorescence during the operation of the molecular pump in line with previously reported observations.[262b-c]

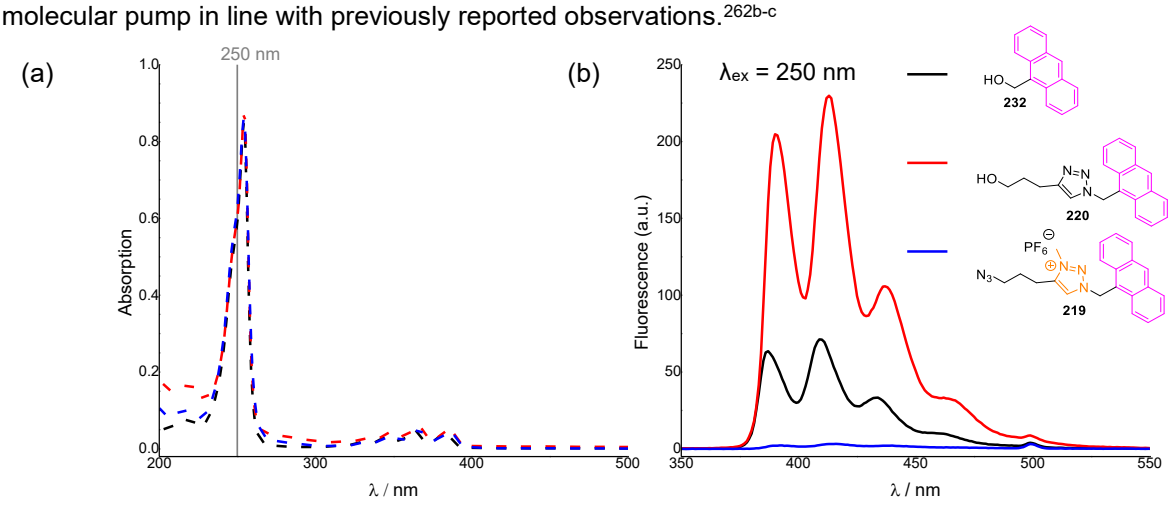

Figure 8.13. Comparing the absorption and fluorescence properties of a series of anthracene-functionalised stopper precursors. (a) UV-vis absorption spectra (CH_3CN, rt) of anthracene stopper precursors **232** (5.6 μM), **220** (5.7 μM) and **219** (2.8 μM). (b) Corresponding fluorescence emission spectra (CH_3CN, rt, λ_{ex} =

250 nm, $\Delta\lambda_{ex}$ = 2.5 nm, $\Delta\lambda_{em}$ = 2.5 nm, A(250 nm) ~ 0.6) for the same solutions of precursors in CH_3CN that were used for UV-vis measurements. Despite similar absorption properties proximity of the methyl triazolium to the anthracene unit of compound **219** (blue) efficiently quenches fluorescence compared to 9-anthracenemethanol **232** (black). An increased fluorescence intensity is observed for triazole bearing anthracene derivative **220** (red) compared to 9-anthracenemethanol **232**.

Encouraged by this observation, the synthesis of the common DBA building block for the creation of left **225** and right energy ratchet part **227** has been undertaken in accordance with previous literature procedures. (Scheme 8.23).[213] First, benzylic amine **235** was prepared from commercially available **234**, by sequential alkylation with 3-bromo-1-propanol then reduction with $LiAlH_4$ in an overall yield of 75%. Aldehyde **237** was made similarly by Williamson ether synthesis of **236** with 3-bromo-1-propanol followed by protection with TBDMS-Cl to give aldehyde **237** in a yield of 52%. With the two intermediates in hand, next, the secondary amine **238** was formed using an adapted two-step reductive amination procedure:[266] First, by condensation of **235** and **237** and then reduction of the generated imine with sodium borohydride. The obtained amine **238** was subsequently protected as *t*-butyl carbamate (Boc). Last the primary alcohol group of Boc-protected amine **238** was converted to the corresponding mesylate **239** with the aid of methanesulfonyl chloride (MsCl).

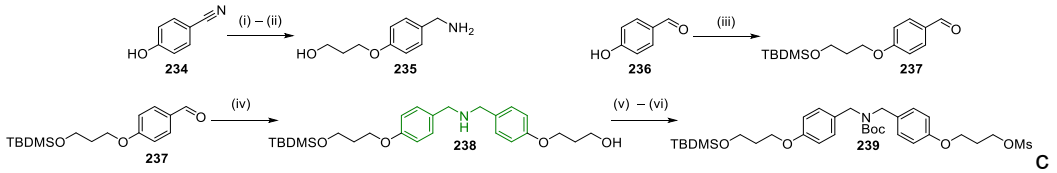

Scheme 8.23. Synthesis of TBDMS-protected DBA fragment **239**. Reagents and conditions: (i) 3-bromo-1-propanol, K_2CO_3, MeCN, 85 °C, 22 h, 77%. (ii) $LiAlH_4$, THF, 0 to 60 °C, 17 h, 97%. (iii) 3-bromo-1-propanol, K_2CO_3, MeCN, 85 °C, 20 h, then TBDMS-Cl, Et_3N, CH_2Cl_2, rt, 27 h, 52% over two steps. (iv) $MgSO_4$, EtOH, THF, rt, 22 h, then $NaBH_4$, 0 °C to rt, 135 min, 72%. (v) Boc anhydride, CH_2Cl_2, rt, 18 h, 74%. (vi) MsCl, CH_2Cl_2, 0 °C, 90 min, 89%.

With this fragment in hand, the synthesis of the alkyne-terminated disulfide barrier precursor **244** was conducted. The six step procedure developed by M. Dommaschk (Scheme 8.24)[267] starts from commercially available methyl 3-bromo-4-ethoxy-5-methoxybenzoate **240** and begins with the protection of the phenol alcohol as the TBDMS ether, followed by palladium-catalysed Sonogashira coupling with mono protected ethynyl(trimethyl)silane to afford the corresponding methyl ester **241** in 75% over two steps. The following series of reduction, Appel, and substitution reactions yields **243**, which when deprotected with TBAF gives the desired trityl-protected benzyl mercaptan **244** in a yield of 46% over four steps.

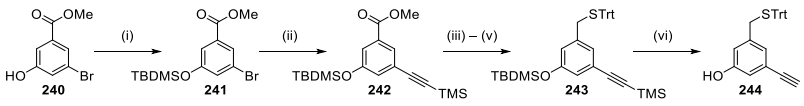

Scheme 8.24. Six-step synthesis of trityl-protected benzyl thiol **244**.[267] Reagents and conditions: (i) TBDMS-Cl, imidazole, CH_2Cl_2, rt, overnight, 96%. (ii) ethynyl(trimethyl)silane, CuI, $Pd(PPh_3)Cl_2$, Et_3N, DMF, 65 °C, overnight, 78%. (iii) $LiAlH_4$, THF, 0 °C to rt, 2 h, then (iv) PPh_3, CBr_4, CH_2Cl_2, 0 °C, 80% over two steps. (v) Trt-SH, Et_3N, DMF, rt, quantitative. (vi) TBAF, THF, rt, 90 min, 57%.

Next, the construction of the left energy ratchet part **225** was performed by repeating the synthesis of adamantane-functionalised 3,5-dihydroxybenzaldehyde **247** and its dimethyl acetal analogue **248** (Scheme 8.25). Compared to the 42% yield reported in the original publication[213] a significantly lower yield of 18% was noticed for the desymmetrisation of 3,5-dihydroxybenzyl alcohol with 1-adamantane methyl bromide via

Williamson ether synthesis (step (ii) in Scheme 8.25). Based on the analysis of the crude for benzyl alcohol **246** this was mainly due to the formation of disubstituted counterparts. Attempts to address this issue by a change of base or polar solvent, however, were not effective and merely left starting material **245** unconverted. Due to later progression of the project the causes for this problem were not further investigated. Continuing with the material the remaining synthesis was completed by oxidizing benzylic alcohol **246** to **247** with manganese oxide and then protecting aldehyde **247** with the aid of trimethyl orthoformate and *p*-toluenesulfonic acid pyridine salt (PPTS). Finishing this last step allowed isolating the desired adamantane barrier fragment **248** in overall four steps in a total yield of 10% from starting 1-adamanatane methanol **245**.

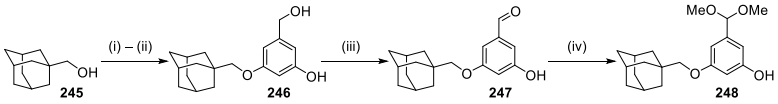

Scheme 8.25. Synthesis of adamantane aldehyde **247** and acetal **248** based on literature protocols.[213] Reagents and conditions: (i) $ZnBr_2$, aq. HBr, neat, 125 °C, 16 h, 97%. (ii) 3,5-dihydroxybenzyl alcohol, K_2CO_3, DMF, 120 °C, 4 d, 18%. (iii) MnO_2, acetone, rt, 105 min, 75%. (iv) $(MeO)_3CH$, PPTS resin, MeOH, 65 °C, 7 h, then Et_3N, rt, 5 min, 76%.

With the building blocks **239**, **244** and **248** in hand, the synthesis of the left energy ratchet part **225** was undertaken (Scheme 8.26). At first, DBA mesylate **239** was combined with trityl-protected benzyl mercaptan **244** using Williamson ether synthesis. This has furnished intermediate **249** whose second alcohol functionality has been subsequently activated via removal of the TBDMS-protecting group with TBAF and then conversion into corresponding mesylate **250** with MsCl. The obtained mesylate was then taken forward to a second Williamson ether synthesis reaction with adamantane dimethyl acetal **248**. Despite losing the acetal protection group this ultimately afforded the left part **251** in excellent yield.

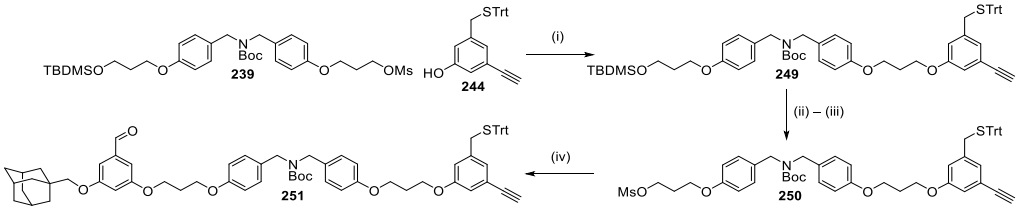

Scheme 8.26. Synthesis of left energy ratchet part **251**. Reagents and conditions: (i) Cs_2CO_3, DMF, 40 °C, 20 h, 62%. (ii) TBAF, THF, rt, 35 min, 83%. (iii) MsCl, Et_3N, CH_2Cl_2, 0 °C, 35 min, 90%. (iv) adamantane dimethyl acetal **248**, Cs_2CO_3, DMF, 40 °C, 20 h, 99%.

Next, the synthesis of the middle part **226** was carried out (Scheme 8.27). Benefiting from the direct resemblance of compound **226** to anthracene azide **219** its synthesis has paralleled previously described protocols for the preparation of the anthracene stopper (Scheme 8.22). Beginning with the CuAAC of TMS-protected 4-ethynylbenzyl azide **252** to 4-ethynylbenzyl alcohol, the corresponding benzylic triazole alcohol **253** was obtained. which when reacted with ADMP gave the benzylic azide in 78%. As a last step, the triazole unit was methylated with trimethyloxonium tetrafluoroborate[255a] to afford final middle triazolium part **226** in an overall yield of 32%.

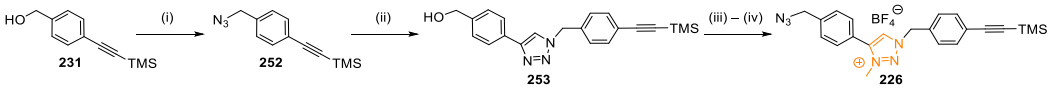

Scheme 8.27. Synthesis of triazolium part **226**. Reagents and conditions: (i) ADMP, DBU, THF, rt, 150 min, 87%. (ii) 4-ethynylbenzyl alcohol, $[Cu(CH_3CN)_4]PF_6$, TBTA, CH_2Cl_2:^{t}BuOH, rt, 17 h, 54%. (iii) ADMP, DBU, THF, rt, 60 min, 78%. (iv) Me_3OBF_4, CH_2Cl_2, 0 °C to rt, 60 min, 86%.

Following this, another CuAAC reaction between the middle part **226** and the left energy ratchet part **251** was performed to give **254** as a mixture of the aldehyde and corresponding methyl hemiacetal as well as dimethyl acetal – presumably as a result of the chromatographic purification when using MeOH as an eluent (Scheme 8.28).

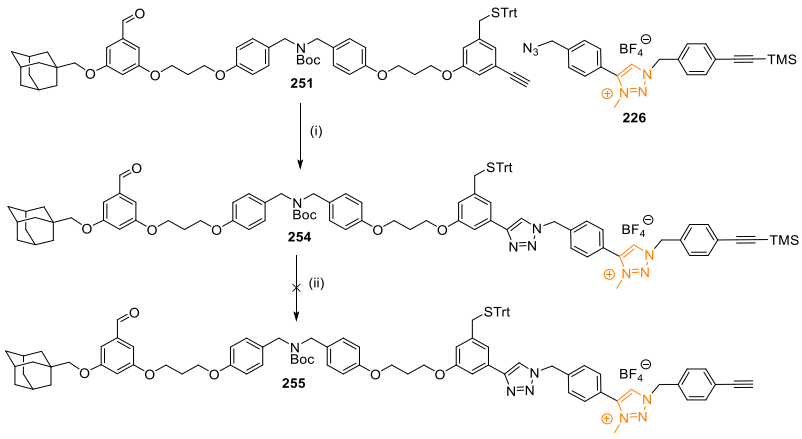

Scheme 8.28. Attempted synthesis of intermediate **255** combining left energy ratchet part **251** and middle triazolium part **226**. Reagents and conditions: (i) $[Cu(CH_3CN)_4]BF_4$, TBTA, CH_2Cl_2:^{t}BuOH, rt, 15 h, 86% obtained as a mixture of aldehyde, methyl hemiacetal, and dimethyl acetal in a ratio of 2:1:3 as determined by NMR. (ii) trialled conditions: K_2CO_3 , MeOH:CH_2Cl_2; or TBAF/TSAF, THF; or F^- on polymer, CH_2Cl_2, rt.

Despite this minor complication an initial test reaction for the removal of the TMS-group was conducted using ^{1}H NMR for analysis. However, regardless of the trailed deprotection methods employed that are known to preserve the trityl group while simultaneously taking of the TMS group,[268] such as when employing either mild basic conditions (K_2CO_3 in MeOH/CH_2Cl) or a fluoride reagent such as tris(dimethylamino)sulfonium difluorotrimethylsilicate (TSAF), TBAF or basic fluoride on an anion-exchange resin (fluoride on amberlyst A-26), the results of the deprotection have remained inconclusive. While the loss of the signal related to the TMS-group was indeed observed via ^{1}H NMR, at the same time, the formation of a range of other unidentifiable signals both in the aromatic and alkylic regions of the spectra indicated decomposition of the material. In neither case, the starting material or the desired terminal alkyne product has been recovered.

To find out whether this unexpected reaction behaviour stems from the concomitant deprotection of the thiol motive and first and foremost, to further investigate the alkyne deprotection, a simplified model system **257** has been prepared in one step from **226** and 4-ethynylbenzaldehyde **256** (Scheme 8.29). This compound does not feature a thiol unit and thus if previous conditions were able to successfully remove the TMS group the positive result would hint at an incompatibility with either the trityl protecting or another functional group.

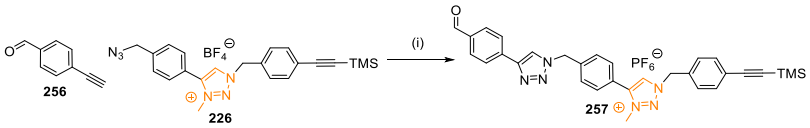

Scheme 8.29. Synthesis of model TMS-protected compound **257**. Reagents and conditions: (i) $[Cu(CH_3CN)_4]PF_6$, TBTA, CH_2Cl_2:^{t}BuOH, rt, 17 h, then KPF_6, THF, rt, 15 min, quantitative.

Repeating the original conditions, the deprotection of compound **257** was indeed observed when monitoring the reaction with ^{1}H NMR. For example, in case of using potassium carbonate as a means for the removal of the silyl protecting group (Scheme 8.30 and Figure 8.14) simultaneous with the disappearance of the

signals related to protons H_{23} and shift of protons H_{15}, and H_{18} a new signal at ~ 0.1 ppm appeared (TMS_2O), which suggested the successful liberation of free (conjugated) alkyne **258**. Similar observations have been with other conditions. The accompanying appearance of additional signals in the reaction shown in Figure 8.14 was traced back to a tris(benzyltriazolylmethyl)amine (TBTA)[270] contamination picked up from the CuAAC. Still, even when removed results for the TMS deprotection have remained identical.

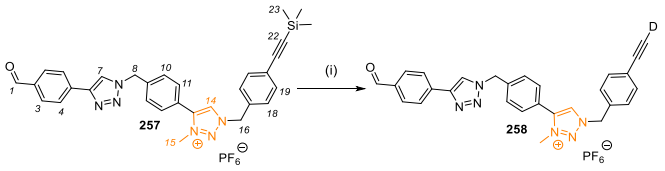

Scheme 8.30. Deprotection of model TMS-protected compound **257**. Reagents and conditions: (i) K_2CO_3, $MeOD:CD_2Cl_2$, rt, 72 h, yield has not been determined.

While these results (re)affirmed the possibility for the intermediate deprotection of the TMS-protected alkyne in presence of a triazole, methyl triazolium and an aldehyde group, it was concluded that to solve the original problems seen for the envisaged deprotection compound **254** an additional effort would be required to find out the actual cause for previous sample decomposition. Given the stability of the Boc-protecting group and the limited reactivity of the adamantyl substituent it seemed likely that the reaction is mainly limited by trityl-protected mercaptan. Yet, to confirm this assumption, further testing would have been required and requisite additional investigations on the reported twofold sequential CuAAC reaction:[265]

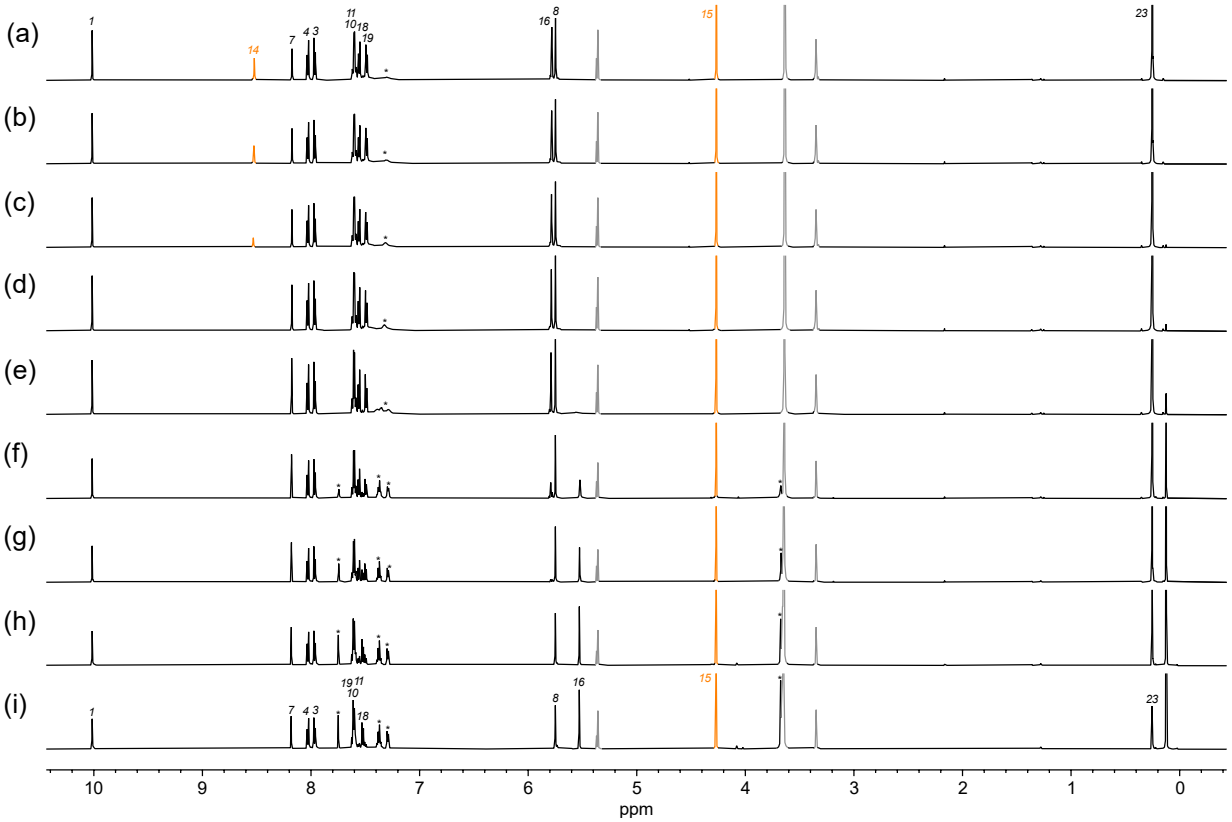

Figure 8.14. Deprotection of TMS-protected model compound **257** with K_2CO_3 in $MeOD:CD_2Cl_2$. Partial ^1H NMR spectra (600 MHz, $MeOD:CD_2Cl_2$ (1:1), 298 K) of (a) model compound **257** (8.5 mM) and (b) upon addition of K_2CO_3. After intervals of (c) 1 h, (d) 2 h, (e) 4 h, (f) 18 h, (g) 36 h, (h) 60 h and (i) 72 h. Labelling corresponding to Scheme 8.30. Peaks of the final spectrum have been assigned with help of additional 2D ^{13}C–^1H correlation experiments. Peaks marked with asterisks (*) correspond to a TBTA contaminant. (Identified with literature values reported for TBTA in reference 270)

8.4.2. 1st Generation Model Pump Design with an Anthracene Stopper

Due to these immediate complications in the synthesis of **223**, we instead turned our attention to the study of the proposed PET effect with 1-barrier pseudo[2]rotaxane pump **260/260**·H⁺ (Scheme 8.31).

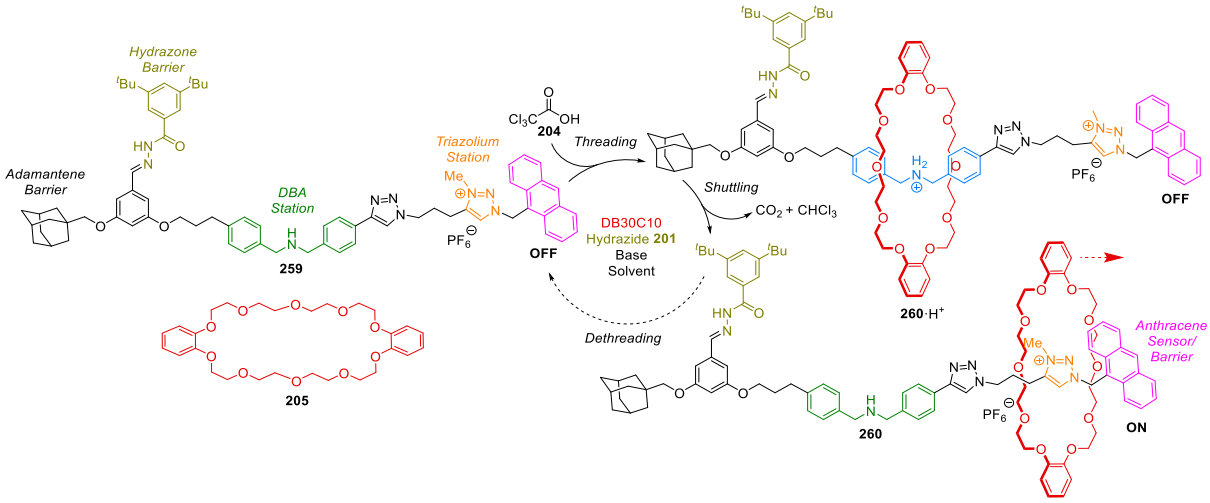

Scheme 8.31. Proposed operation of chemically fuelled crown ether rotaxane pump **260/260**·H⁺ using switchable fluorescence to determine the dethreading kinetics over an anthracene barrier.

In this simplified system the disulfide barrier component of the original 2-barrier design was removed to avoid problems with the synthesis. The updated design relies on the steric effect of an anthracene group and concomitant energy barrier to ensure a unidirectional threading process similar to other pump concepts.[208,211] Besides this, basic building blocks have remained unchanged and it was envisaged that the preparation of the new thread **259** would follow those of the previous design (for its retrosynthesis see Scheme 8.32).

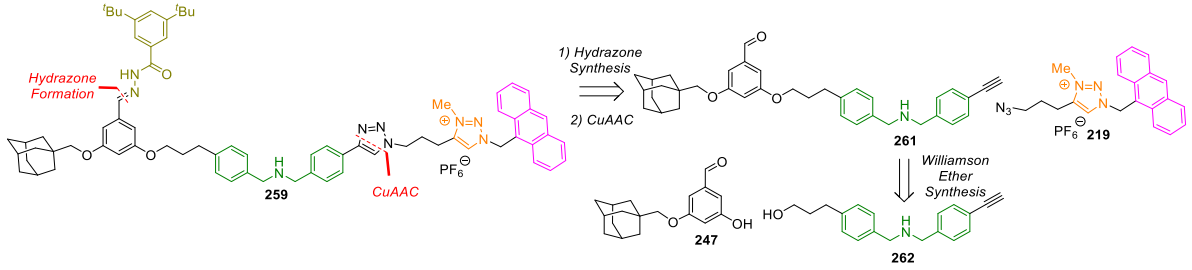

Scheme 8.32. Proposed retrosynthesis of model 1-barrier pump **259** starting from DBA fragment **262** and previously described adamantane aldehyde **247** and anthracene stopper **219**.

Using the adamantyl group as an additional means to prevent macrocycle DB30C10 **205** from moving over the hydrazone barrier, it was hoped that this would direct dethreading of the macrocycle over the anthracene barrier. In addition to it, the incorporation of an already available DBA fragment **262** has been suggested.[271] Bearing an alcohol and the alkyne group this compound offers a basic platform for attaching both adamantane aldehyde **247** and anthracene stopper **219** with previous methods. It was anticipated that once threading with DB30C10 **205**, successfully monitoring the kinetics of the dethreading reaction of the formed bistable (pseudo)[2]rotaxane **260/260**·H⁺ system with fluorescence spectroscopy would then provide a basic understanding of the anticipated PET switching – and concomitantly, shine light on the chemically fuelled pump's transport process. Provided the successful operation of this system, it would establish the essential framework to then allow revisiting the original two component system with an alternative synthetic approach.

In order to access model 1-barrier pump **260**/**260**·H$^+$, we utilised dibenzyl ammonium fragment **261** that was previously developed in the group by S. Kassem (Scheme 8.33).[271]

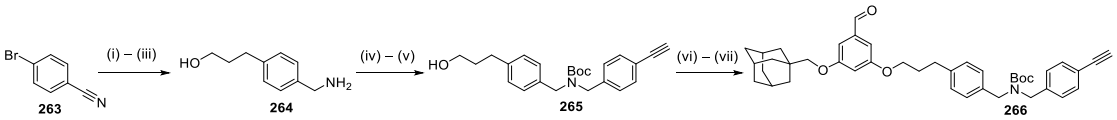

Scheme 8.33. Synthesis of pump fragment **266** from 4-bromobenzonitrile **263** and 4-ethynyl benzaldehyde **256**.[271] Reagents and conditions: (i) propargyl alcohol, $Pd(OAc)_2$, PPh_3, CuI, *N*-butylamine, THF, rt, 4 h, 90%. (ii) H_2, Pd/C, rt, 18 h, 95%. (iii) $LiAlH_4$, THF, 65 °C, 18 h, quantitative. (iv) 4-ethynyl benzaldehyde, STAB, Na_2SO_4, MeOH, rt, 3 h, then (v) Boc_2O, CH_2Cl_2, rt, 16 h, over two steps 80%. (vi) MsCl, Et_3N, THF, 4 h, then (vii) adamantyl aldehyde **247**, Cs_2CO_3, DMF, rt, overnight, 90% over two steps.

The precursor **266** is readily synthesised from 4-bromobenzonitrile **263** by palladium-catalyzed Sonogashira cross-coupling reaction with propargyl alcohol, followed by heterogeneous reduction of the alkyne with hydrogen, subsequent reduction of the nitrile group with $LiAlH_4$ and final reductive amination with 4-ethynyl benzaldehyde. The nonsymmetric dibenzyl amine **262** was further protected as *t*-butyl carbamate to give intermediate **265**, which when activated as the mesylate, allowed carrying out the Williamson ether synthesis with adamantyl aldehyde **266**. Completing this step afforded pump fragment **266** in 62% over seven steps. The anthracene stopper **219** was clicked directly to **266** to give the Boc-protected thread in one step (Scheme 8.34). The Boc-protecting group was then cleaved with TFA to give dibenzyl ammonium salt **267**·H$^+$.

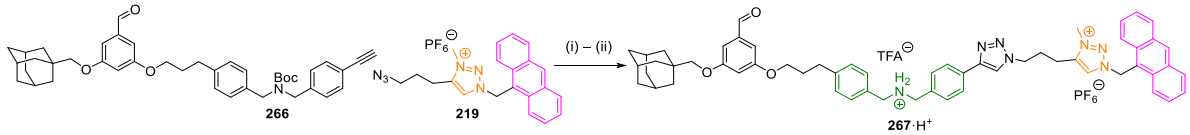

Scheme 8.34. Synthesis of anthracene pump **267**·H$^+$ from DBA mesylate **266** and stopper **219**. Reagents and conditions: (i) $[Cu(CH_3CN)_4]BF_4$, DMSO-d_6, 75 °C, 6 h, 47%. (ii) TFA, CH_2Cl_2, 0 °C, 1 h, quantitative.

With aldehyde thread **267**·H$^+$ prepared and additional components in hand, initial threading studies were conducted. However, any attempts to confirm the (intermediary) formation of the postulated 1-barrier pseudorotaxane **260**·H$^+$ with ^{1}H NMR by first threading macrocycle DB30C10 **205** on the protonated thread **267**·H$^+$ and then capping with reported hydrazide **201**[213] have remained without success (Figure 8.15).

While the first step (i) was confirmed to take place as indicated by the characteristic upfield shifts of benzylic protons H_{20} and H_{21} by approximately 0.2 ppm (Figure 8.15 (b)) and the appearance of a new set of correlated signals H_a–H_f corresponding to threaded macrocycle, addition of hydrazide **201** was always accompanied by immediate precipitation of a sparingly soluble material. In those cases, where some of the remainder after filtration could be redissolved, further examination with ^{1}H NMR failed to provide evidence for the desired formation of pseudorotaxane hydrazone **260**·H$^+$ but rather suggested the isolation of deprotonated free thread hydrazone **259**. It has been reasoned that the cause for this issue is primarily the low solubility of formed hydrazones intensified by the triflate counterion which is known to promote aggregation in contrast to non-coordinating anions such as tetrafluoroborate BF_4 or hexafluorophosphate PF_6.[273]

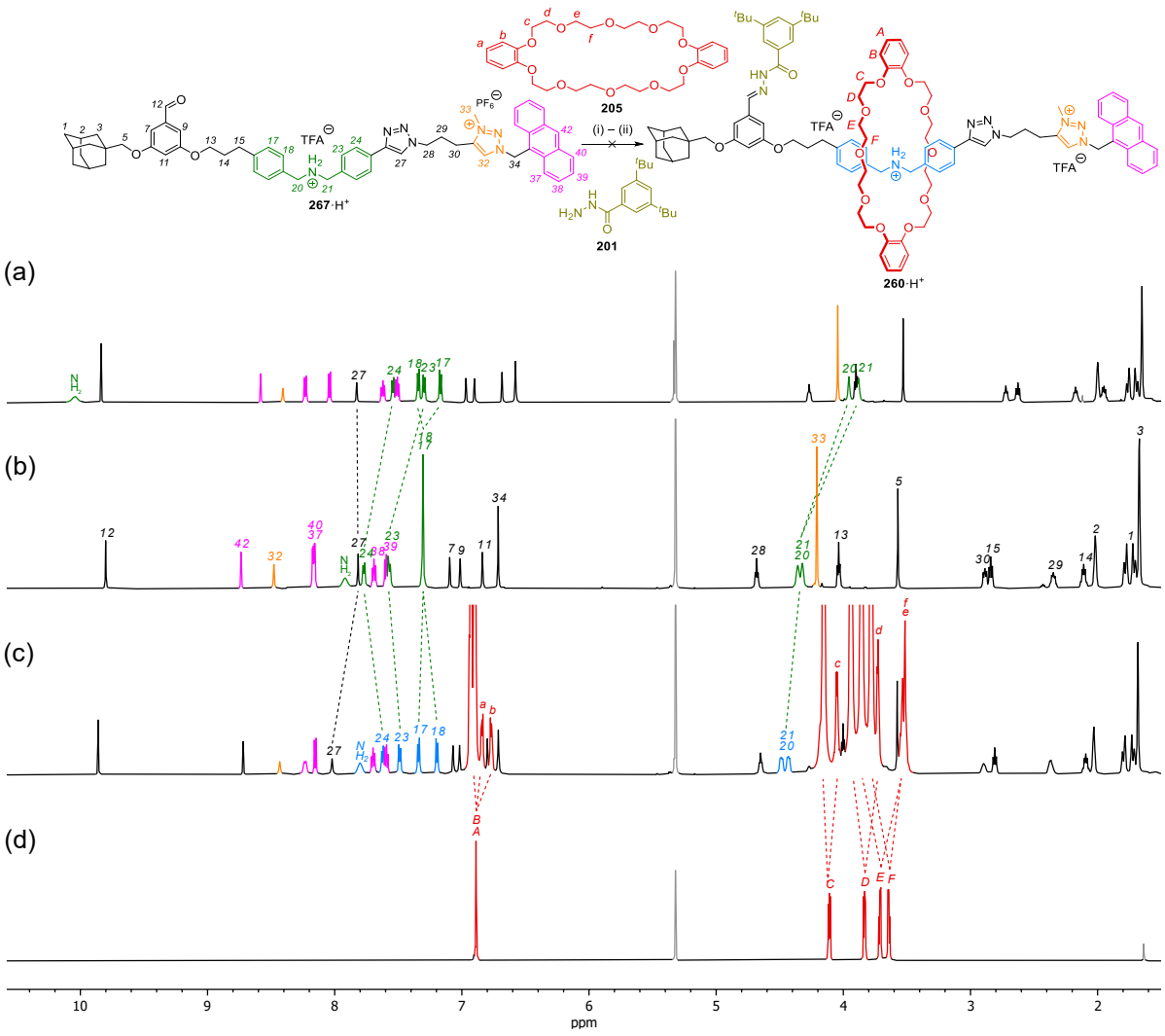

Figure 8.15. Attempted formation of 1-barrier model pseudorotaxane **260**·H⁺ (1st model pump design) ensuing from free thread **267**·H⁺ with macrocycle DB30C10 **205** and reported hydrazide **201**. Reagents and conditions: (i) TFA, DB30C10 **205**, CD_2Cl_2, rt, 2 h, then (ii) addition of hydrazide **201**. Partial ^{1}H NMR spectra (600 MHz, CD_2Cl_2, 298 K) of (a) free thread **267**·H⁺ (27 mM), after addition of (b) 20 equiv. of TFA and (c) 5 equiv. of macrocycle DB30C10. (d) Commercial sample of macrocycle DB30C10 **205**.

To overcome this limitation an alternative methyl glycol functionalised hydrazide **269** was synthesised by a two-step procedure from commercially available methyl 3,5-dihydroxybenzoate **268** to potentially increase solubility of formed hydrazones: First, by twofold alkylation of **268** and subsequently, by hydrazination of the resulting methyl ester in an overall yield of 84% over two steps (Scheme 8.35).

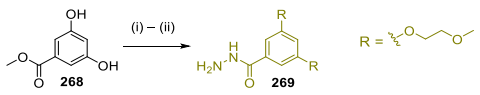

Scheme 8.35. Synthesis of glycol-functionalized hydrazide **269**. Reagents and conditions: (i) 1-bromo-2-methoxyethane, K_2CO_3, CH_3CN, 85 °C, 24 h, 88%. (ii) hydrazine monohydrate, MeOH, 60 °C, 3 d, 96%.

With hydrazide **269** in hand, original threading experiments with thread **267**·H⁺ were repeated. Pleasingly, upon addition of the new hydrazide **267** precipitation did not happen even when leaving the reaction over two days in the presence of excess hydrazide. Importantly, following the reaction with ^{1}H NMR spectra the disappearance of the (sharp) aldehyde signal paralleled characteristic shifted benzylic protons H_{20} and H_{21}

which indicated the retention of the interlocked architecture and, for the first time, suggested the formation of desired pseudo[2]rotaxane **260**·H⁺ (Figure 8.16).

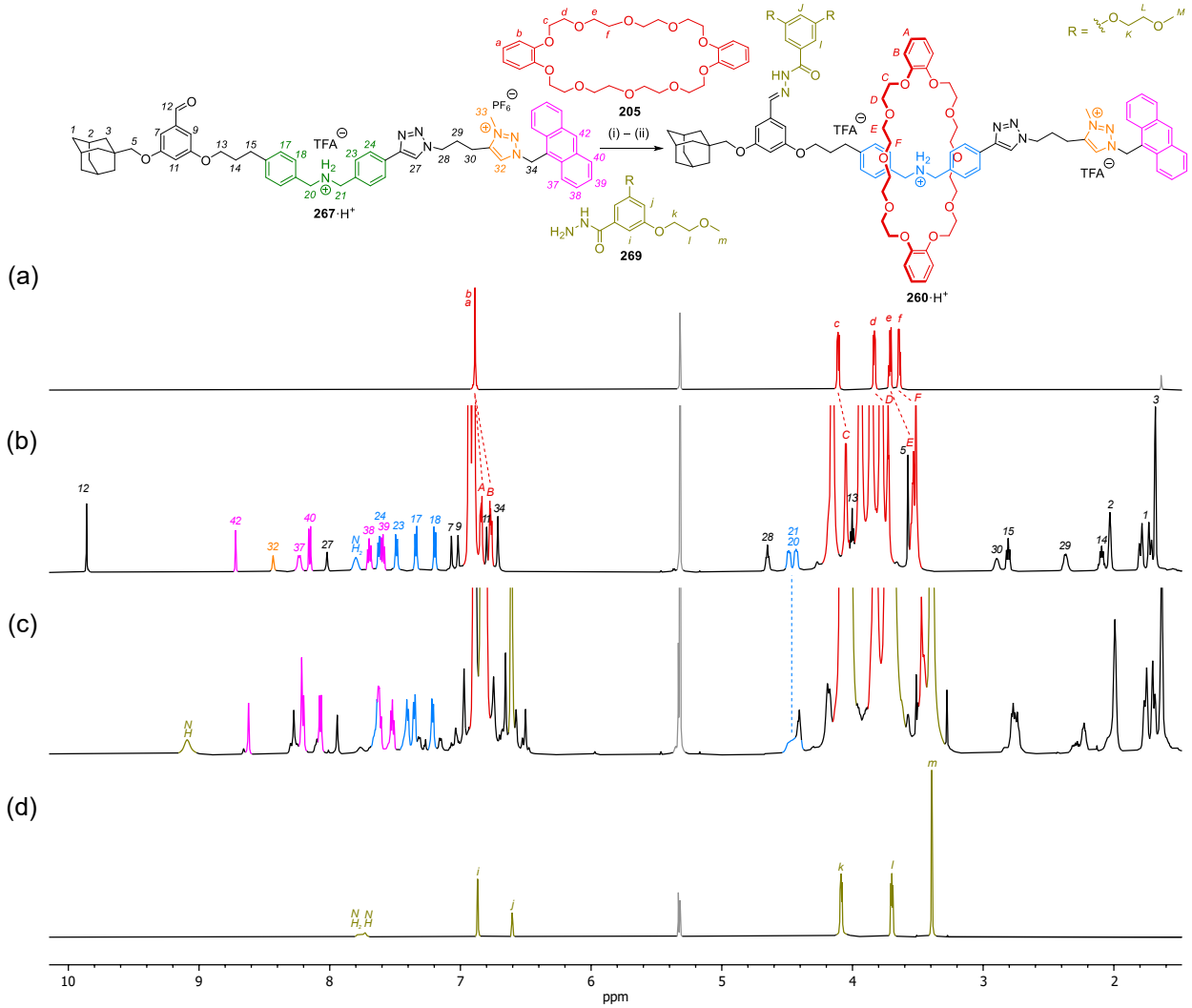

Figure 8.16. Reattempted synthesis of 1-barrier model pseudorotaxane **260**·H⁺ (1st model pump design) from free thread **267**·H⁺, DB30C10 **205** and alternative hydrazide **269**. Reagents and conditions: (i) TFA, DB30C10 **205**, CD_2Cl_2, rt, 2 h, then (ii) addition of hydrazide **269**. Partial ^{1}H NMR spectra (600 MHz, CD_2Cl_2, 298 K) of (a) isolated DB30C10 **205**, (b) free thread **267**·H⁺ (27 mM) in the presence of 20 equivalents of TFA and 5 equiv. of DB30C10 and (c) after addition of 10 equiv. of hydrazide **269**. (d) Hydrazide **269**.

Attempts to substantiate the proposed structure of *in-situ* generated pseudo[2]rotaxane **260**·H⁺ and further confirm the mechanism of the operation have been left without success. Any efforts to isolate the compound via chromatographic methods furnished only the deprotonated free thread hydrazone. Preliminary operation of the thread suggested that dethreading of the macrocycle **205** takes place immediately after addition of the base triethylamine to the crude reaction mixture on the order of the few minutes between the addition and obtaining an ^{1}H NMR spectrum. Furthermore, the interpretation of the crude with ^{1}H NMR spectroscopy has been severely complicated: Due to the presence of excess amounts of hydrazide **269** and macrocycle DB30C10 **205** and the significant signal overlap caused by these components, the critical window of characteristic benzylic protons H_{20} and H_{21} between 4.2 to 4.6 ppm has been almost entirely occluded (Figure 8.16 (c)). Moreover, the occurrence of additional signals, which has been attribute to anion-exchange from $PF6^-$ to TFA^- species, has rendered the taken integration values meaningless. As such, it was concluded that without an additional proof of the intermediate formation of pseudo[2]rotaxane **260**·H⁺ the first pump

system was unsuitable for further kinetic investigations with fluorescence spectroscopy. The main reason for this was first and foremost the lack of an alternative method for studying the operation beyond NMR to verify and also quantify the shuttling and dethreading process.

8.4.3. 2nd Generation Model Pump Design with an Anthracene Stopper

It was reasoned that if an alternative 1-barrier system could be found, which would allow for the separation of the pseudo[2]rotaxane from other system components, the study of the isolated complex would provide the opportunity for developing the operation conditions. Based on the data reported for the kinetic stability of a complexes between DBA motive and DB24C8 **173** [208,243,262d,274] (see Figure 8.17) it was inferred that the stability of the targeted pseudorotaxane system could be similarly increased if smaller macrocycles were used and the size of stopper was kept constant, instead, to refrain from modifying the anthracene stopper.

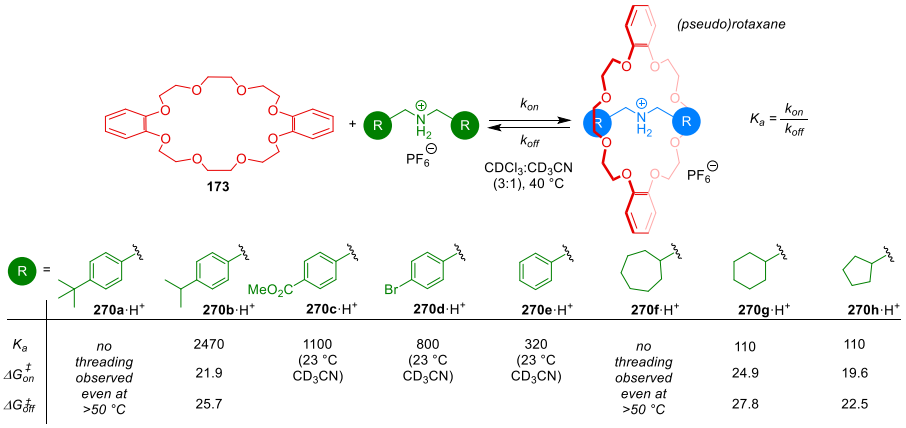

	270a·H+	270b·H+	270c·H+	270d·H+	270e·H+	270f·H+	270g·H+	270h·H+
K_a	*no threading observed even at >50 °C*	2470	1100 (23 °C CD_3CN)	800 (23 °C CD_3CN)	320 (23 °C CD_3CN)	*no threading observed even at >50 °C*	110	110
$\Delta G^{\ddagger}_{on}$		21.9					24.9	19.6
$\Delta G^{\ddagger}_{diff}$		25.7					27.8	22.5

Figure 8.17. Determining the thermodynamics and kinetics of the pseudorotaxane formation via a slipping mechanism with macrocycle DB24C8 **173** and a range of secondary dialkyl- and dibenzyl ammonium salts **270a-h** using ^{1}H NMR.[243,274] Based on the observations reported the stability of detected 1:1 complex is influenced primarily by the steric effects of the different alkyl and benzyl substituents. For example, if threads with either a large t-butyl (**270a**·H$^+$) or a cycloheptyl moiety (**270f**·H$^+$) are employed no mechanically interlocked structure is found even after heating the two components at 50 °C. In contrast, applying a slightly smaller cyclohexyl derivative **270g**·H$^+$ a kinetically stable pseudo[2]rotaxane is formed.

Following this rationale, it was expected that if utilising the next smaller alkylic homologue of DB30C10 in the series of reported crown ethers i.e. macrocycle 27-crown-9 (27C9) **271**, the concomitant increase in the relative energy barrier with respect to the anthracene group would be sufficient to enable isolation of a [2]rotaxane. At the same time, to address the solubility issues encountered with the previous design, the design of the thread has been modified, too (Scheme 8.36).

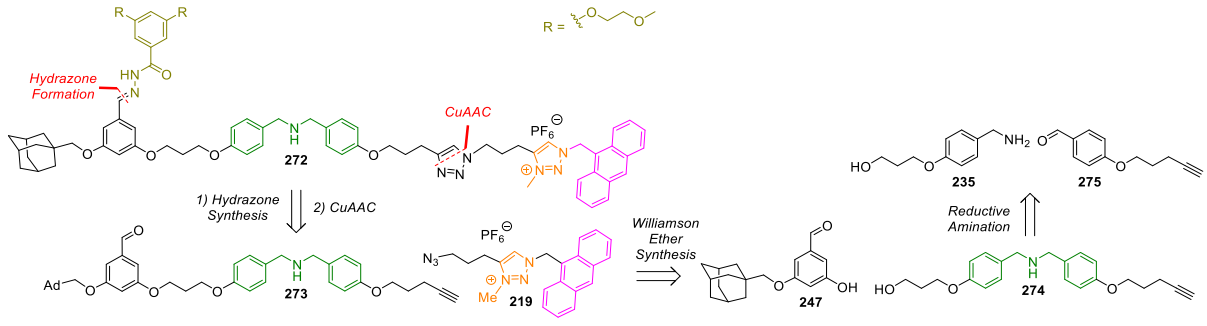

Scheme 8.36. Proposed retrosynthesis of alternate model 1-barrier pump **272**/**272**·H$^+$ (2nd model pump design), starting from elongated DBA fragment **274** and previously described adamantane aldehyde **247** and

anthracene stopper **219**. The synthesis of the DBA unit **274** relies of the reductive amination between established benzyl amine **235** and 1-pentynyl-functionalised aldehyde **275**.

The new thread **272** includes an additional propyl ether connection between the DBA motive and the triazole motive to increase solvent accessibility and provide a more flexible alkyne link for the introduction of anthracene stopper **219**. To begin with the preparation of the altered DBA motive, first of all the alkylation of 4-hydroxybenzaldehyde **276** with pentynyl tosylate was conducted (Scheme 8.37). Completing this step, the required aldehyde **275** was afforded in yields up to 95% and allowed to proceed with the reductive amination of already available benzyl amine **235**. Repeating the previously employed two-step condensation and reduction approach secondary amine **274** was successfully isolated. And after protection with the Boc anhydride and activation with MsCl, building block **277** was obtained in 78% yield over four steps.

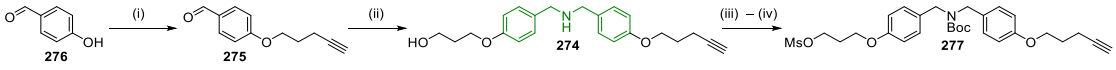

Scheme 8.37. Synthesis of DBA alkyne fragment **277**. Reagents and conditions: (i) pent-4-yn-1-yl tosylate, K_2CO_3, MeCN, 85 °C, 20 h, 95%. (ii) benzyl amine **235**, $MgSO_4$, MeOH, THF, rt, 15 h, then $NaBH_4$, 0 °C to rt, 1 h. (iii) Boc anhydride, CH_2Cl_2, rt, 23 h, 86% over two steps. (iv) MsCl, CH_2Cl_2, 0 °C, 70 min, 95%.

Next, DBA mesylate **277** was forwarded to a Williamson ether synthesis reaction with adamantane acetal **248** to yield acetal product **278** in 67% (Scheme 8.38). Bringing together with the anthracene stopper **219**, the triazole was formed using copper-catalysed click chemistry. Finally, the Boc-protecting group was removed under acidic conditions with TFA to furnish the protonated thread **280**·H^+ after salt-exchange.

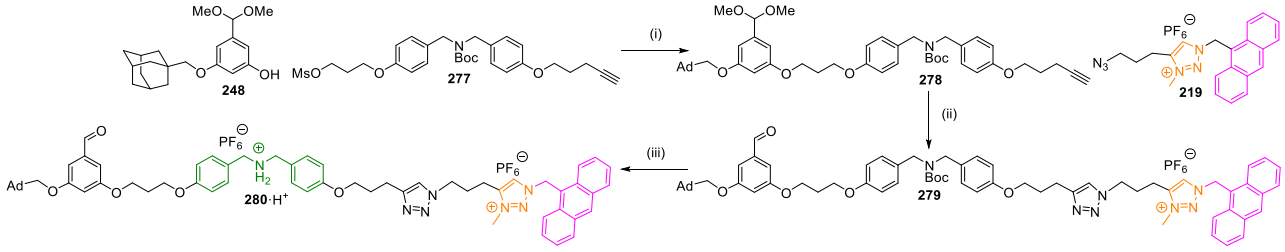

Scheme 8.38. Synthesis of second model anthracene 1-barrier pump **280**·H^+ (2nd model pump design). Reagents and conditions: (i) Cs_2CO_3, DMF, 50 °C, 16 h, 67%. (ii) $[Cu(CH_3CN)_4]BF_4$, DMSO-d_6, 75 °C, 3 h, then KP_6, THF, 15 min, 83%. (iii) TFA, CH_2Cl_2, 0 °C, 1 h, then KP_6, THF, 25 min, quantitative.

Reusing the previously prepared glycol-functionalized hydrazide **269** for the targeted threading studies, the synthesis of the remaining crown ether macrocycle 27C9 was attempted based on earlier reports in the literature (Figure 8.18).[275] Although, the literature procedure, when repeated, gave macrocycle **271** in sufficient amounts, the persistent contamination with unreacted tosylate by products has shown to complicate the initial threading studies (see e.g. Figure 8.19 (d)): For example, it occurs that a spurious proton signal at 4.1 ppm coincides with the expected characteristic protons signals for the benzylic methylene group H_{20} and H_{21} when bound with 27C9. To avoid misinterpretation and to afford **271** in higher purity, the crude has therefore been reacted further with tosyl chloride (TsCl) and hydrazine prior to the separation to facilitate removal of **283** and similar oligomer by products. Although this step reduces the yield of isolated macrocycle, the protocol developed has shown to be superior to other purification techniques examined.

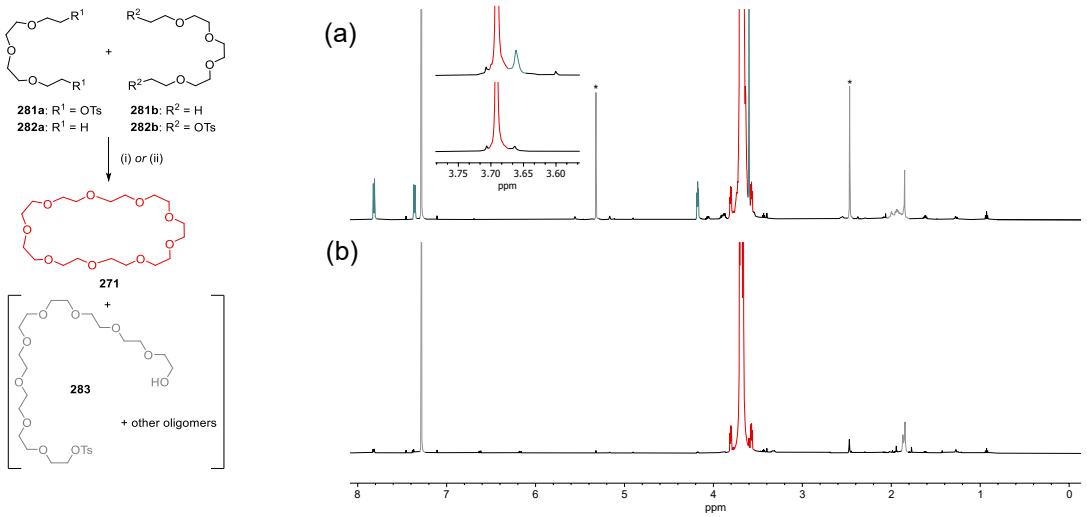

Figure 8.18. Improved synthesis of macrocycle 27C9. Reagents and conditions: (i) NaH, THF, rt, 2 d, 50%. (R^1 = OTs, R^2 = H) (ii) NaH, THF, rt, 7 d, then TsCl, NaH, rt, 1 d, then TsCl, DIPEA, rt, 20 h, then hydrazine, MeOH, rt, 5 h, 34%. (R^1 = H, R^2 = OTs) Corresponding ^{1}H NMR (600 MHz, $CDCl_3$, 298 K) with 27C9 **271** obtained by (a) the reported purification procedure[275] and (b) after additional chemical treatment.

With both new components available threading experiments have been repeated (Figure 8.19).

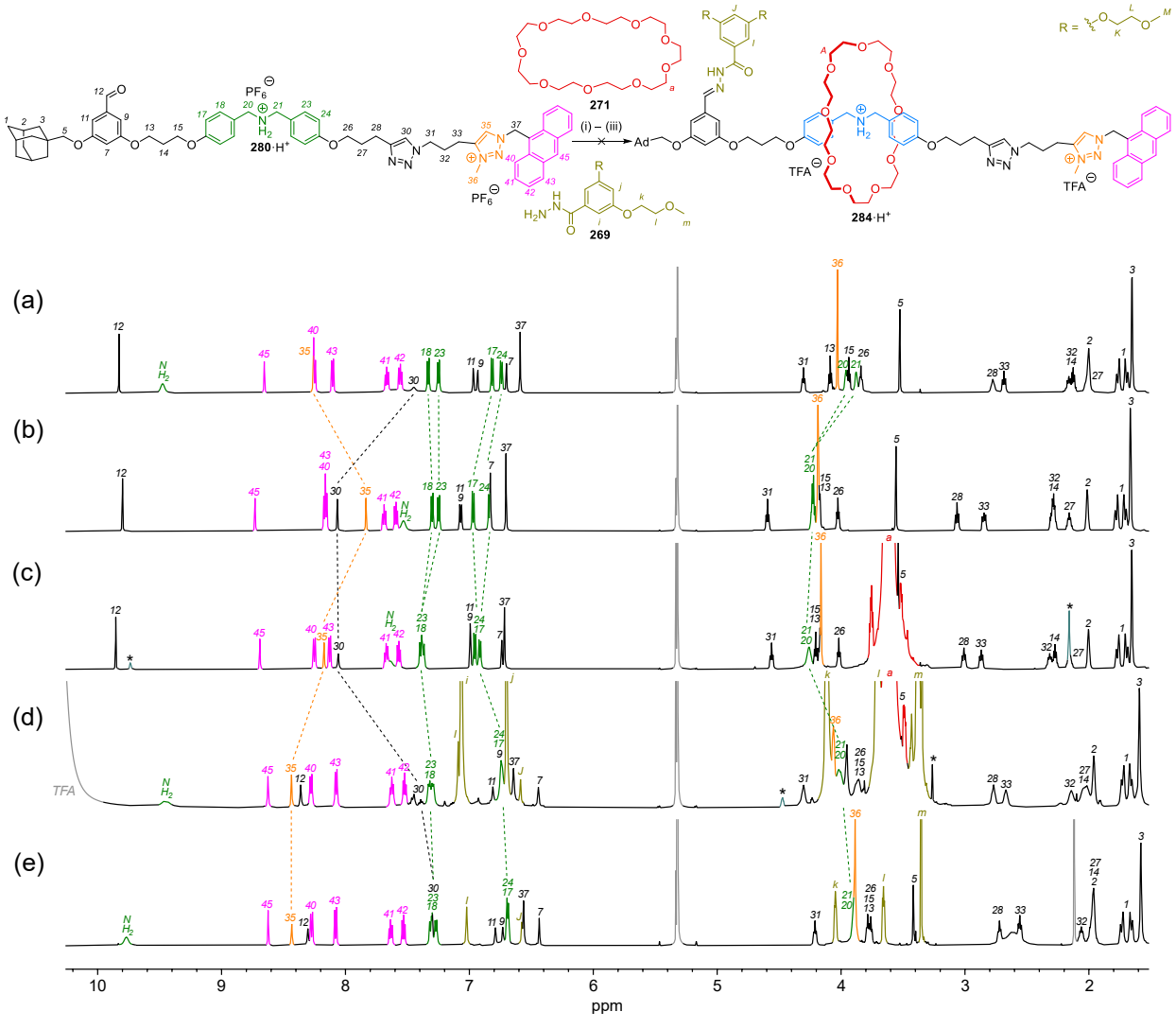

Figure 8.19. Attempted synthesis of 1-barrier model pseudorotaxane **284**·H$^+$ from free thread **280**·H$^+$ (2nd model pump design), macrocycle 27C9 **271** and hydrazide **269**. Reagents and conditions: (i) TFA, (ii) 27C9

271, (iii) hydrazide **269**, CD_2Cl_2, rt. Partial ^1H NMR spectra (600 MHz, CD_2Cl_2, 298 K) of (a) free thread **280**·H^+ (20 mM). After sequential addition of (b) 20 equiv. of TFA, (c) 12 equiv. of macrocycle 27C9 and (d) 12 equiv. of hydrazide **269**. (e) Isolated free thread hydrazone.

While substitution of the original macrocycle DB30C10 **205** with the alkylic counterpart 27C9 **271** facilitated the spectral interpretation and allowed signal assignment of all components at each step of the anticipated pseudorotaxane formation, the addition of the smaller macrocycle **271** had only a modest effect on the signals for the corresponding DBA motive. Characteristic protons signals for the benzylic methylene group H_{20} and H_{21} but also its corresponding aromatic signals H_{17}/H_{18} and H_{23}/H_{24} remained largely unaffected – in spite of the expected increased binding affinity of the smaller, alkylic macrocycle towards the DBA motive.[241,274] Furthermore, attempts to isolate *in-situ* formed rotaxane **284**·H^+, after addition of hydrazide **269** and triethylamine (Figure 8.19 (d)), yielded the unprotonated free thread hydrazone. Neither extending the reaction time nor heating did change the essential outcome of the threading experiments. Increasing the association by using higher concentration of TFA were unsuccessful as well and immediately lead to sample decomposition at concentrations above 1 M. Altogether, these indications suggested that the rotaxane **284**·H^+ was not formed. This was further substantiated by the comparison between an authentic standard of isolated free thread hydrazone (Figure 8.19 (e)) and the crude of the threading experiments after neutralisation with base (Figure 8.19 (d)): Signals in both spectra are in near perfect agreement with each other. To further probe the interaction between free thread **280**·H^+ and macrocycle **205** during threading further experiments based on the nuclear Overhauser effect (NOE) were performed (Figure 8.20).

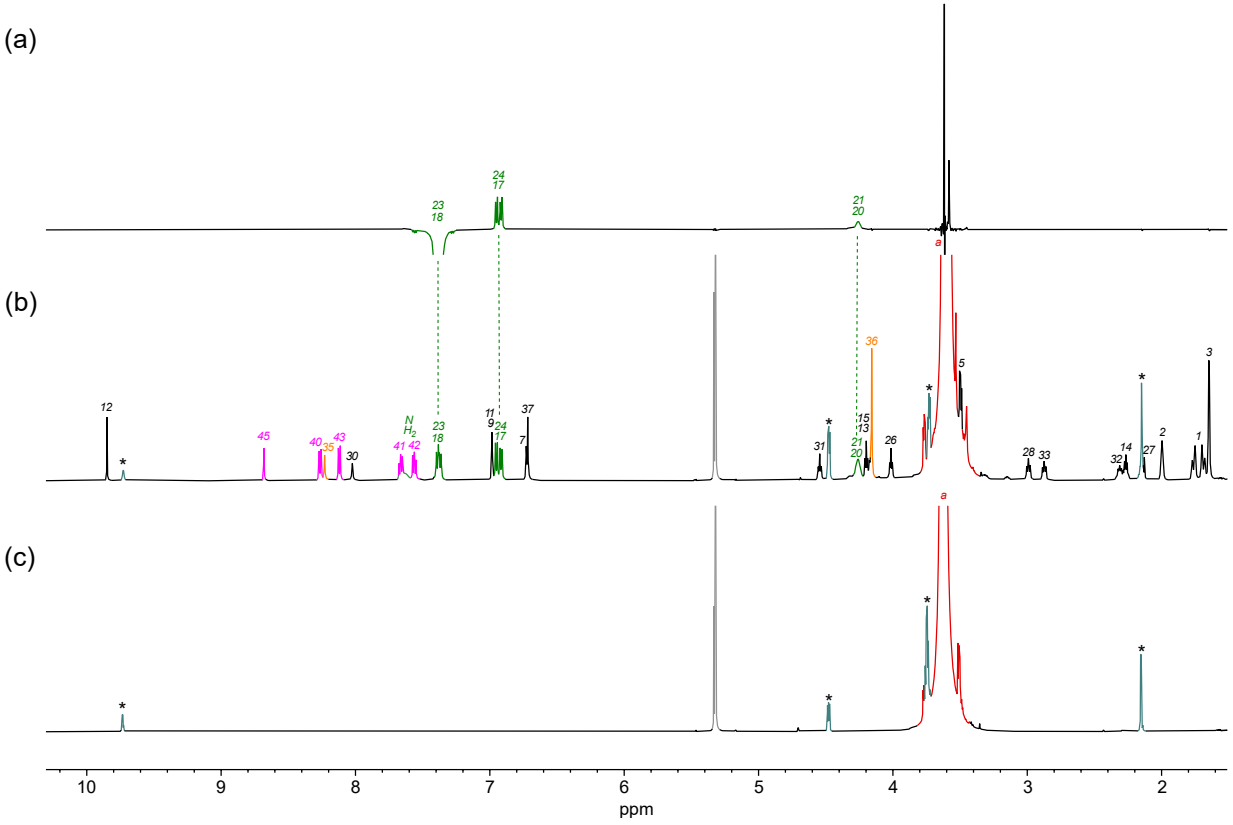

Figure 8.20. Probing the interaction of free thread **280**·H^+ and macrocycle **205** during threading experiments. (a) Partial 1D selective ROESY and corresponding (b) ^1H NMR spectra (600 MHz, CD_2Cl_2, 298 K) of free thread **280**·H^+ (20 mM) in the presence of 12 equiv. of TFA and 17 equiv. of macrocycle 27C9. (c) Corresponding ^1H NMR spectrum of macrocycle **271** in the presence of 12 equiv. of TFA. Peaks marked

with asterisks (*) correspond to remaining open chain tosylate oligomers of the macrocycle **271** (see Figure 8.18). Peak assignments correspond to labelling in Figure 8.19.

Although a weak spatial interaction was found with selective 1D ROESY, as implied by an inverted phase signal at approx. 3.6 ppm in addition to the expected signals for protons H_{17} /H_{24} and H_{20}/H_{21}, this can also result from the adaption of a side-on complex. All in all, it has been concluded that possibly, due to the large energy barrier of the adamantyl motif threading with smaller 27C9 is prevented.

8.4.4. 3rd Generation Model Pump Design with an Anthracene Stopper

Overcoming this limitation, threading of 27C9 onto a modified thread **285**·H⁺ was considered (Scheme 8.39). By removing the adamantyl group, this third design features a reduced steric bulk for the aldehyde and hydrazone moiety that unlike previous designs, is known to allow for threading with 24-crown-8 (24C8) **290** and its derivative DB24C8 **173** (and, consequently, 27C9 **271**). At the same time, it would allow to isolate stable rotaxanes **288**·H⁺ (DB24C8) and **289**·H⁺ (24C8) because of anthracene being an effective stopper unit for those smaller macrocycles.[262c] Additionally, by a direct comparison of deprotonated rotaxanes **288** and **289** with UV-vis spectroscopy it was hoped to get further insight into the requirements for optimal PET disruption and fluorescence enhancement when using various macrocycles of the same size (24C8 vs DB24C8), under high dilution required for UV-vis measurements.

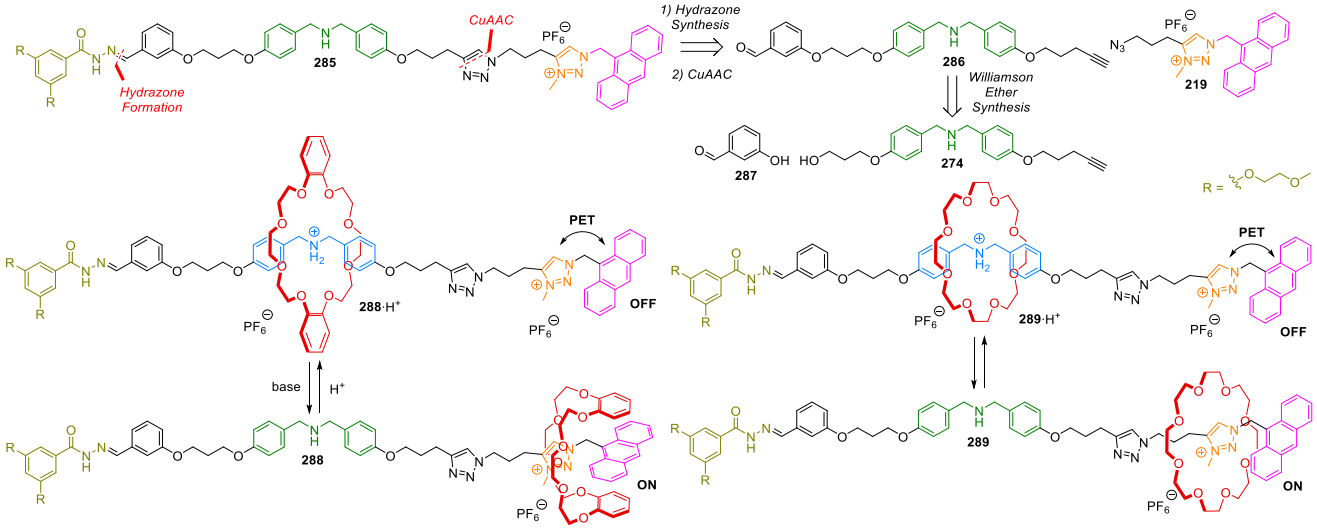

Scheme 8.39. Proposed third model pump design **285**·H⁺/**285** for the formation of rotaxanes **288**·H⁺ and **289**·H⁺. By the using same principal design the influence of various macrocycles such as 27C9, 24C8 and DB24C8 on the anticipated (transient) fluorescence enhancement is expected to allow studying shuttling and if possible, also dethreading kinetics.

Preparation of the new thread **285**·H⁺ (3rd model pump design) was carried out by an analogous protocol to that of the synthesis of the 2nd model pump **280**·H⁺ (Scheme 8.40). First, by linking 3-hydroxybenzaldehyde **287** with Boc-protected dibenzyl ammine mesylate **277** via Williamson ether synthesis and second, by CuAAC with anthracene stopper **219**. Last the obtained intermediate **292** was converted to the corresponding ammonium salts residual **293**·H⁺ by removing the Boc protecting group under acidic conditions. This has allowed isolation of thread **293**·H⁺ in an overall yield of 43% (X = BF_4) or 55% (X = TFA) over the three steps.

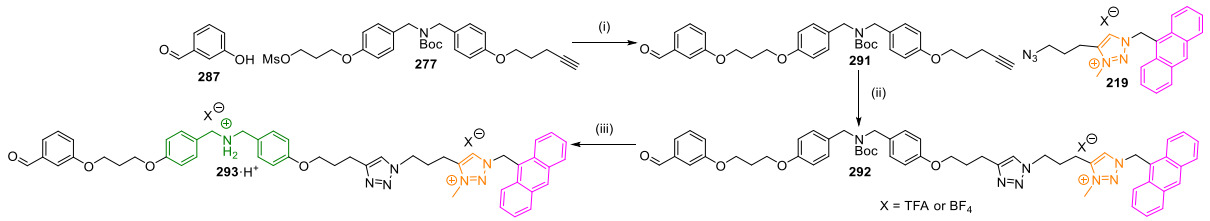

Scheme 8.40. Synthesis of third model anthracene 1-barrier pump **293**·H. Reagents and conditions: (i) K_2CO_3, CH_3CN, 85 °C, 3 d, 65%. (ii) $[Cu(CH_3CN)_4]BF_4$, DMSO-d_6, 70 °C, 3 h, then anion-exchange (amberlyst A26/X^-, CH_3CN), 79% (X = BF_4) or 85%. (X = TFA) (iii) TFA, CH_2Cl_2, 0 °C, 1 h, then anion-exchange (amberlyst A26/X^-, CH_3CN), 83% (X = BF_4) or 99%. (X = TFA)

Next, threading with DB24C8 **173** and 24C8 **290** and using solubilizing hydrazide **269** as a stopper was investigated. In both cases, we were able to isolate corresponding [2]rotaxanes **288**·H^+ and **289**·H^+ in overall very good yields by optimizing the original threading conditions and developing a suitable technique for the separation of hydrazone rotaxanes from reactants and accompanying free thread (Scheme 8.41).

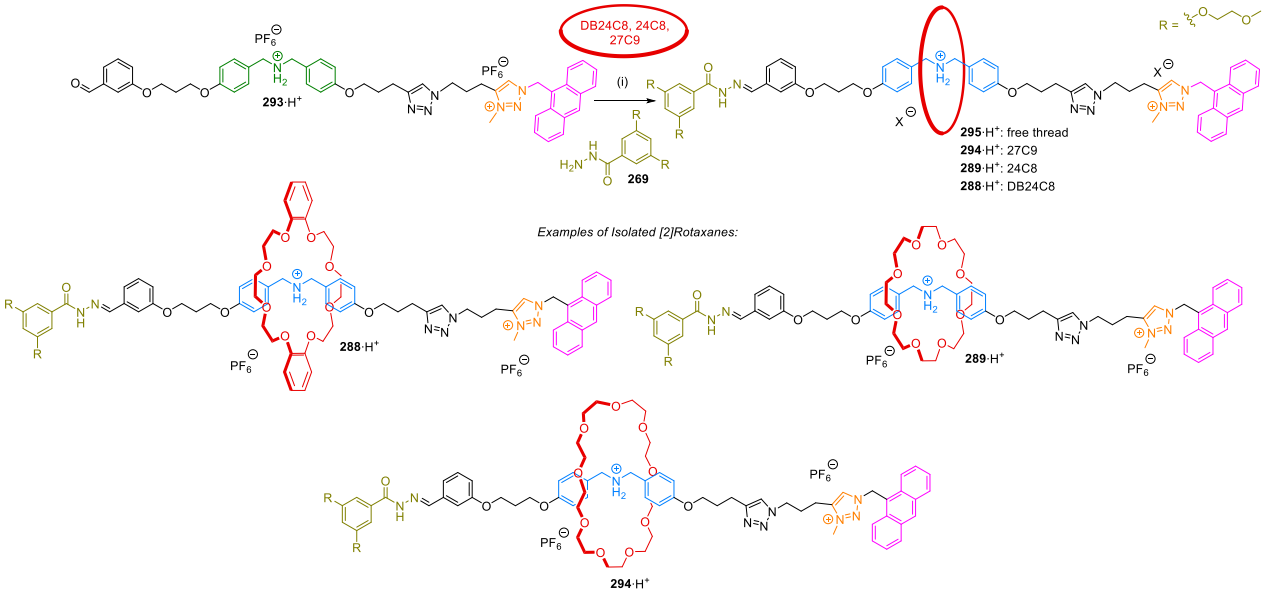

Scheme 8.41. Synthesis of model [2]rotaxanes **294**·H^+, **289**·H^+ and **288**·H^+ by threading 27C9, 24C8 and DB24C8 on thread **293**·H^+ (3rd model pump design) and capping with hydrazide **269**. Reagents and conditions: (i) TFA, macrocycles, CD_2Cl_2, rt, then hydrazide **269**, rt, then Et_3N, rt, then intermediate purification via size exclusion chromatography and final anion-exchange (amberlyst A26/X^-, CH_3CN), 49% (**294**·H^+, 27C9, X = PF_6), 74% (**289**·H^+, 24C8, X = TFA), quantitative (**289**·H^+, 24C8, X = PF_6, **288**·H^+, DB24C8, X = PF_6) and 71% (**295**·H^+, free thread).

The obtained compounds **288**·H^+ and **289**·H^+, after purification with size-exclusion (Bio-Beads S-X resin) and anion-exchange with a strongly basic (type I) quaternary ammonium-functionalized resin (amberlyst A26) loaded with NH_4PF_6 in MeCN, were found to be bench stable, even over a period of months. Only a minor loss of hydrazone and macrocycle **290** were detected for a sample of **289** over multiple days. Rotaxane **294**·H^+ resulting from the threading with 27C9 and free thread hydrazone **295**·H^+ were obtained using similar procedures in yields of 49% and 71%, respectively.

To confirm the anticipated dynamic properties of these molecular switches, **288**·H$^+$ (DB24C8) and **289**·H$^+$ (24C8) were studied under basic and acidic conditions by NMR spectroscopy. Starting from freshly prepared protonated samples, immediate (reversible) shuttling of corresponding macrocycle from the dibenzyl ammonium to the triazolium station was observed for switches **288**·H$^+$/**288** (Figure 8.21) and **289**·H$^+$/**289** (Figure 8.22) in CD_2Cl_2 upon addition of two equivalents of DBU.

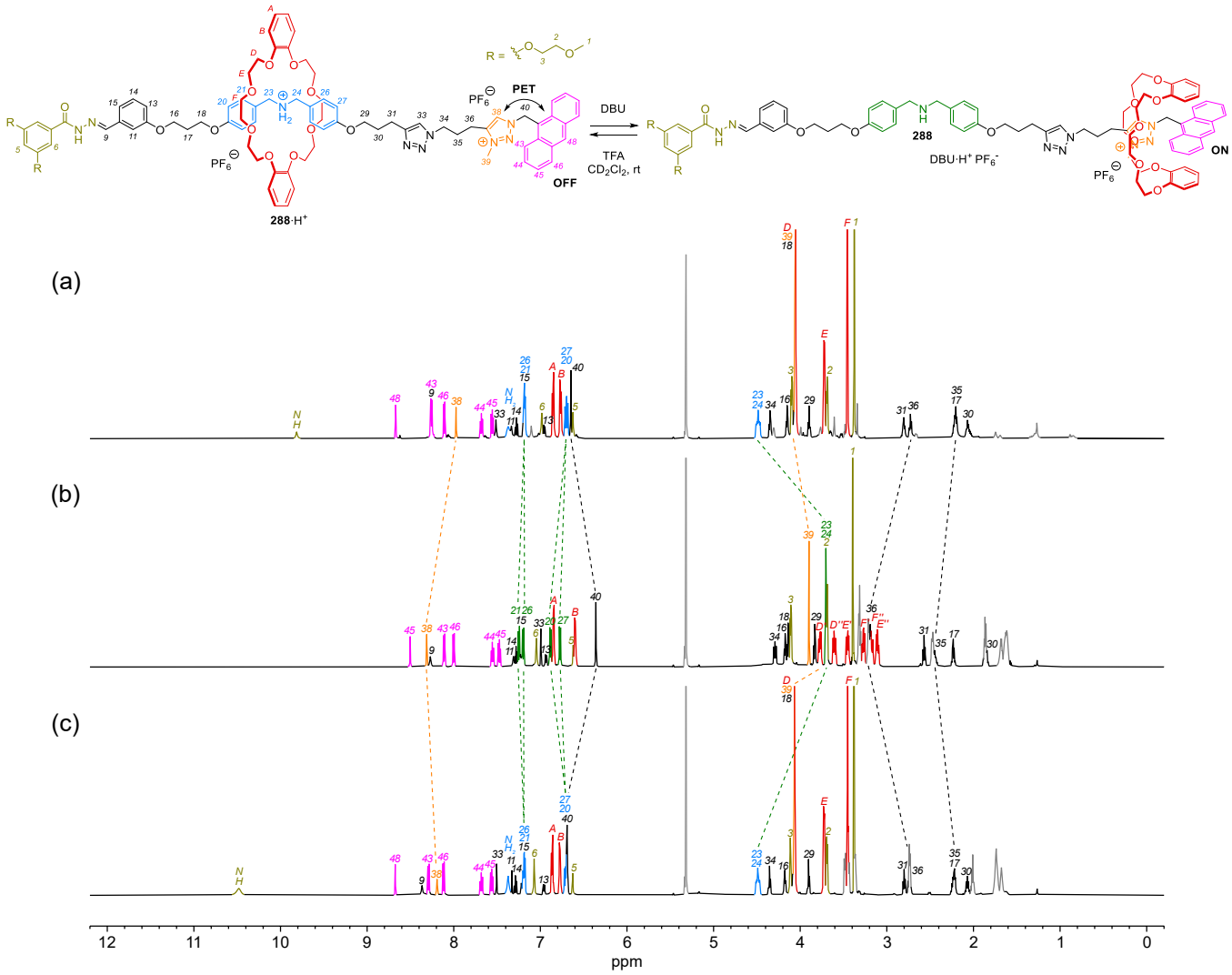

Figure 8.21. ^{1}H NMR (600 MHz, CD_2Cl_2, rt) stack plot comparison of anthracene terminated DB24C8 [2]rotaxane showing (a) **288**·H$^+$ (19 mM) as isolated, (b) **288** (12 mM) after intermediate purification and subsequent deprotonation with DBU (2 eq) and (c) **288**·H$^+$ (12 mM) after re-protonation with TFA (2 eq).

When using a weaker base such as triethylamine, a large excess was required to induce similar quantitative shuttling. This is in line with former observations showing that along with the complexation of the secondary ammonium group by a crown ether macrocycle the immediate acidity of the DBA group decreases.[262b] Moreover, addition of an equimolar amount of an acid such as TFA or TCA fully reverses molecular switches **288** and **289** back to their original position, as indicated by the restitution of original proton shifts for characteristic positions. The minor differences for weakly acidic positions such as protons of the triazole H_{33}, aldehyde H_9 and, most notably, the hydrazide group H_{NH} as seen both in Figure 8.21 and Figure 8.22 may be the result of concomitant anion-exchange from PF_6^- to TFA^- and the presence of protonated DBU.

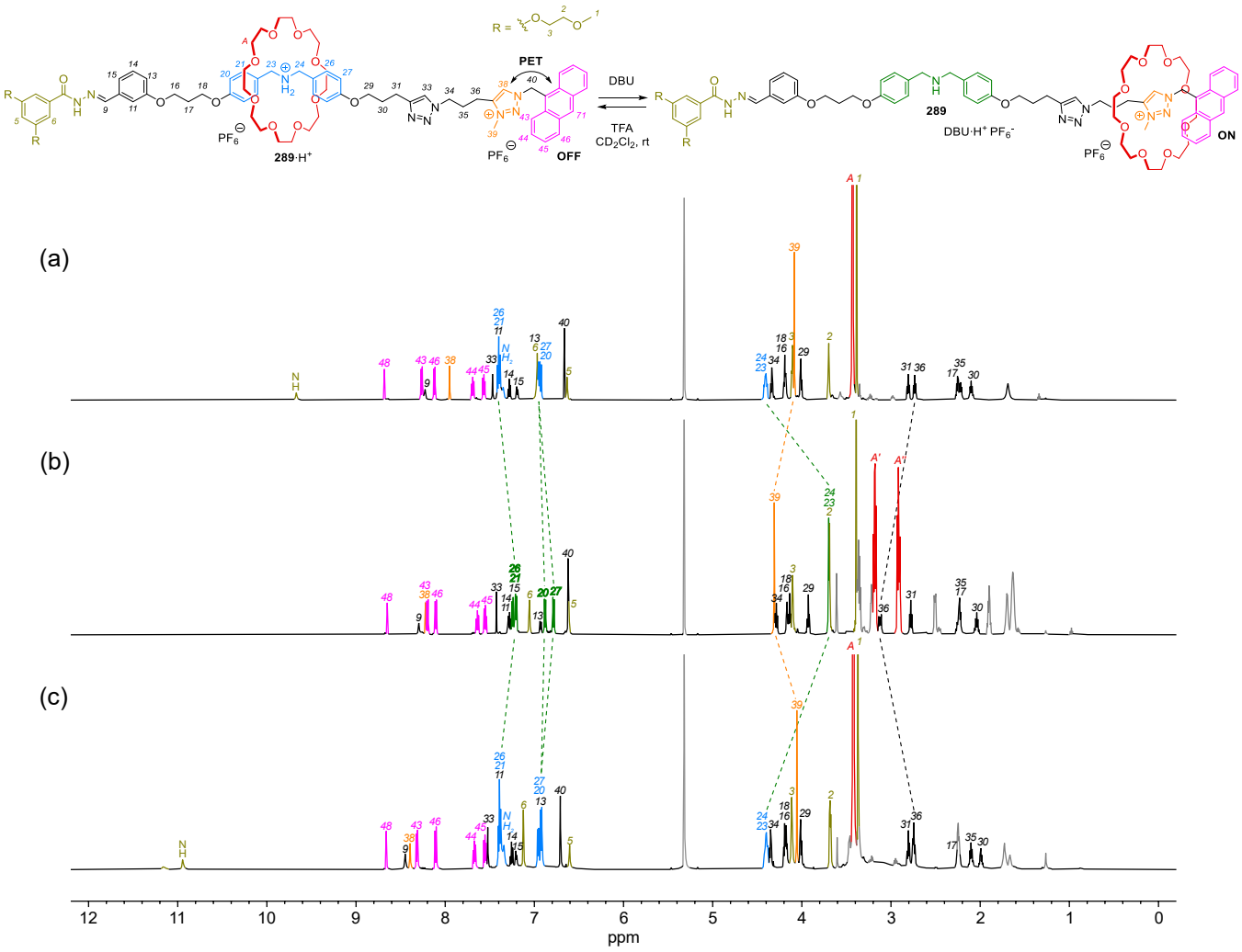

Figure 8.22. ^{1}H NMR (600 MHz, CD_2Cl_2, rt) stack plot comparison of anthracene-terminated 24C8 [2]rotaxane showing (a) **289**·H$^+$ (23 mM) as isolated, (b) **289** after deprotonation with DBU (2 eq) and (c) **289**·H$^+$ (13 mM) after intermediate purification and subsequent re-protonation with TFA (2 eq).

In general, switching the position of the macrocycle from the DBA to the triazolium group was accompanied with a significant upfield shift for protons H_{33} of up to 0.4 ppm comprising the triazole motive and extending to the last methylene protons of the adjacent propylene chain H_{36}, H_{35} and H_{34} with a diminishing effect in the given order. Furthermore, protons associated to the macrocycle (H_a) experienced an overall downfield shift when compared to the protonated rotaxanes **288**·H$^+$ and **289**·H$^+$. This may hint at a weak hydrogen-bonding interaction in the triazole position. The response was echoed also by the methylene groups of the deprotonated dibenzyl ammonium unit for protons at positions H_{24} and H_{25} which move from approximately 4.4 ppm to 3.6 ppm, which the later representing the value of an undisturbed methylene ether group. Simultaneous with the deprotonation of the DBA motive also an effect for the hydrazone protons at positions H_5 and H_6 were seen. It has been observed that those signals varied between freshly prepared **288**·H$^+$, deprotonated **288** and recovered **288**·H$^+$ when looking at, for example, the switching of **288**·H$^+$/**288** (DB24C8, see Figure 8.21). Moreover, significant shifts of up to 0.9 ppm were detected for hydrazide proton H_{NH} when comparing between different experiments (a) and (c) in the same switching state **288**·H$^+$. This finding can be explained by the dynamic nature of the hydrazone bond but also by the acidity of the hydrazone proton H_{NH} – a Schiff's base type analogue – with a pK_a of approx. 19.7 in DMSO-d_6.[276] This peculiarity was found negligible in good approximation for the ensuing studies since proton shifts of the

remaining molecule have otherwise shown to reflect the switching state in a highly consistent manner, for both molecular switches **288**·H^+/**288** (DB24C8) and **289**·H^+/**289** (24C8).

In the former case, additional π-π-stacking between the two catechol moieties and the anthracene unit became apparent in the large downfield shifts seen for the peaks associated with aromatic protons of the macrocycle (Figure 8.21 (b)). At the same time splitting of the methylene peaks of the crown ether bridges into subsets of two smaller peaks was found. This further supported the loss of rotational symmetry due to the restricted confirmation of macrocycle DB24C8 **173** in **288**. Besides this, a significant shielding effect was observed for protons of the methyl group of the triazole H_{39} and the methylene bridge interfacing the anthracene H_{40}. All these findings agreed well with other examples reported in the literature[255a,277] and therefore suggested that in the case of **288** DB24C8 needs to be represented by a more realistic 'folded' structure.

In the latter case, analysing the resonance signals of **289** (24C8) (Figure 8.22 (b)) a split of the single broad macrocycle's peak H_A into a subset of two peaks $H_{A'}$ and $H_{A''}$ was noted. These peaks showed different NOE interactions between the triazolium H_{38} and triazole unit H_{33} and therefore, were assigned to protons on the anthracene facing and turned away side of the macrocycle, respectively. Contrary to **288**, rotaxane **289** displayed a large upfield shift as opposed to a downfield shift for the methyl peak of the triazolium unit under basic conditions. This may be the result of a decreased paramagnetic deshielding of the macrocycle. No sign of a loss of rotational symmetry for threaded 24C8 in state **288** was observed by NMR.

In addition to investigating the switching of **288**·H^+ (DB24C8) and **289**·H^+ (24C8) with ^{1}H NMR samples of both rotaxanes were also examined with UV-vis and fluorescence spectroscopy (Figure 8.23). First, looking at the results of the UV-vis studies (Figure 8.23 (a) and (b)), no significant differences of absorption spectra between protonated **288**·H^+/**289**·H^+ and deprotonated rotaxanes **288**/**289** were observed. Independent whether samples were analysed by diluting concentrated solutions of simultaneous NMR experiments or by directly adding an (excess) amount of DBU and TFA to independent (stock) solutions of **288**·H^+/**289**·H^+ the characteristic absorption spectra of the anthracene with absorption peaks at λ_{max} = 355, 370 and 390 nm as well as main absorption bands at λ_{max} = 300 and 258 nm remained constant. These results are line with the reported results for other rotaxane-based switches[262c,277] and ruled out the possibility of modulating the fluorescence signal by solely varying associated absorption levels with acid and base.

This has allowed continuing with fluorescence studies. Starting from diluted solution of the **288**·H^+ (DB24C8) (Figure 8.21 (c)) and **289**·H^+ (24C8) (Figure 8.22 (d)) reversible switching of the fluorescence signals was observed when treating optical samples with solutions of DBU and TFA sequentially over multiple cycles. Repeatedly, a fivefold and a sevenfold increase of the fluorescence of the deprotonated over the protonated switches were measured for **288**·H^+/**288** and **289**·H^+/**289**, respectively.

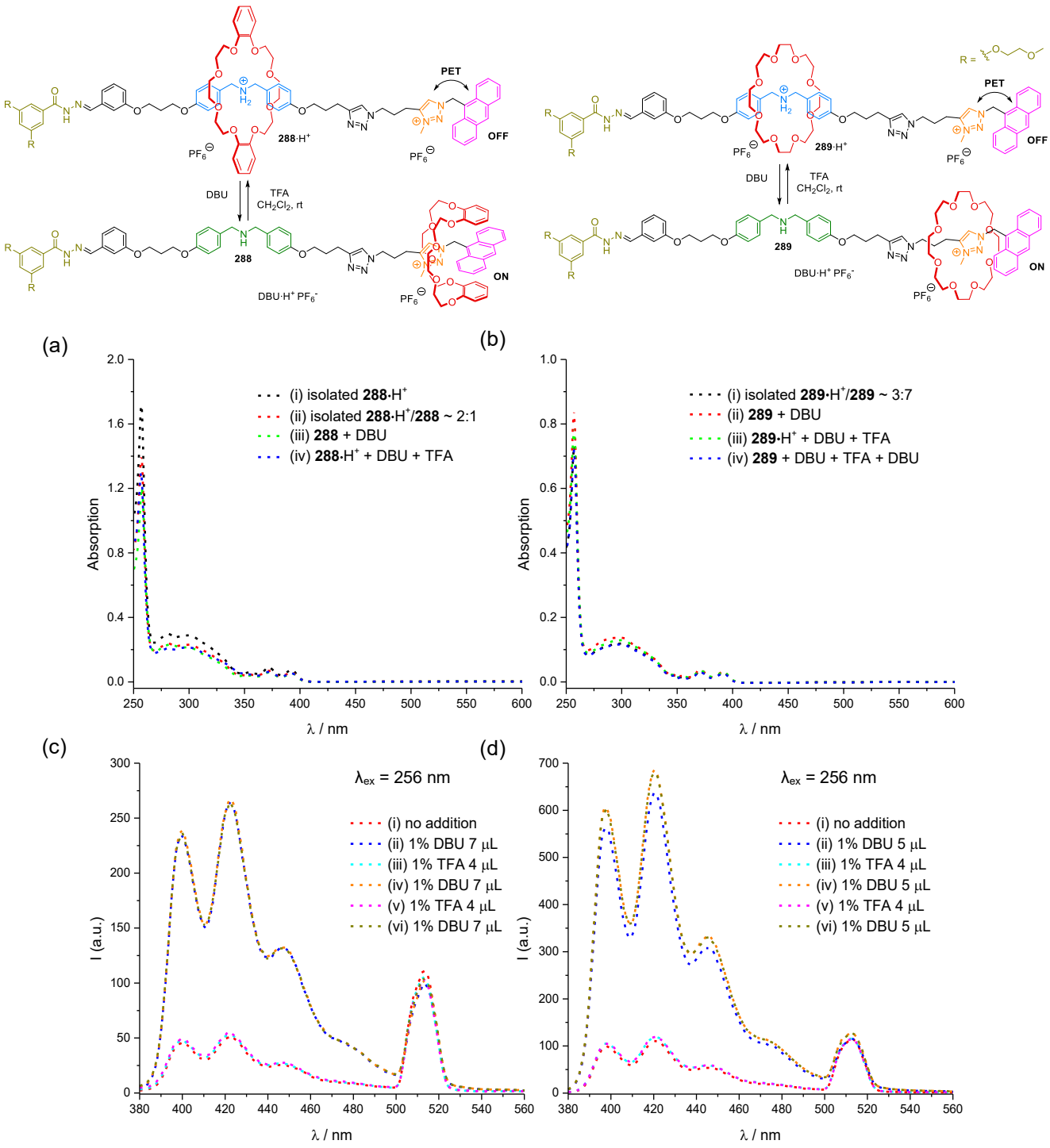

Figure 8.23. Fluorescence switching of the third model pump design with anthracene and (DB)24C8. (a) UV-vis absorption spectra (CH_2Cl_2, rt) of model pump **288**·H⁺/**288** (DB24C8) showing (i) **288**·H⁺ as isolated, (ii) an isolated mixture of **288**·H⁺/**28** in a ratio of 63:37 as determined by ^{1}H NMR integration, (iii) **288** after deprotonation with DBU and (iv) **288**·H⁺ after re-protonation with TFA. In the case of the isolated samples (i) and (ii) aliquots of corresponding NMR solutions were measured. For remaining spectra (iii) DBU and (iv) TFA were directly added to the optical sample. (b) UV-vis absorption spectra (CH_2Cl_2, 4 µM, rt) of pump system **289**·H⁺/**289** (24C8). Aliquots of the NMR solution were taken after each addition to give spectra for (i) the starting mixture of **289**·H⁺/**289** in ratio of 30:70 as determined by ^{1}H NMR integration, (ii) **289** after deprotonation with DBU (0.7 eq), (iii) **289**·H⁺ after re-protonation with TFA (1.6 eq) and (iv) **289** after re-deprotonation with DBU (1.6 eq). Fluorescence emission spectra (CH_2Cl_2, 2 µM, rt, λ_{ex} = 256 nm, $\Delta\lambda_{ex}$ = 5 nm, $\Delta\lambda_{em}$ = 5 nm) of (c) DB24C8 [2]rotaxane **288**·H⁺/**288** and (d) 24C8 [2]rotaxane **289**·H⁺/**289** systems. For each for the samples three switching cycles were performed by (ii) – (vi) sequential addition of appropriate amounts of DBU and TFA (both 1% v/v in CH_2Cl_2) in an alternating manner.

Those values agree well with a similar rotaxane system terminated with anthracene fluorophores on either side of the axle reported by Schmittel and co-workers:[262c] In their case, they noted a sevenfold increase of the fluorescence upon disruption of the PET upon base-mediated shuttling of DB24C8. The comparison drawn is not taking the presence of a second fluorophore into account, but it was speculated that there is no extra contribution of the additional anthracene unit due to the slow movement of the macrocycle by contrast with the fast intramolecular fluorescence quenching via PET.[261g]

In order to provide further evidence for the postulated switching of the macrocycle, fluorescence studies were also repeated with free thread hydrazone **295**·H$^+$. In this case, a different behaviour was found when treating a sample of **295**·H$^+$ with solutions of DBU and TFA under otherwise identical conditions (Figure 8.24).

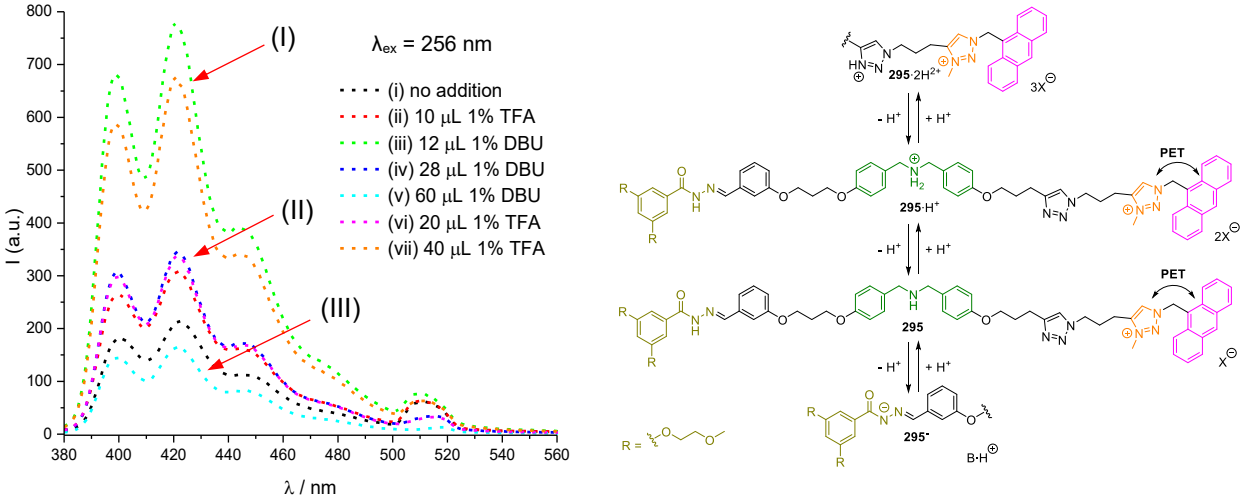

Figure 8.24. Fluorescence switching of free thread hydrazone **295**·H$^+$/**295** system. Measuring the fluorescence emission spectra (CH_2Cl_2, 1 µM, rt, λ_{ex} = 256 nm, $\Delta\lambda_{ex}$ = 5 nm, $\Delta\lambda_{em}$ = 5 nm) of (i) the initial sample and (ii) – (vii) after sequential addition of DBU and TFA (both 1% v/v in CH_2Cl_2) three states of (I) high, (II) intermediate and (III) low fluorescence can be observed.

While small amounts of acid and base did not result into a noticeable change of the fluorescence signal up to three distinct quenching states were noticed when using an excess of TFA and DBU. However, those states observed (marked (I) – (III) in Figure 8.24) could not be assigned to individual states such as **295**·2H^{2+}, **295**·H$^+$, **295** or **295**$^-$ since both (iii) deprotonation and at the same time (vii) protonation from state (II) lead to the state of high fluorescence (I). This observation indicated that switching of the free thread **295**·H$^+$/**295** entails a more complex interplay and suggested the occurrence of potential side reactions at the outer limits of the pH range explored with rotaxanes **288** and **289**. Nevertheless, it was assumed that when keeping within the limit of the small volumes of acid and base required to induce a large amplitude modulation with rotaxanes **288**·H$^+$ (DB24C8) and **289**·H$^+$ (24C8) the extra small modulation stemming from the free thread (**295**·H$^+$/**295**) can be largely treated as constant and therefore negligible for the ensuing analysis.

Based on this, fluorescence switching studies on [2]rotaxane **288**·H$^+$/**288** (DB24C8, which is incapable of dethreading) were performed using 'traceless' chemical fuel TCA **204** in presence of DBU (Figure 8.25). At the start of the experiment the isolated rotaxane **288**·H$^+$ only displayed a modest fluorescence response which, however, after addition of DBU increased by a factor of five due to the relocation of the macrocycle to the triazolium station next to the anthracene (Figure 8.23 (c)). Once an approximately equimolar amount of fuel has been introduced to the system the fluorescence was transiently "turned off" but quickly restored

after a period of about 50 min when all excess fuel had presumably decomposed. The fluorescence spectrum obtained after an interval of three hours (almost) returned to the original “turned on” initial state. It has been expected that multiple additions of fuel would result in a matching sequence of turned on/off cycles to be observed. Altogether, this result nicely demonstrated the anticipated dissipative fluorescence switching.

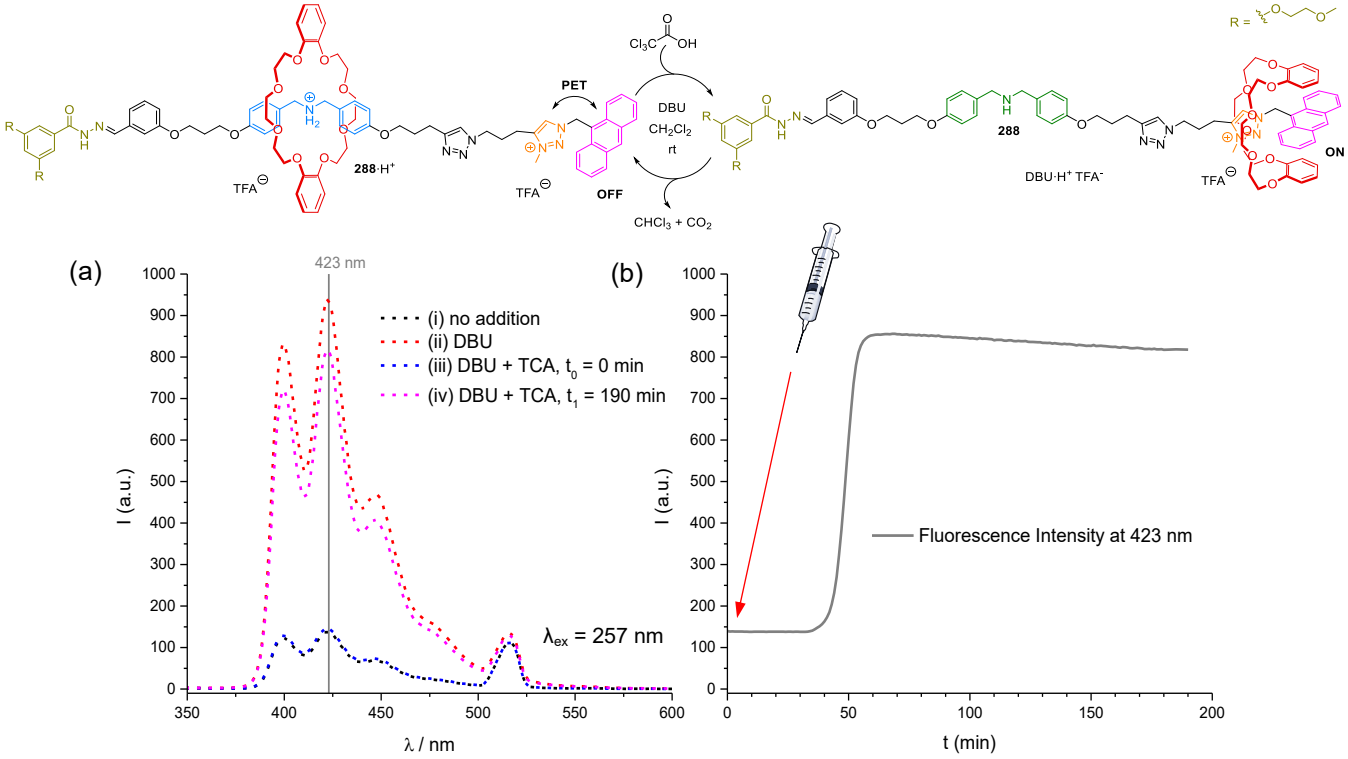

Figure 8.25. Chemically fuelled fluorescence switching of a third model pump design. Fluorescence emission spectra (CH_2Cl_2, 0.6 μM, rt, λ_{ex} = 257 nm, $\Delta\lambda_{ex}$ = 5 nm, $\Delta\lambda_{em}$ = 5 nm) of DB24C8 [2]rotaxane system **288**·H⁺/**288**. An aliquot of a solution of isolated **288**·H⁺ was used as (i) initial sample for following fluorescence experiments. (a) Individual spectra acquired (i) before and after the sequential addition of (ii) DBU and TCA at (iii) t_0 = 0 min and (iv) t_1 = 190 min, respectively. (b) Recorded signal of the fluorescence emission at λ_{em} = 423 nm for the time interval between t_0 and t_1.

Apart from the studies on the isolated rotaxanes **288**·H⁺ (DB24C8) and **289**·H⁺ (24C8) switching was also explored with rotaxane **294**·H⁺ (27C9, Scheme 8.42). Noticing a visual improvement of the acquired spectra by changing the solvent from CD_2Cl_2 to CD_3CN, similarly immediate reversible shuttling of the larger macrocycle could be seen by NMR when successively reacting a freshly prepared sample of **294**·H⁺ with DBU and TFA (Figure 8.26). Identical to shuttling of 24C8, a splitting of the macrocycle’s proton signal H_A into a set of two signals $H_{A'}$ and $H_{A''}$ can be observed under basic conditions. Overall, shifts of characteristic protons largely resembled those of the previous rotaxane **289**·H⁺ (24C8) when performing the switching experiments under comparable conditions.

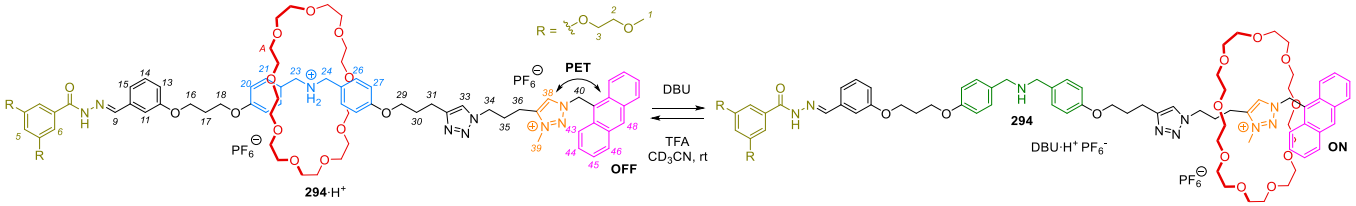

Scheme 8.42. ^{1}H NMR switching experiments performed with model rotaxane **294**·H⁺ (27C9).

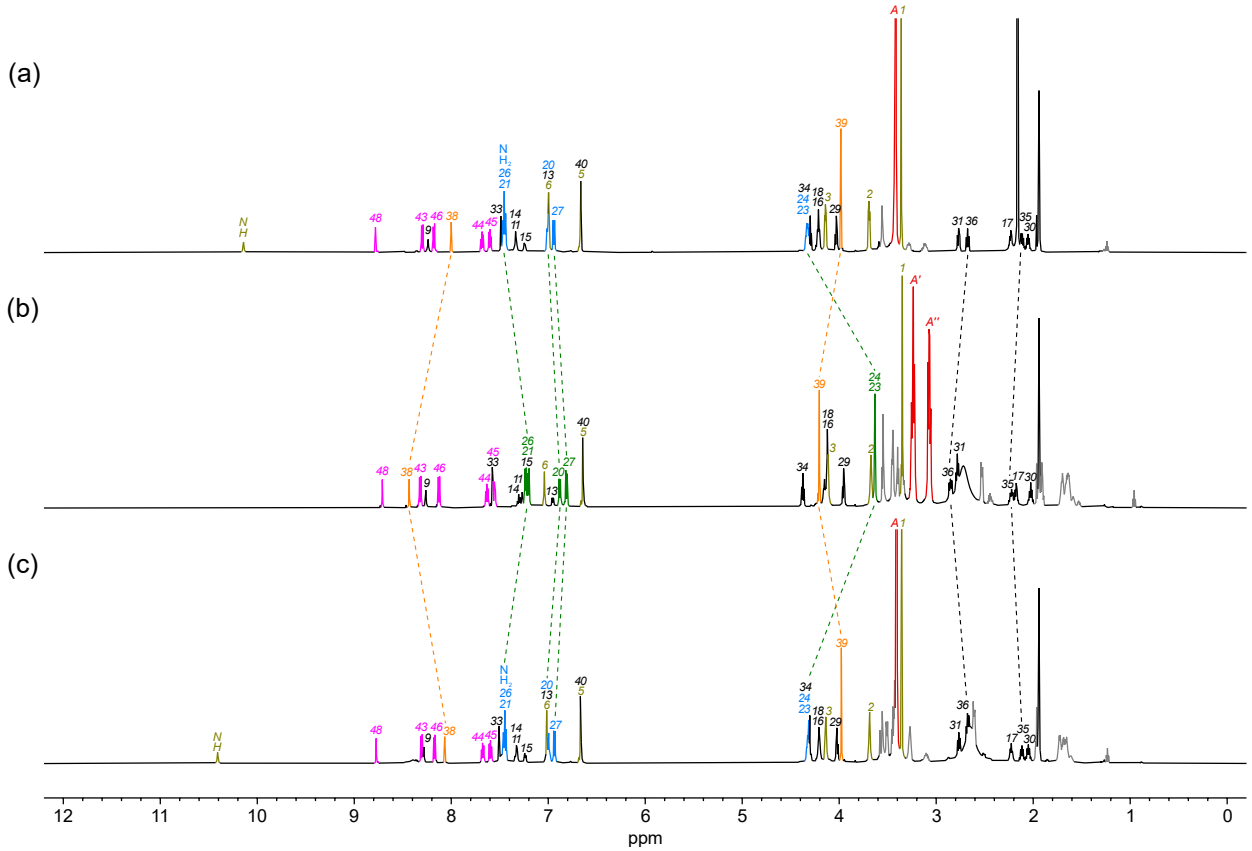

Figure 8.26. ^{1}H NMR (600 MHz, CD_3CN, rt) stack plot comparison of anthracene-terminated 27C9 (pseudo)[2]rotaxane **294**·H$^+$, showing (a) **294**·H$^+$ (8.1 mM) as isolated, (b) **294** after deprotonation with DBU (2 eq) and (c) **294**·H$^+$ after re-protonation of **294** with TFA (2 eq). Labelling corresponding to Scheme 8.42.

With those results in hand, the first dethreading studies were conducted on isolated rotaxanes **289**·H$^+$ (24C8) and **294**·H$^+$ (27C9) (Scheme 8.43). In the former case, stimulated by the repeated observation of a minor but gradually increasing signal corresponding to free macrocycle 24C8 **290** during NMR switching (Figure 8.22), first, dethreading of **289** was attempted by heating a freshly prepared sample of **289**·H$^+$ in CD_2Cl_2 at 40 °C in the presence of DBU. These conditions, however, failed to liberate 24C8 from the thread at a sufficient rate and only a marginal increase of dethreaded macrocycle was seen over one week. Additional efforts to lower the affinity of the macrocycle towards the track and, at the same time, enhance the reaction rate by raising the temperature up to 80 °C by employing more polar solvent CD_3CN, as suggested by the literature for similar crown ether complexes,[278] proved ineffective. In fact, by using these harsh conditions side reactions were promoted and after few days, eventually lead to sample decomposition. All in all, it appeared that macrocycle 24C8 is too small to pass over the anthracene barrier at a sufficient rate for the required for monitoring the operation of a molecular pump system **289**·H$^+$/**289** with fluorescence spectroscopy.

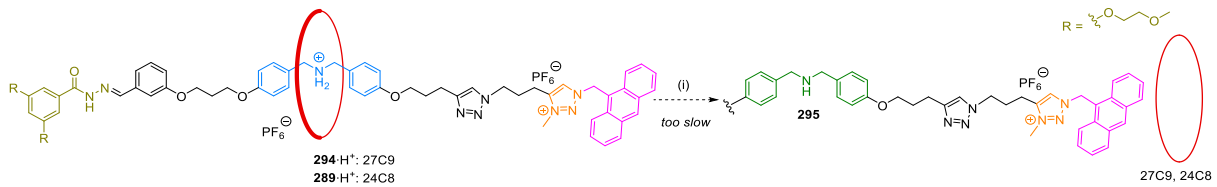

Scheme 8.43. Attempted dethreading of isolated rotaxanes **289**·H$^+$ (24C8) and **294**·H$^+$ (27C9). Reaction conditions trialled: (i) DBU, CD_3CN or CD_2Cl_2, rt up to 80 °C.

Dethreading experiments were also repeated with 27C9 rotaxane analogue **294** and showed promising results but these experiments were similarly affected by an unwanted side reaction. While dethreading occurred at a faster rate compared to rotaxane **289** and appeared to complete after four days by heating a sample of **294** in CD_3CN at 80 °C, as judged by appearance of a signal corresponding to free macrocycle 27C9, upon closer inspection it became apparent that a mixture of both free thread hydrazone **295** and its corresponding free thread aldehyde was formed. Since the loss of the hydrazone could only have occurred under acidic conditions it was speculated that the amount of base decreased over time by a potential (unexpected) side reaction. This finding was independent of the initial amount of DBU and always led to the same outcome. It was concluded that by replacing DBU with another base such as triethylamine clean dethreading with 27C9 would become possible when carefully optimising the reaction conditions. It was evident that macrocycle 27C9 in principle is large enough to pass over the anthracene barrier and thus could eventually be applied for the operation of a molecular pump system (Scheme 8.31).

8.4.5. Revisiting the Two Component Operation with the 3rd Generation Pump Design

As such, with basic fluorescence switching confirmed and protocols for the successful threading and isolation of model pumps **288**·H^+ (DB24C8), **289**·H^+ (24C8) and **294**·H^+ (27C9) established, attention was given to repursue the original main target of the project and develop the required components for the envisaged operation of a 2-barrier machine with 27C9 (see Scheme 8.44 for its retrosynthesis).

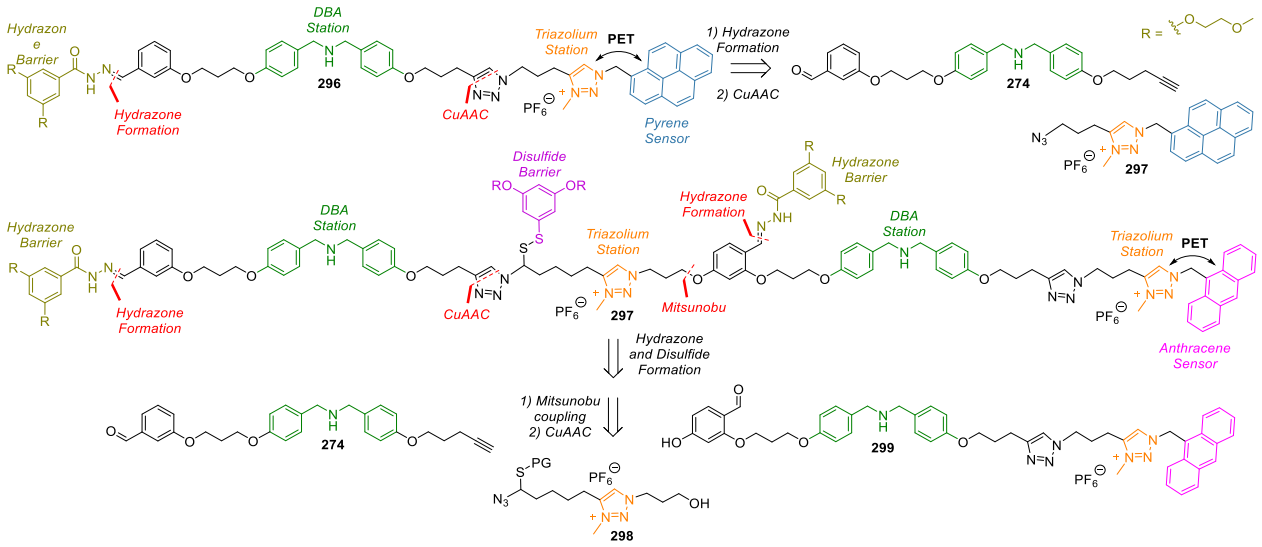

Scheme 8.44. Retrosynthesis of proposed third generation 1- and 2-barrier model pumps **296** and **297** terminated with a pyrene and anthracene fluorophore, respectively.

The updated design **297** takes advantage of previous advancements that have resulted into creation of anthracene free thread **295** (3rd model pump design) and reuses basic chemical building blocks **274** and **219**. The design is complemented by a central triazolium part **298** that incorporates the disulfide barrier and avoids the difficulties of the TMS-deprotection seen earlier by relying on Mitsunobu chemistry for linking with second DBA fragment **299**. In addition to this, an updated internal aldehyde unit is introduced placing the aldehyde group in the 2-position of the corresponding resorcinol ether in **299**. This is due to the fact that, as shown before with the trialled synthesis of second anthracene 1-barrier pump **272**·H^+ (see Figure 8.19),

threading of 27C9 over a dialkylated 3,5-dihydroxybenzyl aldehyde motive appears to be prevented. It was hoped that by changing the substitution pattern and using a 2,4-dihydroxybenzyl aldehyde derivative, reduced steric bulk would reenable passage of 27C9.

To confirm this assumption, test model 1-barrier thread **304**·H⁺ has been synthesised in four steps from starting 2,4-dihydroxybenzyl aldehyde using an *n*-butyl chain as a substitute for the leading track of the envisaged 2-barrier thread **297**·H⁺ (Scheme 8.45). First the statistical alkylation with *n*-butyl bromide was carried out in low yield. Next, Williamson ether synthesis with already available DBA mesylate **277** lead to intermediate alkyne **302** in 99% which when coupled to anthracene azide **222** via CuAAC. Removing the Boc-protecting group furnished the final model thread **304**·H⁺ in a straightforward manner.

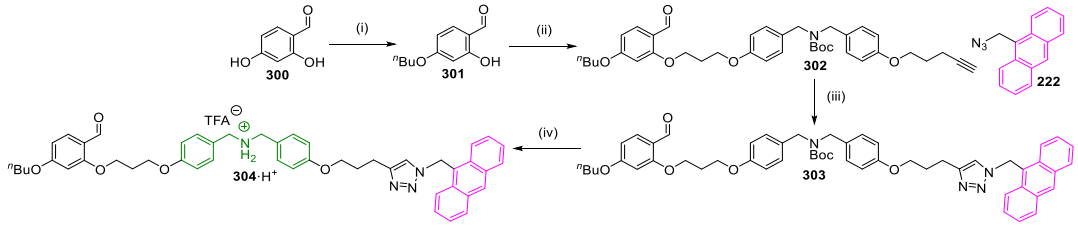

Scheme 8.45. Synthesis of anthracene 1-barrier pump **304**·H⁺ with an internal hydrazone barrier. Reagents and conditions: (i) *n*-butyl bromide, K_2CO_3, acetone, reflux, overnight, 24%. (ii) DBA mesylate **277**, K_2CO_3, CH_3CN, 85 °C, 19 h, 99%. (iii) $[Cu(CH_3CN)_4]BF_4$, DMSO-d_6, 70 °C, 145 min, 92%. (iv) TFA, CH_2Cl_2, 0 °C, 30 min, quantitative.

Following threading experiments with DB24C8 **173**, 24C8 **290** and 27C9 **271** demonstrated that only macrocycle 27C9 can give the desired aldehyde pseudo[2]rotaxane *in-situ*. Smaller macrocycles DB24C8 **173**, 24C8 **290** did not thread even at higher temperature and an extend period (CD_2Cl_2, rt, 21 h, then 40 °C, 6 h). The intermediary complex with 27C9 when capped with glycol functionalised hydrazone **269** was subsequently isolated and characterized by NMR (Scheme 8.46). This demonstrated that salicylic aldehyde motif could indeed be used as a potential internal aldehyde barrier in 2-barrier machine **297**.

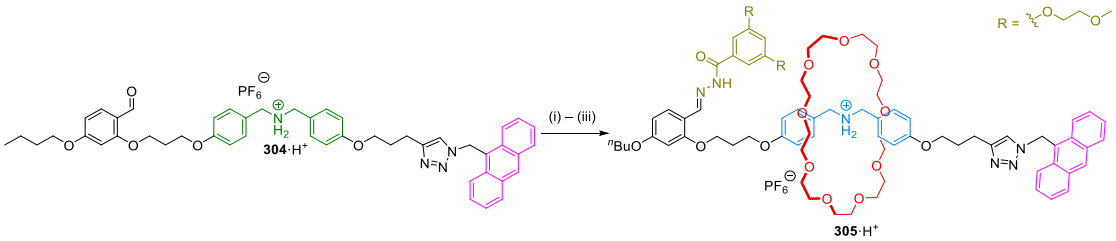

Scheme 8.46. Isolation of anthracene 1-barrier [2]rotaxane **305**·H⁺ from free thread **304**·H⁺ (with internal hydrazone barrier) and macrocycle 27C9 **271.** Reagents and conditions: (i) TFA, macrocycle 27C9, CD_2Cl_2, rt, 19 h, then (ii) hydrazide **269**, rt, 35 min, then (iii) Et_3N, rt, 5 min, 80%.

8.4.6. UV-vis and Fluorescence Studies of a Pyrene Stopper

Taking steps further to make the two component operation reality, a survey of the literature has then suggested that a pyrene motive may be used for the construction of an alternative fluorophore stopper **297** (Scheme 8.47).[262d] Since absorption and fluorescence spectra had been reported to be sufficiently well separated[279] it was anticipated that this chromophore allows for the required second, orthogonal fluorescence read out in the presence of the anthracene unit. Accordingly, the synthesis of a pyrene stopper unit **297** was performed based on previous protocols for the synthesis of corresponding anthracene counterparts (Scheme 8.22). Starting from commercially available 1-pyrenylmethanol **306** and completing a five step reaction sequence combining the preliminary azide formation with a CuAAC to 4-pentyn-1-ol, followed by a second azide formation and final methylation with trimethyloxonium tetrafluoroborate the desired methylated triazolium **297** was obtained in an overall yield of 29%. This result confirmed the generality of the developed synthetic route and allowed to prepare several hundred milligrams of substrate.

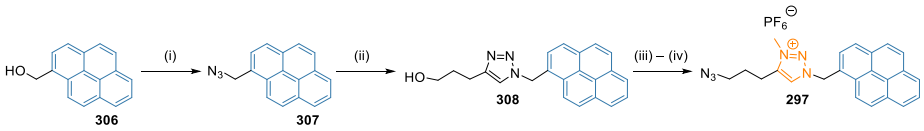

Scheme 8.47. Synthesis of pyrene stopper **297**. Reagents and conditions: (i) ADMP, DBU, THF, –10 °C, 85 min, 49%. (ii) 4-pentyn-1-ol, $[Cu(CH_3CN)_4]BF_4$, CH_2Cl_2:*t*BuOH, rt, 15 h, 93%. (iii) ADMP, DBU, THF, 0 °C, 145 min, 88%. (iv) Me_3OBF_4, CH_2Cl_2, 0 °C, 1 h, then KPF_6, THF, rt, 15 min, 73%.

Next, a series of fluorescence spectra of both pyrene (**308**, **309** and **297**) and anthracene compounds (**220**, **223** and **197**) were measured to initially check the assumed orthogonality of fluorescence read out (Figure 8.27). As evident from the overlay shown in Figure 8.27 (e) spectra of anthracene and pyrene model compounds do not overlap in the proposed ON (**220**, **233**, **308** and **309**) and OFF states (**197** and **297**). In the latter case, independent of the triazole/triazole motive all pyrene intermediates (**308**, **309** and **297**) display main absorption maxima at λ_{abs} = 241, 275 and 343 nm (Figure 8.27 (a)). Irradiating those pyrene intermediates with light at the central absorption band at 275 nm gave rise to a distinct fluorescence with emission maxima at λ_{em} = 375, 395 and 415 nm. Like the anthracene systems (Figure 8.13) methylation of the triazole unit also effectively lowers the measured fluorescence of the adjacent pyrene chromophore in comparison with non-methylated samples (Figure 8.27 (c) and (d)).

Importantly, it became apparent that unlike pyrene anthracene does not exhibit any measurable absorption of light at 275 nm. Similarly, characteristic absorption bands of the anthracene motive at 386 and 367 nm do not overlap with corresponding features of the pyrene spectra. Accordingly, this allowed stimulating the fluorescence in a mixture of anthracene and pyrene compounds **233** and **309** (ON state) independently from another by using different excitation wavelengths at 385 (anthracene) and 275 nm (pyrene), respectively (Figure 8.27 (f)). In both cases, no significant additional spectral contributions stemming from the corresponding second fluorophore were observed.

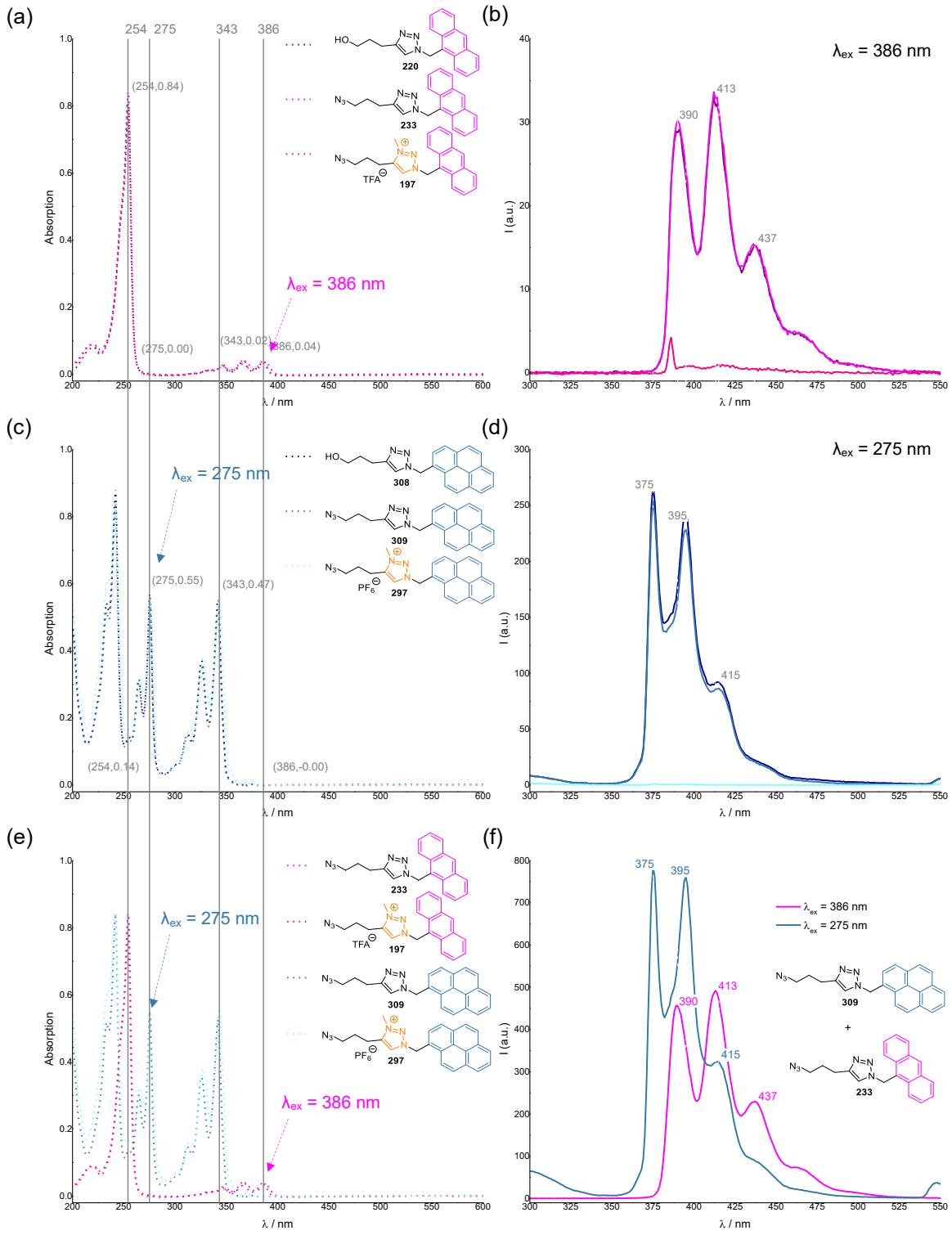

Figure 8.27. Comparison between anthracene and pyrene based stopper precursors. (a) UV-vis absorption spectra (CH_3CN, rt) of anthracene stopper precursors **220** (5.6 μM), **233** (5.7 μM) and **197** (2.8 μM). (b) Corresponding fluorescence emission spectra (CH_3CN, rt, λ_{ex} = 386 nm, $\Delta\lambda_{ex}$ = 2.5 nm, $\Delta\lambda_{em}$ = 2.5 nm, A(386 nm) ~ 0.04) for the same solutions of precursors that were used for UV-vis measurements. (c) UV-vis absorption spectra (CH_3CN, rt) of pyrene stopper precursors **308**, **309** and **297**. (d) Corresponding fluorescence emission spectra (CH_3CN, rt, λ_{ex} = 275 nm, $\Delta\lambda_{ex}$ = 2.5 nm, $\Delta\lambda_{em}$ = 2.5 nm, A(275 nm) ~ 0.5) for the same solutions of precursors that were used for UV-vis measurements. (e) Overlay of UV-vis absorption spectra (CH_3CN, rt) of anthracene stopper precursors **233** and **197** and pyrene analogues **309** and **297**. (f) Fluorescence emission spectra (CH_3CN, rt, $\Delta\lambda_{ex}$ = 5.0 nm, $\Delta\lambda_{em}$ = 5.0 nm) of a mixture of anthracene **233** and pyrene precursor **309** with approx. equal absorbance (A ~ 0.85) in their respective maxima at λ_{max} = 254 nm (anthracene) and λ_{max} = 242 nm (pyrene).

8.4.7. 3rd Generation Model Pump Design with a Pyrene Stopper

Given this positive result for the proposed orthogonal fluorescence read out, synthesis of the first pyrene-terminated 1-barrer pump **296**·H$^+$ (3rd model pump design) was carried out to test the working of the fluorescence switching in a rotaxane system by threading with macrocycle 24C8 and 27C9 (Scheme 8.48).

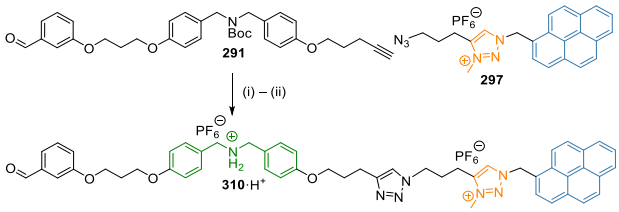

Scheme 8.48. Synthesis of pyrene-terminated 1-barrier pump **310**·H$^+$. Reagents and conditions: (ii) [Cu(CH$_3$CN)$_4$]BF$_4$, DMSO-*d*$_6$, 70 °C, 4 h, 76%. (ii) TFA, CH$_2$Cl$_2$, 0 °C, 50 min, quantitative.

Repeating the synthetic procedure for the construction of the anthracene-based system **293**·H$^+$, preparation of pyrene-terminated thread **296**·H$^+$ was carried out in an analogous manner by connecting pyrene stopper **297** to DBA alkyne precursor **291** via CuAAC and removing the Boc-protecting group with TFA. With this compound in hand threading studies were attempted with 24C8 and 27C9. And using prior established conditions, [2]rotaxanes **311**·H$^+$ (27C9) and **312**·H$^+$ (24C8) were isolated in good yields (Scheme 8.49).

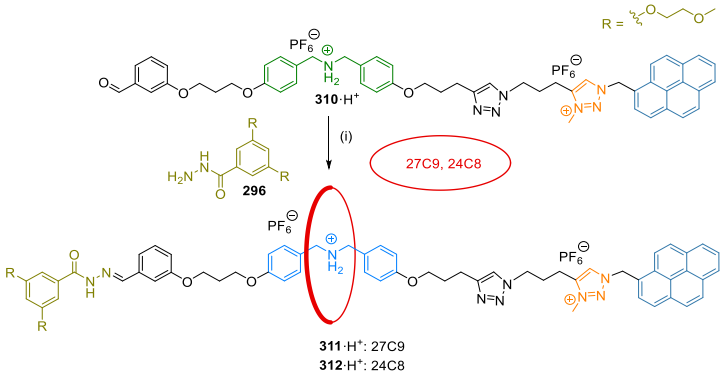

Scheme 8.49. Synthesis of pyrene-terminated (pseudo)[2]rotaxanes **311**·H$^+$ and **312**·H$^+$ by threading 27C9 and 24C8 on thread **310**·H$^+$ and capping with hydrazide **296**. Reagents and conditions: (i) TFA, macrocycles 27C9 or 24C8, CD$_2$Cl$_2$, rt, then hydrazide **296**, rt, then Et$_3$N, rt, then intermediate purification via size exclusion chromatography and final anion-exchange (amberlyst A26/PF$_6^-$, CH$_3$CN), ≤ 51% (**311**·H$^+$, 27C9, note: spontaneous dethreading observed) and 69% (**312**·H$^+$, 24C8).

The switching behaviour of the rotaxanes were then analysed with NMR (Figure 8.28) and fluorescence spectroscopy in the case of **312**·H$^+$ (24C8) (Figure 8.29). In the first case, effecting the shuttling of a freshly prepared sample of rotaxane **312**·H$^+$ (24C8) with base and acid, immediate shuttling of the macrocycle was observed by NMR. This was determined by characteristic upfield shifts for protons of triazolium station H$_{30}$ and H$_{36}$ and also by the concomitant shielding of aromatic H$_{20}$, H$_{21}$, H$_{26}$ and H$_{27}$ as well as benzylic protons H$_{23}$ and H$_{24}$ of the noncomplexed DBA motive when forming **312** with addition of DBU (Figure 8.28 (ii)). Additionally, the proton signal related to the DBA-bound macrocycle H$_A$ split into a set of two peaks H$_{A'}$ and H$_{A''}$ of equal intensity and mirrored coupling patterns when moving the position. Returning to the final state **312**·H$^+$ (Figure 8.28 (iii)), minor dethreading was observed as indicated by the proton signal at 3.6 ppm for the short duration between acquiring the spectra and addition of the reactants. At the same time residual signals for the deprotonated state **312** were seen, most probably, due to an initial over titration with DBU.

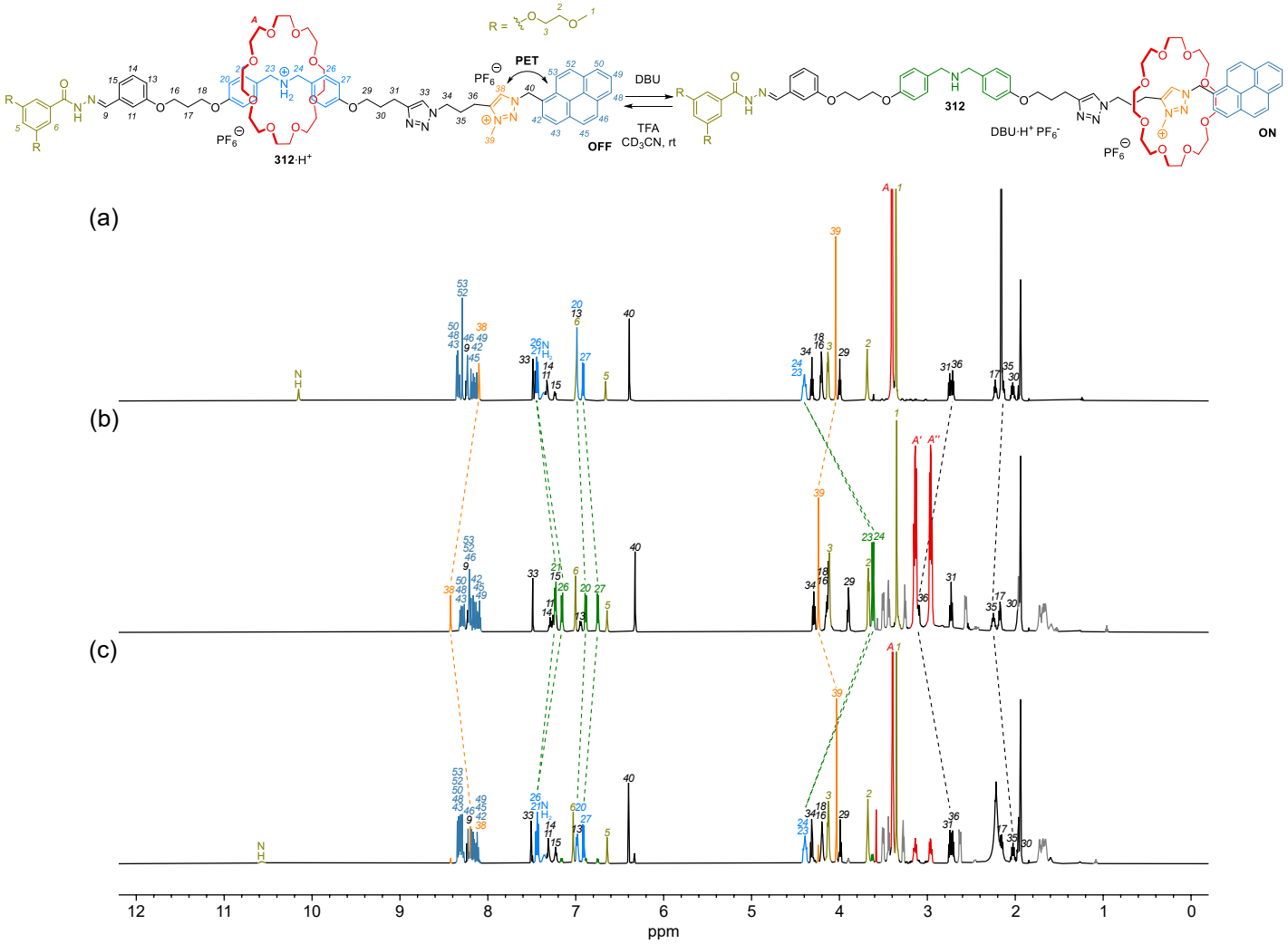

Figure 8.28. ^{1}H NMR (600 MHz, CD_3CN, 11 mM, rt) stack plot comparison of pyrene-terminated 24C8 [2]rotaxane showing (i) **312**·H$^+$ as isolated, (ii) **312** after deprotonation with DBU (1 eq) and (iii) **312**·H$^+$ after subsequent re-protonation with TFA (2 eq).

Carrying on with the fluorescence switching and comparing the response of different rotaxanes terminated with alternative fluorophores **312**·H$^+$ (24C8, pyrene) and **294**·H$^+$ (27C9, anthracene) the orthogonal read out as discovered for their stopper units has been tested (Scheme 8.50 and Figure 8.29).

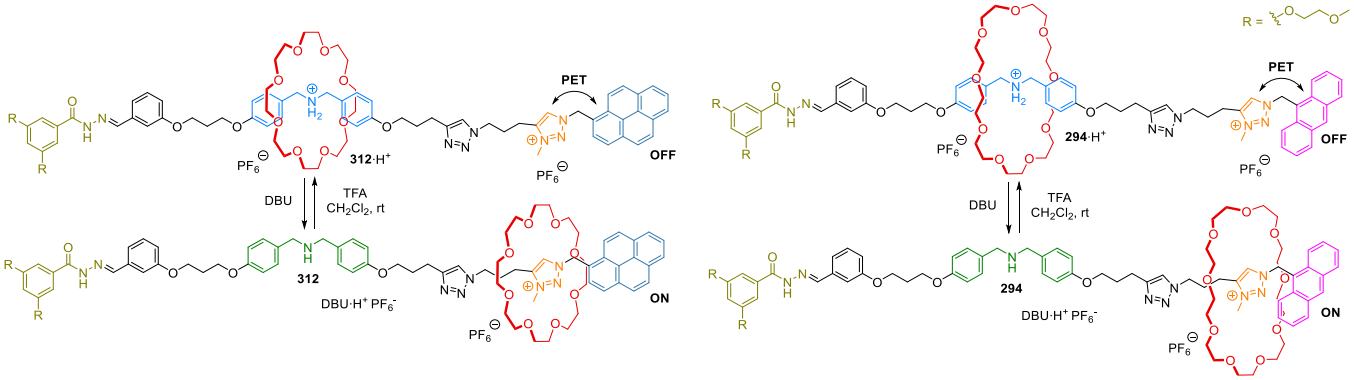

Scheme 8.50.Acid and base-mediated switching of model [2]rotaxanes **312**·H$^+$ (24C8, pyrene) and **294**·H$^+$ (27C9, anthracene).

Looking at the results for individual (Figure 8.29 (a) and (b)) but also a combined system (Figure 8.29 (c)) fully reversible switching of the fluorescence signals was successfully demonstrated over multiple cycles

when adding solution of DBU and TFA in an alternative manner. For both fluorophores approximately a nine-fold increase in the detected signal was measured under basic conditions. In the case of the pyrene system **312**·H⁺/**312** the concentration had to be doubled to reach the same level of fluorescence as detected for the anthracene system **294**·H⁺. These results confirmed previous stopper experiments and enabled monitoring the switching of rotaxanes **312**·H⁺ (24C8, pyrene) and **294**·H⁺ (27C9, anthracene) independent from another by using different excitation wavelengths at 275 and 386 nm for pyrene and anthracene units, respectively.

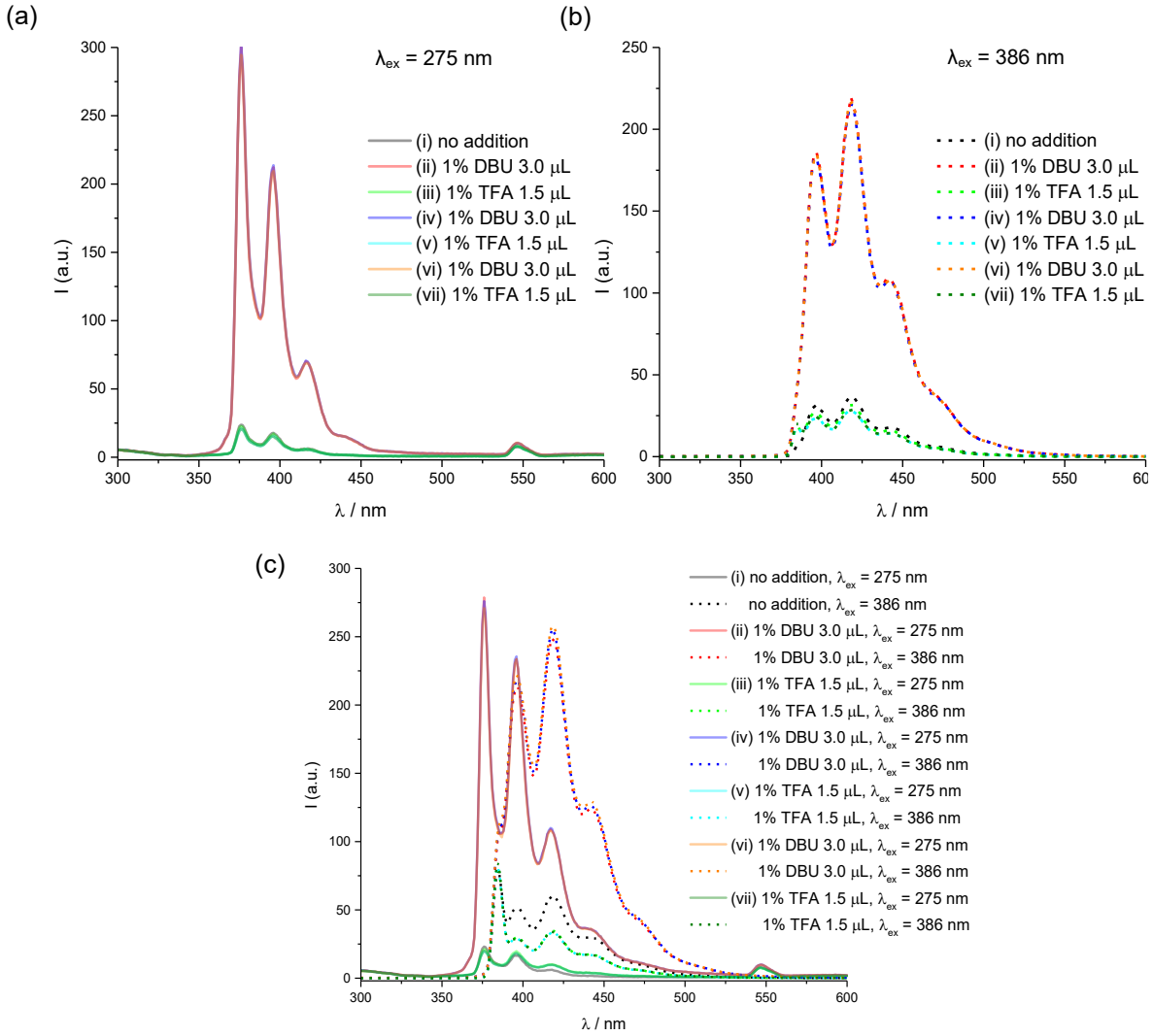

Figure 8.29. Independent simultaneous detection of acid/base modulated fluorescence switching using a mixture of pyrene and anthracene terminated [2]rotaxanes **312**·H⁺/**312** and **294**·H⁺/**294**. (a) Fluorescence emission spectra (CH_2Cl_2, 22 µM, rt, λ_{ex} = 275 nm, $\Delta\lambda_{ex}$ = 5 nm, $\Delta\lambda_{em}$ = 5 nm) of isolated pyrene terminated [2]rotaxane **312**·H⁺/**312** with 24C8. (b) Fluorescence emission spectra (CH_2Cl_2, 11 µM, rt, λ_{ex} = 385 nm, $\Delta\lambda_{ex}$ = 2.5 nm, $\Delta\lambda_{em}$ = 5 nm) of isolated anthracene terminated [2]rotaxane **294**·H⁺/**294** with 27C9. (c) Fluorescence emission spectra (CH_2Cl_2, rt, $\Delta\lambda_{ex}$ = 5 nm, $\Delta\lambda_{em}$ = 5 nm) of the combined mixture of anthracene-**294** (2.5 µM) and pyrene [2]rotaxanes **312** (22 µM) using alternating excitation wavelengths λ_{ex} = 275 nm (pyrene) and λ_{ex} = 386 nm (anthracene) to reveal original emission spectra. Three switching cycles were performed by (ii) – (vii) successive addition of DBU or TFA (both 1% v/v in CH_2Cl_2) in an alternating manner.

Based on this result, synthesis of pyrene-based 1-barrier pseudorotaxane **311**·H⁺ (27C9) was examined. Although **311**·H⁺ could be isolated (in approx. 50% yield) and briefly analysed by ^{1}H NMR and HRMS spontaneous dethreading was noted to give free thread **313** and macrocycle 27C9 (Figure 8.30). Over time,

an increase of proton signal H_a at the expense of H_A was observed potentially due to the reduced binding affinity of the macrocycle **271** towards the DBA station in **311** at low concentration. Addition of DBU to the sample then completed dethreading within few minutes and furnished free thread **313** and macrocycle 27C9.

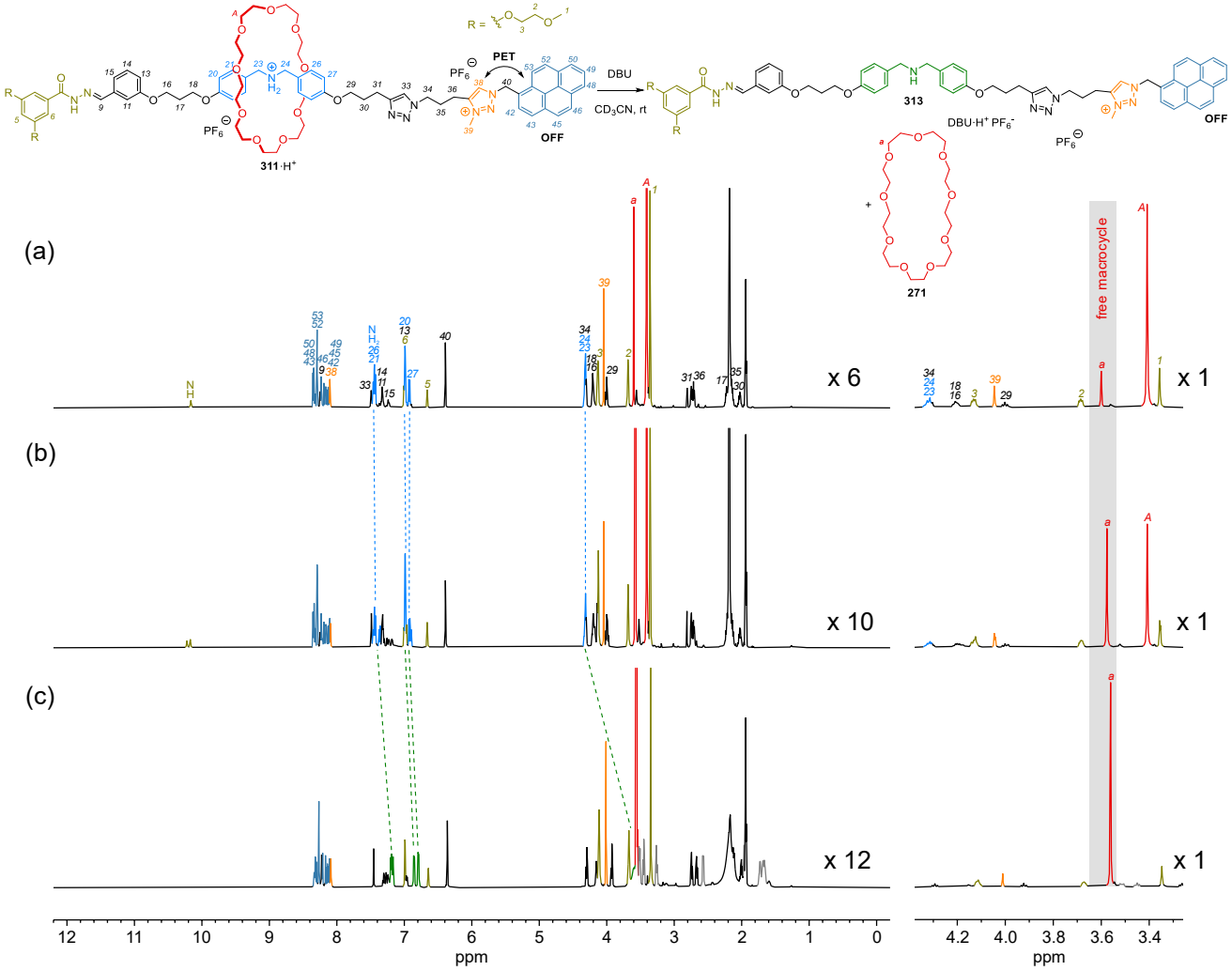

Figure 8.30. Spontaneous dethreading of isolated pseudo[2]rotaxane **311**·H⁺. Full (left) and partial (right) ^{1}H NMR (600 MHz, CD_3CN, 10 mM, rt) stack plots with different scaling factors of pyrene terminated pseudo[2]rotaxane showing (a) **311**·H⁺ as isolated, (b) after 14 hours and (c) after addition of DBU (1 eq). At the start, a mixture of rotaxane **311**·H⁺ and free thread **313** was observed in a ratio of 87:13 and after 14 h this ratio decreased to 54:46 as determined by integration Upon base addition the ratio became zero.

This result suggested that the terminal pyrene unit in **311** is small enough to allow spontaneous dethreading of macrocycle 27C9 at room temperature and thus, it could suit well as a kinetically labile barrier for the third step of the proposed operation of anthracene model pump **258**·H⁺ (see Scheme 8.31). However, it seemed quite likely that concomitant with the reduction of the energy barrier for the dethreading also the energy barrier for opposite threading of 27C9 on free thread **313**·H⁺ would be lowered under acidic conditions (Figure 8.31). As an effect, it would decrease the net amount of anticipated unidirectional movement over the hydrazone barrier in pyrene model pump **311**·H⁺during the initial first step of the operation.

At the same time, previous results implied that the anthracene barrier in **294** is too large to give an appreciable dethreading rate with macrocycle 27C9 under similar conditions. As demonstrated before (Scheme 8.43), macrocycle 27C9 is basically inert to dethreading over the anthracene at room temperature.

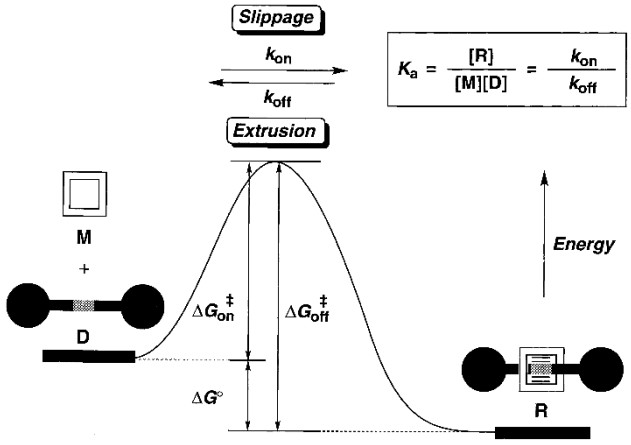

Figure 8.31. Schematic illustration of the self-assembly of rotaxane-like complexes via a slippage approach. If energy barriers for $\Delta G_{on}^{\ddagger}$ and $\Delta G_{off}^{\ddagger}$ are large the system is inert to both slippage and extrusion. On the contrary, at lower values for energy barriers $\Delta G_{on}^{\ddagger}$ and $\Delta G_{off}^{\ddagger}$ the system becomes kinetically labile for either slippage or extrusion depending on whether ΔG^0 is negative or positive, respectively. Energy barriers can be determined by measuring rate constants k_{on} or k_{off} in conjunction with the association constant K_a. Reprinted with permission from reference 243. Copyright 1998 American Chemical Society.

To avoid the complication of going through multiple attempts of improving the final structure of pump systems **311** (pyrene) and **294** (anthracene) and determining their dethreading kinetics (see Scheme 8.51 for a summary of the current results) to ultimately, arrive at pair of matching fluorescent barriers or macrocycles with optimal dethreading kinetics (as recently described by Credi and co-workers for the development of an optimal molecular pump[286]), it was concluded that an alternative approach was necessary.

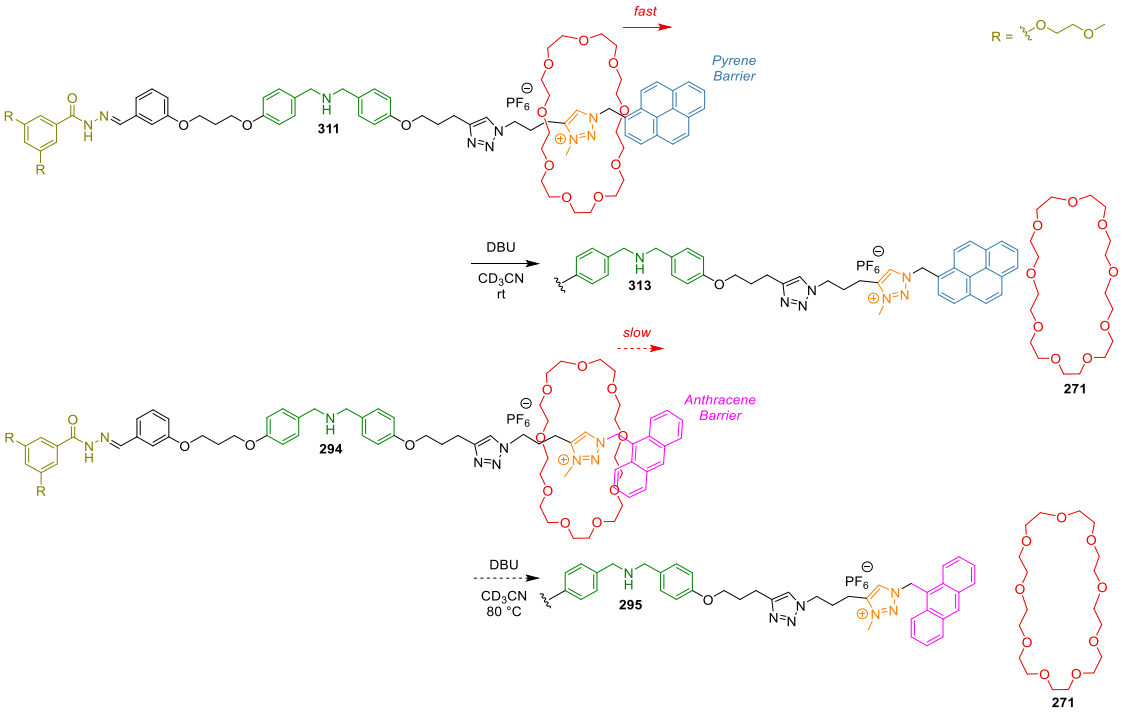

Scheme 8.51. Summary of the results described in this work for dethreading experiments conducted with pyrene (top) and anthracene (bottom) terminated (pseudo)rotaxanes **311** and **294** under basic conditions.

8.4.8. 4th Generation Model Pump Design Based on Pyrene and a Disulfide Stopper

It became clear that nature has already laid out a possible strategy: As highlighted in the introduction of this chapter, ion pumps (Figure 8.2 (c))[181b] or ABC transporter proteins (see Figure 8.6)[192] are able to actively transport particles in a completely unidirectional manner via a “two gate” mechanism. Following their example, as an attempt to solving the dethreading issues, a study of alternative disulfide-terminated pyrene-

based pump **314**·H⁺/**314** was investigated (Scheme 8.52). It was hoped that by reintroducing a disulfide barrier at a position that follows the chromophore/triazolium station the challenging task of finding a suitable chromophore system with an appropriate steric barrier profile for the dethreading with macrocycle 27C9 can entirely be avoided. Instead, in the system proposed substituents on the disulfide terminus dictate the energy barrier for the dethreading of 27C9. Studying the ON/OFF fluorescence signal would then give an indication to the position of the macrocycle as well as the rate of dethreading/disulfide exchange under basic conditions. Each pulse of chemical fuel **204** is expected to initiate a full cycle of unidirectional threading, shuttling and dethreading, which would not be possible if any of the system components are absent.

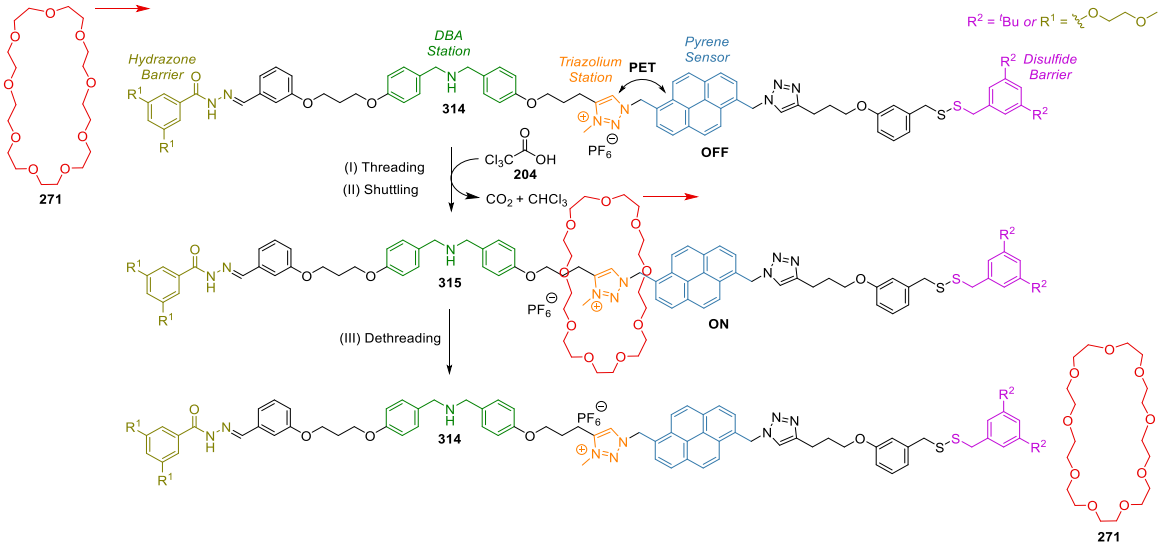

Scheme 8.52. Proposed operation of second pyrene model pump **314**·H⁺/**314** with macrocycle 27C9.

From a synthetic point of view, it was envisaged that preparation of the new pump system **314**·H⁺/**314** could be largely achieved by following previously successful examples of creating pyrene terminated rotaxane thread **313**·H⁺ (Scheme 8.53). The proposed retrosynthetic outline comprised the formation an alkyne terminated disulfide barrier precursor **271** which connected to one side of a bifunctional pyrene unit **316** obtained via sequential CuAAC reactions and methylation would allow reusing previous DBA fragment **291**.

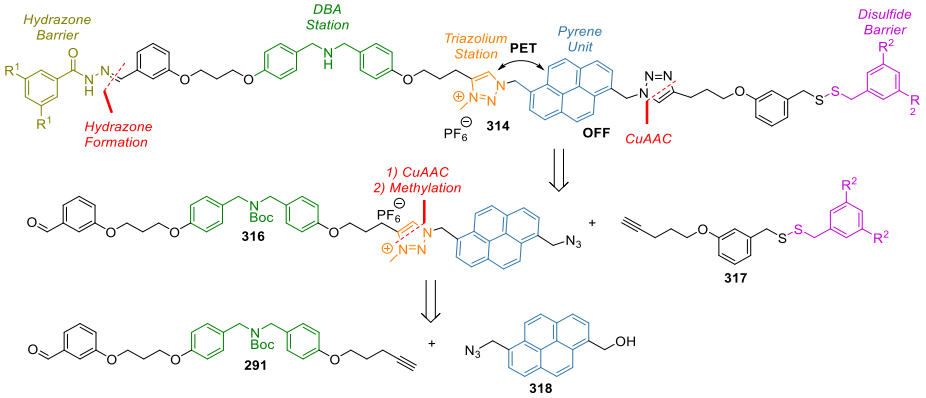

Scheme 8.53. Proposed retrosynthesis of second pyrene model pump **314**·H⁺/**314** starting from available DBA aldehyde fragment **291**, pyrene azide **318** and alkyne disulfide fragment **317**.

As a first step, synthesis of the disulfide precursor **317** was explored (Scheme 8.54). Beginning with commercially available 3-hydroxybenzyl alcohol **319** and alkylating the phenol group with pentynyl tosylate,

intermediate benzylic alcohol **320** was obtained in very good yields. Subsequently conversion of the alcohol group into the corresponding thioacetate via successive Appel reaction and displacement with potassium thioacetate gave **321**. The same substitution was also carried out with benzylic bromide **322** to yield the corresponding acetyl protected benzyl mercaptan. This compound was activated to 2-thiopyridone **323** with 2-aldrithiol to enable the formation of a mixed disulfide with **324**. This has allowed isolating the desired disulfide precursor **317** in 18% over six steps.

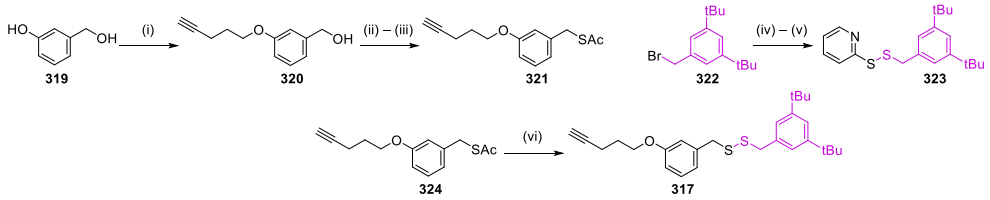

Scheme 8.54. Synthesis of disulfide **317**. Reagents and conditions: (i) pent-4-yn-1-yl tosylate, K_2CO_3, CH_3CN, 85 °C, 16 h, 81%. (ii) Ph_3P, CBr_4, CH_2Cl_2, 0 °C, 15 min, 88%. (iii) KSAc, CH_3CN, 85 °C, 15 h, 91%. (iv) KSAc, CH_3CN, 85 °C, 19 h, 98%. (v) 2,2′-dipyridyl disulfide, pyrrolidine, CH_2Cl_2, rt, 17 h, 70%. (vi) pyrrolidine, CH_2Cl_2, rt, 27 h, then dithiol **323**, rt, 22 h, 43%.

Next, commercially available dibromo pyrene **325** was converted to diol **326** via a combined formylation and reduction reaction based on lithium-bromide exchange and reacting the generated aryl lithium compound with DMF, hydrolysing the imine with HCl, and finally reducing the aldehyde groups with sodium borohydride. The diol was then desymmetrised to mono azide **318** with azide exchange reagent diphenyl phosphoryl azide (Scheme 8.55). Attempts to generate the azide by the reaction with ADMP were unsuccessful.

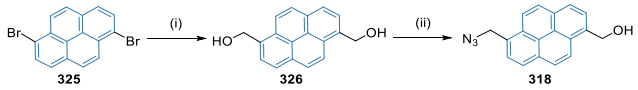

Scheme 8.55. Synthesis of pyrene monoazide **318**. Reagents and conditions: (i) ^{n}BuLi, Et_2O, −78 °C to rt, 85 min, then DMF, −78 °C to rt, 30 min, then HCl, −78 °C to rt, 25 min, then $NaBH_4$, MeOH, −10 °C to rt, 1 h, 57%. (ii) $(PhO)_2PON_3$, DBU, DMF, 0 °C to rt, 3 h, 72%.

With those fragments in hand, the preparation of disulfide-terminated free thread **329**·H^+ was completed in four steps from starting DBA alkyne precursor **291** and pyrene monoazide **318** (Scheme 8.56).

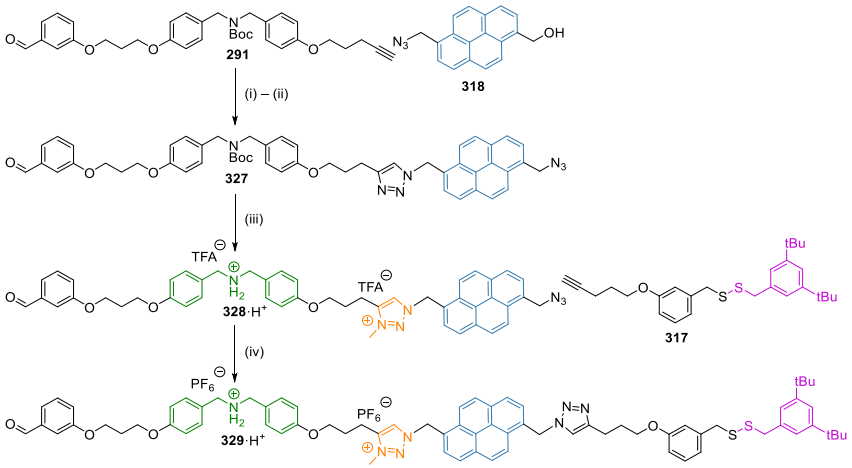

Scheme 8.56. Synthesis of 4th generation pyrene free thread **329**·H^+. Reagents and conditions: (i) $[Cu(CH_3CN)_4]PF_6$, CH_2Cl_2:^{t}BuOH, rt, 2 d, 88%. (ii) ADMP, DBU, THF, 0 °C to rt, 2 h, 68%. (iii) MeOTf, CH_2Cl_2, rt, 19 h, then TFA, CH_2Cl_2, 0 °C, 45 min, quantitative. (iv) $[Cu(CH_3CN)_4]PF_6$, CH_2Cl_2:^{t}BuOH, rt, 3 d, then anion-exchange (amberlyst A26/ PF_6^-, CH_3CN), 84%.

Commencing with CuAAC reaction between with DBA alkyne **291** and mono azide **318** the intermediate alcohol terminated thread was formed which, when reacted with ADMP, afforded azide intermediate **327** in yields of up to 60% over two steps. In the following, methyl triflate was utilised as a methylation agent to yield triazolium intermediate **328**·H^+. Removal of the Boc-protecting group with acid and final CuAAC with previously isolated alkyne **317**, enabled preparation of **329**·H^+ in a yield of 84% over two steps. This method has proved effective in producing several hundred milligrams of pyrene free thread **329**·H^+ repeatedly.

Next, rotaxane formation between aldehyde free thread **329**·H^+ and macrocycle 27C9 was evaluated to study the switching of the isolated model pump by NMR (Scheme 8.57). In a preliminary attempt the desired [2]rotaxane **330**·H^+ was isolated in a yield of 15% using previously established conditions for the threading of 27C9. Interestingly, also the formation of a [3]rotaxane **331**·H^+ was observed in a yield of 19% from the reaction which suggested that disulfide exchange takes places when using TFA in large amounts.

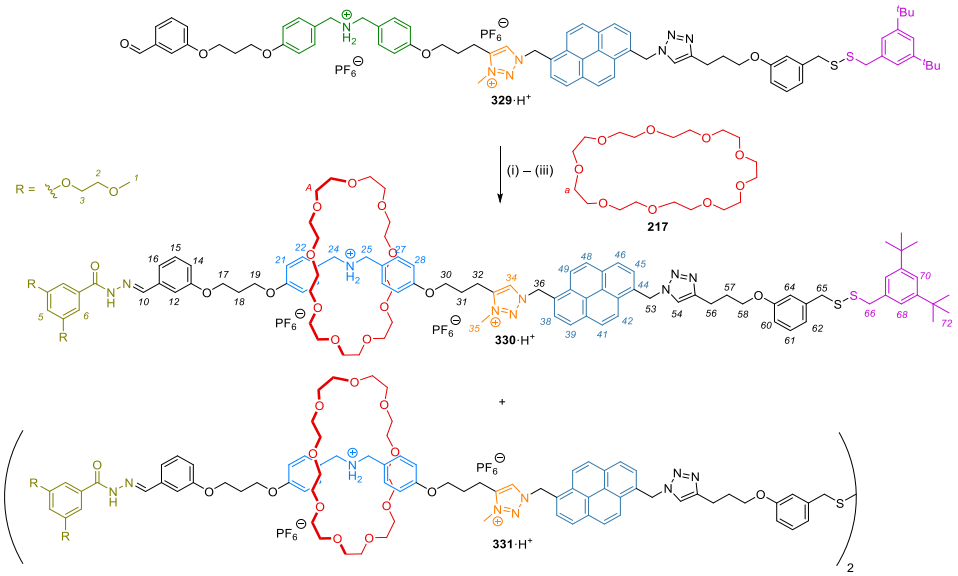

Scheme 8.57. Synthesis of [2]rotaxane **330**·H^+ and [3]rotaxane **331**·H^+ from thread **329**·H^+, 27C9 and hydrazide **269**. Reagents and conditions: (i) TFA, CD_2Cl_2, rt, then (ii) 27C9 (5 eq.), then (iii) hydrazide **269** (2.0 mM), then Et_3N, then anion-exchange (amberlyst A26/ PF_6^-, CH_3CN), 15%.

With the limited material of **330**·H^+ in hand also the following switching with DBU was performed and followed by NMR (Figure 8.32). In a large part, the observed shifting of characteristic protons resembled previous switching studies with for example rotaxane **312**·H^+ (24C8, pyrene) when switching from the protonated **330**·H^+ to the deprotonated state **330** with two equivalents of DBU. As shown in Figure 8.32,^{1}H NMR signals recorded both for the (b) intermediate pseudo[2]rotaxane aldehyde and (c) isolated hydrazone **330**·H^+ agree well with another. Consequently, it was expected that the ensuing operation of rotaxane **330**·H^+/**330** can be easily followed by comparing obtained spectra with the reference data shown in (c) and (d).

In practice, it was envisaged that depending on shuttling of rotaxane **330**·H^+/**330** the position of the macrocycle can be determined by either looking at the proton signals of the methyl group of the triazolium motif H_{35} under basic or the corresponding benzylic protons H_{24} and H_{25} under acidic conditions. In both cases signals are well-resolved and allow for quantification of the shuttling via integration of the signals.

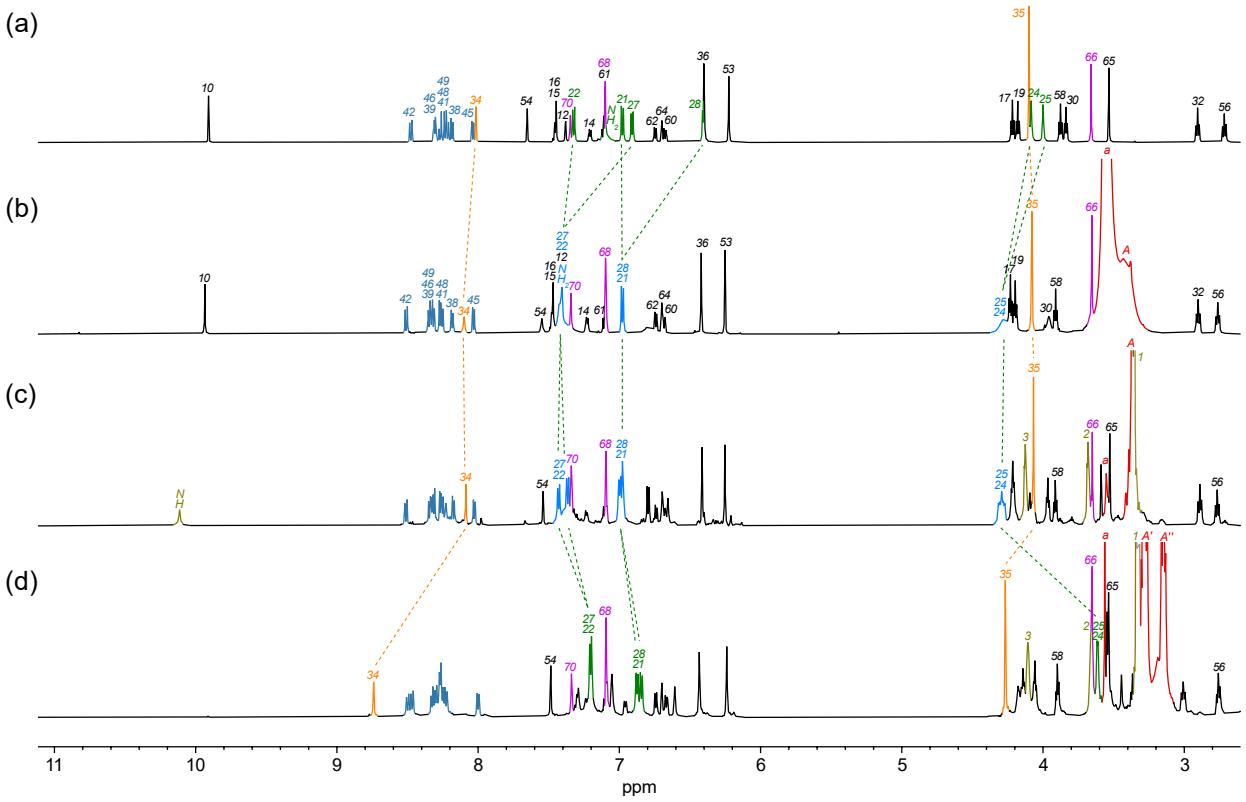

Figure 8.32. Partial ^{1}H NMR spectra (600 MHz, CD_3CN, 298 K) of (a) free thread **329**·H$^+$ (5.0 mM) and (b) after addition of TCA and macrocycle 27C9. (c) Isolated rotaxane **330**·H$^+$ and (d) after switching with DBU (2.0 eq) *in-situ*. Peak assignments correspond to labelling in Scheme 8.57

At this point it was also decided to mask the previously noticed competing binding of the hydrazone motive to the macrocycle by removing the presence of a potentially interfering acidic proton H_{NH} in the final operations. It was hoped that this would also reduce the effective amount of base required to induce shuttling. For this purpose, a methyl-substituted analogue of glycol-functionalised hydrazone **269** was prepared using an adapted literature procedure (Scheme 8.58).[280] Starting from tetrachlorophthalic anhydride the corresponding imide **332** was formed through condensation with hydrazide **269**. Subsequent methylation was achieved using Mitsunobu coupling conditions yielding intermediate **333** in a yield of 68%. Final deprotection with an excess of a hydrazine under Gabriel synthesis conditions furnished the desired methyl-substituted hydrazide **334**.

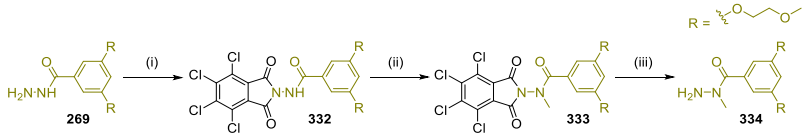

Scheme 8.58. Synthesis of methylated hydrazide **334**. Reagents and conditions: (i) tetrachlorophthalic anhydride, PhMe, 120 °C, 19 h, 98%. (ii) PPh_3, DEAD, MeOH, THF, 0 °C, 2 h, 95%. (iii) hydrazine monohydrate, EtOH, 70 °C, 24 h, 85%.

The operation of pump **329**·H$^+$ was then repeated using alternative hydrazide **334** along with macrocycle 27C9 under otherwise identical conditions (Scheme 8.59) and monitored with ^{1}H NMR (Figure 8.33).

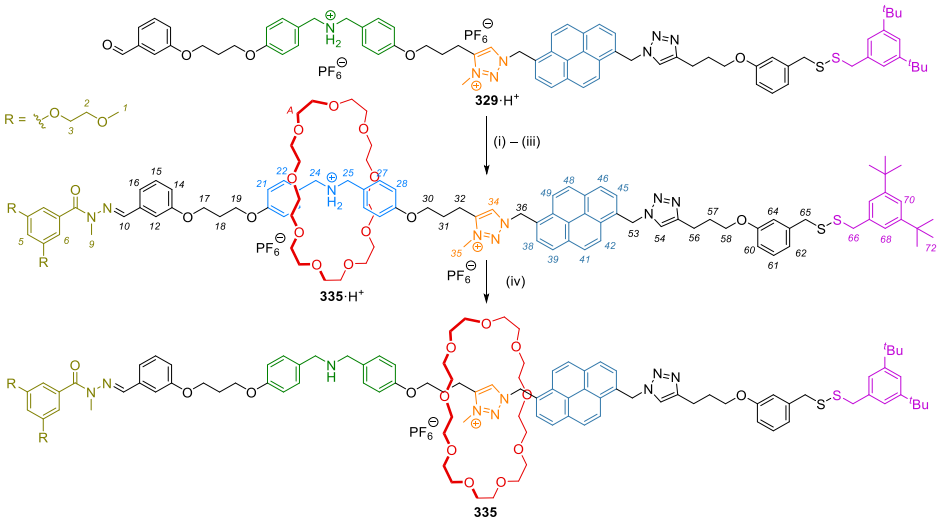

Scheme 8.59. Threading of macrocycle 27C9 onto pyrene free thread **329**·H⁺ using TCA, capping with methylated hydrazide **334** and switching with DBU *in-situ*. Reagents and conditions: (i) 27C9 (5.2 eq.), CD_3CN, rt, then (ii) Me-hydrazide **334** (3.0 eq.), then (iii) TCA (2.0 eq.), then (iv) DBU (2.0 eq.).

As can be seen by indicative proton peaks such as of the triazolium unit H_{34} and H_{35}, as well as DBA peaks H_{24} and H_{25}, in addition to the actual macrocycle peaks H_A and $H_{A'}$/$H_{A''}$, shuttling of 27C9 occurs immediately after the addition of exactly one equivalent of DBU (Figure 8.33 (c)). However, even over a short period of less than one hour disulfide exchange/cleavage occurred (compare Figure 8.33 (c) and (d)) as evident by overall scrambling of signals e.g. of the triazolium peaks H_{34} and H_{35}. Concomitant, an overall broadening of the peaks for threaded 27C9 peaks $H_{A'}$ and $H_{A''}$ was observed.

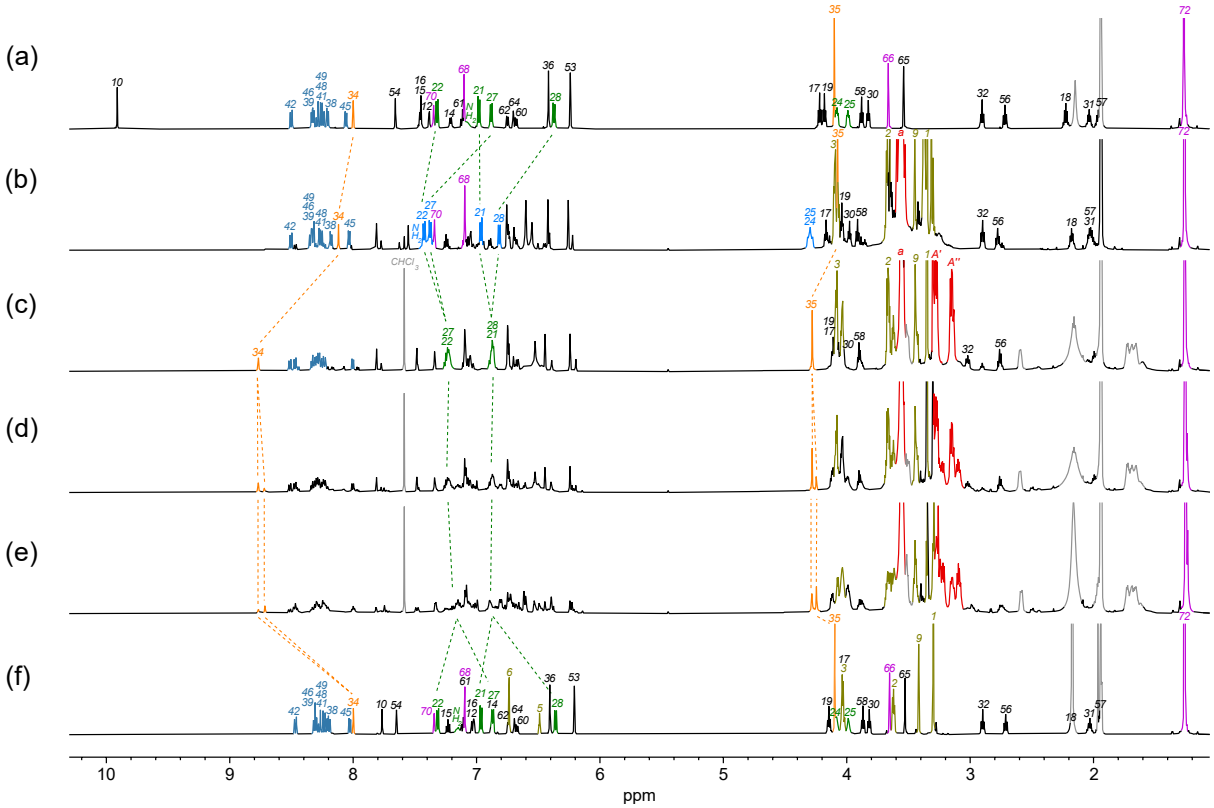

Figure 8.33. Partial ^{1}H NMR spectra (600 MHz, CD_3CN, 298 K) of (a) free thread **329**·H⁺ (5.0 mM), (b) after addition of 27C9, Me-hydrazide **334**, and TCA. [2]rotaxane **335** after switching with DBU (c) immediately at t_0 = 0 h and after an interval of (d) t_1 = 1 h and (e) t_2 = 19 h. (f) Isolated free thread hydrazone **336**·H⁺. Peak assignments correspond to labelling in Scheme 8.59.

It was concluded that a reasonable explanation for this is finding could be the presence of the quite nucleophilic hydrazide **334** during the operation. Under basic conditions this species could promote undesired disulfide exchange/cleavage. In order to avoid the interference of the free hydrazone a survey of the literature suggested that alternatively, hydrazone exchange may be used to for the formation of final rotaxane **335**·H⁺/**335** which may be catalyzed as well by a weakly basic nucleophilic catalyst such as aniline (Scheme 8.60).[281] It was hypothesized that using an excess of a preformed hydrazone substrate such as **338a-c** – see Scheme 8.61 for the preparation of hydrazones conducted – attached hydrazide can be transferred from **338** onto the free thread aldehyde **339**·H⁺ under acidic conditions instead to conclude the formation of intermediary rotaxane **325**·H⁺.

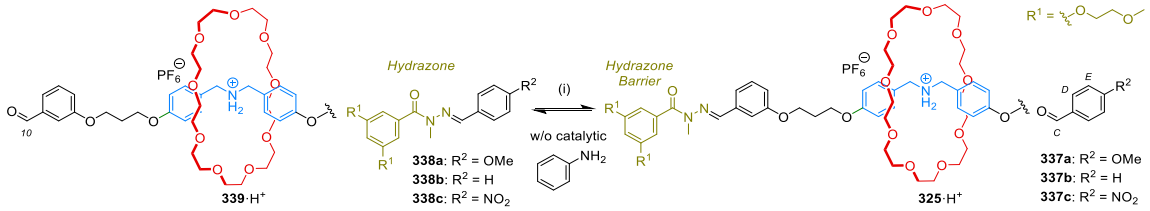

Scheme 8.60. Postulated hydrazone exchange operation scheme with model pump aldehyde **329**·H⁺.

When turned basic hydrazone exchange will come to an end and all hydrazide in the system will be bound as either hydrazone **325** or **338**. Monitoring the exchange reaction can then be conveniently performed with ^{1}H NMR by following proton signal H_{10} for rotaxane aldehyde **339**·H⁺ and similarly for aldehyde protons H_C of starting hydrazone materials **338a-c** (see for example the experiment described Figure 8.34).

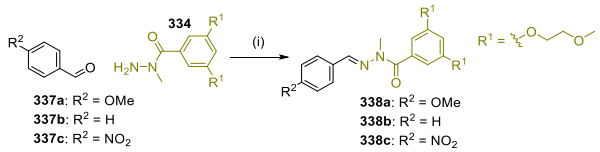

Scheme 8.61. Synthesis of hydrazone surrogates **338a-c** (**338a**: R^2 = OMe, **338b**: R^2 = H, **338c**: R^2 = NO_2). Reagents and conditions: (i) TFA, CH_2Cl_2, rt, 10 to 15 min, then Et_3N, rt, 5 min, 80% (**338a**), 95 % (**338b**) and 91% (**338c**).

And pleasingly, the working of this strategy was confirmed when repeating the previous pre-operation sequence but using hydrazones **338a-c** instead of methyl hydrazide **334** as acid-labile transfer agent. As shown in Figure 8.34 the signal of aldehyde rotaxane **339**·H⁺ diminished over time after TCA was added to a mixture of thread **329**·H⁺, macrocycle 27C9, corresponding Me-hydrazones **338a-c** and disulfide **340** (see Scheme 8.62 for reaction scheme). Qualitatively, anisaldehyde derived hydrazone **338a** showed fastest exchange followed by benzaldehyde derivative **338b**. Electron deficient 4-nitro substituted benzaldehyde **338c** displayed slowest exchange under the conditions studied. A significant rate enhancement was observed with one equivalent of aniline over the uncatalyzed operation. In the case of hydrazone exchange from **338a** to pseudorotaxane **325**·H⁺ the transfer was completed in less than 12 h whereas with **338b** twice the reaction time was required. In case of the nitro derivative 338c the exchange reaction was still not complete after 48 h even with aniline as catalyst. Quantitatively, neither with nor without aniline the order of the reaction kinetics were determined in the first place during this preliminary studies.

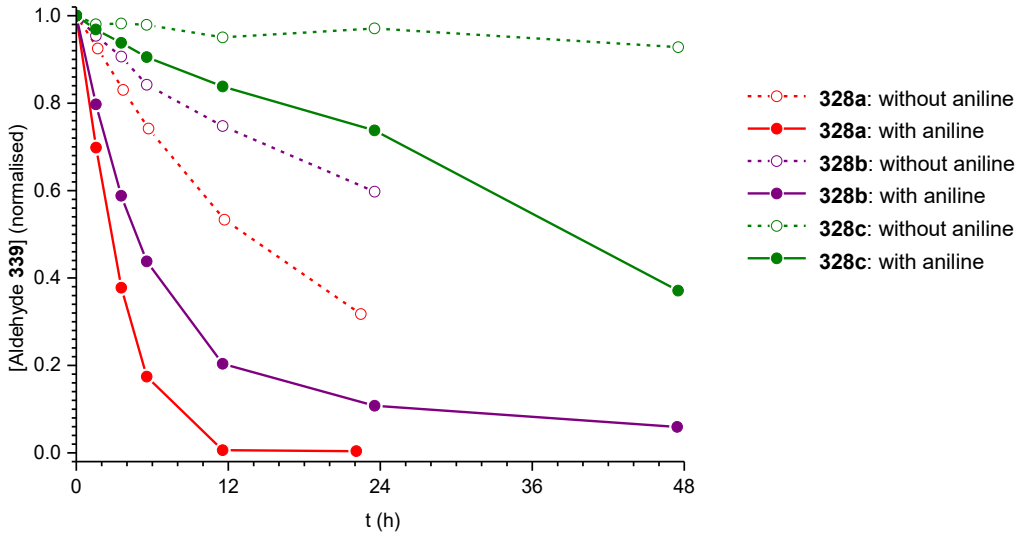

Figure 8.34. Comparison of the hydrazone exchange kinetics of pyrene model pump **329**·H$^+$ for a series of 4-subtituted hydrazones **338** (**338a**: R^2 = OMe, **338b**: R^2 = H, **338c**: R^2 = NO_2) either without or in the presence of 1 equivalent of aniline. Reagents and conditions: (i) thread **329**·H$^+$ (5.0 mM), 27C9, (5.0 eq.) Me-hydrazone **338a-c**, (5.0 eq.) disulfide **340**, (2.0 eq.) w/o aniline, (1.0 eq) TCA, (10.0 eq.) CD_3CN, rt. The conversion of the hydrazone exchange was determined with ^{1}H NMR by integration of the proton signals H_{10} for rotaxane aldehyde **339**·H$^+$ over a duration of up to 48 h.

Nevertheless, building on the hydrazone exchange reaction with anisaldehyde hydrazone **338a** the stepwise operation of pump **329**·H$^+$ was repeated both with and without aniline (Scheme 8.62 and Figure 8.35).

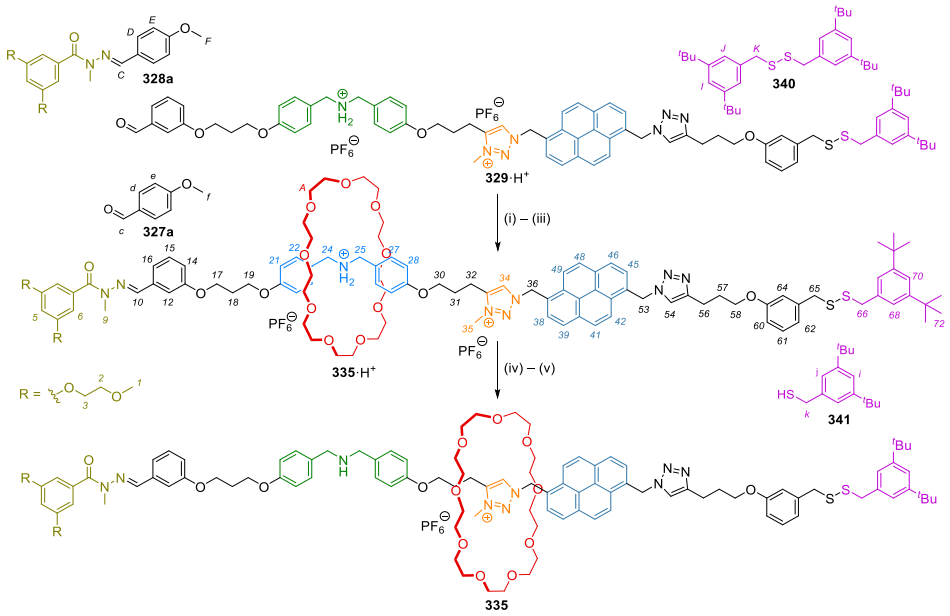

Scheme 8.62. Trialed stepwise operation of pyrene model pump **329**·H$^+$ using TCA, 27C9 and relying on hydrazone exchange with Me-hydrazide **338a** in the presence of disulfide **340** and free thiol **341**. Reagents and conditions: (i) 27C9, (5.0 eq.) CD_3CN, rt, then (ii) hydrazone **338a**, (5.0 eq.) disulfide **340**, (2.0 eq.) aniline, (1.0 eq) then (iii) TCA, (10.0 eq.) then (iv) DBU, (up to 4.0 eq.) then (v) free thiol **341** (up to 1.0 eq.).

As anticipated, shuttling of 27C9 from the DBA to the triazolium station still occurred as indicated by the characteristic shifts of protons for the triazolium unit H_{34} as well as H_{35} and also the pyrene chromophore, particularly for those positions facing towards the triazolium moiety H_{38} as well as H_{49} (determined with additional NOESY experiments). Unlike before (see Scheme 8.59 and Figure 8.33), basic conditions did not

lead to disulfide exchange/cleavage or dethreading, even when reacting over an extended period up to 21 h. Excited by this result, the final dethreading step of the operation cycle was trialled by adding free thiol **341** to the system. However, even after 7 d no sign of dethreading was observed by NMR. Heating the sample at 70 °C for a further 6 d led to apparent sample decomposition as seen by the spectra (j) in Figure 8.35.

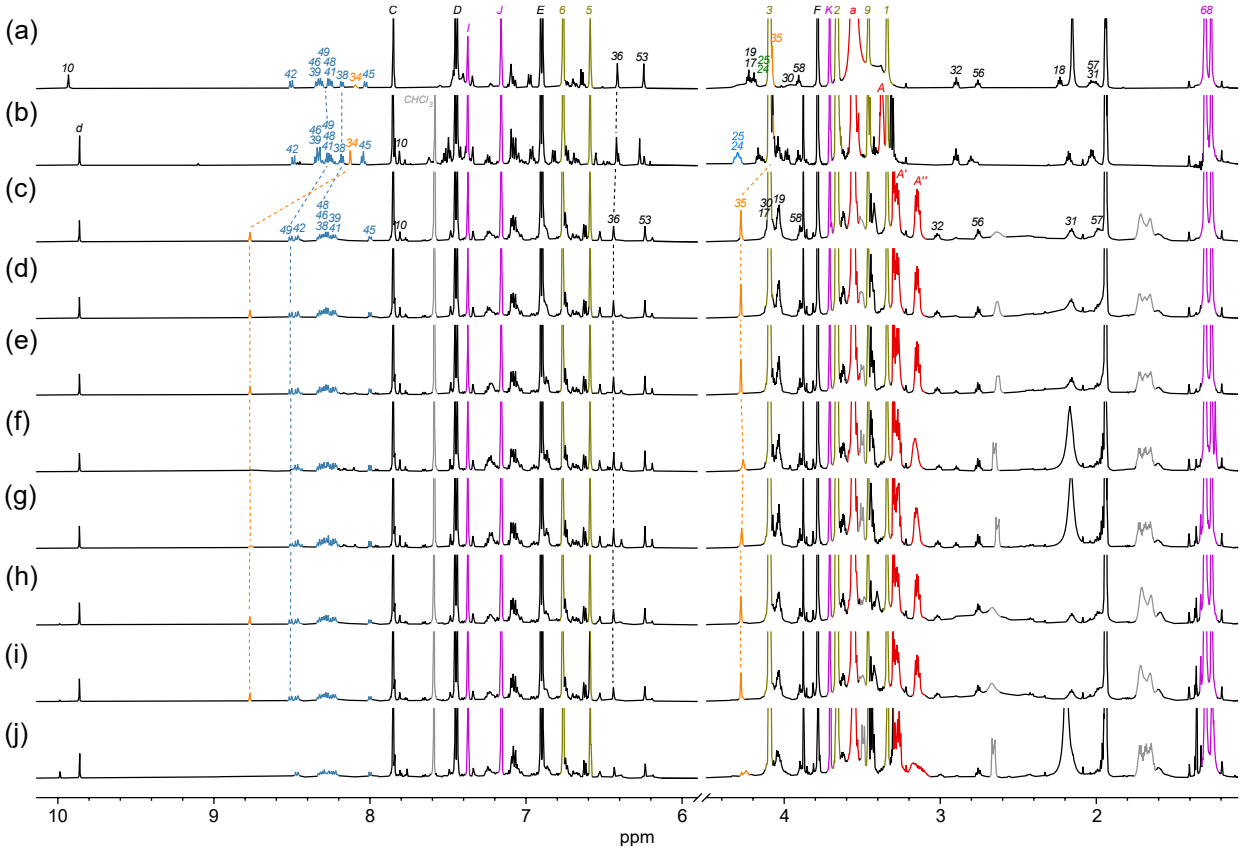

Figure 8.35. Partial ^{1}H NMR spectra (600 MHz, CD_3CN, 298 K) of the operation of pyrene model pump **329**·H^+ (5.0 mM) (a) before and (b) after the addition TCA and a delay of 22 h. (c) Intermediate rotaxane **335** immediately after the addition of DBU (3.0 eq) and (d) after another period of 21 h. After addition of (e) 10 mol% and (f) 1 eq. free thiol **341** as well as (g) after a period of 17 h. (h) After addition of additional DBU. (4.0 eq. in total) (i) After leaving the sample for 2 d at room temperature then (j) heating the sample at 70 °C for another 5 d. Peak assignments correspond to labelling in Scheme 8.62.

Although significant intermediate broadening of the signals for protons H_{38} and H_{49} can be observed after addition of free thiol **341** (Figure 8.35 (f) and (g)) the alluded dynamic exchange of the system[47a] was not accompanied by a qualitative decrease of the split macrocycle signals $H_{A'}$ and $H_{A''}$ at 3.3 and 3.1 ppm. Additionally, once another equivalent of DBU (Figure 8.35 (h)) was added the original state was restored. (compare e.g. with Figure 8.35 (d)) This somewhat unexpected behaviour, may be explained by the oxidation of the free thiol to the corresponding disulfide or another unknown side reaction. Elucidating the cause of this issue by analysing the supplementary $^{13}C^{1}H$ correlation data obtained for the mixture at characteristic intervals, however, did not allow proving this assumption due to the significant overlap and marginal difference between characteristic signals for the free thiol **341** and corresponding disulfide **340**. Trying other solvents for the operation as suggested by literature[282] did not change the outcome of the operation. In all cases (either with or without aniline in CD_3CN, CD_2Cl_2, $CDCl_3$) the first two steps of the operation – threading and shuttling – were successful but dethreading proved elusive. Preliminary results for monitoring reactants in the crude during the operation with LCMS were inclusive giving a range of unidentifiable species.

For that reason, the preparation of an alternative free thiol **344** was investigated. Judged by CPK modelling free thiol **344** would prevent passage of 27C9 once forming the mixed disulfide with pyrene model pump **329**·H^+. It was hoped that with the additional glycol chains monitoring the disulfide exchange with ^{1}H NMR could be simplified by additional characteristic (isolated) signals. Completing the synthesis in five steps from starting 3,5-dihydroxybenzoate **342** via successive hydride reduction, Appel reaction, substitution with thioacetate and deprotection with hydrazine allowed isolating the new glycol functionalised free thiol **344** in several hundred milligrams as a solid (Scheme 8.63).

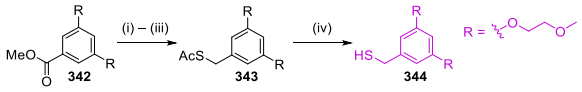

Scheme 8.63. Synthesis of glycol-functionalised free thiol **344**. Reagents and conditions: (i) $LiAlH_4$, THF, 0 °C to 65 °C, 20 h, 81%. (ii) PPh_3, CBr_4, CH_2Cl_2, 0 °C, 20 min, 77%. (iii) KSAc, MeCN, 85 °C, 16 h, 99%. (v) hydrazine, CH_3CN, 0 °C to rt, 6 h, 79%.

Adding this new free thiol **342** (up to two equivalents) to the previous operation, however, did not change the outcome of the dethreading and left the ^{1}H NMR signals of the machine entirely unaffected. As a possible explanation it seemed plausible that the dethreading is prevented by either a slow disulfide exchange reaction of the mixed disulfide in pyrene model pump **329** or by additional side reactions of the machine with both free thiol **341** and **344**. Yet, there was no time left for determining the cause of this issue.

8.5. Conclusion and Outlook

In summary, over the course of the presented study a series of four designs have been tested for the proposed operation of a model 1-barrier pump (see Scheme 8.31 for the basic concept). Relying on the kinetic stability of a hydrazone [2]rotaxane, enabled by the steric bulk of either an anthracene or a pyrene unit, a procedure has been developed that allowed isolation of anthracene [2]rotaxanes **288**·H^+/**288** (DB24C8), **289**·H^+/**289** (24C8) and **294**·H^+/**294** (27C9) and also corresponding pyrene systems **312**·H^+/**312** (24C8) and **311**·H^+/**311** (27C9). This has enabled their switching behaviour under acidic and basic conditions both with NMR and fluorescence spectroscopy to be analysed. It was demonstrated that with both techniques, individual switching states can be identified successfully by large characteristic proton shifts on the one hand and on the other by up to a tenfold increase/decrease of the measured fluorescence signals of the chromophores. Moreover, combining two systems with different fluorophores allowed simultaneous independent monitoring of individual switching states of anthracene and pyrene model pumps using different excitation wavelengths. Fluorescence experiments also revealed that the fluorescence of pyrene is weaker compared to the one of anthracene and would have to be considered for the final operation. Ultimately, it was shown that switching can be performed over multiple cycles fully reversibly either by applying acid and base stepwise or alternatively, using chemical fuel TCA.

The dethreading properties of isolated (pseudo)[2]rotaxanes under basic conditions were scrutinised. The experiments performed showed that in case of the anthracene thermally assisted dethreading is slow with macrocycles 24C8 and 27C9 and leads to additional side reactions. Isolation of the corresponding DB30C10 derived pseudo[2]rotaxanes system was not successful. All in all, this suggested that the optimal size for the dethreading when using an anthracene barrier is comparable if not slightly larger than 27C9 but smaller than

DB30C10, if isolation of the intermediate (pseudo)rotaxane is desired. Opposite to this, dethreading of the pyrene-based is observed already with 24C8 and even more pronounce with 27C9. As such, it remains to be seen whether this allows operating a pyrene-based model 1-barrier pump with 24C8 successfully.

Ensuing studies with an alternative pyrene-based design relying on a disulfide terminus to control the dethreading under basic conditions have manifested the basic possibility to construct a suitable 1-barrier model pump. It was shown that similarly to previous attempts, formation of the intermediate pseudorotaxane takes place under the various conditions trialled and, importantly, switching with acid and base still gives rise to well defined states that can be discerned with NMR. Furthermore, it was revealed that hydrazone exchange can successfully be employed to allow for the intermediate formation of hydrazone rotaxanes from related aldehyde pseudorotaxanes and prevent disulfide scrambling as a result of free nucleophilic hydrazide. A survey of different hydrazone substrates has confirmed that particularly electron rich hydrazones can effectively participate in this type of reaction.

It remains to be seen whether by continuing the studies with free thread **329**·H⁺, subsequent dethreading can be affected with the created model pump system either by using a larger macrocycle such as DB30C10 for the operation or alternatively, finding a suitable kinetic barrier that enables dethreading of 27C9 over the intermediate pyrene unit at sufficient rate but also prevents threading under acidic conditions (Scheme 8.64).

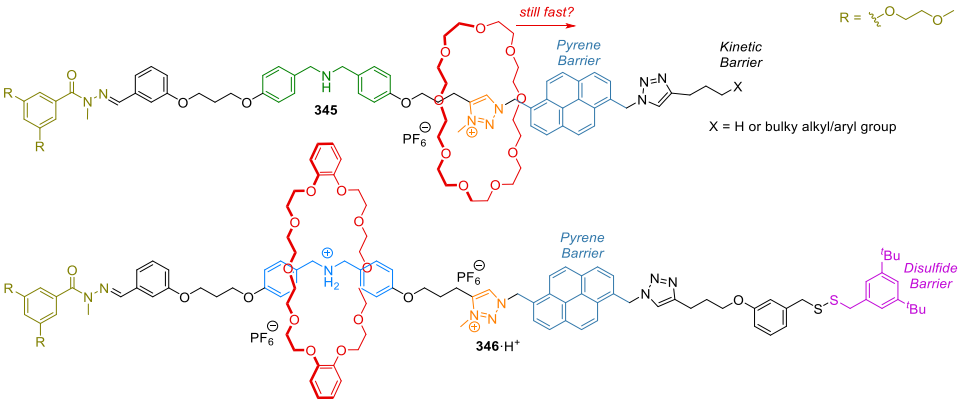

Scheme 8.64. Proposed test experiment for the operation of the original pyrene model pump **329**·H⁺ using surrogate unit X (e.g. a bulky alkyl/aryl group) to confirm dethreading with macrocycle 27C9 and alternative operation of a pyrene pump **346**·H⁺/**346** with larger macrocycle DB30C10.

As an alternative, it has been suggested to examine the substitution of the benzylic disulfide system with a corresponding alkylic system (Scheme 8.65).

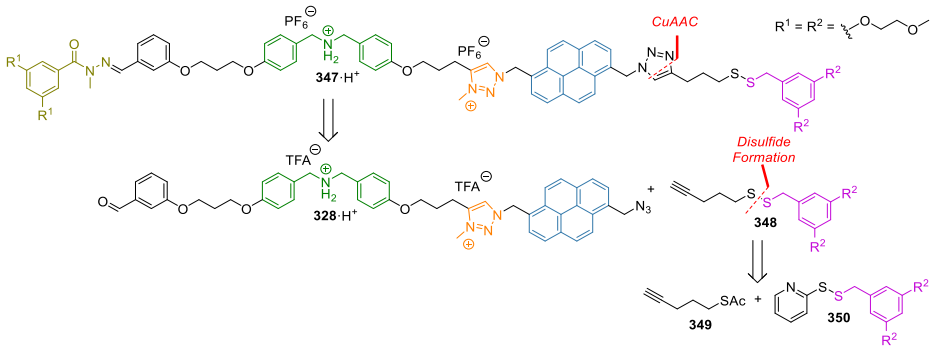

Scheme 8.65. Proposed retrosynthesis of 3rd pyrene model pump **347**·H⁺. The updated design reuses previously established pyrene azide **328**·H⁺ as a building block to connect mixed alkyl benzyl disulfide **348** which may be made from activated thiol stopper **350** and 4-pentynyl-1-thioacetate **349**.

It is hoped that this would not only reduce steric bulk around the disulfide bond (alkyl vs benzyl thiol) but also simplify the overall synthesis of a corresponding a third pyrene-based rotaxane pump **347**·H^+/**347** from components such as **328**·H^+, **349** and **350**. By taking a closer look at the kinetics of the disulfide exchange it may become possible to enable the operation of the proposed model pump. It would also provide the opportunity to contribute to the general understanding of this reaction in non-aqueous media, as literature examples on this topic besides studies in water or DMSO are scarce.

Once these final problems can be overcome, the operation of the proposed pyrene-based bistable rotaxane pump would provide the first example of directly monitoring a molecular transport process in an out-of-equilibrium state with an optical method (Figure 8.36). It is anticipated that once successful, the principal design due its modular components can allow the operation and analysis of more elaborate systems and ultimately, enable studying more complex functional behaviour of created artificial molecular machines.

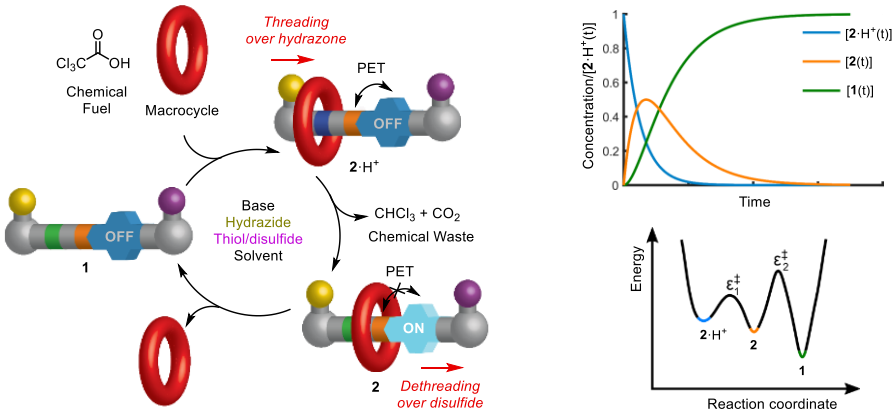

Figure 8.36. Proposed pyrene-based rotaxane pump **2**/**2**·H^+ and its operation with 27C9.

9. Summary and Outlook

Looking back at the results of this work and bringing them into line with the overall context of the study of molecular machines, it is apparent that mimicking nature's sophisticated examples with synthetic methods is a challenging target. Both the development of basic concepts and the necessary chemistry to enable their functioning are still largely based on an intuitive chemical notion. It is evident that developing artificial molecular machines demands rigorous testing and constant revaluation of each machine's operation results; And changing even small aspects in the design can incur an unexpected outcome for their operation. It has been shown that it remains beyond current capabilities to fully project the complex dynamics of biology into artificial molecular systems solely by a rational approach for various practical and theoretical reasons.

Yet, the unprecedent progress that has been made in the understanding of basic principles has opened up the possibility to potentially overcome this limitation in the future. As successfully proven, ratchet designs can be employed to control molecular motion. Based on those ideas several examples have been developed that actively perform unidirectional rotary and translationary movement. Altogether, these efforts have allowed bringing Feynman's goal a significant step closer to the actual realisation of a molecular machinery.

Importantly, taking advantage of this previous knowledge has allowed to create and successfully operate a molecular synthesiser that takes inspiration in the working of the ribosome. With this work, it was shown that by extending reported basic chemical frameworks one can successfully form multiple carbon-carbon bonds in a predetermined manner. In our example, this has allowed preparation of stilbene sequences that can be cyclised to helicenes. These results have proved the generality of this design and suggested that it may be used as platform for further investigations and advanced transformations. It sems likely that by learning how to further control the movement at each step and providing a method to ensure reversibility of each bond formation, ultimately, machines can be created that will take the shape of true "molecular assemblers."[162]

At the same time, the advancements that have been made towards visualising the motion of a chemically fuelled molecular pump design with a fluorescence unit have highlighted an additional aspect for the studies of molecular transporters and motors.[31] Based on the results achieved several opportunities can be imagined that enable exploring the dynamics with this concept in much greater detail: Unlike reasoning from the transition between equilibrium states, this method should be capable to allow monitoring nonequilibrium states and therefore, may be suited to ultimately prove unidirectionality of various pump systems. Due to its unique optical properties particular the use of the pyrene motif appears useful for this endeavour. While the final idea could not be implemented several aspects of the basic methodology were demonstrated. Both suitable fluorophores and a chemical platform have been identified and tested. Furthermore, the first steps towards the operation of a molecular pump have been completed. Once solving the current dethreading issues it can be expected that this would allow completing the project. Achieving this target could then form the basis for studying more advanced systems with these optically active building blocks.

For example, it can be imagined that the extension of this fluorescence switching concept could potentially allow for the construction of light-based information ratchet mechanism whose motion can be detected with fluorescence spectroscopy. It is speculated that by combining the effect of PET from the pyrene fluorophore to the triazolium unit and ET from the fluorophore to a stilbene unit, a system such as **351** (Scheme 9.1) could enable illuminating the path of a moving macrocycle with a position-dependent ratchet mechanism.

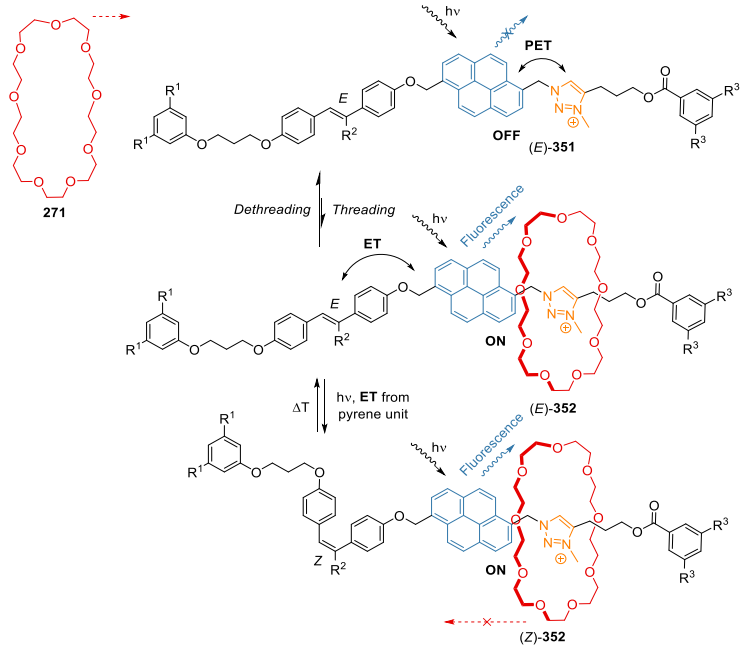

Scheme 9.1. Proposed light-based information ratchet **351** relying on macrocycle-induced modulation of the ET between a stilbene unit and a pyrene fluorophore that acts as a photosensitizer for the double bond isomerisation. Rotaxane formation will be indicated by an increase in fluorescence of the pyrene unit.

As shown earlier, the photoisomerization of methylstilbene **353** in the PSS can be influenced by different photosensitizers such as pyrene via an ET process (see Figure 9.1 for an overview of the effect on the *E*:*Z* ratio of stilbene when using different sensitizers).[107]

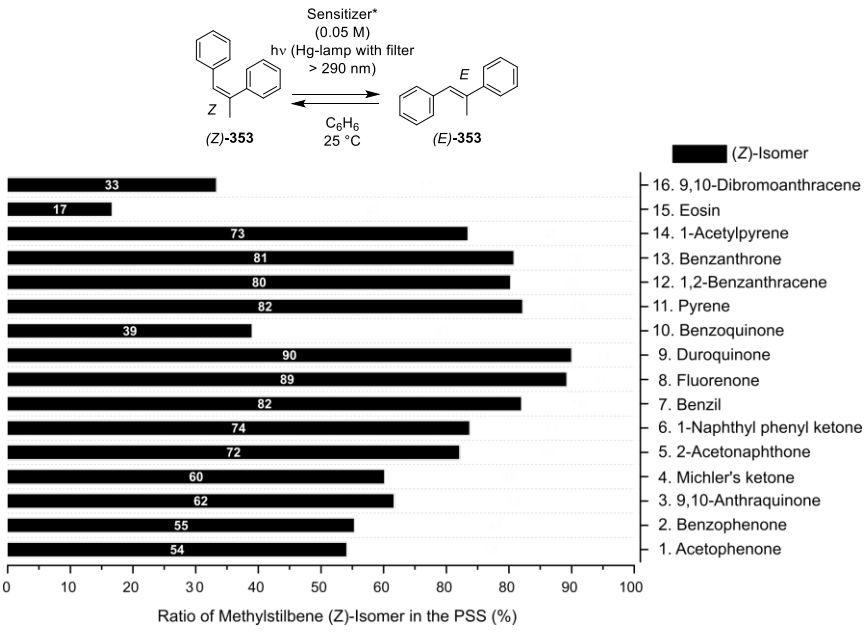

Figure 9.1. Photochemical isomerisation of methylstilbene **353** in the presence of different sensitizers.[107a] Energy transfer (ET) from an excited state of a sensitizer with energy E_T changes the ratio of methylstilbene isomers (*Z*)-353 formed at the PSS.[107]

The idea has been stimulated by the reported cation-recognised photosensitization in the isomerisation of 1,2-dichloroethylene (DCE) **354** as described by Oshima and co-workers (see Figure 9.2 for more details).[283]

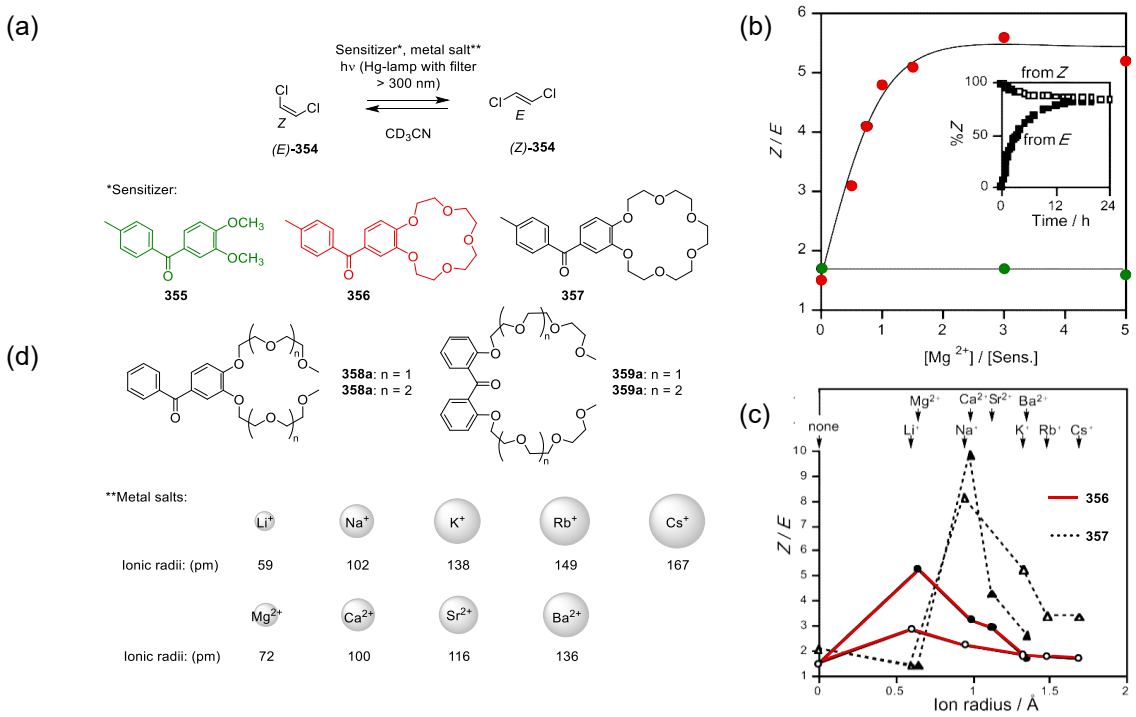

Figure 9.2. Photosensitized isomerization of 1,2-dichloroethylene **354** with 5- and 6-crown ether macrocycle **356** and 357 in comparison to benzophenone **355**.[283] (a) Principal reaction and (b) dependence of the *E*−*Z* ratio in the photo stationary state (PSS, λ >300 nm) on the concentration of $Mg(ClO_4)_2$ for photosensitizer **356** (●) and reference **355** (●). (c) Plot of the (*E*)-**354**:(*Z*)-**354** ratio (10 mM) at the PSS versus the ion radius of alkali (○, ▵) and alkaline earth metal (·, ▲) ions added in the presence of photosensitizer 5-crown **356** (solid line) and 6-crown ether **357**. (dotted line) (d) Effects of metal cation recognition on the isomerisation ratio (*E*)-**354**:(*Z*)-**354** two types of benzophenones **358a-b** and **359a-b** (no shown). With increasing cation size, the ratio of (*Z*)-**354** in the PSS increased from 67 to 91% for **358a-b** but remains unchanged (86−88%) for derivatives **359a-b**. Ionic radii have been taken from literature.[63] Plots (b) and (c) have been adapted with permission from 283a. Copyright (2002) American Chemical Society.

It is hoped that the sensitization effect could be similarly modulated by the binding of a macrocycle to a nearby triazole station instead of an (earth)alkaline metal ion. It is speculated that concomitant with the disruption of the PET effect between the triazolium and the pyrene fluorophore, an ET process from the pyrene to the stilbene gate becomes active. If applicable, this might lead to enhanced *E*–*Z* isomerisation and in turn prevent the macrocycle from reversing into a direction over the fluorophore. The idea is stimulated by the previous light-based information ratchet developed by Leigh et. al. that employs a pair of orthogonal sensitizers to achieve a gate-opening mechanism from the macrocycle's point of view.[105] In the system **351** proposed, a gate-closing mechanism is expected with the prospective position-dependent *E*–*Z* isomerisation of the stilbene gate. (This has been found somewhat reminiscent to the working of a humane mouse trap.) It is postulated that in presence of light, the macrocycle will be entrapped in the rotaxane state once formed. It can relax to its equilibrium state in the absence of light via an additional (thermal) *Z*–*E* isomerisation step. Importantly, due to the incorporated fluorophore it is likely that threading of the macrocycle becomes visible by with fluorescence and thus, could allow detailed kinetic studies of the rotaxane system **351**.

At last, it was noted that this concept could potentially form the basis for another light-based [2]catenane molecular motor **360** (Scheme 9.2). If feasible, this light-based design could potentially form a direct extension and counterpart to the chemically fuelled motor system developed by Leigh and co-workers.[112]

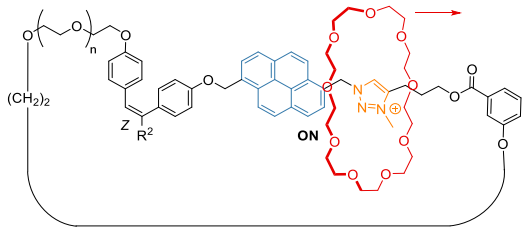

(*E*)-**360**

Scheme 9.2. Directional transport of a light-based [2]catenane rotary motor **360** monitored by fluorescence spectroscopy.

10. References

1. a) “Art Nouveau”, Encyclopædia Britannica. Encyclopædia Britannica, inc., can be found under https://www.britannica.com/art/Art-Nouveau, **2019** (accessed April 30, 2020); b) C. Gontar, “Art Nouveau.” In Heilbrunn Timeline of Art History. New York: The Metropolitan Museum of Art, can be found under http://www.metmuseum.org/toah/hd/artn/hd_artn.htm, **2000** (accessed April 30, 2020).
2. a) A. G. Renstrom and A. G. Renstrom, Wilbur & Orville Wright : a bibliography commemorating the one-hundredth anniversary of the first powered flight, December 17, 1903, National Aeronautics and Space Administration, Office of External Relations, NASA History Office For sale by the U.S. GPO, Supt. of Docs., Washington, D.C., **2002**; b) J. F. V. Vincent, *Proc. Inst. Mech. Eng., Part H* **2009**, *223*, 919–939; c) J. S. Fruton, *Science* **1976**, 192, 327−334; d) D. Needleman, Z. Dogic, *Nat. Rev. Mater.* **2017**, 2, 17048.
3. “Press release: The Nobel Prize in Physiology or Medicine 2019”, Nobelprize.org, Nobel Media AB, can be found under https://www.nobelprize.org/prizes/medicine/2019/press-release, **2020** (accessed April 27, 2020).
4. a) J. M Berg, J. L Tymoczko, G. J. Gatto, L. Stryer, *Biochemistry*, W.H. Freeman, New York, **2019**; b) D. Voet, J. G. Voet, C. W. Pratt, *Voet's Principles of Biochemistry*, John Wiley & Sons, Inc., **2008**.
5. P. Adamski, M. Eleveld, A. Sood, Á. Kun, A. Szilágyi, T. Czárán, E. Szathmáry, S. Otto, *Nat. Rev. Chem.* **2020**, 4, 386–403.
6. F. Mayer in *Biotechnology*, Vol. 1 (Eds.: H.-J. Rehm, G. Reed, A. Pühler, P. Stadler, H. Sahm), VCH Weinheim, Weinheim, **1993**, p. 31.
7. a) A. Pross, *Pure Appl. Chem.* **2015**, 77, 1905–1921; b) R. Pascal, A. Pross, *Synlett* **2017**, 28, 30–35.
8. S. Mann, *Angew. Chem. Int. Ed.* **2008**, 47, 5306–5320.
9. L. M Gierasch, A. Gershenson, *Nat. Chem. Biol.* **2009**, 5, 774–777.
10. J. F. Lutz, M. Ouchi, D. R. Liu, M. Sawamoto, *Science* **2013**, 341, 1238149.
11. C. Bustamante, Y. R. Chemla, N. R. Forde, D. Izhaky, *Annu. Rev. Biochem.* **2004**, 73, 705–748.
12. a) G. Wei, W. Xi, R. Nussinov, B. Ma, *Chem. Rev.* **2016**, 116, 6516−6551; b) V. M. Burger, T. Gurry, C. M. Stultz, *Polymers* **2014**, 6, 2684−2719; c) K. Henzler-Wildman, D. Kern, *Nature* **2007**, 450, 964–972.
13. a) C. Bustamante, D. Keller, G. Oster, *Acc. Chem. Res.* **2001**, 34, 412−420; b) C. Bustamante, Y. R. Chemla, N. R. Forde, D. Izhaky, *Annu. Rev. Biochem.* **2004**, 73, 705–748.
14. C. Mavroidis, A. Dubey, M.L. Yarmush, *Annu. Rev. Biomed. Eng.* **2004**, 6, 363–395.
15. H. Noji, R. Yasuda, M. Yoshida, K. Kinosita, *Nature* **1997**, 386, 299–302.
16. D. S. Goodsell, *Bionanotechnology: Lessons from Nature*, Wiley-Liss, Inc., New Jersey, **2004**.
17. H. Ramezani, H. Dietz, *Nat. Rev. Genet.* **2020**, 21, 5–26.
18. K. Kinbara, T. Aida, Chem. Rev. **2005**, 105, 1377–1400
19. M. Schliwa, G. Woehlke, *Nature* **2003**, 422, 759–765.
20. G. Saper, H. Hess, *Chem. Rev.* **2020**, 120, 288–309.
21. a) J. Robert-Paganin, O. Pylypenko, C. Kikuti, H. L. Sweeney, A. Houdusse, *Chem. Rev.* **2020**, 120, 5−35; b) M. Kneussel, W. Wagner, *Nat. Rev. Neurosci.* **2013**, 14, 233–247.
22. N. Hirokawa, Y. Noda, Y. Tanaka, S. Niwa, *Nat. Rev. Mol. Cell Biol.* **2009**, 10, 682–696.
23. S. L. Reck-Peterson, W. B. Redwine, R. D. Vale, A. P. Carter, *Nat. Rev. Mol. Cell Biol.* **2018**, 19, 382–398.
24. a) C. von Ballmoos, G. M. Cook, P. Dimroth, *Annu. Rev. Biophys.* **2008**, 37, 43–64; b) A. G. Stewart, E. M. Laming, M. Sobti, D. Stock, *Curr. Opin. Struct. Biol.* **2014**, 25, 40–48.

25. a) T. Minamino, K. Imada, *Trends in Microbiol.* **2015**, 23, 267–274; b) T. Mora, H. Yu, Y. Sowa, N. S. Wingreen, *PLoS Comput. Biol.* **2009**, 5, e1000540.
26. a) W. Wu, W. Yang, M. Tsai, *Nat. Rev. Chem.* **2017**, 1, 1–15; b) L. A. Loeb, R. J. Monnat, *Nat. Rev. Genet.* **2008**, 9, 594–604.
27. a) T. M. Schmeing and V. Ramakrishnan, *Nature* **2009**, 461, 1234–1242; b) A. Yonath, *Angew. Chem. Int. Ed.* **2010**, 49, 4340–4354; c) T. A. Steitz, *Angew. Chem. Int. Ed.* **2010**, 49, 4381−4398; d) J. C. Bowman, A. S. Petrov, M. Frenkel-Pinter, P. I. Penev, L. D. Williams, *Chem. Rev.* **2020**, 120, 4848–4878.
28. Y. Seol, K. C. Neuman, *Biophys. Rev.* **2016**, 8, 101–111.
29. a) J. M. Lehn, *Angew. Chem. Int. Ed.* **1988**, 27, 89–112; b) D. J. Cram, *Angew. Chem. Int. Ed.* **1988**, 27, 1009–1020; c) C. J. Pedersen, *Angew. Chem. Int. Ed.* **1988**, 27, 1021–1027; d) J. M. Lehn, *Angew. Chem. Int. Ed.* **1990**, 29, 1304–1319; e) J. M. Lehn, *Supramolecular Chemistry: Concepts and Perspectives*, VCH, Weinheim, **1995**; f) J. W. Steed, J.L. Atwood, *Supramolecular Chemistry*, John Wiley & Sons Ltd., Chichester, **2009**.
30. S. Erbas-Cakmak, D. A. Leigh, C. T. McTernan, A. L. Nussbaumer, *Chem. Rev.* **2015**, 115, 10081−10206.
31. S. Kassem, T. van Leeuwen, A. S. Lubbe, M. R. Wilson, B. L. Feringa, D. A. Leigh, *Chem. Soc. Rev.* **2017**, 46, 2592–2621.
32. a) B. L. Feringa, *J. Org. Chem.* **2007**, 72, 6635–6652; b) B. L. Feringa, *Adv. Mater.* **2020**, 32, 1906416.
33. V. Marcos, L. Zhang, D. A. Leigh, *Proc. Natl. Acad. Sci.* **2018**, 115, 9397–9404.
34. R. D. Astumian, *Chem. Sci.* **2017**, 8, 840–845.
35. a) D. A. Leigh, *Angew. Chem. Int. Ed.* **2016**, 55, 14506–14508; b) J.-P. Sauvage, *Angew. Chem. Int. Ed.* **2017**, 56, 11080–11093; c) J. F. Stoddart, *Angew. Chem. Int. Ed.* **2017**, 56, 11094–11125; d) B. L. Feringa, *Angew. Chem. Int. Ed.* **2017**, 56, 11060–11078.
36. "The Nobel Prize in Chemistry 2016 – Advanced Information", Nobelprize.org, Nobel Media AB, can be found under http://www.nobelprize.org/nobel_prizes/chemistry/laureates/2016/advanced.html, **2020** (accessed April 27, 2020).
37. R. P. Feynman, *Eng. Sci.* **1960**, 23, 22–36.
38. a) J. Robert-Paganin, O. Pylypenko, C. Kikuti, H. L. Sweeney, A. Houdusse, *Chem. Rev.* **2020**, 120, 5−35; b) S. Mohapatra, C. Lin, X. A. Feng, A. Basu, T. Ha, *Chem. Rev.* **2020**, 120, 36–78; c) V. García-López, D. Liu, J. M. Tour, *Chem. Rev.* **2020**, 120, 79−124; d) A. Goswami, S. Saha, P. Biswas, M. Schmittel, *Chem. Rev.* **2020**, 120, 125−199; e) M. Baroncini, S. Silvi. A. Credi, *Chem. Rev.* **2020**, 120, 200−268; f) D. Dattler, G. Fuks, J. Heiser, E. Moulin, A. Perrot, X. Yao, N. Giuseppone, *Chem. Rev.* **2020**, 120, 310−433.
39. a) P. Reimann, *Phys. Rep.* **2002**, 361, 57–265; b) R. D. Astumian, *Science*, **1997**, 276, 917−922. c) R. D. Astumian, *J. Phys., Condens. Matter* **2005**, 17, S3753–S3766; d) R. D. Astumian, *Phys. Chem. Chem. Phys.* **2007**, 9, 5067−5083; e) R. D. Astumian, *Nat. Commun.* **2019**, 10, 3837; f) A. I. Brown, D. A. Sivak, *Chem. Rev.* **2020**, 120, 434−459.
40. E. R. Kay, D. A. Leigh, F. Zerbetto, *Angew. Chem. Int. Ed.* **2007**, 46, 72–191.
41. G. W. Leibnitz, N. Rescher, *G.W. Leibniz's Monadology*, University of Pittsburgh Press, Pittsburgh, **1991**.
42. a) K. E. Drexler, *Engines of creation*, Anchor Press/Doubleday, Garden City, **1986**; b) K. E. Drexler, *Proc. Natl. Acad. Sci.* **1981**, 78, 5275–5278; c) K. E. Drexler, *Nanosystems: molecular machinery, manufacturing, and computation*, Wiley, New York, **1992**; d) K. E. Drexler, *Sci. Am.* **2001**, 285, 74–75.

43. a) R. E. Smalley, *Sci. Am.* **2001**, 285, 76–77; b) C. Tourney, *Nature Nanotech.* **2018**, 13, 2–3.
44. V. Balzani, A. Credi, F. M. Raymo, J. F. Stoddart, *Angew. Chem. Int. Ed.* **2000**, 39, 3348–3391.
45. M. Baroncini, S. Silvi. A. Credi, *Chem. Rev.* **2020**, 120, 200−268.
46. G. S. Kottas, L. I. Clarke, D. Horinek, J. Michl, *Chem. Rev.* **2005**, 105, 1281–1376.
47. a) T. Claridge, *High-resolution NMR techniques in organic chemistry*, Elsevier, Oxford, **2009**; b) I. R. Kleckner, M. P. Foster, *Biochim. Biophys. Acta.* **2011**, 1814, 942–968; c) M. Marušič, J. Schlagnitweit, K. Petzold, *ChemBioChem* **2019**, 20, 2685–2710.
48. G. H. Christie, J. Kenner, *J. Chem. Soc., Trans.* **1922**, 121, 614–620.
49. M. Oki, *Top. Stereochem.* **1983**, 14, 1–81.
50. a) A. K. Colter, I. I. Schuster, R. J. Kurland, *J. Am. Chem. Soc*. **1965**, 87, 2278–2279; b) A. K. Colter, I. I. Schuster, R. J. Kurland, *J. Am. Chem. Soc.* **1965**, 87, 2279–2281; c) I. I. Schuster, A. K. Colter, R. J. Kurland, *J. Am. Chem. Soc.* **1968**, 90, 4679–4687.
51. H. Kwart, S. Alekman, *J. Am. Chem. Soc.* **1968**, 90, 4482–4483.
52. a) D. Gust, K. Mislow, *J. Am. Chem. Soc.* **1973**, 95, 1535–1547; b) J. F. Blount, P. Finocchiaro, D. Gust, K. Mislow, *J. Am. Chem. Soc.* **1973**, 21, 7019–7029; c) K. Mislow, *Acc. Chem. Res.* **1976**, 9, 26–33.
53. a) M. Oki, *Angew. Chem. Int. Ed.* **1976**, 15, 87–93; b) G. Yamamoto, M. Oki, *Chem. Lett.* **1979**, 1251–1254; c) G. Yamamoto, M. Oki, *Chem. Lett.* **1979**, 1255–1258; d) G. Yamamoto, M. Oki, B*ull. Chem. Soc. Jpn.* **1981**, 54, 473–480; e) G. Yamamoto, M. Oki, B*ull. Chem. Soc. Jpn.* **1981**, 54, 481–487; f) G. Yamamoto, M. Oki, *J. Org. Chem.* **1983**, 48, 1233–1236; g) G. Yamamoto, M. Oki, J. Mol. Struct. **1985**, 126, 413–420; h) G. Yamamoto, M. Oki, *Bull. Chem. Soc. Jpn.* **1985**, 58, 1953–1961; i) G. Yamamoto, M. Oki, Bull. Chem. Soc. Jpn. **1986**, 59, 3597–3603; j) G. Yamamoto, *Bull. Chem. Soc. Jpn.* **1989**, 62, 4058–4060.
54. a) Y. Kawada H. Iwamura*, J. Org. Chem.* **1980**, 45, 2547–2548; b) W. D. Hounshell, C. A. Johnson, A. Guenzi, F. Cozzi, K. Mislow, *Proc. Natl. Acad. Sci.* **1980**, 77, 6961–6964; c) H. Iwamura, K. Mislow, *Acc. Chem. Res.* **1988**, 21, 175–182.
55. H. Ube, Y. Yasuda, H. Sato, M. Shionoya, *Nat. Commun.* **2017**, 8, 14296.
56. a) S. Hiraoka, T. Yi, M. Shiro, M. Shionoya*, J. Am. Chem. Soc.* **2002**, 124, 14510–14511; b) S. Hiraoka, K. Harano, T. Tanaka, M. Shiro, M. Shionoya, *Angew. Chem. Int. Ed.* **2003**, *42*, 5182–5185; c) S. Hiraoka, K. Hirata, M. Shionoya, *Angew. Chem. Int. Ed.* **2004**, *43*, 3814–3818; d) S. Hiraoka, M. Shiro, M. Shionoya *J. Am. Chem. Soc.* **2004**, 126, 1214–1218.
57. a) S. Hiraoka, E. Okuno, T. Tanaka, M. Shiro, M. Shionoya, *J. Am. Chem. Soc.* **2008**, 130, 9089–9098; b) S. Hiraoka, Y. Hisanaga, M. Shiro, M. Shionoya, *Angew. Chem. Int. Ed.* **2010**, 49, 1669–1673.
58. E. Okuno, S. Hiraoka, M. Shionoya, *Dalton Trans.* **2010**, 39, 4107–4116.
59. R. Annunziata, M. Benaglia, M. Cinquini, L. Raimondi, F. Cozzi, *J. Phys. Org. Chem.* **2004**, *17*, 749–751.
60. a) N. Zigon, A. Guenet, E. Graf, N. Kyritsakas, M. W. Hossein, *Dalton Trans.* **2013**, 42, 9740–9745; b) A. Guenet, E. Graf, N. Kyritsakas, L. Alloucheb, M. W. Hosseini, *Chem. Commun.* **2007**, 2935–2937; c) A. Guenet, E. Graf, N. Kyritsakas, M. W. Hosseini, *Inorg. Chem.* **2010**, 49, 1872–1883; d) T. Lang, A. Guenet, E. Graf, N. Kyritsakas, M. W. Hosseini, *Chem. Commun.* **2010**, 46, 3508–3510; e) T. Lang, E. Graf, N. Kyritsakas, M. W. Hosseini, *Dalton Trans.* **2011**, 40, 3517–3523; f) N. Zigon, M. W. Hosseini, *Chem. Commun.* **2015**, 51, 12486–12489; g) N. Zigon, A. Guenet, E. Graf, M. W. Hosseini, *Chem. Commun.* **2013**, 49, 3637–3639; h) I. N. Meshkov, V. Bulach, Y. G. Gorbunova, N. Kyritsakas, M. S. Grigoriev, A. Y. Tsivadze, M. W. Hosseini, *Inorg. Chem.* **2016**, 55, 10774–10782.

61. a) G. Wang, H. Xiao, J. He, J. Xiang, Y. Wang, X. Chen, Y. Che, H. Jiang, *J. Org. Chem.* **2016**, 81, 3364–3371; b) C. Yu, L. Ma, J. He, J. Xiang, X. Deng, Y. Wang, X. Chen, H. Jiang, *J. Am. Chem. Soc.* **2016**, 138, 15849–15852.
62. T. R. Kelly, I. Tellitu, J. P. Sestelo, *Angew. Chem. Int. Ed.* **1997**, *36*, 1866−1868.
63. P. W. Atkins, J. De Paula, *Atkins' Physical chemistry*, Oxford University Press, Oxford New York, **2006**.
64. T. R. Kelly, *Acc. Chem. Res.* **2001**, 34, 514–522.
65. B. L. Feringa, *Acc. Chem. Res.* **2001**, 34, 504–513.
66. C. A. Schalley, K. Beizai, F. Vögtle, *Acc. Chem. Res.* **2001**, 34, 465–476.
67. C. P. Mandl, B. König, *Angew. Chem. Int. Ed.* **2004**, 43, 1622–1624.
68. a) T. R. Kelly, M. C, Bowyer, K. V. Bhaskar, D. Bebbington, A. Garcia, F. Lang, M. H. Kim, M. P. Jette, *J. Am. Chem. Soc.* **1994**, 116, 3657–3658; b) T. R. Kelly, *Acc. Chem. Res.* **2001**, 34, 514–522; c) *J. P. Sestelo, T. R. Kelly, Appl. Phys. A **2002**,* 75, 337–343.
69. P. V. Jog, R. E. Brown, D. K. Bates, *J. Org. Chem.* **2003**, 68, 8240–8243.
70. B. E. Dial, P. J. Pellechia, M. D. Smith, K. D. Shimizu, *J. Am. Chem. Soc.* **2012**, 134, 3675–3678.
71. B. E. Dial, R. D. Rasberry, B. N. Bullock, M. D. Smith, P. J. Pellechia, S. Profeta, K. D. Shimizu, *Org. Lett.* **2011**, 13, 244–247.
72. H. Kanazawa, M. Higuchi, K. Yamamoto, *J. Am. Chem. Soc.* **2005**, 127, 16404–16405.
73. Y. Tomohiro, A. Satake, Y. Kobuke*, J. Org. Chem.* **2001**, 66, 8442–8446.
74. D.H. Qu, B. L. Feringa, *Angew. Chem. Int. Ed.* **2010**, 49, 1107–1110.
75. T. R. Kelly, J. P. Sestelo, I. Tellitu, *J. Org. Chem.* **1998**, 63, 3655–3665.
76. K. L. Sebastian, *Phys. Rev. E* **2000**, 61, 937–939.
77. a) T. R. Kelly, H. De Silva, R. A. Silva, *Nature* **1999**, 401, 150–152; b) T. R. Kelly, R. A. Silva, H. De Silva, S. Jasmin, Y. Zhao, *J. Am. Chem. Soc.* **2000**, 122, 6935–6949.
78. M. N. Chatterjee, E. R. Kay, D. A. Leigh, *J. Am. Chem. Soc.* **2006**, 128, 4058–4073.
79. T. R. Kelly, R. A. Silva, H. De Silva, S. Jasmin, Y. Zhao, *J. Am. Chem. Soc.* **2000**, 122, 6935–6949.
80. a) T. R. Kelly, M. Cavero *Org. Lett.* **2002**, 4, 2653–2656; b) T. R. Kelly, X. Cai, F. Damkaci, S. B. Panicker, B. Tu, S. M. Bushell, I. Cornella, M. J. Piggott, R. Salives, M. Cavero, Y. Zhao, S. Jasmin, *J. Am. Chem. Soc.* **2007**, 129, 376–386; c) M. D. Markey, T. R. Kelly, *Tetrahedron* **2008**, 64, 8381–8388.
81. G. Bringmann, A. J. P. Mortimer, P. A. Keller, M. J. Gresser, J. Garner, M. Breuning, *Angew. Chem. Int. Ed.* **2005**, 44, 5384–5427.
82. a) B. J. Dahl, B. P. Branchaud, *Tetrahedron Lett.* **2004**, 45, 9599–9602; b) Y. Lin, B. J. Dahl, B. P. Branchaud, *Tetrahedron Lett.* **2005**, 46, 8359–8362; c) B. J. Dahl, B. P. Branchaud, *Org. Lett.* **2006**, 8, 5841–5844.
83. S. P. Fletcher, F. Dumur, M. M. Pollard, B. L. Feringa, *Science* **2005**, 310, 80–82.
84. B. S. L. Collins, J. C. M. Kistemaker, E. Otten, B. L. Feringa, *Nat. Chem.* **2016**, 8, 860–866.
85. a) B. Feringa, H. Wynberg, *J. Am. Chem. Soc.* **1977**, 99, 602–603; b) N. Harada, A. Saito, N. Koumura, H. Uda, B. de Lange, W. F. Jager, H. Wynberg, B. L. Feringa, *J. Am. Chem. Soc.* **1997**, 119, 7241–7248; c) W. F. Jager, B. de Lange, B. L. Feringa, *Mol. Crysr. Liq. Crysr.* **1992**, 217, 129–132; d) W. F. Jager, B. de Lange, B. L. Feringa, *Mol. Crysr. Liq. Crysr.* **1992**, 217, 133–138; e) N. P. M. Huck, W. F. Jager, B. de Lange, B. L. Feringa, *Science* **1996**, *273*, 1686–1688.
86. N. Koumura, R. W. J. Zijlstra, R. A. van Delden, N. Harada, B. L. Feringa*, Nature* **1999**, 401, 152–155.
87. a) D. Roke, S. J. Wezenberg, B. L. Feringa, *Proc. Natl. Acad. Sci.* **2018**, 115, 9423–9431; b) T. van Leeuwen, A. S. Lubbe, P. Štacko, S. J. Wezenberg, B. L. Feringa, *Nat. Rev. Chem.* **2017**, 1, 0096; c) V. García-Lopez, D. Liu, J. M. Tour, *Chem. Rev.* **2020**, 120, 79−124.

88. J. Conyard, K. Addison, I. A. Heisler, A. Cnossen, W. R. Browne, B. L. Feringa, S. R. Meech, *Nature Chem.* **2012**, 4, 547–551.
89. N. Koumura, E. M. Geertsema, A. Meetsma, B. L. Feringa, *J. Am. Chem. Soc.* **2000**, 122, 12005–12006.
90. N. Ruangsupapichat, M. M. Pollard, S. R. Harutyunyan, B. L. Feringa, *Nature Chem.* **2011**, 3, 53–60.
91. J.-P. Sauvage, *Acc. Chem. Res.* **1998**, 31, 611–619.
92. C. J. Bruns, J. F. Stoddart, *The nature of the mechanical bond: from molecules to machines*, Wiley, Hoboken, New Jersey, **2017**.
93. a) A. Livoreil, C. O. Dietrich-Buchecker and J.-P. Sauvage, *J. Am. Chem. Soc.* **1994**, 116, 9399–9400; b) F. Baumann, A. Livoreil, W. Kaim and J.-P. Sauvage, *Chem. Commun.* **1997**, 35–36; c) A. Livoreil, J.-P. Sauvage, N. Armaroli, V. Balzani, L. Flamigni and B. Ventura, *J. Am. Chem. Soc.* **1997**, 119, 12114–12124; d) D. J. Cardenas, A. Livoreil and J.-P. Sauvage, *J. Am. Chem. Soc.* **1996**, 118, 11980–11981.
94. D. A. Leigh, J. K. Y. Wong, F. Dehez, F. Zerbetto, *Nature* **2003**, 424, 174–179.
95. E. Hänggi, S. Wehner, *Nat. Commun.* **2013**, 4, 1670.
96. P. L. Anelli, N. Spencer, J. F. Stoddart, *J. Am. Chem. Soc.* **1991**, 113, 5131–5133.
97. R. A. Bissell, E. Córdova, A. E. Kaifer, J. F. Stoddart, *Nature* **1994**, 369, 133–137.
98. L. van Dijk, M. J. Tilby, R. Szpera, O. A. Smith, H. A. P. Bunce, S. P. Fletcher, *Nat. Rev. Chem.* **2018**, 2, 0117.
99. A. Martinez-Cuezva, A. Saura-Sanmartin, M. Alajarin, J. Berna, *ACS Catal.* **2020**, 10, 7719–7733.
100. I. Aprahamian, *ACS Cent. Sci.* **2020**, 6, 347–358.
101. R. D. Astumian, I. Derényi, *Eur. Biophys. J.* **1998**, 27, 474–489.
102. A. Altieri, G. Bottari, F. Dehez, D. A. Leigh, J. K. Y. Wong, F. Zerbetto, *Angew. Chem. Int. Ed.* **2003**, 42, 2296–2300.
103. J. V. Hernández, E. R. Kay, D. A. Leigh, *Science* **2004**, 306, 1532–1537.
104. R. D. Astumian, *Nat. Commun.* **2019**, 10, 3837.
105. V. Serreli, C. Lee, E. R. Kay, D. A. Leigh, *Nature* **2007**, 445, 523–527.
106. a) Y. Tokunaga, K. Akasaka, K. Hisada, Y. Shimomura, S. Kakuchi, *Chem. Commun.* **2003**, 2250–2251; b) Y. Tokunaga, K. Akasaka, N. Hashimoto, S. Yamanaka, K. Hisada, Y. Shimomura, S. Kakuchi, *J. Org. Chem.* **2009**, 74, 2374–2379.
107. a) G. S. Hammond, J. Saltiel, A. A. Lamola, N. J. Turro, J. S. Bradshaw, D. O. Cowan, R. C. Counsell, V. Vogt, C. Dalton, *J. Am. Chem. Soc.* **1964**, 86, 3197–3217; b) N. J. Turro, *Photochem. Photobiol.* **1969**, 9, 555–563; c) H. Görner, D. Schult-Frohlinde, *J. Photochem.* **1978**, 6, 91–102; d) S. R. Samanta, A. Parthasarathy and V. Ramamurthy, *Photochem. Photobiol. Sci.* **2012**, 11, 1652.
108. M. Alvarez-Pérez, S. M. Goldup, D. A. Leigh, A. M. Z. Slawin, *J. Am. Chem. Soc.* **2008**, 130, 1836–1838.
109. a) E. M. G. Jamieson, S. M. Goldup, *Nat. Chem.* **2019**, 11, 765–767; b) M. Denis, J. E. M. Lewis, F. Modicom, S. M. Goldup, *Chem* **2019**, 5, 1512–1520; c) E. M. G. Jamieson, F. Modicom, S. M. Goldup, *Chem. Soc. Rev.* **2018**, 47, 5266–5311.
110. a) K. Nakano, M. Kitamura in Separation of Enantiomers, Vol. 5 (Eds.: M. Todd), Wiley-VCH, Weinheim, **2014**, pp. 161–209; b) H. Pellissier, *Tetrahedron* **2011**, 67, 3769–3802.
111. A. Carlone, S. M. Goldup, N. Lebrasseur, D. A. Leigh, A. Wilson, *J. Am. Chem. Soc.* **2012**, 134, 8321−8323.

112. M. R. Wilson, J. Solà, A. Carlone, S. M. Goldup, N. Lebrasseur, D. A. Leigh*, Nature* **2016**, 534, 235–240.
113. R. K. O`Reilly, A. J. Turberfield, T. R. Wilks, *Acc. Chem. Res.* **2017**, 50, 2496–2509.
114. a) B. Lewandowski, G. De Bo, J. W. Ward, M. Papmeyer, S. Kuschel, M. J. Aldegunde, P. M. E. Gramlich, D. Heckmann, S. M. Goldup, D. M. D'Souza, A. E. Fernandes, D. A. Leigh, *Science* **2013**, 339, 189–193; b) G. De Bo, S. Kuschel, D. A. Leigh, B. Lewandowski, M. Papmeyer, J. W. Ward, *J. Am. Chem. Soc.* **2014**, 136, 5811−5814.
115. "The Nobel Prize in Chemistry 2009 – Scientific Background and Information for the public", Nobelprize.org, Nobel Media AB, can be found under "https://www.nobelprize.org/prizes/chemistry /2009/press-release/", **2020** (accessed June 22, 2020).
116. a) A. Ratje, J. Loerke, A. Mikolajka, B. Brünner, P. W. Hildebrand, A. L. Starosta, A. Dönhöfer, S. R. Connell, P. Fucini, T. Mielke, P. C. Whitford, J. N. Onuchic, Y. Yu, K. Y. Sanbonmatsu, R. K. Hartmann, P. A. Penczek, D. N. Wilson, C. M. T. Spahn, *Nature* **2010**, 468, 713−716; b) W. Zhang, J. A. Dunkle, J. H. D. Cate, *Science* **2009**, 325, 1014−1017.
117. J. Murn, Y. Shi, *Nat. Rev. Mol. Cell Biol.* **2017**, 18, 517–527.
118. M. Wang, P. J. Casey, *Nat. Rev. Mol. Cell Biol.* **2016**, 17, 110–122.
119. E. Verdin, M. Ott, *Nat. Rev. Mol. Cell Biol.* **2015**, 16, 258–264.
120. a) M. Johansson, E. Bouakaz, M. Lovmar, M. Ehrenberg, *Mol. Cell* **2008**, 30, 589–598; b) I. L. Volkov, M. Johansson, *Biochemistry* **2019**, 58, 7–14.
121. G. De Bo, M. A. Y. Gall, M. O. Kitching, S. Kuschel, D. A. Leigh, D. J. Tetlow, J. W. Ward, *J. Am. Chem. Soc.* **2017**, 139, 10875−10879.
122. a) P. E. Dawson, T. W. Muir, I. Clark-Lewis, S. B. H. Kent, *Science* **1994**, 266, 776–779; b) S. B. H. Kent, *Chem. Soc. Rev.* **2009**, 38, 338–351; c) V. Agouridas, O. El Mahdi, V. Diemer, M. Cargoet, J.-C. M. Monbaliu, O. Melnyk, *Chem. Rev.* **2019**, 119, 7328–7443; d) R. E. Thompson, T. W. Muir, *Chem. Rev.* **2020**, 120, 3051–3126.
123. a) V. Aucagne, K. D. Hänni, D. A. Leigh, P. J. Lusby, D. B. Walker, *J. Am. Chem. Soc.* **2006**, 128, 2186–2187; b) J. D. Crowley, S. M. Goldup, A. Lee, D. A. Leigh, R. T. McBurney, *Chem. Soc. Rev.* **2009**, 38, 1530–1541; c) M Denis, S. M. Goldup, *Nat. Rev. Chem.* **2017***,* 1, 0061.
124. G. De Bo, M. A. Y. Gall, S. Kuschel, J. De Winter, P. Gerbaux, D. A. Leigh, *Nature Nanotech.* **2018**, 13, 381−385.
125. a) C. T. McTernan, G. De Bo, D. A. Leigh, *Chem* **2020**, 6, 2964−2973; b) R. Costil, A. Guinart, B. L. Feringa, *Chem* **2020**, 6, 2868−2870; c) C. T. McTernan, *Chem* **2020**, 6, 2862−2864.
126. a) G. Wittig, U. Schöllkopf, *Chem. Ber.* **1954**, 87, 1318–1330; b) R. W. Hoffmann, *Angew. Chem. Int. Ed*. **2001**, 40, 1411–1416; c) P. A. Bryne, D. G. Gilheany, *Chem. Soc. Rev.* **2013**, 42, 6670–6696.
127. a) H. C. Kolb, M. G. Finn, K. B. Sharpless, Angew. Chem. Int. Ed. **2001**, 40, 2004–2021; b) C. W. Tornøe, C. Christensen, M. Meldal, *J. Org. Chem.* **2002**, 67, 3057–3064; c) V. V. Rostovtsev, L. G. Green, V. V. Fokin, K. B. Sharpless, *Angew. Chem. Int. Ed.* **2002**, 41, 2596–2599; d) F. Himo, T. Lovell, R. Hilgraf, V. V. Rostovtsev, L. Noodleman, K. B. Sharpless, V. V. Fokin, *J. Am. Chem. Soc.* **2005**, 127, 210–216; e) M. Meldal, C. W. Tornøe, *Chem. Rev.* **2008**, 108, 2952–3015; f) E. Haldón, M. C. Nicasio, P. J. Pérez, *Org. Biomol. Chem.* **2015**, 13, 9528–9550.
128. a) R. Schwesinger, *Chimia* **1985**, 39, 269; b) R. Schwesinger, H. Schlemper, *Angew. Chem. Int. Ed.* **1987**, 26, 1167−1169; c) R. Schwesinger, J. Willaredt, H. Schlemper, M. Keller, D. Schmitt, H. Fritz, *Chem. Ber.* **1994**, 127, 2435−2454.
129. C. T. McTernan, University of Manchester, School of Chemistry, Manchester, **2016**, Unpublished results.

130. S. F. M. van Dongen, J. A. A. W. Elemans, A. E. Rowan, R. J. M. Nolte, *Angew. Chem. Int. Ed.* **2014**, 53, 11420–11428.
131. a) R. Kovall, B. W. Matthews, *Science* **1997**, 277, 1824–1827; b) W. Hwang, J. Yoo, Y. Lee, S. Park, P. Lien Hoang, H. Cho, J. Yu, T. Hoa Vo, M. Shin, M. Jin, D. Park, C. Hyeon, G. Lee, *Nat. Commun.* **2018**, 9, 4404.
132. a) M. A. Trakselis, S. C. Alley, E. Abel-Santos, S. J. Benkovic, *Proc. Natl. Acad. Sci.* **2001**, 98, 8368–8375; b) C. Indiani, M. O'Donnell, *Nat. Rev. Mol. Cell Biol.* **2006**, 7, 751–761; c) B. A. Kelch, *Biopolymers* **2016**, 105, 532–546.
133. P. Thordarson, E. J. A. Bijsterveld, A. E. Rowan, R J. M. Nolte, *Nature* **2003**, 424, 915–918.
134. a) A. B. C. Deutman, C. Monnereau, J. A. A. W. Elemans, G. Ercolani, R. J. M. Nolte, A. E. Rowan, *Science* **2008**, 322, 1668−1671; b) A. B. C. Deutman, S. Cantekin, J. A. A. W. Elemans, A. E. Rowan, R. J. M. Nolte, *J. Am. Chem. Soc.* **2014**, 136, 9165−9172.
135. S. F. M. van Dongen, J. Clerx, K. Nørgaard, T. G. Bloemberg, J. J. L. M. Cornelissen, M. A. Trakselis, S. W. Nelson, S. J. Benkovic, A. E. Rowan, R. J. M. Nolte, *Nature Chem.* **2013**, 5, 945–951.
136. N. Miyagawa, M. Watanabe, T. Matsuyama, Y. Koyama, T. Moriuchi, T. Hirao, Y. Furusho, T. Takata, *Chem. Commun.* **2010**, 46, 1920–1922.
137. M. Ogawa, M. Nagashima, H. Sogawa, S. Kuwata, T. Takata, *Org. Lett.* **2015**, 17, 1664−1667.
138. Y. Takashima, M. Osaki, Y. Ishimaru, H. Yamaguchi, A. Harada, *Angew. Chem. Int. Ed.* **2011**, 50, 7524–7528.
139. S. F. M. van Dongen, J. Clerx, O. I. van den Boomen, M. Pervaiz, M. A. Trakselis, T. Ritschel, L. Schoonen, D. C. Schoenmakers, R. J. M. Nolte, *Biopolymers.* **2018**, 109, e23119.
140. Y. He, D. R. Liu, *Nature Nanotech.* **2010***,* 5, 778–782.
141. M. Madsen, K. V. Gothelf, *Chem. Rev.* **2019**, 119, 6384–6458.
142. J. Bath, A. Tuberfield, *Nature Nanotech.***2007,** 2, 275–284.
143. N. C. Seeman, H. F. Sleiman, *Nat. Rev. Mater.* **2018**, 3, 17068.
144. I. Kaganman, *Nat. Methods* **2010**, 7, 952.
145. a) W. Meng, R. A. Muscat, M. L. McKee, P. J. Milnes, A. H. El-Sagheer, J. Bath, B. G. Davis, T. Brown, R. K. O'Reilly, A. J. Turberfield, *Nature Chem*. **2016**, 8, 542–548; b) M. L. McKee, P. J. Milnes, J. Bath, E. Stulz, R. K. O'Reilly, A. J. Turberfield, *J. Am. Chem. Soc.* **2012**, 134, 1446−1449.
146. A. M. Kushner, Z. Guan, *Angew. Chem. Int. Ed.* **2011**, 50, 9026–9057.
147. L. Montero de Espinosa, W. Meesorn, D. Moatsou, C. Weder, *Chem. Rev.* **2017**, 117, 12851–12892.
148. N. Becker, E. Oroudjev, S. Mutz, J. P. Cleveland, P. K. Hansma, C. Y. Hayashi, D. E. Makarov, H. G. Hansma, *Nat. Mater.* **2003**, 2, 278–283.
149. J. Gershenzon, N. Dudareva, *Nat. Chem. Biol.* **2007**, 3, 408–414.
150. a) R. K. Saiki, D. H. Gelfand, S. Stoffel, S. J. Scharf, R. Higuchi, G. T. Horn, K. B. Mullis, H. A. Erlich, *Science* **1988**, 239, 487–491; b) K. B. Mullis, *Angew. Chem. Int. Ed.* **1994**, 33, 1209–1213.
151. a) R. B. Merrifield, *J. Am. Chem. Soc.* **1963**, 85, 2149–2154; b) F. Sanger, *Angew. Chem.* **1981**, 93, 937–944; c) F. Sanger, *Ann. Rev. Biochem.* **1988**, 57, 1–28; d) R. B. Merrifield, *Angew. Chem. Int. Ed.* **1985**, 24, 799–810.
152. a) B. N. Norris, T. Pan, T. Y. Meyer, *Org. Lett.* **2010**, 12, 5514–5517; b) X. Tong, B. Guo and Y. Huang, *Chem. Commun.* **2011**, 47, 1455–1457; c) B. N. Norris, S. Zhang, C. M. Campbell, J. T. Auletta, P. Calvo-Marzal, G. R. Hutchison, T. Y. Meyer, *Macromolecules* **2013**, 46, 1384–1392; d) Y. Hibi, M. Ouchi, M. Sawamoto, *Nat. Commun.* **2016**, 7, 11064.

153. a) J. C. Barnes, D. J. C. Ehrlich, A. X. Gao, F. A. Leibfarth, Y. Jiang, E. Zhou, T. F. Jamison, J. A. Johnson, *Nature Chem.* **2015**, 7, 810–815; b) J. W. Grate, K. Mo, M. D. Daily, *Angew. Chem. Int. Ed.* **2016**, 55, 3925–3930.
154. J. F. Lutz in *ACS Symposium Series,* Vol. 1170, **2014**, Chapter 1: *Sequence-Controlled Polymers: Synthesis, Self-Assembly, and Properties*, p. 1–11.
155. a) J. Chiefari, Y. K. Chong, F. Ercole, J. Krstina, J. Jeffery, T. P. T. Le, R. T. A. Mayadunne, G. F. Meijs, C. L. Moad, G. Moad, E. Rizzardo, S. H. Thang, M*acromolecules* **1998**, 31, 5559–5562; b) C. Boyer, V. Bulmus, T. P. Davis, V. Ladmiral, J. Liu, S. Perrier, *Chem. Rev.* **2009**, 109, 5402–5436; c) S. Houshyar, D. J. Keddie, G. Moad, R. J. Mulder, S. Sauberna, J. Tsanaktsidisa, *Polym. Chem.* **2012**, 3, 1879–1889.
156. a) M. K. Georges, R. P. N. Veregin, P. M. Kazmaier and G. K. Hamer, *Macromol*. **1993**, 26, 2987–2988; b) G. Moad, E. Rizzardo, *Macromol.* **1995**, 28, 8722–8728; c) C. J. Hawker, J. M. J. Frechet, R. B. Grubbs, J. Dao, *J. Am. Chem. Soc.* **1995**, 117, 10763–10764; d) C. J. Hawker, G. G. Barclay, J. Dao, *J. Am. Chem. Soc.* **1996**, 118, 11467–11471.
157. a) M. Kato, M. Kamigaito, M. Sawamoto, T. Higashimura, *Macromol.* **1995**, 28, 1721–1723; b) J. S. Wang, K. Matyjaszewski, *J. Am. Chem. Soc.* **1995**, 117, 5614–5615; c) D. Konkolewicz, Y. Wang, M. Zhong, P. Krys, A. A. Isse, A. Gennaro, K. Matyjaszewski, *Macromol*. **2013**, 46, 8749–8772.
158. S. Dadashi-Silab, S. Doran, Y. Yagci, *Chem. Rev.* **2016**, 116, 10212–10275.
159. Y.-M. Chuang, A. Ethirajan, T. Junkers, *ACS Macro Lett.* **2014**, 3, 732–737.
160. a) D. J. Hill, M. J. Mio, R. B. Prince, T. S. Hughes, J. S. Moore, *Chem. Rev.* **2001**, 101, 3893–4012; b) J. L. Schmitt, A. M. Stadler, N. Kyritsakas, J. M. Lehn, *Helv. Chim. Acta* **2003**, 86, 1598–1624; c) T. A. Martinek, F. Fulop, *Chem. Soc. Rev.* **2012**, 41, 687–702.
161. T. B. Yu, J. Bai, Z. Guan, *Angew. Chem. Int. Ed.* **2009**, 48, 1097–1101.
162. R. Herges, *Chem. Sci.* **2020**, 11, 9048–9055.
163. M. Frenkel-Pinter, M. Samanta, G. Ashkenasy, L. J. Leman, *Chem. Rev.* **2020**, 120, 4707–4765.
164. a) R. H. Martin, *Angew. Chem. Int. Ed.* **1974**, 13, 649–660; b) R. H. Martin, M. Baes, *Tetrahedron* **1975**, 31, 2135–2137; c) A. Urbano, *Angew. Chem. Int. Ed*. **2003**, 42, 3986–3989; d) P. Sehnal, I. G.Stará , D. Šaman, M. Tichý, J. Míšek, J. Cvačka, L. Rulšek, J. Chocholoušová, J. Vacek, G. Goryl, M. Szymonski, I. Císařová, I. Starý, *Proc. Natl. Acad. Sci.* **2009**, 106, 13169–13174; e) Y. Shen, C.-F. Chen, *Chem. Rev.* **2012**, 112, 1463–1535; f) M. Gingras, *Chem. Soc. Rev.* **2013**, 42, 968–1006; g) M. Gingras, *Chem. Soc. Rev.* **2013**, 42, 1051–1095; h) C.-F. Chen, Y. Shen, *Helicene Chemistry. From Synthesis to Applications*, Springer, Berlin, **2017**.
165. a) L. Liu, B. Yang, T. J. Katz, M. K. Poindexter, *J. Org. Chem*. **1991**, 56, 3769–3775; b) J.-M. Rodier, A. B. Myers, *J. Am. Chem. Soc.* **1993**, 115, 10791–10795; c) N. Hoffman, *J. Photochem. Photobiol., C* **2014**, 19, 1–19.
166. K. Mori, T. Murase, M. Fujita, *Angew. Chem. Int. Ed. **2015***, 45, 6847–6851.
167. a) F. A. Hart, *J. Chem. Soc.* **1960**, 3324–3328; b) E. M. Evleth, L. D. Freeman, R. I. Wagner, *J. Org. Chem.* **1962**, 27, 2192–2197.
168. P. A. Byrne, K. V. Rajendran, J. Muldoon, D. G. Gilheany, *Org. Biomol. Chem.* **2012**, 10, 3531–3537.
169. a) A. I. Khalaf, A. R. Pitt, M. Scobie, C. J. Suckling, J. Urwin, R. D. Waigh, R. V. Fishleigh, S. C. Young, W. A. Wylie, *Tetrahedron* **2000**, 56, 5225–5239; b) S. M. Langenegger, R. Häner, *Helv. Chim. Acta* **2002**, 85, 3414–3421; c) J. Campos Rosa, D. Galanakis, C. R. Ganellin, P. M. Dunn, *J. Med. Chem.* **1996**, 39, 4247–4254.
170. R. B. Du Vernet, O. Wennerström, J. Lawson, T. Otsubo, V. Boekelheide, *J. Am. Chem. Soc.* **1978**, 100, 2457–2464.

171. B. E. Maryanoff, A. B. Reitz, *Chem. Rev.* **1989**, 89, 863–927.
172. a) H. Friebolin, *Basic One- and Two-Dimensional NMR Spectroscopy*, Wiley-VCH, Weinheim, **2011**, p. 89; b) E. Pretsch, P. Bühlmann, M. Badertscher, *Structure Determination of Organic Compounds*, Springer-Verlag, Berlin Heidelberg, **2009**, p. 164.
173. a) A. Ullah Malik, F. Gan, C. Shen, N. Yu, R. Wang, J. Crassous, M. Shu, H. Qiu, *J. Am. Chem. Soc.* **2018**, 140, 2769–2772; b) X. Jiang, S. D. Laffoon, D. Chen, S. Perez-Estrada, A. S. Danis, J. Rodríguez-Lopez, M. A. Garcia-Garibay, J. Zhu, J. S. Moore, *J. Am. Chem. Soc.* **2020**, 142, 6493–6498.
174. a) A. Schnell, J. G. Dawber, J. C. Tebby, *J. Chem. Soc., Perkin Trans. 2* **1976**, 633–636; b) P. A. Byrne, Y. Ortin, D. G. Gilheany, *Chem. Commun.* **2015**, 51, 1147–1150; c) P. A. Byrne, D. G. Gilheany, *Chem. Eur. J.* **2016**, 22, 9140–9154.
175. M. Gingras, C. Collet, *Synlett* **2015**, 15, 2337–2341.
176. a) T. Matsushima, S. Kobayashi, S. Watanabe, *J. Org. Chem.* **2016**, 81, 7799−7806; b) H. Okamoto, H. Takahashia, T. Takanea, Y. Nishiyamab, K. Kakiuchib, S. Gohdac, M. Yamaji, *Synthesis* **2017**, 49, 2949–2957.
177. J. Weber, E. L. Clennan, *J. Org. Chem.* **2019**, 84, 817−830.
178. B. Groh, University of Manchester, School of Chemistry, Manchester, **2017**, Unpublished results.
179. J. Spence, University of Manchester, School of Chemistry, Manchester, **2017**, Unpublished results.
180. R. J. P. Williams, *Dalton Trans.* **2007**, 991−1001.
181. a) E. Gouaux, R. MacKinnon, *Science* **2005**, 310, 1461−1465; b) D. C. Gadsby, *Nat. Rev. Mol. Cell Biol.* **2009**, 10, 344–352.
182. a) D. A. Doyle, J. M. Cabral, R. A. Pfuetzner, A. Kuo, J. M. Gulbis, S. L. Cohen, B. T. Chait, R. MacKinnon, *Science* **1998**, 280, 69–77; b) R. MacKinnon, S. L. Cohen, A. Kuo, A. Lee, B. T. Chait, *Science* **1998**, 280, 106–109.
183. a) T. J. Jentsch, V. Stein, F. Weinreich, A. A. Zdebik, *Physiol. Rev.* **2002**, 82, 503–568; b) R. Dutzler, E. B. Campbell, R. MacKinnon, *Science* **2003**, 300, 108–112; c) V. Faundez, H. C. Hartzell, *Sci. STKE* **2004**, 233, 8; d) L. Feng, E. B. Campbell, Y. Hsiung, R. MacKinnon, *Science* **2010**, 330, 635–641; e) T. J. Jentsch, M. Pusch, *Physiol. Rev.* **2018**, 98, 1493–1590.
184. O. Boudker, G. Verdon, *Trends Pharmacol. Sci.* **2010**, 31, 418–426.
185. D. J. Slotboom, W. N. Konings, J. S. Lolkema, *Microbiol. Mol. Biol. Rev.* **1999**, 63, 293–307.
186. D. Yernool, O. Boudker, Y. Jin, E. Gouaux, *Nature* **2004**, 431, 811–818.
187. a) D. J. Slotboom, W. N. Konings, J. S. Lolkema, *Microbiol. Mol. Biol. Rev.* **1999**, 63, 293–307; b) D. Yernool, O. Boudker, Y. Jin, E. Gouaux, *Nature* **2004**, 431, 811–818.
188. J. E. Walker, *Biochem. Soc. Trans.* **2013**, 41, 1–16.
189. D. Pogoryelov, A. Krah, J. D Langer, Ö. Yildiz, J. D. Faraldo-Gómez, T. Meier, *Nat. Chem. Biol.* **2010**, 6, 891–899.
190. H. Noji, H. Ueno, D. G. G. McMillan, *Biophys. Rev.* **2017**, 9, 103–118.
191. M. Forgac, *Nat. Rev. Mol. Cell Biol.* **2007**, 8, 917–929.
192. a) C. F. Higgins, *Annu. Rev. Cell Biol.* **1992**, 8, 67–113; b) A. L. Davidson, E. Dassa, C. Orelle, J. Chen, *Microbiol. Mol. Biol. Rev.* **2008**, 72, 317−364; c) K. P. Locher, *Phil. Trans. R. Soc. B* **2009**, 364, 239–245; d) K. P. Locher, *Nat. Struct. Mol. Biol.* **2016**, 23, 487–493.
193. R. C. Ford, K. Beis, *Biochem. Soc. Trans.* **2019**, 47, 23–36.
194. I. B. Holland, *Res. Microbiol.* **2019**, 170, 304–320.

195. a) J. Chen, S. Sharma, F. A. Quiocho, A.L. Davidson, *Proc. Natl. Acad. Sci.* **2001**, 98, 1525–1530; b) M. L. Oldham, D. Khare, F. A. Quiocho, A. L. Davidson, J. Chen, *Nature* **2007**, 450, 515–521; c) H. A. Shuman, *J. Biol. Chem.* **1982**, 257, 5455–5461.
196. a) W. Köster, *Res. Microbiol.* **2001**, 152, 291–301; b) K. P. Locher, A. T. Lee, D. C. Rees, *Science* **2002**, 296, 1091–1098; c) V. Braun, K. Hantke, *Curr. Opin. Chem. Biol.* **2011**, 15, 328–334; d) V. M. Korkhov, S. A. Mireku, K. P. Locher, *Nature* **2012**, 490, 367–372.
197. a) P. D. W. Eckford, F. J. Sharom, *Biochem J.* **2010***,* 429, 195–203; b) F. J. Sharom, *IUBMB Life* **2011**, 63, 736–746.
198. M. Herget, C. Baldauf, C. Schölz, D. Parcej, K.-H. Wiesmüller, R. Tampé, R. Abele, E. Bordignon, *Proc. Natl. Acad. Sci.* **2011**, 108, 1349–1354.
199. J. Y. Lee, J. G. Yang, D. Zhitnitsky, O. Lewinson, D. C. Rees, *Science* **2014**, 343, 1133–1136.
200. V. Srinivasan, A. J. Pierik, R. Lill, *Science* **2014**, 343, 1137–1140.
201. D. A. Rodionov, P. Hebbeln, M. S. Gelfand, T. Eitinger, *J. Bacteriol.* **2006**, 188, 317–327.
202. a) S. Matile, A. V. Jentzsch, J. Montenegro, A. Fin, *Chem. Soc. Rev.* **2011**, 40, 2453–2474; b) J.-Y. Chen, J.-L. Hou, *Org. Chem. Front.* **2018**, 5, 1728–1736; c) X. Wu, E. N. W. Howe, P. A. Gale, *Acc. Chem. Res.* **2018**, 51, 1870–1879.
203. M. A. Watson, S. L. Cockroft, *Chem. Soc. Rev.* **2016**, 45, 6118−6129.
204. A. Blanco-Gómez, P. Cortón, L. Barravecchia, I. Neira, E. Pazos, C. Peinador, M. D. García, *Chem. Soc. Rev.* **2020**, 49, 3834–3862.
205. C. Cheng, P. R. McGonigal, J. F. Stoddart, R. D. Astumian, *ACS Nano* **2015**, 9, 8672–8688.
206. J. F. Stoddart, *Chem. Soc. Rev.* **2009**, 38, 1802–1820.
207. A. Coskun, M. Banaszak, R. D. Astumian, J. F. Stoddart, B. A. Grzybowski, *Chem. Soc. Rev.* **2012**, 41, 19–30.
208. M. Baroncini, S. Silvi, M. Venturi, A. Credi, *Angew. Chem. Int. Ed.* **2012**, 51, 4223–4226.
209. C. Cheng, P. R. McGonigal, S. T. Schneebeli, H. Li, N. A. Vermeulen, C. Ke, J. F. Stoddart, *Nature Nanotech.* **2015**, 10, 547–553.
210. Y. Qiu, L. Zhang, C. Pezzato, Y. Feng, W. Li, M. T. Nguyen, C. Cheng, D. Shen, Q.-H. Guo, Y. Shi, K. Cai, F. M. Alsubaie, R. D. Astumian, J. F. Stoddart, *J. Am. Chem. Soc.* **2019**, 141, 17472−17476.
211. G. Ragazzon, M. Baroncini, S. Silvi, M. Venturi, A. Credi, *Nat. Nanotechnol.* **2015**, 10, 70–75.
212. H. Li, C. Cheng, P. R. McGonigal, A. C. Fahrenbach, M. Frasconi, W.-G. Liu, Z. Zhu, Y. Zhao, C. Ke, J. Lei, R. M. Young, S. M. Dyar, D. T. Co, Y.-W. Yang, Y. Y. Botros, W. A. Goddard, M. R. Wasielewski, D. Astumian, J. F. Stoddart, *J. Am. Chem. Soc.* **2013**, 135, 18609−18620.
213. . Erbas-Cakmak, S. D. P. Fielden, U. Karaca, D. A. Leigh, C. T. McTernan, D. J. Tetlow, M. R. Wilson, *Science* **2017**, 358, 340–343.
214. E. R. Kay, D. A. Leigh, *Angew. Chem. Int. Ed.* **2015**, 54, 10080–10088.
215. R. D. Astumian, *Nature Nanotech. **2012,*** 7, 684–688.
216. A. Arduini, R. Bussolati, A. Credi, A. Secchi, S. Silvi, M. Semeraro, M. Venturi, *J. Am. Chem. Soc.* **2013**, 135, 9924–9930.
217. A. Arduini, R. Bussolati, A. Credi, S. Monaco, A. Secchi, S. Silvi, M. Venturi, *Chem. Eur. J.* **2012**, 18, 16203–16213.
218. J. W. Park, H. J. Song, H.-J. Chang, *Tetrahedron Lett.* **2006**, 47, 3831–3834.
219. J. W. Park, H. J. Song, Y. J. Cho, K. K. Park, *J. Phys. Chem. C* **2007**, 111, 18605−18614.
220. A. Harada, *Acc. Chem. Res.* **2001**, 34, 456–464.

221. a) R. Isnin, A. E. Kaifer, *J. Am. Chem. Soc.* **1991**, 113, 8188–8190; b) R. Isnin, A. E. Kaifer, *Pure Appl. Chem.* **1993**, 65, 495–498.
222. J. E. H. Buston, J. R. Young, H. L. Anderson, *Chem. Commun.* **2000**, 905–906.
223. a) H. Yonemura, M. Kasahara, H. Saito, H. Nakamura, T. Matsuo, J. Phys. Chem. **1992**, 96, 5765–5770; b) K. Eliadou, K. Yannakopoulou, A. Rontoyianni, I. M. Mavridis, *J. Org. Chem.* **1999**, 64, 6217–6226.
224. J. W. Park, H. J. Song, *Org. Lett.* **2004**, 6, 4869–4872.
225. M. R. Craig, M. G. Hutchings, T. D. W. Claridge, H. L. Anderson, *Angew. Chem. Int. Ed.* **2001**, 40, 1071–1074.
226. C. A. Stanier, S. J. Alderman, T. D. W. Claridge, H. L. Anderson, *Angew. Chem. Int. Ed.* **2002**, 41, 1769–1772.
227. H. Murakami, A. Kawabuchi, K. Kotoo, M. Kunitake, N. Nakashima, *J. Am. Chem. Soc.* **1997**, 119, 7605–7606.
228. a) Q.-C. Wang, D.-H. Qu, J. Ren, K. Chen, H. Tian, *Angew. Chem. Int. Ed.* **2004**, 43, 2661–2665; b) D.-H. Qu, Q.-C. Wang, J. Ren, H. Tian, *Org. Lett.* **2004**, 6, 2085–2088.
229. Q.-C. Wang, X. Ma, D.-H. Qu, H. Tian, *Chem. Eur. J.* **2006**, 12, 1088–1096.
230. T. Oshikiri, Y. Takashima, H. Yamaguchi, A. Harada, *J. Am. Chem. Soc.* **2005**, 127, 12186–12187.
231. T. Oshikiri, Y. Takashima, H. Yamaguchi, A. Harada, *Chem. Eur. J.* **2007**, 13, 7091–7098.
232. A. Hashidzume, A. Kuse, T. Oshikiri, S. Adachi, M. Okumura, H. Yamaguchi, A. Harada, *Sci. Rep.* **2018**, 8, 8950.
233. T. Oshikiri, H. Yamaguchi, Y. Takashima, A. Harada, *Chem. Commun.* **2009**, 5515−5517.
234. a) A. Arduini, F. Calzavacca, A. Pochini, A. Secchi, *Chem. Eur. J.* **2003**, 9, 793–799; b) A. Credi, S. Dumas, S. Silvi, M. Venturi, A. Arduini, A. Pochini, A. Secchi, *J. Org. Chem.* **2004**, 69, 5881−5887.
235. A. Arduini, F. Ciesa, M. Fragassi, A. Pochini, A. Secchi, *Angew. Chem. Int. Ed.* **2005**, 44, 278–281.
236. a) J. W. Park, *J. Phys. Chem. B* **2006**, 110, 24915–24922; b) A. Arduini, R. Bussolati, A. Credi, G. Faimani, S. Garaude, A. Pochini, A. Secchi, M. Semeraro, S. Silvi, M. Venturi, *Chem. Eur. J.* **2009**, 15, 3230–3242; c) A. Arduini, R. Bussolati, A. Credi, A. Secchi, S. Silvi, M. Semeraro, M. Venturi, *J. Am. Chem. Soc.* **2013**, 135, 9924–9930.
237. Feynman, R. P.; Leighton, R. B.; Sands, M. *The Feynman Lectures on Physics*; Addison-Wesley: Reading MA, **1963**.
238. B. L. Feringa, W. R. Browne, *Molecular Switches*, Wiley-VCH, Weinheim, **2011**.
239. M. Xue, Y. Yang, X. Chi, X. Yan, F. Huan, *Chem. Rev.* **2015**, 115, 7398–7501.
240. Y. Tokunaga, K. Akasaka, K. Hisada, Y. Shimomura, S. Kakuchi, *Chem. Commun.*, **2003**, 2250–2251.
241. S.-H. Chiu, S. J. Rowan, S. J. Cantrill, P. T. Glink, R. L. Garrell, J. F. Stoddart, *Org. Lett.* **2000**, 2, 3631–3634.
242. M. Baroncini, S. Silvi, M. Venturi, A. Credi, *Chem. Eur. J.* **2010**, 16, 11580–1587.
243. P. R. Ashton, I. Baxter, M. C. T. Fyfe, F. M. Raymo, N. Spencer, J. F. Stoddart, A. J. P. White, D. J. Williams, J. *Am. Chem. Soc.* **1998**, 120, 2297–2307.
244. E. Sevick, *Nature Nanotech.* **2015**, 10, 18–19.
245. A. Trabolsi, N. Khashab, A. C. Fahrenbach, D. C. Friedman, M. T. Colvin, K. K. Cotí, D. Benítez, E. Tkatchouk, J.-C. Olsen, M. E. Belowich, R. Carmielli, H. A. Khatib, W. A. Goddard, M. R. Wasielewski, J. F. Stoddart, *Nat. Chem.* **2010**, 2, 42–49.
246. B. Odell, M. V. Reddington, A. M. Z. Slawin, N. Spencer, J. F. Stoddart, D. J. Williams, *Angew. Chem. Int. Ed.* **1988**, 27, 1547–1550.

247. M. Asakawa, W. Dehaen, G. L'abbé, S. Menzer, J. Nouwen, F. M. Raymo, J. F. Stoddart, D. J. Williams, *J. Org. Chem.* **1996**, 61, 9591–9595.
248. V. Balzani, M. Clemente-León, A. Credi, B. Ferrer, M. Venturi, A. H. Flood, J. F. Stoddart, *Proc. Natl. Acad. Sci.* **2006**, 103, 1178–1183.
249. a) A. Trabolsi, N. Khashab, A. C. Fahrenbach, D. C. Friedman, M. T. Colvin, K. K. Cotí, D. Benítez, E. Tkatchouk, J.-C. Olsen, M. E. Belowich, R. Carmielli, H. A. Khatib, W. A. Goddard, M. R. Wasielewski, J. F. Stoddart, *Nat. Chem.* **2010**, 2, 42–49; b) H. Li, A. C. Fahrenbach, S. K. Dey, S. Basu, A. Trabolsi, Z. Zhu, Y. Y. Botros, J. F. Stoddart, *Angew. Chem. Int. Ed.* **2010**, 49, 8260–8265; c) A. C. Fahrenbach, J. C. Barnes, D. A. Lanfranchi, H. Li, A. Coskun, J. J. Gassensmith, Z. Liu, D. Benítez, A. Trabolsi, W. A. Goddard, M. Elhabiri, J. F. Stoddart, *J. Am. Chem. Soc.* **2012**, 134, 3061–3072; d) H. Li, Z. Zhu, A. C. Fahrenbach, B. M. Savoie, C. Ke, J. C. Barnes, J. Lei, Y.-L. Zhao, L. M. Lilley, T. J. Marks, M. A. Ratner, J. F. Stoddart, *J. Am. Chem. Soc.* **2013**, 135, 456–467.
250. C. Cheng, P. R. McGonigal, W.-G. Liu, H. Li, N. A. Vermeulen, C. Ke, M. Frasconi, C. L. Stern, W. A. Goddard, J. F. Stoddart, *J. Am. Chem. Soc.* **2014**, 136, 14702–14705.
251. K. Cai, Y. Shi, G.-W. Zhuang, L. Zhang, Y. Qiu, D. Shen, H. Chen, Y. Jiao, H. Wu, C. Cheng, J. F. Stoddart, *J. Am. Chem. Soc.* **2020**, 142, 10308−10313.
252. S. Goldup, *Nat. Nanotechnol.* **2015**, 10, 488−489.
253. C. Pezzato, M. T. Nguyen, C. Cheng, D. J. Kim, M. T. Otley, J. F. Stoddart, *Tetrahedron* **2017**, 73, 4849–4857.
254. C. Pezzato, M. T. Nguyen, D. J. Kim, O. Anamimoghadam, L. Mosca, J. F. Stoddart, *Angew. Chem. Int. Ed.* **2018**, *57*, 9325–9329.
255. a) F. Coutrot, E. Busseron, *Chem. Eur. J.* **2008**, 14, 4784–4787; b) F. Coutrot, *ChemistryOpen* **2015**, 4, 556–576.
256. P. L. Houston, *Chemical kinetics and reaction dynamics*, Dover Publications, Mineola New York, **2006**.
257. A. M. George, P. M. Jones, *Prog. Biophys. Mol. Biol.* **2012**, 109, 95–107.
258. a) U. A. Hellmich, S. Lyubenova, E. Kaltenborn, R. Doshi, H. W. van Veen,T. F. Prisner, C. Glaubitz, *J. Am. Chem. Soc.* **2012**, 134, 5857–5862; b) E. Lehnert, J. Mao, A. R. Mehdipour, G. Hummer, R. Abele, C. Glaubitz, R. Tampe, *J. Am. Chem. Soc.* **2016**, 138, 13967–13974; c) A. Nöll, C. Thomas, V. Herbring, T. Zollmann, K. Barth, A. R. Mehdipour, T. M. Tomasiak, S. Brüchert, B. Joseph, R. Abele, V. Oliéric, M. Wang, K. Diederichs, G. Hummer, R. M. Stroud, K. M. Pos, R. Tampé, *Proc. Natl. Acad. Sci.* **2017**, 114, E438–E447.
259. H. Göddeke, L. V. Schäfer, *J. Am. Chem. Soc.* **2020**, 142, 12791–12801.
260. Y. Cheng, *Science* **2018**, 361, 876-880.
261. a) K. H. Grellmann, A. R. Watkins, A. Weller, *J. Phys. Chem.* **1972**, 76, 469–473; b) M. Julliard, M. Chanon, *Chem. Rev.* **1983**, 83, 425–506; c) R. A. Bissell, A. Prasanna de Silva, H. Q. N. Gunaratne, P. L. M. Lynch, G. E. M. Maguire, K. R. A. S. Sandanayake, *Chem. Soc. Rev.* **1992**, 21, 187–195; d) A. P. de Silva, H. Q. N. Gunaratne, T. Gunnlaugsson, A. J. M. Huxley, C. P. McCoy; e) J. T. Rademacher, T. E. Rice, *Chem. Rev.* **1997**, 97, 1515−1566; f) A. P. de Silva, D. B. Fox, T. S. Moody, S. M.Weir, *Trends Biotechnol.* **2001**, 19, 29–34; g) J. R. Lakowicz, *Principles of Fluorescence Spectroscopy*, Springer, New York, **2006**.
262. For example: a) D. A. Leigh, M. A. F. Morales, E. M. Pérez, J. K. Y. Wong, C. G. Saiz, A. M. Z. Slawin, A. J. Carmichael, D. M. Haddleton, A. M. Brouwer, W. Jan Buma, G. W. H. Wurpel, S. León, F. Zerbetto, *Angew. Chem. Int. Ed.* **2005**, 44, 3062–3067; b) C.-S. Kwan, A. S. C. Chan, K. Cham-Fai Leung, *Org. Lett.* **2016**, 18, 976–979; c) A. Ghosh, I. Paul, M. Adlung, C. Wickleder, M. Schmittel, *Org. Lett.* **2018**,

20, 1046–1049; d) S. Corra, C. de Vet, J. Groppi, M. La Rosa, S. Silvi, M. Baroncini, A. Credi, *J. Am. Chem. Soc.* **2019**, 141, 9129–9133.

263. a) D. E. Stack, A. L. Hill, C. B. Diffendaffer, N. M. Burns, *Org. Lett.* **2002**, 4, 4487–4490; b) P. Lan, D. Berta, J. A. Porco, Jr, M. S. South, J. J. Parlow *J. Org. Chem.* **2003**, 68, 9678–9686; c) O. Tosic, J. Mattay, *Eur. J. Org. Chem.* **2011**, 371–376; d) A. Borissov, J. Y. C. Lim, A. Brown, K. E. Christensen, A. L. Thompson, M. D. Smith, P. D. Beer, *Chem. Commun.* **2017**, 53, 2483–2486.
264. a) M. Kitamura, T. Koga, M. Yano, T. Okauchi, *Synlett* **2012**, 23, 1335–1338; b) M. Kitamura, K. Murakami, *Org. Synth.* **2015**, 92, 171–181.
265. a) P. M. E. Gramlich, S. Warncke, J. Gierlich, T. Carell, *Angew. Chem. Int. Ed.* **2008**, 47, 3442–3444; b) I. E. Valverde, A. F. Delmas, V. Aucagne, *Tetrahedron* **2009**, 65, 7597–7602; c) J. Iehl, J.-F. Nierengarten, *Chem. Commun*. **2010**, 46, 4160-4162; d) I. E. Valverde, F. Lecaille, G. Lalmanach, V. Aucagne, A. F. Delmas, *Angew. Chem. Int. Ed.* **2012**, 51, 718–722.
266. H. Zheng, Y. Li, C. Zhou, Y. Li, W. Yang, W. Zhou, Z. Zuo, H. Liu, *Chem. Eur. J.* **2011**, 17, 2160–2167.
267. M. Dommaschk, University of Manchester, School of Chemistry, Manchester, **2019**, Unpublished results.
268. P. G. M. Wuts, *Greene's protective groups in organic synthesis*, John Wiley & Sons, Hoboken, New Jersey, **2014**, pp. 1195–1197.
269. Z. Meng, J.-F. Xiang, C.-F. Chen, *J. Am. Chem. Soc.* **2016**, 138, 5652−5658.
270. T. R. Chan, R. Hilgraf, K. B. Sharpless, V. V. Fokin, *Org. Lett.* **2004**, 6, 2853–2855.
271. S. Kassem, University of Manchester, School of Chemistry, Manchester, **2017**, Unpublished results.
272. A. F. Abdel-Magid, K. G. Carson, B. D. Harris, C. A. Maryanoff, R. D. Shah, *J. Org. Chem.* **1996**, 61, 3849–3862.
273. T. B. Gasa, C. Valente, J. F. Stoddart, *Chem. Soc. Rev.* **2011**, 40, 57–78.
274. P. R. Ashton, R. A. Bartsch, S. J. Cantrill, R. E. Hanes, Jr. S. K. Hickingbottom, J. N. Lowe, J. A. Preece, J. F. Stoddart, V. S. Talanovb, Z.-H. Wanga, *Tetrahedron Lett.* **1999**, 40, 3661–3664.
275. R. Chênevert, L. D'Astous, L., *J. Heterocyclic Chem.* **1986***,* 23, 1785–1787.
276. F. G. Bordwell, H. E. Fried, D. L. Hughes, T. Yun Lynch, A. V. Satish, Y. E. Whang, *J. Org. Chem.* **1990**, 55, 3330–3336.
277. W. Yang, Y. Li, J. Zhang, Y. Yu, T. Liu, H. Liua, Y. Li, *Org. Biomol. Chem.* **2011**, 9, 6022–6026.
278. P. R. Ashton, P. J. Campbell, E. J. T. Chrystal, P. T. Glink, S. Menzer, D. Philp, N. Spencer, J. F. Stoddart, P. A. Tasker, D. J. Williams, *Angew. Chem. Int. Ed.* **1995**, *34*, 1865–1869.
279. Y.-H. Huang, Q.-M. Ge, Y.-Y. Zhao, H. Cong, J.-L. Zhao, Z. Tao, Q.-Y. Luo, *Spectrochim. Acta, Part A,* **2019**, 218, 213–220.
280. a) N. Brosse, M.-F. Pinto, B. Jamart-Grégoire, *J. Org. Chem.* **2000**, 65, 4370–4374; b) M.-F. Pinto, N. Brosse, B. Jamart-Grégoire, *Syn. Commun.* **2002**, 32, 3603–3610.
281. a) A. Dirksen, S. Dirksen, T. M. Hackeng, P. E. Dawson, *J. Am. Chem. Soc.* **2006**, 128, 15602–15603; b) A. Dirksen, P. E. Dawson, *Bioconjugate Chem.* **2008**, 19, 2543–2548; c) V. T. Bhat, A. M. Caniard, T. Luksch, R. Brenk, D. J. Campopiano, M. F. Greaney, *Nature Chem.* **2010**, 2, 490–497; d) S. H. Hewitt, A. J. Wilson, *Eur. J. Org. Chem.* **2018**, 16, 1872–1879.
282. a) R. P. Szajewski, G. M. Whitesides, *J. Am. Chem. Soc.* **1980**, 102, 2011–2026; b) J. Houk, G. M. Whitesides, *J. Am. Chem. Soc.* **1987**, 109, 6825–6836; c) R. Singh, G. M. Whitesides, *J. Am. Chem. Soc.* **1990**, 109, 1190–1197.
283. a) K. Kokubo, H. Kakimoto, T. Oshima, *J. Am. Chem. Soc.* **2002**, 124, 6548–6549; b) K. Kokubo, K. Kitasaka, T. Oshima, *Org. Lett.* **2006**, 8, 1597–1600.

284. X. Cheng, J. C. Smith, *Chem. Rev.* **2019**, 119, 5849–5880.
285. a) J. A. Pitcher, N. J. Freedman, R. J. Lefkowitz, *Annu. Rev. Biochem.* **1998**, 67, 653–692; b) D. M. Rosenbaum, S. G. F. Rasmussen, B. K. Kobilka, *Nature* **2009**, 459, 356–363.
286. J. Groppi, L. Casimiro, M. Canton, S. Corra, M. Jafari-Nasab, G. Tabacchi, L. Cavallo, M. Baroncini, S. Silvi, E. Fois, A. Credi, *Angew. Chem. Int. Ed.* **2020**, 59, 2–12.
287. D. H. Waldeck, *Chem. Rev.* **1991**, 91, 415–436.
288. a) G. Fischer, *Chem. Soc. Rev.* **2000**, 29, 119–127; b) I. Ledneczki, P. Forgo, J.T. Kiss, Á. Molnár, I. Pálinkó, *J. Mol. Struct.* **2007**, 834–836, 349–354.
289. E. J. Corey, C. J. Helal, *Angew. Chem. Int. Ed.* **1998**, *37*, 1986–2012.
290. Q.-H. Guo, Y. Qiu, X. Kuang, J. Liang, Y. Feng, L. Zhang, Y. Jiao, D. Shen, R. D. Astumian, J. F. Stoddart, *J. Am. Chem. Soc.* **2020**, 142, 14443−14449.
291. Y. Zhang, Z. Chang, H. Zhao, S. Crespi, B. L. Feringa, D. Zhao, *Chem* **2020**, 6, 2420–2429.

11. Appendix

11.1. Experimental Procedures

11.1.1. General Methods

Unless stated otherwise, reagents were obtained from commercial sources and used without purification. Unless otherwise stated, all reactions were carried out in anhydrous solvents and under an N_2 or Ar atmosphere. Anhydrous THF (HPLC grade, Fischer Scientific), $CHCl_3$ (99.8+%, Fischer Scientific), CH_2Cl_2 (HPLC grade, Fischer Scientific), CH_3CN (HPLC grade, Fischer Scientific), and toluene (>99%, Fischer Scientific) were obtained by passing the solvent through an activated alumina column on a Phoenix SDS (solvent drying system; JC Meyer Solvent Systems, CA, USA). DMF (peptide synthesis grade, Merck) was used unless otherwise stated. Solutions were irradiated with a 365 nm LED source (FWHM =15 nm, ThorLabs M395L4). ^{1}H NMR spectra were recorded on a Bruker Avance III instrument with an Oxford AS600 magnet equipped with a cryoprobe [5mm CPDCH 13C-1H/D] (600 MHz) at 298 K. Chemical shifts are reported in parts per million (ppm) from high to low frequency using the residual solvent peak as the internal reference CD_3CN = 1.94 ppm, ($(CD_3)_2SO$ = 2.50 ppm, $CDCl_3$ = 7.26 ppm, CD_2Cl_2 = 5.32 ppm, toluene-d_8 = 2.08 ppm and $(CD_3)_2CO$ = 2.05 ppm). All ^{1}H resonances are reported to the nearest 0.01 ppm. The multiplicity of ^{1}H signals are indicated as: s = singlet; d = doublet; t = triplet; quint. = quintet; sex. = sextet; sept. = septet; m = multiplet; br = broad; or combinations thereof. Coupling constants (*J*) are quoted in Hz and reported to the nearest 0.1 Hz. ^{13}C NMR spectra (151 Mhz) were recorded on the same spectrometer at 298 K with the central resonance of the solvent peak as the internal reference (CD_3CN = 1.32 ppm, $(CD_3)_2SO$ = 39.52 ppm, $CDCl_3$ = 77.16 ppm, CD_2Cl_2 = 53.84 ppm and toluene-d_8 = 20.43 ppm). All ^{13}C resonances are reported to the nearest 0.1 ppm in general, or to 0.01 ppm to aid in the differentiation of close but resolved signals. ^{11}B, ^{19}F and ^{31}P NMR spectra were recorded on a Bruker Ascend 500, Ascend 400 or Avance II instrument: at base frequencies of 128(^{11}B), 471(^{19}F), 202(^{31}P) MHz (Bruker Ascend 500 and Bruker Avance II) or 376(^{19}F), 162(^{31}P) MHz (Bruker Ascend 400) without referencing. DEPT, COSY, NOESY, ROESY, HSQC, HSQC-TOCSY and HMBC experiments (standard Bruker library, Topspin 3.6.x) were used to aid structural determination and spectral assignment. Flash column chromatography was carried out using Silica 60 Å (particle size 40 – 63 µm, Sigma Aldrich, UK) as the stationary phase. Preparative TLC was performed using either PLC 20 × 20 cm, 60 F254 preparatory plates (Merck). Analytical TLC was performed on precoated silica gel plates (0.25 mm thick, 60 F254, Merck, Germany) and visualized using both short and long waved ultraviolet light in combination with standard laboratory stains (permanganate or ceric ammonium molybdate). Size-exclusion chromatography was carried out under gravity using a neutral, porous styrene divinylbenzene resin (1% crosslinked linked, Bio-Rad, Bio-Beads, S-X1) as stationary phase and CH_2Cl_2 as an eluent. Anion-exchange was carried out by passing a concentrated solution of the organic salt through a bed of anion-exchange resin (amberlyst A26, Sigma-Aldrich) with CH_3CN as an eluent. The appropriate anion-exchange resin is obtained by eluting the resin (OH form) with a concentrated aqueous solution of the corresponding NH_4X salt (where X represents the anion), then washed with deionised water till neutral, followed by anhydrous MeOH and finally, CH_3CN. UV-vis spectra were acquired on a Varian Cary 100 and fluorescence spectra on a Varian Cary Eclipse instrument and data as shown is unprocessed. Low resolution ESI mass spectrometry was performed with a Thermo Scientific LCQ Fleet Ion Trap Mass Spectrometer or an Agilent Technologies 1200 LC system with either an Agilent 6130 single quadrupole MS detector or an Advion Expression LCMS single quadrupole MS detector. High-resolution mass spectrometry was carried out by the Mass Spectrometry Service, School of Chemistry, the University of Manchester. Compounds **74**,[114a] **75**,[123a] **134**,[169,170] and **123**[125] were synthesized according to literature procedures.

11.1.2. Helicene Synthesis by a Rotaxane-Based Molecular Machine

Synthesis of One-Barrier Rotaxanes 122a and 122b

Synthesis of **126b**

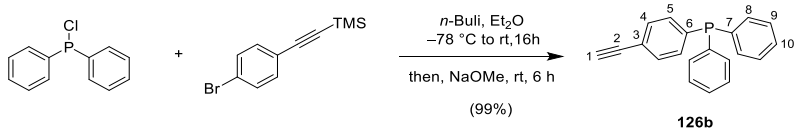

126b

To a solution of 4-((trimethylsilyl)ethynyl)bromobenzene (500 mg, 1.97 mmol) in dry degassed Et_2O (20 ml) at –78 °C was added *n*-BuLi (2.5 M in hexanes, 0.79 mL, 1.97 mmol) dropwise and the reaction mixture was warmed to –10 °C and stirred for 15 minutes. The reaction mixture was then cooled to –78 °C and diphenylchlorophosphine (0.24 mL, 1.32 mmol) was added dropwise. The reaction mixture was warmed to room temperature and stirred for 16 h. MeOH (2 mL) was added followed by NaOMe (53 mg, 0.99 mmol) and the reaction mixture was stirred at room temperature for 6 h. The reaction was concentrated *in vacuo* and purified by flash chromatography under argon (all tubes and flasks were purged with argon) (SiO_2, petroleum ether/ EtOAc, 100:1) to afford **126b** (375 mg, 99%) as a colourless oil that was stored as a solution in benzene under argon in the freezer.

^{1}H NMR (600 MHz, $CDCl_3$) δ 7.44 (dd, *J* = 8.2, 1.5 Hz, 2H, H-5), 7.38 – 7.32 (m, 6H, H-9 and H-10), 7.31 – 7.28 (m, 4H, H-8), 7.25 – 7.22 (m, 2H, H-4), 3.11 (s, 1H, H-1).

^{31}P NMR (162 MHz, $CDCl_3$) δ −5.46.

^{13}C NMR (151 MHz, $CDCl_3$) δ 138.8 (d, $J_{C\text{-}P}$ = 12.9 Hz), 136.6 (d, $J_{C\text{-}P}$ = 10.7 Hz), 134.0 (d, $J_{C\text{-}P}$ = 19.8 Hz), 133.5 (d, $J_{C\text{-}P}$ = 19.3 Hz), 132.1 (d, $J_{C\text{-}P}$ = 6.6 Hz), 129.1, 128.8 (d, $J_{C\text{-}P}$ = 7.1 Hz), 122.4, 83.5, 78.3.

HRMS (ESI^+): Calculated for $C_{20}H_{16}P$: 287.0984 $[M+H]^+$, found 287.0972.

Synthesis of **126a**

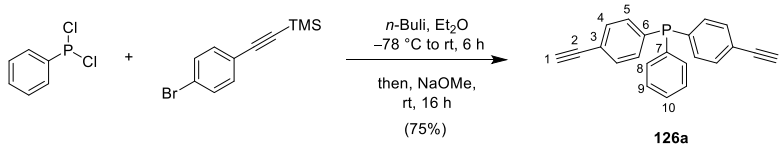

126a

To a solution of 4-((trimethylsilyl)ethynyl)bromobenzene (2 .00 g, 7.90 mmol) in dry degassed Et_2O (80 ml) at –78 °C was added *n*-BuLi (2.5 M in hexanes, 3.16 mL, 7.90 mmol) dropwise and the reaction mixture was warmed to –10 °C and stirred for 15 minutes. The reaction mixture was then cooled to –78 °C and dichlorophenylphosphine (0.43 mL, 3.16 mmol) was added dropwise. The reaction mixture was warmed to room temperature and stirred for 5 h. MeOH (10 mL) was added followed by NaOMe (85 mg, 1.58 mmol) and the reaction mixture was stirred at room temperature for 16 h. The reaction was concentrated *in vacuo* and purified by flash chromatography (SiO_2, petroleum ether/ EtOAc, 100:1) under argon (all tubes and flasks were purged with argon) to afford **126a** (742 mg, 75%) as a clear yellow oil that was stored under argon in benzene in the freezer. Data consistent with that previously reported.[125]

^{1}H NMR (600 MHz, $CDCl_3$) δ 7.48 – 7.43 (m, 4H, H-5), 7.40 – 7.33 (m, 3H, H-9 and H-10), 7.31 – 7.27 (m, 2H, H-8), 7.26 – 7.20 (m, 4H, H-4), 3.12 (s, 2H, H-1).

^{13}C NMR (151 MHz, $CDCl_3$) δ 138.1 (d, $J_{C\text{-}P}$ = 12.7 Hz), 136.0 (d, $J_{C\text{-}P}$ = 10.5 Hz), 134.0 (d, $J_{C\text{-}P}$ = 20.2 Hz), 133.6 (d, $J_{C\text{-}P}$ = 19.5 Hz), 132.3 (d, $J_{C\text{-}P}$ = 7.1 Hz), 129.4, 129.2, 128.9 (d, $J_{C\text{-}P}$ = 7.4 Hz), 128.4, 125.4, 122.7, 83.4, 78.5.

Synthesis of **135b**

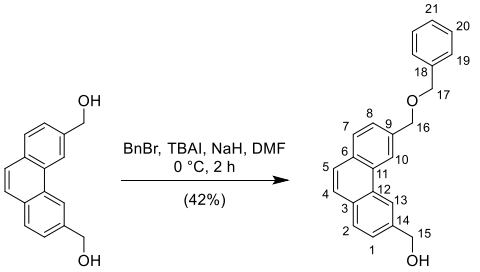

134 **135b**

To a solution of **134**[169,170] (100 mg, 0.42 mmol) and TBAI (16 mg, 0.042 mmol) in DMF (5 mL) at 0 °C was added NaH (60% in mineral oil, 17.5 mg, 0.44 mmol) and benzyl bromide (50 µL, 0.42 mmol). The reaction was stirred at 0 °C for 2 h. The reaction was quenched by the slow addition of saturated aqueous NH_4Cl (10 mL) and diluted with CH_2Cl_2 (20 mL). The organic layer was separated, and the aqueous layer was extracted with CH_2Cl_2 (2 × 10 mL). The combined organic layers were washed with brine (3 × 20 mL), dried over $MgSO_4$, filtered, and concentrated *in vacuo*. The resultant residue was purified by flash chromatography (SiO_2, petroleum ether/EtOAc, 2:1) to give **135b** (58 mg, 42%) as a white solid.

^{1}H NMR (600 MHz, $CDCl_3$) δ 8.69 (s, 2H, H-10 and H-13), 7.90 (d, *J* = 8.1 Hz, 2H, H-2 and H-7), 7.74 (s, 2H, H-4 and H-5), 7.65 – 7.59 (m, 2H, H-1 and H-8), 7.43 (d, *J* = 7.4 Hz, 2H, H-19), 7.39 (t, *J* = 7.5 Hz, 2H, H-20), 7.32 (t, *J* = 7.3 Hz, 1H, H-21), 4.98 (d, *J* = 6.0 Hz, 2H, H-15), 4.84 (s, 2H, H-16), 4.66 (s, 2H, H-17), 1.81 (t, *J* = 6.0 Hz, 1H, C-1 OH).

^{13}C NMR (151 MHz, $CDCl_3$) δ 139.2, 138.4, 136.7, 131.9, 131.8, 130.4, 130.3, 129.1, 129.0, 128.6, 128.1, 127.9, 126.9, 126.8, 126.7, 125.9, 122.0, 121.0, 72.7, 72.4, 66.0.

HRMS (ASAP): Calculated for $C_{23}H_{20}O_2$: 328.1458 $[M]^+$, found 328.1459.

Synthesis of **125b**

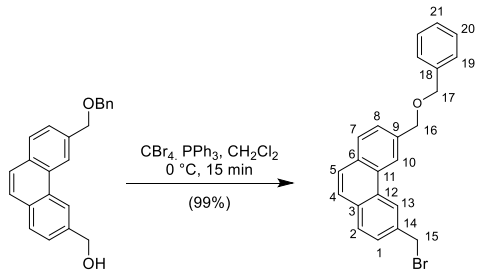

135b **125b**

To a solution of **135b** (52 mg, 0.16 mmol) in CH_2Cl_2 (10 mL) at 0 °C was added CBr_4 (105 mg, 0.40 mmol) and PPh_3 (105 mg, 0.32 mmol) and the reaction was stirred at 0 °C for 15 minutes. The resultant mixture was evaporated from SiO_2 and purified by flash chromatography (SiO_2, petroleum ether/EtOAc, 5:1) to give **125b** (61 mg, 99%) as a white solid.

^{1}H NMR (600 MHz, $CDCl_3$) δ 8.69 (s, 1H, H-13), 8.65 (s, 1H, H-10), 7.90 (d, *J* = 5.6 Hz, 1H, H-2 or H-7), 7.88 (d, *J* = 5.5 Hz, 1H, H-2 or H-7), 7.78 – 7.70 (m, 2H, H-4 and H-5), 7.63 – 7.64 (s, 1H, H-1 and H-8), 7.43 (d, *J* = 7.2 Hz, 2H, H-19), 7.40 (t, *J* = 7.5 Hz, 2H, H-20), 7.33 (t, *J* = 7.3 Hz, 1H, H-21), 4.84 (s, 2H, H-16), 4.79 (s, 2H, H-15), 4.66 (s, 2H, H-17).

^{13}C NMR (151 MHz, $CDCl_3$) δ 138.3, 137.0, 136.0, 132.1, 131.9, 130.4, 130.1, 129.5, 129.0, 128.7, 128.1, 127.9, 127.62, 127.58, 126.8, 126.6, 123.4, 121.8, 72.6, 72.5, 34.5.

HRMS (APPI): Calculated for $C_{23}H_{19}OBr$: 390.0614 $[M]^+$, found 390.0601.

Synthesis of **124b**

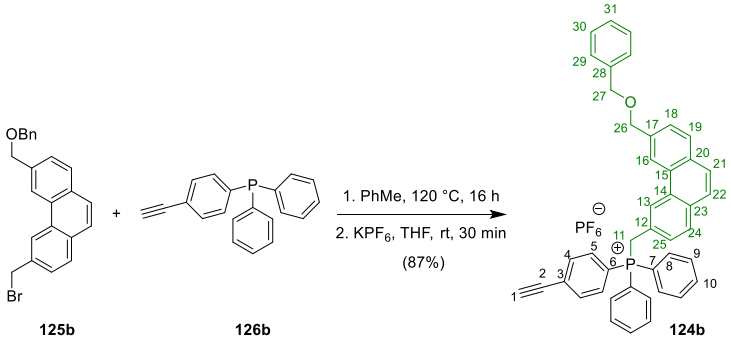

125b (82 mg, 0.21 mmol) and **126b** (90 mg, 0.31 mmol) were dissolved in degassed toluene (3 mL) and heated at 120 °C in a sealed tube for 16 h. The solvent was removed *in vacuo* and the residue was taken up in THF (10 mL). KPF_6 (100 mg, 0.51 mmol) was added and the solution stirred at room temperature for 30 minutes. The solvent was removed *in vacuo* and the residue was taken up in CH_2Cl_2 and filtered under reduced pressure. The filtrate was concentrated *in vacuo* and purified by size exclusion chromatography (S-X1, CH_2Cl_2) to give **124b** (136 mg, 87%) as a yellow glassy solid.

^{1}H NMR: (600 MHz, $CDCl_3$) δ 8.05 (s, 1H, H-13), 8.01 (s, 1H, H-16), 7.76 (d, *J* = 8.1 Hz, 1H, H-19), 7.69 – 7.66 (m, 2H, H-10), 7.63 (dd, *J* = 8.4, 3.0 Hz, 2H, H-4), 7.64 – 7.61 (m, 2H, H-18 and H-21), 7.59 – 7.49 (m, 11H, H-5, H-8, H-9 and H-24), 7.45 (d, *J* = 8.8 Hz, 1H, H-22), 7.43 – 7.42 (m, 2H, H-29), 7.39 (t, *J* = 7.6 Hz, 2H, H-30), 7.31 (t, *J* = 7.2 Hz, 1H, H-31), 7.05 (dt, *J* = 8.2, 1.9 Hz, 1H, H-25), 4.78 (d, J_{H-P} = 14.1 Hz, 2H, H-11), 4.75 (s, 2H, H-26), 4.62 (s, 2H, H-27), 3.29 (s, 1H, H-1).

^{31}P NMR: (202 MHz, $CDCl_3$) δ 22.5, −144.1 (sept, J_{P-F} = 713.7 Hz).

^{13}C NMR: (151 MHz, $CDCl_3$) δ 138.6, 137.4, 135.5 (d, J_{C-P} = 3.3 Hz), 134.2 (d, J_{C-P} = 9.6 Hz), 134.1 (d, J_{C-P} = 9.9 Hz), 133.6 (d, J_{C-P} = 12.8 Hz), 131.8 (d, J_{C-P} = 3.5 Hz), 131.5, 130.5 (d, J_{C-P} = 12.6 Hz), 130.1 (d, J_{C-P} = 3.4 Hz), 129.6 (d, J_{C-P} = 3.4 Hz), 129.4, 129.3, 129.3, 128.7, 128.7 (d, J_{C-P} = 4.6 Hz), 128.6, 128.2, 127.8, 127.1, 126.1, 126.0 (d, J_{C-P} = 7.0 Hz), 124.0 (d, J_{C-P} = 9.0 Hz), 122.1, 117.3 (d, J_{C-P} = 86.3 Hz), 116.7 (d, J_{C-P} = 86.1 Hz), 83.0, 81.5, 72.7, 72.5, 30.9 (d, J_{C-P} = 47.9 Hz).

HRMS (ESI$^+$): Calculated for $C_{43}H_{34}OP$: 597.2342 $[M-PF_6]^+$, found 597.2328.

Synthesis of 1-barrier rotaxane **122b** and free thread **139b**

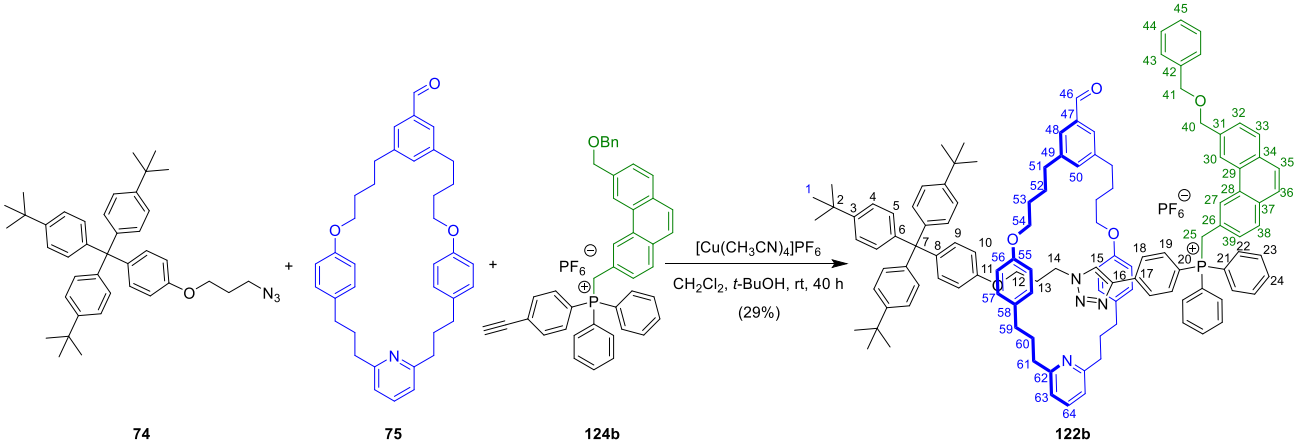

Aldehyde macrocycle **75** (45 mg, 0.080 mmol) and $[Cu(CH_3CN)_4]PF_6$ (4.5 mg, 0.012 mmol) were dissolved in degassed CH_2Cl_2 (2 ml) in a flame dried flask and stirred at room temperature for 20 min. Azide stopper **74** (14 mg, 0.024 mmol) and **124b** (15 mg, 0.020 mmol) in degassed CH_2Cl_2 (2 ml) and *t*-BuOH (0.5 mL) were added to the reaction mixture and the reaction was stirred at room temperature for 40 h. The reaction mixture was diluted with CH_2Cl_2 (40 ml) and washed with pH 7 aqueous Na_4EDTA solution (1M, 20 mL). The organic layer was separated and dried over $MgSO_4$, filtered, and concentrated *in vacuo*. The resultant residue was purified by size exclusion chromatography (S-X1, CH_2Cl_2) to give **122b** (10.9 mg, 29%) as an opaque white glassy solid.

^{1}H NMR: (600 MHz, $CDCl_3$) δ 9.78 (s, 1H, H-46), 8.18 (m, 1H, H-30), 8.12 (s, 1H, H-27), 7.82 – 7.76 (m, 3H, H-38 and H-48), 7.70 (td, *J* = 7.3, 1.6 Hz, 2H, H-33 and H-35), 7.66 (d, *J* = 8.7 Hz, 2H, H-18), 7.60 (d, *J* = 8.1, 1H, H-36), 7.60 – 7.49 (m, 9H, H-15, H-18, H-22, H-32 and H-50), 7.42 – 7.34 (m, 9H, H-23, H24, H-43 and H-64), 7.34 (t, *J* = 7.7 Hz, 2H, H-44), 7.33 – 7.27 (m, 1H, H-45), 7.23 (d, *J* = 8.6 Hz, 6H, H-4), 7.09 (d, *J* = 8.6 Hz, 6H, H-5), 7.07 (d, *J* = 8.7 Hz, 1H, H-39), 6.98 (d, *J* = 8.9 Hz, 2H, H-9), 6.85 (d, *J* = 7.7 Hz, 2H, H-63), 6.70 (d, *J* = 8.5 Hz, 4H, H-57), 6.44 (d, *J* = 8.9 Hz, 2H, H-10), 6.37 (d, *J* = 8.5 Hz, 4H, H-56), 4.77 (d, $J_{H\text{-}P}$ = 14.1 Hz, 2H, H-25), 4.72 (s, 2H, H-40), 4.58 (s, 2H, H-41), 3.77 (t, *J* = 7.6 Hz, 2H, H-14), 3.73 – 3.67 (m, 4H, H-54), 3.31 (t, *J* = 5.8 Hz, 2H, H-12), 2.61 (t, *J* = 7.5 Hz, 4H, H-51), 2.58 – 2.53 (m, 4H, H-61), 2.48 (t, *J* = 7.4 Hz, 4H, H-59), 1.78 – 1.73 (m, 4H, H-60), 1.72 – 1.66 (m, 10H, H-13, H-52, H-53), 1.30 (s, 27H, H-1).

^{31}P NMR: (162 MHz, $CDCl_3$) δ 21.80, −144.0 (quin, $J_{P\text{-}F}$ = 713.5 Hz).

^{13}C NMR: (151 MHz, $CDCl_3$) δ 192.9, 161.5, 157.0, 156.2, 148.5, 144.7, 144.3, 143.8, 139.9, 138.6, 137.8, 137.4, 137.0, 136.6, 135.4 (d, $J_{C\text{-}P}$ = 3.2 Hz), 134.9, 134.4 (d, $J_{C\text{-}P}$ = 10.0 Hz), 134.2 (d, $J_{C\text{-}P}$ = 9.8 Hz), 133.8, 132.2, 131.8 (d, $J_{C\text{-}P}$ = 2.6 Hz), 131.6, 130.8, 130.4 (d, $J_{C\text{-}P}$ = 12.5 Hz), 130.3 (d, $J_{C\text{-}P}$ = 3.2 Hz), 129.5 (d, $J_{C\text{-}P}$ = 15.7 Hz), 129.2, 128.8, 128.6, 128.19, 128.15, 127.8, 127.5, 127.1, 126.8 (d, $J_{C\text{-}P}$ = 12.7 Hz), 126.1, 124.5 (d, $J_{C\text{-}P}$ = 8.7 Hz), 124.2, 122.3, 122.1, 120.3, 120.1, 117.5 (d, $J_{C\text{-}P}$ = 86.2 Hz), 115.2 (d, $J_{C\text{-}P}$ = 87.5 Hz),114.4, 114.1, 113.1, 113.0, 72.6, 72.5, 67.4, 63.9, 63.2, 47.1, 37.9, 35.2, 35.0, 34.5, 32.6, 31.5, 31.1 (d, $J_{C\text{-}P}$ = 48.0 Hz), 29.4, 29.0, 28.4.

HRMS (ESI$^+$): Calculated for $C_{121}H_{127}N_4O_5P$: 1746.9539 $[M\text{-}PF_6]^+$, found 1746.9439.

Free thread **139b** was also isolated as a colourless film (4.2 mg, 16%).

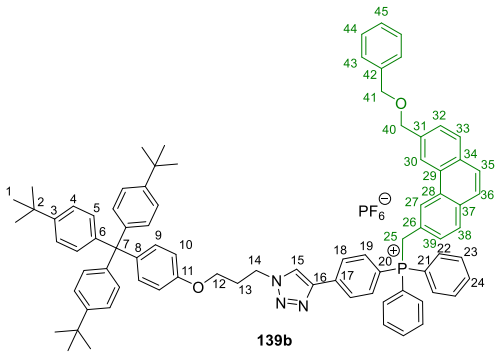

^{1}H NMR: (600 MHz, $CDCl_3$) δ 8.08 (s, 1H, H-27), 8.07 – 8.04 (m, 4H, H-15, H-18 and H-30), 7.77 (d, *J* = 8.4 Hz, H-33), 7.69 – 7.66 (m, 2H, H-24), 7.64 (d, *J* = 8.4 Hz, H-35), 7.58 – 7.51 (m, 9H, H-19, H-23, H-32, H-36 and H-38), 7.49 – 7.44 (m, 4H, H-22), 7.41 – 7.35 (m, 4H, H-43 and H-44), 7.31 – 7.27 (m, 1H, H-45), 7.22 (d, *J* = 8.4 Hz, 6H, H-4), 7.10 – 7.06 (m, 8H, H-5 and H-9), 7.22 (d, *J* = 8.4 Hz, 1H, H-39), 4.69 – 4.64 (m, 4H, H-25 and H-40), 4.58 (t, *J* = 7.2 Hz, H-14), 4.57 (s, 2H, H-41), 3.98 (t, *J* = 6.0 Hz, H-12), 2.39 (p, *J* = 6.3 Hz, 2H, H-13), 1.29 (s, 27H, H-1).

^{13}C NMR: (151 MHz, $CDCl_3$) δ 156.3, 148.3, 145.2, 144.1, 140.0, 138.4, 137.8 (d, $J_{C\text{-}P}$ = 2.8 Hz), 137.2, 135.3 (d, $J_{C\text{-}P}$ = 2.6 Hz)), 134.5 (d, $J_{C\text{-}P}$ = 10.0 Hz), 134.0 (d, $J_{C\text{-}P}$ = 9.7 Hz), 132.3, 131.7 (d, $J_{C\text{-}P}$ = 3.2 Hz), 131.5, 130.7, 130.3 (d, $J_{C\text{-}P}$ = 12.6 Hz), 130.1 (d, $J_{C\text{-}P}$ = 3.1 Hz), 129.3 (d, $J_{C\text{-}P}$ = 4.3 Hz), 129.3, 128.7, 128.5, 128.4 (d, $J_{C\text{-}P}$ = 4.7 Hz), 128.1, 127.8, 127.8, 127.1 (d, $J_{C\text{-}P}$ = 12.9 Hz), 127.0, 126.0, 125.8 (d, $J_{C\text{-}P}$ = 6.5 Hz), 124.2 (d, $J_{C\text{-}P}$ = 8.8 Hz), 124.1, 122.5, 121.8, 117.1 (d, $J_{C\text{-}P}$ = 86.1 Hz) , 115.2 (d, $J_{C\text{-}P}$ = 88.1 Hz), 112.9, 72.5, 72.4, 64.0, 63.1, 47.6, 34.3, 31.4, 31.1 (d, $J_{C\text{-}P}$ = 53.0 Hz) 30.0.

HRMS (ESI^+): calculated for $C_{83}H_{83}O_2N_3P$ 1184.6217 $[M\text{-}PF_6]^+$, found 1184.6211.

Synthesis of **135a**

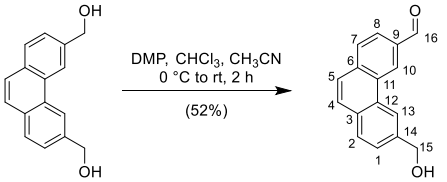

134 **135a**

To a solution of **134** (100 mg, 0.42 mmol) in $CHCl_3$ (10 ml) and CH_3CN (5 mL) at 0 °C was added Dess-Martin periodinane (180 mg, 0.42 mmol). The reaction was gradually warmed to room temperature and stirred for 2 h. The reaction was quenched by the addition of saturated aqueous $Na_2S_2O_3$ (5 mL) and 2M aqueous NaOH (5 mL) were added and the mixture was diluted with CH_2Cl_2 (20 mL). The organic layer was separated, and the aqueous layer was extracted with CH_2Cl_2 (2 × 10 mL). The combined organic layers were dried over $MgSO_4$, filtered, and concentrated *in vacuo*. The resultant residue was purified by flash chromatography (SiO_2, pet ether/EtOAc, 2:1 – 1:1) to give **135a** (52 mg, 52 %) as a white solid.

^{1}H NMR: (600 MHz, $CDCl_3$) δ 10.29 (s, 1H, H-16), 9.22 (s, 1H, H-10), 8.79 (s, 1H, H-13), 8.09 (dd, *J* = 8.2, 1.5 Hz, 1H, H-8), 8.02 (d, *J* = 8.2 Hz, 1H, H-7), 7.95 (d, *J* = 8.1 Hz, 1H, H-2), 7.91 (d, *J* = 8.8 Hz, 1H, H-4), 7.80 (d, *J* = 8.8 Hz, 1H, H-5), 7.68 (d, *J* = 8.1 Hz, 1H, H-1), 5.03 (d, *J* = 5.9 Hz, 2H, H-15), 1.90 (t, *J* = 5.9 Hz, 1H, OH).

^{13}C NMR: (151 MHz, $CDCl_3$) δ 192.6, 140.3, 136.3, 134.4, 131.8, 130.7, 130.3, 130.2, 129.7, 129.4, 127.5, 126.55, 126.52, 125.4, 120.8, 65.7.

HRMS (ASAP): Calculated for $C_{16}H_{13}O_2$: 237.0910 $[M+H]^+$, found 237.0901.

Synthesis of **125a**

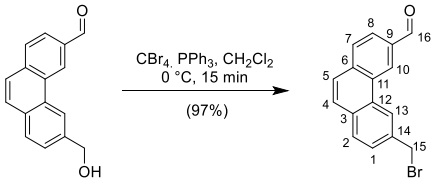

135a **125a**

To a solution of **135a** (111 mg, 0.470 mmol) in CH_2Cl_2 (15 mL) at 0 °C was added CBr_4 (388 mg, 1.17 mmol) and PPh_3 (247 mg, 0.941 mmol) and the reaction was stirred at 0 °C for 15 minutes. The resultant mixture was evaporated from SiO_2 and purified by flash chromatography (SiO_2, CH_2Cl_2, neat) to give **125a** (137 mg, 97%) as a white solid.

^{1}H NMR: (600 MHz, $CDCl_3$) δ 10.30 (s, 1H, H-16), 9.19 (s, 1H, H-10), 8.79 (s, 1H, H-13), 8.11 (dd, *J* = 8.2, 1.5 Hz, 1H, H-8), 8.02 (d, *J* = 8.2 Hz, H-7), 7.94 (d, *J* = 8.2 Hz, 1H, H-2), 7.90 (d, *J* = 8.8 Hz, 1H, H-4), 7.82 (d, *J* = 8.8 Hz, 1H, H-5), 7.71 (dd, *J* = 8.1, 1.6 Hz, 1H, H-1), 4.80 (s, 2H, H-15).

^{13}C NMR: (151 MHz, $CDCl_3$) δ 192.5, 137.2, 136.3, 134.5, 132.2, 130.7, 130.04, 129.97, 129.8, 129.8, 128.4, 127.3, 127.1, 125.7, 123.3, 33.9.

HRMS (ASAP): Calculated for $C_{16}H_{12}OBr$: 299.0066 $[M+H]^+$, found 299.0055.

Synthesis of **124a**

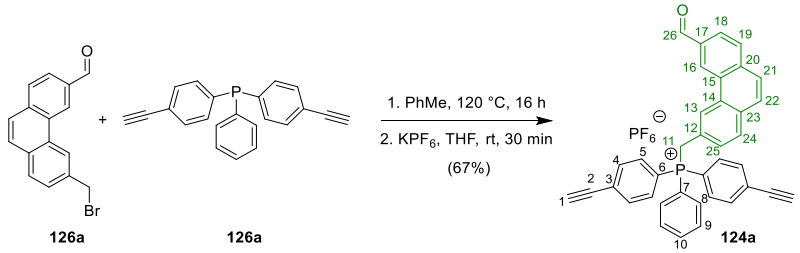

125a (40 mg, 0.13 mmol) and **126a** (46 mg, 0.15 mmol) were dissolved in degassed toluene (5 mL) and heated at 120 °C in a sealed tube for 16 h. The solvent was removed *in vacuo* and the residue was taken up in THF (10 mL). KPF_6 (100 mg, 0.51 mmol) was added and the solution stirred at room temperature for 30 minutes. The solvent was removed *in vacuo* and the residue was taken up in CH_2Cl_2 and filtered under reduced pressure. The filtrate was concentrated *in vacuo* and purified by size exclusion chromatography (S-X1, CH_2Cl_2) to give **124a** (61 mg, 67%) as a yellow glassy solid.

^{1}H NMR: (600 MHz, DMSO-d_6) δ 10.20 (s, 1H, H-26), 8.57 (s, 1H, H-16), 8.32 (s, 1H. H-13), 8.19 (d, J = 8.2 Hz, 1H, H-18), 8.10 (dd, J = 8.2, 1.4 Hz, 1H, H-19), 8.04 – 7.96 (m, 3H, , H-21, H-22 and H-24), 7.91 (td, J = 7.3, 1.8 Hz, 1H, H-10), 7.86 – 7.68 (m, 12H, H-4, H-5. H-8 and H-9), 7.43 (d, J = 8.2 Hz, 1H, H-25), 5.46 (d, J_{H-P} = 15.8 Hz, 2H, H-11), 4.67 (s, 2H, H-1).

^{31}P NMR: (162 MHz, DMSO-d_6) δ 23.61, −144.22 (sept, J_{P-F} = 711.2 Hz).

^{13}C NMR: (151 MHz, DMSO-d_6) δ 192.6, 135.6, 135.5 (d, J_{C-P} = 3.3 Hz), 134.5 (d, J_{C-P} = 10.3 Hz), 134.3, 134.2 (d, J_{C-P} = 3.7 Hz), 133.0 (d, J_{C-P} = 13.0 Hz), 131.3 (d, J_{C-P} = 3.2 Hz), 130.3 (d, J_{C-P} = 12.5 Hz), 129.8, 129.7, 129.55 (d, J_{C-P} = 2.8 Hz), 129.49 (d, J_{C-P} = 3.3 Hz), 128.7, 128.5 (d, J_{C-P} = 3.3 Hz), 127.3, 126.8 (d, J_{C-P} = 8.9 Hz), 126.0, 125.7 (d, J_{C-P} = 6.5 Hz), 125.6, 117.8 (d, J_{C-P} = 86.5 Hz), 117.0 (d, J_{C-P} = 85.8 Hz), 86.0, 81.7, 28.6 (d, J_{C-P} = 45.9 Hz).

HRMS (ESI$^+$): Calculated for $C_{38}H_{26}OP$ 529.1716 $[M\text{-}PF_6]^+$, found 529.1691.

Synthesis of 1-barrier rotaxane **122a** and free thread **139a**

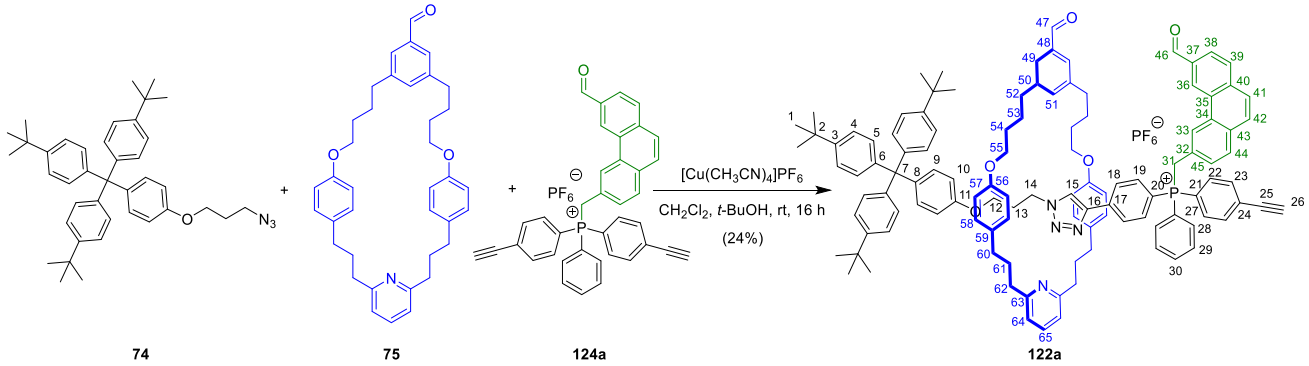

Aldehyde macrocycle **75** (51 mg, 0.091 mmol) and $[Cu(CH_3CN)_4]PF_6$ (5.1 mg, 0.014 mmol) were dissolved in degassed CH_2Cl_2 (10 ml) in a flame dried flask and stirred at room temperature for 30 min. Azide stopper **74** (13 mg, 0.022 mmol) and **124a** (40 mg, 0.059 mmol) in degassed CH_2Cl_2 (5 ml) and *t*-BuOH (1 mL) were added to the reaction mixture and the reaction was stirred at room temperature for 16 h. The reaction mixture was diluted with CH_2Cl_2 (40 ml) and washed with pH 7 aqueous Na_4EDTA solution (1M, 20 mL). The organic layer was separated and dried over $MgSO_4$, filtered, and concentrated *in vacuo*. The resultant residue was purified by iterative size exclusion chromatography (S-X1, CH_2Cl_2) to give **122a** (10 mg, 24%) as a white glassy solid.

^{1}H NMR: (600 MHz, $CDCl_3$) δ 10.14 (s, 1H, H-46), 9.79 (s, 1H, H-47), 8.71 (s, 1H, H-36), 8.37 (s, 1H, H-33), 8.02 (d, *J* = 8.2 Hz, 1H, H-38), 7.88 (d, *J* = 8.2 Hz, 1H, H-39), 7.85 – 7.79 (m, 3H, H-30 and H-49), 7.75 – 7.64 (m, 8H, H-41, H-42, H18, H-19 and H-23), 7.64 – 7.54 (m, 4H, H-22 and H-29,), 7.50 – 7.42 (m, 2H, H-28), 7.41 (s, 2H, H-15, H-44), 7.40 – 7.34 (m, 2H, H-51 and H-65), 7.23 (d, *J* = 8.5 Hz, 6H, H-4), 7.12 (d, *J* = 8.6 Hz, 1H, H-45), 7.08 (d, *J* = 8.2 Hz, 6H, H-5), 6.99 (d, *J* = 8.4 Hz, 2H, H-9), 6.87 (d, *J* = 7.7 Hz, 2H, H-64), 6.69 (d, *J* = 8.0 Hz, 4H, H-58), 6.43 (d, *J* = 8.4 Hz, 2H, H-10), 6.35 (d, *J* = 7.4 Hz, 4H, H-57), 4.96 (d, $J_{H\text{-}P}$ = 14.1 Hz, 2H, H-31), 3.77 (t, *J* = 7.5 Hz, 2H, H-14), 3.74 – 3.66 (m, 4H, H-55), 3.38 (s, 1H, H-26), 3.31 (t, *J* = 5.8 Hz, 2H, H-12), 2.61 (s, 4H, H-52), 2.56 (t, *J* = 8.7 Hz, 4H, H-62), 2.48 (t, *J* = 7.4 Hz, 4H, H-60), 1.79 – 1.73 (m, 4H, H-61), 1.69 (s, 10H, H-13, H-53 and H-54), 1.30 (s, 27H, H-1).

^{1}H NMR: (600 MHz, DMSO-d_6) δ 10.11 (s, 1H), 9.83 (s, 1H), 8.63 (s, 1H), 8.43 (s, 1H), 8.27 (s, 1H), 8.17 (d, *J* = 8.3 Hz, 1H), 8.07 (dd, *J* = 8.0, 1.3 Hz, 1H), 8.03 – 7.90 (m, 4H), 7.81 (ddd, *J* = 15.4, 8.4, 3.1 Hz, 3H), 7.79 – 7.72 (m, 3H), 7.70 (dd, *J* = 12.4, 8.2 Hz, 2H), 7.53 (dd, *J* = 12.3, 8.2 Hz, 2H), 7.46 (s, 2H), 7.42 (t, *J* = 7.7 Hz, 1H), 7.37 (d, *J* = 8.2 Hz, 1H), 7.33 (s, 1H), 7.23 (d, *J* = 8.7 Hz, 6H), 6.97 (d, *J* = 8.6 Hz, 6H), 6.91 (d, *J* = 7.7 Hz, 2H), 6.76 (d, *J* = 8.5 Hz, 2H), 6.61 (d, *J* = 8.0 Hz, 4H), 6.33 (d, *J* = 8.6 Hz, 2H), 6.24 (d, *J* = 7.1 Hz, 4H), 5.43 (d, $J_{H\text{-}P}$ = 15.6 Hz, 2H), 4.69 (s, 1H), 4.14 (t, *J* = 7.0 Hz, 2H), 3.60 – 3.50 (m, 4H), 3.41 (t, *J* = 6.3 Hz, 3H), 2.46 – 2.30 (m, 10H), 1.94 – 1.84 (m, 2H), 1.63 (q, *J* = 7.6, 7.2 Hz, 5H), 1.55 (s, 8H), 1.24 (s, 27H).

^{31}P NMR: (162 MHz, $CDCl_3$) δ 22.46, −143.86 (sept, $J_{P\text{-}F}$ = 714.4 Hz).

^{13}C NMR: (151 MHz, $CDCl_3$) δ 192.91, 192.87, 161.5, 157.0, 156.2, 148.5, 144.6, 144.3, 144.2, 143.8, 139.9, 137.9, 136.6, 135.6, 134.95, 134.85, 134.5 (d, $J_{C\text{-}P}$ = 10.0 Hz), 134.2 (d, $J_{C\text{-}P}$ = 9.7 Hz), 134.1, 133.8, 133.6 (d, $J_{C\text{-}P}$ = 12.8 Hz), 132.5, 132.2, 131.6 (d, $J_{C\text{-}P}$ = 3.7 Hz), 130.83, 130.80, 130.5 (d, $J_{C\text{-}P}$ = 12.7 Hz), 130.3 (d, $J_{C\text{-}P}$ = 3.0 Hz), 129.7 (d, $J_{C\text{-}P}$ = 3.3 Hz), 129.4 (d, $J_{C\text{-}P}$ = 2.2 Hz), 129.3, 129.2, 129.1, 128.9, 127.5, 126.8 (d, $J_{C\text{-}P}$ = 12.6 Hz), 126.3 (d, $J_{C\text{-}P}$ = 7.1 Hz), 125.4 (d, $J_{C\text{-}P}$ = 8.7 Hz), 122.3, 120.1, 117.6 (d, $J_{C\text{-}P}$ = 86.8 Hz),

117.1 (d, $J_{C\text{-}P}$ = 86.5 Hz), 114.5 (d, $J_{C\text{-}P}$ = 87.7 Hz), 114.1, 113.1, 113.0, 83.3, 81.4, 69.4, 67.4, 63.9, 63.2, 47.1, 38.0, 35.2, 35.0, 34.5, 31.5, 31.4, 29.6 (d, $J_{C\text{-}P}$ = 63.7 Hz), 29.0, 28.4.
HRMS (ESI): calculated for $C_{116}H_{118}O_5N_4P$ 1677.8834 $[M\text{-}PF_6]^+$, found 1677.8804.

Free thread **139a** was also isolated as a glassy film (11.4 mg, 40%).

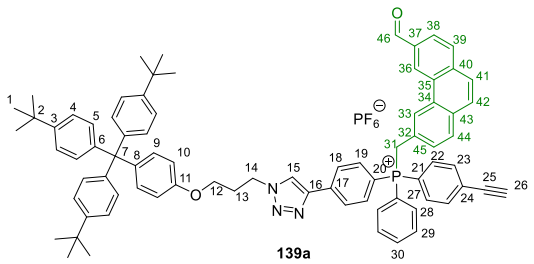

139a

^{1}H NMR: (600 MHz, DMSO-d_6) δ 10.04 (s, 1H, H-46), 8.85 (s, 1H, H-15), 8.53 (s, 1H, H-36), 8.30 (s, 1H, H-33), 8.17 – 8.14 (m, 3H, H-18 and H-38), 8.04 (d, J = 9.0 Hz, 1H, H-39), 8.01 – 7.93 (m, 3H, H-41, H-42 and H-44), 7.91 (t, J = 6.6 Hz, 1H, H-30), 7.85 – 7.73 (m, 10H, H-19, H-22, H23, H-28 and H-29), 7.46 (d, J = 8.4 Hz, 1H, H-45), 7.29 (d, J = 8.6 Hz, 6H, H-4), 7.06 (d, J = 8.5 Hz, 6H, H-5), 7.03 (d, J = 8.9 Hz, 4H, H-9), 6.84 (d, J = 8.9 Hz, 4H, H-10), 5.45 (d, $J_{H\text{-}P}$ = 16.2 Hz, 2H, H-31), 4.66 (s, 1H, H-26), 4.59 (t, J = 6.8 Hz, 2H, H-14), 3.99 (t, J = 6.0 Hz, 2H, H-12), 2.33 (p, J = 6.4 Hz, 2H, H-13), 1.24 (s, 27H, H-1).
^{13}C NMR: (151 MHz, DMSO-d_6) δ 192.4, 156.0, 147.8, 144.4, 144.0, 139.2, 137.2, 135.6, 135.4, 135.1 (d, $J_{C\text{-}P}$ = 10.3 Hz), 134.4 (d, $J_{C\text{-}P}$ = 10.5 Hz), 134.2, 134.1, 133.0 (d, $J_{C\text{-}P}$ = 12.8 Hz), 131.4, 131.3 (d, $J_{C\text{-}P}$ = 3.0 Hz), 130.3 (d, $J_{C\text{-}P}$ = 12.6 Hz), 130.0, 129.8 (d, $J_{C\text{-}P}$ = 5.2 Hz), 129.7, 129.50 (d, $J_{C\text{-}P}$ = 2.7 Hz), 129.46 (d, $J_{C\text{-}P}$ = 3.5 Hz), 128.7, 128.4 (d, $J_{C\text{-}P}$ = 3.3 Hz), 127.2, 127.0 (d, $J_{C\text{-}P}$ = 8.9 Hz), 126.2 (d, $J_{C\text{-}P}$ = 13.0 Hz), 126.0, 125.8 (d, $J_{C\text{-}P}$ = 6.6 Hz), 125.5, 124.4, 123.7, 118.2 (d, $J_{C\text{-}P}$ = 86.4 Hz), 117.5 (d, $J_{C\text{-}P}$ = 85.4 Hz), 115.6 (d, $J_{C\text{-}P}$ = 88.0 Hz), 113.5, 85.9, 81.8, 64.2, 62.6, 47.0, 40.1, 34.1, 31.1, 29.5, 28.8 (d, $J_{C\text{-}P}$ = 46.2 Hz).
HRMS (ESI^+): calculated for $C_{78}H_{75}O_2N_3P$ 1116.5591 $[M\text{-}PF_6]^+$, found 1116.5563.

One-Barrier Operation and Cyclisation of 122b

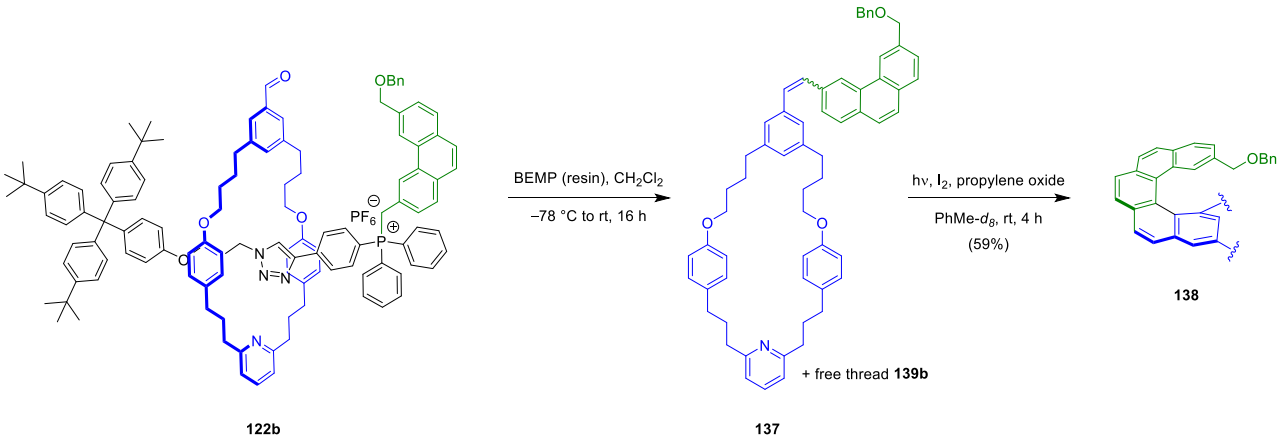

122b 137 138

To a solution of one-barrier rotaxane **122b** (4.5 mg, 2.4 μmol) in dry degassed CH_2Cl_2 (100 mL) at – 78 °C was added BEMP (resin bound, ~2.0 mmol/g, 12 mg, 0.024 mmol). The reaction was gradually warmed to room temperature and stirred for 16 h. The reaction was filtered, and the filtrate was concentrated *in vacuo*. ^{1}H NMR (Figure 7.19) confirmed the formation of **137** with a 89:11 ratio of *E:Z* isomers. The crude residue was dissolved in toluene-d_8 (1.5 mL) and I_2 (1 mg, 3 μmol) and propylene oxide (17 μL, 0.24 mmol) were added and the reaction was irradiated (365 nm, 212 mA, 50 mW) in a quartz cuvette for 4 h. The reaction was concentrated *in vacuo* and purified by size exclusion chromatography (S-X1, CH_2Cl_2) to remove free thread **139b** (1.5 mg, 71%), and then purified by PTLC (SiO_2, 250 μm, CH_2Cl_2/MeOH, 50:1) to give [5]helicene **138** (1.2 mg, 59%) as a colourless solid.

Data consistent with product isolated from conventional stepwise synthesis (see Scheme 7.16, Figure 7.17, Figure 7.18 and Figure 7.20).

The reacted free thread **140** was also isolated as a film (1.5 mg, 71%).

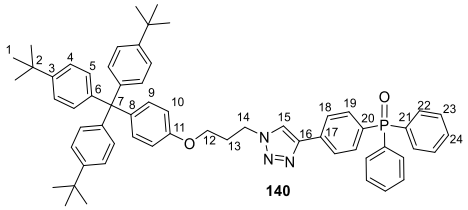

140

^{1}H NMR: (600 MHz, $CDCl_3$) δ 7.92 (dd, *J* = 8.3 and 2.3 Hz, 2H, H-18), 7.85 (s, 1H, H-15), 7.72 (dd, *J* = 11.6 and 8.3 Hz, 2H, H-19), 7.70 – 7.66 (m, 4H, H-22), 7.57 – 7.53 (m, 2H, H-24), 7.49 – 7.44 (m, 4H, H-23), 7.22 (d, *J* =8.6 Hz, 6H, H-4), 7.09 (d, *J* = 8.9 Hz, 2H, H-9), 7.07 (d, *J* = 8.6 Hz, 6H, H-5), 6.75 (d, *J* = 8.9 Hz, 2H, H10), 4.54 (t, *J* = 6.9 Hz, H-14), 3.99 (t, *J* = 5.6 Hz, 2H, H-12), 2.44 (p, *J* = 6.0 Hz, 2H, H-13), 1.29 (s, 27H, H-1).

^{13}C NMR: (151 MHz, $CDCl_3$) δ 156.3, 148.5, 146.8, 144.2, 140.4, 134.2(d, $J_{C\text{-}P}$ = 2.9 Hz), 133.0, 132.8 (d, $J_{C\text{-}P}$ = 10.1 Hz), 132.5, 132.2 (d, $J_{C\text{-}P}$ = 9.9 Hz), 132.1 (d, $J_{C\text{-}P}$ = 2.6 Hz), 130.8, 128.7 (d, $J_{C\text{-}P}$ = 12.2 Hz), 125.7 (d, $J_{C\text{-}P}$ = 12.4 Hz), 124.2, 121.1, 113.1, 64.0, 63.2, 47.6, 34.5, 31.5.

HRMS (ESI$^+$): calculated for $C_{60}H_{64}O_2N_3PNa$ 912.4628 $[M+Na]^+$, found 912.4655.

Synthesis of Two-Barrier Rotaxane 142

Synthesis of **141**

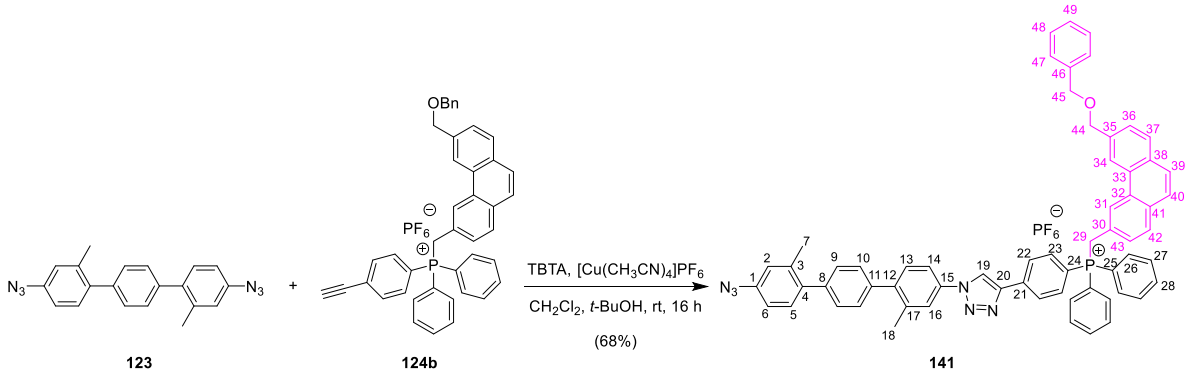

A solution of TBTA (36 mg, 0.067 mmol) and $[Cu(CH_3CN)_4]PF_6$ (23 mg, 0.061 mmol) was stirred in degassed CH_2Cl_2 (5 mL) for 20 minutes. Diazide linker **123**[125] (183 mg, 0.54 mmol) and terminal barrier **124b** (100 mg, 0.13 mmol) were dissolved in degassed CH_2Cl_2 (10 mL) and *t*-BuOH (3 mL) and then added to the reaction mixture. The reaction was stirred at room temperature for 16 h. The reaction was poured into pH 7 aqueous Na_4EDTA (1M, 20 mL) and CH_2Cl_2 (20 mL). The organic layer was separated, and the aqueous layer was extracted with CH_2Cl_2 (2 × 10 mL). The combined organic layers were dried over Na_2SO_4, filtered, and concentrated *in vacuo*. The residue was purified by size exclusion chromatography (S-X1, CH_2Cl_2) to give **141** (99 mg, 68 %) as a white solid.

^{1}H NMR: (600 MHz, CD_2Cl_2) δ 8.54 (s, 1H, H-19), 8.24 (dd, *J* = 8.3, 3.1 Hz, 2H, H-22), 8.15 (s, 1H, H-31), 8.05 (s, 1H, H-34), 7.88 (d, *J* = 8.1 Hz, 1H, H-37), 7.85 – 7.77 (m, 4H, H-2, H-39, H-40, H-42), 7.72 – 7.68 (m, 1H, H-6), 7.67 – 7.60 (m, 8H, H-23, H-26, H-28 and H-36), 7.56 (ddd, *J* = 12.7, 8.3, 1.3 Hz, 4H, H-27), 7.49 (d, *J* = 8.2 Hz, 1H, H-5), 7.44 – 7.36 (m, 8H, H-9, H-10, H-47 and H-48), 7.33 – 7.30 (m, 2H, H-13, H-49), 7.19 (dt, *J* = 8.2, 1.9 Hz, 1H, H-43), 7.00 (d, *J* = 2.4 Hz, 1H, H-16), 6.97 (dd, *J* = 8.0, 2.4 Hz, 1H, H-14), 4.73 (d, $J_{H\text{-}P}$ = 13.8 Hz, 2H, H-29), 4.69 (s, 2H, H-44), 4.60 (s, 2H, H-45), 2.45 (s, 3H, H-7), 2.35 (s, 3H, H-18).

^{31}P NMR: (162 MHz, CD_2Cl_2) δ 21.56, −144.27 (sept, $J_{P\text{-}F}$ = 711.4 Hz).

^{13}C NMR: (151 MHz, CD_2Cl_2) δ 146.1, 143.1, 140.6, 139.5 (d, $J_{C\text{-}P}$ = 12.5 Hz), 139.0, 138.9, 138.4, 138.3 (d, $J_{C\text{-}P}$ = 3.1 Hz), 138.04, 137.98, 136.3 (d, $J_{C\text{-}P}$ = 3.0 Hz), 136.1, 135.3 (d, $J_{C\text{-}P}$ = 10.0 Hz), 134.6 (d, $J_{C\text{-}P}$ = 9.7 Hz), 132.7 (d, $J_{C\text{-}P}$ = 3.4 Hz), 132.2, 131.7 (d, $J_{C\text{-}P}$ = 4.9 Hz), 131.0 (d, $J_{C\text{-}P}$ = 12.6 Hz), 130.7 (d, $J_{C\text{-}P}$ = 3.2 Hz), 130.2 (d, $J_{C\text{-}P}$ = 2.8 Hz), 129.9, 129.7, 129.4, 129.3, 129.1 (d, $J_{C\text{-}P}$ = 4.6 Hz), 129.0, 128.6, 128.4, 128.3, 127.7 (d, $J_{C\text{-}P}$ = 12.9 Hz), 127.6, 126.6, 126.0 (d, $J_{C\text{-}P}$ = 6.4 Hz), 124.6 (d, $J_{C\text{-}P}$ = 8.7 Hz), 122.7, 121.7, 121.2, 120.6, 118.3, 117.4 (d, $J_{C\text{-}P}$ = 86.3 Hz), 117.0, 116.0 (d, $J_{C\text{-}P}$ = 88.1 Hz), 73.0, 72.9, 32.5 (d, $J_{C\text{-}P}$ = 49.0 Hz), 21.1, 21.0.

HRMS (ASAP): Calculated for $C_{63}H_{50}OP$: 937.3778 $[M\text{-}PF_6]^+$, found 937.3747.

Synthesis of 2-barrier rotaxane **142**

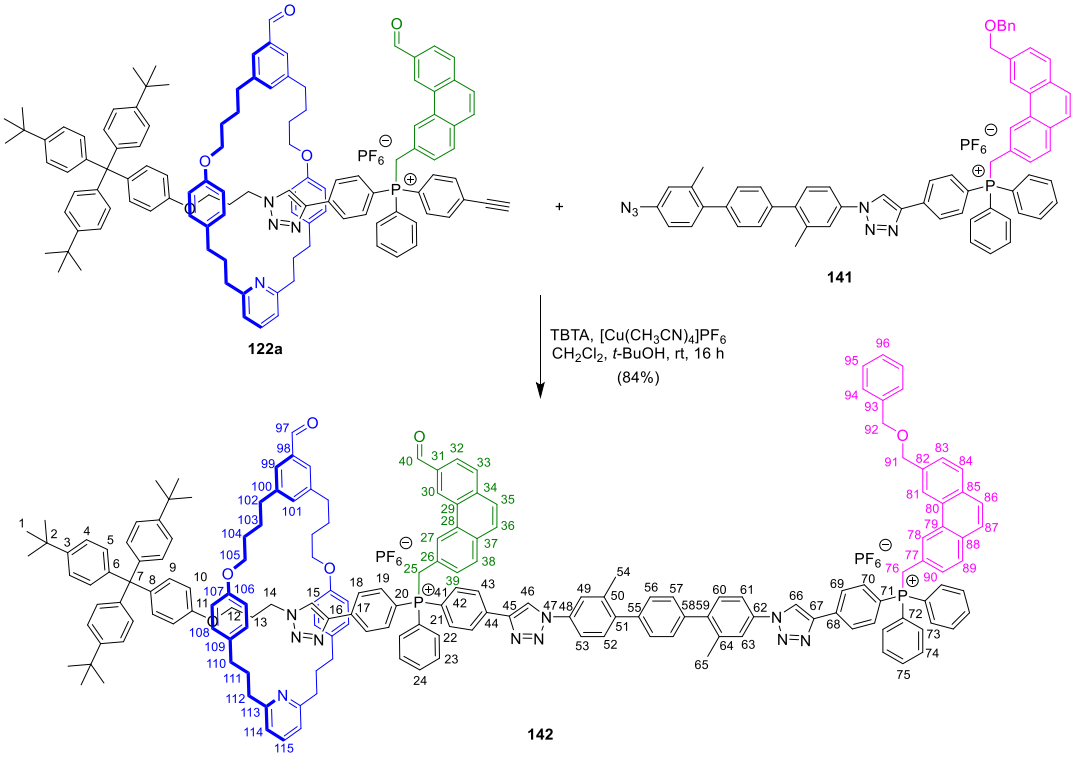

A solution of TBTA (0.7 mg, 1.4 μmol) and $[Cu(CH_3CN)_4]PF_6$ (0.5 mg, 1.2 μmol) was stirred in degassed CH_2Cl_2 (1 mL) for 20 minutes. Rotaxane **122a** (5 mg, 2.7 μmol) and tail piece **141** (3.6 mg, 3.3 μmol) were dissolved in degassed CH_2Cl_2 (2 mL) and *t*-BuOH (0.5 mL) and then added to the reaction mixture. The reaction was stirred at room temperature for 16 h. The reaction was poured into pH 7 aqueous Na_4EDTA (1M, 10 mL) and CH_2Cl_2 (10 mL). The organic layer was separated, and the aqueous layer was extracted with CH_2Cl_2 (2 × 5 mL). The combined organic layers were dried over Na_2SO_4, filtered, and concentrated *in vacuo*. The residue was purified by size exclusion chromatography (S-X1, CH_2Cl_2) to give two-barrier rotaxane **142** (6.7 mg, 84%) as a white solid.

^{1}H NMR: (600 MHz, $CDCl_3$) δ 9.96 (s, 1H, H-40 or H-97), 9.77 (s, 1H, H-40 or H-97), 8.76 (s, 1H, H46 or H-66), 8.72 (s, 1H, H46 or H-66), 8.52 (s, 1H, H-30), 8.40 – 8.34 (m, 2H, H-43 or H-69), 8.33 – 8.29 (m, 2H, H-43 or H-69), 8.16 (s, 1H, H-27), 7.89 (s, 2H. H-78 and H-81), 7.84 – 7.68 (m, 10H, H-24, H-42, H-70, H-75, H-83 and H-99), 7.66 – 7.53 (m, 8H, H-18 and H-19, H-32, H-33, H-35 and H-36), 7.53 – 7.33 (m, 29H, H-15, H-22, H-23, H-38, H-56, H-57, H-73, H-74, H-84, H-86, H-87, H-89, H-94, H-95, H-96, H-101 and H-115), 7.33 – 7.27 (m, 2H, H-53 and H-61), 7.22 (d, *J* = 8.3 Hz, 8H, H-4, H-39 and H-49 or H-63), 7.08 (d, *J* = 8.1 Hz, 8H, H-5, H-90 and H-49 or H-63), 6.97 (d, *J* = 8.3 Hz, 2H, H-9), 6.94 (d, *J* = 8.0 Hz, 2H, H-114), 6.83 (d, *J* = 7.6 Hz, 1H, H-52 or H-60), 6.80 (d, *J* = 7.7 Hz, 1H, H-52 or H-60), 6.67 (dd, *J* = 13.1, 8.1 Hz, 4H, H-108), 6.42 (d, *J* = 8.4 Hz, 2H, H-10), 6.34 (d, *J* = 8.0 Hz, 4H, H-107), 4.82 (d, $J_{H\text{-}P}$ = 14.8 Hz, 2H, H-25), 4.64 (d, $J_{H\text{-}P}$ = 12.1 Hz, 2H, H-76), 4.62 (s, 2H, H-91), 4.56 (s, 2H, H-92), 3.72 (t, *J* = 6.4 Hz, 2H, H-14), 3.70 – 3.62 (m, 4H, H-105), 3.30 (t, *J* = 6.0 Hz, 2H, H-12), 2.62 – 2.56 (m, 4H, H-102), 2.56 – 2.50 (m, 4H, H-112), 2.49 – 2.42 (m, 4H, H-110), 2.42 (m, 3H, H-54 or H-65), 2.41 (s, 3H, H-54 or H-65), 1.76 – 1.62 (m, 14H, H-13, H-103, H-104 and H-111), 1.30 (s, 27H, H-1).

^{31}P NMR: (202 MHz, $CDCl_3$) δ 22.12, 22.10, −143.80 (sept, $J_{P\text{-}F}$ = 711.0 Hz).

^{13}C NMR: (151 MHz, $CDCl_3$) δ 193.0, 192.8, 161.51, 161.45, 157.01, 157.00, 156.2, 148.5, 146.1, 144.7, 144.2 (d, J_{C-P} = 7.5 Hz), 143.78, 143.77, 142.4, 142.3, 139.9, 139.6 (d, J_{C-P} = 2.3 Hz), 138.6, 137.8, 137.5 (d, J_{C-P} = 2.2 Hz), 137.2, 136.9, 136.6, 135.9 (d, J_{C-P} = 5.6 Hz), 135.5, 135.4, 134.8, 134.72, 134.70, 134.64, 134.61, 134.57, 134.50, 134.41, 134.3 (d, J_{C-P} = 9.5 Hz), 133.8 (d, J_{C-P} = 8.3 Hz), 132.5 (d, J_{C-P} = 3.6 Hz), 132.2 (d, J_{C-P} = 2.2 Hz), 131.5 (d, J_{C-P} = 11.3 Hz), 131.3 (d, J_{C-P} = 2.6 Hz), 130.82, 130.79, 130.3 (d, J_{C-P} = 12.8 Hz), 129.9, 129.2, 128.9, 128.6, 128.1, 127.80, 127.53, 127.48, 127.2, 127.0, 126.8, 126.7, 126.0, 124.2, 124.1, 122.6 (d, J_{C-P} = 19.1 Hz), 122.0, 120.5, 120.0 (d, J_{C-P} = 6.0 Hz), 118.2 (d, J_{C-P} = 18.4 Hz), 116.91 (d, J_{C-P} = 85.6 Hz), 116.85, 114.1, 113.0, 80.2, 72.7, 72.6, 67.4, 63.9, 63.2, 47.1, 37.9, 35.2, 35.0, 34.5, 32.6, 31.54, 31.52, 29.6 (d, J_{C-P} = 67.2 Hz), 28.7 (d, J_{C-P} = 82.3 Hz), 28.4, 20.91, 20.89.
HRMS (ESI^+): Calculated for $C_{179}H_{168}O_6P_2$: 1308.1325 $[M\text{-}2PF_6]^{2+}$, found 1308.1302.

Two-Barrier Operation of 142

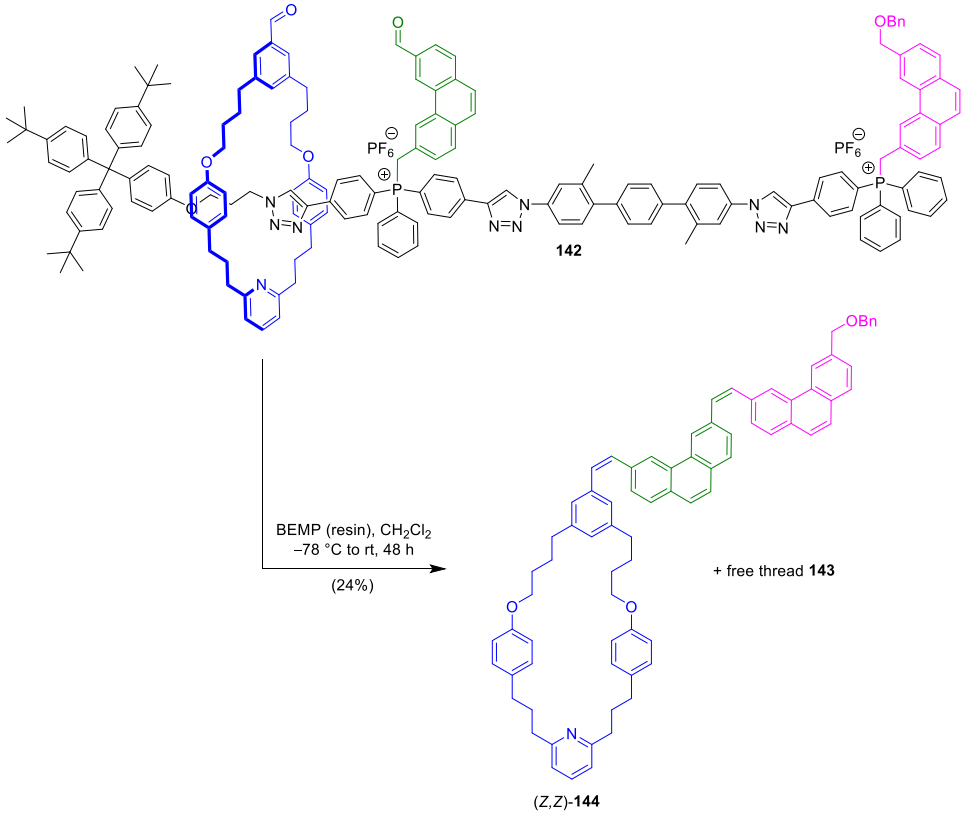

To a solution of two-barrier rotaxane **142** (4.5 mg, 1.5 μmol) in dry degassed CH_2Cl_2 (200 mL) at –78 °C was added BEMP (resin bound, ~2.0 mmol/g, 30 mg, 0.060 mmol). The reaction was gradually warmed to room temperature and stirred for 48 h. The reaction was filtered, and the filtrate was concentrated *in vacuo*. The residue was purified by size exclusion chromatography (S-X1, CH_2Cl_2) to yield free thread **143** (1.6 mg). Further elution gave the desired compound **144** (0.38 mg, 24%) as a white solid as an inseparable 80:20 ratio of (*Z,Z)* to another *E*/*Z* configurational isomer.

Data consistent with product isolated from conventional stepwise synthesis (see Scheme 7.22, Figure 7.21 and Figure 7.23). Due the complexity of the aromatic region of the spectrum the minor product's *E*/*Z* configuration was unable to be assigned.

Also recovered free thread **143** as a yellow film (1.6 mg, 66%).

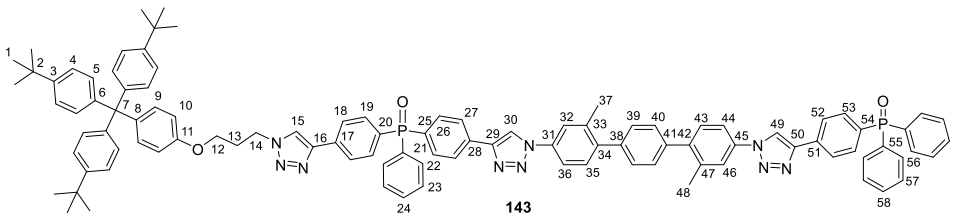

^{1}H NMR: (600 MHz, $CDCl_3$) δ 8.31 (s, 1H, H-30/49), 8.29 (s, H-30/49), 8.06 – 8.02 (m, 4H, H-18 and H-27), 7.97 – 7.93 (m, 2H, H-52), 7.87 (s, 1H, H-15), 7.82 – 7.67 (m, 18H, H-19, H-22, H-25, H-32, H-36, H-44, H-46, H-53 and H-56), 7.60 – 7.56 (m, 3H, H-24 and H-58), 7.52 – 7.47 (m, 8H, H-23, H-35, H-43 and H-57), 7.44 (s, 4H, H-39 and H-40), 7.22 (d, *J* = 8.5 Hz, 6H, H-4), 7.10 (d, *J* = 8.8 Hz, 2H, H-9), 7.07 (d, *J* = 8.5 Hz,

6H, H-5), 6.76 (d, *J* = 8.8 Hz, 2H, H-10), 4.67 (t, *J* = 6.8 Hz, 2H, H-14), 4.02 (t, *J* = 5.8 Hz, 2H, H-12), 2.50 – 2.44 (m, 8H, H-13, H-37 and H-48), 1.31 (s, 27H, H-1).

^{13}C NMR: (151 MHz, $CDCl_3$) δ 156.2, 148.4, 147.3, 147.29, 147.27, 147.25, 146.9, 146.6, 145.7, 144.0, 142.3, 141.4, 140.2, 135.9, 132.9, 132.8, 132.7, 132.4, 132.2, 132.1, 131.2, 130.7, 129.1, 128.7, 128.63, 128.60, 128.55, 125.83, 125.81, 125.79, 125.75, 125.72, 125.71, 125.68, 125.64, 124.1, 122.4, 121.0, 118.43, 118.41, 118.40, 117.9, 113.0, 63.8, 63.1, 47.4, 34.3, 31.4, 30.1, 29.7, 20.8.

Synthesis of Standards of Operation

Synthesis of **361**

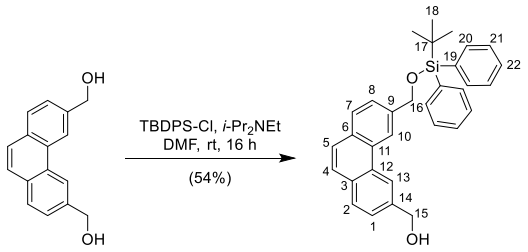

134 **361**

To a solution of **134** (200 mg, 0.85 mmol) in DMF (5 mL) was added *i*-Pr_2NEt (1.48 ml, 8.50 mmol) and TBDPS-Cl (240 µL, 0.92 mmol) sequentially and the reaction mixture was stirred at room temperature for 16 h. The reaction was poured into saturated aqueous NH_4Cl (10 mL) and diluted with CH_2Cl_2 (20 mL). The organic layer was separated, and the aqueous layer was extracted with CH_2Cl_2 (2 × 10 mL). The combined organic layers were washed with brine (3 × 20 mL), dried over $MgSO_4$, filtered, and concentrated *in vacuo*. The resultant residue was purified by flash chromatography (SiO_2, pet ether/EtOAc, 5:1) to give **361** (216 mg, 54%) as a white solid.

^{1}H NMR: (600 MHz, $CDCl_3$) δ 8.67 (s, 1H, H-10), 8.60 (s, 1H, H-13), 7.89 (d, *J* = 8.1 Hz, 1H, H-2 or H-7), 7.87 (d, *J* = 8.1 Hz, 1H, H-2 or H-7), 7.80 – 7.75 (m, 4H, H-20), 7.76 – 7.69 (m, 2H, H-4 and H-5), 7.61 – 7.59 (m, 2H. H-1 and H-8), 7.47 – 7.43 (m, 2H, H-22), 7.42 – 7.37 (m, 4H, H-21), 5.05 (s, 2H, H-16), 4.95 (s, 2H, H-15), 1.83 (d, *J* = 5.9 Hz, 1H, C-15 OH), 1.17 (s, 9H, H-18).

^{13}C NMR: (151 MHz, $CDCl_3$) δ 139.5, 139.0, 135.8, 133.7, 131.8, 131.4, 130.4, 130.2, 129.9, 129.1, 127.9, 126.9, 126.4, 125.7, 125.2, 121.0, 119.9, 66.1, 66.0, 27.1, 19.6.

HRMS (ESI^+): Calculated for $C_{32}H_{32}O_2SiNa$: 499.2064 $[M+Na]^+$, found 499.2050.

Synthesis of **147**

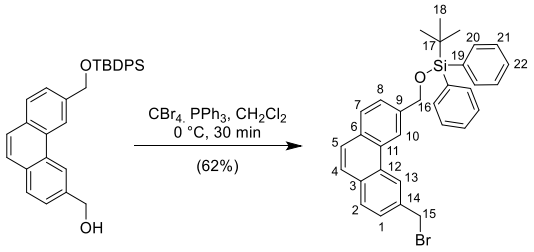

361 **147**

To a solution of **361** (194 mg, 0.407 mmol) in CH_2Cl_2 (20 mL) at 0 °C was added CBr_4 (213 mg, 0.814 mmol) and PPh_3 (213 mg, 0.814 mmol) and the reaction was stirred at 0 °C for 30 minutes. The resultant mixture was evaporated from SiO_2 and purified by flash chromatography (SiO_2, pet ether/EtOAc, 20:1) to give **147** (135 mg, 62%) as a white solid.

^{1}H NMR: (600 MHz, $CDCl_3$) δ 8.61 (s, 1H, H-10), 8.59 (s, 1H, H-13), 7.87 (t, *J* = 7.8 Hz, 2H, H-2 and H-7), 7.79 – 7.73 (m, 5H, H-20 and H-4), 7.70 (d, *J* = 8.8 Hz, 1H, H-5), 7.64 – 7.58 (m, 2H, H-1 and H-8), 7.46 (t, *J* = 7.3 Hz, 2H, H-22), 7.41 (t, *J* = 7.2 Hz, 4H, H-21), 5.06 (s, 2H, H-16), 4.76 (s, 2H, H-15), 1.18 (s, 9H, H-18).

^{13}C NMR: (151 MHz, $CDCl_3$) δ 139.7, 135.8, 133.7, 132.1, 131.4, 130.4, 130.0, 129.9, 129.4, 128.7, 127.9, 127.6, 127.4, 126.2, 125.5, 123.4, 120.0, 66.1, 34.5, 29.9, 27.1, 19.6.

HRMS (ESI^+): Calculated for $C_{32}H_{31}{}^{81}BrOSi$: 540.1307 $[M]^+$, found 540.1298.

Synthesis of **148**

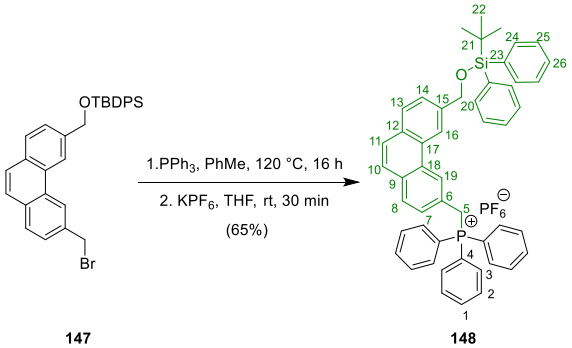

147 **148**

147 (245 mg, 0.454 mmol) and PPh_3 (226 mg, 0.681 mmol) were dissolved in degassed toluene (5 mL) and heated at 120 °C in a sealed tube for 16 h. The solvent was removed *in vacuo* and the residue was taken up in THF (10 mL). KPF_6 (200 mg, 1.08 mmol) was added and the solution stirred at room temperature for 30 minutes. The solvent was removed *in vacuo* and the residue was taken up in CH_2Cl_2 and filtered under reduced pressure. The filtrate was concentrated *in vacuo* and purified by size exclusion chromatography (S-X1, CH_2Cl_2) to give **148** (257 mg, 65%) as a yellow glassy solid.

^{1}H NMR: (600 MHz, CD_2Cl_2) δ 8.02 (s, 1H, H-19), 7.95 – 7.92 (m, 2H, H-13 and H-16), 7.85 – 7.74 (m, 10H, H-1, H-8, H-10/11, H-14 and H-24), 7.72 (d, J = 8.8 Hz, 1H, H-10/11), 7.65 – 7.60 (m, 6H, H-2), 7.54 – 7.45 (m, 12H, H-3, H-25 and H-26), 7.18 (d, J = 8.1 Hz, 1H, H-7), 5.02 (s, 2H, H-20), 4.68 (d, $J_{H\text{-}P}$ = 13.9 Hz, H-5), 1.19 (s, 9H, H-22).

^{31}P NMR: (168 MHz, CD_2Cl_2) δ 21.64 (s), −144.31 (sept, $J_{P\text{-}F}$ = 739.2 Hz).

^{13}C NMR: (151 MHz, $CDCl_3$) δ 140.4, 136.1, 136.0 (d, $J_{C\text{-}P}$ = 2.7 Hz), 134.5 (d, $J_{C\text{-}P}$ = 9.7 Hz), 134.1, 132.5 (d, $J_{C\text{-}P}$ = 2.9 Hz), 131.9, 130.9 (d, $J_{C\text{-}P}$ = 12.6 Hz), 130.6 (d, $J_{C\text{-}P}$ = 2.9 Hz), 130.4, 130.1 (d, $J_{C\text{-}P}$ = 2.3 Hz), 129.7, 129.3, 129.1 (d, $J_{C\text{-}P}$ = 4.7 Hz), 128.5, 128.4, 126.4, 125.8 (d, $J_{C\text{-}P}$ = 6.3 Hz), 124.6 (d, $J_{C\text{-}P}$ = 8.7 Hz), 120.0, 117.4 (d, $J_{C\text{-}P}$ = 86.0 Hz), 66.6, 32.2 (d, $J_{C\text{-}P}$ = 49.0 Hz), 27.3, 19.8.

HRMS (ASAP): Calculated for $C_{50}H_{46}OPSi$: 721.3050 $[M\text{-}PF_6]^+$, found 721.3021.

Synthesis of **149**

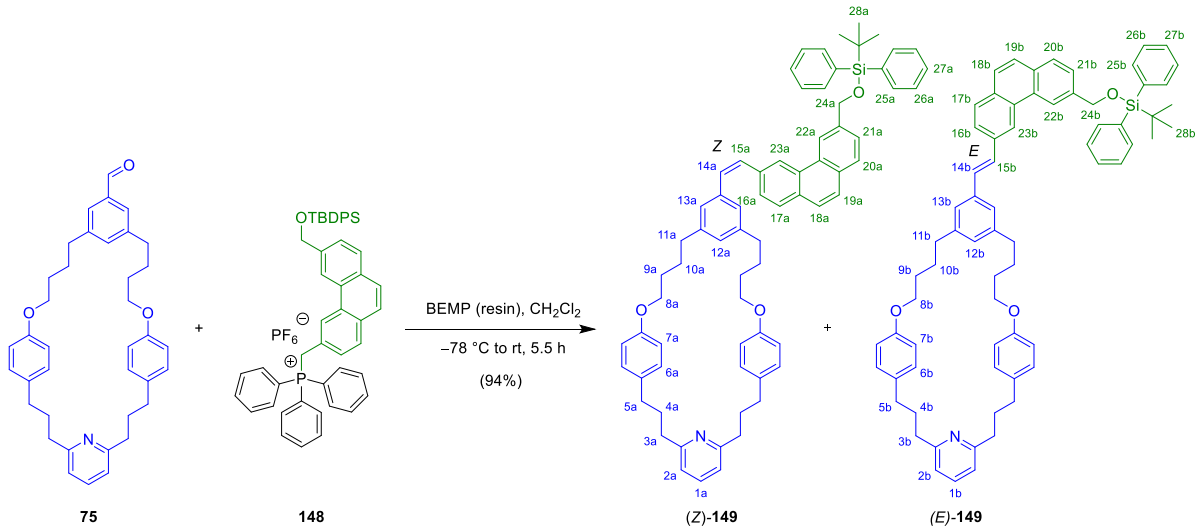

To a solution of **148** (428 mg, 0.534 mmol) and aldehyde macrocycle **74** (200 mg, 0.356 mmol) in CH_2Cl_2 (10 mL) at –78 °C was added BEMP (resin bound, ~2.0 mmol/g, 356 mg, 0.712 mmol) under argon and the reaction stirred for 40 minutes. The reaction mixture was gradually warmed to room temperature and stirred for 5.5 h. The reaction was filtered, and the filtrate was concentrated *in vacuo*. The residue was purified by flash chromatography (SiO_2, petroleum ether/ EtOAc, 85:15) to give **149** (335 mg, 94%, mixture of constitutional isomers: *E*:*Z* ~ 1:1, ratio determined by integration of NMR signals for benzylic positions H-24b and H-24a at δ = 5.11 and δ = 5.01 ppm respectively) as a colourless solid.

^{1}H NMR (600 MHz, CD_2Cl_2): δ 8.78 (s, 1H, H-22b), 8.75 (s, 1H, H-23b), 8.53 (s, 1H, H-23a), 8.40 (s, 1H, H-22a), 7.91 – 7.88 (m, 2H, H-17b and H-20b), 7.86 (d, *J* = 8.2 Hz, 1H, H-20a), 7.84 (d, *J* = 8.3, 1H, H-16b), 7.81 – 7.79 (m, 4H, H-25b), 7.77 – 7.73 (m, 6H, H-18b, H-19b and 25a), 7.70 (d, *J* = 8.8 Hz, 1H, H-19a), 7.68 (d, *J* = 8.3 Hz, 1H, H-17a), 7.64 (d, *J* = 8.8 Hz, 1H, H-18a), 7.63 – 7.59 (m, 2H, H-21a/b), 7.52 – 7.47 (m, 3H, H-1a/b and H-16a), 7.47 – 7.37 (m, 13H, H-14b, H-26b and H-27a/b), 7.33 (d, *J* = 16.3 Hz, 1H, H-15b), 7.29 (s, 2H, H-13b), 7.07 – 7.04 (m, 9H, H-6a/b and H-12b), 6.99 – 6.95 (m, 6H, H-2a/b and H13a), 6.88 (s, 1H, H-12a), 6.83 (d, *J* = 12.2 Hz, 1H, H-15a), 6.77 – 6.74 (m, 5H, H-7b and H-14a), 6.73 (d, *J* = 8.5 Hz, 4H, H-7a), 5.11 (s, 2H, H-24b), 5.01 (s, 2H, H-24a), 3.95 (t, *J* = 5.9 Hz, 4H, H-8b), 3.82 (t, *J* = 5.7 Hz, 4H, H-8a), 2.78 – 2.70 (m, 12H, H-3a/b and H-11b), 2.58 – 2.53 (m, 8H, H-5a/b), 2.49 (t, *J* = 7.0 Hz, 4H, H-11a), 2.04 – 1.97 (m, 8H, H-4a/b), 1.89 – 1.83 (m, 4H, H-10b), 1.83 – 1.78 (m, 4H, H-9b), 1.68 – 1.58 (m, 8H, H-9a and H-10a), 1.21 (s, 9H, H-28b), 1.15 (s, 9H, H-28a).

^{13}C NMR (151 MHz, CD_2Cl_2): δ 161.69, 161.68, 157.69, 157.66, 143.27, 142.82, 139.89, 139.79, 137.69, 137.62, 136.66, 136.07, 136.04, 136.02, 135.99, 134.91, 134.87, 133.97, 133.94, 132.08, 131.80, 131.63, 131.56, 131.54, 130.85, 130.49, 130.44, 130.38, 130.36, 130.20, 130.18, 129.78, 129.63, 129.27, 128.93, 128.88, 128.76, 128.54, 128.36, 128.19, 128.17, 128.00, 127.80, 127.02, 126.99, 126.97, 126.61, 126.59, 125.50, 124.94, 124.87, 123.74, 121.40, 120.36, 120.16, 120.11, 114.58, 114.57, 68.02, 67.92, 66.40, 66.33, 37.94, 35.60, 35.34, 34.82, 32.40, 28.94, 28.70, 28.46, 28.31, 27.17, 27.07.

HRMS (ESI$^+$): Calculated for $C_{70}H_{74}NO_3Si$: 1004.5432 $[M+H]^+$, found 1004.5408.

Synthesis of **362**

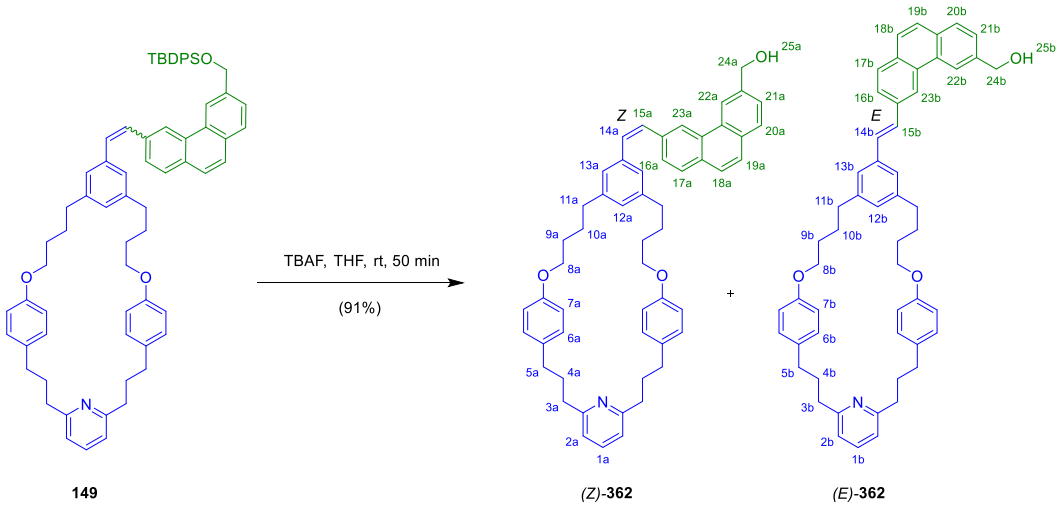

To a solution of **149** (156 mg, 0.155 mmol) in THF (10 mL) was added TBAF (1M in THF, 0.47 mL, 0.47 mmol) dropwise at room temperature under argon and the reaction was stirred for 50 minutes. The reaction was quenched by the addition of saturated aqueous NH_4Cl (10 mL) and diluted with CH_2Cl_2 (20 mL). The organic layer was separated, and the aqueous layer was extracted with CH_2Cl_2 (2 × 15 mL). The combined organic layers were washed with brine and dried over Na_2SO_4, filtered, and concentrated *in vacuo*. The residue was purified by flash chromatography (SiO_2, petroleum ether/ EtOAc, 7:3) to give **362** (108 mg, 91%, mixture of constitutional isomers: *E*:*Z* ~ 1:1.25, ratio determined by integration of NMR signals for benzylic positions H-24b and H-24a at δ = 4.98 and δ = 4.73 ppm respectively) as a white solid.

^{1}H NMR (600 MHz, $CDCl_3$): δ 8.74 (s, 1H, H-23b), 8.73 (s, 1H, H-22b), 8.62 (s, 1H, H-23a), 8.24 (s, 1H, H-22a), 7.90 – 7.83 (m, 3H, H-16b, H-17b and H-20b), 7.78 (d, *J* = 8.1 Hz, 1H, H-20a), 7.74 (d, J = 8.2 Hz, 1H, H-17a), 7.72 – 7.70 (m, 2H, H-18b and H-19b), 7.67 – 7.64 (m, 2H, H-18a and H-19a), 7.59 (d, *J* = 8.1, 1H, H-21b), 7.53 – 7.47 (m, 3H, H-1a/b and H-16a), 7.42 – 7.37 (m, 2H, H-15b and H-21a), 7.30 (d, *J* = 16.4 Hz, 1H, H-14b), 7.28 (s, 2H, H-13b), 7.05 (d, *J* = 8.2 Hz, 8H, H-6a/b), 7.02 (s, 1H, H-12b), 7.00 (s, 2H, H-13a), 6.97 (t, *J* = 8.1 Hz, 4H, H-2a/b), 6.94 (s, 1H, H-12a), 6.80 (d, *J* = 12.1 Hz, 1H, H-15a), 6.77 (d, *J* = 8.3 Hz, 4H, H-7b), 6.76 – 6.71 (m, 5H, H-7a and H-14a), 4.98 (s, 2H, H-24b), 4.73 (s, 2H, H-24a), 3.95 (t, *J* = 5.7 Hz, 4H, H-8b), 3.72 (t, *J* = 5.7 Hz, 4H, H-8a), 2.82 (q, J = 8.0 Hz, 8H, H-3a/b), 2.71 (t, *J* = 7.3 Hz, 4H, H-11b), 2.60 – 2.55 (m, 8H, H-5a/b), 2.52 (t, *J* = 7.1 Hz, 4H, H-11a), 2.29 (s, 1H, H-25a), 2.24 (s, 1H, H-25b), 2.08 – 1.98 (m, 8H, H-4/b), 1.90 – 1.80 (m, 8H, H-9b and H-10b), 1.66 – 1.56 (m, 8H, H-9a and H-10a).

^{13}C NMR (151 MHz, $CDCl_3$): δ 161.51, 157.30, 157.12, 142.86, 142.58, 139.39, 139.32, 137.48, 137.37, 136.65, 136.63, 135.88, 135.56, 134.64, 134.59, 131.87, 131.78, 131.55, 131.24, 130.57, 130.38, 130.22, 130.01, 129.60, 129.40, 129.06, 128.77, 128.71, 128.35, 128.13, 128.01, 127.62, 126.77, 126.72, 126.66, 126.57, 125.79, 124.64, 124.37, 123.12, 121.63, 120.76, 120.71, 120.28, 120.24, 114.45, 114.42, 67.75, 67.65, 65.79, 65.48, 38.03, 37.96, 35.41, 35.24, 34.78, 34.72, 32.54, 32.51, 28.75, 28.50, 28.23, 28.19.

HRMS (ESI^+): Calculated for $C_{54}H_{56}NO_3$: 766.4255 $[M+H]^+$, found 766.4234.

Synthesis of **145**

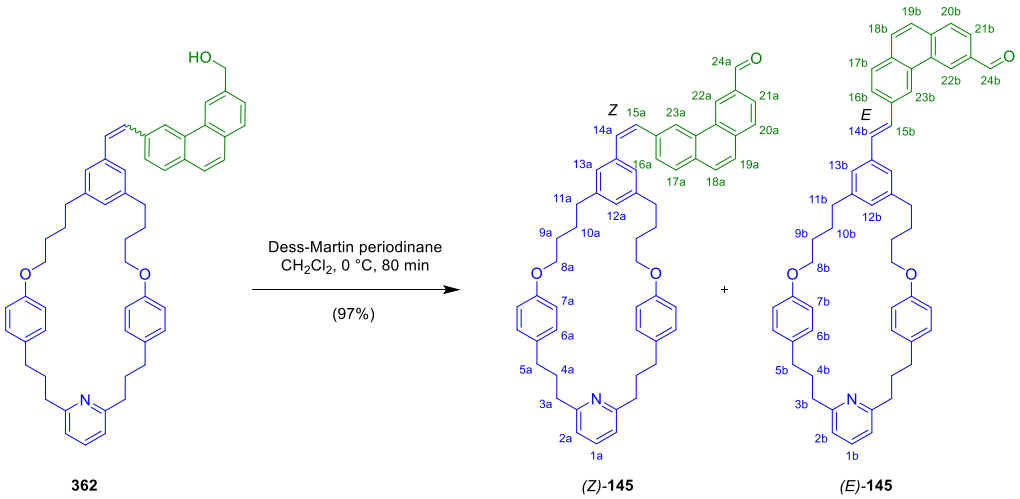

To a solution of **S13** (88.7 mg, 0.116 mmol) in CH_2Cl_2 (10 mL) at 0 °C was added Dess-Martin periodinane (98.2 mg, 0.232 mmol) under argon and the reaction was continued stirring for 80 minutes. The reaction was quenched by the addition of saturated aqueous $NaHCO_3$ (10 mL). The biphasic mixture was extracted with CH_2Cl_2 (3 × 25 mL). The combined organic layers were washed with brine and dried over Na_2SO_4, filtered, and concentrated *in vacuo*. The residue was purified by flash chromatography (SiO_2, petroleum ether/ EtOAc, 7:3) to give **145** (85.9 mg, 97%, mixture of constitutional isomers: *E*:*Z* ~ 1:1, ratio determined by integration of NMR signals for methylene positions H-8b and H-8a at δ = 3.94 and δ = 3.79 ppm respectively) as a yellow solid.

^{1}H NMR (600 MHz, CD_2Cl_2): δ 10.30 (s, 1H, H-24b), 10.12 (s, 1H, H-24a), 9.26 (s, 1H, H-22b), 8.86 (s, 1H, H-23b), 8.85 (s, 1H, H-22a), 8.68 (s, 1H, H-23a), 8.09 (dd, *J* = 8.2, 1.5 Hz, 1H, H-21b), 8.04 (d, *J* = 8.2 Hz, 1H, H-20b), 7.99 – 7.95 (m, 3H, H-17b, H20a and H-21a), 7.95 – 7.90 (m, 2H, H-16b and H18b), 7.82 (d, *J* = 8.8 Hz, 1H, H-18a), 7.80 (d, *J* = 8.8 Hz, 1H, H-19b), 7.76 (d, *J* = 8.3 Hz, 1H, H-17a), 7.74 (d, *J* = 8.7 Hz, 1H, H-19a), 7.56 (dd, *J* = 8.2, 1.6 Hz, 1H, H-16a), 7.52 – 7.48 (m, 2H, H-1a/b), 7.45 (d, *J* = 16.3 Hz, 1H, H-15b), 7.39 (d, *J* = 16.3 Hz, 1H, H-14b), 7.31 (s, 2H, H-13b), 7.07 – 7.02 (m, 9H, H-6a/b and H-12b), 7.01 – 6.94 (m, 7H, H-2a/b, H-12a and H-13a), 6.86 (d, *J* = 12.2 Hz, 1H, H-15a), 6.82 (d, *J* = 12.2 Hz, 1H, H-14a), 6.78 – 6.73 (m, 4H, H-7b), 6.69 (d, *J* = 8.6 Hz, 4H, H-7a), 3.94 (t, *J* = 5.9 Hz, 2H, H-, H-8b), 3.79 (t, *J* = 5.8 Hz, 2H, H-8a), 2.77 – 2.71 (m, 12H, H-3a/b and H-11b), 2.57 – 2.51 (m, 8H, H-5a and H11a), 1.99 (s, 8H, H-4a/b), 1.89 – 1.83 (m, 4H, H-10b), 1.82 – 1.77 (m, 4H, H-9b), 1.68 – 1.58 (m, 8H, H-9a and H-10a).

^{13}C NMR (151 MHz, CD_2Cl_2): δ 192.62, 192.40, 161.69, 157.69, 157.67, 157.61, 143.35, 143.05, 137.66, 137.43, 137.19, 137.04, 136.69, 136.43, 134.88, 134.78, 134.76, 132.33, 132.06, 131.57, 131.19, 130.69, 130.66, 130.38, 130.36, 130.30, 130.28, 129.99, 129.97, 129.83, 129.64, 129.60, 128.90, 128.77, 128.35, 128.17, 127.68, 127.53, 126.89, 126.66, 126.62, 125.44, 125.05, 124.98, 124.96, 123.46, 121.61, 120.37, 114.59, 114.56, 68.04, 67.89, 37.92, 35.60, 35.39, 34.82, 34.80, 32.43, 32.41, 28.95, 28.73, 28.46, 28.39.

HRMS (ESI$^+$): Calculated for $C_{54}H_{54}NO_3$: 764.4098 $[M+H]^+$, found 764.4078.

Synthesis of **136**

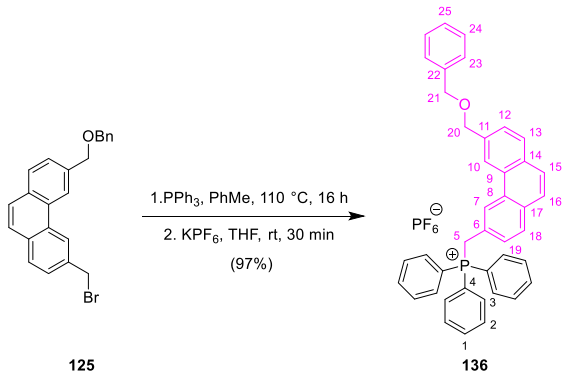

125b (130 mg, 0.33 mmol) and triphenylphosphine (131 mg, 0.50 mmol) were dissolved in degassed toluene (8 mL) and heated at 110 °C in a sealed tube for 16 h. The solvent was removed *in vacuo* and the residue was taken up in THF (10 mL). KPF_6 (100 mg, 0.54 mmol) was added and the solution stirred at room temperature for 30 minutes. The solvent was removed *in vacuo* and the residue was taken up in CH_2Cl_2 and filtered under reduced pressure. The filtrate was concentrated *in vacuo* and purified by size exclusion chromatography (S-X1, CH_2Cl_2) to give **136** (233 mg, 97%) as a yellow glassy solid.

^{1}H NMR: (600 MHz, $CDCl_3$) δ 8.05 (s, 1H, H-7), 8.02 (s, 1H, H-10), 7.77 (d, *J* = 8.4 Hz, 1H, H-13), 7.70 – 7.66 (m, *3*H, H-1), 7.62 (d, *J* = 8.8 Hz, 1H, H-15), 7.59 (d, *J* = 8.0 Hz, 1H, H-12), 7.57 – 7.47 (m, 14H, H-2, H-3, H-16 and H-18), 7.44 – 7.41 (m, 2H, H-23), 7.39 (t, *J* = 7.4 Hz, 2H, H-24), 7.32 (t, *J* = 7.2 Hz, 1H, H-25), 7.04 (d, *J* = 8.2 Hz, 1H, H-19), 4.74 (s, 2H, H-20), 4.72 (d, $J_{H\text{-}P}$ = 13.8 Hz, 2H, H-5), 4.62 (s, 2H, H-21).

^{31}P NMR: (202 MHz, $CDCl_3$) δ 22.36, −144.03 (sept, $J_{P\text{-}F}$ = 713.0 Hz).

^{13}C NMR: (151 MHz, $CDCl_3$) δ 138.6, 137.3, 135.4 (d, $J_{C\text{-}P}$ = 2.8 Hz), 134.2 (d, $J_{C\text{-}P}$ = 9.6 Hz), 131.8 (d, $J_{C\text{-}P}$ = 2.8 Hz), 134.2 (d, $J_{C\text{-}P}$ = 9.6 Hz), 131.7 (d, $J_{C\text{-}P}$ = 3.1 Hz), 131.6, 130.4 (d, $J_{C\text{-}P}$ = 12.5 Hz), 130.1 (d, $J_{C\text{-}P}$ = 3.3 Hz), 129.5, 129.3, 129.3, 128.7 (d, $J_{C\text{-}P}$ = 3.3 Hz), 128.6, 128.2, 128.1, 127.9, 127.8, 127.1, 126.1, 126.1, 125.9 (d, $J_{C\text{-}P}$ = 6.3 Hz), 124.3 (d, $J_{C\text{-}P}$ = 8.9 Hz), 122.2, 117.2 (d, $J_{C\text{-}P}$ = 85.8 Hz), 72.7, 72.6, 31.1 (d, $J_{C\text{-}P}$ = 48.5 Hz).

HRMS (ESI$^+$): Calculated for $C_{41}H_{34}OP$: 573.2342 $[M\text{-}PF_6]^+$, found 573.2322.

Synthesis of **144**

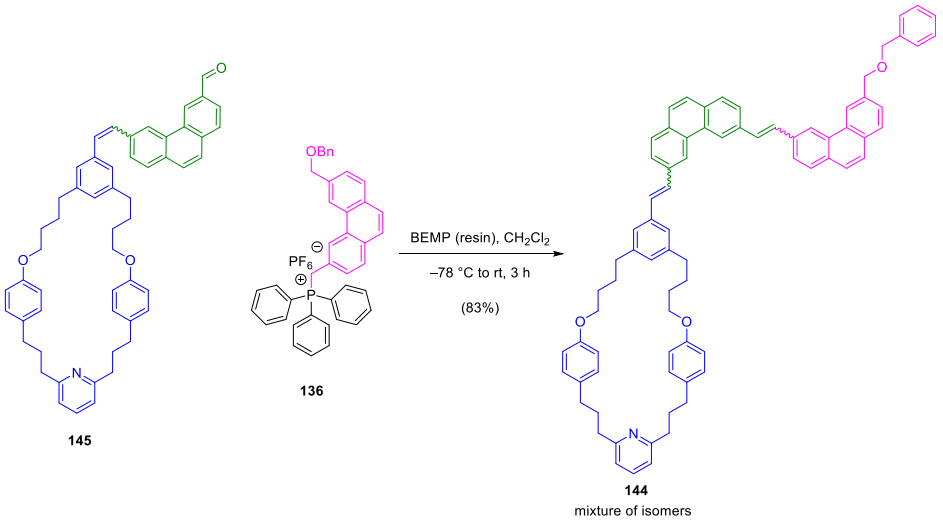

To a solution of **136** (120 mg, 0.167 mmol) and **145** (85.9 mg, 0.112 mmol) in CH_2Cl_2 (3 mL) at –78 °C was added BEMP (resin bound, ~2.0 mmol/g, 112 mg, 0.225 mmol) under argon and the reaction continued stirring for 30 minutes. In the following, the reaction mixture was gradually warmed to room temperature and stirred for 2.5 h. The reaction was filtered, and the filtrate was concentrated *in vacuo*. The residue was purified by flash chromatography (SiO_2, CH_2Cl_2/MeOH, 100:1) followed by size exclusion chromatography (S-X1, CH_2Cl_2) to give **144** (98.2 mg, 83%, mixture of four constitutional isomers – approx. in equal ratio) as a white solid.

Note: Due to the complexity of the obtained mixture of four configurational isomers assignment of the ^{1}H NMR for this compound was omitted. A list of multiplet ranges is provided instead. For an assignment of single isomer (*Z,Z)*-**144** please see below. For a comparison between the ^{1}H NMR and ^{13}C NMR of the four configurational isomers of **144** and pure (*Z,Z)*-**144** please see Figure 7.23.

^{1}H NMR (600 MHz, $CDCl_3$): δ 8.88 – 8.84 (m, 4H), 8.82 – 8.79 (m, 4H), 8.76 (d, *J* = 4.9 Hz, 2H), 8.72 (s, 1H), 8.65 (s, 1H), 8.51 (s, 1H), 8.47 (s, 1H), 8.42 (d, *J* = 1.6 Hz, 1H), 8.29 (s, 1H), 8.22 (s, 2H), 7.99 – 7.27 (m, 107H), 7.14 (d, *J* = 7.9 Hz, 3H), 7.09 – 6.91 (m, 48H), 6.87 (d, *J* = 12.2 Hz, 1H), 6.79 – 6.76 (m, 12H), 6.74 – 6.71 (m, 5H), 6.65 – 6.61 (m, 6H), 6.51 (d, *J* = 12.1 Hz, 1H), 4.89 (d, *J* = 11.1 Hz, 5H), 4.68 (s, 6H), 4.55 (s, 2H), 4.51 (s, 2H), 4.44 (s, 2H), 4.41 (s, 2H), 3.95 (t, *J* = 5.8 Hz, 12H), 3.81 (t, *J* = 5.6 Hz, 4H), 3.75 (t, *J* = 5.9 Hz, 4H), 2.84 – 2.77 (m, 24H), 2.75 – 2.67 (m, 12H), 2.60 – 2.49 (m, 32H), 2.06 – 1.96 (m, 24H), 1.91 – 1.77 (m, 24H), 1.71 – 1.59 (m, 24H).

^{13}C NMR (151 MHz, $CDCl_3$): δ 161.53, 157.36, 157.34, 157.26, 142.90, 142.79, 142.68, 142.55, 138.40, 138.37, 137.73, 137.60, 137.50, 137.45, 137.39, 136.79, 136.77, 136.71, 136.68, 136.60, 136.04, 135.98, 135.93, 135.87, 135.79, 135.77, 135.72, 135.70, 135.68, 135.47, 134.64, 134.58, 134.47, 132.18, 132.06, 132.02, 132.00, 131.95, 131.83, 131.79, 131.70, 131.55, 131.51, 131.46, 131.41, 131.27, 131.17, 131.13, 131.11, 131.09, 130.73, 130.70, 130.67, 130.60, 130.43, 130.40, 130.37, 130.26, 130.22, 130.20, 130.14, 130.12, 129.79, 129.76, 129.73, 129.64, 129.57, 129.44, 129.40, 129.37, 129.33, 129.29, 129.24, 129.21, 129.11, 129.06, 129.03, 128.92, 128.80, 128.76, 128.69, 128.67, 128.65, 128.60, 128.54, 128.50, 128.46, 128.35, 128.18, 128.14, 128.11, 128.09, 128.06, 128.02, 127.99, 127.97, 127.95, 127.87, 127.83, 127.78, 127.76, 127.70, 127.60, 127.06, 126.93, 126.89, 126.87, 126.84, 126.82, 126.76, 126.74, 126.73, 126.71, 126.69, 126.66, 126.63, 126.62, 126.55, 126.53, 124.72, 124.69, 124.67, 124.36, 124.33, 124.31, 124.26,

123.44, 123.36, 123.25, 123.20, 123.03, 122.08, 121.93, 121.89, 121.83, 121.80, 121.68, 121.61, 120.25, 114.50, 114.46, 114.41, 114.39, 72.69, 72.64, 72.58, 72.54, 72.41, 72.37, 72.18, 72.16, 67.80, 67.79, 67.65, 67.59, 38.07, 35.45, 35.43, 35.25, 35.19, 34.83, 34.81, 32.51, 28.79, 28.59, 28.23, 28.11.

HRMS (ASAP): Calculated for $C_{77}H_{71}NO_3$: 1058.5525 $[M+H]^+$, found 1058.5514.

Irradiation of **144** (mixture of configurational isomers) to give isomer *(Z,Z)*-**144**

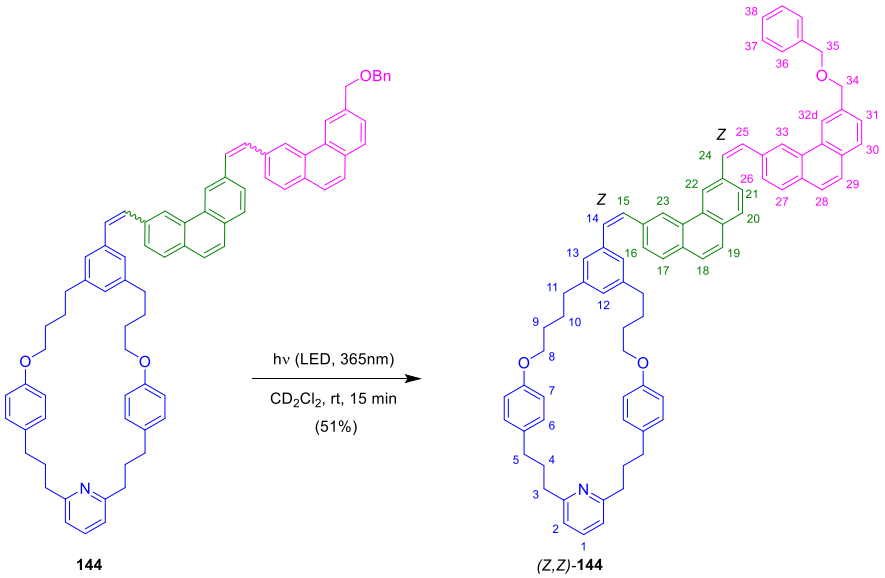

A solution of **144** (16 mg, 15 µmol) in CD_2Cl_2 (550 µL) was irradiated (LED, 365 nm, 195 mA, 50 mW) in an NMR tube for 15 min. The reaction was concentrated *in vacuo* and then purified by PTLC (SiO_2, 250 µm, CH_2Cl_2/Et_2O, 19:1, the collected silica was extracted with CH_2Cl_2/MeOH, 200:1) to give *(Z,Z)*-**144** (8.2 mg, 51%) as a yellow solid.

^{1}H NMR (600 MHz, $CDCl_3$): δ 8.86 (s, 1H, H-22), 8.84 (s, 1H, H-33), 8.79 (s, 2H, H-23 and H-32), 7.98 – 7.86 (m, 7H, H-16, H-17, H-20, H-21, H-26, H-27 and H-30), 7.75 (s, 2H, H-18 and H-29), 7.73 (s, 2H, H-19 and H-28), 7.67 – 7.61 (m, 3H, H-24, H-25 and H-31), 7.50 – 7.43 (m, 4H, H-1, H-15 and H-36), 7.41 – 7.37 (m, 2H, H-37), 7.35 – 7.30 (m, 2H, H-14 and H-38), 7.29 (s, 2H, H-13), 7.07 – 7.04 (m, 4H, H-6), 7.02 (s, 1H, H-12), 6.95 (d, *J* = 7.6 Hz, 2H, H-2), 6.81 – 6.74 (m, 4H, H-7), 4.90 (s, 2H, H-34), 4.68 (s, 2H, H-35), 3.95 (t, *J* = 5.8 Hz, 4H, H-8), 2.81 (t, *J* = 7.5 Hz, 4H, H-3), 2.72 (t, *J* = 7.4 Hz, 4H, H-11), 2.59 – 2.53 (m, 4H, H-5), 2.05 – 1.98 (m, 4H, H-4), 1.91 – 1.79 (m, 8H, H-9 and H-10).

^{13}C NMR (151 MHz, $CDCl_3$): δ 161.5, 157.4, 142.9, 138.4, 137.4, 136.8, 136.6, 136.0, 135.8, 134.6, 132.2, 132.1, 132.0, 130.72, 130.69, 130.7, 130.4, 129.76, 129.75, 129.71, 129.43, 129.40, 129.32, 129.27, 129.23, 129.20, 129.1, 128.8, 128.71, 128.69, 128.64, 128.54, 128.17, 128.13, 127.99, 127.97, 126.92, 126.84, 126.81, 126.76, 126.72, 126.70, 124.72, 124.68, 124.32, 124.25, 122.1, 121.87, 121.83, 121.80, 121.67, 120.2, 114.49, 114.45, 72.6, 72.4, 67.8, 38.1, 38.1, 35.5, 34.8, 32.5, 28.8, 28.2.

HRMS (ASAP): Calculated for $C_{77}H_{71}NO_3$: 1058.5525 $[M+H]^+$, found 1058.5514.

Irradiation of **144** to give [9]helicene **146**

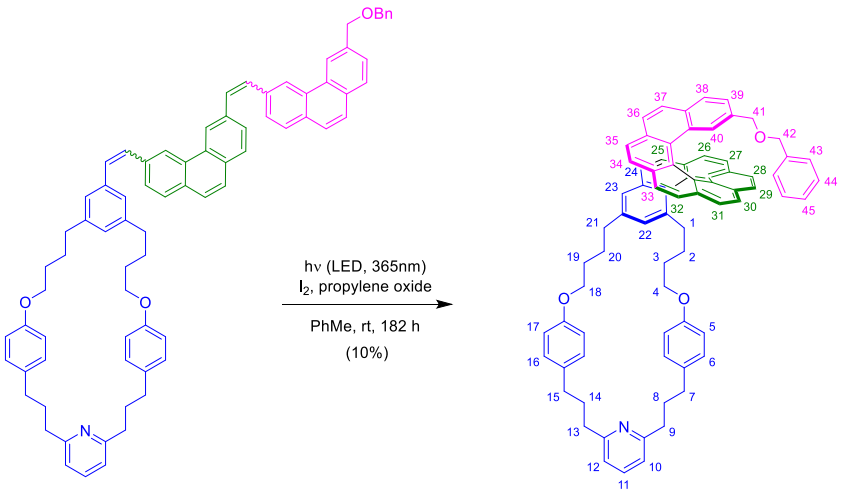

144 **146**

144 (20 mg, 19 μmol, mixture of four configurational isomers) was dissolved in degassed toluene (20 mL) under argon and iodine (12.2 mg, 48.1 μmol) and propylene oxide (66 μL, 0.945 mmol) were added. The reaction was irradiated (LED, 365 nm, 195 mA, 50 mW) through the side of a Schlenk tube for 182 h. Throughout the course of the reaction the precipitate that formed on the interface of the glassware was removed by briefly sonicating the reaction mixture. The reaction was quenched by the addition of saturated aqueous $NaHCO_3$ (10 mL) and saturated aqueous $Na_2S_2O_3$ (10 mL). The biphasic mixture was extracted with CH_2Cl_2 (3 × 15 mL). The combined organic layers were washed with brine and dried over Na_2SO_4, filtered, and concentrated *in vacuo*. The residue was purified by flash chromatography (SiO_2, petroleum ether/ EtOAc, 4:1) and then further purified by PTLC (SiO_2, 250 μm, CH_2Cl_2/Et_2O, 15:3) to give [9]helicene **146** (1.9 mg, 10%) as a yellow solid.

^{1}H NMR: (600 MHz, $CDCl_3$) δ 7.88 (d, *J* = 8.1 Hz, 1H, H-30), 7.82 (d, *J* = 8.1 Hz, 1H, H-31), 7.69 (d, *J* = 8.1 Hz, 1H, H-32), 7.67 (d, *J* = 8.1 Hz, 1H, H-29), 7.46 (t, *J* = 7.5 Hz, 1H, H-11), 7.42 (d, *J* = 8.1 Hz, 1H, H-28), 7.34 (d, *J* = 8.0 Hz, 1H, H-38), 7.34 (d, *J* = 8.1 Hz, 1H, H-33), 7.31 (d, *J* = 8.4 Hz, 1H, H-37), 7.28 – 7.25 (m, 2H, H-44), 7.25 – 7.22 (m, 2H, H-36 and H45), 7.19 (d, *J* = 8.1 Hz, 1H, H-35), 7.16 – 7.09 (m, 5H, H-24, H-27 and H-43), 7.08 (d, *J* = 7.9 Hz, 1H, H-39), 7.05 (d, *J* = 8.0 Hz, 1H, H-26), 7.04 – 7.00 (m, 3H, H-16, H-25 and H-27), 6.98 – 6.94 (m, 1H, H-23), 6.96 – 6.90 (m, 4H, H-6, H-10 and H-12), 6.84 (s, 1H, H-40), 6.72 (d, *J* = 8.6 Hz, 2H, H-17), 6.48 (d, *J* = 8.7 Hz, 2H, H-5), 6.36 (s, 1H, H-22), 4.24 (d, *J* = 12.0 Hz, 1H, H-41), 4.14 (d, *J* = 11.8 Hz, 1H, H-42), 4.08 (d, *J* = 11.8 Hz, 1H, H-42'), 3.91 (q, *J* = 5.9 Hz, 2H, H-18), 3.77 (d, *J* = 12.0 Hz, 1H, H-41'), 3.32 – 3.20 (m, 2H, H-4), 2.83 – 2.72 (m, 4H, H-9 and H-13), 2.70 – 2.63 (m, 2H, H-21), 2.52 (dd, *J* = 10.0, 6.2 Hz, 2H, H-15), 2.50 – 2.44 (m, 2H, H-7), 2.04 – 1.92 (m, 4H, H-8 and H-14), 1.92 – 1.72 (m, 4H, H-19 and H-20), 1.22 – 1.14 (m, 1H, H-1), 0.99 – 0.91 (m, 1H, H-1'), 0.82 – 0.72 (m, 1H, H-2), 0.69 – 0.59 (m, 1H, H-3), 0.53 – 0.43 (m, 1H, H-3'), 0.41 – 0.30 (m, 1H, H-2').

^{13}C NMR: (151 MHz, $CDCl_3$) δ 161.5, 157.3, 157.2, 138.5, 137.9, 136.6, 136.3, 134.7, 134.4, 133.5, 132.5, 131.8, 131.6, 131.3, 131.2, 131.01, 130.99, 130.88, 129.4, 129.2, 128.5, 128.4, 127.8, 127.51, 127.48, 127.26, 127.17, 126.83, 126.80, 126.72, 126.68, 126.55, 126.42, 126.24, 126.21, 126.02, 125.90, 125.81, 125.70, 125.4, 125.1, 125.0, 124.9, 124.5, 124.1, 123.9, 120.3, 114.5, 114.2, 72.5, 71.6, 67.9, 67.5, 38.0, 35.2, 34.66, 34.64, 32.8, 32.4, 29.1, 28.3, 28.0, 27.9.

HRMS (ESI$^+$): Calculated for $C_{77}H_{67}NONa$: 1076.5013 $[M+Na]^+$, found 1076.4987.

Synthesis of **137**

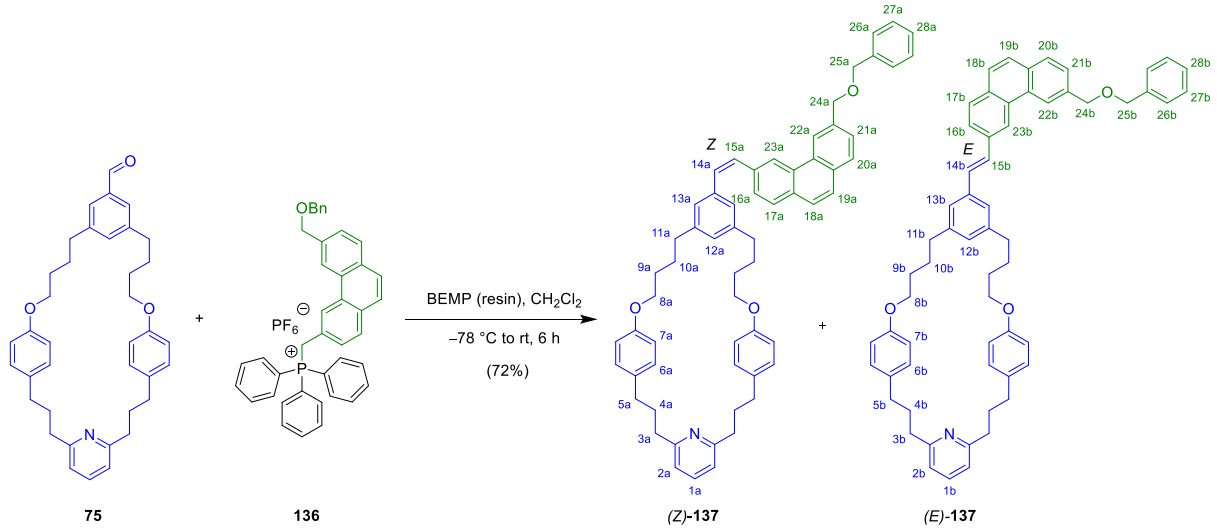

To a solution of **136** (64.3 mg, 89.5 µmmol) and aldehyde macrocycle **75** (41.9 mg, 74.6 µmol) in CH_2Cl_2 (5 mL) at –78 °C was added BEMP (resin bound, ~2.0 mmol/g, 74.6 mg, 149.1 µmol) under argon and the reaction was stirred for 25 minutes. After this period, the reaction mixture was gradually warmed to room temperature and stirred for 6 hours. The reaction was filtered, and the filtrate was concentrated *in vacuo*. The residue was purified by PTLC (SiO_2, 500 µm, CH_2Cl_2/Et_2O, 95:5) to give **137** (46.0 mg, 72.0%, mixture of constitutional isomers: *E*:*Z* ~ 1:1.1, ratio determined by integration of NMR signals for benzylic positions H-24b and H-24a at δ = 4.89 and δ = 4.77 ppm respectively) as a colourless foam.

^{1}H NMR (600 MHz, $CDCl_3$): δ 8.77 (s, 1H, H-23b), 8.76 (s, 1H, H-22b), 8.65 (s, 1H, H-23a), 8.43 (s, 1H, H-22a), 7.94 – 7.86 (m, 4H, H-16b, H-17b and H-20a/b), 7.74 (s, 2H, H-18b and H-19b), 7.72 (d, *J* = 8.6 Hz, 2H, H-17a and H-18a), 7.68 (d, *J* = 8.8 Hz, 1H, H-19a), 7.66 (dd, *J* = 8.0, 1.5 Hz, 1H, H-21b), 7.61 (dd, *J* = 8.1, 1.5 Hz, 1H, H-21a), 7.54 – 7.47 (m, 5H, H-1a/b, H-16a and H-26b), 7.46 – 7.30 (m, 11H, H-13b, H-14b, H-15b, H-26a, H-27a/b and H-28a/b), 7.09 (t, *J* = 8.0 Hz, 8H, H-6a/b), 7.06 (s, 1H, H-12b), 7.02 (d, *J* = 1.6 Hz, 2H, H-13a), 6.98 (dd, *J* = 7.7, 3.9 Hz, 4H, H-2a/b), 6.95 (d, *J* = 2.1 Hz, 1H, H-12a), 6.86 (d, *J* = 12.2 Hz, 1H, H-15a), 6.84 – 6.80 (m, 4H, H-7b), 6.77 (dd, *J* = 9.0, 2.6 Hz, 4H, H-7a and H-14a), 4.89 (s, 2H, H-24b), 4.77 (s, 2H, H-24a), 4.71 (s, 2H, H-25b), 4.62 (s, 2H, H-25a), 3.99 (t, *J* = 5.8 Hz, 4H, H-8b), 3.85 (t, *J* = 5.5 Hz, 4H, H-8a), 2.85 (td, *J* = 7.6, 2.5 Hz, 8H, H-3a/b), 2.75 (t, *J* = 7.4 Hz, 4H, H-11b), 2.62 – 2.58 (m, 8H, H-5a/b), 2.54 (t, *J* = 7.1 Hz, 4H, H-11a), 2.09 – 2.03 (m, 8H, H-4a/b), 1.94 – 1.83 (m, 8H, H-9b and H-10b), 1.72 – 1.64 (m, 8H, H-9a and H-10a).

^{13}C NMR (151 MHz, $CDCl_3$): δ 161.47, 157.29, 157.26, 142.83, 142.47, 138.36, 138.33, 137.37, 136.63, 136.61, 136.56, 135.83, 135.71, 134.58, 134.52, 131.95, 131.76, 131.73, 131.25, 130.55, 130.28, 130.19, 130.14, 129.55, 129.39, 129.36, 129.04, 128.97, 128.86, 128.71, 128.61, 128.54, 128.18, 128.10, 128.03, 127.96, 127.85, 127.78, 127.75, 127.59, 126.75, 126.70, 126.57, 126.53, 124.63, 124.35, 123.36, 121.84, 121.80, 121.60, 120.19, 114.42, 114.39, 72.61, 72.29, 72.27, 67.71, 67.57, 38.04, 35.40, 35.15, 34.77, 32.52, 28.73, 28.52, 28.19, 28.09.

HRMS (ASAP): Calculated for $C_{61}H_{62}NO_3$: 856.4724 $[M+H]^+$, found 856.4723.

Synthesis of **138**

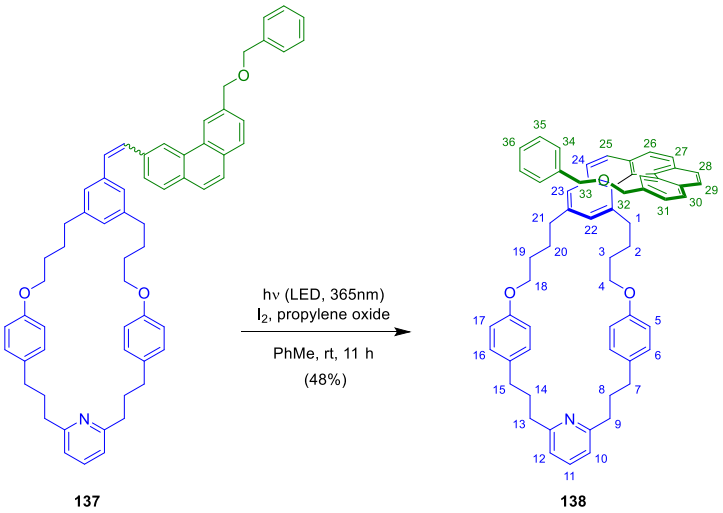

137 **138**

137 (46.0 mg, 53.7 µmol) was dissolved in degassed toluene (50 mL) under argon and iodine (16.4 mg, 64.5 µmol) and propylene oxide (190 µL, 2.69 mmol) were added. The reaction was irradiated (LED, 365 nm, 195 mA, 50 mW) through the side of a Schlenk tube for 11 h. The crude reaction was concentrated *in vacuo*. The residue was purified by PTLC (SiO_2, 500 µm, CH_2Cl_2/Et_2O, 95:5, then CH_2Cl_2/MeOH, 99:1) to give [5]helicene **138** (21.9 mg, 48%) as a colourless solid.

^{1}H NMR (600 MHz, $CDCl_3$): δ 7.93 – 7.90 (m, 3H, H-26, H-27 and H-30), 7.89 (s, 2H, H-28 and H-29), 7.87 (s, 1H, H-17), 7.84 (d, *J* = 8.4 Hz, 1H, H-24), 7.78 (d, *J* = 8.4 Hz, 1H, H-25), 7.64 (d, *J* = 1.8 Hz, 1H, H-23), 7.52 (dd, *J* = 8.1, 1.6 Hz, 1H, H-31), 7.46 (t, *J* = 7.6 Hz, 1H, H-11), 7.30 – 7.27 (m, 2H, H-35), 7.26 – 7.21 (m, 3H, H-34 and H-36), 7.15 – 7.13 (m, 1H, H-22), 7.00 (d, *J* = 8.6 Hz, 2H, H-16 and H-33), 6.96 – 6.90 (m, 4H, H-6, H-10 and H-12), 6.70 (d, *J* = 8.7 Hz, 2H, H-17 and H-34), 6.51 (d, *J* = 8.7 Hz, 2H, H-5), 4.40 – 4.34 (m, 4H, H-32 and H-33), 3.92 – 3.87 (m, 2H, H-18), 3.44 – 3.36 (m, 2H, H-4), 2.82 (t, *J* = 7.5 Hz, 2H, H-21), 2.81 – 2.75 (m, 4H, H-9 and H-13), 2.54 – 2.50 (m, 2H, H-15), 2.49 – 2.45 (m, 2H, H-7), 2.14 – 2.07 (m, 1H, H-1), 2.03 – 1.77 (m, 9H, H-8, H-14, H-19 and H-20), 1.14 – 1.06 (m, 1H, H-2), 0.99 – 0.91 (m, 1H, H-2'), 0.90 – 0.74 (m, 2H, H-3).

^{13}C NMR (151 MHz, $CDCl_3$): δ 161.5, 157.3, 157.1, 140.6, 140.4, 138.5, 136.6, 135.1, 134.7, 134.5, 133.4, 132.2, 131.7, 131.3, 130.7, 129.4, 129.3, 129.2, 128.53, 128.48, 128.33, 127.8, 127.7, 127.64, 127.55, 126.92, 126.86, 126.7, 126.3, 126.1, 125.8, 125.7, 124.9, 120.3, 114.4, 114.2, 72.8, 71.9, 67.9, 67.6, 37.9, 35.3, 34.6, 34.5, 32.4, 28.9, 28.6, 28.2, 27.8.

HRMS (ASAP): Calculated for $C_{61}H_{60}NO_3$: 854.4568 $[M+H]^+$, found 854.4567.

11.1.3. Unidirectional Linear Transport with a Fluorescence Read Out

Synthesis of Anthracene Azide Stopper 219

Synthesis of **222**

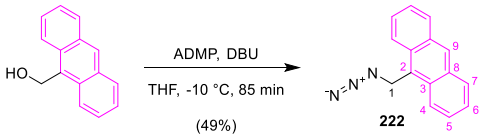

To a solution of 9-anthracenemethanol (2.00 g, 9.60 mmol) and ADMP (3.29 g, 11.5 mmol) in dry THF (50 mL, 0.2 M) at –10 °C was added DBU (2.15 mL, 14.4 mmol) dropwise and the reaction was continued stirring at –10 °C for 85 minutes. The reaction was quenched by the addition of saturated aqueous NH_4Cl (5 mL). The biphasic mixture was extracted with CH_2Cl_2 (3 × 50 mL). The combined organic layers were washed with brine and dried over Na_2SO_4, filtered, and concentrated *in vacuo*. The residue was purified by flash chromatography (SiO_2, CH_2Cl_2) to afford **222** (1.10 g, 49%) as a brown solid.

^{1}H NMR (600 MHz, $CDCl_3$) δ 8.52 (s, 1H, H-9), 8.30 (d, J = 8.9 Hz, 2H, H-4), 8.06 (d, J = 8.4 Hz, 2H, H-7), 7.63 – 7.57 (m, 2H, H-5), 7.55 – 7.49 (m, 2H, H-6), 5.35 (s, 2H, H-1).

^{13}C NMR (151 MHz, $CDCl_3$) δ 131.54 (C-8), 130.88 (C-3), 129.46 (C-7), 129.16 (C-9), 127.01 (C-5), 125.94 (C-2), 125.37 (C-6), 123.68 (C-4), 46.53 (C-1).

HRMS (APCI$^+$): Calculated for $C_{15}H_{12}N_3$: 234.1026 $[M+H]^+$, found 234.1029.

Synthesis of **220**

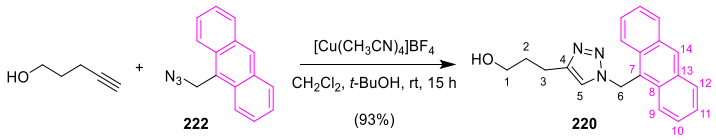

To a solution of **222** (206.1 mg, 0.88 mmol) and 4-pentyn-1-ol (0.12 mL, 1.32 mmol) in degassed CH_2Cl_2 (8 mL) and *t*-BuOH (2 mL) was added $[Cu(CH_3CN)_4]BF_4$ (55.6 mg, 177 µmol) and the reaction was stirred at room temperature for 15 hours. The reaction was quenched by the addition of saturated aqueous EDTA (10 mL, pH = 7). The biphasic mixture was extracted with CH_2Cl_2 (3 × 25 mL). The combined organic layers were washed with brine and dried over Na_2SO_4, filtered, and concentrated *in vacuo*. The residue was purified by flash chromatography (SiO_2, CH_2Cl_2/ MeOH, 39:1) to give **220** (259 mg, 93%) as a colourless solid.

^{1}H NMR (600 MHz, $CDCl_3$) δ 8.59 (s, 1H, H-14), 8.32 (d, J = 8.9 Hz, 2H, H-9), 8.09 (d, J = 8.4 Hz, 2H, H-12), 7.62 – 7.58 (m, 2H, H-10), 7.57 – 7.51 (m, 2H, H-11), 6.88 (s, 1H, H-5), 6.51 (s, 2H, H-6), 3.60 (q, J = 6.0 Hz, 2H, H-1), 2.64 (t, J = 7.2 Hz, 2H, H-3), 2.06 (t, J = 5.7 Hz, 1H, C-1 OH), 1.82 – 1.75 (m, 2H, H-2).

^{13}C NMR (151 MHz, $CDCl_3$) δ 147.66 (C-4), 131.59 (C-13), 130.96 (C-8), 129.95 (C-14), 129.62 (C-12), 127.79 (C-10), 125.58 (C-11), 124.08 (C-7), 123.17 (C-9), 120.52 (C-5), 62.20 (C-1), 46.49 (C-6), 31.82 (C-2), 22.33 (C-3).

HRMS (ASAP$^-$): Calculated for $C_{20}H_{18}ON_3$: 316.1455 $[M-H]^-$, found 316.1453.

Synthesis of **233**

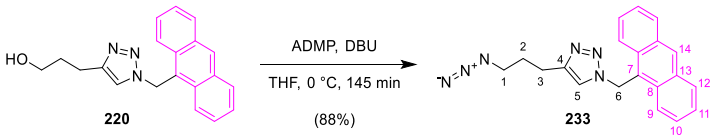

To a suspension of **220** (252.2 mg, 795 µmol) and ADMP (453 mg, 1.59 mmol) in dry THF (4.0 mL, 0.2 M) at 0 °C was added DBU (0.36 mL, 2.38 mmol) and the reaction was continued stirring at 0 °C for 145 minutes. The reaction was quenched by the addition of saturated aqueous NH_4Cl (10 mL). The biphasic mixture was extracted with CH_2Cl_2 (3 × 30 mL). The combined organic layers were washed with brine and dried over Na_2SO_4, filtered, and concentrated *in vacuo*. The residue was purified by flash chromatography (SiO_2, CH_2Cl_2/ MeOH, 99:1) to afford **233** (239 mg, 88%) as a yellow solid.

^{1}H NMR (600 MHz, $CDCl_3$) δ 8.59 (s, 1H, H-14), 8.31 (d, J = 8.8 Hz, 2H, H-9), 8.09 (d, J = 8.4 Hz, 2H, H-12), 7.64 – 7.58 (m, 2H, H-10), 7.57 – 7.51 (m, 2H, H-11), 6.88 (s, 1H, H-5), 6.52 (s, 2H, H-6), 3.23 (t, J = 6.8 Hz, 2H, H-1), 2.61 (t, J = 7.5 Hz, 2H, H-3), 1.83 (dt, J = 14.2, 6.9 Hz, 2H, H-2).

^{13}C NMR (151 MHz, $CDCl_3$) δ 146.86 (C-4), 131.59 (C-13), 130.95 (C-8), 129.97 (C-14), 129.63 (C-12), 127.80 (C-10), 125.58 (C-11), 124.05 (C-7), 123.15 (C-9), 120.58 (C-5), 50.76 (C-1), 46.49 (C-6), 28.52 (C-2), 22.78 (C-3).

HRMS (ASAP$^+$): Calculated for $C_{20}H_{19}N_6$: 343.1666 $[M+H]^+$, found 343.1662.

Synthesis of **219** ($PF6^-$ salt)

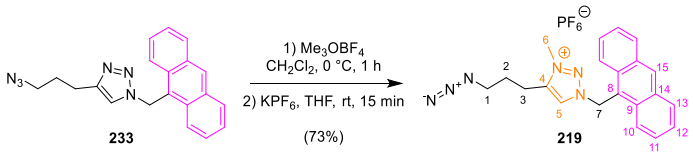

To a solution of **233** (228.9 mg, 669 µmol) in dry degassed CH_2Cl_2 (7 mL, 0.1 M) at 0 °C was added trimethyloxonium tetrafluoroborate (148 mg, 1.00 mmol) and the reaction was stirred for 60 minutes. The reaction mixture was quenched with MeOH (1 mL) and concentrated *in vacuo*. The resultant residue was purified by flash chromatography. (SiO_2, CH_2Cl_2/ MeOH, 39:1) The intermediate product was then taken up in THF (10 mL) and KPF_6 (1.29 g, 7.00 mmol) was added. The solution was stirred at room temperature for 15 minutes. The solvent was removed *in vacuo* and the residue was taken up in CH_2Cl_2 and filtered under reduced pressure. The filtrate was concentrated *in vacuo* to give **219** (245 mg, 73%, $PF6^-$ salt) as a yellow solid.

^{1}H NMR (600 MHz, CD_2Cl_2) δ 8.73 (s, 1H, H-15), 8.27 (d, J = 8.9 Hz, 2H, H-10), 8.16 (d, J = 8.5 Hz, 2H, H-13), 7.78 (s, 1H, H-5), 7.75 – 7.69 (m, 2H, H-11), 7.63 – 7.58 (m, 2H, H-12), 6.72 (s, 2H, H-7), 4.18 (s, 3H, H-6), 3.39 (t, J = 6.2 Hz, 2H, H-1), 2.82 – 2.77 (m, 2H, H-3), 1.88 – 1.81 (m, 2H, H-2).

^{13}C NMR (151 MHz, CD_2Cl_2) δ 144.37 (C-5), 131.98 (C-15), 131.78 (C-14), 131.51 (C-9), 130.12 (C-13), 129.09 (C-11), 127.69 (C-5), 126.15 (C-12), 122.60 (C-10), 120.09 (C-8), 50.59 (C-7), 50.40 (C-1), 38.16 (C-6), 26.48 (C-2), 21.07 (C-3).

^{19}F NMR (376 MHz, CD_2Cl_2) δ -73.51 (d, J = 710.9 Hz).

^{31}P NMR (162 MHz, CD_2Cl_2) δ -144.63 (hept, J = 710.9 Hz).

HRMS (HESI$^+$): Calculated for $C_{21}H_{21}N_6$: 357.1822 $[M\text{-}PF_6]^+$, found 357.1811.

Synthesis of **219** (TFA^- salt)

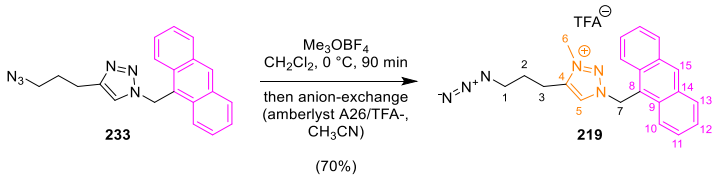

To a solution of **233** (283.3 mg, 827 µmol) in dry degassed CH_2Cl_2 (10 mL, 0.1 M) at 0 °C was added trimethyloxonium tetrafluoroborate (183.6 mg, 1.24 mmol) and the reaction was stirred for 90 minutes. The reaction mixture was quenched with MeOH (10 mL) and concentrated *in vacuo*. The resultant residue was purified by flash chromatography (SiO_2, CH_2Cl_2/ MeOH, 39:1) and then anion-exchange chromatography (amberlyst A-26 TFA^-, CH_3CN) to give **219** (264 mg, 70%, TFA^- salt) as a light brown solid.

^{1}H NMR (600 MHz, CD_2Cl_2) δ 8.72 (s, 1H, H-15), 8.28 (d, J = 8.9 Hz, 2H, H-10), 8.15 (d, J = 8.5 Hz, 2H, H-13), 7.84 (s, 1H, H-5), 7.74 – 7.68 (m, 2H, H-11), 7.64 – 7.57 (m, 2H, H-12), 6.72 (s, 2H, H-7), 4.17 (s, 3H, H-6), 3.41 – 3.36 (m, 2H, H-1), 2.84 – 2.77 (m, 2H, H-3), 1.90 – 1.82 (m, 2H, H-2).

^{13}C NMR (151 MHz, CD_2Cl_2) δ 144.36 (C-4), 131.93 (C-15), 131.81 (C-14), 131.55 (C-9), 130.11 (C-13), 129.06 (C-11), 127.83 (C-5), 126.15 (C-12), 122.69 (C-10), 120.24 (C-8), 50.58 (C-7), 50.43 (C-1), 38.14 (C-6), 26.50 (C-2), 21.08 (C-3).

^{19}F NMR (471 MHz, CD_2Cl_2) δ -73.46 (d, J = 710.9 Hz).

HRMS (HESI$^+$): Calculated for $C_{21}H_{21}N_6$: 357.1822 $[M\text{-}TFA]^+$, found 357.1811.

Synthesis of TBDMS-Protected DBA Fragment 239

Synthesis of **362**

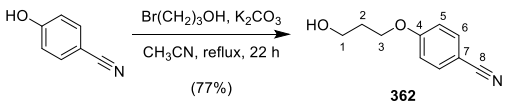

362

To a solution of 3-bromo-1-propanol (3.0 mL, 34 mmol) and 4-hydroxybenzonitrile (4.0 g, 34 mmol) in CH_3CN (100 mL, 0.3 M) was added K_2CO_3 (granulate, 13.9 g, 101 mmol) and the reaction mixture was heated to reflux (heating set to 85 °C; using a reflux condenser and drying tube charged with $CaCl_2$) for 22 hours. The reaction mixture was cooled to room temperature, filtrated through a plug of celite and the residue washed with additional EtOAc. (100 mL) The combined organic phases were concentrated *in vacuo*. The residue was purified by flash chromatography (SiO_2, petroleum ether/ EtOAc, 2:3) give **362** (4.57 g, 77%) as a colourless solid.

^{1}H NMR (600 MHz, $CDCl_3$) δ 7.58 (d, *J* = 8.9 Hz, 2H, H-6), 6.96 (d, *J* = 8.9 Hz, 2H, H-5), 4.17 (t, *J* = 6.1 Hz, 2H, H-3), 3.87 (q, *J* = 5.8 Hz, 2H, H-1), 2.07 (p, *J* = 6.0 Hz, 2H, H-2), 1.51 (td, *J* = 5.1, 2.9 Hz, 1H, C-1 OH).
^{13}C NMR (151 MHz, $CDCl_3$) δ 162.28 (C-4), 134.16 (C-6), 119.37 (C-8), 115.31 (C-5), 104.12 (C-7), 65.66 (C-3), 59.77 (C-1), 31.88 (C-2).
HRMS (HESI$^-$): Calculated for $C_{10}H_{10}O_2N$: 176.0717 $[M-H]^-$, found 176.0714.

Synthesis of **235**

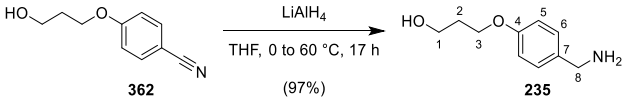

To a suspension of lithium aluminium hydride (crushed pellets, 1.98 g, 52.2 mmol) in dry THF (100 mL) at 0 °C was added a solution of **362** (4.56 g, 25.7 mmol) in dry THF (30 mL, 0.2 M in total) over 15 minutes via a syringe pump (2 mL/min) and the reaction mixture was continued stirring for 50 minutes at 0 °C. The reaction was warmed to room temperature and then slowly heated to reflux (heating set to 60 °C, using a reflux condenser, under argon) for 16 hours. The reaction mixture was cooled to 0 °C and distilled water (2.0 mL), an aqueous solution of sodium hydroxide (15% w/w, 2.0 mL) and more distilled water (6.0 mL) were added one after each other. Na_2SO_4 was added, and the reaction mixture was gradually warmed to room temperature and stirred for 15 minutes. The resulting suspension was filtrated through a plug of celite, the residue washed with EtOAc (150 mL) and the combined organic phases were dried over Na_2SO_4, filtered, and concentrated *in vacuo* to afford **235** (4.53 g, 97%) as a yellow solid.

^{1}H NMR (600 MHz, $CDCl_3$) δ 7.22 (d, *J* = 8.1 Hz, 2H, H-6), 6.88 (d, *J* = 8.4 Hz, 2H, H-5), 4.12 (t, *J* = 5.8 Hz, 2H, H-3), 3.87 (t, *J* = 5.3 Hz, 2H, H-1), 3.80 (s, 2H, H-8), 2.05 (p, *J* = 5.7 Hz, 2H, H-2), 1.49 (s, 2H, C-8 NH_2), 1.26 (t, *J* = 7.1 Hz, 1H, C-1 OH).

^{13}C NMR (151 MHz, $CDCl_3$) δ 157.81 (C-4), 135.97 (C-7), 128.43 (C-6), 114.65 (C-5), 66.05 (C-3), 60.74 (C-1), 46.06 (C-8), 32.13 (C-2).

HRMS (HESI$^+$): Calculated for $C_{10}H_{13}O_2$: 165.0910 $[M\text{-}NH_2]^+$, found 165.0905.

Synthesis of **237**

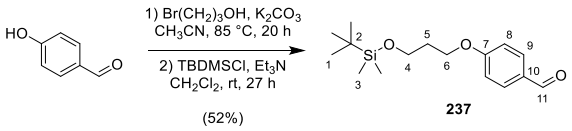

237

To a solution of 3-bromo-1-propanol (0.95 mL, 10.5 mmol) and 4-hydroxybenzaldehyde (854.8 mg, 7.00 mmol) in CH_3CN (70 mL, 0.1 M) was added K_2CO_3 (granulate, 1.93 g, 14.0 mmol) and the reaction mixture was heated to reflux (heating set to 85 °C; using a reflux condenser and drying tube charged with $CaCl_2$) for 20 hours. The reaction mixture was cooled to room temperature and the solvent removed *in vacuo*. The crude was resuspended in $CHCl_3$, filtrated through a plug of celite and the residue washed with additional $CHCl_3$. (100 mL in total) The combined organic phases were concentrated *in vacuo.*

The intermediate product was dissolved in dry CH_2Cl_2 (70 mL, 0.1 M) and TBDPS-Cl (50% in PhMe, 2.91 mL, 8.4 mmol) followed by triethylamine (1.46 mL, 10.5 mmol) were added at room temperature and the reaction was stirred for 27 hours. The reaction was quenched by the addition of saturated aqueous NH_4Cl (25 mL). The biphasic mixture was extracted with CH_2Cl_2 (3 × 50 mL). The combined organic layers were washed with brine and dried over Na_2SO_4, filtered, and concentrated *in vacuo*. The residue was purified by flash chromatography (SiO_2, petroleum ether/ EtOAc, 19:1) give **237** (1.07 g, 52% over two steps) as a colourless liquid.

^{1}H NMR (600 MHz, $CDCl_3$) δ 9.88 (s, 1H, H-11), 7.83 (d, J = 7.8 Hz, 2H, H-9), 7.00 (d, J = 7.9 Hz, 2H, H-8), 4.16 (t, J = 5.4 Hz, 2H, H-6), 3.81 (t, J = 5.9 Hz, 2H, H-4), 2.04 – 1.97 (m, 2H, H-5), 0.88 (s, 9H, H-1), 0.04 (s, 6H, H-3).

^{13}C NMR (151 MHz, $CDCl_3$) δ 190.99 (C-11), 164.35 (C-7), 132.15 (C-9), 129.95 (C-10), 114.90 (C-8), 65.03 (C-6), 59.30 (C-4), 32.27 (C-5), 26.04 (C-1), 18.45 (C-2), -5.26 (C-3).

HRMS ($ASAP^+$): Calculated for $C_{16}H_{27}O_3Si$: 295.1724 $[M+H]^+$, found 295.1716.

Synthesis of **238**

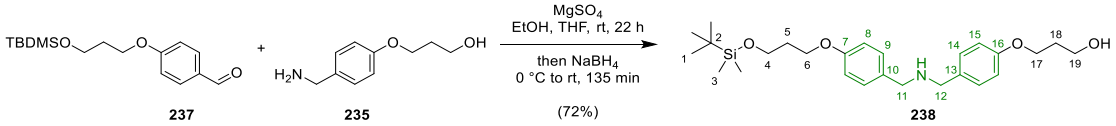

To a solution of **235** (1.06 g, 5.52 mmol) and **237** (2.44 g, 8.28 mmol) in dry EtOH (39 mL) and dry THF (5 mL, 0.1 M in total) was added $MgSO_4$ (anhydrous, *excess*) at room temperature and the reaction was stirred for 22 hours. The reaction mixture ware cooled to 0 °C and $NaBH_4$ (626 mg, 16.6 mmol) was added dropwise. The reaction was stirred for 30 minutes, warmed to room temperature, and stirred for 105 minutes. The reaction was quenched with distilled water (25 mL) and the biphasic mixture was extracted with CH_2Cl_2 (3 × 50 mL). The combined organic layers were washed with brine and dried over Na_2SO_4, filtered, and concentrated *in vacuo*. The residue was purified by flash chromatography (SiO_2, CH_2Cl_2/ MeOH, 9:1) to afford **238** (1.82 g, 72%) as a colourless solid.

^{1}H NMR (600 MHz, $CDCl_3$) δ 7.26 (d, J = 14.7 Hz, 4H, H-9 and H-14, *overlapped with solvent peak*), 6.86 (d, J = 7.4 Hz, 4H, H-8 and H-15), 4.10 (t, J = 5.9 Hz, 2H, H-17), 4.04 (t, J = 6.2 Hz, 2H, H-6), 3.86 (t, J = 5.8 Hz, 2H, H-19), 3.79 (t, J = 6.0 Hz, 2H, H-4), 3.73 (m, 4H, H-11 and H-12), 2.04 (p, J = 5.8 Hz, 2H, H-18), 1.97 (p, J = 6.1 Hz, 2H, H-5), 0.88 (s, 9H, H-1), 0.04 (s, 6H, H-3).

^{13}C NMR (151 MHz, $CDCl_3$) δ 158.48 (d, *2 rotomers*, C-7), 158.15 (d, *2 rotomers*, C-16), 131.11 (C-10 and C-13, *weak*), 129.96 – 129.73 (m, C-9 and C-14), 114.64 – 114.52 (m, C-8 and C-15), 65.97 (d, *2 rotomers*, C-17), 64.63 (C-6), 60.73 (d, *2 rotomers*, C-19), 59.68 (C-4), 52.06 – 51.78 (m, C-11 and C-12), 32.55 (C-5), 32.10 (C-18), 26.07 (C-1), 18.47 (C-2), -5.23 (C-3).

HRMS ($APCI^+$): Calculated for $C_{26}H_{42}O_4NSi$: 460.2878 $[M+H]^+$, found 460.2877.

Synthesis of **363**

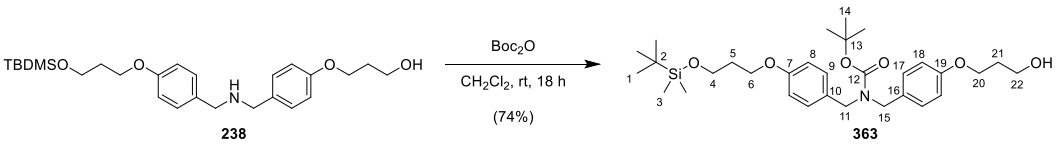

To a solution of **238** (2.32 g, 5.06 mmol) in dry CH_2Cl_2 (70 mL, 0.1 M) was added Boc anhydride (2.0 M in THF, 3.04 mL, 6.08 mmol) at room temperature and the reaction was stirred for 18 hours. The reaction was quenched with distilled water (40 mL) and the biphasic mixture was extracted with CH_2Cl_2 (3 × 50 mL). The combined organic layers were washed with brine and dried over Na_2SO_4, filtered, and concentrated *in vacuo*. The residue was purified by flash chromatography (SiO_2, petroleum ether/ EtOAc, 3:2) to afford **363** (2.10 g, 74%) as a colourless liquid.

^{1}H NMR (600 MHz, $CDCl_3$) δ 7.15 (s, 2H, H-17), 7.10 (s, 2H, H-9), 6.87 (d, J = 8.3 Hz, 2H, H-18), 6.85 (d, J = 8.4 Hz, 2H, H-8), 4.32 (s, 2H, H-15), 4.23 (s, 2H, H-11), 4.13 (t, J = 5.9 Hz, 2H, H-20), 4.05 (t, J = 6.1 Hz, 2H, H-6), 3.88 (q, J = 5.7 Hz, 2H, H-22), 3.80 (t, J = 6.0 Hz, 2H, H-4), 2.05 (p, J = 7.1, 6.5 Hz, 2H, H-21), 1.98 (p, J = 6.0 Hz, 2H, H-5), 1.74 (t, J = 5.4 Hz, 1H, C-22 OH), 1.50 (s, 9H, H-14), 0.89 (s, 9H, H-1), 0.05 (s, 6H, H-3).

^{13}C NMR (151 MHz, $CDCl_3$) δ 158.45 (C-7), 158.11 (C-19), 156.09 (C-12), 130.52 (C-16), 130.00 (C-10), 129.50 (C-17), 128.93 (C-9), 114.59 (C-8 and C-18), 80.04 (C-13), 66.01 (C-20), 64.65 (C-6), 60.79 (C-22), 59.68 (C-4), 48.50 (C-11), 48.13 (C-15), 32.56 (C-5), 32.11 (C-21), 28.64 (C-14), 26.07 (C-1), 18.48 (C-2), -5.22 (C-3).

HRMS (HESI$^+$): Calculated for $C_{31}H_{49}O_6NNaSi$: 582.3221 $[M+Na]^+$, found 582.3204.

Synthesis of **239**

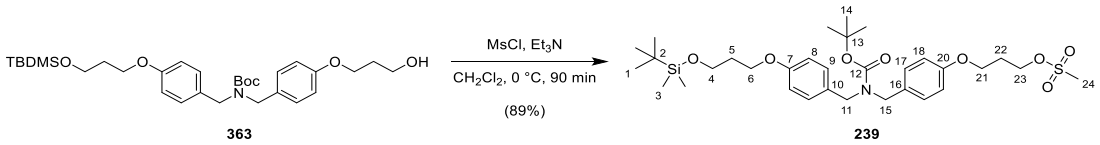

To a solution of **363** (216.7 mg, 387 µmol) in dry CH_2Cl_2 (4 mL, 0.1 M) was added MsCl (0.04 mL, 464 µmol) and triethylamine (0.08 mL, 581 µmol) sequentially at 0 °C and the reaction was stirred for 90 minutes. The reaction was quenched with saturated aqueous NH_4Cl (15 mL) and the biphasic mixture was extracted with CH_2Cl_2 (3 × 25 mL). The combined organic layers were washed with brine and dried over Na_2SO_4, filtered, and concentrated *in vacuo* to give **239** (219 mg, 89%) as a colourless oil.

^{1}H NMR (600 MHz, $CDCl_3$) δ 7.15 (s, 2Hz, H-9), 7.10 (s, 2H, H-17), 6.86 (d, J = 8.6 Hz, 2H, H-8), 6.85 (d, J = 8.5 Hz, 2H, H-18), 4.46 (t, J = 6.1 Hz, 2H, H-23), 4.32 (s, 2H, H-11), 4.23 (s, 2H, H-15), 4.09 (t, J = 5.8 Hz, 2H, H-21), 4.06 (t, J = 6.2 Hz, 2H, H-6), 3.80 (t, J = 6.0 Hz, 2H, H-4), 3.00 (s, 3H, H-24), 2.23 (p, J = 6.0 Hz, 2H, H-22), 1.98 (p, J = 6.1 Hz, 2H, H-5), 1.50 (s, 9H, H-14), 0.89 (s, 9H, H-1), 0.05 (s, 6H, H-3).

^{13}C NMR (151 MHz, $CDCl_3$) δ 158.49 (C-7), 157.85 (C-20), 156.09 (C-12), 130.82 (C-16), 130.02 (C-10), 129.53 (d, *2 rotomers*, C-9), 128.96 (d, *2 rotomers*, C-17), 114.62 (C-8/18), 114.58 (C-8/18), 80.06 (C-13), 66.89 (C-23), 64.68 (C-6), 63.36 (C-21), 59.68 (C-4), 48.93 – 47.67 (m, C-11 and C-15), 37.41 (C-24), 32.57 (C-5), 29.29 (C-22), 28.64 (C-14), 26.08 (C-1), 18.47 (C-2), -5.22 (C-3).

HRMS (HESI$^+$): Calculated for $C_{32}H_{51}O_8NNaSSi$: 660.2997 $[M+Na]^+$, found 660.2978.

Synthesis of Trityl-Protected Benzyl Thiol 244

Synthesis of **241**

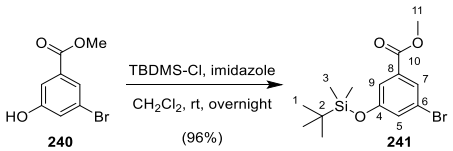

To a suspension of **240** (11.0 g, 47.6 mmol) in CH_2Cl_2 (240 mL, 0.2 M in total) was added imidazole (3.57 g, 52.4 mmol) and a solution of TBDMS-Cl (7.89 g, 52.4 mmol) in CH_2Cl_2 (40 mL) sequentially at room temperature and the reaction was stirred overnight. The reaction was filtrated, and the collected filtrate was washed with distilled water, saturated aqueous $NaHCO_3$ and brine. The combined organic layers were dried over $MgSO_4$, filtered, and concentrated *in vacuo*. The residue was purified by flash chromatography (SiO_2, CH_2Cl_2/ MeOH, 20:1) to afford **241** (15.75 g, 96%) as a colourless solid.

^{1}H NMR (600 MHz, $(CD_3)_2CO$) δ 7.75 – 7.71 (m, 1H, H-7), 7.44 (dd, *J* = 2.3, 1.4 Hz, 1H, H-9), 7.35 – 7.31 (m, 1H, H-5), 3.89 (s, 3H, H-11), 1.01 (s, 9H, H-1), 0.27 (s, 6H, H-3).

^{13}C NMR (151 MHz, $(CD_3)_2CO$) δ 165.68 (C-10), 157.62 (C-4), 134.09 (C-8), 128.39 (C-5), 126.02 (C-7), 123.04 (C-6), 120.64 (C-9), 52.84 (C-11), 25.88 (C-1), 18.77 (C-2), -4.48 (C-3).

HRMS (ASAP$^+$): Calculated for $C_{14}H_{22}O_3BrSi$: 345.0516 $[M+H]^+$, found 345.0514.

Synthesis of **242**

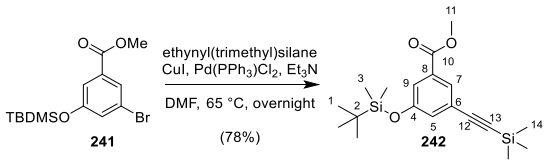

To a solution copper(I) iodide (275 mg, 1.45 mmol) and $Pd(PPh_3)Cl2$ (510 mg, 0.73 mmol) in a degassed mixture of triethylamine and dry DMF in equal ratio (50 mL in total, 0.2 mM in total) were added ethynyl(trimethyl)silane (2.3 mL, 15.95 mmol) and a solution of **241** (5.00 g, 14.5 mmol) in a degassed mixture of triethylamine and dry DMF in equal ratio (25 mL in total) at room temperature and the reaction mixture was stirred at 65 °C overnight under an atmosphere of nitrogen. The crude reaction was cooled to room temperature and concentrated *in vacuo*. The residue was purified by flash chromatography (SiO_2, petroleum ether/ CH_2Cl_2, 3:1) to afford **242** (4.1 g, 78%) as a colourless solid.

^{1}H NMR (600 MHz, $CDCl_3$) δ 7.74 (t, *J* = 1.4 Hz, 1H, H-7), 7.43 (dd, *J* = 2.4, 1.5 Hz, 1H, H-9), 7.09 (dd, *J* = 2.4, 1.4 Hz, 1H, H-5), 3.90 (s, 2H, H-11), 0.98 (s, 9H, H-1), 0.25 (s, 9H, H-14), 0.21 (s, 6H, H-3).

^{13}C NMR (151 MHz, $CDCl_3$) δ 166.38 (C-8), 155.66 (C-4), 131.70 (C-8), 127.72 (C-5), 126.58 (C-7), 124.60 (C-6), 121.61 (C-9), 103.89 (C-12), 95.18 (C-13), 52.45 (C-11), 25.73 (C-1), 18.29 (C-2), 0.03 (C-14), -4.31 (C-3).

HRMS (ASAP$^+$): Calculated for $C_{19}H_{31}O_3Si_2$: 363.1806 $[M+H]^+$, found 363.1803.

Synthesis of **364**

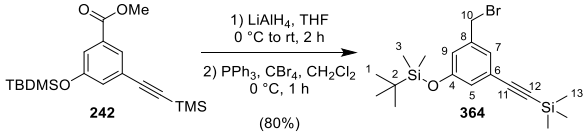

To a suspension of lithium aluminium hydride (crushed pellets, 858 mg, 22.6 mmol) in dry THF (100 mL) at 0 °C was added a solution of **242** (4.10 g, 11.3 mmol) in dry THF (25 mL, 0.1 M in total) and the reaction mixture was continued stirring for 2 hours while slowly allowed warming to room temperature. The reaction mixture was added to saturated aqueous NH_4Cl and extracted with CH_2Cl_2 (3 × 50 mL). The combined organic layers were dried over $MgSO_4$, filtered, and concentrated *in vacuo*. The intermediate product (4.0 g) was redissolved in CH_2Cl_2 (50 mL), cooled to at 0 °C and a solution of CBr_4 (5.95 g, 17.9 mmol) and PPh_3 (4.69 g, 17.9 mmol) in CH_2Cl_2 (100 mL, 0.1 mM in total) was added. The reaction was continued stirring at 0 °C for 1 hour. The resultant mixture was concentrated *in vacuo* and purified by flash chromatography (SiO_2, petroleum ether/ CH_2Cl_2, 3:1) to give **364** (3.80 g, 80%) as a yellow solid.

^{1}H NMR (600 MHz, $CDCl_3$) δ 7.10 (t, *J* = 1.4 Hz, 1H, H-7), 6.85 (dd, *J* = 2.2, 1.4 Hz, 1H, H-9), 6.84 – 6.80 (m, 1H, H-5), 4.37 (s, 2H, H-10), 0.98 (s, 9H, H-1), 0.24 (s, 9H, H-13), 0.20 (s, 6H, H-3).

^{13}C NMR (151 MHz, $CDCl_3$) δ 155.76 (C-4), 139.29 (C-8), 125.91 (C-7), 124.64 (C-6), 123.43 (C-9), 121.56 (C-5), 104.33 (C-11), 94.65 (C-12), 32.73 (C-10), 25.75 (C-1), 18.28 (C-2), 0.06 (C-13), -4.29 (C-3).

HRMS (ASAP$^+$): Calculated for $C_{18}H_{30}OBrSi_2$: 397.1013 $[M+H]^+$, found 397.1006.

Synthesis of **243**

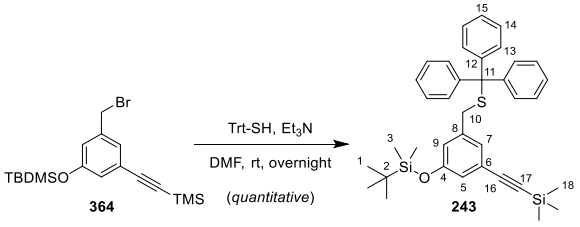

To a solution of **364** (784 mg, 1.97 mmol) in DMF (10 mL, 0.2 mM) were added triethylamine (366 µL, 2.56 mmol) and trityl mercaptan (655 mg, 2.37 mmol) and the reaction was stirred at room temperature overnight. The reaction mixture was diluted with ethyl acetate and washed with distilled water and brine. The combined organic layers were dried over Na_2SO_4, filtered, and concentrated *in vacuo* to yield **243** (1.2 g, *assumed quantitative*) as a yellow solid.

^{1}H NMR (600 MHz, $CDCl_3$) δ 7.45 (d, *J* = 7.8 Hz, 6H, H-13), 7.30 (t, *J* = 7.7 Hz, 6H, H-14), 7.23 (t, *J* = 7.3 Hz, 3H, H-15), 6.84 (s, 1H, H-7), 6.75 (s, 1H, H-9), 6.55 (s, 1H, H-6), 3.20 (s, 2H, H-10), 0.97 (s, 9H, H-1), 0.24 (s, 9H, H-18), 0.17 (s, 6H, H-3).

^{13}C NMR (151 MHz, $CDCl_3$) δ 155.47 (C-4), 144.74 (C-12), 138.74 (C-8), 129.74 (C-13), 128.11 (C-14), 126.88 (C-15), 126.08 (C-7), 124.12 (C-6), 122.01 (C-9), 121.72 (C-5), 104.89 (C-16), 94.00 (C-17), 67.56 (C-11), 25.77 (C-1), 18.27 (C-2), 0.11 (C-18), -4.27 (C-3).

HRMS (ESI^+): Calculated for $C_{37}H_{44}ONaSSi_2$: 615.2544 $[M+Na]^+$, found 615.2513.

Synthesis of **244**

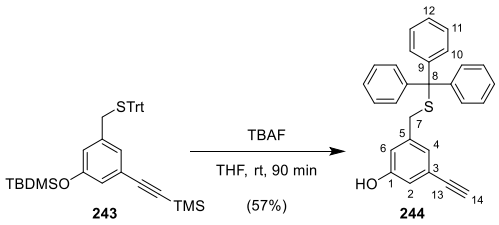

To a solution of **243** (1.2 g, 1.97 mmol) in THF (21.5 mL, 0.1 mM) was added TBAF (1 M in THF, 5.91 mL, 5.91 mmol) and the reaction was stirred at room for 90 minutes. The reaction mixture was diluted with ethyl acetate and the biphasic mixture was extracted with $CHCl_3$ (2 × 50 mL). The combined organic layers were dried over Na_2SO_4, filtered, and concentrated *in vacuo*. The resultant residue was purified by flash chromatography (SiO_2, CH_2Cl_2) to give **244** (460 mg, 57%) as a colourless solid.

^{1}H NMR (600 MHz, $CDCl_3$) δ 7.46 – 7.44 (m, 6H, H-10), 7.30 (t, *J* = 7.7 Hz, 6H, H-11), 7.25 – 7.21 (m, 3H, H-12), 6.83 (s, 1H, H-4), 6.78 (dd, *J* = 2.3, 1.2 Hz, 1H, H-6), 6.58 – 6.56 (m, 1H, H-2), 4.82 (s, 1H, C-1 OH), 3.23 (s, 2H, H-7), 3.02 (s, 1H, H-14).

^{13}C NMR (151 MHz, $CDCl_3$) δ 155.37 (C-1), 144.62 (C-9), 139.25 (C-6), 129.70 (C-10), 128.13 (C-11), 126.92 (C-12), 125.64 (C-4), 123.35 (C-3), 117.62 (C-6), 117.15 (C-2), 83.17 (C-14), 67.59 (C-8), 36.52 (C-7).

HRMS (ASAP$^-$): Calculated for $C_{28}H_{21}OS$: 405.1319 [M-H]$^-$, found 405.1315.

Synthesis of Adamantyl Aldehyde 247 and Acetal 248

Synthesis of **365**

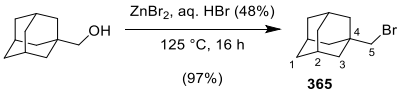

365

To a suspension of 1-adamantanemethanol (5.00 g, 30.1 mmol) in aqueous HBr (48%, 100 mL, 0.3 M) was added $ZnBr_2$ (98%, anhydr., 17.6 g, 78.2 mmol) and the reaction mixture was heated to reflux (heating set to 125 °C; using a reflux condenser) for 16 hours. The reaction mixture was cooled to room temperature and then diluted with distilled water (100 mL). The formed colourless precipitate was removed by filtration, washed with distilled water, and dried *in vacuo* to give **365** (6.67 g, 97%) as a colourless solid.

^{1}H NMR (600 MHz, $CDCl_3$) δ 3.15 (s, 2H, H-5), 2.00 (s, 3H, H-2), 1.73 – 1.59 (m, 6H, H-1), 1.56 (d, J = 2.3 Hz, 6H, H-3).

^{13}C NMR (151 MHz, $CDCl_3$) δ 48.65 (C-5), 40.82 (C-3), 36.82 (C-1), 33.71 (C-4), 28.49 (C-2).

HRMS ($APCI^+$): Calculated for $C_{11}H_{18}Br$: 229.0587 $[M+H]^+$, found 229.0588.

Synthesis of **246**

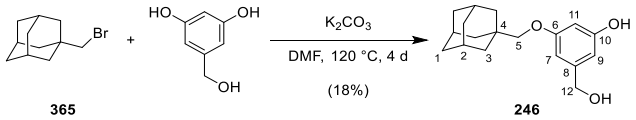

365 246

To a solution of **365** (2.98 g, 13.0 mmol) and 5-(hydroxymethyl)-1,3-benzenediol (5.47 g, 39.0 mmol) in dry, degassed DMF (50 mL, 0.3 M) was added K_2CO_3 (granulate, 8.99 g, 65.0 mmol) and the reaction mixture was stirred at 120 °C for 4 days. The reaction mixture was cooled to room temperature and then diluted with distilled water (100 mL). The pH of the suspension was adjusted to 4 and the reaction mixture was extracted with EtOAc (3 × 150 mL). The combined organic layers were washed with brine and dried over Na_2SO_4, filtered, and concentrated *in vacuo*. The residue was purified by flash chromatography (SiO_2, petroleum ether/ EtOAc, 3:2) give **246** (668 mg, 18%) as a colourless solid.

^{1}H NMR (600 MHz, $CDCl_3$) δ 6.48 (s, 1H, H-7), 6.41 (s, 1H, H-9), 6.33 (s, 1H, H-11), 5.52 (s, 1H, C-10 OH), 4.59 (s, 2H, H-12), 3.45 (s, 2H, H-5), 2.01 (s, 4H, H-2 and C-12 OH), 1.77 – 1.67 (m, 6H, H-1), 1.63 (s, 6H, H-3).

^{13}C NMR (151 MHz, $CDCl_3$) δ 161.38 (C-6), 157.11 (C-10), 143.32 (C-8), 105.98 (C-9), 105.65 (C-7), 101.34 (C-11), 78.51 (C-5), 65.27 (C-12), 39.58 (C-), 37.24 (C-1), 33.86 (C-4), 28.31 (C-3).

HRMS (ASAP$^-$): Calculated for $C_{18}H_{23}O_3$: 287.1648 $[M-H]^-$, found 287.1653.

Synthesis of **247**

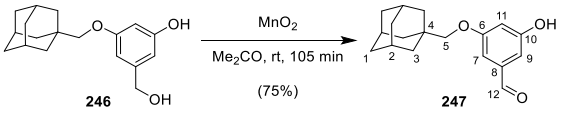

To a solution of **246** (297.0 mg, 1.03 mmol) in acetone (2.5 mL, 0.4 M) was added MnO_2 (technical grade, 1.12 g, 12.9 mmol) and the reaction mixture was stirred at room temperature for 60 minutes. A second portion of MnO_2 (technical grade, 564 mg, 6.50 mmol) and the reaction mixture was stirred for another 45 minutes The resulting suspension was filtrated through a plug of celite, the residue washed with acetone and the combined organic phases were dried over Na_2SO_4, filtered and concentrated *in vacuo*. The residue was purified by flash chromatography (SiO_2, petroleum ether/ EtOAc, 4:1) give **247** (221 mg, 75%) as a colourless solid.

^{1}H NMR (600 MHz, $CDCl_3$) δ 9.88 (s, 1H, H-12), 7.00 (dd, J = 2.2, 1.2 Hz, 1H, H-7), 6.91 (dd, J = 2.3, 1.2 Hz, 1H, H-9), 6.67 (t, J = 2.3 Hz, 1H, H-11), 4.99 (s, 1H, C-10 OH), 3.53 (s, 2H, H-5), 2.02 (s, 3H, H-2), 1.78 – 1.68 (m, 6H, H-1), 1.65 (d, J = 2.3 Hz, 6H, H-3).

^{13}C NMR (151 MHz, $CDCl_3$) δ 192.05 (C-12), 161.65 (C-6), 157.23 (C-10), 138.62 (C-8), 108.71 (C-9), 108.60 (C-11), 108.07 (C-7), 78.85 (C-5), 39.55 (C-3), 37.20 (C-1), 33.90 (C-4), 28.27 (C-2).

HRMS (HESI$^-$): Calculated for $C_{18}H_{21}O_3$: 285.1485 $[M-H]^-$, found 285.1491.

Synthesis of **248**

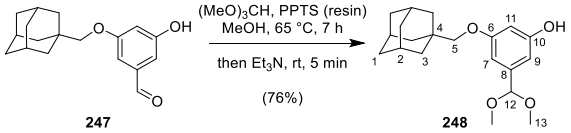

To a solution of **247** (204.1 mg, 0.71 mmol) and PPTS (resin-bound, 2.0-3.0 mmol/g, 35 mg, 70 µmol in dry MeOH (10 mL, 0.1 M) was added trimethoxy methane (0.78 mL, 7.1 mmol) and the reaction mixture was stirred at 65 °C for 7 hours. The reaction was cooled to room temperature and then quenched by the addition of Et_3N (0.10 mL, 0.71 mmol). The reaction was filtrated through a plug of cotton, the residue washed with CH_2Cl_2 and the combined organic phases were concentrated *in vacuo* to give **248** (180 mg, 76%) as a brown solid.

^{1}H NMR (600 MHz, $CDCl_3$) δ 6.59 (s, 1H, H-7), 6.50 (s, 1H, H-9), 6.37 (t, J = 2.2 Hz, 1H, H-11), 5.28 (s, 1H, H-12), 4.75 (s, 1H, C-1 OH), 3.47 (s, 2H, H-5), 3.33 (s, 6H, H-13), 2.01 (s, 3H, H-2), 1.77 – 1.67 (m, 6H, H-1), 1.64 (d, J = 2.1 Hz, 6H, H-3).

^{13}C NMR (151 MHz, $CDCl_3$) δ 161.21 (C-6), 156.64 (C-10), 140.77 (C-8), 105.87 (C-9), 105.59 (C-7), 102.97 (C-12), 102.17 (C-11), 78.50 (C-5), 52.94 (C-13), 39.60 (C-3), 37.27 (C-1), 33.88 (C-4), 28.33 (C-2).

HRMS (ASAP$^-$): Calculated for $C_{20}H_{27}O_4$: 331.1915 $[M-H]^-$, found 331.1915.

Synthesis of Left Energy Ratchet Part 251

Synthesis of **249**

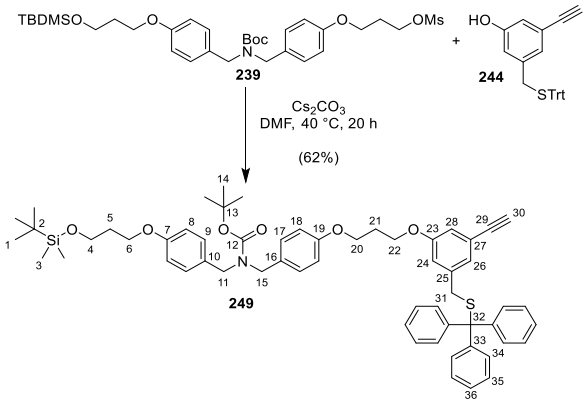

To a solution of **239** (556.8 mg, 873 µmol) and **244** (374.0 mg, 920 µmol) in dry DMF (10 mL, 0.1 M) was added Cs_2CO_3 (846.5 mg, 2.60 mmol) and the reaction mixture was heated to 40 °C and stirred for 20 hours. The reaction mixture was cooled to room temperature and quenched with distilled water. (25 mL) The biphasic mixture was extracted with CH_2Cl_2 (3 × 25 mL). The combined organic layers were washed with brine and dried over Na_2SO_4, filtered, and concentrated *in vacuo*. The residue was purified by flash chromatography (SiO_2, CH_2Cl_2/ MeOH, 99:1) to afford **249** (511 mg, 62%) as a colourless solid.

^{1}H NMR (600 MHz, $CDCl_3$) δ 7.46 – 7.43 (m, 6H, H-34), 7.30 (t, J = 7.7 Hz, 6H, H-25), 7.24 – 7.20 (m, 3H, H-36), 7.14 (s, 2H, H-9/17), 7.09 (d, J = 7.2 Hz, 2H, H-9/17), 6.88 – 6.83 (m, 6H, H-8, H-18, H-26 and H-28), 6.65 (s, 1H, H-24), 4.31 (s, 2H, H-11/15), 4.22 (s, 2H, H-11/15), 4.12 (t, J = 6.0 Hz, 2H, H-20), 4.09 (t, J = 6.1 Hz, 2H, H-22), 4.05 (t, J = 6.2 Hz, 2H, H-6), 3.80 (t, J = 6.0 Hz, 2H, H-4), 3.24 (s, 2H, H-31), 3.02 (s, 1H, H-30), 2.23 (p, J = 5.9 Hz, 2H, H-21), 1.98 (p, J = 6.1 Hz, 2H, H-5), 1.50 (s, 9H, H-14), 0.89 (s, 9H, H-1), 0.05 (s, 6H, H-3).

^{13}C NMR (151 MHz, $CDCl_3$) δ 158.72 (C-23), 158.45 (C-7), 158.19 (C-19), 156.10 (C-12), 144.67 (C-33), 138.98 (C-25), 130.37 (C-10/16), 130.03 (C-10/16), 129.72 (C-34), 129.54 (C-9/17), 128.93 (C-9/17), 128.13 (C-35), 126.92 (C-36), 125.53 (C-26), 123.14 (C-27), 116.71 (C-24), 116.42 (C-28), 114.59 (C-8 and C-18), 83.49 (C-29), 80.02 (C-13), 77.16 (C-30, *overlapped with solvent peak*), 67.62 (C-32), 64.64 (C-6 and C-22), 64.42 (C-20), 59.69 (C-4), 48.39 (C-11/15), 48.07 (C-11/15), 36.72 (C-31), 32.56 (C-5), 29.35 (C-21), 28.65 (C-14), 26.08 (C-1), 18.48 (C-2), -5.22 (C-3).

HRMS (HESI$^+$): Calculated for $C_{59}H_{69}O_6NNaSSi$: 970.4508 $[M+Na]^+$, found 970.4520.

Synthesis of **366**

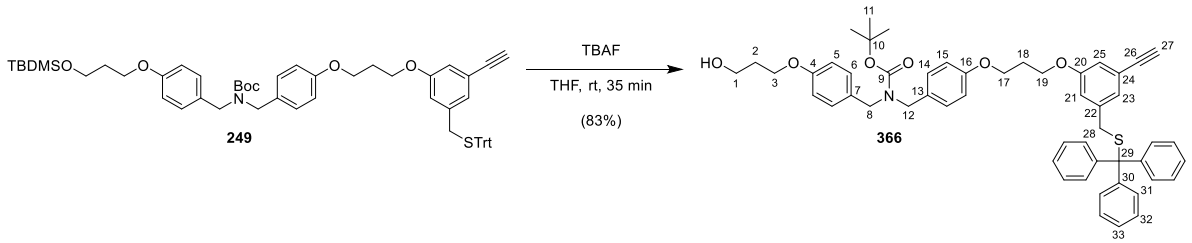

To a solution of **249** (491.2 mg, 518 µmol) in dry degassed THF (5 mL, 0.1 M) was added TBAF (1.0 M in THF, 0.78 mL, 777 µmol) at room temperature and the reaction was stirred for 35 minutes. The reaction was quenched by the addition of saturated aqueous $NaHCO_3$ (15 mL). The biphasic mixture was extracted with CH_2Cl_2 (3 × 25 mL). The combined organic layers were washed with brine and dried over Na_2SO_4, filtered, and concentrated *in vacuo*. The residue was purified by flash chromatography (SiO_2, CH_2Cl_2/ MeOH, 99:1) to afford **366** (358 mg, 83%) as a colourless solid.

^{1}H NMR (600 MHz, $CDCl_3$) δ 7.45 (d, J = 7.4 Hz, 6H, H-31), 7.30 (t, J = 7.7 Hz, 6H, H-32), 7.22 (t, J = 7.3 Hz, 3H, H-33), 7.14 (s, 2H, H-6/14), 7.10 (s, 2H, H-6/14), 6.89 – 6.83 (m, 6H, H-5, H-15, H-23 and H-25), 6.65 (s, 1H, H-21), 4.32 (s, 2H, H-8/12), 4.23 (s, 2H, H-8/12), 4.12 (t, J = 5.9 Hz, 4H, H-3 and H-17/19), 4.09 (t, J = 6.1 Hz, 2H, H-17/19), 3.87 (q, J = 5.7 Hz, 2H, H-1), 3.24 (s, 2H, H-28), 3.02 (s, 1H, H-27), 2.23 (p, J = 5.9 Hz, 2H, H-18), 2.05 (p, J = 5.9 Hz, 2H, H-2), 1.73 (t, J = 5.3 Hz, 1H, C-1 OH), 1.50 (s, 9H, H-11).

^{13}C NMR (151 MHz, $CDCl_3$) δ 158.72 (C-20), 158.19 (C-4/16), 158.12 (C-4/16), 156.09 (C-9), 144.66 (C-30), 138.98 (C-22), 130.50 (C-7/13), 130.33 (C-7/13), 129.72 (C-31), 129.57 (C-6/14), 128.95 (C-6/14), 128.13 (C-32), 126.92 (C-33), 125.54 (C-23), 123.14 (C-24), 116.71 (C-21), 116.42 (C-25), 114.59 (C-5 and C-15), 83.49 (C-26), 80.06 (C-10), 77.16 (C-27, *overlapped with solvent peak*), 67.62 (C-29), 66.01 (C-3), 64.63 (C-17/19), 64.42 (C-17/19), 60.79 (C-1), 48.44 (C-8/12), 48.10 (C-8/12), 36.72 (C-28), 32.11 (C-2), 29.35 (C-18), 28.64 (C-11).

HRMS (HESI$^+$): Calculated for $C_{53}H_{55}O_6NNaS$: 856.3642 $[M+Na]^+$, found 856.3619.

Synthesis of **250**

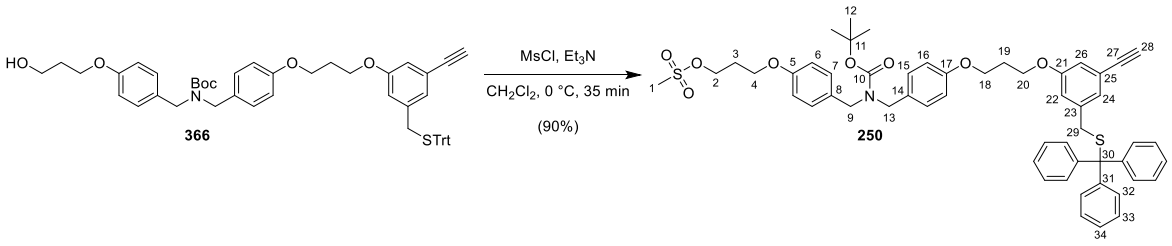

To a solution of **366** (354.0 mg, 424 µmol) in dry CH_2Cl_2 (2 mL, 0.2 M) was added MsCl (0.05 mL, 646 µmol) and triethylamine (0.06 mL, 424 µmol) sequentially at 0 °C and the reaction was stirred for 35 minutes. The reaction was quenched with saturated aqueous NH_4Cl (15 mL) and the biphasic mixture was extracted with CH_2Cl_2 (3 × 15 mL). The combined organic layers were washed with brine and dried over Na_2SO_4, filtered, and concentrated *in vacuo* to give **250** (347 mg, 90%) as a colourless solid.

^{1}H NMR (600 MHz, $CDCl_3$) δ 7.45 (d, J = 7.4 Hz, 6H, H-32), 7.30 (t, J = 7.7 Hz, 6H, H-33), 7.22 (t, J = 7.3 Hz, 3H, H-34), 7.15 (s, 2H, H-7/15), 7.10 (s, 2H, H-7/15), 6.89 – 6.82 (m, 6H, H-6, H-16, H-24 and H-26), 6.65 (s, 1H, H-22), 4.45 (t, J = 6.1 Hz, 2H, H-2), 4.32 (s, 2H, H-9/13), 4.23 (s, 2H, H-9/13), 4.12 (t, J = 6.1 Hz, 2H, H-18), 4.11 – 4.07 (m, 4H, H-4 and H-20), 3.24 (s, 2H, H-29), 3.02 (s, 1H, H-28), 3.00 (s, 3H, H-1), 2.23 (p, J = 5.9 Hz, 4H, H-3 and H-19), 1.50 (s, 9H, H-12).

^{13}C NMR (151 MHz, $CDCl_3$) δ 158.72 (C-21), 158.21 (C-17), 157.84 (C-5), 156.08 (C-10), 144.66 (C-31), 138.98 (C-23), 130.76 (C-8), 130.28 (C-14), 129.72 (C-32), 129.58 (C-7/15), 129.02 (C-7/15), 128.13 (C-33), 126.92 (C-34), 125.54 (C-24), 123.14 (C-25), 116.70 (C-22), 116.42 (C-26), 114.61 (C-6/16), 114.56 (C-6/16), 83.49 (C-27), 80.09 (C11-), 77.16 (C-28), 67.62 (C-30), 66.90 (C-2), 64.62 (C-20), 64.42 (C-18), 63.32 (C-4), 48.50 (C-9/13), 48.09 (C-9/13), 37.40 (C-1), 36.72 (C-29), 29.35 (C-3/19), 29.27 (C-3/19), 28.64 (C-12).

HRMS (HESI$^+$): Calculated for $C_{54}H_{57}O_8NNaS_2$: 934.3418 $[M+Na]^+$, found 934.3388.

Synthesis of **251**

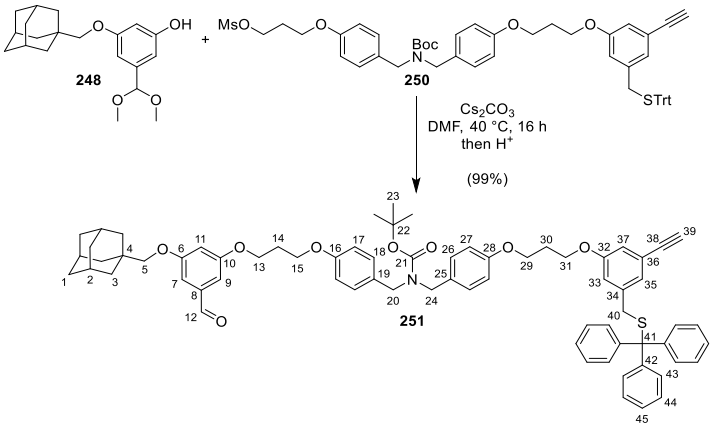

To a solution of **250** (347.0 mg, 380 µmol) and **248** (179.6 mg, 540 µmol) in dry DMF (10 mL, 38 mM) was added Cs_2CO_3 (371.4 mg, 1.14 mmol) and the reaction mixture was heated to 40 °C and stirred for 16 hours. The reaction mixture was cooled to room temperature and quenched with distilled water. (25 mL) The biphasic mixture was extracted with CH_2Cl_2 (3 × 25 mL). The combined organic layers were washed with brine and dried over Na_2SO_4, filtered, and concentrated *in vacuo*. The residue was purified by flash chromatography (SiO_2, CH_2Cl_2/ MeOH, 99:1, then petroleum ether/ EtOAc, 4:1) to afford **251** (417 mg, 99%) as a colourless solid.

^{1}H NMR (600 MHz, CD_2Cl_2) δ 9.87 (s, 1H, H-12), 7.45 (d, J = 7.4 Hz, 6H, H-43), 7.31 (t, J = 7.7 Hz, 6H, H-44), 7.24 (t, J = 7.3 Hz, 3H, H-45), 7.12 (s, 4H, H-18 and H-26), 7.00 (d, J = 2.2 Hz, 2H, H-7 and H-9), 6.88 – 6.85 (m, 5H, H-17, H-27 and H-37), 6.83 (s, 1H, H-35), 6.75 (t, J = 2.2 Hz, 2H, H-11), 6.65 (s, 1H, H-33), 4.27 (s, 2H, H-20/24), 4.21 (t, J = 6.2 Hz, 4H, H-20/24 and H-13), 4.15 (t, J = 6.1 Hz, 2H, H-15), 4.12 (t, J = 6.1 Hz, 2H, H-29), 4.09 (t, J = 6.0 Hz, 2H, H-31), 3.55 (s, 2H, H-5), 3.24 (s, 2H, H-40), 3.09 (s, 1H, H-39), 2.26 (p, J = 6.1 Hz, 2H, H-14), 2.22 (p, J = 6.1 Hz, 2H, H-30), 2.00 (s, 3H, H-2), 1.78 – 1.69 (m, 6H, H-3), 1.67 – 1.65 (m, 6H, H-1), 1.47 (s, 9H, H-23).

^{13}C NMR (151 MHz, CD_2Cl_2) δ 192.27 (C-12), 161.75 (C-6), 160.93 (C-10), 159.10 (C-32), 158.49 (C-28), 156.09 (C-21), 144.96 (C-42), 139.44 (C-34), 138.83 (C-8), 130.82 (C-19/26), 130.78 (C-19/26), 129.93 (C-43), 129.50 (C-18/26), 129.24 (C-18/26), 128.35 (C-44), 127.15 (C-45), 125.59 (C-35), 123.29 (C-36), 116.88 (C-33), 116.66 (C-37), 114.74 (C-17 and C-27), 108.06 (C-11), 107.91 (C-7), 107.79 (C-9), 83.51 (C-38), 80.00 (C-22), 79.08 (C-5), 77.28 (C-39), 67.82 (C-41), 65.34 (C-13), 65.04 (C-31), 64.73 (C-29), 64.69 (C-15), 48.83 (C-20/24), 48.38 (C-20/24), 39.71 (C-3), 37.43 (C-1), 36.78 (C-40), 34.09 (C-4), 29.57 (C-14 and C-30), 28.71 (C-2), 28.56 (C-23).

HRMS (HESI$^+$): Calculated for $C_{71}H_{75}O_8NNaS$: 1124.5106 $[M+Na]^+$, found 1124.5074.

Synthesis of Middle Triazolium Part 226

Synthesis of **252**

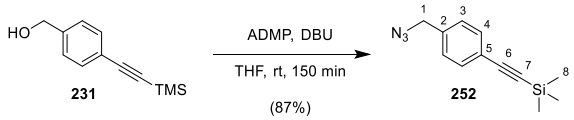

To a solution of TMS-protected 4-ethynylbenzyl alcohol **231** (406.7 mg, 2.00 mmol) and ADMP (684 mg, 2.40 mmol) in dry THF (10.0 mL, 0.2 M) at room temperature was added DBU (0.33 mL, 2.60 mmol) and the reaction was stirred for 150 minutes. The reaction was quenched by the addition of saturated aqueous NH_4Cl (10 mL). The biphasic mixture was extracted with CH_2Cl_2 (3 × 25 mL). The combined organic layers were washed with brine and dried over Na_2SO_4, filtered, and concentrated *in vacuo*. The residue was purified by flash chromatography (SiO_2, petroleum ether/ EtOAc, 19:1) to afford **252** (380 mg, 87%) as a colourless oil.

^{1}H NMR (600 MHz, $CDCl_3$) δ 7.48 (d, J = 7.9 Hz, 2H, H-4), 7.25 (s, 2H, H-3, *overlapped with solvent peak*), 4.33 (s, 2H, H-1), 0.25 (s, 9H, H-8).

^{13}C NMR (151 MHz, $CDCl_3$) δ 135.77 (C-2), 132.53 (C-4), 128.14 (C-3), 123.30 (C-5), 104.58 (C-6), 95.11 (C-7), 54.59 (C-1), 0.07 (C-8).

HRMS (APCI$^+$): Calculated for $C_{12}H_{16}N_3Si$: 230.1108 $[M+H]^+$, found 230.1112.

Synthesis of **253**

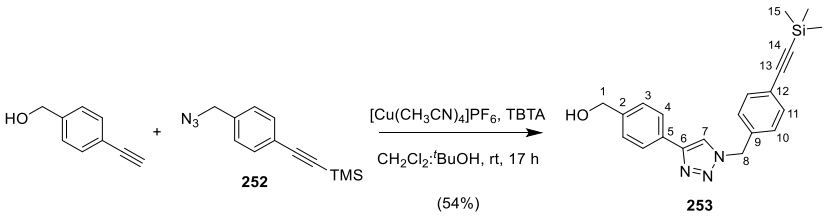

To a solution of **252** (396.8 mg, 1.73 mmol), TBTA (110.2 mg, 0.21 mmol) and 4-ethynylbenzyl alcohol (343.0 mg, 2.60 mmol) in degassed CH_2Cl_2 (8 mL) and *t*-BuOH (2 mL) was added $[Cu(CH_3CN)_4]PF_6$ (64.5 mg, 0.17 mmol) and the reaction was stirred at room temperature for 17 hours. The reaction mixture was concentrated *in vacuo* and purified by flash chromatography (SiO_2, petroleum ether/ EtOAc, 13:7) to give **253** (337 mg, 54%) as a colourless solid.

^{1}H NMR (600 MHz, $CDCl_3$) δ 7.79 (d, J = 8.2 Hz, 2H, H-4), 7.64 (s, 1H, H-7), 7.48 (d, J = 8.3 Hz, 2H, H-11), 7.41 (d, J = 8.3 Hz, 2H, H-3), 7.24 (d, J = 8.3 Hz, 2H, H-10), 5.57 (s, 2H, H-8), 4.72 (d, J = 5.0 Hz, 2H, H-1), 1.68 (s, 1H, C-1 OH), 0.24 (s, 9H, H-15).

^{13}C NMR (151 MHz, $CDCl_3$) δ 148.21 (C-6), 141.02 (C-2), 134.86 (C-9), 132.90 (C-11), 129.95 (C-5), 128.11 (C-10), 127.57 (C-3), 126.19 (C-4), 123.98 (C-12), 119.57 (C-7), 104.17 (C-13), 95.73 (C-14), 65.23 (C-1), 54.06 (C-8), 0.03 (C-15).

HRMS (HESI$^+$): Calculated for $C_{21}H_{24}ON_3Si$: 362.1683 $[M+H]^+$, found 362.1672.

Synthesis of **367**

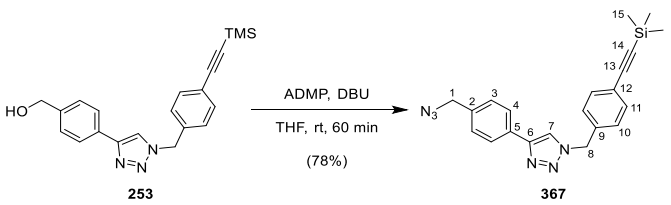

To a solution of **253** (332.5 mg, 920 µmol) and ADMP (314.7 mg, 1.10 mmol) in dry THF (4.6 mL, 0.2 M) at room temperature was added DBU (0.18 mL, 1.20 mmol) and the reaction was stirred for 60 minutes. The reaction was quenched by the addition of saturated aqueous NH_4Cl (15 mL). The biphasic mixture was extracted with CH_2Cl_2 (3 × 15 mL). The combined organic layers were washed with brine and dried over Na_2SO_4, filtered, and concentrated *in vacuo*. The residue was purified by flash chromatography (SiO_2, petroleum ether/ EtOAc, 7:3) to afford **367** (278 mg, 78%) as a colourless solid.

^{1}H NMR (600 MHz, $CDCl_3$) δ 7.82 (d, J = 7.7 Hz, 2H, H-4), 7.66 (s, 1H, H-7), 7.48 (d, J = 7.8 Hz, 2H, H-11), 7.36 (d, J = 7.7 Hz, 2H, H-3), 7.23 (d, J = 7.8 Hz, 2H, H-10), 5.57 (s, 2H, H-8), 4.36 (s, 2H, H-1), 0.24 (s, 9H, H-15).

^{13}C NMR (151 MHz, $CDCl_3$) δ 147.92 (C-6), 135.43 (C-2), 134.80 (C-9), 132.83 (C-11), 130.62 (C-5), 128.87 (C-3), 128.01 (C-10), 126.25 (C-4), 124.01 (C-12), 119.74 (C-7), 104.15 (C-13), 95.75 (C-14), 54.65 (C-1), 54.08 (C-8), 0.03 (C-15).

HRMS (ASAP$^+$): Calculated for $C_{21}H_{23}N_6Si$: 387.1748 $[M+H]^+$, found 387.1746.

Synthesis of **226**

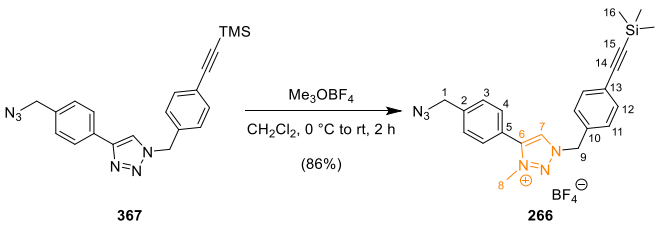

To a solution of **367** (277.9 mg, 719 µmol) in dry degassed CH_2Cl_2 (19 mL, 38 mM) at 0 °C was added trimethyloxonium tetrafluoroborate (117.0 mg, 791 µmol) and the reaction was stirred for 60 minutes. The reaction mixture was concentrated *in vacuo* and purified by flash chromatography (SiO_2, CH_2Cl_2/ MeOH, 49:1) to give **266** (303 mg, 86%, calculated for the BF_4^- salt) as a yellow solid.

^{1}H NMR (600 MHz, $CDCl_3$) δ 8.57 (s, 1H, H-7), 7.59 (d, J = 8.2 Hz, 2H, H-4), 7.49 (s, 4H, H-11 and H-12), 7.47 (d, J = 8.1 Hz, 2H, H-3), 5.73 (s, 2H, H-9), 4.44 (s, 2H, H-1), 4.22 (s, 3H, H-8), 0.24 (s, 9H, H-16).

^{13}C NMR (151 MHz, $CDCl_3$) δ 143.21 (C-6), 140.05 (C-2), 133.05 (C-12), 131.14 (C-10), 130.04 (C-4), 129.86 (C-11), 129.24 (C-3), 128.77 (C-7), 125.29 (C-13), 121.68 (C-5), 103.84 (C-14), 96.62 (C-15), 57.42 (C-9), 54.08 (C-1), 38.64 (C-8), 0.00 (C-16).

HRMS (HESI$^+$): Calculated for $C_{22}H_{25}N_6Si$: 401.1904 $[M\text{-}BF_4]^+$, found 401.1893.

Attempted Synthesis of Intermediate 255

Synthesis of **254**

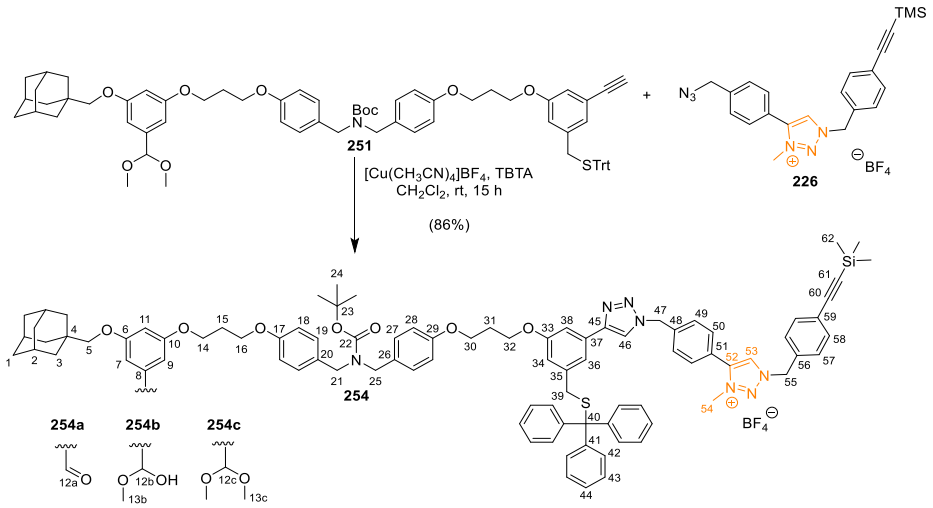

To a solution of **251** (208.3 mg, 189 µmol) and **226** (106.0 mg, 217 µmol) in degassed CH_2Cl_2 (1.5 mL, 0.1 M) were added $[Cu(CH_3CN)_4]BF_4$ (26.5 mg, 84.2 µmol) and TBTA (53.6 mg, 101 µmol) and the reaction was stirred at room temperature for 15 hours. The reaction was quenched by the addition of saturated aqueous EDTA (10 mL, pH = 7). The biphasic mixture was extracted with CH_2Cl_2 (3 × 15 mL). The combined organic layers were washed with brine and dried over Na_2SO_4, filtered, and concentrated *in vacuo*. The resultant residue was purified by size exclusion chromatography (S-X1, CH_2Cl_2) followed by flash chromatography (SiO_2, CH_2Cl_2/ MeOH, 19:1) to afford **254** (264 mg, 86%, calculated for the BF_4^- salt, mixture of **254a**:**254b**:**254c** ~ 2:1:3, ratio determined by integration of NMR signals for methine protons H-5a, H-5b and H-5c at δ = 3.54, 3.52 and 3.48 ppm respectively) as a colourless solid.

^{1}H NMR (600 MHz, $CDCl_3$) δ 9.87 (s, 2H, H-12a), 8.55 (s, 6H, H-53), 7.79 (s, 6H, H-46), 7.59 (d, J = 8.2 Hz, 12H, H-50), 7.54 – 7.49 (m, 36H, H-49, H-57 and H-58), 7.46 (d, J = 7.4 Hz, 36H, H-42), 7.30 (t, J = 7.7 Hz, 36H, H-43), 7.27 (s, 6H, H-38), 7.23 (t, J = 7.3 Hz, 18H, H-44), 7.13 (d, J = 10.0 Hz, 32H, H-19 and H-27), 6.99 (d, J = 2.3 Hz, 4H, H-7a and H-9a), 6.89 – 6.83 (m, 24H, H-18 and H-28), 6.74 (t, J = 2.3 Hz, 2H, H-11a), 6.67 (t, J = 2.3 Hz, 1H, H-11b), 6.63 (s, 6H, H-34), 6.57 (d, J = 2.1 Hz, 6H, H-7c and H-9c), 6.43 (t, J = 2.2 Hz, 3H, H-11c), 5.80 (s, 12H, H-55), 5.66 (s, 12H, H-47), 5.24 (s, 4H, H-12c), 4.29 – 4.11 (m, 90H, H-14, H-16, H-21, H-25, H-30, H-32 and H-54), 3.86 (s, 3H, H-13b), 3.54 (s, 4H, H-5a), 3.52 (s, 2H, H-5b), 3.48 (s, 6H, H-5c), 3.31 (s, 12H, H-39), 3.28 (s, 18H, H-13c), 2.28 – 2.20 (m, 24H, H-, H-15 and H-31), 2.00 (s, 18H, H-2), 1.78 – 1.68 (m, 36H, H-1), 1.65 (d, J = 4.7 Hz, 36H, H-3), 1.47 (s, 54H, H-24), 0.23 (s, 54H, H-62).

^{13}C NMR (151 MHz, $CDCl_3$) δ 192.29 (C-12a), 166.93 (C-12b), 161.75 (C-6a), 161.20 (C-6c), 160.93 (C-6b), 160.35 (C-10), 159.85 (C-33), 158.53 (C-17 and C-28), 156.10 (C-22), 148.18 (C-45), 145.01 (C-41), 143.54 (C-52), 141.04 (C-8b), 139.91 (C-48), 139.71 (C-35), 138.82 (C-8a), 133.18 (C-58), 132.13 (C-37), 131.38 (C-56), 130.74 (C-20 and C-26), 130.42 (C-50), 130.10 (C-57), 129.94 (C-42), 129.52 (C-49), 129.25 (C-19 and C-27), 129.09 (C-53), 128.35 (C-43), 127.14 (C-44), 125.60 (C-59), 122.24 (C-51), 120.74 (C-46), 119.07 (C-36), 115.60 (C-34), 114.75 (C-18 and C-28), 110.55 (C-38), 108.06 (C-11a), 107.92 (C-7b and C-9b), 107.77 (C-7a and C-9a), 106.51 (C-11b), 105.54 (C-7c), 105.27 (C-C9c), 103.91 (C-60), 103.47 (C-12c), 101.57 (C-11c), 96.85 (C-61), 80.00 (C-23), 79.08 (C-5a), 78.98 (C-5b), 78.75 (C-5c), 67.77 (C-40),

65.34 (C-14/16/30/32), 65.22 (C-14/16/30/32), 65.03 (C-14/16/30/32), 64.95 (C-14/16/30/32), 64.88 (C-14/16/30/32), 64.80 (C-14/16/30/32), 64.76 (C-14/16/30/32), 64.70 (C-14/16/30/32), 57.92 (C-55), 53.66 (C-47), 53.04 (C-13c), 52.43 (C-13b), 48.90 (C-21/25), 48.21 (C-21/25), 39.77 (C-3c), 39.73 (C-3b), 39.71 (C-3a), 39.13 (C-54), 37.48 (C-1c), 37.45 (C-1b), 37.43 (C-a), 37.11 (C-39), 34.08 (C-4a/4b/4c), 34.07 (C-4a/4b/4c), 29.69 (C-15/31), 29.66 (C-15/31), 29.60 (C-15/31), 29.57 (C-15/31), 28.75 (C-2c), 28.72 (C-2b), 28.70 (C-a), 28.56 (C-24), -0.15 (C-62).

HRMS (HESI$^+$): Calculated for $C_{93}H_{100}O_8N_7SSi$: 1502.7118 $[M\text{-}BF_4]^+$, found 1502.7087, (**254a**) Calculated for $C_{95}H_{106}O_8N_9SSi$: 1548.7537 $[M\text{-}BF_4]^+$, found 1548.7505. (**254c**)

Synthesis of **257**

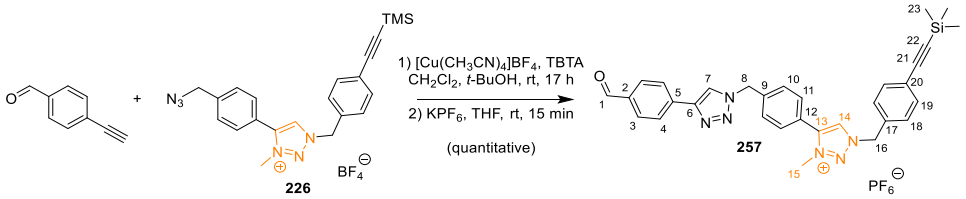

To a solution of **226** (52.3 mg, 107 µmol) and 4-ethynylbenzaldehyde (20.9 mg, 161 µmol) in degassed CH_2Cl_2 (4 mL) and *t*-BuOH (1 mL) were added $[Cu(CH_3CN)_4]BF_4$ (11.8 mg, 73.5 µmol) and TBTA (22.7 mg, 42.8 µmol) sequentially and the reaction was stirred at room temperature for 17 hours. The reaction was quenched by the addition of saturated aqueous EDTA (10 mL, pH = 7). The biphasic mixture was extracted with CH_2Cl_2 (3 × 15 mL). The combined organic layers were washed with brine and dried over Na_2SO_4, filtered, and concentrated *in vacuo*. The resultant residue was purified by flash chromatography (SiO_2, CH_2Cl_2/ MeOH, 39:1) The intermediate product was taken up in THF (10 mL) and KPF_6 (200 mg, 1.09 mmol) was added. The solution was stirred at room temperature for 15 minutes. The solvent was removed *in vacuo* and the residue was taken up in CH_2Cl_2 and filtered under reduced pressure. The filtrate was concentrated *in vacuo* and purified by size exclusion chromatography (S-X1, CH_2Cl_2) to afford **257** (73.6 mg, *assumed quantitative*) as a colourless solid.

^{1}H NMR (600 MHz, CD_2Cl_2) δ 10.01 (s, 1H, H-1), 8.29 (s, 1H, H-14), 8.02 – 7.98 (m, 3H, H-4 and H-7), 7.93 (d, J = 8.2 Hz, 2H, H-3), 7.58 – 7.52 (m, 6H, H-11, H-18 and H-19), 7.47 (d, J = 8.1 Hz, 2H, H-10), 5.75 (s, 2H, H-8), 5.70 (s, 2H, H-16), 4.23 (s, 3H, H-15), 0.24 (s, 9H, H-23).

^{13}C NMR (151 MHz, CD_2Cl_2) δ 191.91 (C-1), 147.37 (C-6), 143.69 (C-13), 139.80 (C-9), 136.49 (C-5), 136.39 (C-2), 133.30 (C-19), 130.88 (C-17), 130.64 (C-3), 130.40 (C-11), 130.04 (C-10), 129.64 (C-18), 128.54 (C-14), 126.34 (C-4), 125.81 (C-12), 122.13 (C-20), 121.83 (C-7), 103.76 (C-21), 97.07 (C-22), 58.08 (C-8), 53.84 (C-16, *overlapped with solvent peak*), 39.18 (C-15), -0.17 (C-23).

^{19}F NMR (376 MHz, CD_2Cl_2) δ -72.32 (d, J = 711.9 Hz).

^{31}P NMR (162 MHz, CD_2Cl_2) δ -144.25 (p, J = 711.3 Hz).

HRMS (HESI$^+$): Calculated for $C_{31}H_{31}ON_6Si$: 531.2323 $[M\text{-}PF_6]^+$, found 531.2312.

Synthesis of First Model Anthracene One-Barrier Pump 267·H$^+$

Synthesis of **368**

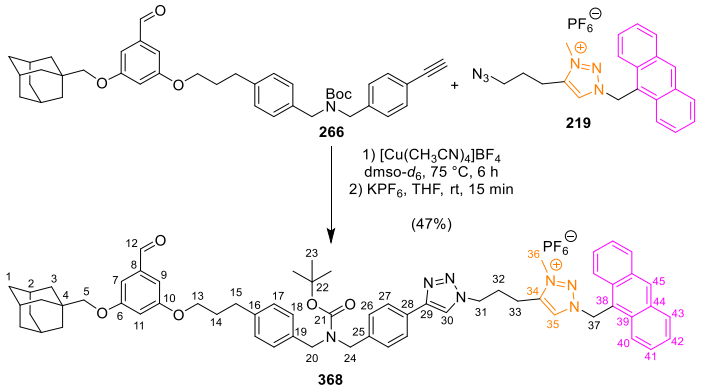

To a solution of **219** (63.6 mg, 126 µmol) and **266** (90.0 mg, 139 µmol) in degassed DMSO (3.0 mL, 42 mM) was added $[Cu(CH_3CN)_4]BF_4$ (7.9 mg, 25 µmol) and the reaction was stirred at 75 °C for 6 hours. The reaction was quenched by the addition of saturated aqueous EDTA (20 mL, pH = 7). The biphasic mixture was extracted with CH_2Cl_2 (3 × 25 mL). The combined organic layers were washed with brine and dried over Na_2SO_4, filtered, and concentrated *in vacuo*. The resultant residue was purified by flash chromatography (SiO_2, CH_2Cl_2/ MeOH, 39:1). The intermediate product was taken up in THF (10 mL) and KPF_6 (258 mg, 1.40 mmol) was added. The solution was stirred at room temperature for 15 minutes. The solvent was removed *in vacuo* and the residue was taken up in CH_2Cl_2 and filtered under reduced pressure. The filtrate was concentrated *in vacuo* and purified by size exclusion chromatography (S-X1, CH_2Cl_2) to give **368** (68.4 mg, 47%) as a yellow solid.

^{1}H NMR (600 MHz, CD_2Cl_2) δ 9.87 (s, 1H, H-12), 8.70 (s, 1H, H-45), 8.20 (d, J = 8.8 Hz, 2H, H-40), 8.14 (d, J = 8.4 Hz, 2H, H-43), 7.94 (s, 1H, H-30), 7.89 (s, 1H, H-35), 7.79 (d, J = 8.0 Hz, 2H, H-27), 7.72 – 7.68 (m, 2H, H-41), 7.60 – 7.56 (m, 2H, H-42), 7.29 (s, 2H, H-26), 7.17 (d, J = 7.9 Hz, 2H, H-17), 7.12 (s, 2H, H-18), 7.00 – 6.98 (m, 1H, H-7), 6.96 – 6.95 (m, 1H, H-9), 6.72 (t, J = 2.2 Hz, 1H, H-11), 6.60 (s, 2H, H-37), 4.48 (t, J = 6.0 Hz, 2H, H-31), 4.42 – 4.28 (m, 4H, H-20 and H-24), 4.16 (s, 3H, H-36), 3.99 (t, J = 6.2 Hz, 2H, H-13), 3.55 (s, 2H, H-5), 2.84 – 2.76 (m, 4H, H-15 and H-33), 2.37 – 2.31 (m, 2H, H-32), 2.09 (dt, J = 13.8, 6.4 Hz, 2H, H-14), 2.01 (s, 3H, H-2), 1.79 – 1.69 (m, 6H, H-1), 1.67 – 1.66 (m, 6H, H-3), 1.46 (s, 9H, H-23).

^{13}C NMR (151 MHz, CD_2Cl_2) δ 192.33 (C-12), 161.74 (C-6), 161.07 (C-10), 156.14 (C-21), 148.17 (C-29), 143.74 (C-34), 140.87 (C-16), 139.00 (C-26), 138.81 (C-8), 136.14 (C-19), 131.98 (C-45), 131.74 (C-44), 131.43 (C-39), 130.11 (C-43), 129.62 (C-28), 129.09 (C-41), 128.98 (C-17), 128.61 (d, J = 39.0 Hz, C-26), 128.16 (d, J = 27.7 Hz, C-18), 127.91 (C-35), 126.13 (C-42), 126.02 (C-27), 122.57 (C-40), 121.00 (C-30), 120.06 (C-38), 108.08 (C-11), 107.85 (C-7), 107.71 (C-9), 80.24 (C-22), 79.08 (C-5), 67.74 (C-13), 50.58 (C-37), 49.79 (C-20/24), 49.43 (C-20/24), 49.03 (C-31), 39.72 (C-3), 38.35 (C-36), 37.43 (C-1), 34.09 (C-4), 32.01 (C-15), 31.14 (C-14), 28.71 (C-2), 28.51 (C-23), 27.28 (C-32), 20.97 (C-33).

^{19}F NMR (376 MHz, CD_2Cl_2) δ -72.91 (d, J = 711.3 Hz).

^{31}P NMR (162 MHz, CD_2Cl_2) δ -144.47 (hept, J = 711.2 Hz).

HRMS (HESI$^+$): Calculated for $C_{63}H_{70}O_5N_7$: 1004.5433 $[M\text{-}PF_6]^+$, found 1004.5410.

Synthesis of **267**·H⁺

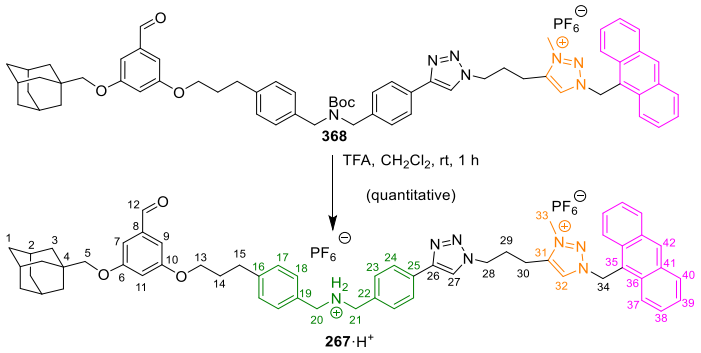

To a solution of **368** (19.9 mg, 17.3 µmol) in dry CH_2Cl_2 (2 mL, 10 mM) was added TFA (0.40 mL, 5.12 mmol) at room temperature and the reaction was stirred for 60 minutes. The reaction mixture was concentrated *in vacuo*. The residue was resuspended in PhMe (5 mL) and concentrated *in vacuo* under high vacuum. The last step was repeated two times to afford **267**·H⁺ (20.7 mg, *assumed quantitative*) as a colourless solid.

Note: Due to incomplete removal of TFA after deprotection of compound **267**·H⁺ the ^{19}F NMR spectrum shows both TFA^- and PF_6^- anions in a ratio of 20:80 as determined by integration.

^{1}H NMR (600 MHz, CD_3CN) δ 9.86 (s, 1H, H-12), 8.83 (s, 2H, C-20/21 NH_2^+), 8.78 (s, 1H, H-42), 8.28 (d, J = 8.9 Hz, 2H, H-37), 8.18 (d, J = 8.5 Hz, 2H, H-40), 8.08 (s, 1H, H-27), 7.98 (s, 1H, H-32), 7.85 (d, J = 8.2 Hz, 2fH, H-24), 7.69 – 7.65 (m, 2H, H-38), 7.62 – 7.58 (m, 2H, H-39), 7.56 (d, J = 8.2 Hz, 2H, H-23), 7.41 (d, J = 8.1 Hz, 2H, H-18), 7.29 (d, J = 8.1 Hz, 2H, H-17), 7.01 (dd, J = 2.2, 1.2 Hz, 1H, H-7), 6.97 (dd, J = 2.2, 1.2 Hz, 1H, H-9), 6.74 (t, J = 2.3 Hz, 1H, H-11), 6.64 (s, 2H, H-34), 4.40 (t, J = 6.6 Hz, 2H, H-28), 4.19 (s, 2H, H-21), 4.16 (s, 2H, H-20), 4.01 (d, J = 4.3 Hz, 5H, H-13 and H-33), 3.58 (s, 2H, H-5), 2.83 – 2.80 (m, 2H, H-15), 2.73 – 2.70 (m, 2H, H-30), 2.17 (dt, J = 14.2, 6.9 Hz, 2H, H-29), 2.10 – 2.04 (m, 2H, H-14), 1.99 (s, 3H, H-2), 1.80 – 1.68 (m, 6H, H-1), 1.68 – 1.65 (m, 6H, H-3).

^{13}C NMR (151 MHz, CD_3CN) δ 193.29 (C-12), 162.36 (C-6), 161.67 (C-10), 147.43 (C-16), 144.53 (C-31), 144.20 (C-26), 139.68 (C-8), 132.86 (C-25), 132.43 (C-41), 132.09 (C-36/42), 132.08 (C-36/42), 131.87 (C-22 and C-23), 131.28 (C-18), 130.52 (C-40), 129.99 (C-17), 129.72 (C-19), 129.04 (C-38), 128.79 (C-32), 126.69 (C-24), 126.64 (C-39), 123.96 (C-37), 122.35 (C-27), 122.00 (C-35), 108.55 (C-7), 108.33 (C-11), 108.17 (C-9), 79.44 (C-5), 68.28 (C-13), 51.58 (C-20), 51.41 (C-21), 50.69 (C-34), 49.60 (C-28), 39.96 (C-3), 38.54 (C-33), 37.72 (C-1), 34.52 (C-4), 32.29 (C-15), 31.27 (C-14), 29.15 (C-2), 27.94 (C-29), 21.00 (C-30).

^{19}F NMR (376 MHz, CD_2Cl_2) δ -72.66 (d, J = 711.8 Hz), -75.63 (TFA).

^{31}P NMR (162 MHz, CD_2Cl_2) δ -144.50 (hept, J = 711.4 Hz).

HRMS (HESI⁺): Calculated for $C_{58}H_{62}O_3N_7$: 904.4909 $[M-H]^+$, found 904.4895.

Synthesis of Glycol-Functionalized Hydrazide 269

Synthesis of **369**

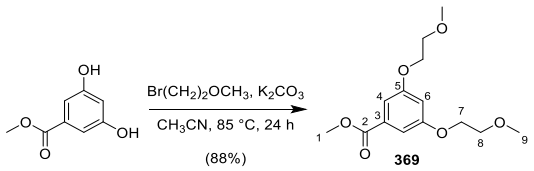

To a suspension of 1-bromo-2-methoxyethane (4.20 mL, 44.6 mmol) and 3,5-dihydroxybenzoate (3.00 g, 17.8 mmol) in CH_3CN (180 mL, 0.1 M) was added K_2CO_3 (granulate, 7.40 g, 53.5 mmol) and the reaction mixture was heated to reflux (heating set to 85 °C; using a reflux condenser and drying tube charged with $CaCl_2$) for 24 hours. The reaction mixture was cooled to room temperature and the solvent removed *in vacuo*. The resultant residue was purified by flash chromatography (SiO_2, petroleum ether/ EtOAc, 3:1) give **369** (4.44 g, 88%) as a colourless liquid.

^{1}H NMR (600 MHz, $CDCl_3$) δ 7.21 (d, J = 2.2 Hz, 2H, H-4), 6.73 (t, J = 2.2 Hz, 1H, H-6), 4.15 – 4.10 (m, 4H, H-7), 3.89 (s, 3H, H-1), 3.75 (dd, J = 5.4, 3.7 Hz, 4H, H-8), 3.45 (s, 6H, H-9).

^{13}C NMR (151 MHz, $CDCl_3$) δ 166.92 (C-2), 159.85 (C-5), 132.01 (C-3), 108.18 (C-4), 106.99 (C-6), 70.98 (C-8), 67.68 (C-7), 59.38 (C-9), 52.38 (C-1).

HRMS (HESI$^+$): Calculated for $C_{14}H_{21}O_6$: 285.1333 $[M+H]^+$, found 285.1334.

Synthesis of **269**

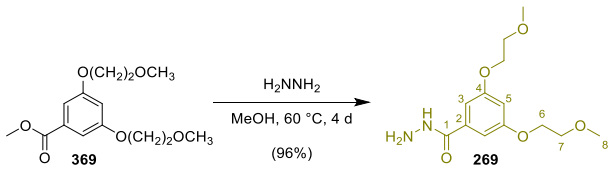

To a solution of **369** (5.97 g, 21.0 mmol) in MeOH (100 mL, 0.2 M) was added hydrazine (monohydrate, 1.53 mL, 31.5 mmol) and the reaction mixture was heated to reflux (heating set to 60 °C; using a reflux condenser) for 3 days. The reaction mixture was cooled to room temperature and the solvent removed *in vacuo*. The resultant residue was purified by flash chromatography (SiO_2, CH_2Cl_2/ MeOH, 19:1) give **269** (5.43 g, 96%) as a colourless solid.

^{1}H NMR (600 MHz, $CDCl_3$) δ 7.26 (s, C-1 NH, *overlapped with solvent peak*), 6.88 (d, *J* = 2.2 Hz, 2H, H-3), 6.67 (t, *J* = 2.2 Hz, 1H, H-5), 4.12 (dd, *J* = 5.3, 3.9 Hz, 4H, H-6), 4.06 (s, 2H, C-1 NH_2), 3.74 (dd, *J* = 5.3, 3.8 Hz, 4H, H-7), 3.45 (s, 6H, H-8).

^{13}C NMR (151 MHz, $CDCl_3$) δ 168.58 (C-1), 160.23 (C-4), 134.76 (C-2), 105.77 (C-3), 105.23 (C-5), 70.98 (C-7), 67.72 (C-6), 59.39 (C-8).

HRMS (ASAP$^+$): Calculated for $C_{13}H_{21}O_5N_2$: 285.1445 $[M+H]^+$, found 285.1444.

Synthesis of DBA Alkyne Fragment 277

Synthesis of pent-4-yn-1-yl tosylate

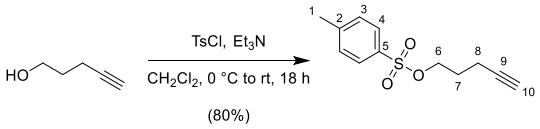

To a solution of 4-pentyn-1-ol (2.20 mL, 23.8 mmol) in dry CH_2Cl_2 (150 mL, 0.2 M) was added TsCl (5.44 g, 28.5 mmol) and triethylamine (6.60 mL, 47.6 mmol) sequentially at 0 °C and the reaction was stirred for 25 minutes. The reaction was warmed to room temperature and stirred for 18 hours. The reaction mixture was quenched with distilled water (50 mL) and the biphasic mixture was extracted with CH_2Cl_2 (3 × 75 mL). The combined organic layers were washed with brine and dried over Na_2SO_4, filtered, and concentrated *in vacuo.* The resultant residue was purified by flash chromatography (SiO_2, petroleum ether/ EtOAc, 17:3) give 4-yn-1-yl tosylate (4.56 g, 80%) as a colourless liquid.

^{1}H NMR (600 MHz, $CDCl_3$) δ 7.80 (d, *J* = 8.2 Hz, 2H, H-3), 7.35 (d, *J* = 8.2 Hz, 2H, H-4), 4.15 (t, *J* = 6.1 Hz, 2H, H-6), 2.45 (s, 3H, H-1), 2.26 (td, *J* = 6.9, 2.6 Hz, 2H, H-8), 1.90 – 1.82 (m, 3H, H-7 and H-10).

^{13}C NMR (151 MHz, $CDCl_3$) δ 144.95 (C-2), 133.07 (C-5), 130.00 (C-3), 128.09 (C-4), 82.25 (C-9), 69.57 (C-10), 68.85 (C-6), 27.85 (C-7), 21.80 (C-1), 14.84 (C-8).

HRMS (ASAP$^+$): Calculated for $C_{12}H_{15}O_3S$: 239.0736 $[M+H]^+$, found 239.0742.

Synthesis of **275**

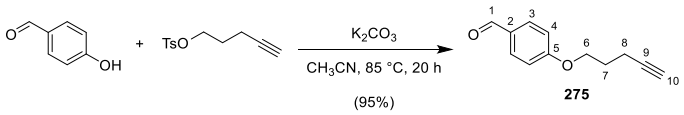

To a solution of 4-yn-1-yl tosylate (3.88 g, 16.3 mmol) and 4-hydroxybenzaldehyde (2.39 g, 19.5 mmol) in CH_3CN (150 mL, 0.1 M) was added K_2CO_3 (granulate, 6.75 g, 48.8 mmol) and the reaction mixture was heated to reflux (heating set to 85 °C; using a reflux condenser and drying tube charged with $CaCl_2$) for 20 hours. The reaction mixture was cooled to room temperature and the solvent removed *in vacuo*. The crude was resuspended in $CHCl_3$, filtrated through a plug of celite and the residue washed with additional $CHCl_3$. (150 mL in total) The combined organic phases were concentrated *in vacuo* to give **275** (2.91 g, 95%) as a colourless solid.

^{1}H NMR (600 MHz, $CDCl_3$) δ 9.89 (s, 1H, H-1), 7.84 (d, *J* = 8.7 Hz, 2H, H-3), 7.01 (d, *J* = 8.7 Hz, 2H, H-4), 4.17 (t, *J* = 6.1 Hz, 2H, H-6), 2.43 (td, *J* = 6.9, 2.6 Hz, 3H, H-8), 2.04 (p, *J* = 6.5 Hz, 2H, H-7), 1.99 (t, *J* = 2.6 Hz, 1H, H-10).

^{13}C NMR (151 MHz, $CDCl_3$) δ 190.95 (C-1), 164.09 (C-5), 132.15 (C-3), 130.13 (C-2), 114.92 (C-4), 83.19 (C-9), 69.32 (C-10), 66.63 (C-6), 28.06 (C-7), 15.24 (C-8).

HRMS (ASAP$^+$): Calculated for $C_{12}H_{13}O_2$: 189.0910 $[M+H]^+$, found 189.0909.

Synthesis of **370**

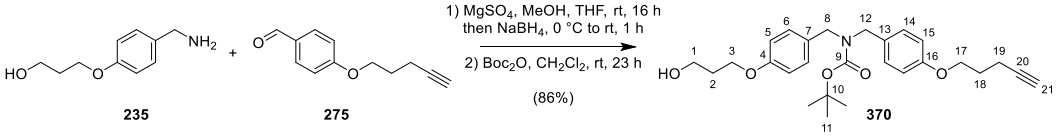

To a solution of **235** (2.33 g, 12.9 mmol) and **275** (2.91 g, 15.5 mmol) in dry MeOH (111 mL) and dry THF (14 mL, 0.1 M in total) was added $MgSO_4$ (anhydrous, *excess*) at room temperature and the reaction was stirred for 16 hours. The reaction mixture ware cooled to 0 °C and $NaBH_4$ (99%, 1.95 g, 51.6 mmol) was added dropwise. The reaction was stirred for 45 minutes, warmed to room temperature, and stirred for 25 minutes. Next, the reaction was quenched with distilled water (*approx.* 5 mL) and filtered through a plug of celite and the residue washed with additional CH_2Cl_2. The combined organic phases were dried over Na_2SO_4, filtered, and concentrated *in vacuo.* The residue was resuspended in PhMe (20 mL) and concentrated *in vacuo* under high vacuum. The last step was repeated two times.

To a suspension of the crude in dry CH_2Cl_2 (100 mL, 0.1 M) was Boc anhydride (2.0 M in THF, 7.1 mL, 14.2 mmol) at room temperature and the reaction was stirred for 23 hours. The resultant mixture was evaporated from SiO_2 and purified by flash chromatography (SiO_2, petroleum ether/ EtOAc, 7:3) give **370** (5.03 g, 86%) as a colourless oil.

^{1}H NMR (600 MHz, $CDCl_3$) δ 7.14 (s, 2H, H-6/14), 7.10 (s, 2H, H-6/14), 6.87 – 6.85 (m, 4H, H-5 and H-15), 4.32 (s, 2H, H-8/12), 4.24 (s, 2H, H-8/12), 4.12 (t, *J* = 5.9 Hz, 2H, H-3), 4.06 (t, *J* = 6.1 Hz, 2H, H-17), 3.87 (q, *J* = 5.7 Hz, 2H, H-1), 2.41 (td, *J* = 7.0, 2.6 Hz, 2H, H-19), 2.05 (p, *J* = 5.9 Hz, 2H, H-2), 2.00 (p, *J* = 6.8 Hz, 2H, H-18), 1.97 (t, *J* = 2.6 Hz, 1H, H-21), 1.88 – 1.81 (m, 1H, C-1 OH), 1.50 (s, 9H, H-11).

^{13}C NMR (151 MHz, $CDCl_3$) δ 158.27 (C-16), 158.14 (C-4), 156.08 (C-9), 130.48 (C-7/13), 130.29 (C-7/13), 129.52 (C-6/14), 128.92 (C-6/14), 114.64 (C-5/15), 114.61 (C-5/15), 83.63 (C-20), 80.06 (C-10), 68.99 (C-21), 66.30 (C-17), 65.96 (C-3), 60.67 (C-1), 48.48 (C-8/12), 48.15 (C-8/12), 32.13 (C-2), 28.63 (C-11), 28.33 (C-18), 15.32 (C-19).

HRMS ($HESI^+$): Calculated for $C_{27}H_{35}O_5NNa$: 476.2407 $[M+Na]^+$, found 476.2394.

Synthesis of **277**

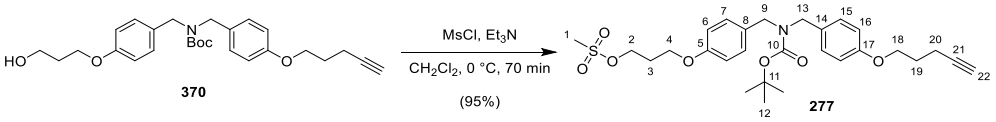

To a solution of **370** (2.73 g, 6.03 mmol) in dry CH_2Cl_2 (20 mL, 0.3 M) was added MsCl (0.75 mL, 9.64 mmol) and triethylamine (0.92 mL, 6.63 mmol) sequentially at 0 °C and the reaction was stirred for 70 minutes. The reaction was quenched with distilled water (15 mL) and the biphasic mixture was extracted with CH_2Cl_2 (3 × 25 mL). The combined organic layers were washed with brine and dried over Na_2SO_4, filtered, and concentrated *in vacuo* to give **277** (3.05 g, 95%) as a colourless oil.

^{1}H NMR (600 MHz, $CDCl_3$) δ 7.15 (s, 2H, H-7/15), 7.11 (s, 2H, H-7/15), 6.88 – 6.83 (m, 4H, H-6 and H-16), 4.45 (t, *J* = 6.1 Hz, 2H, H-2), 4.32 (s, 2H, H-9/13), 4.24 (s, 2H, H-9/13), 4.11 – 4.04 (m, 4H, H-4 and H-18), 3.00 (s, 3H, H-1), 2.41 (td, *J* = 7.0, 2.6 Hz, 2H, H-20), 2.23 (p, *J* = 5.9 Hz, 2H, H-3), 2.00 (p, *J* = 6.6 Hz, 2H, H-19), 1.97 (t, *J* = 2.6 Hz, 1H, H-22), 1.50 (s, 9H, H-12).

^{13}C NMR (151 MHz, $CDCl_3$) δ 158.30 (C-17), 157.86 (C-5), 156.08 (C-10), 130.79 (C-8/14), 130.28 (C-8/14), 129.56 (C-7/15), 129.01 (C-7/15), 114.66 (C-6/16), 114.60 (C-6/16), 83.64 (C-21), 80.09 (C-11), 69.00 (C-22), 66.89 (C-2), 66.31 (C-18), 63.37 (C-4), 48.47 (C-9/13), 48.17 (C-9/13), 37.42 (C-1), 29.30 (C-3), 28.64 (C-12), 28.34 (C-19), 15.33 (C-20).

HRMS (HESI$^+$): Calculated for $C_{28}H_{38}O_7NS$: 532.2363 $[M+H]^+$, found 532.2364.

Synthesis of Second Model Anthracene One-Barrier Pump 280·H$^+$

Synthesis of **278**

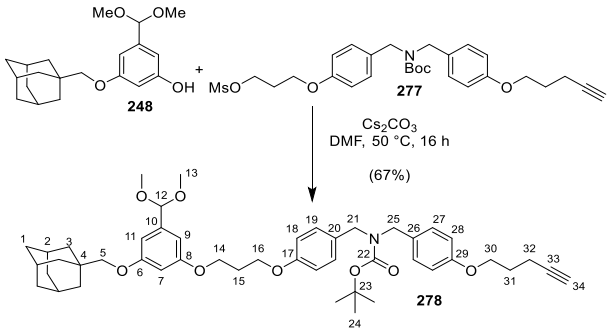

To a degassed solution of **277** (1.87 g, 3.08 mmol) and **248** (665 mg, 2.00 mmol) in dry DMF (20 mL, 0.2 M) was added Cs_2CO_3 (1.96 g, 6.00 mmol) and the reaction mixture was heated to 50 °C for 16 h under argon. The reaction mixture was cooled to room temperature and the reaction was quenched with distilled water (40 mL) and the biphasic mixture was extracted with CH_2Cl_2 (3 × 50 mL). The combined organic layers were washed with a saturated aqueous solution of LiCl (50 mL) then brine, dried over Na_2SO_4, filtered, and concentrated *in vacuo*. The resultant residue was purified by flash chromatography (SiO_2, petroleum ether/ EtOAc, 9:1) give **278** (1.02 g, 67%) as a colourless solid.

^{1}H NMR (600 MHz, $CDCl_3$) δ 7.14 (s, 2H, H-19/27), 7.10 (s, 2H, H-19/27), 6.87 – 6.84 (m, 4H, H-18 and H-28), 6.60 (s, 2H, H-9 and H-11), 6.44 (t, *J* = 2.1 Hz, 1H, H-7), 5.28 (s, 1H, H-12), 4.32 (s, 2H, H-21/25), 4.23 (s, 2H, H-21/25), 4.18 – 4.12 (m, 4H, H-14 and H-16), 4.06 (t, *J* = 6.1 Hz, 2H, H-30), 3.48 (s, 2H, H-5), 3.33 (s, 6H, H-13), 2.41 (td, *J* = 7.0, 2.5 Hz, 2H, H-32), 2.25 (p, *J* = 5.9 Hz, 2H, H-15), 2.03 – 1.98 (m, 5H, H-2 and H-31), 1.97 (t, *J* = 2.6 Hz, 1H, H-34), 1.77 – 1.66 (m, 6H, H-1), 1.65 – 1.63 (m, 6H, H-3), 1.50 (s, 9H, H-24).

^{13}C NMR (151 MHz, $CDCl_3$) δ 161.01 (C-6), 160.09 (C-8), 158.25 (C-17 and C-29), 156.09 (C-22), 140.44 (C-10), 130.29 (C-20 and C-26), 129.55 (C-19/27), 128.91 (C-19/27), 114.61 (C-18 and C-28), 105.35 (C-9/11), 104.98 (C-9/11), 103.28 (C-12), 101.62 (C-7), 83.65 (C-33), 80.04 (C-23), 78.48 (C-5), 69.00 (C-34), 66.27 (C-30), 64.60 (C-14 and C-16), 53.01 (C-13), 48.41 (C-21/25), 48.07 (C-21/253), 39.62 (C-3), 37.28 (C-1), 33.89 (C-4), 29.47 (C-15), 28.65 (C-24), 28.33 (C-2), 15.33 (C-32).

HRMS (HESI$^+$): Calculated for $C_{47}H_{61}O_8NNa$: 790.4289 $[M+Na]^+$, found 790.4254.

Synthesis of **279**

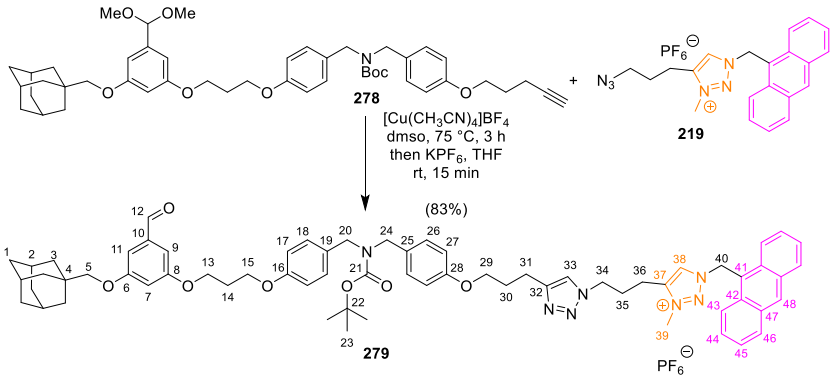

To a solution of **219** (80.0 mg, 159 µmol) and **278** (146.8 mg, 191 µmol) in degassed DMSO (3.0 mL, 0.1 M) was added $[Cu(CH_3CN)_4]BF_4$ (10.0 mg, 32.0 µmol) and the reaction was stirred at 75 °C for 3 hours. The reaction was quenched by the addition of saturated aqueous EDTA (10 mL, pH = 7). The biphasic mixture was extracted with CH_2Cl_2 (3 × 25 mL). The combined organic layers were washed with brine and dried over Na_2SO_4, filtered, and concentrated *in vacuo*. The resultant residue was purified by flash chromatography (SiO_2, CH_2Cl_2/ MeOH, 19:1) The intermediate product was then taken up in THF (10 mL) and KPF_6 (703 mg, 3.82 mmol) was added. The solution was stirred at room temperature for 15 minutes. The solvent was removed *in vacuo* and the residue was taken up in CH_2Cl_2 and filtered. The filtrate was concentrated *in vacuo* and purified by size exclusion chromatography (S-X1, CH_2Cl_2) to give **279** (161 mg, 83%) as a colourless solid.

^{1}H NMR (600 MHz, CD_2Cl_2) δ 9.86 (s, 1H, H-12), 8.70 (s, 1H, H-48), 8.27 (d, *J* = 8.8 Hz, 2H, H-43), 8.14 (d, *J* = 8.4 Hz, 2H, H-46), 7.90 (s, 1H, H-38), 7.74 – 7.69 (m, 2H, H-44), 7.60 – 7.56 (m, 2H, H-45), 7.41 (s, 1H, H-33), 7.15 – 7.07 (m, 4H, H-18 and H-25), 6.99 (d, *J* = 2.3 Hz, 2H, H-9 and H-11), 6.87 (d, *J* = 8.6 Hz, 2H, H-17), 6.82 (d, *J* = 8.2 Hz, 2H, H-27), 6.74 (t, *J* = 2.3 Hz, 1H, H-7), 6.69 (s, 2H, H-40), 4.36 (t, *J* = 6.1 Hz, 2H, H-34), 4.28 – 4.19 (m, 6H, H-13, H-20 and H-24), 4.15 (t, *J* = 6.1 Hz, 2H, H-15), 4.13 (s, 3H, H-35), 3.97 (t, *J* = 5.9 Hz, 2H, H-29), 3.54 (s, 2H, H-5), 2.82 (t, *J* = 7.6 Hz, 2H, H-31), 2.74 (s, 2H, H-36), 2.26 (p, *J* = 6.1 Hz, 4H, H-14 and H-35), 2.09 (p, *J* = 6.7 Hz, 2H, H-30), 2.01 (s, 3H, H-2), 1.80 – 1.68 (m, 6H, H-1), 1.67 – 1.65 (m, 6H, H-3), 1.47 (s, 9H, H-23).

^{13}C NMR (151 MHz, CD_2Cl_2) δ 192.28 (C-12), 161.75 (C-6), 160.93 (C-8), 158.58 (C-28), 158.49 (C-16), 156.09 (C-21), 147.93 (C-32), 143.84 (C-37), 138.81 (C-10), 131.96 (C-), 131.76 (C-48), 131.47 (C-42), 130.80 (C-19), 130.65 (C-25), 130.11 (C-46), 129.27 (C-18 and), 129.08 (C-44), 127.99 (C-38), 126.13 (C-45), 122.64 (C-43), 122.22 (C-33), 120.14 (C-41), 114.74 (C-17 and C-27), 108.05 (C-7), 107.92 (C-11), 107.77 (C-), 80.02 (C-22), 79.08 (C-5), 67.30 (C-29), 65.34 (C-13), 64.70 (C-15), 50.59 (C-40), 48.85 (C-20/24), 48.65 (C-34), 48.38 (C-20/24), 39.71 (C-3), 38.25 (C-39), 37.43 (C-1), 34.08 (C-4), 29.57 (C-14), 29.24 (C-30), 28.71 (C-2), 28.56 (C-23), 27.35 (C-35), 22.34 (C-31), 20.80 (C-36).

^{19}F NMR (471 MHz, CD_2Cl_2) -72.96 (d, *J* = 711.3 Hz).

^{31}P NMR (202 MHz, CD_2Cl_2) δ -144.56 (hept, *J* = 711.3 Hz).

HRMS (HESI$^+$): Calculated for $C_{66}H_{76}O_7N_7$: 1078.5801 $[M\text{-}PF_6]^+$, found 1078.5769.

Synthesis of **280**·H⁺

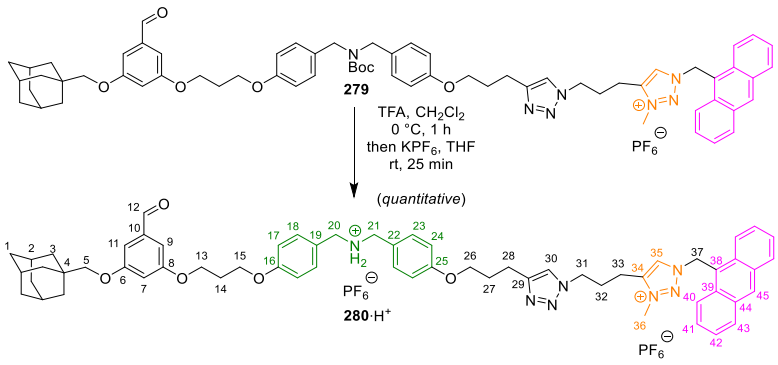

To a solution of **279** (153 mg, 125 µmol) in dry CH_2Cl_2 (14 mL, 0.1 M) was added TFA (2.9 mL, 38 mmol) at 0 °C and the reaction was stirred for 60 minutes. The reaction mixture was concentrated *in vacuo*. The residue was resuspended in PhMe (20 mL) and concentrated *in vacuo* under high vacuum. The last step was repeated two times. The residue was taken up in THF (10 mL) and KPF_6 (1.14 g, 6.20 mmol) was added. The solution was stirred at room temperature for 25 minutes. The solvent was removed *in vacuo* and the residue was taken up in CH_2Cl_2 and filtered. The filtrate was concentrated *in vacuo* to yield **280**·H⁺ (172 mg, *assumed quantitative)* as a yellow solid.

Note: Due to incomplete removal of TFA the ^{19}F NMR shows signals corresponding to both TFA and PF_6^- anions in a ratio of 36:64 as determined by integration.

^{1}H NMR (600 MHz, CD_2Cl_2) δ 9.83 (s, 1H, H-12), 9.45 (s, 2H, C20/21 NH_2^+), 8.67 (s, 1H, H-45), 8.29 (s, 1H, H-36), 8.26 (d, *J* = 8.8 Hz, 2H, H-40), 8.12 (d, *J* = 8.4 Hz, 2H, H-43), 7.70 – 7.65 (m, 2H, H-41), 7.60 – 7.54 (m, 2H, H-42), 7.40 (d, *J* = 8.2 Hz, 3H, H-18 and H-30), 7.31 (d, *J* = 8.0 Hz, 2H, H-23), 6.97 (dd, *J* = 2.1, 1.1 Hz, 1H, H-11), 6.93 (dd, *J* = 2.1, 1.1 Hz, 1H, H-9), 6.81 (d, *J* = 8.5 Hz, 2H, H-17), 6.73 (d, *J* = 8.5 Hz, 2H, H-24), 6.70 (t, *J* = 2.3 Hz, 1H, H-7), 6.56 (s, 2H, H-37), 4.31 (t, *J* = 6.2 Hz, 2H, H-31), 4.07 (t, *J* = 6.1 Hz, 2H, H-13), 4.05 (s, 2H, H-20), 4.00 (s, 3H, H-35), 3.93 (s, 2H, H-21), 3.89 (q, *J* = 6.2 Hz, 4H, H-15 and H-26), 3.53 (s, 2H, H-5), 2.84 (t, *J* = 6.4 Hz, 2H, H-28), 2.65 (t, *J* = 7.4 Hz, 2H, H-33), 2.14 (dd, *J* = 14.0, 6.8 Hz, 2H, H-32), 2.12 – 2.09 (m, 2H, H-14), 2.09 – 2.05 (m, 2H, H-27), 2.00 (s, 3H, H-2), 1.78 – 1.68 (m, 6H, H-1), 1.66 – 1.64 (m, 6H, H-3).

^{13}C NMR (151 MHz, CD_2Cl_2) δ 192.30 (C-12), 161.73 (C-6), 160.83 (C-8), 159.99 (C-16), 159.86 (C-25), 147.00 (C-29, *low S/N*), 143.44 (C-34), 138.77 (C-10), 132.10 (C-18), 131.94 (C-23), 131.73 (C-45), 131.41 (C-39), 130.02 (C-43), 128.85 (C-41), 128.57 (C-44), 126.08 (C-42), 123.31 (C-22), 123.11 (C-19), 122.81 (C-40), 120.62 (C-38), 115.10 (C-17), 115.03 (C-24), 108.05 (C-7 and C-11), 107.59 (C-9), 79.07 (C-5), 66.94 (C-26), 65.15 (C-13), 64.60 (C-15), 50.76 (C-20), 50.44 (C-21), 50.33 (C-37), 49.06 (C-31), 39.70 (C-3), 38.05 (C-36), 37.42 (C-1), 34.07 (C-4), 29.33 (C-14), 28.70 (C-2), 28.35 (C-27), 27.28 (C-32), 21.88 (C-28), 20.53 (C-33).

^{19}F NMR (471 MHz, CD_2Cl_2) δ -73.01 (d, *J* = 711.2 Hz), -75.50 (TFA).

^{31}P NMR (202 MHz, CD_2Cl_2) δ -144.49 (hept, *J* = 711.2 Hz).

HRMS (HESI⁺): Calculated for $C_{61}H_{69}O_5N_7$: 489.7675 $[M\text{-}2PF_6]^{2+}$, found 489.7681.

Improved Synthesis of Macrocycle 27C9

Synthesis of **271**

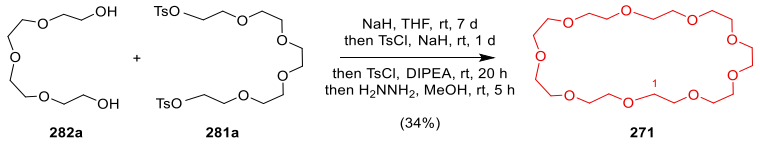

To a solution of pentaethylene glycol ditosylate**281a** (4.63 g, 8.47 mmol) and tetraethylene glycol **282a** (1.65 g, 8.50 mmol) in dry THF (424 mL, 20 mM) was added NaH (60% in mineral oil, 1.7 g, 43 mmol) dropwise over 100 minutes at room temperature and the reaction was stirred for 7 days. To the crude reaction mixture was added TsCl (1.61 g, 8.47 mmol) and NaH (60% in mineral oil, 1.7 g, 43 mmol) and the reaction was stirred for another day at room temperature. The reaction was quenched by the addition of saturated aqueous NH_4Cl (100 mL). The biphasic mixture was extracted with CH_2Cl_2 (3 × 150 mL) and then a mixture of $CHCl_3$ and *i*-PrOH (3:1, 150 mL). The combined organic layers were washed with brine and dried over Na_2SO_4, filtered, and concentrated *in vacuo*. Leftover tosylate **283** (see Figure 8.18) was removed by flash chromatography (SiO_2, CH_2Cl_2/ MeOH, 19:1) and fractions containing macrocycle **271** were further treated with TsCl (excess) and DIPEA (excess) in CH_2Cl_2 for 20 hours at room temperature. The solvent was removed *in vacuo* and excess TsCl removed by flash chromatography. (SiO_2, CH_2Cl_2/ MeOH, 19:1) The residue was dissolved in MeOH and hydrazine (monohydrate, excess) was added. The resulting reaction mixture was stirred for 5 hours at room temperature. The reaction was concentrated *in vacuo* and purified flash chromatography (SiO_2, CH_2Cl_2/ MeOH, 19:1) to give **271** (1.14 g, 34%) as a colourless liquid.

^{1}H NMR (600 MHz, $CDCl_3$) δ 3.67 (s, 36H, H-1).

^{13}C NMR (151 MHz, $CDCl_3$) δ 70.90 (C-1).

Synthesis of Third Model Anthracene One-Barrier Pump 293·H$^+$

Synthesis of **281**

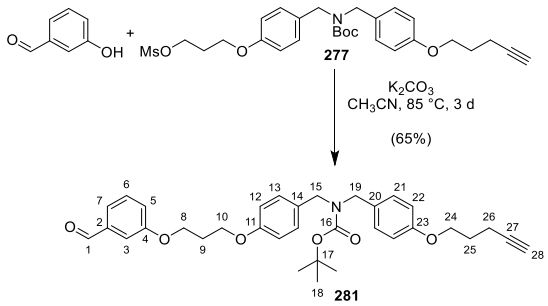

To a solution of **277** (3.05 g, 5.02 mmol) and 3-hydroxybenzaldehyde (676 mg, 5.54 mmol) in CH_3CN (50 mL, 0.1 M) was added K_2CO_3 (granulate, 2.08 g, 15.1 mmol) and the reaction mixture was heated to reflux (heating set to 85 °C; using a reflux condenser and drying tube charged with $CaCl_2$) for 3 days. The reaction mixture was cooled to room temperature and the reaction was quenched with distilled water (50 mL) and the biphasic mixture was extracted with CH_2Cl_2 (3 × 50 mL). The combined organic layers were washed with brine and dried over Na_2SO_4, filtered, and concentrated *in vacuo*. The resultant residue was purified by flash chromatography (SiO_2, petroleum ether/ EtOAc, 4:1) give **281** (1.82 g, 65%) as a colourless oil.

^{1}H NMR (600 MHz, $CDCl_3$) δ 9.97 (s, 1H, H-1), 7.47 – 7.43 (m, 2H, H-6 and H-7), 7.42 (d, *J* = 1.8 Hz, 1H, H-3), 7.19 (dt, *J* = 7.1, 2.3 Hz, 1H, H-5), 7.14 (s, 2H, H-13/21), 7.10 (s, 2H, H-13/21), 6.89 – 6.84 (m, 4H, H-12 and H-22), 4.32 (s, 2H, H-15/19), 4.26 – 4.20 (m, 4H, H-8 and H-15/19), 4.17 (t, *J* = 6.0 Hz, 2H, H-10), 4.06 (t, *J* = 6.1 Hz, 2H, H-24), 2.41 (td, *J* = 7.0, 2.6 Hz, 2H, H-26), 2.29 (p, *J* = 6.0 Hz, 2H, H-9), 2.00 (p, *J* = 6.5 Hz, 2H, H-25), 1.97 (t, *J* = 2.6 Hz, 1H, H-28), 1.50 (s, 9H, H-18).

^{13}C NMR (151 MHz, $CDCl_3$) δ 192.26 (C-1), 159.60 (C-4), 158.28 (C-23), 158.18 (C-11), 156.09 (C-16), 137.96 (C-2), 130.45 (C-14/20), 130.31 (C-14/20), 130.22 (C-6), 129.54 (C-13/21), 128.94 (C-13/21), 123.69 (C-7), 122.02 (C-5), 114.65 (C-12/22), 114.62 (C-12/22), 112.98 (C-3), 83.64 (C-27), 80.06 (C-17), 68.99 (C-28), 66.30 (C-24), 64.88 (C-8), 64.36 (C-10), 48.44 (C-15/19), 48.13 (C-15/19), 29.35 (C-9), 28.64 (C-18), 28.34 (C-25), 15.33 (C-26).

HRMS (APCI$^+$): Calculated for $C_{34}H_{40}O_6N$: 558.2850 $[M+H]^+$, found 558.2852.

Synthesis of **292** (BF_4^- salt)

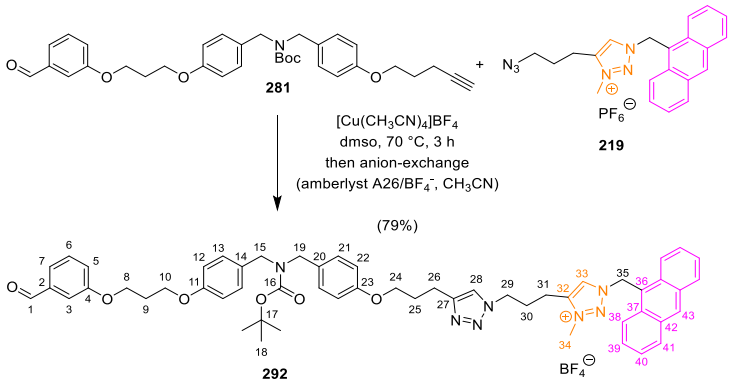

To a solution of **219** (94.5 mg, 188 µmol) and **281** (125.9 mg, 226 µmol) in degassed DMSO (3.0 mL, 0.1 M) was added $[Cu(CH_3CN)_4]BF_4$ (59.2 mg, 188 µmol) and the reaction was stirred at 70 °C for 3 hours. The reaction was quenched by the addition of saturated aqueous EDTA (10 mL, pH = 7). The biphasic mixture was extracted with CH_2Cl_2 (3 × 25 mL). The combined organic layers were washed with brine and dried over Na_2SO_4, filtered, and concentrated *in vacuo*. The resultant residue was purified by flash chromatography (SiO_2, CH_2Cl_2/ MeOH, 19:1), size exclusion chromatography (S-X1, CH_2Cl_2) and then anion-exchange chromatography (amberlyst A-26 BF_4^-, CH_3CN) to give **292** (149 mg, 79%, $BF4^-$ salt) as a beige solid.

^{1}H NMR (600 MHz, CD_2Cl_2) δ 9.94 (s, 1H, H-1), 8.66 (s, 1H, H-43), 8.33 (d, *J* = 8.9 Hz, 2H, H-38), 8.18 (s, 1H, H-28), 8.11 (d, *J* = 8.4 Hz, 2H, H-41), 7.71 – 7.67 (m, 2H, H-39), 7.58 – 7.55 (m, 2H, H-40), 7.49 (s, 1H, H-33), 7.47 – 7.43 (m, 2H, H-6 and H-7), 7.41 – 7.39 (m, 1H, H-3), 7.20 (dt, *J* = 6.2, 2.8 Hz, 1H, H-5), 7.14 – 7.08 (m, 4H, H-13 and H-21), 6.87 (d, *J* = 8.6 Hz, 2H, H-12), 6.82 (d, *J* = 8.2 Hz, 2H, H-22), 6.71 (s, 2H, H-35), 4.38 (t, *J* = 6.4 Hz, 2H, H-29), 4.28 – 4.20 (m, 6H, H-8, H-15 and H-19), 4.16 (t, *J* = 6.1 Hz, 2H, H-10), 4.09 (s, 3H, H-34), 3.96 (t, *J* = 5.8 Hz, 2H, H-24), 2.81 – 2.75 (m, 4H, H-26 and H-31), 2.31 – 2.24 (m, 4H, H-9 and H-30), 2.08 (p, *J* = 6.3 Hz, 2H, H-25), 1.47 (s, 9H, H-18).

^{11}B NMR (160 MHz, CD_2Cl_2) δ -1.08.

^{13}C NMR (151 MHz, CD_2Cl_2) δ 192.37 (C-1), 159.93 (C-4), 158.62 (C-23), 158.51 (C-11), 156.11 (C-16), 147.97 (C-32), 143.81 (C-27), 138.33 (C-2), 131.76 (C-42), 131.70 (C-43), 131.51 (C-37), 130.84 (C-14), 130.65 (C-20), 130.48 (C-6), 129.99 (C-41), 129.31 (C-13 and C-21), 128.87 (C-39), 128.47 (C-28), 126.06 (C-40), 123.47 (C-7), 122.97 (C-38), 122.40 (C-33), 121.91 (C-5), 120.79 (C-36), 114.78 (C-12 and C-22), 113.46 (C-3), 80.02 (C-17), 67.38 (C-24), 65.25 (C-8), 64.73 (C-10), 50.46 (C-35), 48.92 (C-15/19), 48.71 (C-29), 48.45 (C-15/19), 38.13 (C-34), 29.59 (C-9), 29.29 (C-25), 28.57 (C-18), 27.41 (C-30), 22.41 (C-26), 20.81 (C-31).

^{19}F NMR (471 MHz, CD_2Cl_2) δ -152.13 ($^{10}BF_4$), -152.18 (q, *J* = *approx.* 1.5 Hz, $^{11}BF_4$).

HRMS ($HESI^+$): Calculated for $C_{55}H_{60}O_6N_7$: 914.4600 $[M+BF_4]^+$, found 914.4586.

Synthesis of **292** (TFA^- salt)

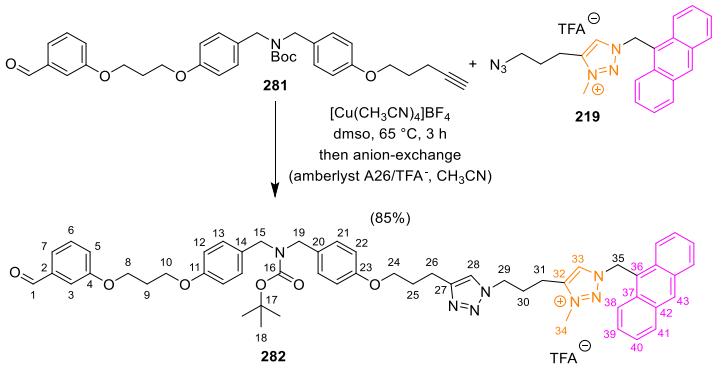

To a solution of **219** (218.7 mg, 481 µmol) and **281** (322.0 mg, 577 µmol) in degassed DMSO (3.4 mL, 0.1 M) was added $[Cu(CH_3CN)_4]PF_6$ (179.8 mg, 481 µmol) and the reaction was stirred at 65 °C for 3 hours. The reaction was quenched by the addition of saturated aqueous EDTA (10 mL, pH = 7). The biphasic mixture was extracted with CH_2Cl_2 (3 × 25 mL). The combined organic layers were washed with brine and dried over Na_2SO_4, filtered, and concentrated *in vacuo*. The resultant residue was purified by flash chromatography (SiO_2, CH_2Cl_2/ MeOH, 39:1), size exclusion chromatography (S-X1, CH_2Cl_2) and then anion-exchange chromatography (amberlyst A-26 TFA^-, CH_3CN) to give **282** (421 mg, 85%, TFA^- salt) as a colourless solid.

^{1}H NMR (600 MHz, CD_2Cl_2) δ 9.94 (s, 1H, H-1), 8.69 (s, 1H, H-43), 8.28 (d, *J* = 8.9 Hz, 2H, H-38), 8.13 (d, *J* = 8.4 Hz, 2H, H-41), 7.99 (s, 1H, H-33), 7.71 (t, *J* = 7.6 Hz, 2H, H-39), 7.58 (t, *J* = 7.3 Hz, 2H, H-40), 7.48 – 7.42 (m, 3H, H-6, H-7 and H-28), 7.40 (s, 1H, H-3), 7.20 (dt, *J* = 6.0, 2.8 Hz, 1H, H-5), 7.15 – 7.08 (m, 4H, H-13 and H-21), 6.87 (d, *J* = 8.5 Hz, 2H, H-12), 6.82 (d, *J* = 7.8 Hz, 2H, H-22), 6.70 (s, 2H, H-35), 4.36 (t, *J* = 6.0 Hz, 2H, H-29), 4.28 – 4.20 (m, 6H, H-15, H-19 and H-8), 4.16 (t, *J* = 6.0 Hz, 2H, H-10), 4.12 (s, 3H, H-34), 3.97 (s, 2H, H-24), 2.82 (t, *J* = 7.3 Hz, 2H, H-26), 2.75 (t, *J* = 6.7 Hz, 2H, H-31), 2.30 – 2.22 (m, 4H, H-9 and H-30), 2.09 (p, *J* = 7.6 Hz, 2H, H-25), 1.47 (s, 9H, H-18).

^{13}C NMR (151 MHz, CD_2Cl_2) δ 192.38, 159.95, 158.61, 158.52, 156.13, 147.83, 143.84, 138.34, 131.91, 131.78, 131.51, 130.85, 130.69, 130.48, 130.09, 129.31, 129.03, 128.16, 126.13, 123.49, 122.74, 122.31, 121.93, 120.32, 114.79, 113.46, 80.04, 67.34, 65.26, 64.74, 50.58, 48.97, 48.73, 48.46, 38.22, 29.60, 29.25, 28.58, 27.38, 22.33, 20.81.

^{19}F NMR (471 MHz, CD_2Cl_2) δ -72.96 (d, *J* = 711.4 Hz).

HRMS (HESI$^+$): Calculated for $C_{55}H_{60}O_6N_7$: 914.4600 $[M\text{-}TFA]^+$, found 914.4583.

Synthesis of **293**·H^+ ($BF4^-$ salt)

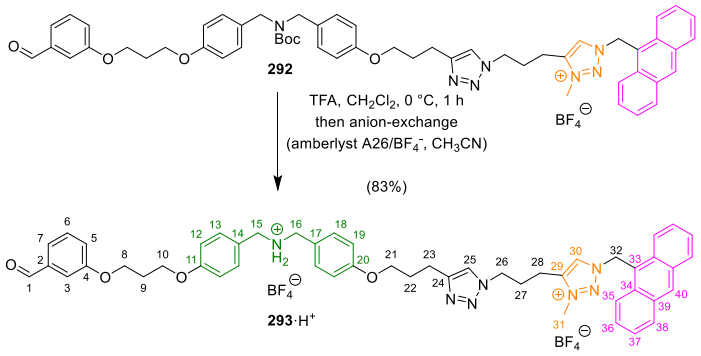

To a solution of **292** (140.6 mg, 140 µmol) in dry CH_2Cl_2 (16 mL, 0.1 M) was added TFA (3.3 mL, 42 mmol) at 0 °C and the reaction was stirred for 60 minutes. The reaction mixture was concentrated *in vacuo*. The residue was resuspended in PhMe (20 mL) and concentrated *in vacuo* under high vacuum. The last step was repeated two times. The resultant was purified by anion-exchange chromatography (amberlyst A-26 BF_4^-, CH_3CN) and then size exclusion chromatography (S-X1, CH_2Cl_2) to give **293**·H^+ (115.0 mg, 83%, $BF4^-$ salt) as a colourless solid.

Note: Due to incomplete removal of TFA the ^{19}F NMR shows ^{19}F signals corresponding to both TFA and BF_4^- anions in a ratio of 42:58 as determined by integration.

^{1}H NMR (600 MHz, CD_2Cl_2) δ 9.93 (s, 1H, H-1), 8.66 (s, 1H, H-40), 8.32 (d, *J* = 8.9 Hz, 2H, H-35), 8.18 (s, 1H, H-30), 8.10 (d, *J* = 8.4 Hz, 2H, H-38), 7.70 – 7.67 (m, 2H, H-36), 7.57 – 7.54 (m, 2H, H-37), 7.45 – 7.42 (m, 3H, H-5, H-7 and H-25), 7.38 (d, *J* = 1.9 Hz, 1H, H-3), 7.27 (d, *J* = 8.4 Hz, 2H, H-13), 7.21 (d, *J* = 8.3 Hz, 2H, H-18), 7.18 (dt, *J* = 6.1, 2.9 Hz, 1H, H-6), 6.86 (d, *J* = 8.5 Hz, 2H, H-12), 6.79 (d, *J* = 8.5 Hz, 2H, H-19), 6.68 (s, 2H, H-32), 4.34 (t, *J* = 6.5 Hz, 2H, H-26), 4.20 (t, *J* = 6.1 Hz, 2H, H-8), 4.12 (t, *J* = 6.1 Hz, 2H, H-10), 4.06 (s, 3H, H-31), 3.92 (t, *J* = 6.2 Hz, 2H, H-21), 3.75 (s, 2H, H-15), 3.71 (s, 2H, H-16), 2.77 (t, *J* = 7.5 Hz, 2H, H-23), 2.73 (t, *J* = 7.6 Hz, 2H, H-28), 2.27 – 2.21 (m, 4H, H-9 and H-27), 2.05 (p, *J* = 6.4 Hz, 2H, H-22).

^{11}B NMR (128 MHz, CD_2Cl_2) δ -1.09.

^{13}C NMR (151 MHz, CD_2Cl_2) δ 192.38 (C-1), 159.92 (C-4), 158.76 (C-20), 158.68 (C-11), 147.76 (C-24), 143.78 (C-29), 138.32 (C-2), 131.75 (C-39), 131.68 (C-40), 131.51 (C-34), 130.99 (C-14), 130.88 (C-17), 130.47 (C-25), 130.25 (C-13), 130.18 (C-18), 129.98 (C-38), 128.85 (C-36), 128.48 (C-30), 126.06 (C-37), 123.46 (C-5), 122.99 (C-35), 122.28 (C-7), 121.91 (C-6), 120.83 (C-33), 114.77 (C-12/19), 114.75 (C-12/19), 113.46 (C-3), 67.27 (C-21), 65.23 (C-8), 64.71 (C-10), 52.36 (C-15), 52.24 (C-16), 50.41 (C-32), 48.62 (C-26), 38.08 (C-31), 29.56 (C-9), 29.18 (C-22), 27.43 (C-27), 22.34 (C-23), 20.76 (C-28).

^{19}F NMR (471 MHz, CD_2Cl_2) δ -75.58 (TFA), -151.36 ($^{10}BF_4$), -151.41 ($^{11}BF_4$).

HRMS (HESI$^+$): Calculated for $C_{50}H_{52}O_4N_7$: 814.4069 $[M-H]^+$, found 814.4051.

Synthesis of **293**·H^+ (TFA^- salt)

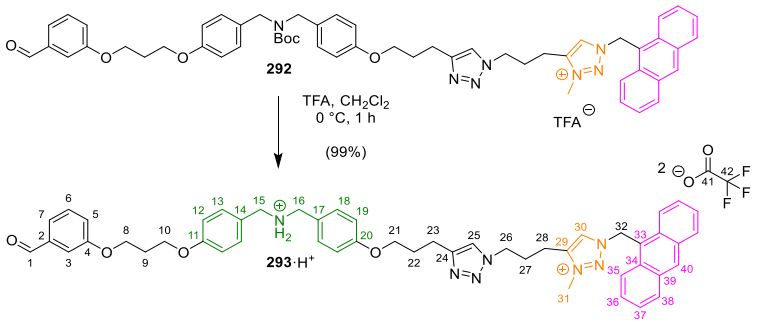

To a solution of **292** (410 mg, 399 µmol) in dry CH_2Cl_2 (48 mL, 0.1 M) was added TFA (9.5 mL, 122 mmol) at 0 °C and the reaction was stirred for 65 minutes. The reaction mixture was concentrated *in vacuo*. The residue was resuspended in PhMe (20 mL) and concentrated *in vacuo* under high vacuum. The last step was repeated two times. Finally, the residue was redissolved in CH_2Cl_2 and precipitated with Et_2O and concentrated *in vacuo* to give **293**·H^+ (412 mg, 99%, TFA^- salt) as a yellow solid.

^{1}H NMR (600 MHz, CD_2Cl_2) δ 9.91 (s, 1H, H-1), 9.21 (s, 2H, C15/16 NH_2^+), 8.67 (s, 1H, H-40), 8.25 (d, *J* = 8.9 Hz, 2H, H-35), 8.18 (s, 1H, H-30), 8.11 (d, *J* = 8.4 Hz, 2H, H-38), 7.70 – 7.65 (m, 2H, H-36), 7.59 – 7.53 (m, 2H, H-37), 7.46 (s, 1H, H-25), 7.44 – 7.41 (m, 2H, H-6 and H-7), 7.33 (d, *J* = 8.5 Hz, 3H, H-3 and H-13), 7.24 (d, *J* = 8.4 Hz, 2H, H-18), 7.16 (dq, *J* = 6.1, 3.5, 2.7 Hz, 1H, H-5), 6.84 (d, *J* = 8.6 Hz, 2H, H-12), 6.74 (d, *J* = 8.5 Hz, 2H, H-19), 6.61 (s, 2H, H-32), 4.32 (t, *J* = 6.3 Hz, 2H, H-26), 4.12 (t, *J* = 6.1 Hz, 2H, H-8), 4.04 (s, 3H, H-31), 4.03 – 3.96 (m, 4H, H-10 and H-15), 3.90 (s, 2H, H-16), 3.86 (t, *J* = 5.9 Hz, 2H, H-21), 2.80 (t, *J* = 7.3 Hz, 2H, H-23), 2.70 (t, *J* = 7.4 Hz, 2H, H-28), 2.21 – 2.12 (m, 4H, H-9 and H-27), 2.03 (p, *J* = 6.5 Hz, 2H, H-22).

^{13}C NMR (151 MHz, CD_2Cl_2) δ 192.43 (C-1), 160.82 (q, *J* = 37.2 Hz, C-41), 160.05 (C-11), 159.88 (C-20), 159.81 (C-4), 146.86 (C-24), 143.53 (C-29), 138.24 (C-2), 131.98 (C-13), 131.86 (C-18), 131.79 (C-40), 131.72 (C-39), 131.42 (C-34), 130.46 (C-6), 130.03 (C-38), 128.88 (C-36), 128.45 (C-30), 126.07 (C-37), 123.58 (C-7), 123.41 (C-25), 123.13 (C-17), 122.97 (C-14), 122.75 (C-35), 121.92 (C-5), 120.48 (C-33), 116.31 (q, *J* = 290.2 Hz, C-42), 115.17 (C-12), 115.08 (C-19), 113.26 (C-3), 66.94 (C-21), 65.03 (C-8), 64.64 (C-10), 50.69 (C-15), 50.42 (C-16), 50.39 (C-32), 49.26 (C-26), 38.07 (C-31), 29.34 (C-9), 28.45 (C-22), 27.20 (C-27), 21.74 (C-23), 20.55 (C-28).

^{19}F NMR (376 MHz, CD_2Cl_2) δ -72.59 (d, *J* = 706.4 Hz), -76.20.

HRMS (HESI$^+$): Calculated for $C_{50}H_{52}O_4N_7$: 814.4075 $[M-H]^+$, found 814.4051.

Synthesis of Anthracene Free Thread 295·H⁺

Synthesis of **295**

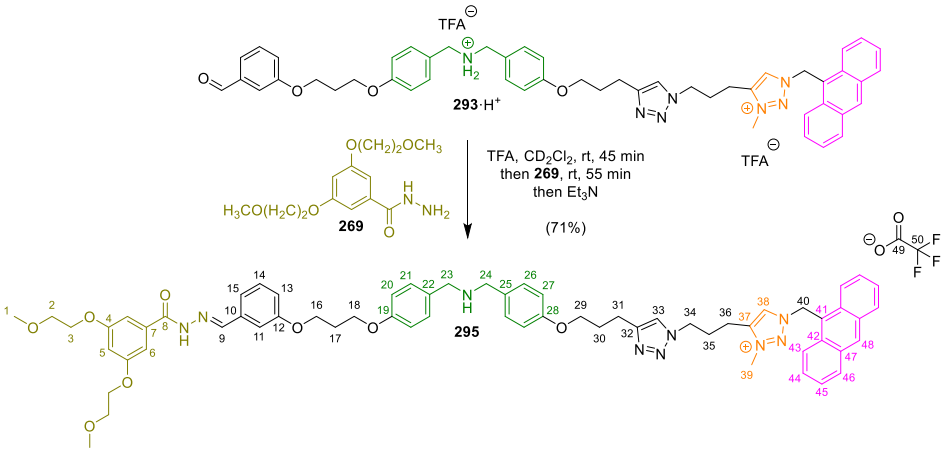

To a solution of **293**·H⁺ (12.1 mg, 12.0 µmol) in CD_2Cl_2 (500 µl, 24 mM) at room temperature was added TFA (27.4 µl, 240 µmol) and the reaction was thoroughly mixed and left standing for 45 minutes. Hydrazide **269** (10.2 mg, 36 µmol) was added and after 55 minutes the reaction was basified with Et_3N. (50.2 µl, 360 µmol) The crude reaction mixture was purified by size exclusion chromatography (S-X1, CH_2Cl_2) to give **295** (10.1 mg, 71%, *yield calculated for the TFA⁻ salt*) as a yellow solid.

^{1}H NMR (600 MHz, CD_2Cl_2) δ 11.04 (s, 1H, C-8 NH), 8.60 (s, 1H, H-48), 8.54 (s, 1H, H-38), 8.39 (s, 1H, H-9), 8.28 (d, *J* = 8.2 Hz, 2H, H-43), 8.06 (d, *J* = 8.4 Hz, 2H, H-46), 7.62 (t, *J* = 7.3 Hz, 2H, H-44), 7.54 – 7.48 (m, 2H, H-45), 7.30 – 7.24 (m, 5H, H-21, H-25 and H-33), 7.19 – 7.13 (m, 2H, H-11 and H-14), 7.12 – 7.08 (m, 3H, H-6 and H-15), 6.82 (d, *J* = 7.3 Hz, 1H, H-13), 6.70 – 6.62 (m, 4H, H-20 and H-27), 6.58 (s, 1H, H-5), 6.54 (s, 2H, H-40), 4.19 (s, 2H, H-34), 4.08 – 4.04 (m, 4H, H-3), 3.89 (s, 6H, H-16/18, H-23 and H-24), 3.82 (s, 3H, H-39), 3.79 – 3.72 (m, 4H, H-16/18 and H-29), 3.67 – 3.63 (m, 4H, H-2), 3.34 (s, 6H, H-1), 2.69 (t, *J* = 6.8 Hz, 2H, H-31), 2.52 (s, 2H, H-36), 2.04 (s, 2H, H-35), 1.96 (s, 4H, H-17 and H-30).

^{13}C NMR (151 MHz, CD_2Cl_2) δ 164.20 (C-8), 161.41 (q, *J* = 33.6 Hz, C-49), 160.46 (C-4), 159.64 – 159.53 (m, C-12, C-19 and C-28), 149.31 (C-9), 147.39 (C-32), 143.39 (C-37), 135.90 (C-10), 135.58 (C-7), 131.84 (C-47), 131.71 (C-21 and C-26), 131.48 – 131.41 (m, C-42 and C-48), 130.13 (C-14), 129.89 (C-46), 128.95 (C-38), 128.65 (C-44), 126.02 (C-45), 124.96 (C-22 and C-25), 123.21 (C-43), 122.41 (C-33), 121.30 (C-41), 121.18 (C-15), 117.54 (q, *J* = 295.1 Hz, C-50), 117.53 (C-13), 114.86 (C-20 and C-27), 112.31 (C-11), 106.54 (C-6), 105.69 (C-5), 71.21 (C-2), 68.09 (C-3), 67.01 (C-29), 64.81 (C-16/18), 64.56 (C-16/18), 59.14 (C-1), 51.05 (C-23/24), 50.93 (C-23/24), 50.17 (C-40), 48.51 (C-34), 37.78 (C-39), 29.37 (C-17), 28.69 (C-30), 27.38 (C-35), 22.17 (C-31), 20.58 (C-36).

^{19}F NMR (471 MHz, CD_2Cl_2) δ -75.51.

HRMS (HESI⁺): Calculated for $C_{63}H_{70}O_8N_9$: 1080.5342 [M-TFA⁻]⁺, found 1080.5316.

Synthesis and Switching of Anthracene [2]Rotaxanes 294·H⁺, 289·H⁺ and 288·H⁺

Synthesis of **288**·H⁺ (TFA⁻ salt)

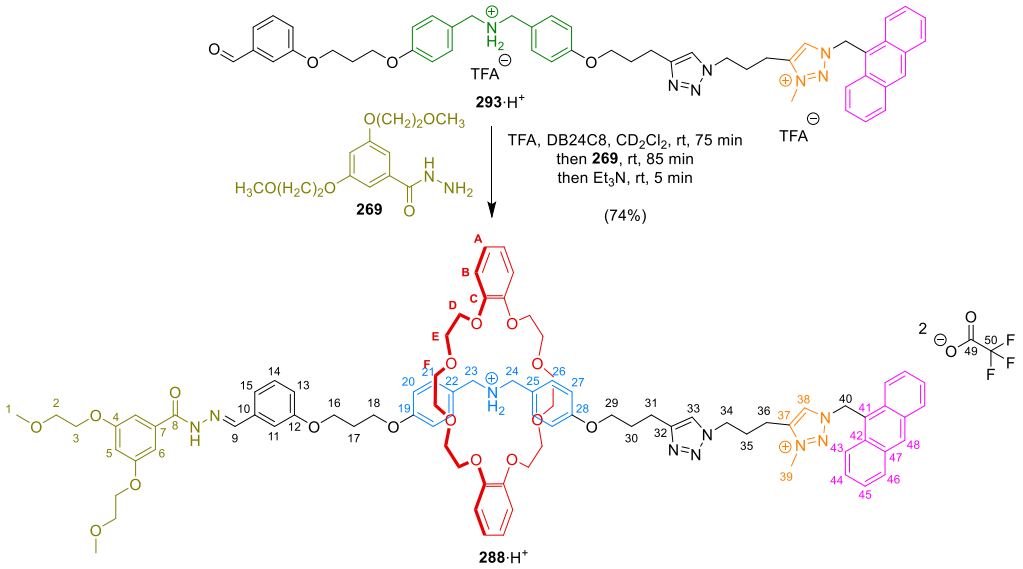

To a solution of **293**·H⁺ (12.1 mg, 12.0 µmol) and DB24C8 (26.9 mg, 60 µmol) in CD_2Cl_2 (500 µl, 24 mM) at room temperature was added TFA (18.7 µl, 240 µmol) and the reaction was thoroughly mixed and left standing for 75 minutes. Hydrazide **269** (34.1 mg, 120 µmol) was added and after 85 minutes the reaction was basified with Et_3N. (50.2 µl, 360 µmol) The crude was purified by size exclusion chromatography (S-X1, CH_2Cl_2) to give **288**·H⁺ (15.3 mg, 74%) as a yellow solid.

^{1}H NMR (600 MHz, CD_2Cl_2) δ 11.96 (s, 1H, C-8 NH), 9.03 (s, 1H, H-38), 8.68 (s, 1H, H-9), 8.63 (s, 1H, H-48), 8.40 (d, J = 8.8 Hz, 2H, H-43), 8.08 (d, J = 8.4 Hz, 2H, H-46), 7.68 – 7.62 (m, 3H, H-33 and H-44), 7.57 – 7.51 (m, 2H, H-45), 7.38 – 7.31 (m, 3H, H-15 and C-23/24 NH_2^+), 7.26 (d, J = 6.6 Hz, 2H, H-6), 7.23 (d, J = 7.0 Hz, 2H, H-11 and H-14), 7.18 – 7.15 (m, 4H, H-21 and H-26), 6.91 (dt, J = 7.0, 2.4 Hz, 1H, H-13), 6.87 – 6.82 (m, 4H, H-*A*), 6.78 – 6.74 (m, 6H, H-40 and H-*B*), 6.71 (d, J = 8.5 Hz, 2H, H-20/27), 6.68 (d, J = 8.6 Hz, 2H, H-H-20/27), 6.58 (s, 1H, H-5), 4.50 – 4.43 (m, 4H, H-23 and H-24), 4.38 (t, J = 6.5 Hz, 2H, H-34), 4.16 (t, J = 5.8 Hz, 2H, H-16), 4.14 – 4.10 (m, 4H, H-3), 4.08 (t, J = 6.0 Hz, 2H, H-18), 4.06 – 4.02 (m, 8H, H-*D*), 3.99 (s, 3H, H-39), 3.91 (t, J = 6.3 Hz, 2H, H-29), 3.72 – 3.69 (m, 8H, H-*E*), 3.68 – 3.65 (m, 4H, H-2), 3.42 (s, 8H, H-*F*), 3.35 (s, 6H, H-1), 2.78 (t, J = 7.5 Hz, 2H, H-31), 2.75 (t, J = 7.4 Hz, 2H, H-36), 2.28 (q, J = 6.8 Hz, 2H, H-35), 2.19 (p, J = 5.9 Hz, 2H, H-17), 2.07 (p, J = 6.7 Hz, 2H, H-35).

^{13}C NMR (151 MHz, CD_2Cl_2) δ 163.89 (C-8), 160.72 (q, J = 32.4 Hz, C-49), 160.34 (C-4), 159.99 (C-19), 159.94 (C-28), 159.61 (C-12), 149.23 (C-9), 147.93 (C-*C*), 147.63 (C-32), 143.52 (C-37), 136.78 (C-7), 135.90 (C-10), 131.73 (C-47), 131.52 (C-42), 131.39 (C-48), 131.15 (C-21/26), 131.06 (C-21/26), 130.01 (C-14), 129.84 (C-46), 129.55 (C-38), 128.60 (C-44), 125.98 (C-45), 124.16 (C-22/25), 124.08 (C-22/25), 123.39 (C-43), 122.40 (C-33), 121.95 (C-*A*), 121.55 (C-41), 121.20 (C-15), 116.96 (C-13), *approx.* 115.96 (q, J = *approx.* 301 Hz, C-50), 114.88 (C-20/27), 114.85 (C-20/27), 113.03 (C-*B*), 112.25 (C-11), 106.60 (C-6), 106.00 (C-5), 71.28 (C-2), 71.07 (C-*F*), 70.61 (C-*E*), 68.57 (C-*D*), 68.10 (C-3), 67.38 (C-29), 64.67 (C-18), 64.52 (C-16), 59.09 (C-1), 52.33 (C-23/24), 52.31 (C-23/24), 50.29 (C-40), 48.71 (C-34), 37.99 (C-39), 29.59 (C-17), 29.08 (C-30), 27.37 (C-35), 22.31 (C-31), 20.88 (C-36).

^{19}F NMR (471 MHz, CD_2Cl_2) δ -72.71 (d, J = 711.7 Hz), -76.20.

HRMS (HESI⁺): Calculated for $C_{87}H_{103}O_{16}N_9$: 764.8756 $[M+H]^+$, found 764.8743.

Switching from **288**·H^+ to **288** (TFA^- salt)

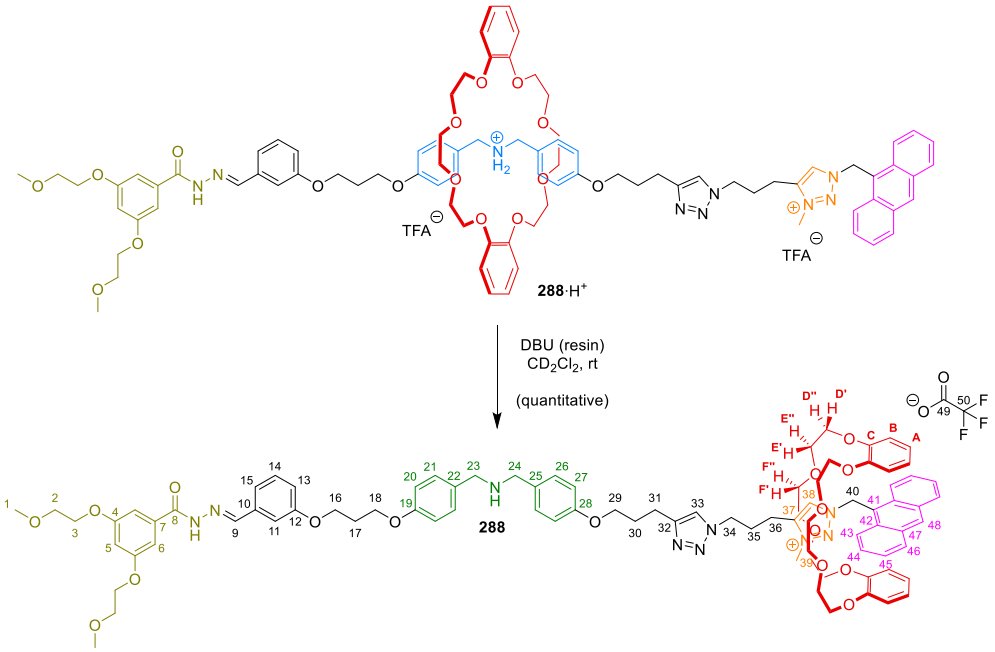

A solution of **288**·H^+ (15.3 mg, 8.9 µmol, TFA^- salt) in CD_2Cl_2 (600 µl, 15 mM) at room temperature was filtered through a plug of DBU (polymer-bound, 100-200 mesh, 1.5-2.5 mmol/g, *approx*. 0.5 cm filling height) and cotton wool hold in a glass Pasteur pipette to give a yellow solution of **288** (*quantitative by NMR*).

^{1}H NMR (600 MHz, CD_2Cl_2) δ 8.63 (s, 1H, H-9), 8.43 (s, 1H, H-48), 8.29 (s, 1H, H-38), 8.11 (d, J = 8.8 Hz, 2H, H-43), 7.94 (d, J = 8.4 Hz, 2H, H-46), 7.51 – 7.47 (m, 2H, H-44), 7.44 – 7.39 (m, 2H, H-45), 7.29 – 7.14 (m, 10H, H-6, H-11, H-14, H-15, H-21 and H-25), 6.95 (s, 1H, H-33), 6.89 (d, J = 8.5 Hz, 2H, H-20), 6.85 (d, J = 7.1 Hz, 1H, H-13), 6.83 – 6.79 (m, 4H, H-*A*), 6.73 (d, J = 8.4 Hz, 2H, H-27), 6.59 (s, 1H, H-5), 6.56 – 6.52 (m, 4H, H-*B*), 6.39 (s, 2H, H-40), 4.25 (t, J = 8.8 Hz, 2H, H-29), 4.16 – 4.09 (m, 8H, H-3, H-16 and H-18), 3.83 – 3.77 (m, 5H, H-29 and H-39), 3.73 – 3.66 (m, 14H, H-2, H-23, H-24 and H-*D'/D''*), 3.59 – 3.53 (m, 4H, H-*D'/D''*), 3.42 – 3.36 (m, 12H, H-1 and H-*E'/E'''*), 3.20 (dd, J = 10.4, 6.2 Hz, 4H, H-*F'/F'''*), 3.14 – 3.09 (m, 6H, H-36 and H-*E'/E'''*), 3.04 (dd, J = 10.4, 6.2 Hz, 4H, H-*F'/F'''*), 2.57 (t, J = 7.2 Hz, 2H, H-31), 2.43 – 2.34 (m, 2H, H-35), 2.20 (p, J = 5.9 Hz, 2H, H-17), 1.87 (p, J = 6.7 Hz, 2H, H-30).

^{13}C NMR (151 MHz, CD_2Cl_2) δ 163.88 (C-8), 160.52 (q, J = 32.3 Hz, C-49), 160.32 (C-4), 159.56 (C-12), 158.37 (C-19), 158.20 (C-28), 149.07 (C-9), 147.67 (C-*C*), 147.06 (C-37), 146.62 (C-33), 136.48 (C-19), 135.93 (C-7), 133.23 (C-22/25), 133.22 (C-22/25), 131.59 (C-42), 131.31 (C-48), 131.19 (C-47), 129.86 (C-46), 129.67 (C-21), 129.62 (C-26), 128.83 (C-38), 128.51 (C-44), 125.93 (C-45), 122.98 (C-43), 121.47 (C-*A*), 121.18 (C-41), 121.12 (C-33), 121.07 (C-15), 117.03 (C-13), 114.70 (C-20), 114.50 (C-27), 112.38 (C-*B*), 112.20 (C-11), 106.60 (C-6), 105.81 (C-5), 71.27 (C-2), 71.04 (C-*F*), 69.95 (C-*E*), 68.24 (C-*D*), 68.09 (C-3), 66.76 (C-29), 64.76 (C-16), 64.72 (C-18), 59.13 (C-1), 52.93 (C-23), 52.81 (C-24), 49.69 (C-40), 49.57 (C-34), 37.16 (C-39), 29.65 (C-17), 28.91 (C-30), 25.76 (C-35), 21.95 (C-31), 20.73 (C-36).

Synthesis of **288**·H$^+$ (PF_6^- salt)

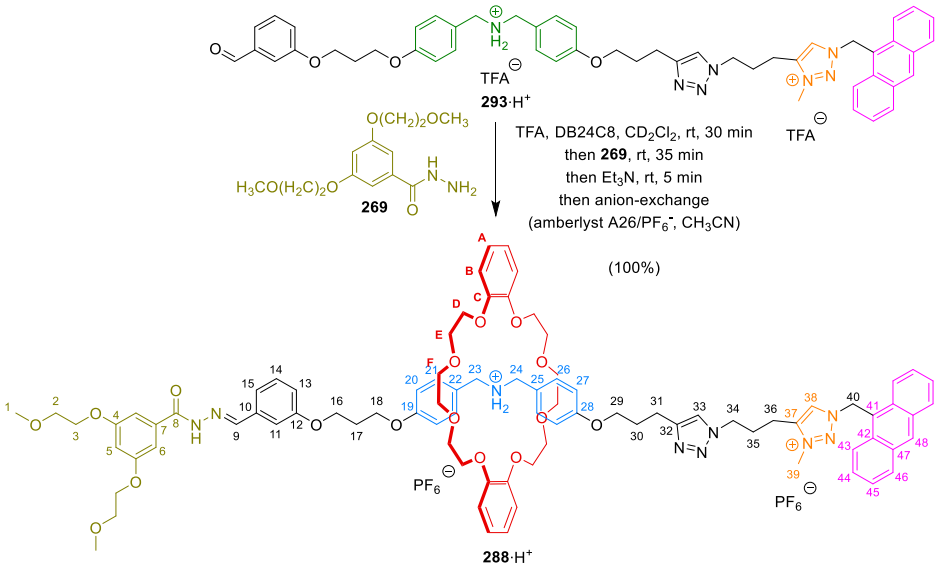

To a solution of **293**·H$^+$ (11.5 mg, 11.6 µmol) and DB24C8 (26.1 mg, 116 µmol) in CD_2Cl_2 (500 µl, 23 mM) at room temperature was added TFA (18.2 µl, 232 µmol) and the reaction was thoroughly mixed and left standing for 30 minutes. Hydrazide **269** (33.0 mg, 116 µmol) was added and after 35 minutes the reaction was basified with Et_3N. (48.6 µl, 349 µmol) The crude reaction mixture was purified by size exclusion chromatography (S-X1, CH_2Cl_2) and then anion-exchange chromatography (amberlyst A-26 PF_6^-, CH_3CN) to give **288**·H$^+$ (21.1 mg, 100%) as a yellow solid.

^{1}H NMR (600 MHz, CD_2Cl_2) δ 9.81 (s, 1H, C-8 NH), 8.67 (s, 1H, H-48), 8.26 (d, J = 8.8 Hz, 3H, H-9 and H-43), 8.11 (d, J = 8.4 Hz, 2H, H-46), 7.97 (s, 1H, H-38), 7.70 – 7.66 (m, 2H, H-44), 7.60 – 7.53 (m, 2H, H-45), 7.51 (s, 1H, H-33), 7.41 – 7.32 (m, 3H, H-11 and C-23/24 NH_2^+), 7.28 (t, J = 7.9 Hz, 1H, H-14), 7.22 – 7.15 (m, 5H, H-15, H-21 and H-26), 6.98 (s, 2H, H-6), 6.95 (dd, J = 8.2, 2.0 Hz, 1H, H-13), 6.87 – 6.83 (m, 4H, H-*A*), 6.80 – 6.74 (m, 4H, H-*B*), 6.73 – 6.68 (m, 4H, H-20 and H-27), 6.65 (s, 2H, H-40), 6.62 (s, 1H, H-5), 4.52 – 4.45 (m, 4H, H-23/24), 4.35 (t, J = 6.6 Hz, 2H, H-29), 4.15 (t, J = 5.9 Hz, 2Hz, H-16), 4.11 – 4.08 (m, 4H, H-3), 4.07 – 4.04 (m, 13H, H-18, H-39 and H-*D*), 3.90 (t, J = 6.2 Hz, 2H, H-29), 3.73 – 3.71 (m, 8H, H-*E*), 3.70 – 3.68 (m, 4H, H-2), 3.46 (s, 8H, H-*F*), 3.38 (s, 6H, H-1), 2.80 (t, J = 7.3 Hz, 2H, H-31), 2.73 (t, J = 7.6 Hz, 2H, H-36), 2.25 – 2.17 (m, 4H, H-17 and H-35), 2.09 – 2.04 (m, 2H, H-30).

^{13}C NMR (151 MHz, CD_2Cl_2) δ 163.95 (C-8), 160.59 (C-4), 159.92 (C-28), 159.90 (C-19), 159.69 (C-12), 148.90 (C-9), 147.94 (C-*C*), 147.59 (C-32), 143.86 (C-37), 135.75 (C-10), 135.56 (C-7), 131.80 (C-48), 131.74 (C-47), 131.53 (C-42), 131.14 (C-21/26), 131.10 (C-21/26), 130.21 (C-14), 130.00 (C-46), 128.95 (C-44), 128.03 (C-38), 126.08 (C-45), 124.26 (C-27), 124.09 (C-25), 122.83 (C-43), 122.54 (C-33), 121.93 (C-*A*), 121.31 (C-15), 120.37 (C-41), 117.53 (C-13), 114.88 (C-20), 114.79 (C-27), 113.02 (C-*B*), 112.30 (C-11), 106.30 (C-6), 105.58 (C-5), 71.21 (C-2), 71.10 (C-*F*), 70.64 (C-*E*), 68.55 (C-*D*), 68.12 (C-3), 67.33 (C-29), 64.72 (C-16 and C-18), 59.17 (C-1), 52.35 (C-23/24), 52.33 (C-23/24), 50.47 (C-40), 48.88 (C-34), 38.06 (C-39), 29.55 (C-17), 28.97 (C-34), 27.33 (C-35), 22.20 (C-31), 20.69 (C-36).

Switching from **288**·H$^+$ to **288** (PF_6^- salt)

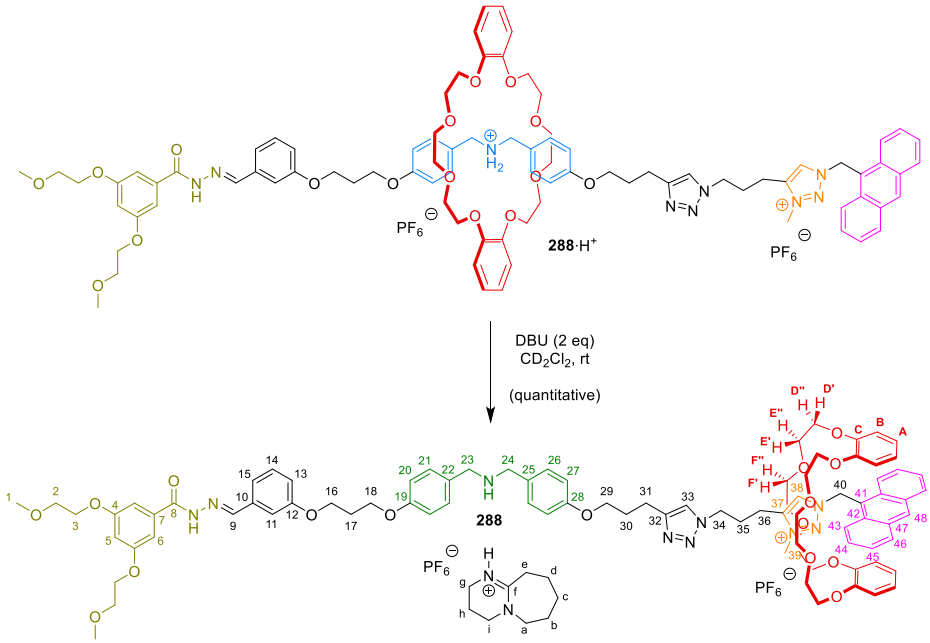

To a solution of **288**·H$^+$ (21.1 mg, 11.6 µmol, PF_6^- salt) in CD_2Cl_2 (600 µl, 19 mM) at room temperature was added DBU (3.46 µL, 23.2 µmol) to give a yellow solution of **288** (*quantitative by NMR*).

^{1}H NMR (600 MHz, CD_2Cl_2) δ 8.50 (s, 1H, H-48), 8.31 (s, 1H, H-38), 8.27 (s, 1H, H-9), 8.11 (d, J = 8.8 Hz, 2H, H-43), 8.00 (d, J = 8.4 Hz, 2H, H-45), 7.58 – 7.53 (m, 2H, H-44), 7.50 – 7.44 (m, 2H, H-45), 7.31 (s, 1H, H-11), 7.28 (t, J = 7.9 Hz, 1H, H-14), 7.25 (d, J = 8.6 Hz, 2H, H-21), 7.24 – 7.20 (m, 1H, H-15), 7.20 (d, J = 8.5 Hz, 2H, H-26), 7.04 (s, 2H, H-6), 6.99 (s, 1H, H-33), 6.94 (dd, J = 8.1, 1.8 Hz, 1H, H-13), 6.88 (d, J = 8.6 Hz, 2H, H-20), 6.85 (dt, J = 7.4, 3.7 Hz, 4H, H-*A*), 6.77 (d, J = 8.6 Hz, 2H, H-27), 6.62 (s, 1H, H-5), 6.60 (dd, J = 5.9, 3.6 Hz, 4H, H-*B*), 6.36 (s, 2H, H-40), 4.31 – 4.27 (m, 2H, H-34), 4.17 (t, J = 6.0 Hz, 2H, H-16), 4.14 (t, J = 6.2 Hz, 2H, H-18), 4.12 – 4.09 (m, 4H, H-3), 3.90 (s, 3H, H-39), 3.83 (t, J = 6.2 Hz, 2H, H-29), 3.77 (dd, J = 11.1, 5.9 Hz, 4H, H-*D'/D''*), 3.71 – 3.68 (m, 8H, H-2, H-23 and H-24), 3.61 (dd, J = 11.2, 6.4 Hz, 4H, H-*D'/D''*), 3.45 (dd, J = 11.6, 6.4 Hz, 4H, H-*E'/E''*), 3.39 (s, 6H, H-1), 3.32 (q, J = 6.7, 6.0 Hz, 8H, H-*a* and H-*i*), 3.27 (dd, J = 10.8, 6.4 Hz, 4H, H-*F'/F''*), 3.24 – 3.19 (m, 5H, H-36 and H-*g*), 3.18 (dd, J = 11.6, 5.8 Hz, 4H, *E'/E''*), 3.11 (dd, J = 10.8, 6.3 Hz, 4H, H-*F'/F''*), 2.57 (t, J = 7.5 Hz, 2H, H-31), 2.50 – 2.42 (m, 6H, H-35 and H-*e*), 2.23 (p, J = 6.1 Hz, 2H, H-17), 1.87 (p, J = 6.0 Hz, 6H, H-30 and H-*e*), 1.71 – 1.66 (m, 4H, H-*c*), 1.62 (dd, J = 9.8, 4.0 Hz, 8H, H-*b* and H-*d*).

^{13}C NMR (151 MHz, CD_2Cl_2) δ 164.61 (C-8), 164.37 (C-*f*), 160.46 (C-4), 159.71 (C-12), 158.34 (C-19/28), 158.31 (C-19/28), 148.71 (C-9), 147.75 (C-*C*), 147.40 (C-32), 146.90 (C-32), 136.72 (C-7), 136.25 (C-10), 133.33 (C-22), 133.26 (C-25), 131.66 (C-47), 131.55 (C-48), 131.21 (C-42), 130.06 (C-14), 130.04 (C-46), 129.65 (C-21), 129.59 (C-26), 128.86 (C-33), 128.71 (C-44), 126.04 (C-45), 122.75 (C-43), 121.55 (C-*A*), 121.07 (C-15), 120.83 (C-41), 117.29 (C-13), 114.70 (C-20), 114.55 (C-27), 112.49 (C-*B*), 112.38 (C-11), 106.44 (C-6), 105.18 (C-5), 71.26 (C-2), 71.12 (C-*F*), 70.01 (C-*E*), 68.36 (C-*D*), 68.09 (C-3), 67.12 (C-29), 65.04 (C-16), 64.84 (C-18), 59.20 (C-1), 54.02 (C-*a*, *overlapped with solvent peak*), 52.93 (C-23/24), 52.87 (C-23/24), 49.66 (C-34), 48.84 (C-*i*), 40.98 (C-*g*), 37.28 (C-39), 34.71 (C-*e*), 29.70 (C-*c* and C-17), 29.23 (C-30), 27.89 (C-*b*), 25.88 (C-35), 25.29 (C-*d*), 22.20 (C-31), 21.27 (C-*h*), 20.85 (C-36).

Synthesis of **289**·H^+ (PF_6^- salt)

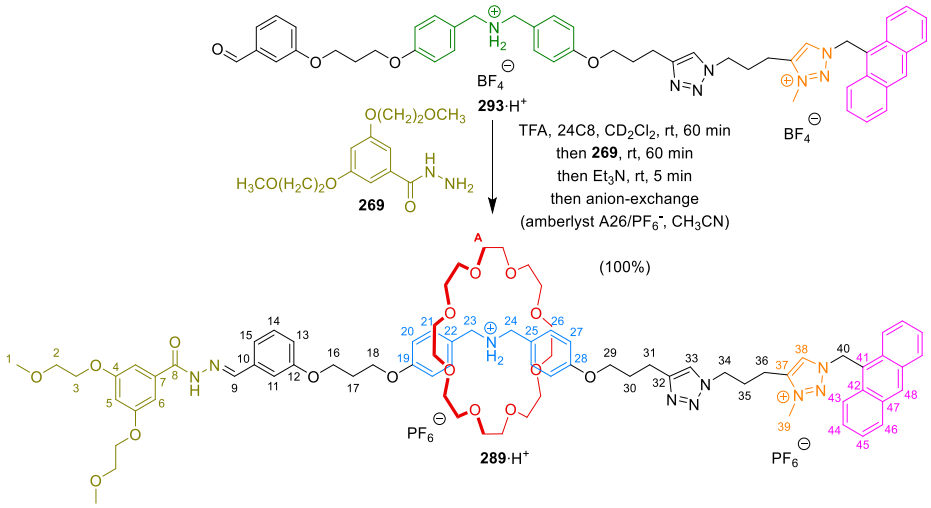

To a solution of **293**·H^+ (11.5 mg, 11.6 µmol) and 24C8 (20.5 mg, 58.1 µmol) in CD_2Cl_2 (500 µl, 23 mM) at room temperature was added TFA (18.2 µl, 232 µmol) and the reaction was thoroughly mixed and left standing for 60 minutes. Hydrazide **269** (33.0 mg, 116 µmol) was added and after 60 minutes the reaction was basified with Et_3N. (48.6 µl, 349 µmol) The crude reaction mixture was purified by size exclusion chromatography (S-X1, CH_2Cl_2) and then anion-exchange chromatography (amberlyst A-26 PF_6^-, CH_3CN) to give **289**·H^+ (20.0 mg, 100%) as a yellow solid.

^{1}H NMR (600 MHz, CD_2Cl_2) δ 9.67 (s, 1H, C-8 NH), 8.68 (s, 1H, H-48), 8.26 (d, *J* = 8.8 Hz, 2H, H-43), 8.22 (s, 1H, H-9), 8.12 (d, *J* = 8.4 Hz, 2H, H-46), 7.95 (s, 1H, H-38), 7.71 – 7.67 (m, 2H, H-44), 7.59 – 7.55 (m, 2H, H-45), 7.47 (s, 1H, H-33), 7.42 – 7.34 (m, 7H, H-11, H-21, H-26 and C-23/24 NH_2^+), 7.28 (t, *J* = 7.9 Hz, 1H, H-14), 7.19 (d, *J* = 7.5 Hz, 1H, H-15), 6.99 – 6.90 (m, 7H, H-6, H-13, H-20 and H-27), 6.66 (s, 2H, H-40), 6.63 (t, *J* = 2.1 Hz, 2H, H-5), 4.44 – 4.38 (m, 4H, H-23 and H-24), 4.34 (t, *J* = 6.6 Hz, 2H, H-34), 4.21 – 4.17 (m, 4H, H-16 and H-18), 4.12 – 4.09 (m, 4H, H-3), 4.08 (s, 3H, H-39), 4.01 (t, *J* = 6.3 Hz, 2H, H-29), 3.71 – 3.69 (m, 4H, H-2), 3.43 (s, 32H, H-*A*), 3.38 (s, 6H, H-1), 2.81 (t, *J* = 7.4 Hz, 2H, H-31), 2.73 (t, *J* = 7.6 Hz, 2H, H-36), 2.28 – 2.19 (m, 4H, H-17 and H-35), 2.10 (p, *J* = 6.7 Hz, 2H, H-35).

^{13}C NMR (151 MHz, CD_2Cl_2) δ 163.85 (C-8), 160.61 (C-4), 160.13 (C-28), 160.09 (C-19), 159.68 (C-12), 148.67 (C-9), 147.74 (C-32), 143.91 (C-37), 135.73 (C-10), 135.67 (C-7), 132.20 (C-21/26), 132.17 (C-21/26), 131.82 (C-48), 131.75 (C-47), 131.53 (C-42), 130.17 (C-14), 130.01 (C-46), 128.97 (C-44), 128.00 (C-38), 126.09 (C-45), 124.63 (C-22), 124.42 (C-25), 122.80 (C-43), 122.22 (C-33), 121.41 (C-15), 120.33 (C-41), 117.63 (C-13), 114.90 (C-27), 114.82 (C-20), 112.08 (C-11), 106.26 (C-6), 105.50 (C-5), 71.21 (C-2), 70.86 (C-*A*), 68.13 (C-3), 67.54 (C-29), 64.93 (C-16), 64.80 (C-18), 59.18 (C-1), 52.13 (C-23), 52.08 (C-24), 50.49 (C-40), 48.67 (C-34), 38.09 (C-39), 29.62 (C-17), 29.10 (C-30), 27.38 (C-35), 22.32 (C-31), 20.73 (C-36).

^{19}F NMR (471 MHz, CD_2Cl_2) δ -72.87 (d, *J* = 706.5 Hz).

^{31}P NMR (202 MHz, CD_2Cl_2) δ -144.63 (hept, *J* = 706.5 Hz).

HRMS (ESI^+): Calculated for $C_{79}H_{103}N_9O_{16}$: 716.8756 $[M\text{-}2PF_6]^{2+}$, found 716.8755.

Switching from **289**·H^+ to **289** (PF_6^- salt)

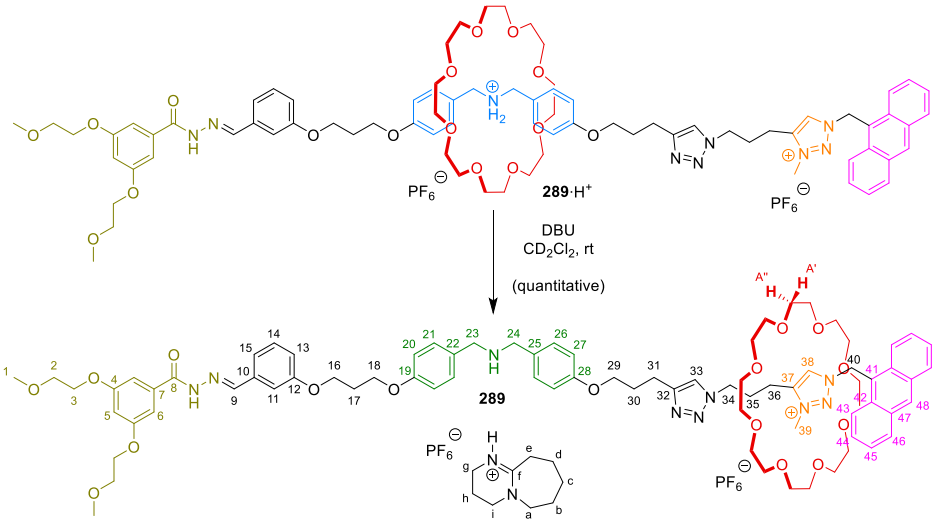

To a solution of **289**·H^+ (20.0 mg, 11.6 µmol, PF_6^- salt) in CD_2Cl_2 (500 µl, 23 mM) at room temperature was added DBU (3.46 µL, 23.2 µmol) to give a yellow solution of **289** (*quantitative by NMR*).

^{1}H NMR (600 MHz, CD_2Cl_2) δ 8.65 (s, 1H, H-48), 8.30 (s, 1H, H-9), 8.24 – 8.18 (m, 3H, H-38 and H-43), 8.11 (d, *J* = 8.4 Hz, 2H, H-46), 7.66 – 7.61 (m, 2H, H-44), 7.57 – 7.53 (m, 2H, H-45), 7.43 (s, 1H, H-33), 7.31 – 7.19 (m, 7H, H-11, H-14, H-15, H-21 and H-26), 7.05 (s, 2H, H-6), 6.95 – 6.91 (m, 1H, H-13), 6.88 (d, *J* = 8.5 Hz, 2H, H-20), 6.79 (d, *J* = 8.5 Hz, 2H, H-27), 6.64 – 6.59 (m, 3H, H-5 and H-40), 4.31 (s, 3H, H-39), 4.29 (t, *J* = 7.6 Hz, 2H, H-34), 4.17 (t, *J* = 6.0 Hz, 2H, H-16), 4.14 (t, *J* = 6.2 Hz, 2H, H-18), 4.12 – 4.09 (m, 4H, H-3), 3.93 (t, *J* = 6.2 Hz, 2H, H-29), 3.71 – 3.68 (m, 8H, H-2, H-23 and H-24), 3.39 (s, 6H, H-1), 3.39 – 3.34 (m, 8H, H-*a* and H-*i*), 3.23 – 3.21 (m, 4H, H-*g*), 3.21 – 3.16 (m, 14H, H-*A′/A″*, *part. dethreading obs.*), 3.14 – 3.10 (m, 2H, H-36), 2.94 – 2.89 (m, 14H, H-*A′/A″*, *part. dethreading obs.*), 2.78 (t, *J* = 7.5 Hz, 2H, H-31), 2.52 – 2.49 (m, 4H, H-*e*), 2.28 – 2.20 (m, 4H, H-17 and H-35), 2.04 (p, *J* = 6.6 Hz, 2H, H-30), 1.90 (p, *J* = 5.9 Hz, 4H, H-*h*), 1.72 – 1.67 (m, 4H, H-*c*), 1.67 – 1.60 (m, 8H, H-*b* and H-*d*).

^{13}C NMR (151 MHz, CD_2Cl_2) δ 165.04 (C-*f*), 164.92 (C-8), 160.42 (C-4), 159.69 (C-12), 158.32 (C-19), 158.29 (C-28), 148.93 (C-9), 147.27 (C-37), 146.92 (C-32), 136.88 (C-7), 136.37 (C-10), 133.33 (C-22), 133.28 (C-25), 131.88 (C-47), 131.52 (C-42), 131.50 (C-48), 130.06 (C-46), 129.95 (C-38), 129.63 (C-21), 129.58 (C-26), 128.67 (C-44), 126.09 (C-45), 123.04 (C-43), 121.74 (C-33), 120.98 (C-15), 120.87 (C-41), 117.13 (C-13), 114.68 (C-20), 114.55 (C-27), 112.44 (C-11), 106.46 (C-6), 105.13 (C-5), 71.26 (C-2), 70.98 (C-*A′/A″*), 68.07 (C-3), 67.13 (C-29), 65.03 (C-16), 64.83 (C-18), 59.18 (C-1), 54.20 (C-*a*, *overlapped with solvent peak*), 52.90 (C-23), 52.85 (C-24), 50.25 (C-34), 49.89 (C-40), 48.85 (C-*i*), 40.20 (C-*g*), 37.97 (C-39), 34.12 (C-*e*), 29.70 (C-17), 29.56 (C-*c*), 29.40 (C-30), 27.59 (C-*b*), 25.82 (C-35), 24.99 (C-*d*), 22.37 (C-31), 20.88 (C-36), 20.82 (C-*h*).

Synthesis of **294**·H^+ (PF_6^- salt)

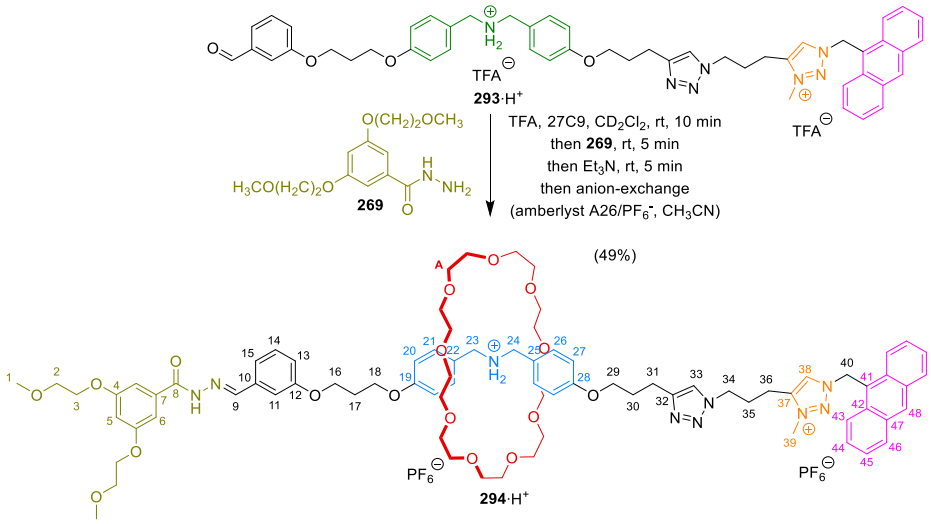

To a solution of **293**·H^+ (15.1 mg, 14.9 µmol) and 27C9 (59.3 mg, 150 µmol) in CD_2Cl_2 (598 µl, 25 mM) at room temperature was added TFA (35.0 µl, 449 µmol) and the reaction was thoroughly mixed and left standing for 10 minutes. Hydrazide **269** (42.5 mg, 150 µmol) was added and after 5 minutes the reaction was basified with Et_3N. (64.6 µl, 463 µmol) The crude reaction mixture was purified by size exclusion chromatography (S-X1, CH_2Cl_2) and then anion-exchange chromatography (amberlyst A-26 PF_6^-, CH_3CN) to give **294**·H^+ (12.9 mg, 49%) as a yellow solid.

^{1}H NMR (600 MHz, CD_3CN) δ 10.16 (s, 1H, C-8 NH), 8.78 (s, 1H, H-48), 8.30 (d, J = 8.8 Hz, 2H, H-43), 8.24 (s, 1H, H-9), 8.18 (d, J = 8.5 Hz, 2H, H-46), 8.00 (s, 1H, H-38), 7.71 – 7.65 (m, 2H, H-44), 7.63 – 7.57 (m, 2H, H-45), 7.49 (s, 1H, H-33), 7.48 – 7.40 (m, 6H, H-21, H-26 and C-23/24 NH_2^+), 7.36 – 7.31 (m, 2H, H-14 and H-11), 7.24 (d, J = 7.4 Hz, 1H, H-15), 7.03 – 6.97 (m, 5H, H-6, H-13 and H-20), 6.94 (d, J = 8.7 Hz, 2H, H-27), 6.70 – 6.64 (m, 3H, H-5 and H-40), 4.36 – 4.27 (m, 6H, H-23, H-24 and H-34), 4.21 (t, J = 5.8 Hz, 4H, H-16 and H-18), 4.16 – 4.12 (m, 4H, H-3), 4.03 (t, J = 6.4 Hz, 2H, H-29), 3.98 (s, 3H, H-39), 3.71 – 3.67 (m, 4H, H-2), 3.42 (s, 36H, H-*A*), 3.36 (s, 6H, H-1), 2.77 (t, J = 7.8 Hz, 2H, H-31), 2.68 (t, J = 7.7 Hz, 2H, H-36), 2.23 (p, J = 6.0 Hz, 2H, H-17), 2.11 (p, J = 7.8 Hz, 2H, H-35), 2.05 (p, J = 7.2 Hz, 2H, H-30).

^{13}C NMR (151 MHz, CD_3CN) δ 164.14 (C-8), 161.19 (C-4), 160.70 (C-28), 160.67 (C-19), 160.30 (C-12), 148.69 (C-9), 148.09 (C-32), 144.59 (C-37), 136.84 (C-10), 136.69 (C-7), 133.16 (C-21), 133.09 (C-26), 132.45 (C-47), 132.13 (C-42), 132.08 (C-48), 131.02 (C-14), 130.53 (C-46), 129.04 (C-44), 128.86 (C-38), 126.70 (C-45), 125.12 (C-22/25), 125.06 (C-C-22/25), 124.00 (C-43), 122.61 (C-33), 122.04 (C-41), 121.55 (C-15), 118.33 (C-13, *overlapped with solvent peak*), 115.48 (C-20), 115.39 (C-27), 112.56 (C-11), 107.06 (C-6), 105.56 (C-6), 71.57 (C-2), 71.17 (C-*A*), 68.69 (C-3), 68.10 (C-29), 65.51 (C-16), 65.39 (C-18), 59.07 (C-1), 52.65 (C-23/24), 52.62 (C-23/24), 50.73 (C-40), 49.19 (C-34), 38.48 (C-39), 29.83 (C-17), 29.75 (C-30), 28.03 (C-35), 22.66 (C-31), 21.02 (C-36).

^{19}F NMR (471 MHz, CD_3CN) δ -72.87 (d, J = 706.4 Hz).

^{31}P NMR (203 MHz, CD_3CN) δ -144.65 (hept, J = 706.5 Hz).

HRMS (ESI^+): Calculated for $C_{81}H_{107}N_9O_{17}$: 738.8887 $[M\text{-}2PF_6]^{2+}$, found 738.8874.

Switching from **294**·H^+ to **294** (PF_6^- salt)

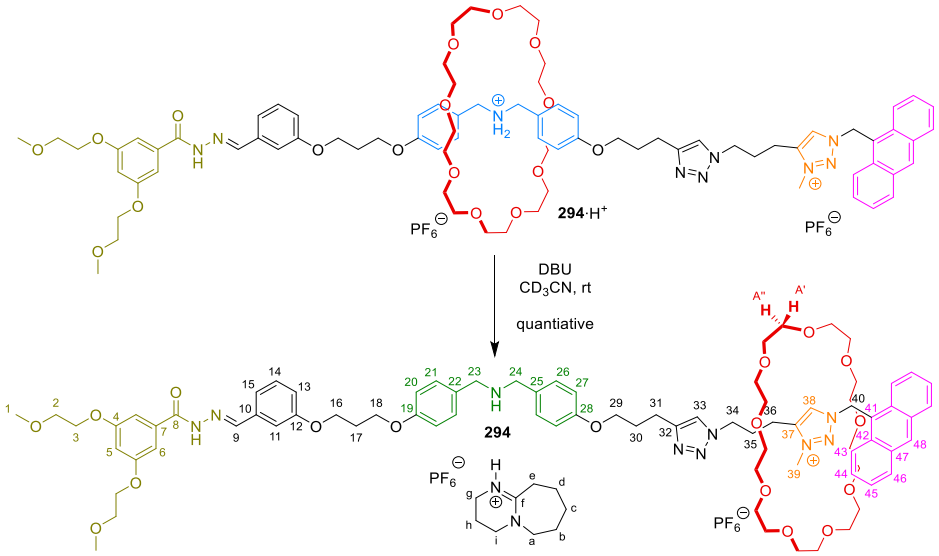

To a solution of **294**·H^+ (10.6 mg, 6.0 µmol, PF_6^- salt) in CD_3CN (550 µl, 11 mM) at room temperature was added DBU (1.8 µL, 12.0 µmol) to give a yellow solution of **294** (*quantitative by NMR*).

^{1}H NMR (600 MHz, CD_3CN) δ 8.71 (s, 1H, H-48), 8.43 (s, 1H, H-38), 8.34 – 8.27 (m, 3H, H-9 and H-43), 8.12 (d, *J* = 8.4 Hz, 2H, H-46), 7.65 – 7.61 (m, 2H, H-43), 7.59 – 7.53 (m, 3H, H-33 and H-45), 7.28 (t, *J* = 7.9 Hz, 1H, H-14), 7.25 (s, 1H, H-11), 7.24 – 7.18 (m, 5H, H-15, H-21 and H-26), 7.09 (s, 2H, H-6), 6.93 (dd, *J* = 8.0, 2.1 Hz, 1H, H-13), 6.87 (d, *J* = 8.6 Hz, 2H, H-20), 6.81 (d, *J* = 8.6 Hz, 2H, H-27), 6.64 (s, 2H, H-40), 6.61 (t, *J* = 2.1 Hz, 1H, H-5), 4.37 (t, *J* = 7.3 Hz, 2H, H-34), 4.20 (s, 3H, H-39), 4.13 – 4.09 (m, 8H, H-16, H-18 and H-3), 3.95 (t, *J* = 6.3 Hz, 2H, H-29), 3.67 – 3.65 (m, 4H, H-2), 3.63 (s, 4H, H-23 and H-24), 3.41 – 3.39 (m, 5H, H-*a*), 3.36 (t, *J* = 6.0 Hz, 6H, H-*i*), 3.34 (s, 6H, H-1), 3.26 – 3.22 (m, 18H, H-*A'/A''*), 3.21 – 3.18 (m, 6H, H-*g*), 3.09 – 3.05 (m, 18H, H-*A'/A''*), 2.87 – 2.84 (m, 2H, H-36), 2.78 (t, *J* = 7.4 Hz, 2H, H-31), 2.51 – 2.48 (m, 5H, H-*e*), 2.25 – 2.19 (m, 2H, H-35), 2.16 (p, *J* = 6.2 Hz, 2H, H-17), 2.03 (p, *J* = 6.6 Hz, 2H, H-30), 1.87 (p, *J* = 5.9 Hz, 5H, H-*h*), 1.68 (h, *J* = 5.7 Hz, 6H, H-*c*), 1.66 – 1.56 (m, 12H, H-*b* and H-*d*).

^{13}C NMR (151 MHz, CD_3CN) δ 165.62 (C-*f*), 165.07 (C-8), 161.01 (C-4), 160.26 (C-12), 158.82 (C-28), 158.78 (C-19), 148.91 (C-9), 147.62 (C-32), 145.58 (C-37), 137.89 (C-7), 137.44 (C-10), 134.20 (C-22), 134.12 (C-25), 132.44 (C-47), 132.12 (C-42), 131.81 (C-48), 131.13 (C-38), 130.87 (C-14), 130.40 (C-44), 130.28 (C-26), 130.25 (C-21), 128.93 (C-44), 126.61 (C-45), 124.40 (C-43), 122.78 (C-33), 122.53 (C-41), 121.21 (C-15), 117.61 (C-13), 115.26 (C-20/27), 115.21 (C-20/27), 112.77 (C-11), 107.14 (C-6), 105.32 (C-5), 71.60 (C-2), 71.17 (C-*A*), 68.60 (C-3), 67.57 (C-29), 65.51 (C-16), 65.35 (C-18), 59.07 (C-1), 54.56 (C-*A*), 52.97 (C-23 and C-24), 50.34 (C-40), 50.13 (C-34), 49.16 (C-*i*), 40.52 (C-*g*), 38.57 (C-39), 34.60 (C-*e*), 29.96 (C-17), 29.73 (C-*c*), 29.71 (C-30), 27.63 (C-*b*), 27.55 (C-35), 25.12 (C-*d*), 22.57 (C-31), 21.28 (C-36), 20.91 (C-*h*).

Synthesis of Model Anthracene One-Barrier Pump 304 with Internal Hydrazone Barrier

Synthesis of **301**

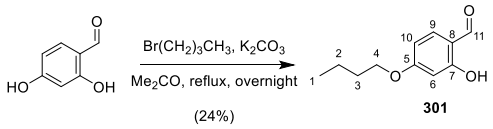

To a solution of *n*-butyl bromide (14.0 mL, 17.9 mmol) and 2,4-dihydroxybenzyl aldehyde (1.00 g, 7.24 mmol) in acetone (25 mL, 0.3 M) were added 1-bromobutane (1.40 mL, 13.0 mmol) and K_2CO_3 (granulate, 800 mg, 7.24 mmol) and the reaction mixture was heated to reflux overnight. The reaction was diluted with CH_2Cl_2 and 1 M aqueous HCl was added. The biphasic mixture was extracted with CH_2Cl_2 (two times). The combined organic layers were washed with brine and dried over $MgSO_4$, filtered, and concentrated *in vacuo*. The residue was purified by flash chromatography (SiO_2, petroleum ether/ CH_2Cl_2, 1:1) to give **301** (342 mg, 24%) as a colourless solid.

^{1}H NMR (600 MHz, DMSO-d_6) δ 9.99 (s, 1H, H-11), 7.60 (d, J = 8.7 Hz, 1H, H-9), 6.55 (dd, J = 8.7, 2.2 Hz, 1H, H-10), 6.46 (d, J = 2.2 Hz, 1H, H-6), 4.02 (t, J = 6.5 Hz, 2H, H-4), 1.69 (p, J = 6.6 Hz, 2H, H-3), 1.42 (h, J = 7.4 Hz, 2H, H-2), 0.92 (t, J = 7.4 Hz, 3H, H-1).

^{13}C NMR (151 MHz, DMSO-d_6) δ 191.16 (C-11), 165.48 (C-5), 163.15 (C-7), 132.31 (C-9), 116.11 (C-8), 107.79 (C-10), 101.21 (C-6), 67.78 (C-4), 30.50 (C-3), 18.67 (C-2), 13.68 (C-1).

HRMS (ASAP$^-$): Calculated for $C_{11}H_{13}O_3$: 193.0870 $[M-H]^-$, found 193.0870.

Synthesis of **302**

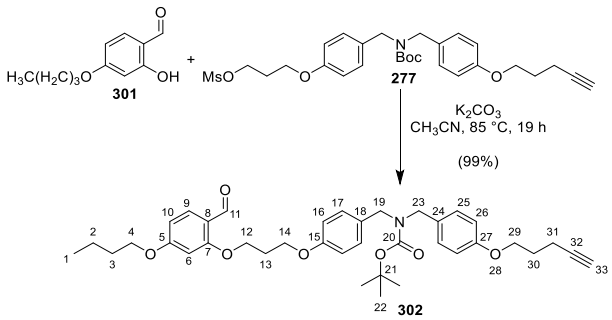

To a solution of **277** (297.1 mg, 0.559 mmol) and **301** (132.2 mg, 0.681 mmol) in CH_3CN (10 mL, 56 mM) was added K_2CO_3 (granulate, 231.7 mg, 1.68 mmol) and the reaction mixture was heated to reflux (heating set to 85 °C; using a reflux condenser and drying tube charged with $CaCl_2$) for 19 hours. The reaction mixture was cooled to room temperature and the solvent removed *in vacuo*. The residue was purified by flash chromatography (SiO_2, petroleum ether/ EtOAc, 4:1) to give **302** (349 mg, 99%) as a colourless solid.

^{1}H NMR (600 MHz, $CDCl_3$) δ 10.32 (s, 1H, H-11), 7.80 (d, J = 8.7 Hz, 1H, H-9), 7.19 – 7.07 (m, 4H, H-17 and H-25), 6.87 – 6.85 (m, 4H, H-16 and H-26), 6.53 (dd, J = 8.7, 1.7 Hz, 1H, H-10), 6.47 (d, J = 2.0 Hz, 1H, H-6), 4.31 (s, 2H, H-19/20), 4.25 (q, J = 5.7 Hz, 2H, H-12), 4.23 (s, 2H, H-19/20), 4.17 (t, J = 5.9 Hz, 2H, H-14), 4.06 (t, J = 6.1 Hz, 2H, H-29), 4.02 (t, J = 6.5 Hz, 2H, H-4), 2.41 (td, J = 7.0, 2.6 Hz, 2H, H-31), 2.33 (p, J = 5.9 Hz, 2H, H-13), 2.01 (q, J = 6.5 Hz, 2H, H-30), 1.97 (t, J = 2.6 Hz, 1H, H-33), 1.82 – 1.74 (m, 2H, H-3), 1.54 – 1.45 (m, 12H, H-2 and H-22), 0.98 (t, J = 7.4 Hz, 3H, H-1).

^{13}C NMR (151 MHz, $CDCl_3$) δ 188.27 (C-11), 165.95 (C-6), 163.14 (C-7), 158.28 (C-27), 158.10 (C-15), 156.08 (C-20), 130.61 (C-9), 130.55 (C-18/24), 130.30 (C-18/24), 129.55 (C-17/25), 128.98 (C-17/25), 119.02 (C-8), 114.65 (C-16/26), 114.59 (C-16/26), 106.65 (C-10), 99.14 (C-6), 83.64 (C-32), 80.06 (C-21), 68.99 (C-33), 68.29 (C-29), 66.30 (C-4), 65.14 (C-12), 64.26 (C-14), 48.41 (C-19/23), 48.10 (C-19/23), 31.25 (C-3), 29.30 (C-13), 28.64 (C-22), 28.35 (C-30), 19.31 (C-2), 15.33 (C-31), 13.94 (C-1).

HRMS (HESI$^+$): Calculated for $C_{38}H_{47}O_7NNa$: 652.3245 $[M+Na]^+$, found 652.3224.

Synthesis of **303**

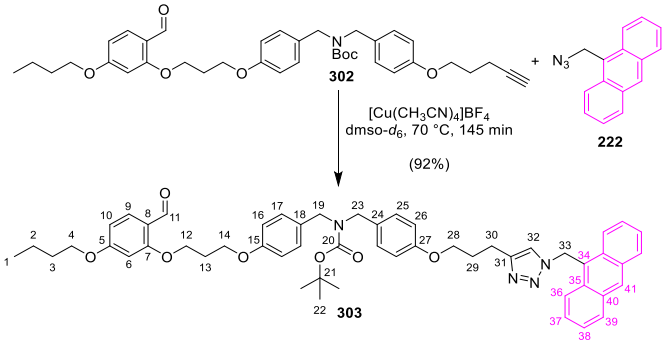

To a solution of **222** (148.8 mg, 0.638 mmol) and **302** (334.7 mg, 0.531 mmol) in degassed DMSO (2.5 mL, 0.2 M) was added $[Cu(CH_3CN)_4]BF_4$ (33.4 mg, 106 µmol) and the reaction was stirred at 70 °C for 145 minutes. The reaction was quenched by the addition of saturated aqueous EDTA (10 mL, pH = 7). The biphasic mixture was extracted with CH_2Cl_2 (4 × 15 mL). The combined organic layers were washed with brine and dried over Na_2SO_4, filtered, and concentrated *in vacuo*. The resultant residue was purified by flash chromatography (SiO_2, CH_2Cl_2/ MeOH, 99:1) to give **303** (420 mg, 92%) as a yellow solid.

^{1}H NMR (600 MHz, $CDCl_3$) δ 10.32 (s, 1H, H-11), 8.58 (s, 1H, H-41), 8.31 (d, J = 8.8 Hz, 2H, H-36), 8.08 (d, J = 8.4 Hz, 2H, H-39), 7.79 (d, J = 8.7 Hz, 1H, H-9), 7.62 – 7.56 (m, 2H, H-37), 7.55 – 7.50 (m, 2H, H-38), 7.15 – 7.07 (m, 2H, H-17), 7.07 – 7.00 (m, 2H, H-25), 6.89 (s, 1H, H-32), 6.86 (d, J = 8.6 Hz, 2H, H-16), 6.68 (d, J = 6.5 Hz, 2H, H-26), 6.55 – 6.50 (m, 3H, H-10 and H-33), 6.47 (d, J = 2.0 Hz, 1H, H-6), 4.29 (s, 2H, H-19), 4.25 (t, J = 6.0 Hz, 2H, H-12), 4.20 (s, 2H, H-23), 4.17 (t, J = 5.9 Hz, 2H, H-14), 4.01 (t, J = 6.5 Hz, 2H, H-4), 3.87 (s, 2H, H-28), 2.73 (t, J = 7.5 Hz, 2H, H-30), 2.33 (p, J = 5.9 Hz, 2H, H-13), 2.01 (p, J = 6.5 Hz, 2H, H-29), 1.78 (p, J = 6.5 Hz, 2H, H-4), 1.56 – 1.43 (m, 12H, H-2 and H-22), 0.98 (t, J = 7.4 Hz, 3H, H-1).

^{13}C NMR (151 MHz, $CDCl_3$) δ 188.25 (C-11), 165.94 (C-5), 163.13 (C-7), 158.21 (C-15), 158.09 (C-27), 156.06 (C-20), 147.54 (C-31), 131.59 (C-35), 130.95 (C-40), 130.59 (C-9), 130.53 (C-18), 130.05 (C-24), 129.91 (C-41), 129.70 – 129.30 (m, C-17 and C-39), 129.04 – 128.77 (m, C-25), 127.75 (C-37), 125.55 (C-38), 124.14 (C-34), 123.18 (C-36), 120.57 (C-32), 119.01 (C-8), 114.57 (C-16), 114.50 (C-26), 106.64 (C-10), 99.13 (C-6), 80.03 (C-21), 68.28 (C-4), 67.03 (C-28), 65.13 (C-12), 64.26 (C-14), 48.36 (C-23), 48.01 (C-19), 46.46 (C-33), 31.24 (C-3), 29.29 (C-13), 28.90 (C-29), 28.64 (C-22), 22.38 (C-30), 19.30 (C-2), 13.94 (C-1).

HRMS (HESI$^+$): Calculated for $C_{53}H_{58}O_7N_4Na$: 885.4198 $[M+Na]^+$, found 885.4203.

Synthesis of **304**·H⁺

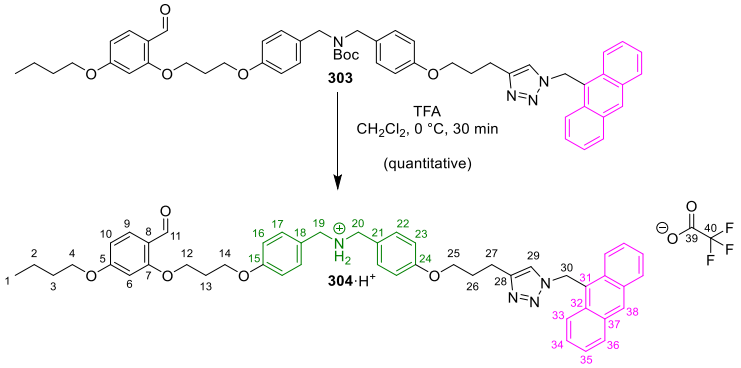

To a solution of **303** (408 mg, 0.47 mmol) in dry CH_2Cl_2 (18 mL, 26 mM) was added TFA (3.70 mL, 47.3 mmol) at 0 °C and the reaction was stirred for 30 minutes. The reaction mixture was concentrated *in vacuo*. The residue was resuspended in PhMe (20 mL) and concentrated *in vacuo* under high vacuum. The last step was repeated two times to furnish **304**·H⁺ (437 mg, ≤108%, *contains residual TFA*) as a colourless solid.

^{1}H NMR (600 MHz, CD_2Cl_2) δ 10.07 (s, 1H, H-11), 9.23 (s, 2H, C19/20 NH_2^+), 8.60 (s, 1H, H-38), 8.30 (d, J = 8.8 Hz, 2H, H-33), 8.08 (d, J = 8.4 Hz, 2H, H-36), 7.69 (d, J = 8.7 Hz, 1H, H-9), 7.63 – 7.58 (m, 2H, H-34), 7.57 – 7.50 (m, 2H, H-35), 7.23 (d, J = 8.6 Hz, 2H, H-17), 7.15 (d, J = 8.6 Hz, 2H, H-22), 7.06 (s, 1H, H-29), 6.85 (d, J = 8.6 Hz, 2H, H-18), 6.64 (d, J = 8.6 Hz, 2H, H-23), 6.52 – 6.49 (m, 3H, H-10 and H-30), 6.44 (d, J = 2.1 Hz, 1H, H-6), 4.18 (t, J = 5.9 Hz, 2H, H-12), 4.10 (t, J = 6.0 Hz, 2H, H-14), 4.00 (t, J = 6.5 Hz, 2H, H-4), 3.87 (s, 4H, H-19 and H-20), 3.75 (t, J = 6.1 Hz, 2H, H-25), 2.67 (t, J = 7.6 Hz, 2H, H-27), 2.25 (p, J = 5.9 Hz, 2H, H-13), 1.88 (p, J = 6.3 Hz, 3H, H-26), 1.75 (p, J = 6.6 Hz, 2H, H-3), 1.47 (h, J = 7.4 Hz, 2H, H-2), 0.96 (t, J = 7.4 Hz, 3H, H-1).

^{13}C NMR (151 MHz, CD_2Cl_2) δ 188.44 (C-11), 166.41 (C-5), 163.49 (C-7), 160.98 (q, J = 37.4 Hz, C-39), 160.05 (C-15), 159.98 (C-24), 147.08 (C-28), 131.87 (C-37), 131.80 (C-17), 131.67 (C-22), 131.18 (C-32), 130.46 (C-9), 130.43 (C-38), 129.89 (C-36), 128.13 (C-34), 125.85 (C-35), 123.87 (C-31), 123.26 (C-33), 123.03 (C-18), 122.77 (C-21), 121.84 (C-29), 119.01 (C-8), 116.32 (q, J = 289.8 Hz, C-40), 115.31 (C-16), 115.11 (C-23), 107.06 (C-10), 99.22 (C-6), 68.66 (C-4), 67.19 (C-25), 65.46 (C-12), 64.80 (C-14), 50.04 (C-19/20), 50.01 (C-19/20), 47.24 (C-30), 31.48 (C-3), 29.21 (C-13), 28.83 (C-26), 21.92 (C-27), 19.53 (C-2), 13.95 (C-1).

^{19}F NMR (471 MHz, CD_2Cl_2) δ -76.06.

HRMS (HESI⁺): Calculated for $C_{48}H_{51}O_5N_4$: 763.3854 [M-TFA]⁺, found 763.3831.

Synthesis of Anthracene One-Barrier [2]Rotaxane 305·H⁺ with Internal Hydrazone Barrier

Synthesis of **305**·H⁺

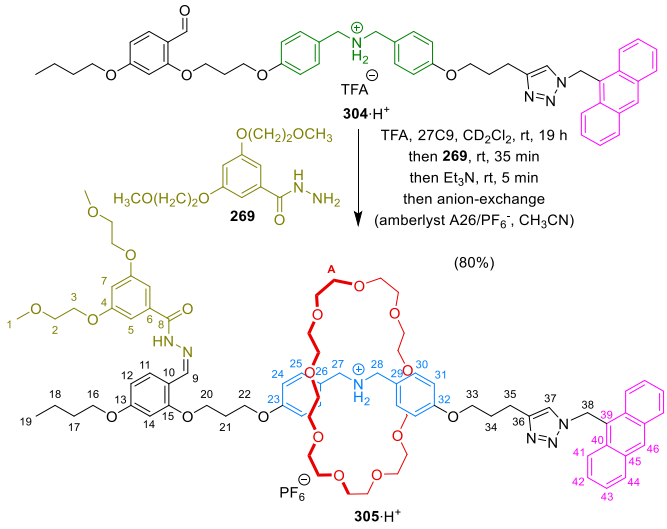

To a solution of **304**·H⁺ (11.8 mg, 13.7 μmol) and TFA (21.5 μl, 275 μmol) in CD_2Cl_2 (549 μl, 25 mM) at room temperature was added 27C9 (27.2 mg, 68.7 μmol) and the reaction was thoroughly mixed and left standing for 19 hours. Hydrazide **269** (39.1 mg, 137 μmol) was added and after 35 minutes the reaction was basified with Et_3N. (40.2 μl, 289 μmol) The crude reaction mixture was purified by size exclusion chromatography (S-X1, CH_2Cl_2) and then anion-exchange chromatography (amberlyst A-26 PF_6^-, CH_3CN) to give **305**·H⁺ (15.3 mg, 80%) as a yellow solid.

^{1}H NMR (600 MHz, CD_3CN) δ 10.05 (s, 1H, C-8 NH), 8.63 (s, 1H, H-9), 8.61 (s, 1H, H-46), 8.43 (d, J = 8.9 Hz, 2H, H-41), 8.09 (d, J = 8.3 Hz, 2H, H-44), 7.76 (d, J = 8.5 Hz, 1H, H-11), 7.62 – 7.58 (m, 2H, H-42), 7.55 – 7.51 (m, 2H, H-43), 7.39 (d, J = 8.5 Hz, 2H, H-24), 7.36 – 7.29 (m, 4H, H-31 and C-27/28 NH_2^+), 7.27 (s, 1H, H-37), 7.00 – 6.95 (m, 4H, H-5 and H-25), 6.80 (d, J = 8.6 Hz, 2H, H-30), 6.63 (s, 1H, H-7), 6.54 – 6.46 (m, 4H, H-12, H-14 and H-38), 4.30 – 4.24 (m, 6H, H-22, H-27 and H-28), 4.22 (t, J = 5.7 Hz, 2H, H-20), 4.12 – 4.09 (m, 4H, H-3), 3.99 – 3.92 (m, 4H, H-16 and H-33), 3.68 – 3.65 (m, 4H, H-2), 3.34 (s, 6H, H-1), 3.32 (s, 36H, H-*A*), 2.66 (t, J = 7.6 Hz, 2H, H-35), 2.26 (p, J = 5.7 Hz, 2H, H-21), 1.92 – 1.87 (m, 2H, H-34), 1.71 (p, J = 6.6 Hz, 2H, H-17), 1.45 (h, J = 7.4 Hz, 2H, H-18), 0.95 (t, J = 7.4 Hz, 3H, H-19).

^{13}C NMR (151 MHz, CD_3CN) δ 163.77 (C-8), 163.53 (C-13), 161.16 (C-4), 160.72 (C-23), 160.35 (C-32), 159.96 (C-15), 148.02 (C-36), 144.87 (C-9), 136.93 (C-6), 133.07 (C-25), 133.03 (C-30), 132.47 (C-45), 131.57 (C-40), 130.35 (C-46), 130.27 (C-44), 128.25 (C-42), 128.10 (C-11), 126.45 (C-39), 126.42 (C-43), 125.14 (C-26), 124.93 (C-29), 124.52 (C-41), 121.94 (C-37), 116.17 (C-10), 115.52 (C-31), 115.39 (C-24), 108.01 (C-12), 106.94 (C-5), 105.30 (C-7), 100.14 (C-14), 71.58 (C-2), 71.09 (C-*A*), 68.87 (C-16), 68.67 (C-3), 67.97 (C-33), 65.80 (C-20), 65.54 (C-22), 59.09 (C-1), 52.58 (C-27/28), 52.52 (C-27/28), 46.82 (C-38), 31.93 (C-17), 29.93 (C-21), 29.24 (C-34), 22.60 (C-35), 19.89 (C-18), 14.11 (C-19).

^{19}F NMR (376 MHz, CD_3CN) δ -73.18 (d, J = 706.4 Hz).

^{31}P NMR (162 MHz, CD_3CN) δ -144.62 (hept, J = 706.4 Hz).

HRMS (HESI⁺): Calculated for $C_{79}H_{105}N_6O_{18}$: 1425.7480 $[M\text{-}PF_6]^+$, found 1425.7483.

Synthesis of Pyrene Stopper 297

Synthesis of **306**

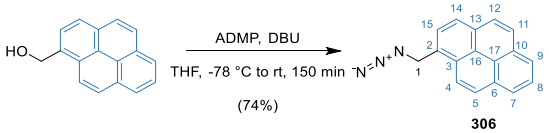

To a solution of 1-pyrenylmethanol (400 mg, 1.72 mmol) and ADMP (589 mg, 2.07 mmol) in dry THF (10 mL, 0.2 M) at –78 °C was added DBU (0.39 mL, 2.58 mmol) and the reaction was continued stirring at –78 °C for 2 hours. The reaction was warmed to room temperature and stirred for another 30 minutes. The reaction was quenched by the addition of saturated aqueous NH_4Cl (10 mL). The biphasic mixture was extracted with CH_2Cl_2 (3 × 15 mL). The combined organic layers were washed with brine and dried over Na_2SO_4, filtered, and concentrated *in vacuo*. The residue was purified by flash chromatography (SiO_2, petroleum ether/ EtOAc, 19:1) to afford **306** (328 mg, 74%) as a pale-yellow solid.

^{1}H NMR (600 MHz, $CDCl_3$) δ 8.28 (d, J = 9.2 Hz, 1H, H-4), 8.25 – 8.21 (m, 2H, H-7 and H-9), 8.19 (d, J = 9.2 Hz, 1H, H-5), 8.17 (d, J = 7.7 Hz, 1H, H-14), 8.10 (d, J = 8.9 Hz, 1H, H-11), 8.07 (d, J = 8.9 Hz, 1H, H-12), 8.04 (t, J = 7.6 Hz, 1H, H-8), 7.98 (d, J = 7.7 Hz, 1H, H-15), 5.04 (s, 2H, H-1).

^{13}C NMR (151 MHz, $CDCl_3$) δ 131.95 (C-13), 131.37 (C-10), 130.88 (C-6), 129.42 (C-3), 128.55 (C-5), 128.42 (C-2), 128.05 (C-11), 127.64 (C-15), 127.49 (C-12), 126.35 (C-8), 125.78 (C-7/9), 125.71 (C-7/9), 125.21 (C-16), 124.80 (C-14), 124.79 (C-17), 122.84 (C-4), 53.25 (C-1).

HRMS (APCI$^+$): Calculated for $C_{17}H_{12}N_3$: 258.1026 $[M+H]^+$, found 258.1026.

Synthesis of **307**

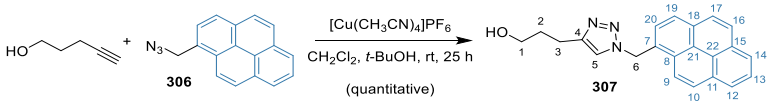

To a solution of **306** (322 mg, 1.25 mmol) and 4-pentyn-1-ol (0.17 mL, 1.86 mmol) in degassed CH_2Cl_2 (8 mL) and *t*-BuOH (2 mL) was added $[Cu(CH_3CN)_4]PF_6$ (92.6 mg, 248 µmol) and the reaction was stirred at room temperature for 25 hours. The reaction was quenched by the addition of saturated aqueous EDTA (10 mL, pH = 7). The biphasic mixture was extracted with CH_2Cl_2 (3 × 25 mL). The combined organic layers were washed with brine and dried over Na_2SO_4, filtered, and concentrated *in vacuo*. The residue was purified by flash chromatography (SiO_2, CH_2Cl_2/ MeOH, 39:1) to give **307** (434 mg, 102%) as a colourless solid.

^{1}H NMR (600 MHz, $CDCl_3$) δ 8.25 – 8.21 (m, 3H, H-9, H-12 and H-14), 8.19 (d, J = 7.8 Hz, 1H, H-19), 8.15 (d, J = 9.2 Hz, 1H, H-10), 8.13 (d, J = 8.9 Hz, 1H, H-16), 8.08 (d, J = 8.9 Hz, 1H, H-17), 8.05 (t, J = 7.6 Hz, 1H, H-13), 7.95 (d, J = 7.7 Hz, 1H, H-20), 7.05 (s, 1H, H-5), 6.22 (s, 2H, H-6), 3.63 (q, J = 6.0 Hz, 2H, H-), 2.71 (t, J = 7.2 Hz, 2H, H-3), 2.09 (t, J = 5.7 Hz, 1H, C-1 OH), 1.83 (p, J = 6.5 Hz, 2H, H-2).

^{13}C NMR (151 MHz, $CDCl_3$) δ 147.94 (C-4), 132.27 (C-18), 131.32 (C-15), 130.73 (C-11), 129.51 (C-8), 129.21 (C-10), 128.45 (C-16), 127.82 (C-20), 127.37 (C-17), 127.10 (C-7), 126.56 (C-13), 126.09 (C-14), 125.99 (C-12), 125.25 (C-21), 125.07 (C-19), 124.64 (C-22), 122.12 (C-9), 120.91 (C-5), 62.12 (C-1), 52.55 (C-6), 31.89 (C-2), 22.32 (C-3).

HRMS (HESI$^+$): Calculated for $C_{22}H_{19}ON_3Na$: 364.1420 $[M+Na]^+$, found 364.1406.

Synthesis of **308**

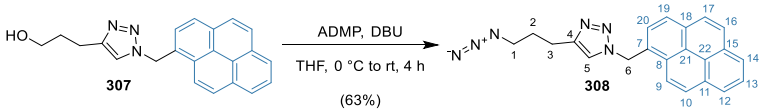

To a suspension of **307** (430 mg, 1.26 mmol) and ADMP (714 mg, 2.50 mmol) in dry THF (15 mL, 0.1 M) at 0 °C was added DBU (0.56 mL, 3.75 mmol) and the reaction was continued stirring at 0 °C for 3 hours. The reaction was warmed to room temperature and stirred for another 1 hour. The reaction was quenched by the addition of saturated aqueous NH_4Cl (10 mL). The biphasic mixture was extracted with CH_2Cl_2 (3 × 25 mL). The combined organic layers were washed with brine and dried over Na_2SO_4, filtered, and concentrated *in vacuo*. The residue was purified by flash chromatography (SiO_2, petroleum ether/ EtOAc, 3:1) to afford **308** (292 mg, 63%) as a fluorescent colourless solid.

^{1}H NMR (600 MHz, CD_3CN) δ 8.35 (d, J = 9.2 Hz, 1H, H-9), 8.27 – 8.24 (m, 2H, H-12 and H-14), 8.21 (d, J = 7.8 Hz, 1H, H-19), 8.19 (d, J = 9.2 Hz, 1H, H-10), 8.13 (d, J = 8.9 Hz, 1H, H-16), 8.09 (d, J = 8.9 Hz, 1H, H-17), 8.05 (t, J = 7.6 Hz, 1H, H-13), 7.93 (d, J = 7.8 Hz, 1H, H-20), 7.48 (s, 1H, H-5), 6.20 (s, 2H, H-6), 3.26 (t, J = 6.8 Hz, 2H, H-1), 2.64 (t, J = 7.5 Hz, 2H, H-3), 1.81 (p, J = 7.1 Hz, 2H, H-2).

^{13}C NMR (151 MHz, CD_3CN) δ 147.82 (C-5), 132.63 (C-18), 132.16 (C-15), 131.56 (C-11), 129.87 (C-8), 129.74 (C-7), 129.37 (C-10), 128.88 (C-16), 128.56 (C-20), 128.26 (C-17), 127.46 (C-13), 126.74 (C-14), 126.61 (C-12), 126.01 (C-19), 125.57 (C-21), 125.15 (C-22), 123.45 (C-9), 122.70 (C-5), 52.43 (C-6), 51.36 (C-1), 29.21 (C-2), 23.27 (C-3).

HRMS (HESI$^+$): Calculated for $C_{22}H_{18}N_6Na$: 389.1485 $[M+Na]^+$, found 389.1472.

Synthesis of **297**

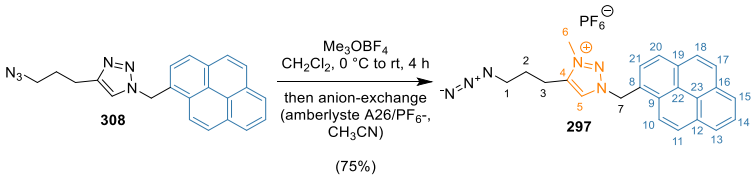

To a solution of **308** (284 mg, 0.78 mmol) in dry degassed CH_2Cl_2 (10 mL, 0.1 M) at 0 °C was added trimethyloxonium tetrafluoroborate (171 mg, 1.16 mmol) and the reaction was stirred for 3 hours. The reaction was warmed to room temperature and stirred for another 1 hour. The reaction mixture was quenched with MeOH (5 mL) and concentrated *in vacuo*. The resultant residue was purified by flash chromatography (SiO_2, CH_2Cl_2/ MeOH, 19:1) and then anion-exchange chromatography (amberlyst A-26 PF_6^-, CH_3CN) to give **297** (308 mg, 75%) as a light brown solid.

^{1}H NMR (600 MHz, CD_3CN) δ 8.38 – 8.33 (m, 3H, H-13, H-15 and H-20), 8.33 – 8.28 (m, 2H, H-10 and H-11), 8.25 (d, J = 9.0 Hz, 1H, H-17), 8.20 (d, J = 9.0 Hz, 1H, H-18), 8.18 (d, J = 7.8 Hz, 1H, H-21), 8.14 (t, J = 7.6 Hz, 1H, H-14), 8.09 (s, 1H, H-5), 6.41 (s, 2H, H-7), 4.09 (s, 3H, H-6), 3.34 (t, J = 6.6 Hz, 2H, H-1), 2.78 (t, J = 7.8 Hz, 2H, H-3), 1.86 – 1.80 (m, 2H, H-2).

^{13}C NMR (151 MHz, CD_3CN) δ 145.06 (C-4), 133.72 (C-19), 132.14 (C-16), 131.49 (C-12), 130.63 (C-9), 130.16 (C-11), 130.01 (C-21), 129.77 (C-17), 128.99 (C-5), 128.25 (C-18), 127.85 (C-14), 127.36 (C-15), 127.12 (C-13), 126.20 (C-20), 125.72 (C-22), 125.31 (C-8), 125.03 (C-23), 123.07 (C-10), 55.98 (C-7), 50.75 (C-1), 38.52 (C-6), 26.81 (C-2), 21.19 (C-3).

^{19}F NMR (376 MHz, CD_3CN) δ -72.94 (d, J = 706.4 Hz).

^{31}P NMR (162 MHz, CD_3CN) δ -144.63 (hept, J = 706.4 Hz).

HRMS (HESI$^+$): Calculated for $C_{23}H_{21}N_6$: 381.1822 $[M\text{-}PF_6]^+$, found 381.1805.

Synthesis of Model Pyrene-Terminated One-Barrier Pump 310·H$^+$

Synthesis of **372**

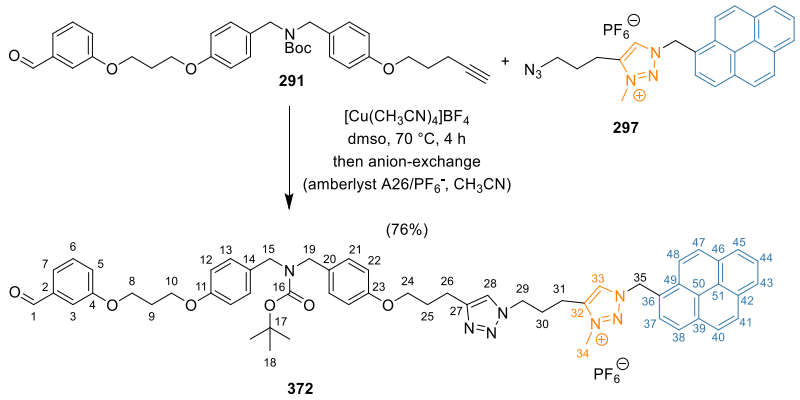

To a solution of **297** (290.7 mg, 0.550 mmol) and **291** (255.7 mg, 0.458 mmol) in degassed DMSO (2.5 mL, 0.2 M) was added $[Cu(CH_3CN)_4]BF_4$ (28.8 mg, 91.7 µmol) and the reaction was stirred at 70 °C for 4 hours. The reaction was quenched by the addition of saturated aqueous EDTA (10 mL, pH = 7). The biphasic mixture was extracted with CH_2Cl_2 (3 × 15 mL). The combined organic layers were washed with brine and dried over Na_2SO_4, filtered, and concentrated *in vacuo*. The resultant residue was purified by flash chromatography (SiO_2, CH_2Cl_2/ MeOH, 39:1), followed by size exclusion chromatography (S-X1, CH_2Cl_2) and finally, by anion-exchange chromatography (amberlyst A-26 PF_6^-, CH_3CN) to give **372** (378 mg, 76%) as a colourless solid.

^{1}H NMR (600 MHz, CD_3CN) δ 9.93 (s, 1H, H-1), 8.36 – 8.32 (m, 3H, H-38, H-43 and H-45), 8.32 – 8.28 (m, 2H, H-47 and H-48), 8.24 (d, J = 9.0 Hz, 1H, H-41), 8.19 (d, J = 8.9 Hz, 1H, H-40), 8.16 (d, J = 7.8 Hz, 1H, H-37), 8.13 (t, J = 7.6 Hz, 1H, H-44), 8.07 (s, 1H, H-33), 7.49 – 7.45 (m, 3H, H-6, H-7 and H-28), 7.41 – 7.40 (m, 1H, H-3), 7.23 (dt, J = 6.1, 2.8 Hz, 1H, H-5), 7.13 – 7.09 (m, 4H, H-12 and H-22), 6.88 (d, J = 8.6 Hz, 2H, H-13), 6.82 (d, J = 8.6 Hz, 2H, H-21), 6.39 (s, 2H, H-35), 4.31 (t, J = 6.7 Hz, 2H, H-29), 4.27 – 4.20 (m, 6H, H-15, H-19 and H-8), 4.15 (t, J = 6.2 Hz, 2H, H-10), 4.04 (s, 3H, H-34), 3.95 (t, J = 6.3 Hz, 2H, H-24), 2.75 (t, J = 7.6 Hz, 2H, H-26), 2.70 (t, J = 7.7 Hz, 2H, H-31), 2.21 (p, J = 6.2 Hz, 2H, H-9), 2.16 – 2.12 (m, 2H, H-30, *overlapped with resid. H_2O peak*), 2.02 (p, J = 6.8 Hz, 2H, H-25), 1.43 (s, 9H, H-18).

^{13}C NMR (151 MHz, CD_3CN) δ 193.42 (C-1), 160.50 (C-4), 159.18 (C-23), 159.12 (C-11), 156.60 (C-16), 148.11 (C-27), 144.65 (C-32), 139.09 (C-2), 133.72 (C-39), 132.13 (C-42), 131.62 (C-14/20, *weak*), 131.51 (C-14/20, *weak*), 131.48 (C-46), 131.30 (C-28), 130.62 (C-49), 130.17 (C-47), 130.02 (C-37), 129.95 (C-12 and C-22), 129.78 (C-41), 129.04 (C-33), 128.24 (C-40), 127.86 (C-44), 127.37 (C-43), 127.12 (C-45), 126.20 (C-38), 125.72 (C-50), 125.25 (C-36), 125.02 (C-51), 123.58 (C-7), 123.08 (C-48), 122.64 (C-6), 122.27 (C-5), 115.42 (C-13/21), 115.37 (C-13/21), 114.46 (C-3), 80.39 (C-17), 67.83 (C-24), 65.80 (C-8), 65.33 (C-10), 55.97 (C-35), 49.71 (C-15/19, *weak*), 49.41 (C-15/19, *weak*), 49.17 (C-31), 38.53 (C-34), 29.83 (C-9), 29.74 (C-25), 28.61 (C-18), 27.99 (C-30), 22.63 (C-26), 21.06 (C-29).

^{19}F NMR (376 MHz, CD_3CN) δ -72.94 (d, J = 706.4 Hz).

^{31}P NMR (162 MHz, CD_3CN) δ -144.63 (hept, J = 706.1 Hz).

HRMS (HESI$^+$): Calculated for $C_{57}H_{60}N_7O_6$: 938.4600 $[M\text{-}PF_6]^+$, found 938.4570.

Synthesis of **310**·H⁺

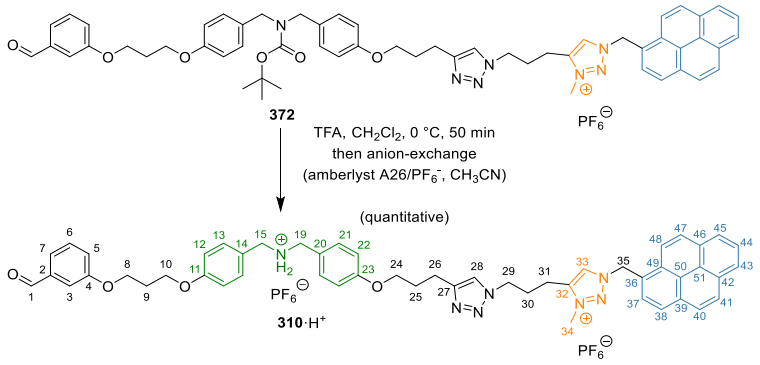

To a solution of **372** (372 mg, 0.34 mmol) in dry CH_2Cl_2 (15 mL, 23 mM) was added TFA (2.68 mL, 34.3 mmol) at 0 °C and the reaction was stirred for 50 minutes. The reaction mixture was concentrated *in vacuo*. The residue was resuspended in PhMe (20 mL) and concentrated *in vacuo* under high vacuum. The last step was repeated two times. The residue obtained was subjected to anion-exchange chromatography (amberlyst A-26 PF_6^-, CH_3CN) to give **310**·H⁺ (388 mg, 100%) as a colourless solid.

^{1}H NMR (600 MHz, CD_3CN) δ 9.94 (s, 1H, H-1), 8.37 – 8.33 (m, 3H, H-38, H-43 and H-45), 8.33 – 8.28 (m, 2H, H-47 and H-48), 8.25 (d, J = 8.9 Hz, 1H, H-41), 8.20 (d, J = 8.9 Hz, 1H, H-40), 8.17 (d, J = 7.8 Hz, 1H, H-37), 8.14 (t, J = 7.6 Hz, 1H, H-44), 8.09 (s, 1H, H-33), 7.50 – 7.46 (m, 3H, H-5, H-6 and H-28), 7.41 – 7.39 (m, 1H, H-3), 7.38 – 7.33 (m, 4H, H-15 and H-21), 7.23 (dt, J = 6.2, 2.8 Hz, 1H, H-7), 6.99 (d, J = 8.7 Hz, 2H, H-12), 6.94 (d, J = 8.7 Hz, 2H, H-22), 6.87 (s, 2H, C-15/19 NH_2^+), 6.40 (s, 2H, H-35), 4.31 (t, J = 6.7 Hz, 2H, H-29), 4.23 (t, J = 6.2 Hz, 2H, H-8), 4.19 (t, J = 6.2 Hz, 2H, H-10), 4.12 (s, 4H, H-15 and H-19), 4.05 (s, 3H, H-34), 4.01 (t, J = 6.3 Hz, 2H, H-24), 2.76 (t, J = 7.7 Hz, 2H, H-26), 2.71 (t, J = 7.7 Hz, 2H, H-31), 2.24 (p, J = 6.2 Hz, 2H, H-9), 2.17 – 2.12 (m, 2H, H-30, *overlapped with resid. H_2O peak*), 2.04 (p, J = 6.4 Hz, 2H, H-25).

^{13}C NMR (151 MHz, CD_3CN) δ 193.44 (C-1), 161.03 (C-23), 160.96 (C-11), 160.46 (C-4), 148.06 (C-27), 144.66 (C-32), 139.10 (C-2), 133.73 (C-39), 132.84 (C-13/21), 132.81 (C-13/21), 132.14 (C-42), 131.48 (C-46), 131.34 (C-28), 130.63 (C-49), 130.17 (C-47), 130.02 (C-37), 129.79 (C-41), 129.04 (C-33), 128.25 (C-40), 127.87 (C-44), 127.38 (C-43), 127.12 (C-45), 126.20 (C-38), 125.72 (C-50), 125.27 (C-36), 125.02 (C-51), 123.79 (C-5), 123.32 (C-14), 123.22 (C-20), 123.09 (C-48), 122.61 (C-6), 122.30 (C-7), 115.85 (C-12), 115.79 (C-22), 114.25 (C-3), 68.09 (C-24), 65.67 (C-8), 65.49 (C-10), 55.98 (C-35), 51.70 (C-15 and C-19), 49.18 (C-29), 38.54 (C-34), 29.77 (C-25), 29.72 (C-9), 28.01 (C-30), 22.63 (C-26), 21.07 (C-31).

^{19}F NMR (471 MHz, CD_3CN) δ -72.88 (d, J = 706.5 Hz).

^{31}P NMR (203 MHz, CD_3CN) δ -144.61 (hept, J = 706.5 Hz).

HRMS (HESI⁺): Calculated for $C_{52}H_{53}F_6N_7O_4P$: 984.3795 $[M\text{-}PF_6]^+$, found 984.3789.

Synthesis and Switching of Pyrene (Pseudo)[2]Rotaxanes 312·H⁺ and 311·H⁺

Synthesis of **312**·H⁺

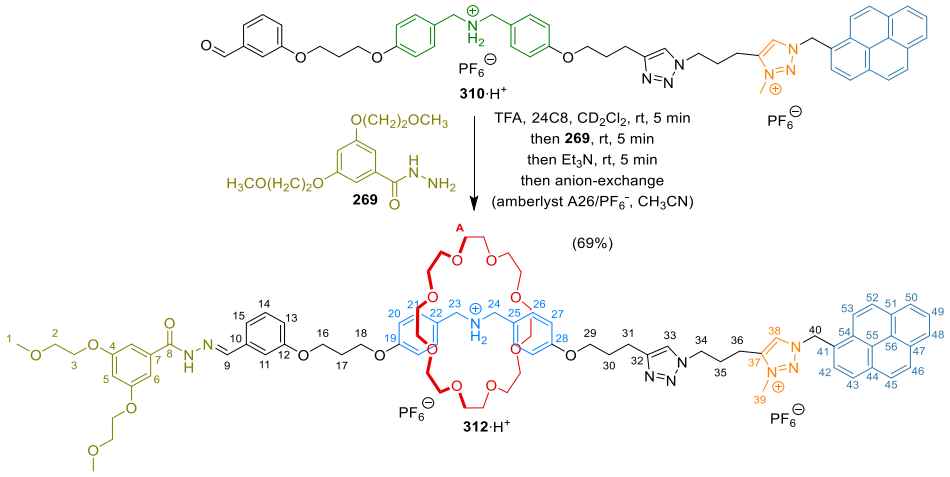

To a solution of **310**·H⁺ (10.5 mg, 9.3 µmol) and 24C8 (16.7 mg, 46.5 µmol) in CD_2Cl_2 (464 µl, 25 mM) at room temperature was added TFA (14.5 µl, 186 µmol) and the reaction was thoroughly mixed and left standing for 5 minutes. Hydrazide **269** (26.4 mg, 92.9 µmol) was added and after 5 minutes the reaction was basified with Et_3N. (27.2 µl, 195 µmol) The crude reaction mixture was purified by size exclusion chromatography (S-X1, CH_2Cl_2) and then anion-exchange chromatography (amberlyst A-26 PF_6^-, CH_3CN) to give **312**·H⁺ (11.3 mg, 69%) as a yellow solid.

Note: The ^{19}F NMR spectrum has been acquired after switching *in-situ* with DBU/TFA.

^{1}H NMR (600 MHz, CD_3CN) δ 10.15 (s, 1H, C-8 NH), 8.35 (d, J = 7.7 Hz, 2H, H-48 and H-50), 8.33 (d, J = 7.9 Hz, 1H, H-43), 8.31 – 8.27 (m, 2H, H-52 and H-53), 8.25 – 8.22 (m, 2H, H-9 and H-46), 8.19 (d, J = 9.0 Hz, 1H, H-45), 8.16 (d, J = 7.8 Hz, 1H, H-42), 8.13 (t, J = 7.6 Hz, 1H, H-49), 8.10 (s, 1H, H-38), 7.49 (s, 1H, H-33), 7.45 (d, J = 8.8 Hz, 2H, H-21), 7.44 (d, J = 8.8 Hz, 2H, H-26), 7.40 – 7.30 (m, 4H, H-11, H-14 and C-23/24 NH_2^+), 7.24 (d, J = 7.4 Hz, 1H, H-15), 7.01 – 6.96 (m, 5H, H-6, H-13 and H-20), 6.92 (d, J = 8.7 Hz, 2H, H-27), 6.66 (s, 1H, H-5), 6.39 (s, 2H, H-40), 4.43 – 4.36 (m, 4H, H-23 and H-24), 4.31 (t, J = 6.7 Hz, 2H, H-34), 4.21 (t, J = 6.1 Hz, 4H, H-16 and H-18), 4.16 – 4.12 (m, 4H, H-3), 4.04 (s, 3H, H-39), 4.00 (t, J = 6.4 Hz, 2H, H-29), 3.71 – 3.66 (m, 4H, H-2), 3.40 (s, 32H, H-*A*), 3.36 (s, 6H, H-1), 2.75 (t, J = 7.6 Hz, 2H, H-31), 2.71 (t, J = 7.7 Hz, 2H, H-36), 2.23 (p, J = 6.0 Hz, 2H, H-17), 2.15 (p, J = 6.7 Hz, 2H, H-35, *overlapped with solvent peak*), 2.03 (p, J = 6.5 Hz, 2H, H-30).

^{13}C NMR (151 MHz, CD_3CN) δ 164.13 (C-8), 161.18 (C-4), 160.55 (C-19), 160.52 (C-28), 160.29 (C-12), 148.67 (C-9), 148.09 (C-32), 144.66 (C-37), 136.84 (C-10), 136.68 (C-7), 133.70 (C-44), 133.15 (C-21), 133.07 (C-26), 132.13 (C-47), 131.48 (C-51), 131.01 (C-14), 130.61 (C-54), 130.16 (C-52), 130.00 (C-42), 129.76 (C-46), 129.06 (C-38), 128.25 (C-45), 127.85 (C-49), 127.36 (C-48), 127.12 (C-50), 126.19 (C-43), 125.70 (C-55), 125.53 (C-22), 125.46 (C-52), 125.28 (C-41), 125.01 (C-56), 123.09 (C-53), 122.62 (C-33), 121.53 (C-15), 118.33 (C-13, *overlapped with solvent peak*), 115.36 (C-20), 115.28 (C-27), 112.57 (C-11), 107.05 (C-6), 105.54 (C-5), 71.57 (C-2), 71.27 (C-*A*), 68.68 (C-3), 68.04 (C-29), 65.46 (C-16), 65.39 (C-18), 59.07 (C-1), 55.96 (C-40), 52.53 (C-23/24), 52.50 (C-23/24), 49.20 (C-34), 38.52 (C-39), 29.84 (C-17), 29.74 (C-30), 28.00 (C-35), 22.64 (C-31), 21.08 (C-36).

^{19}F NMR (471 MHz, CD_3CN) δ -72.85 (d, *J* = 706.6 Hz), -75.54 (TFA).

^{31}P NMR (202 MHz, CD_3CN) δ -144.62 (hept, *J* = 706.6 Hz).

HRMS (HESI$^+$): Calculated for $C_{81}H_{103}N_9O_{16}$: 728.8755 $[M\text{-}2PF_6]^{2+}$, found 728.8756.

Switching from **312**·H⁺ to **312**

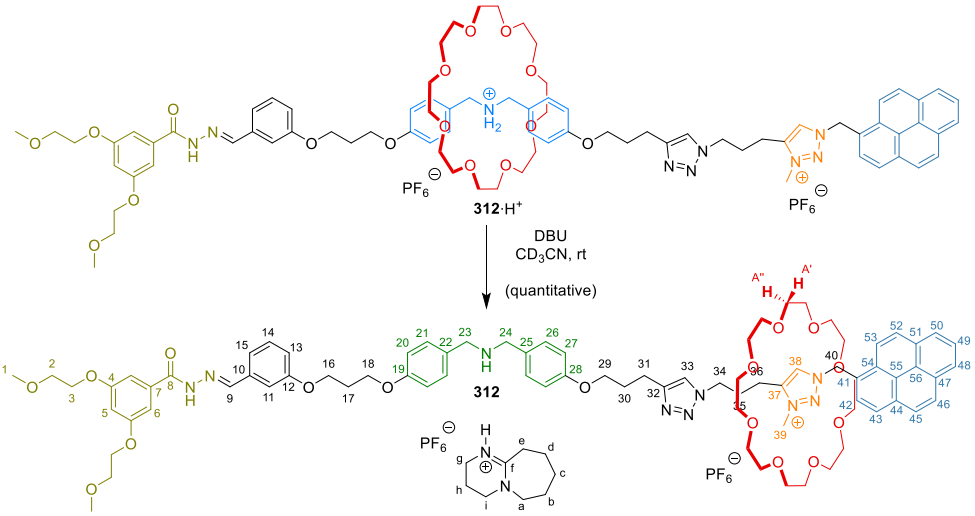

To a solution of **312**·H⁺ (11.3 mg, 6.5 µmol) in CD_3CN (592 µl, 11 mM) at room temperature was added DBU (1.0 µL, 6.7 µmol) to give a yellow solution of **312** (*quantitative by NMR*).

^{1}H NMR (600 MHz, CD_3CN) δ 8.42 (s, 1H, H-38), 8.31 (d, J = 7.7 Hz, 1H, H-48), 8.29 (d, J = 7.8 Hz, 1H, H-50), 8.27 (d, J = 7.9 Hz, 1H, H-43), 8.23 (s, 1H, H-9), 8.22 – 8.21 (m, 2H, H-52 and H-53), 8.20 (d, J = 9.2 Hz, 1H, H-46), 8.16 (d, J = 7.8 Hz, 1H, H-42), 8.13 (d, J = 8.9 Hz, 1H, H-45), 8.10 (t, J = 7.6 Hz, 1H, H-49), 7.49 (s, 1H, H-33), 7.29 (t, J = 7.8 Hz, 1H, H-14), 7.26 (s, 1H, H-11), 7.25 – 7.19 (m, 3H, H-15 and H-21), 7.16 (d, J = 8.5 Hz, 2H, H-26), 7.00 (d, J = 2.0 Hz, 2H, H-6), 6.95 (d, J = 7.1 Hz, 1H, H-13), 6.89 (d, J = 8.5 Hz, 2H, H-20), 6.75 (d, J = 8.5 Hz, 2H, H-27), 6.64 (s, 1H, H-5), 6.33 (s, 2H, H-40), 4.29 (t, J = 7.7 Hz, 2H, H-34), 4.24 (s, 3H, H-39), 4.16 – 4.10 (m, 9H, H-3, H-16, H-18 and C-*f*/*g* NH), 3.90 (t, J = 6.3 Hz, 2H, H-29), 3.68 – 3.66 (m, 4H, H-2), 3.63 (s, 2H, H-23), 3.61 (s, 2H, H-24), 3.52 – 3.49 (m, 2H, H-*a*), 3.44 (t, J = 5.9 Hz, 2H, H-*i*), 3.35 (s, 6H, H-1), 3.26 (t, J = 5.8 Hz, 2H, H-*g*), 3.16 – 3.08 (m, 18H, H-36 and H-*A'/A''*), 2.99 – 2.93 (m, 16H, H-*A'/A''*), 2.73 (t, J = 7.4 Hz, 2H, H-31), 2.58 – 2.55 (m, 2H, H-*e*), 2.25 (dt, J = 16.1, 8.3 Hz, 2H, H-35), 2.17 (p, J = 6.1 Hz, 2H, H-17), 2.00 – 1.95 (m, 4H, H-30 and H-*h*), 1.74 – 1.71 (m, 2H, H-*c*), 1.70 – 1.63 (m, 4H, H-*b* and H-*d*).

^{13}C NMR (151 MHz, CD_3CN) δ 166.99 (C-*f*), 164.25 (C-8), 161.15 (C-4), 160.29 (C-12), 158.82 (C-19), 158.72 (C-28), 148.79 (C-9), 147.46 (C-37), 147.35 (C-32), 136.85 (C-10), 136.77 (C-7), 134.22 (C-22), 134.07 (C-25), 133.74 (C-44), 132.03 (C-47), 131.42 (C-51), 131.00 (C-14), 130.94 (C-38), 130.71 (C-42), 130.57 (C-54), 130.28 (C-21), 130.22 (C-52), 130.21 (C-26), 129.69 (C-46), 128.15 (C-45), 127.81 (C-49), 127.31 (C-48), 127.06 (C-50), 126.20 (C-43), 125.73 (C-55), 125.30 (C-41), 124.98 (C-56), 123.04 (C-53), 122.62 (C-33), 121.27 (C-15), 117.98 (C-13), 115.26 (C-20), 115.15 (C-27), 112.84 (C-11), 107.05 (C-6), 105.59 (C-5), 71.57 (C-2), 71.41 (C-*A*), 68.66 (C-3), 67.46 (C-29), 65.55 (C-16), 65.33 (C-18), 59.07 (C-1), 55.94 (C-40), 55.21 (C-*a*), 52.94 (C-23 and C-24), 50.50 (C-29), 49.34 (C-*i*), 39.22 (C-*g*), 38.38 (C-39), 33.95 (C-*e*), 29.95 (C-17), 29.67 (C-30), 29.44 (C-*c*), 26.97 (C-*b*), 26.69 (C-35), 24.36 (C-*d*), 22.50 (C-31), 21.26 (C-36), 19.93 (C-*h*).

Synthesis of **311**·H⁺

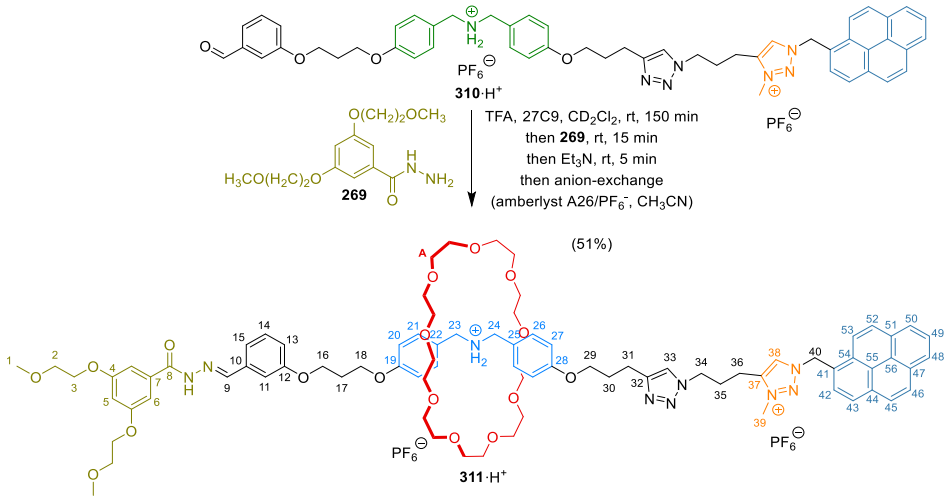

To a solution of **310**·H⁺ (12.4 mg, 11.0 µmol) and TFA (25.7 µl, 330 µmol) in CD_2Cl_2 (550 µl, 20 mM) at room temperature was added 27C9 (43.6 mg, 110 µmol) and the reaction was thoroughly mixed and left standing for 150 minutes. Hydrazide **269** (31.3 mg, 110 µmol) was added and after 15 minutes the reaction was basified with Et_3N. (47.5 µl, 341 µmol) The crude reaction mixture was purified by size exclusion chromatography (S-X1, CH_2Cl_2) and then anion-exchange chromatography (amberlyst A-26 PF_6^-, CH_3CN) to give **X** (10.0 mg, ≤ 51%, *part. dethreading obs.*) as a yellow solid.

Note: Due to observed instability i.e. fast dethreading of compound **311**·H⁺ in solution (CD_3CN) characterisation is based ^{1}H NMR and HRMS only.

^{1}H NMR (600 MHz, CD_3CN) δ 10.16 (s, 1Hz, C-8 NH), 8.36 – 8.32 (m, 3H, H-43, H-48 and H-50), 8.29 (s, 2H, H-52 and H-53), 8.26 – 8.22 (m, 2H, H-9 and H-46), 8.19 (d, *J* = 8.9 Hz, 1H, H-45), 8.16 (d, *J* = 7.8 Hz, 1H, H-42), 8.13 (t, *J* = 7.6 Hz, 1H, H-49), 8.10 (s, 1H, H-38), 7.51 – 7.42 (m, 6H, H-21, H-26 and C23/24 NH_2^+), 7.39 – 7.29 (m, 2H, H-11 and H-14), 7.23 (d, *J* = 7.2 Hz, 1H, H-15), 7.02 – 6.96 (m, 5H, H-6, H-13 and H-20), 6.93 (d, *J* = 8.6 Hz, 2H, H-27), 6.66 (s, 1H, H-5), 6.39 (s, 2H, H-40), 4.35 – 4.29 (m, 6H, H-23, H-24 and H-34), 4.23 – 4.18 (m, 4H, H-16 and H-18), 4.15 – 4.11 (m, 4H, H-3), 4.05 (s, 3H, H-35), 4.00 (t, *J* = 6.4 Hz, 2H, H-29), 3.70 – 3.67 (m, 5H, H-2), 3.60 (s, 4H, *dethreaded macrocycle*), 3.41 (s, 32H, H-*A, part. dethreading obs.*), 3.36 (s, 6H, H-1), 2.77 – 2.70 (m, 4H, H-31 and H-36), 2.24 – 2.12 (m, 4H, H-17 and H-35, *overlapped with solvent peak*), 2.03 (p, *J* = 6.4 Hz, 2H, H-30).

HRMS (ESI⁺): Calculated for $C_{83}H_{107}F_6N_9O_{17}P$: 1646.7421 $[M\text{-}PF_6]^+$, found 1646.7358.s

Synthesis of Disulfide Stopper 317

Synthesis of **319**

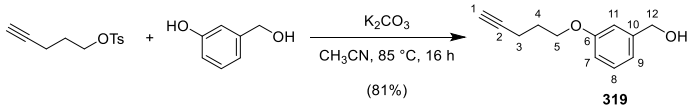

To a solution of pent-4-yn-1-yl tosylate (1.50 g, 6.29 mmol) and 3-hydroxybenzyl alcohol (938 mg, 7.55 mmol) in CH_3CN (60 mL, 0.1 M) was added K_2CO_3 (granulate, 1.31 g, 9.44 mmol) and the reaction mixture was heated to reflux (heating set to 85 °C; using a reflux condenser and drying tube charged with $CaCl_2$) for 16 hours. The reaction mixture was cooled to room temperature and the solvent removed *in vacuo*. The crude was resuspended in $CHCl_3$, filtrated through a plug of celite and the residue washed with additional $CHCl_3$. (100 mL in total) The combined organic phases were concentrated *in vacuo* and the resulting residue was purified by flash chromatography (SiO_2, petroleum ether/ EtOAc, 4:1) to give **319** (972 mg, 81%) as a colourless oil.

^{1}H NMR (600 MHz, $CDCl_3$) δ 7.29 – 7.25 (m, 1H, H-8, *overlapped by solvent peak*), 6.96 – 6.92 (m, 2H, H-9 and H-11), 6.84 (dd, J = 8.4, 2.3 Hz, 1H, H-7), 4.68 (d, J = 6.0 Hz, 2H, H-12), 4.08 (t, J = 6.1 Hz, 2H, H-5), 2.41 (td, J = 7.0, 2.7 Hz, 1H, H-3), 2.01 (p, J = 6.5 Hz, 2H, H-4), 1.97 (t, J = 2.7 Hz, 1H, H-1), 1.61 (t, J = 6.0 Hz, 1H, C-12 OH).

^{13}C NMR (151 MHz, $CDCl_3$) δ 159.34 (C-6), 142.67 (C-10), 129.78 (C-8), 119.30 (C-9), 113.99 (C-7), 113.05 (C-11), 83.62 (C-2), 69.01 (C-1), 66.23 (C-5), 65.47 (C-12), 28.34 (C-4), 15.33 (C-3).

HRMS (ASAP$^+$): Calculated for $C_{12}H_{15}O_2$: 191.1067 $[M+H]^+$, found 191.1065.

Synthesis of **373**

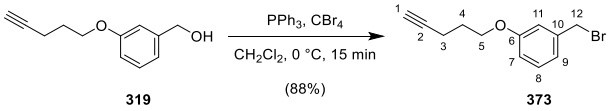

To a solution of **319** (964 mg, 5.07 mmol) in CH_2Cl_2 (50 mL, 0.1 M) at 0 °C was added CBr_4 (4.20 g, 12.7 mmol) and PPh_3 (2.66 g, 10.1 mmol) and the reaction was stirred at 0 °C for 15 minutes. The resultant mixture was evaporated from SiO_2 and purified by flash chromatography (SiO_2, petroleum ether/ EtOAc, 9:1) give **373** (1.13 g, 88%) as a colourless oil.

^{1}H NMR (600 MHz, $CDCl_3$) δ 7.26 – 7.22 (m, 1H, H-8, *overlapped by solvent peak*), 6.97 (dt, J = 7.5, 1.3 Hz, 1H, H-9), 6.94 (t, J = 2.1 Hz, 1H, H-11), 6.84 (dd, J = 8.3, 1.6 Hz, 1H, H-7), 4.46 (s, 2H, H-8), 4.08 (t, J = 6.1 Hz, 2H, H-12), 2.42 (td, J = 7.0, 2.7 Hz, 3H, H-3), 2.01 (p, J = 6.6 Hz, 2H, H-4), 1.98 (t, J = 2.7 Hz, 1H, H-1).

^{13}C NMR (151 MHz, $CDCl_3$) δ 159.22 (C-6), 139.29 (C-10), 129.97 (C-8), 121.48 (C-9), 115.22 (C-11), 114.81 (C-7), 83.55 (C-2), 69.07 (C-1), 66.27 (C-5), 33.63 (C-12), 28.29 (C-4), 15.31 (C-3).

HRMS (ASAP$^+$): Calculated for $C_{12}H_{14}OBr$: 253.0223 $[M+H]^+$, found 253.0220.

Synthesis of **321**

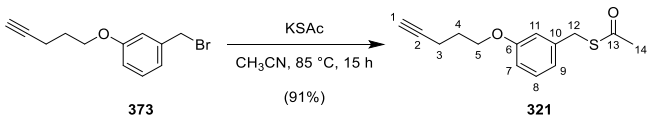

To a solution of **373** (1.07 g, 4.22 mmol) in CH_3CN (45 mL, 0.1 M) was added KSAc (578 mg, 5.06 mmol) and the reaction mixture was heated to reflux (heating set to 85 °C; using a reflux condenser and drying tube charged with $CaCl_2$) for 15 hours. The reaction mixture was cooled to room temperature and the solvent removed *in vacuo*. The residue was purified by flash chromatography (SiO_2, petroleum ether/ EtOAc, 9:1) to give **321** (953 mg, 91%) as an orange, brown liquid.

^{1}H NMR (600 MHz, $CDCl_3$) δ 7.20 (t, J = 7.9 Hz, 1H, H-8), 6.86 (d, J = 7.6 Hz, 1H, H-9), 6.83 (t, J = 2.1 Hz, 1H, H-11), 6.78 (dd, J = 7.8, 2.1 Hz, 1H, H-7), 4.09 (s, 2H, H-12), 4.05 (t, J = 6.1 Hz, 2H, H-5), 2.40 (td, J = 7.0, 2.7 Hz, 2H, H-3), 2.35 (s, 3H, H-14), 2.02 – 1.95 (m, 3H, H-1 and H-4).

^{13}C NMR (151 MHz, $CDCl_3$) δ 195.24 (C-13), 159.19 (C-6), 139.22 (C-10), 129.79 (C-8), 121.30 (C-9), 115.11 (C-11), 113.49 (C-7), 83.63 (C-2), 69.01 (C-1), 66.18 (C-5), 33.58 (C-12), 30.47 (C-14), 28.33 (C-4), 15.32 (C-3).

HRMS ($ASAP^+$): Calculated for $C_{14}H_{17}O_2S$: 249.0944 $[M+H]^+$, found 249.0944.

Synthesis of **374**

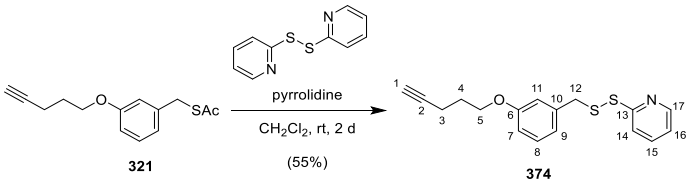

To a solution of **321** (953 mg, 3.84 mmol) and 2,2′-dipyridyl disulfide (1.27 g, 5.76 mmol) in degassed CH_2Cl_2 (19 mL, 0.2 M) was added pyrrolidine (0.64 mL, 7.67 mmol) dropwise and the reaction mixture was stirred for 2 days at room temperature. The reaction was quenched by the addition of saturated aqueous NH_4Cl (10 mL). The biphasic mixture was extracted with CH_2Cl_2 (3 × 25 mL). The combined organic layers were washed with brine and dried over Na_2SO_4, filtered, and concentrated *in vacuo*. The residue was purified by flash chromatography (SiO_2, $CHCl_3$/ Et_2O, 97:3) to afford **374** (661 mg, 55%) as a colourless solid.

^{1}H NMR (600 MHz, $CDCl_3$) δ 8.43 (d, J = 4.6 Hz, 1H, H-17), 7.54 – 7.47 (m, 2H, H-14 and H-15), 7.16 (t, J = 7.9 Hz, 1H, H-8), 7.04 – 7.01 (m, 1H, H-16), 6.88 (d, J = 7.5 Hz, 1H, H-9), 6.84 (t, J = 2.1 Hz, 1H, H-11), 6.75 (dd, J = 8.3, 2.5 Hz, 1H, H-7), 4.02 – 3.97 (m, 4H, H-5 and H-12), 2.39 (td, J = 7.0, 2.7 Hz, 2H, H-3), 2.00 – 1.94 (m, 3H, H-1 and H-4).

^{13}C NMR (151 MHz, $CDCl_3$) δ 160.24 (C-13), 159.13 (C-6), 149.58 (C-17), 138.16 (C-10), 136.87 (C-15), 129.71 (C-8), 121.88 (C-9), 120.59 (C-16), 119.65 (C-14), 115.44 (C-11), 113.97 (C-7), 83.62 (C-2), 69.03 (C-1), 66.18 (C-5), 44.00 (C-12), 28.30 (C-4), 15.31 (C-3).

HRMS (ASAP$^+$): Calculated for $C_{17}H_{18}ONS_2$: 316.0824 $[M+H]^+$, found 316.0822.

Synthesis of **375**

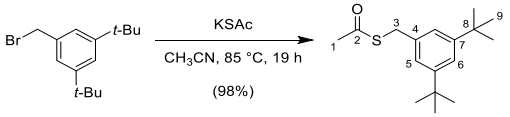

322 **375**

To a solution of **322** (847 mg, 3.00 mmol) in CH_3CN (30 mL, 0.1 M) was added KSAc (377 mg, 3.30 mmol) and the reaction mixture was heated to reflux (heating set to 85 °C; using a reflux condenser and drying tube charged with $CaCl_2$) for 19 hours. The reaction mixture was cooled to room temperature and the solvent removed *in vacuo*. The residue was purified by flash chromatography (SiO_2, petroleum ether/ EtOAc, 39:1) to give **375** (816 mg, 98%) as a yellow oil.

^{1}H NMR (600 MHz, $CDCl_3$) δ 7.31 (t, J = 1.8 Hz, 1H, H-6), 7.12 (d, J = 1.8 Hz, 2H, H-4), 4.13 (s, 2H, H-3), 2.35 (s, 3H, H-1), 1.31 (s, 18H, H-9).

^{13}C NMR (151 MHz, $CDCl_3$) δ 195.55 (C-2), 151.26 (C-7), 136.45 (C-4), 123.21 (C-5), 121.56 (C-6), 34.96 (C-8), 34.25 (C-3), 31.56 (C-9), 30.50 (C-1).

HRMS (ASAP$^+$): Calculated for $C_{17}H_{27}OS$: 279.1777 $[M+H]^+$, found 279.1777.

Synthesis of **323**

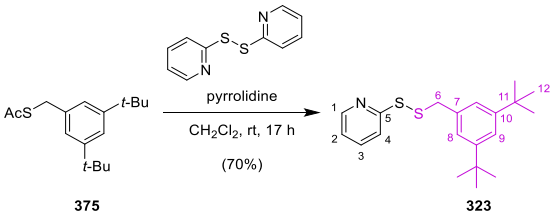

375 **323**

To a solution of **375** (806 mg, 2.89 mmol) and 2,2′-dipyridyl disulfide (956 mg, 4.34 mmol) in degassed CH_2Cl_2 (60 mL, 0.04 M) was added pyrrolidine (0.24 mL, 2.89 mmol) dropwise and the reaction mixture was stirred for 17 hours at room temperature. The reaction was quenched by the addition of saturated aqueous NH_4Cl (10 mL). The biphasic mixture was extracted with CH_2Cl_2 (4 × 25 mL). The combined organic layers were washed with brine and dried over Na_2SO_4, filtered, and concentrated *in vacuo*. The residue was purified by flash chromatography (SiO_2, petroleum ether/ Et_2O, 19:1) to afford **323** (702 mg, 70%) as a colourless solid.

^{1}H NMR (600 MHz, $CDCl_3$) δ 8.37 (d, J = 3.9 Hz, 1H, H-1), 7.39 – 7.35 (m, 1H, H-3), 7.26 – 7.23 (m, 2H, H-4 and H-9), 7.13 (d, J = 1.8 Hz, 2H, H-8), 6.97 – 6.94 (m, 1H, H-2), 4.01 (s, 2H, H-6), 1.25 (s, 18H, H-12).

^{13}C NMR (151 MHz, $CDCl_3$) δ 160.74 (C-5), 151.31 (C-10), 149.26 (C-1), 136.67 (C-3), 135.89 (C-7), 123.51 (C-8), 121.73 (C-9), 120.25 (C-2), 119.00 (C-4), 44.82 (C-6), 34.87 (C-11), 31.58 (C-12).

HRMS (ASAP$^+$): Calculated for $C_{20}H_{28}NS_2$: 346.1658 $[M+H]^+$, found 346.1654.

Synthesis of **317**

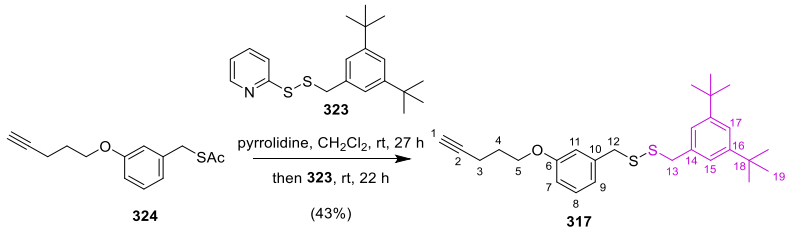

To a solution of **324** (686 mg, 2.76 mmol) in degassed CH_2Cl_2 (6 mL, 0.5 M) was added pyrrolidine (0.28 mL, 3.31 mmol) dropwise and the reaction mixture was stirred for 21 hours at room temperature. Another portion of pyrrolidine (0.18 mL, 2.21 mmol) was added the reaction was stirred for 6 hours. In the following, a solution of **323** (702 mg, 2.03 mmol) in degassed CH_2Cl_2 (3 mL, 0.7 M) was added and the solution stirred for 22 hours. The reaction was quenched by the addition of saturated aqueous NH_4Cl (10 mL). The biphasic mixture was extracted with CH_2Cl_2 (4 × 25 mL). The combined organic layers were washed with brine and dried over Na_2SO_4, filtered, and concentrated *in vacuo*. The residue was purified by flash chromatography (SiO_2, petroleum ether/ Et_2O, 39:1) to afford **317** (386 mg, 43%) as a colourless solid.

^{1}H NMR (600 MHz, $CDCl_3$) δ 7.33 (t, J = 1.8 Hz, 1H, H-17), 7.20 (t, J = 8.0 Hz, 1H, H-9), 7.11 (d, J = 1.8 Hz, 2H, H-15), 6.82 – 6.76 (m, 3H, H-7, H-8 and H-11), 4.05 (t, J = 6.1 Hz, 2H, H-5), 3.68 (s, 2H, H-13), 3.52 (s, 2H, H-12), 2.40 (td, J = 6.9, 2.6 Hz, 2H, H-3), 1.99 (p, J = 7.1, 6.6 Hz, 1H, H-4), 1.96 (t, J = 2.7 Hz, 1H, H-1), 1.33 (s, 18H, H-19).

^{13}C NMR (151 MHz, $CDCl_3$) δ 159.10 (C-6), 151.10 (C-16), 139.19 (C-10), 136.37 (C-14), 129.48 (C-7), 123.84 (C-15), 121.98 (C-9), 121.56 (C-17), 115.68 (C-11), 113.44 (C-8), 83.62 (C-2), 69.02 (C-1), 66.19 (C-5), 44.13 (C-13), 43.29 (C-12), 34.96 (C-18), 31.61 (C-19), 28.34 (C-4), 15.32 (C-3).

HRMS (ASAP$^+$): Calculated for $C_{27}H_{37}OS_2$: 441.2280 $[M+H]^+$, found 441.2284.

Synthesis of Thiol 341 and Disulfide 340

Synthesis of **341**

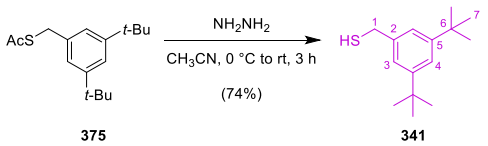

375 **341**

To a solution of **375** (907.6 mg, 3.26 mmol) in degassed CH_3CN (33 mL, 0.1 M) at 0 °C was added hydrazine (monohydrate, 0.32 mL, 6.52 mmol) dropwise under argon and stirred for 2 hours. The reaction was warmed to room temperature and stirred for another 1 h. The reaction was concentrated *in vacuo* and purified by flash chromatography (SiO_2, petroleum ether/ EtOAc, 39:1) to afford **341** (570 mg, 74%) as a colourless oil.
Note: Due to (slow) oxidation of the sample the NMR during the closure of the department in course of the COVID-19 pandemics data presented was acquired for a mixtures of thiol **341** and disulfide **340** in a ratio of approx. 66:33 as determined by integration.
^{1}H NMR (600 MHz, $CDCl_3$) δ 7.32 – 7.30 (m, 1H, H-4), 7.17 (d, *J* = 1.7 Hz, 2H, H-3), 3.75 (d, *J* = 7.4 Hz, 2H, H-1), 1.77 (t, *J* = 7.4 Hz, C-1 SH), 1.33 (s, 18H, H-7).
^{13}C NMR (151 MHz, $CDCl_3$) δ 151.25 (C-5), 140.25 (C-2), 122.38 (C-3), 121.32 (C-4), 35.01 (C-6), 31.60 (C-7), 29.68 (C-1).
HRMS (HESI$^-$): Calculated for $C_{15}H_{23}S$: 235.1526 $[M-H]^-$, found 235.1523.

Synthesis of **340**

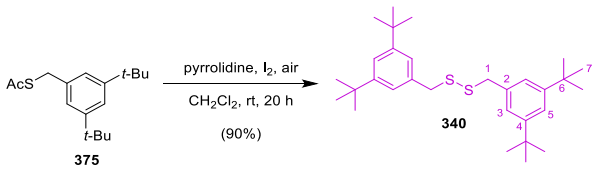

To a solution of **375** (653 mg, 2.35 mmol) in CH_2Cl_2 (10 mL, 0.2 M) was added pyrrolidine (0.39 mL, 4.69 mmol) dropwise and the reaction mixture was stirred for 17 hours at room temperature exposed to air. Iodine (60 mg, 0.24 mmol) was added, and the reaction was stirred for another 3 hours. The resultant mixture was evaporated from SiO_2 and purified by flash chromatography (SiO_2, petroleum ether/ EtOAc, 39:1) to give **340** (497 mg, 90%) as a colourless oil.

^{1}H NMR (600 MHz, $CDCl_3$) δ 7.31 (t, J = 1.8 Hz, 2H, H-5), 7.11 (d, J = 1.8 Hz, 4H, H-3), 3.65 (s, 4H, H-1), 1.32 (s, 36H, H-7).

^{13}C NMR (151 MHz, $CDCl_3$) δ 151.10 (C-4), 136.66 (C-2), 123.63 (C-3), 121.51 (C-5), 44.43 (C-1), 34.94 (C-6), 31.61 (C-7).

HRMS (ASAP$^-$): Calculated for $C_{30}H_{45}S_2$: 469.2968 $[M-H]^-$, found 469.2970.

Synthesis of Pyrene Monoazide 318

Synthesis of **326**

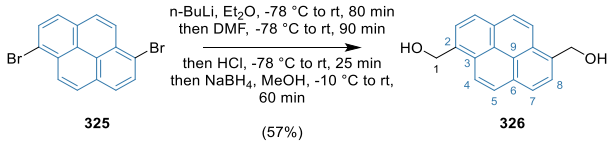

325 (57%) **326**

To a solution of **325** (1.00 g, 2.78 mmol) in dry degassed Et_2O (20 mL, 0.1 M) at –78 °C was added *n*-BuLi (2.5 M in hexanes, 2.78 mL, 6.95 mmol) dropwise and the reaction mixture was continued stirring for 25 minutes at –78 °C, warmed to –10 °C, stirred for 35 minutes and in addition, warmed to room temperature and stirred for another 25 minutes. The reaction mixture was then cooled to –78 °C and DMF (2.14 mL, 278 mmol) was added dropwise over 10 minutes. The reaction mixture was warmed to room temperature and stirred for 80 minutes. The reaction mixture was cooled to –78 °C and HCl (2.0 M in Et_2O, 3.48 mL, 6.95 mmol) was added dropwise over 5 minutes and the reaction mixture was warmed to room temperature and stirred for 20 minutes. Finally, the reaction mixture was cooled to –10 °C, diluted with dry MeOH (20 mL) and $NaBH_4$ (1.05 g, 278 mmol) was added dropwise. The reaction mixture was warmed to room temperature and stirred for 60 minutes, in total. Leftover $NaBH_4$ was carefully quenched by the addition of an aqueous 1 M HCl solution and the reaction was neutralized with an aqueous 2 M NaOH solution. The colourless precipitate formed during was separated and the biphasic mixture was extracted with CH_2Cl_2 (3 × 150 mL). The combined organic layers were dried over Na_2SO_4, filtered, combined with the separated precipitate, and concentrated *in vacuo*. The residue was purified by flash chromatography (SiO_2, CH_2Cl_2/ DMF, 40:1) to give **326** (417 mg, 57%) as a colourless solid.

^{1}H NMR (600 MHz, DMSO-d_6) δ 8.34 (d, J = 9.2 Hz, 2H, H-4), 8.27 (d, J = 7.8 Hz, 2H, H-7), 8.20 (d, J = 9.2 Hz, 2H, H-5), 8.14 (d, J = 7.8 Hz, 2H, H-8), 5.51 (t, J = 5.5 Hz, 2H, C-1 OH), 5.24 (d, J = 5.3 Hz, 4H, H-1).

^{13}C NMR (151 MHz, DMSO-d_6) δ 135.97 (C-2), 129.70 (C-6), 127.89 (C-3), 127.32 (C-5), 125.55 (C-8), 124.65 (C-7), 124.15 (C-9), 122.89 (C-4), 61.40 (C-1).

HRMS (APCI$^-$): Calculated for $C_{18}H_{13}O_2$: 261.0921 $[M-H]^-$, found 261.0918.

Synthesis of **318**

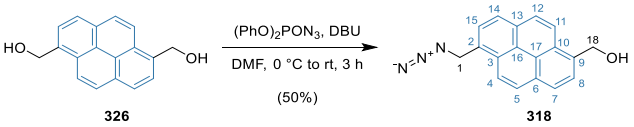

To a solution of **326** (415 mg, 1.58 mmol) and DBU (0.28 mL, 1.90 mmol) in DMF (40 mL) was added a solution of $(PhO)_2PON_3$ (0.38 mL, 1.74 mmol) in DMF (20 mL) over 1 hour via a syringe pump (20 mL/h) at 0 °C. Then, the reaction was warmed to room temperature and stirred for 2 hours. The reaction volume was reduced *in vacuo* to about 5 mL in total and the residue was purified by flash chromatography (SiO_2, CH_2Cl_2) to give **318** (226 mg, 50%) as a yellow solid.

^{1}H NMR (600 MHz, DMSO-d_6) δ 8.41 (d, J = 9.2 Hz, 1H, H-11), 8.37 – 8.31 (m, 3H, H-4, H-7 and H-14), 8.28 (d, J = 9.2 Hz, 1H, H-5), 8.23 (d, J = 9.2 Hz, 1H, H-12), 8.19 (d, J = 7.8 Hz, 1H, H-8), 8.14 (d, J = 7.7 Hz, 1H, H-15), 5.54 (t, J = 5.5 Hz, 1H, C-18 OH), 5.26 (d, J = 5.5 Hz, 2H, H-18), 5.22 (s, 2H, H-1).

^{13}C NMR (151 MHz, DMSO-d_6) δ 136.64 (C-9), 130.81 (C-13), 129.58 (C-6), 128.97 (C-2 and C-3), 128.25 (C-5), 127.99 (C-15), 127.79 (C-10), 127.19 (C-12), 125.83 (C-8), 125.19 (C-7), 124.80 (C-14), 124.32 (C-16), 123.93 (C-17), 123.80 (C-11), 122.58 (C-4), 61.33 (C-18), 51.79 (C-1).

HRMS (APCI$^-$): Calculated for $C_{18}H_{12}ON_3$: 286.0985 $[M-H]^-$, found 286.0987.

Synthesis of Model Pyrene One-Barrier Pump 329·H$^+$

Synthesis of **327**

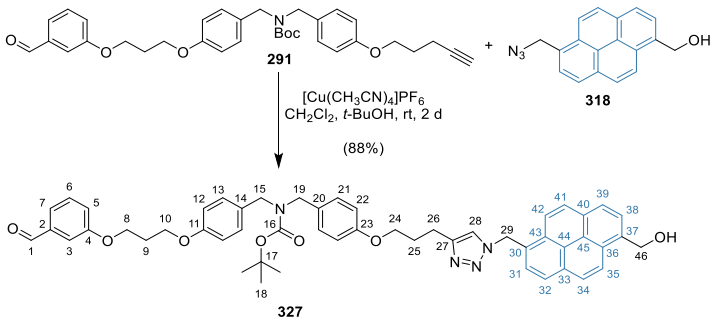

To a solution of **291** (159.5 mg, 286 µmol) and **318** (68.5 mg, 238 µmol) in degassed CH_2Cl_2 (8 mL) and *t*-BuOH (2 mL) was added $[Cu(CH_3CN)_4]PF_6$ (17.8 mg, 48 µmol) and the reaction was stirred at room temperature for 2 days. The reaction was quenched by the addition of saturated aqueous EDTA (10 mL, pH = 7). The biphasic mixture was extracted with CH_2Cl_2 (3 × 15 mL). The combined organic layers were washed with brine and dried over Na_2SO_4, filtered, and concentrated *in vacuo*. The residue was purified by flash chromatography (SiO_2, CH_2Cl_2/ MeOH, 40:1) followed by size exclusion chromatography (S-X1, CH_2Cl_2) to give **327** (178 mg, 88%) as a yellow solid.

^{1}H NMR (600 MHz, DMSO-d_6) δ 9.97 (s, 1H, H-1), 8.46 (d, J = 9.2 Hz, 1H, H-42), 8.40 (d, J = 9.2 Hz, 1H, H-35), 8.32 – 8.29 (m, 2H, H-32 and H-39), 8.25 (d, J = 9.2 Hz, 1H, H-41), 8.22 (d, J = 9.2 Hz, 1H, H-34), 8.17 (d, J = 7.8 Hz, 1H, H-38), 7.97 (d, J = 7.9 Hz, 1H, H-31), 7.95 (s, 1H, H-28), 7.53 – 7.49 (m, 2H, H-5 and H-6), 7.47 – 7.43 (m, 1H, H-3), 7.29 (dt, J = 7.4, 2.4 Hz, 1H, H-7), 7.11 (s, 2H, H-13), 7.06 (s, 2H, H-21), 6.92 (d, J = 8.6 Hz, 2H, H-12), 6.81 (d, J = 8.5 Hz, 2H, H-22), 6.32 (s, 2H, H-29), 5.53 (t, J = 5.5 Hz, 1H, C-46 OH), 5.25 (d, J = 5.5 Hz, 2H, H-46), 4.26 – 4.10 (m, 8H, H-8, H-10, H-15 and H-19), 3.93 (t, J = 6.4 Hz, 2H, H-24), 2.73 (t, J = 7.5 Hz, 2H, H-26), 2.19 (p, J = 6.3 Hz, 2H, H-9), 1.99 (p, J = 6.7 Hz, 2H, H-25), 1.39 (s, 9H, H-18).

^{13}C NMR (151 MHz, DMSO-d_6) δ 192.98 (C-1), 158.99 (C-4), 157.68 (C-11), 157.62 (C-23), 155.00 (C-16), 146.48 (C-27), 137.64 (C-2), 136.66 (C-37), 130.68 (C-33), 130.40 (C-6), 130.11 (*broad*, C-14), 129.92 (*broad*, C-20), 129.49 (C-40), 129.26 (C-30), 128.89 (*broad*, C-13), 128.67 (*broad*, C-21), 128.59 (C-43), 128.36 (C-41), 127.79 (C-36), 127.45 (C-31), 127.14 (C-34), 125.82 (C-38), 125.16 (C-32/39), 125.02 (C-32/39), 124.25 (C-44), 123.89 (C-45), 123.81 (C-35), 122.36 (C-5), 122.30 (C-28), 122.20 (C-42), 121.37 (C-7), 114.44 (C-12), 114.35 (C-22), 113.73 (C-3), 79.08 (C-17), 66.62 (C-24), 64.59 (C-8), 64.09 (C-10), 61.32 (C-46), 50.85 (C-29), 48.41 (C-15/19), 47.98 (C-15/19), 28.53 (C-9), 28.42 (C-25), 28.04 (C-18), 21.61 (C-26).

HRMS (HESI$^+$): Calculated for $C_{52}H_{52}O_7N_4Na$: 867.3728 $[M+Na]^+$, found 867.3724.

Synthesis of **327**

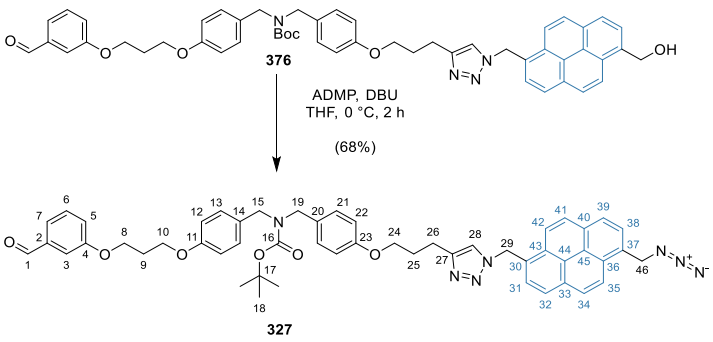

To a solution of **376** (392 mg, 464 µmol) in THF (15 mL, 31 mM) was added ADMP (265 mg, 929 µmmol) at 0 °C followed by DBU (208 µL, 1.39 mmol) and the reaction was continued stirring at 0 °C for 2 hours. The reaction was quenched by the addition of saturated aqueous NH_4Cl (10 mL). The biphasic mixture was extracted with CH_2Cl_2 (4 × 20 mL). The combined organic layers were washed with brine and dried over Na_2SO_4, filtered, and concentrated *in vacuo*. The residue was purified by flash chromatography (SiO_2, CH_2Cl_2/ Et_2O, 9:1) to afford **327** (273 mg, 68%) as a yellow solid.

^{1}H NMR (600 MHz, CD_2Cl_2) δ 9.95 (s, 1H, H-1), 8.34 (d, J = 9.2 Hz, 1H, H-35), 8.31 (d, J = 9.2 Hz, 1H, H-42), 8.26 (d, J = 7.8 Hz, 1H, H-32), 8.24 (d, J = 7.8 Hz, 1H, H-39), 8.22 (d, J = 9.2 Hz, 1H, H-34), 8.17 (d, J = 9.2 Hz, 1H, H-41), 8.05 (d, J = 7.8 Hz, 1H, H-38), 7.97 (d, J = 7.8 Hz, 1H, H-31), 7.48 – 7.41 (m, 2H, H-5 and H-6), 7.42 – 7.38 (m, 1H, H-3), 7.22 – 7.17 (m, 2H, H-7 and H-28), 7.10 (s, 2H, H-13), 7.02 (d, J = 8.0 Hz, 2H, H-21), 6.86 (d, J = 8.6 Hz, 2H, H-12), 6.72 (d, J = 8.3 Hz, 2H, H-22), 6.23 (s, 2H, H-29), 5.07 (s, 2H, H-46), 4.29 – 4.12 (m, 8H, H-8, H-10, H-15 and H-19), 3.91 (t, J = 6.3 Hz, 2H, H-24), 2.79 (t, J = 7.5 Hz, 2H, H-26), 2.27 (p, J = 6.1 Hz, 2H, H-9), 2.04 (p, J = 6.5 Hz, 2H, H-25), 1.46 (s, 9H, H-18).

^{13}C NMR (151 MHz, CD_2Cl_2) δ 192.36 (C-1), 159.94 (C-4), 158.55 (C-23), 158.50 (C-11), 156.10 (C-16), 147.98 (C-27), 138.34 (C-2), 131.91 (C-33), 131.59 (C-40), 130.85 (C-14), 130.58 (C-20), 130.47 (C-6), 129.92 (C-36), 129.74 (C-37 and C-43), 129.41 (C-13), 129.21 (C-21), 129.14 (C-41), 128.78 (C-30), 128.57 (C-34), 128.39 (C-38), 128.25 (C-31), 125.96 (C-32), 125.86 (C-39), 125.39 (C-44), 125.27 (C-45), 123.89 (C-35), 123.49 (C-5), 122.97 (C-42), 121.93 (C-7), 121.39 (C-28), 114.77 (C-12), 114.68 (C-22), 113.43 (C-3), 80.01 (C-17), 67.30 (C-24), 65.25 (C-8), 64.73 (C-10), 53.42 (C-46), 52.58 (C-29), 48.87 (C-15/19), 48.44 (C-15/19), 29.59 (C-9), 29.25 (C-25), 28.57 (C-18), 22.53 (C-26).

HRMS (HESI$^+$): Calculated for $C_{52}H_{51}O_6N_7Na$: 892.3793 $[M+Na]^+$, found 892.3762.

Synthesis of **328**·H⁺

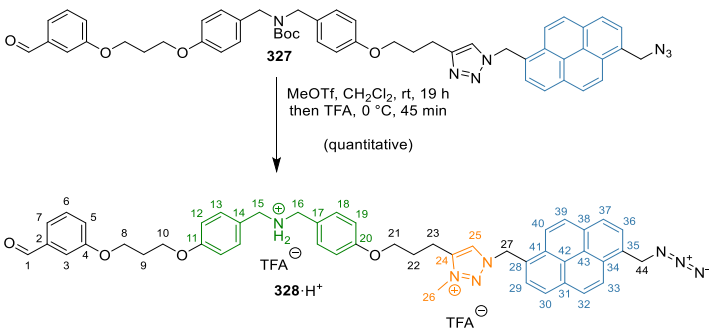

To a solution of **327** (271 mg, 0.31 mmol) in degassed CH_2Cl_2 (20 mL, 16 mM) was added MeOTf (0.18 mL, 1.56 mmol) and the reaction was stirred at room temperature for 19 hours. The reaction mixture was concentrated *in vacuo* and the resultant residue was purified by size exclusion chromatography (S-X1, CH_2Cl_2). The crude triazolium intermediate was redissolved in degassed CH_2Cl_2 (20 mL, 16 mM) and TFA (2.43 mL, 31.1 mmol) was added at 0 °C. The reaction was continued stirring at 0 °C for 45 minutes and then concentrated *in vacuo.* The crude reaction was resuspended in PhMe (10 mL) and concentrated *in vacuo* under high vacuum. The last step was repeated two times **328**·H⁺ (330 mg, 109%, *with residual TFA*) was obtained as a yellow glossy solid.

^{1}H NMR (600 MHz, CD_2Cl_2) δ 9.90 (s, 1H, H-1), 8.52 (s, 2H, C15/16 NH_2^+), 8.34 (d, J = 9.2 Hz, 1H, H-33), 8.32 (s, 1H, H-25), 8.30 – 8.24 (m, 3H, H-30, H-37 and H-40), 8.22 – 8.16 (m, 3H, H-29, H-32 and H-39), 8.05 (d, J = 7.8 Hz, 2H, H-36), 7.43 (d, J = 8.6 Hz, 2H, H-13), 7.41 – 7.40 (m, 2H, H-5 and H-6), 7.36 (d, J = 8.7 Hz, 2H, H-18), 7.32 (d, J = 2.6 Hz, 1H, H-3), 7.13 (td, J = 4.7, 2.7 Hz, 1H, H-7), 6.90 (d, J = 8.7 Hz, 2H, H-12), 6.68 (d, J = 8.7 Hz, 2H, H-19), 6.30 (s, 2H, H-27), 5.05 (s, 2H, H-44), 4.15 (s, 2H, H-15), 4.13 – 4.08 (m, 5H, H-8 and H-26), 4.06 – 3.99 (m, 6H, H-16, H-10 and H-21), 2.86 (t, J = 7.1 Hz, 2H, H-23), 2.15 (p, J = 6.1 Hz, 2H, H-9), 2.09 (p, J = 6.6 Hz, 2H, H-22).

^{13}C NMR (151 MHz, CD_2Cl_2) δ 192.41 (C-1), 160.26 (C-11), 159.83 (C-4), 158.62 (C-20), 144.54 (C-24), 138.26 (C-2), 132.76 (C-31), 132.41 (C-18), 132.15 (C-13), 131.38 (C-38), 130.44 (C-6), 130.41 (C-35), 130.16 (C-28), 129.89 (C-39), 129.77 (C-29), 129.59 (C-34), 128.86 (C-25), 128.56 (C-36), 128.48 (C-32), 126.25 (C-37), 126.17 (C-30), 125.25 (C-43), 125.03 (C-42), 124.79 (C-41), 124.58 (C-33), 123.74 (C-17), 123.46 (C-5), 122.61 (C-14), 122.44 (C-40), 121.91 (C-7), 115.34 (C-12), 115.24 (C-19), 113.42 (C-3), 66.46 (C-21), 65.05 (C-8), 64.74 (C-10), 55.66 (C-27), 53.32 (C-44), 51.51 (C-15), 50.87 (C-16), 38.03 (C-26), 29.37 (C-9), 26.14 (C-22), 20.90 (C-23).

^{19}F NMR (376 MHz, CD_2Cl_2) δ −76.0 (3F), −78.07 (3F).

HRMS (ESI^+): Calculated for $C_{48}H_{47}O_4N_7$: 392.6839 $[M\text{-}2TFA]^{2+}$, found 392.6832.

Synthesis of **329**·H⁺

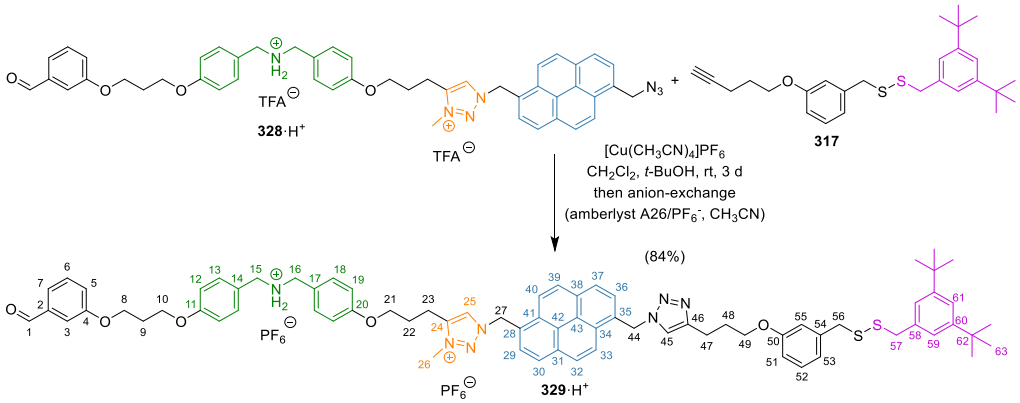

To a solution of **328**·H⁺ (328.7 mg, 0.335 mmol) and **217** (221.4 mg, 0.503 mmol) in degassed CH_2Cl_2 (20 mL) and *t*-BuOH (5 mL) was added $[Cu(CH_3CN)_4]PF_6$ (25 mg, 67 µmol) and the reaction was stirred at room temperature for 3 days. The reaction mixture was concentrated *in vacuo* and anion-exchange was performed (amberlyst A-26 PF_6^-, CH_3CN). The resultant residue was purified by size exclusion chromatography (S-X1, CH_2Cl_2) to give **329**·H⁺ (429 mg, 84%) as a yellow brown solid.

^{1}H NMR (600 MHz, CD_3CN) δ 9.91 (s, 1H, H-1), 8.50 (d, J = 9.3, 1H, H-33), 8.34 – 8.31 (m, 2H, H-30 and H-37), 8.30 – 8.23 (m, 3H, H-32, H-39 and H-40), 8.20 (d, J = 7.9, 1H, H-29), 8.05 (d, J = 7.9, 1H, H-36), 8.00 (s, 1H, H-25), 7.66 (s, 1H, H-45), 7.49 – 7.42 (m, 2H, H-6 and H-7), 7.39 – 7.37 (m, 1H, H-3), 7.35 (t, J = 1.9, 1H, H-61), 7.32 (d, J = 8.7, 2H, H-13), 7.21 (dt, J = 6.1, 2.8, 1H, H-5), 7.13 – 7.03 (m, 5H, C15/16 NH_2^+, H-52 and H-59), 6.98 (d, J = 8.7, 2H, H-12), 6.89 (d, J = 8.7, 2H, H-18), 6.75 (d, J = 8.1, 1H, H-53), 6.70 (t, J = 2.0, 1H, H-55), 6.69 – 6.66 (m, 1H, H-51), 6.41 (s, 2H, H-27), 6.38 (d, J = 8.7, 2H, H-19), 6.24 (s, 2H, H-44), 4.22 (t, J = 6.2, 2H, H-8), 4.18 (t, J = 6.2, 2H, H-10), 4.10 (s, 3H, H-26), 4.08 (t, J = 6.1, 2H, H-15), 3.99 (t, J = 6.1, 2H, H-16), 3.88 (t, J = 6.3, 2H, H-49), 3.83 (t, J = 5.8, 2H, H-21), 3.66 (s, 2H, H-57), 3.54 (s, 2H, H-56), 2.90 (t, J = 7.1, 2H, H-23), 2.72 (t, J = 7.5, 2H, H-47), 2.23 (p, J = 6.1, 2H, H-9), 2.04 (p, J = 7.1, 2H, H-22), 1.99 – 1.96 (m, 2H, H-48), 1.27 (s, 18H, H-63).

^{13}C NMR (151 MHz, CD_3CN) δ 193.40 (C-1), 160.95 (C-11), 160.44 (C-4), 160.19 (C-20), 159.95 (C-50), 152.00 (C-50), 148.12 (C-46), 145.54 (C-24), 140.28 (C-54), 139.07 (C-2), 137.61 (C-58), 133.18 (C-31), 132.82 (C-13), 132.50 (C-18), 132.00 (C-38), 131.32 (C-6), 131.21 (C-34), 130.71 (C-41), 130.46 (C-52), 130.42 (C-29), 130.16 (C-39), 130.03 (C-43), 129.48 (C-36), 129.28 (C-32), 128.97 (C-25), 127.19 (C-37), 126.81 (C-30), 125.99 (C-42), 125.69 (C-28), 125.43 (C-35), 125.03 (C-33), 124.67 (C-59), 123.77 (C-7), 123.52 (C-40), 123.38 (C-17), 123.36 (C-14), 123.26 (C-45), 122.64 (C-53), 122.44 (C-61), 122.27 (C-5), 116.57 (C-55), 115.84 (C-12), 115.22 (C-19), 114.25 (C-3), 114.04 (C-51), 67.72 (C-49), 67.40 (C-21), 65.65 (C-8), 65.49 (C-10), 56.01 (C-27), 52.51 (C-44), 51.74 (C-15), 51.52 (C-16), 43.75 (C-57), 43.06 (C-56), 38.52 (C-), 35.45 (C-62), 31.66 (C-63), 29.72 (C-9), 29.52 (C-48), 26.82 (C-22), 22.58 (C-47), 21.11 (C-23).

^{19}F NMR (376 MHz, CD_3CN) δ -72.93 (d, J = 706.3 Hz).

^{31}P NMR (162 MHz, CD_3CN) δ -144.62 (hept, J = 706.3 Hz).

HRMS (ESI^+): Calculated for $C_{75}H_{83}N_7O_5S_2$: 612.7943 $[M\text{-}2PF_6]^{2+}$, found 612.7947.

Synthesis of Methyl Hydrazide 334

Synthesis of **332**

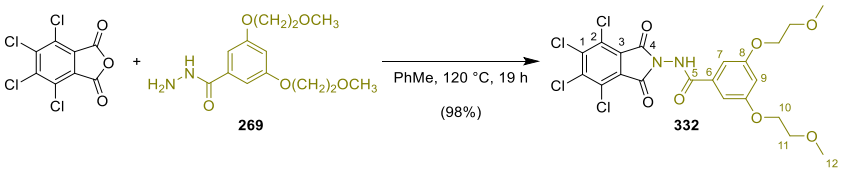

A suspension of **269** (1.00 g, 3.50 mmol) and tetrachlorophthalic anhydride (1.00 g, 352 mmol) in PhMe (50 mL, 0.1 M) was heated at 120 °C for 19 hours. The reaction was cooled to room temperature and concentrated *in vacuo*. The residue was purified by flash chromatography (SiO_2, CH_2Cl_2/ MeOH, 49:1) to afford **332** (1.90 g, 98%) as a colourless solid.

^{1}H NMR (600 MHz, DMSO-d_6) δ 11.44 (s, 1H, C-5 NH), 7.13 (d, J = 2.3 Hz, 2H, H-7), 6.83 (t, J = 2.3 Hz, 1H, H-9), 4.19 – 4.14 (m, 4H, H-10), 3.70 – 3.65 (m, 4H, H-11), 3.32 (s, 6H, H-12).

^{13}C NMR (151 MHz, DMSO-d_6) δ 164.79 (C-5), 161.02 (C-4), 159.80 (C-8), 139.35 (C-1), 132.24 (C-6), 129.03 (C-3), 126.18 (C-2), 106.32 (C-7), 105.68 (C-9), 70.23 (C-11), 67.38 (C-10), 58.18 (C-12).

HRMS (ASAP$^+$): Calculated for $C_{21}H_{19}O_7N_2Cl_4$: 550.9941 $[M+H]^+$, found 550.9945.

Synthesis of **333**

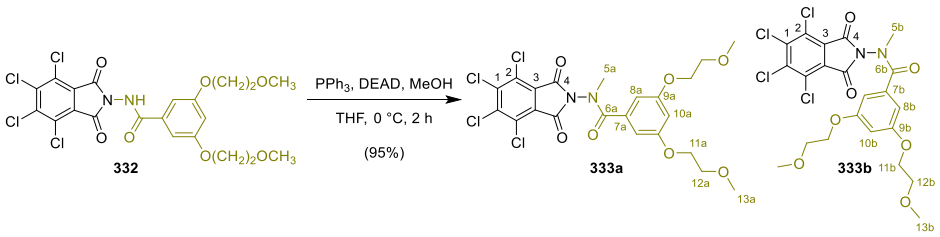

To a suspension of **332** (553 mg, 1.00 mmol) and triphenylphosphine (394 mg, 1.50 mmol) in dry degassed THF (14 mL, 0.1 M) was added diethyl azodicarboxylate (0.26 mL, 1.50 mmol) and MeOH (0.06 mL, 1.50 mmol) dropwise at 0 °C under argon and the reaction was stirred for 2 hours. The reaction was quenched by the addition of saturated aqueous $NaHCO_3$ (10 mL). The biphasic mixture was extracted with CH_2Cl_2 (3 × 15 mL). The combined organic layers were washed with brine and dried over Na_2SO_4, filtered, and concentrated *in vacuo*. The residue was purified by flash chromatography (SiO_2, CH_2Cl_2/ Et_2O, 9:1) to afford **333** (538 mg, 95%) as a colourless solid.

Note: Two sets of signals have been observed with ^{1}H NMR both in CD_3CN and DMSO-d_6 ascribed to the occurrence of two acetamide-based rotamers **333a** (*major*) and **333b** (*minor*) in slow exchange (298K) and in an unequal ratio of approx. 3:1 (CD_3CN) and 4:1. (DMSO-d_6) It is assumed that *major* signals correspond to the thermodynamically more favourable *(E)* rotamer **333a** and *minor* signals to *(Z)* rotamer **333b** in accordance with the literature.[288]

^{1}H NMR (600 MHz, CD_3CN) δ 6.77 – 6.70 (m, 2H, H-8b), 6.66 (s, 1H, H-10b), 6.48 (s, 2H, H-8a), 6.45 (s, 1H, H-10a), 4.18 – 4.11 (m, 4H, H-11b), 3.97 (s, 4H, H-11a), 3.71 – 3.66 (m, 4H, H-12b), 3.60 (s, 4H, H-12a), 3.36 (s, 9H, H-5b and H-13b), 3.30 (s, 9H, H- H-5a and H-13a).

^{13}C NMR (151 MHz, CD_3CN) δ 172.85 (C-6), 161.49 (C-4), 160.80 (C-9), 141.45 (C-7), 136.28 (C-1), 130.83 (C-3), 126.75 (C-2), 106.75 (C-8b), 105.71 (C-8a), 105.04 (C-10), 71.38 (C-12), 68.53 (C-11), 59.00 (C-13), 40.60 (C-5b), 35.97 (C-5a).

HRMS (ASAP$^-$): Calculated for $C_{22}H_{20}O_7N_2Cl_4$: 564.0019 [M]$^-$, found 564.0031.

Synthesis of **334**

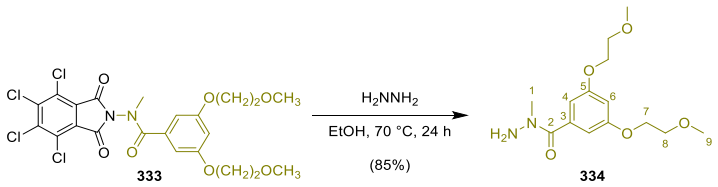

To a suspension of **333** (508.6 mg, 0.898 mmol) in EtOH (10 mL, 0.1 M) was added hydrazine (monohydrate, 87.1 µL, 1.80 mmol) dropwise and the reaction mixture was stirred and heated at 70 °C for 24 hours. The reaction was cooled to room temperature and concentrated *in vacuo*. The residue was resuspended in $CHCl_3$, filtrated through a plug of celite and concentrated *in vacuo*. The crude product was purified by flash chromatography (SiO_2, $CHCl_3$/ MeOH, 19:1) to afford **334** (226.6 mg, 85%) as a colourless oil.

^{1}H NMR (600 MHz, $CDCl_3$) δ 6.62 – 6.55 (m, 3H, H-4 and H-6), 4.61 (s, 2H, NH_2), 4.12 – 4.08 (m, 4H, H-7), 3.76 – 3.71 (m, 4H, H-8), 3.44 (s, 6H, H-9), 3.18 (s, 3H, H-1).

^{13}C NMR (151 MHz, $CDCl_3$) δ 169.74 (C-2), 159.97 (C-5), 136.96 (C-3), 106.24 (C-4), 103.41 (C-6), 71.01 (C-8), 67.65 (C-7), 59.37 (C-9), 40.60 (C-1).

HRMS (ASAP$^+$): Calculated for $C_{14}H_{23}O_5N_2$: 299.1601 $[M+H]^+$, found 299.1600.

Synthesis of Pyrene Free Thread 336·H⁺

Synthesis of **336**·H⁺

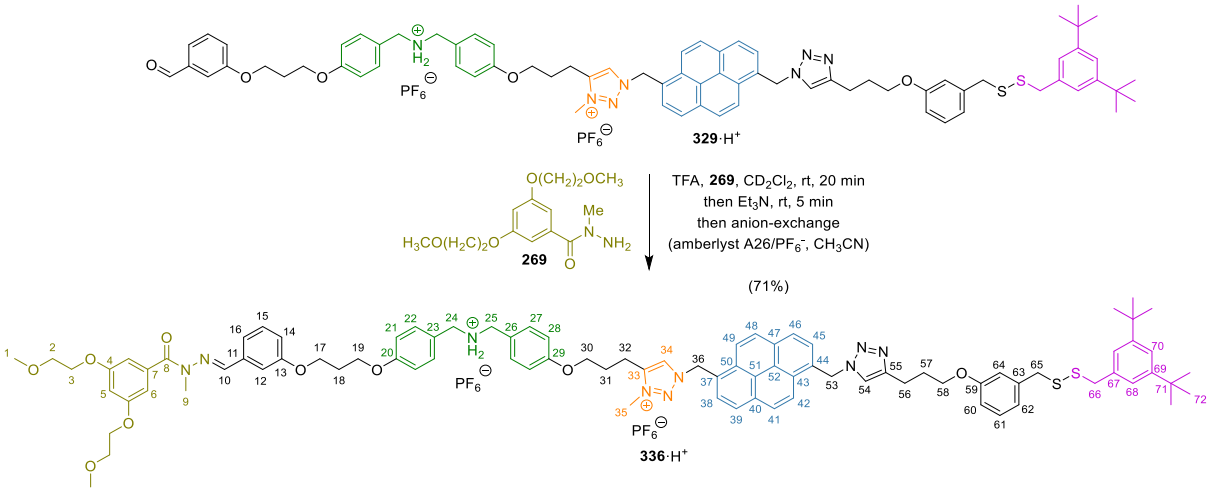

To a solution of **329**·H⁺ (10.6 mg, 7.0 μmol) in CD_2Cl_2 (450 μl, 15 mM) at room temperature were added Hydrazide **334** (6.9 mg, 23.1 μmol) and TFA (0.5 μl, 7.0 μmol) and the reaction was thoroughly mixed and left standing for 20 minutes. The reaction was basified with Et_3N, (2.0 μl, 14.0 μmol) purified by size exclusion chromatography (S-X1, CH_2Cl_2) and then anion-exchange chromatography (amberlyst A-26 PF_6^-, CH_3CN) to give **336**·H⁺ (8.9 mg, 71%) as a yellow solid.

^{1}H NMR (600 MHz, CD_3CN) δ 8.47 (d, *J* = 9.3 Hz, 1H, H-42), 8.31 (t, *J* = 7.8 Hz, 2H, H-39 and H-46), 8.27 (d, *J* = 9.3 Hz, 1H, H-49), 8.25 – 8.21 (m, 2H, H-41 and H-48), 8.19 (d, *J* = 7.9 Hz, 1H, H-38), 8.03 (d, *J* = 7.9 Hz, 1H, H-45), 8.00 (s, 1H, H-34), 7.77 (s, 1H, H-10), 7.65 (s, 1H, H-54), 7.34 (t, *J* = 1.7 Hz, 1H, H-70), 7.31 (d, *J* = 8.7 Hz, 2H, H-22), 7.23 (t, *J* = 7.9 Hz, 1H, H-15), 7.18 – 7.13 (m, 2H, C24/25 NH_2^+), 7.12 – 7.08 (m, 3H, H-61 and H-68), 7.05 – 7.01 (m, 2H, H-12 and H-16), 6.96 (d, *J* = 8.7 Hz, 2H, H-21), 6.89 – 6.86 (m, 3H, H-14 and H-27), 6.75 – 6.73 (m, 3H, H-6 and H-62), 6.69 (s, 1H, H-64), 6.67 (dd, *J* = 8.2, 1.9 Hz, 1H, H-60), 6.49 (t, *J* = 2.3 Hz, 1H, H-5), 6.41 (s, 2H, H-36), 6.36 (d, *J* = 8.7 Hz, 2H, H-28), 6.21 (s, 2H, H-53), 4.14 (t, *J* = 6.1 Hz, 2H, H-19), 4.10 (s, 3H, H-35), 4.08 (s, 2H, H-24), 4.05 – 4.01 (m, 6H, H-17 and H-3), 3.99 (s, 2H, H-25), 3.87 (t, *J* = 6.3 Hz, 2H, H-58), 3.82 (t, *J* = 5.8 Hz, 2H, H-30), 3.65 (s, 2H, H-66), 3.64 – 3.61 (m, 4H, H-2), 3.53 (s, 2H, H-65), 3.42 (s, 3H, H-9), 3.30 (s, 6H, H-1), 2.90 (t, *J* = 7.0 Hz, 2H, H-32), 2.71 (t, *J* = 7.5 Hz, 2H, H-56), 2.19 – 2.15 (m, 2H, H-18, *overlapped with solvent peak*), 2.03 (p, *J* = 6.7 Hz, 2H, H-31), 1.96 – 1.95 (m, 2H, H-67, *overlapped with solvent peak*), 1.26 (s, 18H, H-72).

^{13}C NMR (151 MHz, CD_3CN) δ 171.13 (C-8), 160.93 (C-29), 160.15 – 160.09 (m, C-4, C-13 and C-20), 159.92 (C-59), 151.97 (C-69), 148.09 (C-55), 145.51 (C-33), 140.25 (C-10 and C-63), 139.23 (C-7), 137.66 (C-11), 137.58 (C-67), 133.14 (C-40), 132.82 (C-22), 132.45 (C-27), 131.96 (C-47), 131.17 (C-44), 130.86 (C-15), 130.66 (C-50), 130.44 (C-61), 130.40 (C-38), 130.14 (C-48), 129.98 (C-43), 129.44 (C-45), 129.25 (C-41), 128.95 (C-34), 127.16 (C-46), 126.79 (C-39), 125.95 (C-37), 125.64 (C-51), 125.38 (C-52), 124.99 (C-42), 124.66 (C-68), 123.48 (C-49), 123.39 (C-26), 123.33 (C-23), 123.24 (C-54), 122.62 (C-62), 122.42 (C-70), 121.40 (C-16), 117.38 (C-14), 116.54 (C-64), 115.83 (C-21), 115.18 (C-28), 113.99 (C-60), 111.64 (C-12), 108.78 (C-6), 103.80 (C-5), 71.56 (C-2), 68.52 (C-3), 67.68 (C-58), 67.36 (C-30), 65.52 (C-19), 65.10 (C-17), 59.05 (C-1), 55.97 (C-36), 52.46 (C-53), 51.71 (C-24), 51.45 (C-25), 43.70 (C-66), 43.01 (C-65),

38.50 (C-35), 35.43 (C-71), 31.64 (C-72), 29.79 (C-18), 29.50 (C-57), 29.17 (C-9), 26.77 (C-31), 22.56 (C-56), 21.09 (C-32).

^{19}F NMR (376 MHz, CD_3CN) δ -72.86 (d, *J* = 706.5 Hz).

^{31}P NMR (162 MHz, CD_3CN) δ -144.61 (hept, *J* = 706.5 Hz).

HRMS (ESI^+): Calculated for $C_{75}H_{83}N_7O_5S_2$: 752.8655 $[M\text{-}2PF_6]^{2+}$, found 752.8654.

Synthesis of Hydrazone Surrogates 338a-c

Synthesis of **338a**

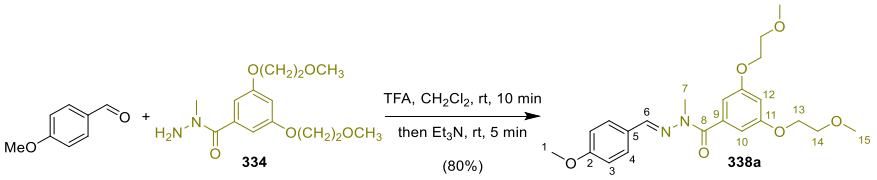

To a solution of **334** (60.8 mg, 204 µmol) in CH_2Cl_2 (2.0 mL, 0.1 M) were added 4-methoxybenzaldehyde (210 µL, 1.70 mmol) and TFA (13.3 µL, 170 µmol) at room temperature and the reaction was stirred for 10 minutes. After addition of Et_3N (35.5 µL, 255 µmol), the crude reaction mixture was concentrated *in vacuo* and purified by flash chromatography (SiO_2, CH_2Cl_2/ MeOH/ Et_3N, 200:3:1) to afford **338** (68.2 mg, 80%) as a colourless solid.

^{1}H NMR (600 MHz, $CDCl_3$) δ 7.71 (s, 1H, H-6), 7.45 (d, J = 8.7 Hz, 2H, H-4), 6.88 – 6.84 (m, 4H, H-3 and H-10), 6.66 (t, J = 2.3 Hz, 1H, H-12), 4.13 – 4.09 (m, 4H, H-13), 3.81 (s, 3H, H-1), 3.75 – 3.70 (m, 4H, H-14), 3.53 (s, 3H, H-7), 3.43 (s, 6H, H-15).

^{13}C NMR (151 MHz, $CDCl_3$) δ 170.79 (C-6), 160.96 (C-2), 159.06 (C-11), 139.18 (C-6), 137.39 (C-9), 128.80 (C-4), 127.63 (C-5), 114.31 (C-3), 108.55 (C-10), 104.41 (C-12), 71.04 (C-14), 67.62 (C-13), 59.33 (C-15), 55.47 (C-1), 28.88 (C-7).

HRMS (ASAP$^+$): Calculated for $C_{22}H_{29}O_6N_2$: 417.2020 $[M+H]^+$, found 417.2022.

Synthesis of **338b**

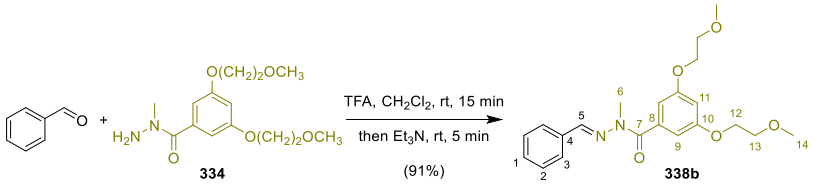

To a solution of **334** (69.2 mg, 232 µmol) in CH_2Cl_2 (2.0 mL, 0.1 M) were added benzaldehyde (70.7 µL, 696 µmol) and TFA (18.1 µL, 232 µmol) at room temperature and the reaction was stirred for 15 minutes. After addition of Et_3N (48.5 µL, 348 µmol), the crude reaction mixture was concentrated *in vacuo* and purified by flash chromatography (SiO_2, CH_2Cl_2/ MeOH/ Et_3N, 200:3:1) to afford **338b** (85.0 mg, 95%) as a colourless solid.

^{1}H NMR (600 MHz, $CDCl_3$) δ 7.75 (s, 1H, H-5), 7.55 – 7.49 (m, 2H, H-2), 7.37 – 7.30 (m, 3H, H-1 and H-3), 6.88 (d, J = 2.3 Hz, 2H, H-9), 6.67 (t, J = 2.3 Hz, 1H, H-11), 4.14 – 4.09 (m, 4H, H-12), 3.74 – 3.71 (m, 4H, H-13), 3.55 (s, 3H, H-5), 3.43 (s, 6H, H-14).

^{13}C NMR (151 MHz, $CDCl_3$) δ 170.96 (C-7), 159.12 (C-10), 139.36 (C-5), 137.21 (C-8), 134.83 (C-4), 129.80 (C-1), 128.88 (C-3), 127.35 (C-2), 108.65 (C-9), 104.56 (C-11), 71.05 (C-13), 67.66 (C-12), 59.33 (C-14), 28.97 (C-6).

HRMS (ASAP$^+$): Calculated for $C_{21}H_{27}O_5N_2$: 387.1914 $[M+H]^+$, found 387.1915.

Synthesis of **338c**

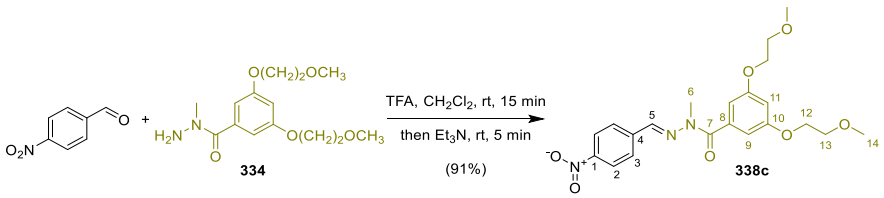

To a solution of **334** (69.2 mg, 232 µmol) in CH_2Cl_2 (2.0 mL, 0.1 M) were added 4-nitrobenzaldehyde (105.1 mg, 696 µmol) and TFA (18.1 µL, 232 µmol) at room temperature and the reaction was stirred for 15 minutes. After addition of Et_3N (48.5 µL, 348 µmol), the crude reaction mixture was concentrated *in vacuo* and purified by flash chromatography (SiO_2, CH_2Cl_2/ MeOH/ Et_3N, 200:3:1) to afford **338c** (90.9 mg, 91%) as a yellow solid.

^{1}H NMR (600 MHz, $CDCl_3$) δ 8.20 (d, J = 8.8 Hz, 2H, H-2), 7.76 (s, 1H, H-5), 7.65 (d, J = 8.8 Hz, 2H, H-3), 6.85 (d, J = 2.3 Hz, 2H, H-9), 6.69 (t, J = 2.3 Hz, 1H, H-11), 4.14 – 4.10 (m, 4H, H-12), 3.76 – 3.71 (m, 4H, H-13), 3.57 (s, 3H, H-6), 3.44 (s, 6H, H-14).

^{13}C NMR (151 MHz, $CDCl_3$) δ 171.10 (C-7), 159.28 (C-10), 148.19 (C-1), 140.88 (C-4), 136.57 (C-6), 136.14 (C-5), 127.76 (C-3), 124.28 (C-2), 108.72 (C-9), 104.44 (C-11), 71.03 (C-13), 67.73 (C-12), 59.37 (C-14), 29.25 (C-6).

HRMS (ASAP$^+$): Calculated for $C_{21}H_{25}O_7N_3$: 431.1687 $[M]^+$, found 431.1701.

Synthesis of Glycol-Functionalised Free Thiol 344

Synthesis of **377**

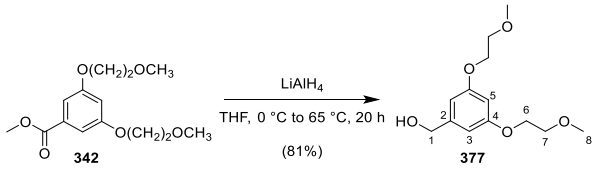

To a suspension of lithium aluminium hydride (crushed pellets, 1.19 g, 31.3 mmol) in THF (100 mL) at 0 °C was added a solution of **342** (4.44 g, 15.6 mmol) in THF (20 mL, 0.1 M in total) dropwise over 5 minutes under argon and stirred for 30 minutes. The reaction mixture was warmed to room temperature, stirred for 60 minutes, and then heated at 65 °C under reflux for 18 h. The reaction mixture was cooled to 0 °C and distilled water (1.5 mL), an aqueous solution of sodium hydroxide (15% w/w, 1.5 mL) and another portion of distilled water (4.5 mL) were added sequentially. $MgSO_4$ (excess) was added, and the reaction mixture was gradually warmed to room temperature and stirred for 30 minutes. The resulting suspension was filtrated through a plug of celite, the residue washed with EtOAc (100 mL) and the combined organic phases were concentrated *in vacuo* to afford **377** (3.25 g, 81%) as a yellow oil.

^{1}H NMR (600 MHz, $CDCl_3$) δ 6.55 (d, J = 2.3 Hz, 2H, H-3), 6.45 (t, J = 2.3 Hz, 1H, H-5), 4.62 (d, J = 6.1 Hz, 2H, H-1), 4.12 – 4.08 (m, 4H, H-6), 3.76 – 3.70 (m, 4H, H-7), 3.44 (s, 6H, H-8), 1.65 – 1.60 (m, 1H, C-1 OH).

^{13}C NMR (151 MHz, $CDCl_3$) δ 160.22 (C-4), 143.41 (C-2), 105.60 (C-3), 100.96 (C-5), 71.10 (C-7), 67.42 (C-6), 65.49 (C-1), 59.37 (C-8).

HRMS (ASAP$^+$): Calculated for $C_{13}H_{21}O_5$: 257.1384 $[M+H]^+$, found 257.1380.

Synthesis of **378**

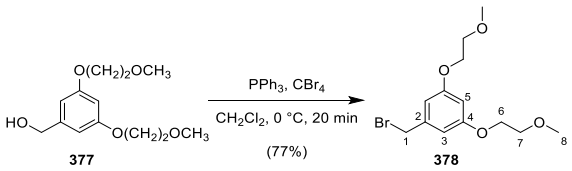

To a solution of **377** (1.44 g, 5.62 mmol) in CH_2Cl_2 (56 mL, 0.1 M) at 0 °C was added CBr_4 (4.66 g, 14.1 mmol) and PPh_3 (2.95 g, 11.2 mmol) and the reaction was stirred at 0 °C for 20 minutes. The resultant mixture was evaporated from SiO_2 and purified by flash chromatography (SiO_2, CH_2Cl_2/ MeOH, 99:1) to give **378** (1.38 g, 77%) as a yellow oil.

^{1}H NMR (600 MHz, $CDCl_3$) δ 6.56 (d, J = 2.3 Hz, 2H, H-3), 6.46 (t, J = 2.3 Hz, 1H, H-5), 4.39 (s, 2H, H-1), 4.12 – 4.07 (m, 4H, H-6), 3.76 – 3.71 (m, 4H, H-7), 3.44 (s, 6H, H-8).

^{13}C NMR (151 MHz, $CDCl_3$) δ 160.11 (C-4), 139.76 (C-2), 108.06 (C-3), 101.83 (C-5), 71.05 (C-7), 67.50 (C-6), 59.37 (C-8), 33.71 (C-1).

HRMS (ASAP$^+$): Calculated for $C_{13}H_{20}O_4Br$: 319.0539 $[M+H]^+$, found 319.0539.

Synthesis of **343**

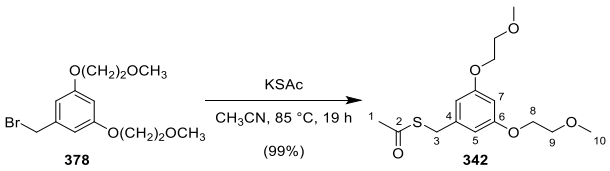

378 **342**

A suspension of **378** (1.62 g, 5.08 mmol) and potassium thioacetate (696 mg, 6.09 mmol) in CH_3CN (51 mL, 0.1 M) was heated at 85 °C under reflux for 16 h. The solvent was removed *in vacuo* and the resulting residue purified by flash chromatography (SiO_2, CH_2Cl_2/ MeOH, 39:1) to afford **343** (1.59 g, 99%) as a yellow oil.

^{1}H NMR (600 MHz, $CDCl_3$) δ 6.46 (d, J = 2.2 Hz, 2H, H-5), 6.40 (t, J = 2.2 Hz, 1H, H-7), 4.10 – 4.05 (m, 4H, H-8), 4.03 (s, 2H, H-3), 3.74 – 3.70 (m, 4H, H-9), 3.44 (s, 6H, H-10), 2.34 (s, 3H, H-1).

^{13}C NMR (151 MHz, $CDCl_3$) δ 195.20 (C-2), 160.09 (C-6), 139.80 (C-4), 107.83 (C-5), 100.64 (C-7), 71.08 (C-9), 67.40 (C-8), 59.35 (C-10), 33.74 (C-3), 30.44 (C-1).

HRMS (ASAP$^+$): Calculated for $C_{15}H_{23}O_5S$: 315.1261 $[M+H]^+$, found 315.1259.

Synthesis of **344**

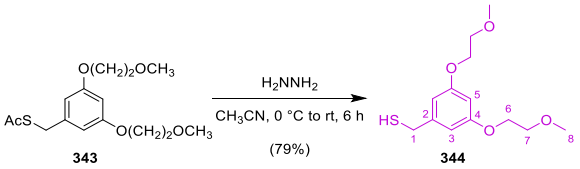

To a solution of **343** (1.59 g, 5.04 mmol) in degassed CH_3CN (50 mL, 0.1 M) at 0 °C was added hydrazine (monohydrate, 0.49 mL, 10.1 mmol) dropwise under argon and stirred for 25 minutes. The reaction was warmed to room temperature and stirred for 5 h. The reaction was concentrated *in vacuo* and purified by flash chromatography (SiO_2, $CHCl_3$/ diethyl ether, 17:3) to afford **344** (1.08 g, 79%) as a colourless oil.

^{1}H NMR (600 MHz, $CDCl_3$) δ 6.51 (d, J = 2.2 Hz, 2H, H-3), 6.40 (t, J = 2.2 Hz, 1H, H-5), 4.11 – 4.06 (m, 4H, H-5), 3.76 – 3.70 (m, 4H, H-7), 3.65 (d, J = 7.6 Hz, 2H, H-1), 3.44 (s, 6H, H-8), 1.73 (t, J = 7.6 Hz, 1H, C-1 SH).

^{13}C NMR (151 MHz, $CDCl_3$) δ 160.15 (C-4), 143.43 (C-2), 107.12 (C-2), 100.36 (C-5), 71.10 (C-7), 67.42 (C-6), 59.37 (C-8), 29.35 (C-1).

HRMS (ASAP$^+$): Calculated for $C_{13}H_{21}O_4S$: 273.1155 $[M+H]^+$, found 273.1152.

11.2. ^{1}H, ^{11}B, ^{13}C, ^{19}F and ^{31}P NMR spectra

11.2.1. Helicene Synthesis by a Rotaxane-Based Molecular Machine

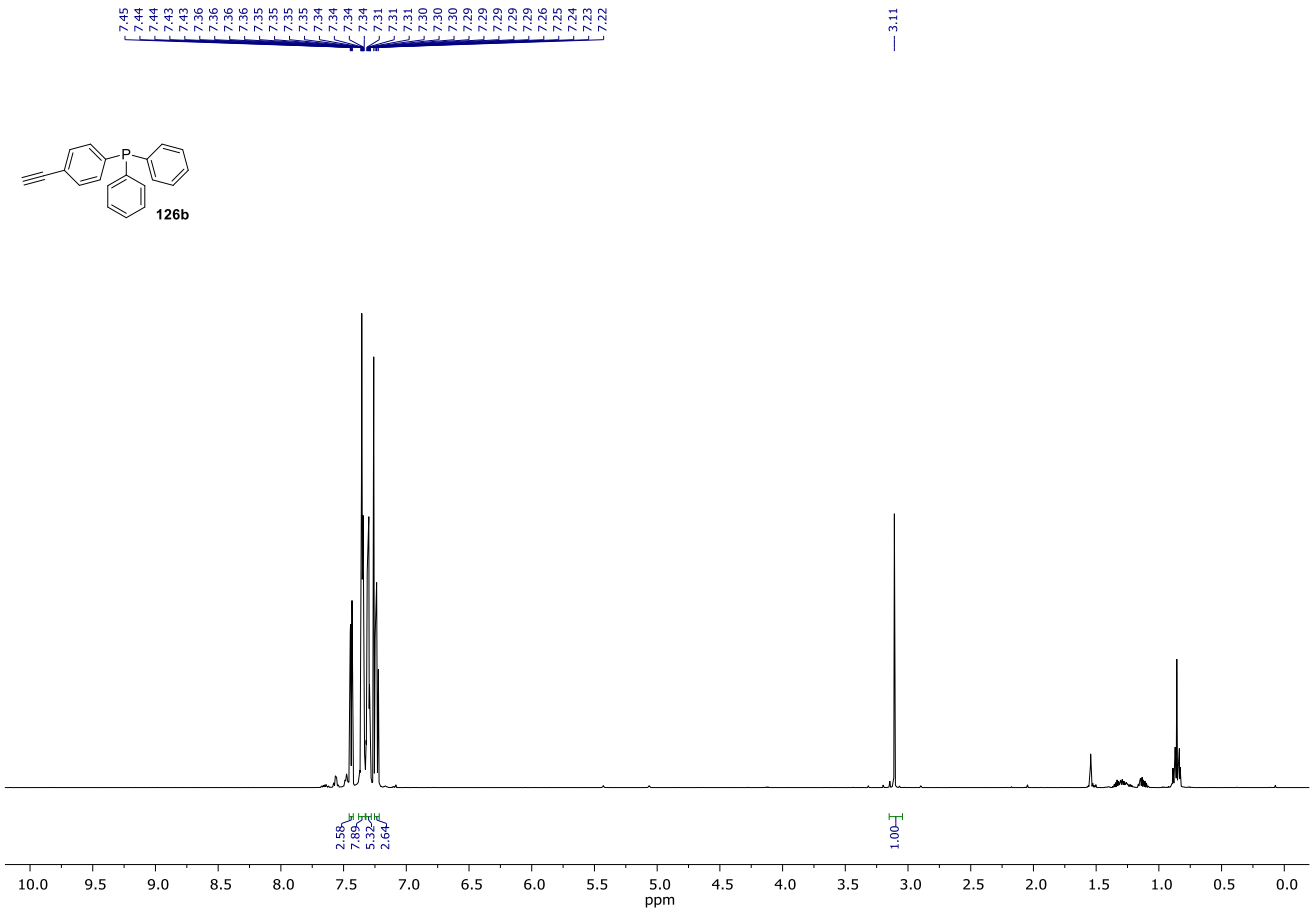

Spectrum 1. ^{1}H NMR (600 MHz, $CDCl_3$) of **126b**.

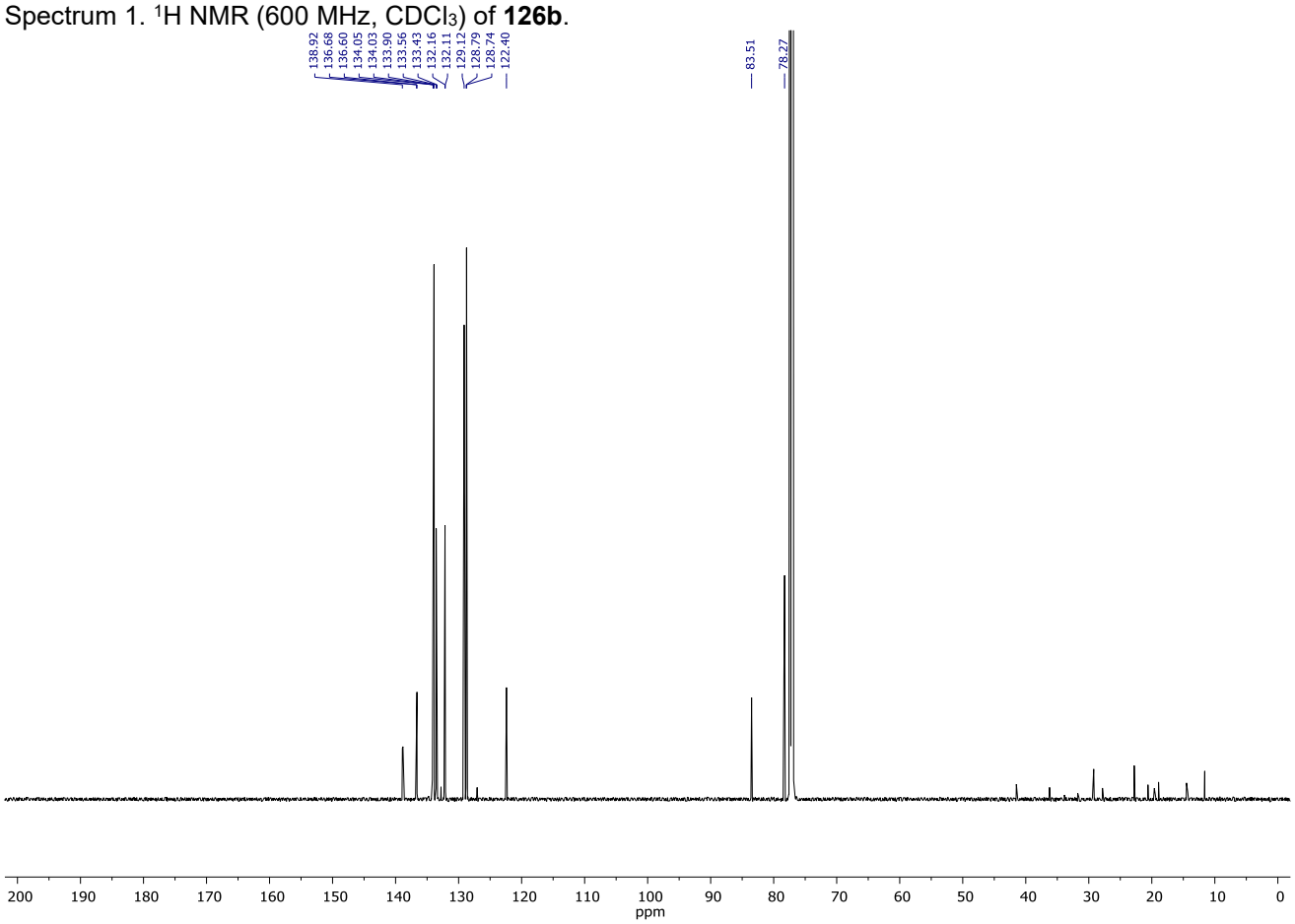

Spectrum 2. ^{13}C NMR (151 MHz, $CDCl_3$) of **126b**.

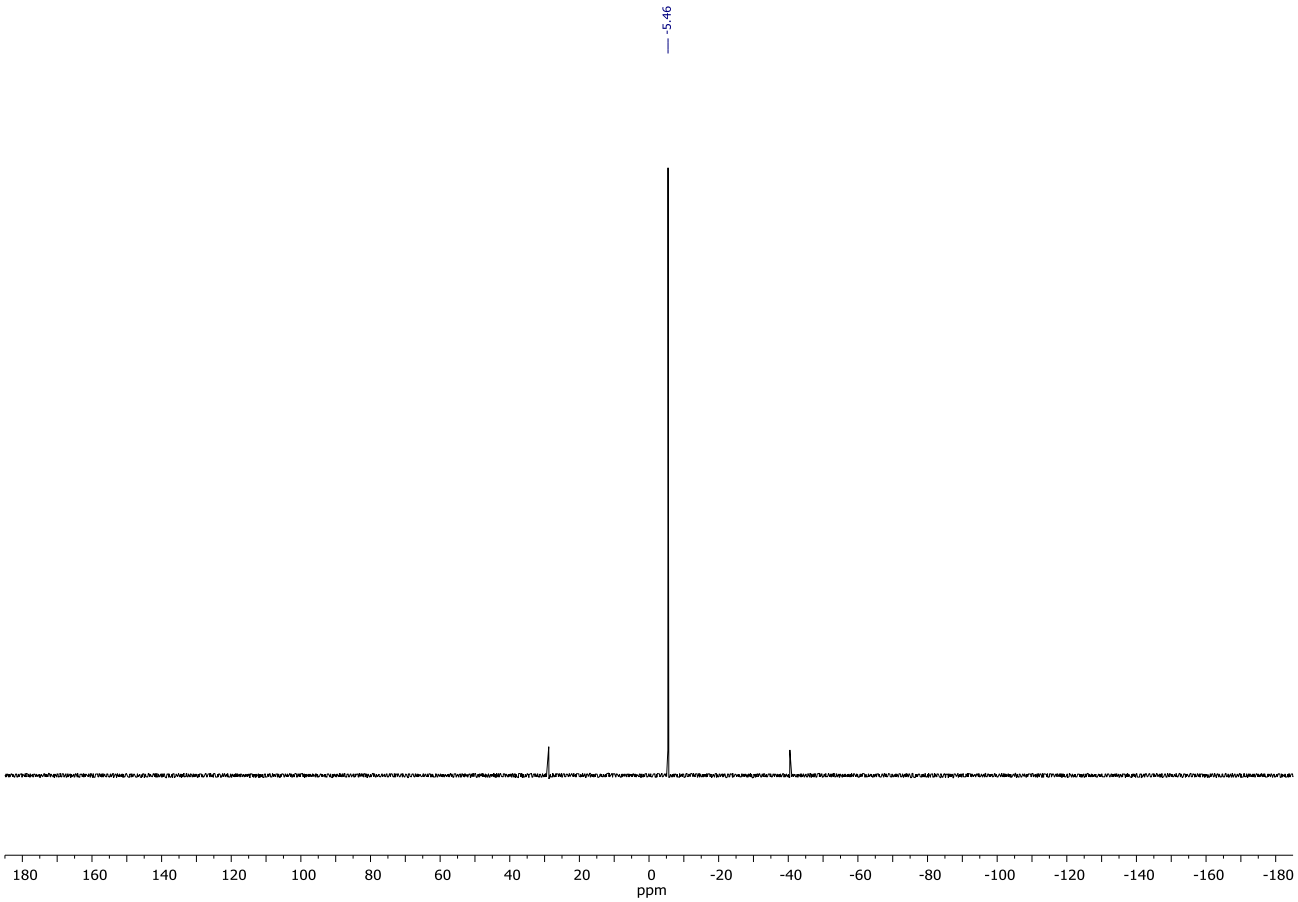

Spectrum 3. ^{31}P NMR (162 MHz, $CDCl_3$) of **126b**.

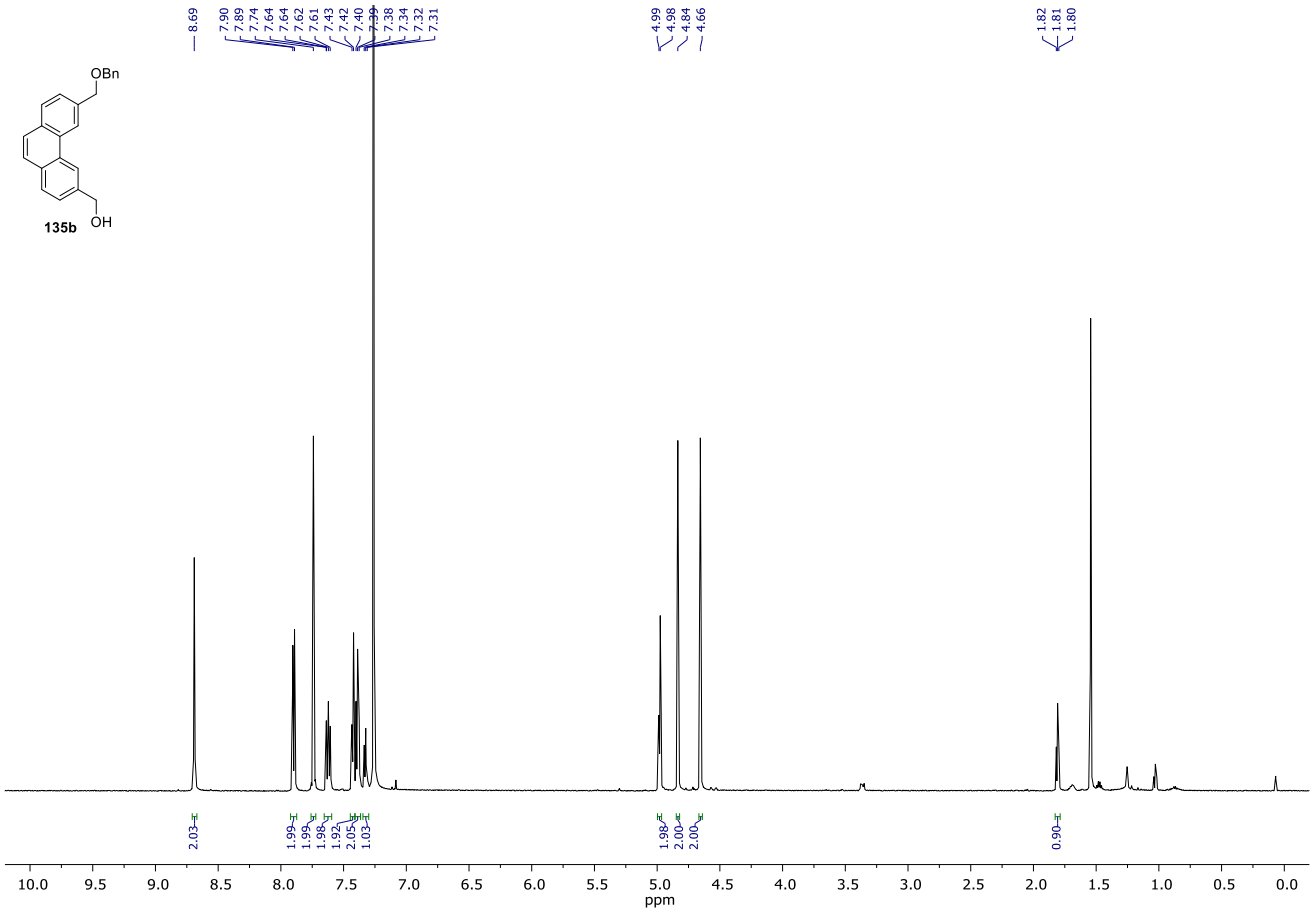

Spectrum 4. ^{1}H NMR (600 MHz, $CDCl_3$) of **135b**.

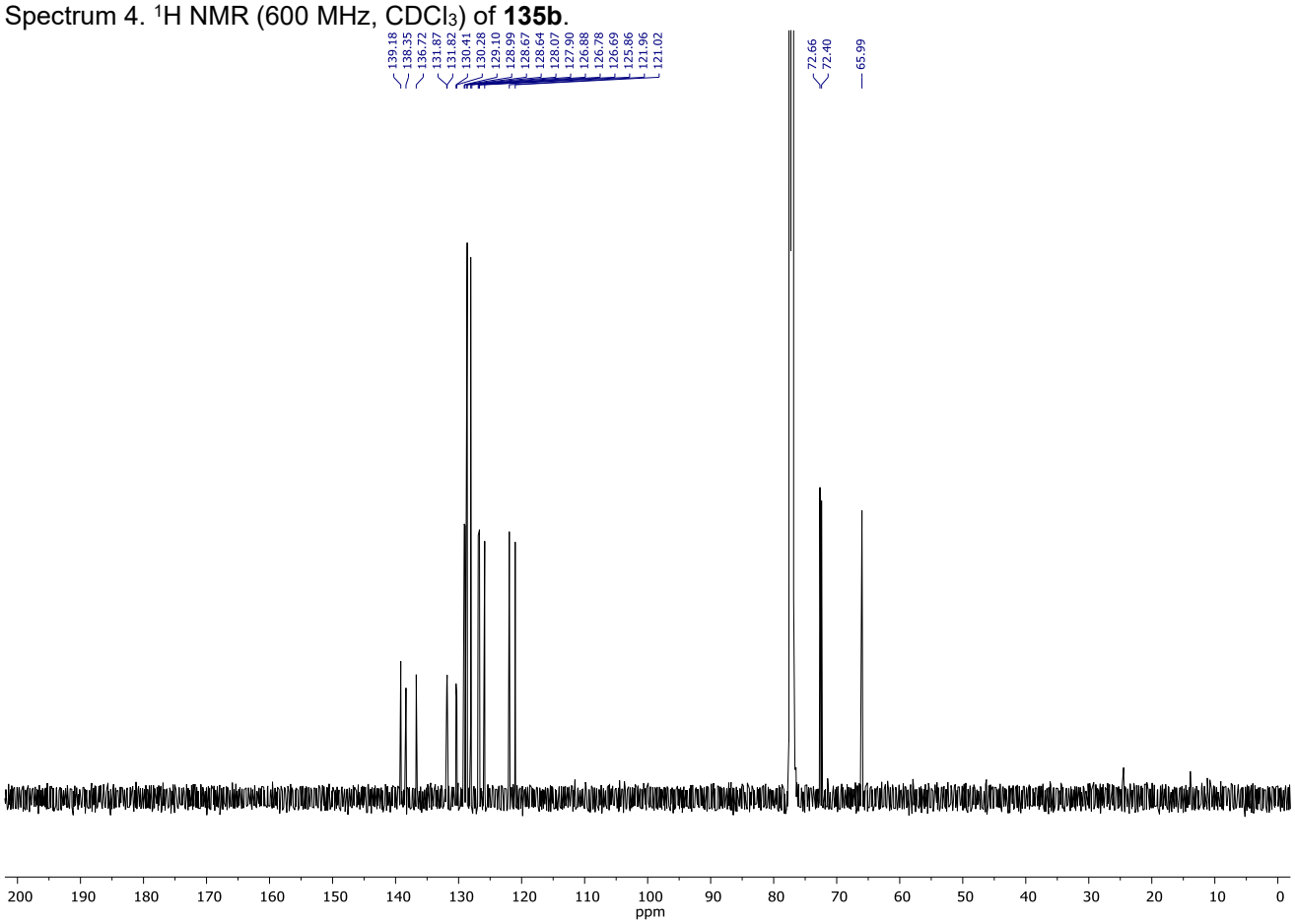

Spectrum 5. ^{13}C NMR (151 MHz, $CDCl_3$) of **135b**.

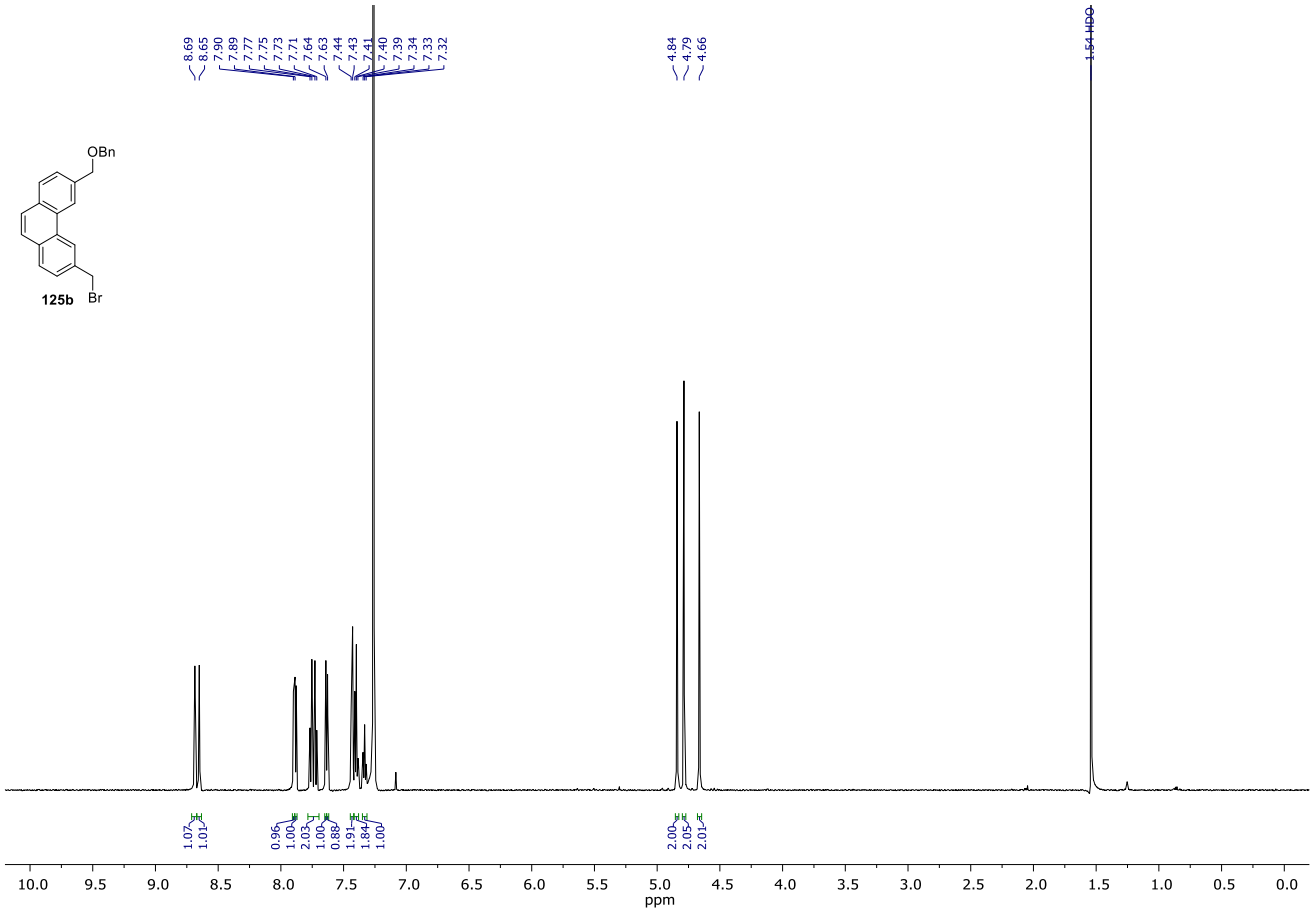

Spectrum 6. ^{1}H NMR (600 MHz, $CDCl_3$) of **125b**.

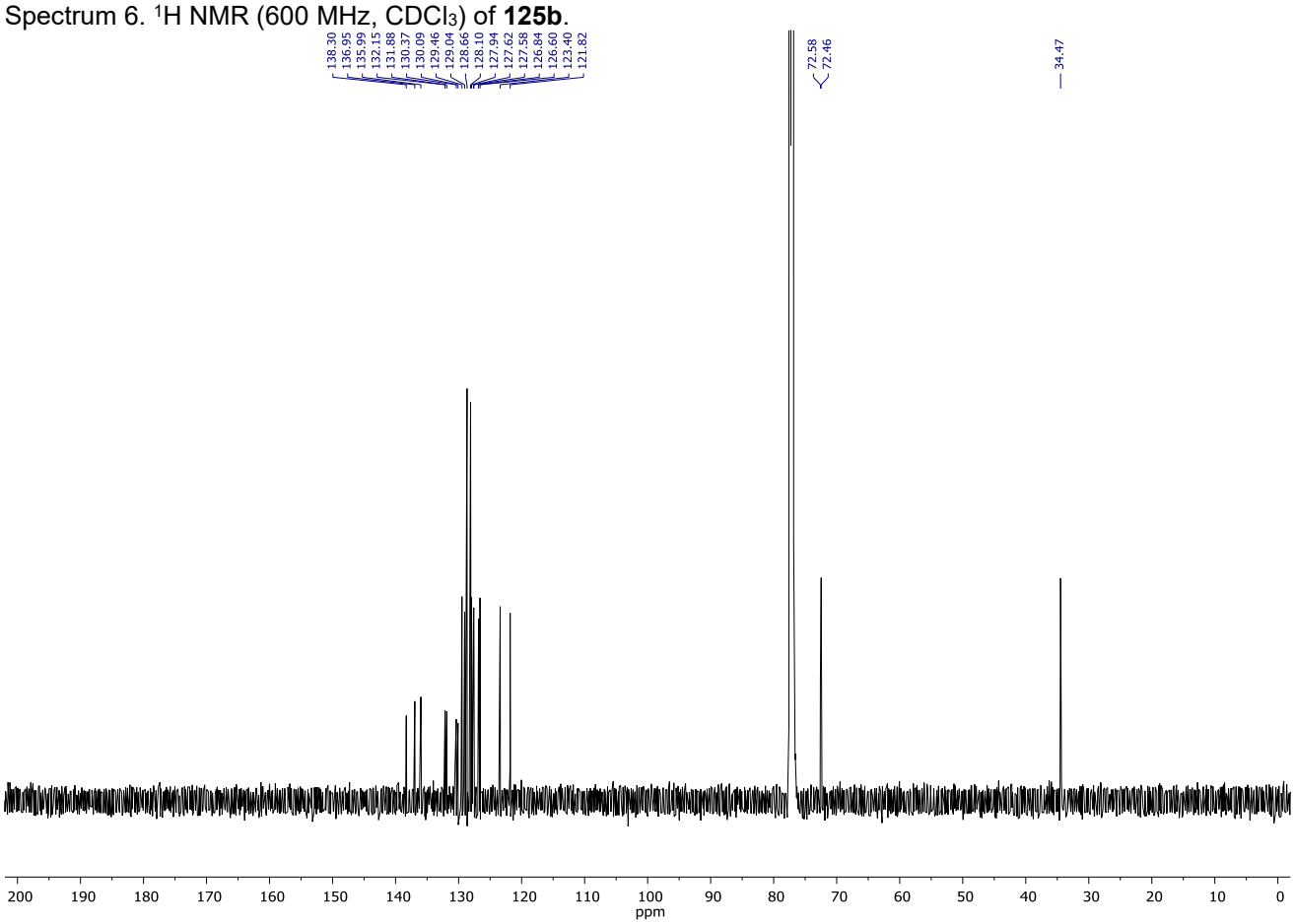

Spectrum 7. ^{13}C NMR (151 MHz, $CDCl_3$) of **125b**.

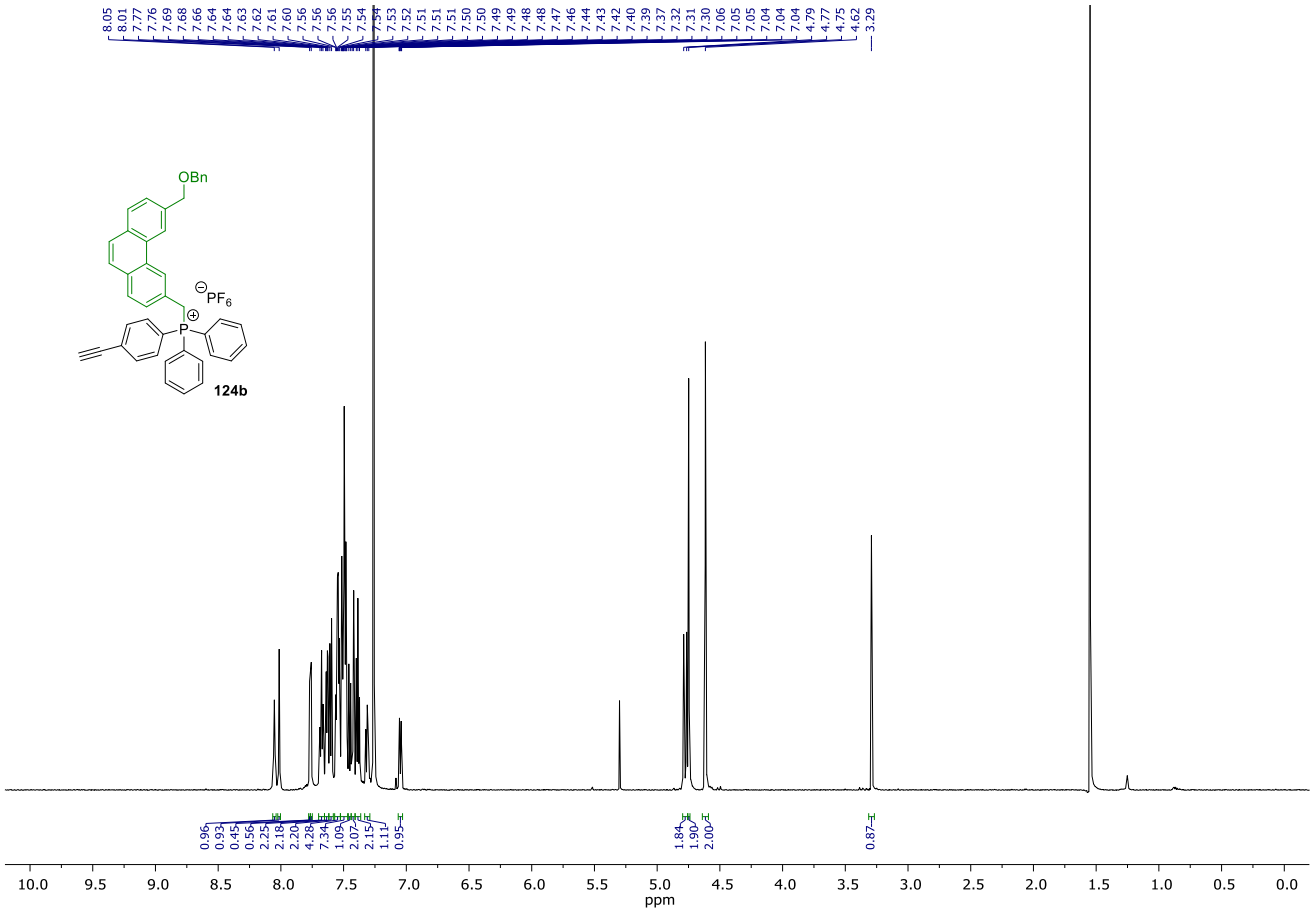

Spectrum 8. ^{1}H NMR (600 MHz, $CDCl_3$) of **124b**.

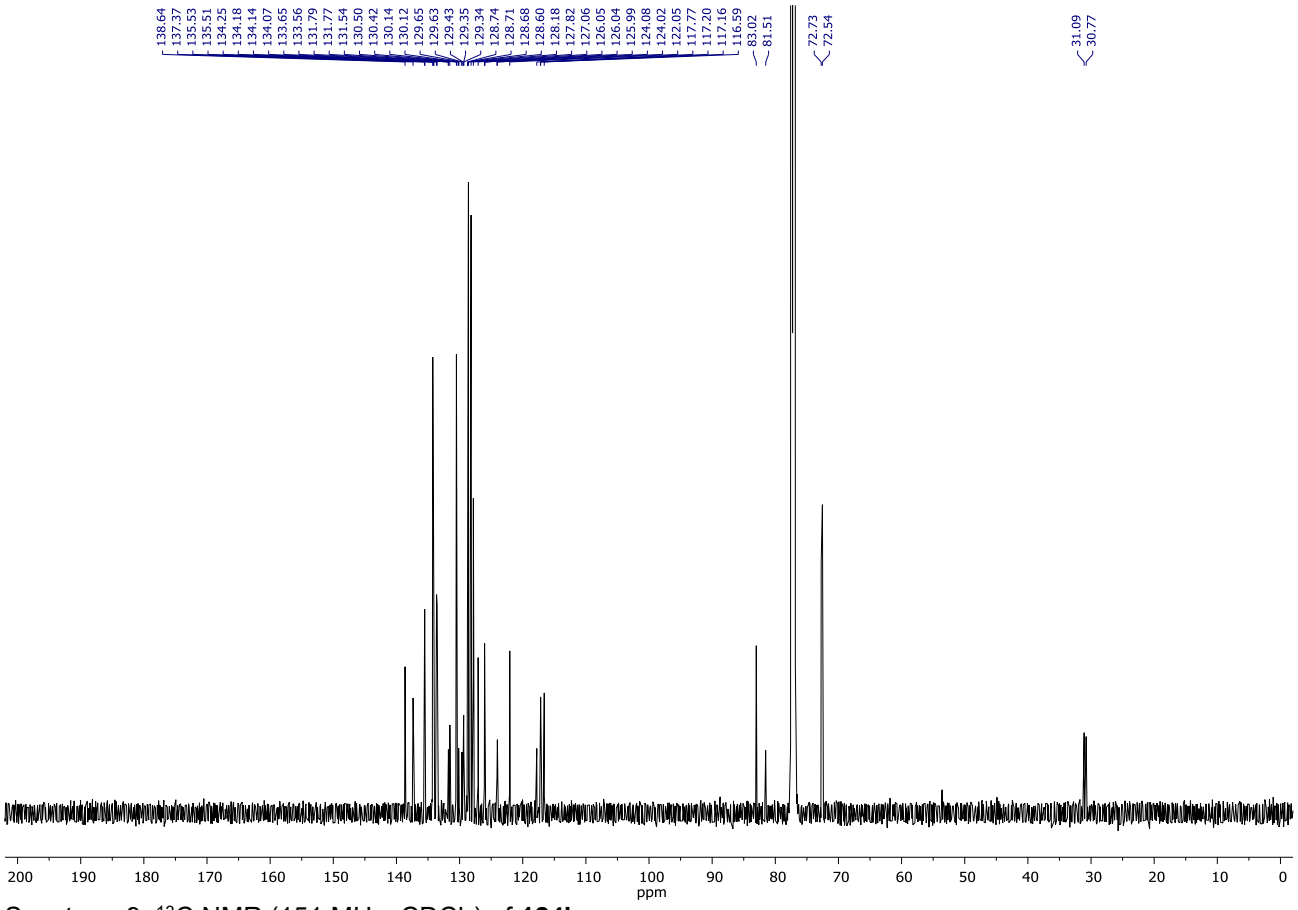

Spectrum 9. ^{13}C NMR (151 MHz, $CDCl_3$) of **124b**.

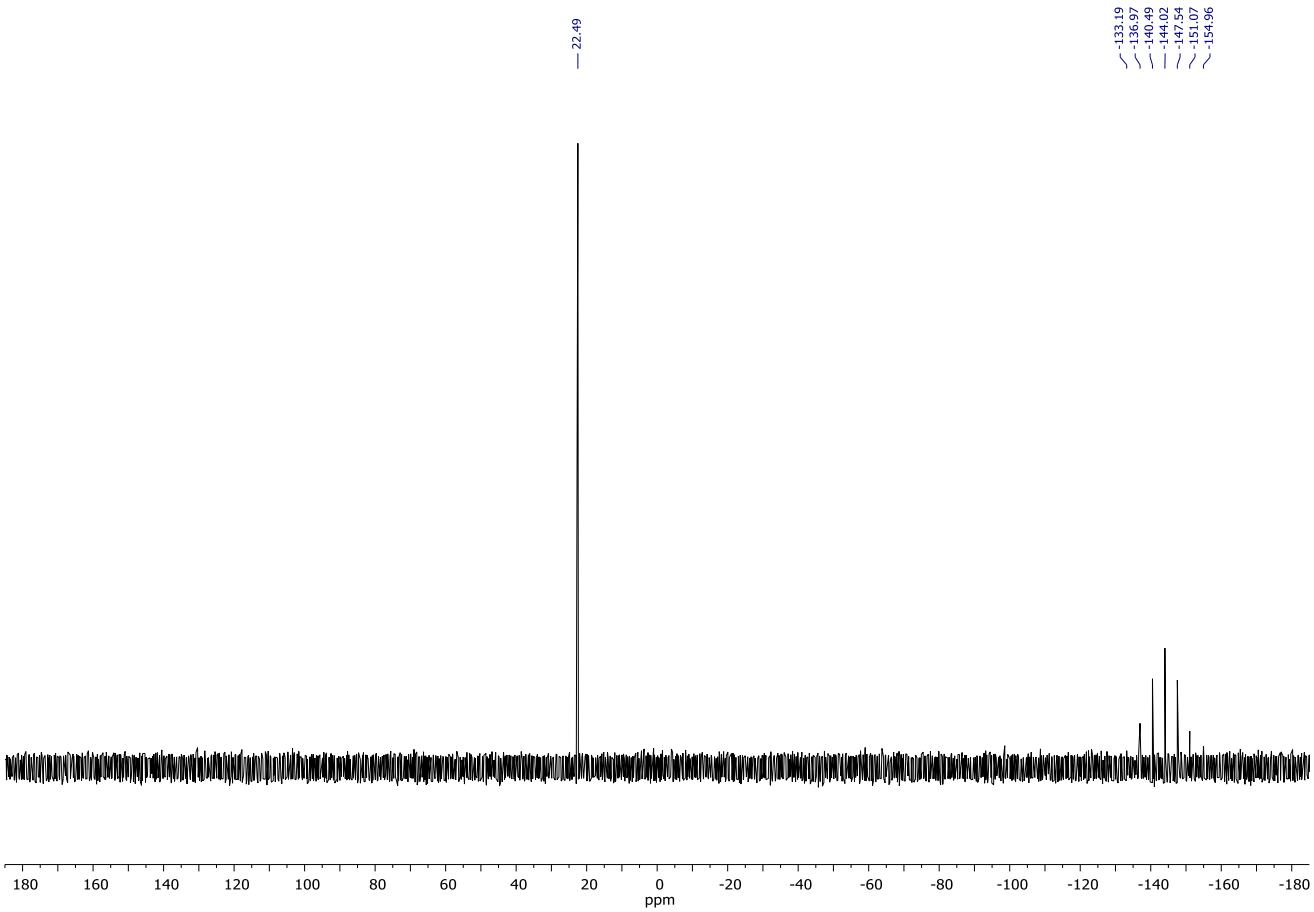

Spectrum 10. ^{31}P NMR (162 MHz, $CDCl_3$) of **124b**.

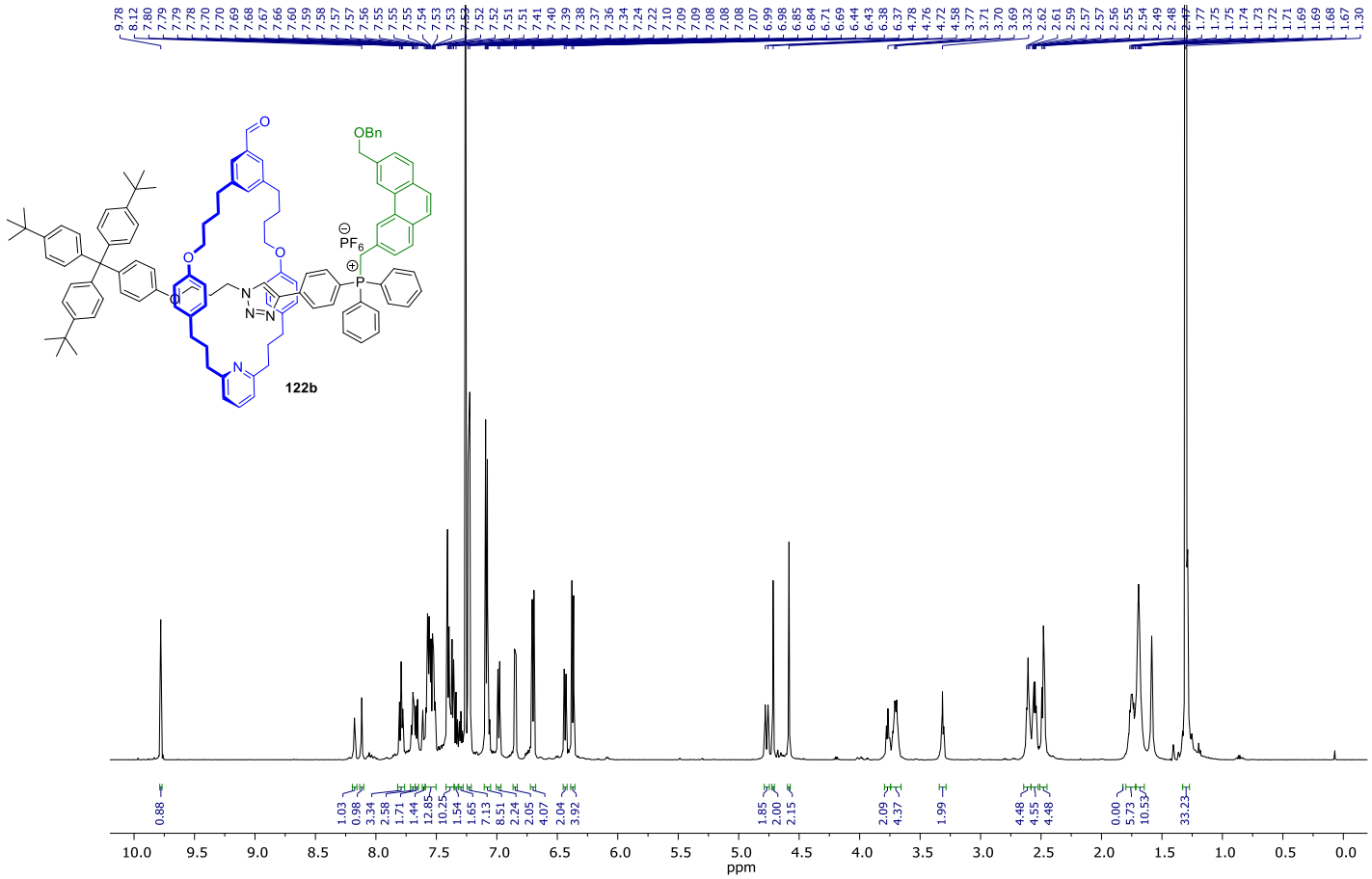

Spectrum 11. ^{1}H NMR (600 MHz, $CDCl_3$) of **122b**.

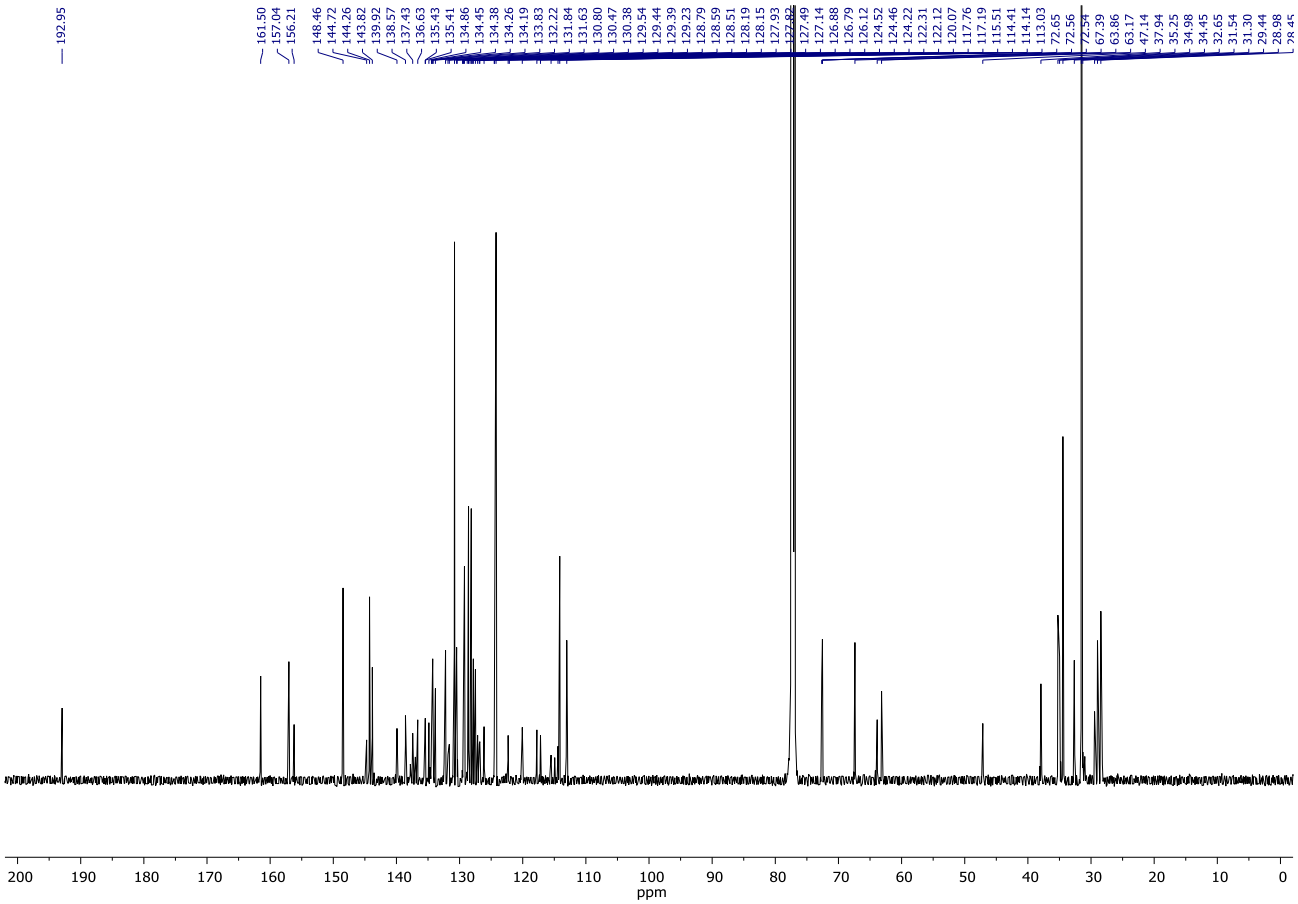

Spectrum 12. ^{13}C NMR (151 MHz, $CDCl_3$) of **122b**.

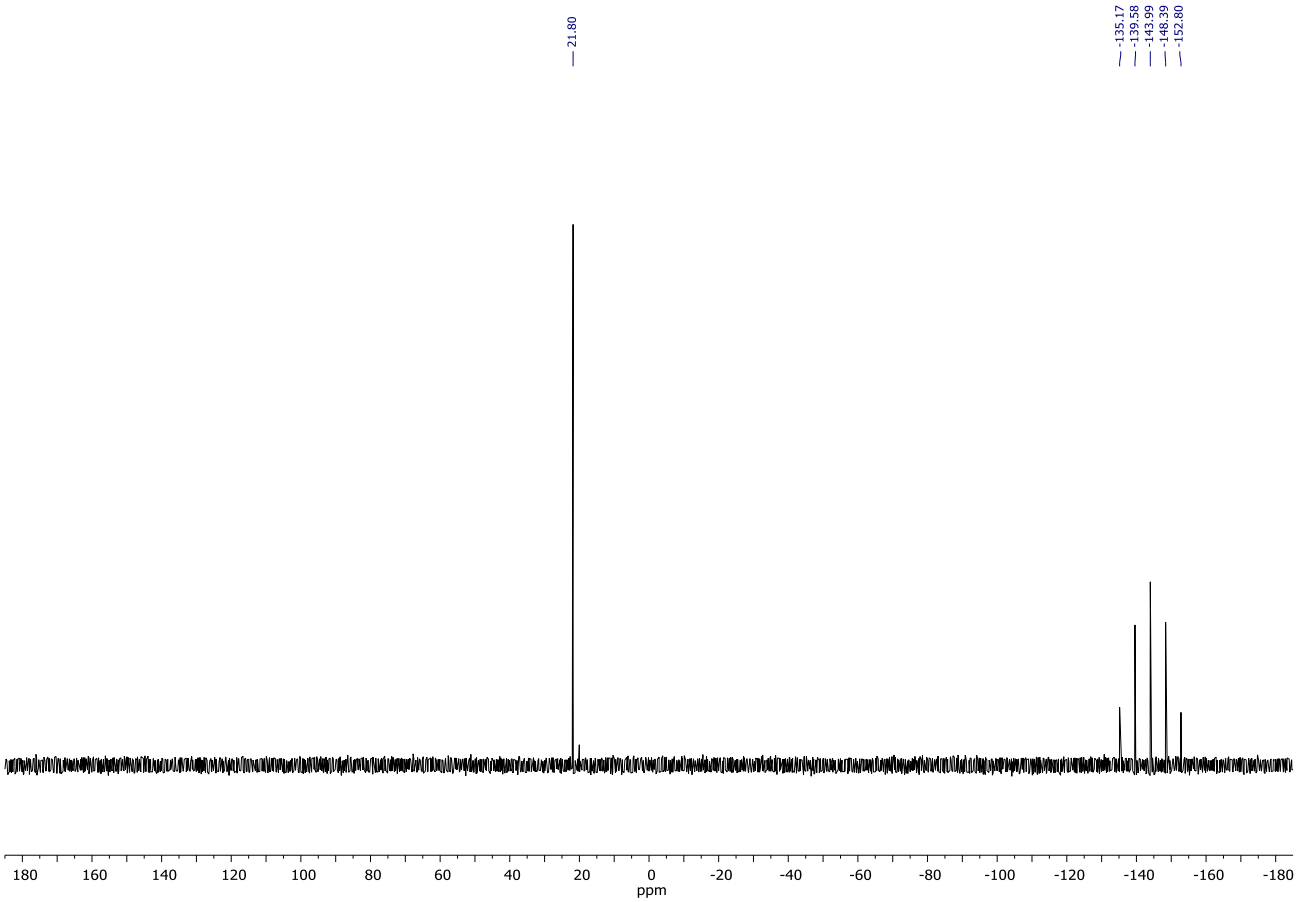

Spectrum 13. ^{31}P NMR (162 MHz, $CDCl_3$) of **122b**.

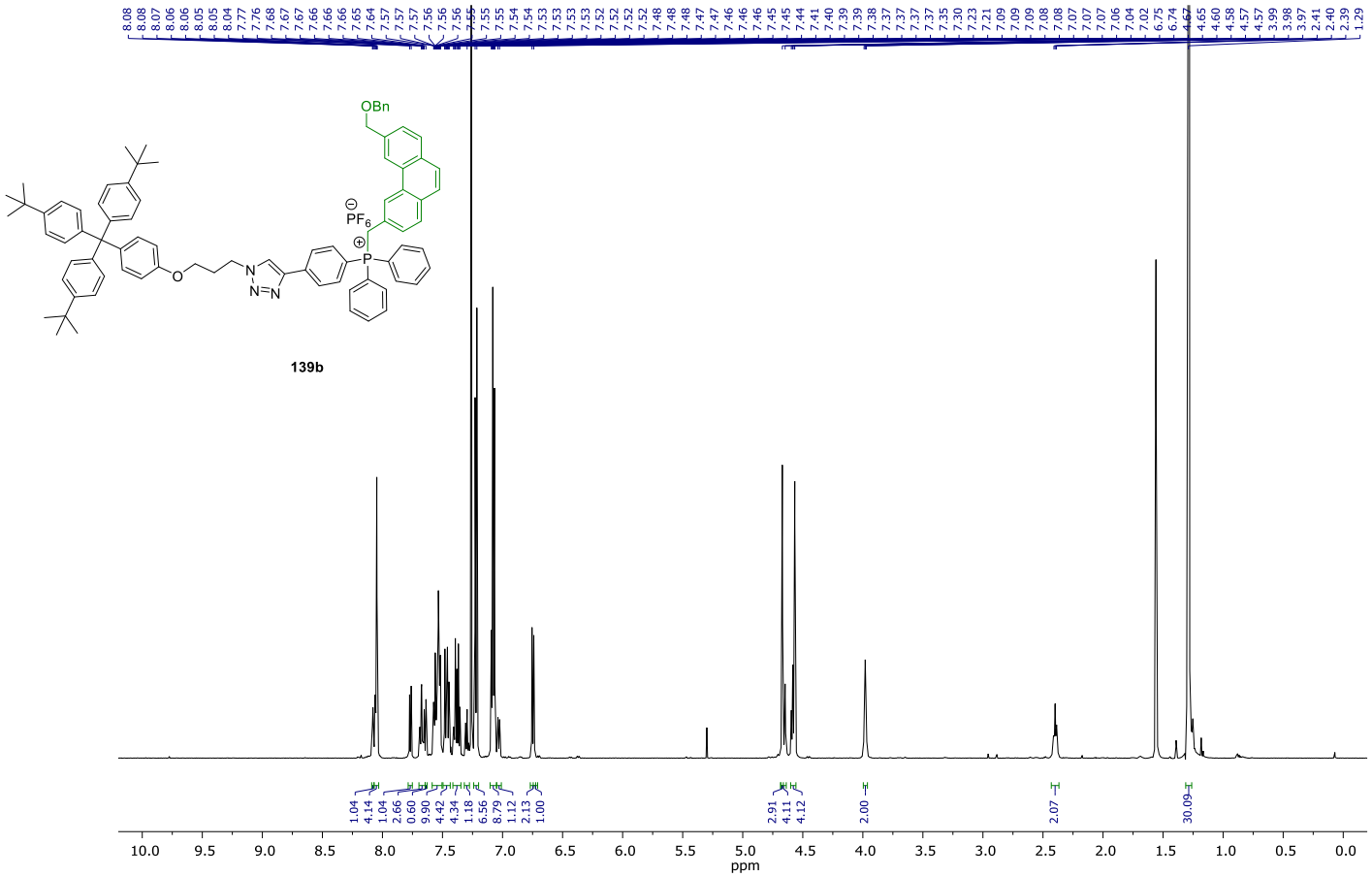

Spectrum 14. ^{1}H NMR (600 MHz, $CDCl_3$) of **139b**.

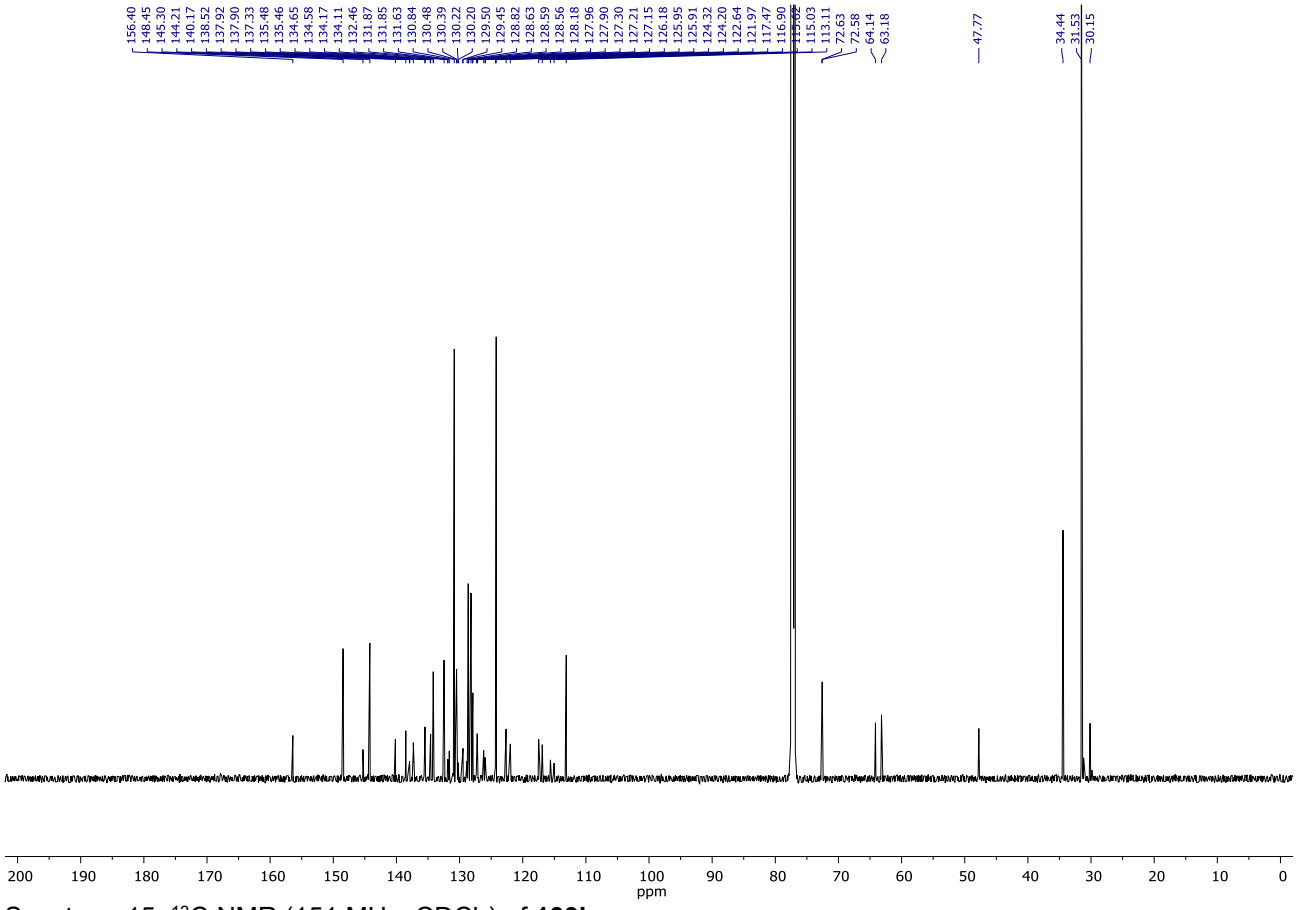

Spectrum 15. ^{13}C NMR (151 MHz, $CDCl_3$) of **139b**.

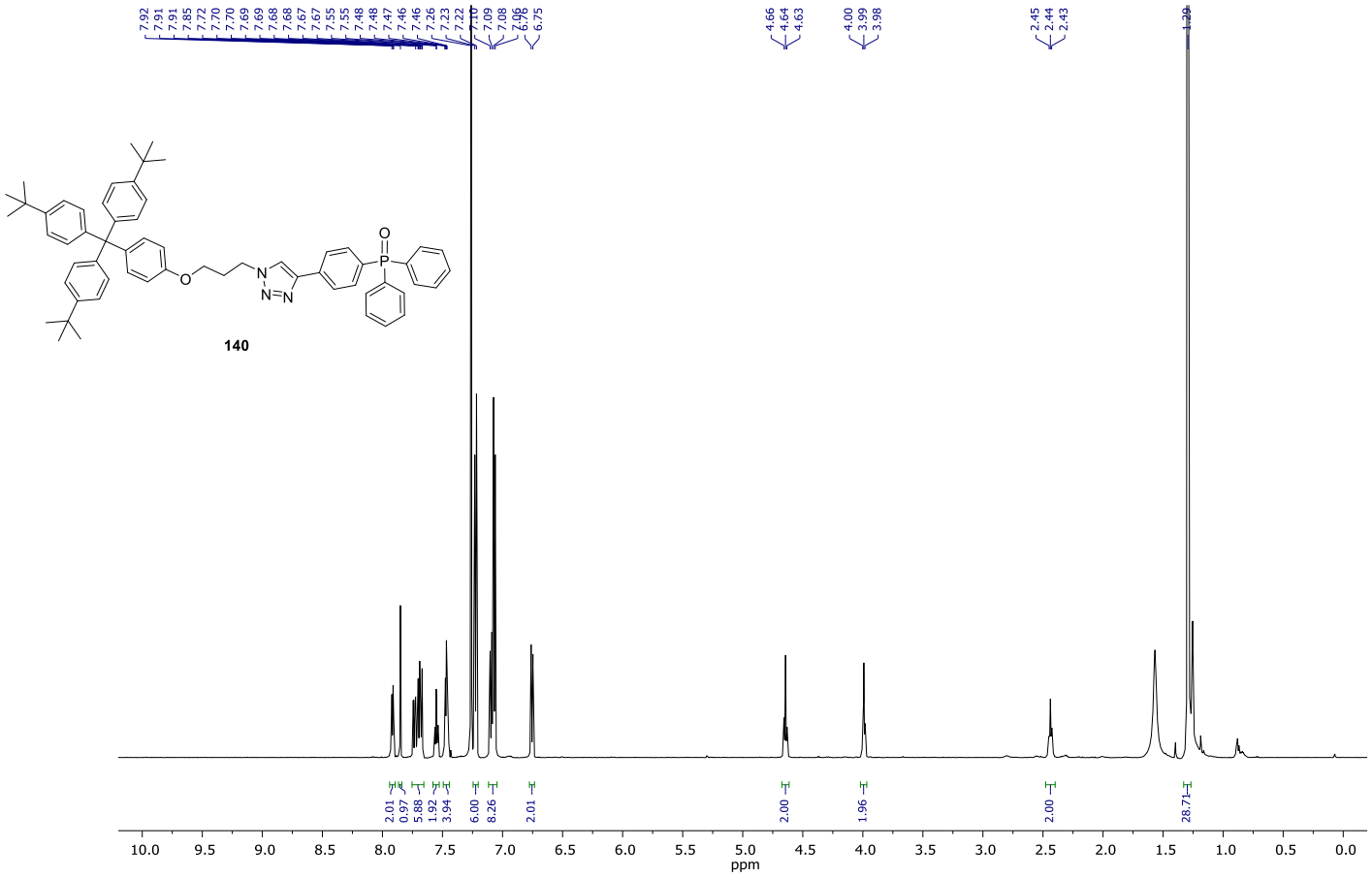

140

Spectrum 16. ^{1}H NMR (600 MHz, $CDCl_3$) of **140**.

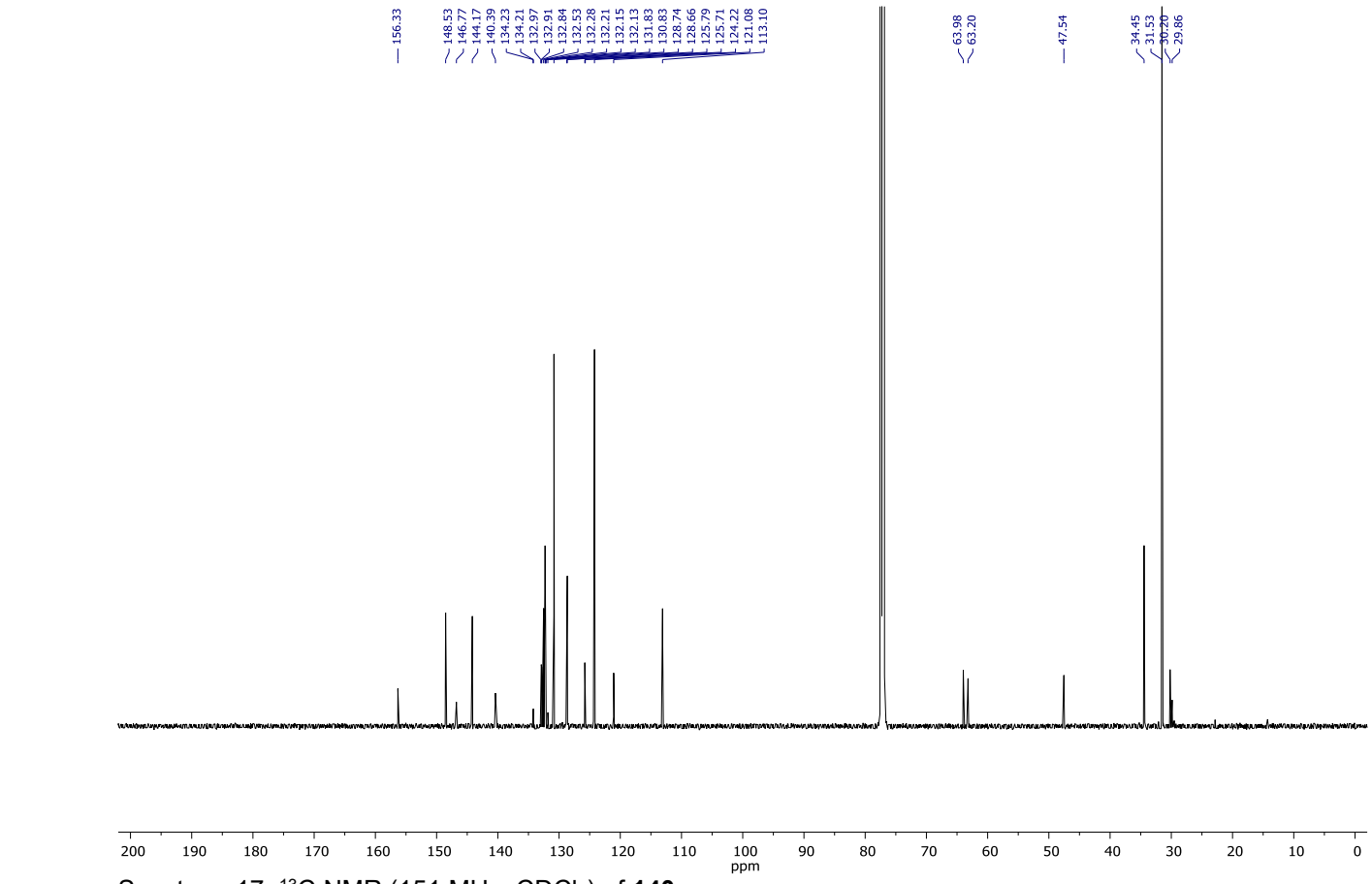

Spectrum 17. ^{13}C NMR (151 MHz, $CDCl_3$) of **140**.

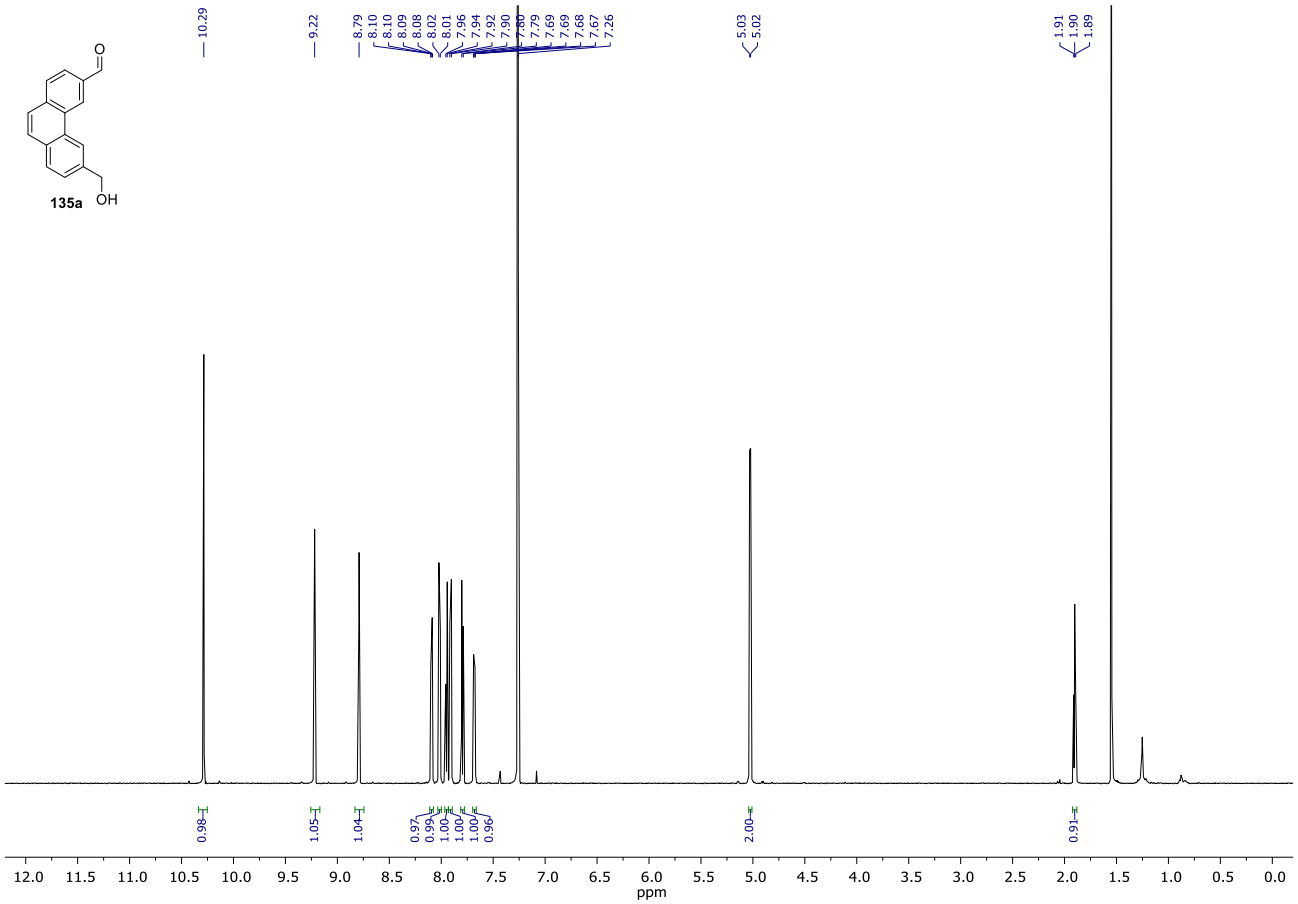

Spectrum 18. ^{1}H NMR (600 MHz, $CDCl_3$) of **135a**.

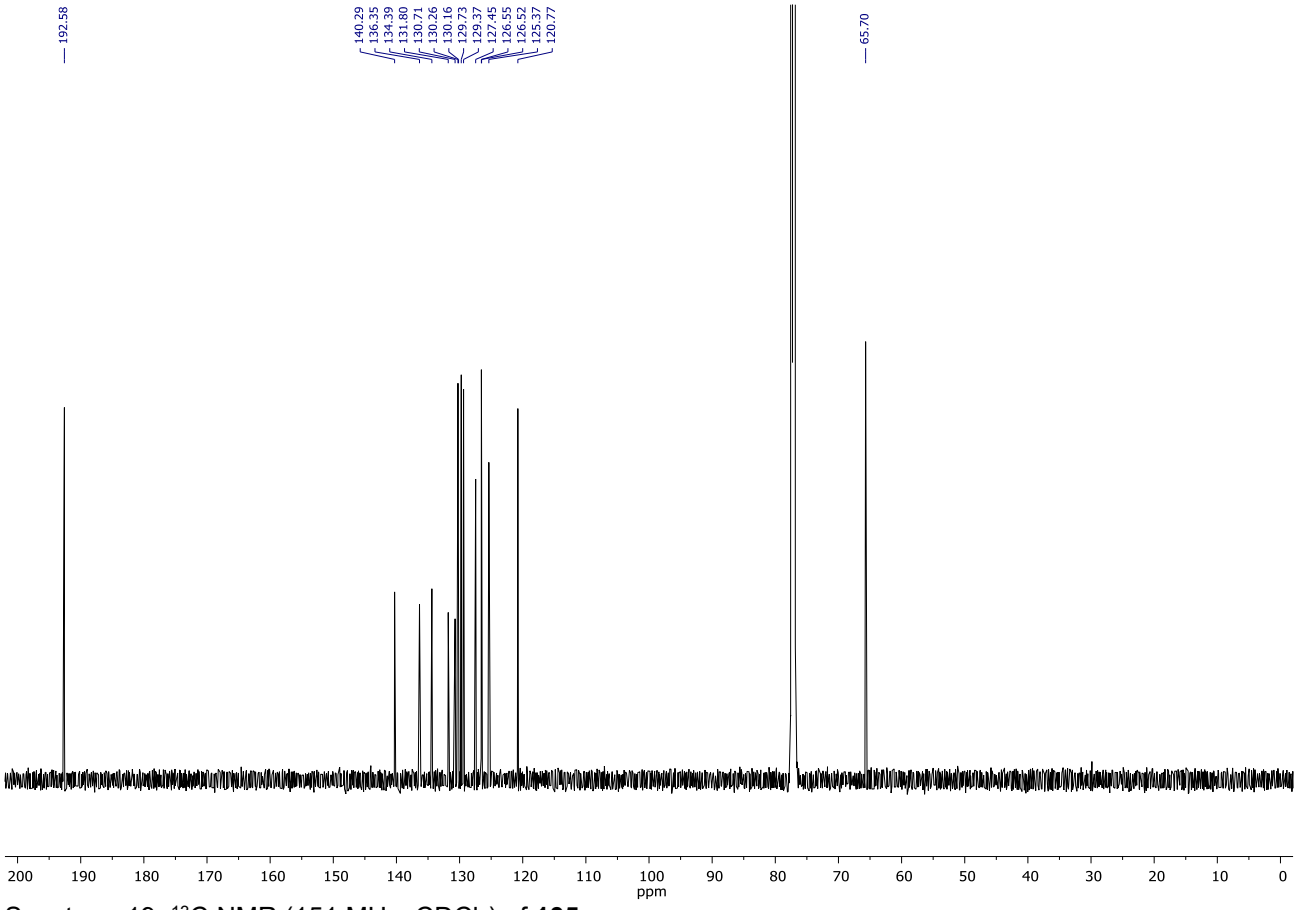

Spectrum 19. ^{13}C NMR (151 MHz, $CDCl_3$) of **135a**.

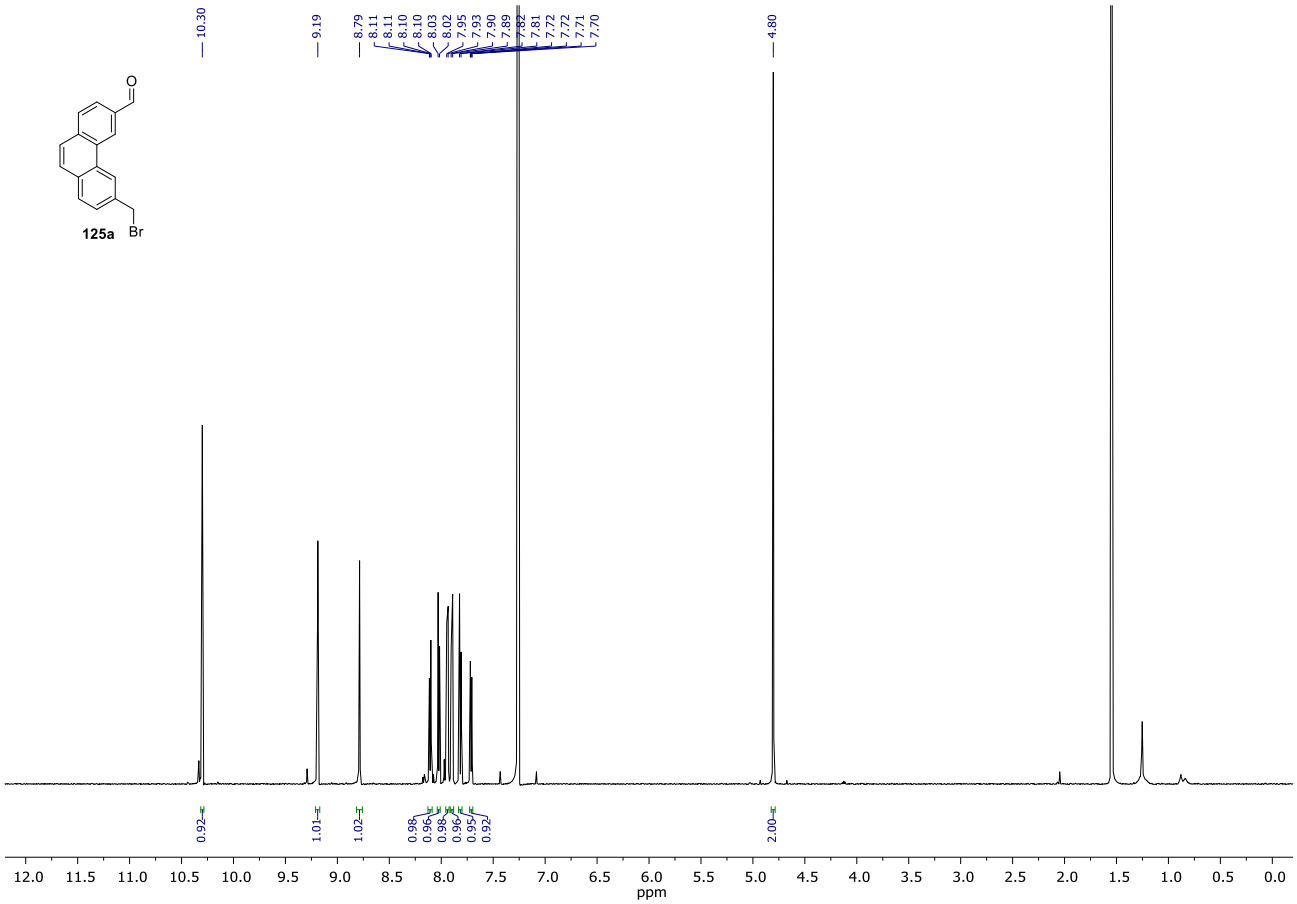

Spectrum 20.[1]H NMR (600 MHz, $CDCl_3$) of **125a**.

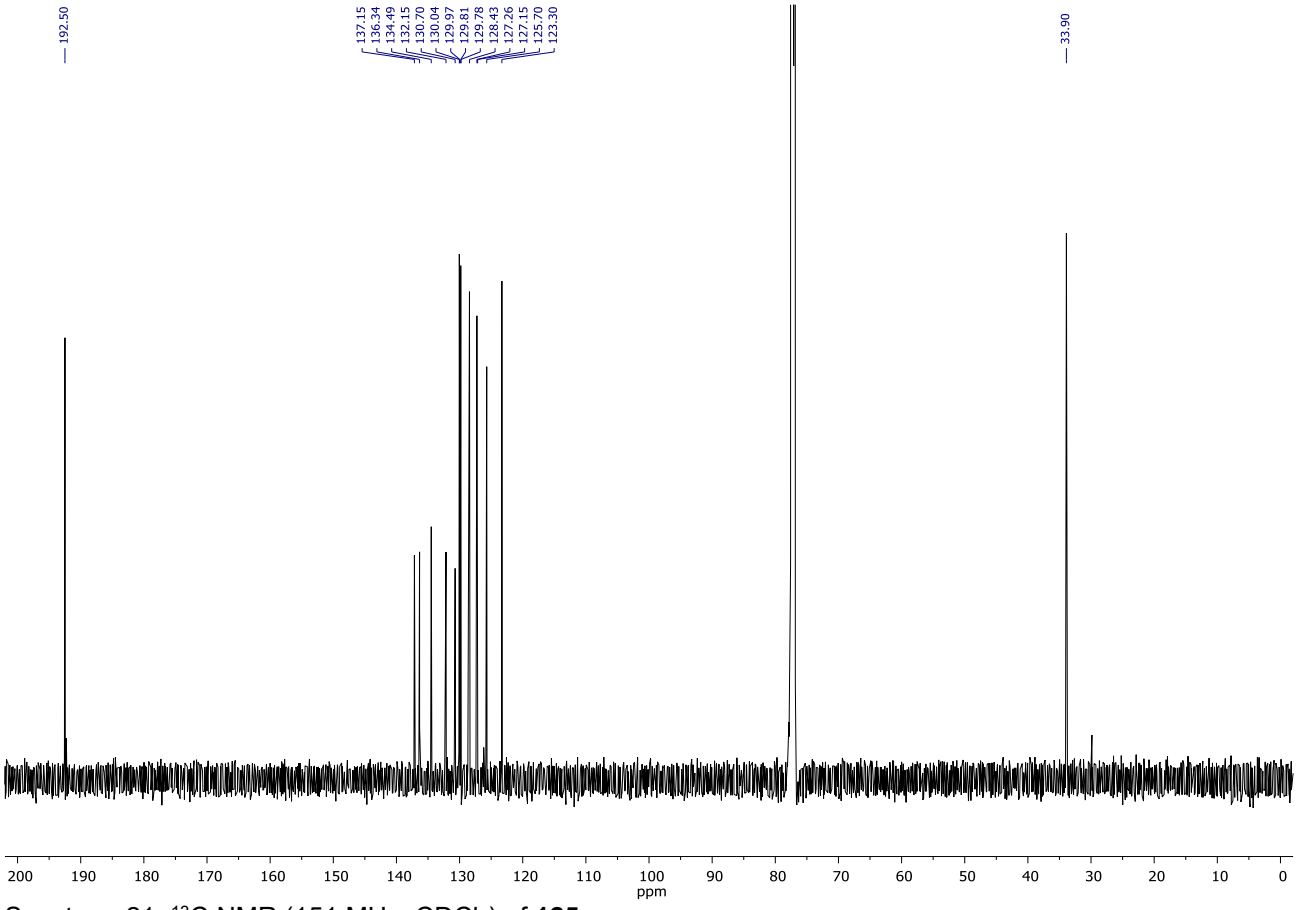

Spectrum 21. [13]C NMR (151 MHz, $CDCl_3$) of **125a**.

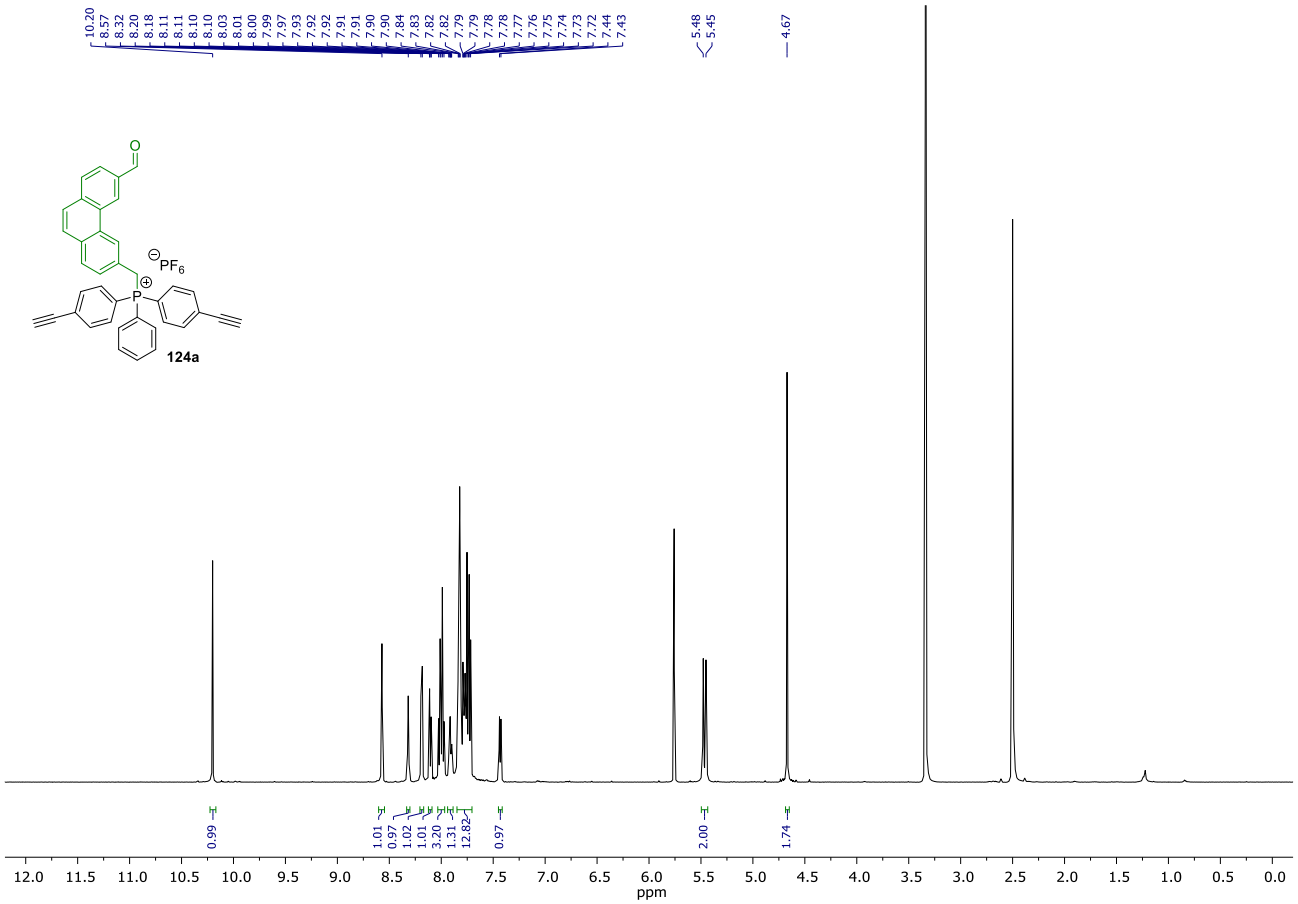

Spectrum 22. ^{1}H NMR (600 MHz, DMSO-d_6) of **124a**.

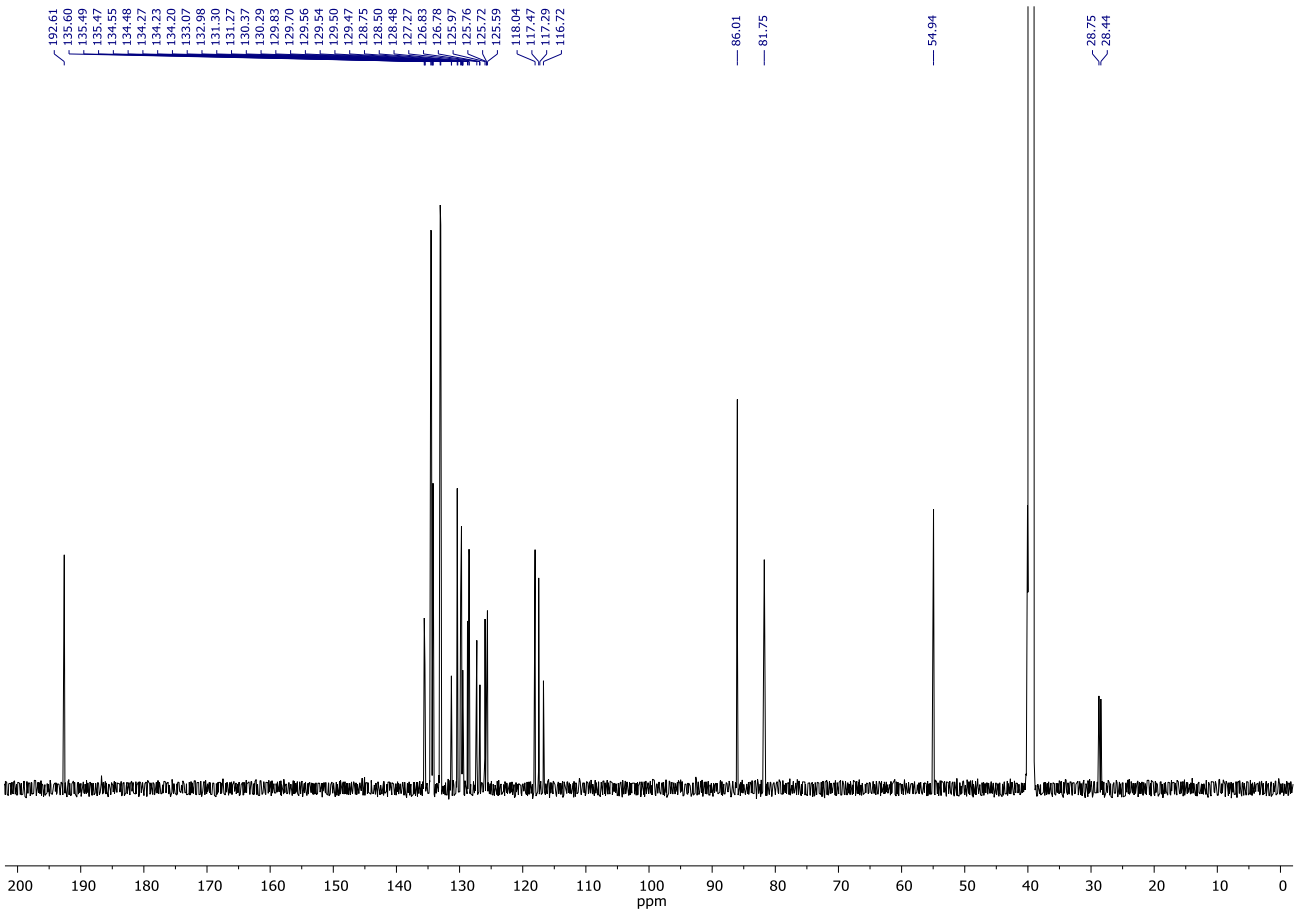

Spectrum 23. ^{13}C NMR (151 MHz, DMSO-d_6) of **124a**.

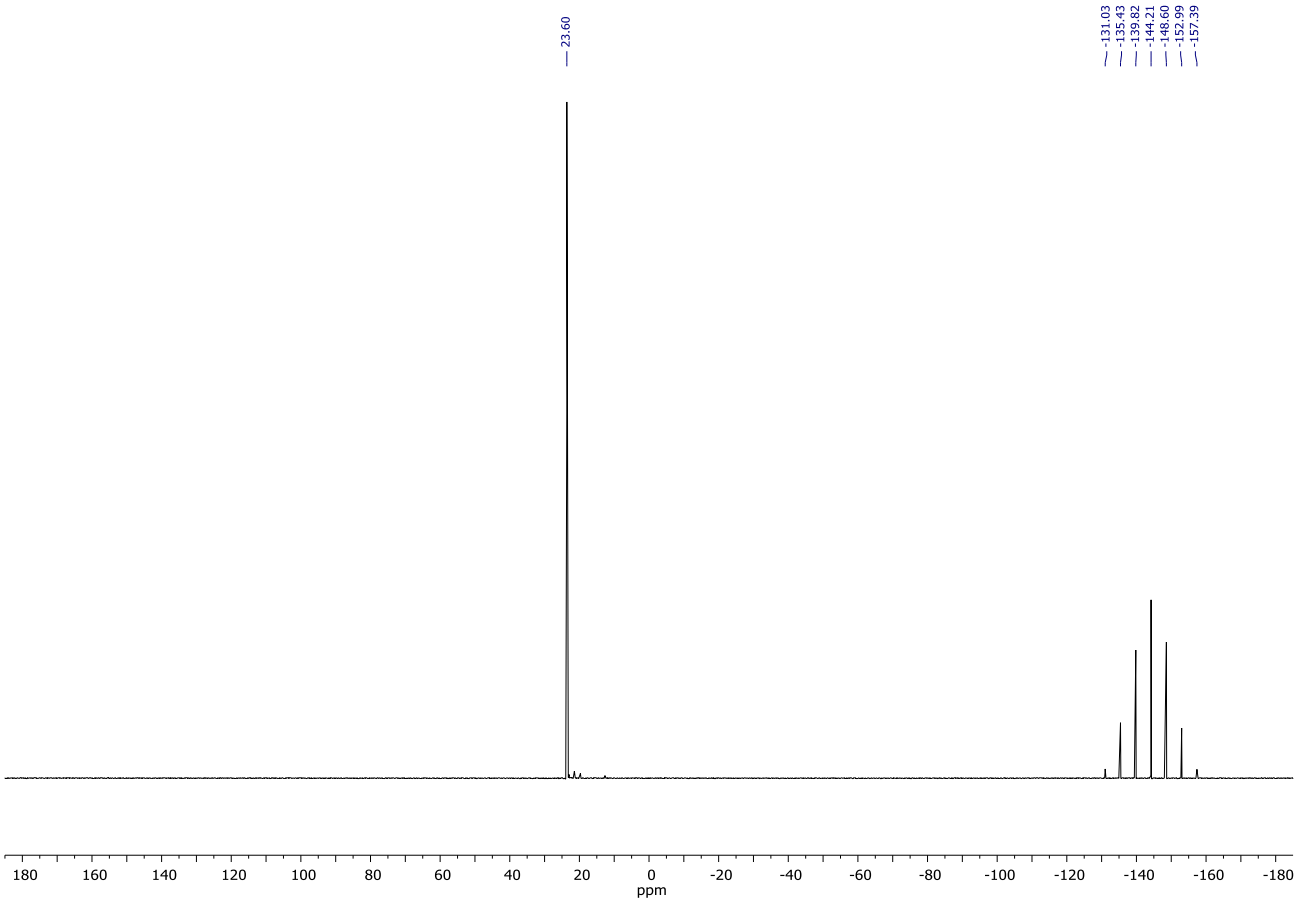

Spectrum 24. ^{31}P NMR (162 MHz, DMSO-d_6) of **124a**.

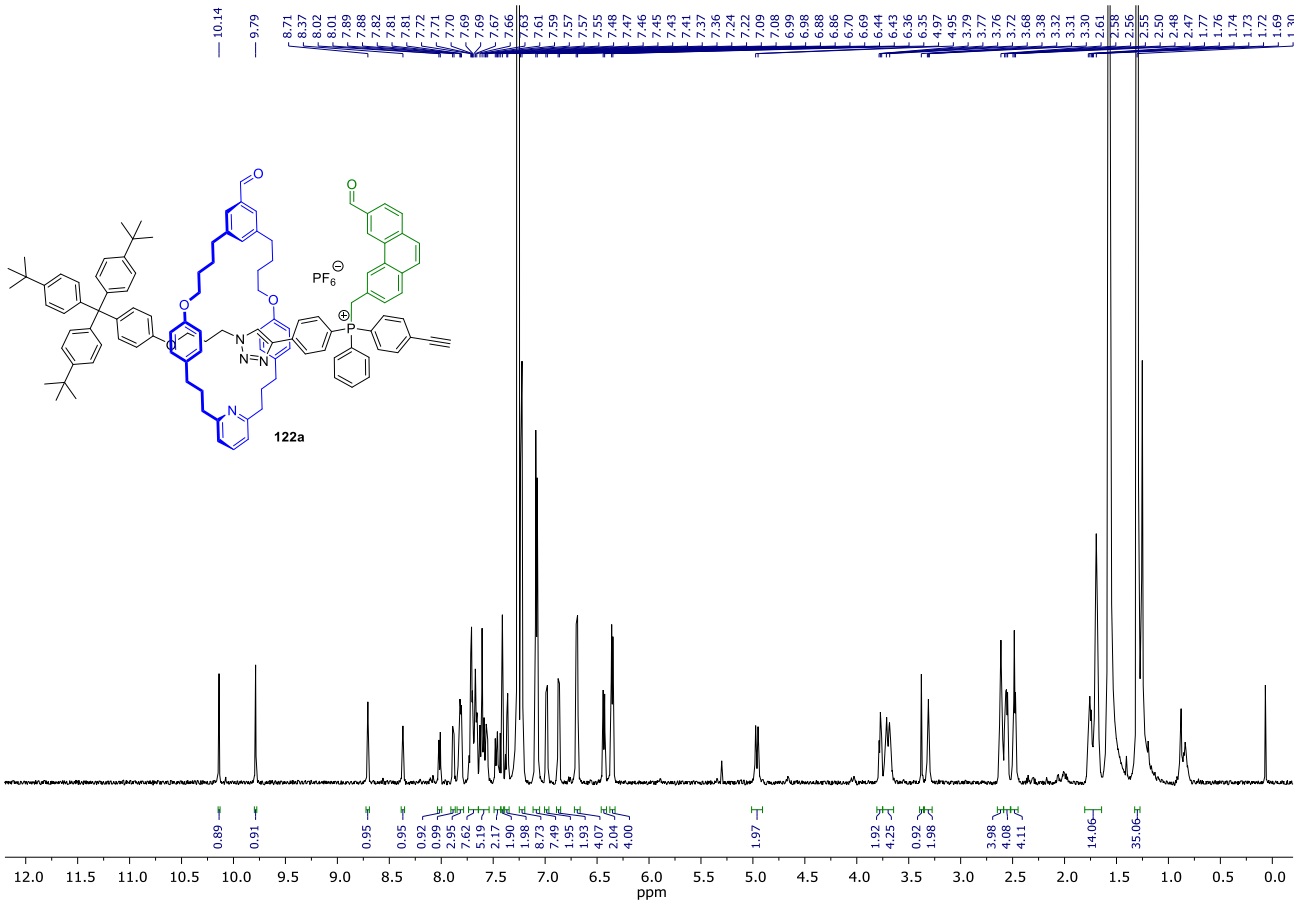

Spectrum 25. ^{1}H NMR (600 MHz, $CDCl_3$) of **122a**.

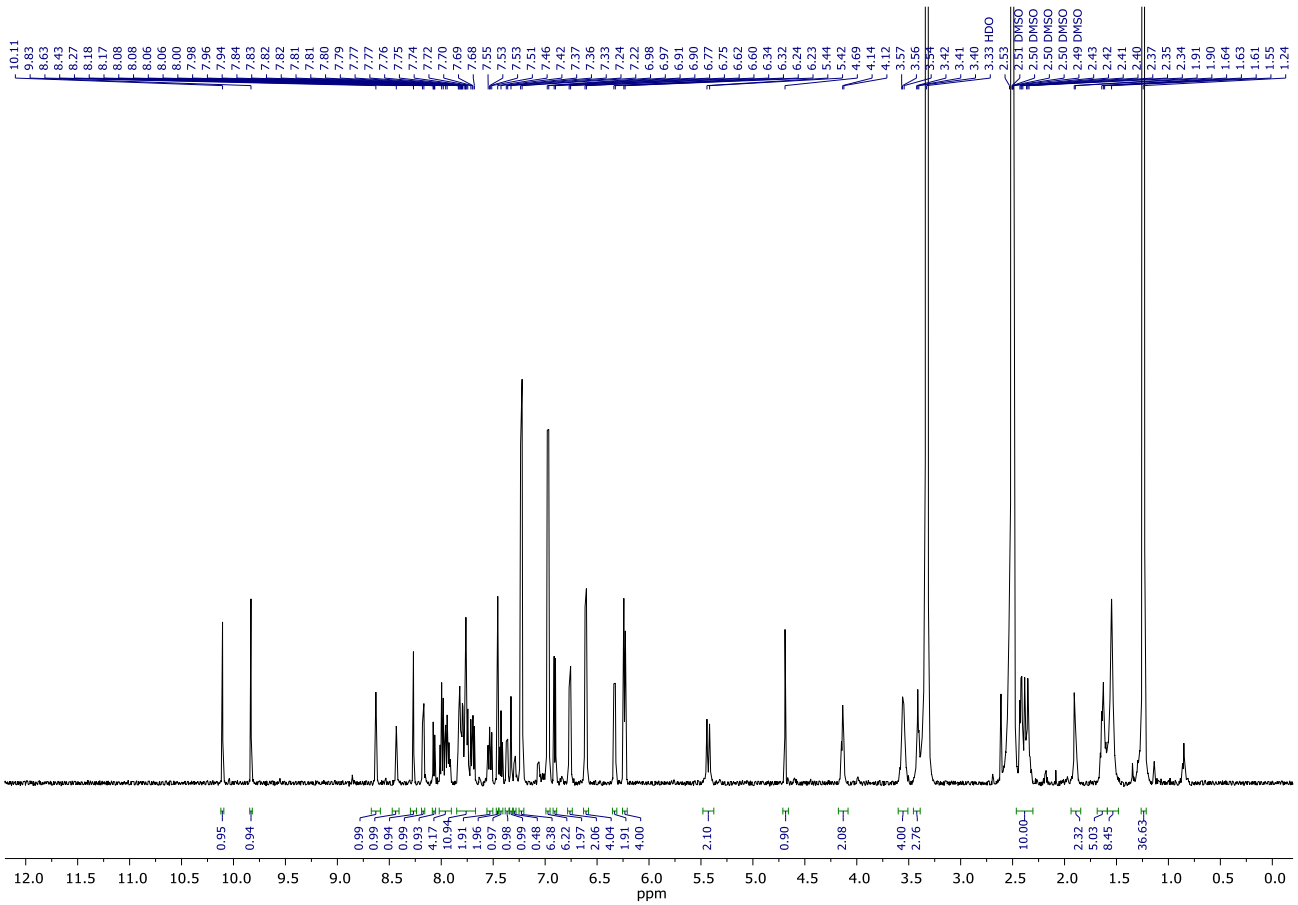

Spectrum 26. ^{1}H NMR (600 MHz, DMSO-d_6) of **122a**.

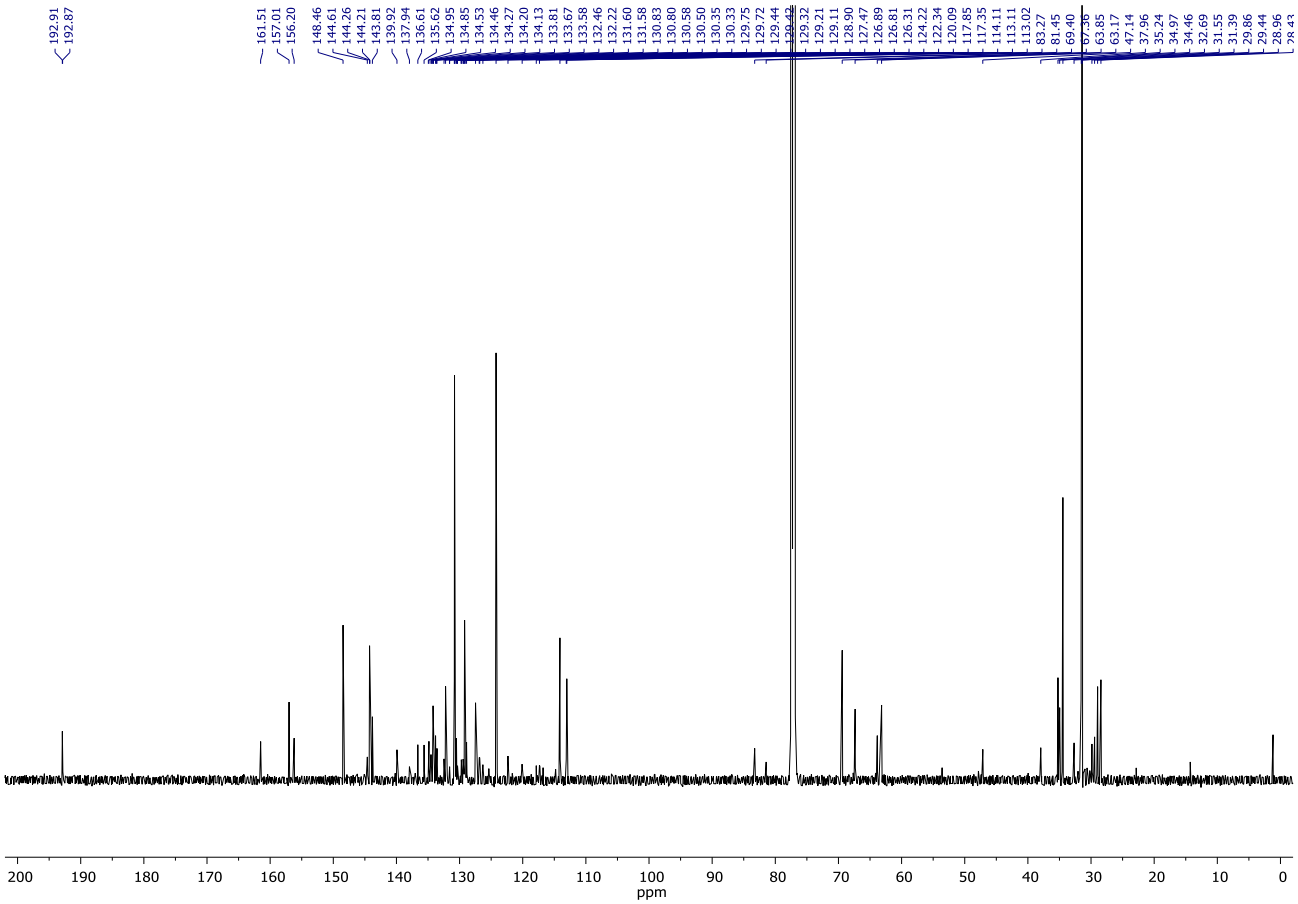

Spectrum 27. ^{13}C NMR (151 MHz, $CDCl_3$) of **122a**.

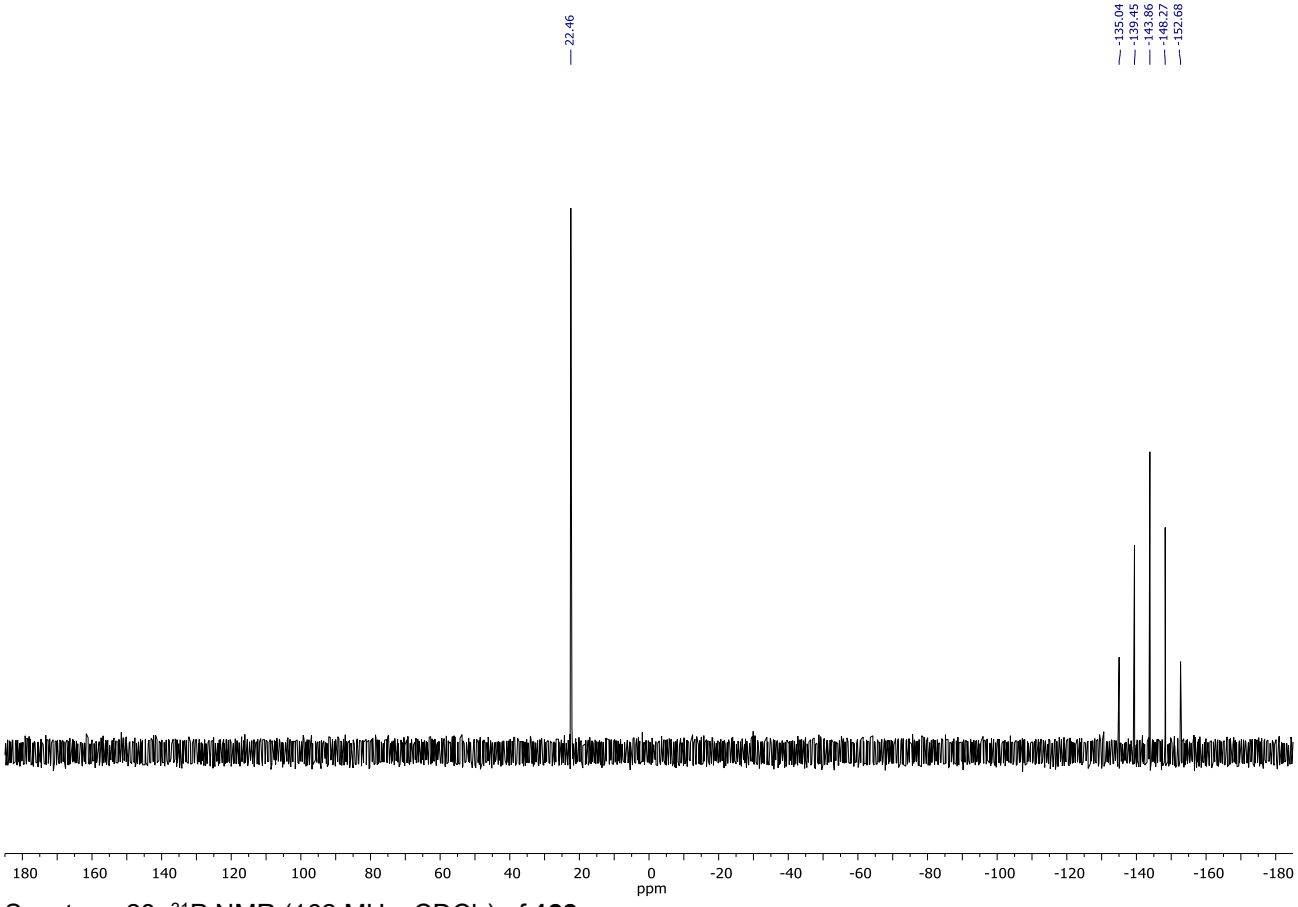

Spectrum 28. ^{31}P NMR (162 MHz, $CDCl_3$) of **122a**.

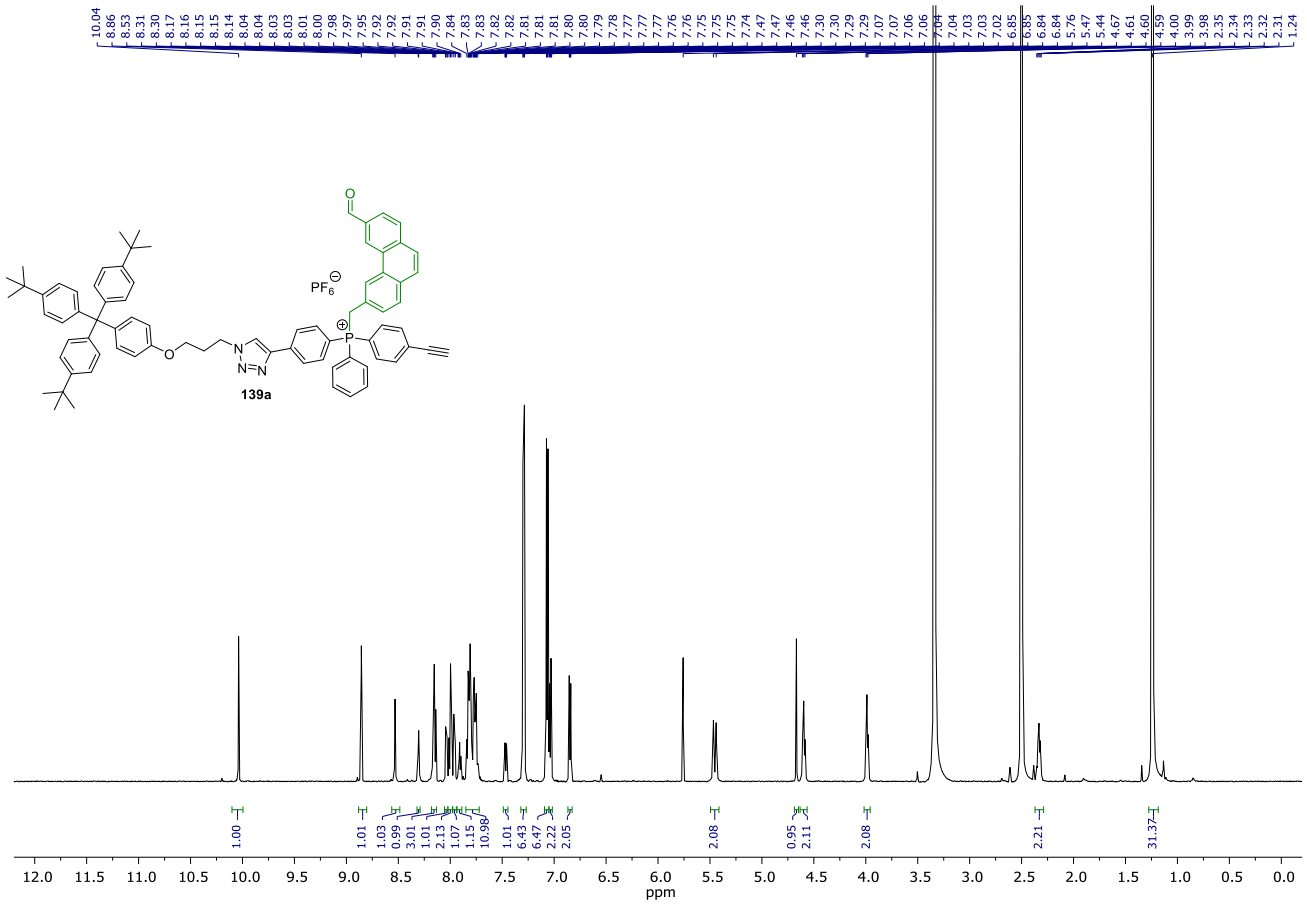

Spectrum 29. ^{1}H NMR (600 MHz, DMSO-d_6) of **139a**.

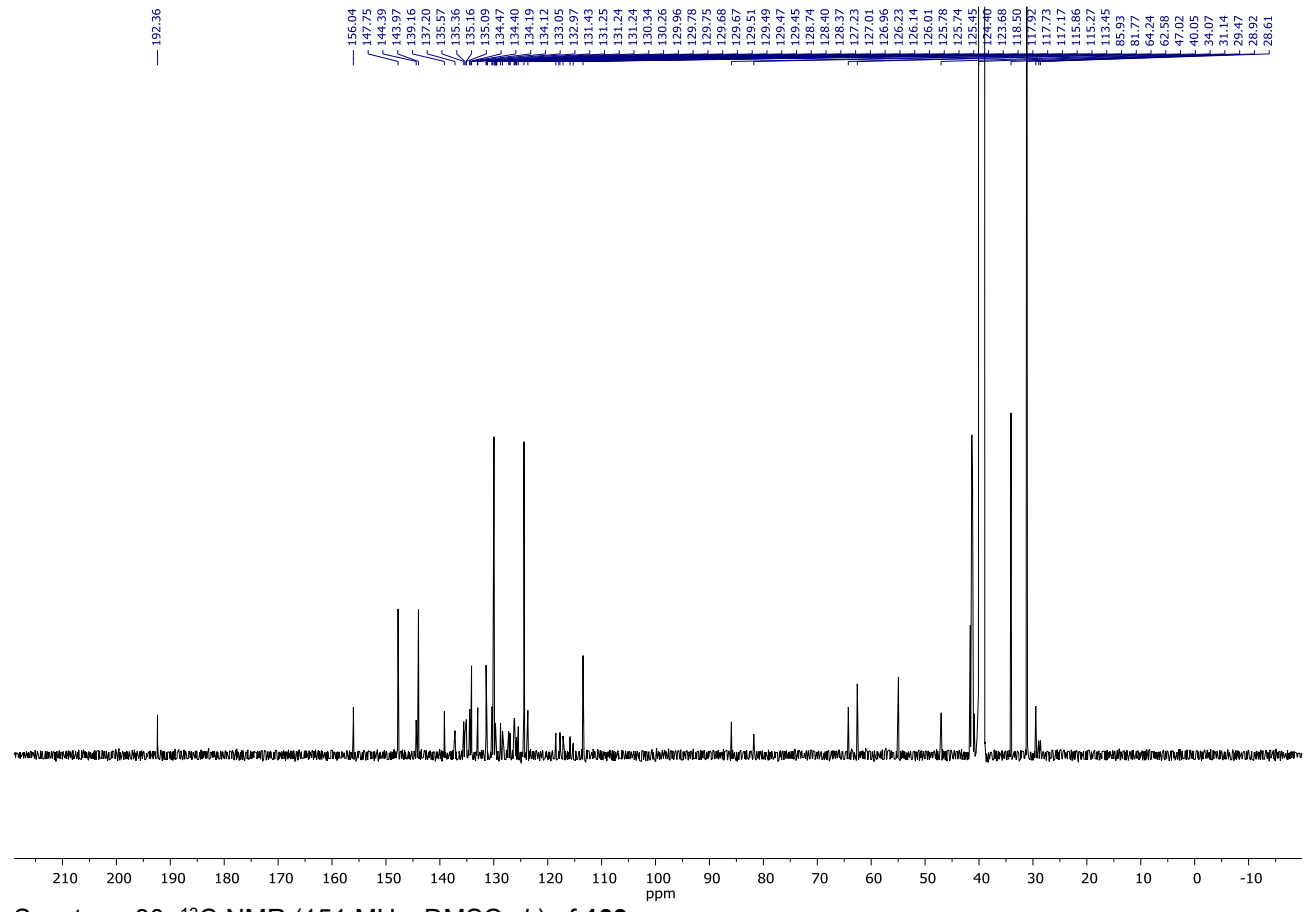

Spectrum 30. ^{13}C NMR (151 MHz, DMSO-d_6) of **139a**.

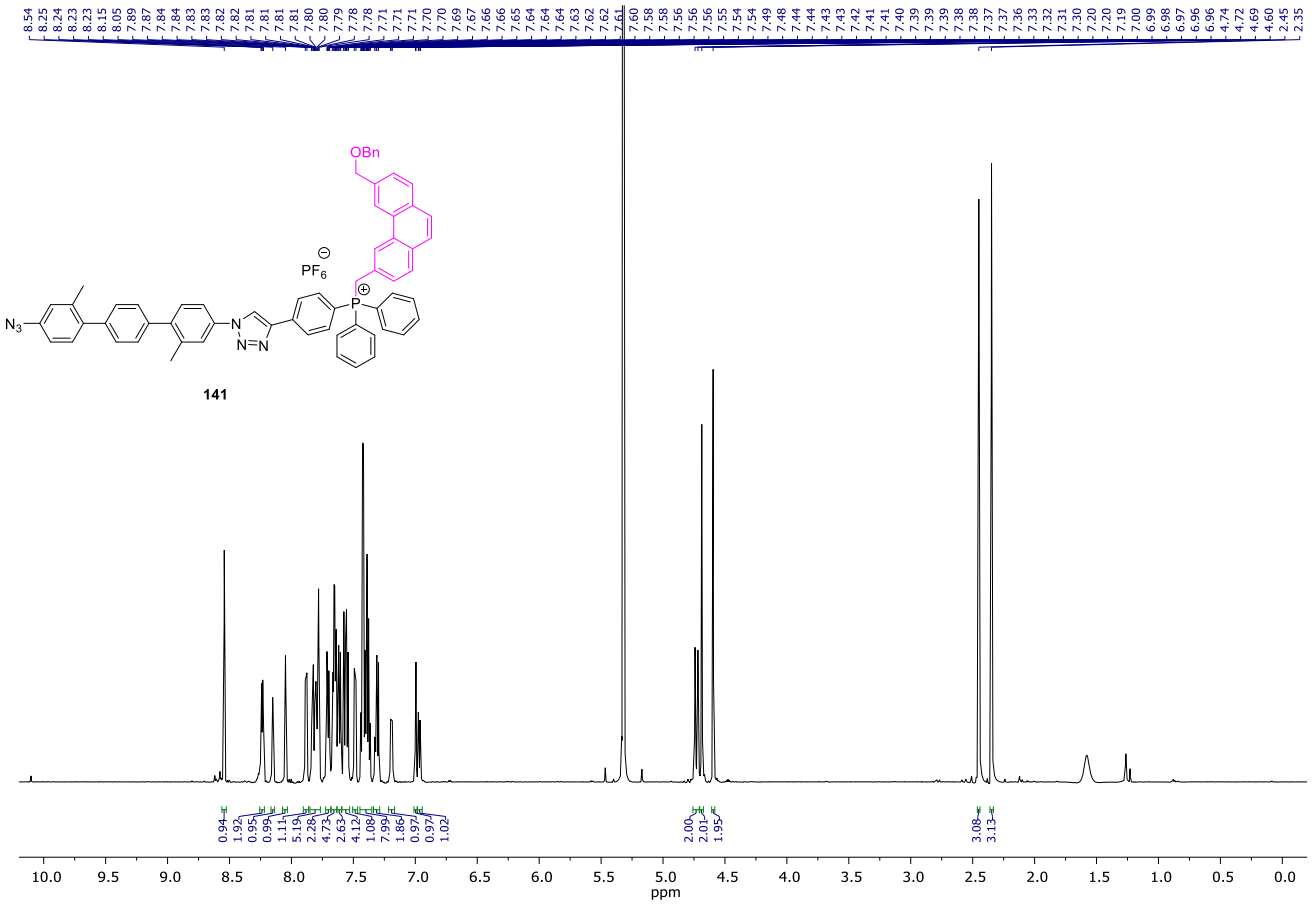

Spectrum 31. ^{1}H NMR (600 MHz, CD_2Cl_2) of **141**.

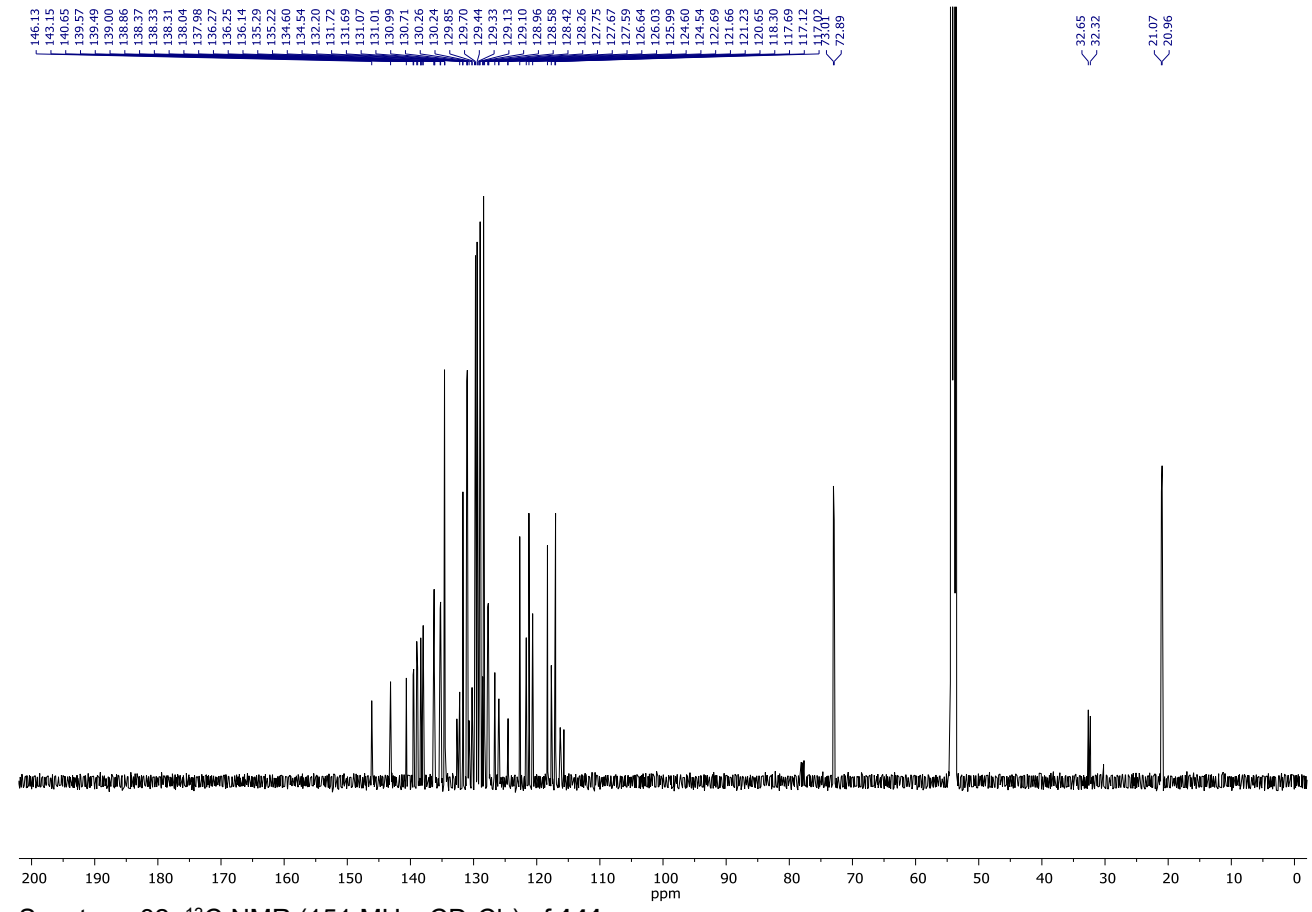

Spectrum 32. ^{13}C NMR (151 MHz, CD_2Cl_2) of **141**.

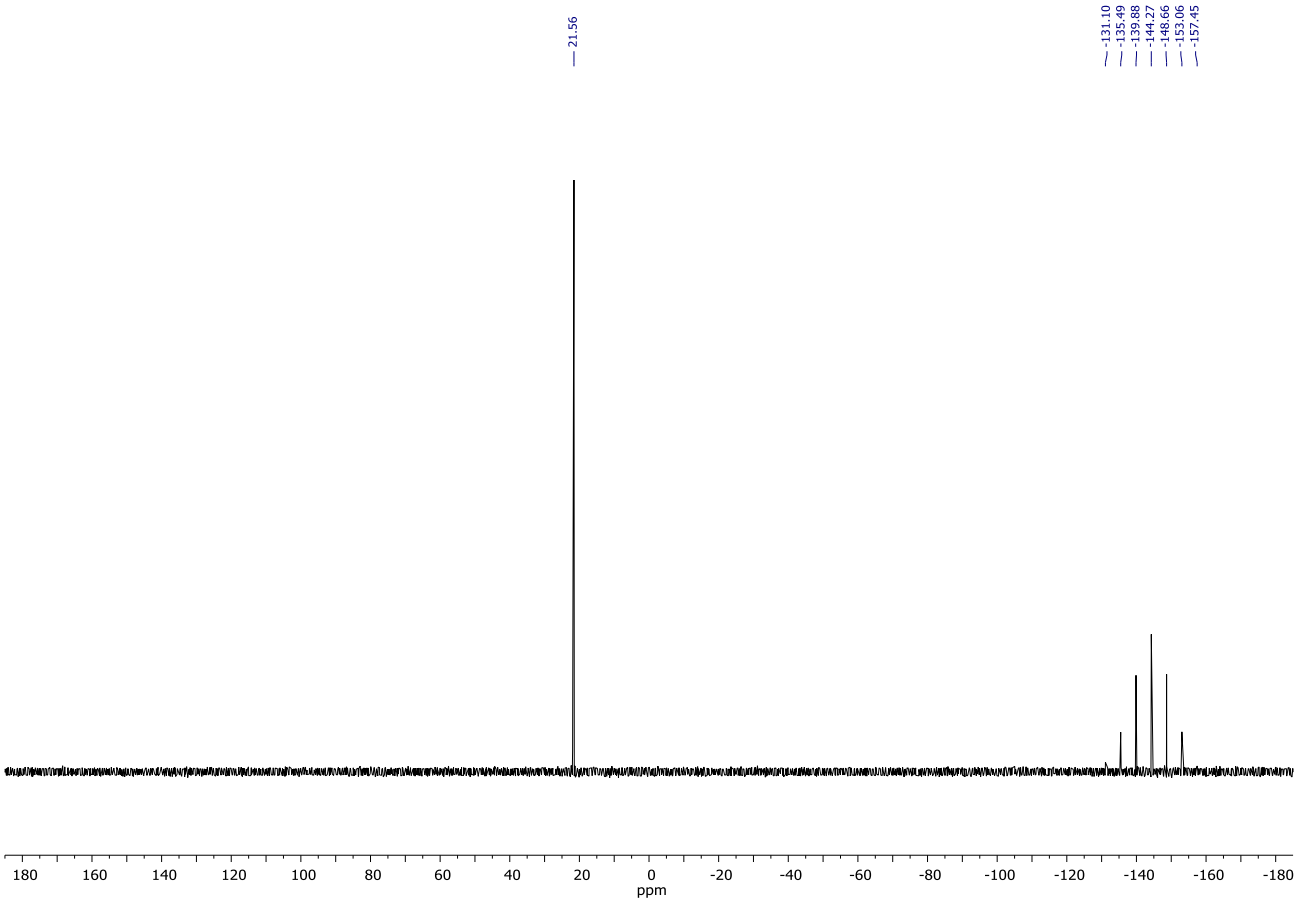

Spectrum 33. ^{31}P NMR (162 MHz, CD_2Cl_2) of **141**.

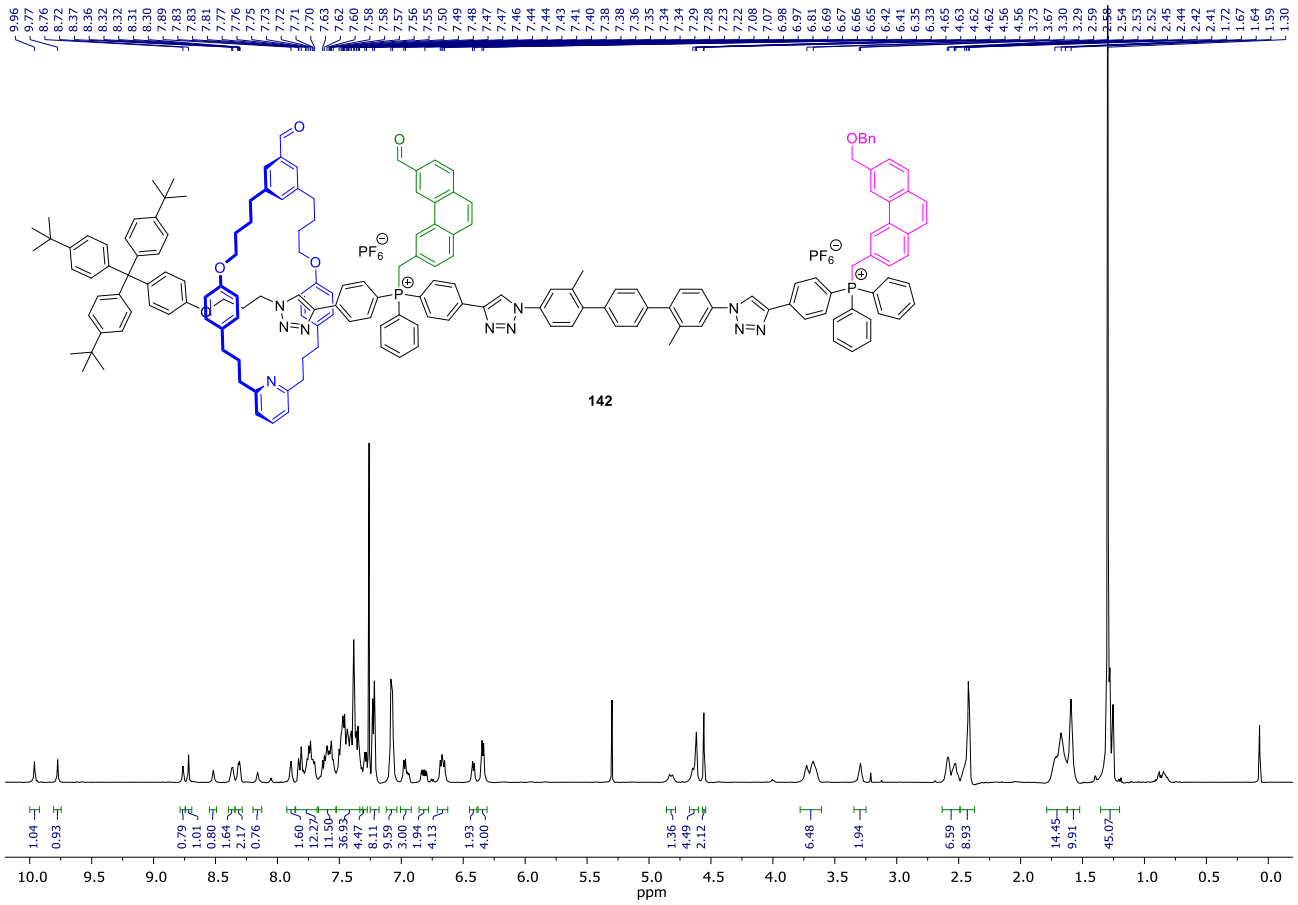

Spectrum 34. ^{1}H NMR (600 MHz, $CDCl_3$) of **142**.

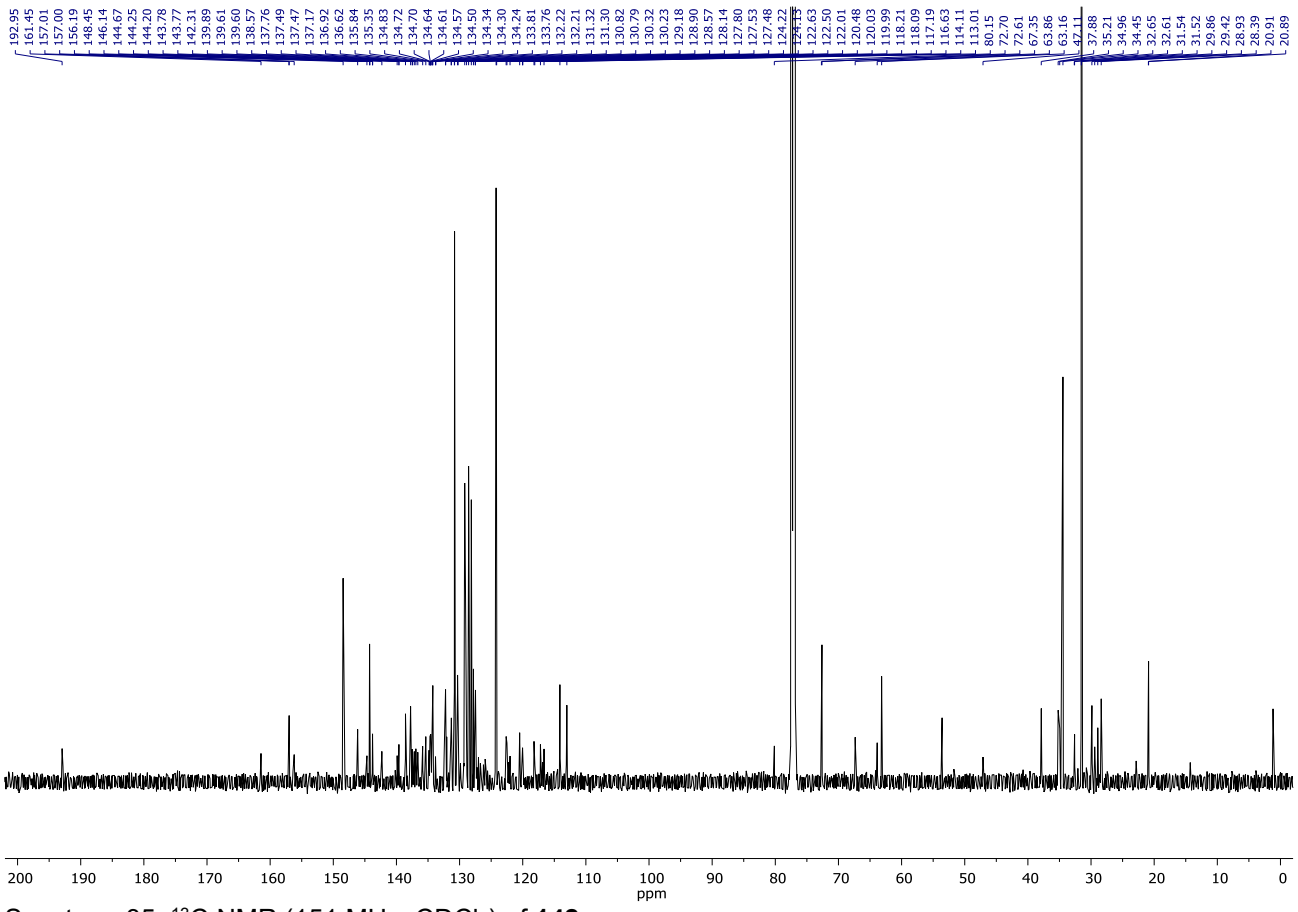

Spectrum 35. ^{13}C NMR (151 MHz, $CDCl_3$) of **142**.

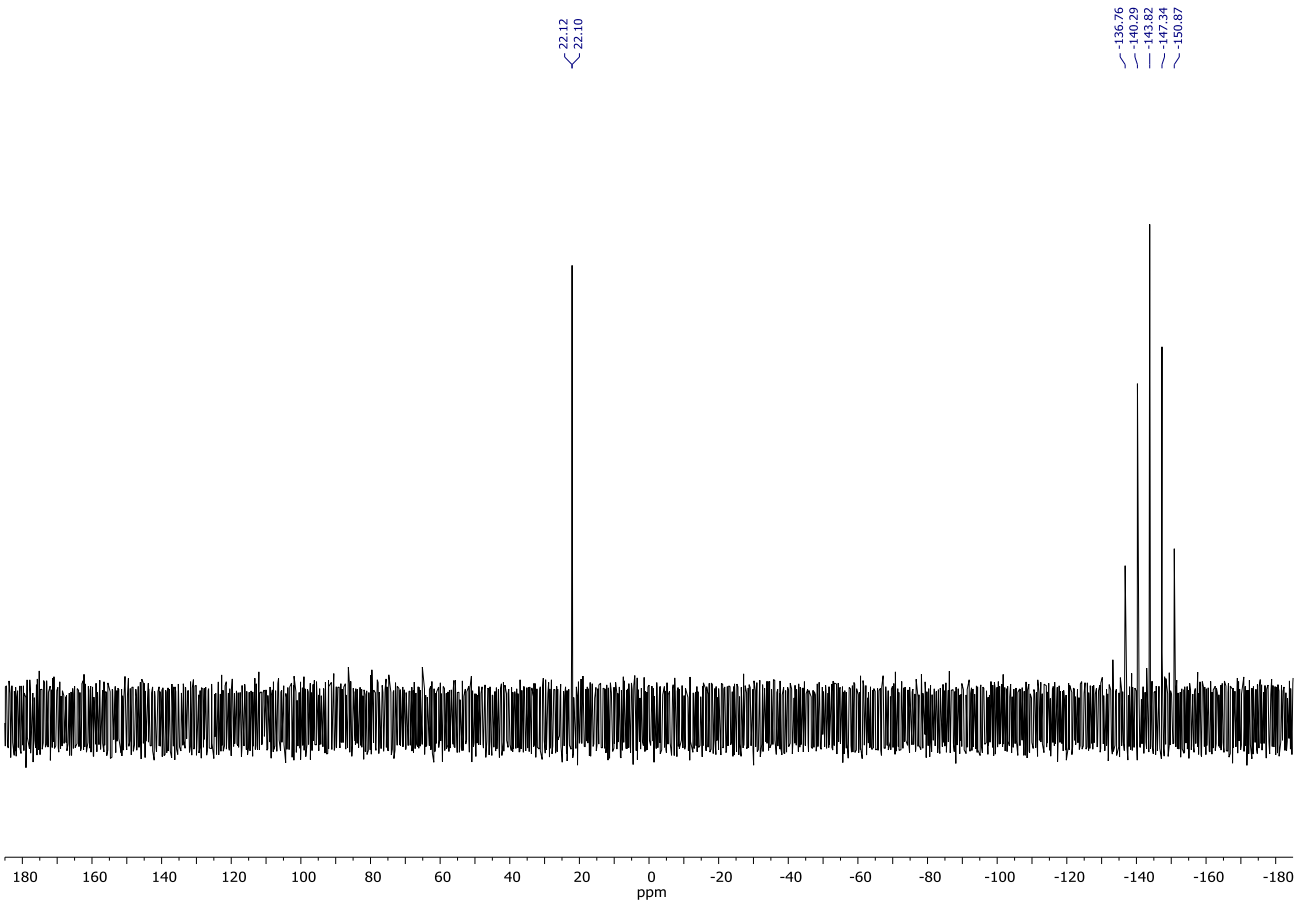

Spectrum 36. ^{31}P NMR (162 MHz, DMSO-d_6) of **142**.

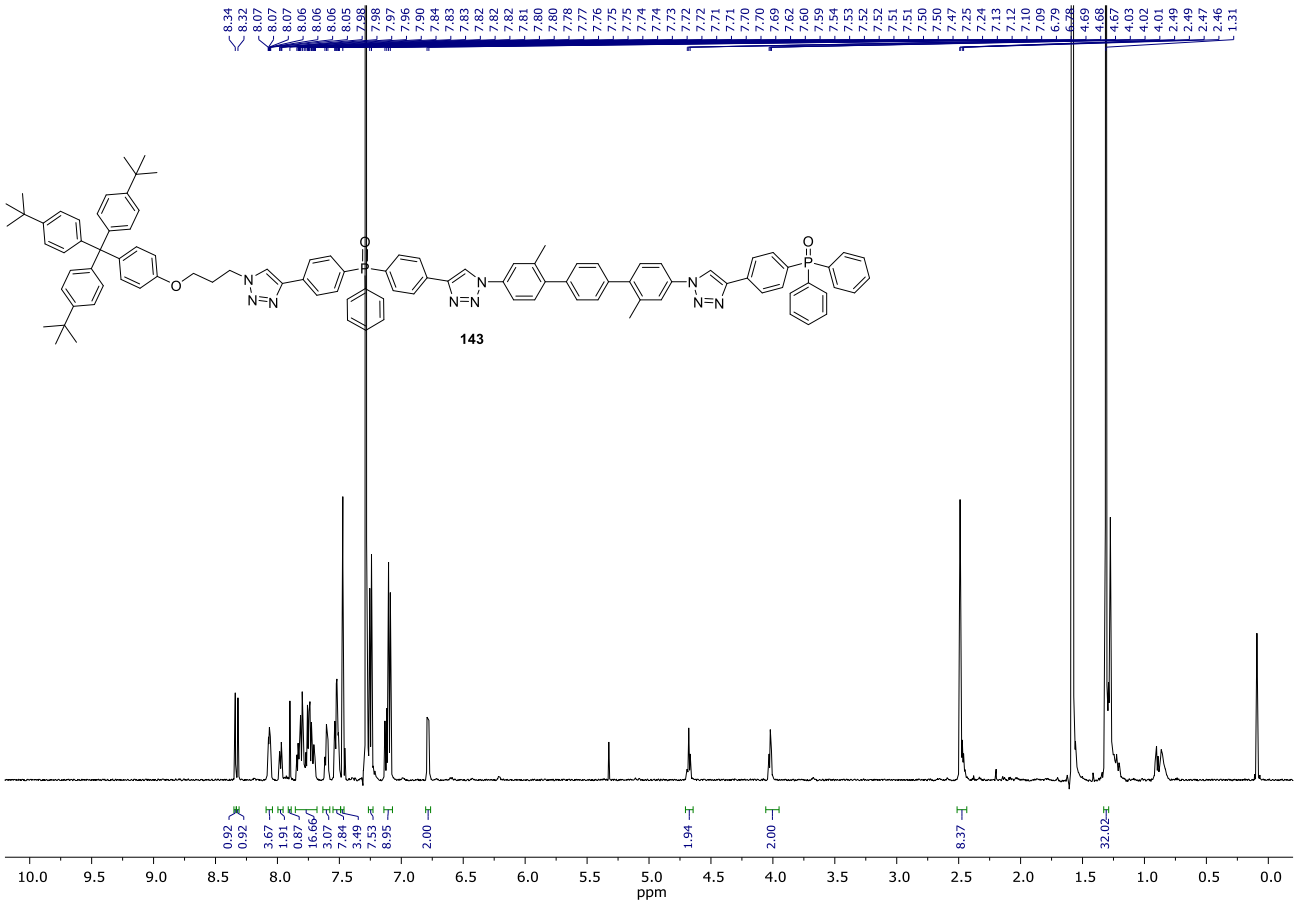

Spectrum 37. ^{1}H NMR (600 MHz, $CDCl_3$) of **143**.

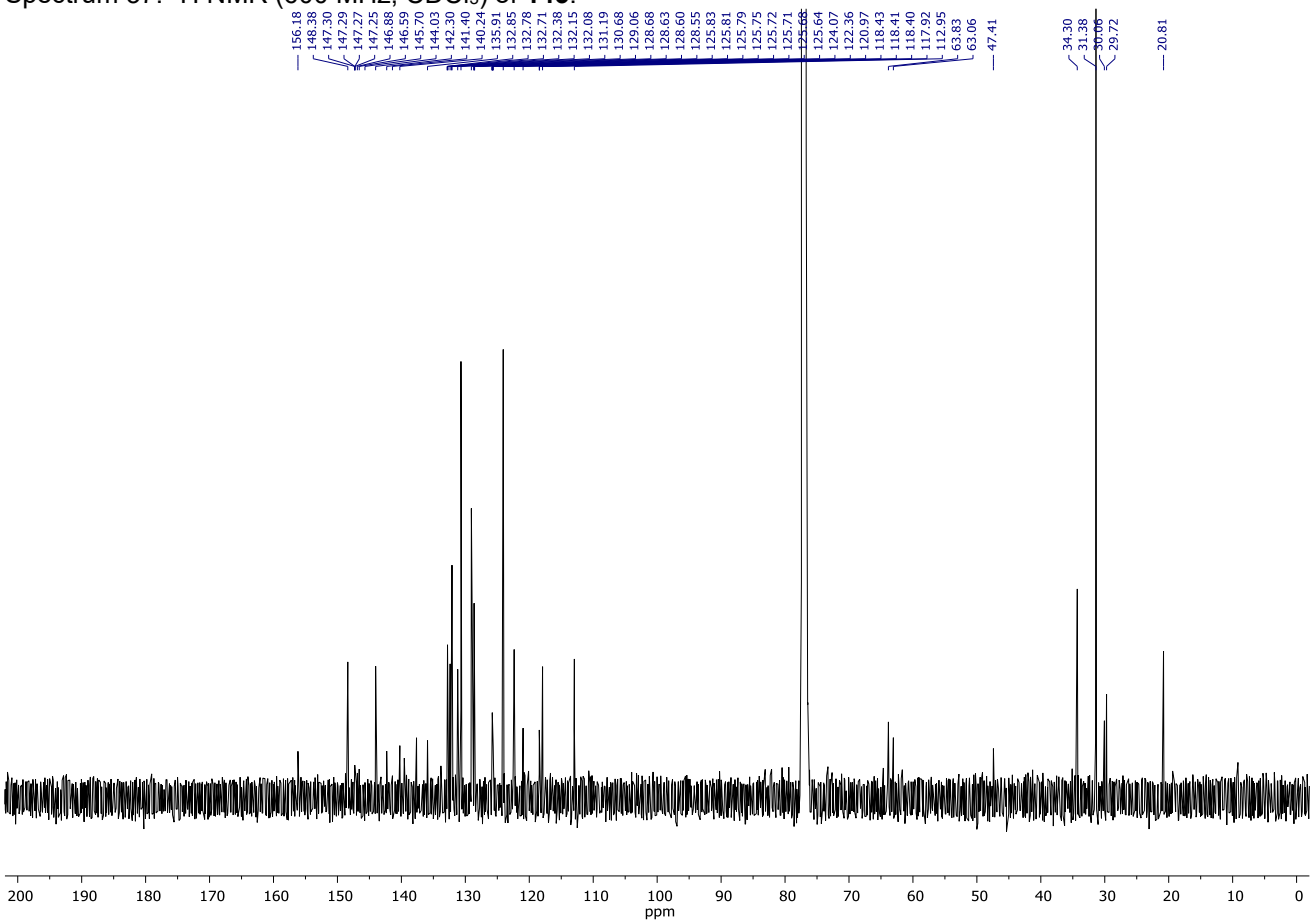

Spectrum 38. ^{13}C NMR (151 MHz, CD_2Cl_2) of **143**.

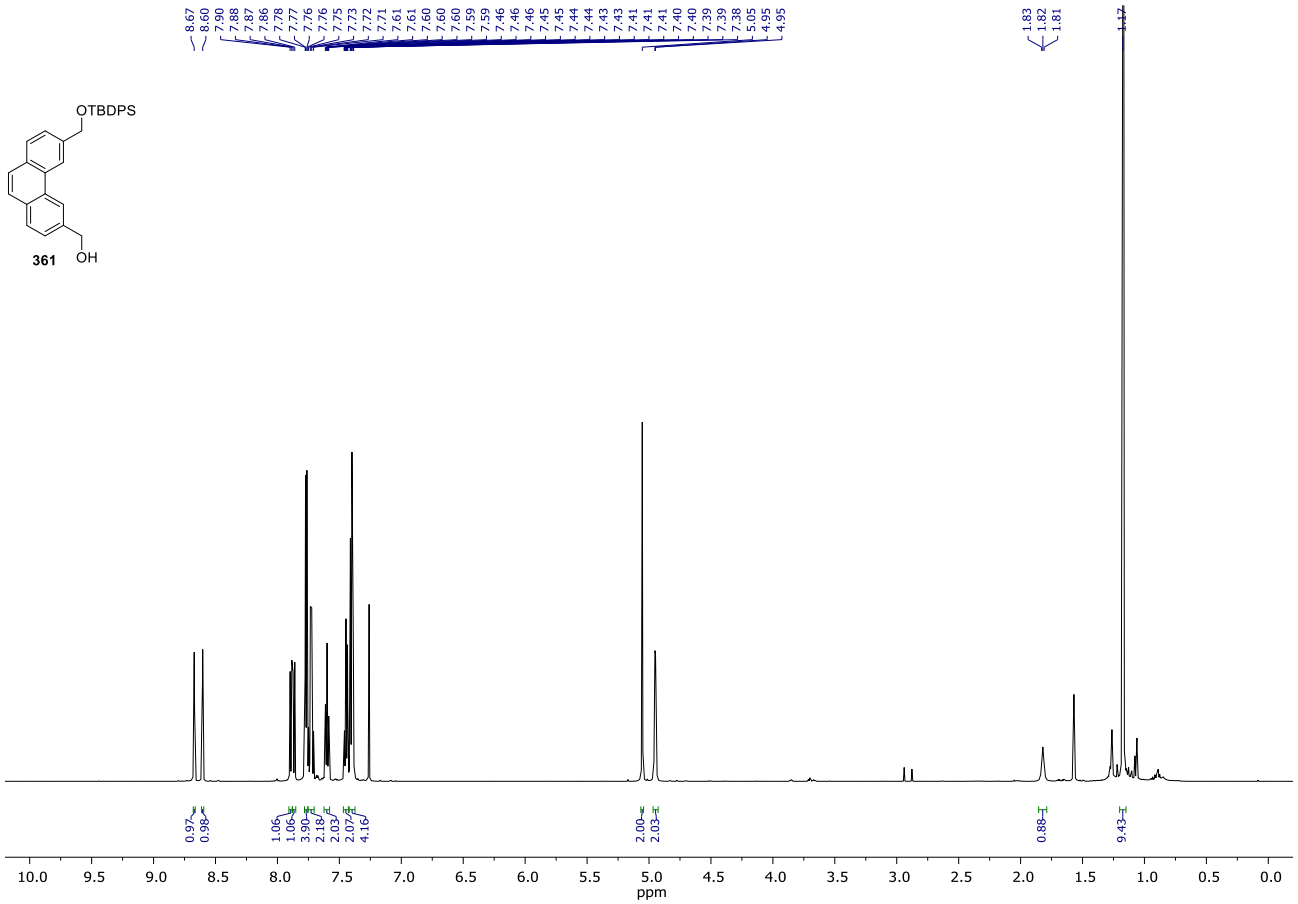

Spectrum 39. ^{1}H NMR (600 MHz, $CDCl_3$) of **361**.

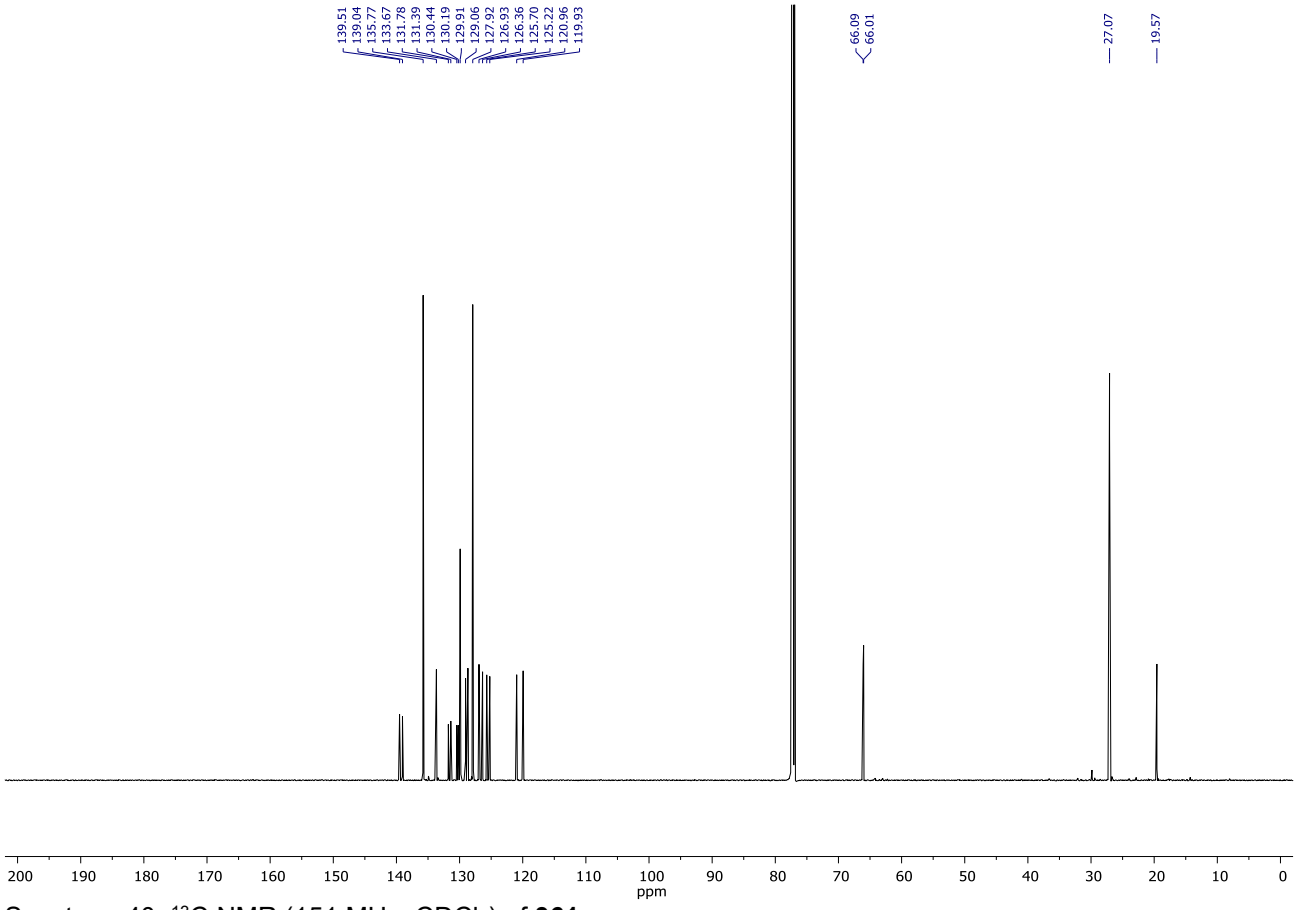

Spectrum 40. ^{13}C NMR (151 MHz, $CDCl_3$) of **361**.

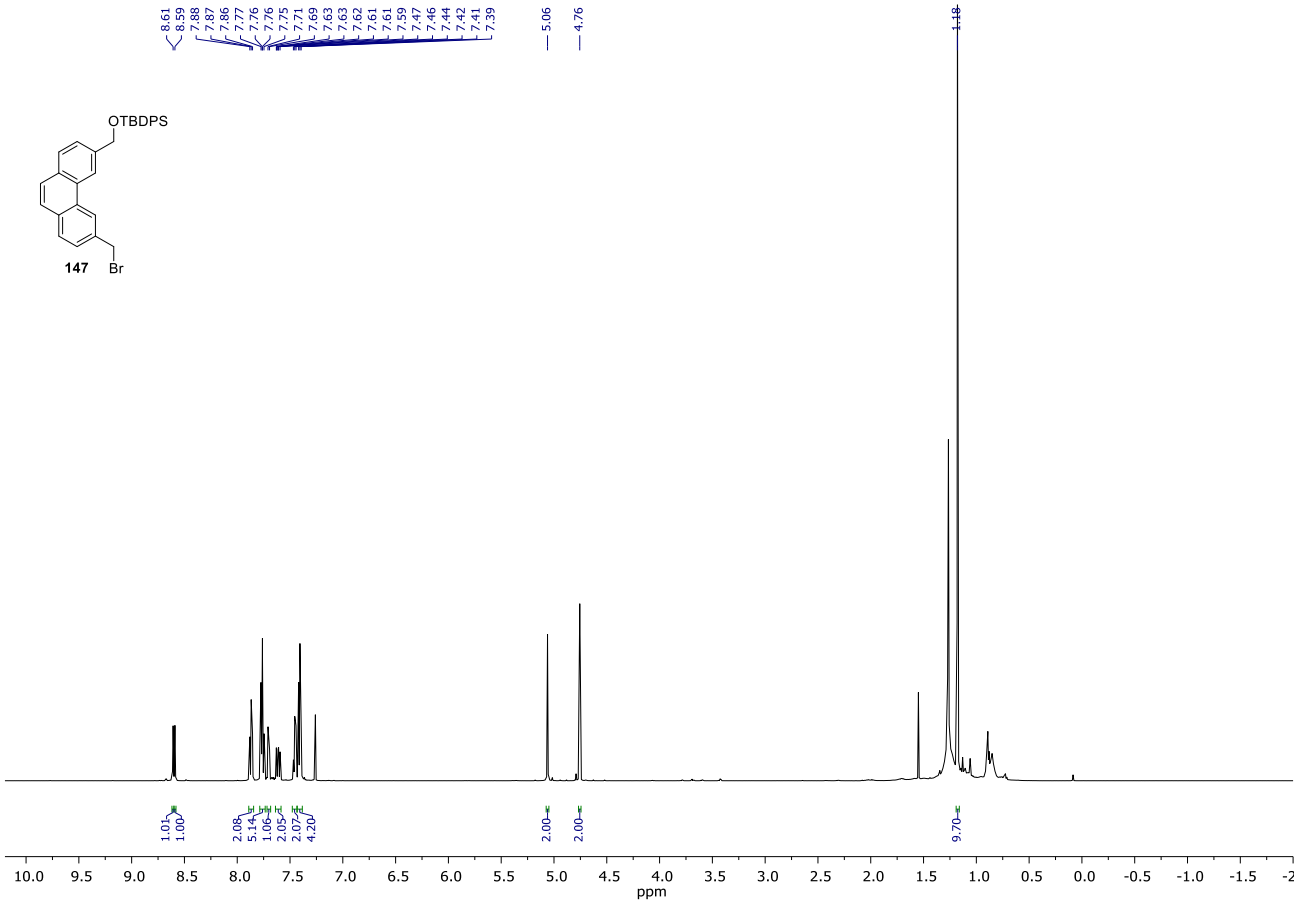

Spectrum 41. ^{1}H NMR (600 MHz, $CDCl_3$) of **147**.

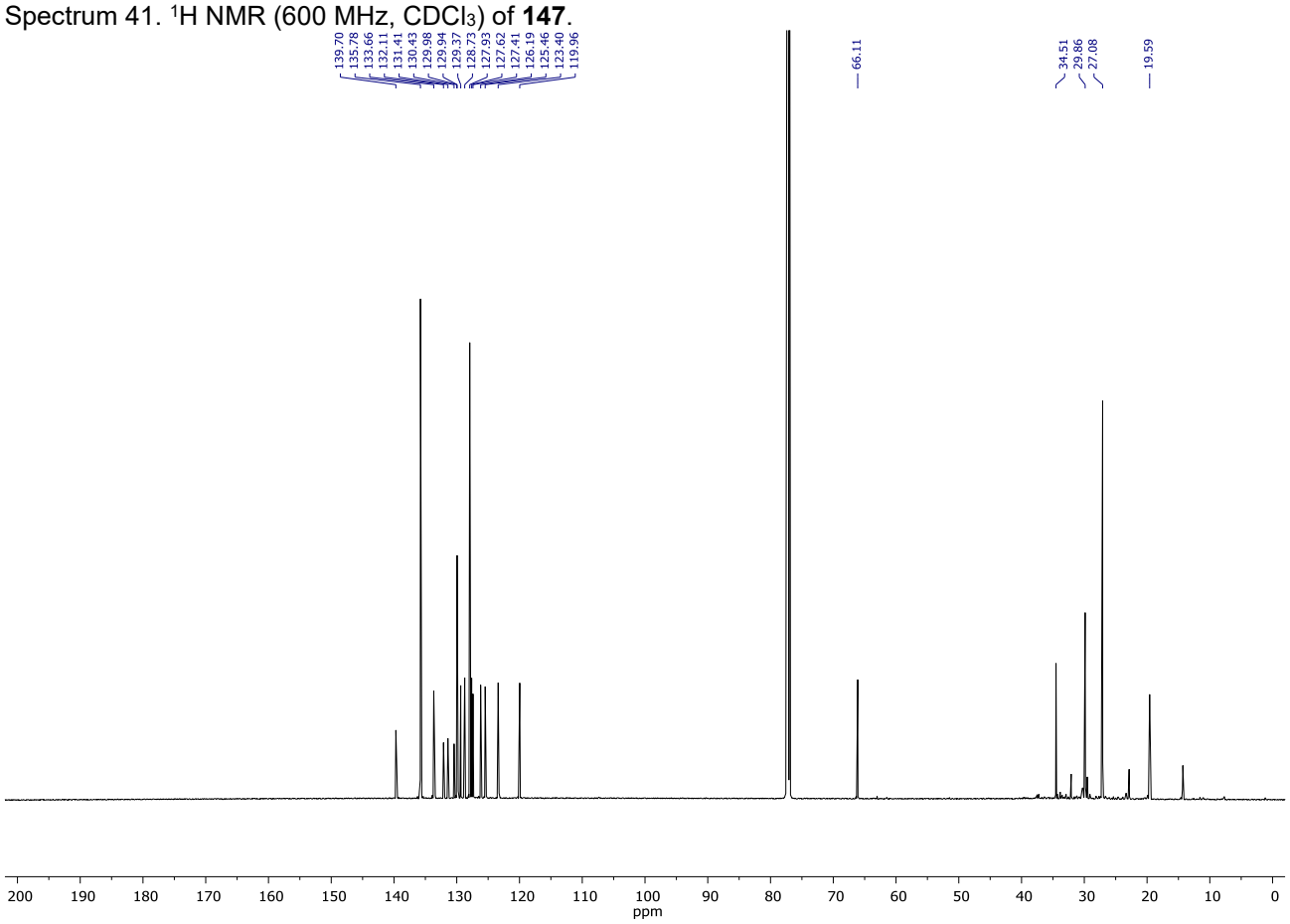

Spectrum 42.^{13}C NMR (151 MHz, $CDCl_3$) of **147**.

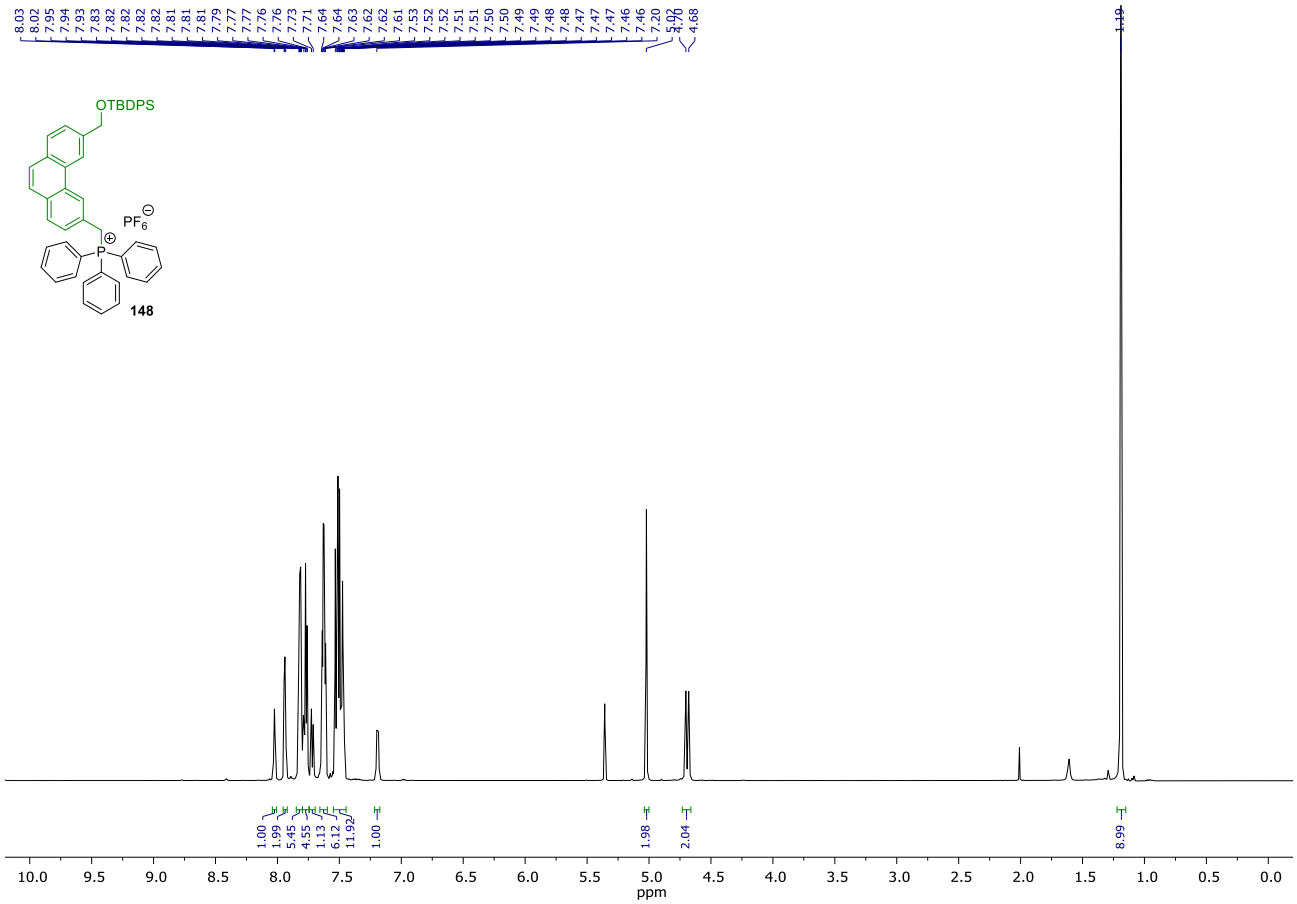

Spectrum 43. ^{1}H NMR (600 MHz, CD_2Cl_2) of **148**.

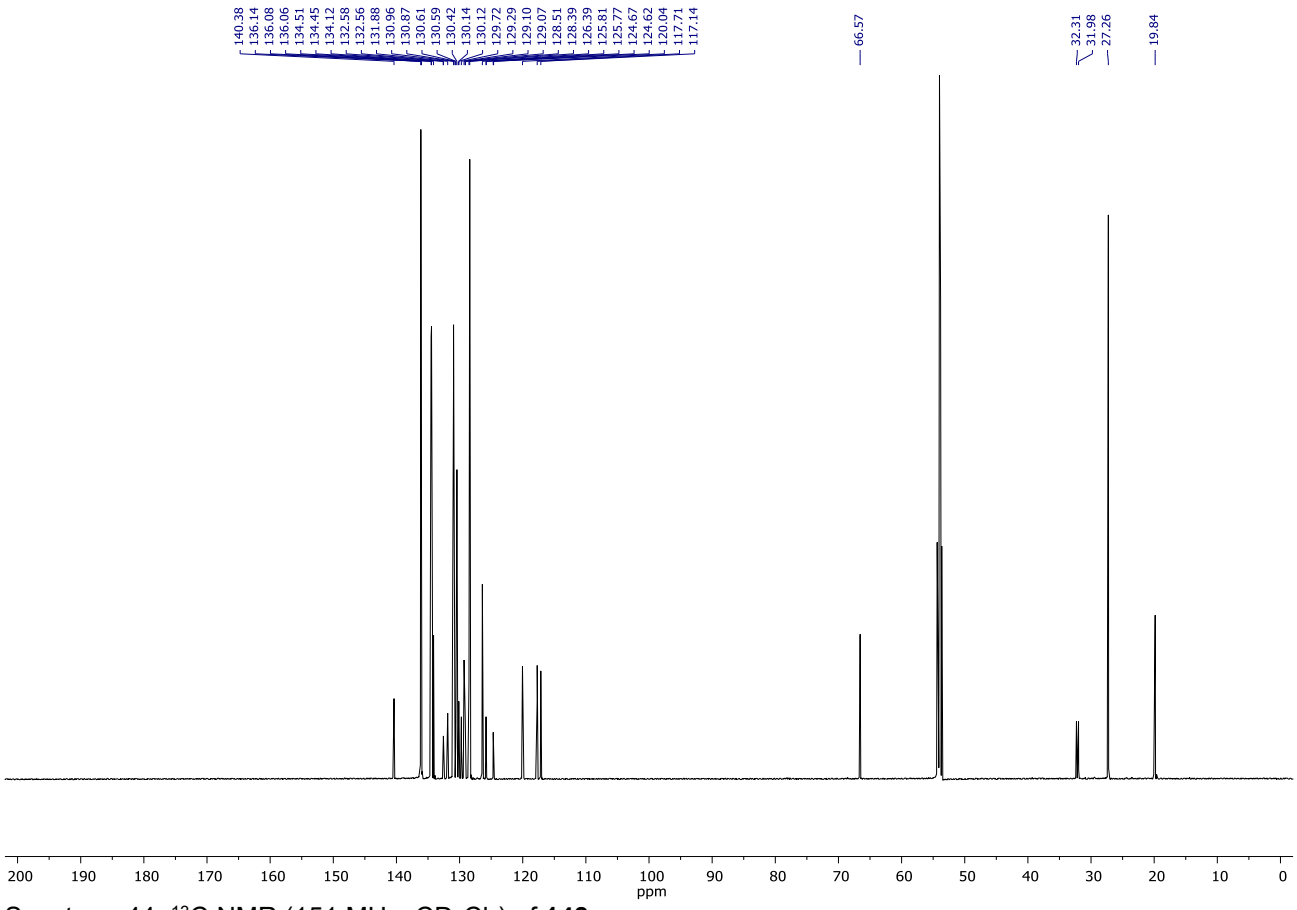

Spectrum 44. ^{13}C NMR (151 MHz, CD_2Cl_2) of **148**.

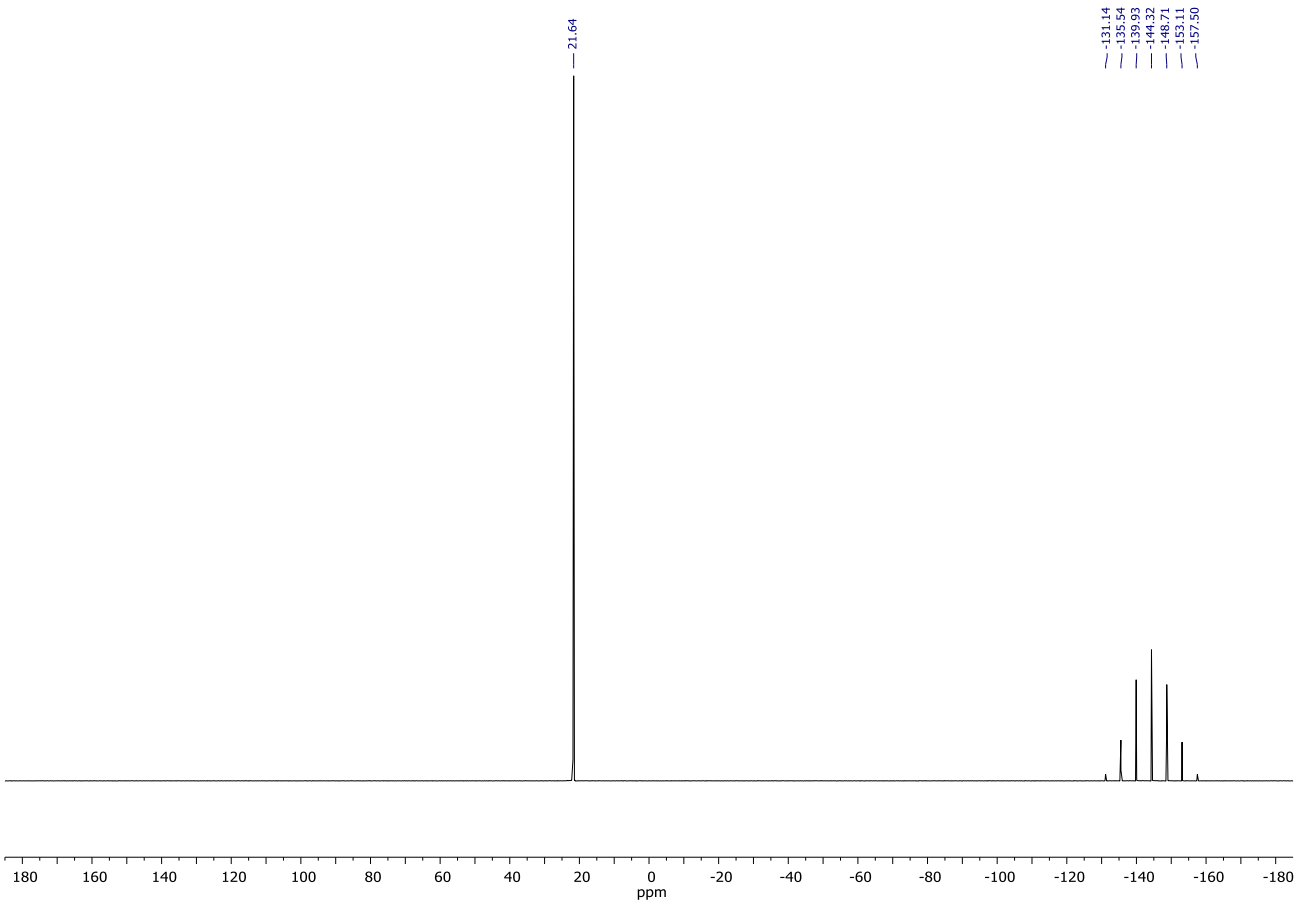

Spectrum 45. ^{31}P NMR (162 MHz, CD_2Cl_2) of **148**.

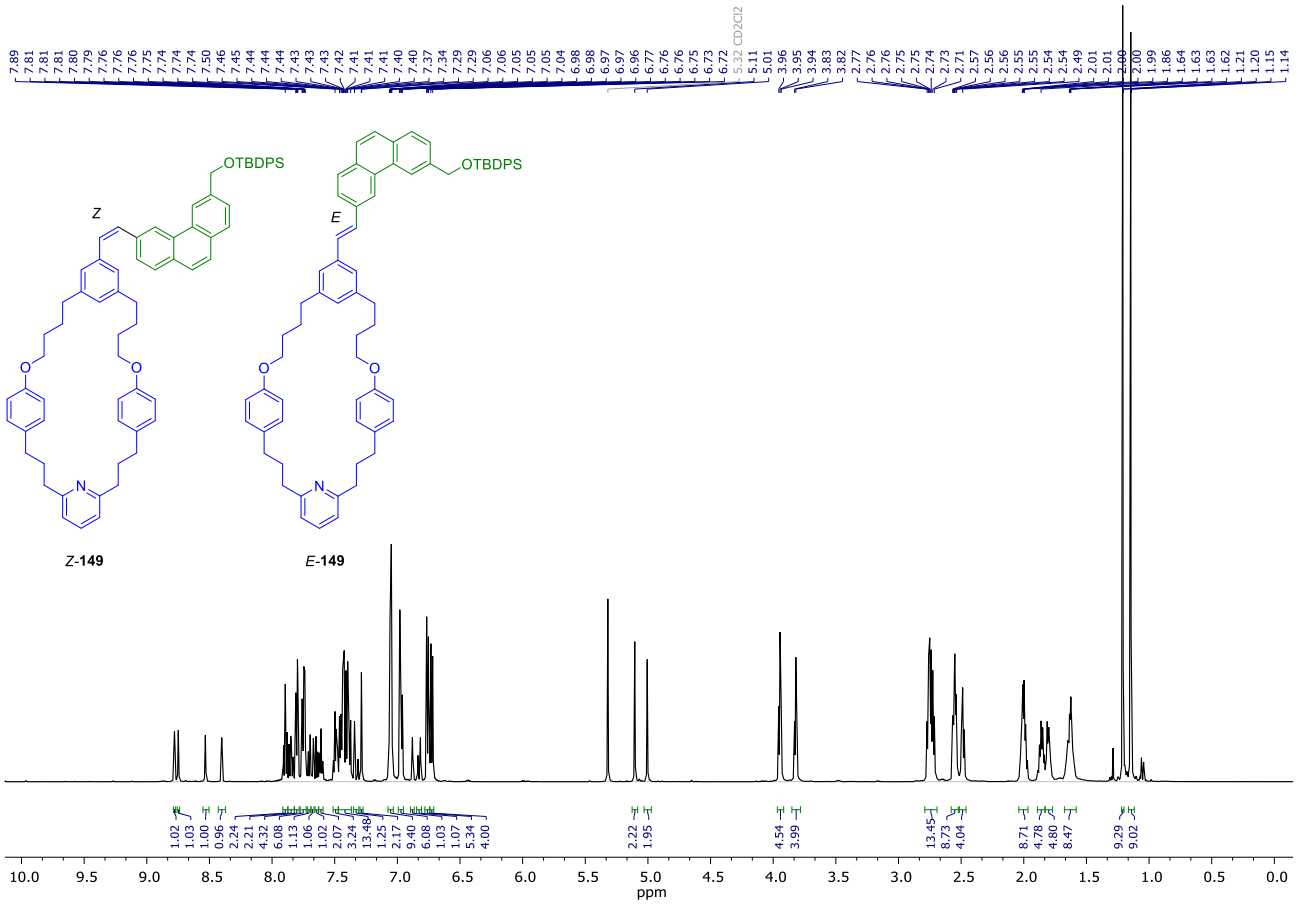

Spectrum 46. ^{1}H NMR (600 MHz, CD_2Cl_2) of **149**.

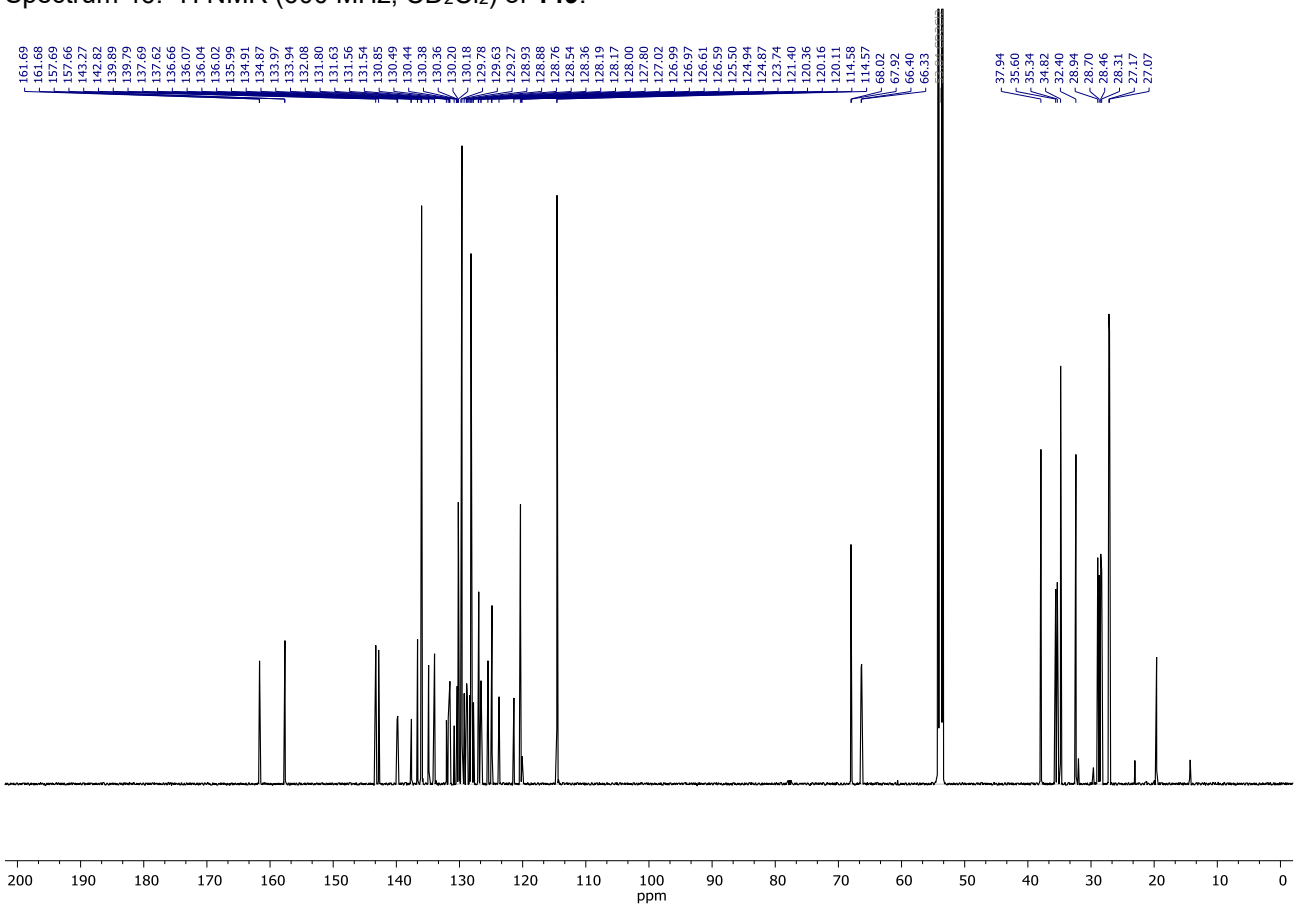

Spectrum 47. ^{13}C NMR (151 MHz, CD_2Cl_2) of **149**.

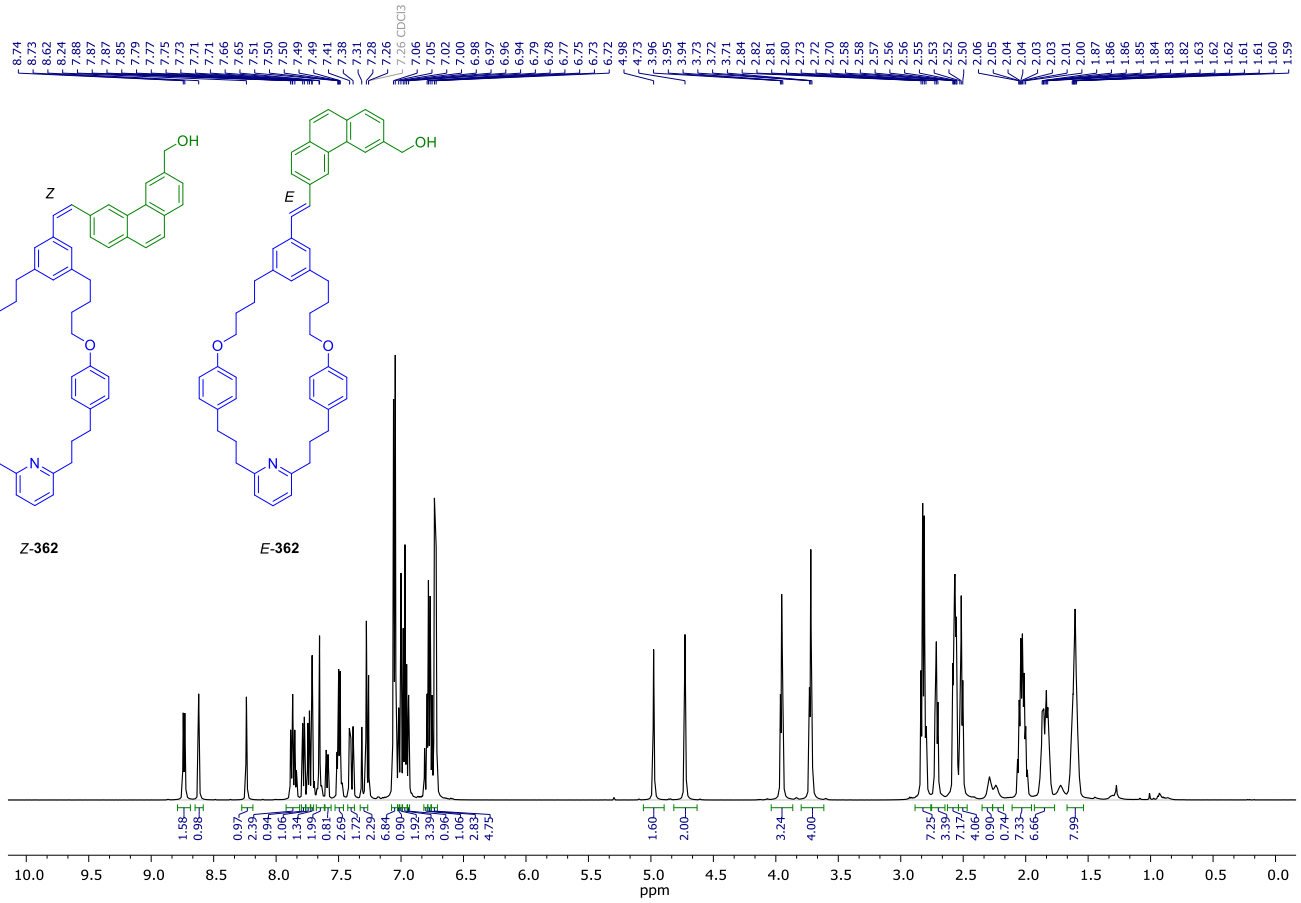

Spectrum 48. ^{1}H NMR (600 MHz, $CDCl_3$) of **362**.

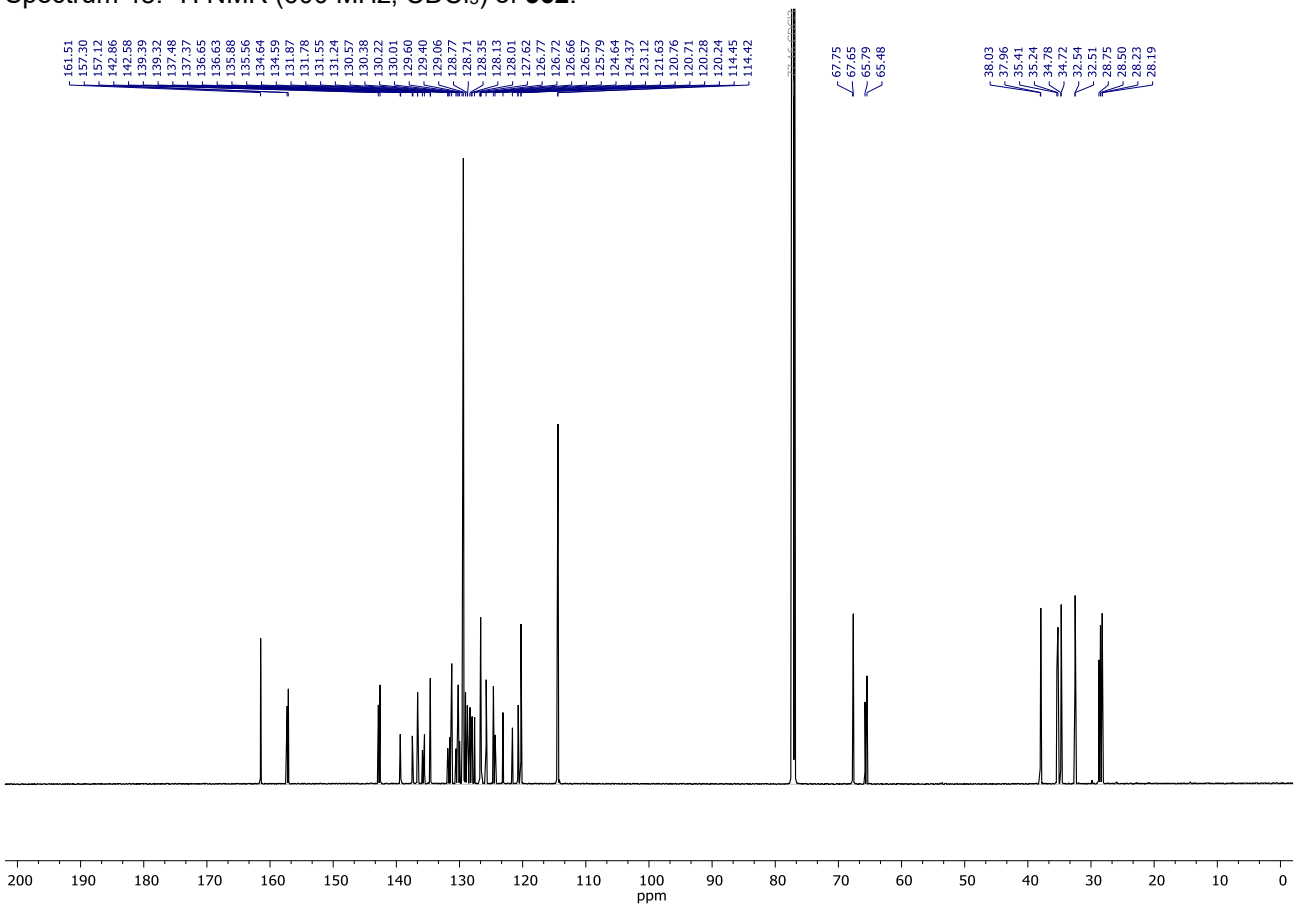

Spectrum 49. ^{13}C NMR (151 MHz, $CDCl_3$) of **362**.

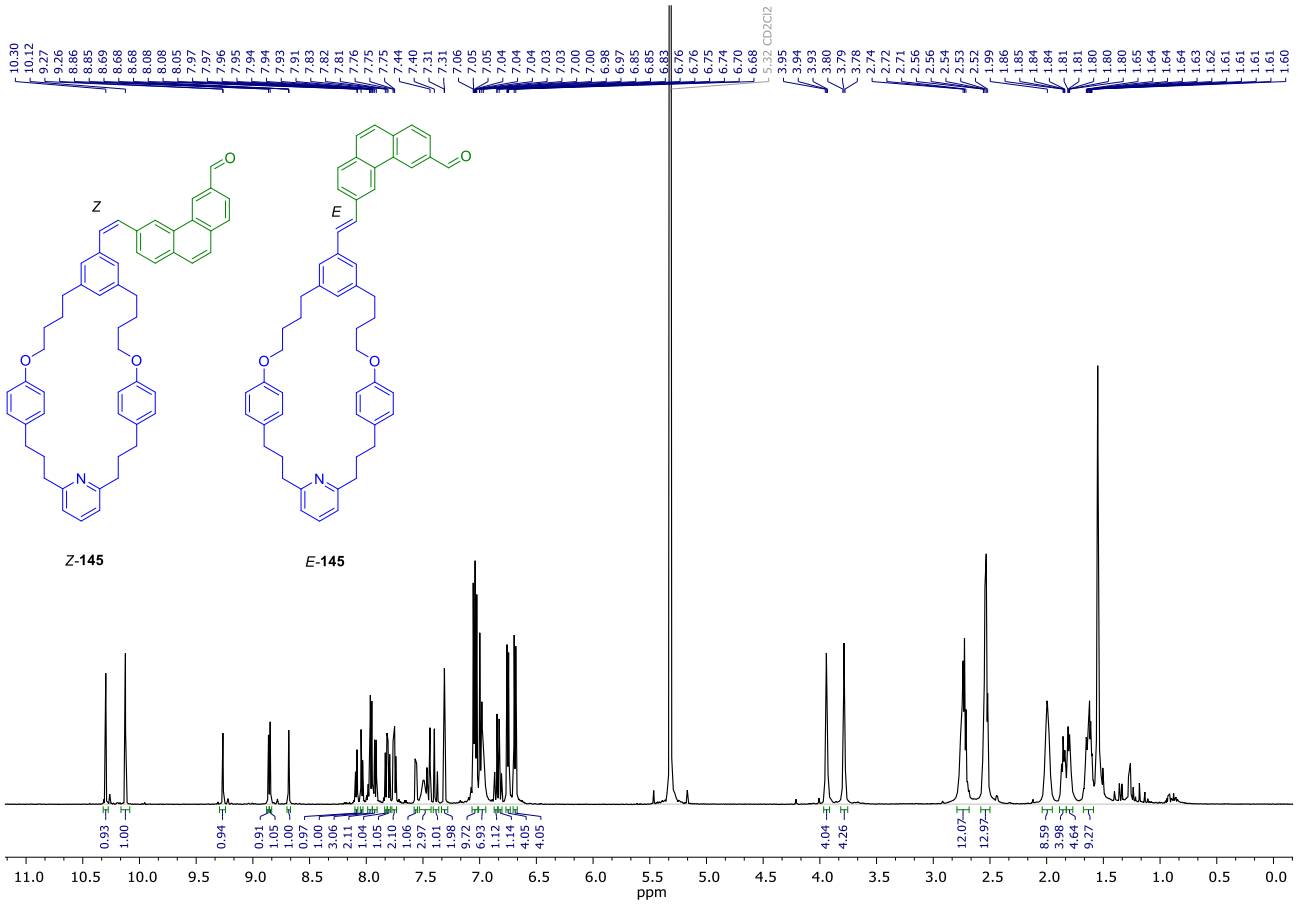

Spectrum 50. ^{1}H NMR (600 MHz, $CDCl_3$) of **145**.

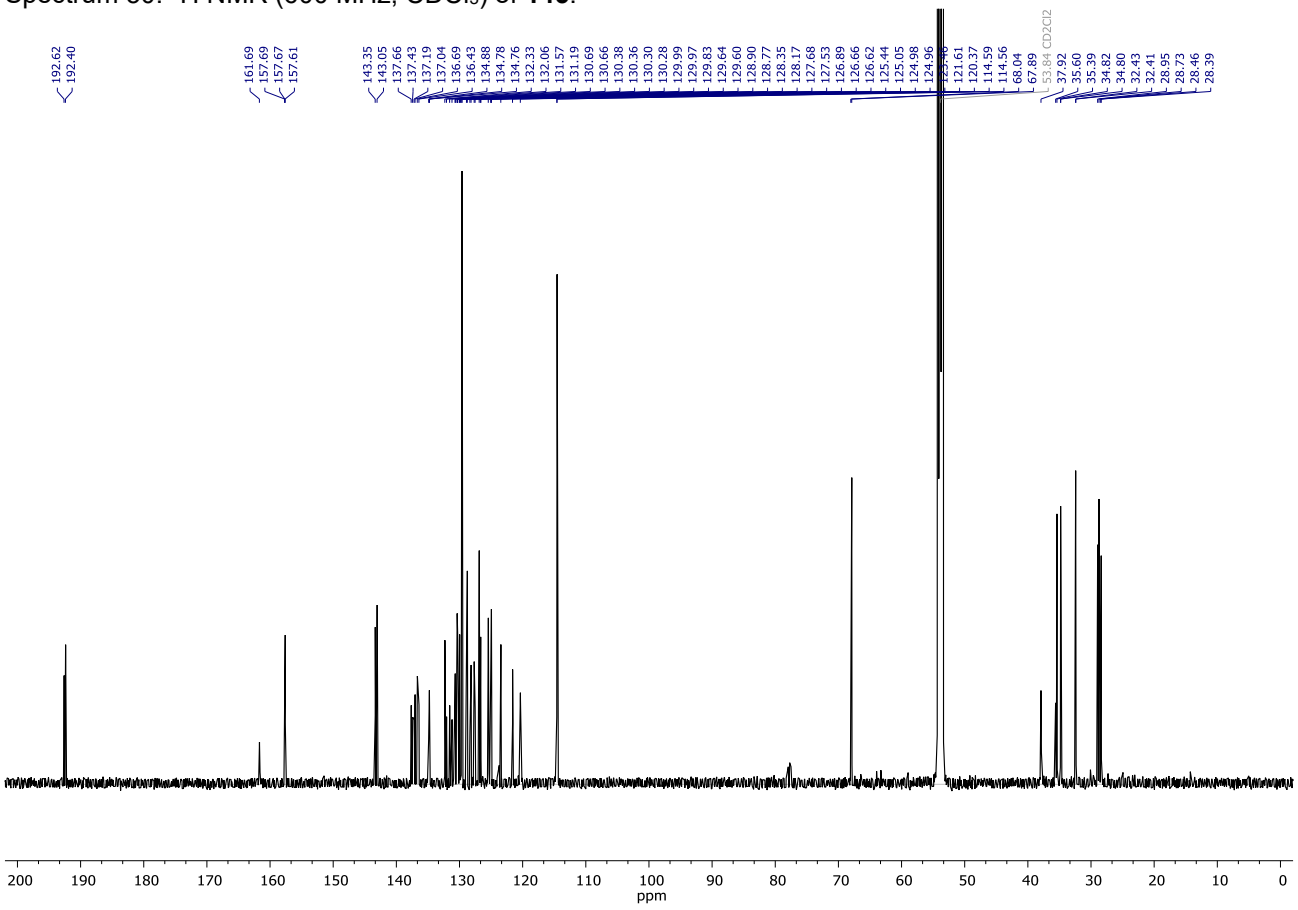

Spectrum 51. ^{13}C NMR (151 MHz, $CDCl_3$) of **145**.

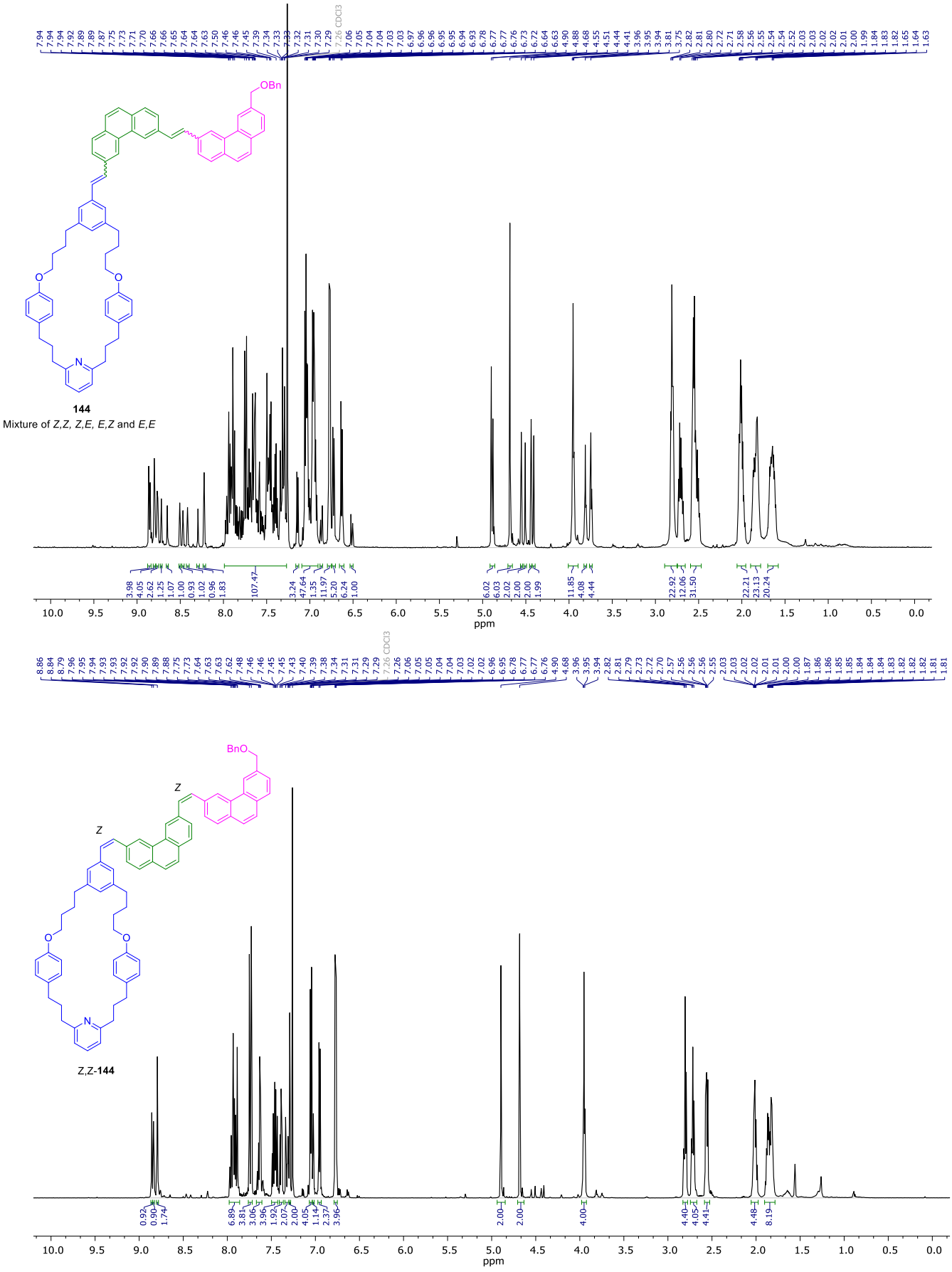

Spectrum 52. ^{1}H NMR (600 MHz, $CDCl_3$) comparison between **144** (mixture of 4 isomers, top) and *Z,Z*-**144** (bottom) after isomerization.

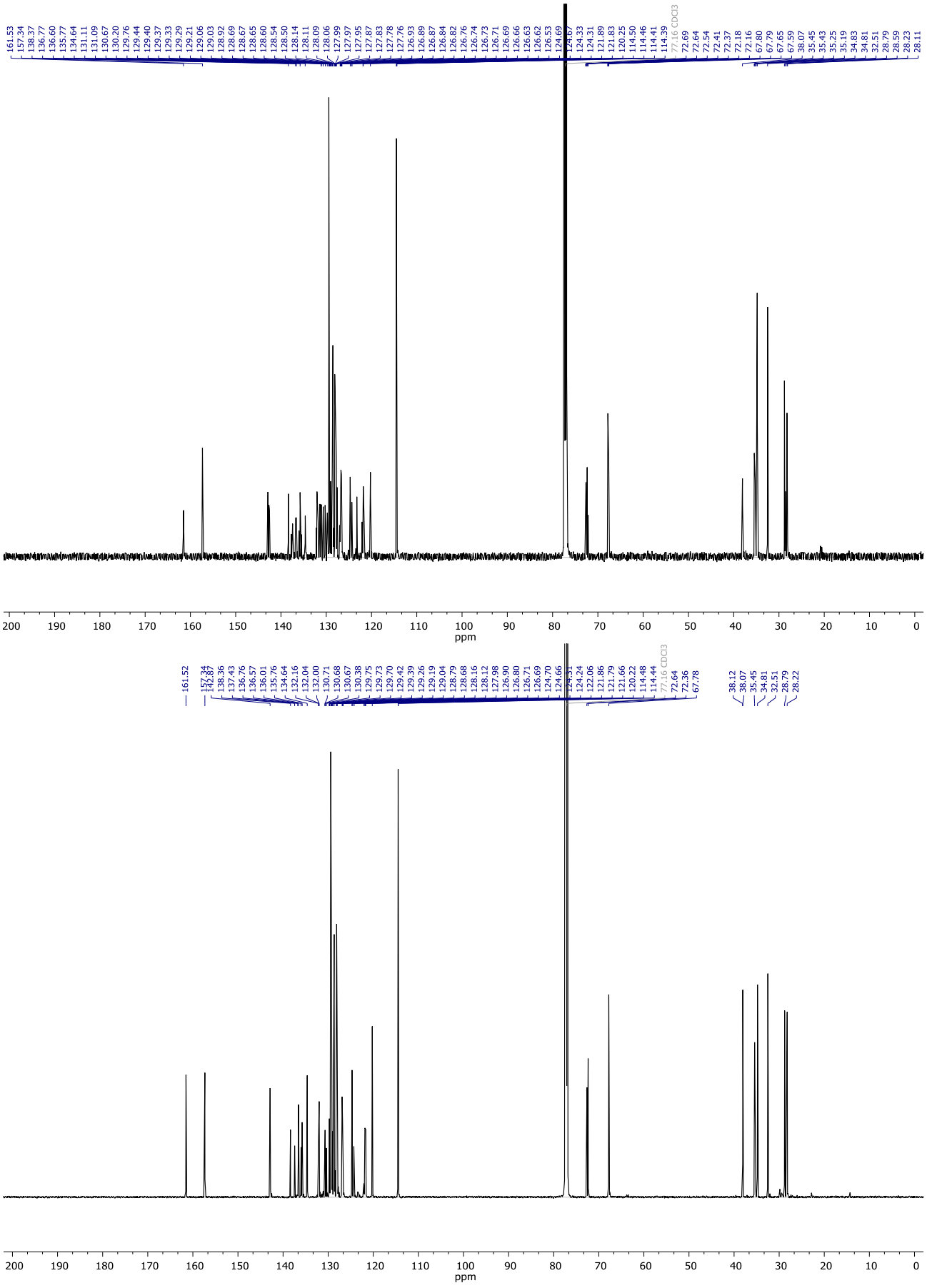

Spectrum 53. ^{13}C NMR (151 MHz, $CDCl_3$) comparison between **144** (mixture of 4 isomers, top) and *Z,Z*-**144** (bottom) after isomerization.

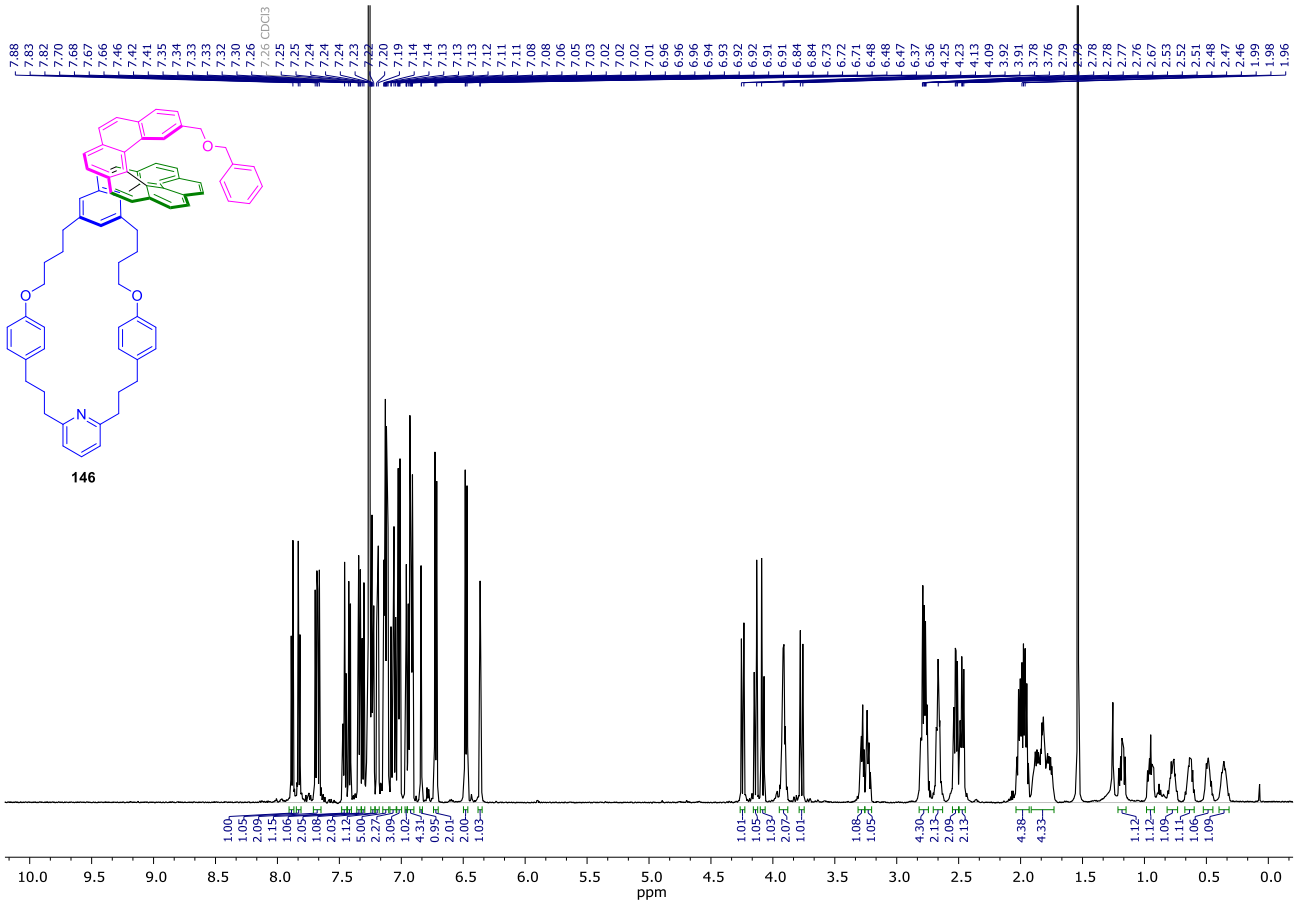

Spectrum 54. ^{1}H NMR (600 MHz, $CDCl_3$) of **146**.

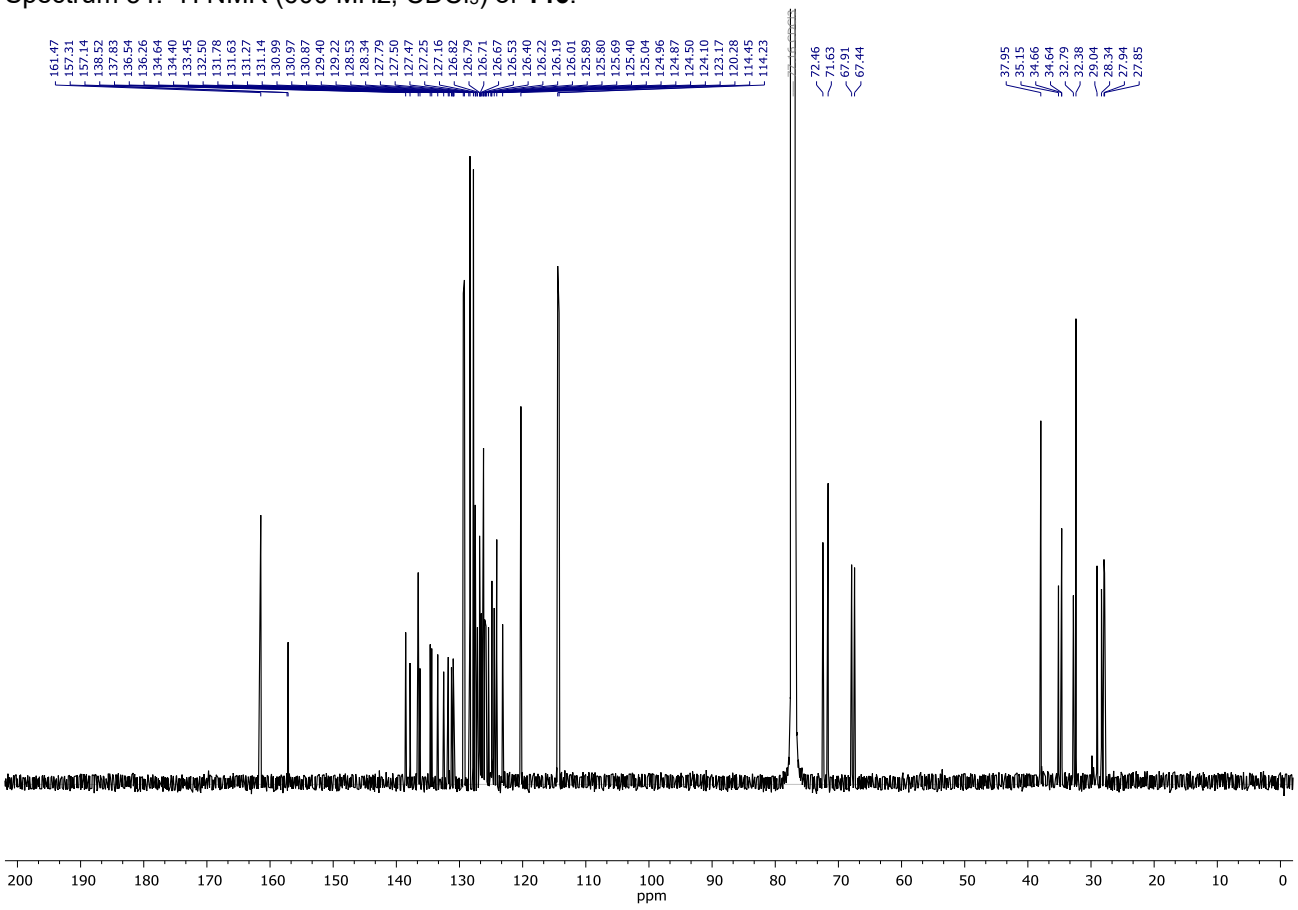

Spectrum 55. ^{13}C NMR (151 MHz, $CDCl_3$) of **146**.

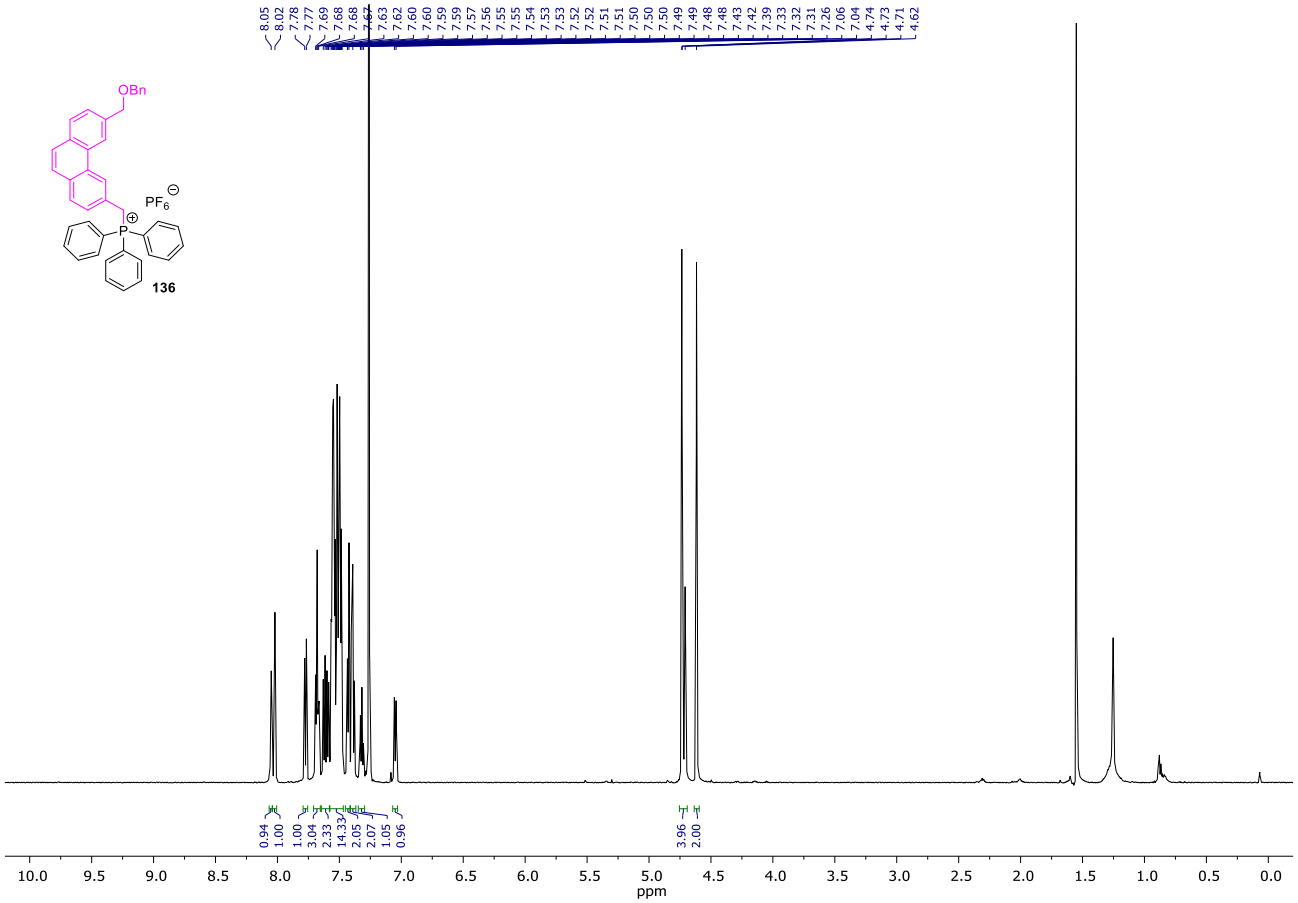

Spectrum 56. ^{1}H NMR (600 MHz, $CDCl_3$) of **136**.

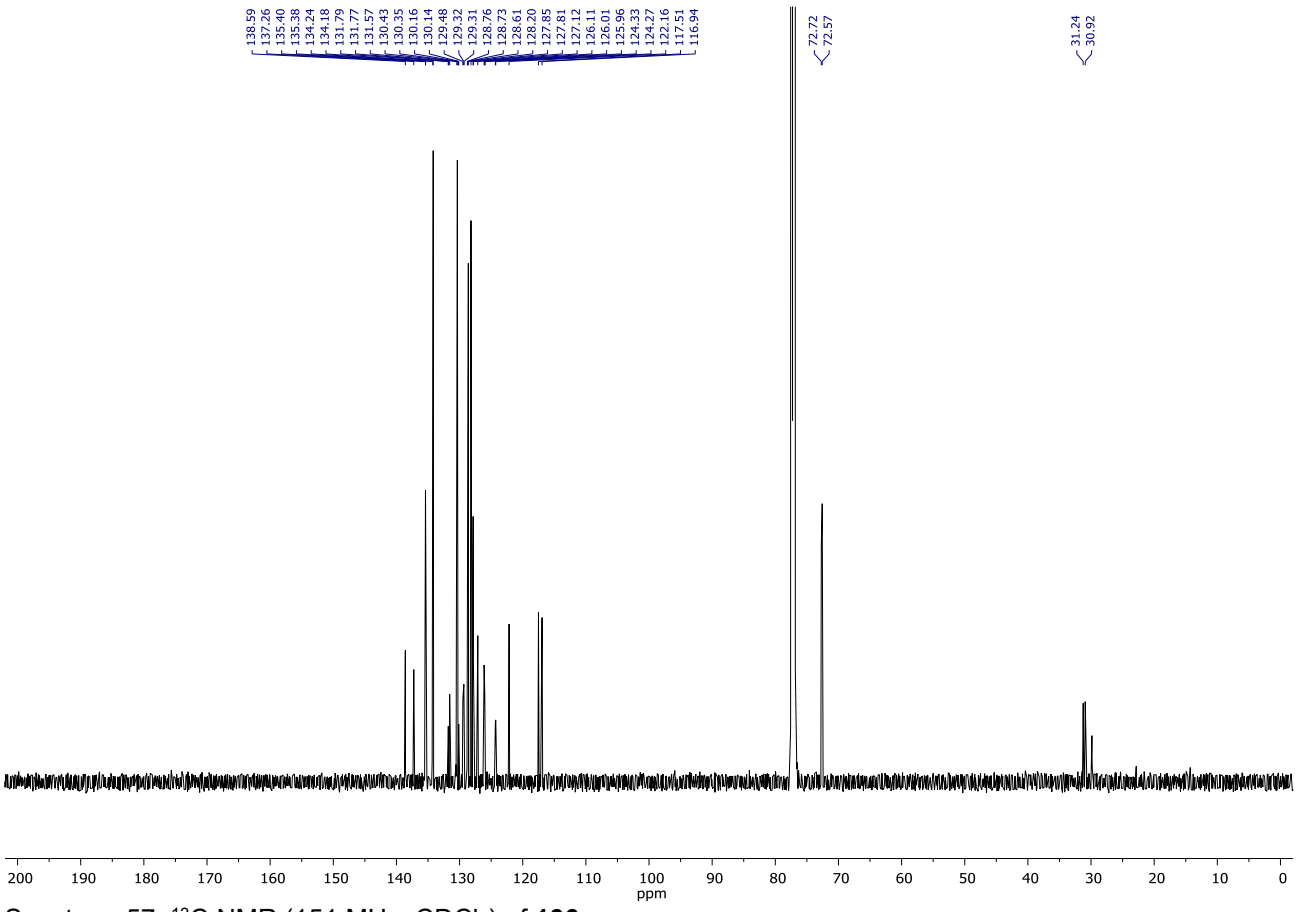

Spectrum 57. ^{13}C NMR (151 MHz, $CDCl_3$) of **136**.

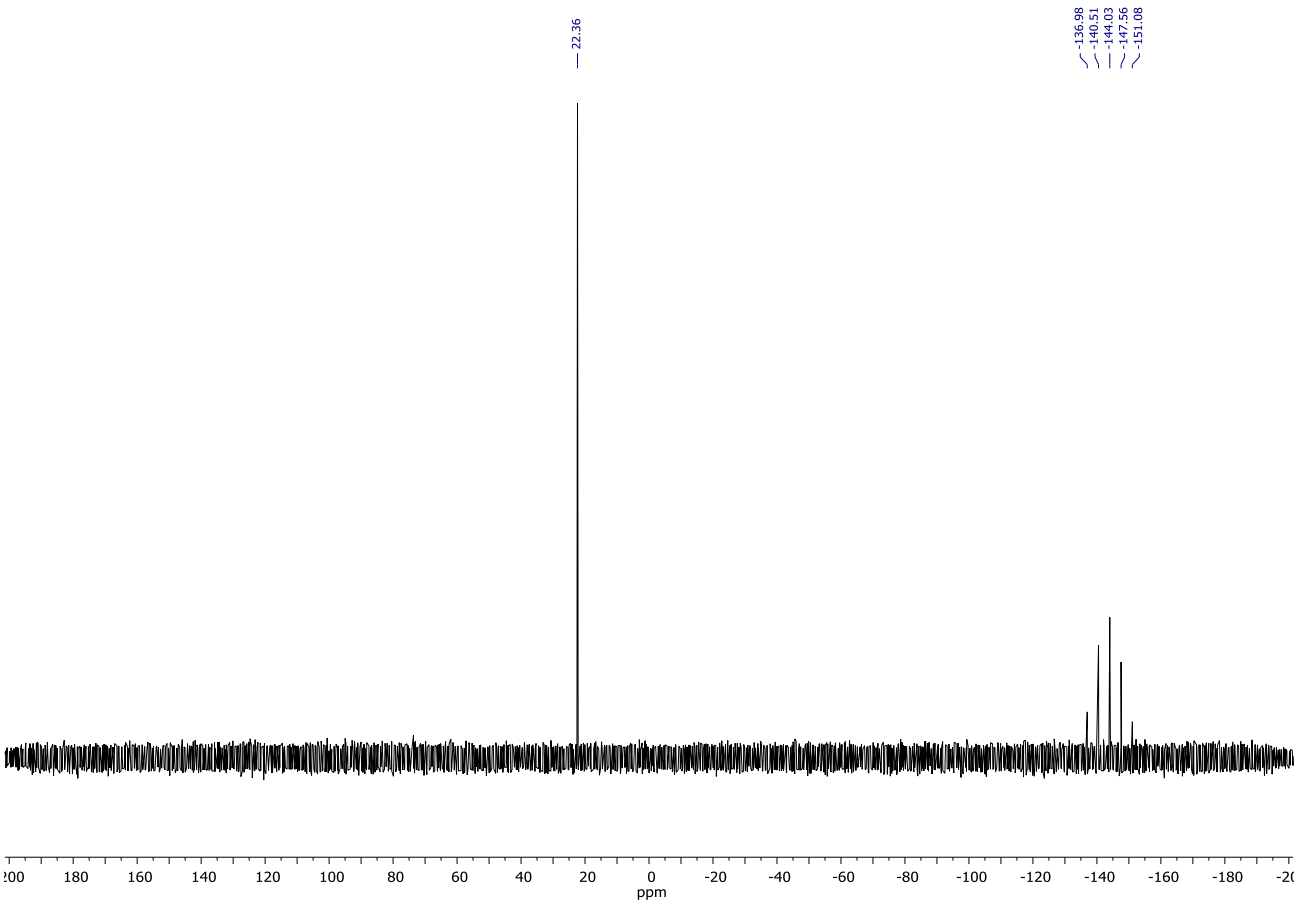

Spectrum 58. ^{31}P NMR (162 MHz, $CDCl_3$) of **136**.

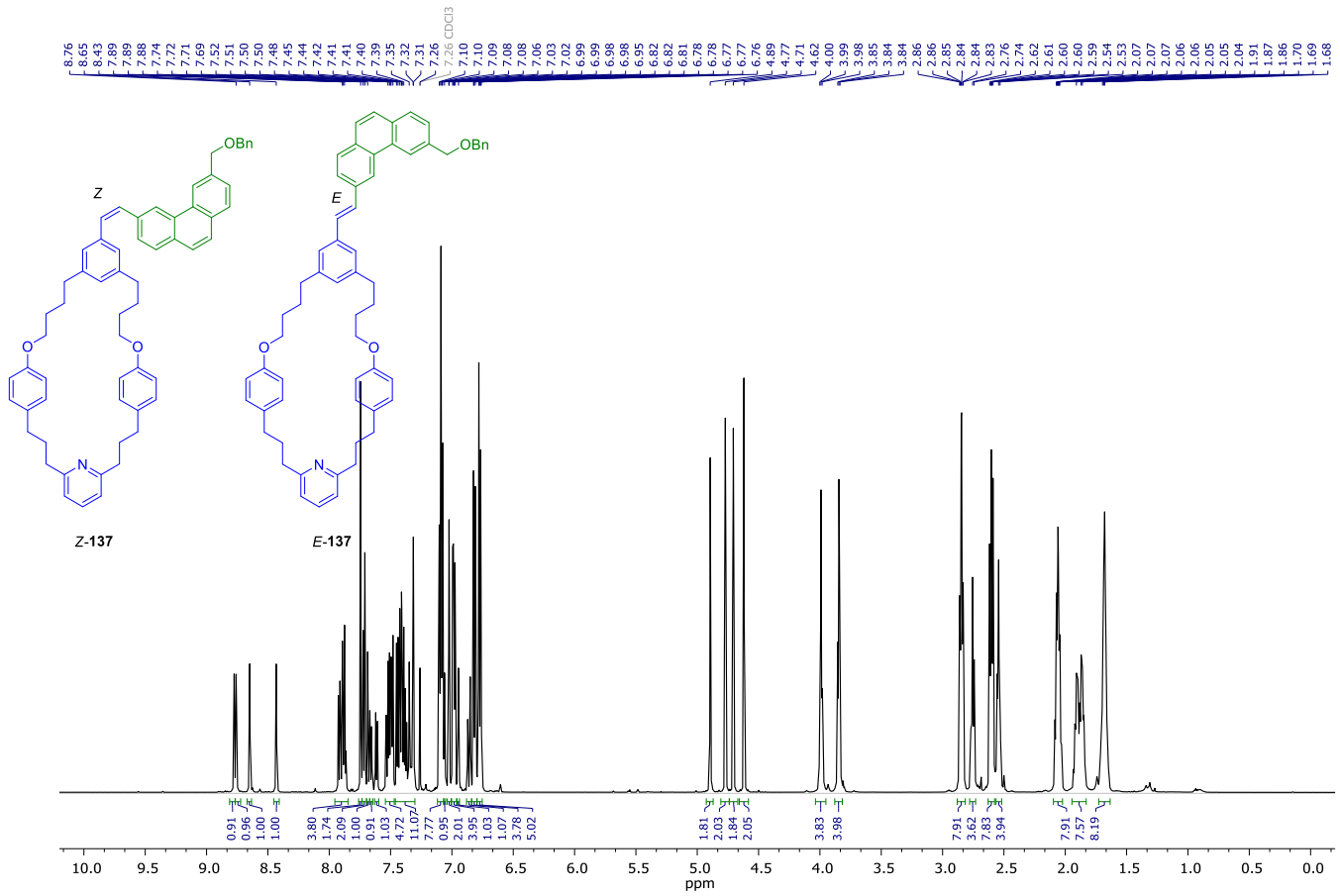

Spectrum 59. ^{1}H NMR (600 MHz, $CDCl_3$) of **137**.

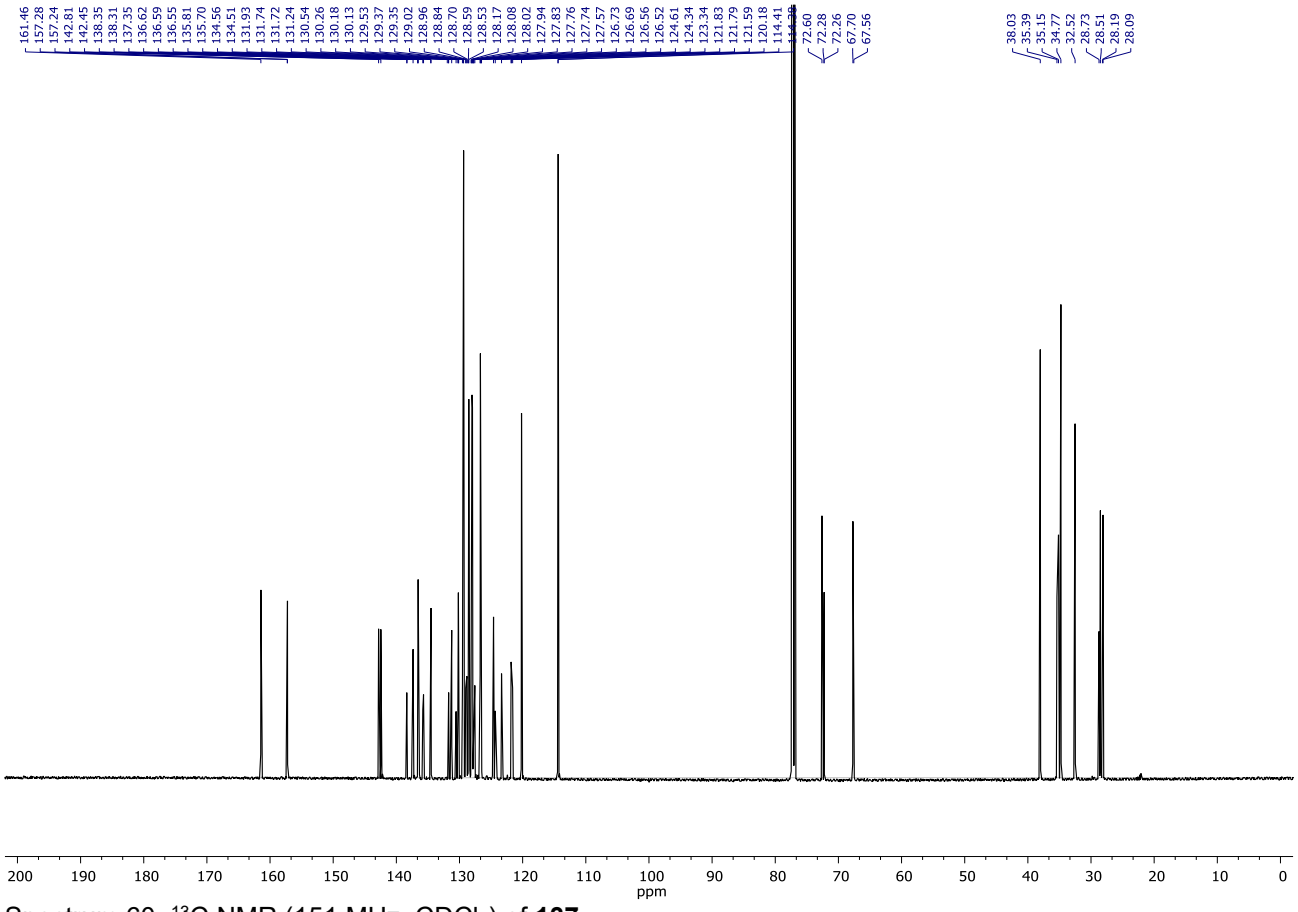

Spectrum 60. ^{13}C NMR (151 MHz, $CDCl_3$) of **137**.

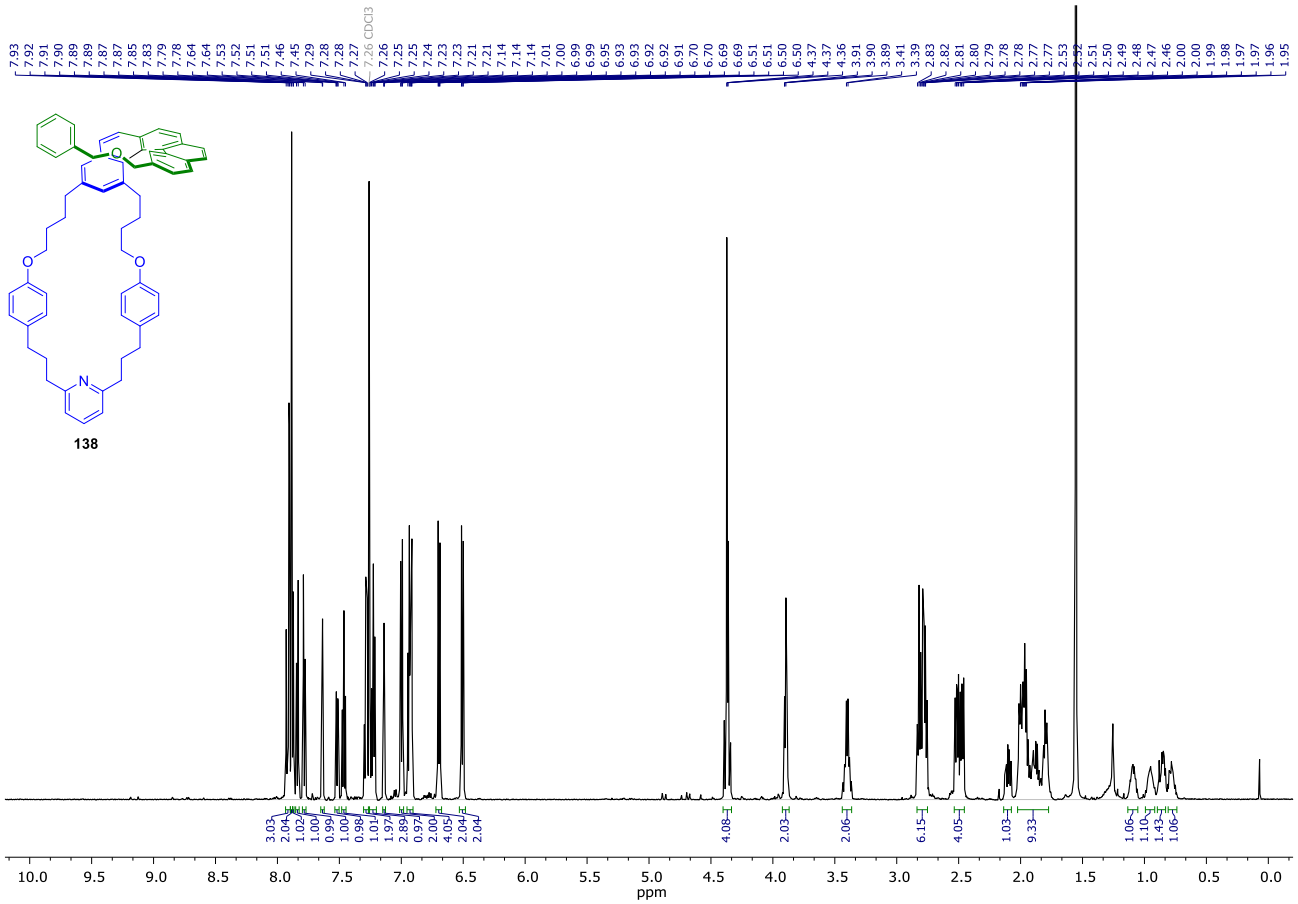

Spectrum 61. ^{1}H NMR (600 MHz, $CDCl_3$) of **138**.

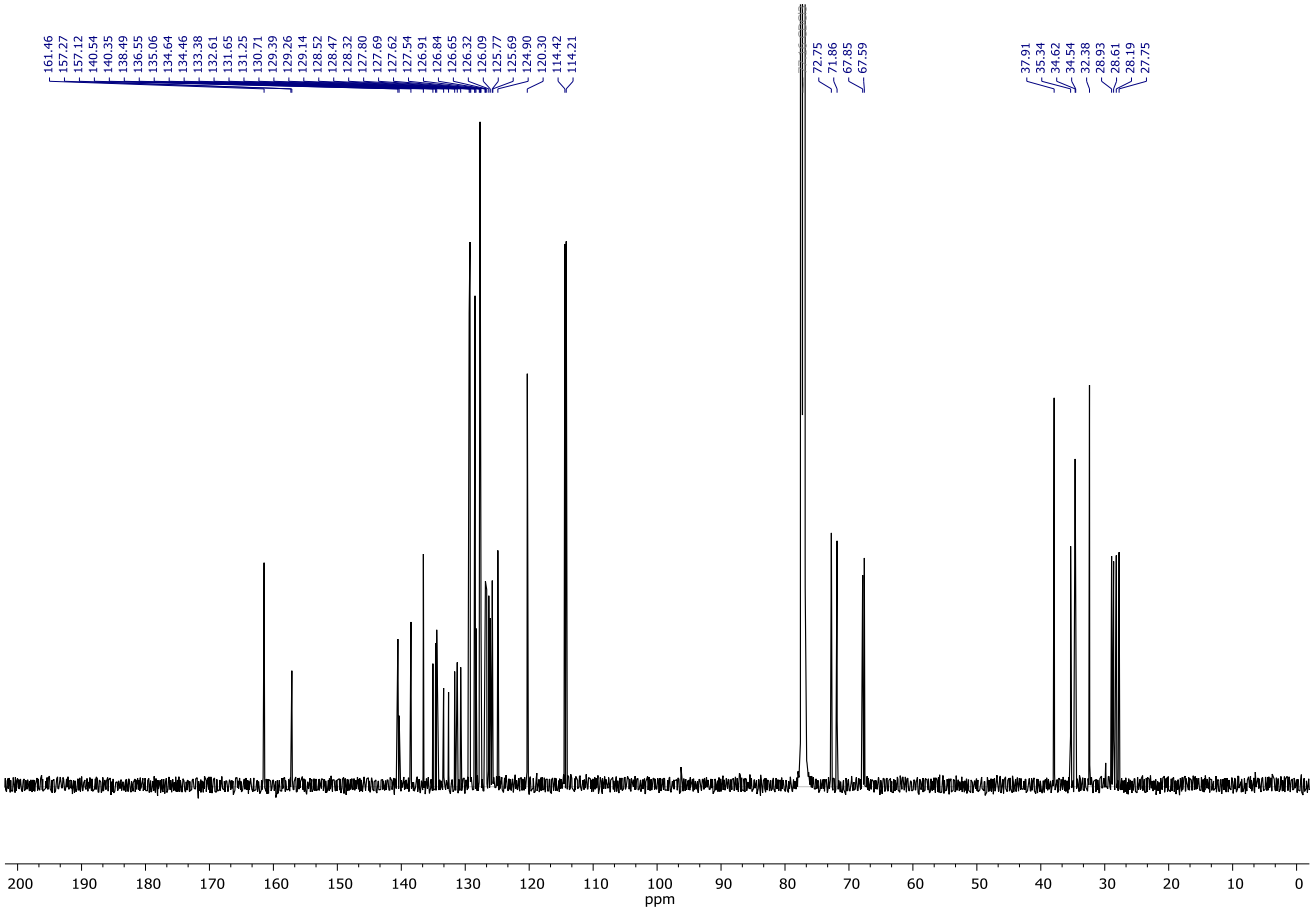

Spectrum 62. ^{13}C NMR (151 MHz, $CDCl_3$) of **138**.

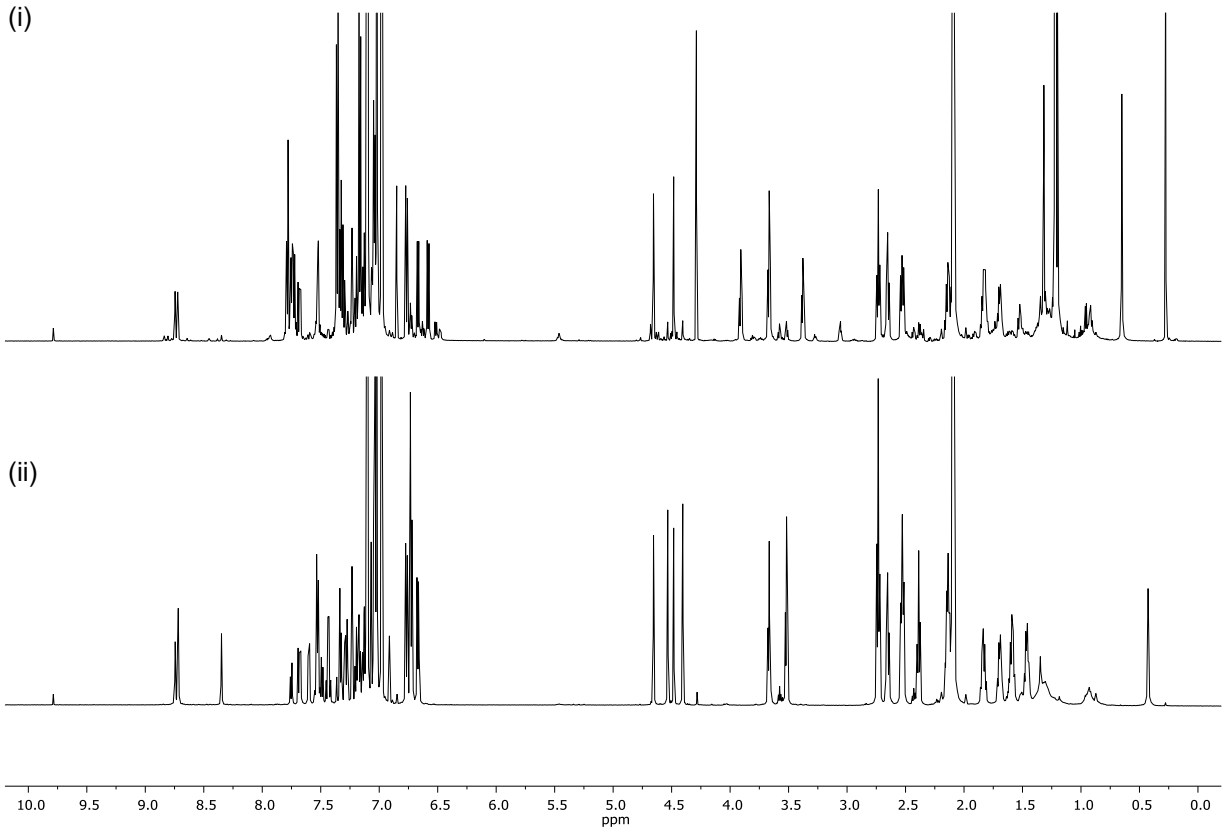

Spectrum 63. ^{1}H NMR (600 MHz, toluene-d_8) stack plot of (i) crude 1-barrier operation vs (ii) 1-barrier authentic standard.

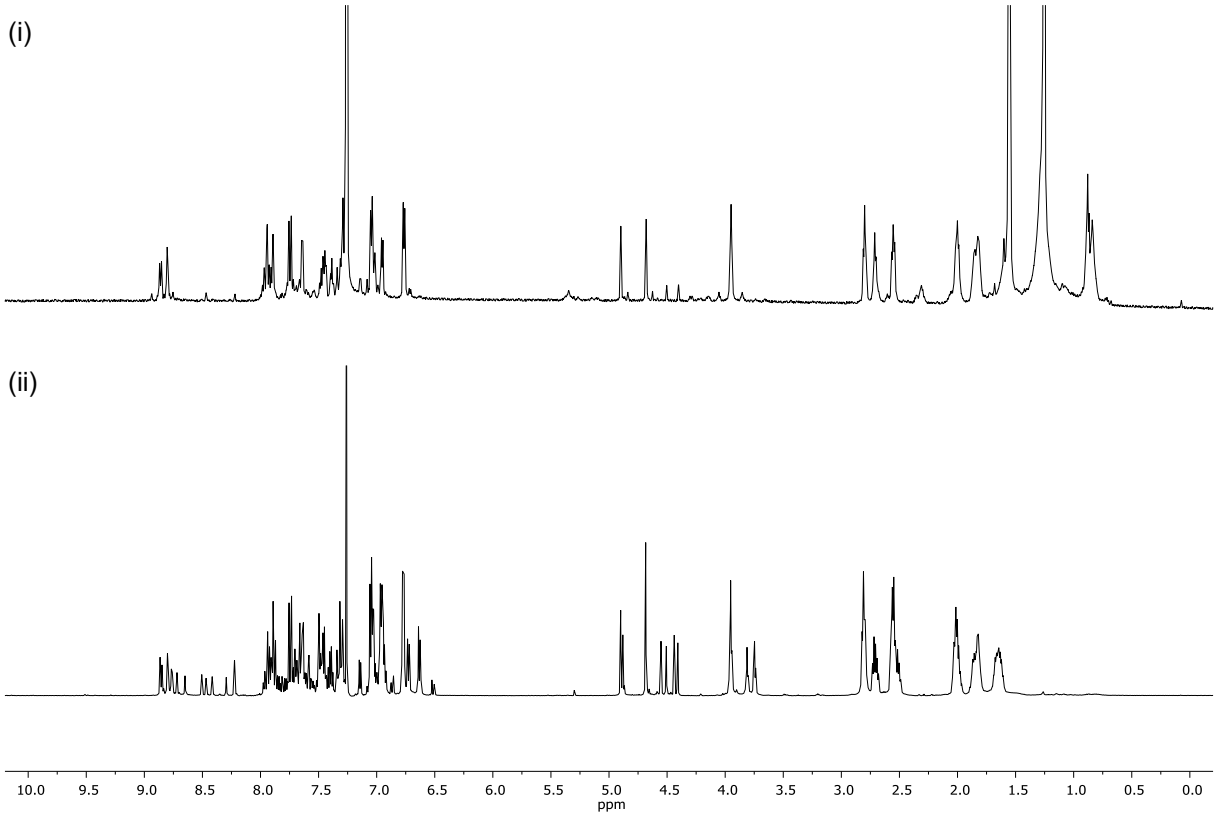

Spectrum 64. ^{1}H NMR (600 MHz, $CDCl_3$) stack plot of (i) 2-barrier operation product vs (ii) 2-barrier authentic standard

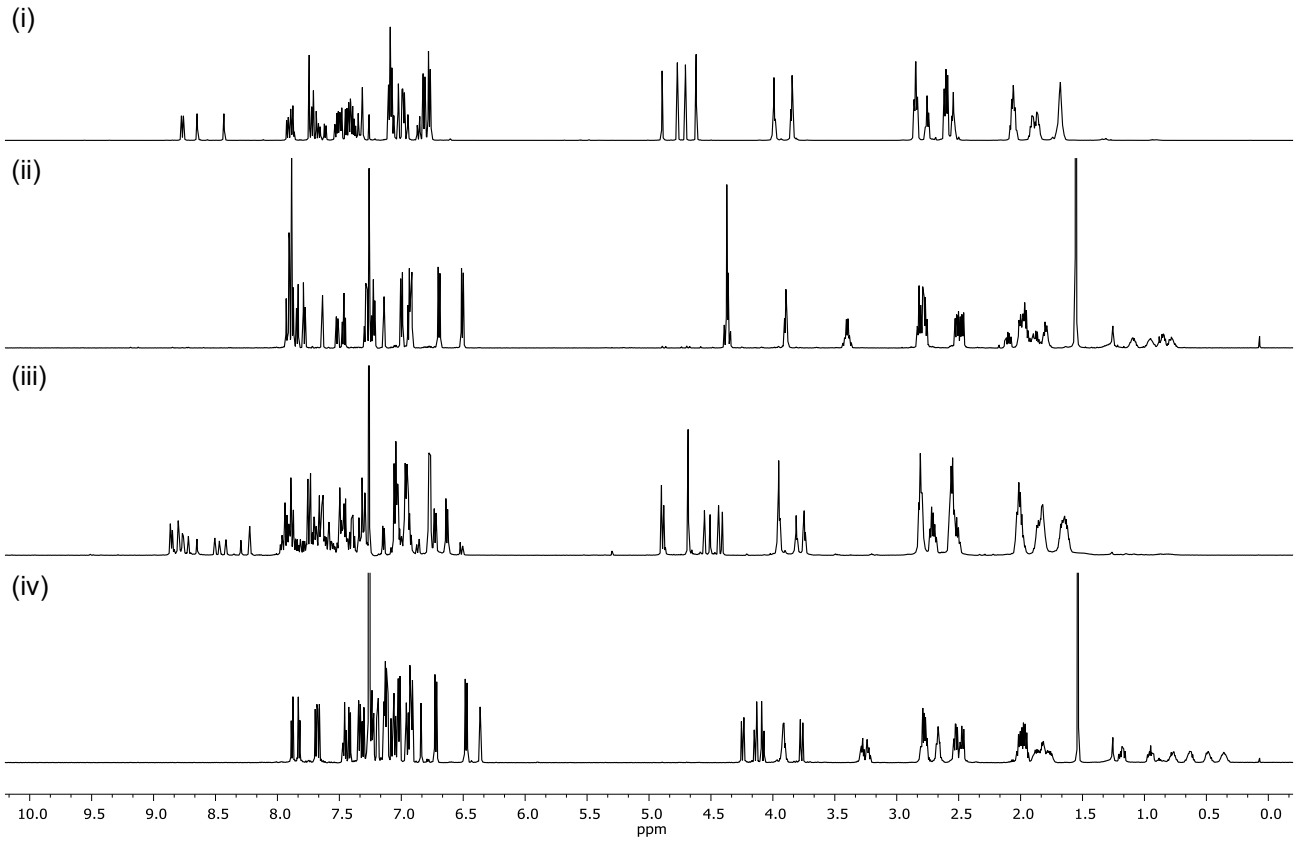

Spectrum 65. ^{1}H NMR (600 MHz, $CDCl_3$) stack plot comparison of (i) 1-barrier operation standard **137** (E/Z mixture), (ii) [5]helicene **138**, (iii) 2-barrier operation standard **144** (Mixture of 4 isomers) and (iv) [9]helicene **146**.

11.2.2. Unidirectional Linear Transport with a Fluorescence Read Out

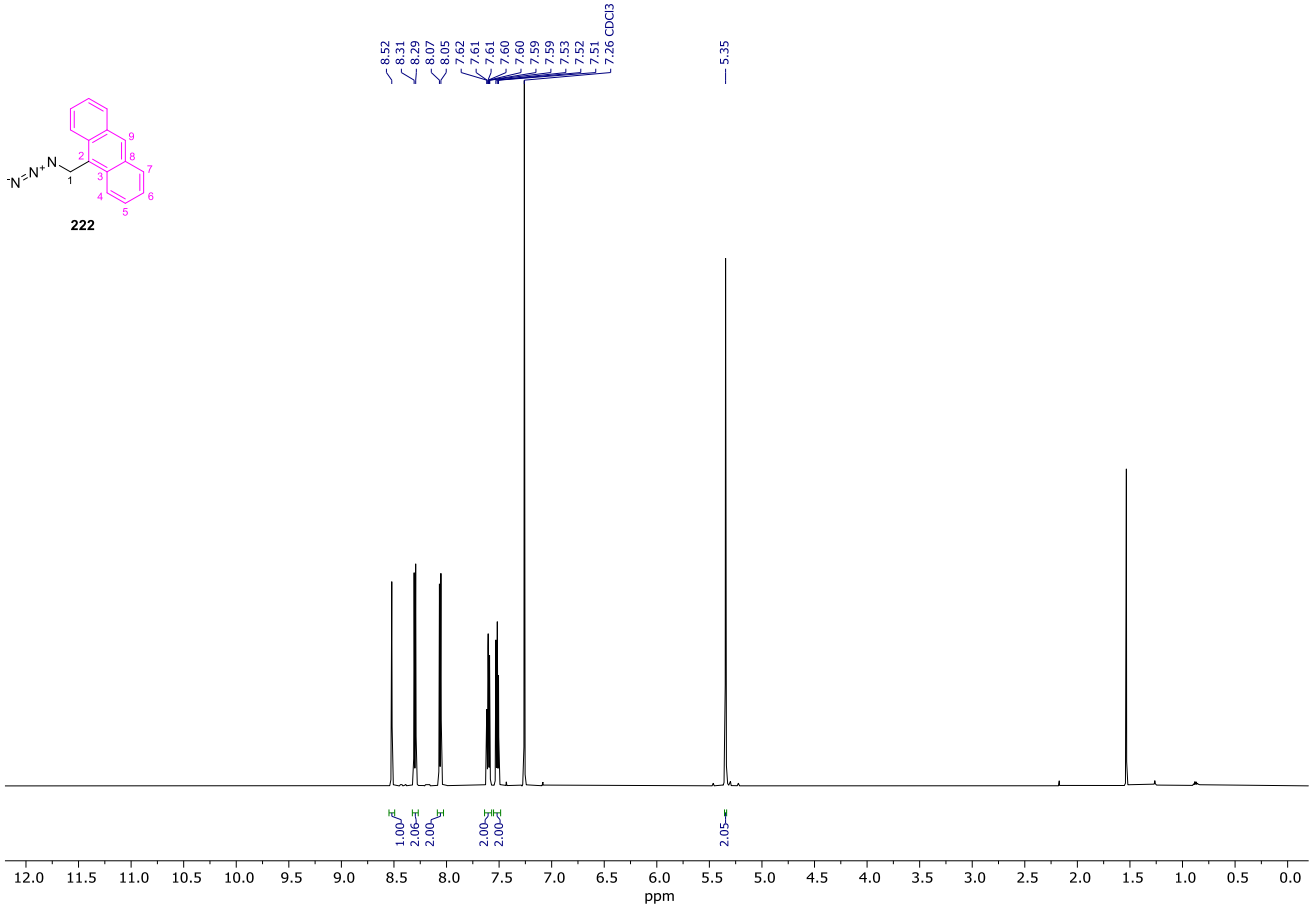

222

Spectrum 66. ^{1}H NMR (600 MHz, $CDCl_3$) of **222**.

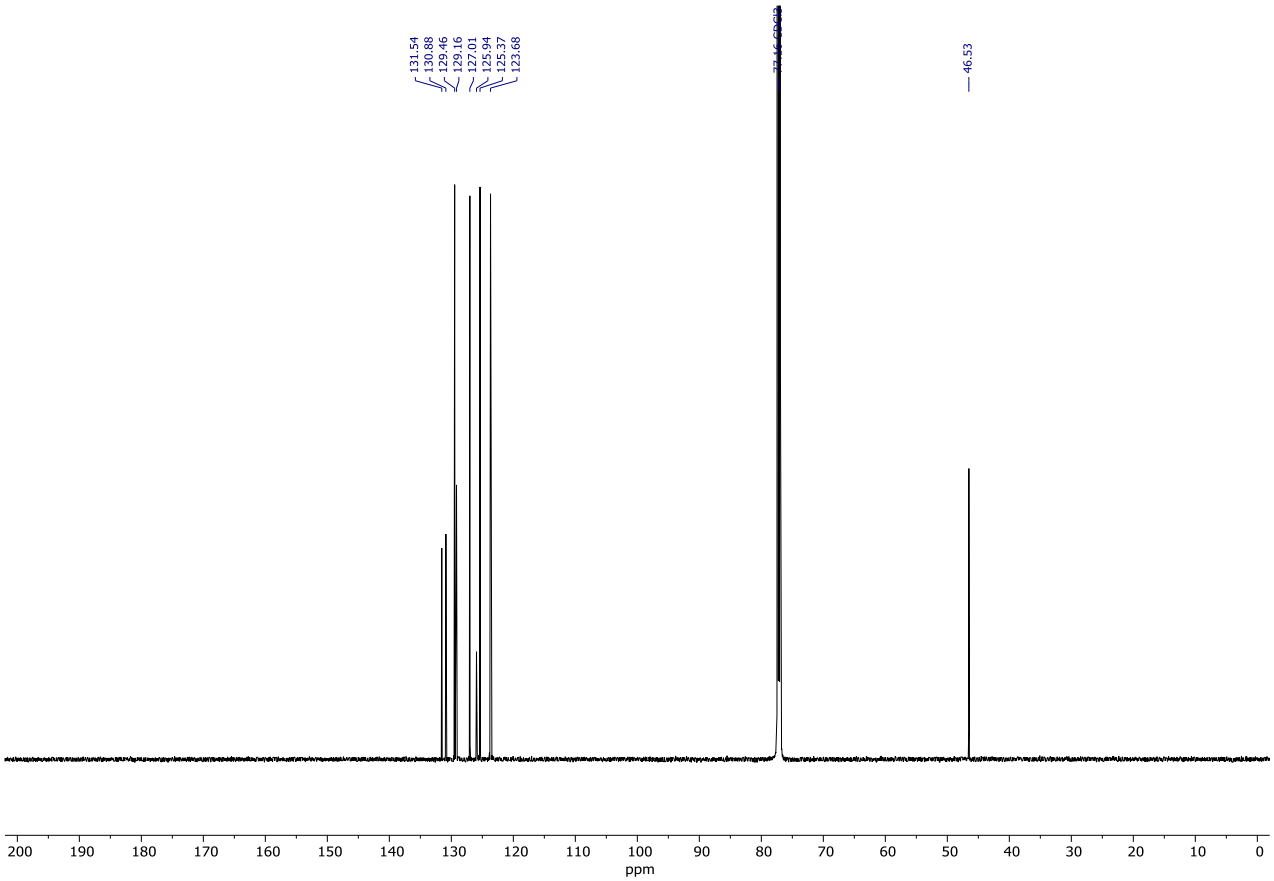

Spectrum 67. ^{13}C NMR (151 MHz, $CDCl_3$) of **222**.

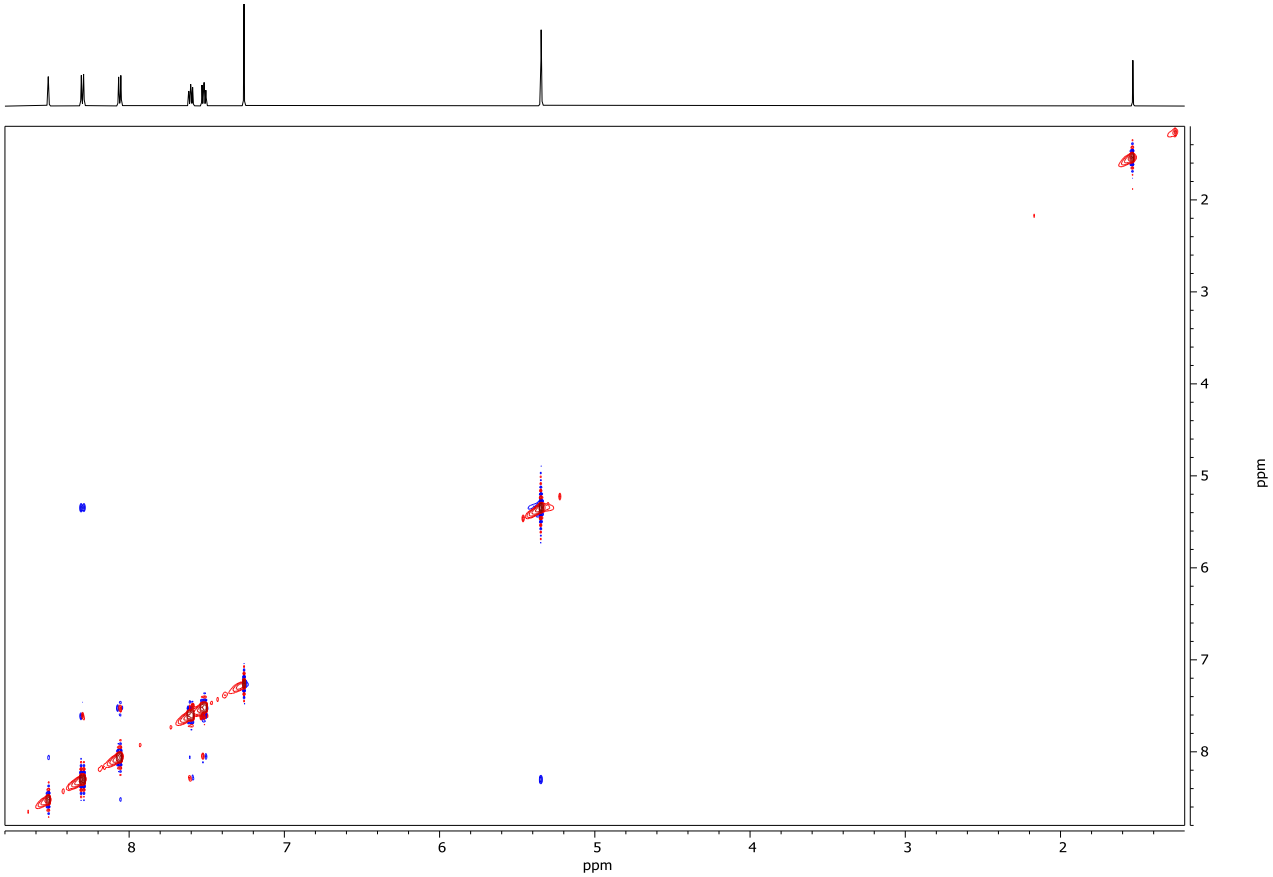

Spectrum 68. 2D NOESY (600 MHz, $CDCl_3$) of **222**. Data was recorded with a 300 ms mixing time and a relaxation delay of 1.99 s. 2K data points were collected for 256 increments of 4 scans.

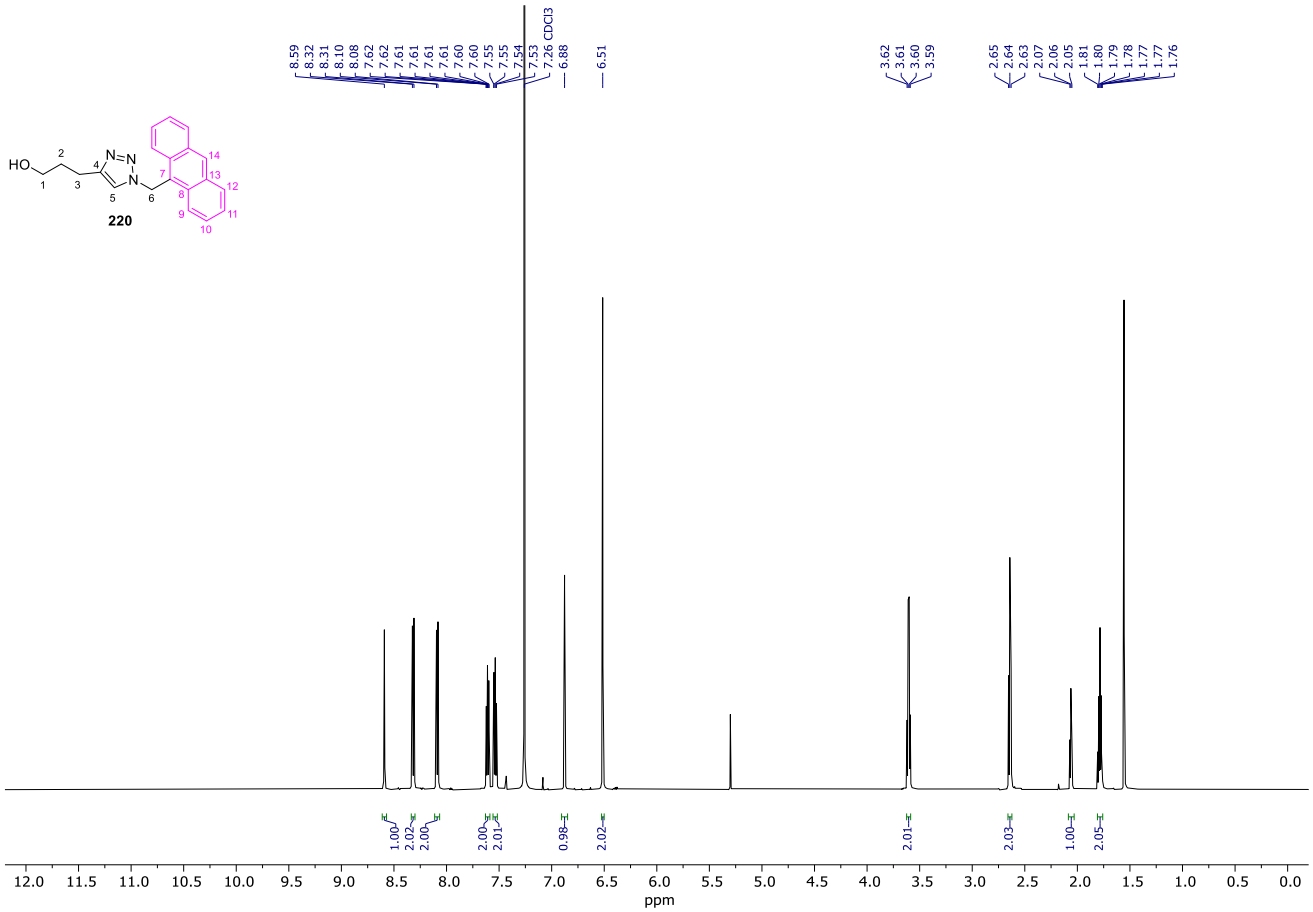

Spectrum 69. ^{1}H NMR (600 MHz, $CDCl_3$) of **220**.

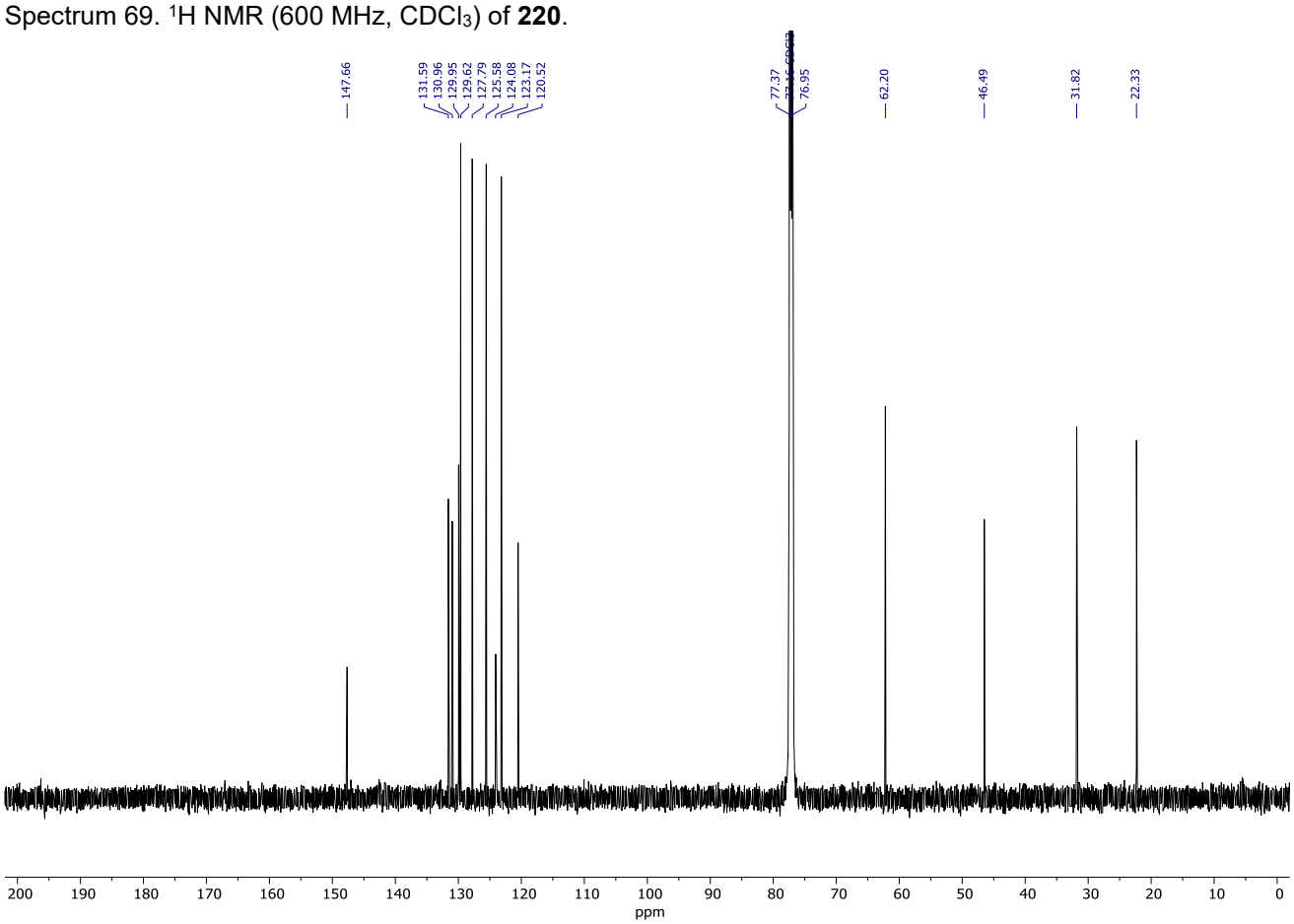

Spectrum 70. ^{13}C NMR (151 MHz, $CDCl_3$) of **220**.

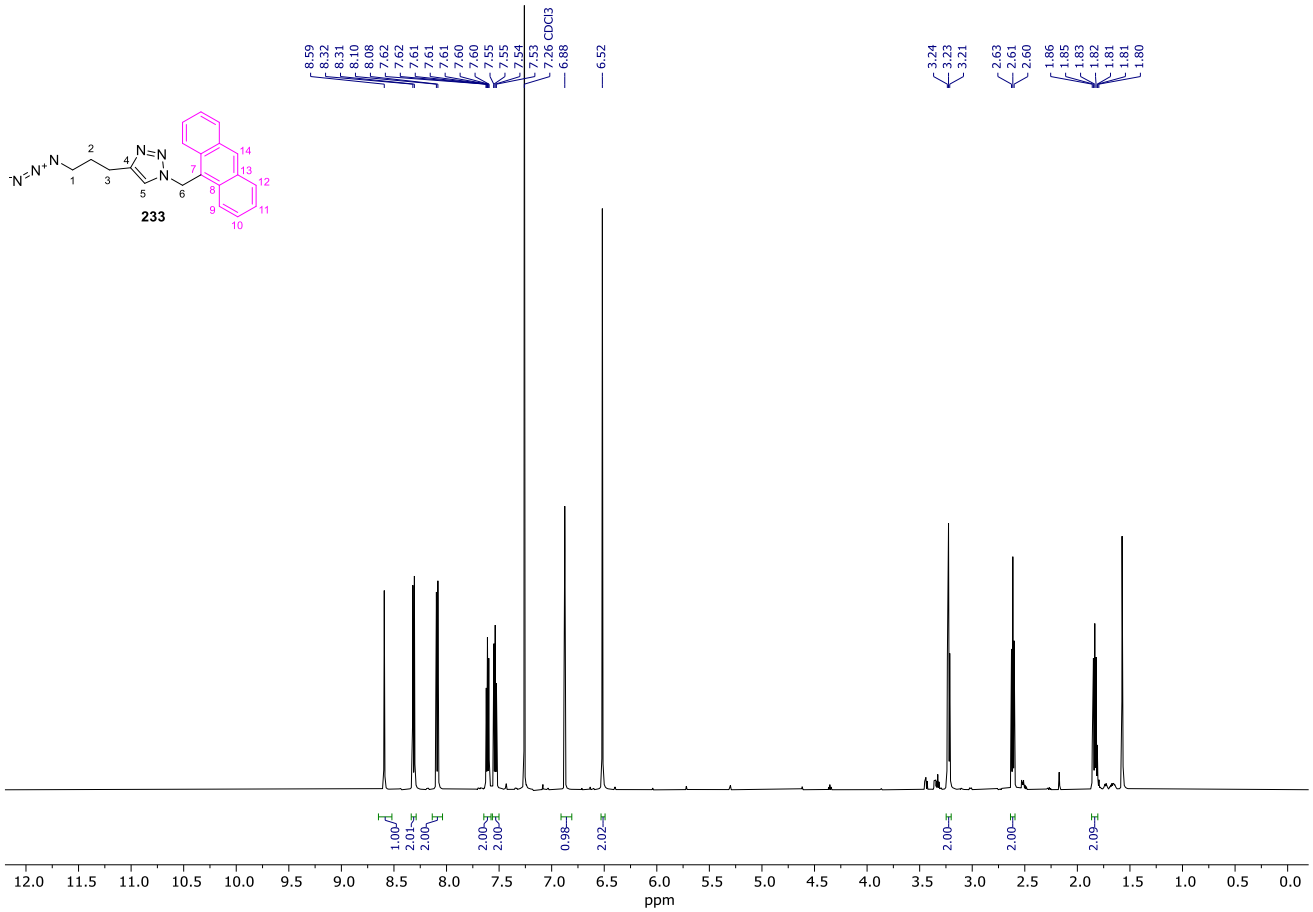

Spectrum 71. ^{1}H NMR (600 MHz, $CDCl_3$) of **233**.

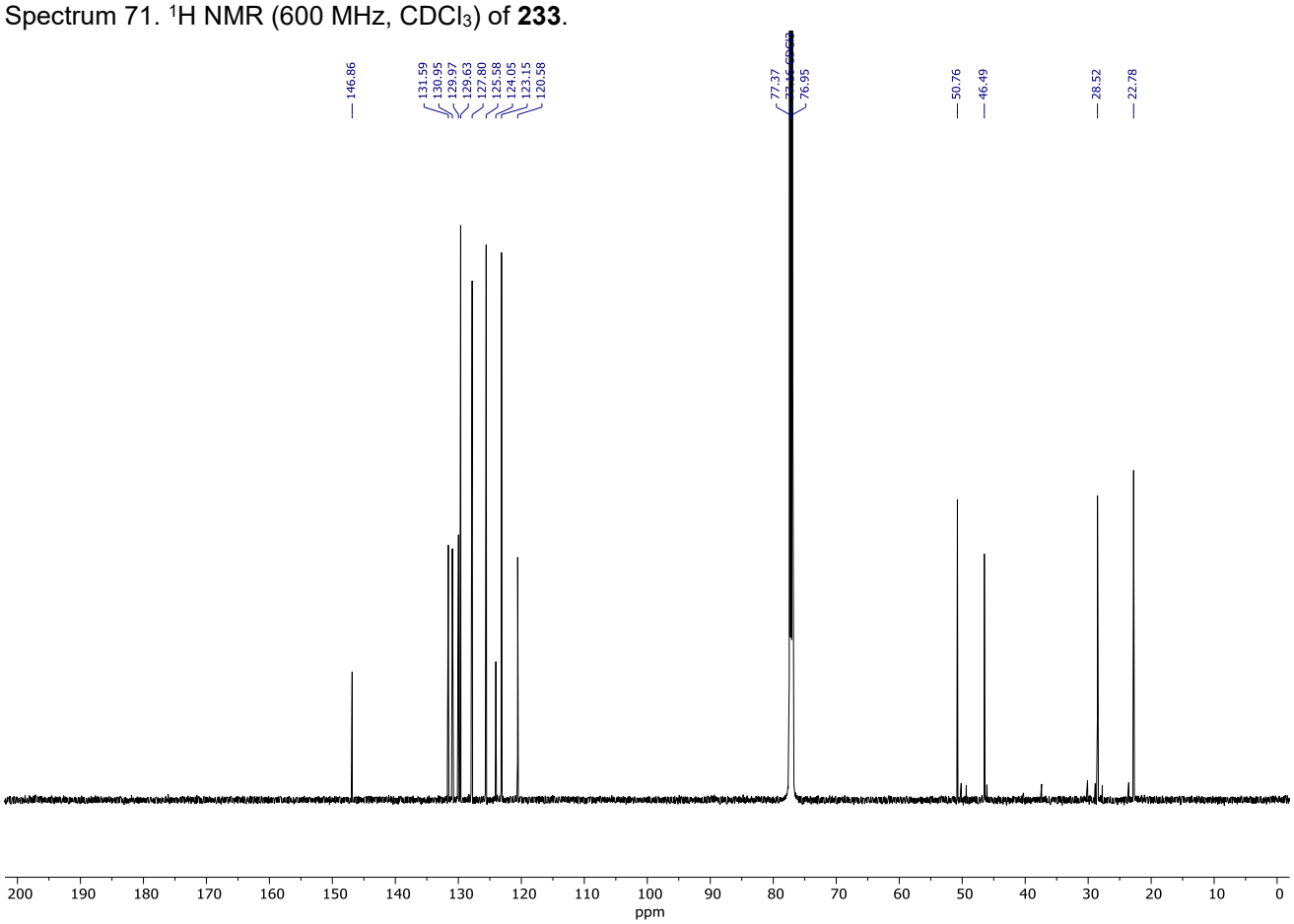

Spectrum 72. ^{13}C NMR (151 MHz, $CDCl_3$) of **233**.

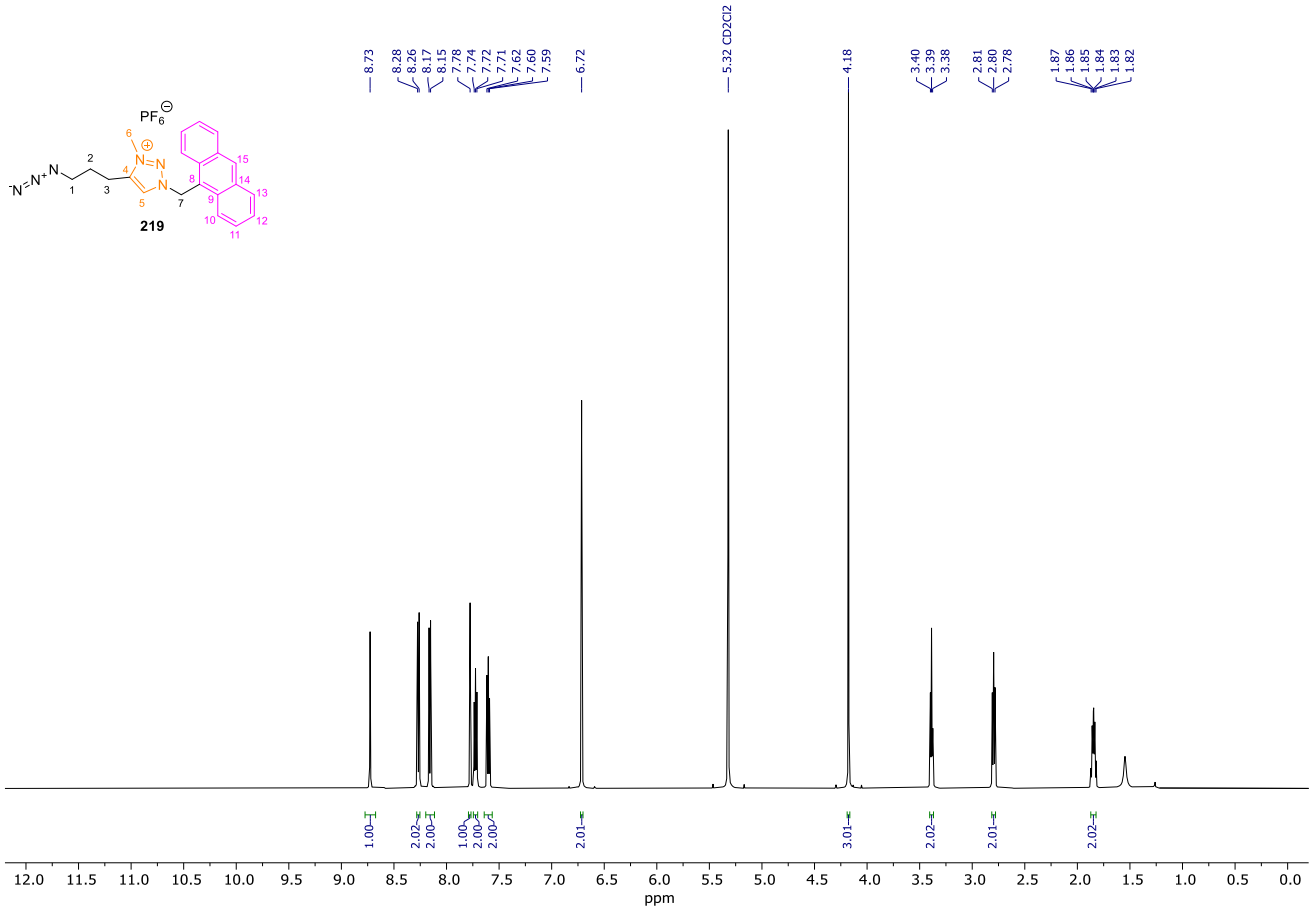

Spectrum 73. ^{1}H NMR (600 MHz, CD_2Cl_2) of **219** ($PF6^-$ salt).

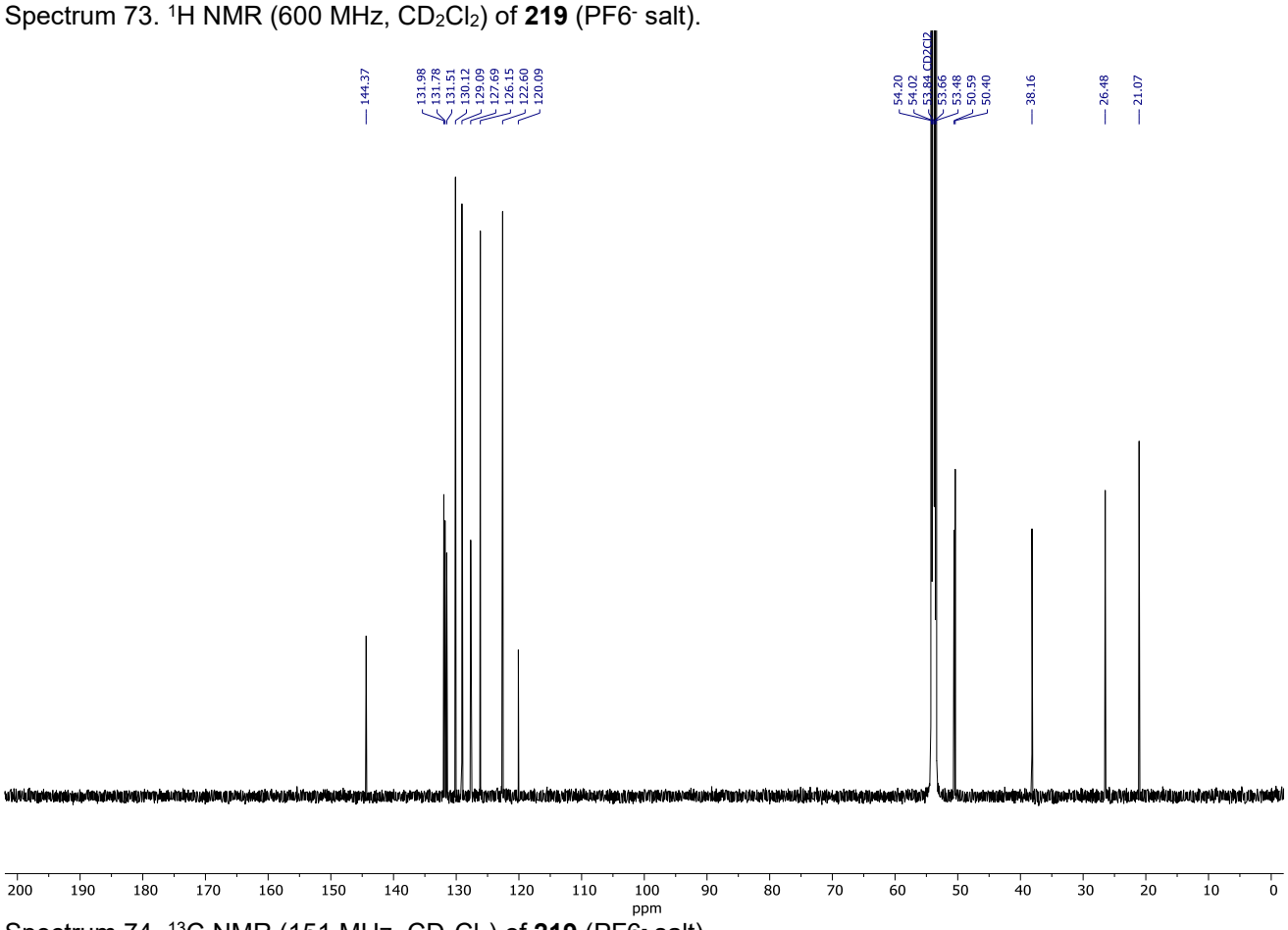

Spectrum 74. ^{13}C NMR (151 MHz, CD_2Cl_2) of **219** ($PF6^-$ salt).

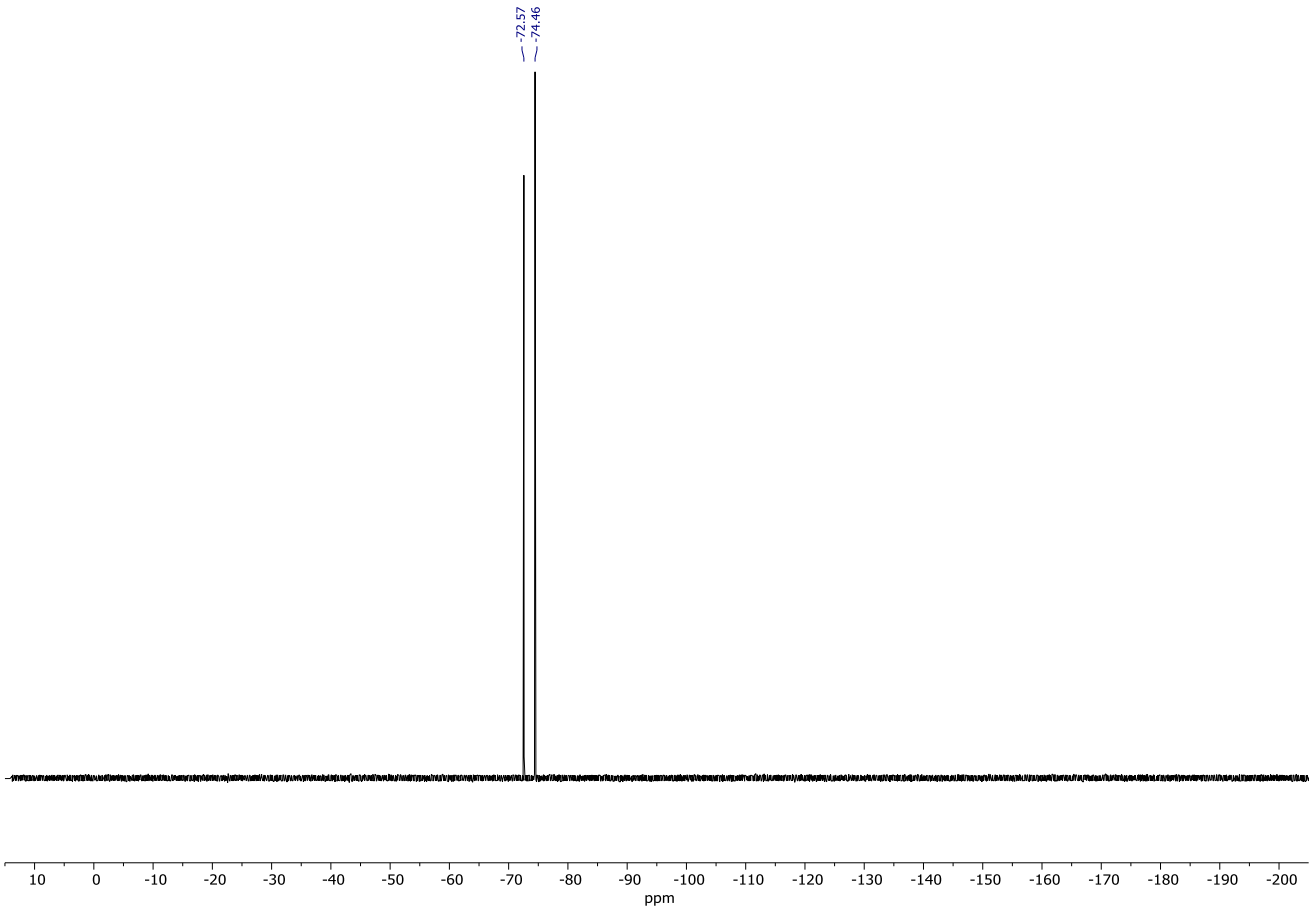

Spectrum 75. ^{19}F NMR (376 MHz, CD_2Cl_2) of **219** ($PF6^-$ salt).

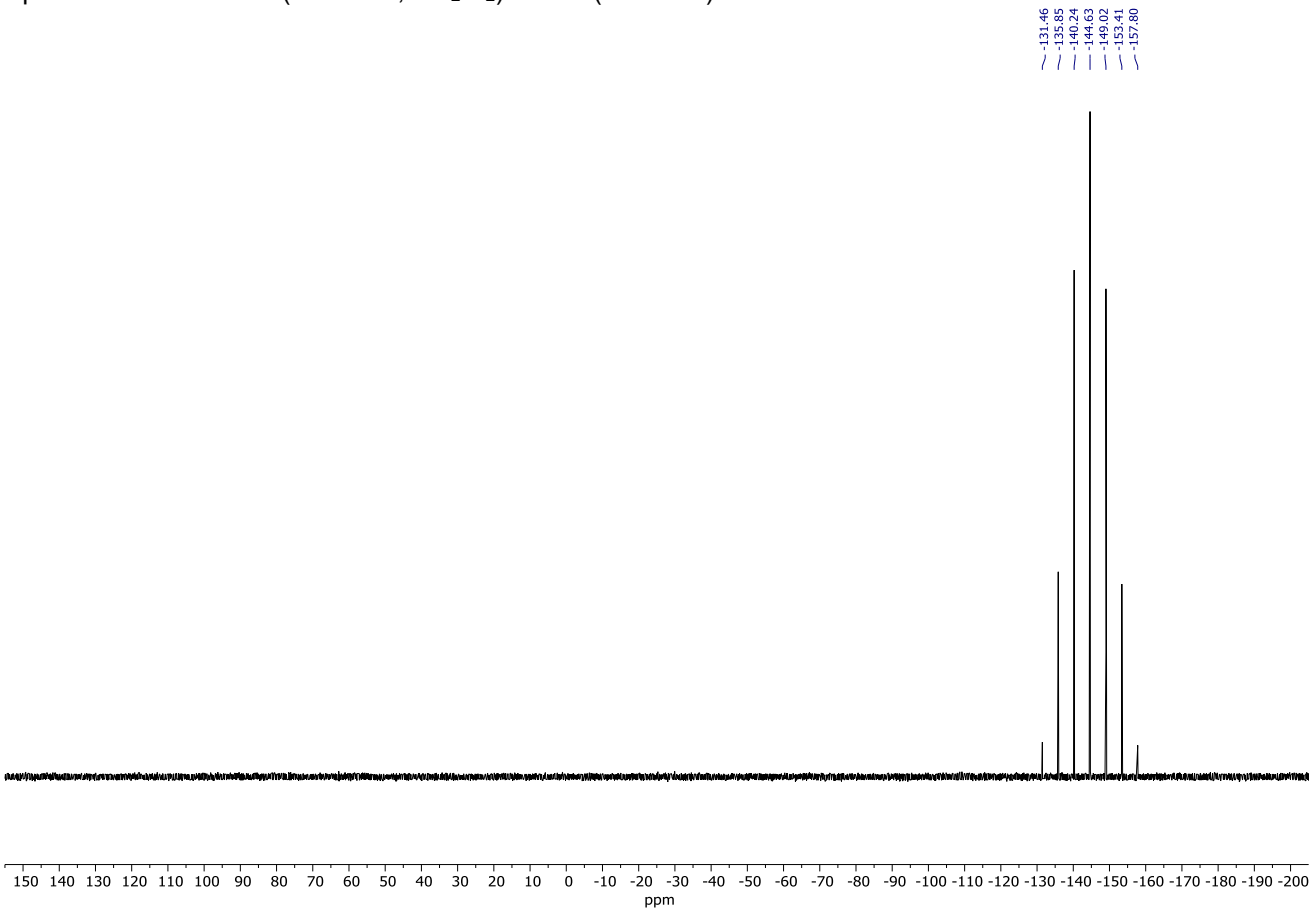

Spectrum 76. ^{31}P NMR (162 MHz, CD_2Cl_2) of **219** ($PF6^-$ salt).

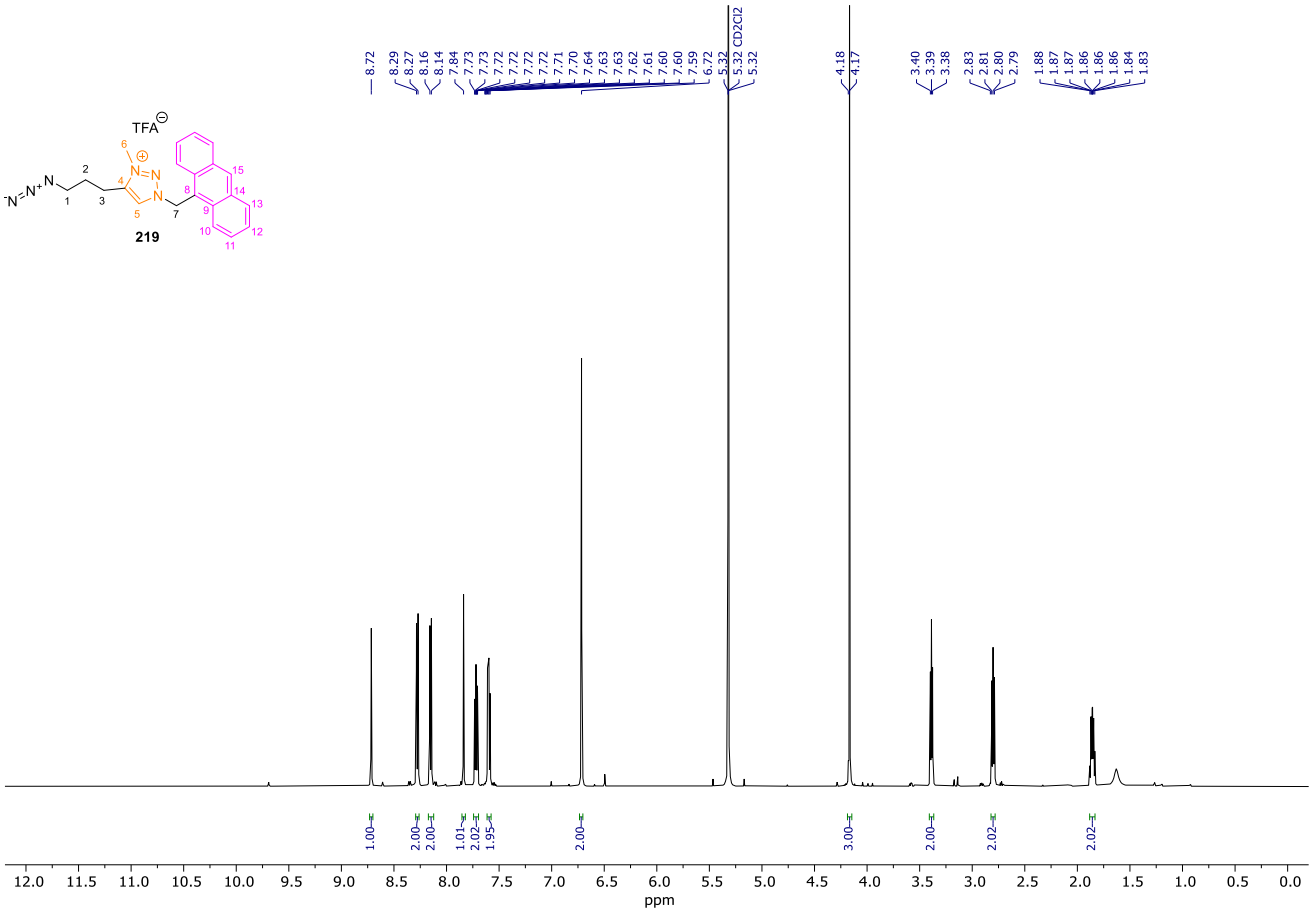

Spectrum 77. ^{1}H NMR (600 MHz, CD_2Cl_2) of **219** (TFA^- salt).

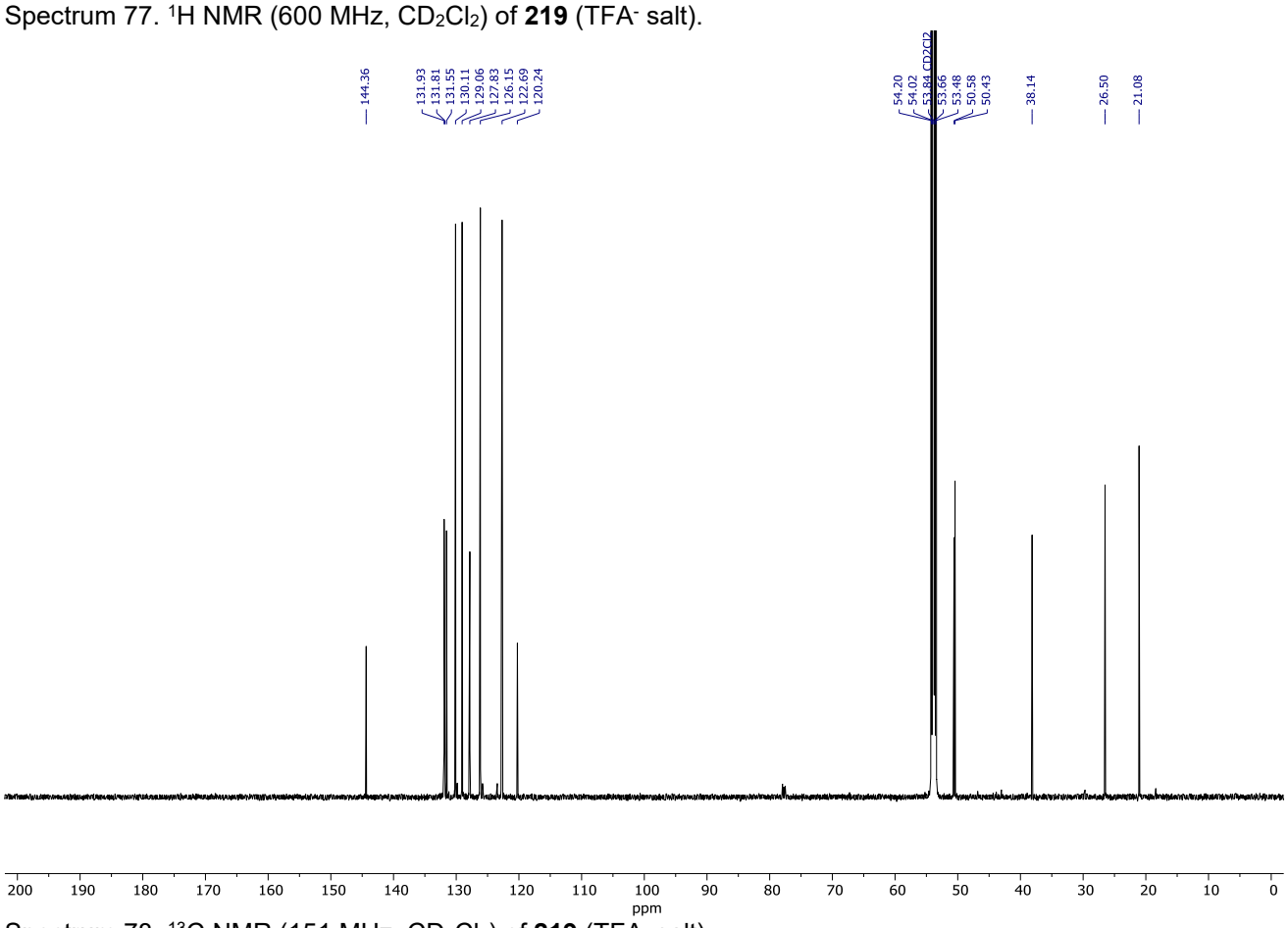

Spectrum 78. ^{13}C NMR (151 MHz, CD_2Cl_2) of **219** (TFA^- salt).

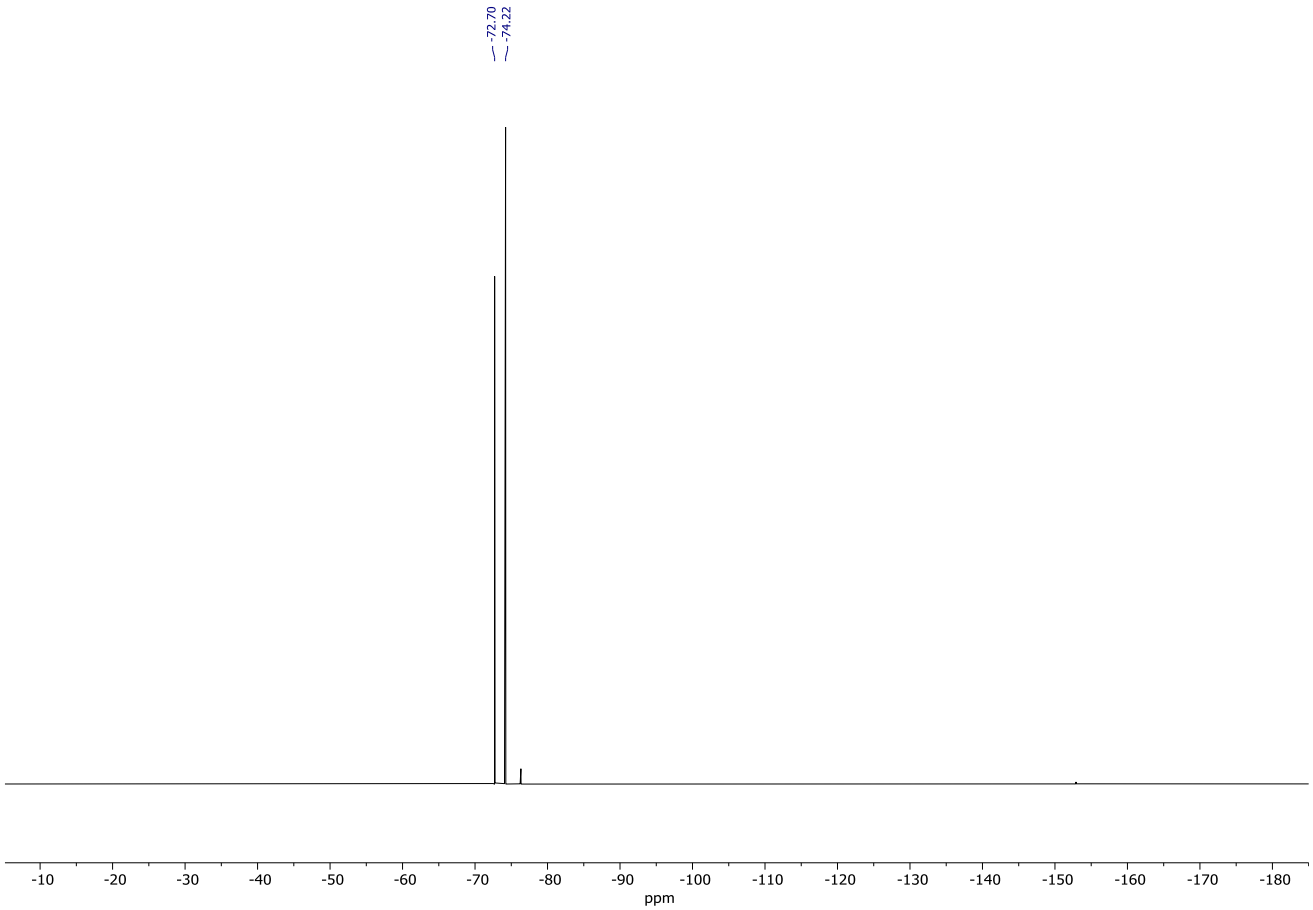

Spectrum 79. ^{19}F NMR (471 MHz, CD_2Cl_2) of **219** (TFA^- salt).

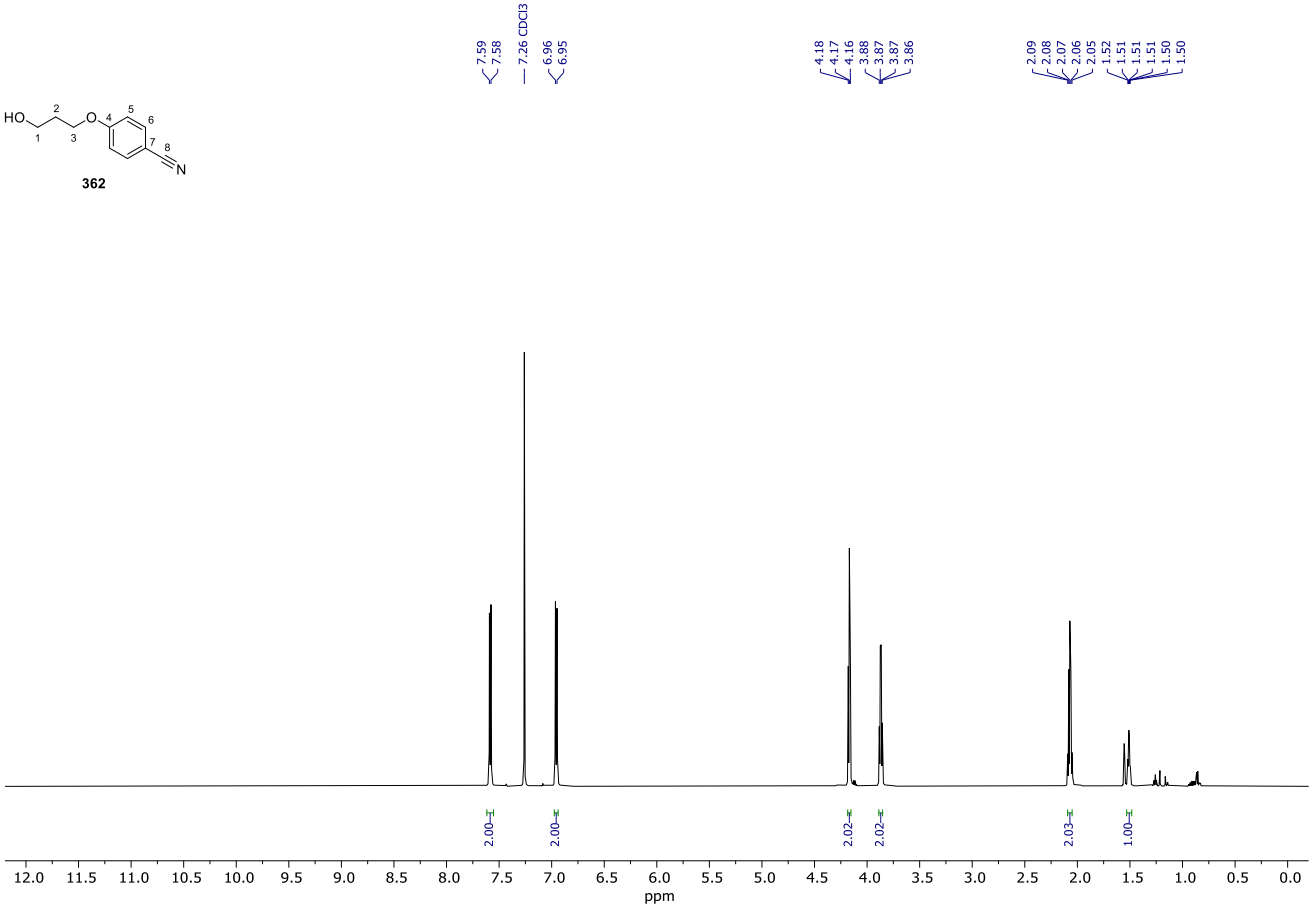

Spectrum 80. ^{1}H NMR (600 MHz, $CDCl_3$) of **362**.

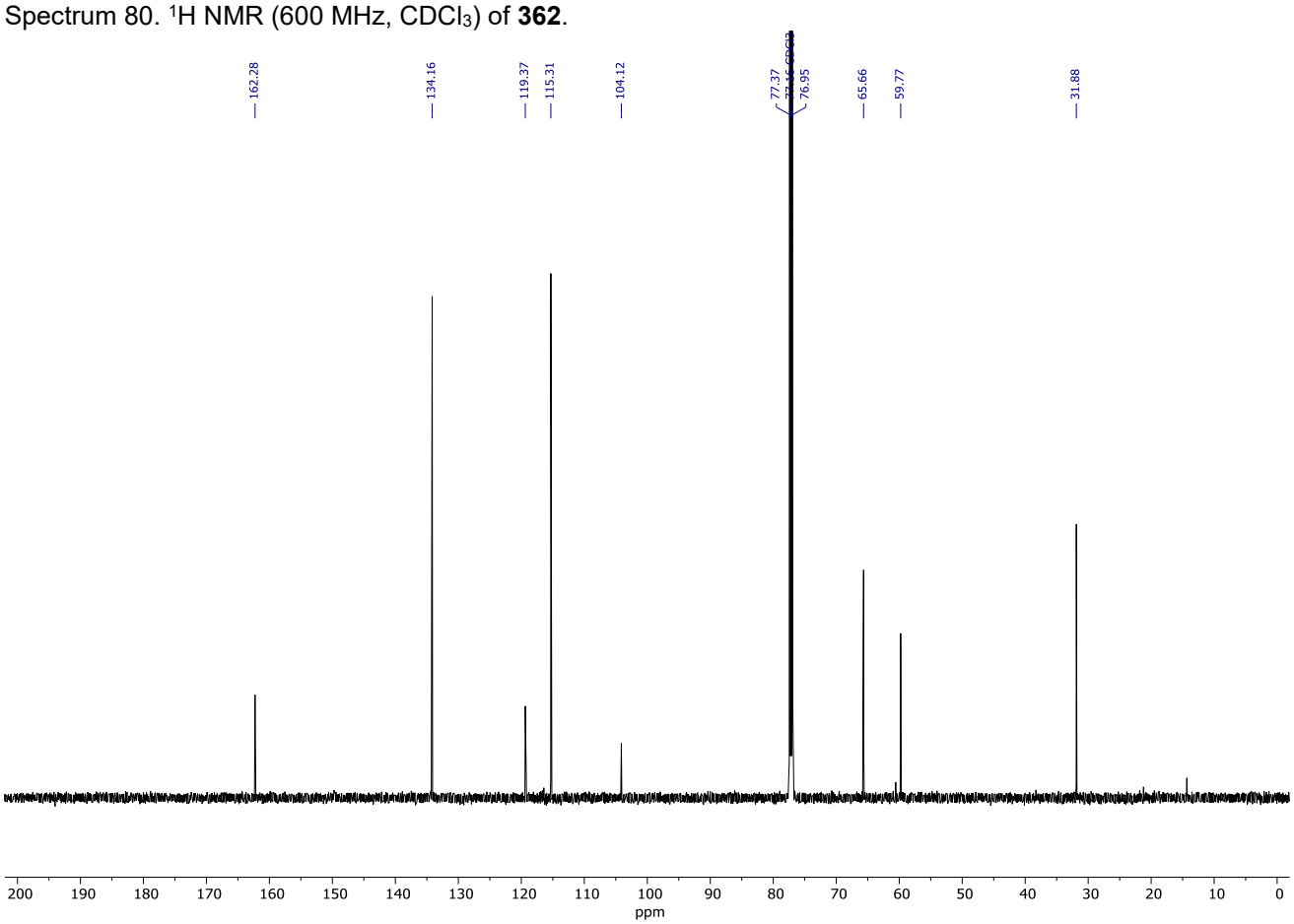

Spectrum 81. ^{13}C NMR (151 MHz, $CDCl_3$) of **362**.

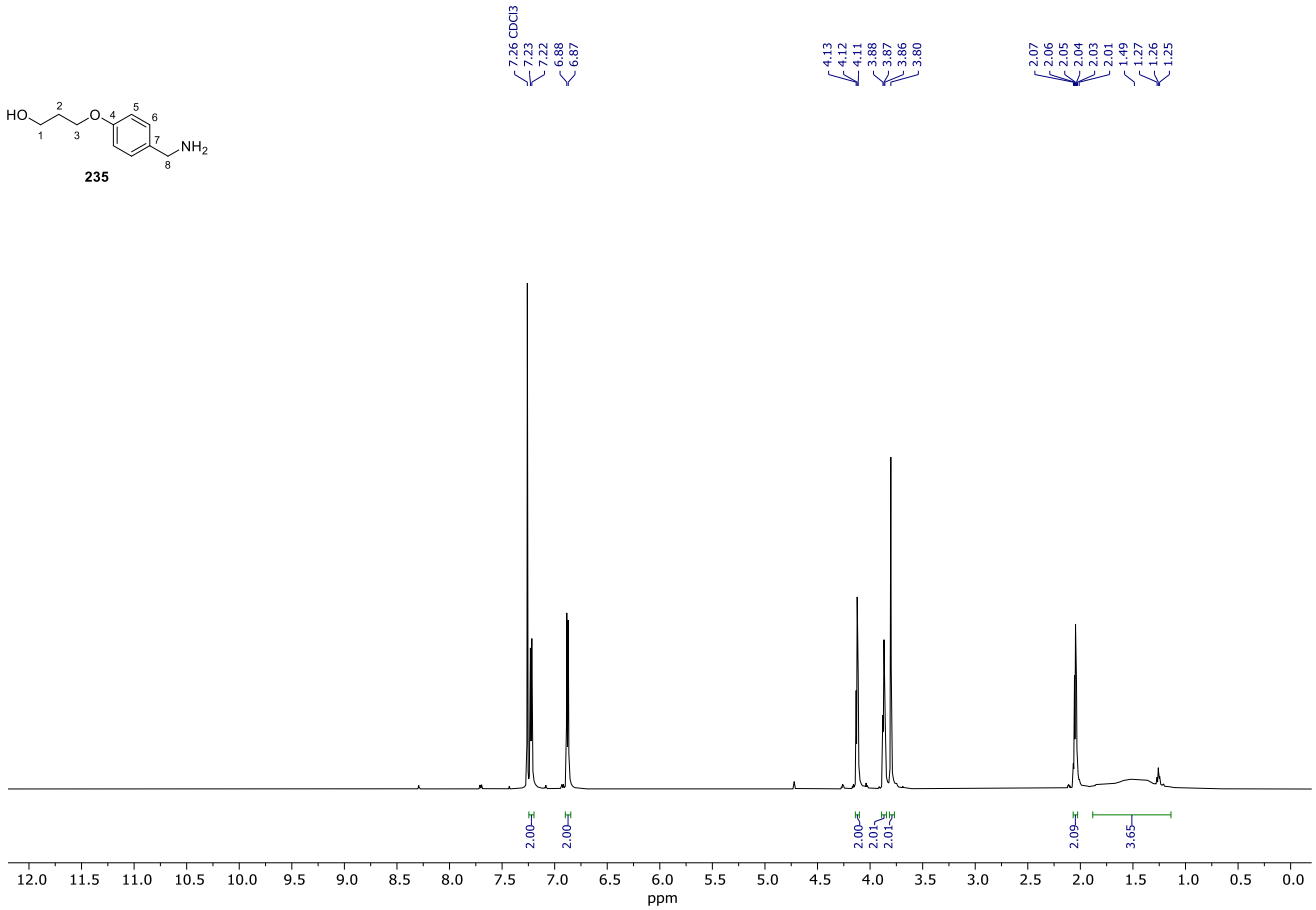

Spectrum 82. ^{1}H NMR (600 MHz, $CDCl_3$) of **235**.

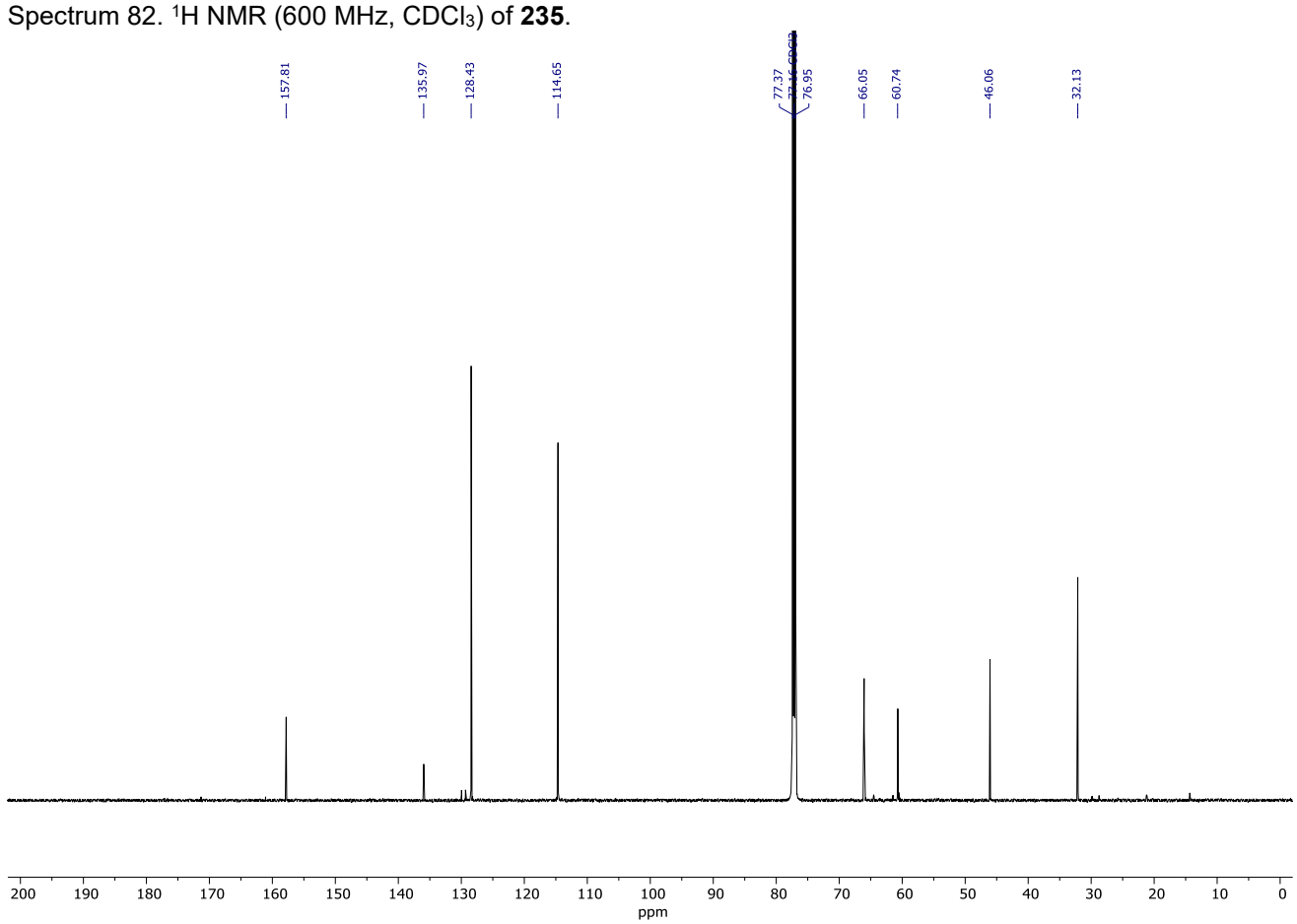

Spectrum 83. ^{13}C NMR (151 MHz, $CDCl_3$) of **235**.

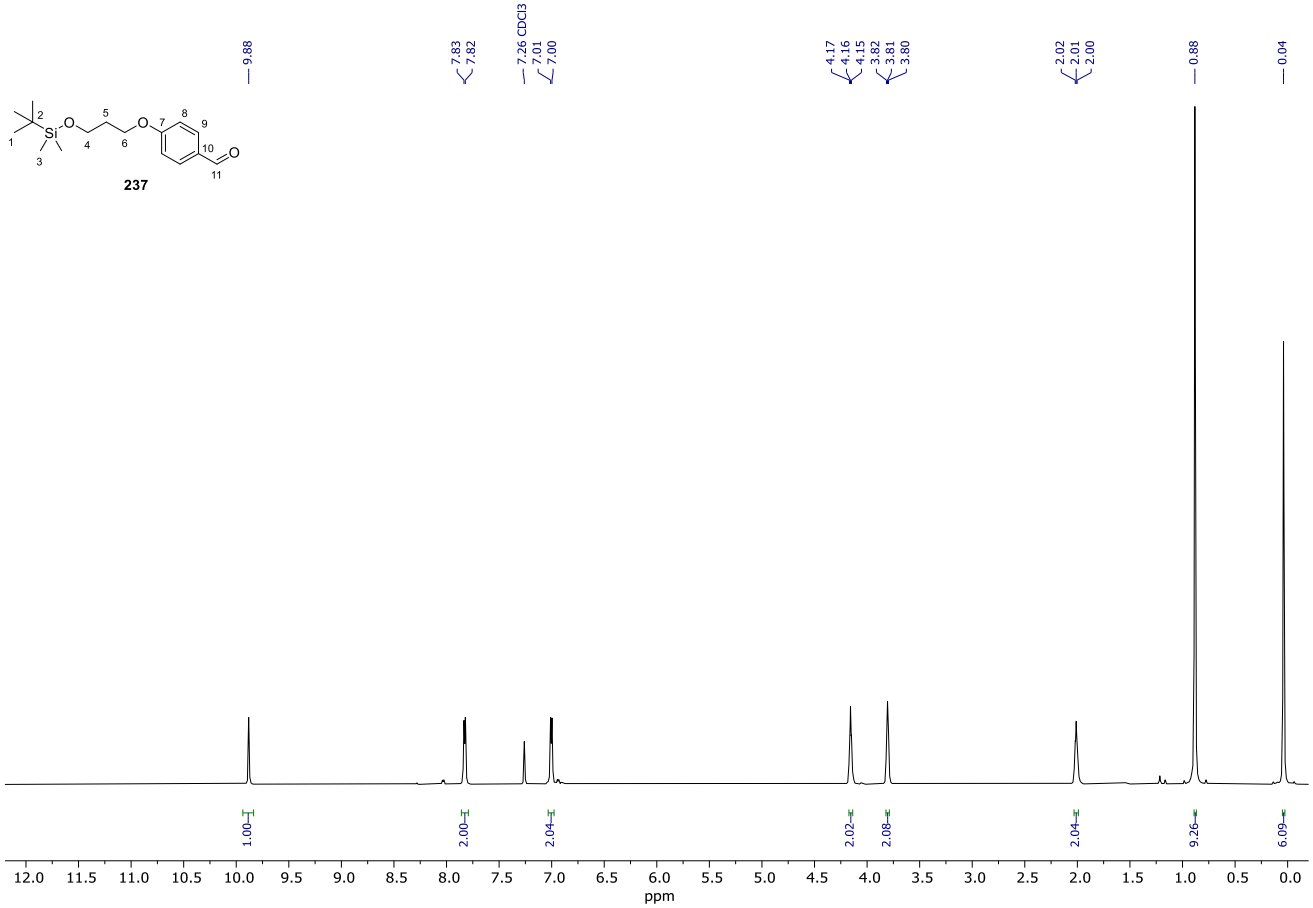

Spectrum 84. ^{1}H NMR (600 MHz, $CDCl_3$) of **237**.

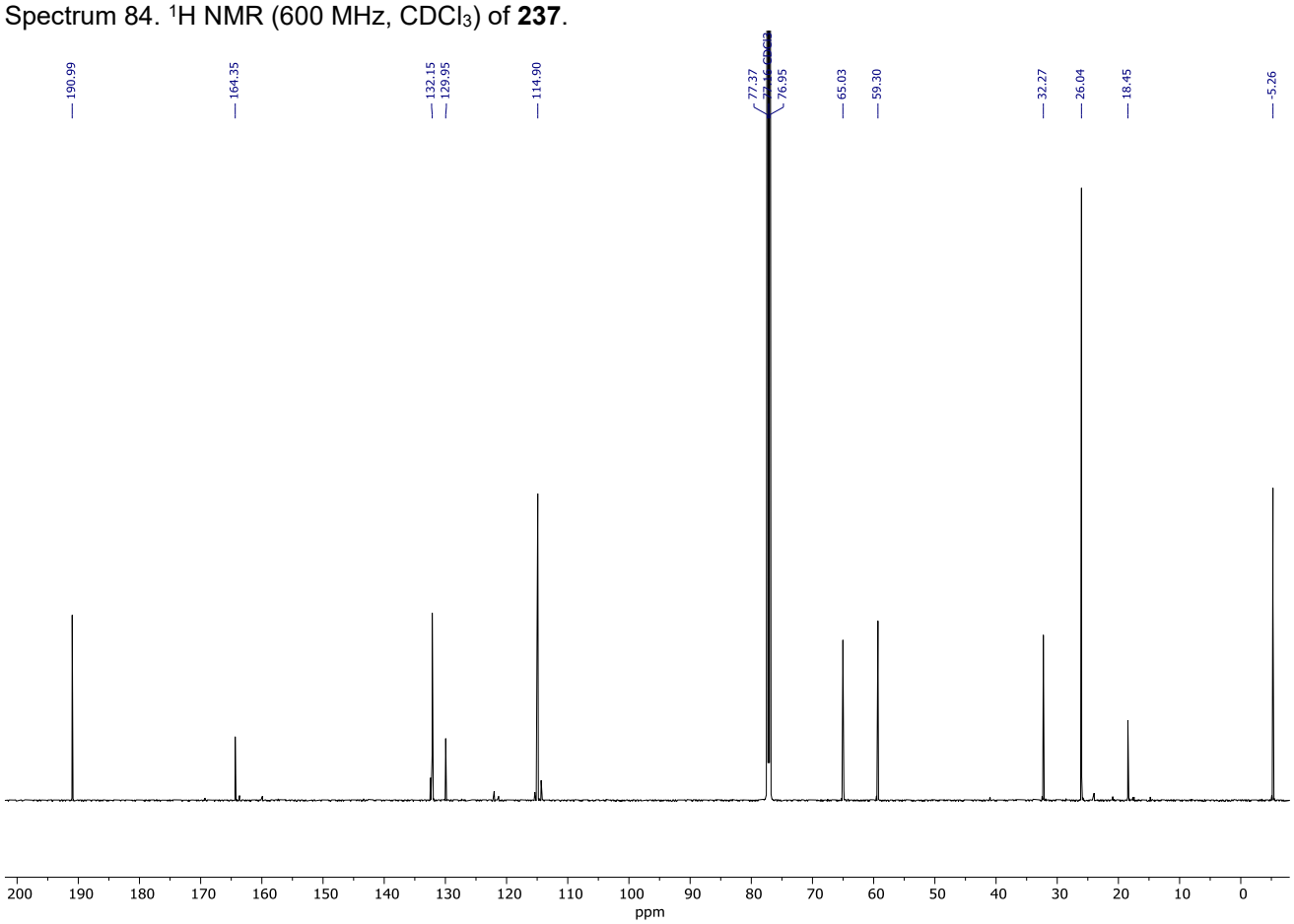

Spectrum 85. ^{13}C NMR (151 MHz, $CDCl_3$) of **237**.

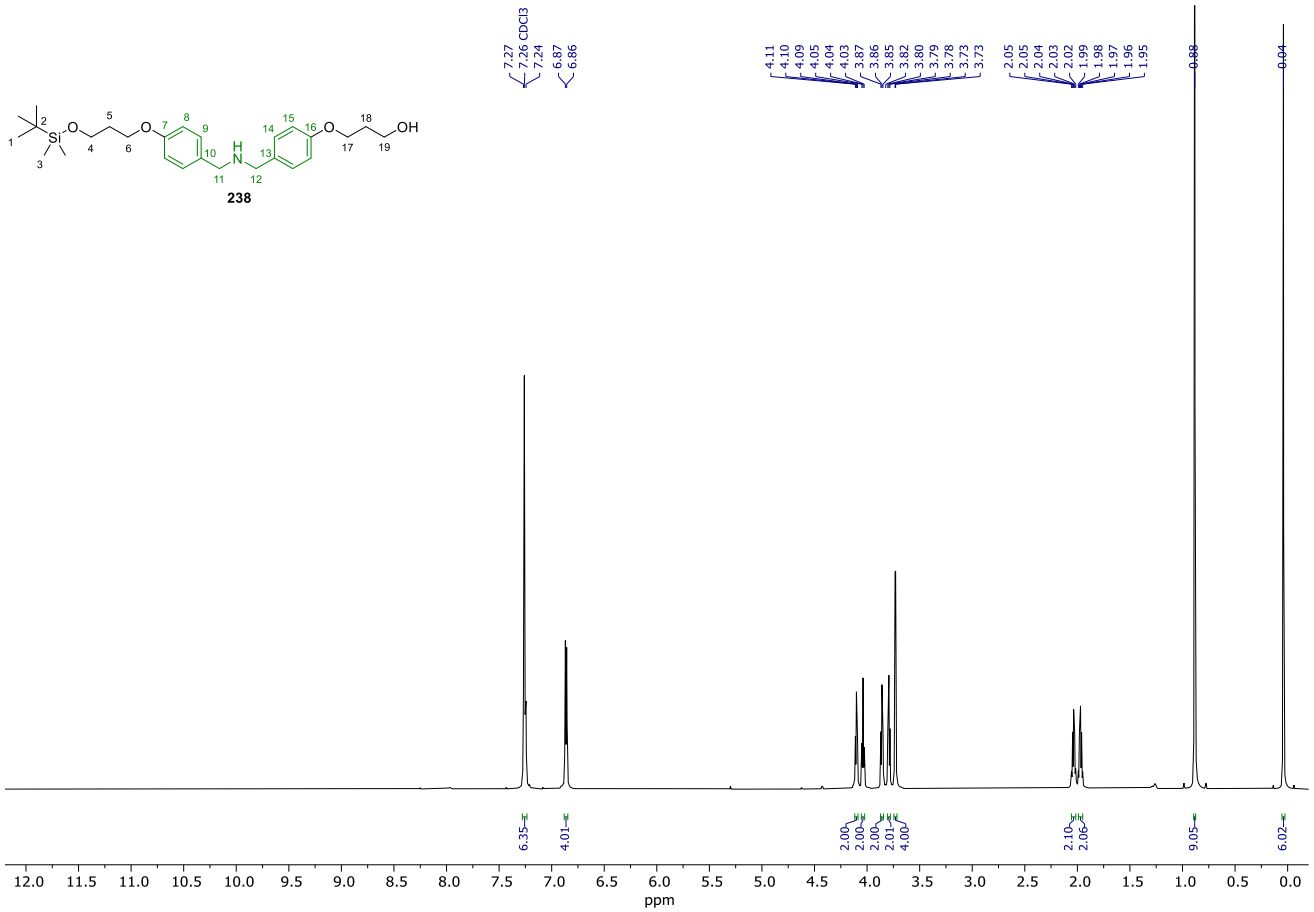

Spectrum 86. ^{1}H NMR (600 MHz, $CDCl_3$) of **238**.

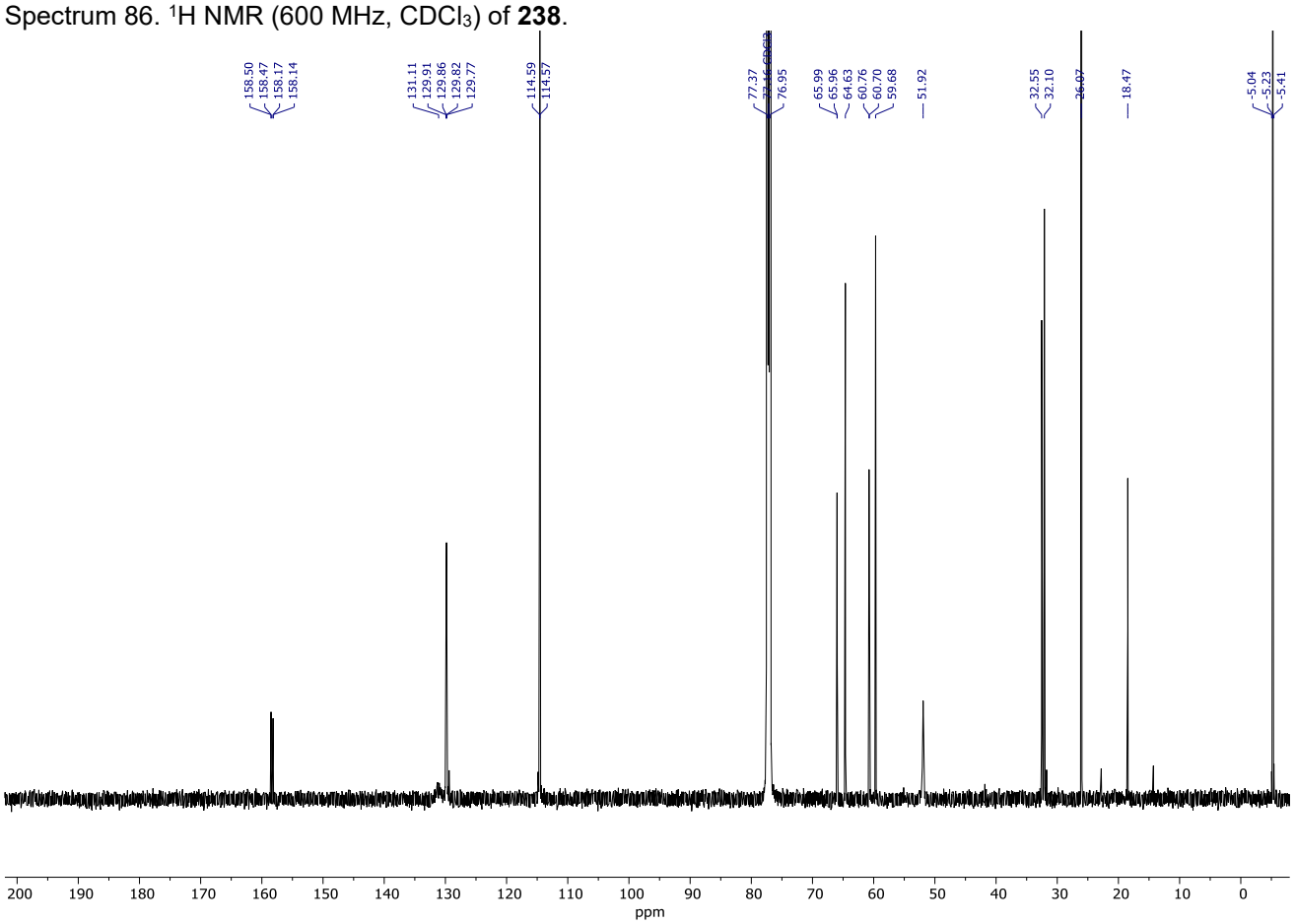

Spectrum 87. ^{13}C NMR (151 MHz, $CDCl_3$) of **238**.

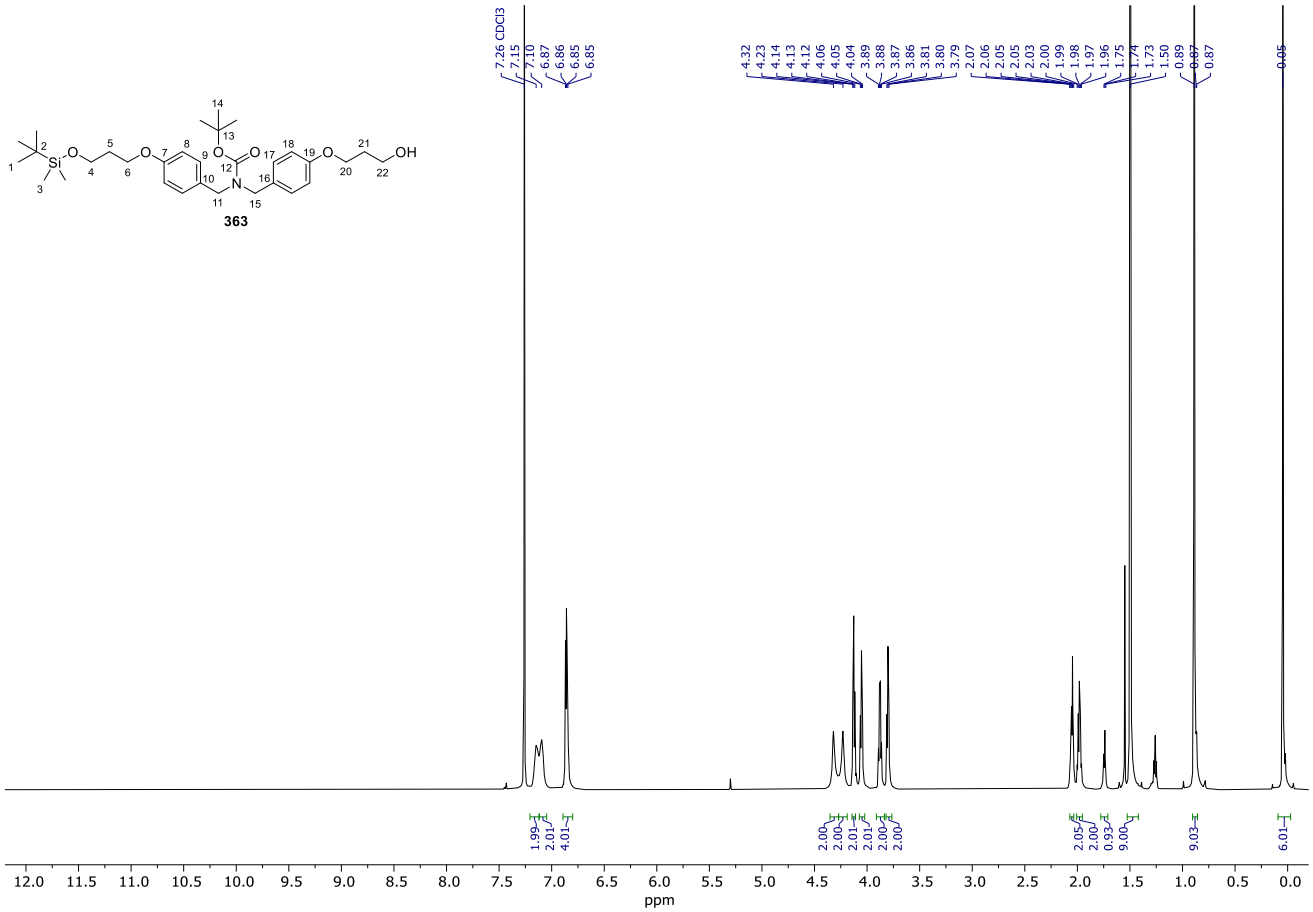

Spectrum 88. ^{1}H NMR (600 MHz, $CDCl_3$) of **363**.

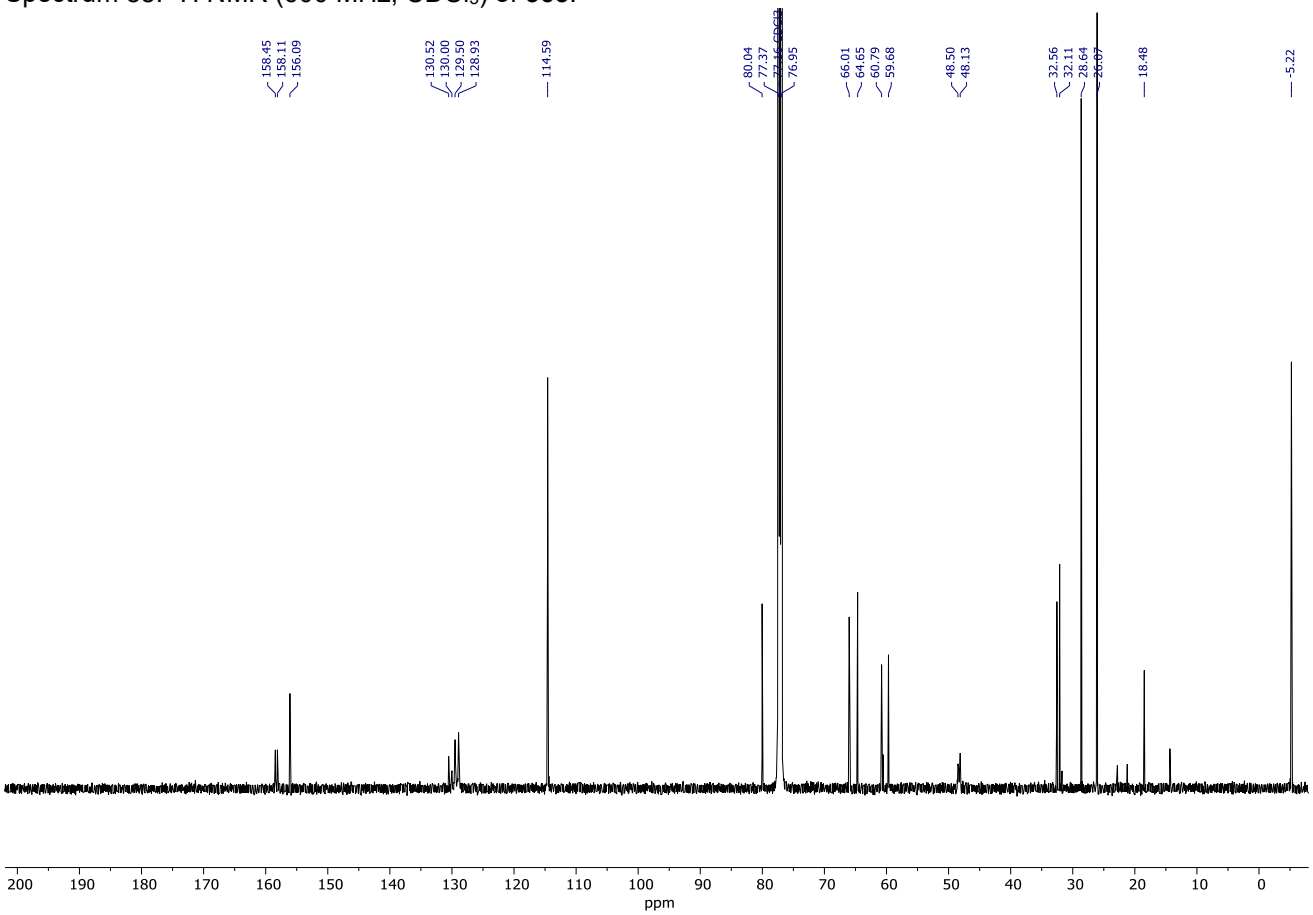

Spectrum 89. ^{13}C NMR (151 MHz, $CDCl_3$) of **363**.

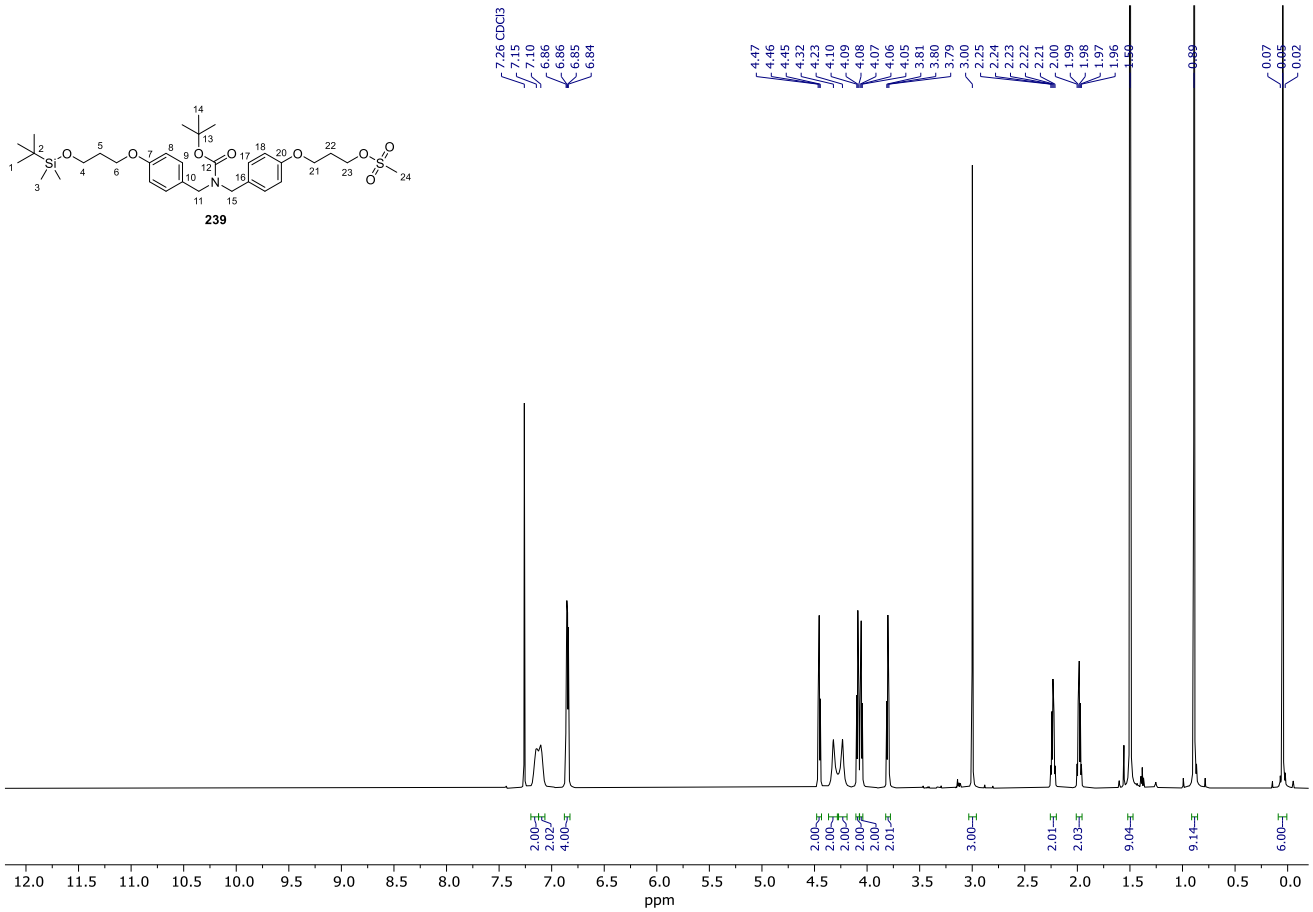

Spectrum 90. ^{1}H NMR (600 MHz, $CDCl_3$) of **239**.

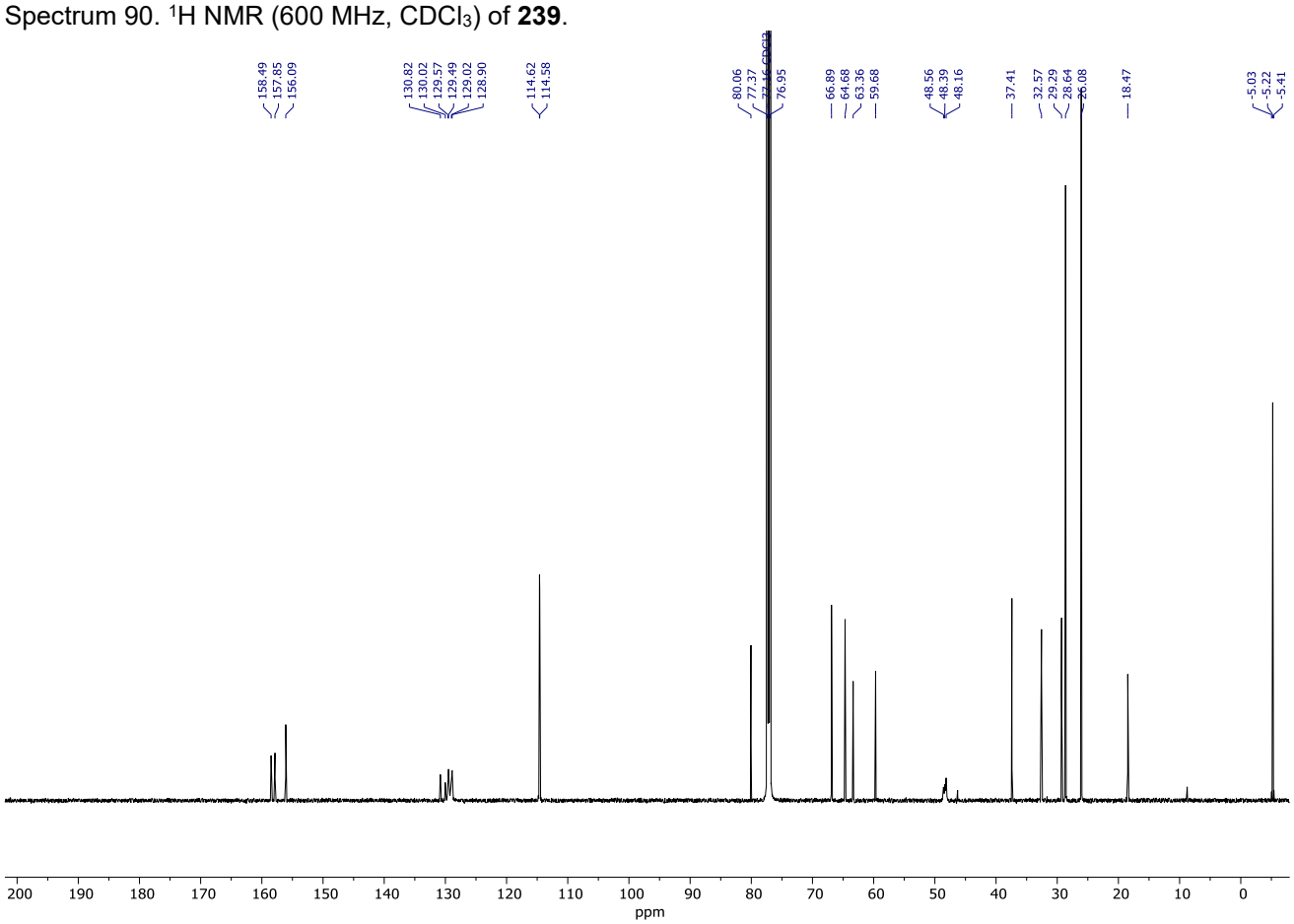

Spectrum 91. ^{13}C NMR (151 MHz, $CDCl_3$) of **239**.

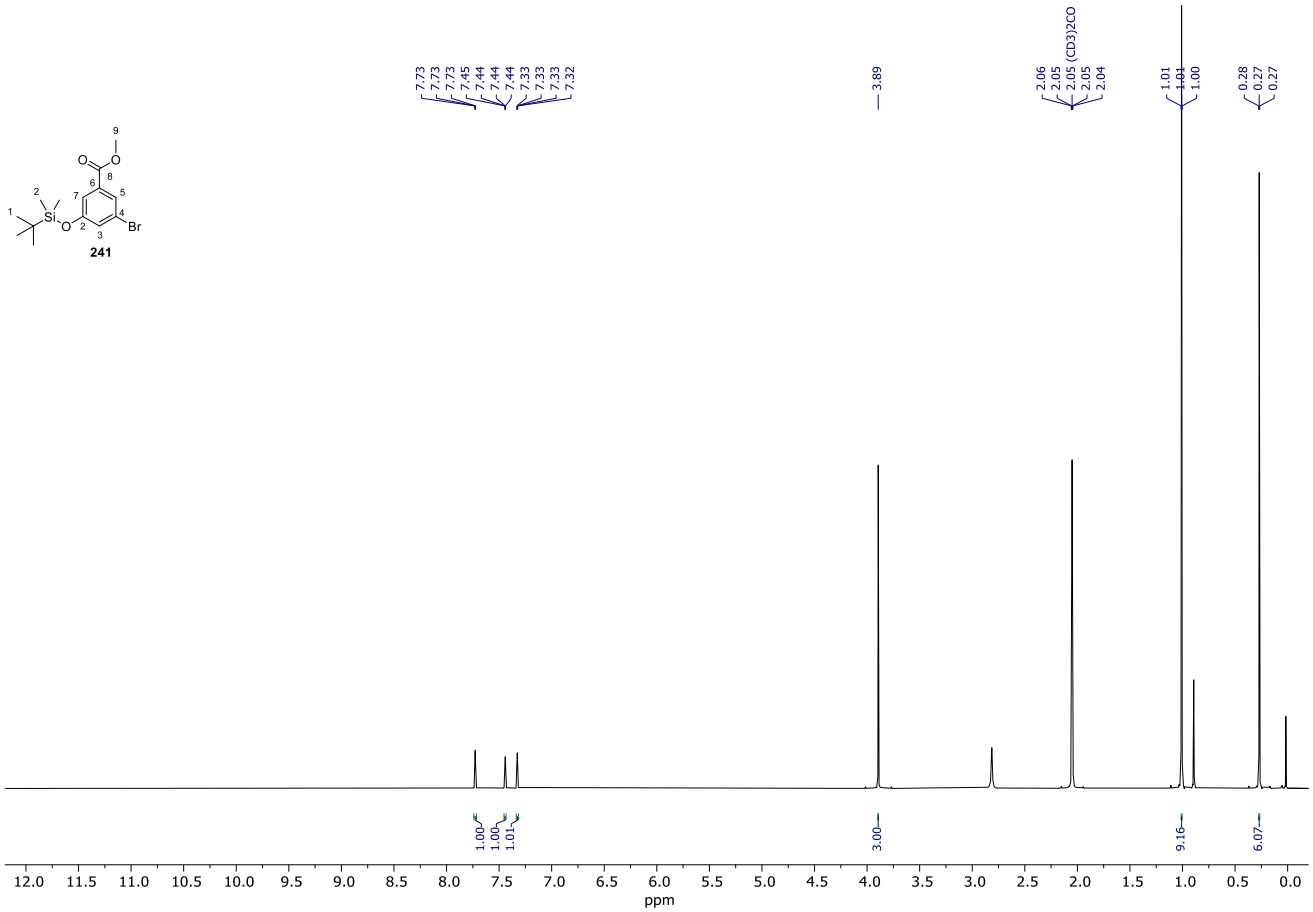

Spectrum 92. ^{1}H NMR (600 MHz, $(CD_3)_2CO$) of **241**.

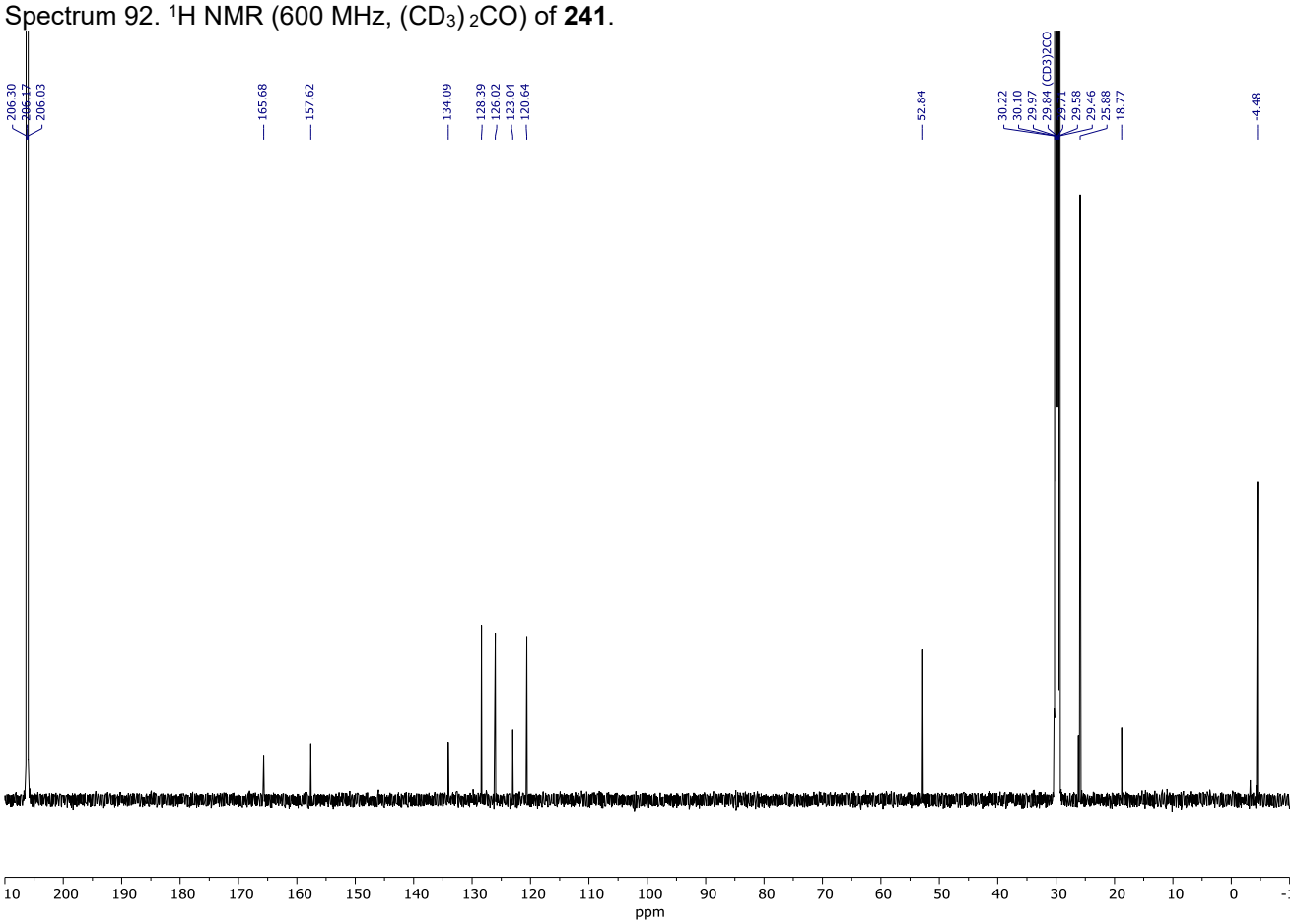

Spectrum 93. ^{13}C NMR (151 MHz, $(CD_3)_2CO$) of **241**.

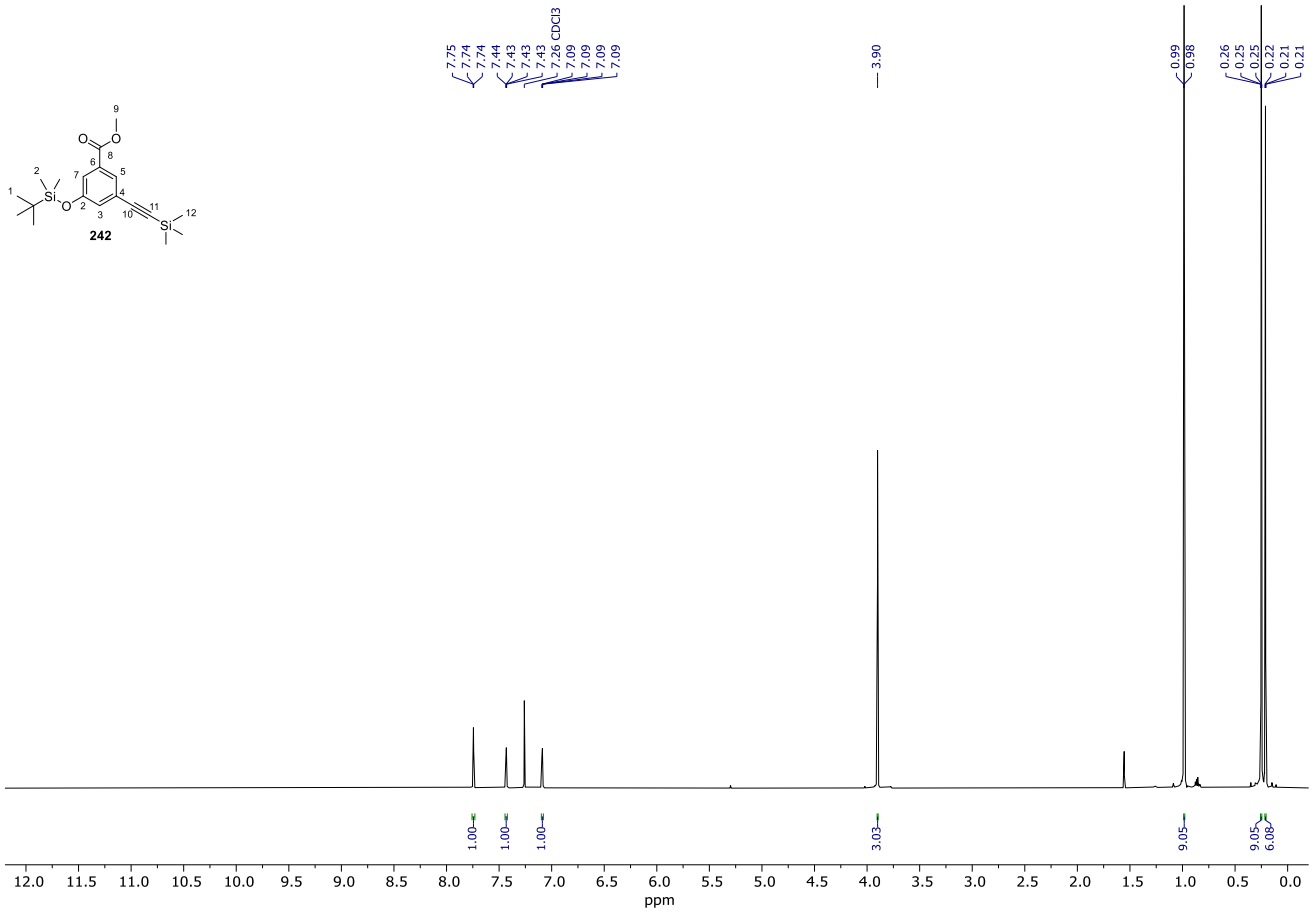

Spectrum 94. ^{1}H NMR (600 MHz, $CDCl_3$) of **242**.

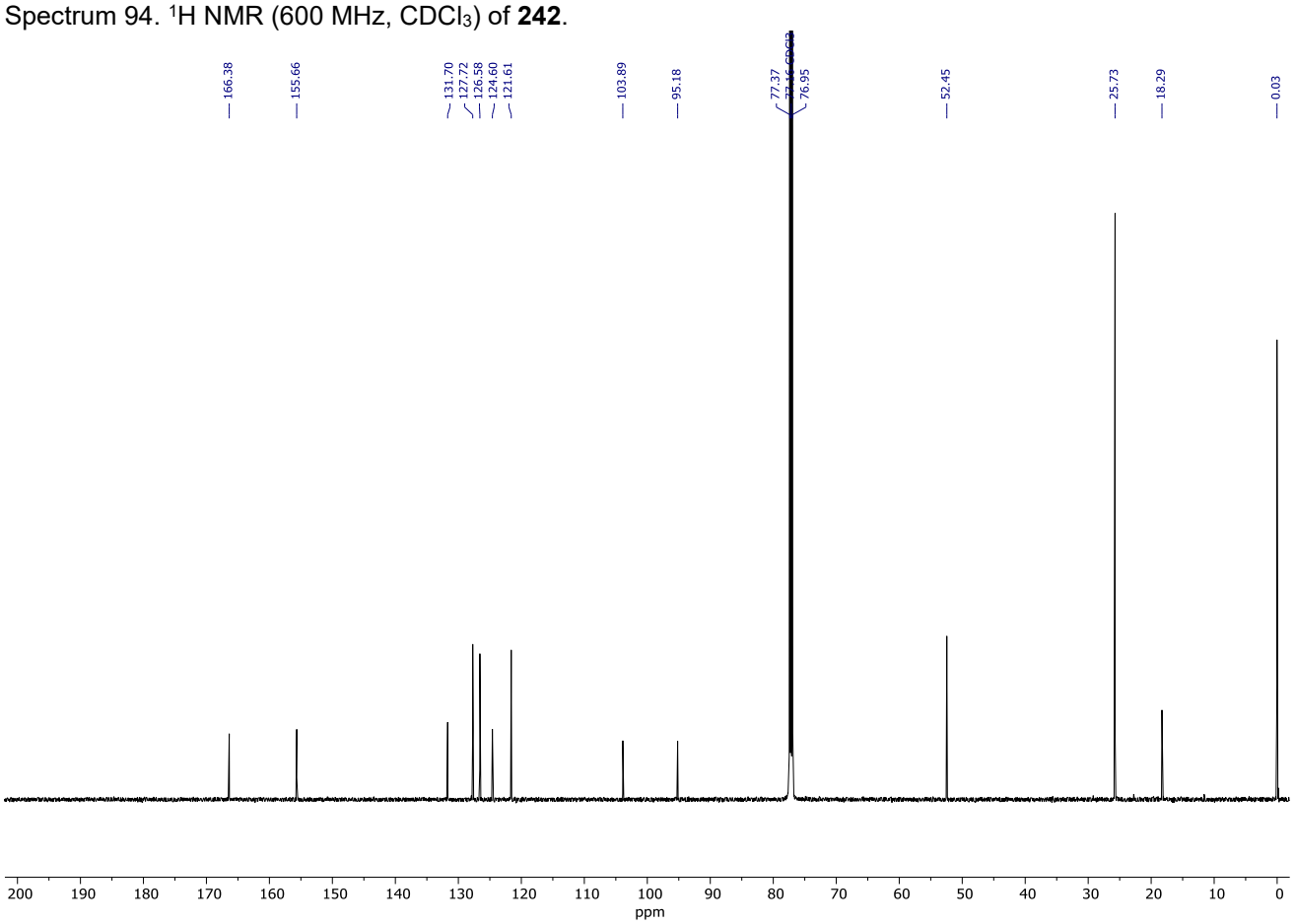

Spectrum 95. ^{13}C NMR (151 MHz, $CDCl_3$) of **242**.

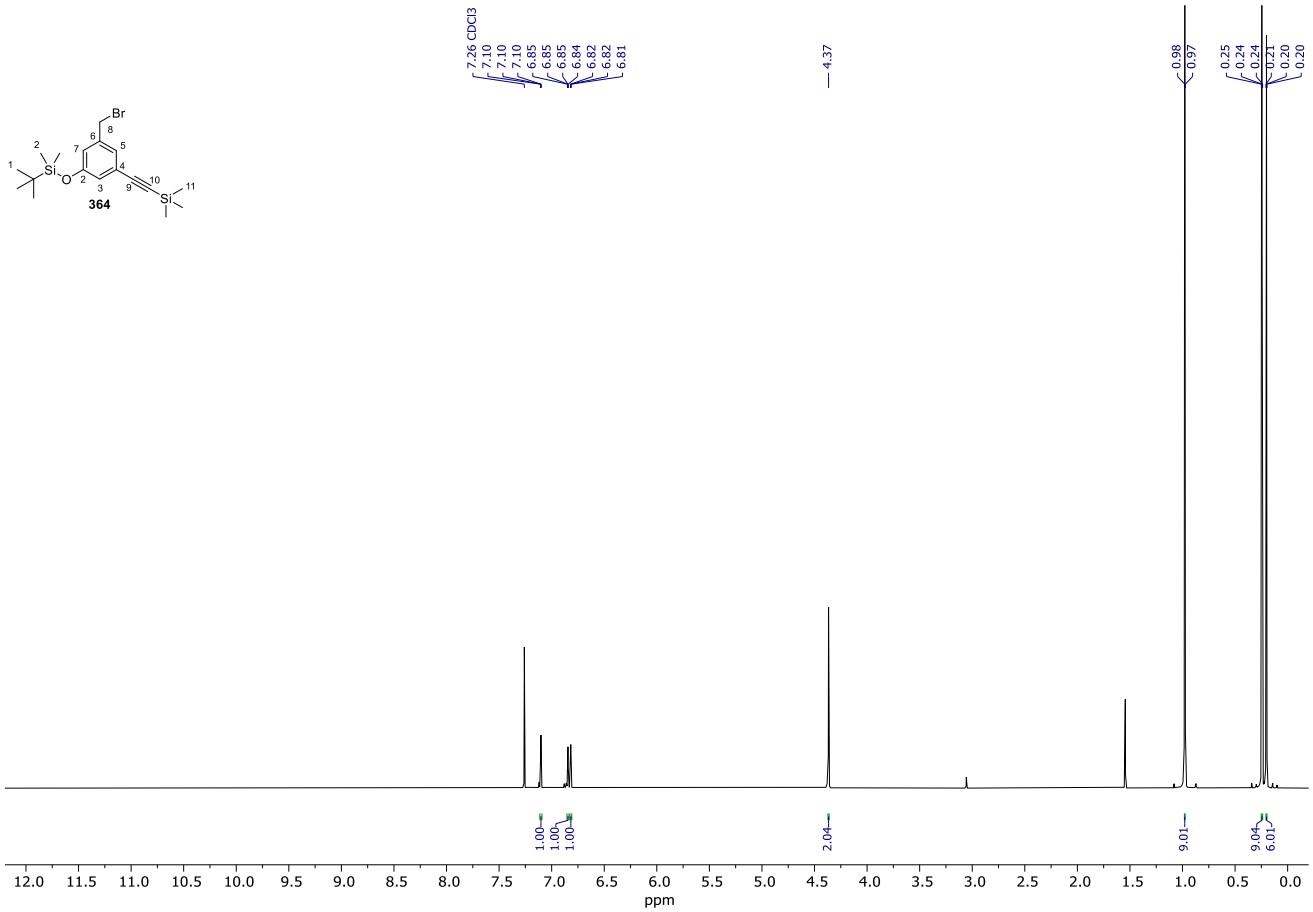

Spectrum 96. ^{1}H NMR (600 MHz, $CDCl_3$) of **364**.

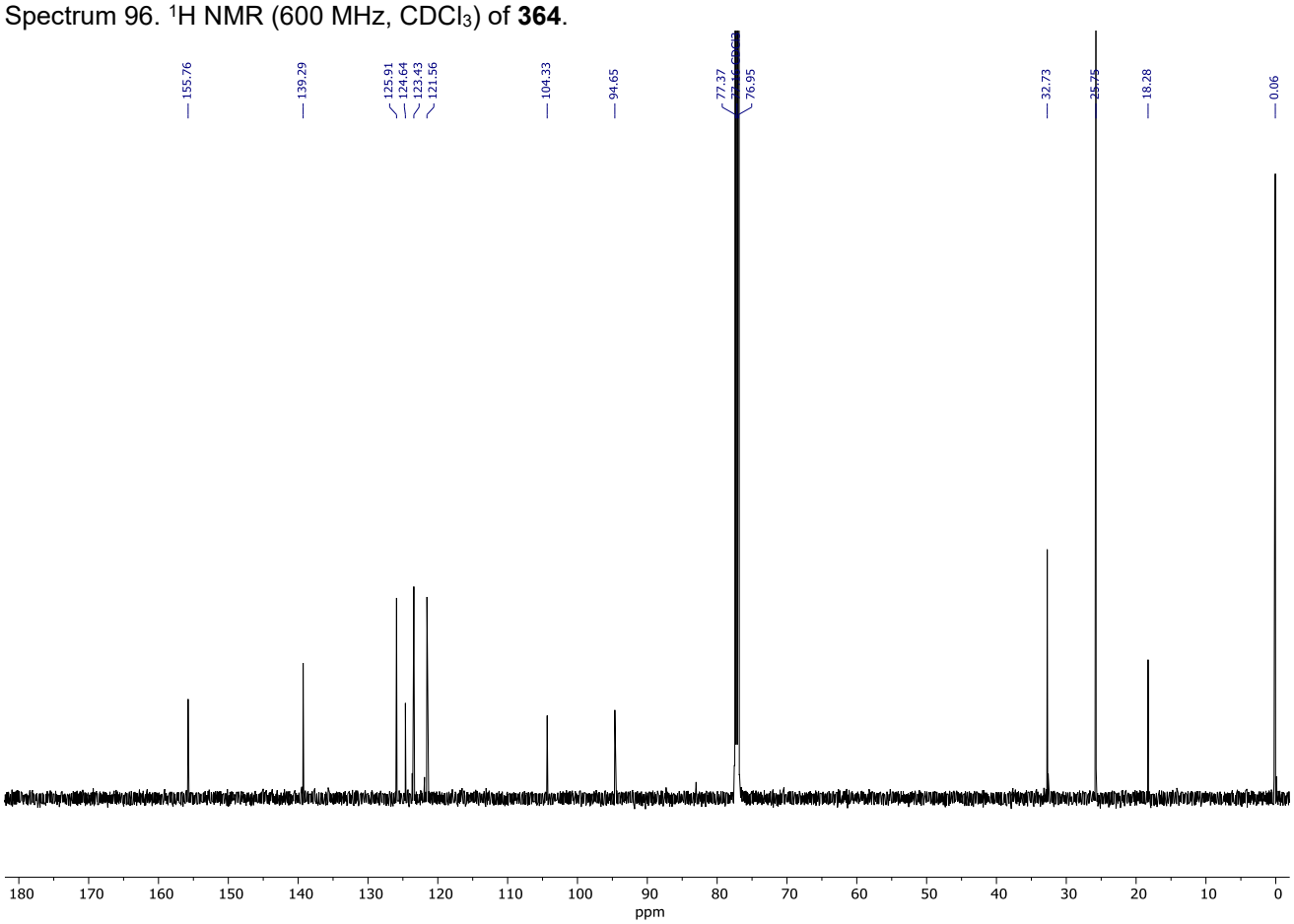

Spectrum 97. ^{13}C NMR (151 MHz, $CDCl_3$) of **364**.

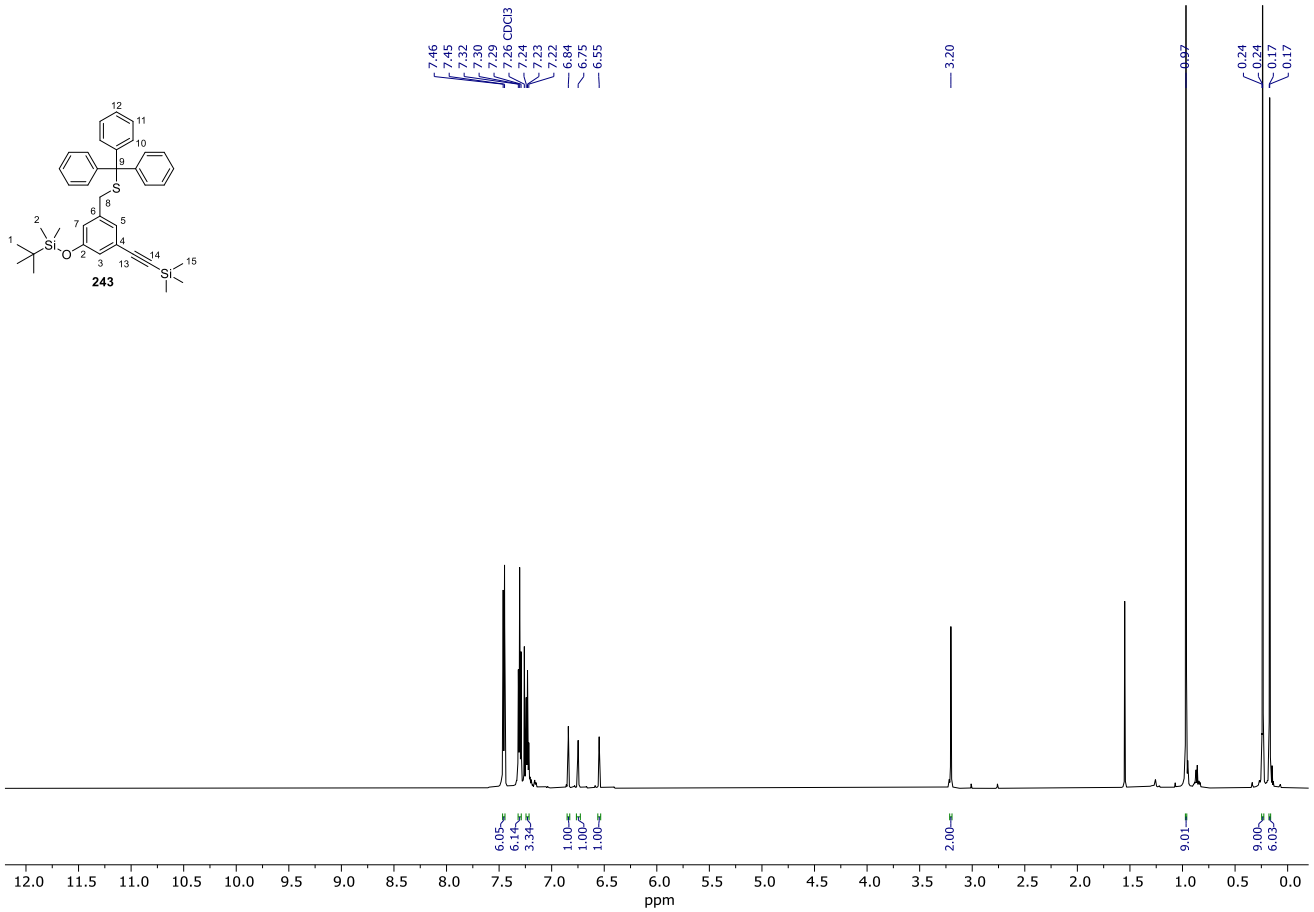

Spectrum 98. ^{1}H NMR (600 MHz, $CDCl_3$) of **243**.

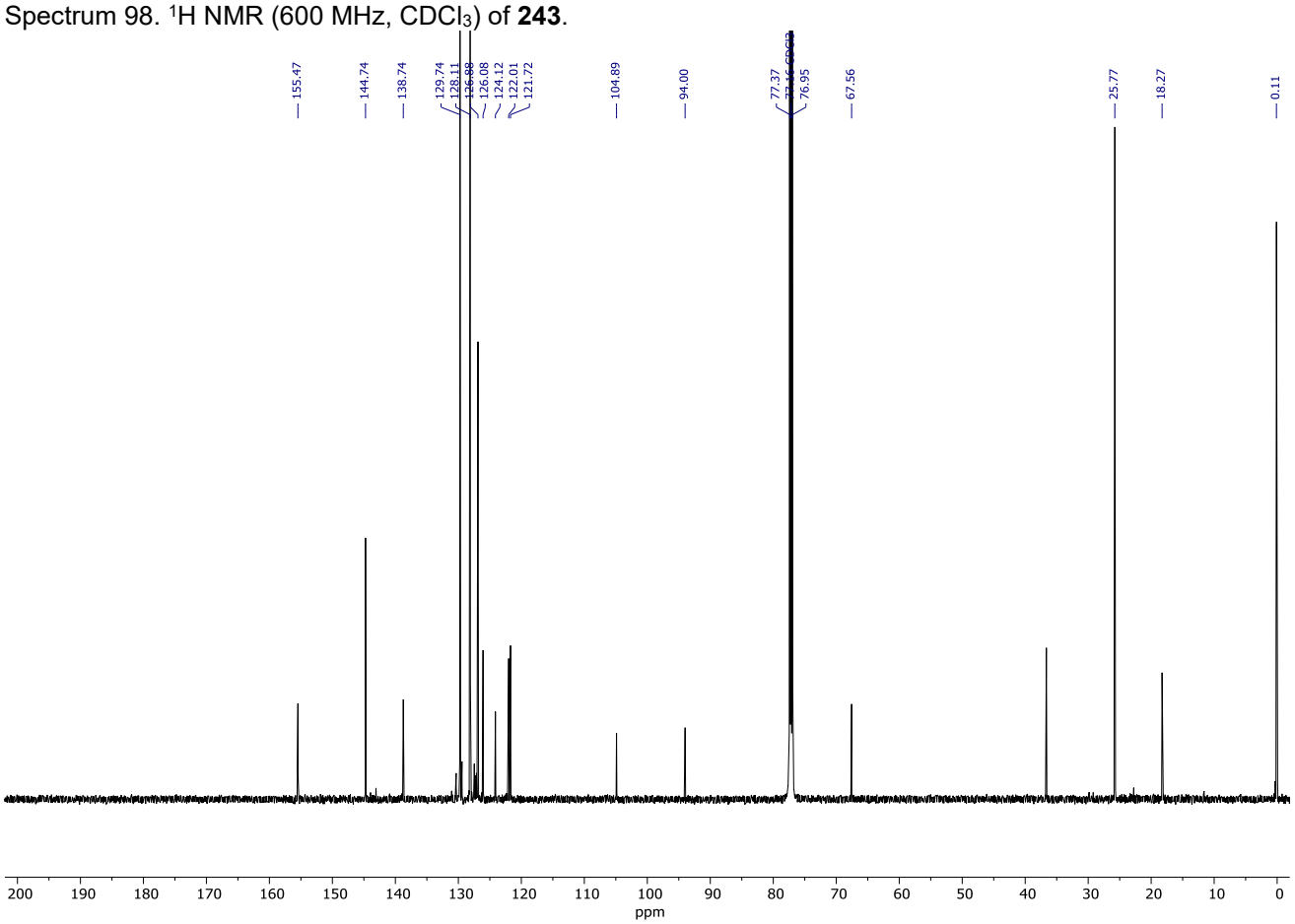

Spectrum 99. ^{13}C NMR (151 MHz, $CDCl_3$) of **243**.

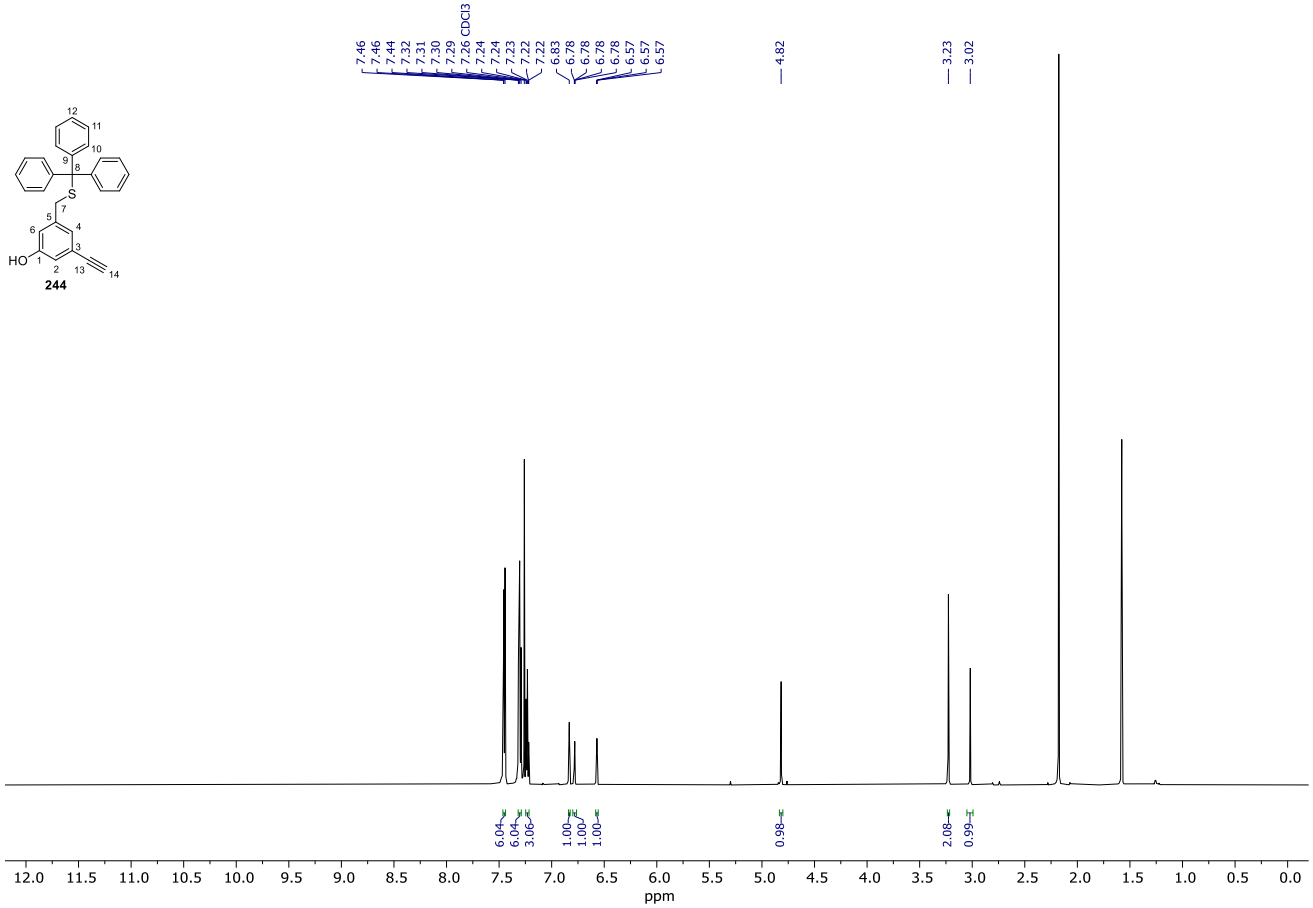

Spectrum 100. ^{1}H NMR (600 MHz, $CDCl_3$) of **244**.

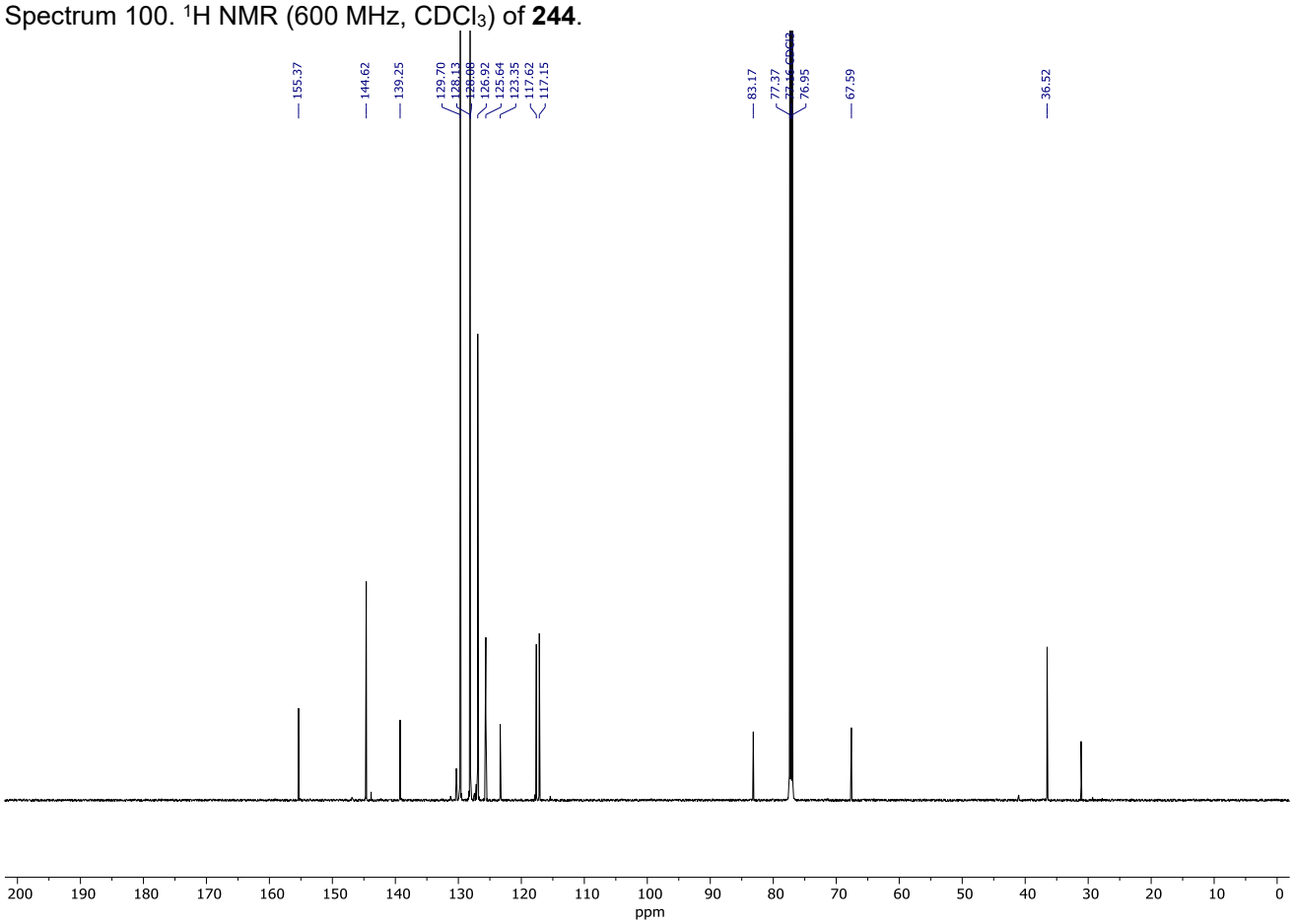

Spectrum 101. ^{13}C NMR (151 MHz, $CDCl_3$) of **244**.

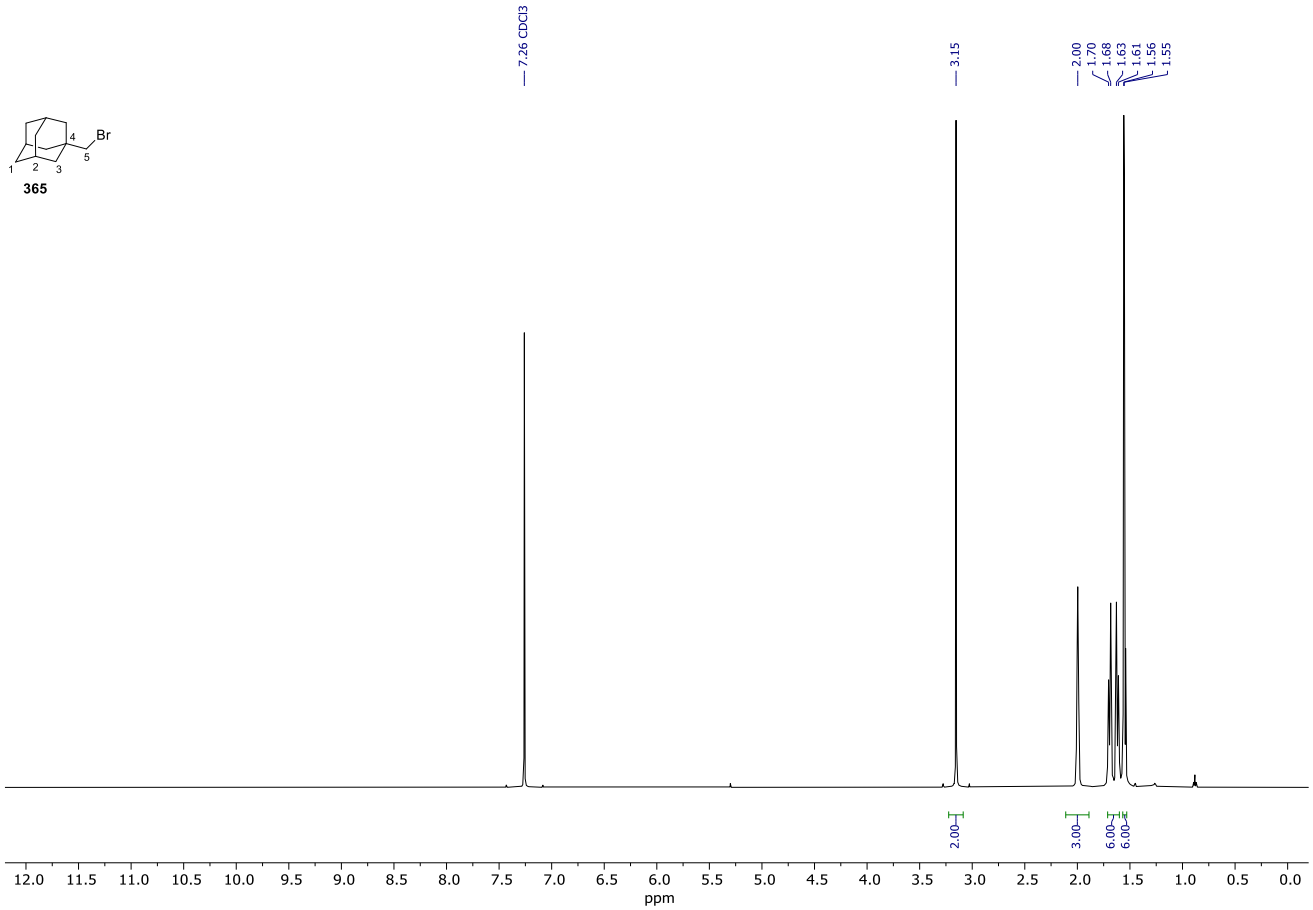

Spectrum 102. ^{1}H NMR (600 MHz, $CDCl_3$) of **365**.

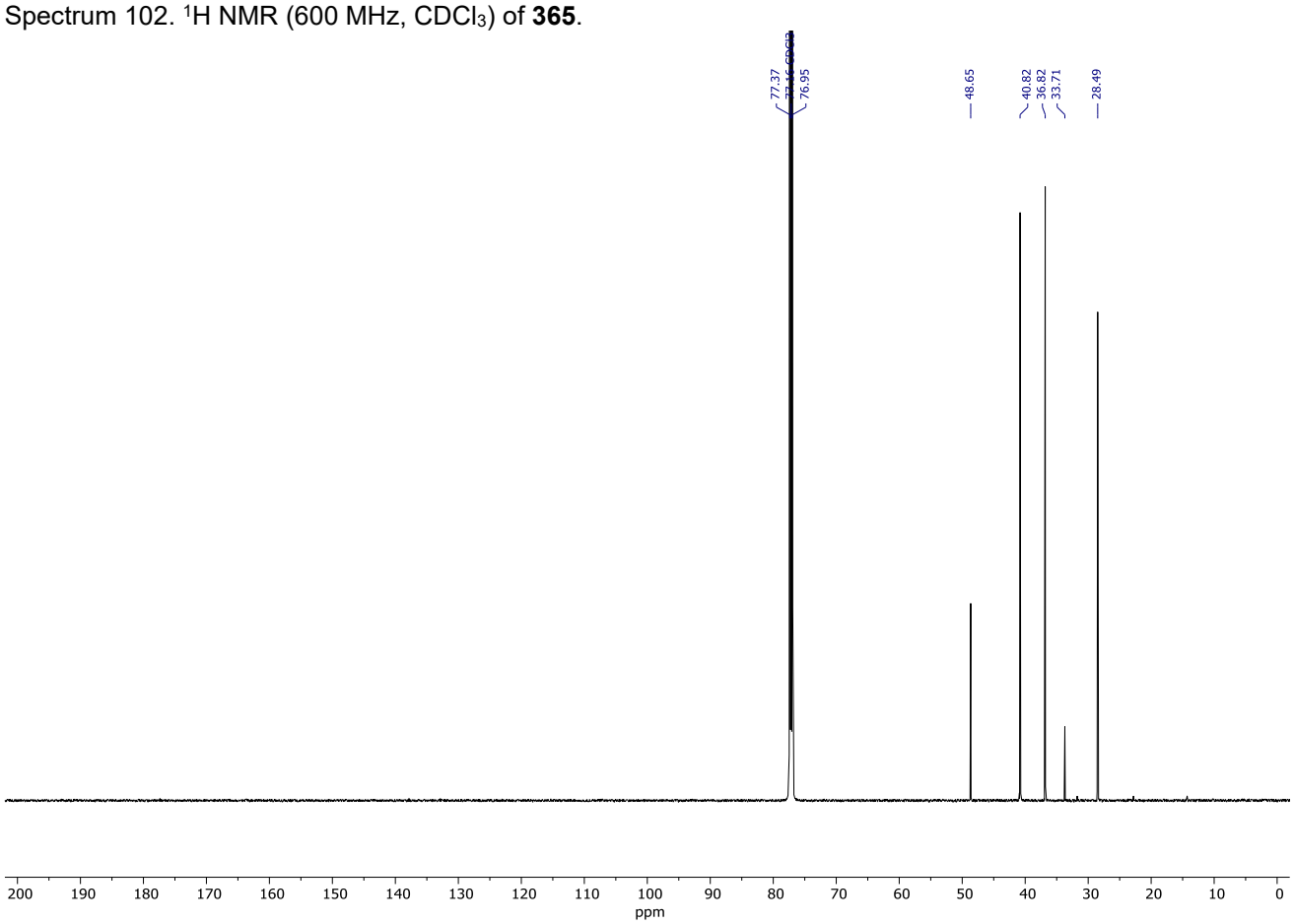

Spectrum 103. ^{13}C NMR (151 MHz, $CDCl_3$) of **365**.

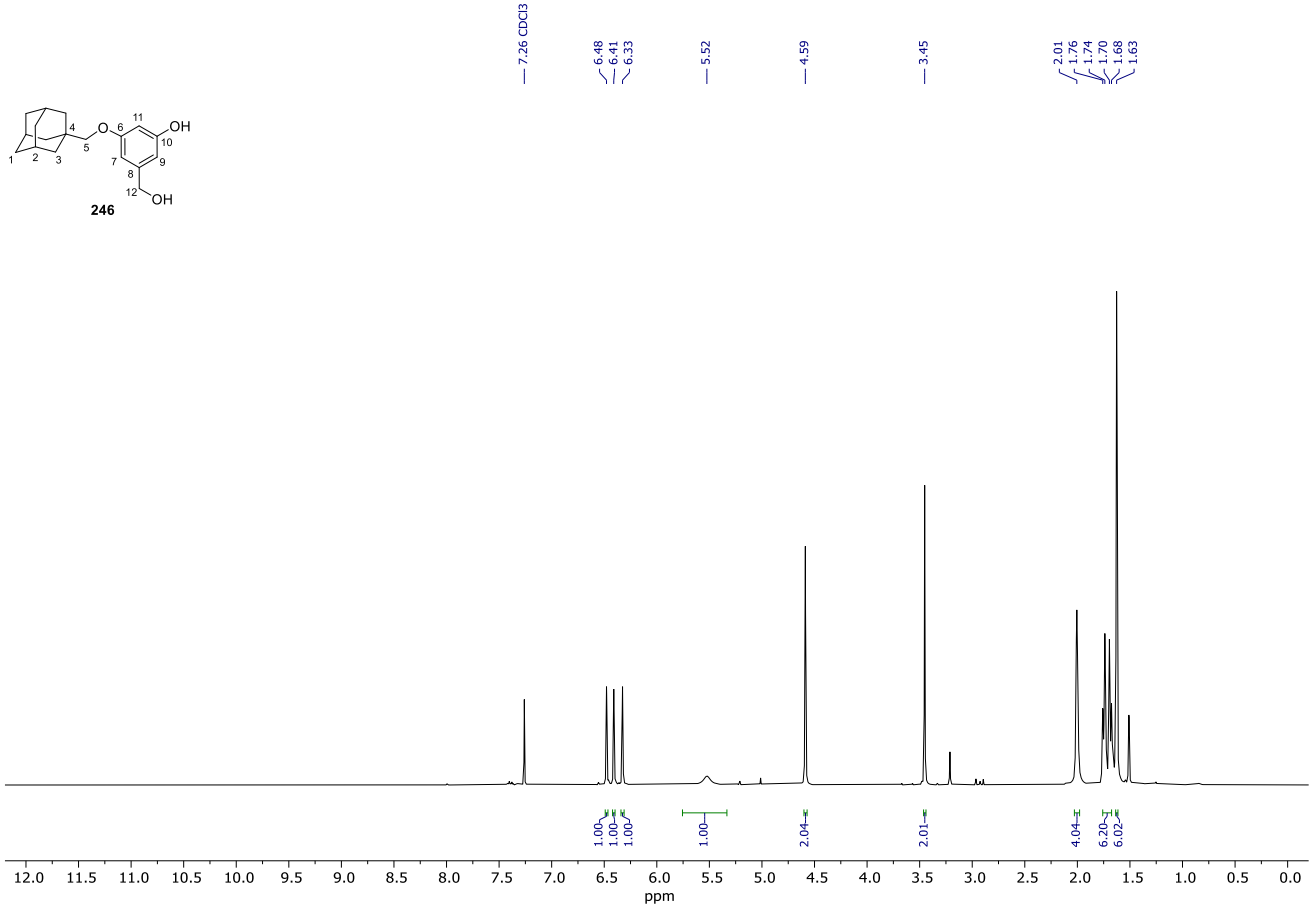

Spectrum 104. ^{1}H NMR (600 MHz, $CDCl_3$) of **246**.

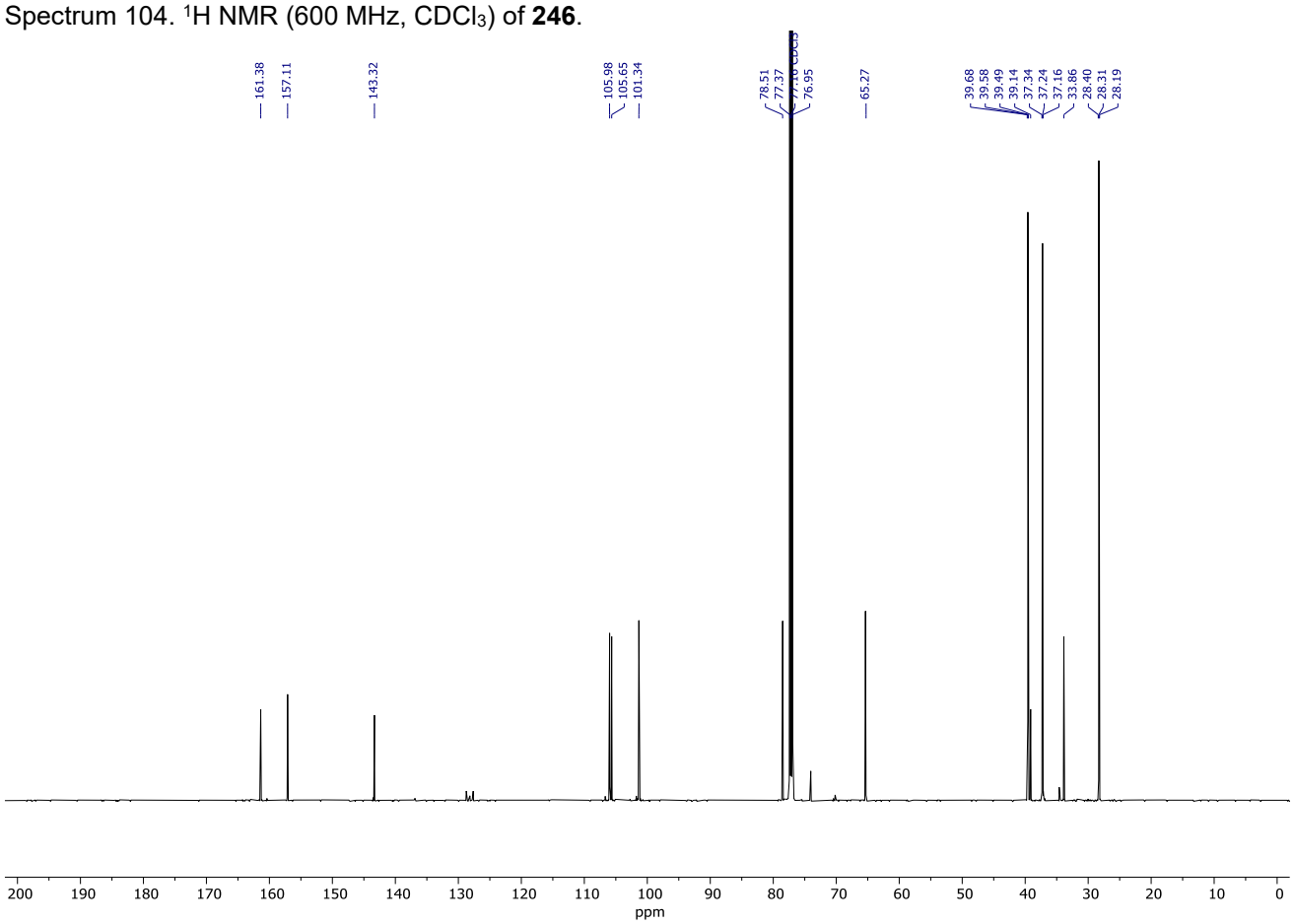

Spectrum 105. ^{13}C NMR (151 MHz, $CDCl_3$) of **246**.

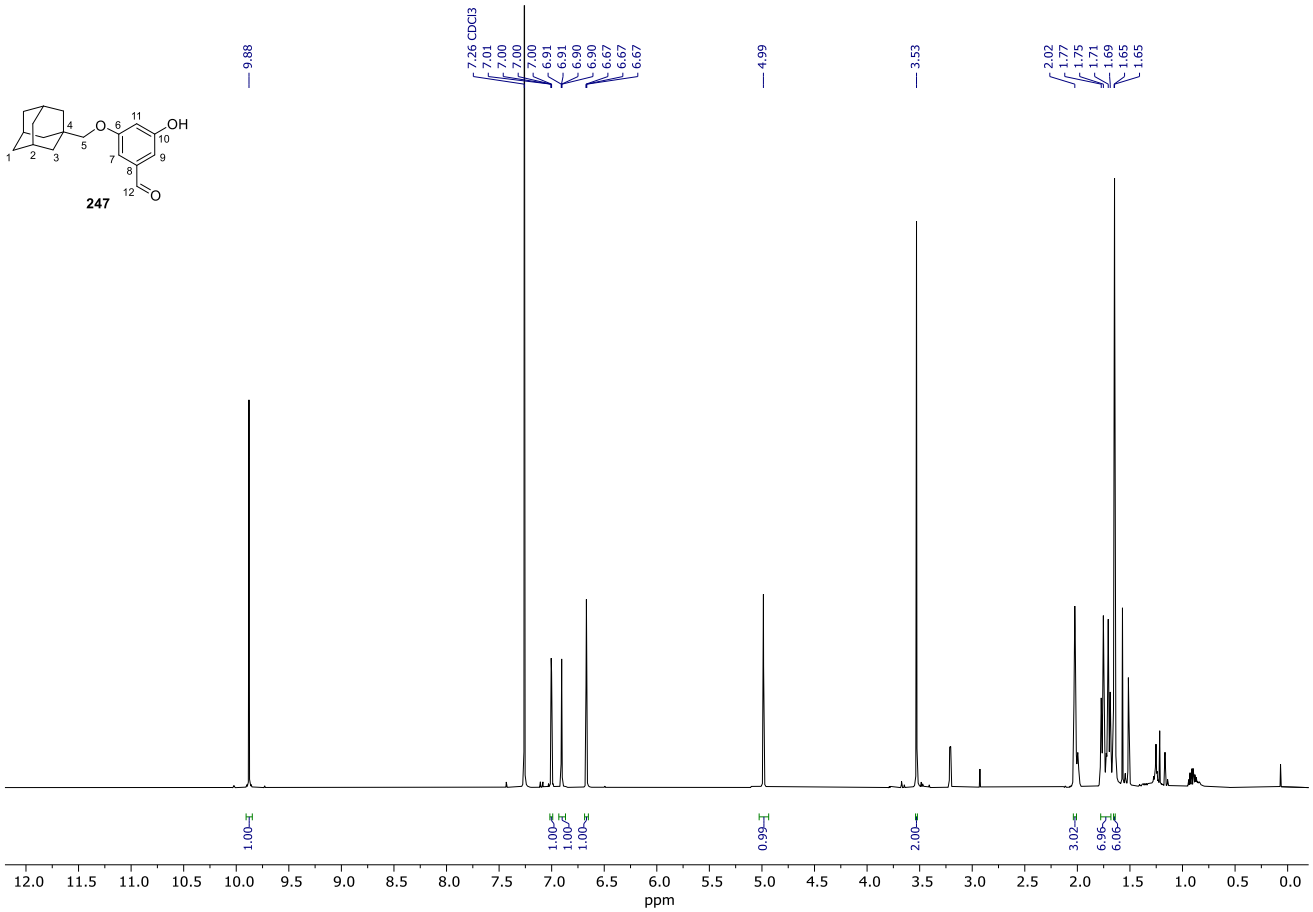

Spectrum 106. ^{1}H NMR (600 MHz, $CDCl_3$) of **247**.

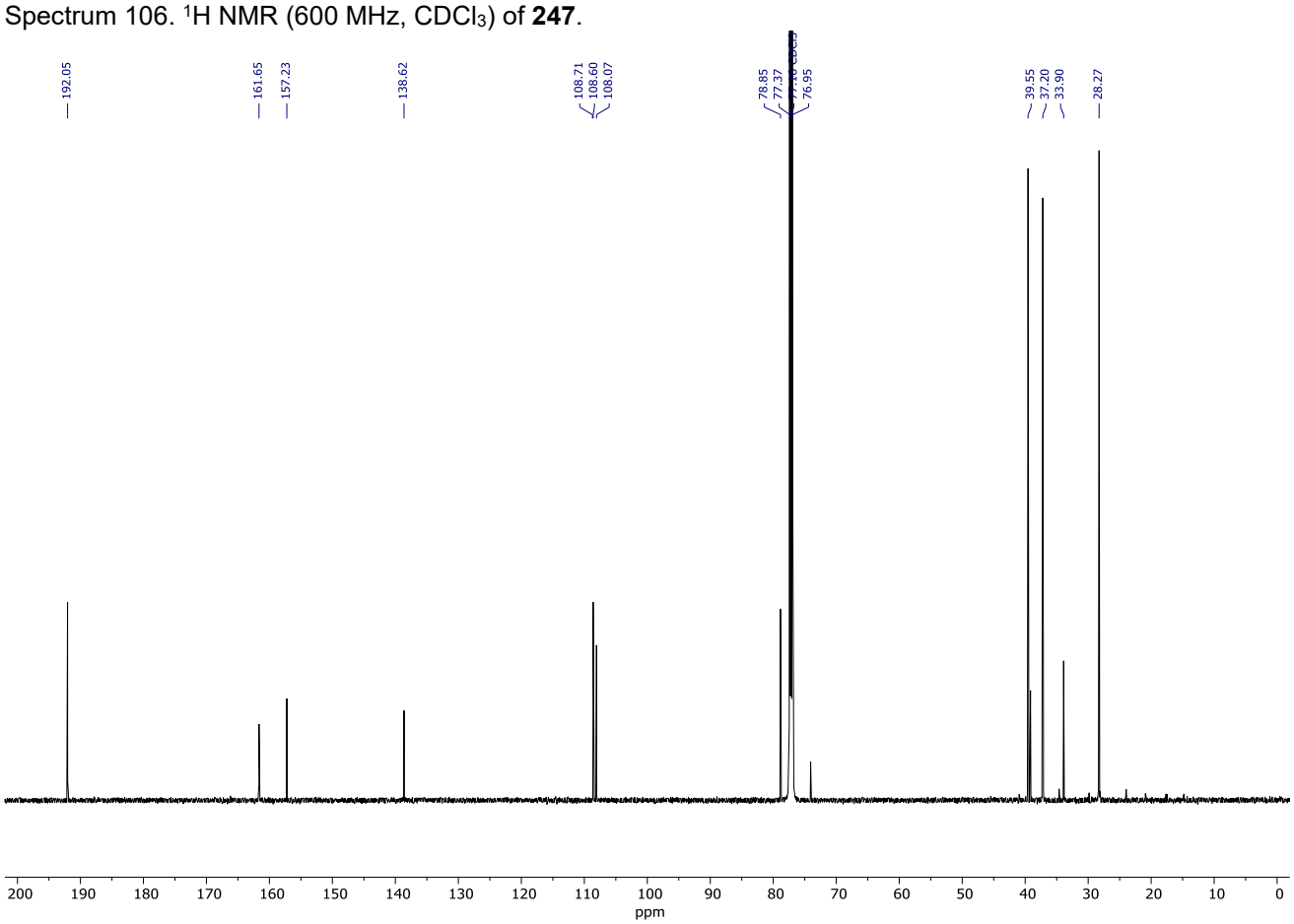

Spectrum 107. ^{13}C NMR (151 MHz, $CDCl_3$) of **247**.

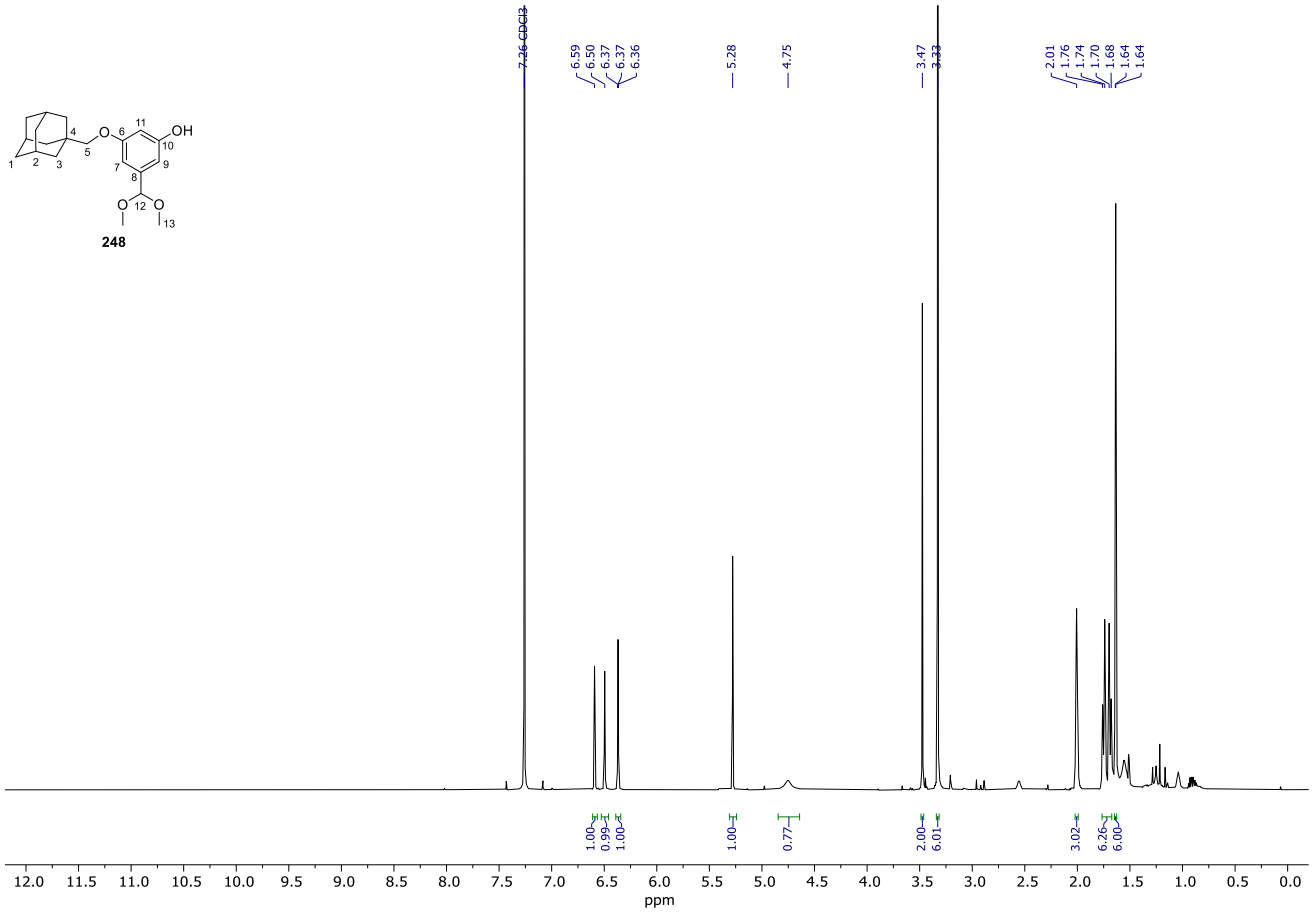

Spectrum 108.[1]H NMR (600 MHz, $CDCl_3$) of **248**.

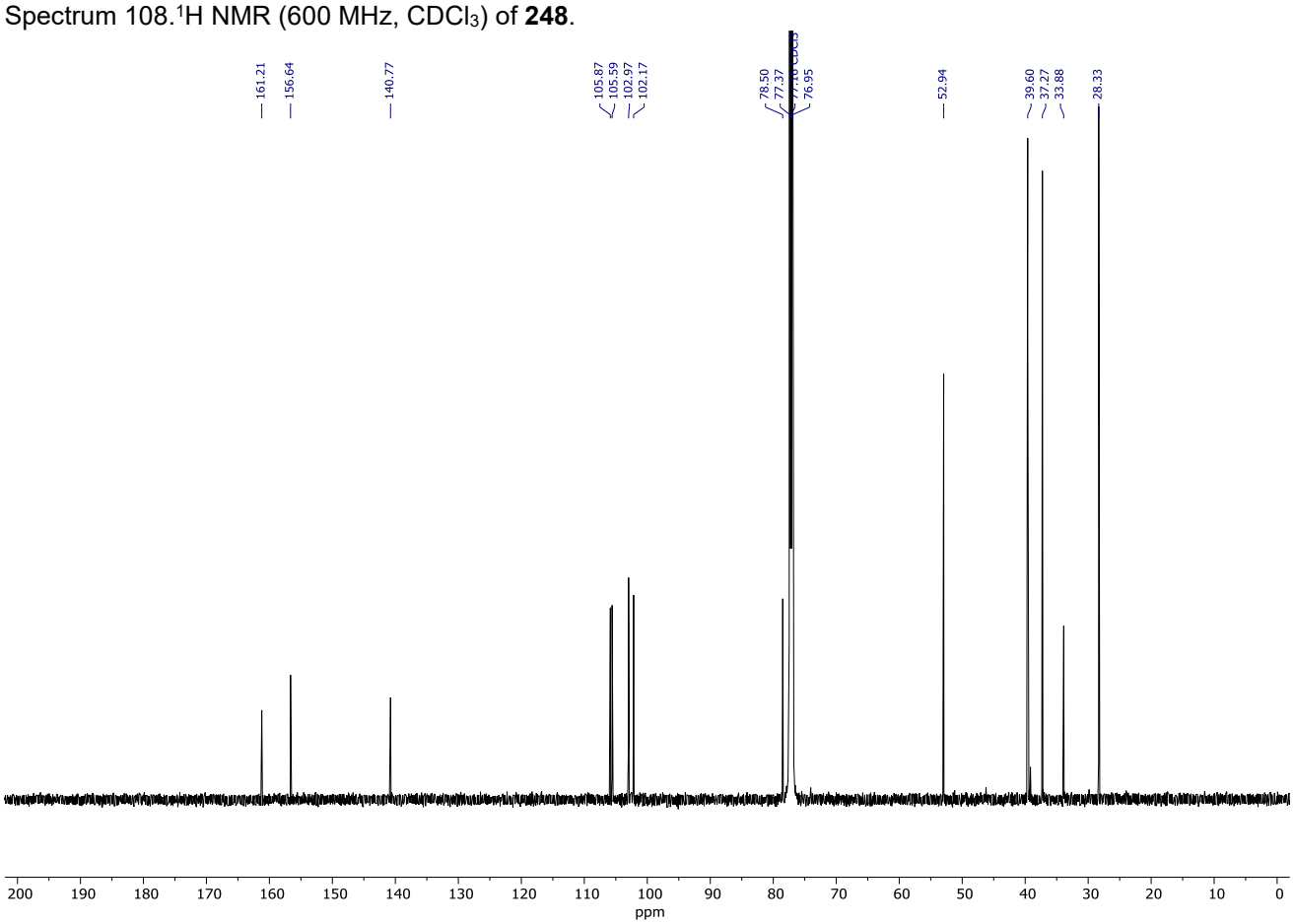

Spectrum 109. [13]C NMR (151 MHz, $CDCl_3$) of **248**.

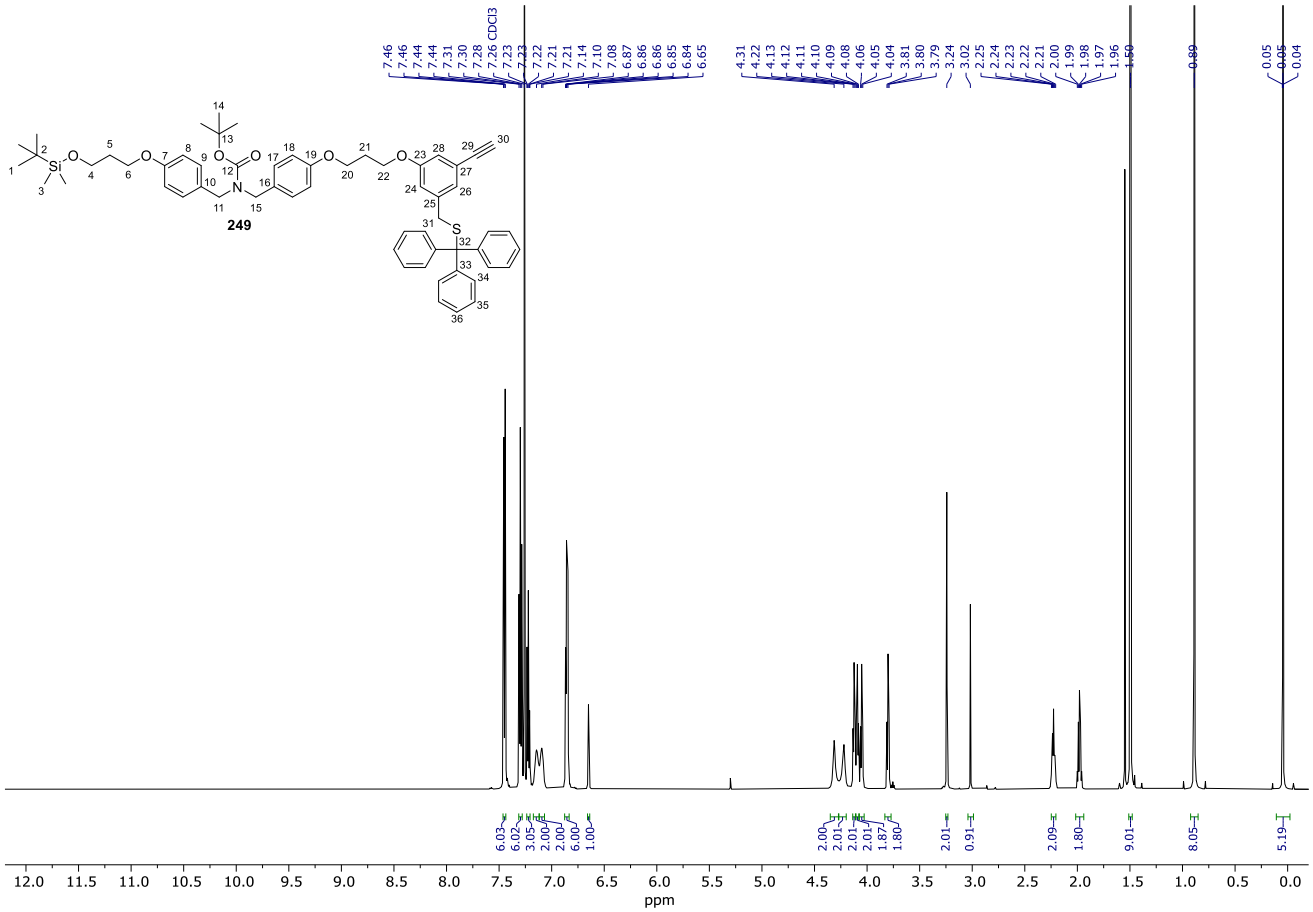

Spectrum 110. ^{1}H NMR (600 MHz, $CDCl_3$) of **249**.

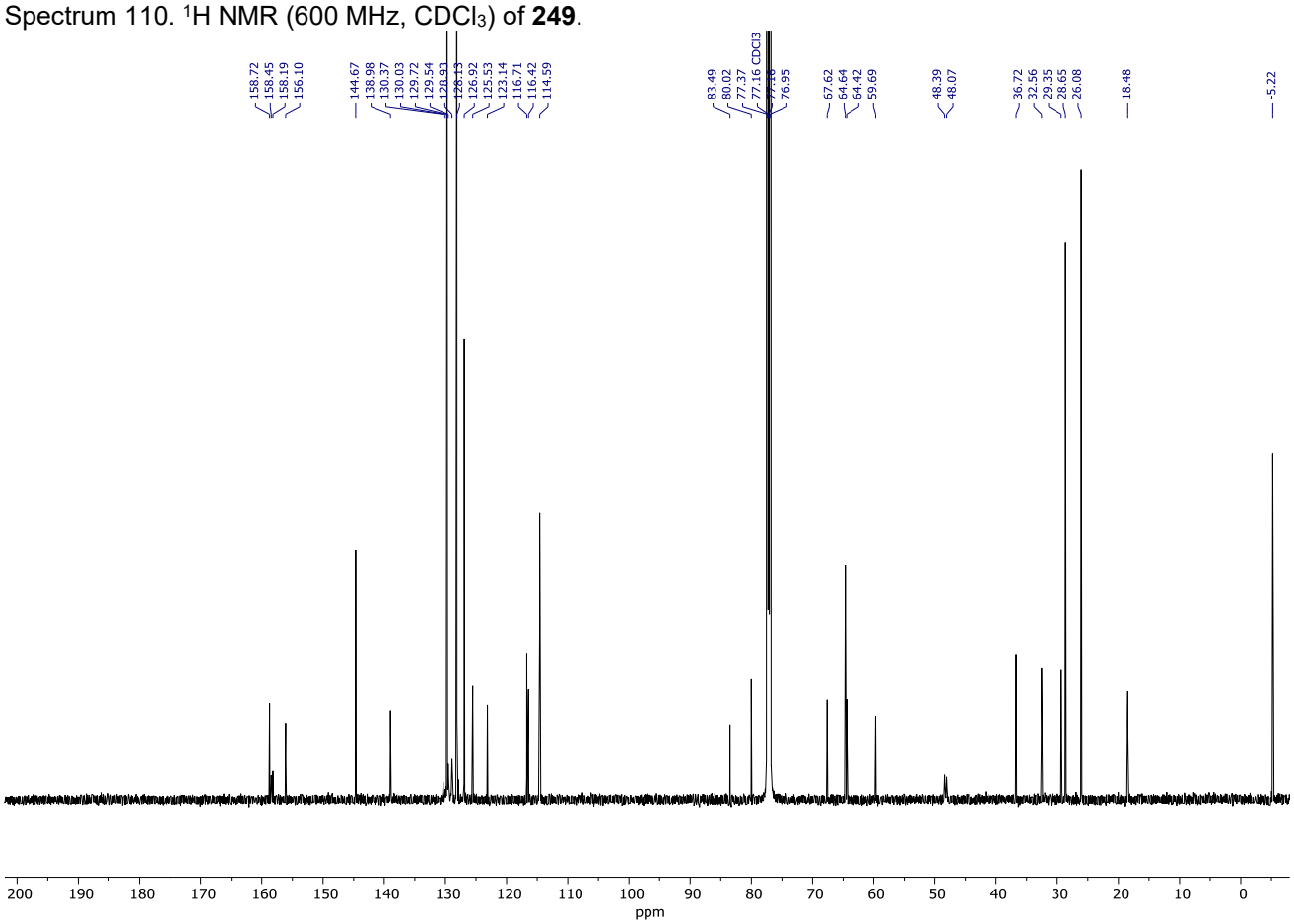

Spectrum 111. ^{13}C NMR (151 MHz, $CDCl_3$) of **249**.

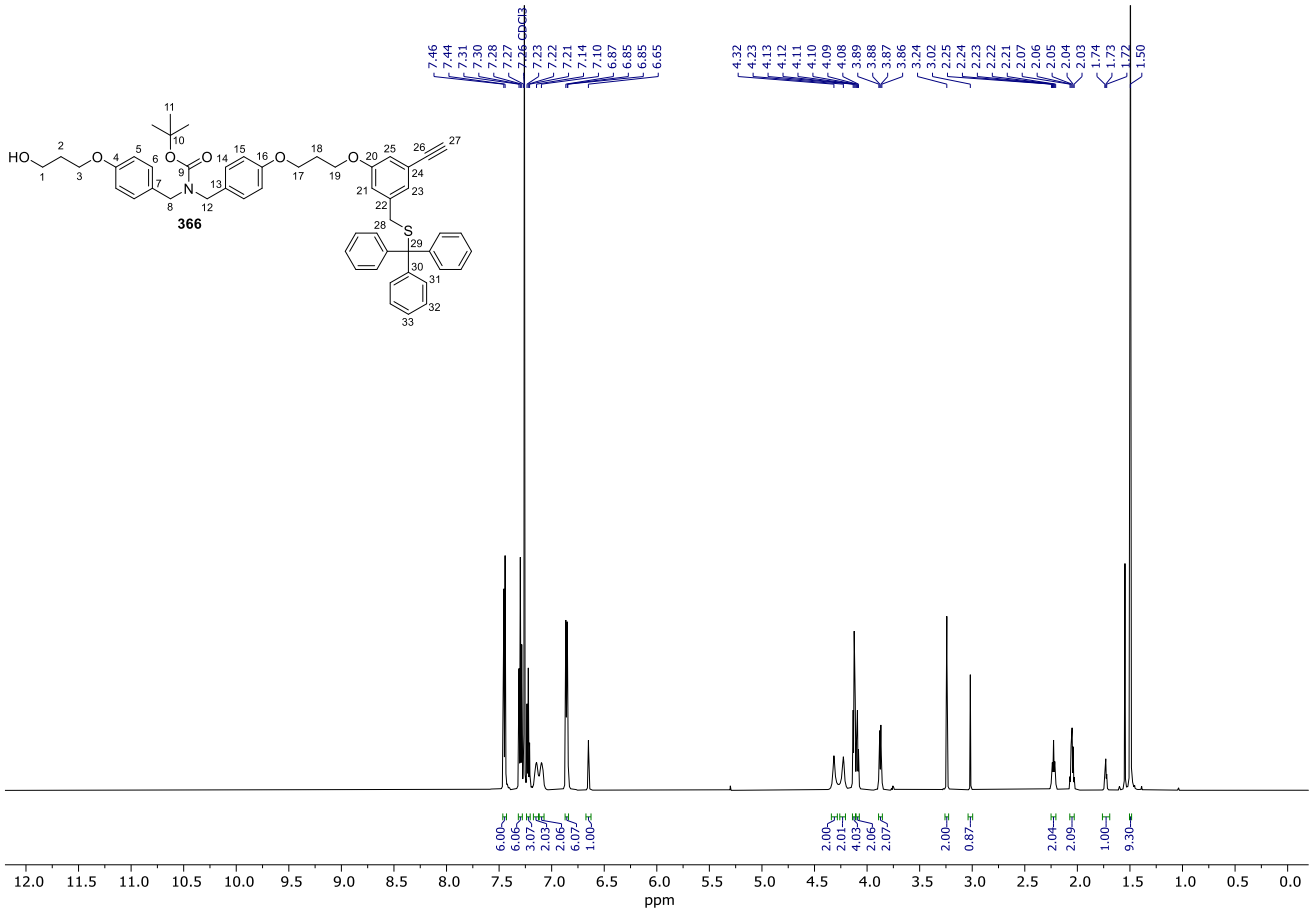

Spectrum 112. ^{1}H NMR (600 MHz, $CDCl_3$) of **366**.

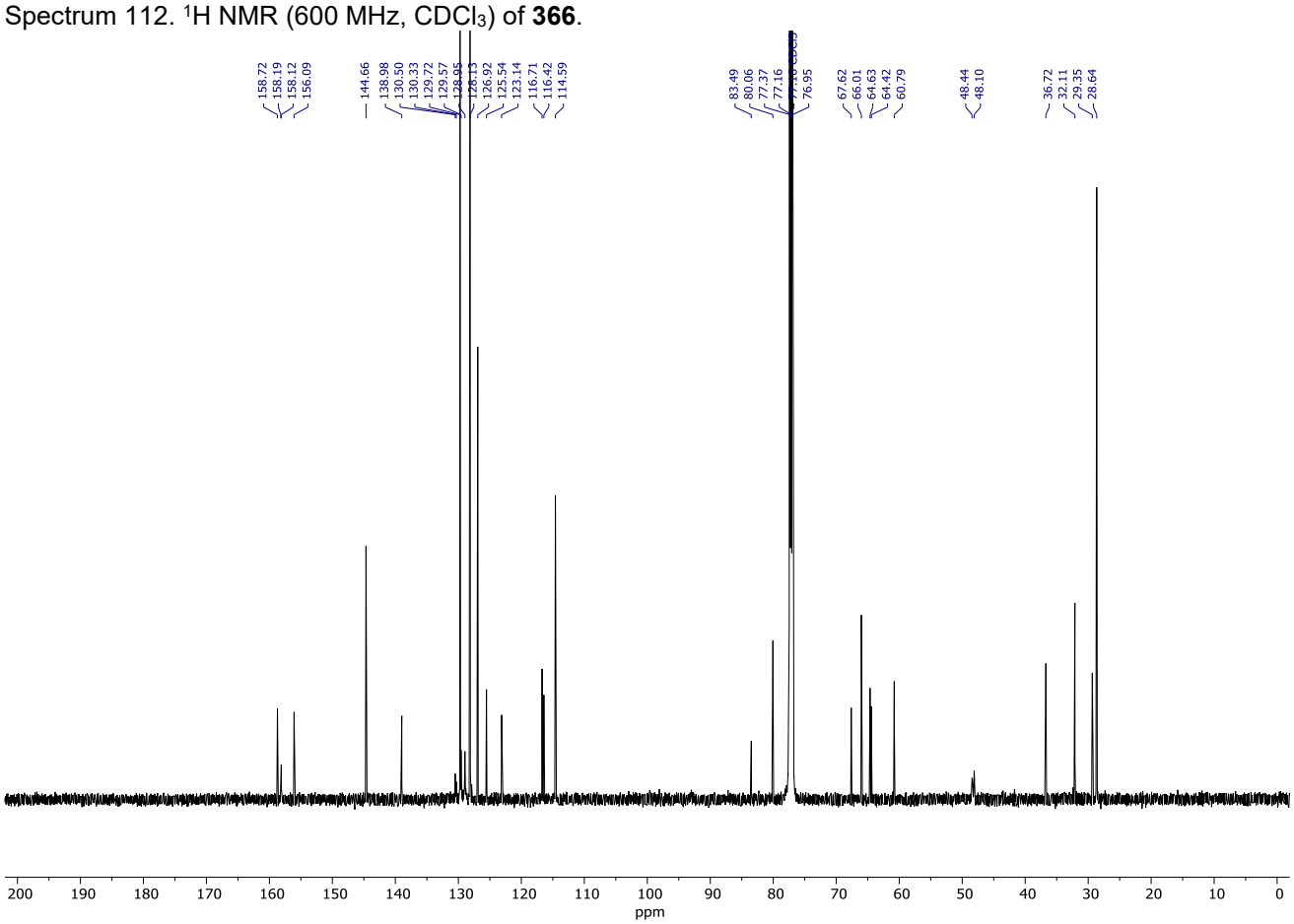

Spectrum 113. ^{13}C NMR (151 MHz, $CDCl_3$) of **366**.

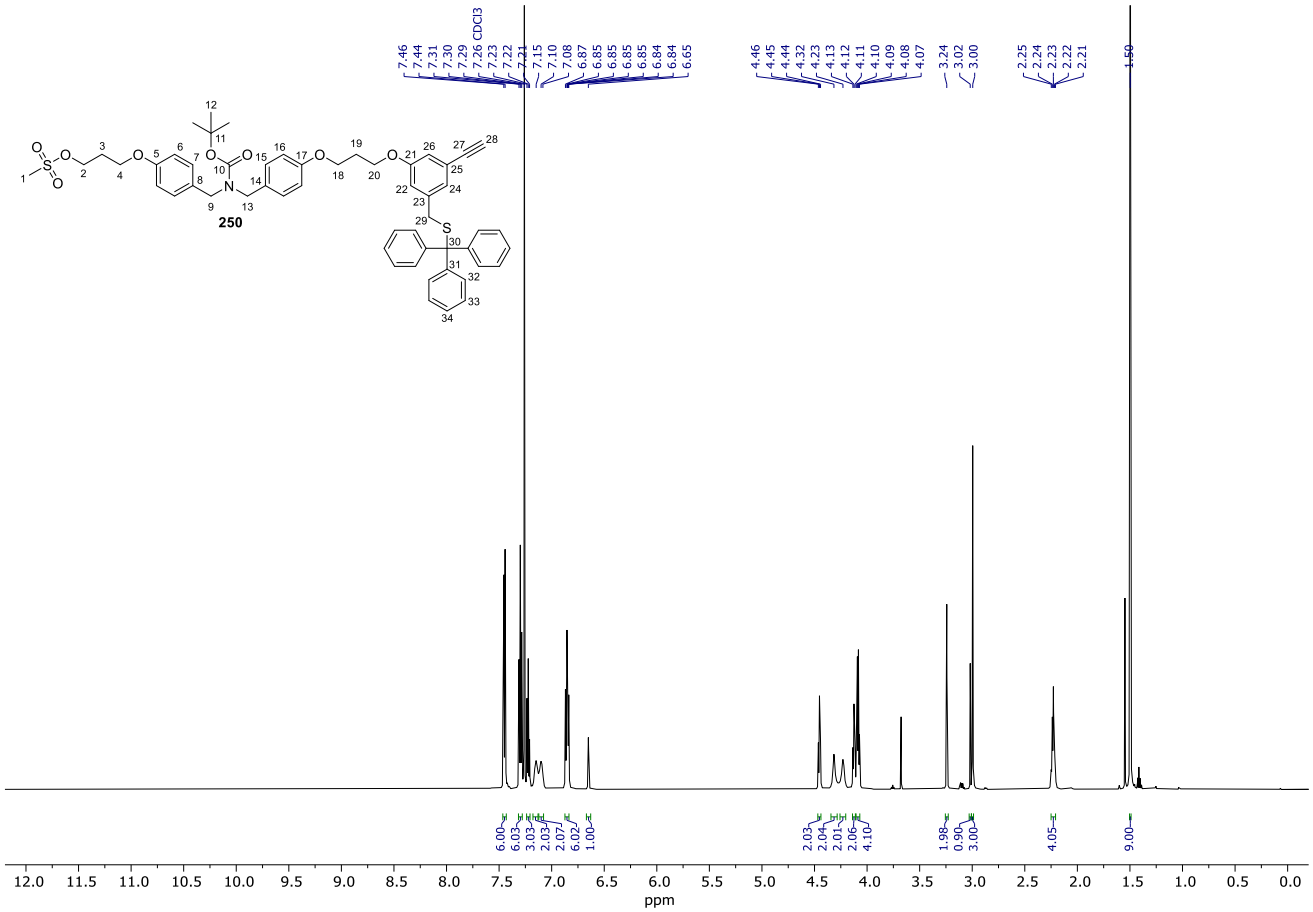

Spectrum 114. ^{1}H NMR (600 MHz, $CDCl_3$) of **250**.

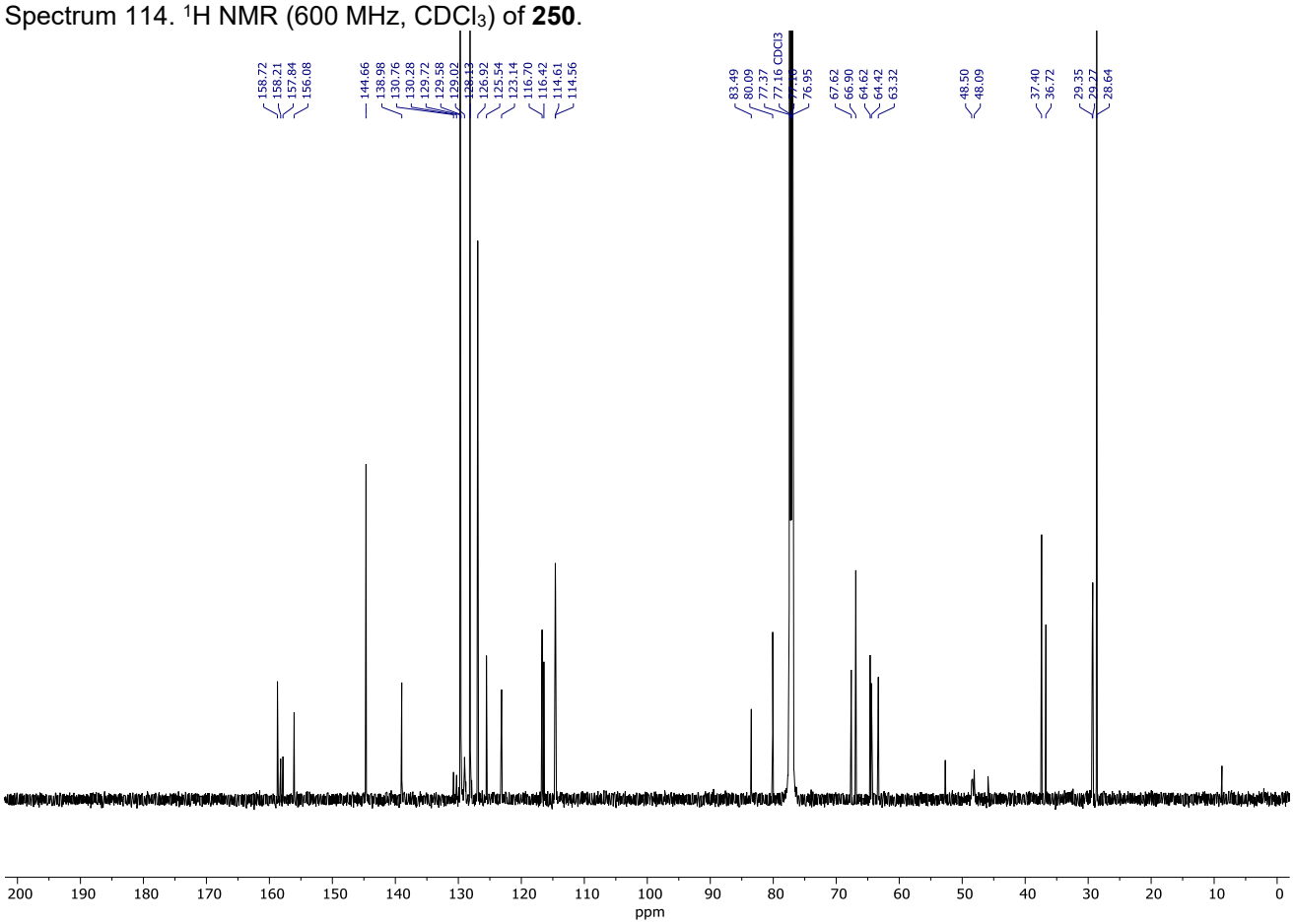

Spectrum 115. ^{13}C NMR (151 MHz, $CDCl_3$) of **250**.

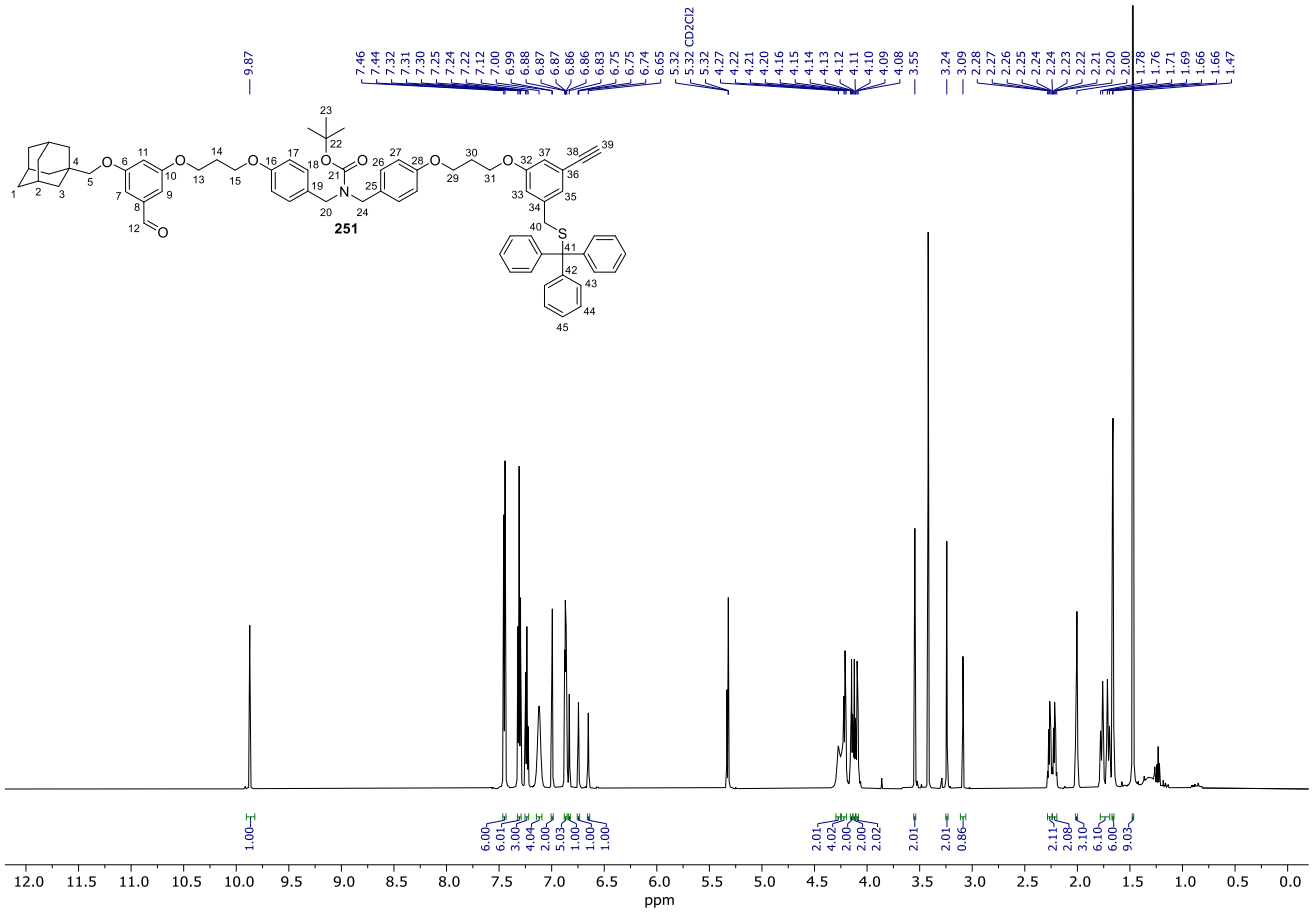

Spectrum 116. ^{1}H NMR (600 MHz, CD_2Cl_2) of **251**.

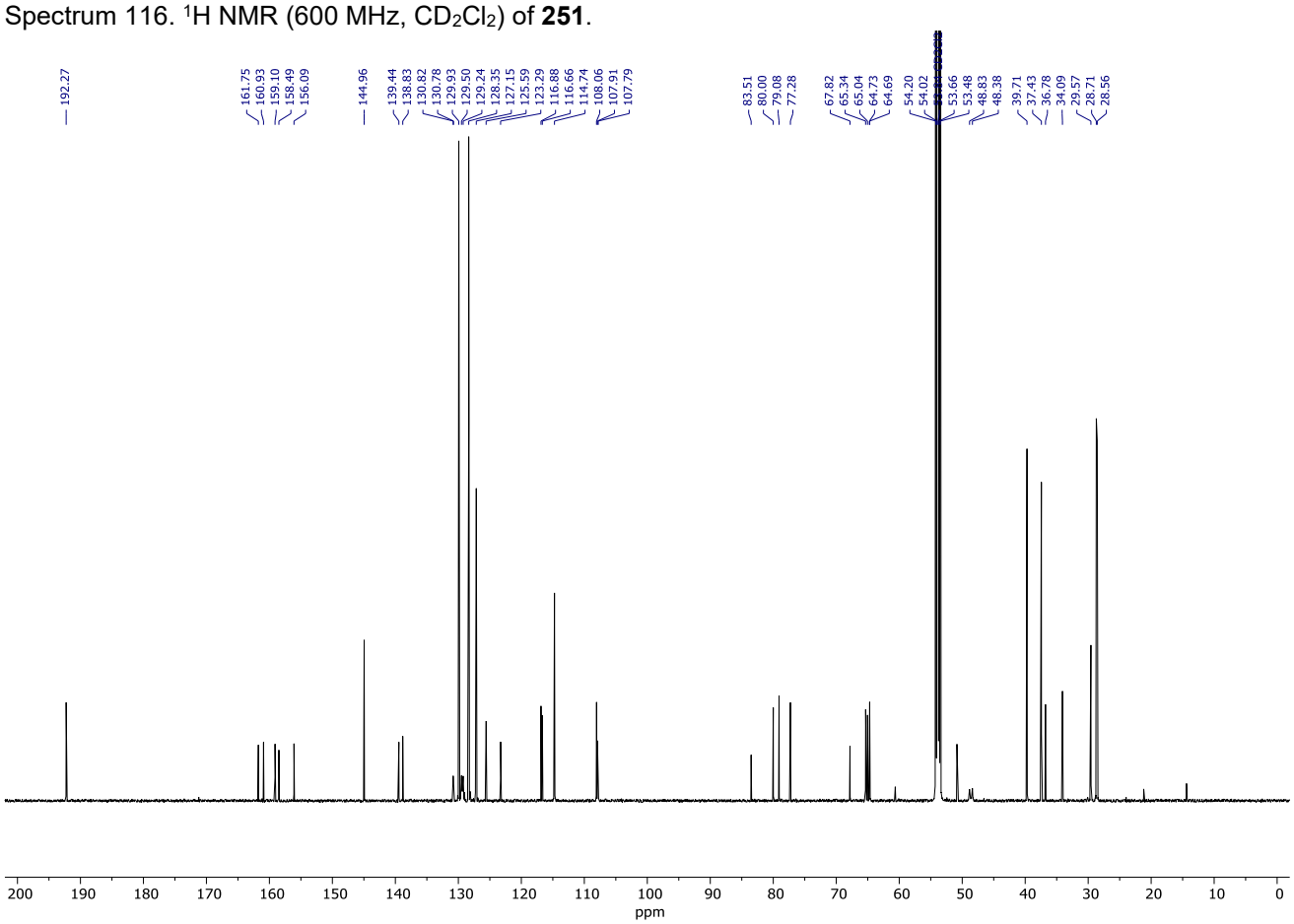

Spectrum 117. ^{13}C NMR (151 MHz, CD_2Cl_2) of **251**.

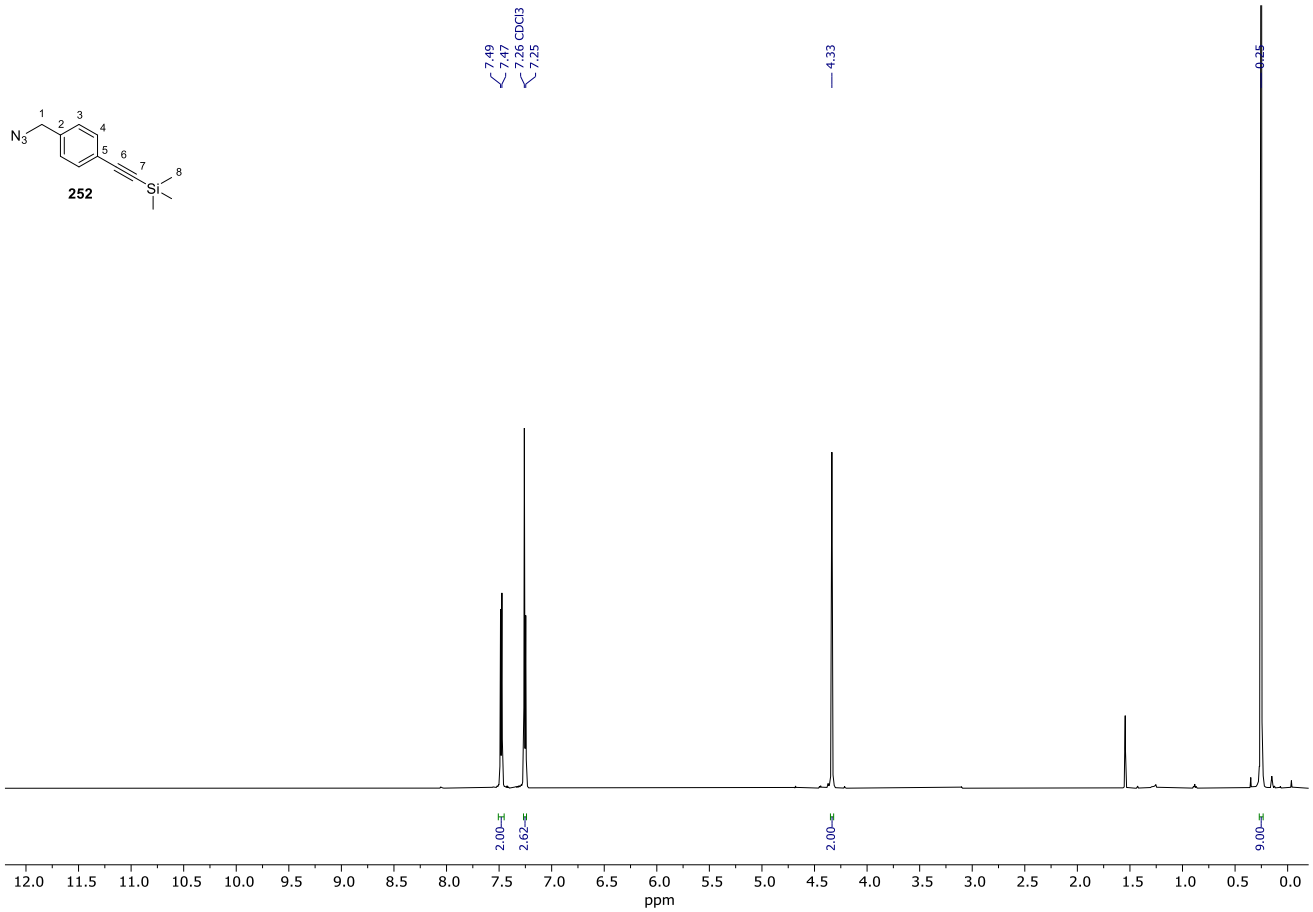

Spectrum 118. ^{1}H NMR (600 MHz, $CDCl_3$) of **252**.

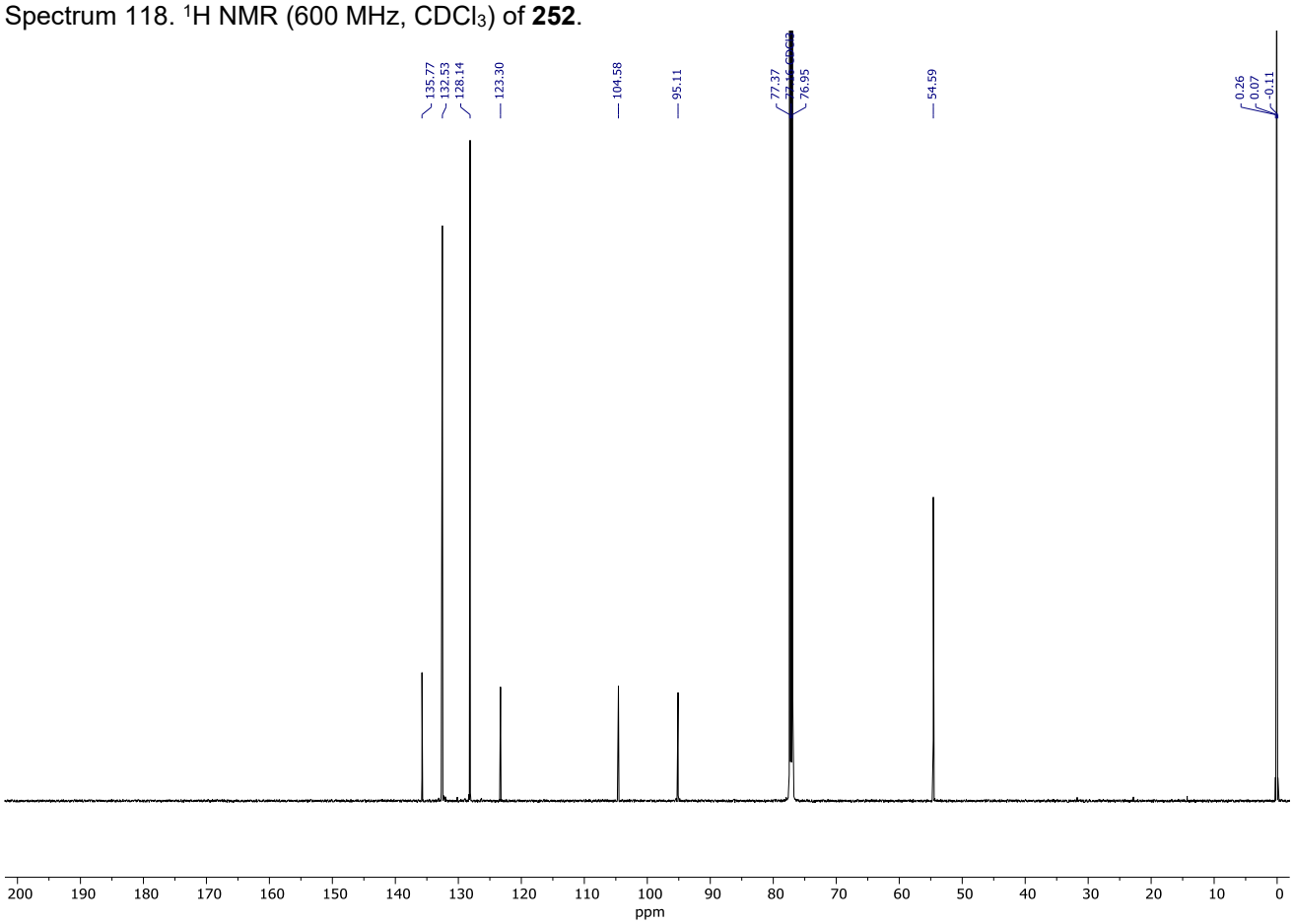

Spectrum 119. ^{13}C NMR (151 MHz, $CDCl_3$) of **252**.

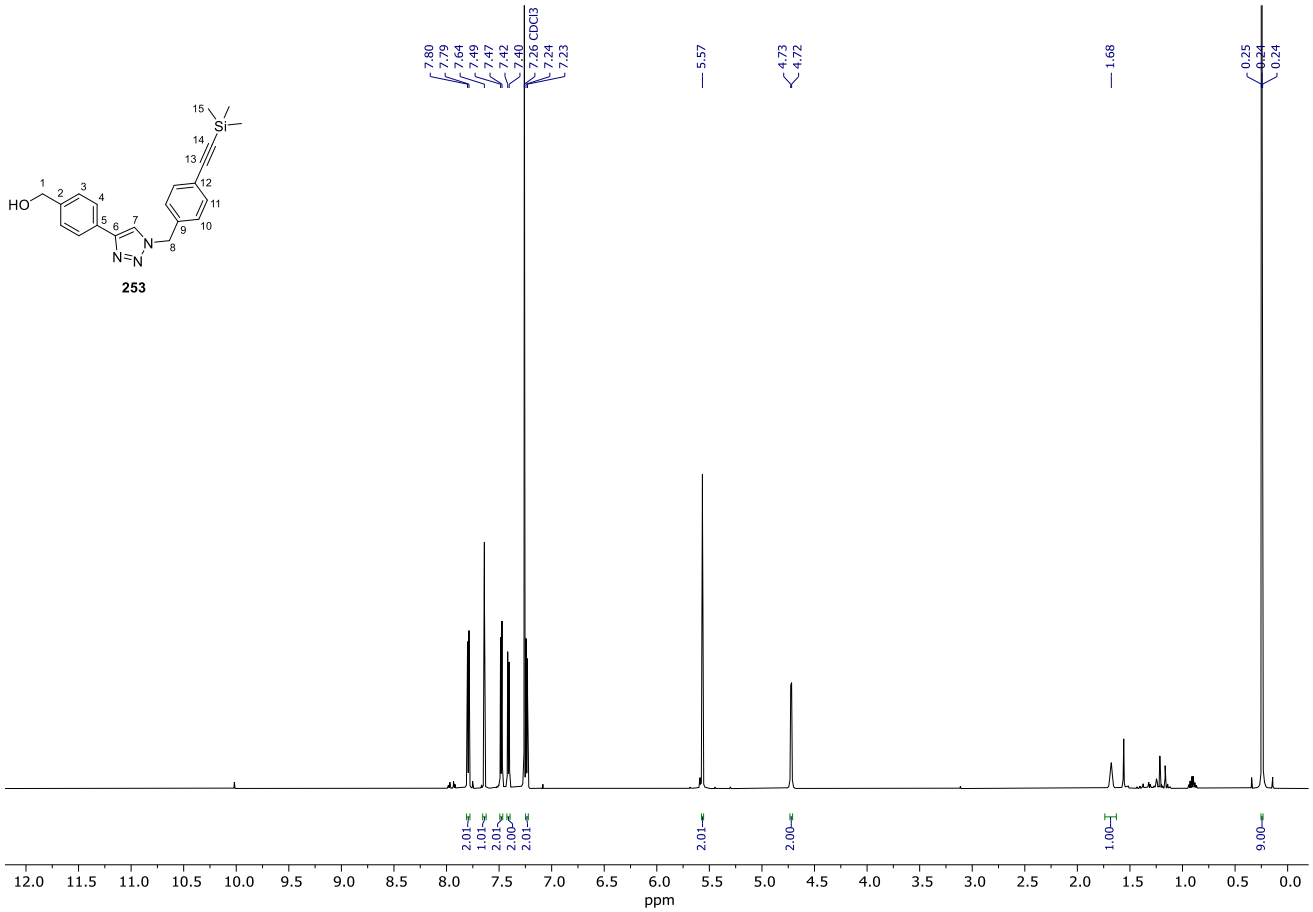

Spectrum 120. ^{1}H NMR (600 MHz, $CDCl_3$) of **253**.

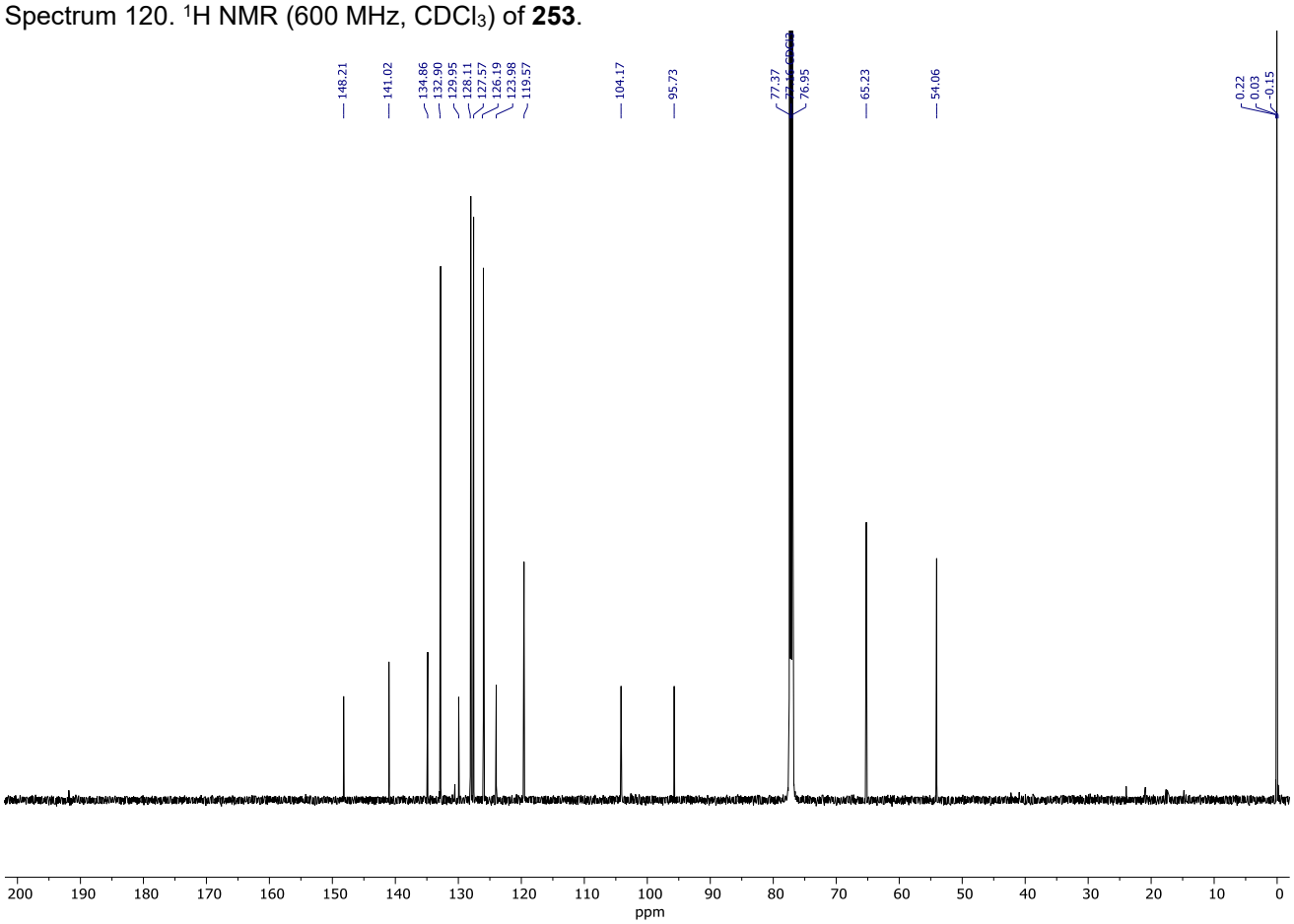

Spectrum 121. ^{13}C NMR (151 MHz, $CDCl_3$) of **253**.

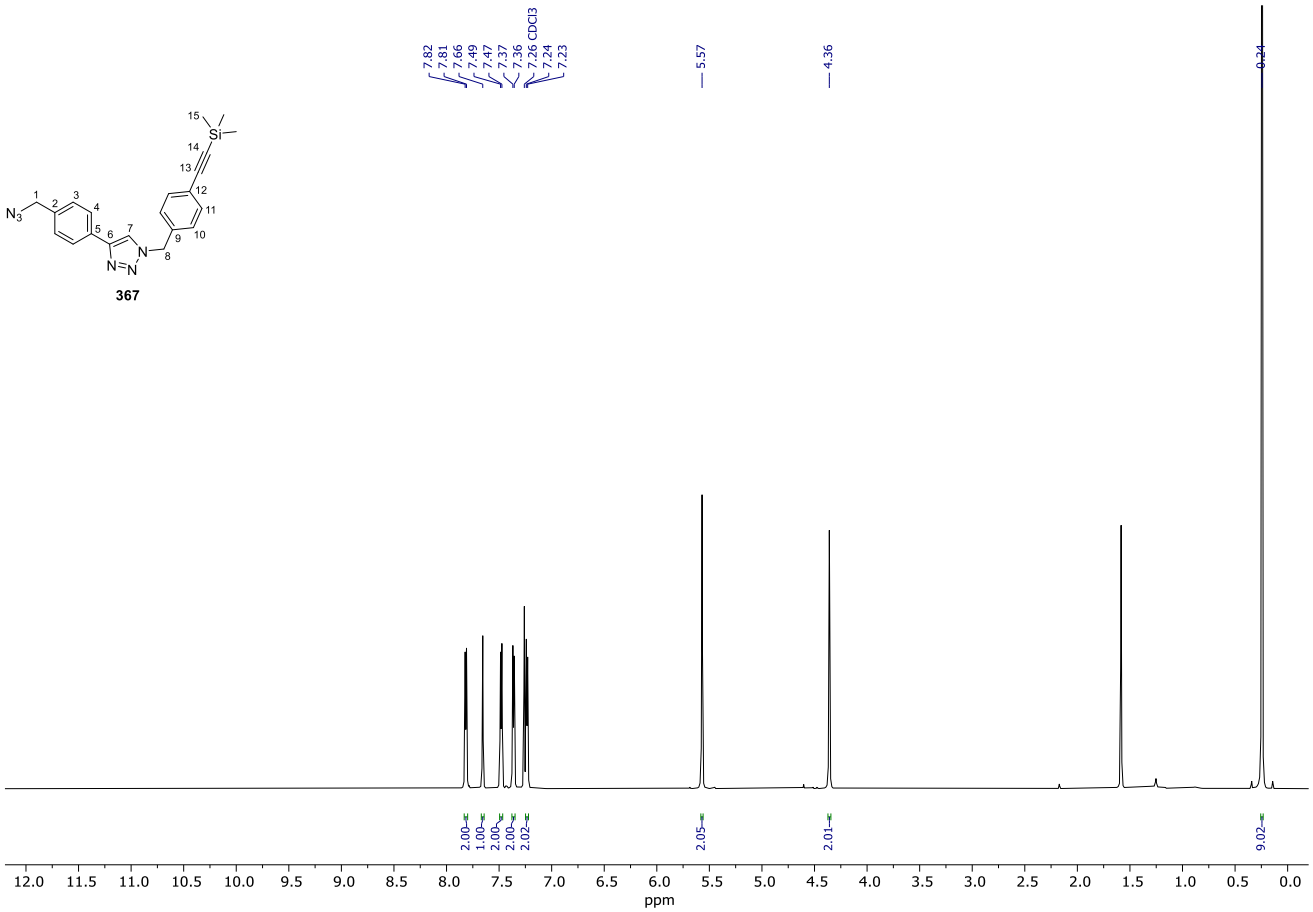

367

Spectrum 122. ^{1}H NMR (600 MHz, $CDCl_3$) of **367**.

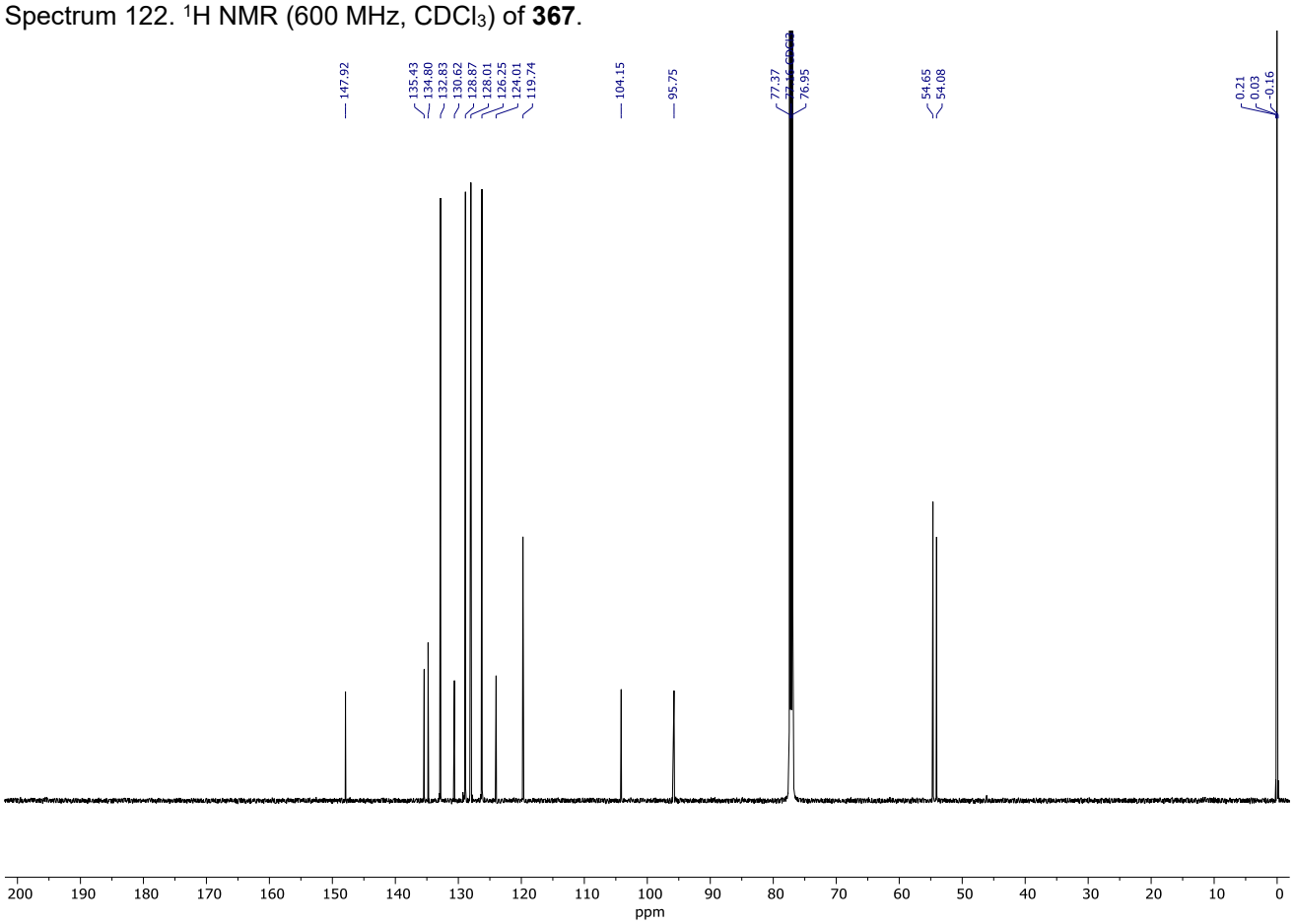

Spectrum 123. ^{13}C NMR (151 MHz, $CDCl_3$) of **367**.

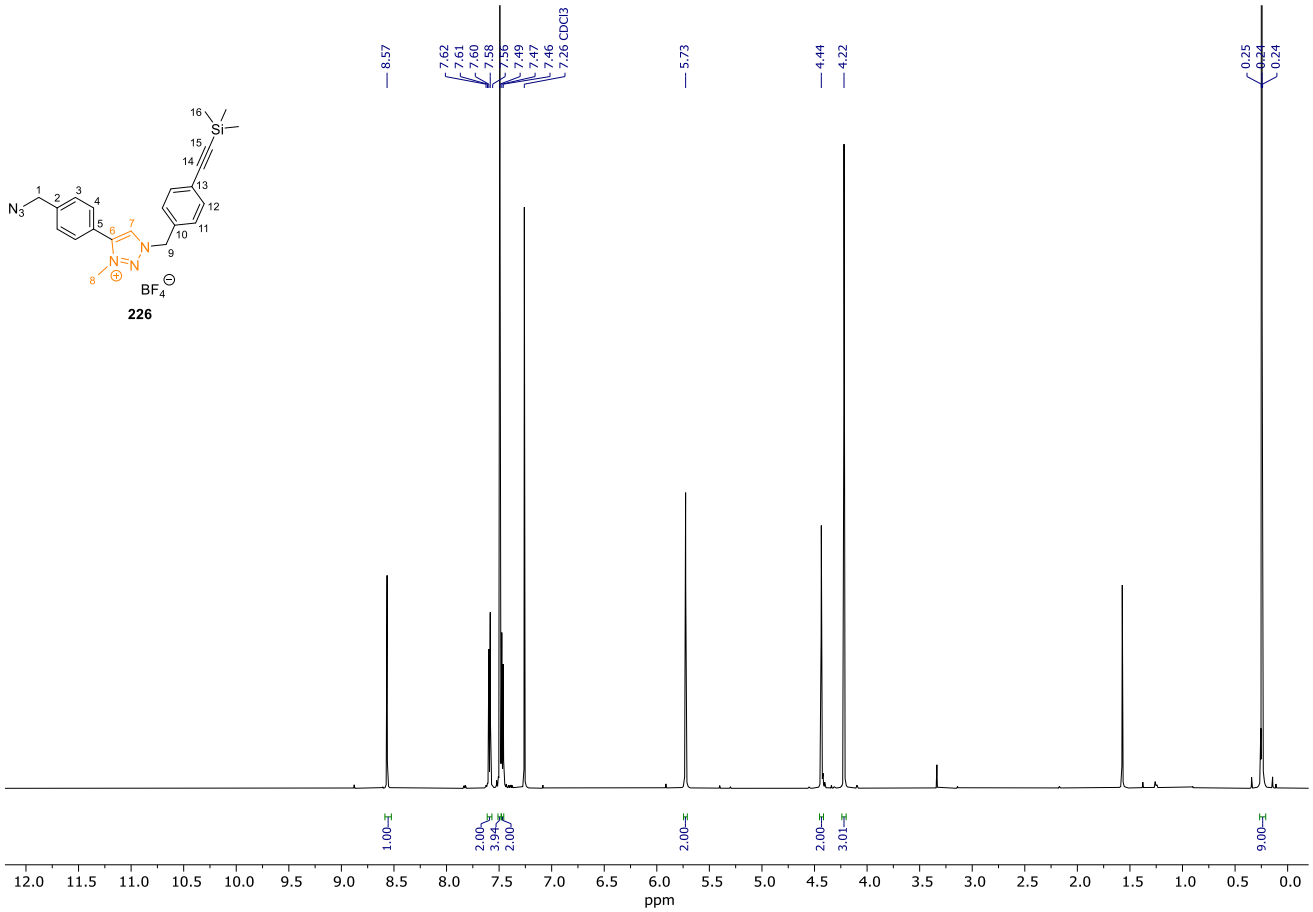

226

Spectrum 124. ^{1}H NMR (600 MHz, $CDCl_3$) of **226**.

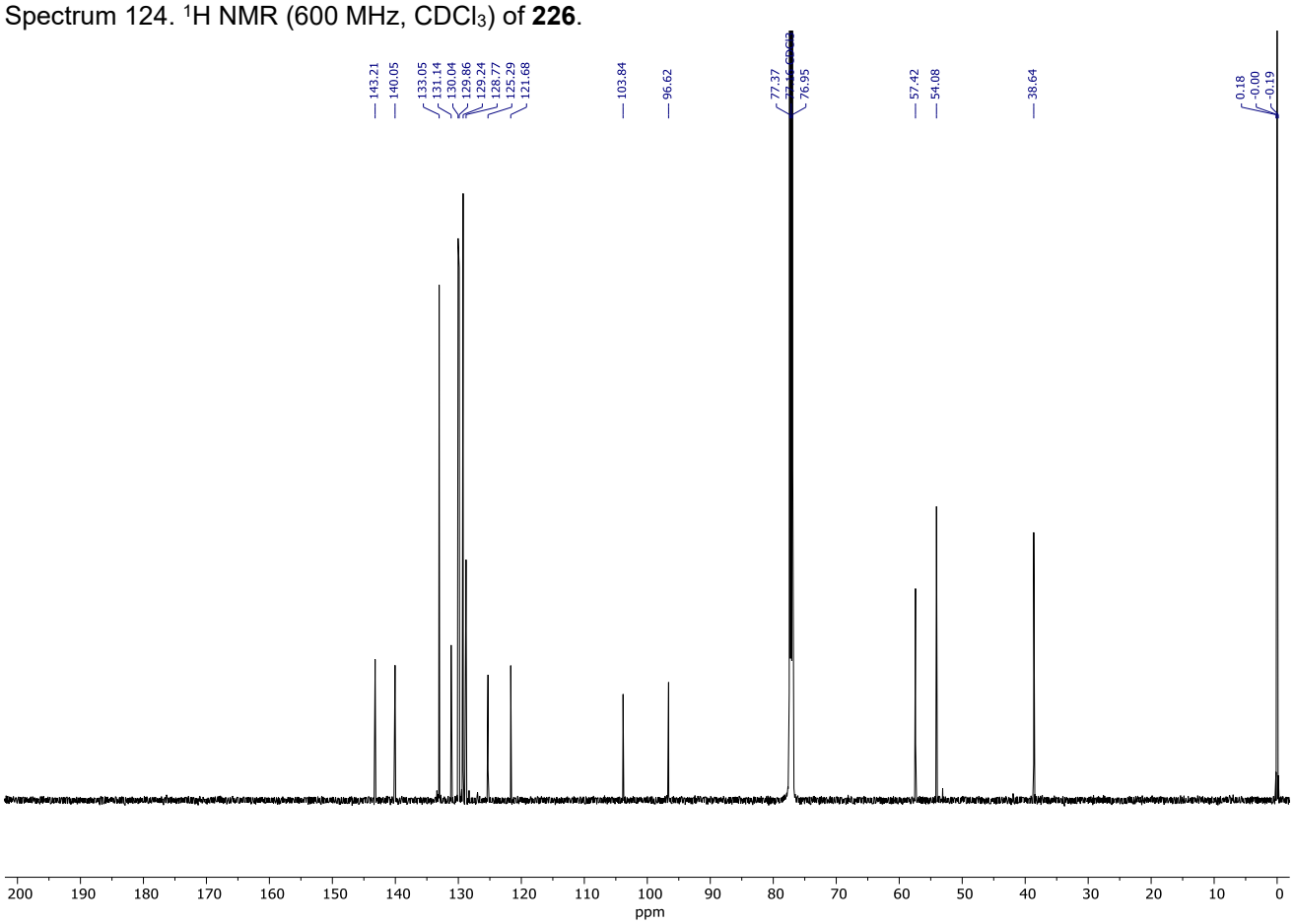

Spectrum 125. ^{13}C NMR (151 MHz, $CDCl_3$) of **226**.

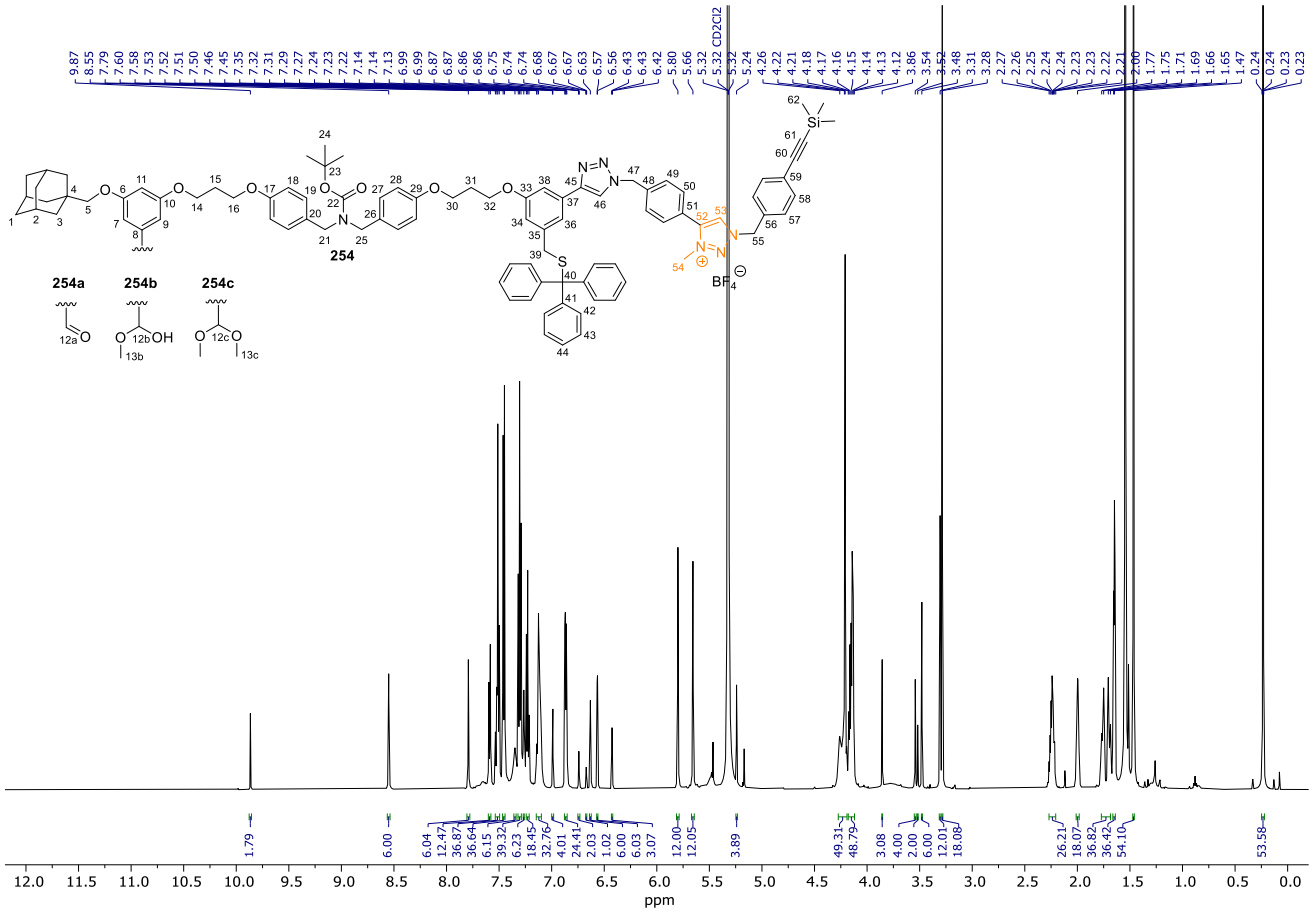

Spectrum 126. ^{1}H NMR (600 MHz, $CDCl_3$) of **254**.

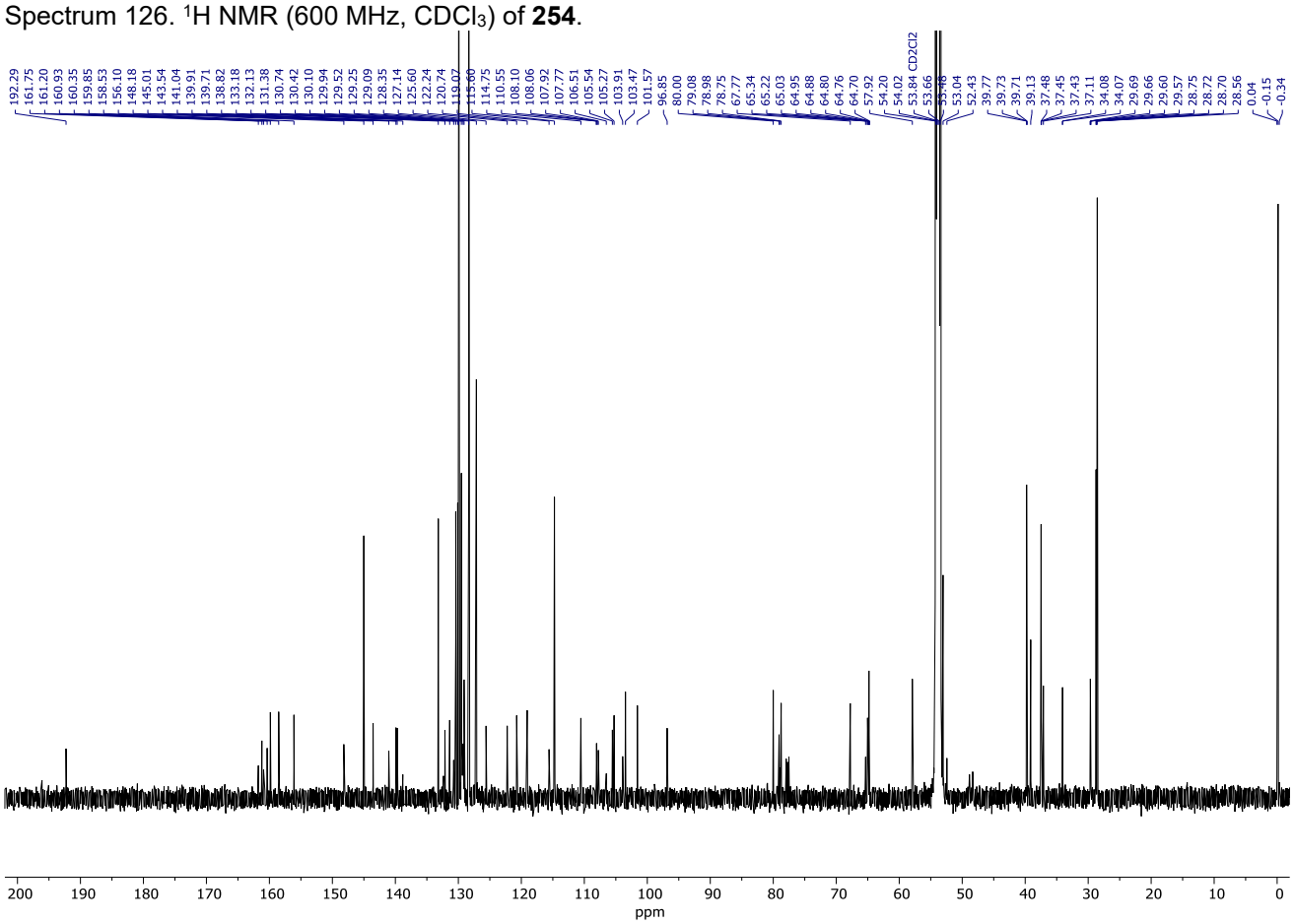

Spectrum 127. ^{13}C NMR (151 MHz, $CDCl_3$) of **254**.

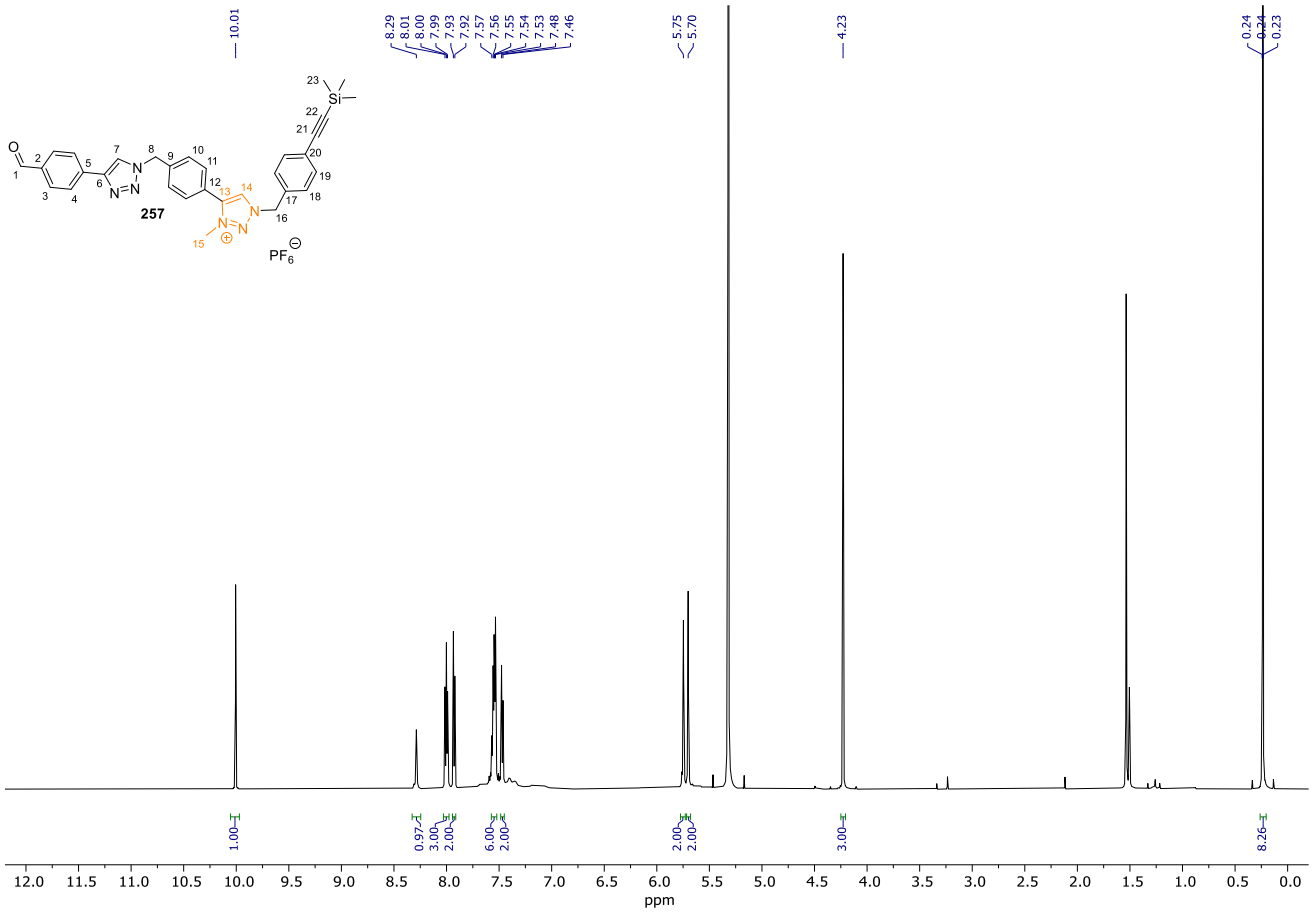

Spectrum 128. ^{1}H NMR (600 MHz, $CDCl_3$) of **257**.

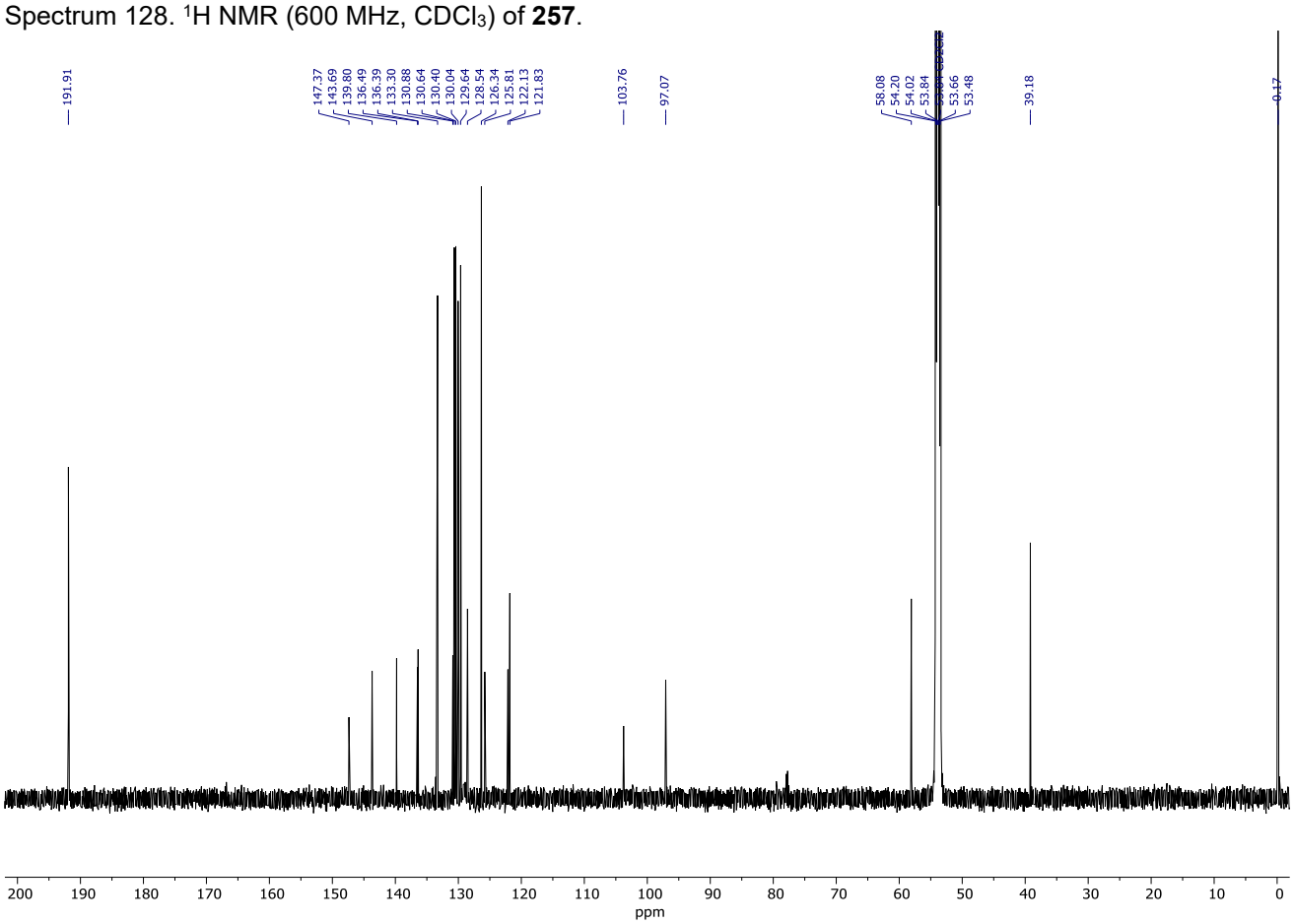

Spectrum 129. ^{13}C NMR (151 MHz, $CDCl_3$) of **257**.

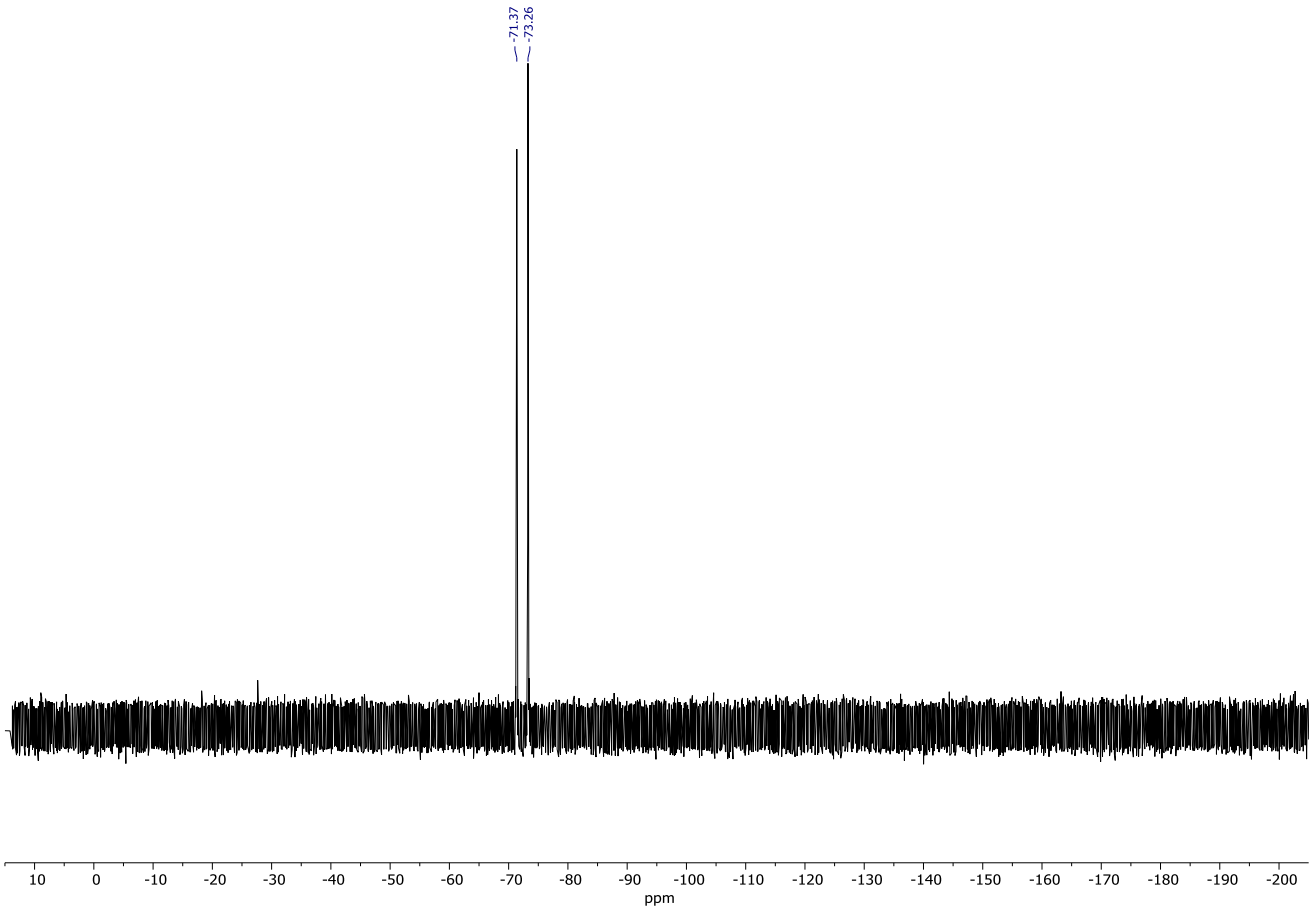

Spectrum 130. ^{19}F NMR (376 MHz, CD_2Cl_2) of **257**.

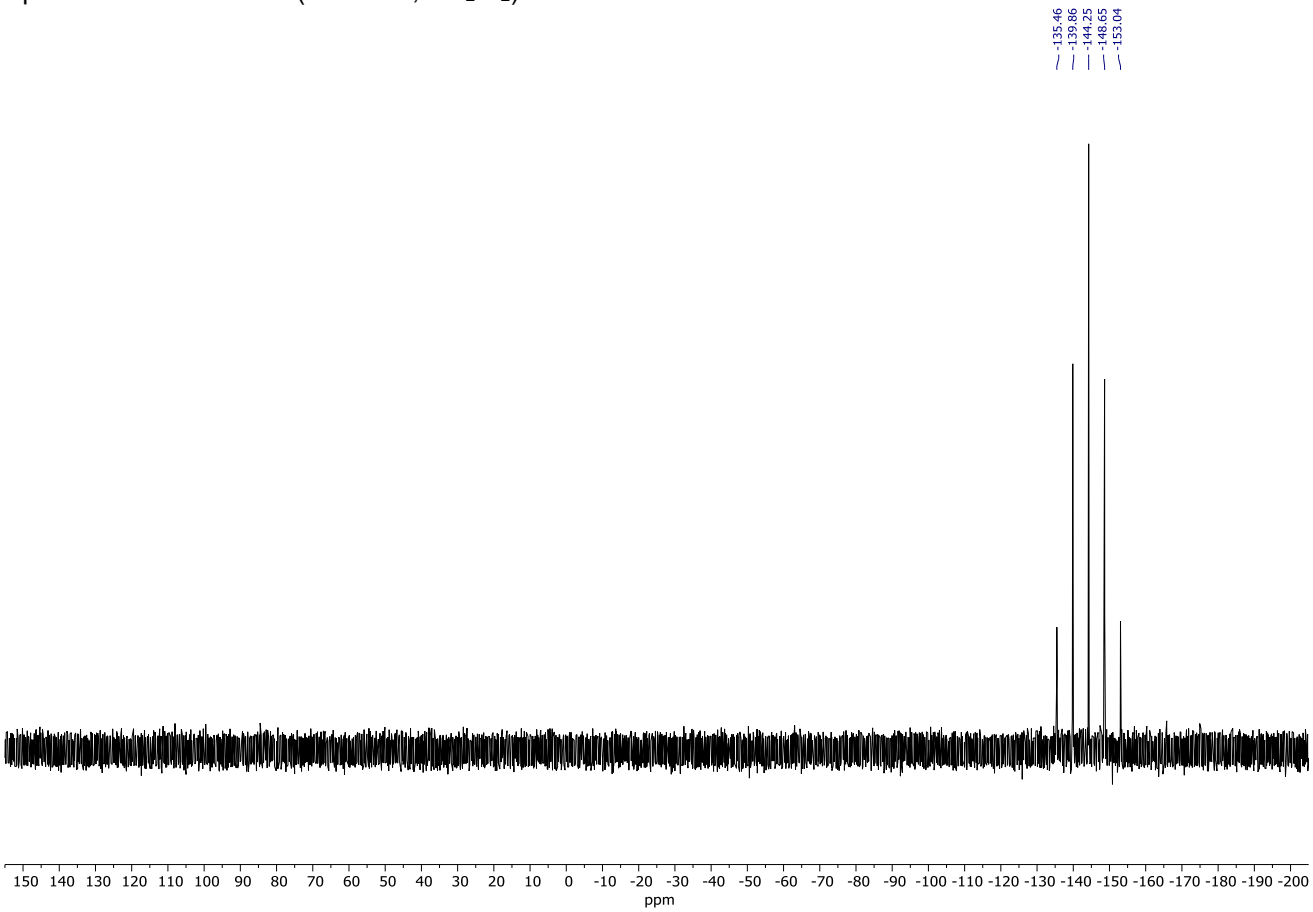

Spectrum 131. ^{31}P NMR (162 MHz, CD_2Cl_2) of **257**.

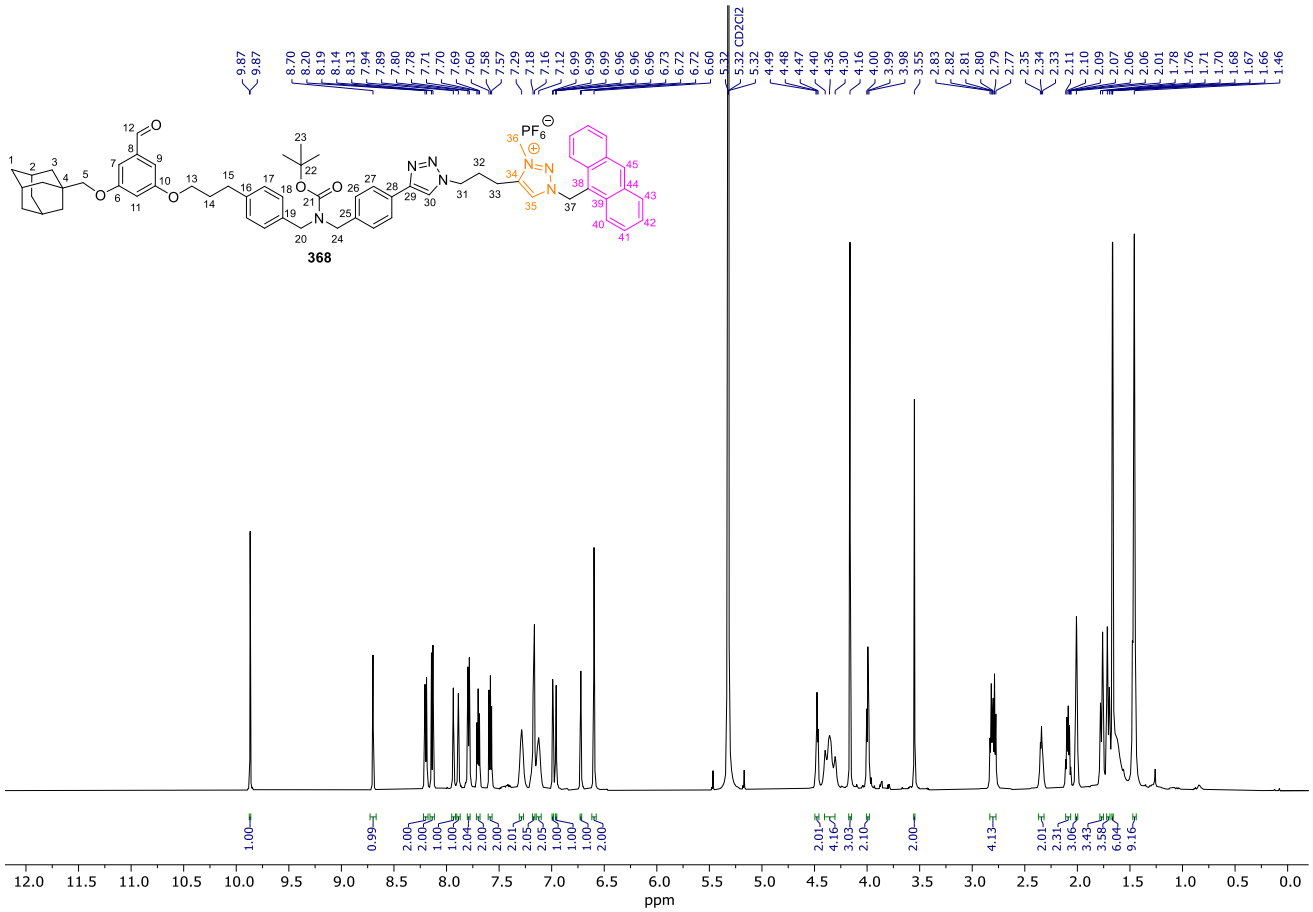

Spectrum 132. ^{1}H NMR (600 MHz, CD_2Cl_2) of **368**.

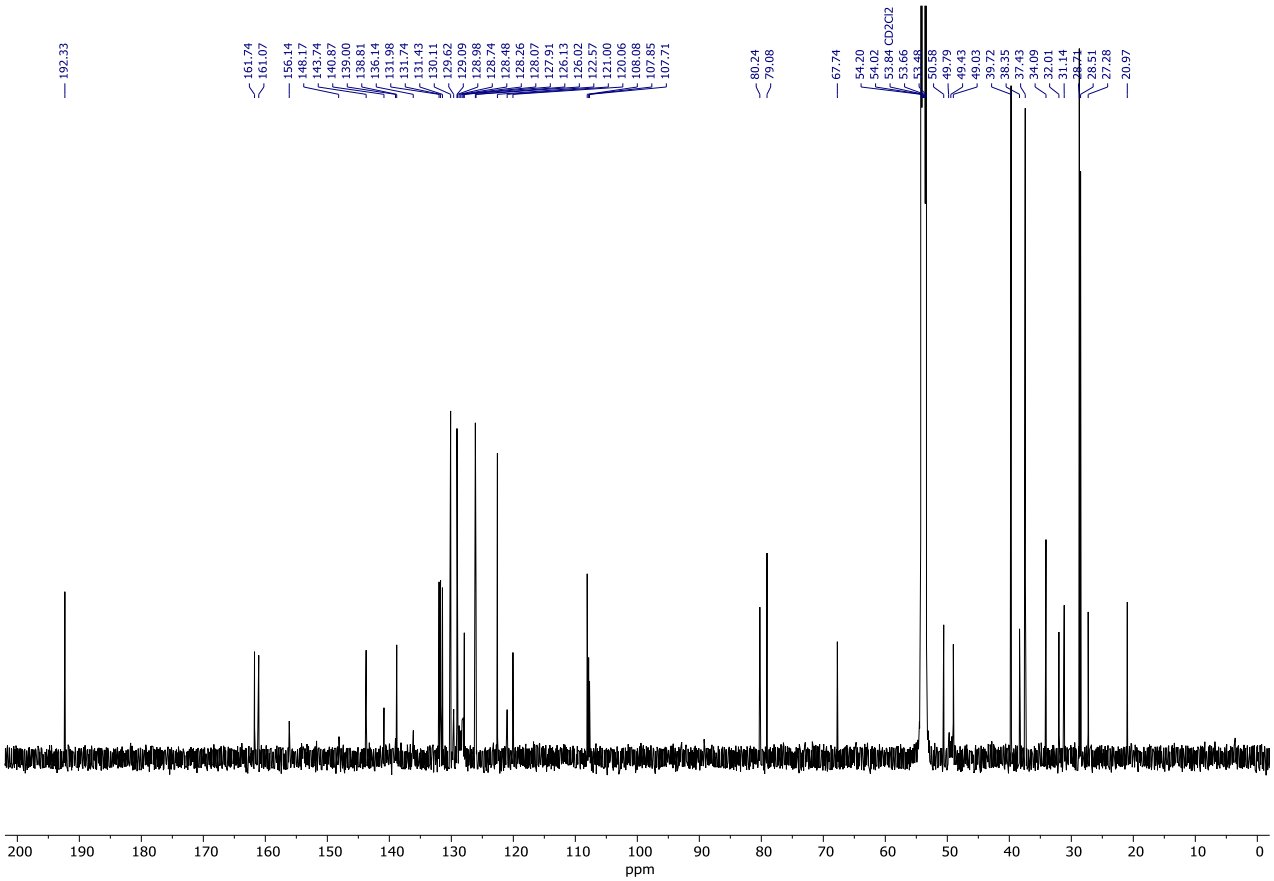

Spectrum 133. ^{13}C NMR (151 MHz, CD_2Cl_2) of **368**.

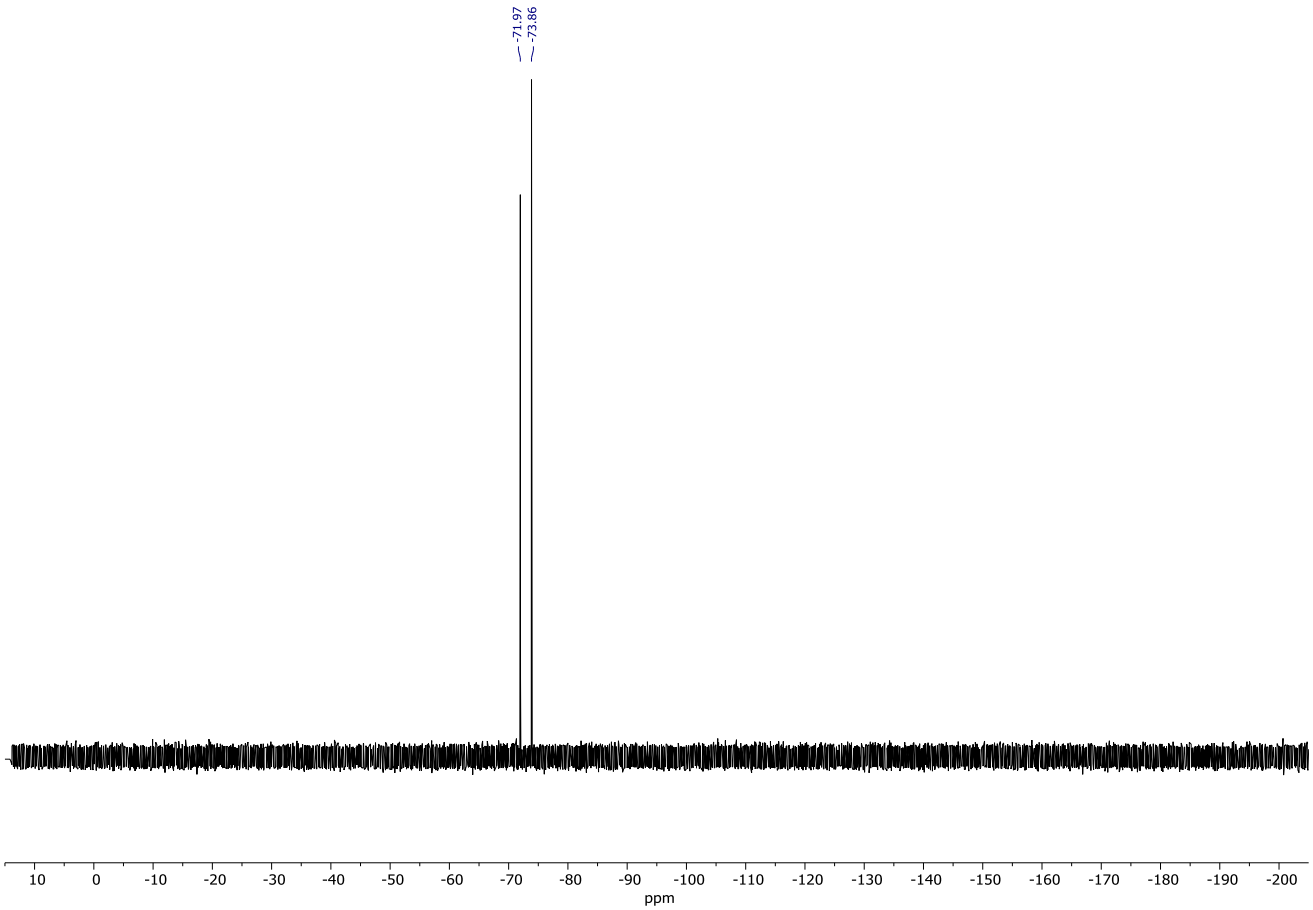

Spectrum 134. ^{19}F NMR (376 MHz, CD_2Cl_2) of **368**.

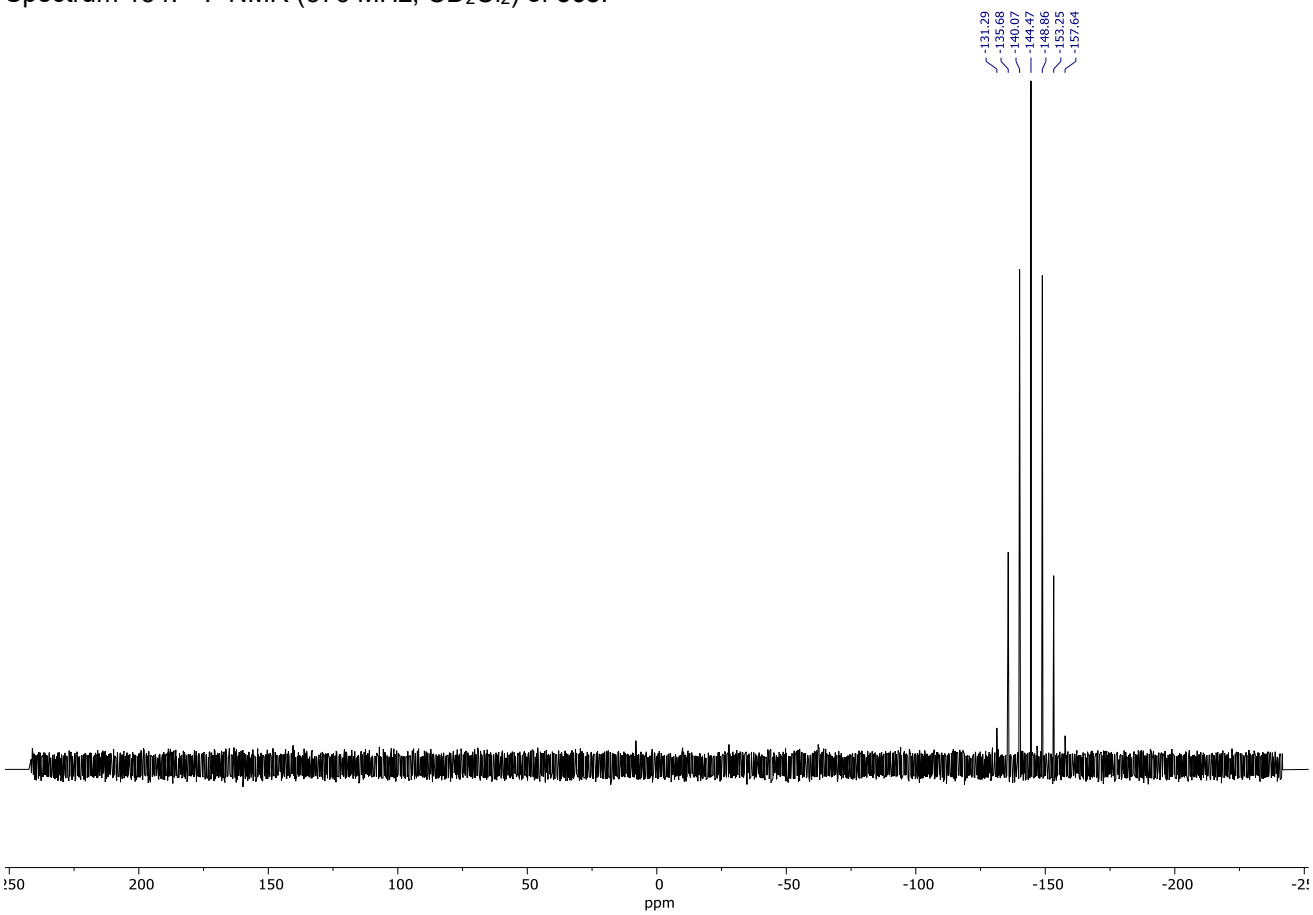

Spectrum 135. ^{31}P NMR (162 MHz, CD_2Cl_2) of **368**.

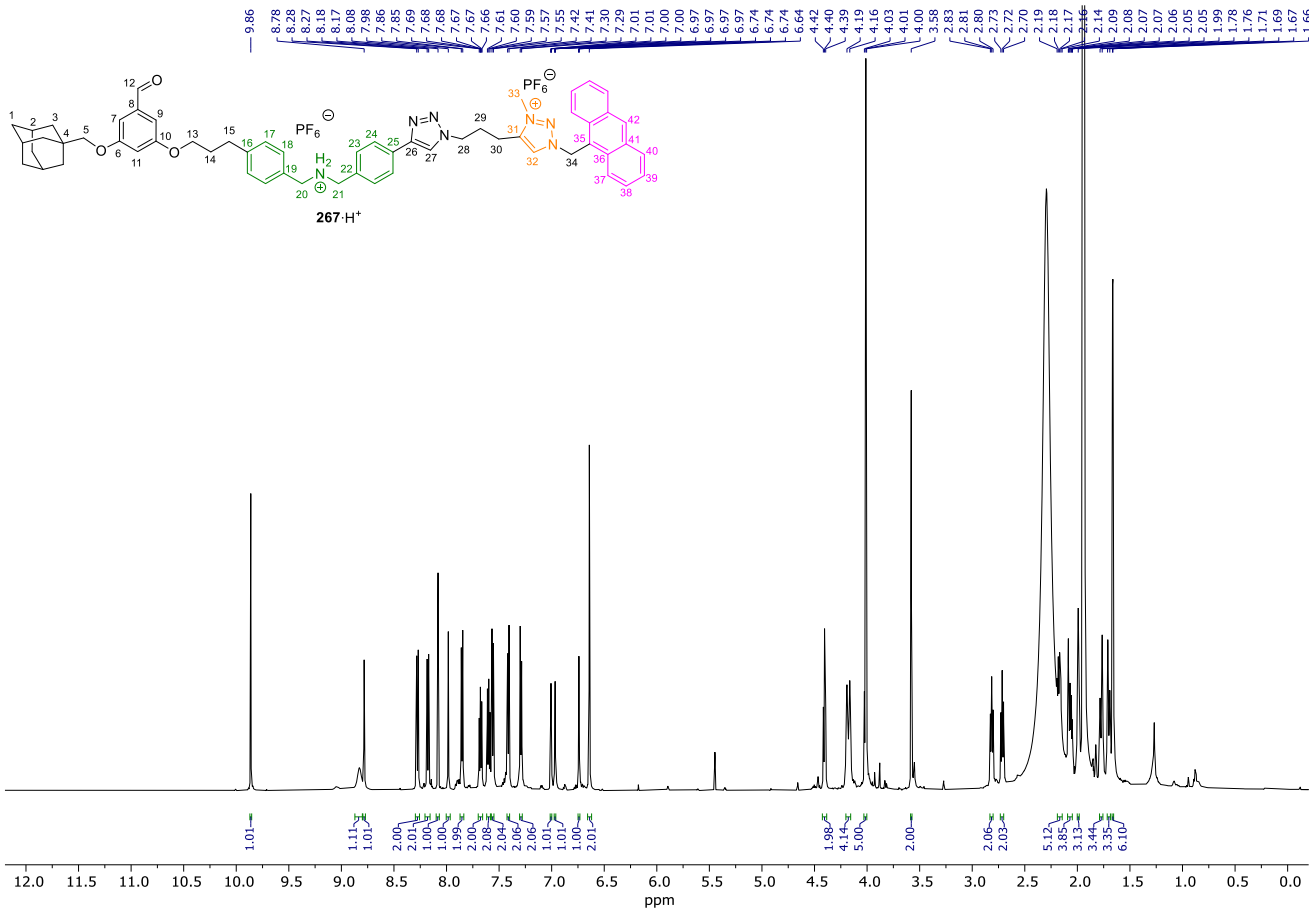

Spectrum 136. ^{1}H NMR (600 MHz, CD_3CN) of **267**·H^+.

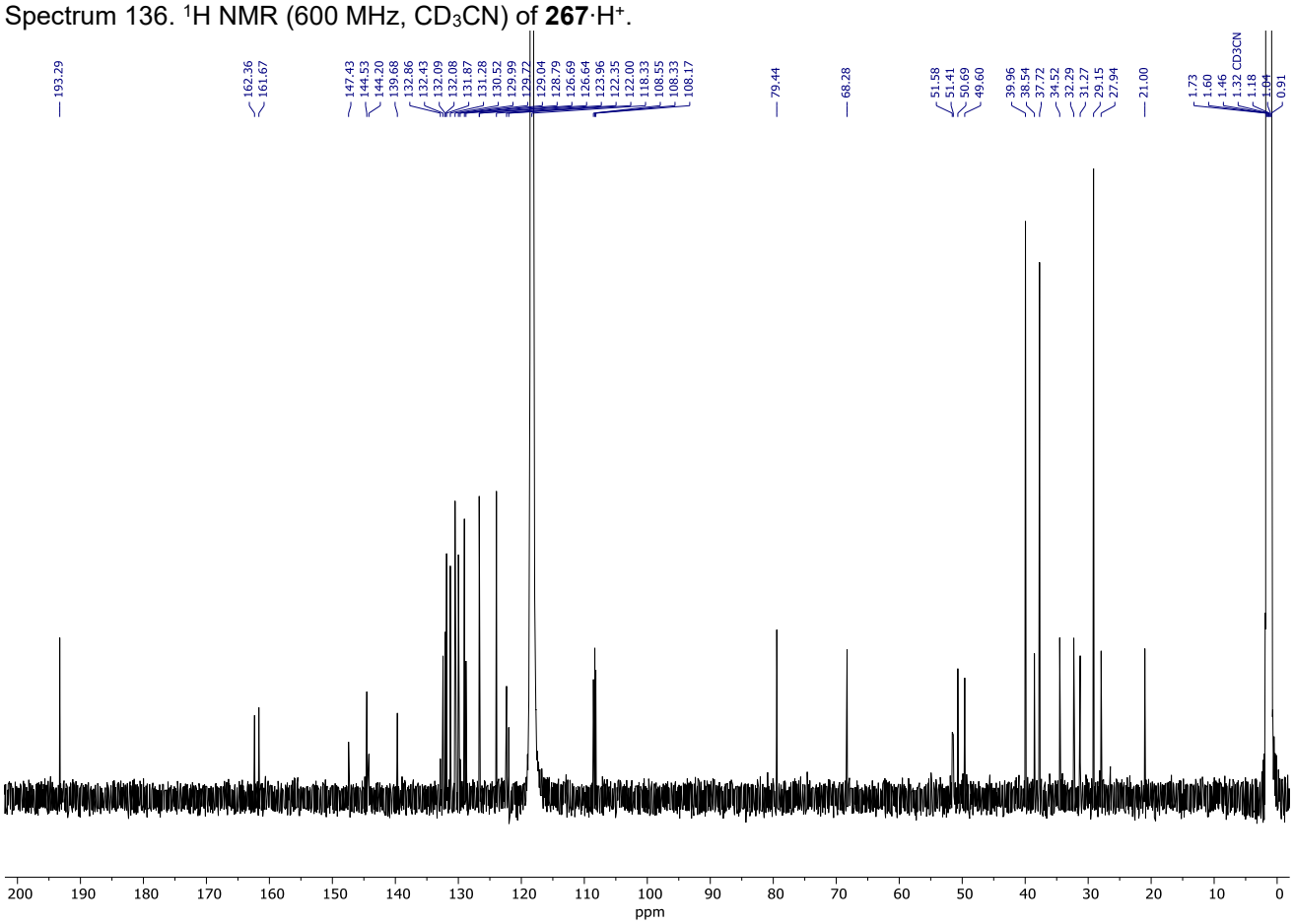

Spectrum 137. ^{13}C NMR (151 MHz, CD_3CN) of **267**·H^+.

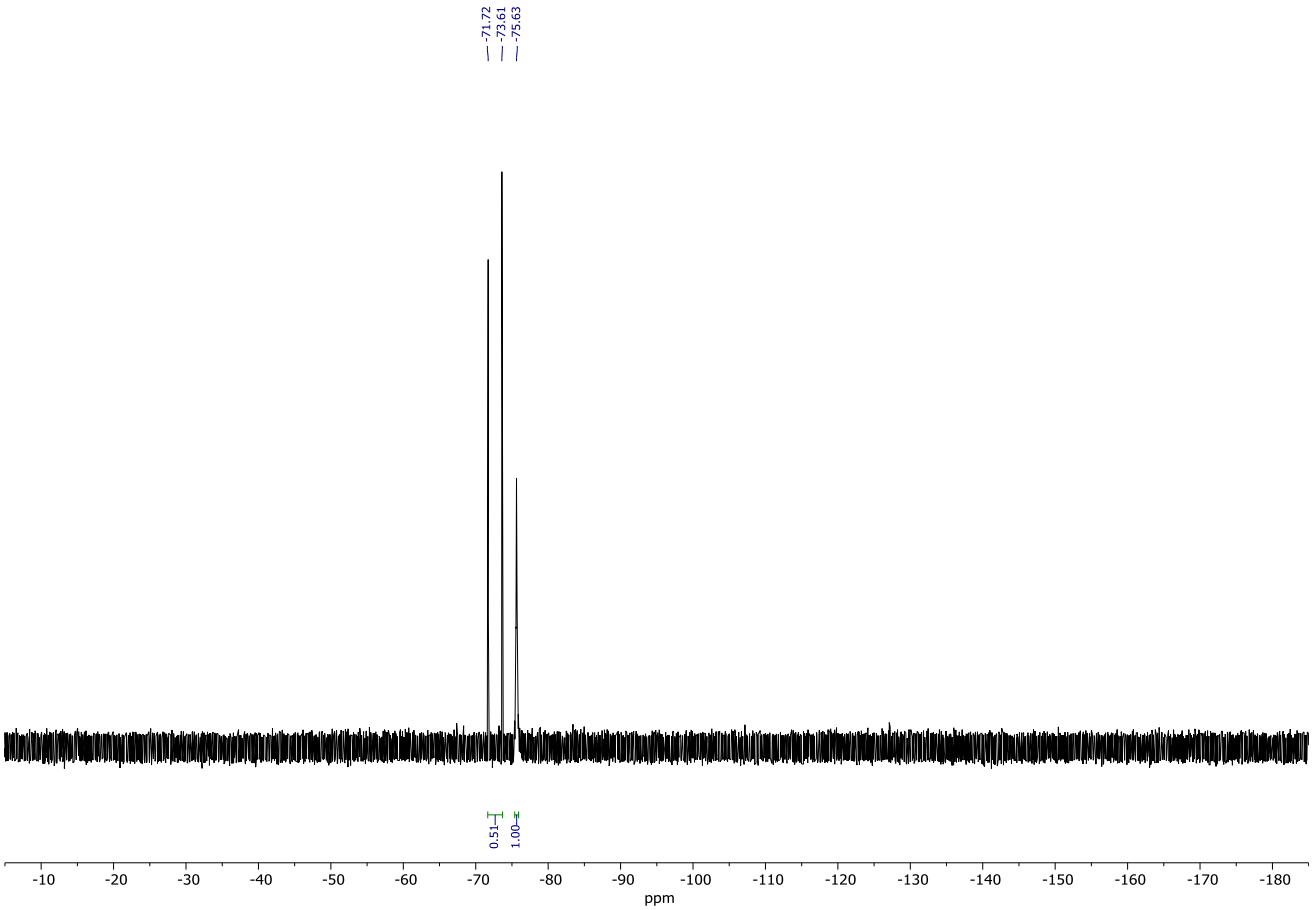

Spectrum 138. ^{19}F NMR (376 MHz, CD_2Cl_2) of **267**·H^+.

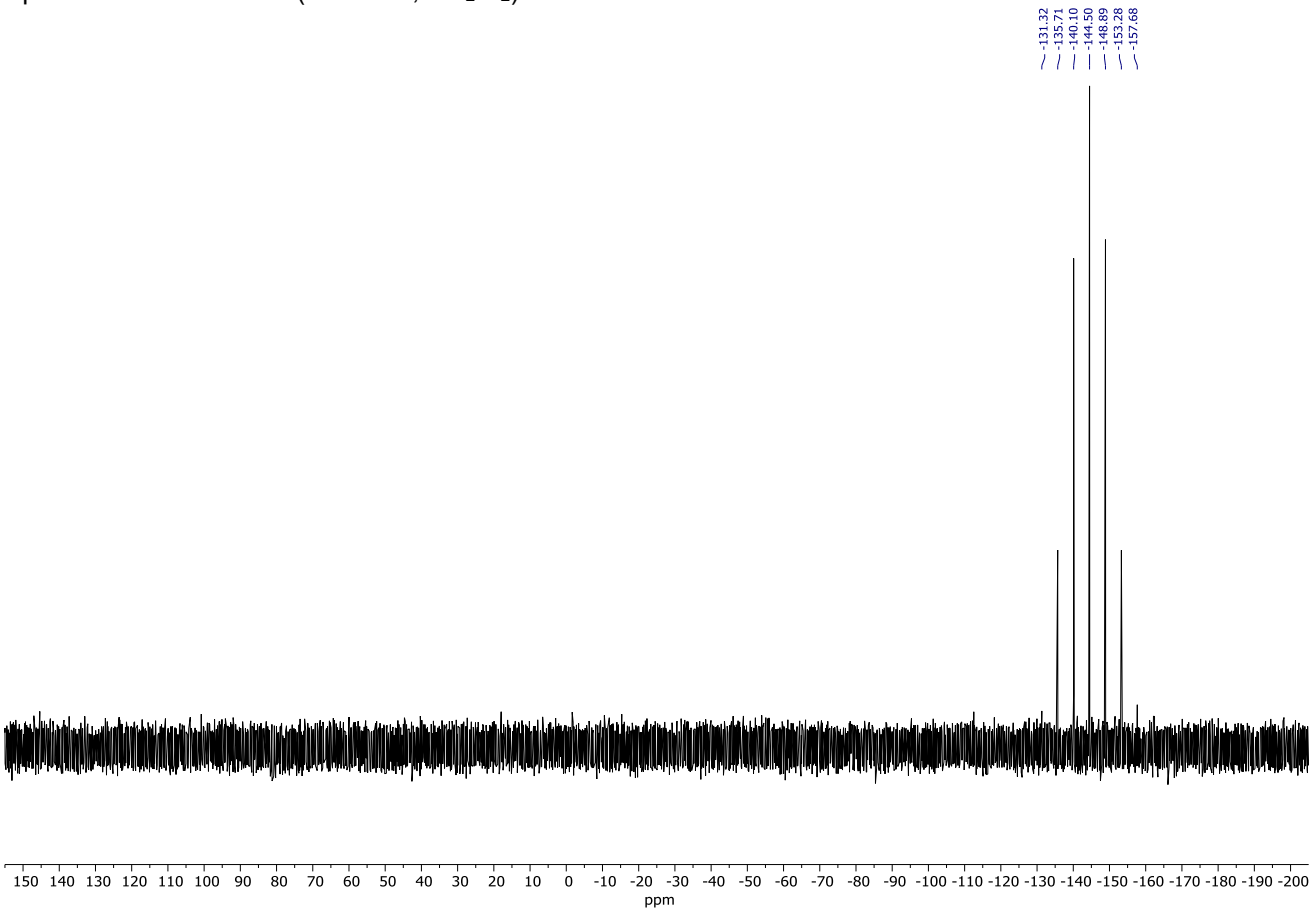

Spectrum 139. ^{31}P NMR (162 MHz, CD_2Cl_2) of **267**·H^+.

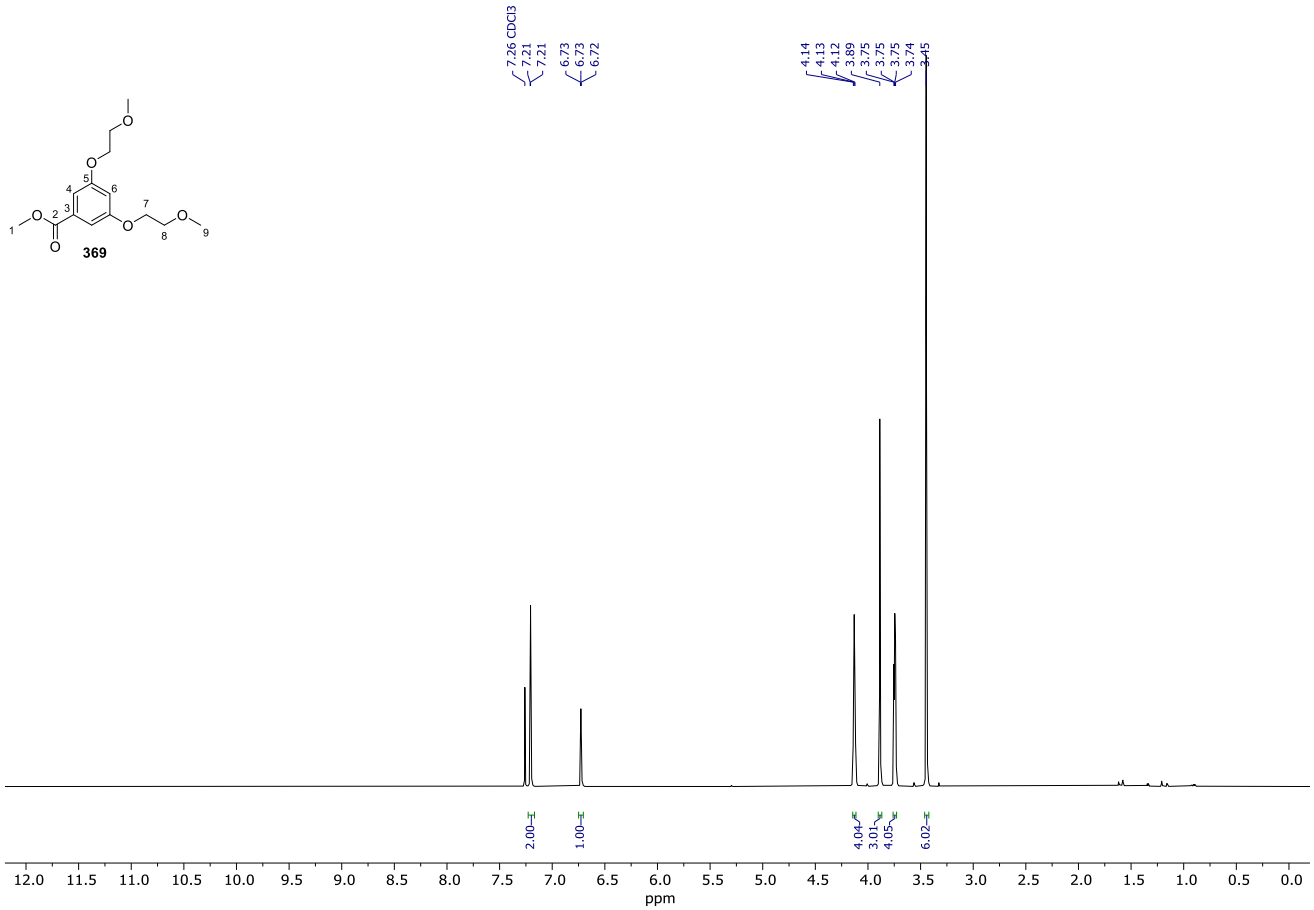

Spectrum 140. ^{1}H NMR (600 MHz, $CDCl_3$) of **369**.

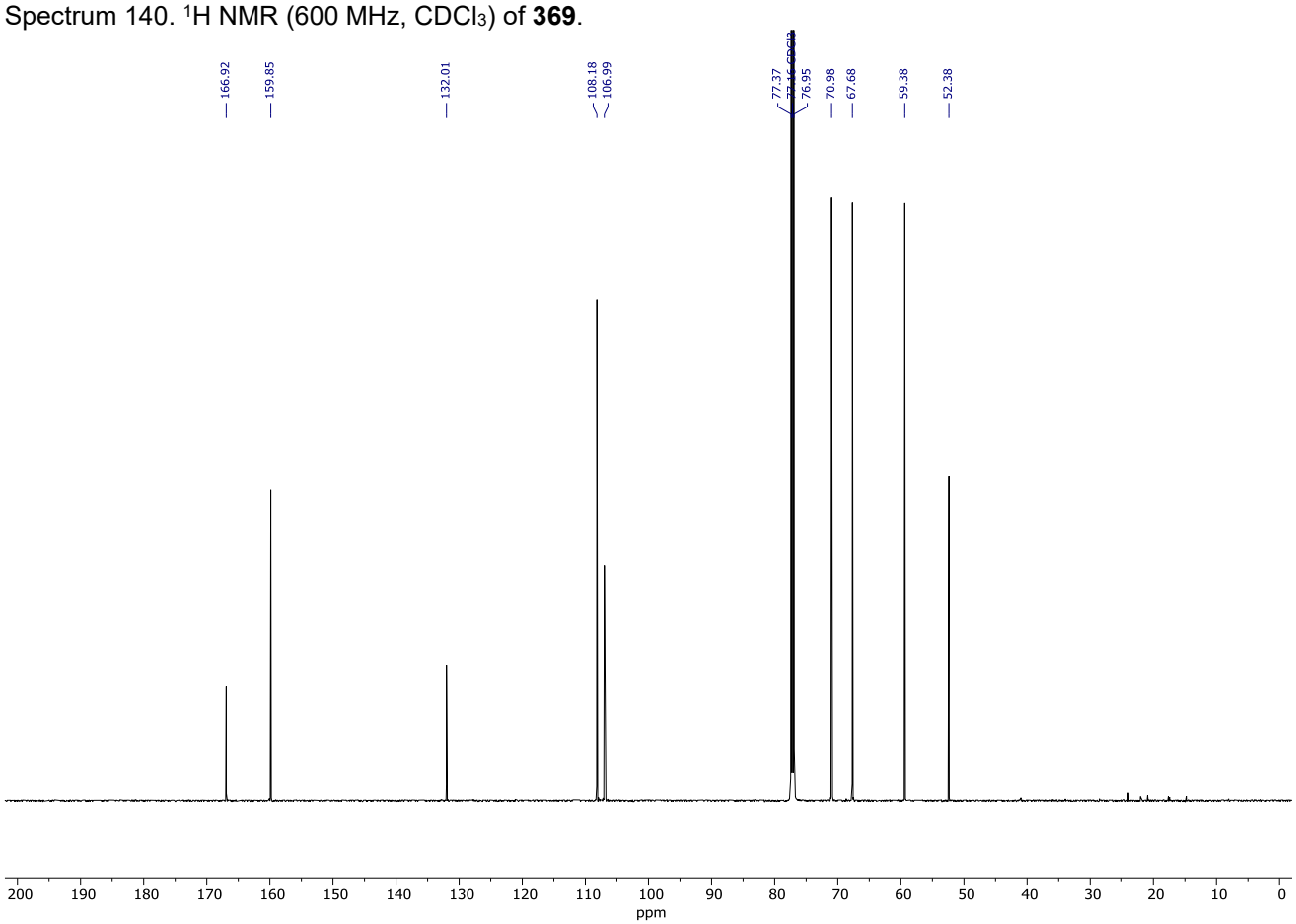

Spectrum 141. ^{13}C NMR (151 MHz, $CDCl_3$) of **369**.

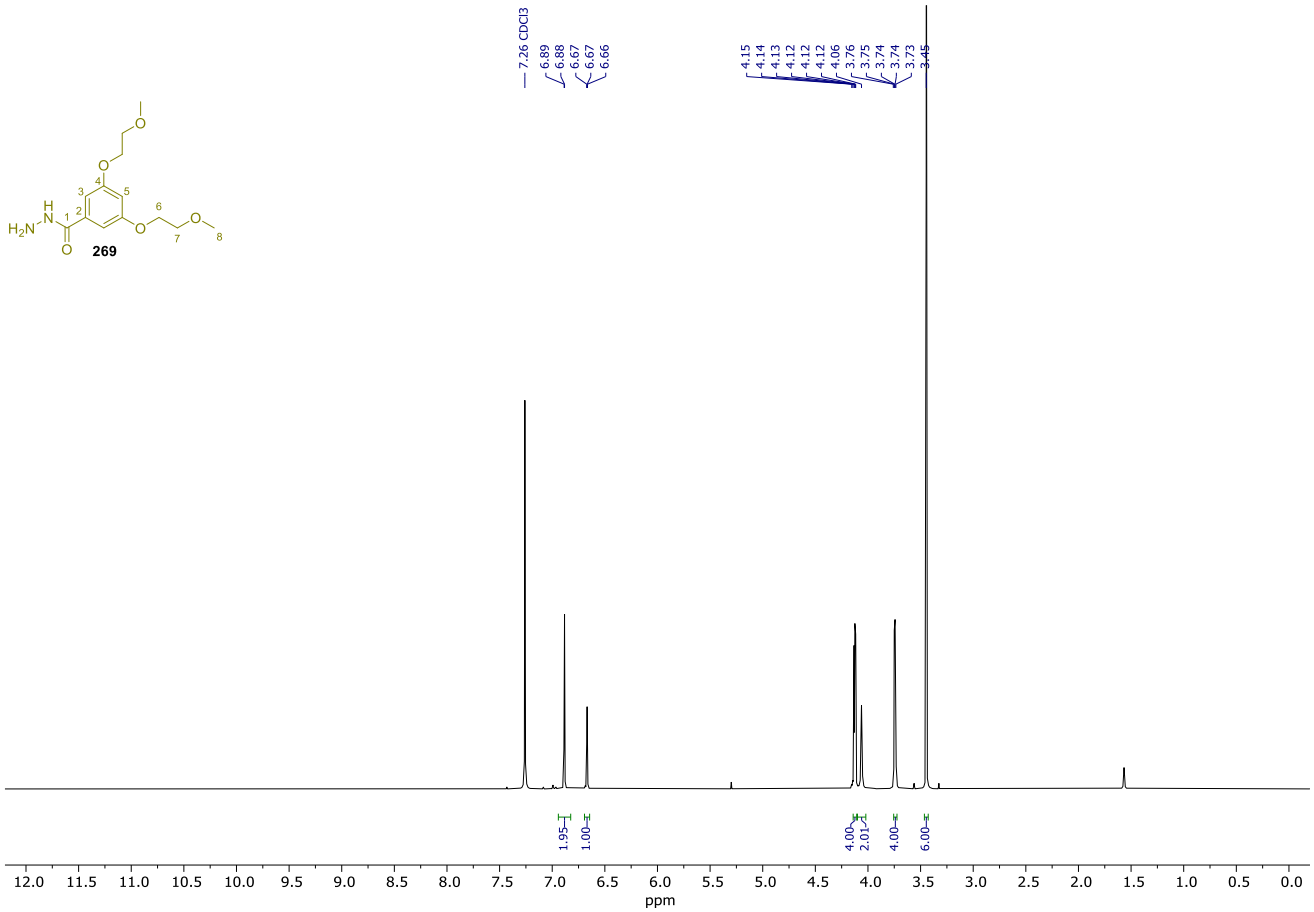

269

Spectrum 142. ^{1}H NMR (600 MHz, $CDCl_3$) of **269**.

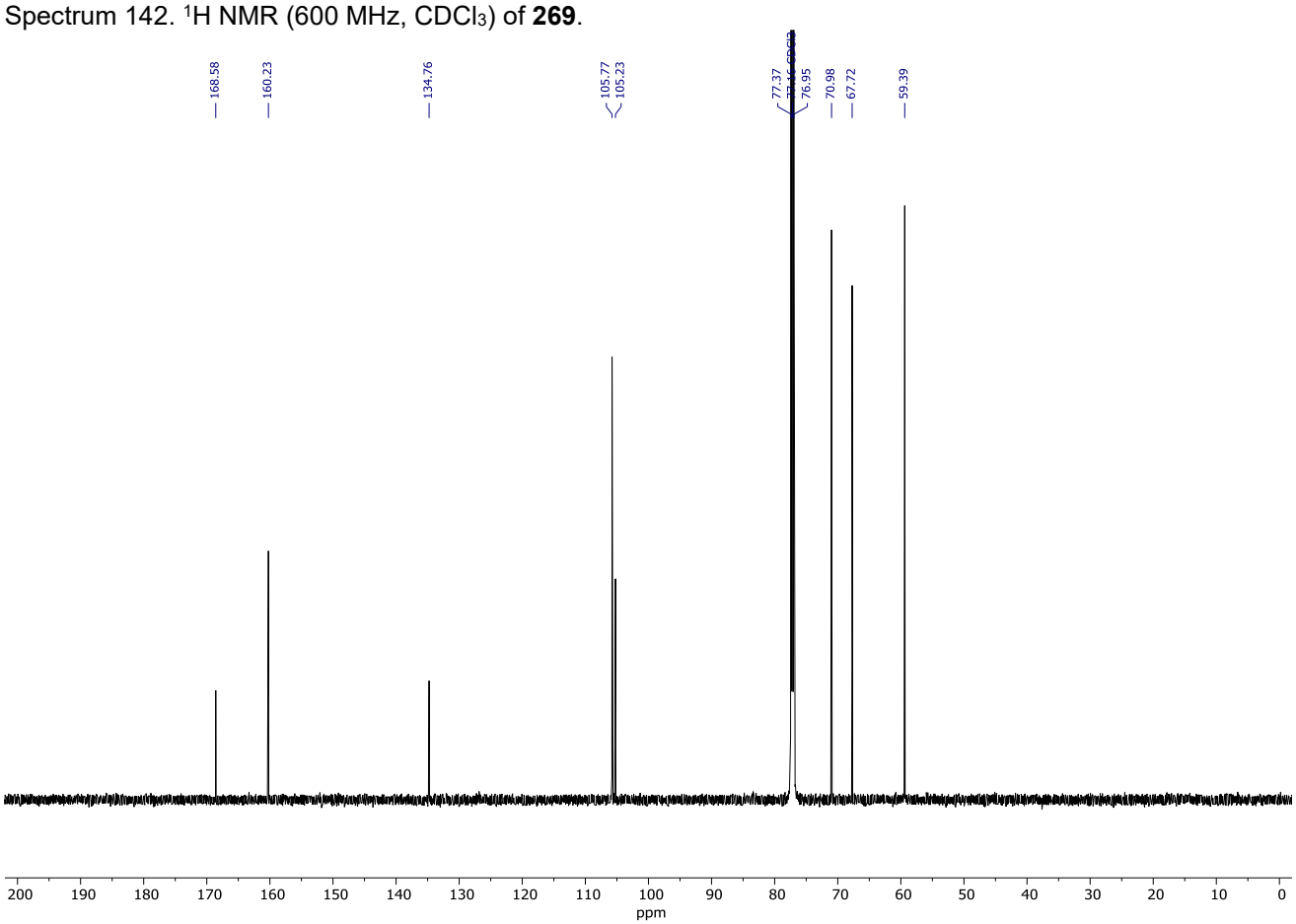

Spectrum 143. ^{13}C NMR (151 MHz, $CDCl_3$) of **269**.

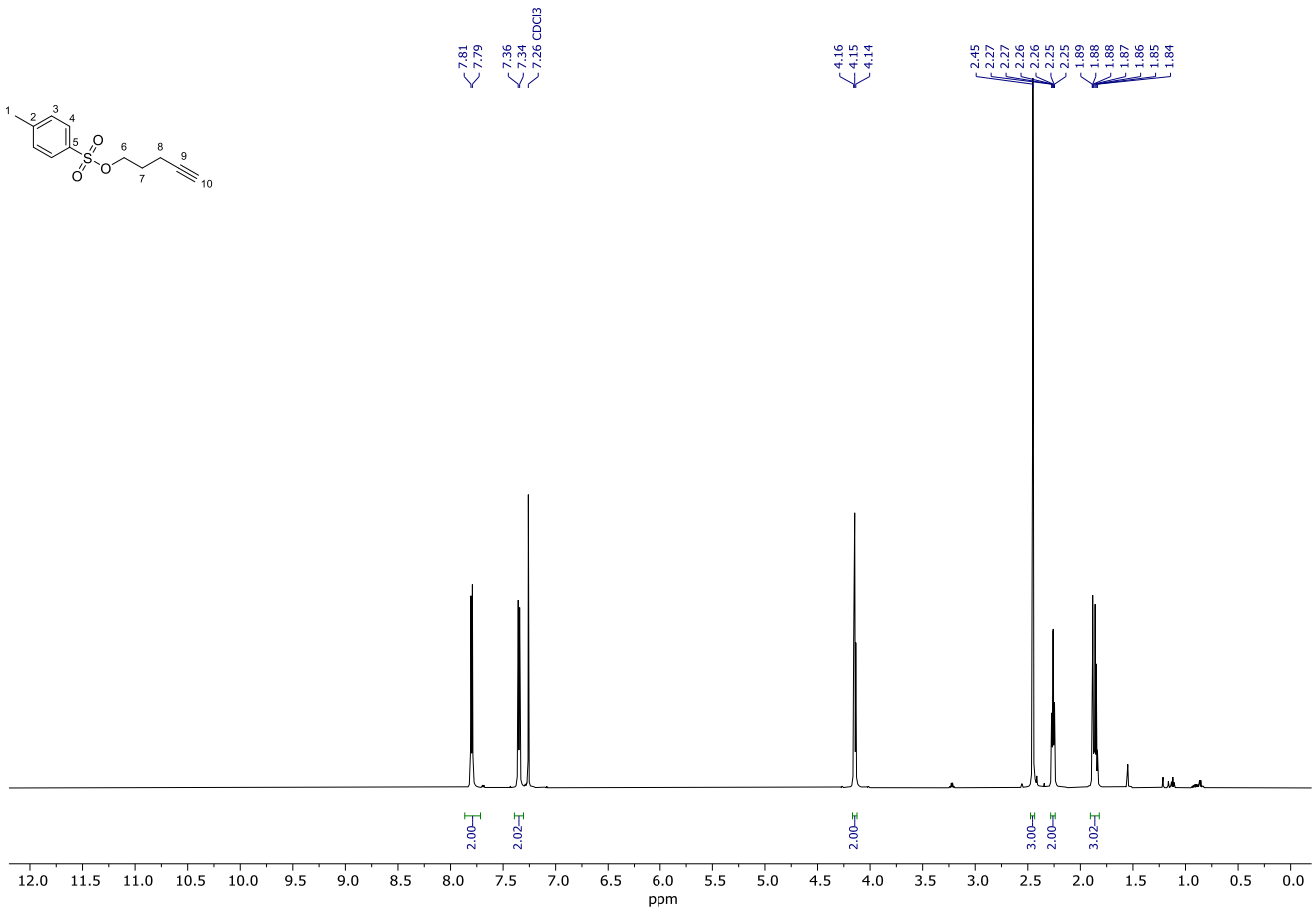

Spectrum 144. ^{1}H NMR (600 MHz, $CDCl_3$) of 4-yn-1-yl tosylate.

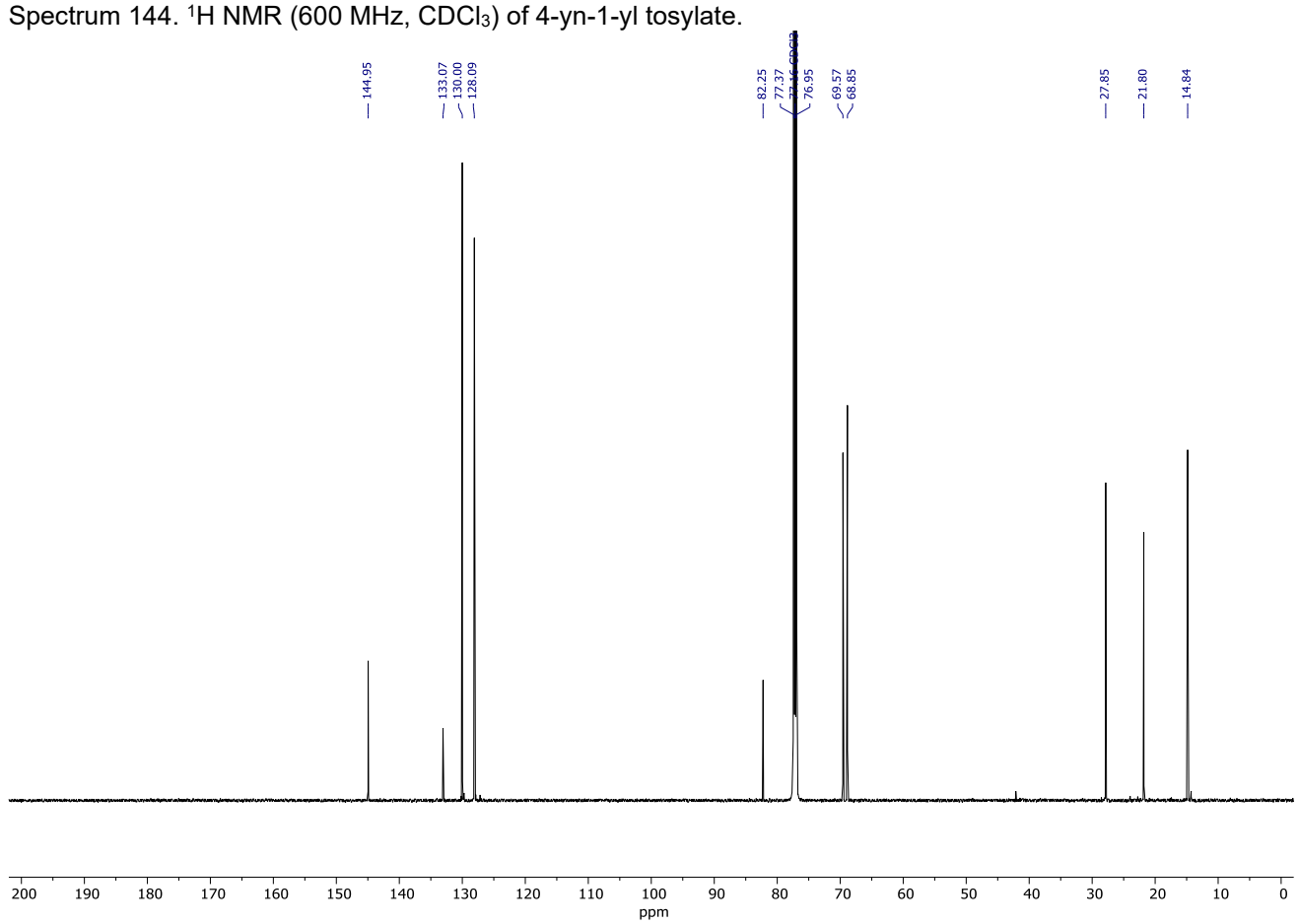

Spectrum 145. ^{13}C NMR (151 MHz, $CDCl_3$) of 4-yn-1-yl tosylate.

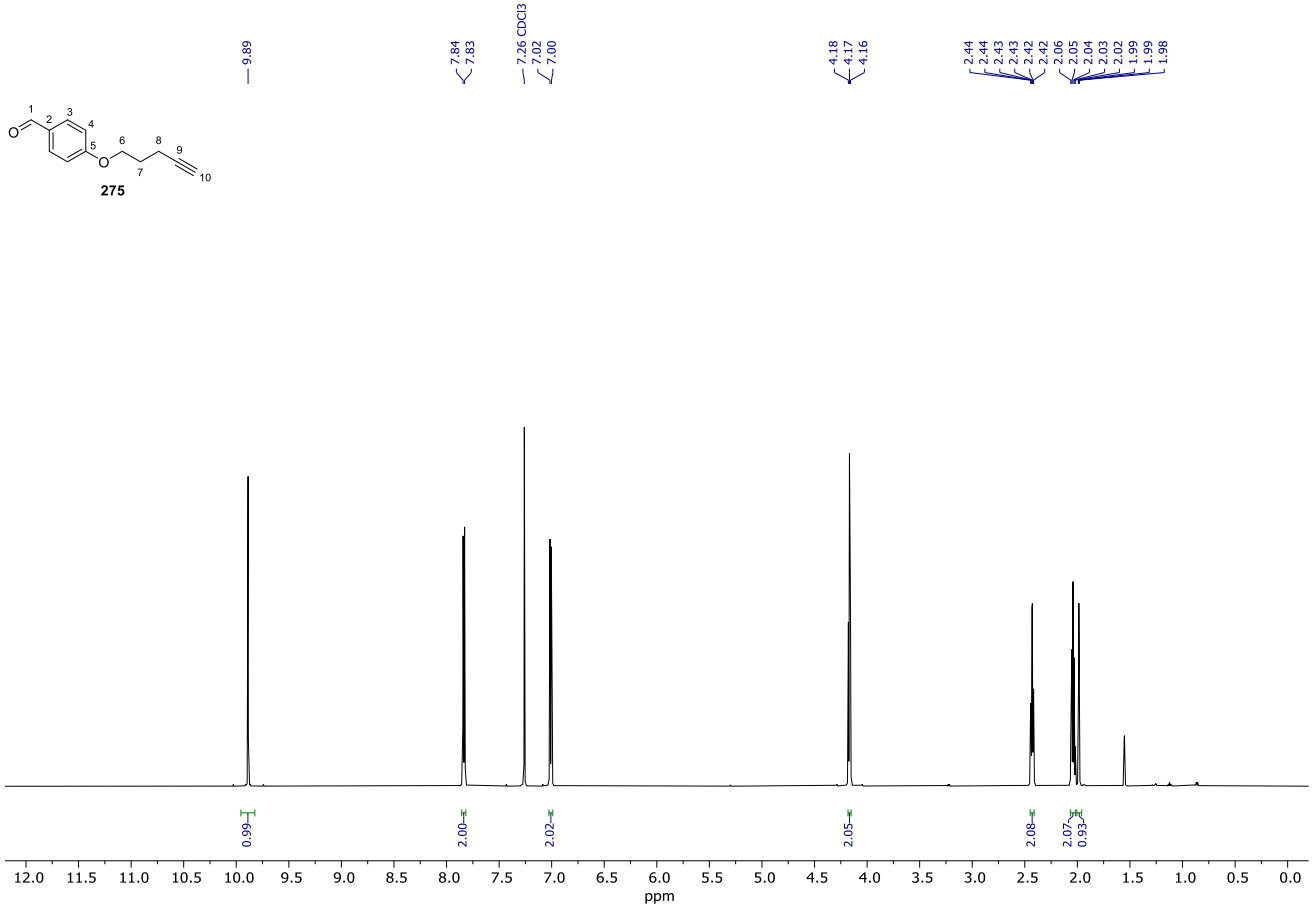

275

Spectrum 146. ^{1}H NMR (600 MHz, $CDCl_3$) of **275**.

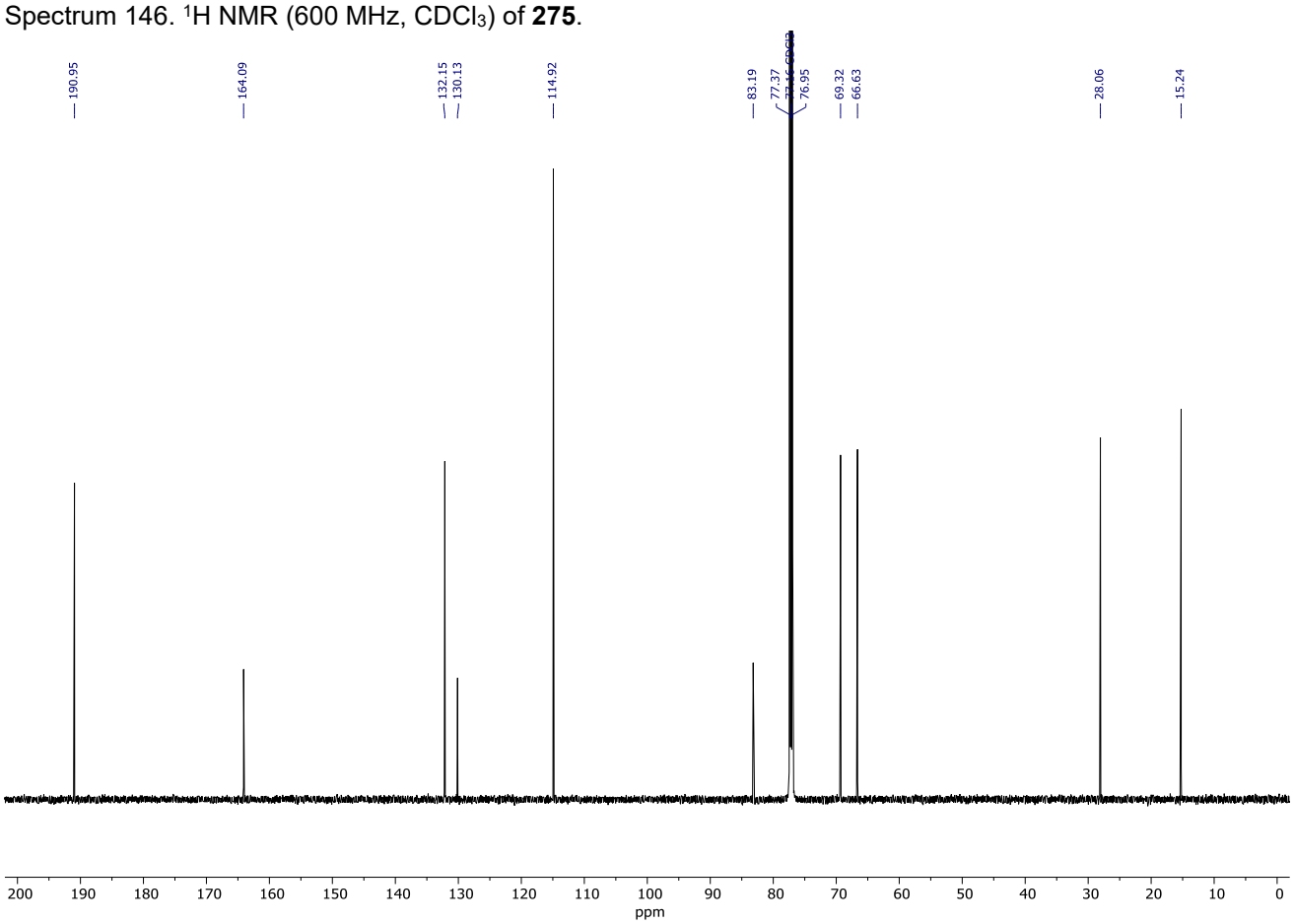

Spectrum 147. ^{13}C NMR (151 MHz, $CDCl_3$) of **275**.

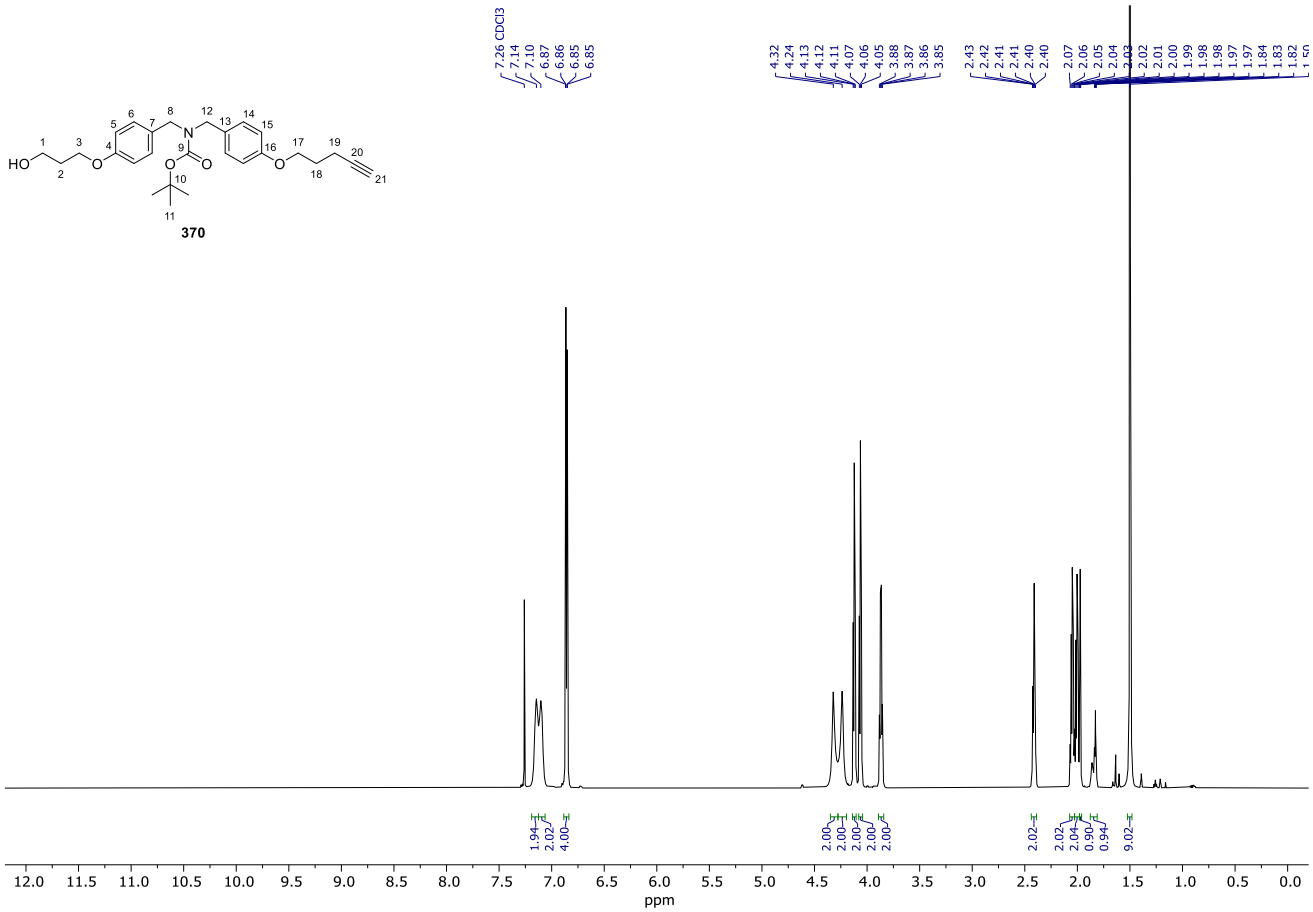

Spectrum 148. ^{1}H NMR (600 MHz, $CDCl_3$) of **370**.

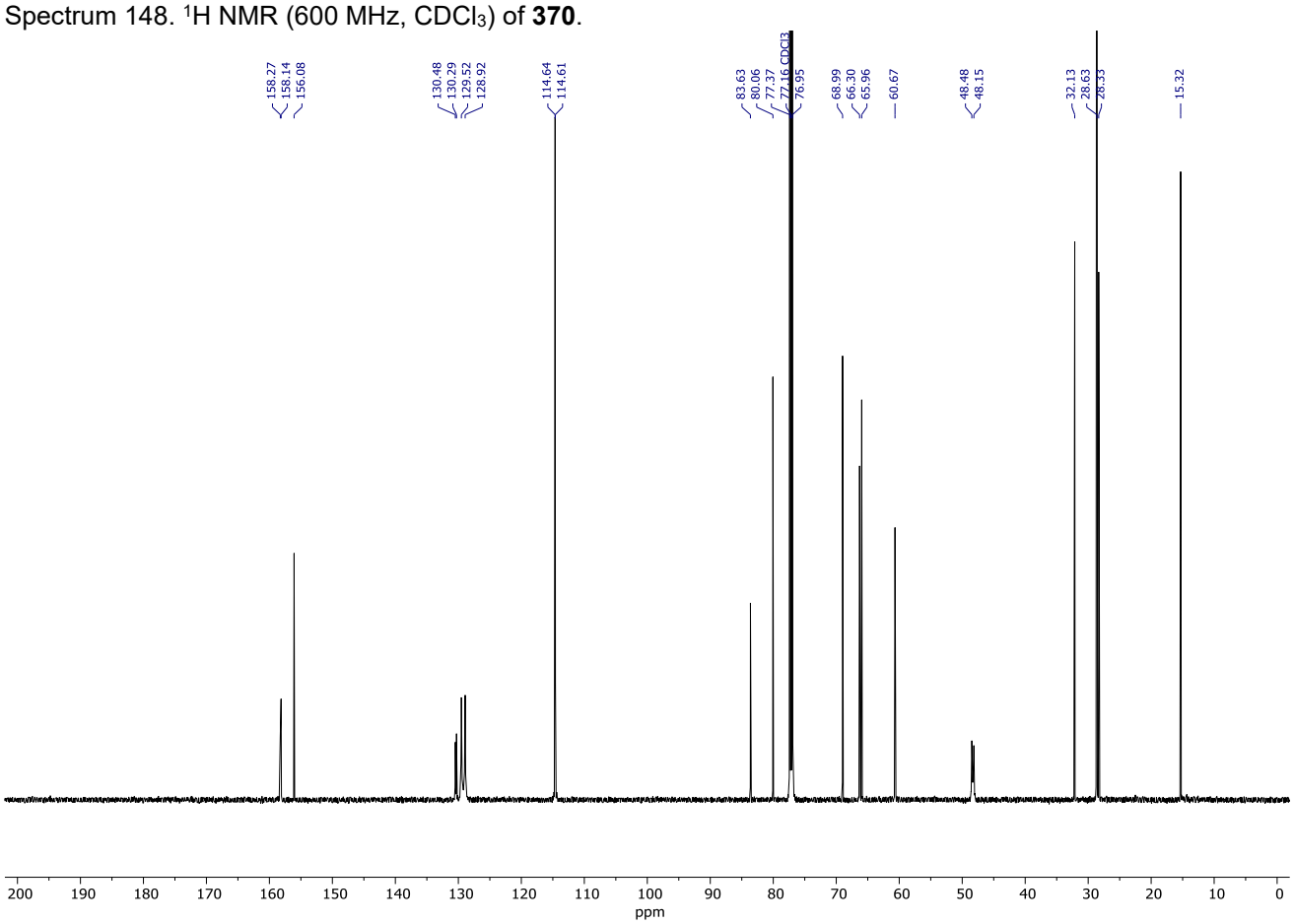

Spectrum 149. ^{13}C NMR (151 MHz, $CDCl_3$) of **370**.

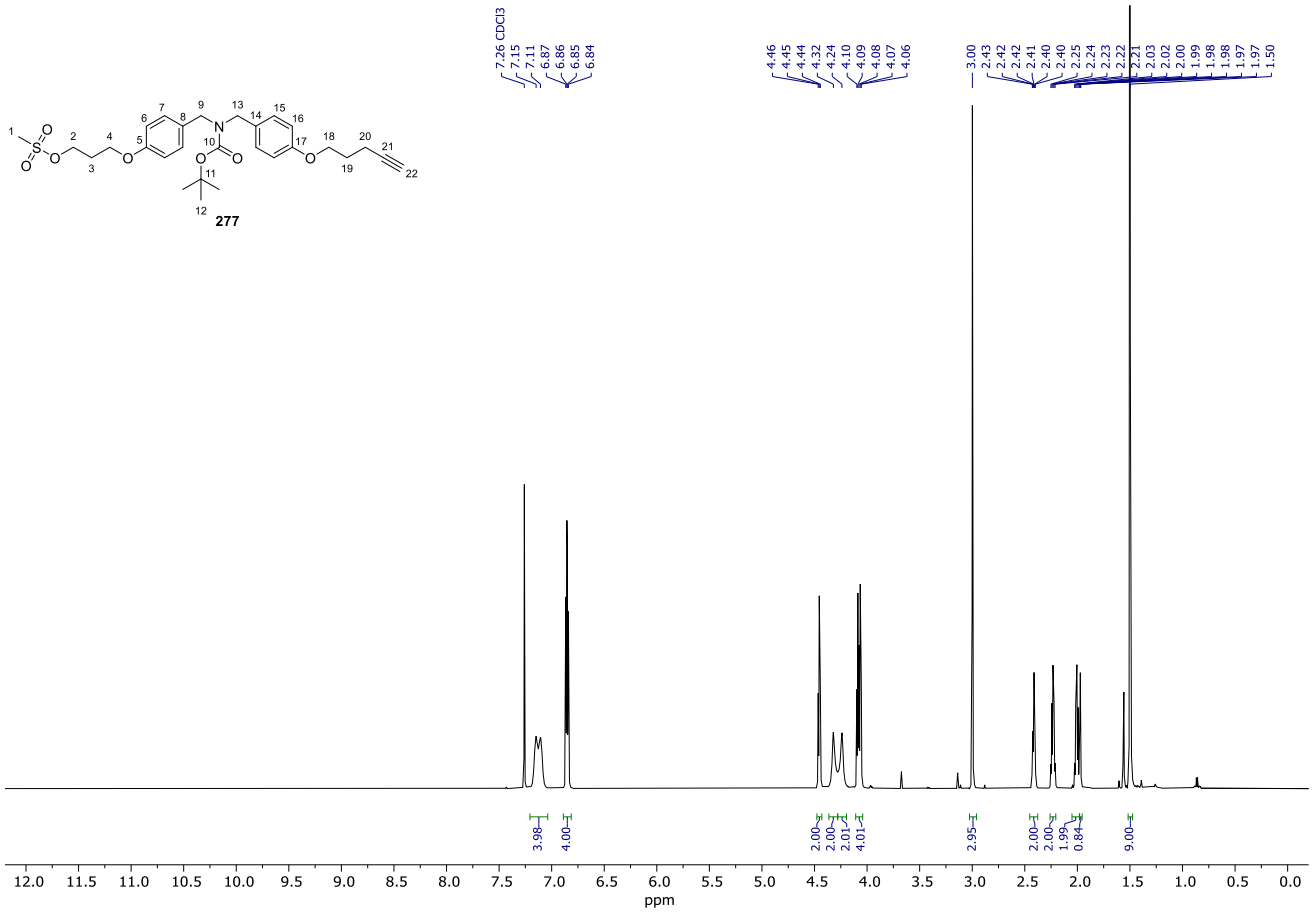

Spectrum 150. ^{1}H NMR (600 MHz, $CDCl_3$) of **277**.

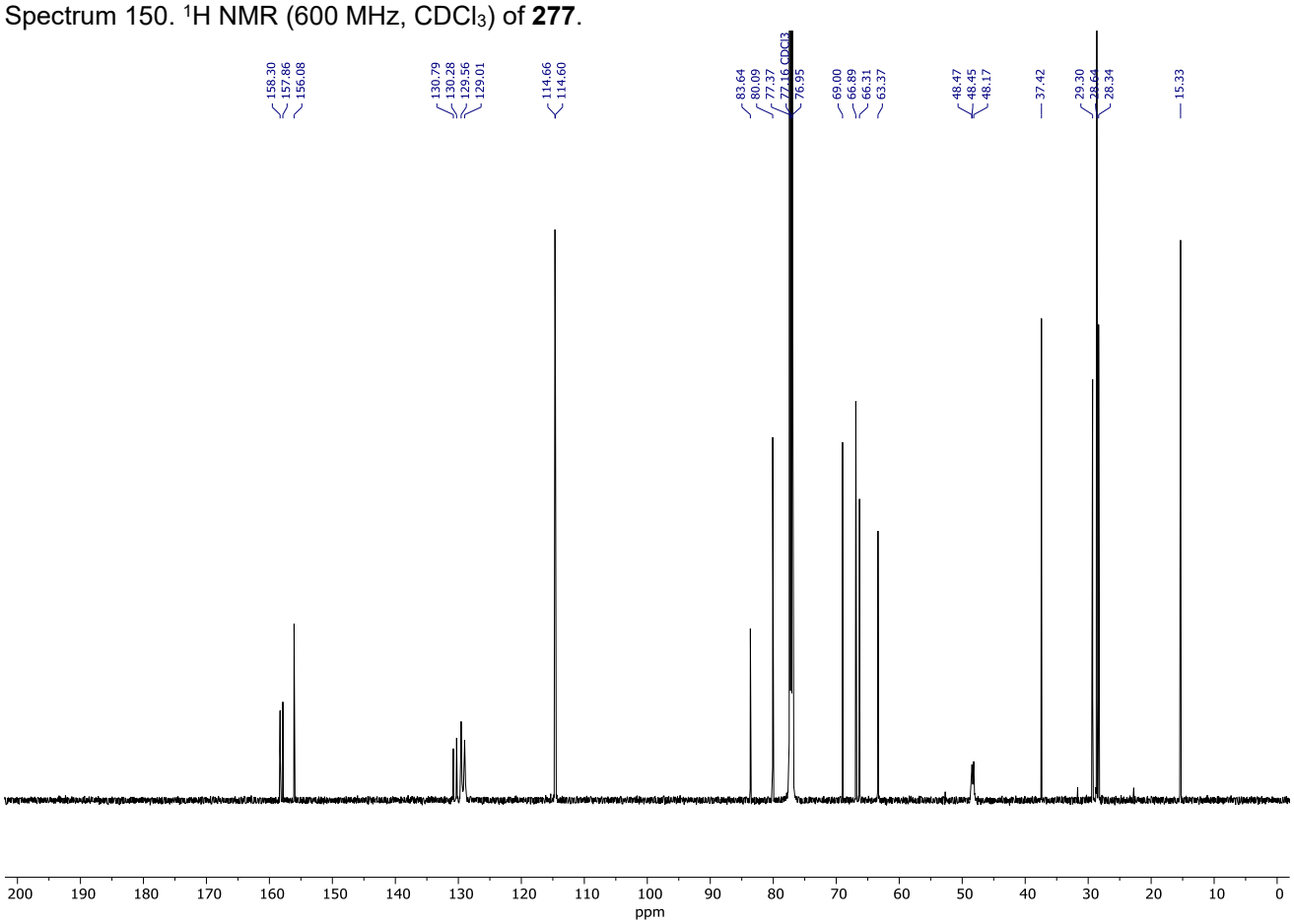

Spectrum 151. ^{13}C NMR (151 MHz, $CDCl_3$) of **277**.

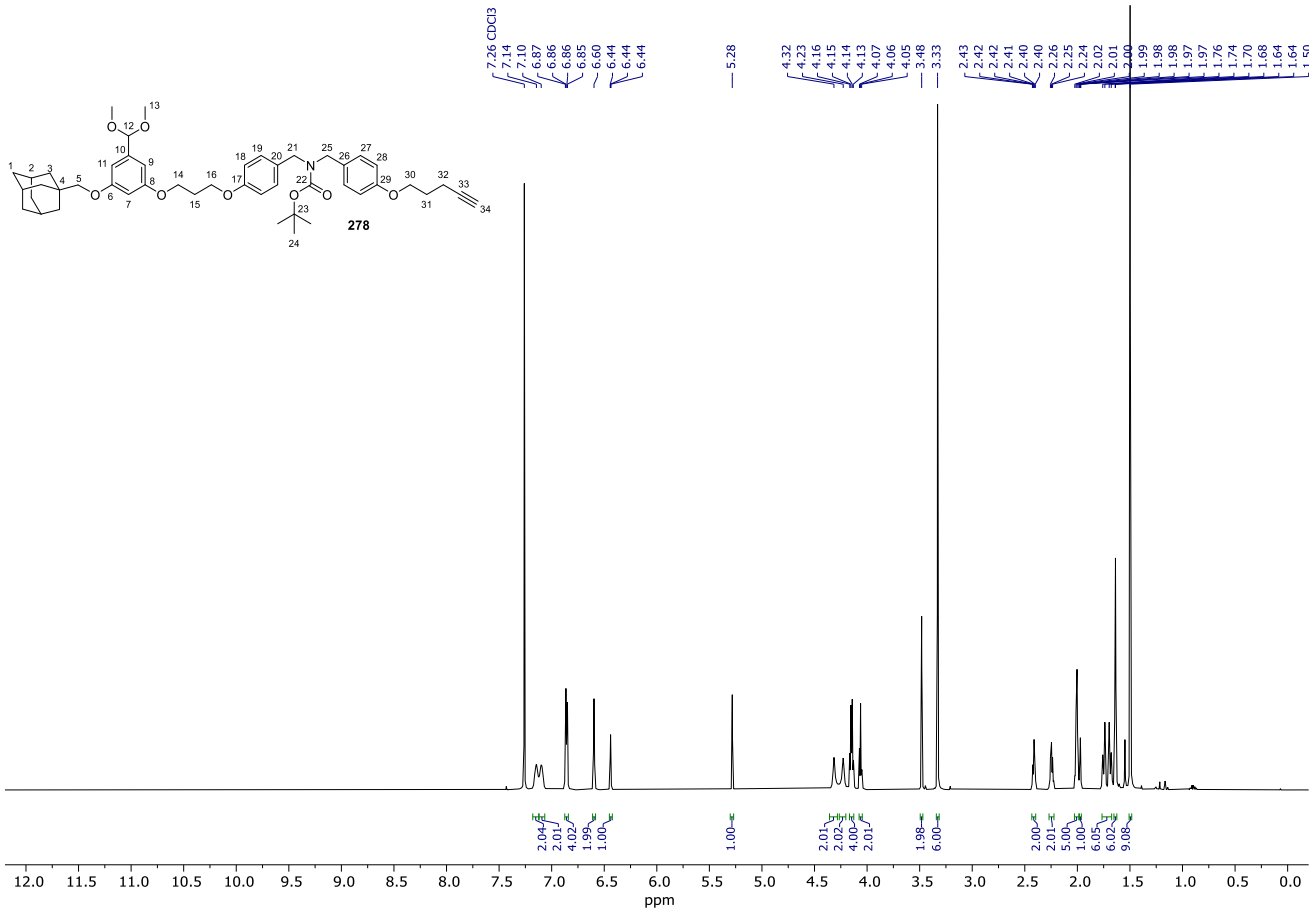

Spectrum 152. ^{1}H NMR (600 MHz, $CDCl_3$) of **278**.

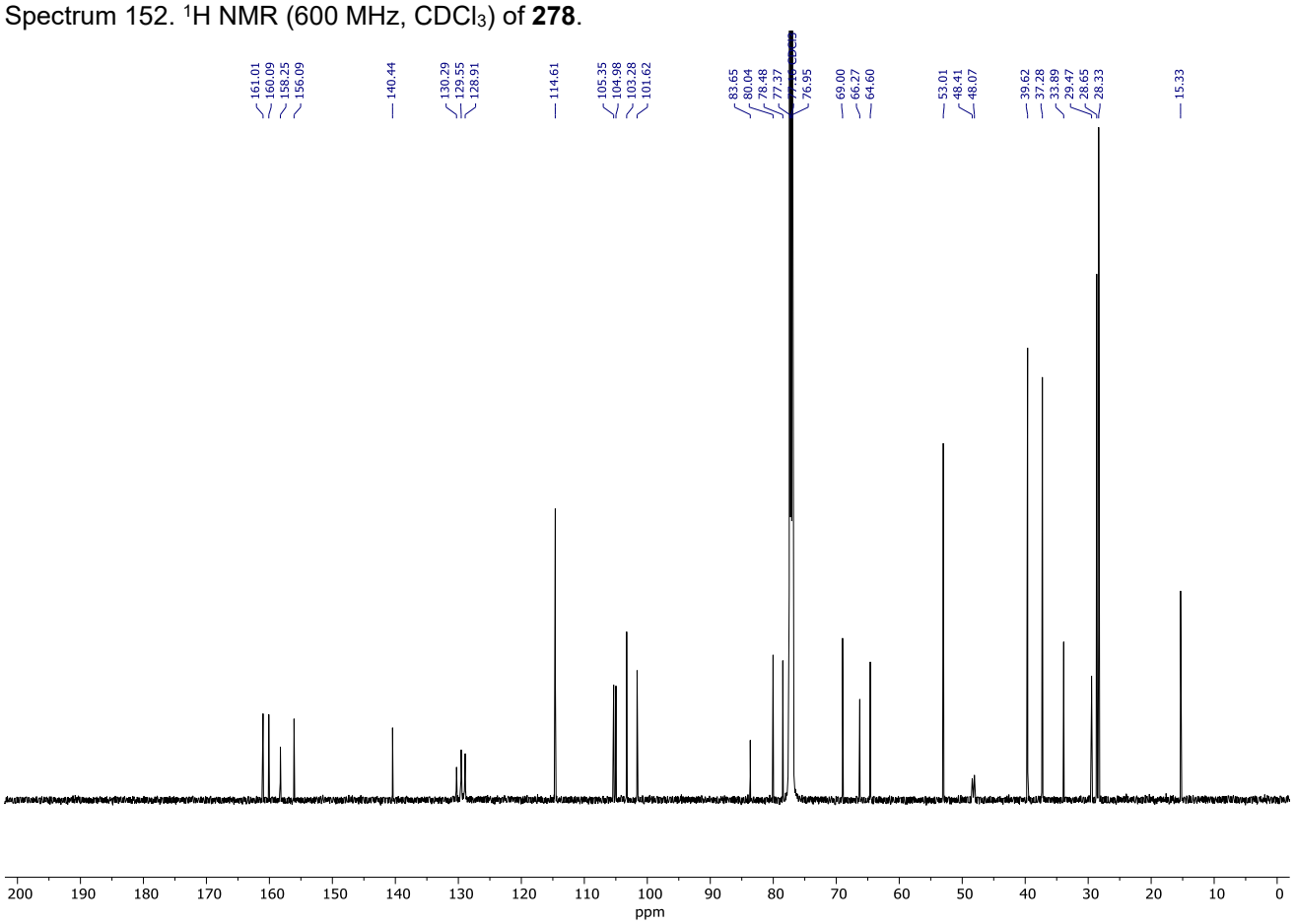

Spectrum 153. ^{13}C NMR (151 MHz, $CDCl_3$) of **278**.

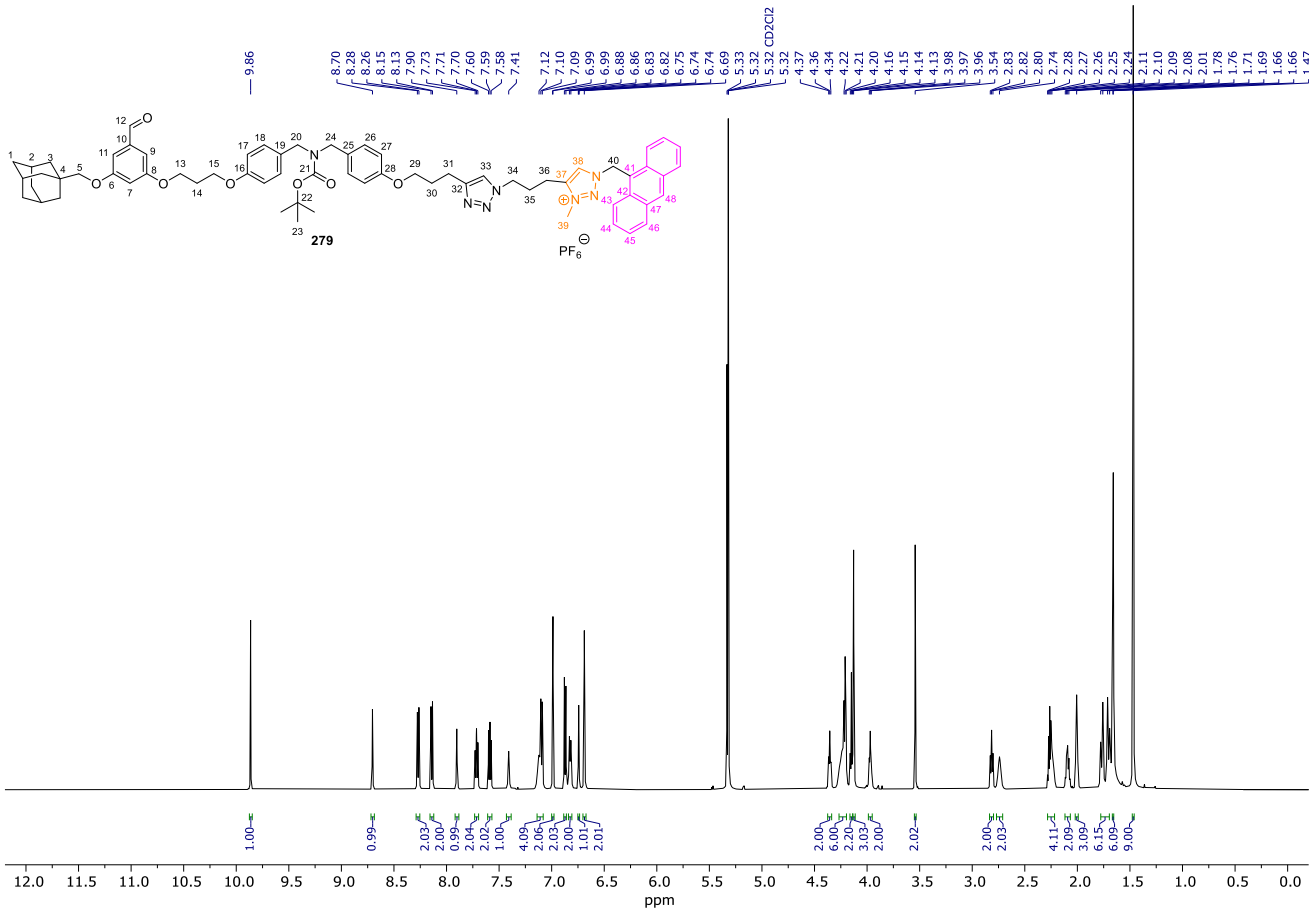

Spectrum 154. ^{1}H NMR (600 MHz, CD_2Cl_2) of **279**.

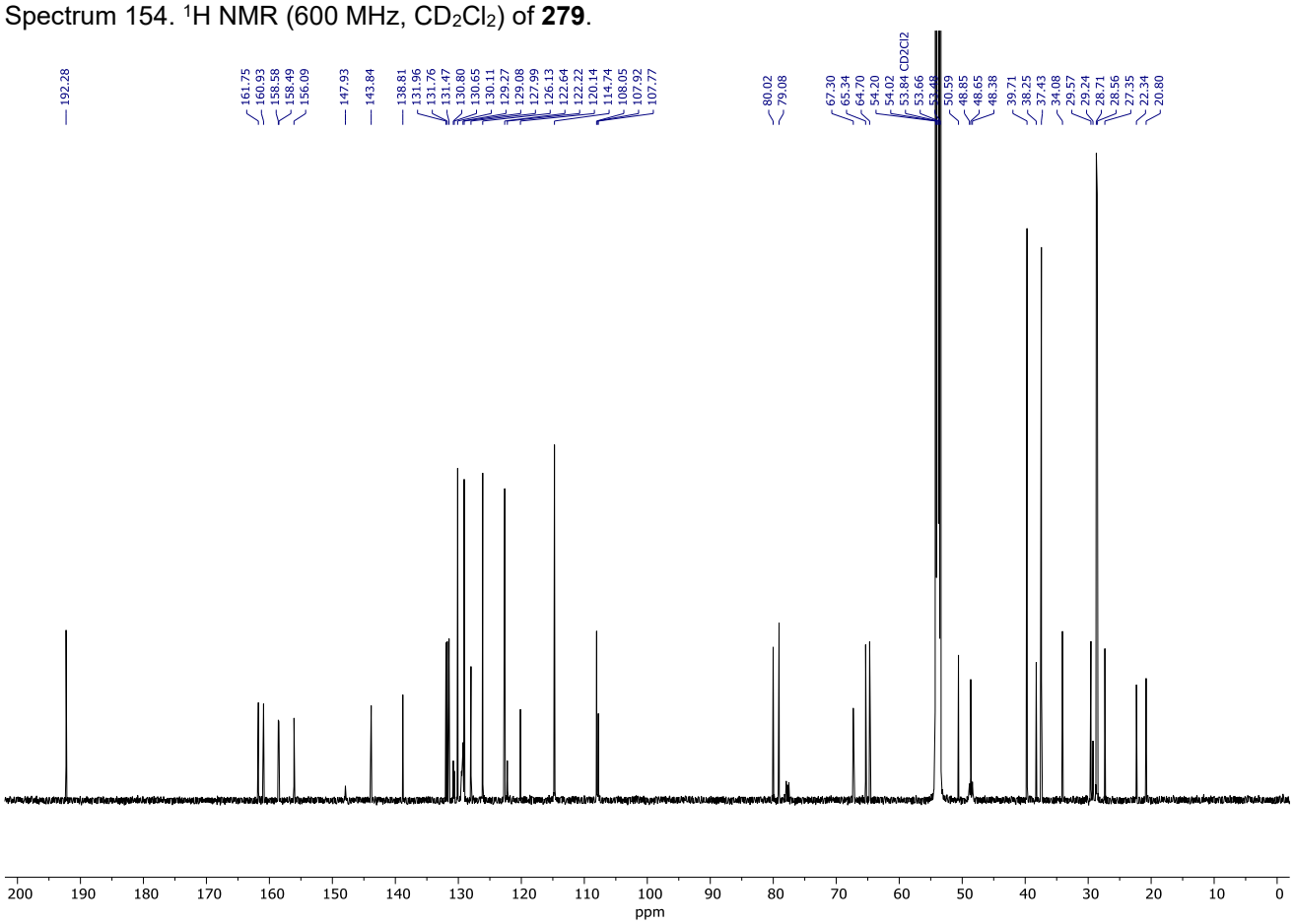

Spectrum 155. ^{13}C NMR (151 MHz, CD_2Cl_2) of **279**.

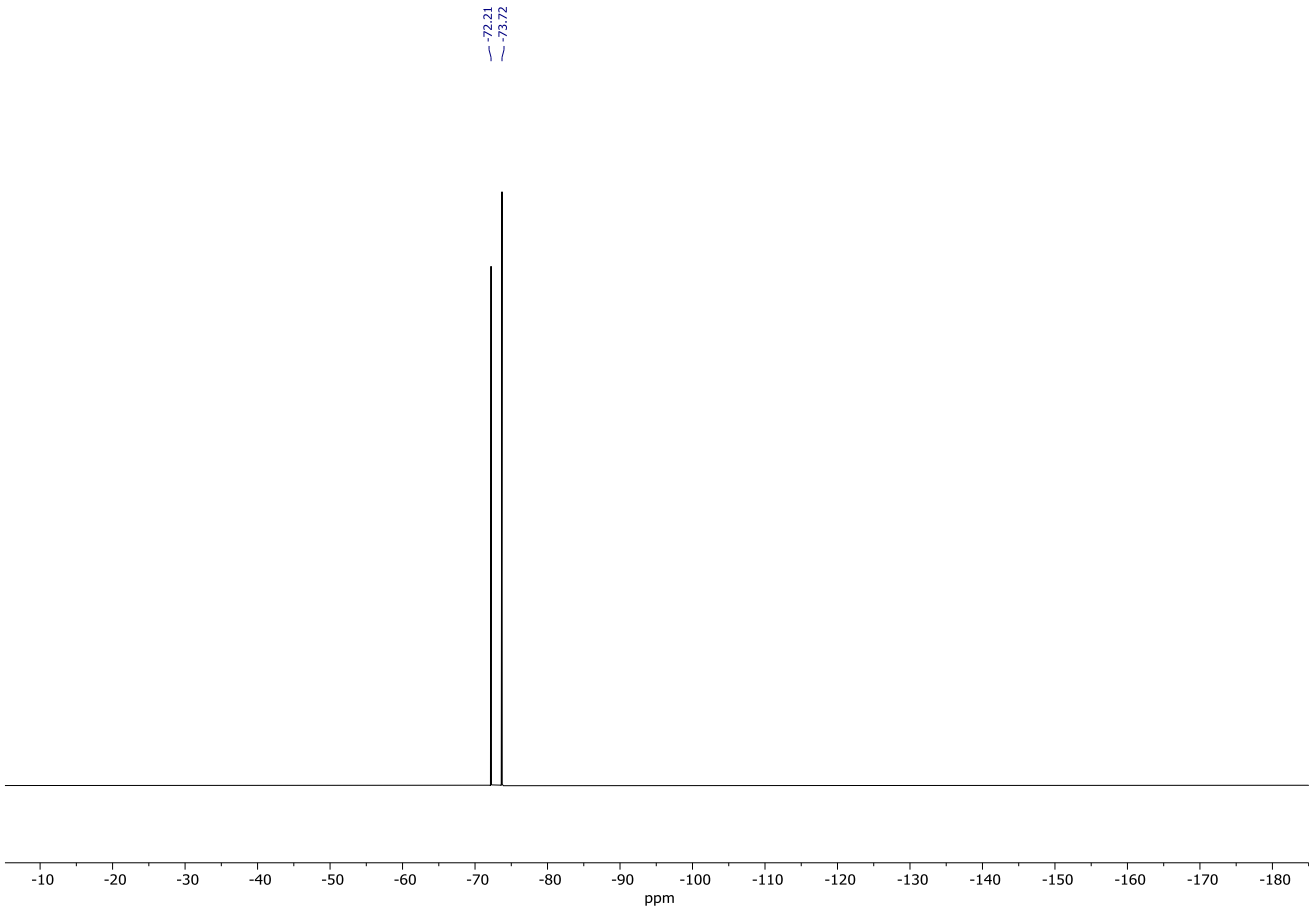

Spectrum 156. ^{19}F NMR (376 MHz, CD_2Cl_2) of **279**.

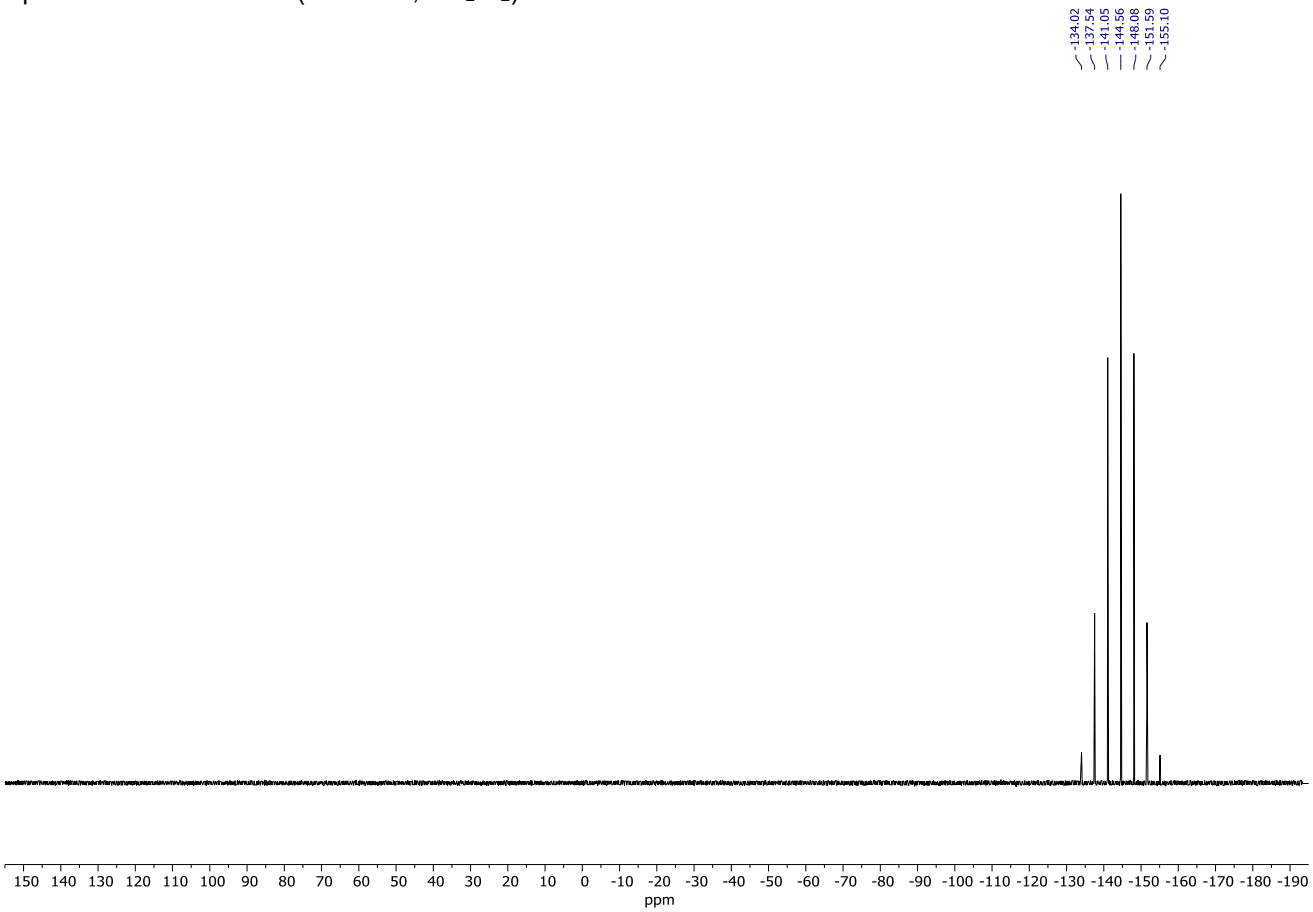

Spectrum 157. ^{31}P NMR (162 MHz, CD_2Cl_2) of **279**.

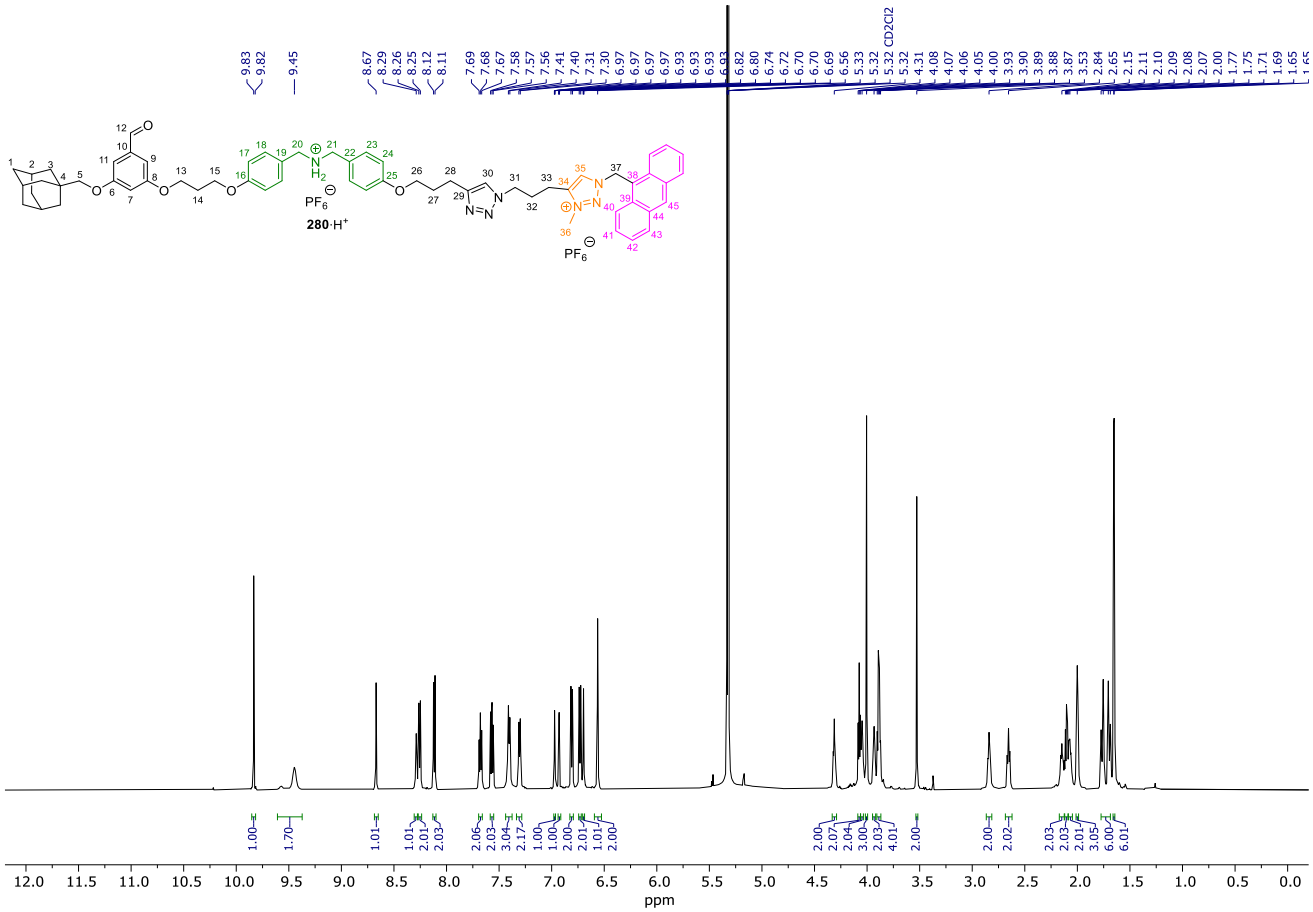

Spectrum 158. ^{1}H NMR (600 MHz, CD_2Cl_2) of **280**·H^+.

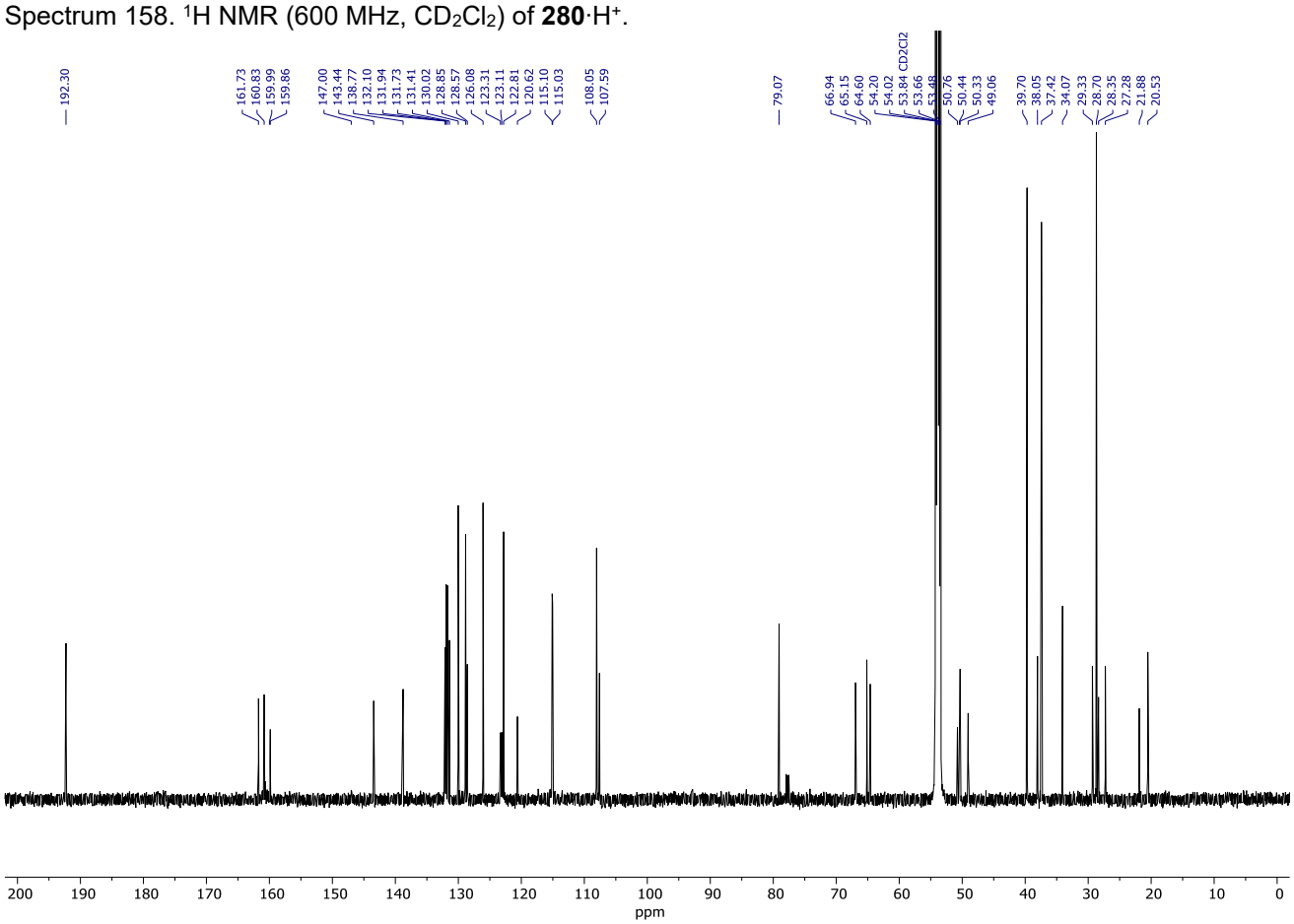

Spectrum 159. ^{13}C NMR (151 MHz, CD_2Cl_2) of **280**·H^+.

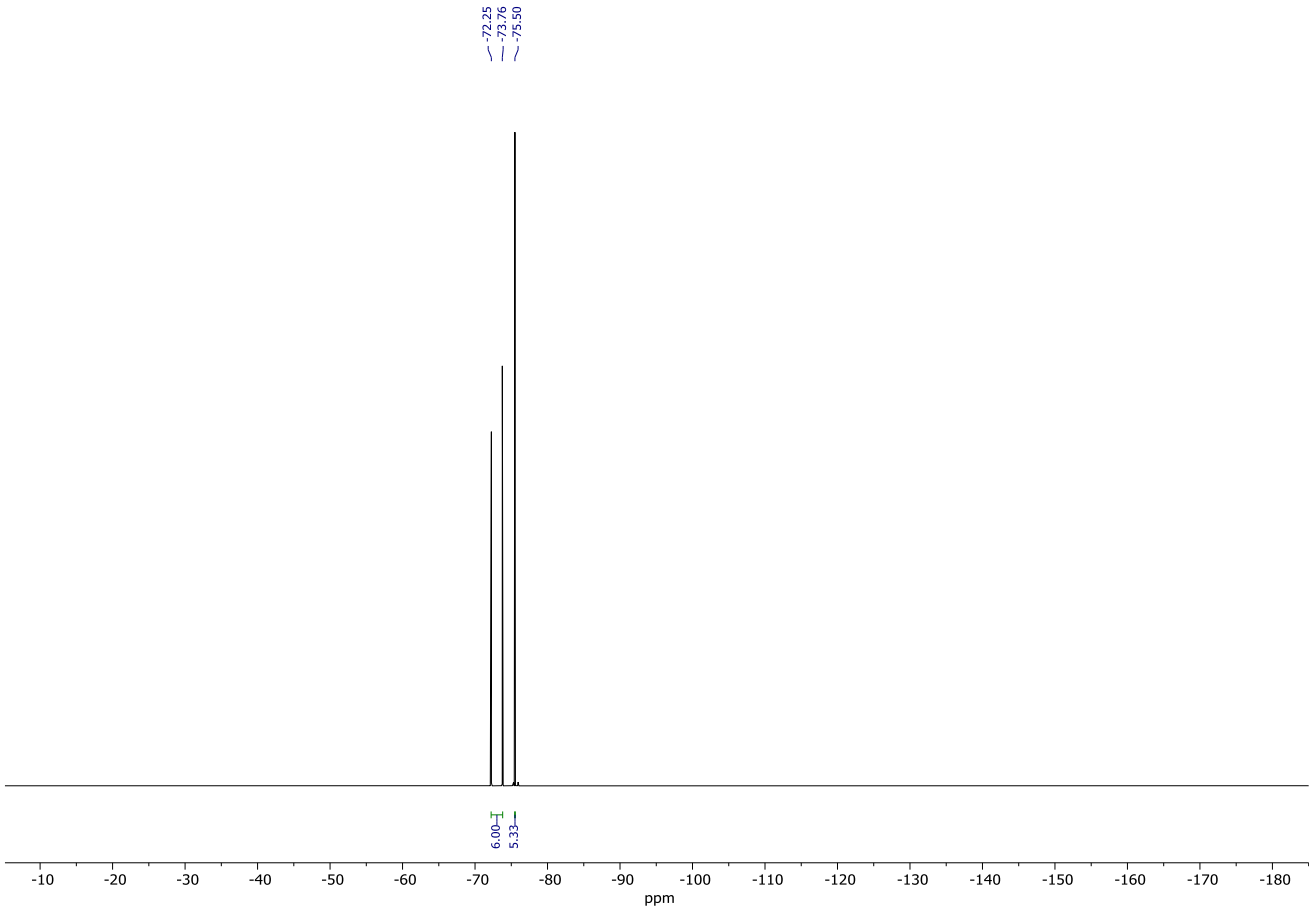

Spectrum 160. ^{19}F NMR (471 MHz, CD_2Cl_2) of **280**·H^+.

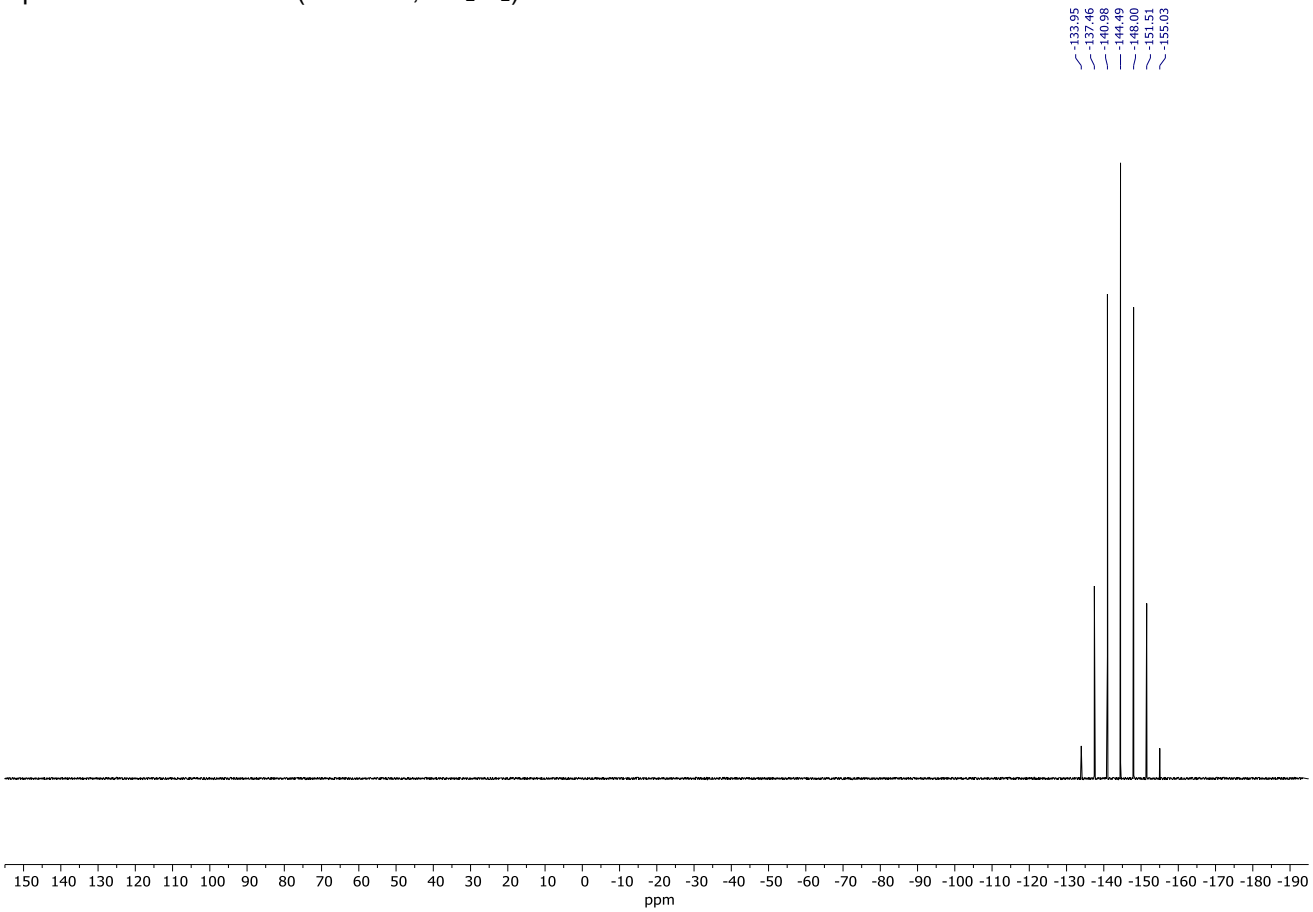

Spectrum 161. ^{31}P NMR (202 MHz, CD_2Cl_2) of **280**·H^+.

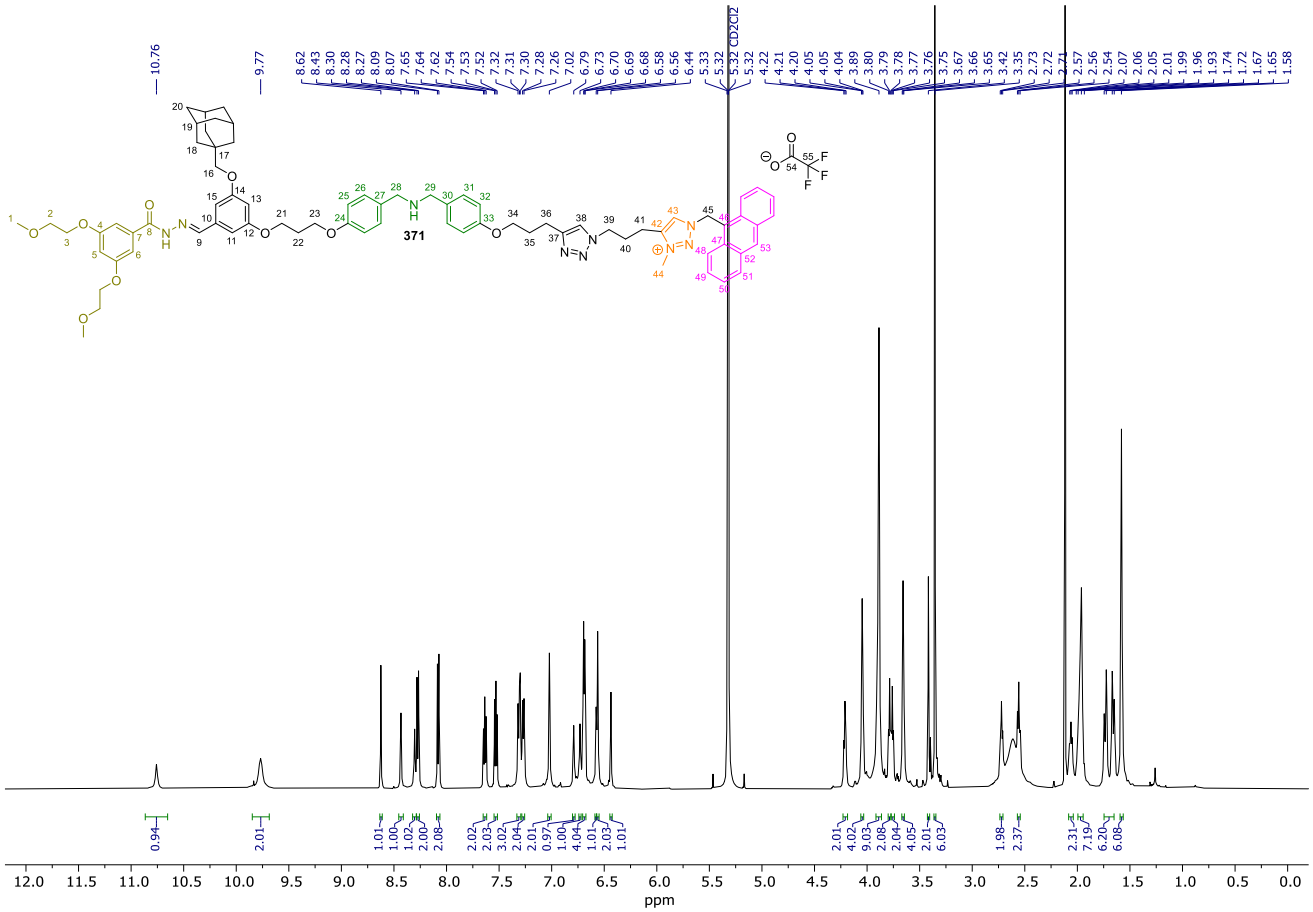

Spectrum 162. ^{1}H NMR (600 MHz, $CDCl_3$) of **371**.

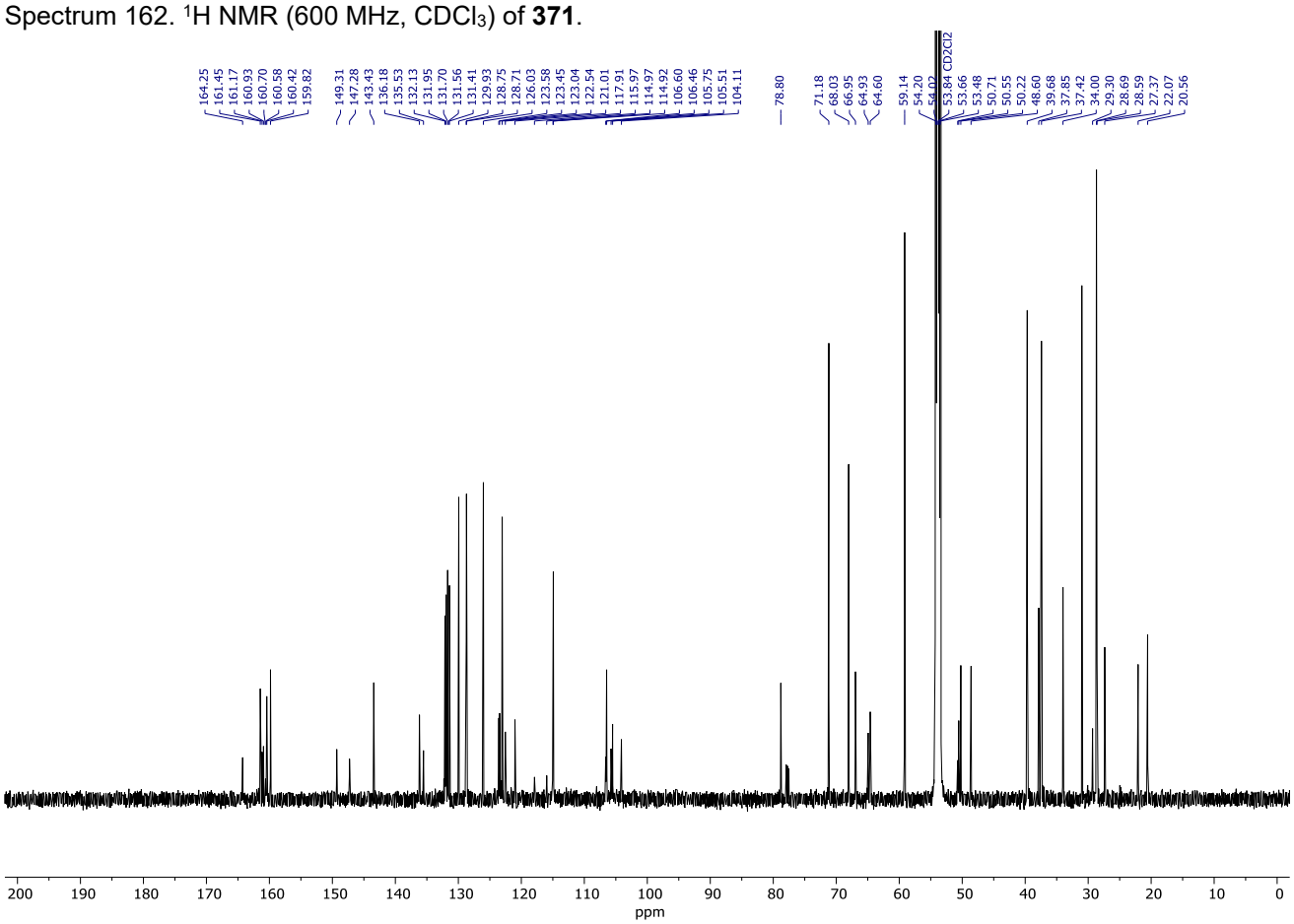

Spectrum 163. ^{13}C NMR (151 MHz, $CDCl_3$) of **371**.

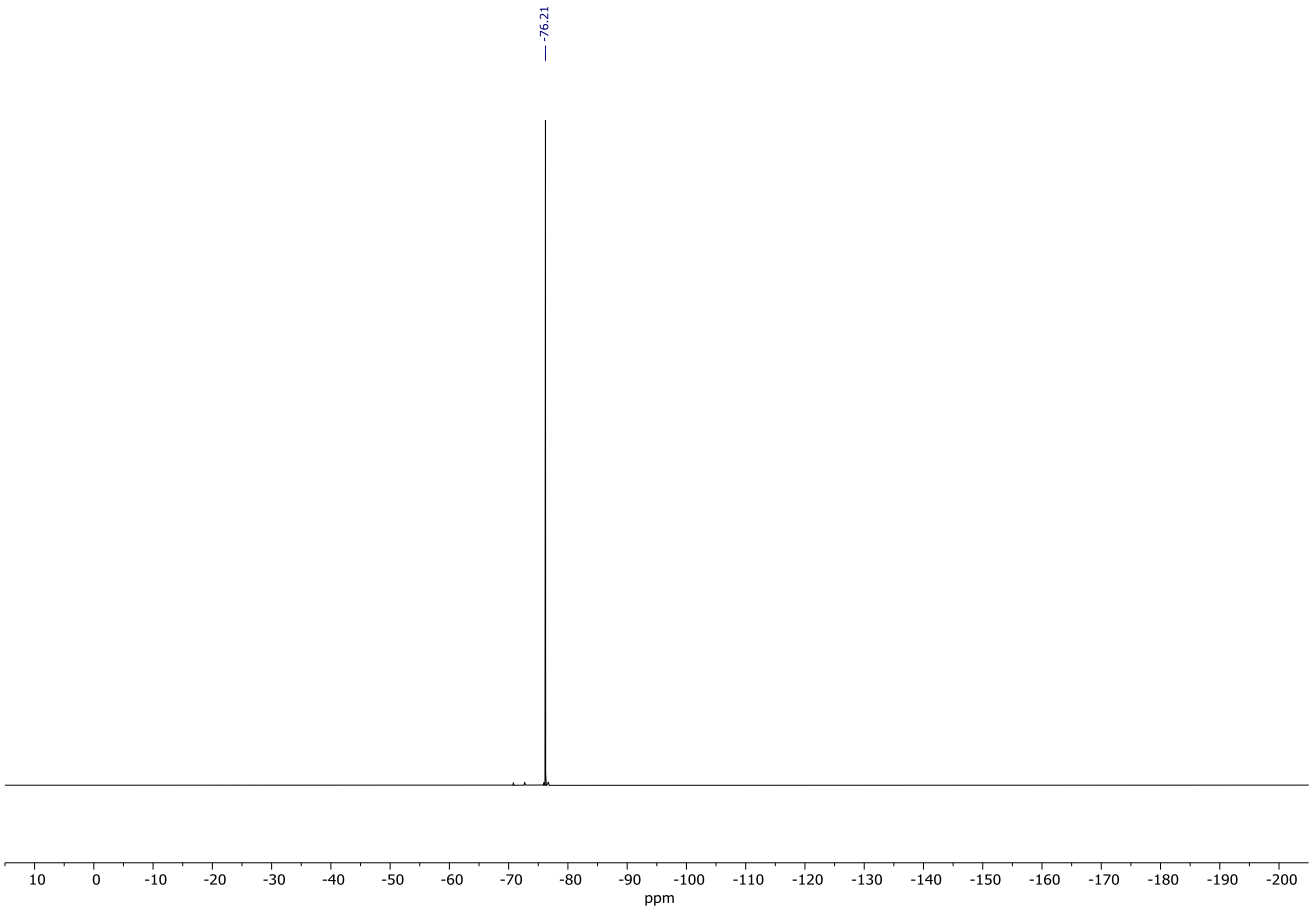

Spectrum 164. ^{19}F NMR (376 MHz, CD_2Cl_2) of **371**.

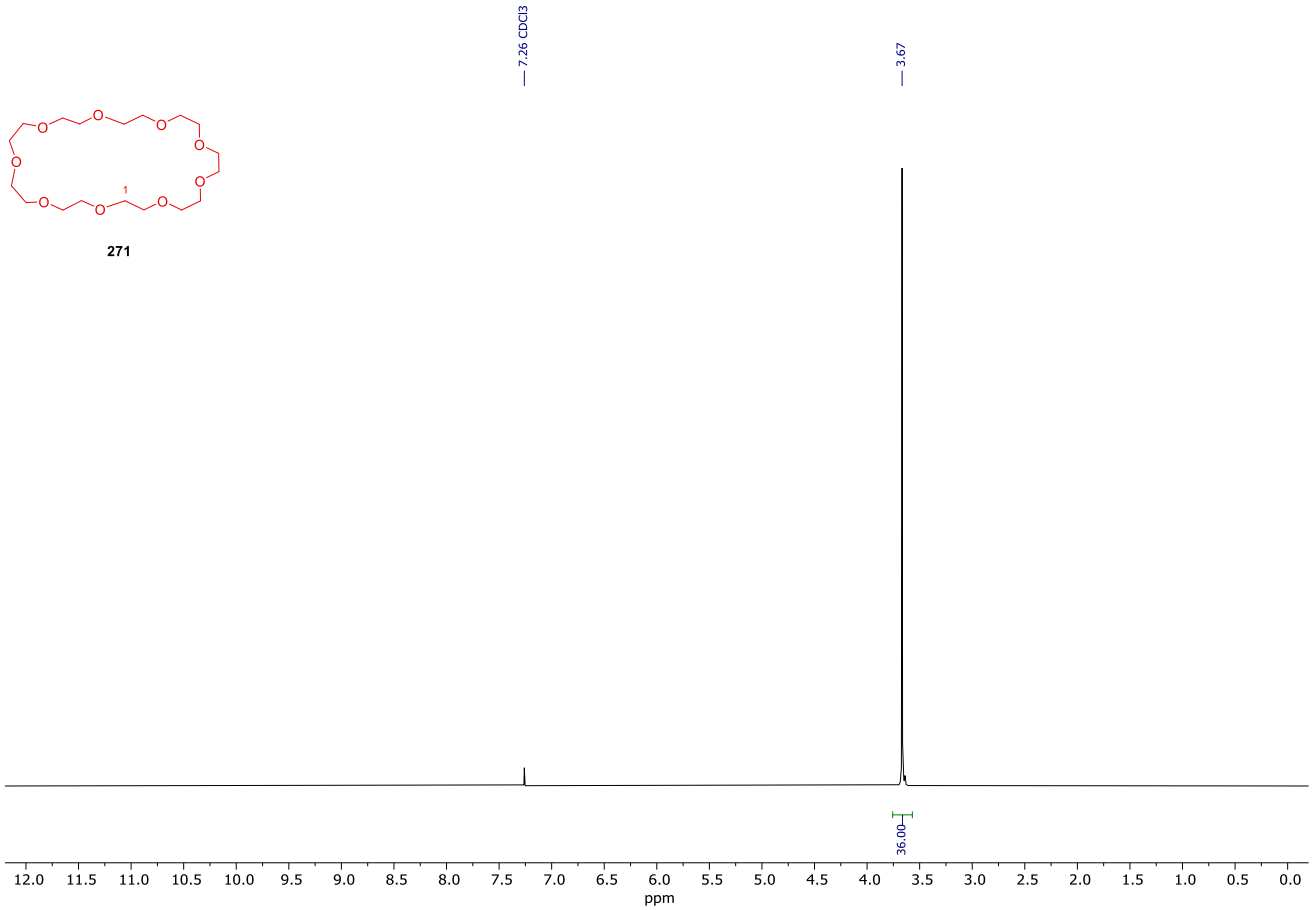

271

Spectrum 165. ^{1}H NMR (600 MHz, $CDCl_3$) of **271**.

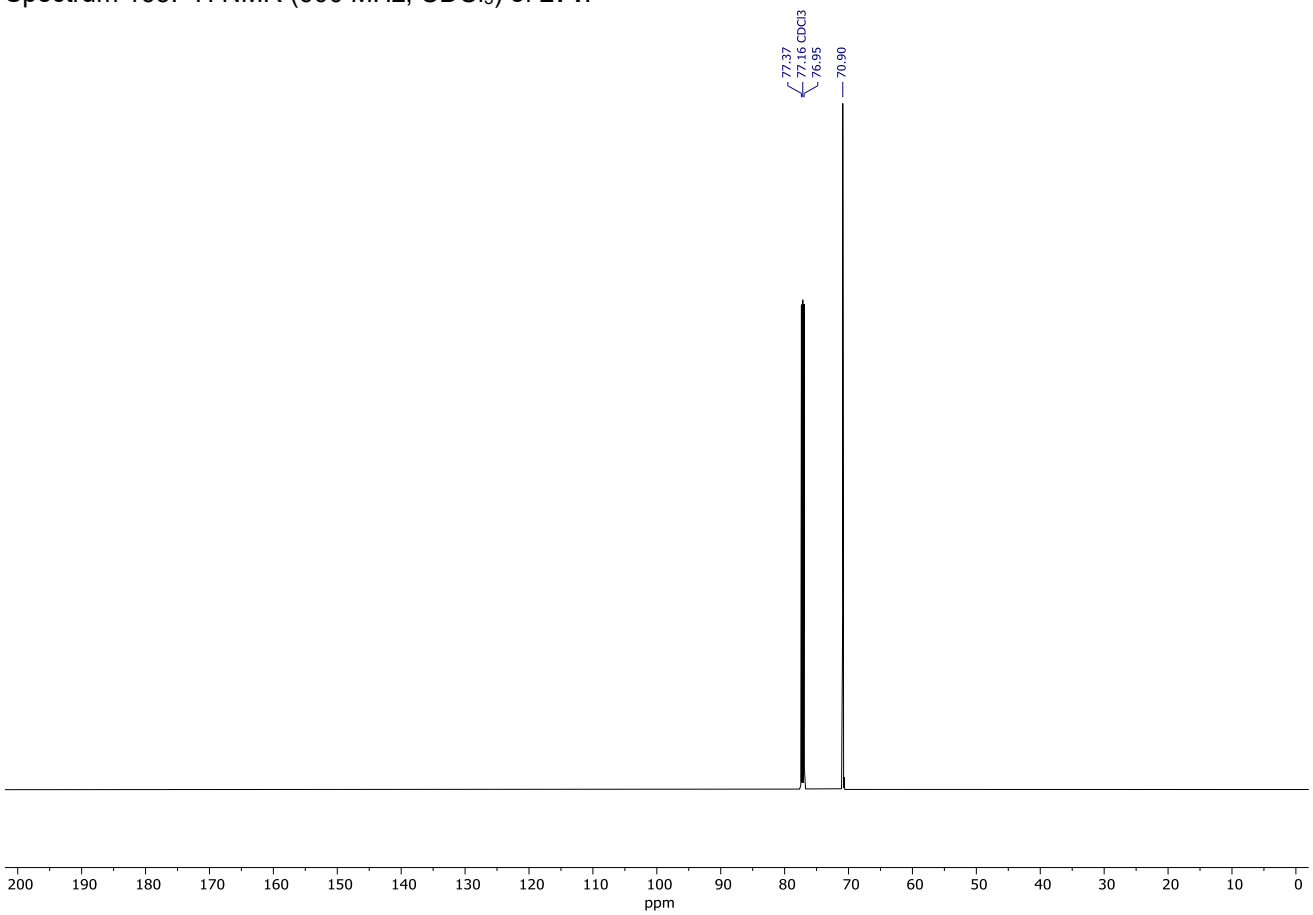

Spectrum 166. ^{13}C NMR (151 MHz, $CDCl_3$) of **271**.

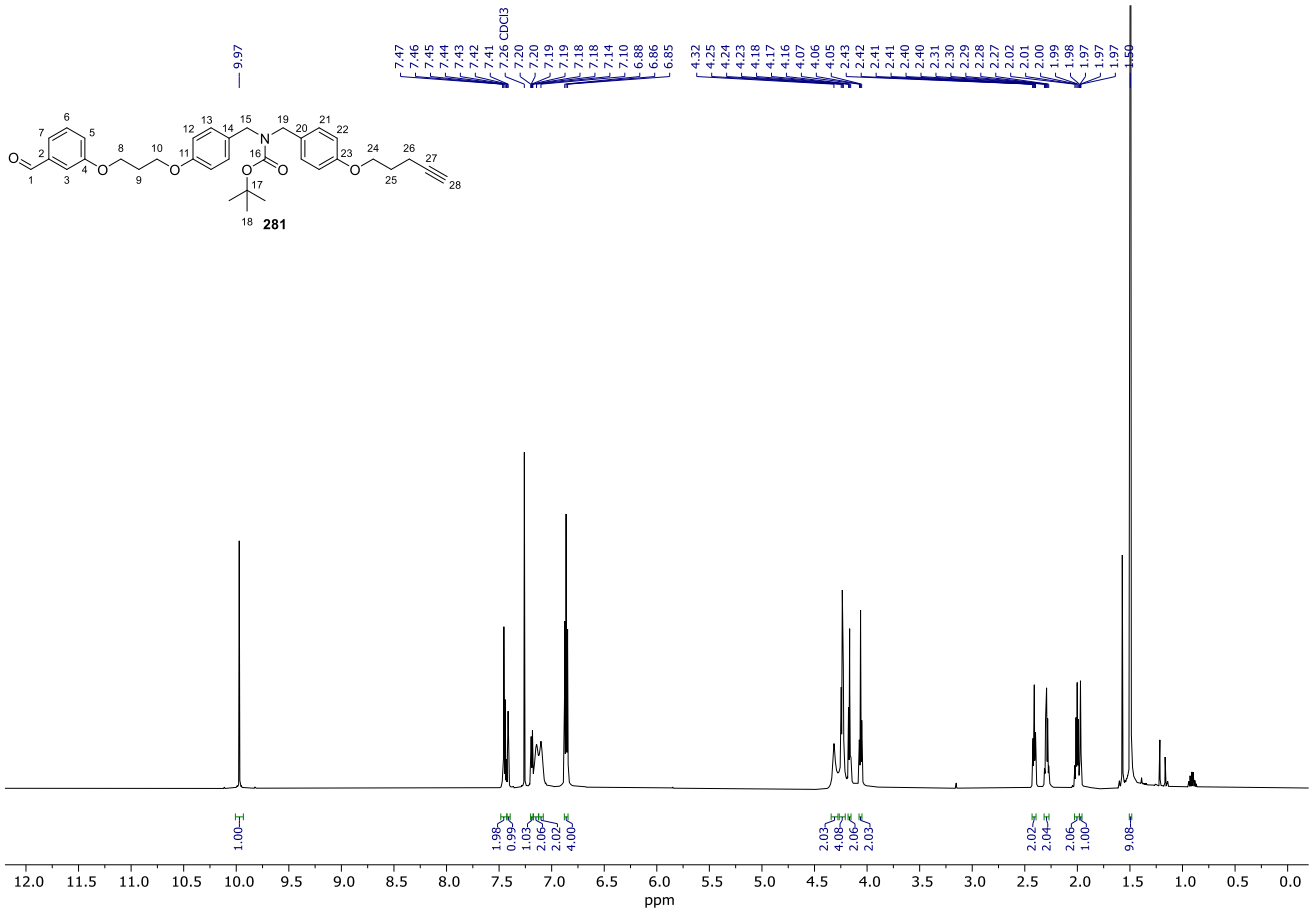

Spectrum 167. ^{1}H NMR (600 MHz, $CDCl_3$) of **281**.

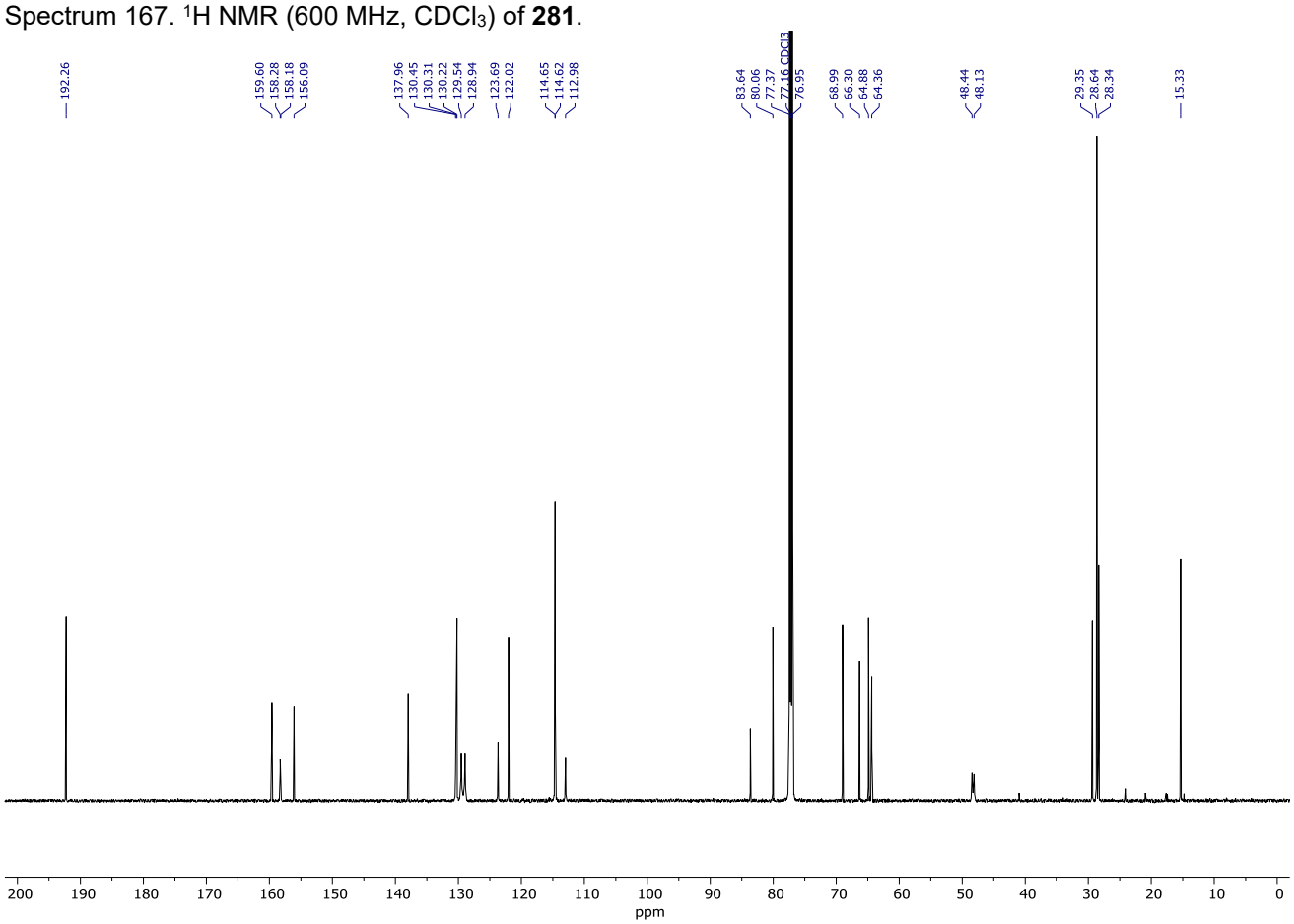

Spectrum 168. ^{13}C NMR (151 MHz, $CDCl_3$) of **281**.

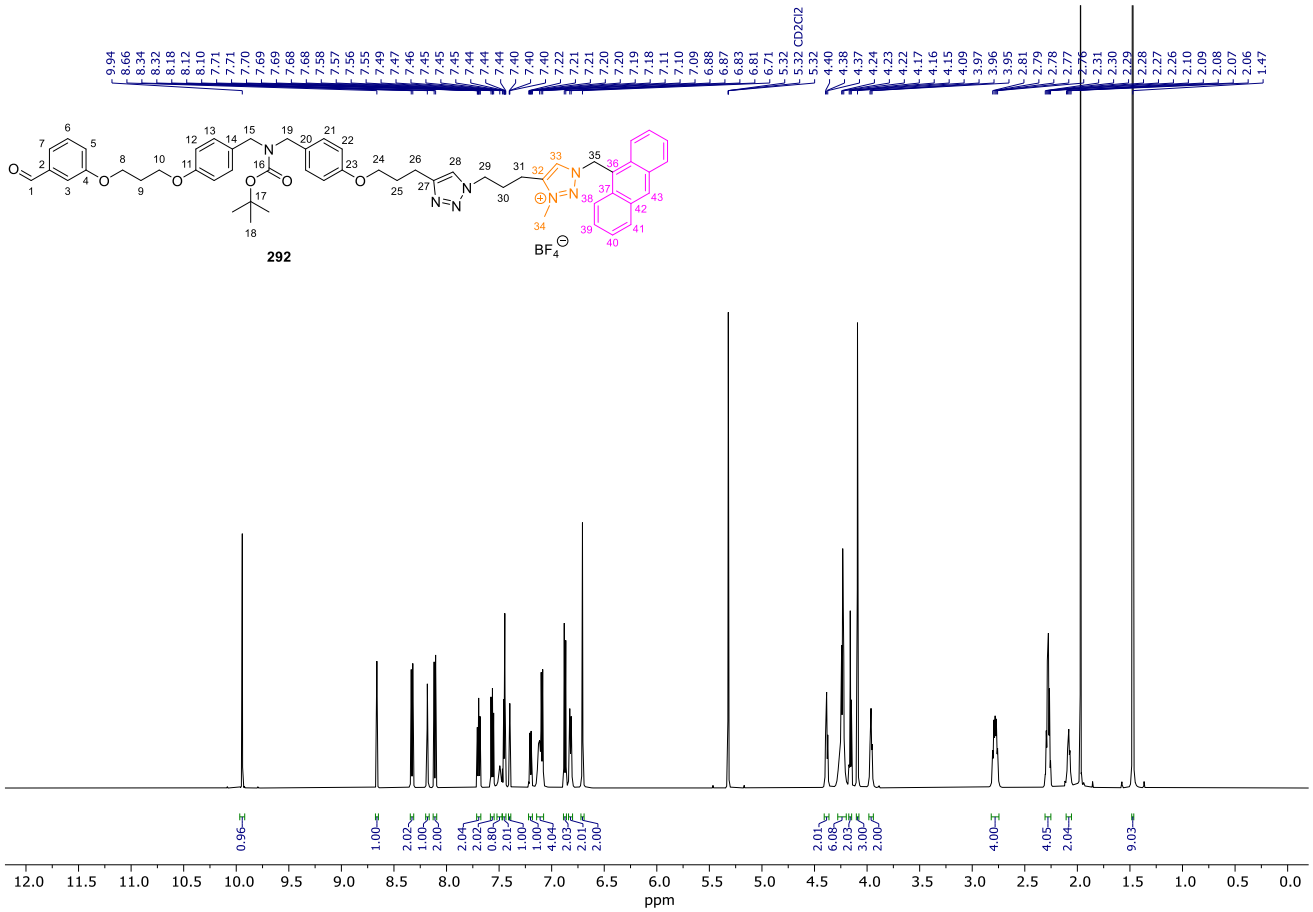

Spectrum 169. ^{1}H NMR (600 MHz, CD_2Cl_2) of **292** ($BF4^-$ salt).

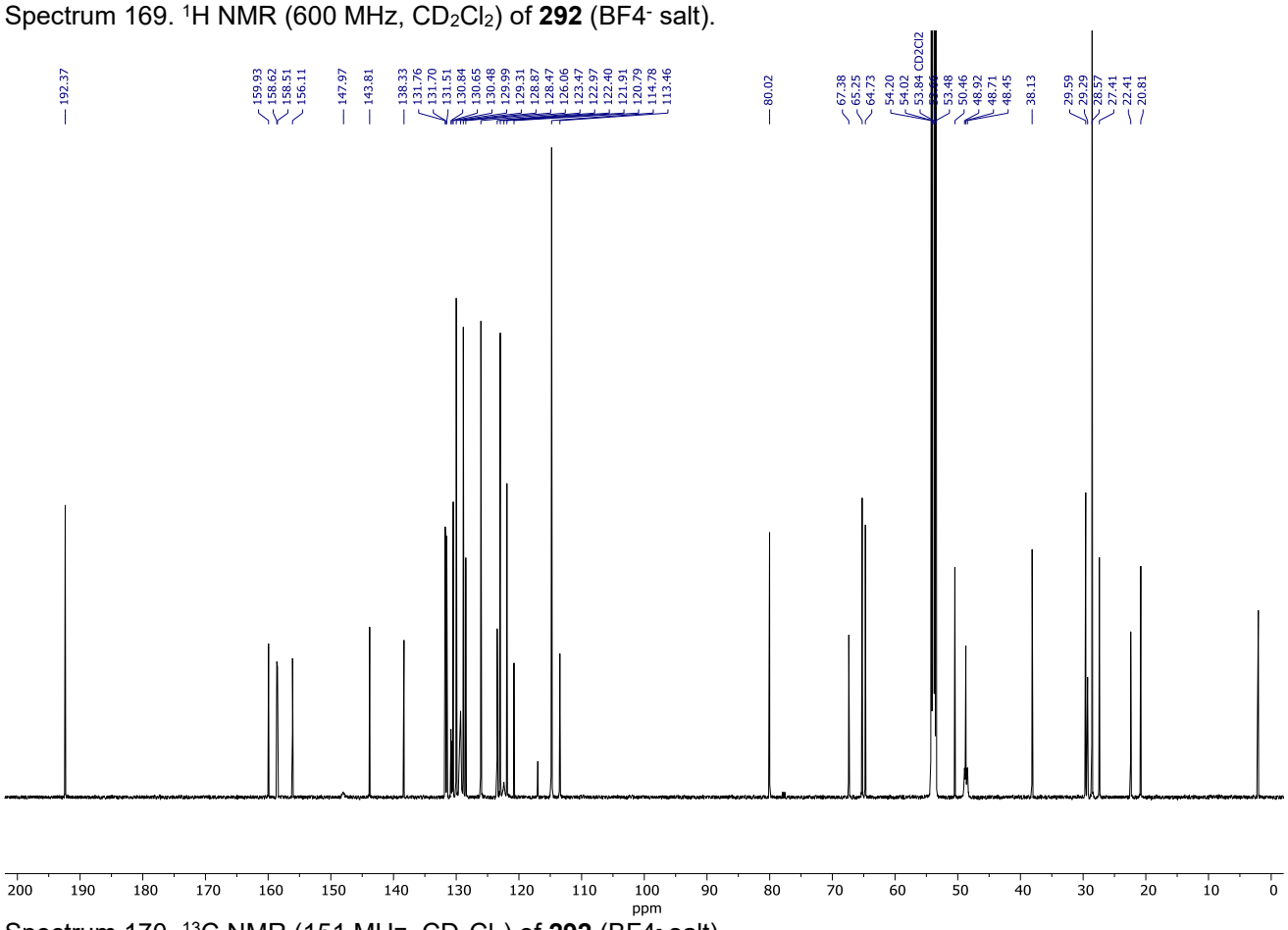

Spectrum 170. ^{13}C NMR (151 MHz, CD_2Cl_2) of **292** ($BF4^-$ salt).

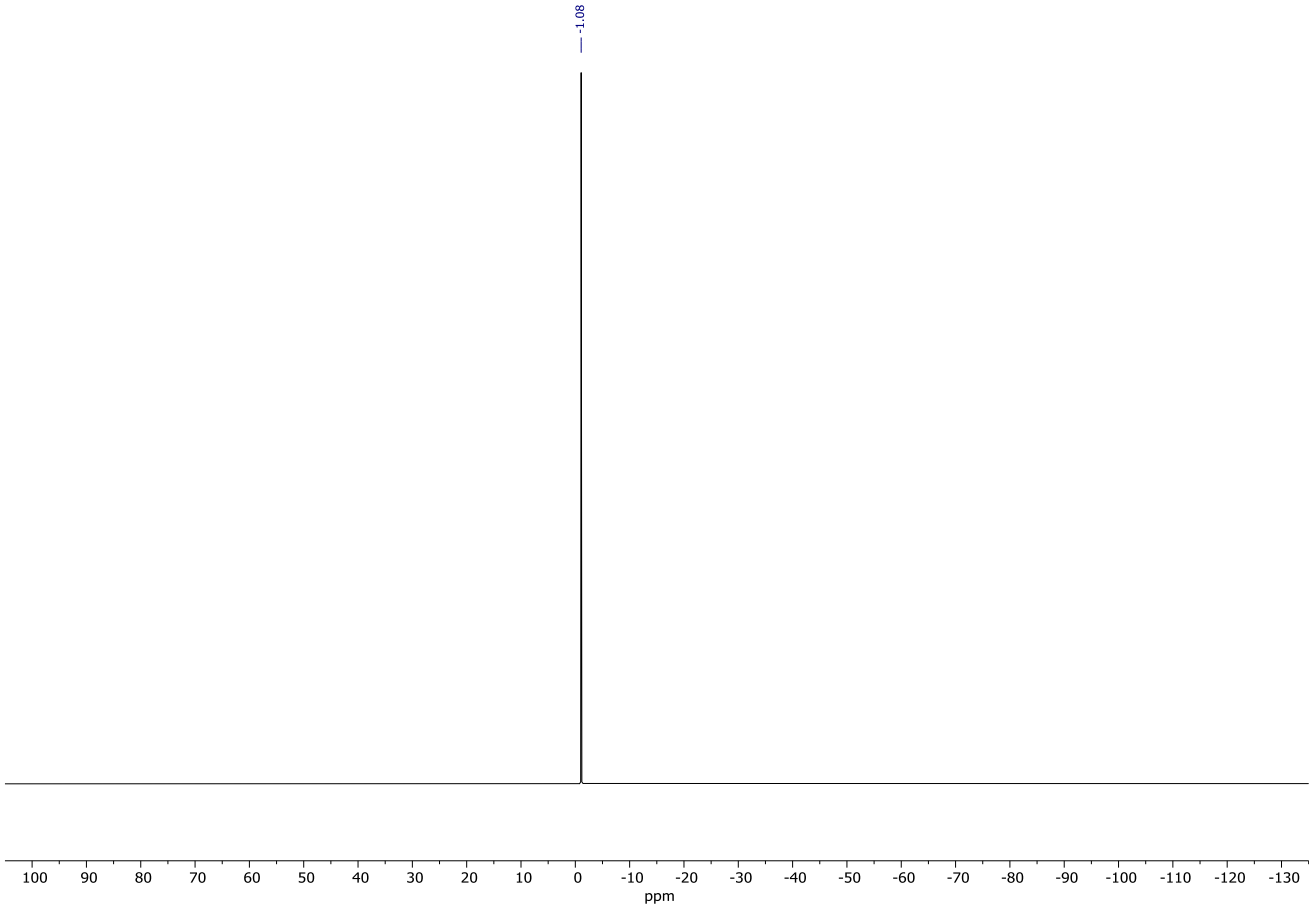

Spectrum 171. ^{11}B NMR (160 MHz, CD_2Cl_2) of **292** ($BF4^-$ salt).

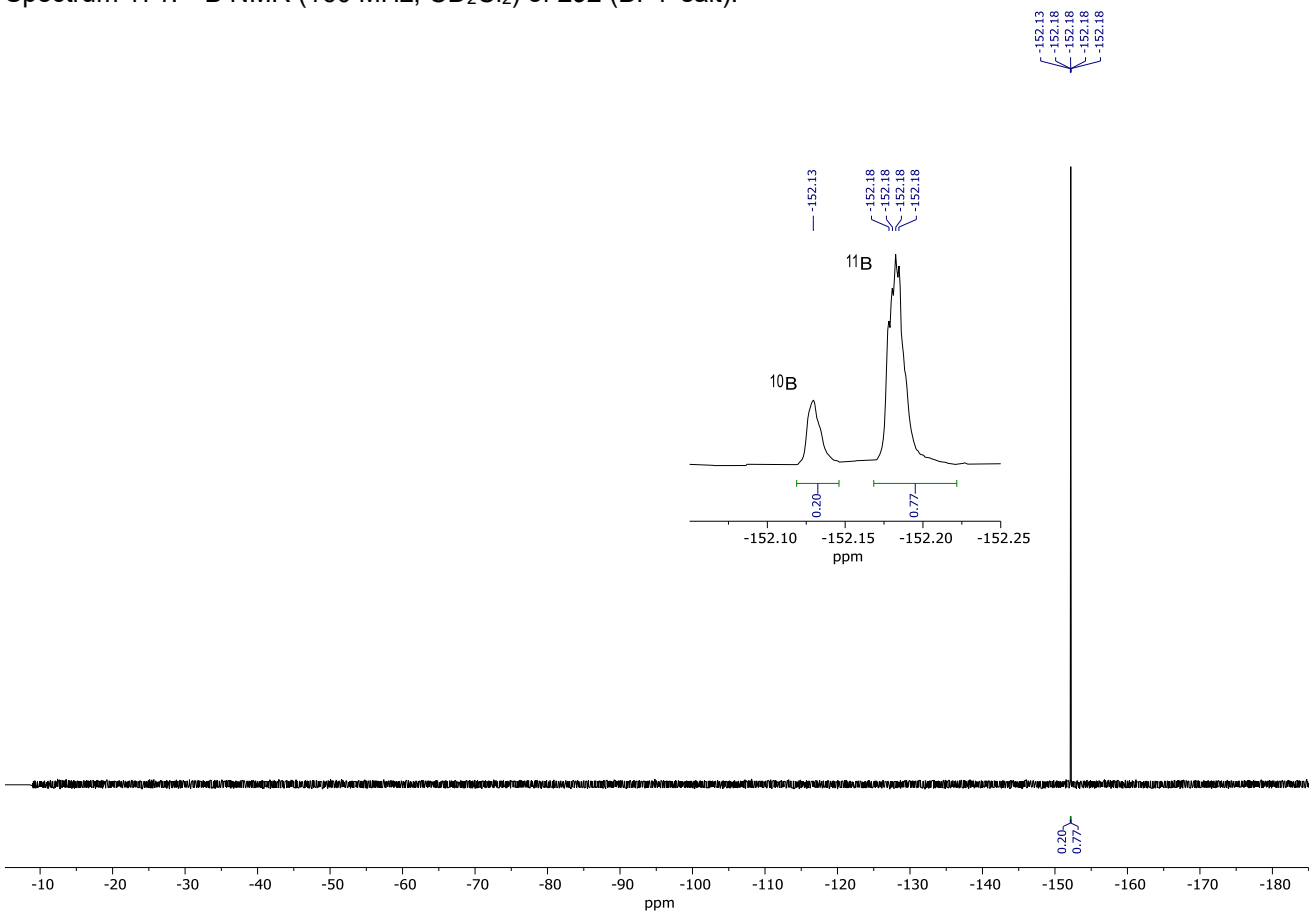

Spectrum 172. ^{19}F NMR (471 MHz, CD_2Cl_2) of **292** ($BF4^-$ salt).

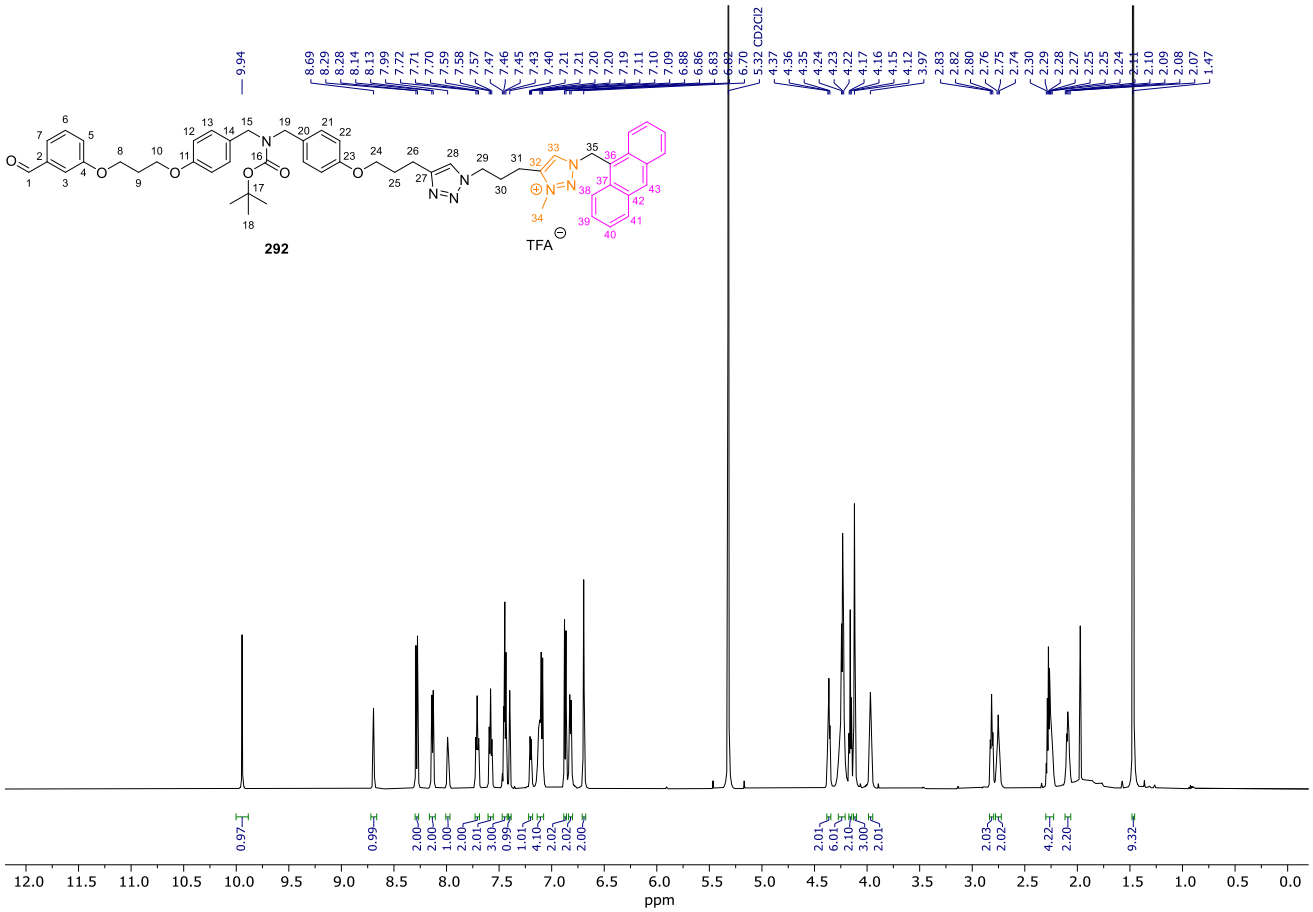

Spectrum 173. ^{1}H NMR (600 MHz, CD_2Cl_2) of **292** (TFA^- salt).

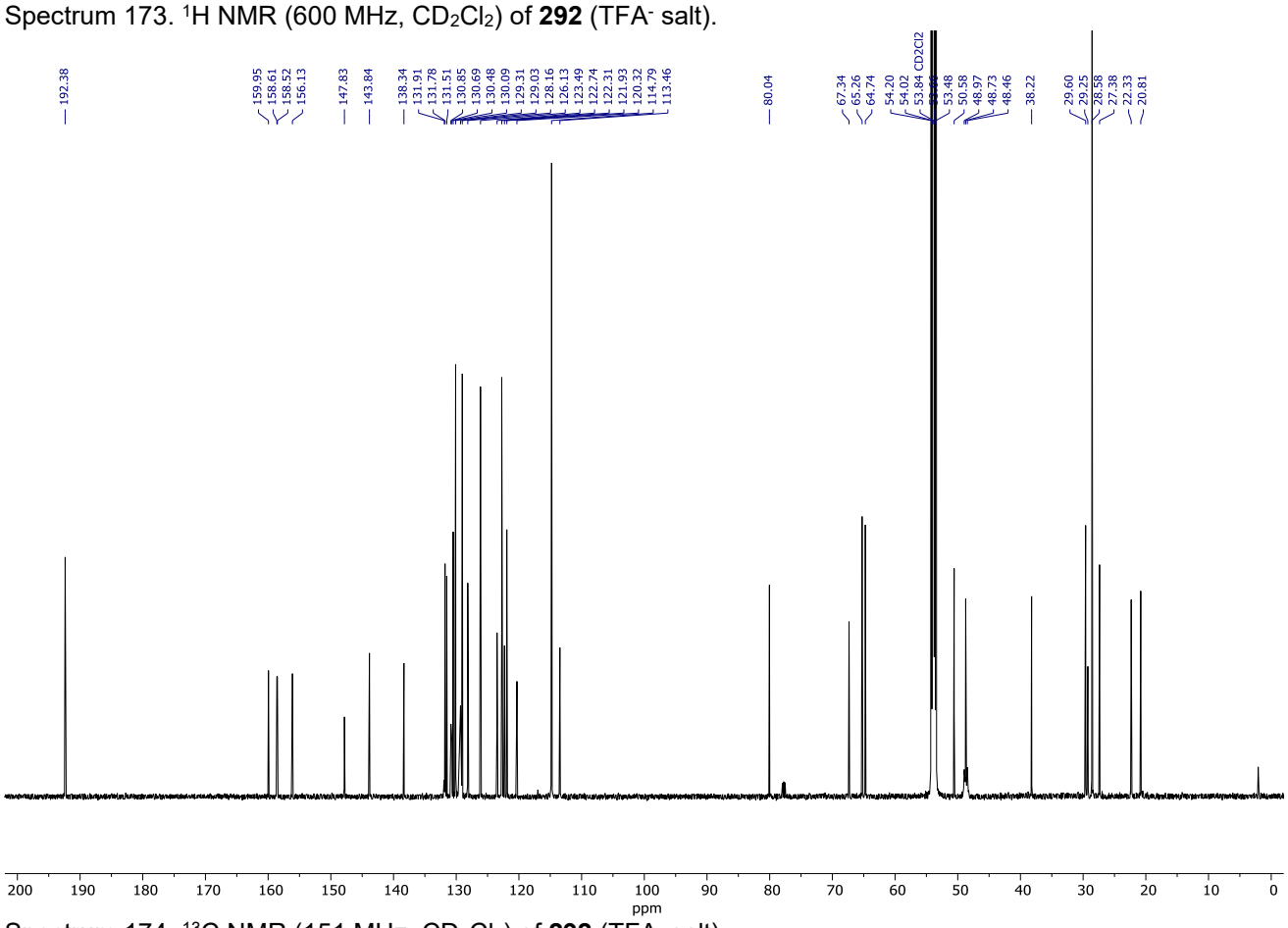

Spectrum 174. ^{13}C NMR (151 MHz, CD_2Cl_2) of **292** (TFA^- salt).

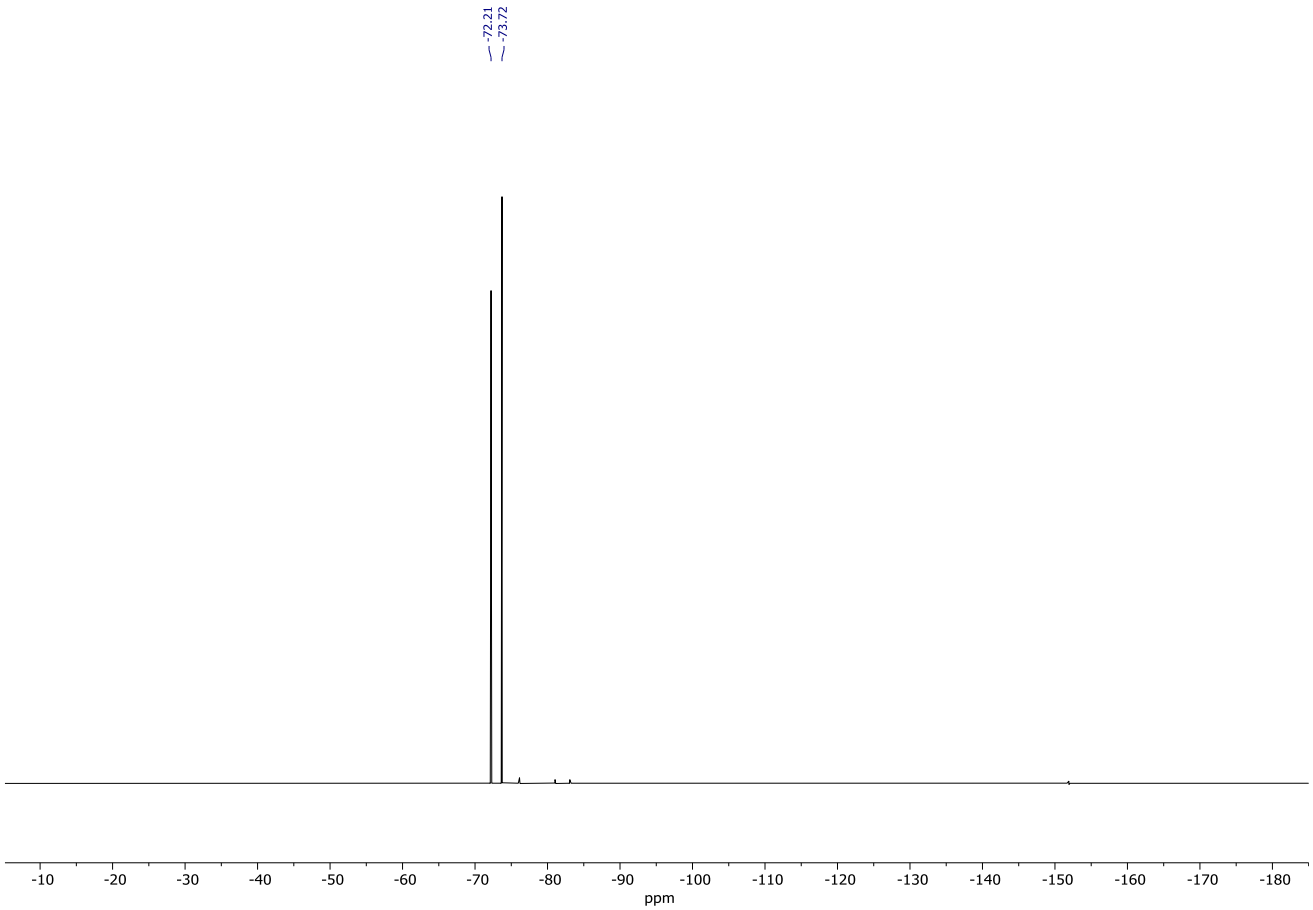

Spectrum 175. ^{19}F NMR (471 MHz, CD_2Cl_2) of **292** (TFA^- salt).

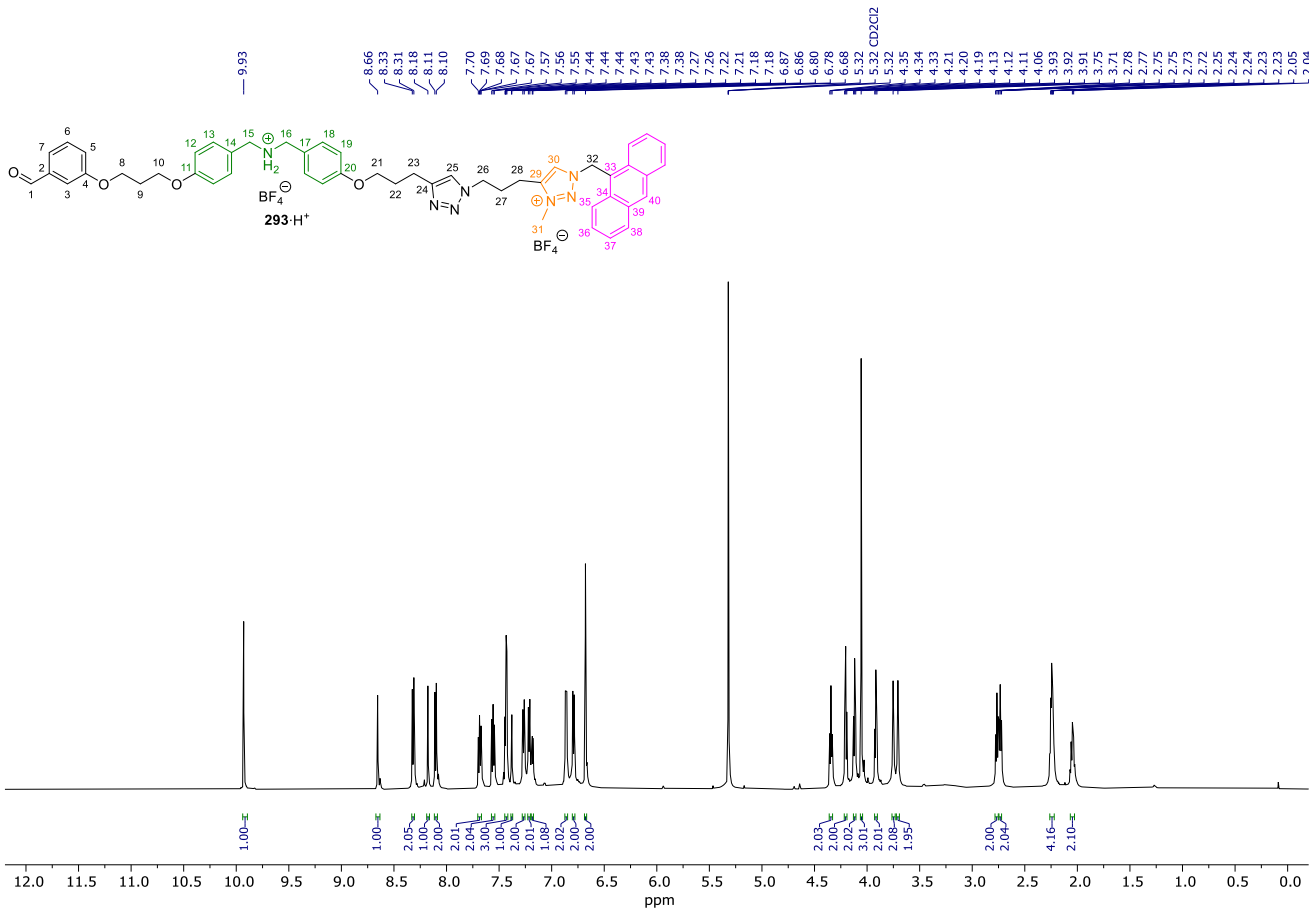

Spectrum 176. ^{1}H NMR (600 MHz, $CDCl_3$) of **293**·H^+ ($BF4^-$ salt).

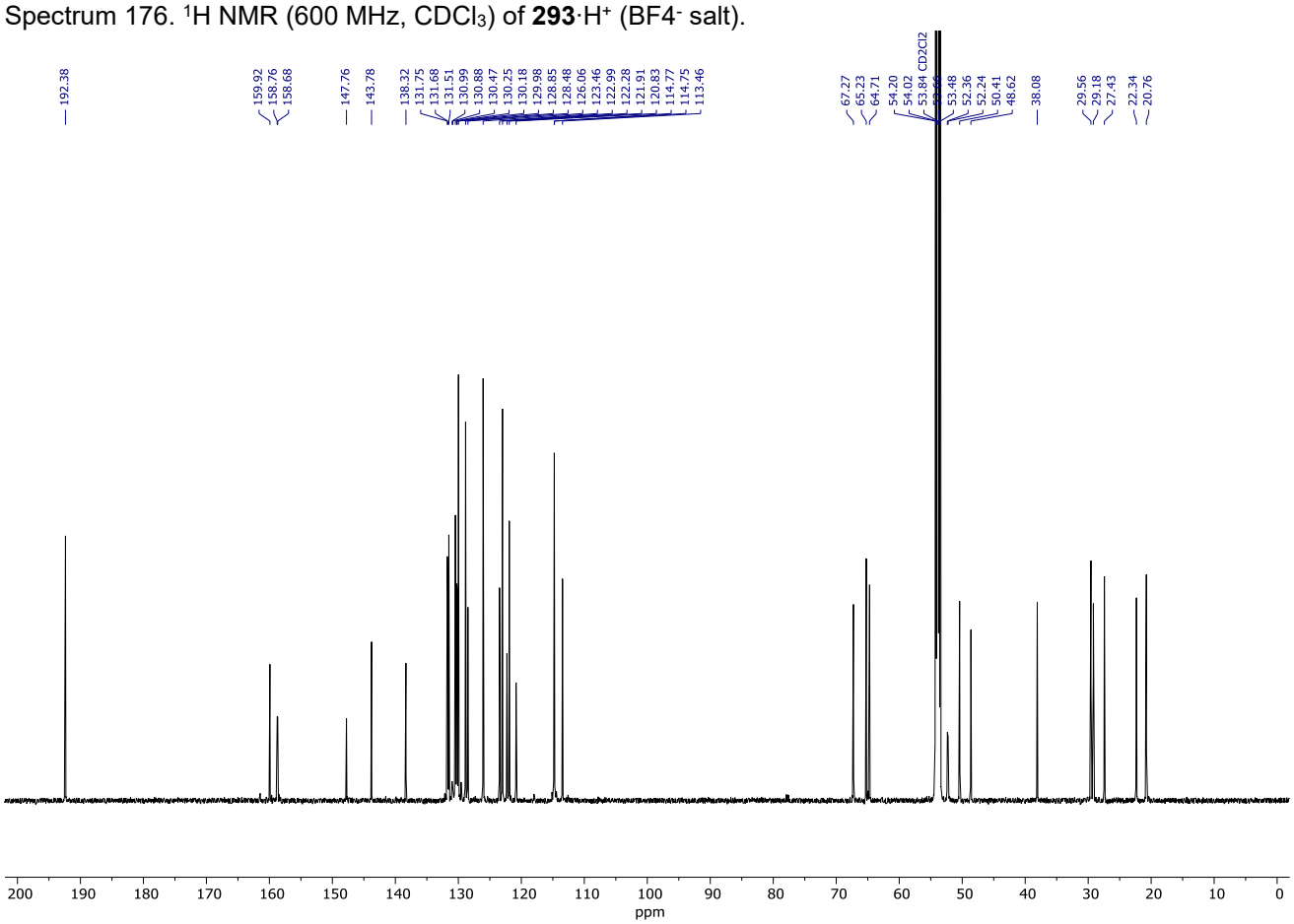

Spectrum 177. ^{13}C NMR (151 MHz, $CDCl_3$) of **293**·H^+ ($BF4^-$ salt).

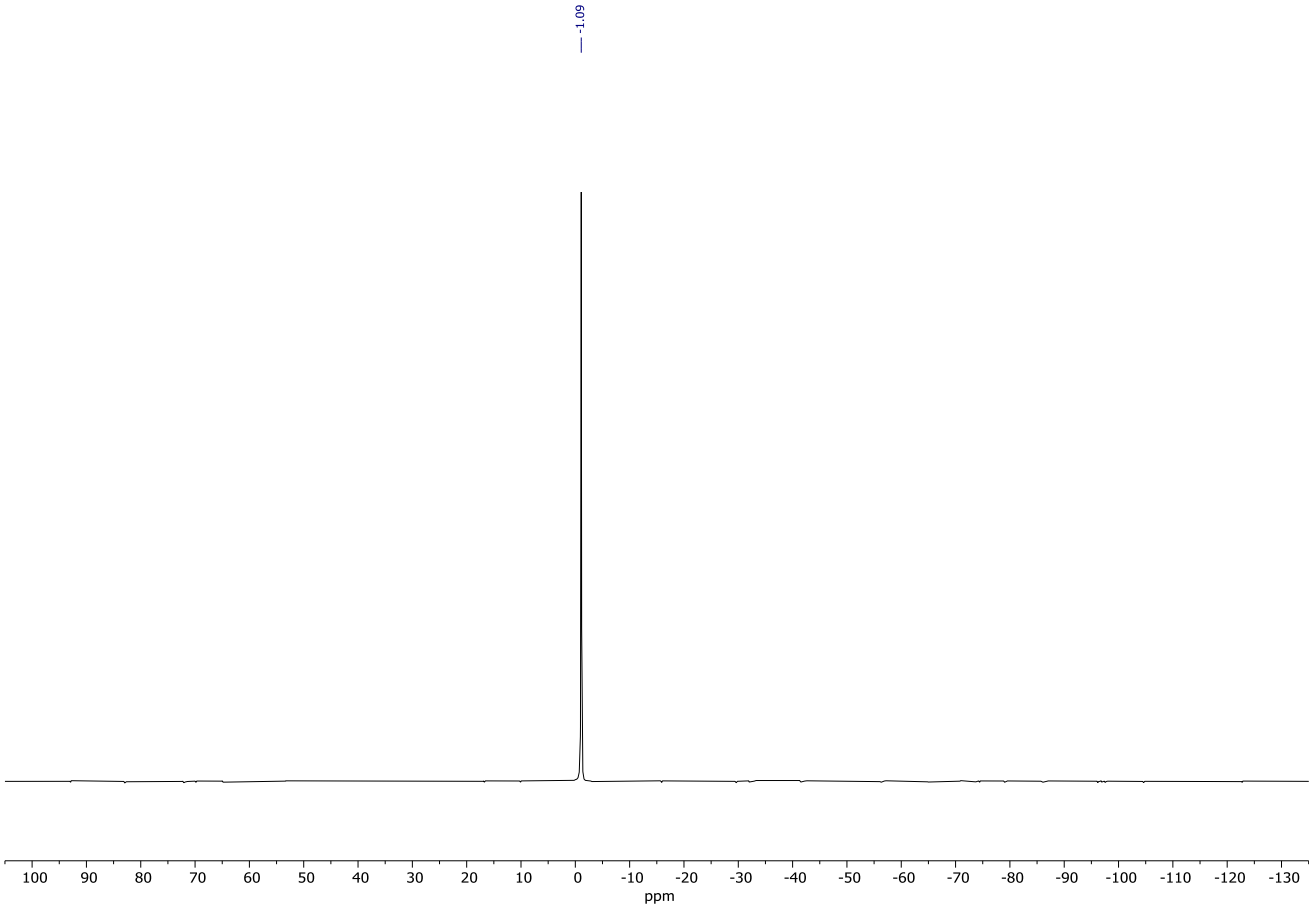

Spectrum 178. ^{11}B NMR (128 MHz, CD_2Cl_2) of **293**·H^+ ($BF4^-$ salt).

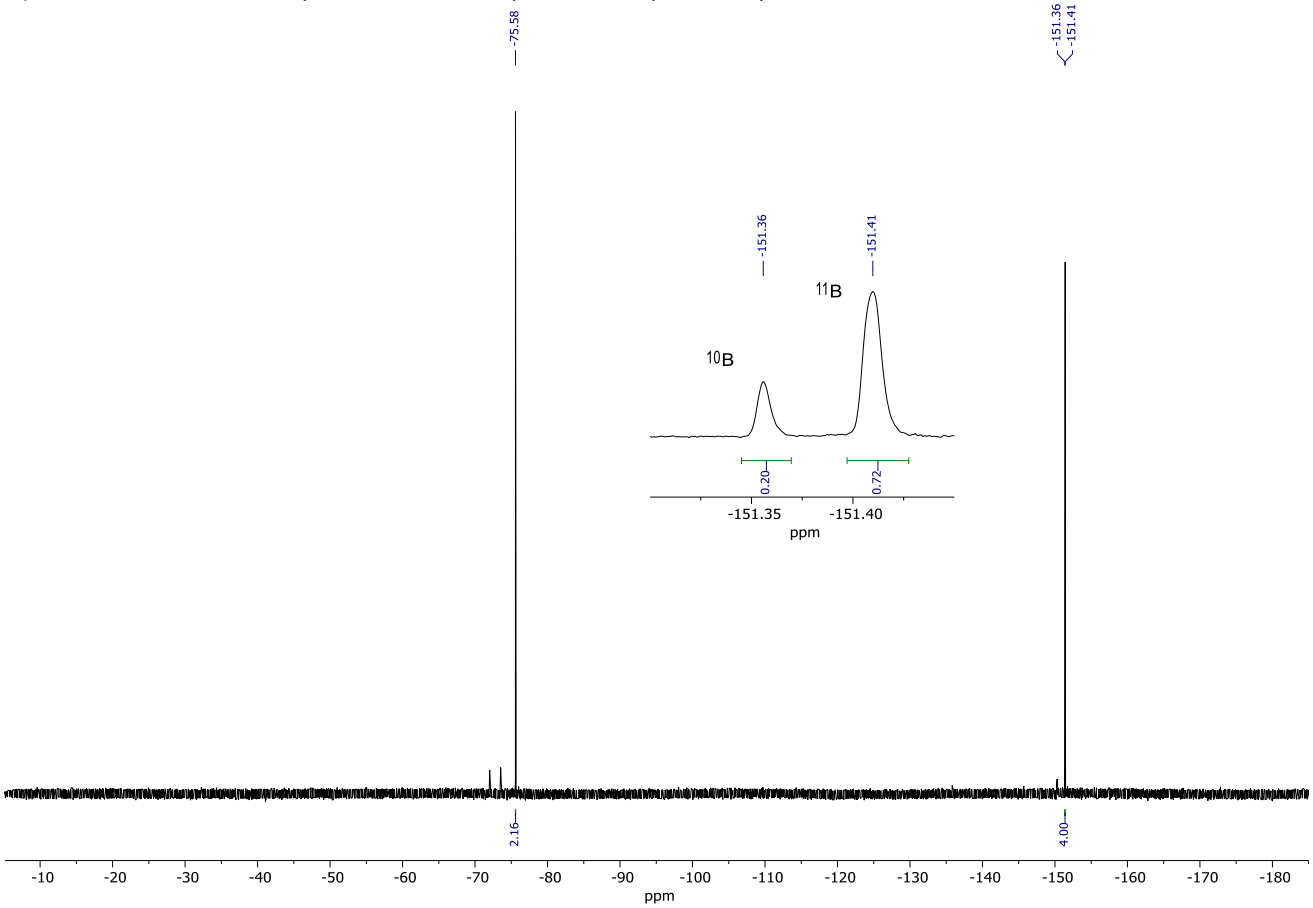

Spectrum 179. ^{19}F NMR (471 MHz, CD_2Cl_2) of **293**·H^+ ($BF4^-$ salt).

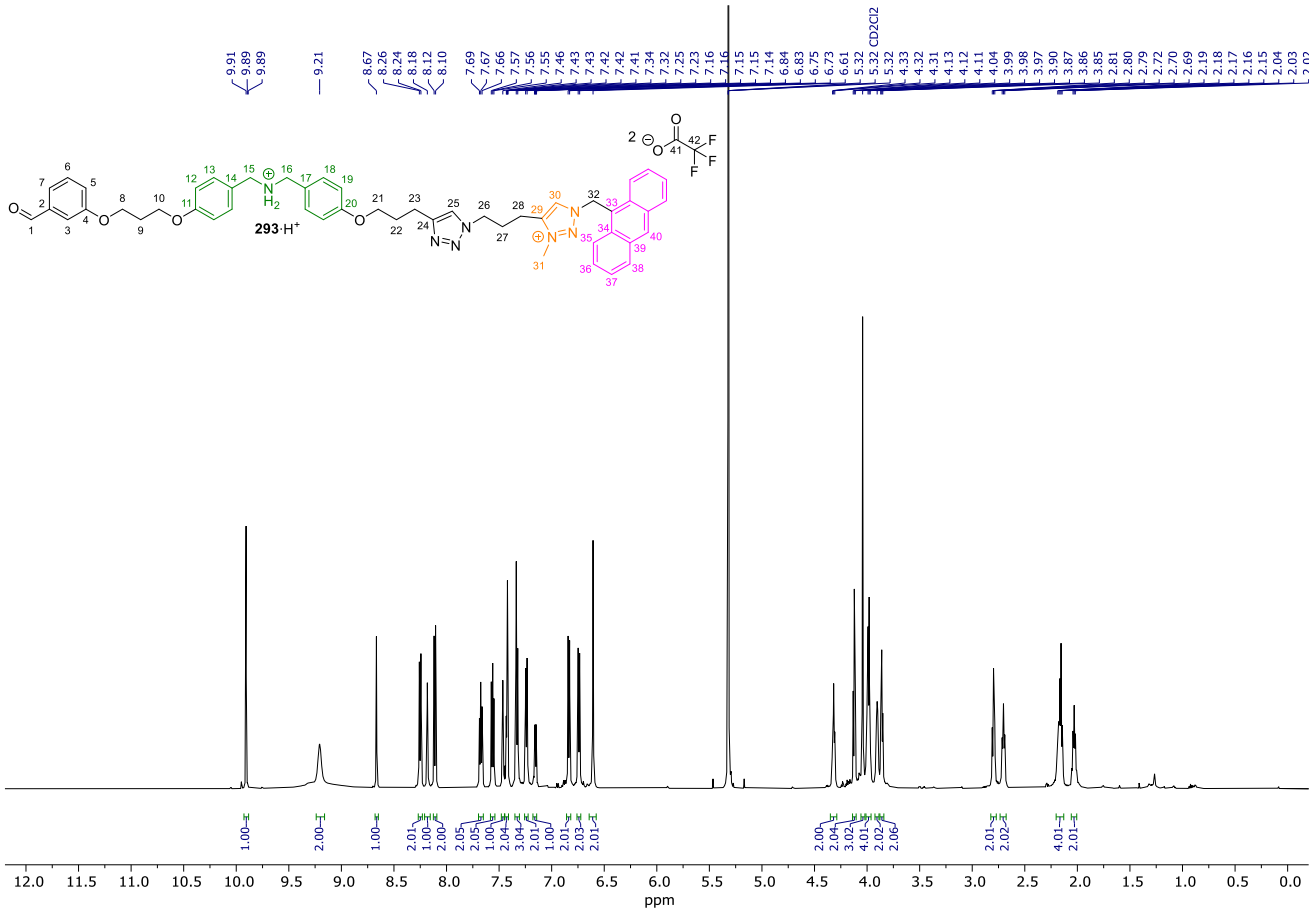

Spectrum 180. ^{1}H NMR (600 MHz, CD_2Cl_2) of **293**·H^+ (TFA^- salt).

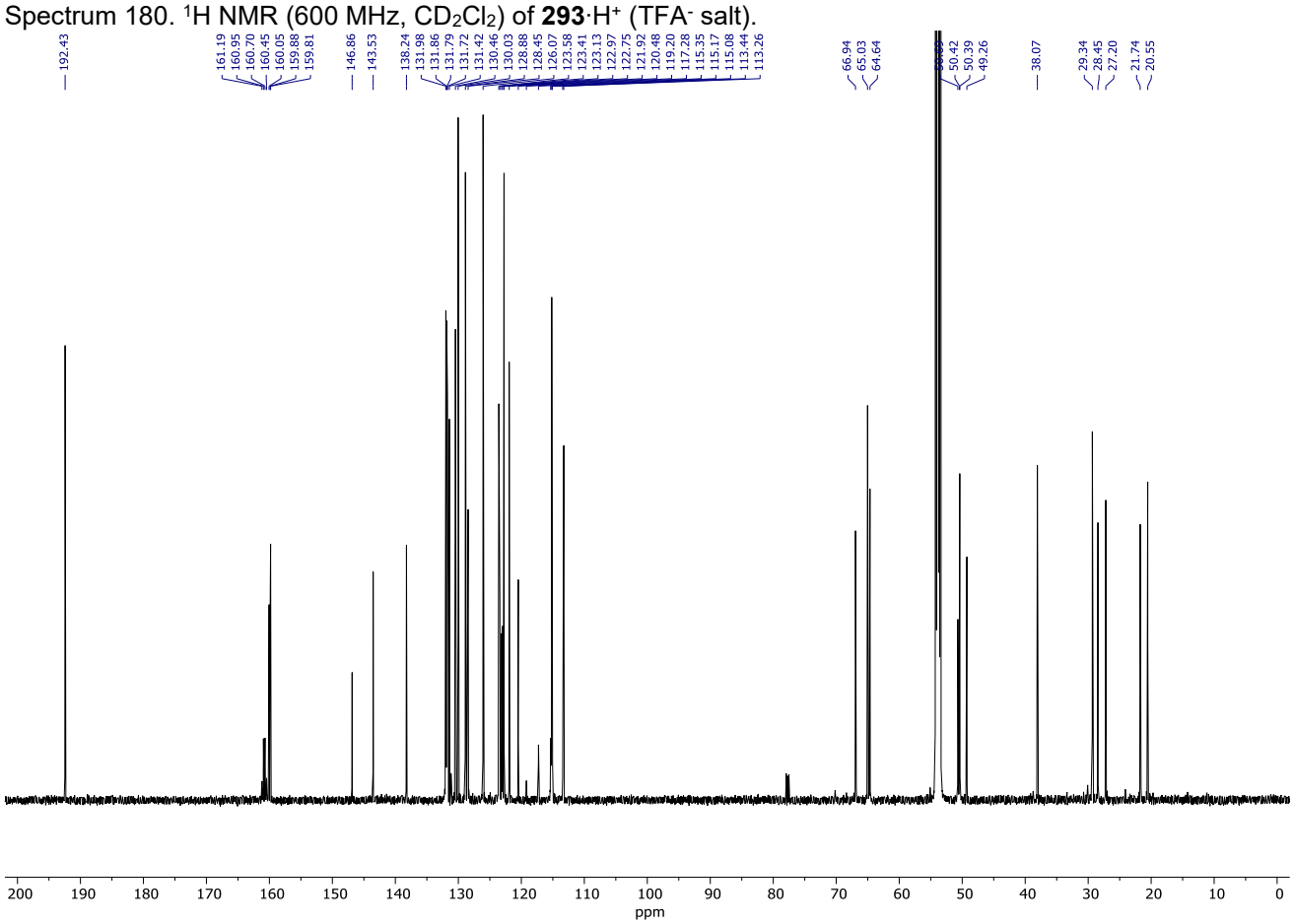

Spectrum 181. ^{13}C NMR (151 MHz, CD_2Cl_2) of **293**·H^+ (TFA^- salt).

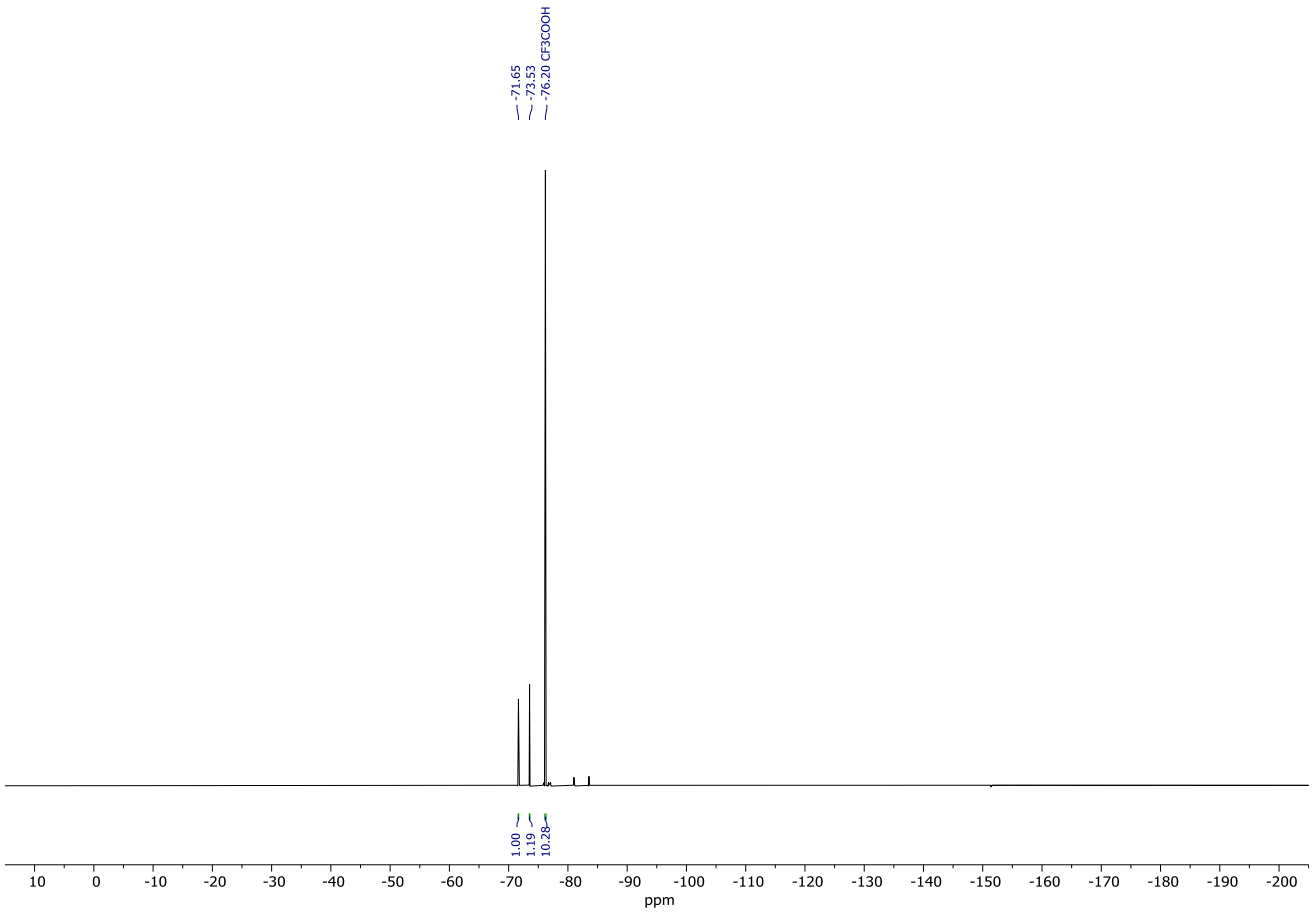

Spectrum 182. ^{19}F NMR (376 MHz, CD_2Cl_2) of **293**·H^+ (TFA^- salt).

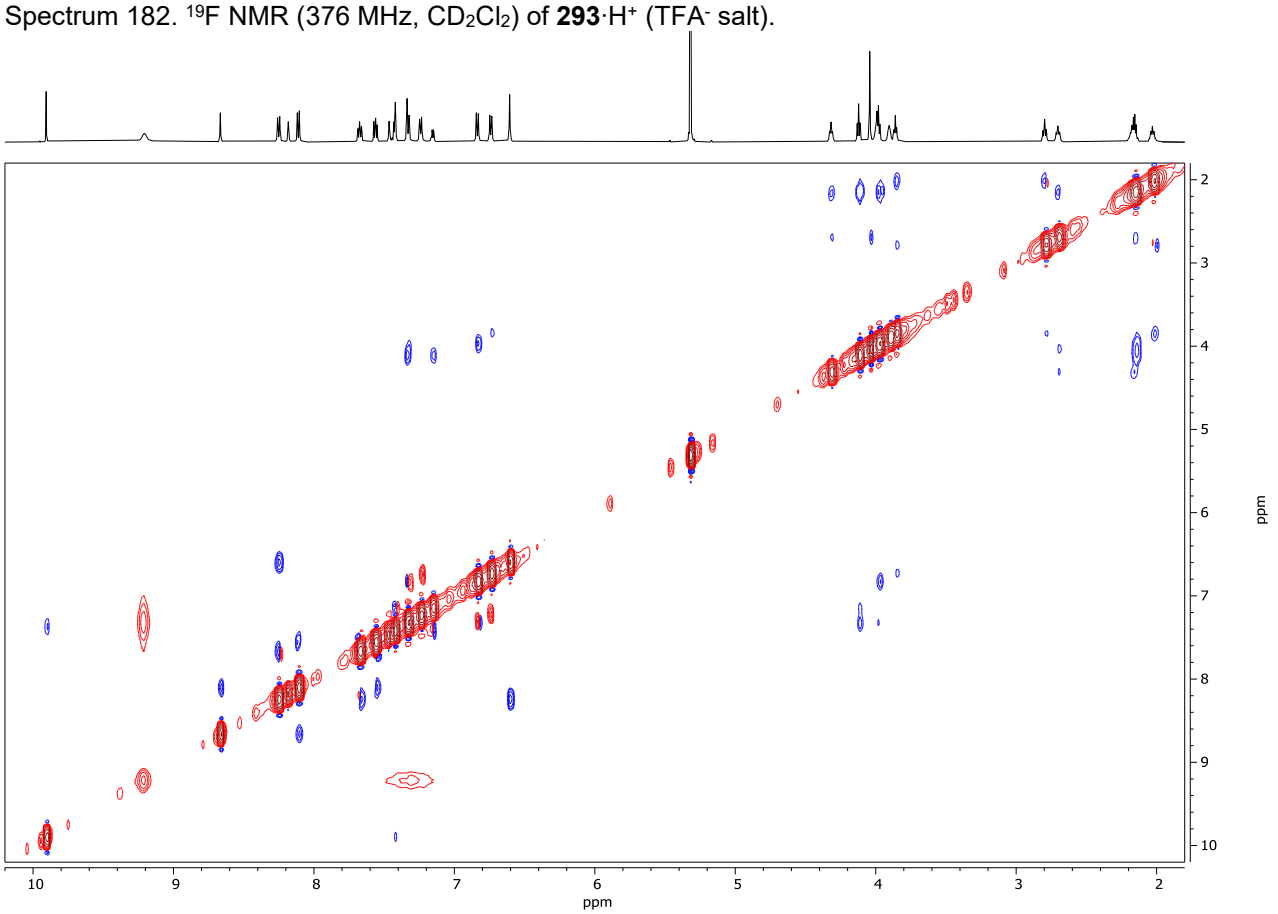

Spectrum 183. 2D NOESY (600 MHz, CD_2Cl_2) of **293**·H^+ Data was recorded with a 300 ms mixing time and a relaxation delay of 2.07 s. 2K data points were collected for 256 increments of 4 scans.

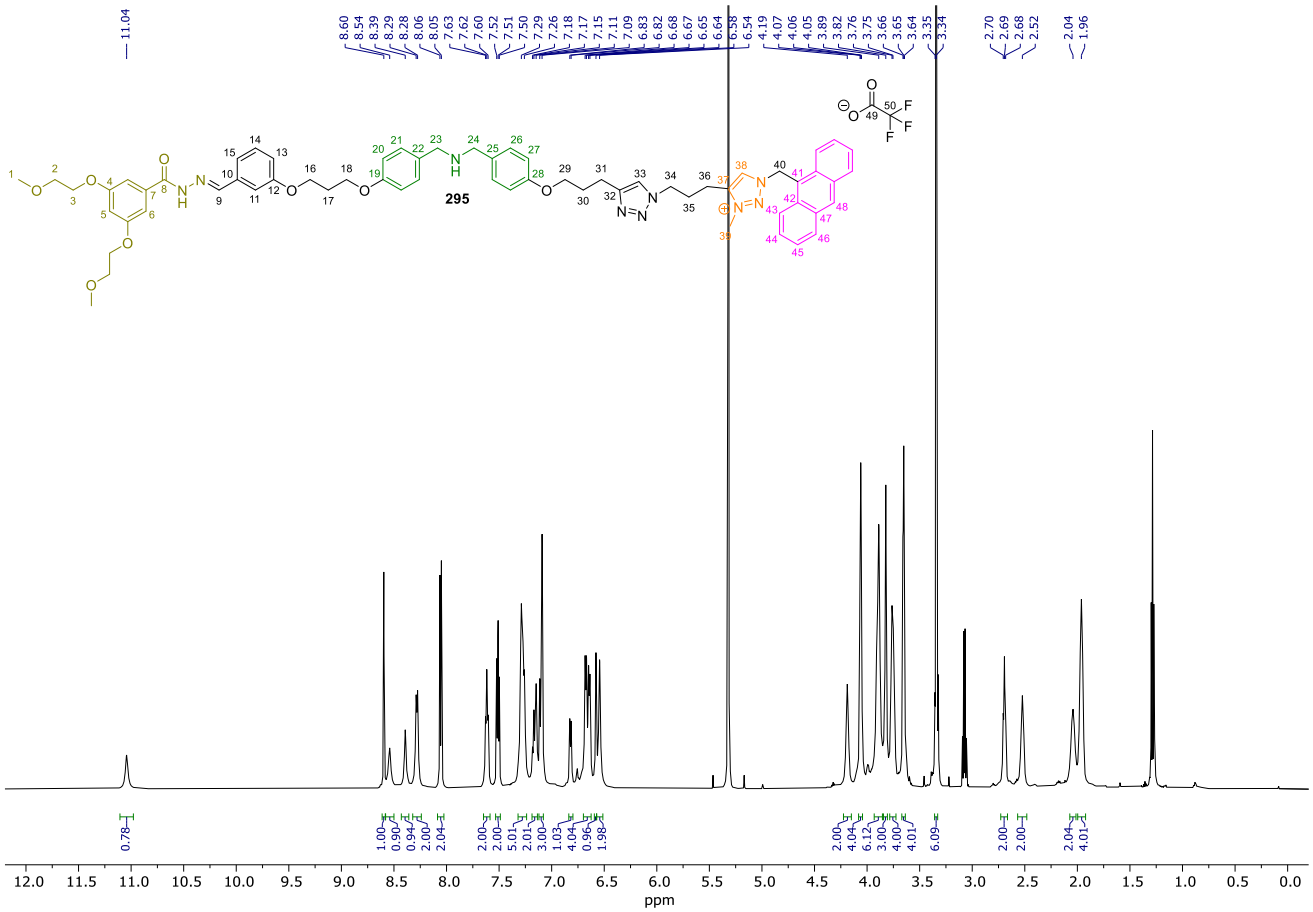

Spectrum 184. ^{1}H NMR (600 MHz, CD_2Cl_2) of **295**.

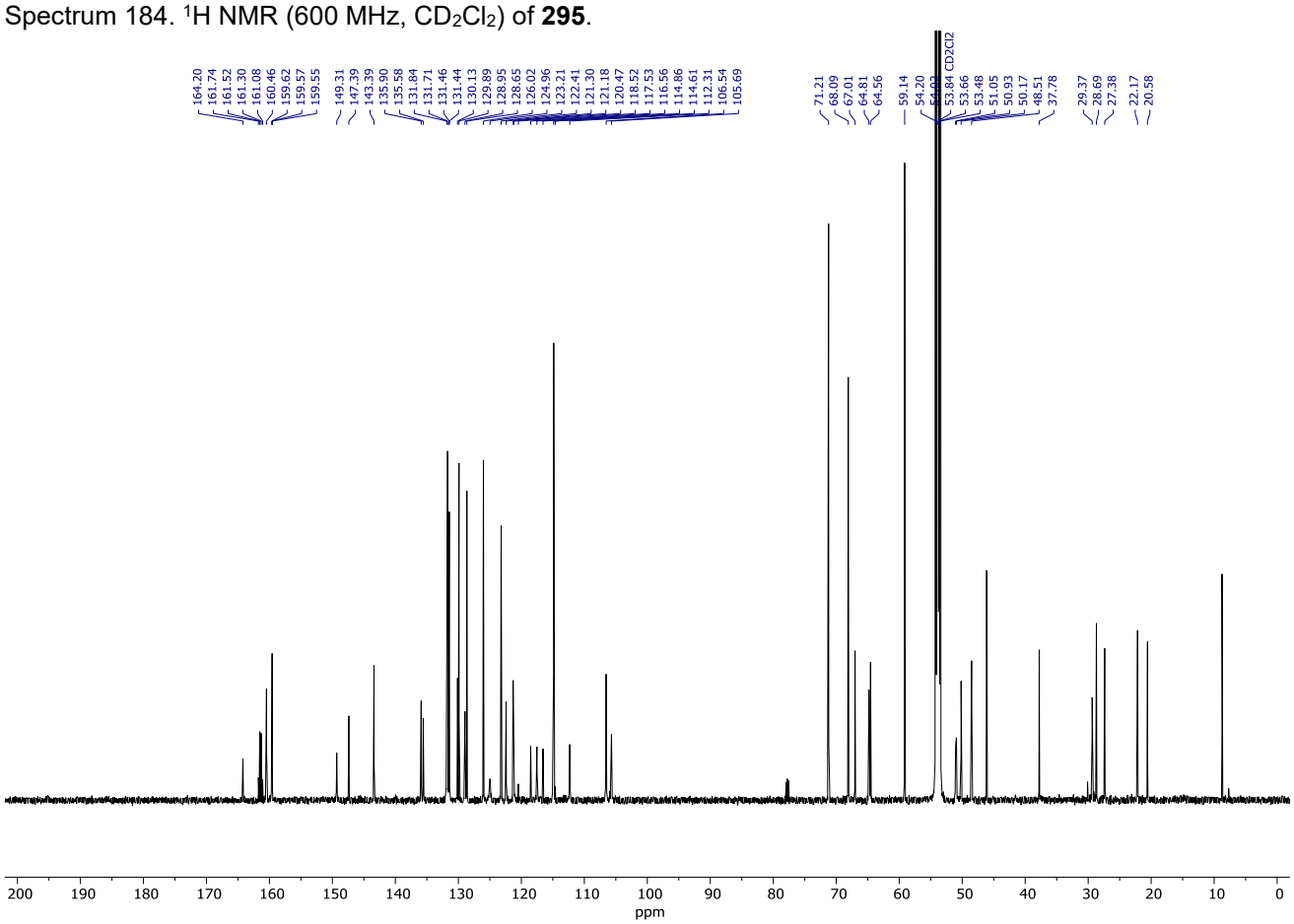

Spectrum 185. ^{13}C NMR (151 MHz, CD_2Cl_2) of **295**.

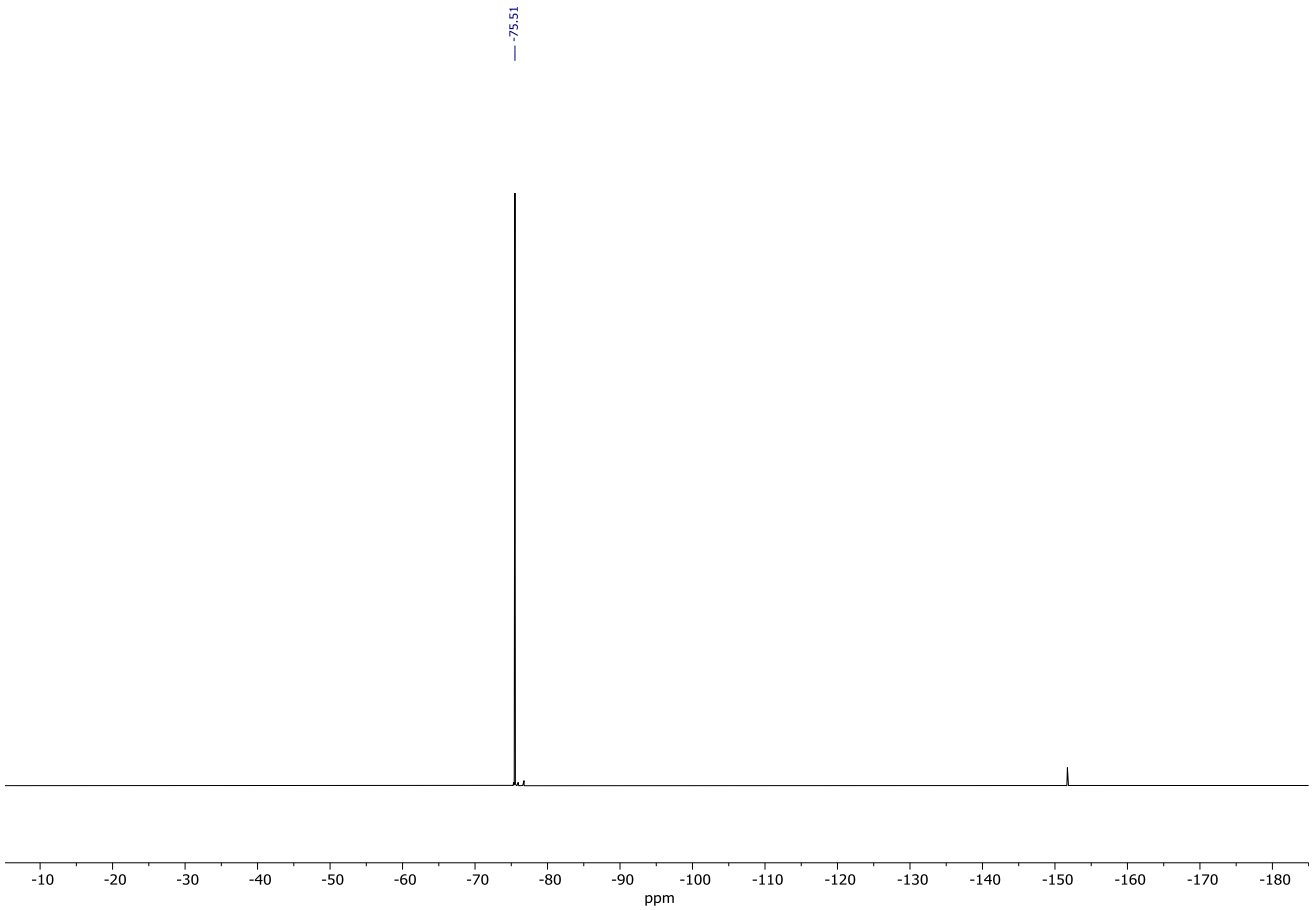

Spectrum 186. ^{19}F NMR (471 MHz, CD_2Cl_2) of **295**.

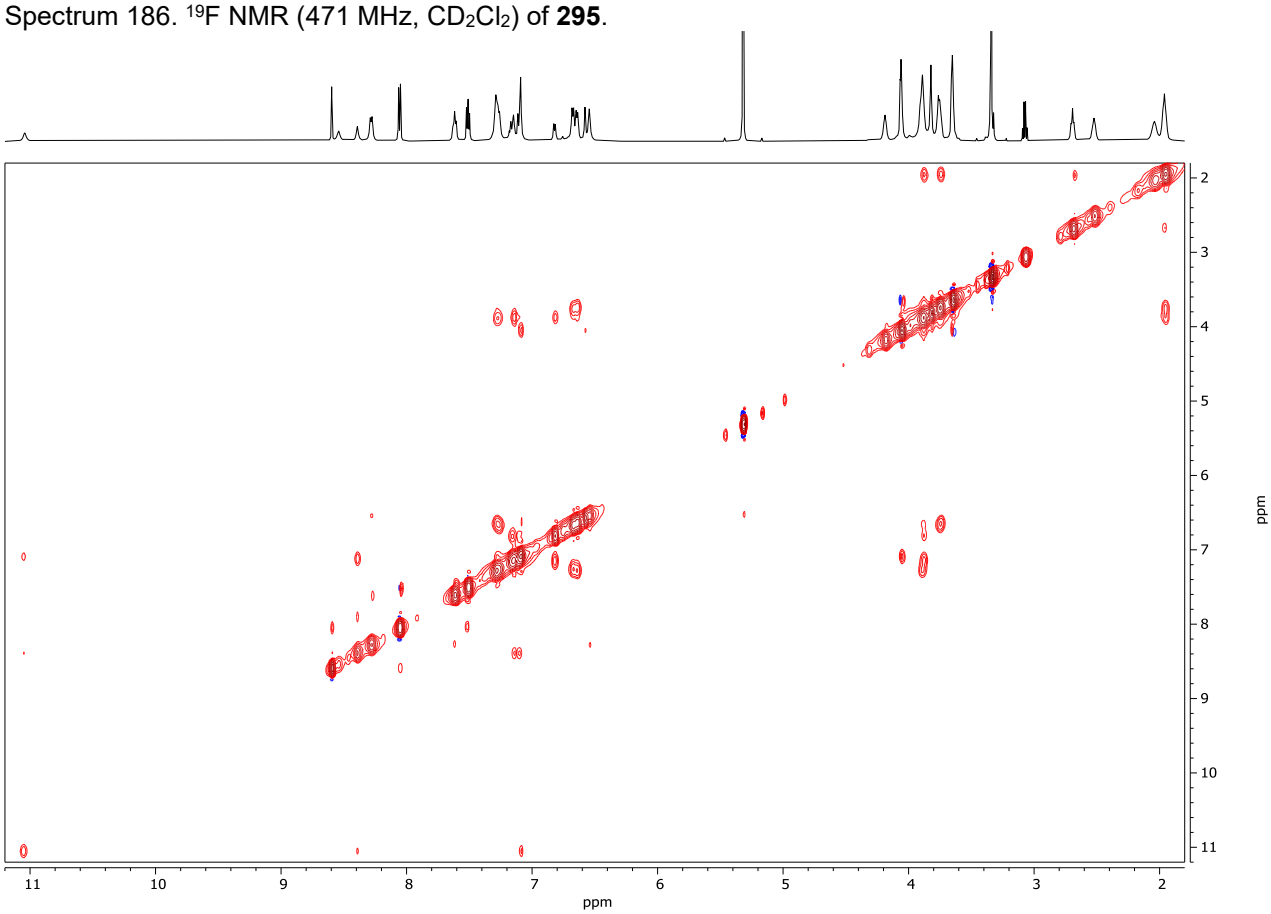

Spectrum 187. 2D NOESY (600 MHz, CD_2Cl_2) of **295**. Data was recorded with a 300 ms mixing time and a relaxation delay of 2.05 s. 2K data points were collected for 256 increments of 4 scans.

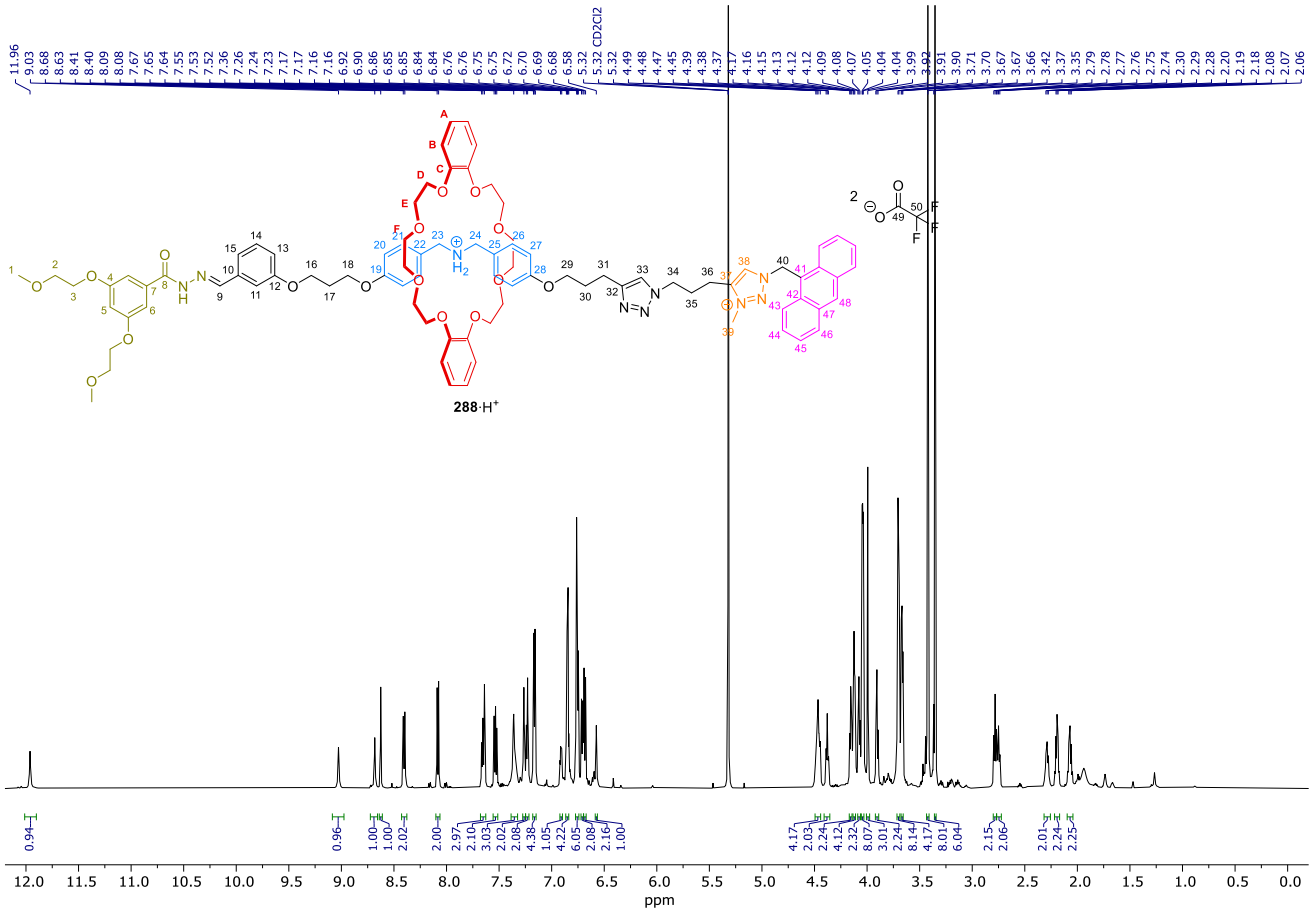

Spectrum 188. ^{1}H NMR (600 MHz, CD_2Cl_2) of **288**·H^+ (TFA^- salt).

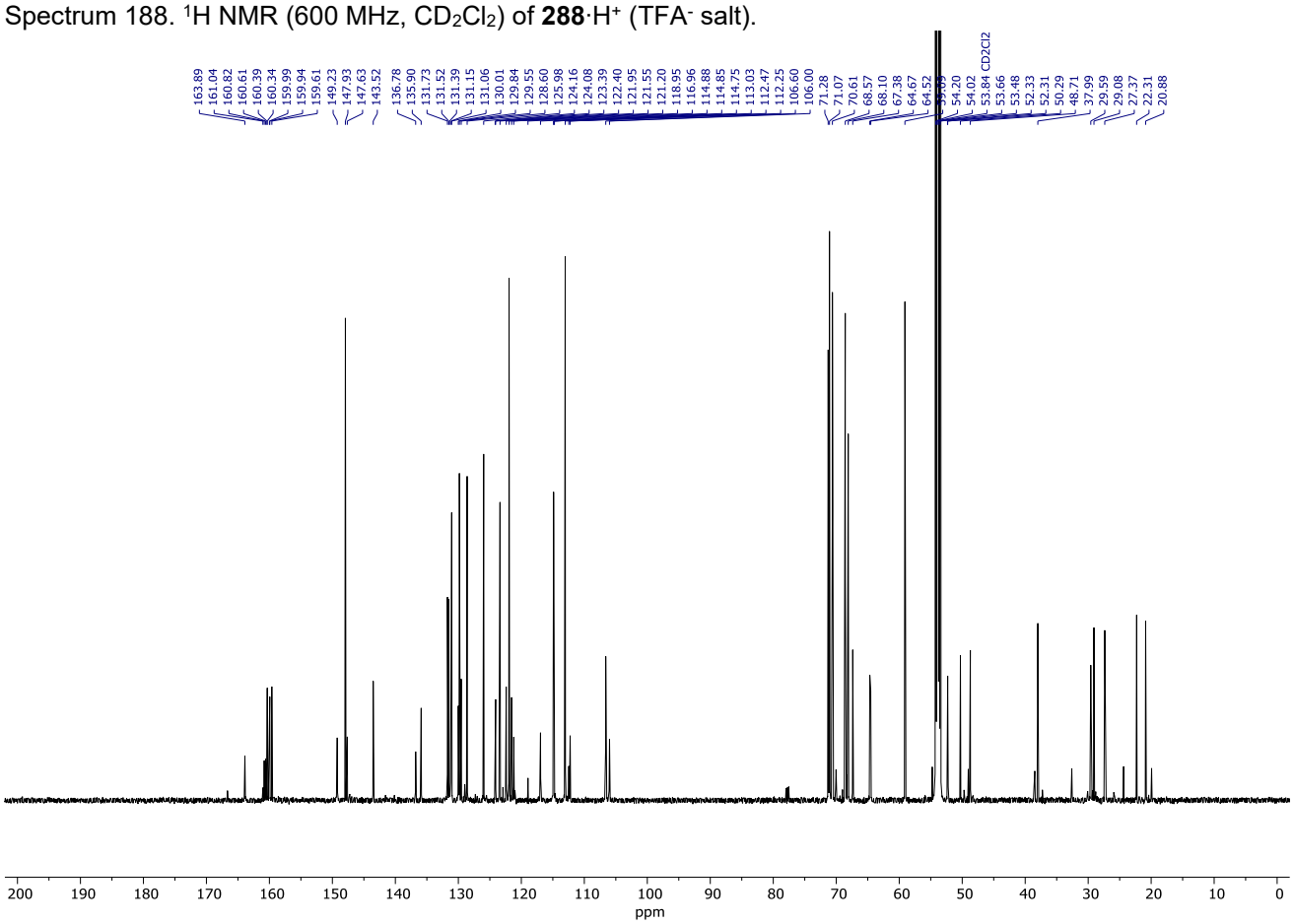

Spectrum 189. ^{13}C NMR (151 MHz, CD_2Cl_2) of **288**·H^+ (TFA^- salt).

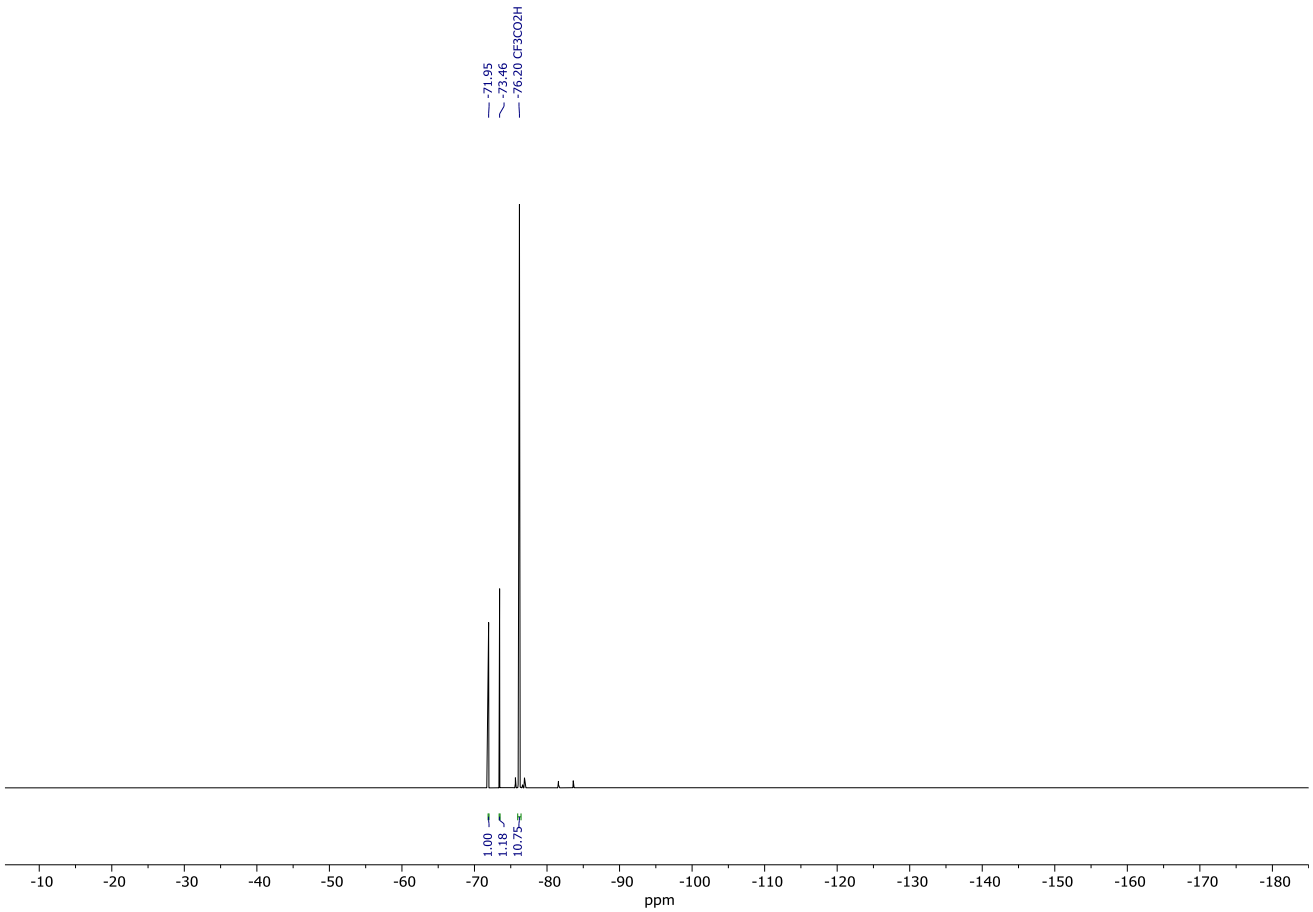

Spectrum 190. ^{19}F NMR (471 MHz, CD_2Cl_2) of **288**·H^+ (TFA^- salt).

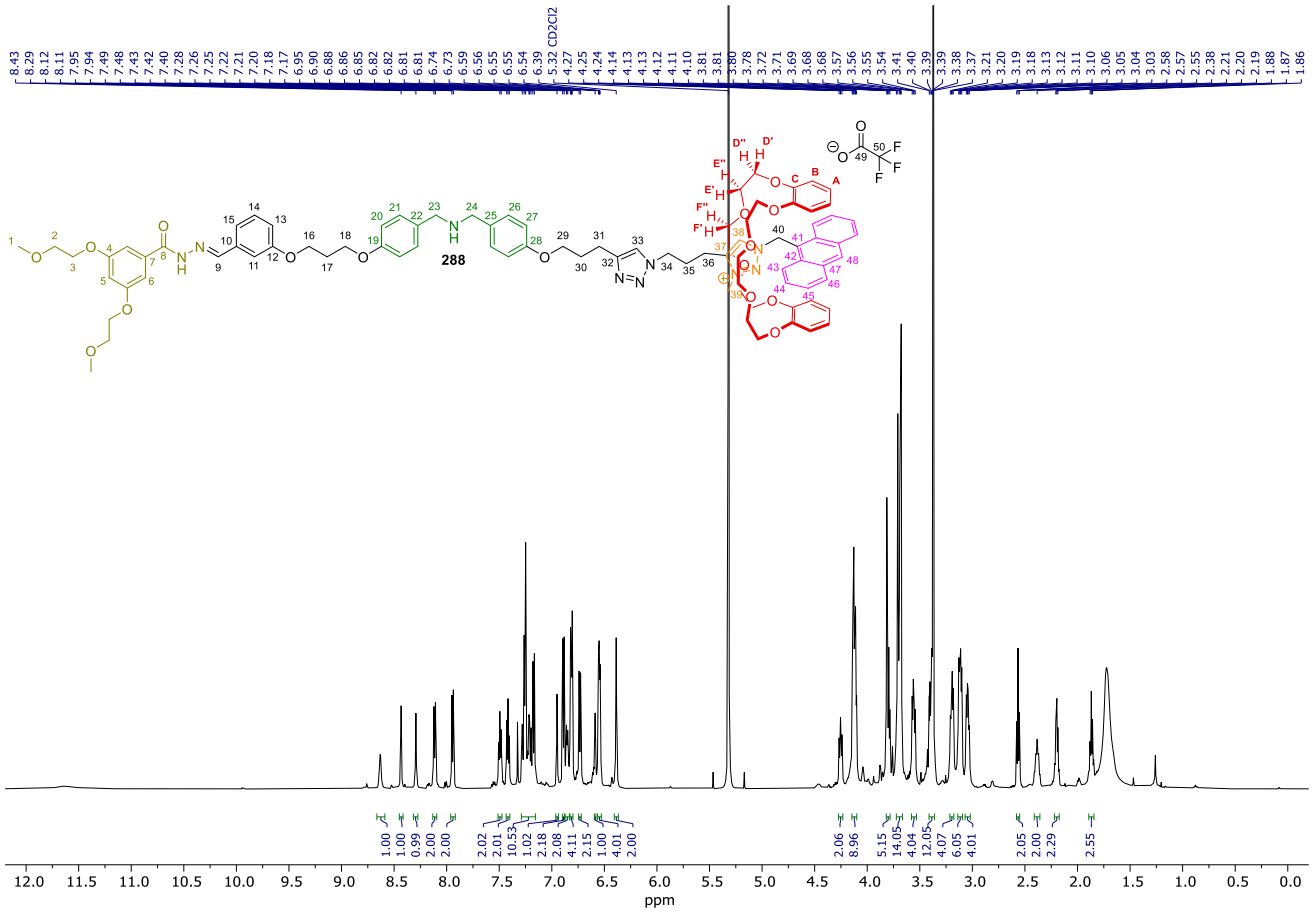

Spectrum 191. ^{1}H NMR (600 MHz, CD_2Cl_2) of **288** (TFA^- salt).

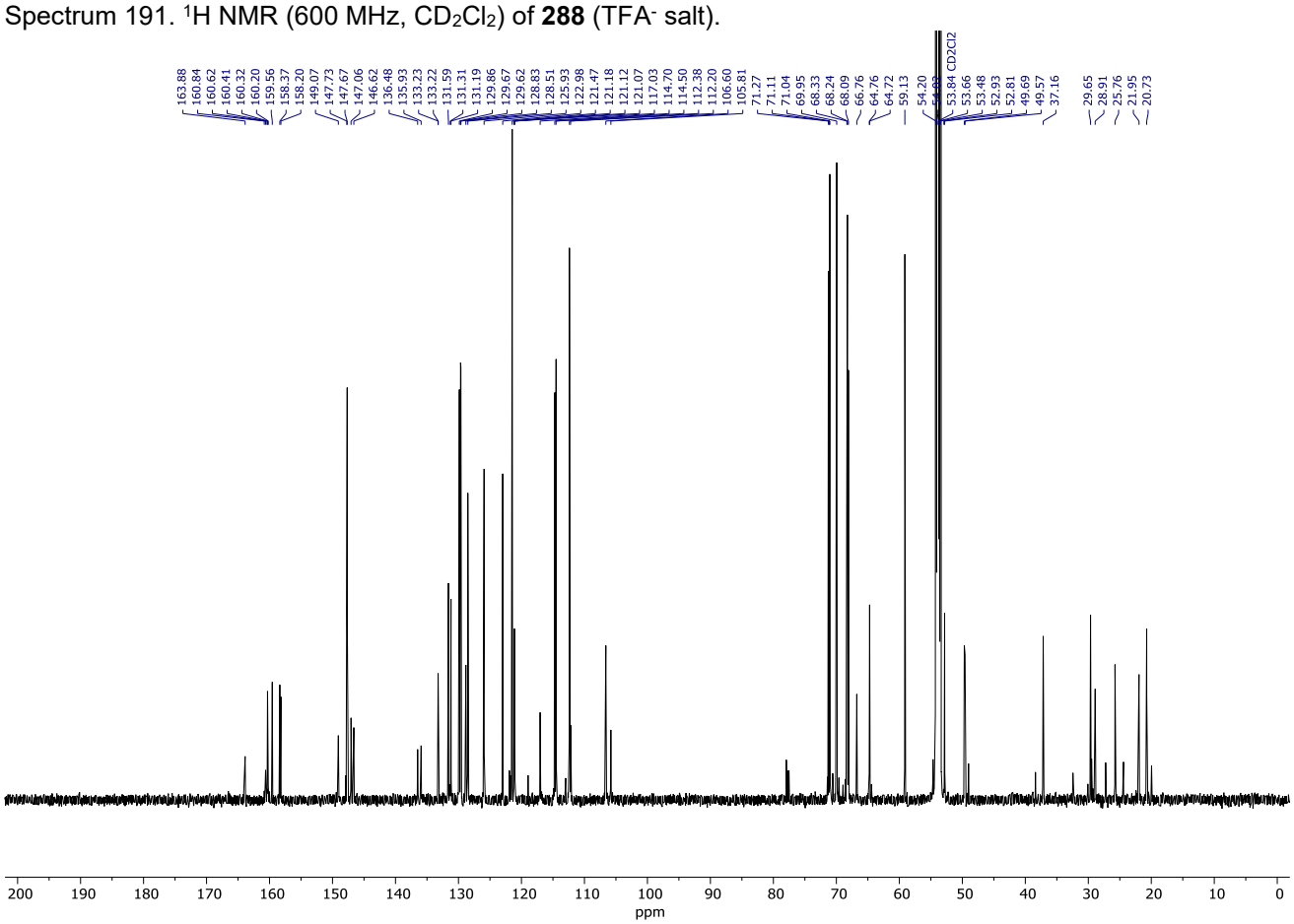

Spectrum 192. ^{13}C NMR (151 MHz, CD_2Cl_2) of **288** (TFA^- salt).

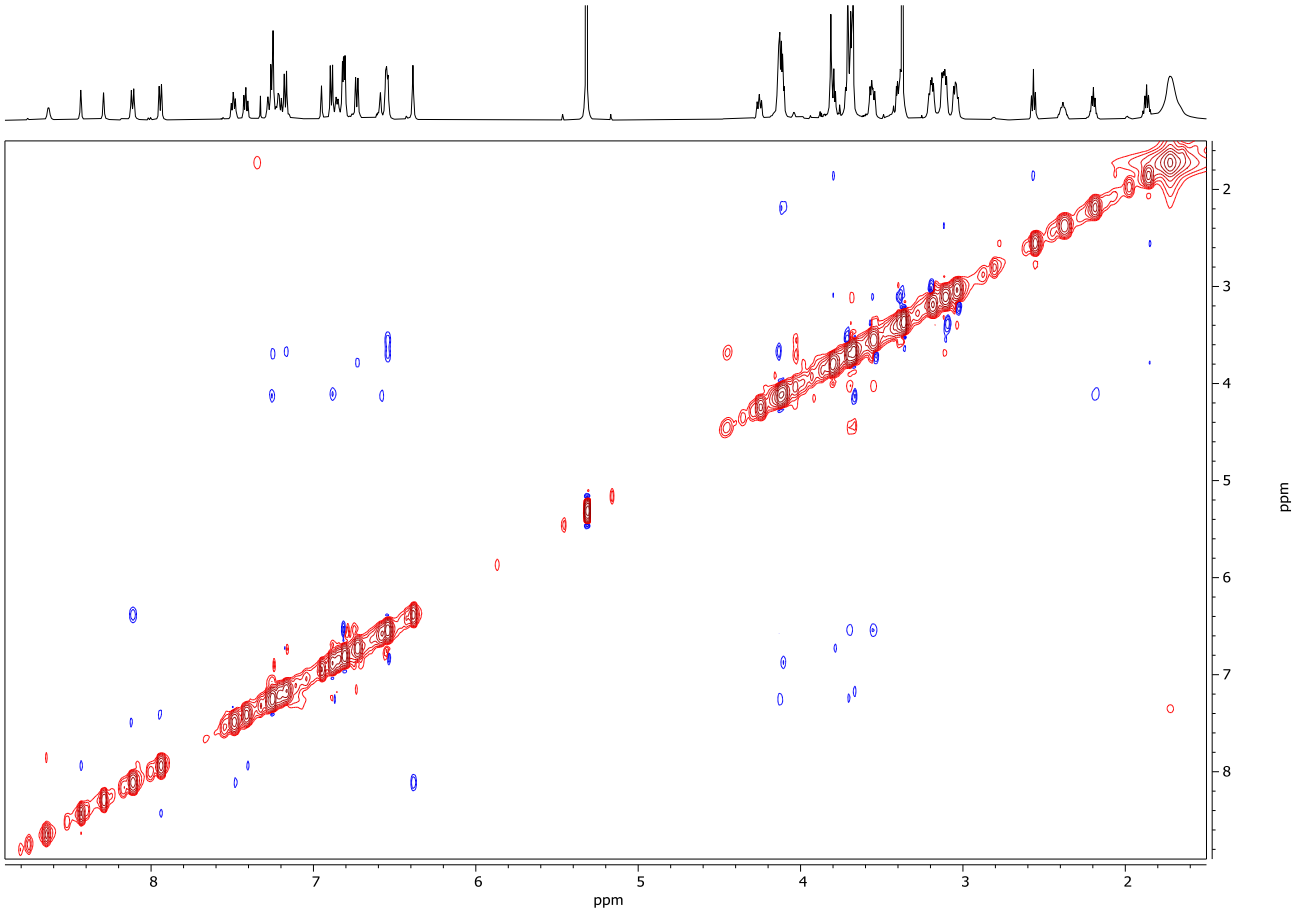

Spectrum 193. 2D NOESY (600 MHz, CD_2Cl_2) of **288**. Data was recorded with a 300 ms mixing time and a relaxation delay of 2.00 s. 2K data points were collected for 256 increments of 4 scans.

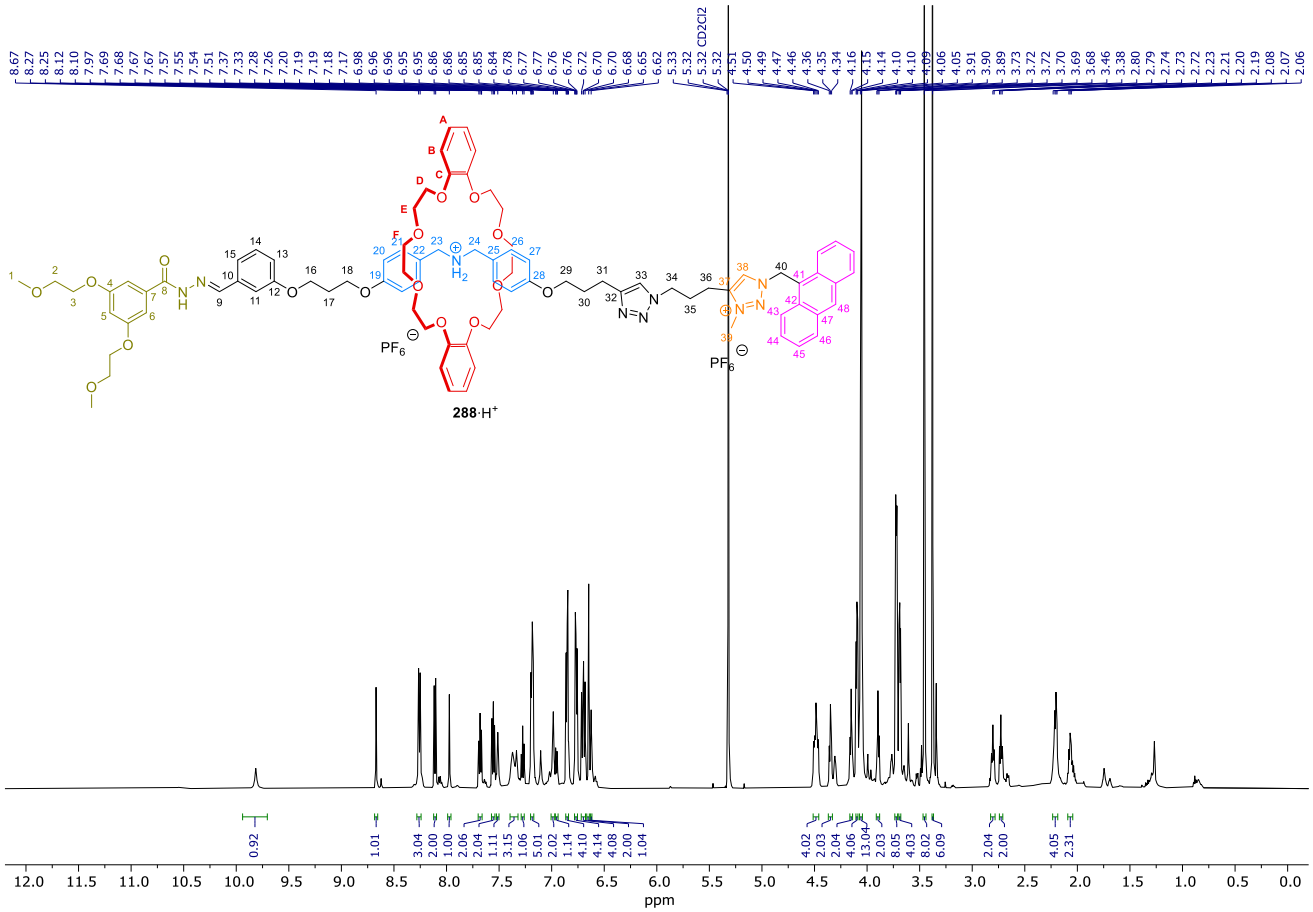

Spectrum 194. ^{1}H NMR (600 MHz, CD_2Cl_2) of **288**·H^+ (PF_6^- salt).

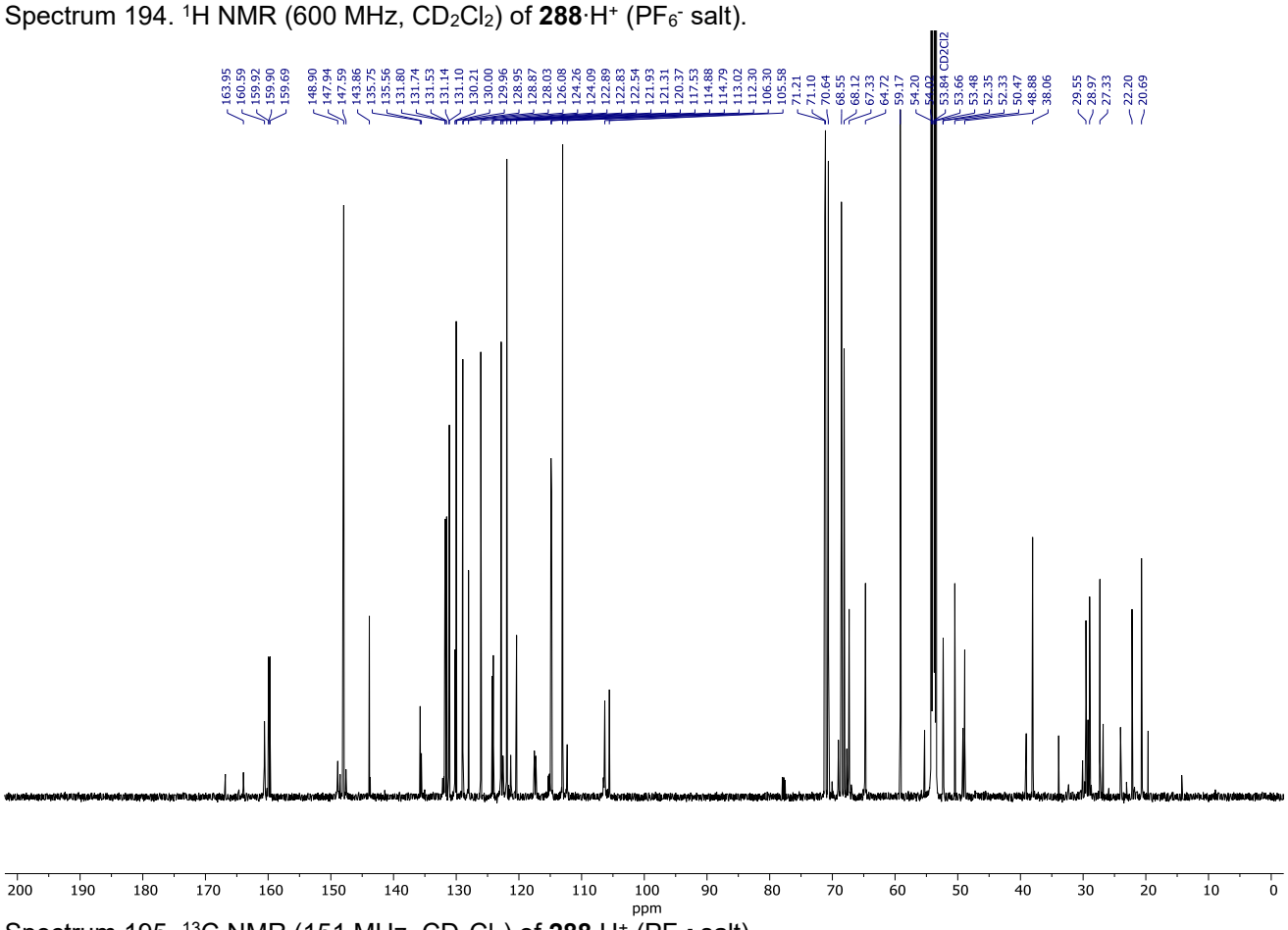

Spectrum 195. ^{13}C NMR (151 MHz, CD_2Cl_2) of **288**·H^+ (PF_6^- salt).

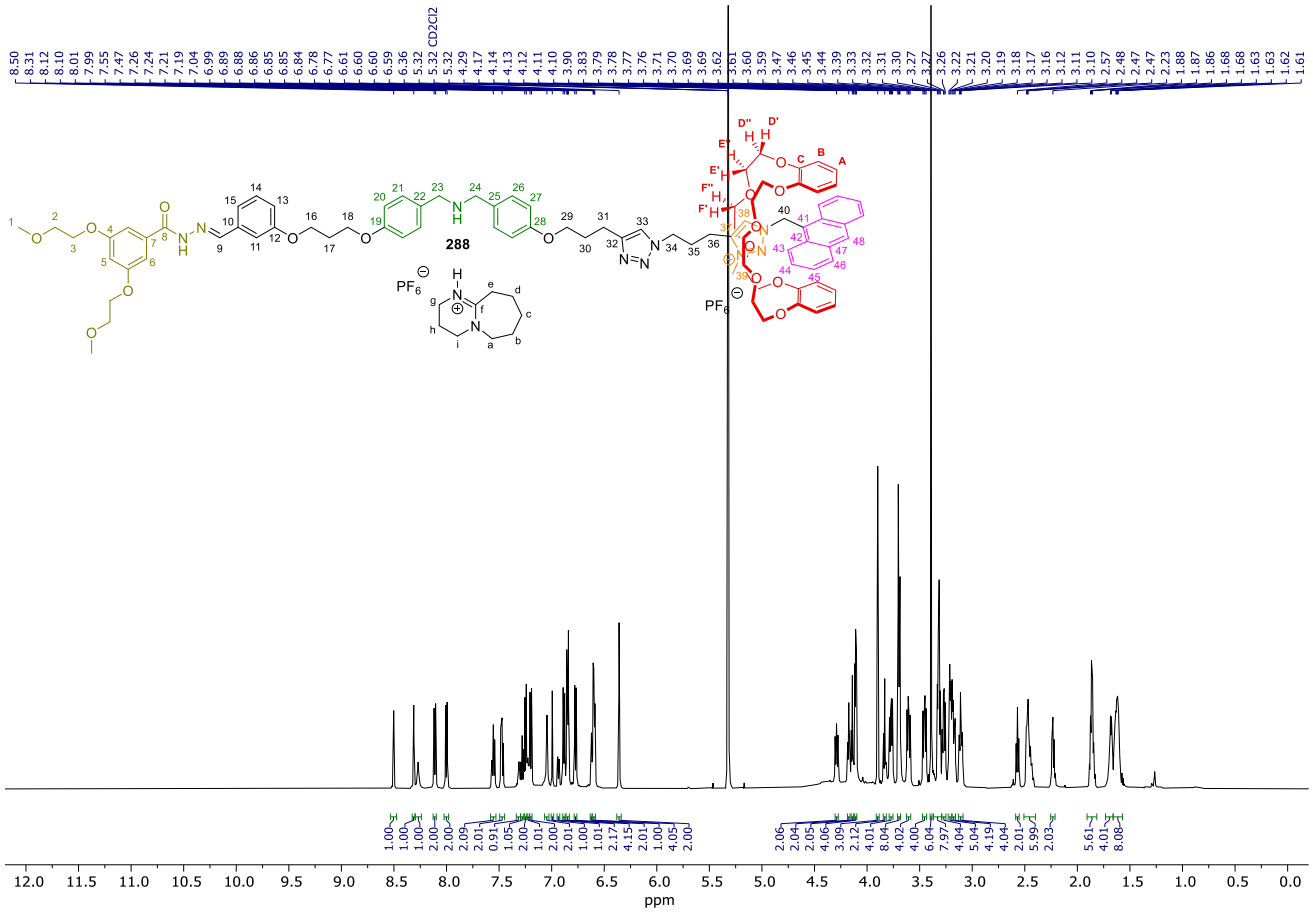

Spectrum 196. ^{1}H NMR (600 MHz, CD_2Cl_2) of **288** (PF_6^- salt).

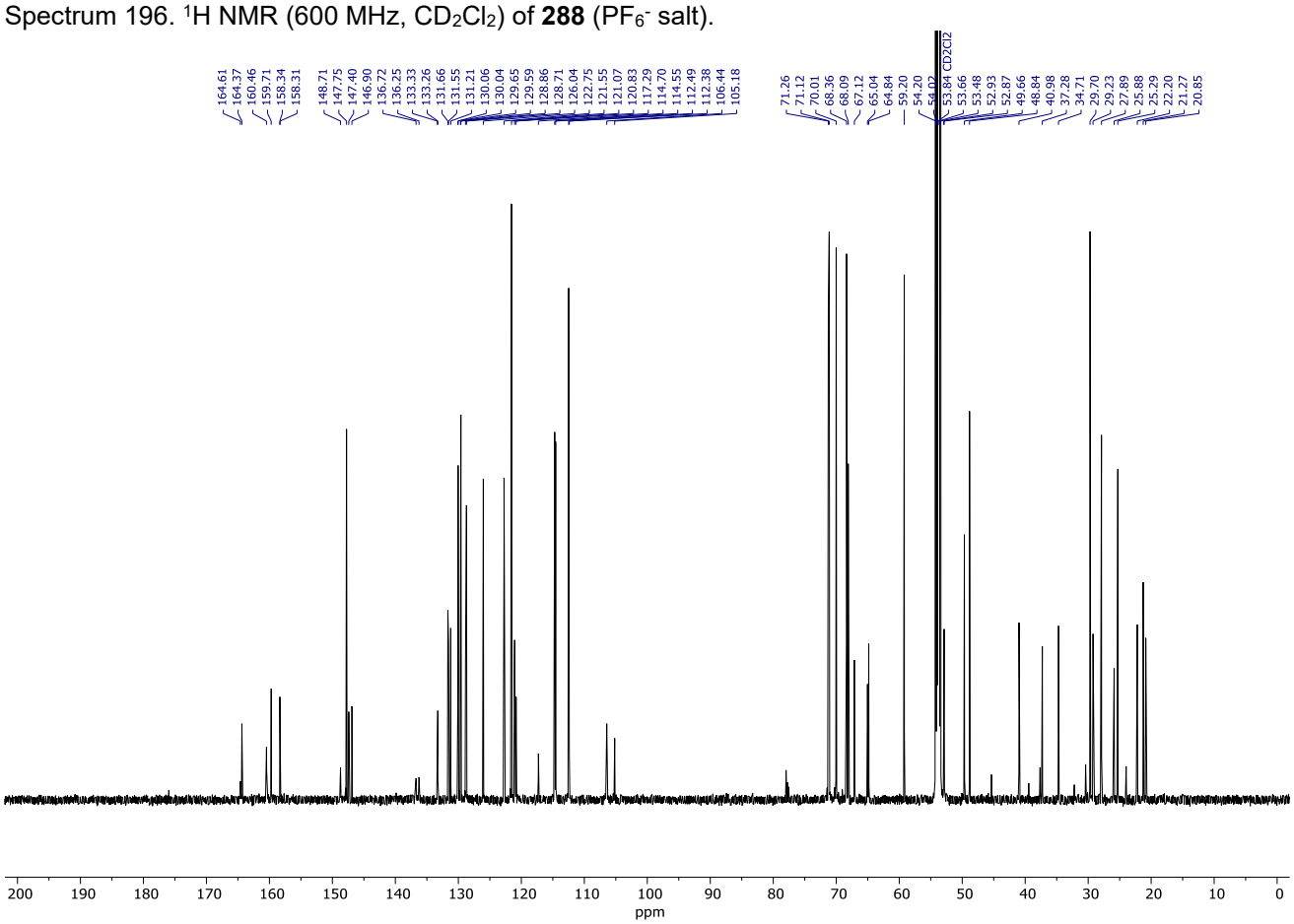

Spectrum 197. ^{13}C NMR (151 MHz, CD_2Cl_2) of **288** (PF_6^- salt).

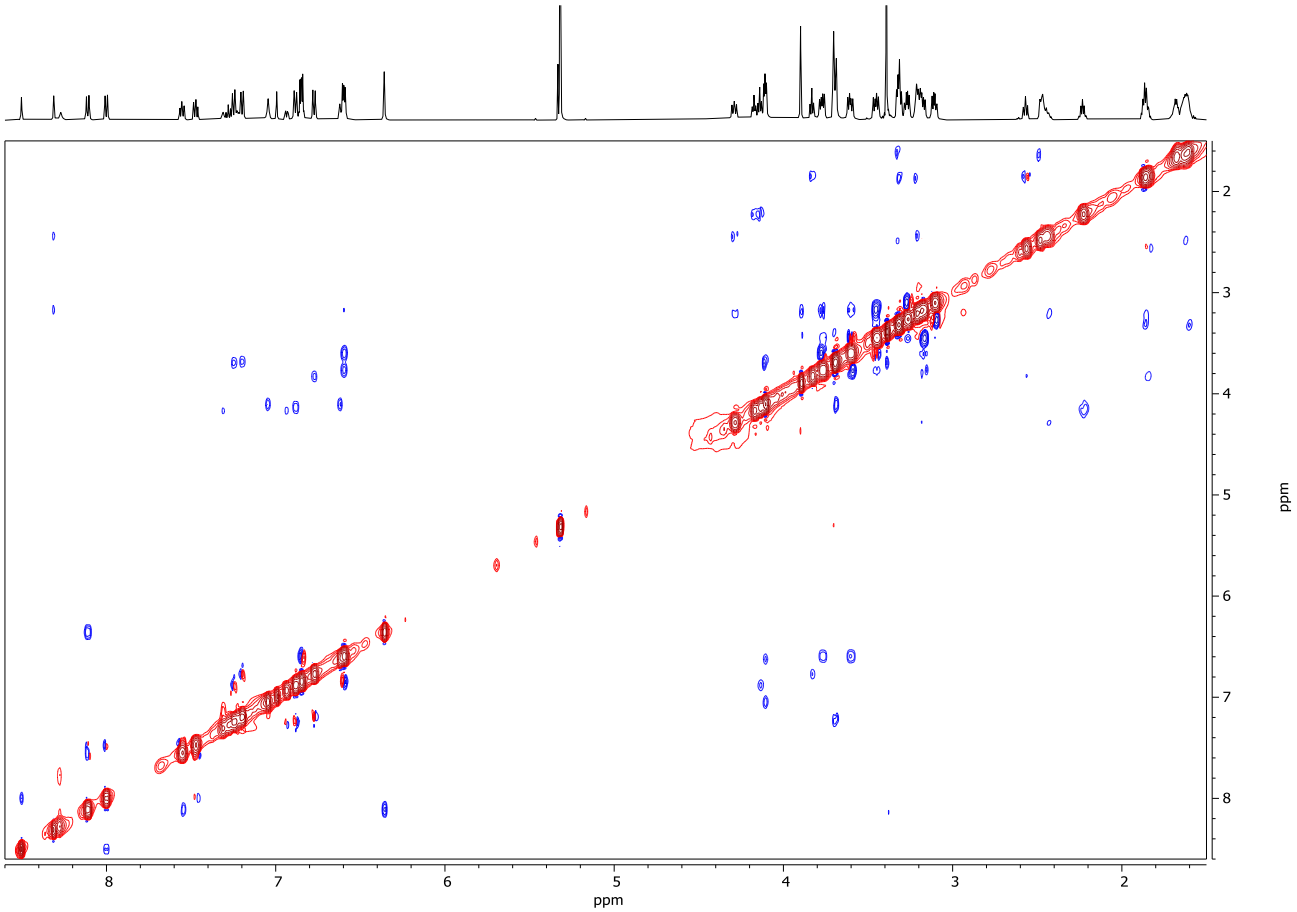

Spectrum 198. 2D NOESY (600 MHz, CD_2Cl_2) of **288**. Data was recorded with a 300 ms mixing time and a relaxation delay of 2.00 s. 2K data points were collected for 256 increments of 4 scans.

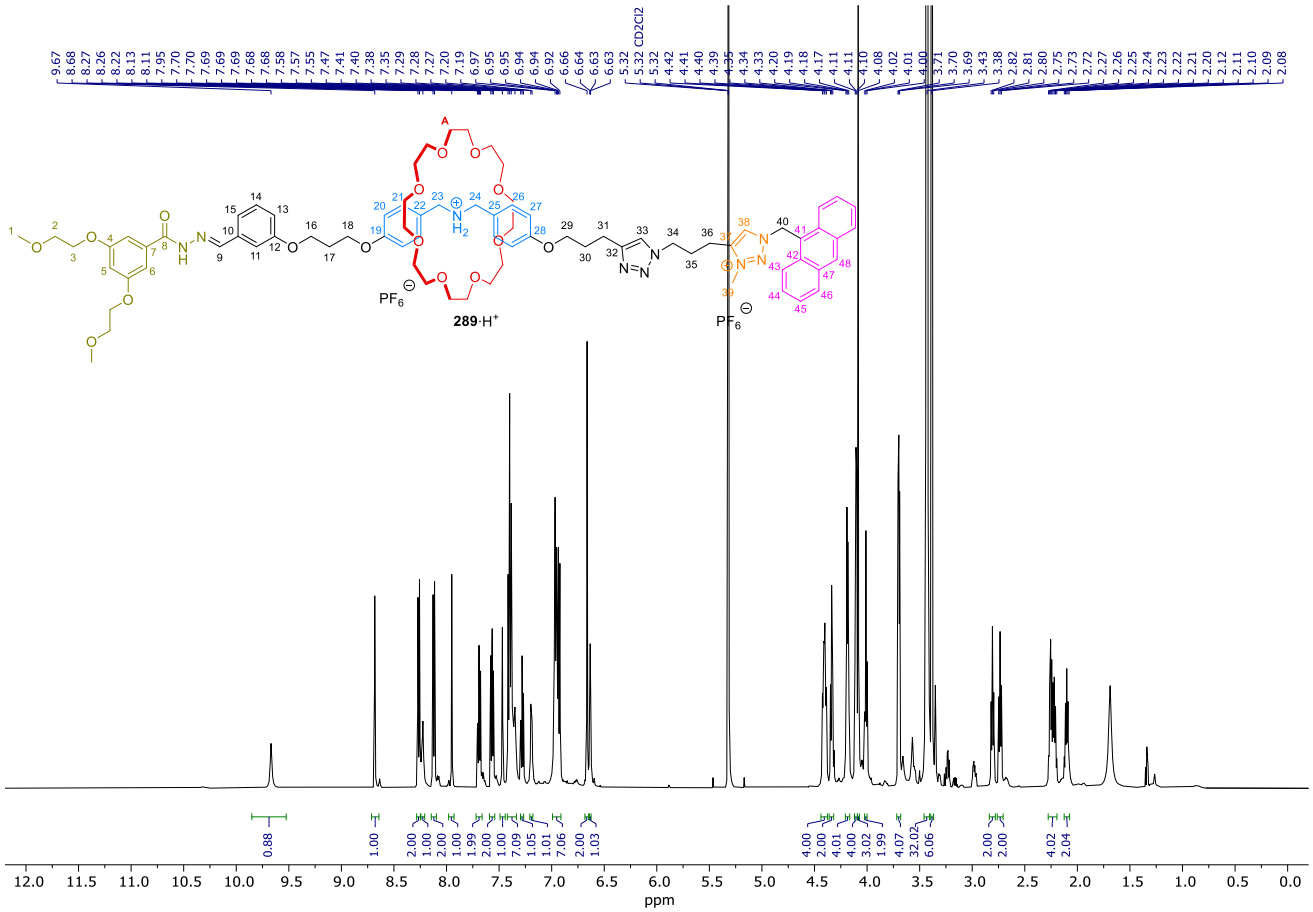

Spectrum 199. ^{1}H NMR (600 MHz, CD_2Cl_2) of **289**·H^+ (PF_6^- salt).

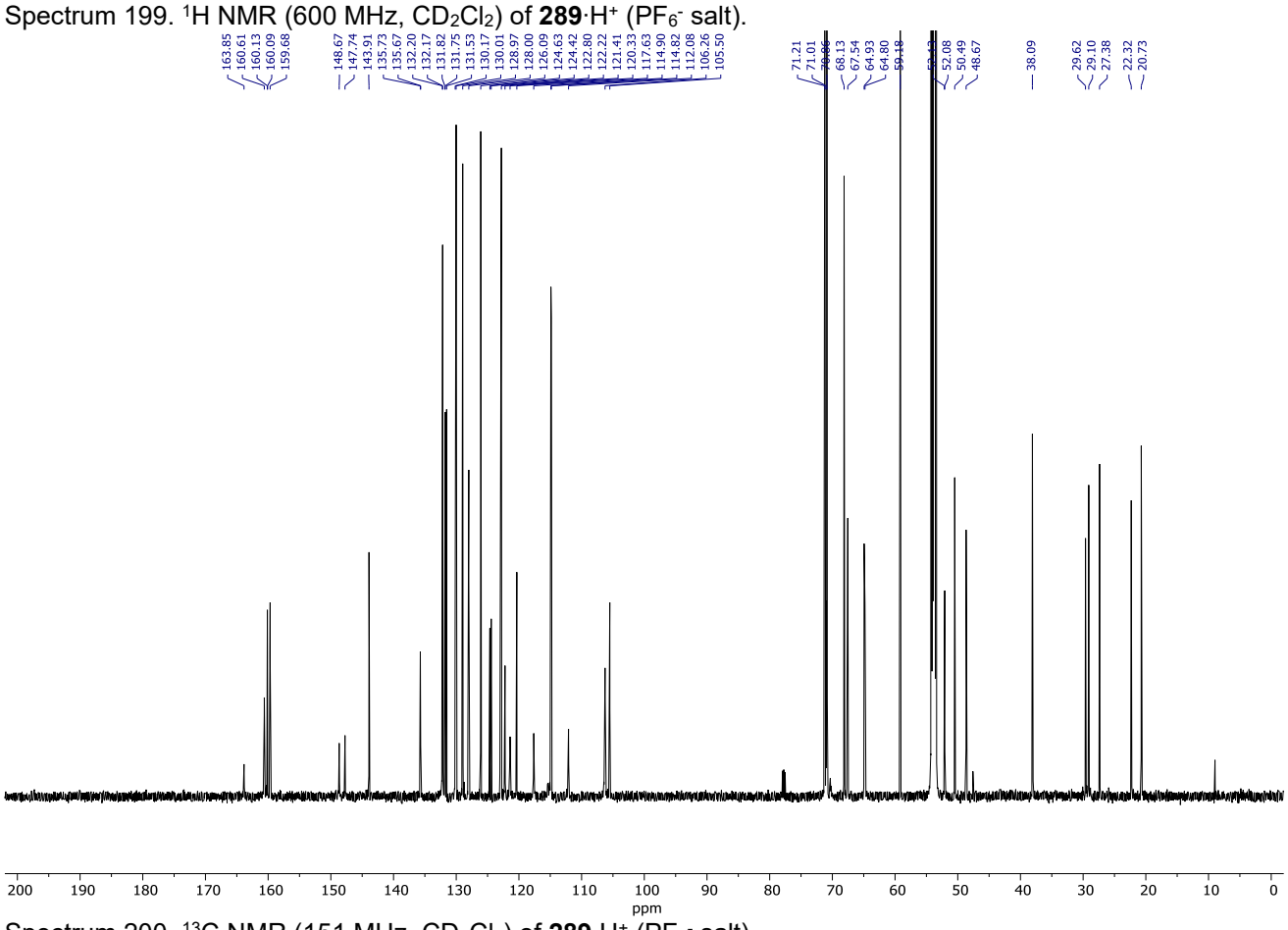

Spectrum 200. ^{13}C NMR (151 MHz, CD_2Cl_2) of **289**·H^+ (PF_6^- salt).

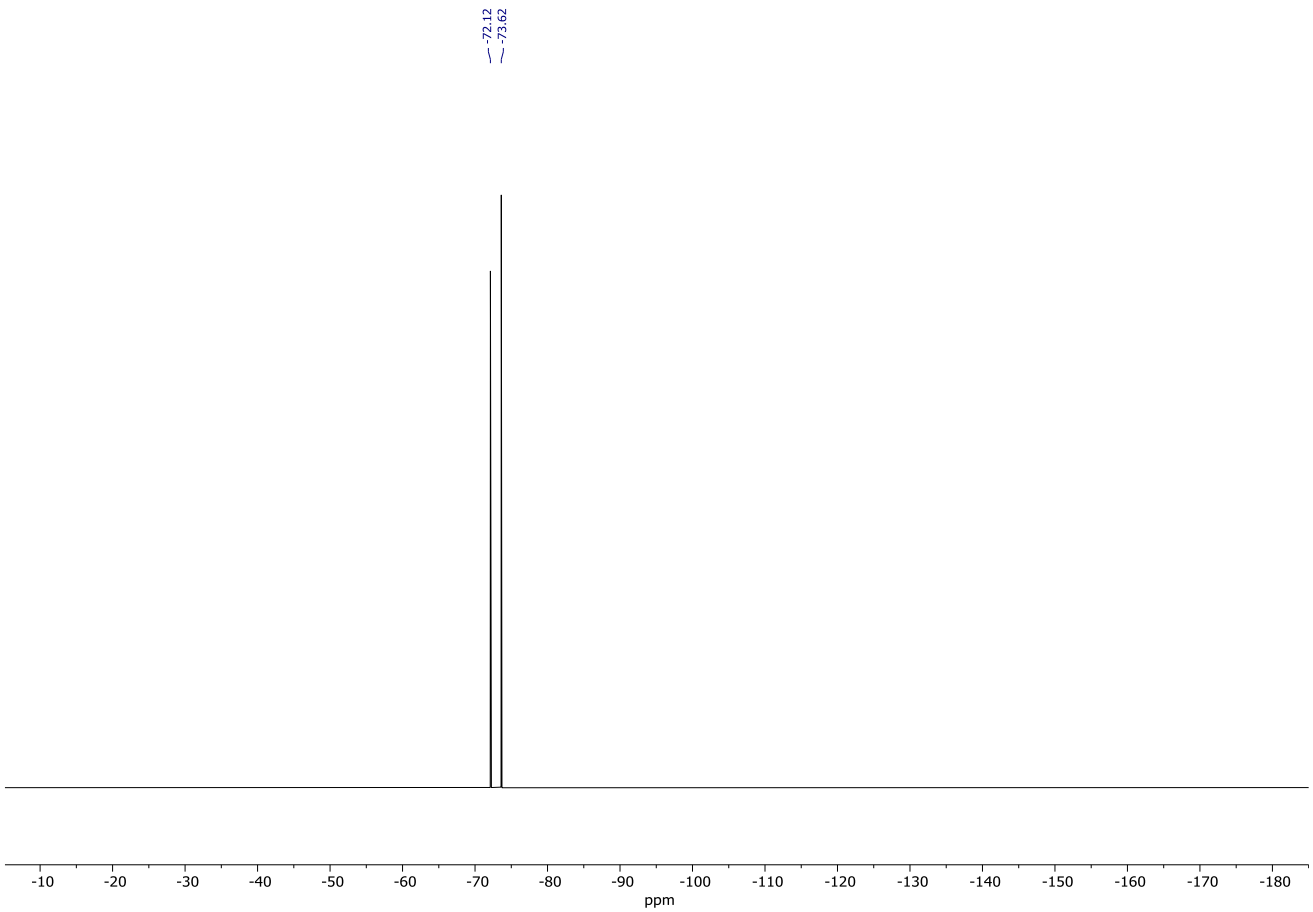

Spectrum 201. ^{19}F NMR (471 MHz, CD_2Cl_2) of **289**·H^+ (PF_6^- salt).

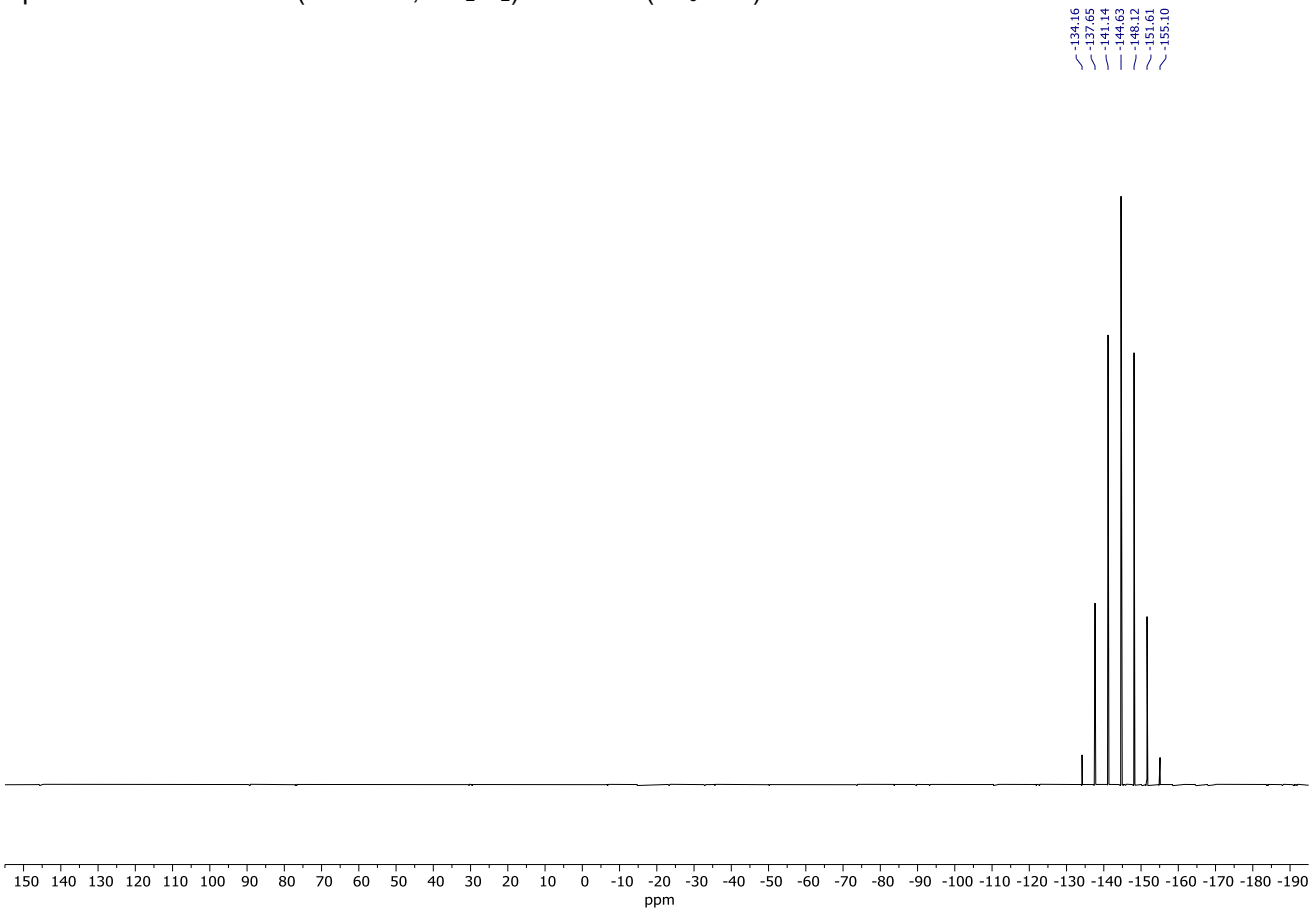

Spectrum 202. ^{31}P NMR (202 MHz, CD_2Cl_2) of **289**·H^+ (PF_6^- salt).

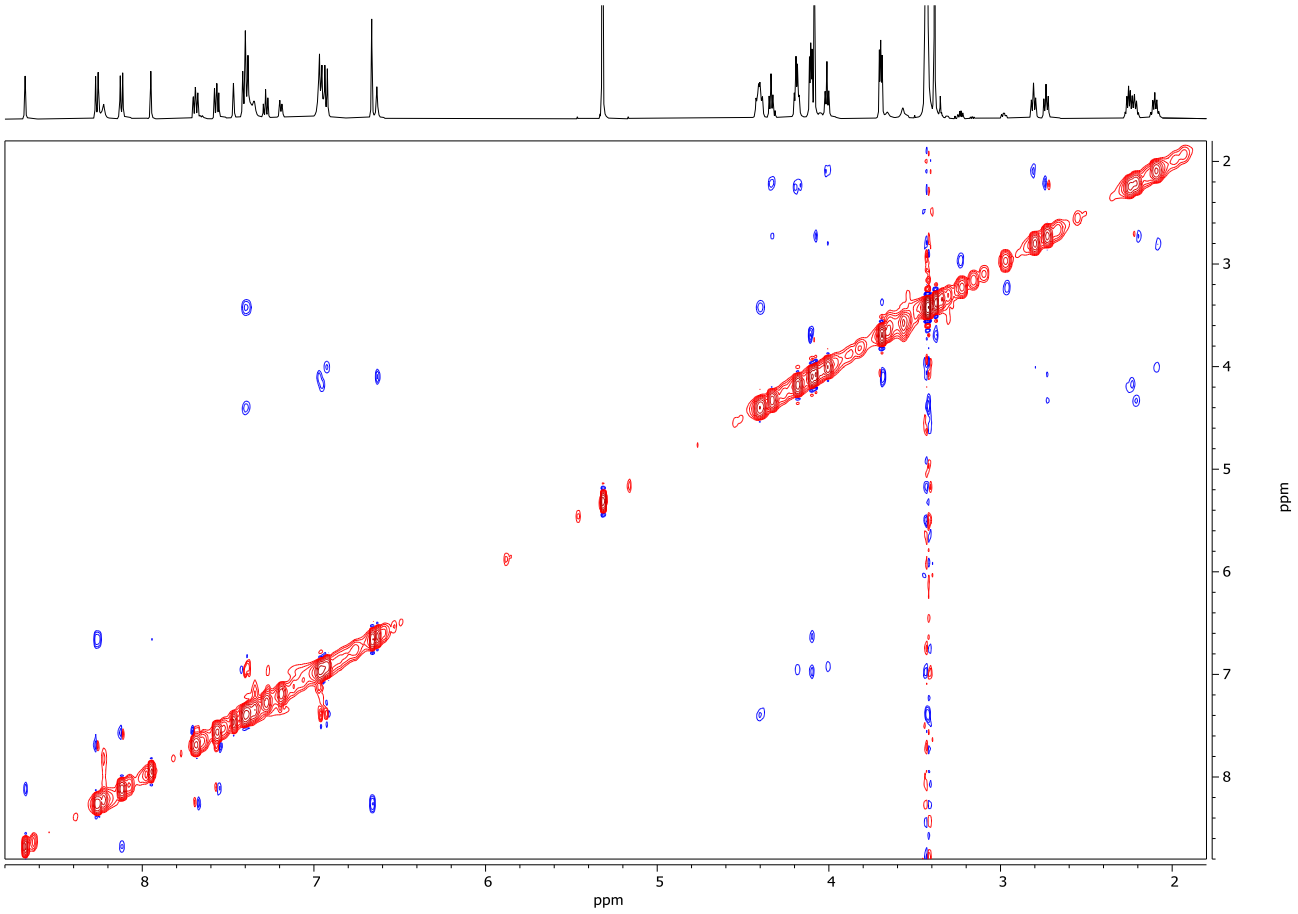

Spectrum 203. 2D NOESY (600 MHz, CD_2Cl_2) of **289**. Data was recorded with a 300 ms mixing time and a relaxation delay of 2.02 s. 2K data points were collected for 256 increments of 4 scans.

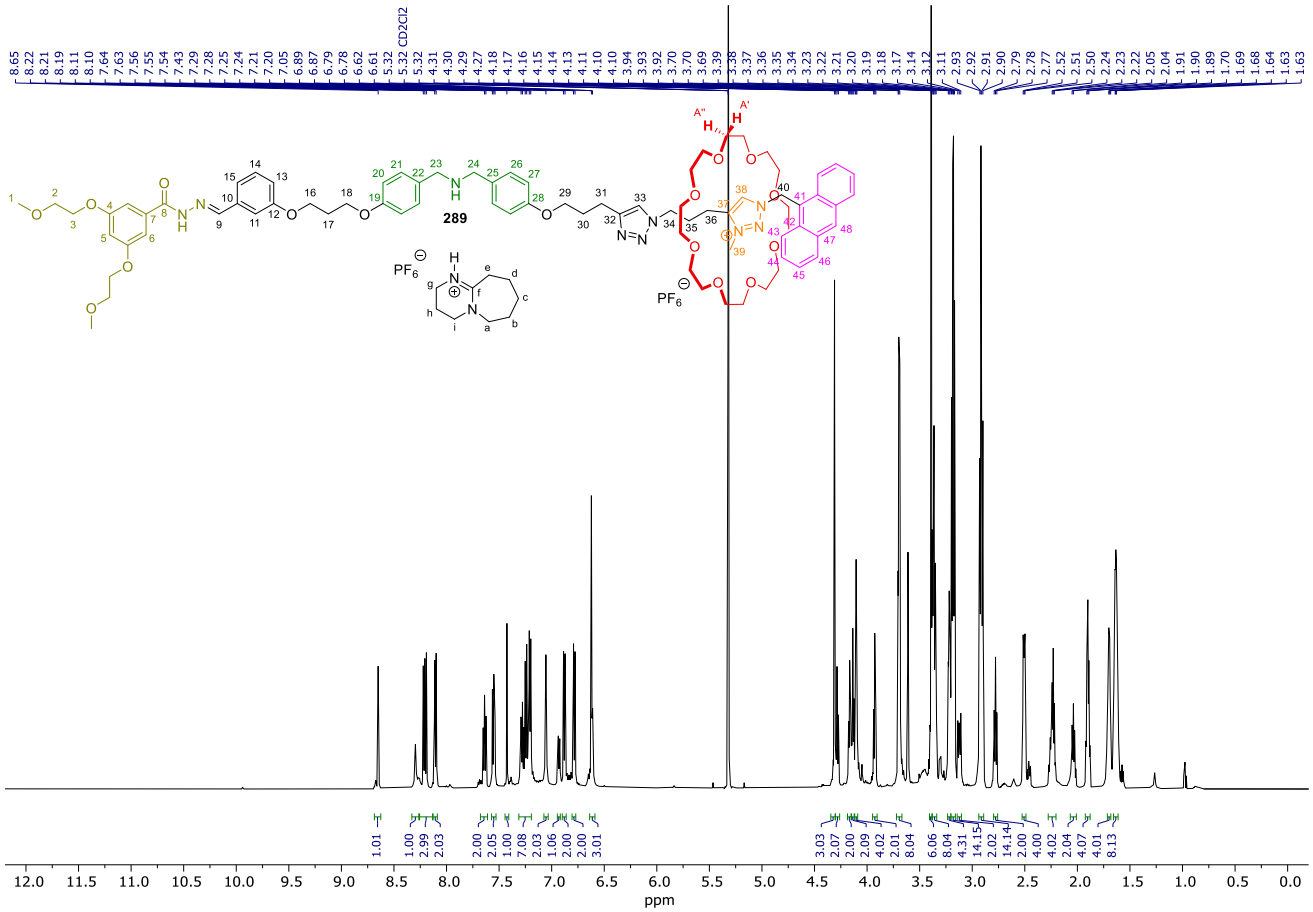

Spectrum 204. ^{1}H NMR (600 MHz, CD_2Cl_2) of **289** (PF_6^- salt).

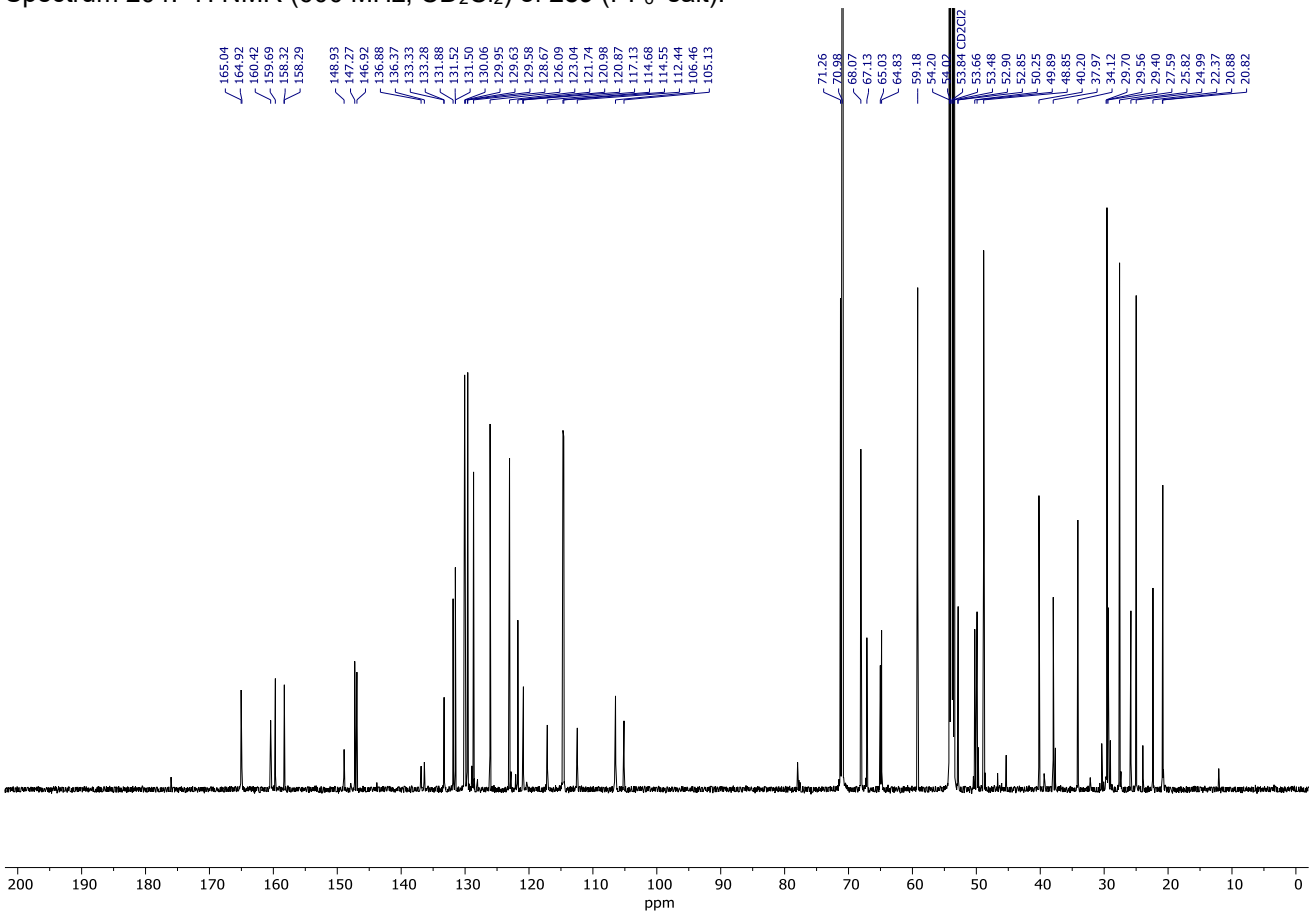

Spectrum 205. ^{13}C NMR (151 MHz, CD_2Cl_2) of **289** (PF_6^- salt).

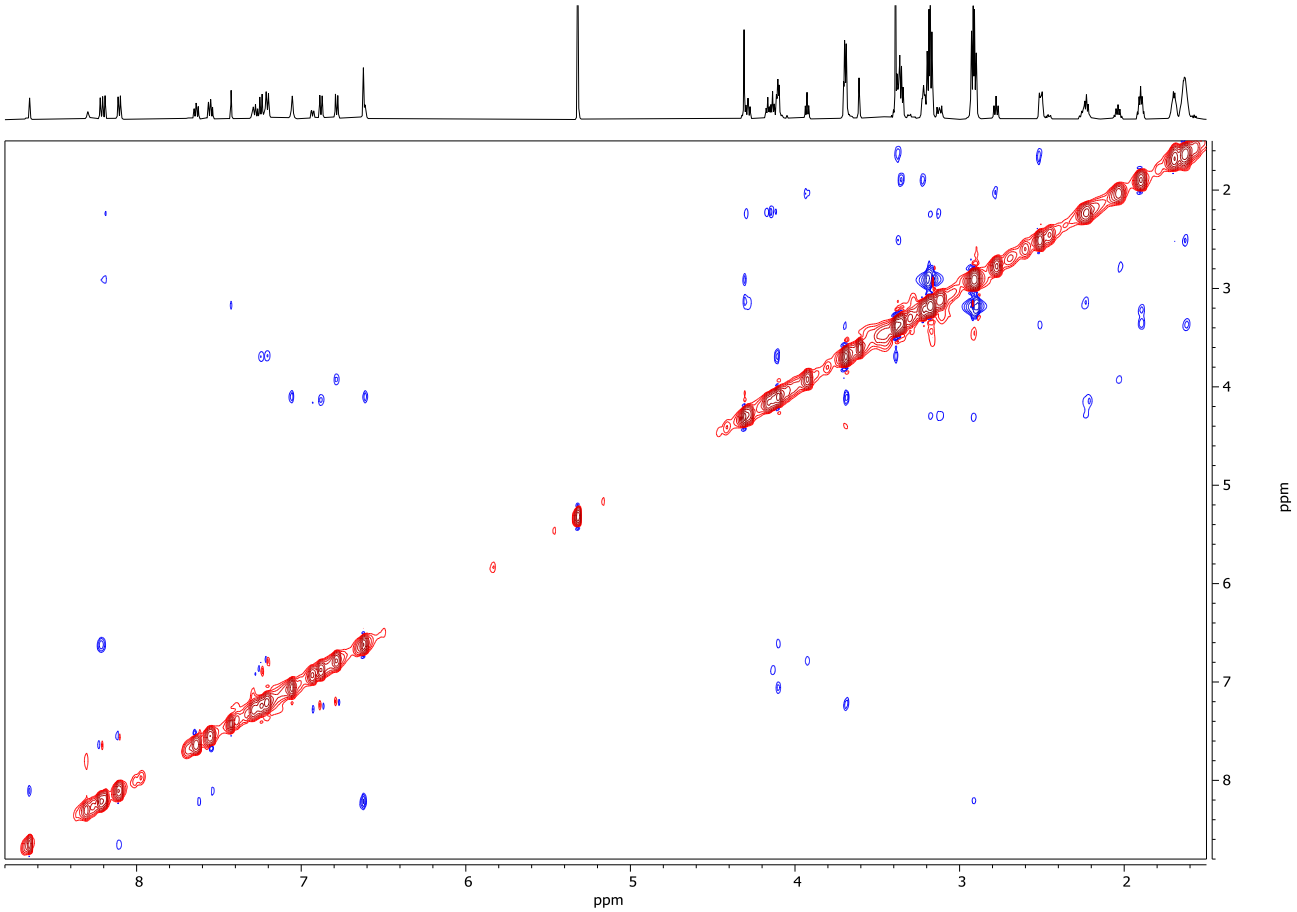

Spectrum 206. 2D NOESY (600 MHz, CD_2Cl_2) of **289**. Data was recorded with a 300 ms mixing time and a relaxation delay of 2.01 s. 2K data points were collected for 256 increments of 4 scans.

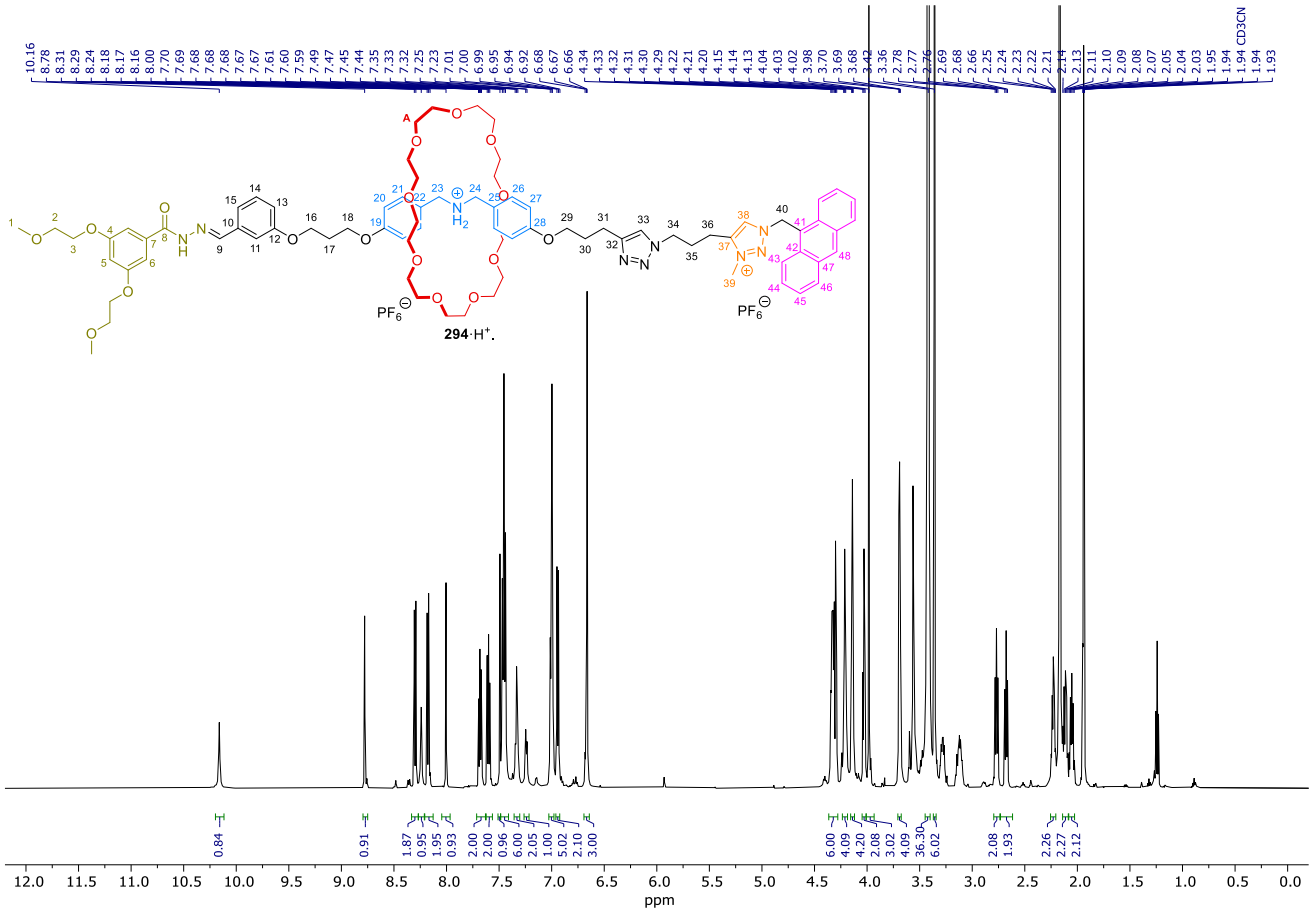

Spectrum 207. ^{1}H NMR (600 MHz, CD_3CN) of **294**·H^+ (PF_6^- salt).

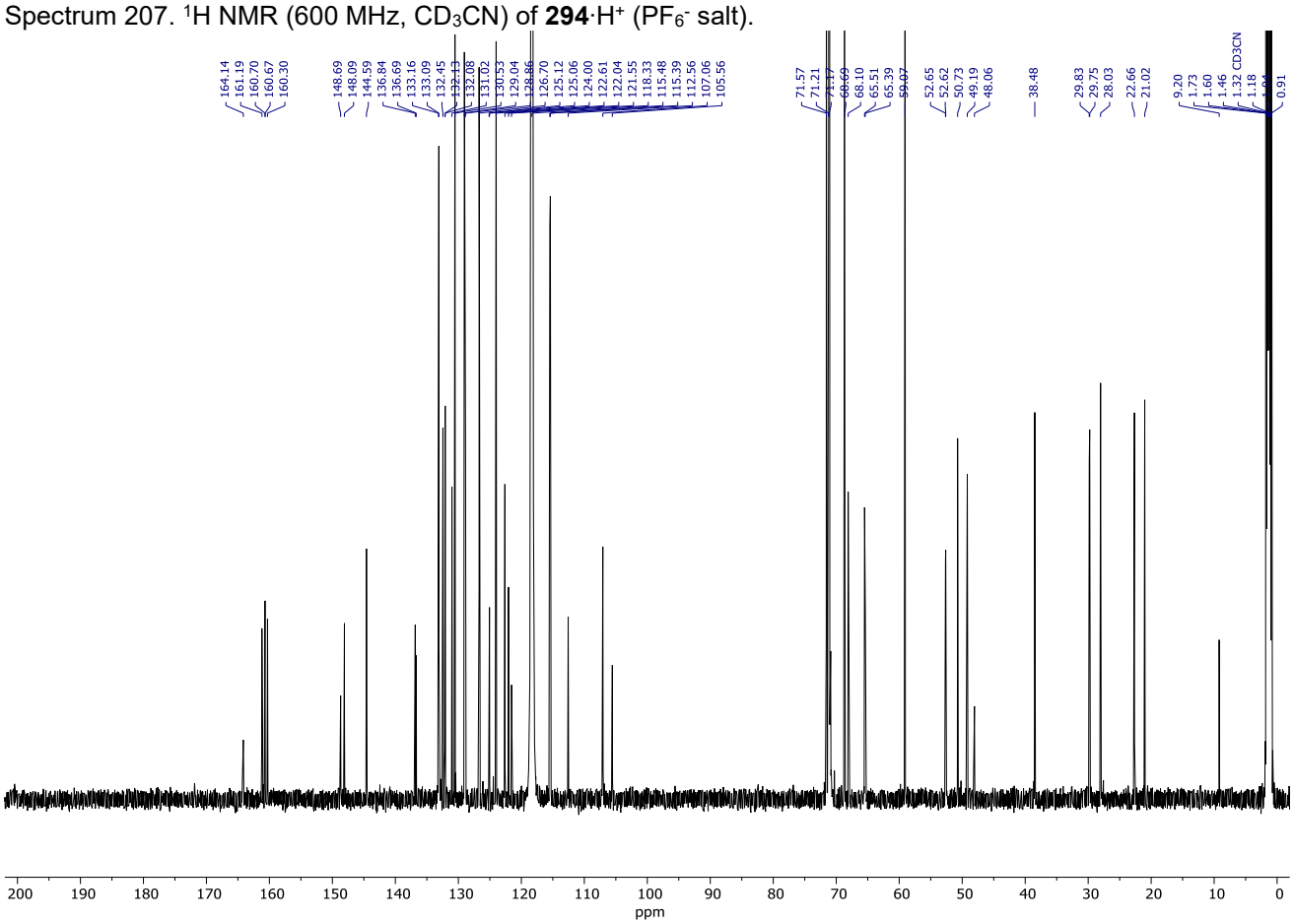

Spectrum 208. ^{13}C NMR (151 MHz, CD_3CN) of **294**·H^+ (PF_6^- salt).

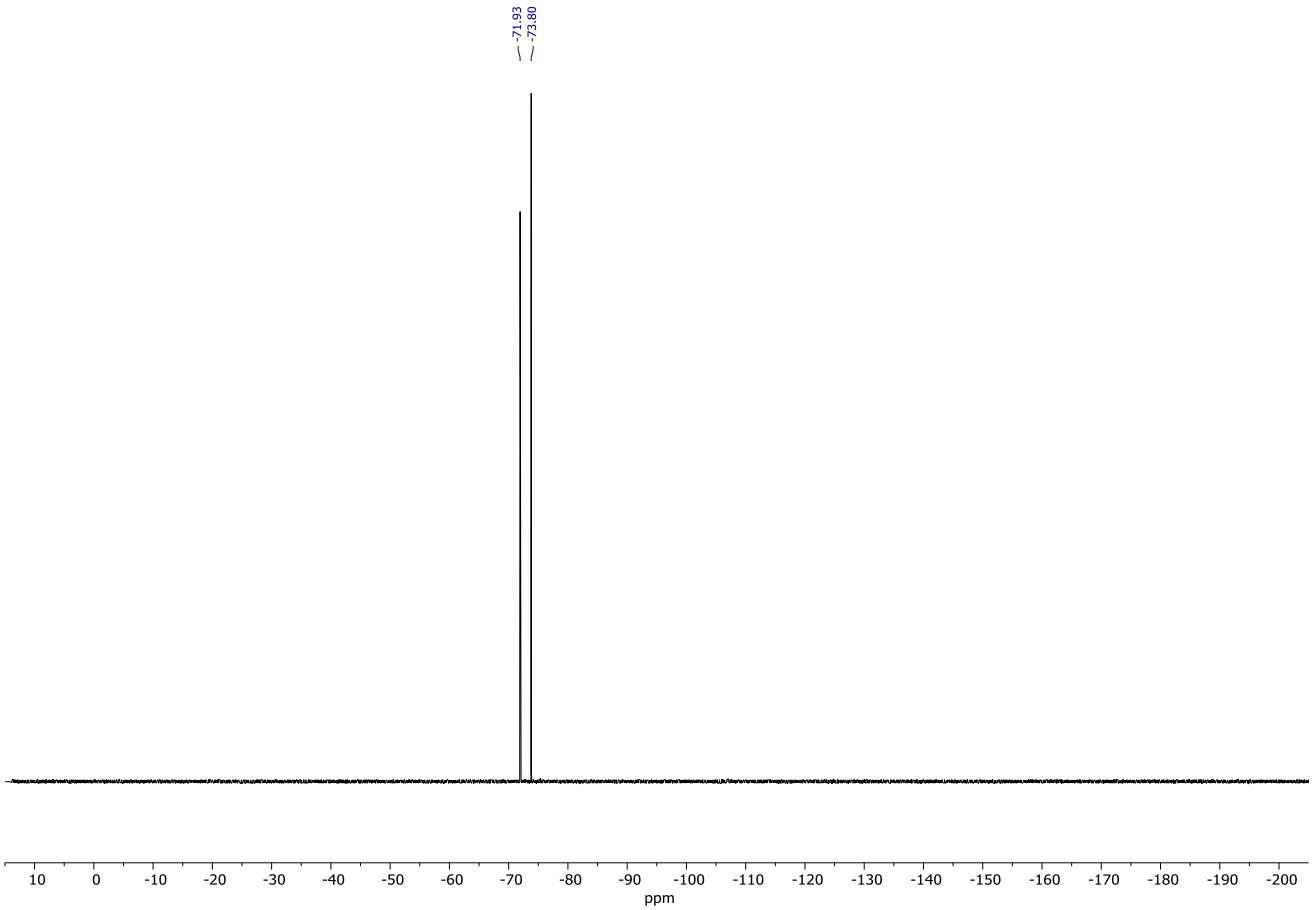

Spectrum 209. ^{19}F NMR (376 MHz, CD_3CN) of **294**·H^+ (PF_6^- salt).

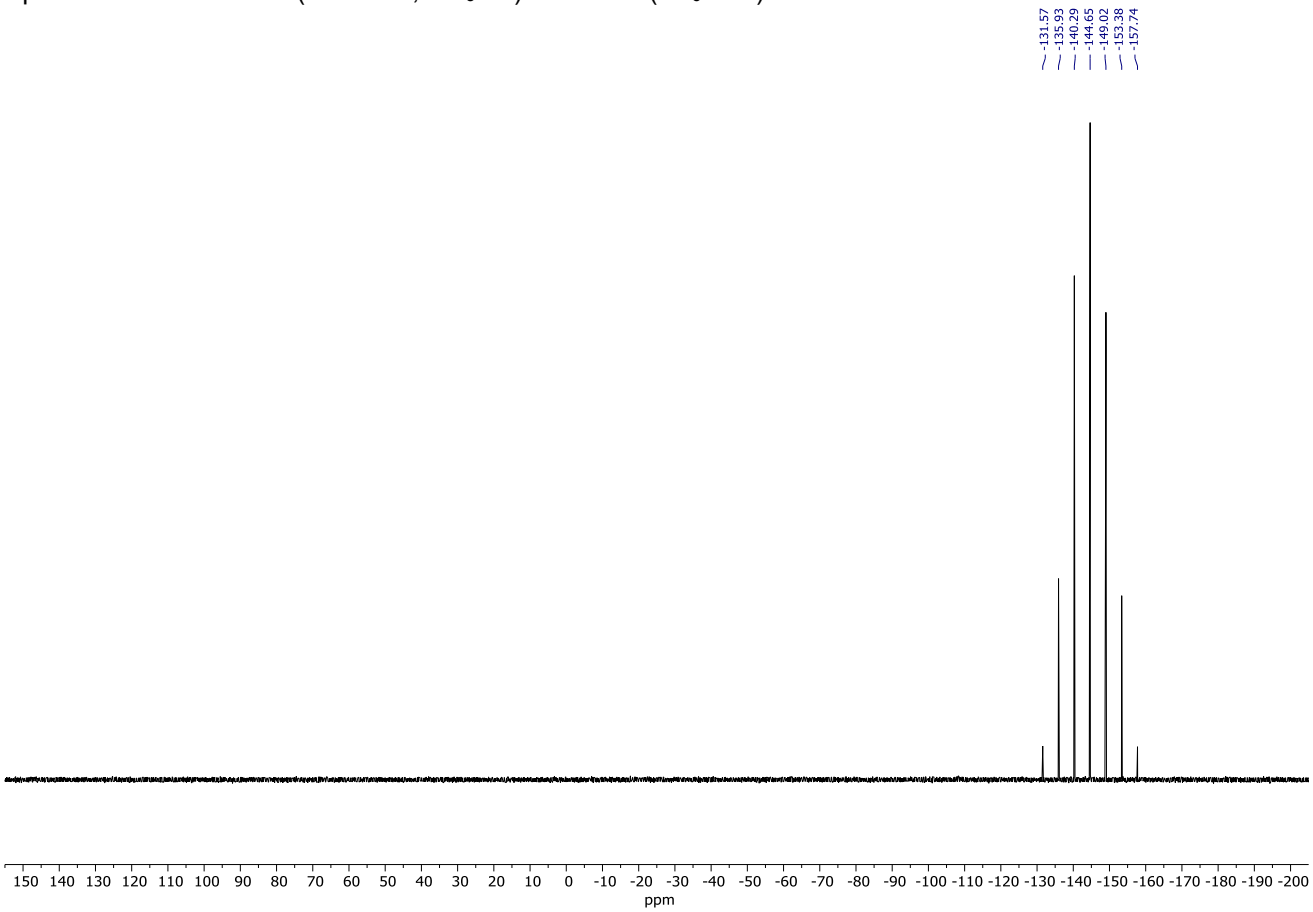

Spectrum 210. ^{31}P NMR (162 MHz, CD_3CN) of **294**·H^+ (PF_6^- salt).

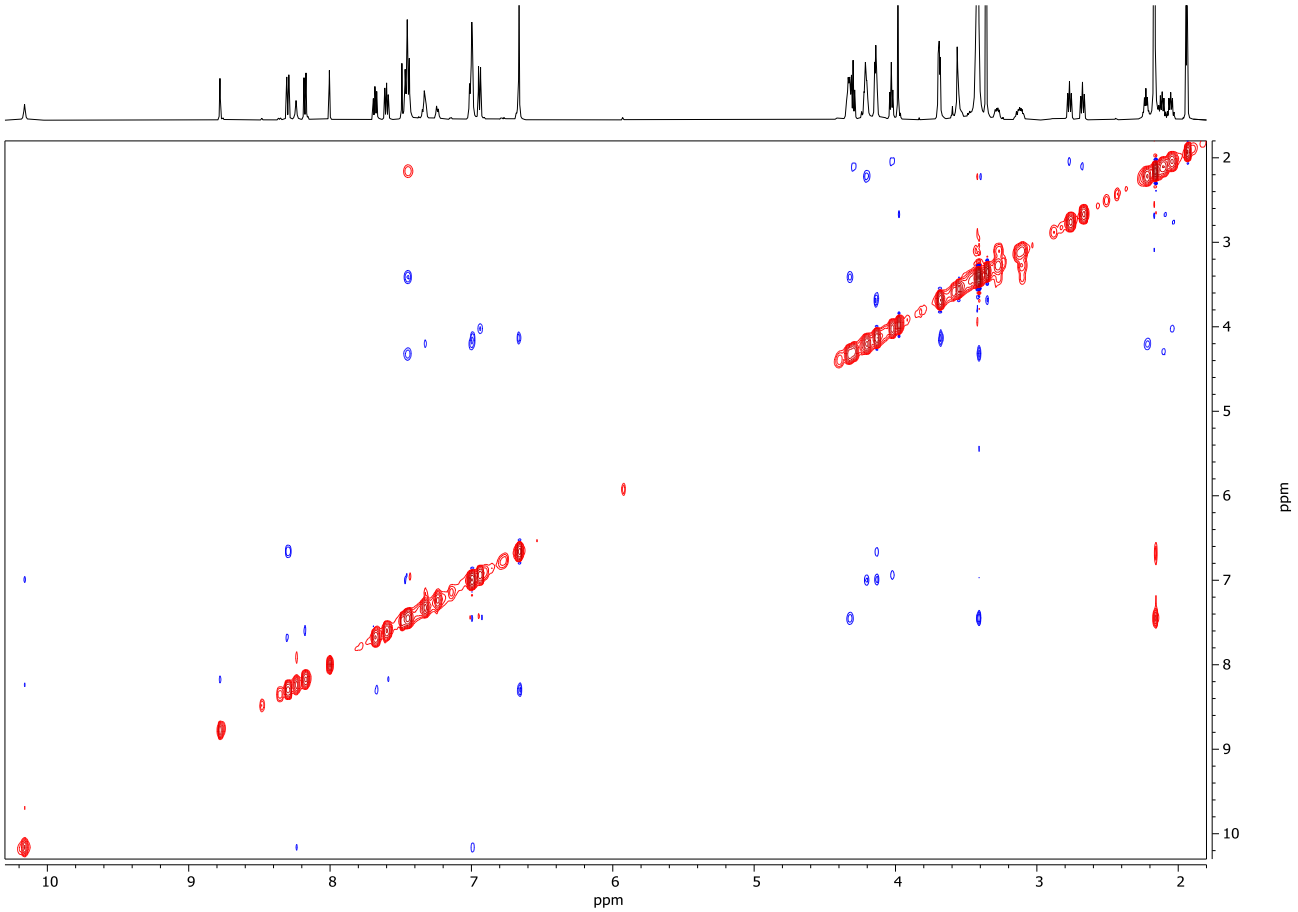

Spectrum 211. 2D NOESY (600 MHz, CD_3CN) of **294**·H^+. Data was recorded with 400 ms mixing time and a relaxation delay of 2.03 s. 2K data points were collected for 256 increments of 4 scans.

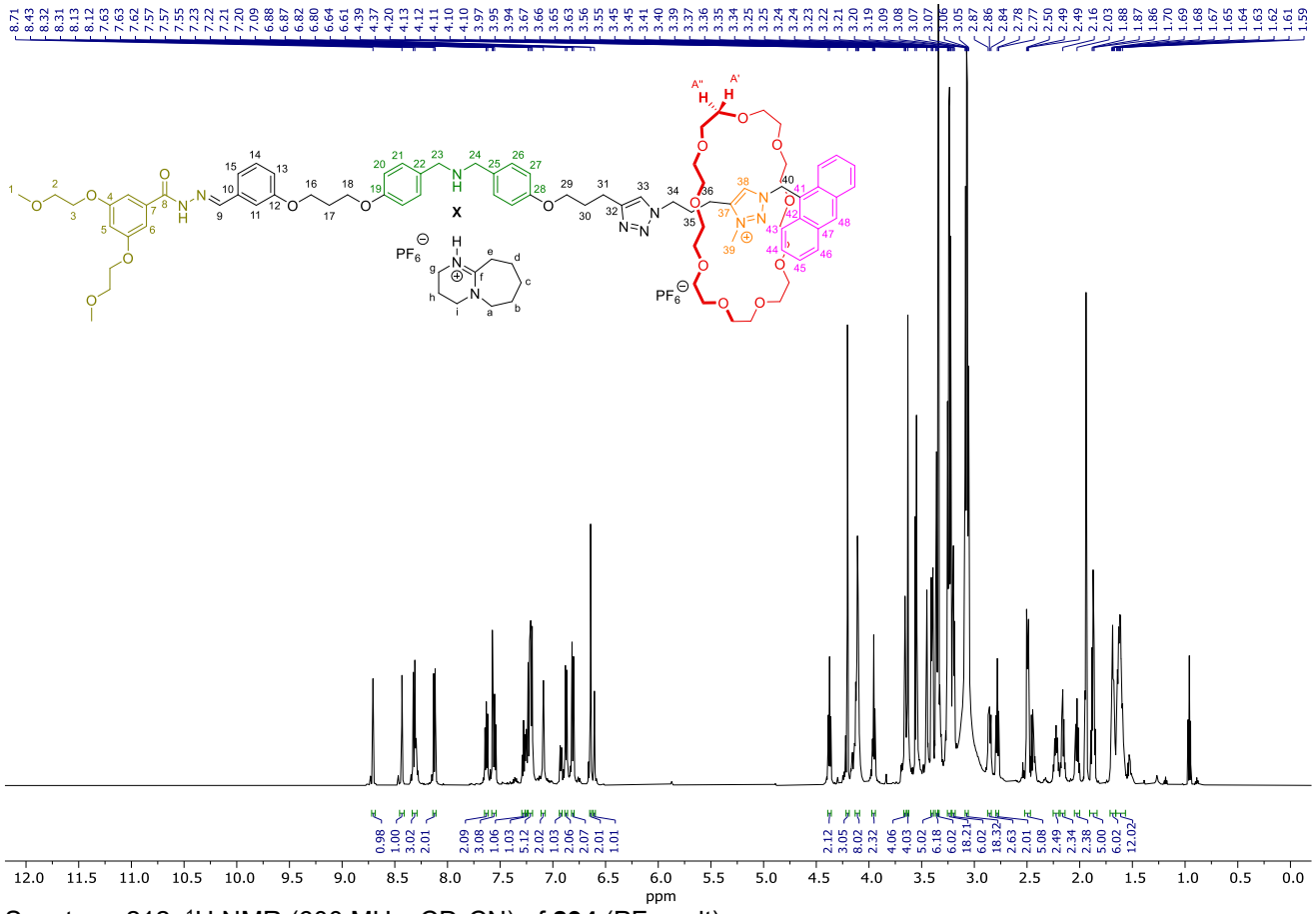

Spectrum 212. ^{1}H NMR (600 MHz, CD_3CN) of **294** (PF_6^- salt).

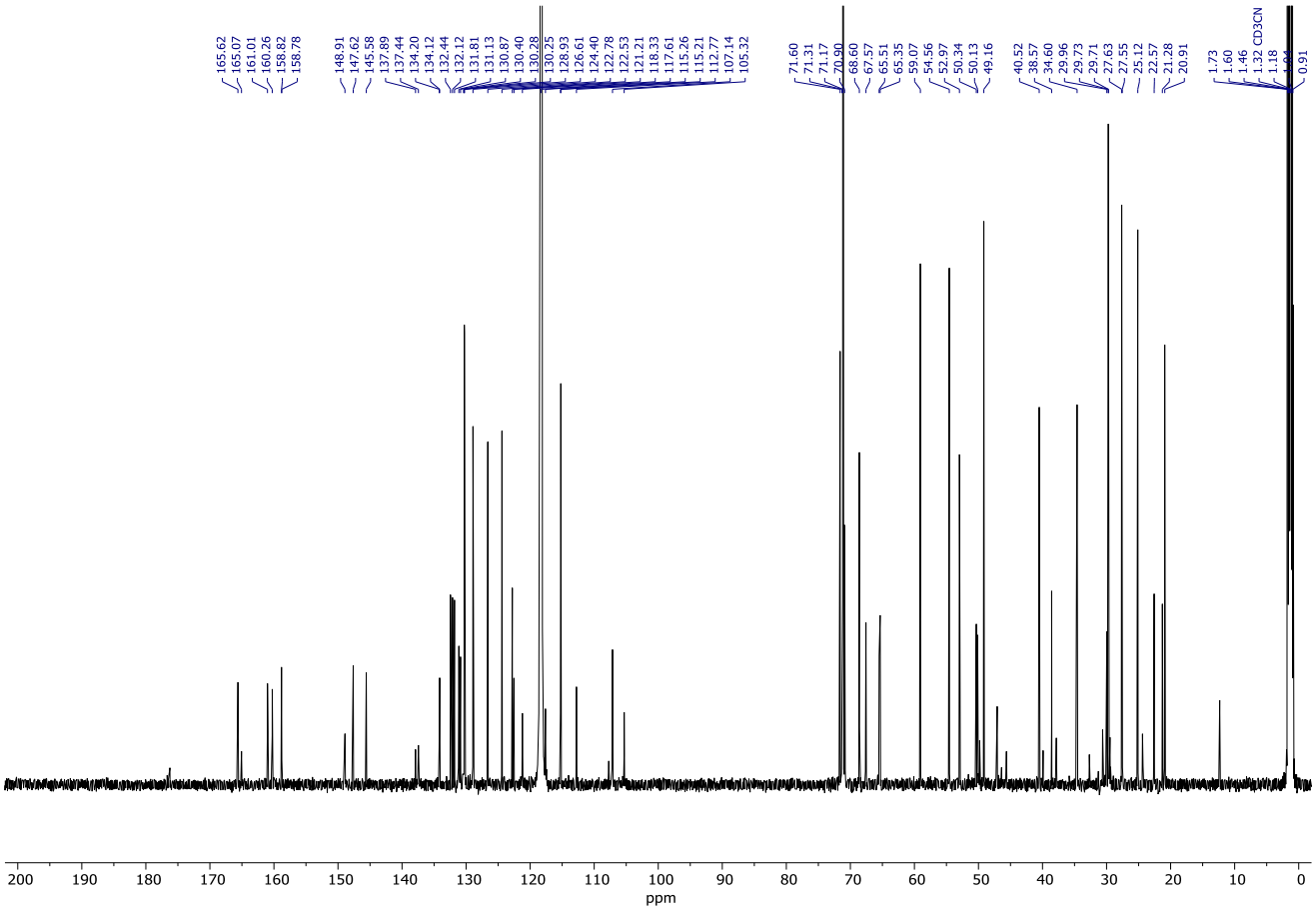

Spectrum 213. ^{13}C NMR (151 MHz, CD_3CN) of **294** (PF_6^- salt).

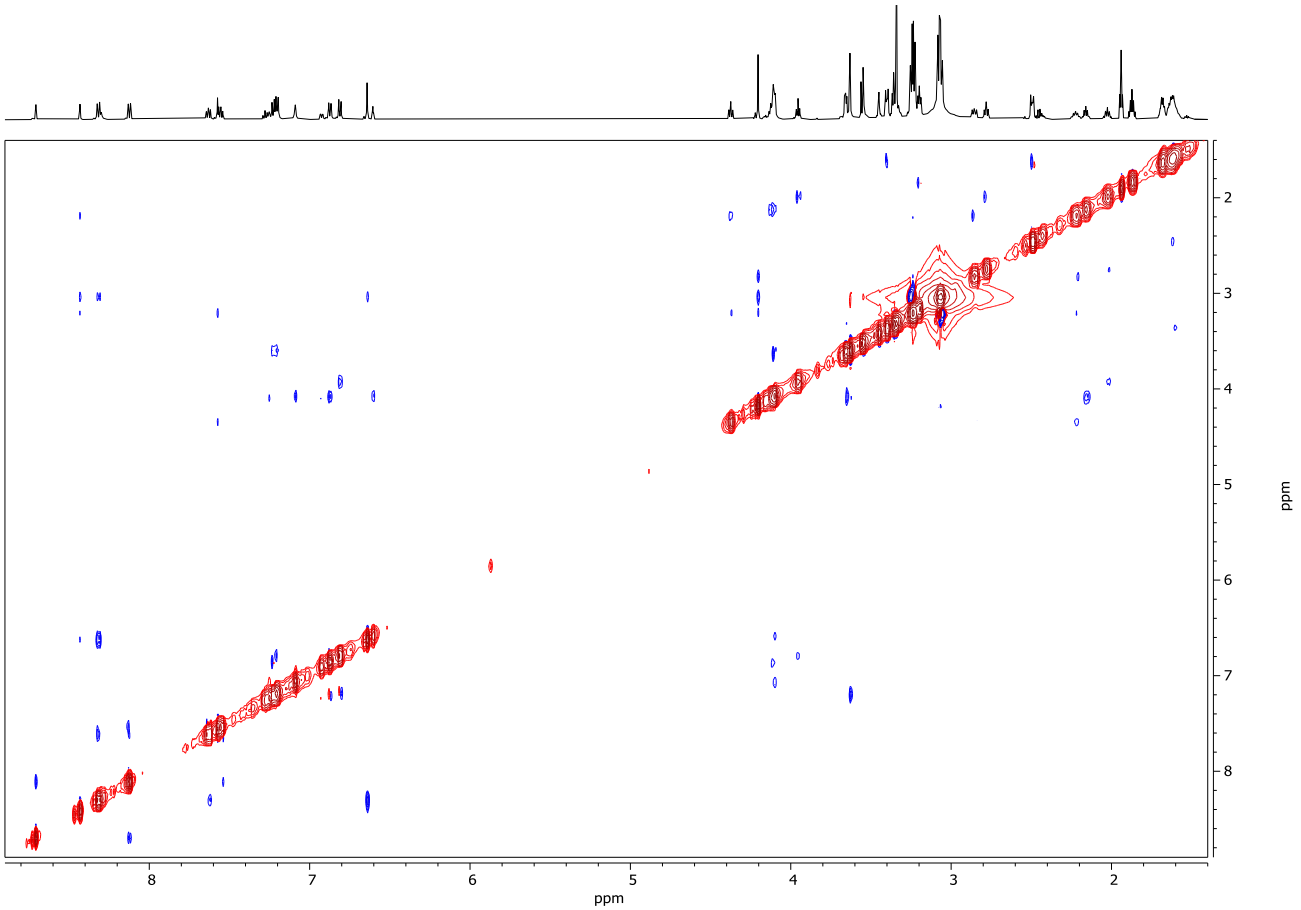

Spectrum 214. 2D NOESY (600 MHz, CD_3CN) of **294**. Data was recorded with a 400 ms mixing time and a relaxation delay of 2.05 s. 4K data points were collected for 256 increments of 4 scans.

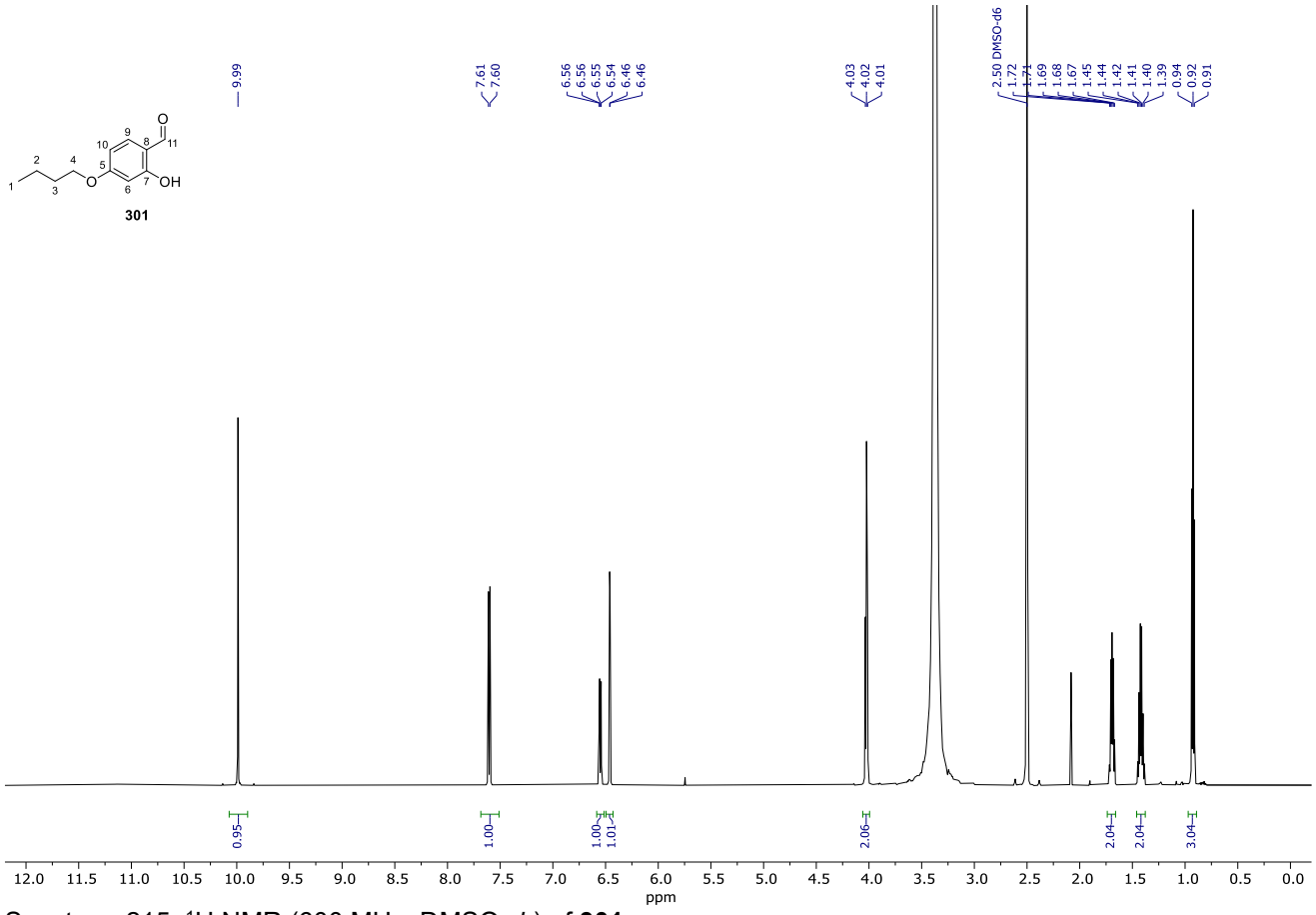

301

Spectrum 215. ^{1}H NMR (600 MHz, DMSO-d_6) of **301**.

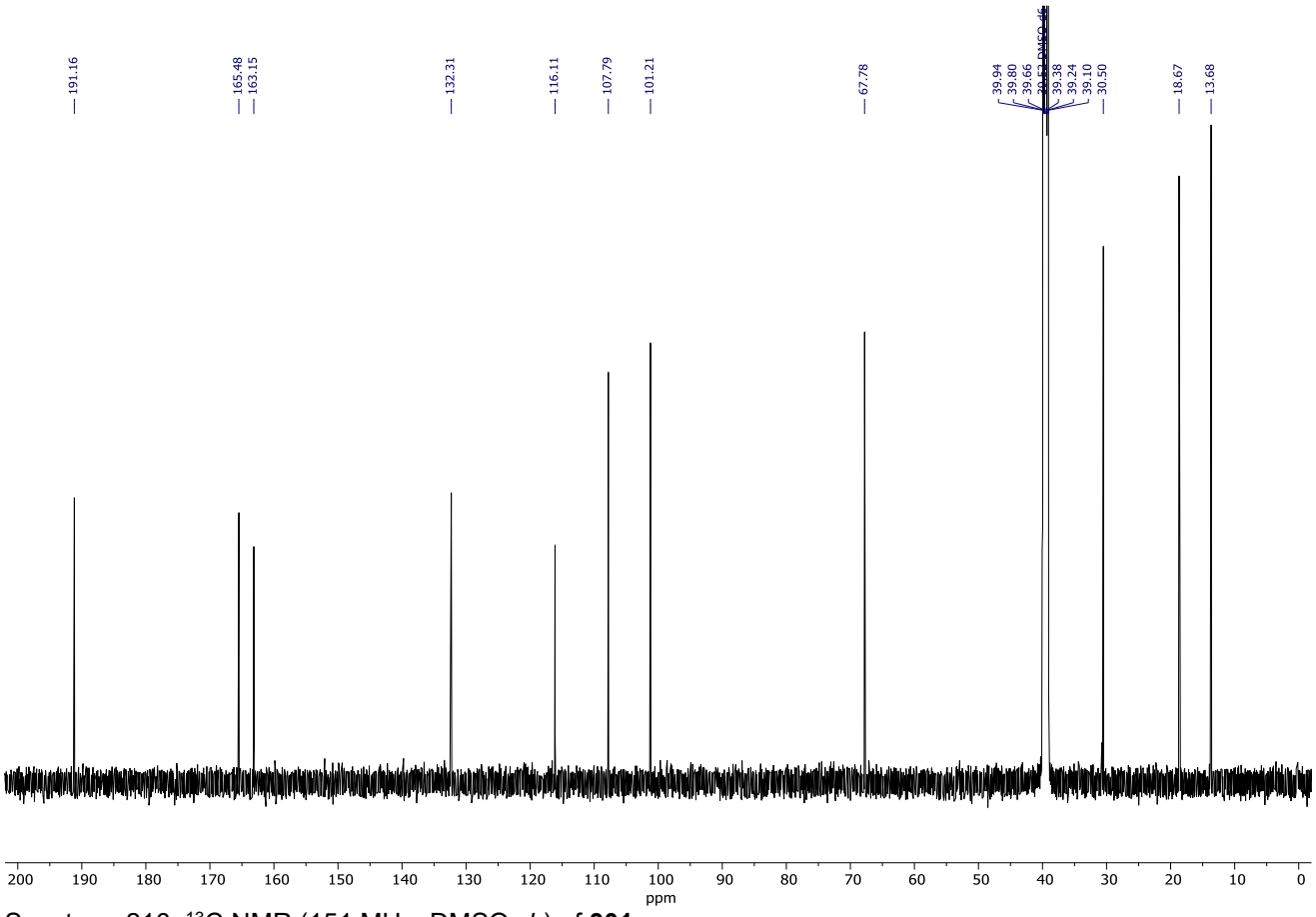

Spectrum 216. ^{13}C NMR (151 MHz, DMSO-d_6) of **301**.

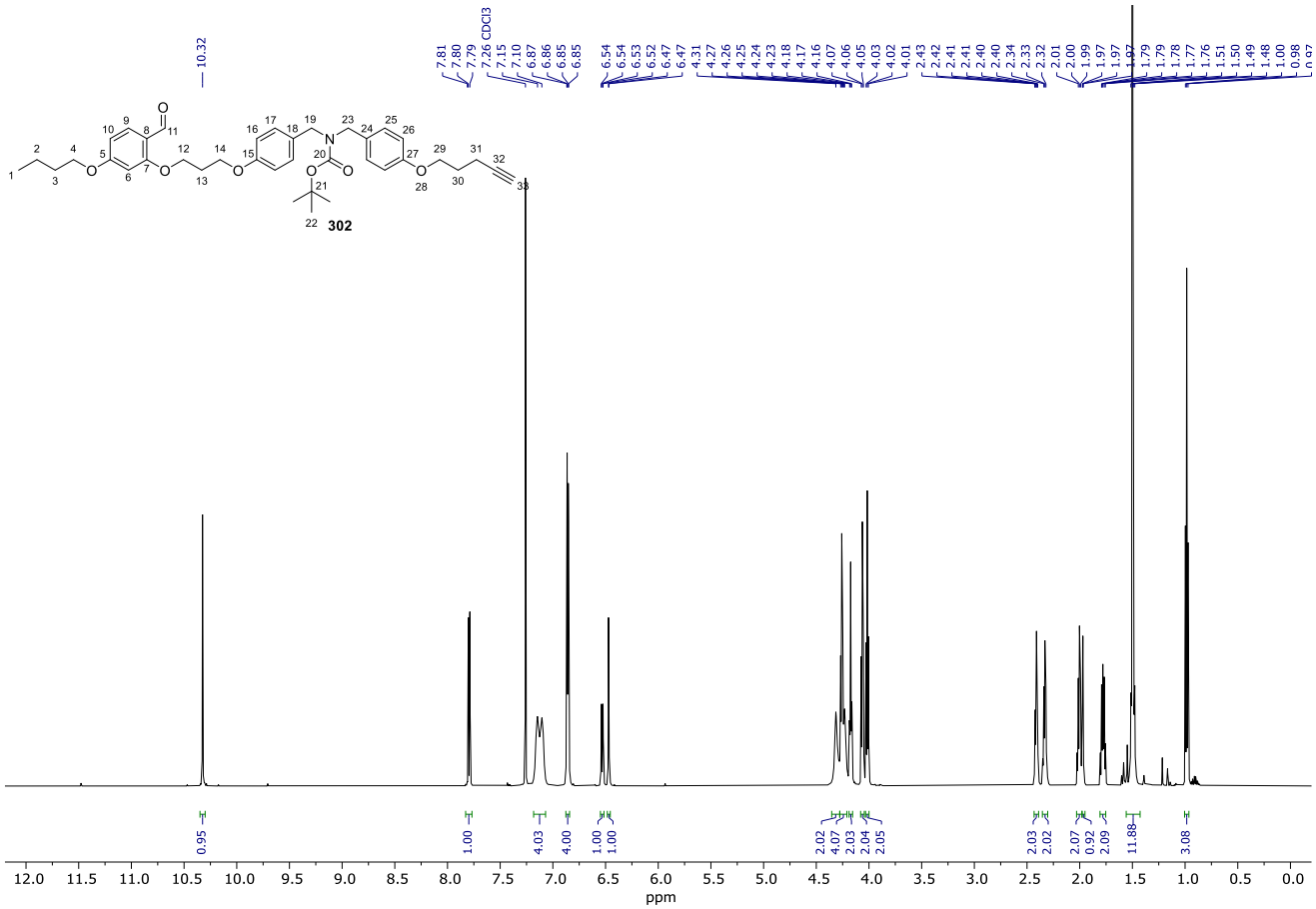

Spectrum 217. ^{1}H NMR (600 MHz, $CDCl_3$) of **302**.

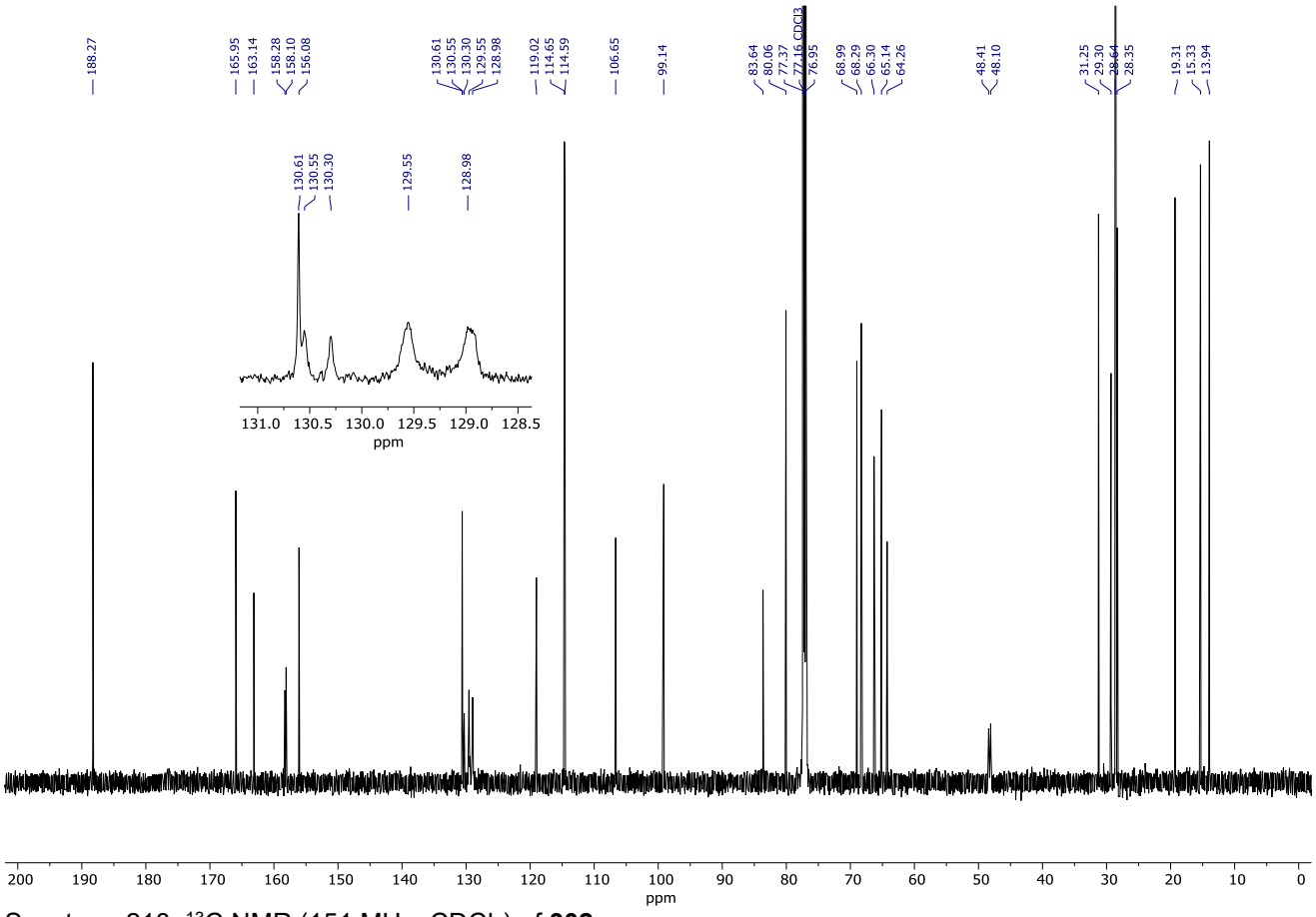

Spectrum 218. ^{13}C NMR (151 MHz, $CDCl_3$) of **302**.

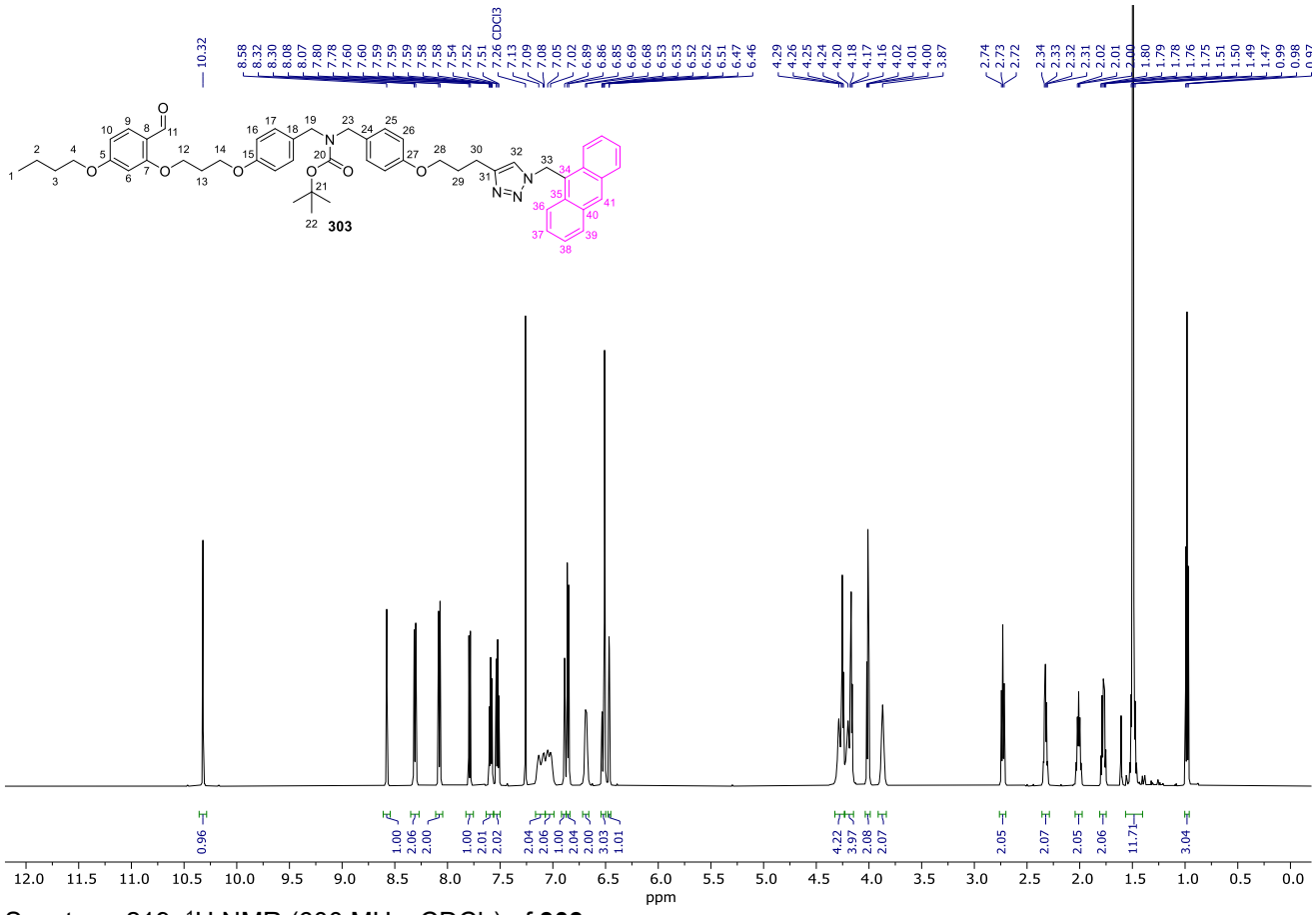

Spectrum 219. ^{1}H NMR (600 MHz, $CDCl_3$) of **303**.

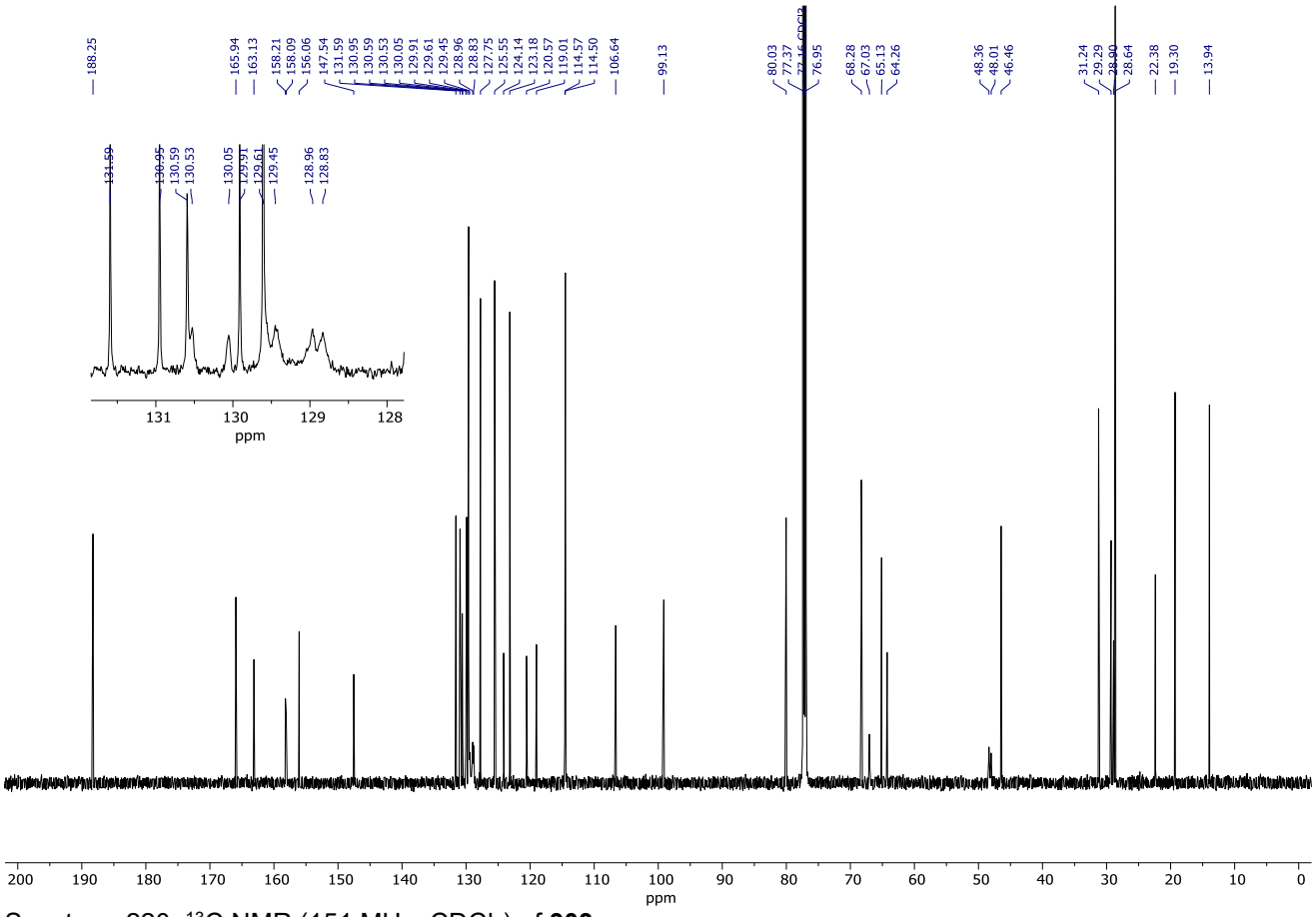

Spectrum 220. ^{13}C NMR (151 MHz, $CDCl_3$) of **303**.

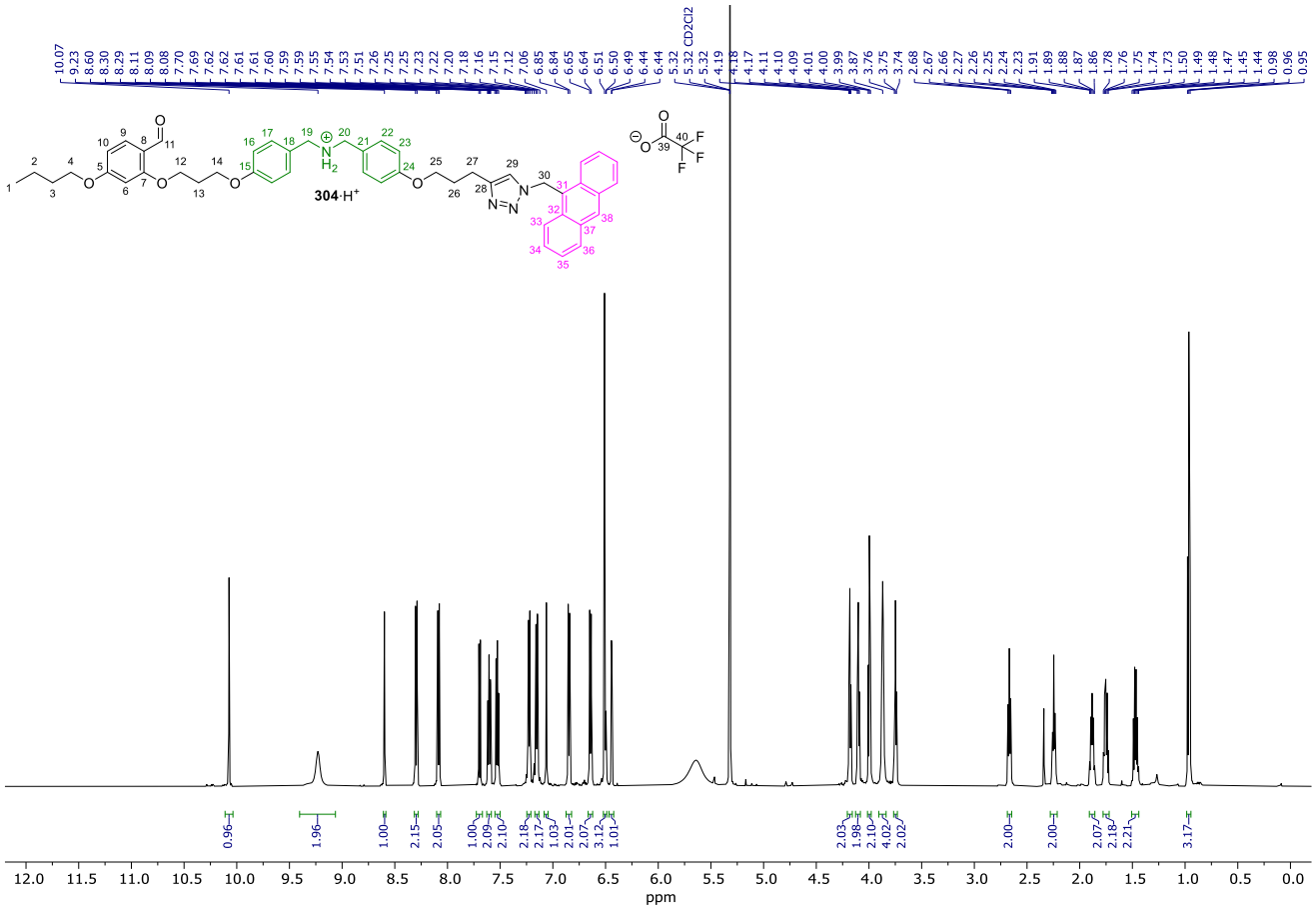

Spectrum 221. ^{1}H NMR (600 MHz, CD_2Cl_2) of **304**·H^+.

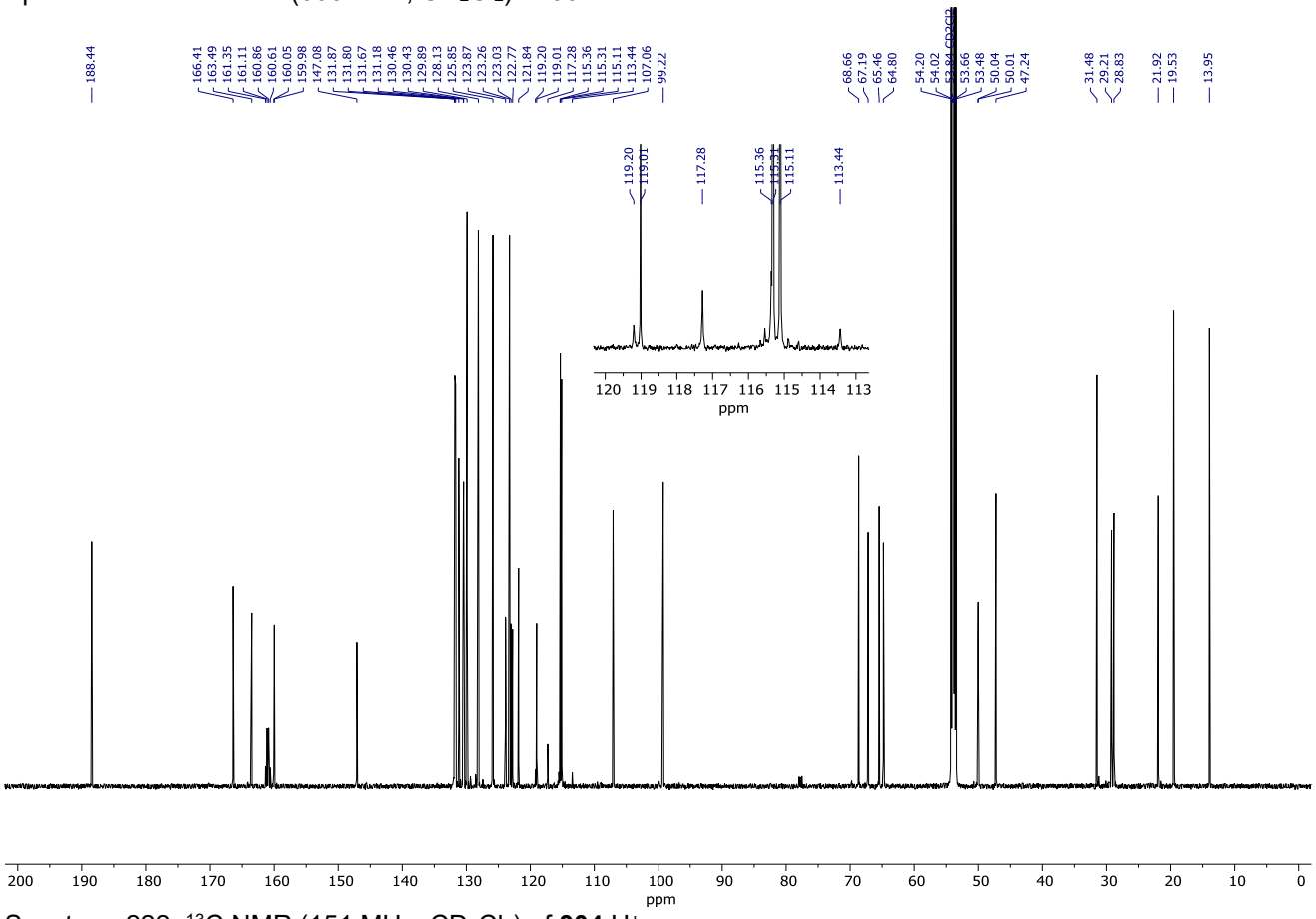

Spectrum 222. ^{13}C NMR (151 MHz, CD_2Cl_2) of **304**·H^+.

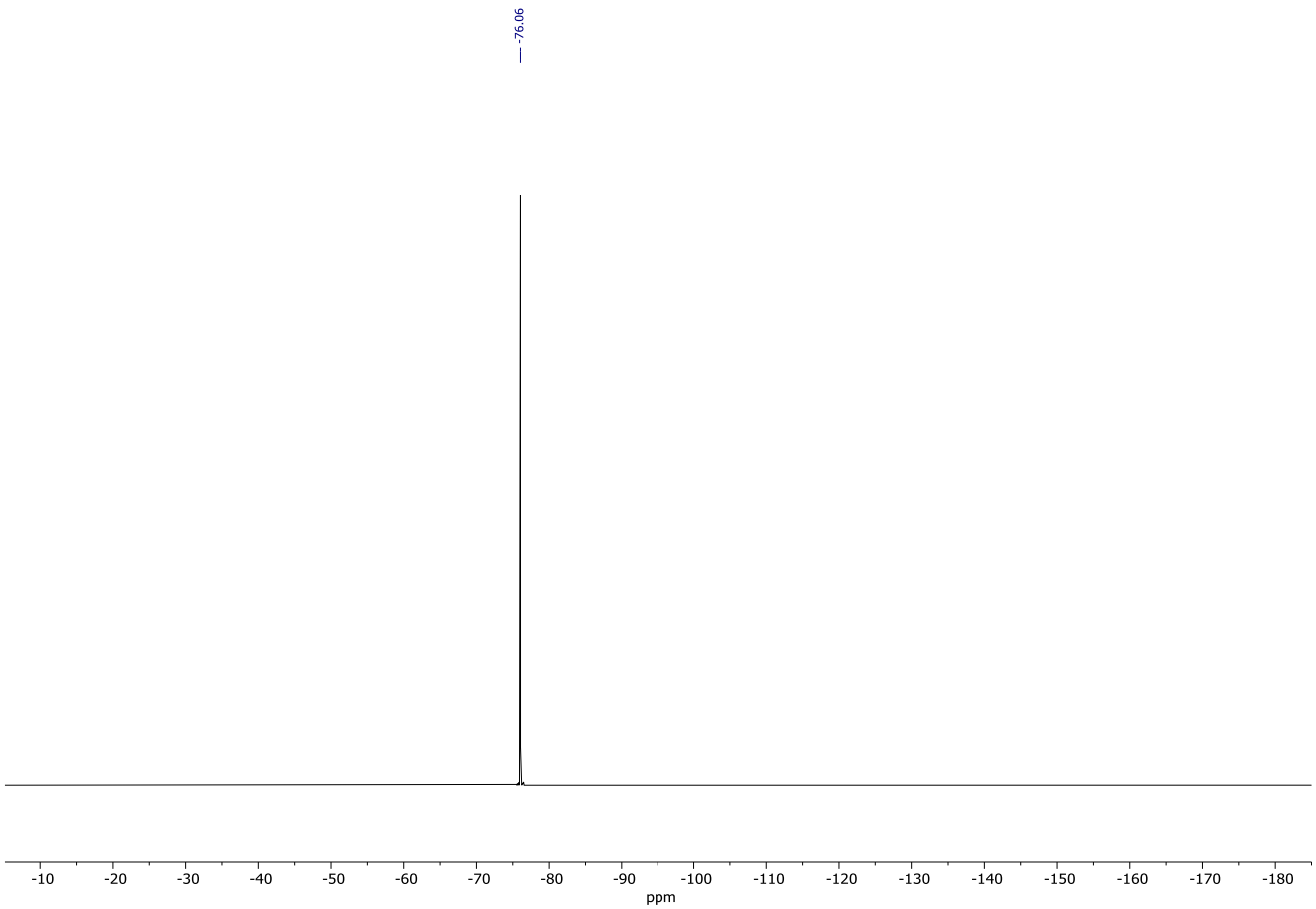

Spectrum 223. ^{19}F NMR (471 MHz, CD_2Cl_2) of **304**·H^+.

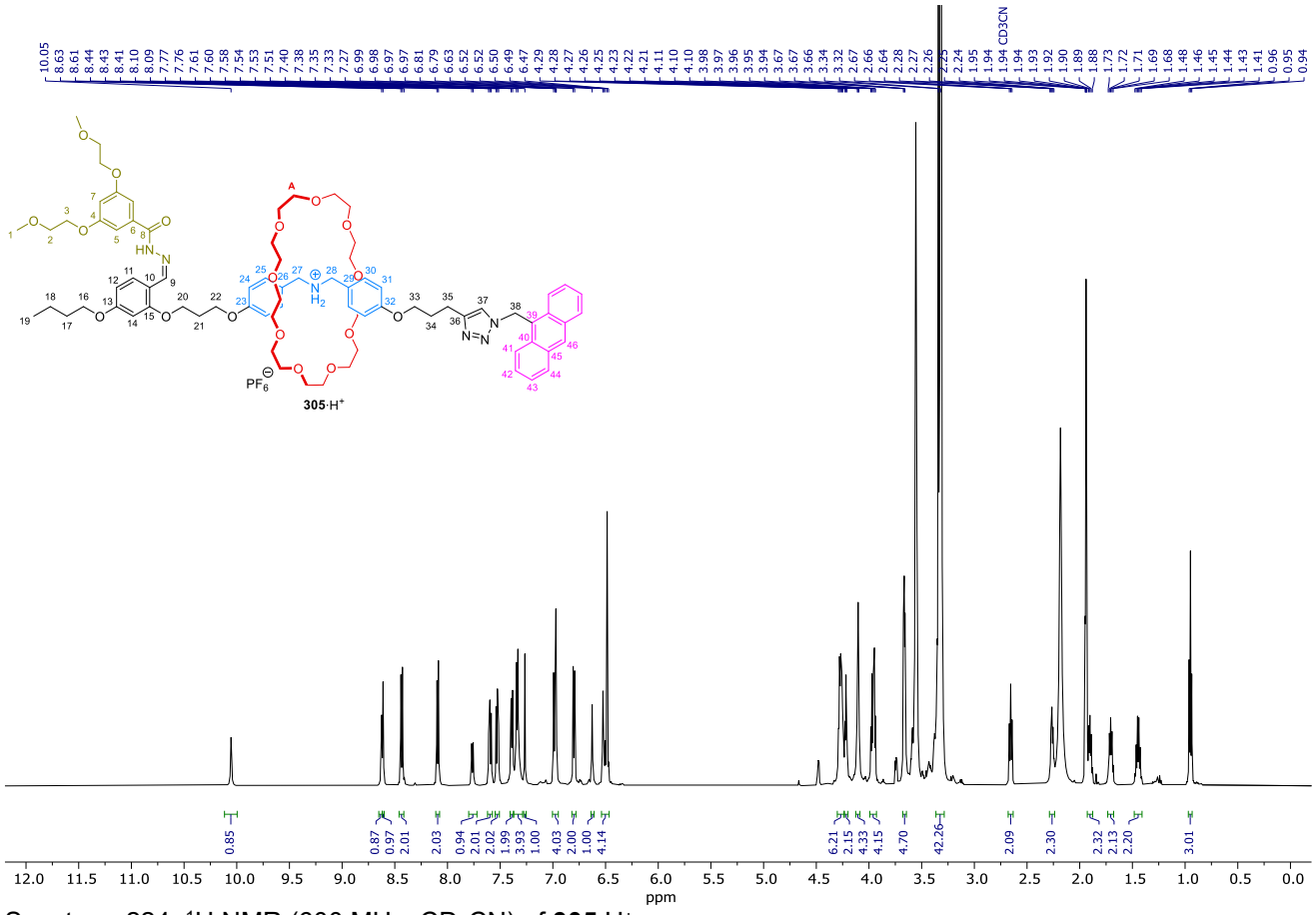

Spectrum 224. ^{1}H NMR (600 MHz, CD_3CN) of **305**·H^+.

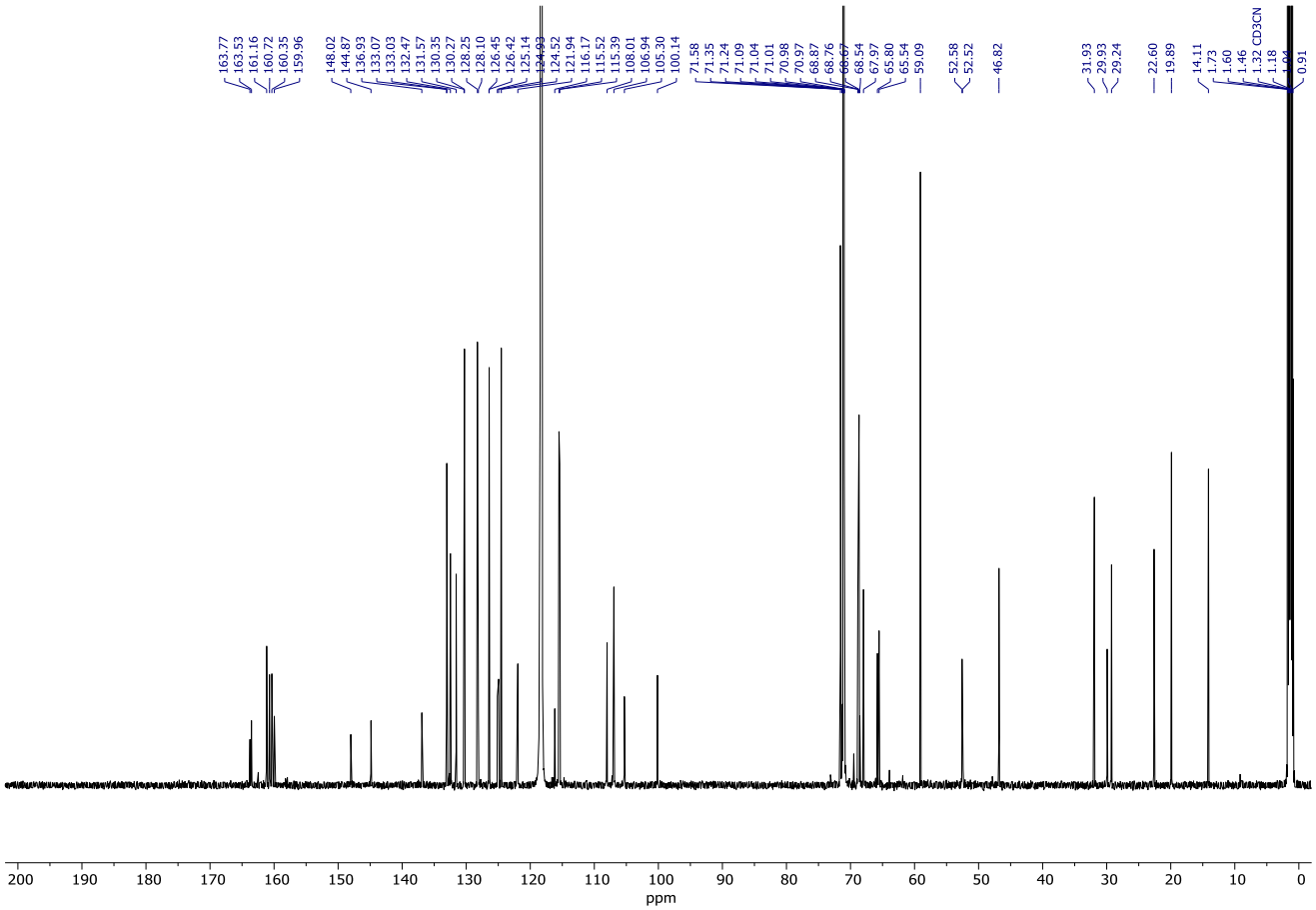

Spectrum 225. ^{13}C NMR (151 MHz, CD_3CN) of **305**·H^+.

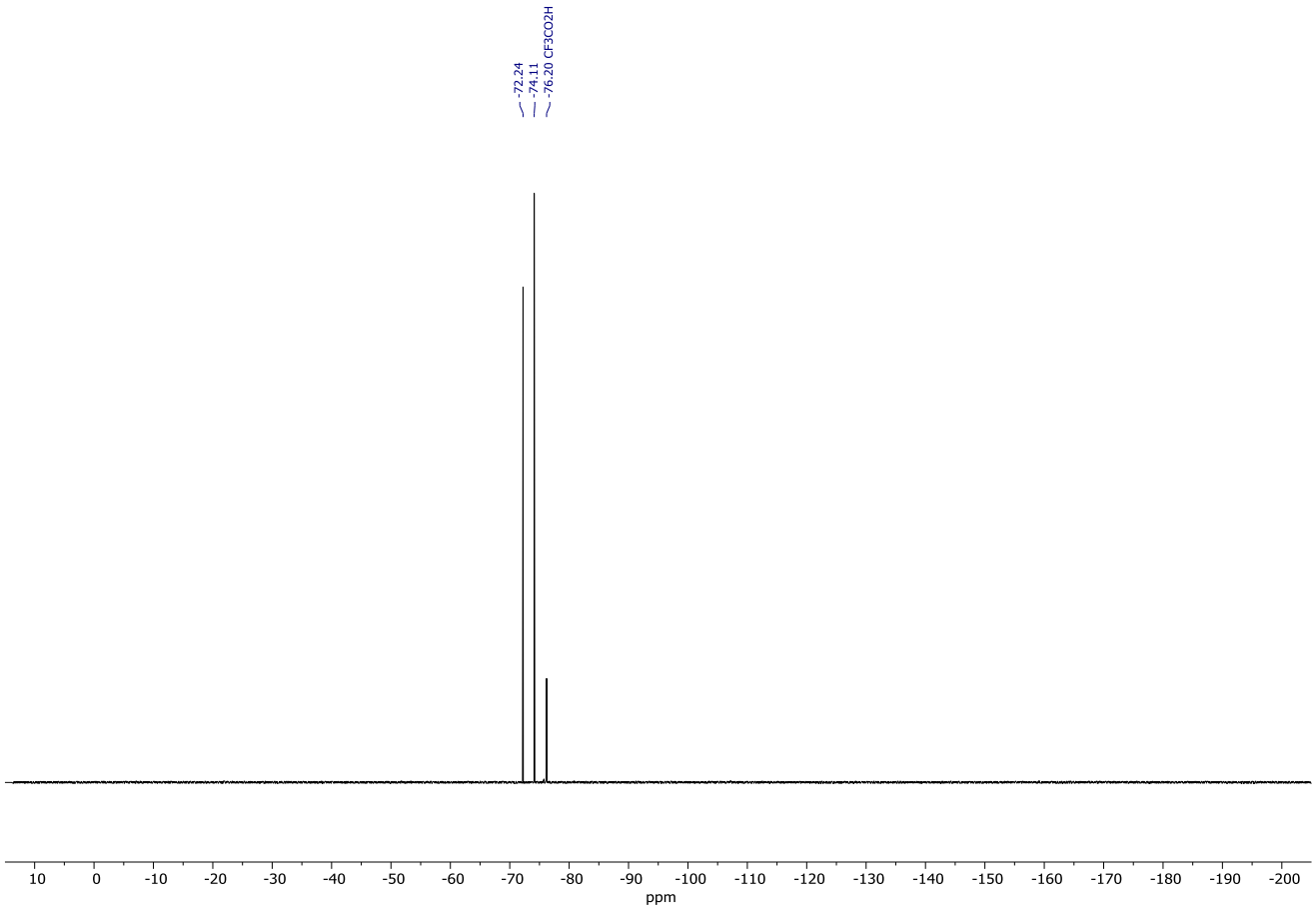

Spectrum 226. ^{19}F NMR (376 MHz, CD_3CN) of **305**·H^+.

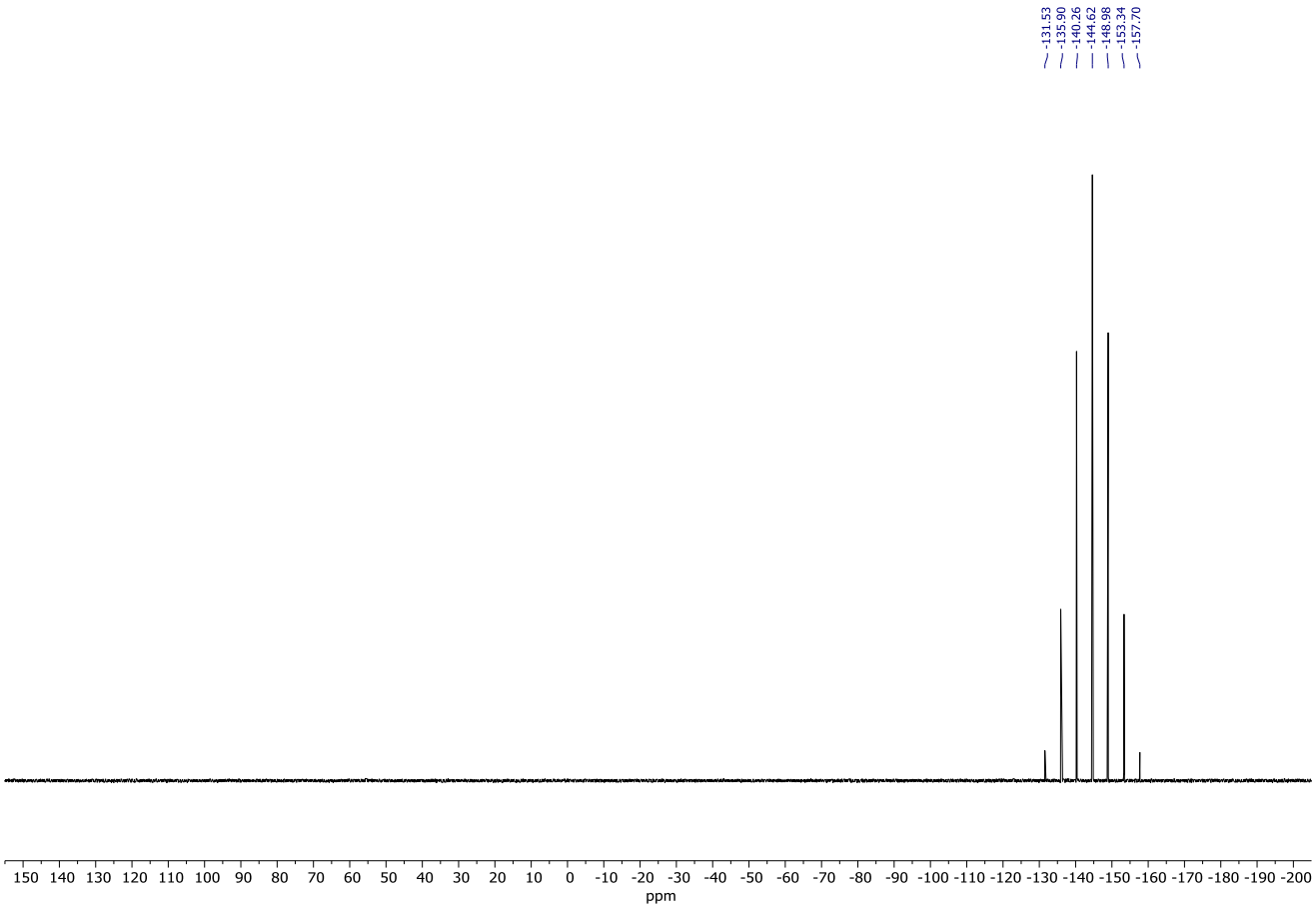

Spectrum 227. ^{31}P NMR (162 MHz, CD_3CN) of **305**·H^+.

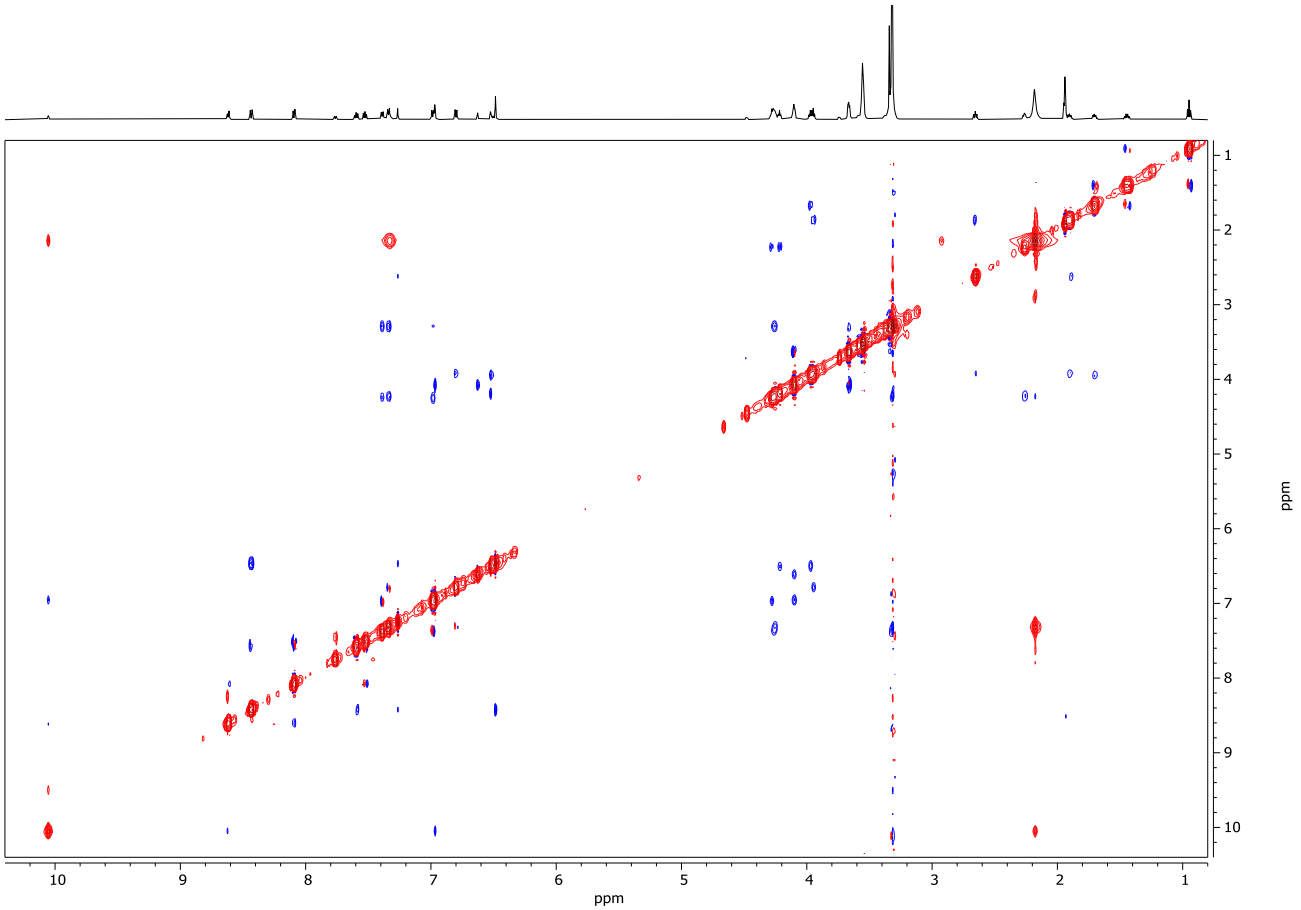

Spectrum 228. 2D NOESY (600 MHz, CD_3CN) of **305**. Data was recorded with a 400 ms mixing time and a relaxation delay of 2.03 s. 2K data points were collected for 256 increments of 4 scans.

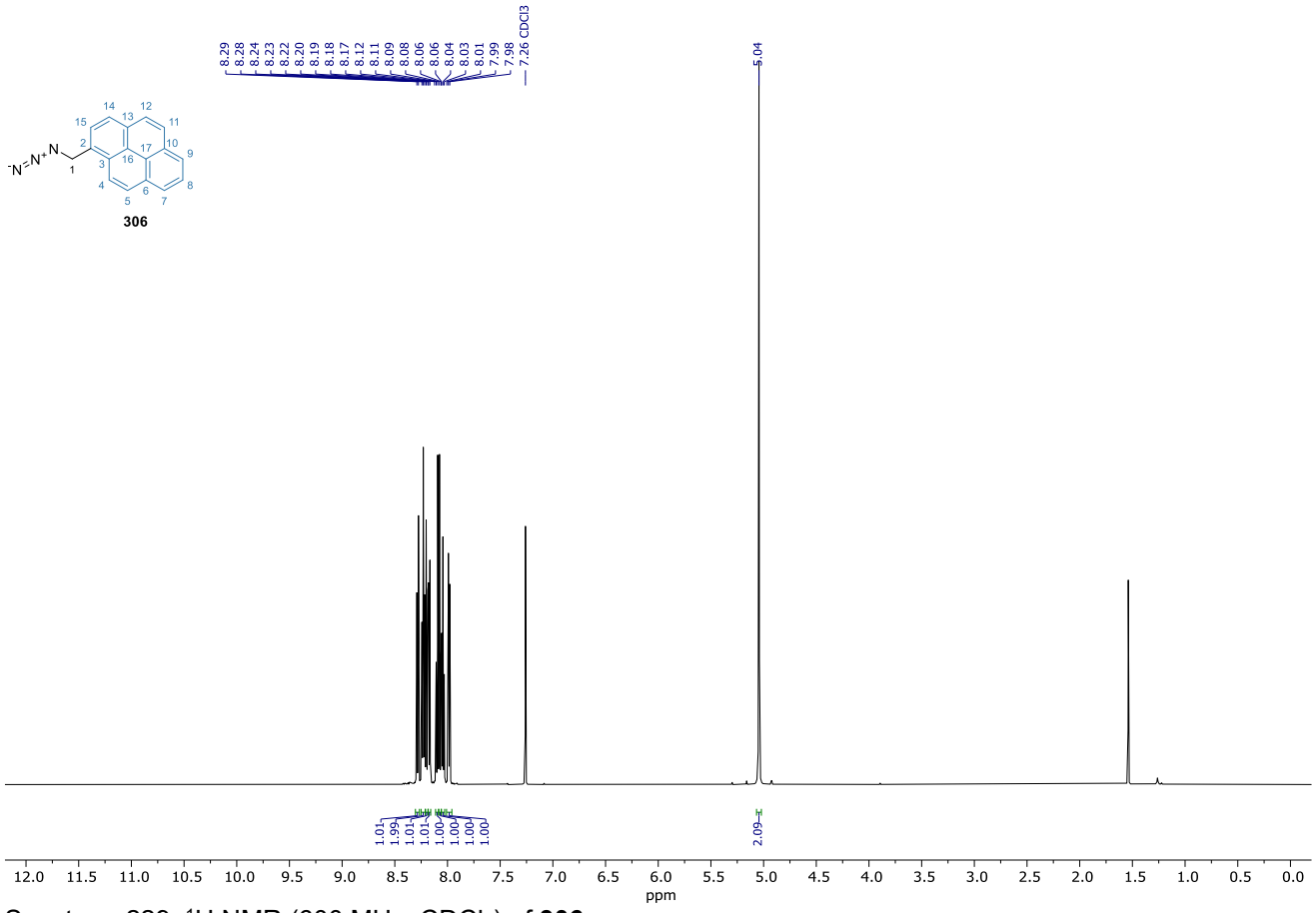

Spectrum 229. ^{1}H NMR (600 MHz, $CDCl_3$) of **306**.

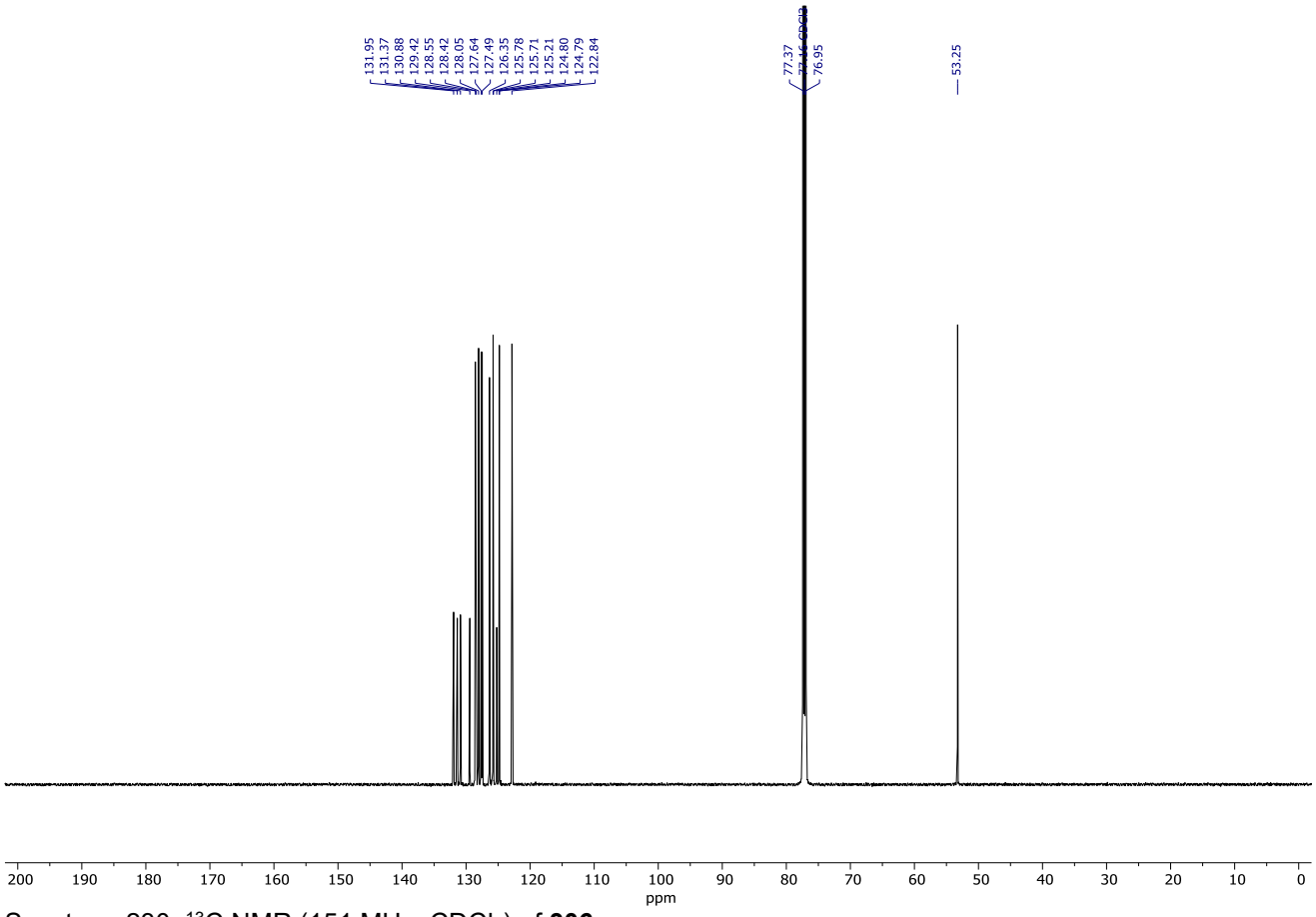

Spectrum 230. ^{13}C NMR (151 MHz, $CDCl_3$) of **306**.

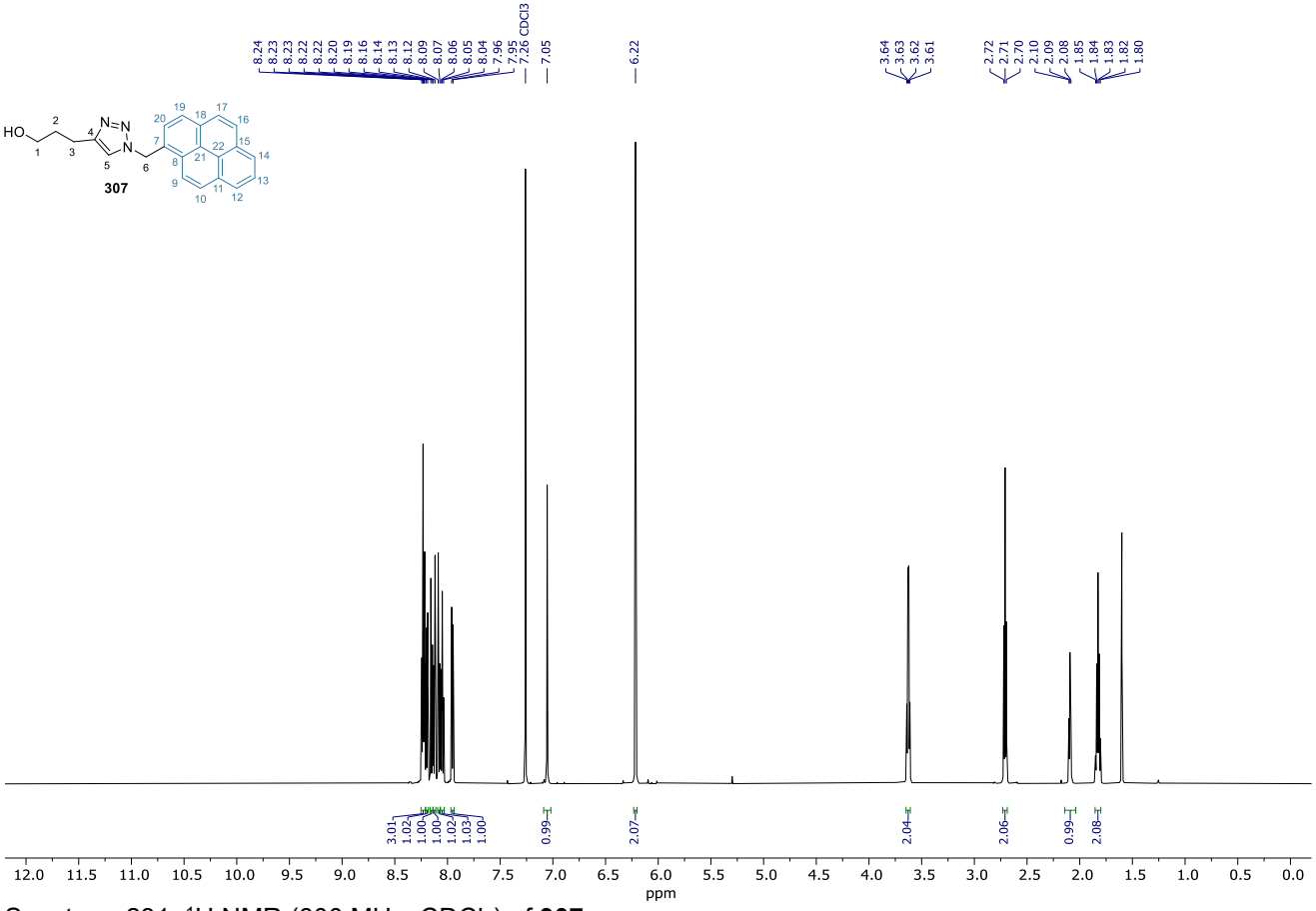

Spectrum 231. ^{1}H NMR (600 MHz, $CDCl_3$) of **307**.

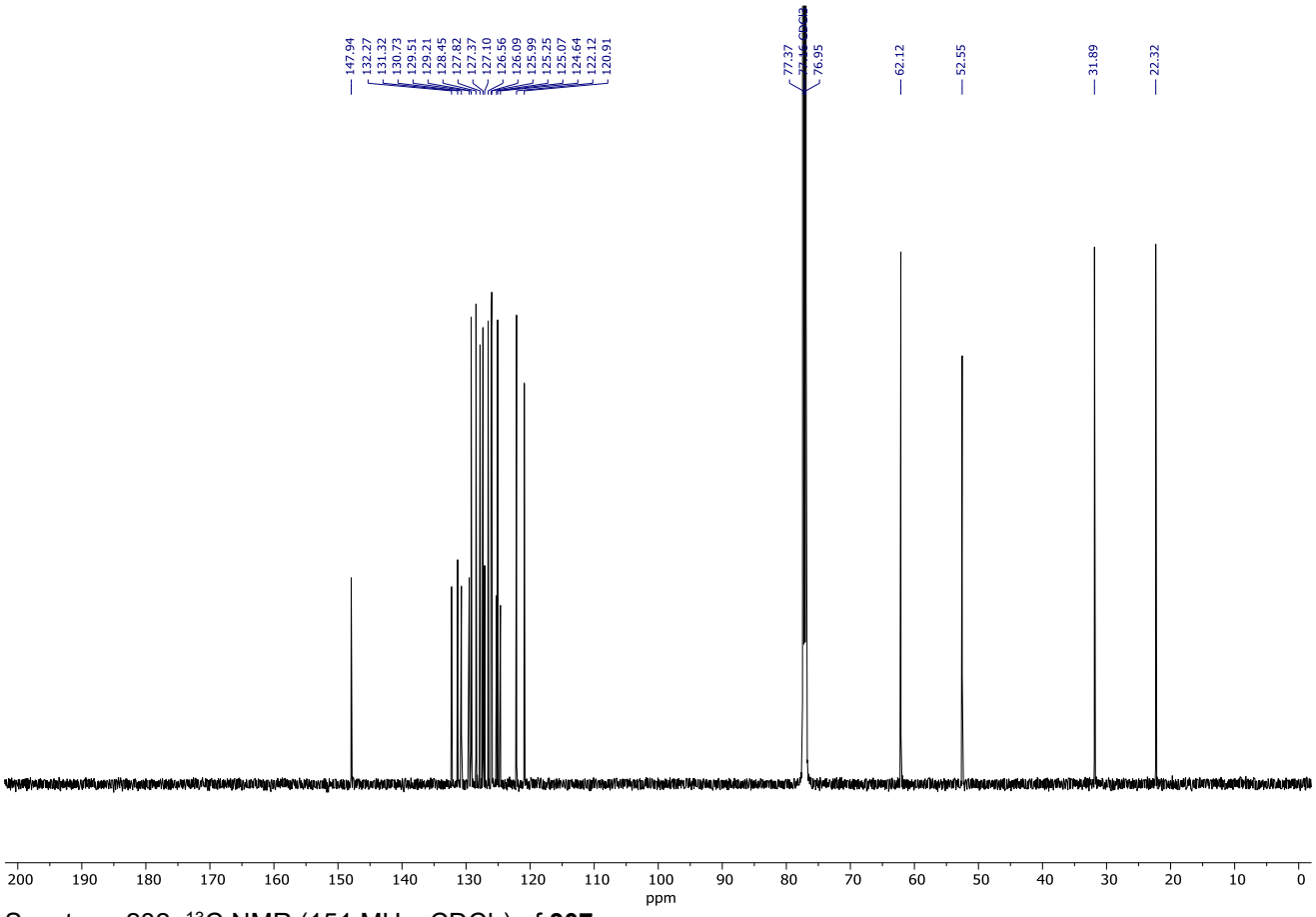

Spectrum 232. ^{13}C NMR (151 MHz, $CDCl_3$) of **307**.

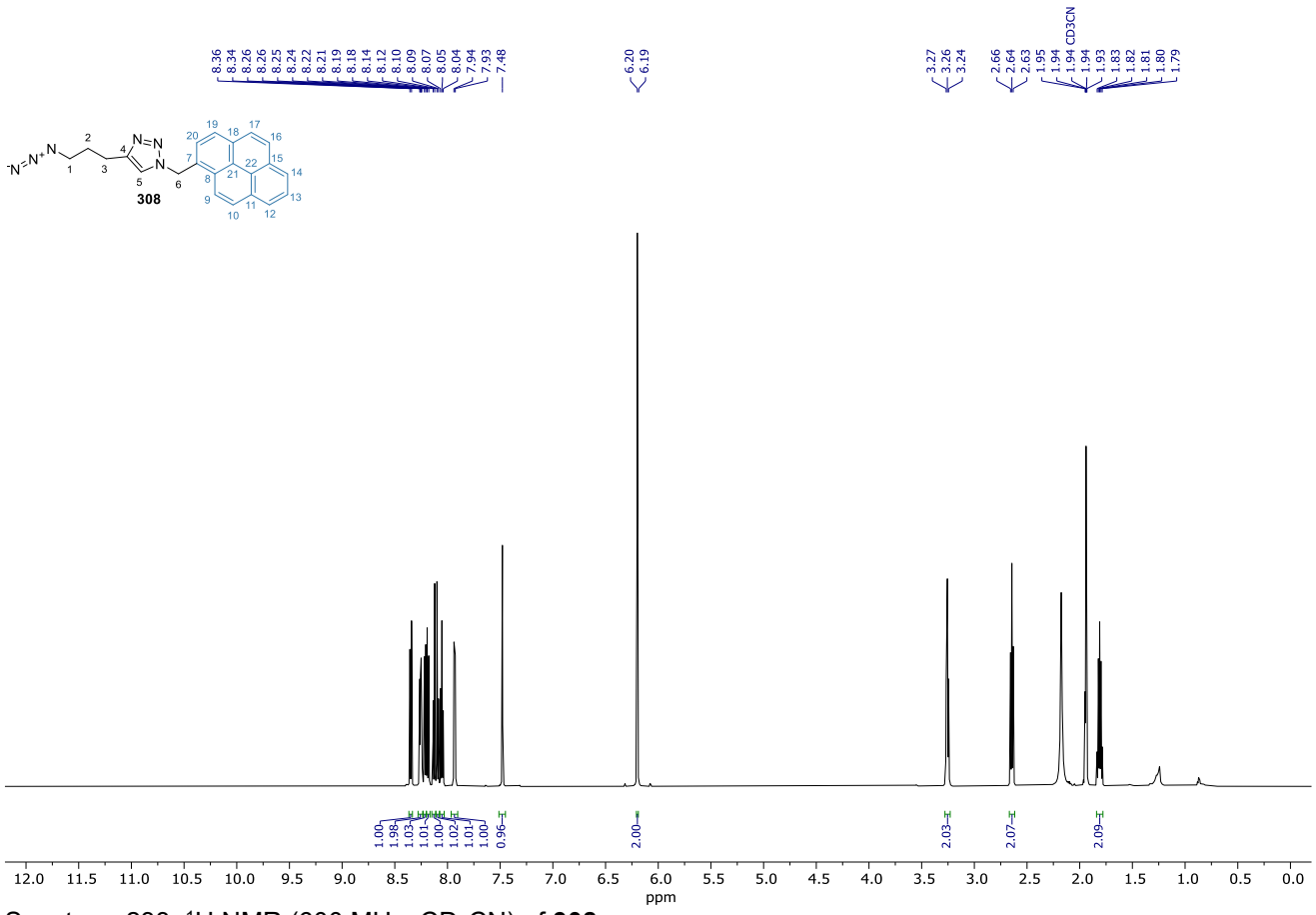

Spectrum 233. ^{1}H NMR (600 MHz, CD_3CN) of **308**.

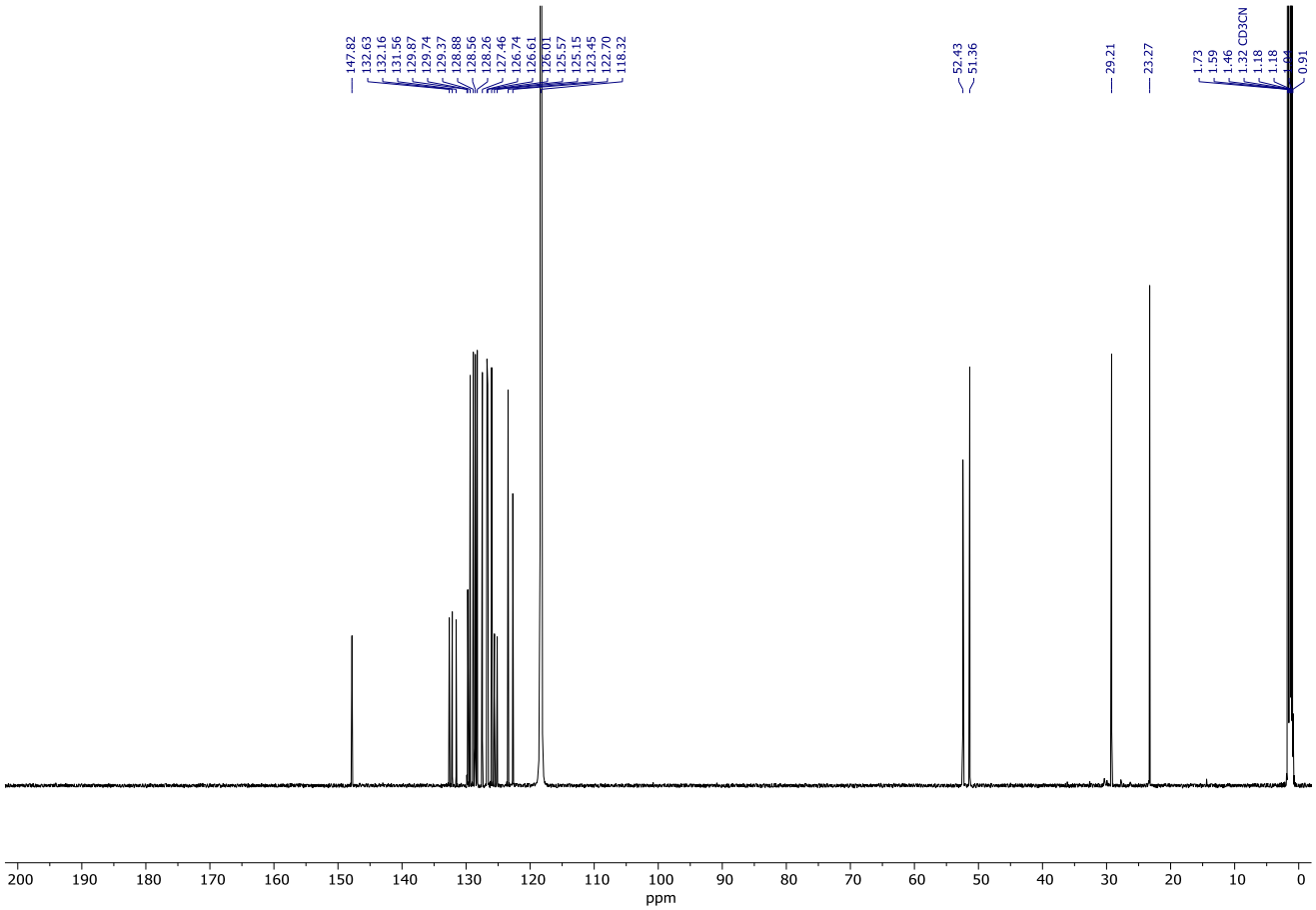

Spectrum 234. ^{13}C NMR (151 MHz, CD_3CN) of **308**.

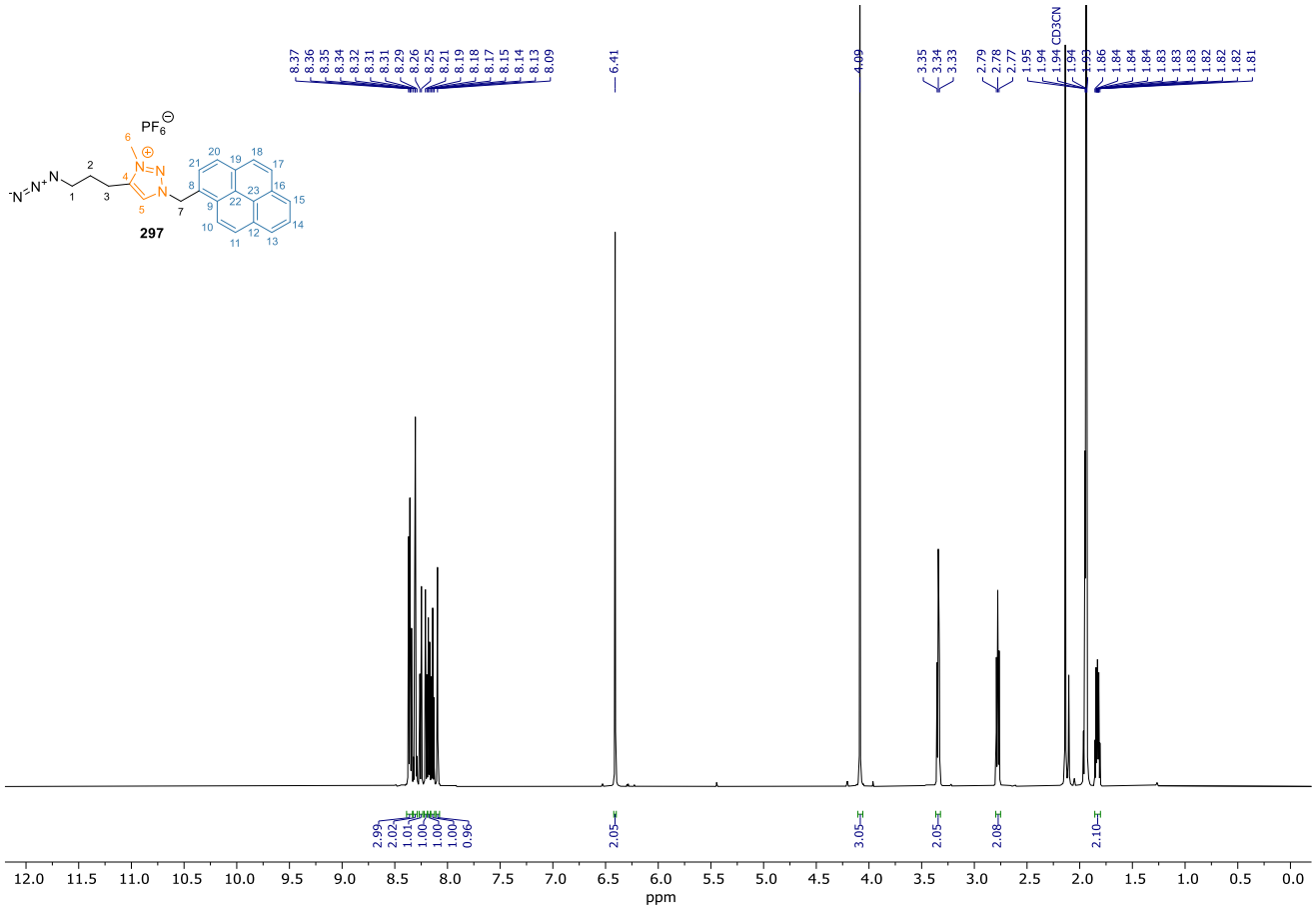

Spectrum 235. ^{1}H NMR (600 MHz, CD_3CN) of **297**.

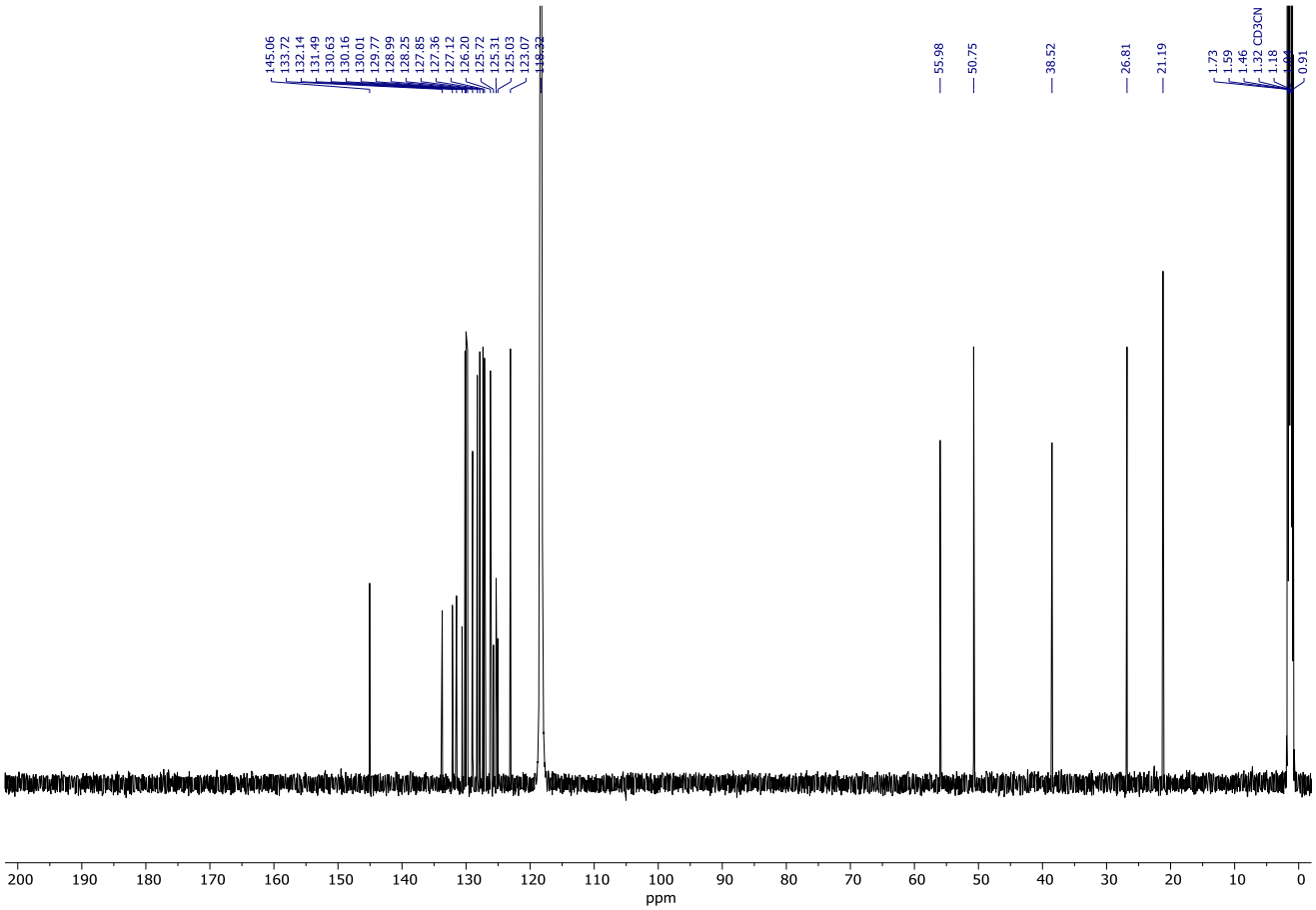

Spectrum 236. ^{13}C NMR (151 MHz, CD_3CN) of **297**.

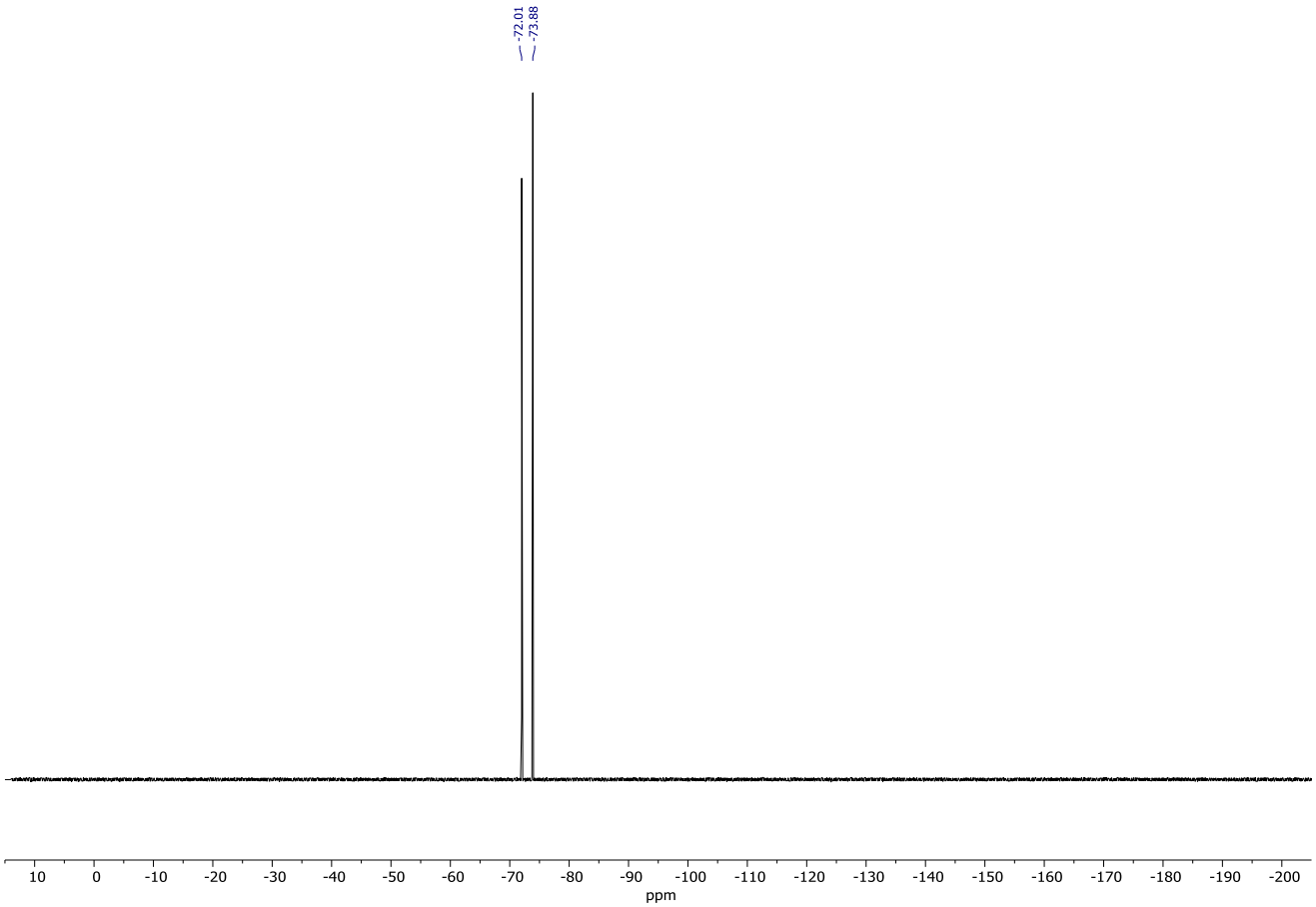

Spectrum 237. ^{19}F NMR (376 MHz, CD_3CN) of **297**.

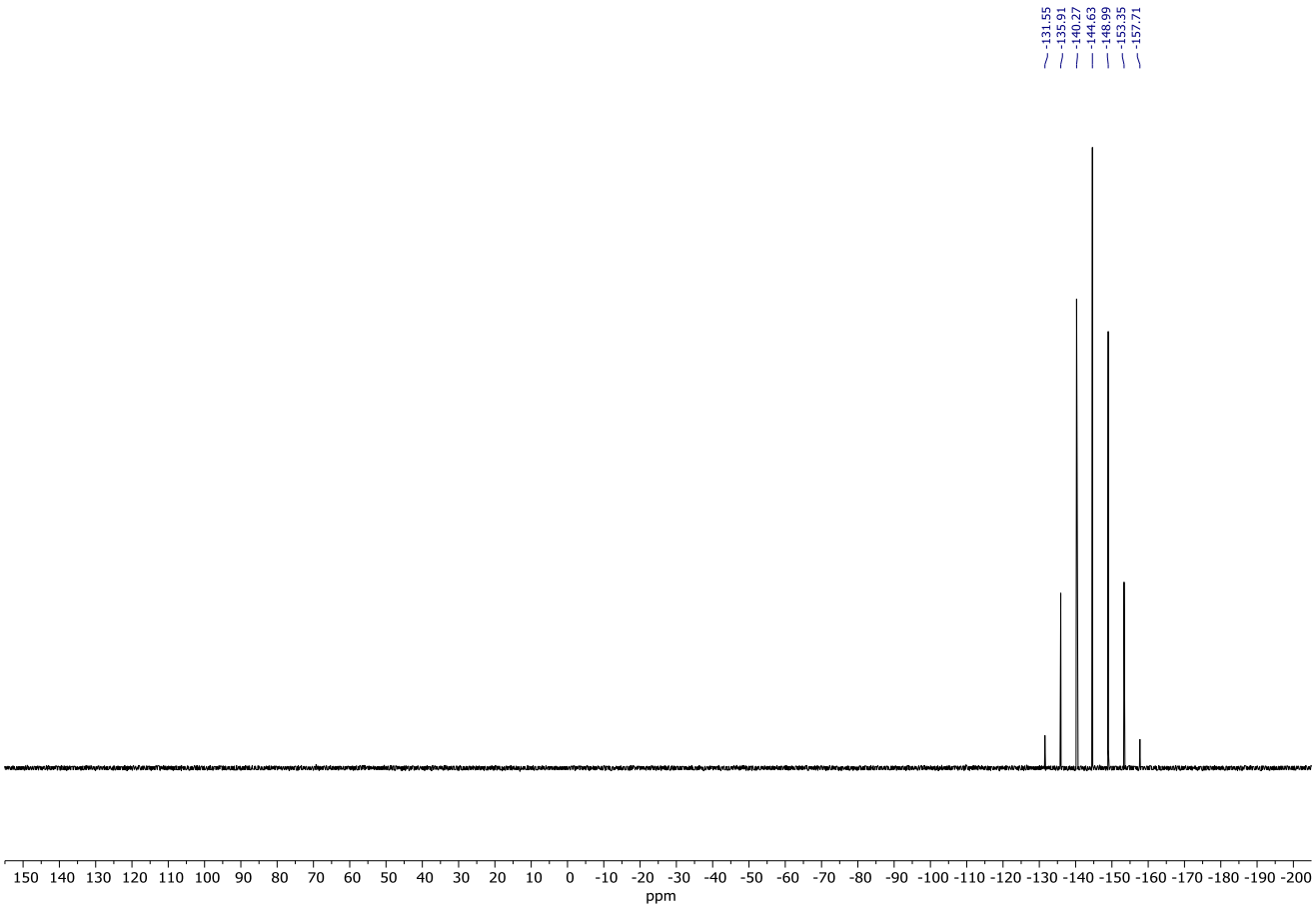

Spectrum 238. ^{31}P NMR (162 MHz, CD_3CN) of **297**.

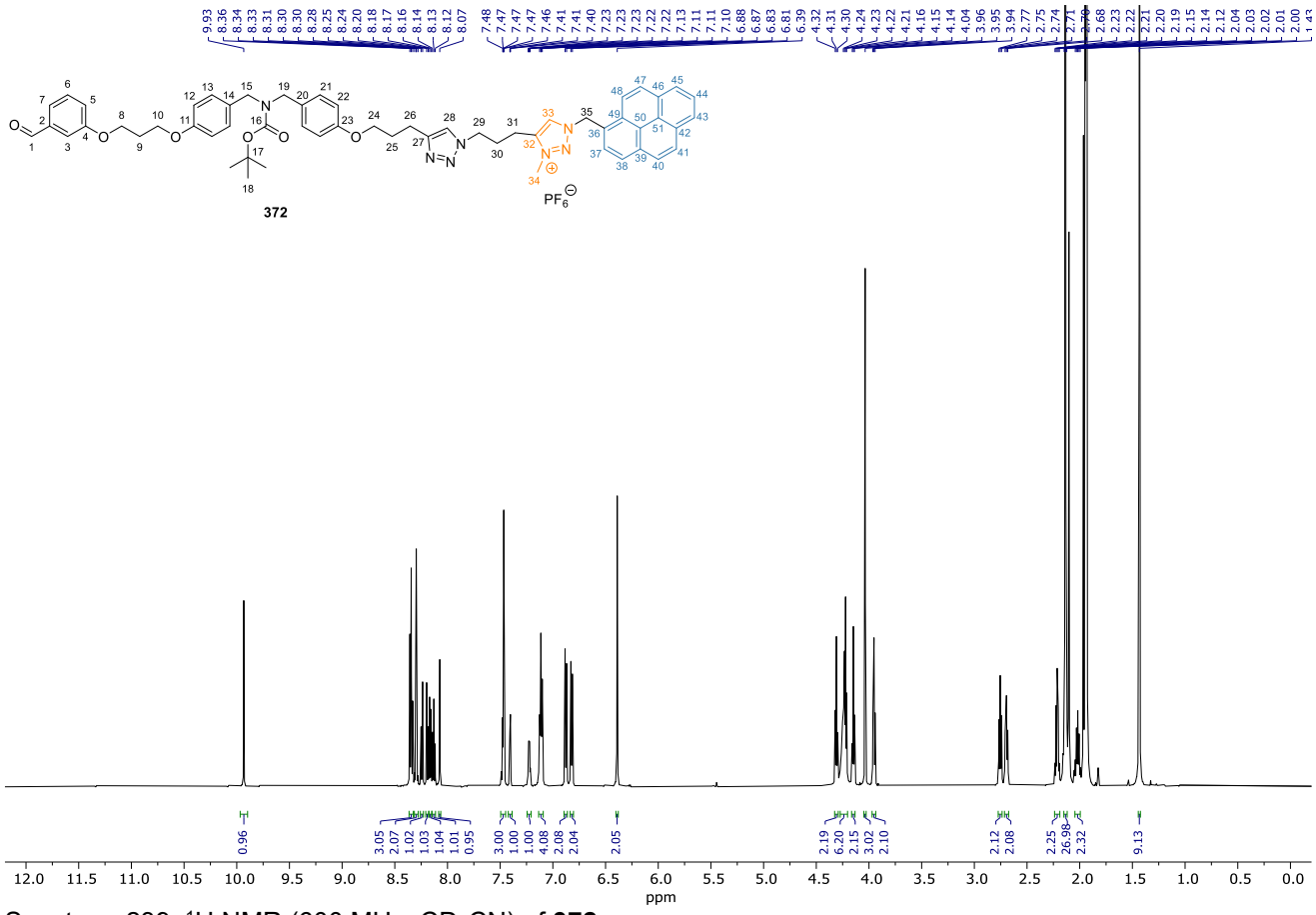

Spectrum 239. ^{1}H NMR (600 MHz, CD_3CN) of **372**.

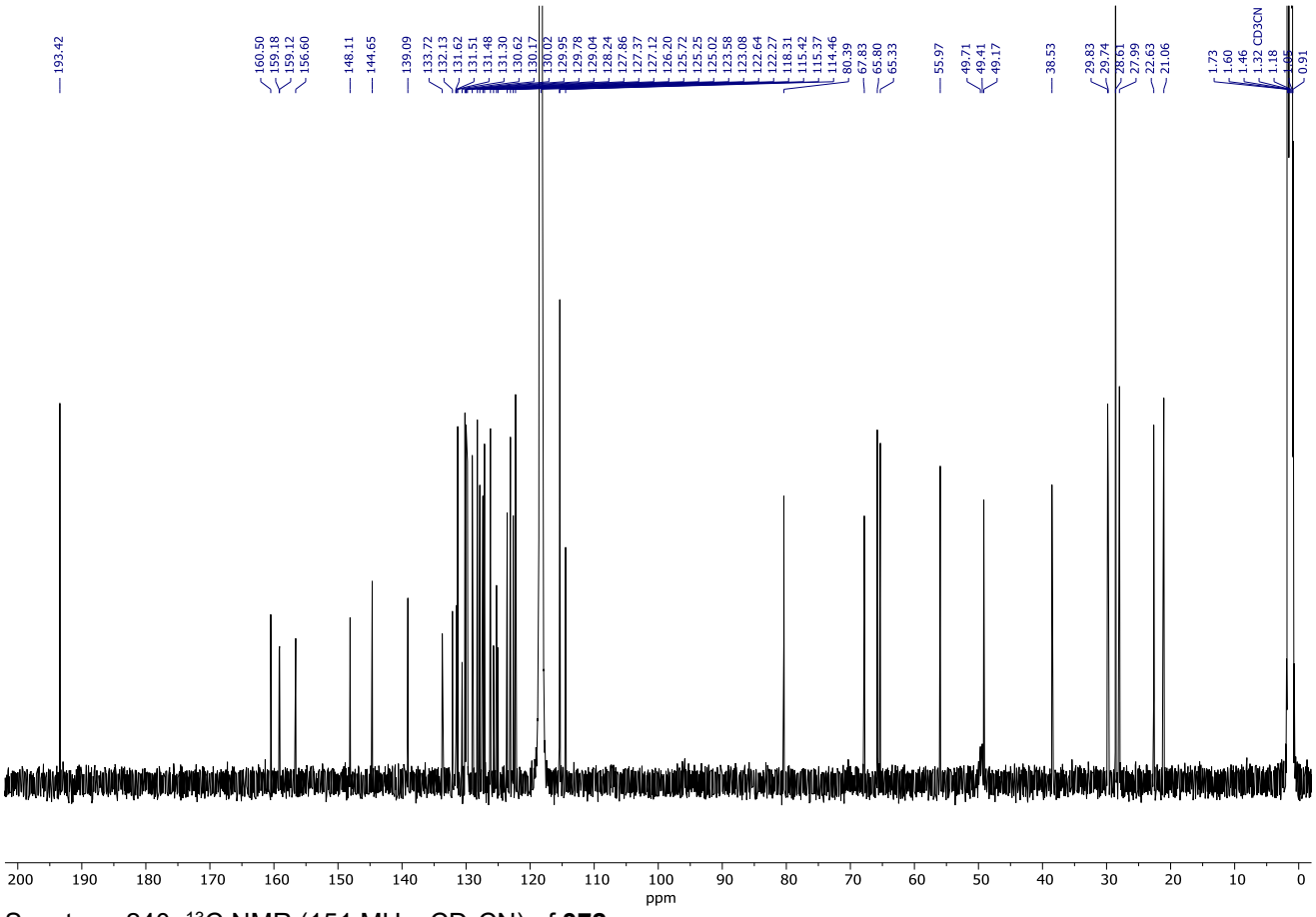

Spectrum 240. ^{13}C NMR (151 MHz, CD_3CN) of **372**.

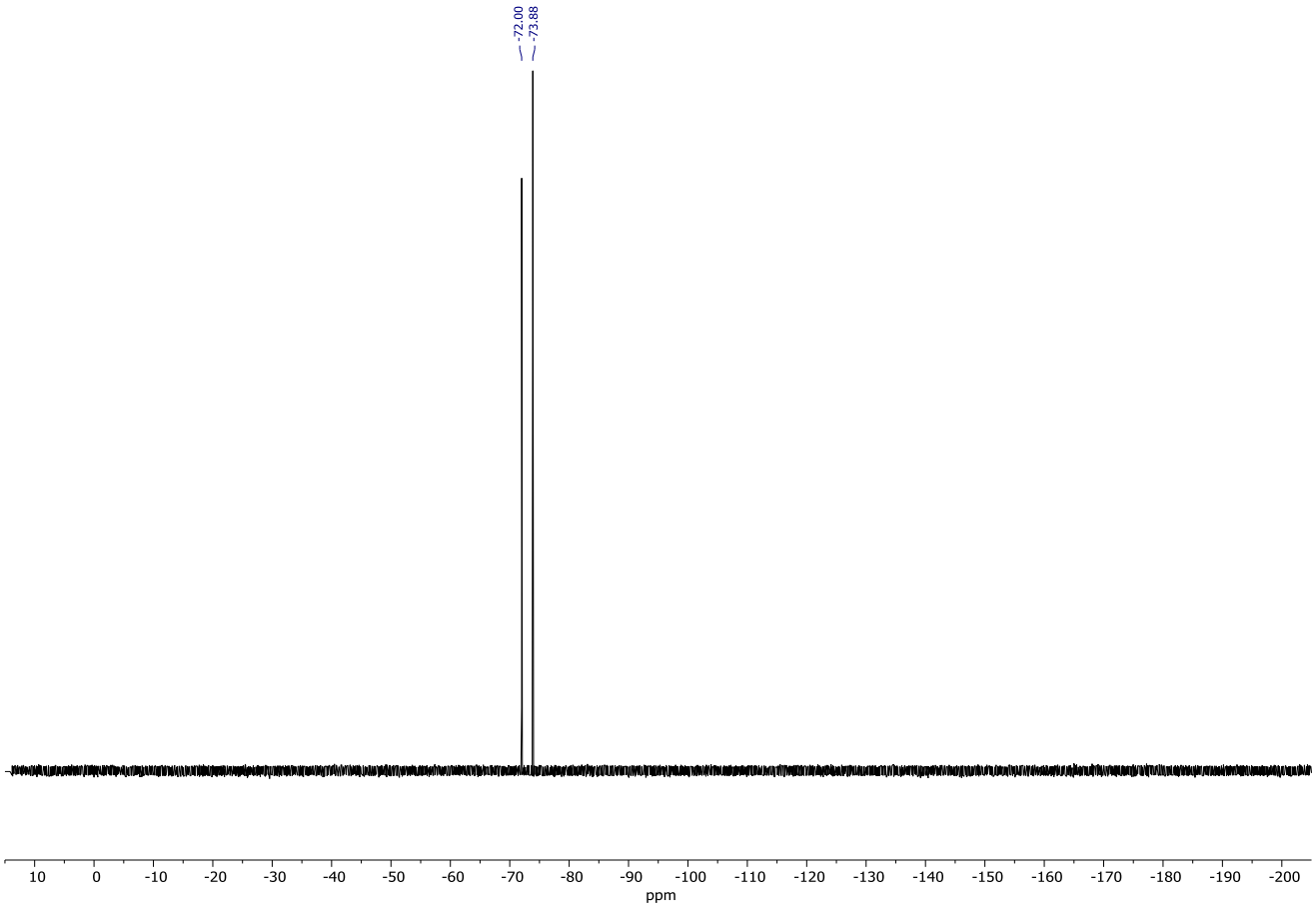

Spectrum 241. ^{19}F NMR (376 MHz, CD_3CN) of **372**.

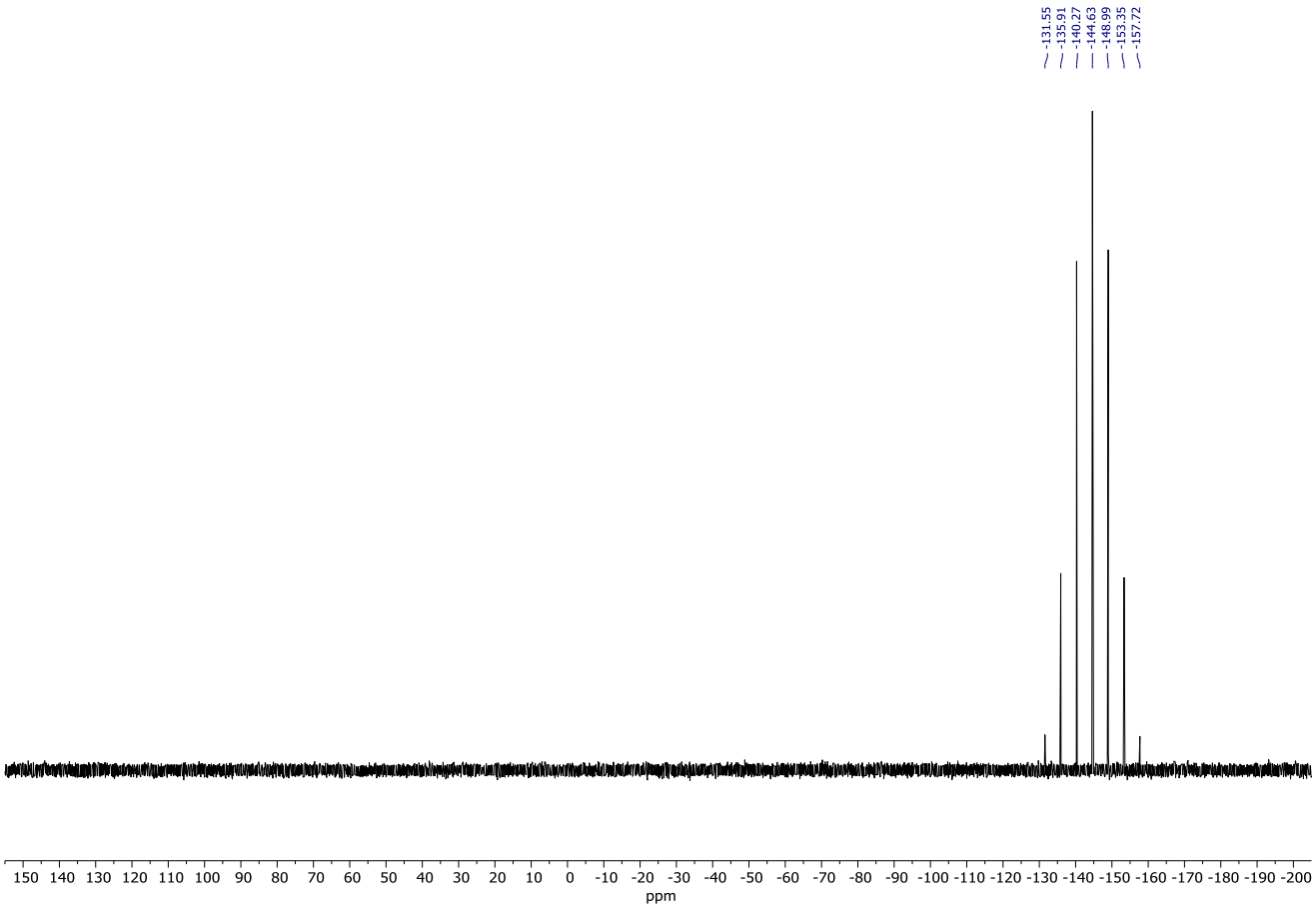

Spectrum 242. ^{31}P NMR (162 MHz, CD_3CN) of **372**.

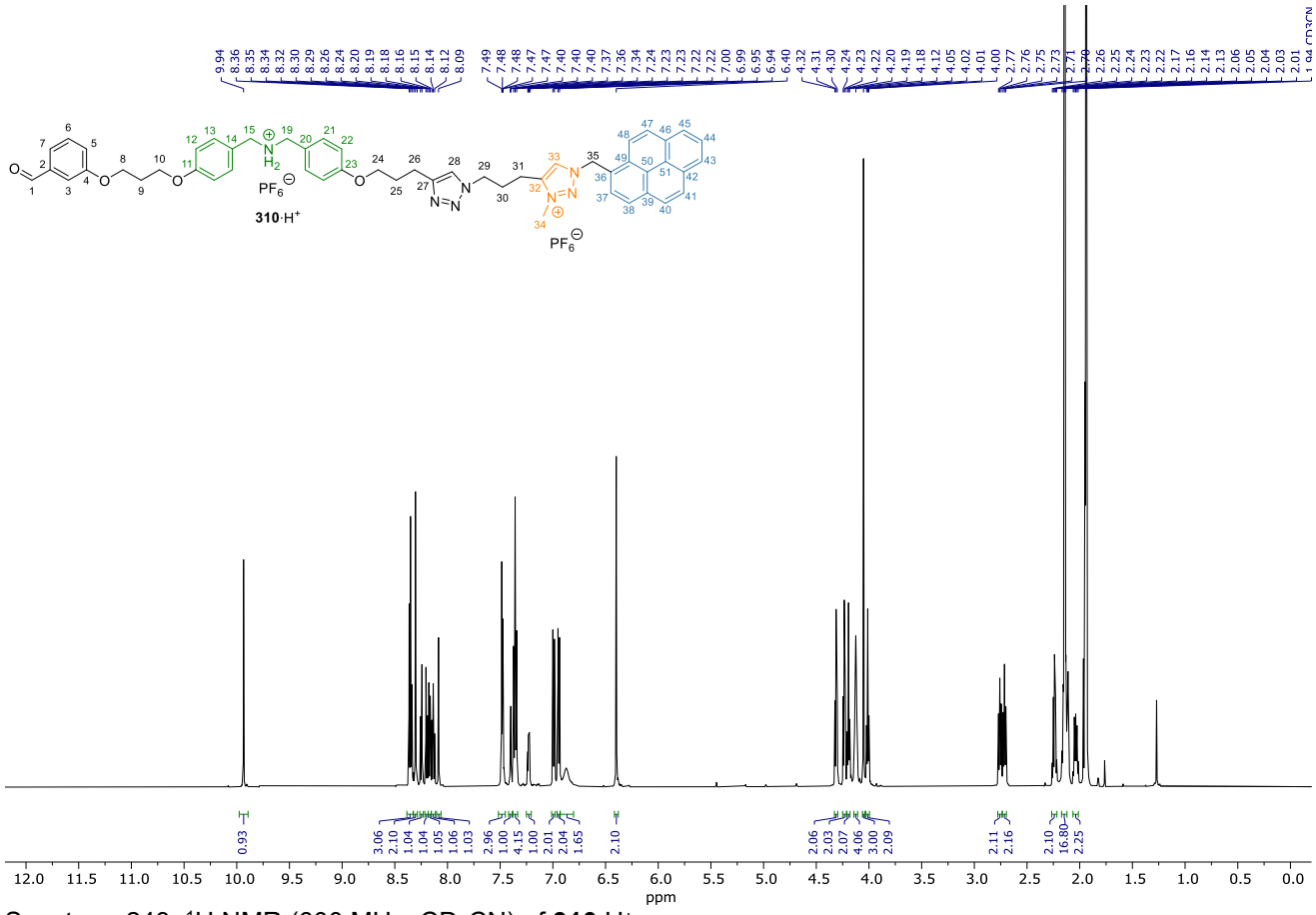

Spectrum 243. ^{1}H NMR (600 MHz, CD_3CN) of **310**·H^+.

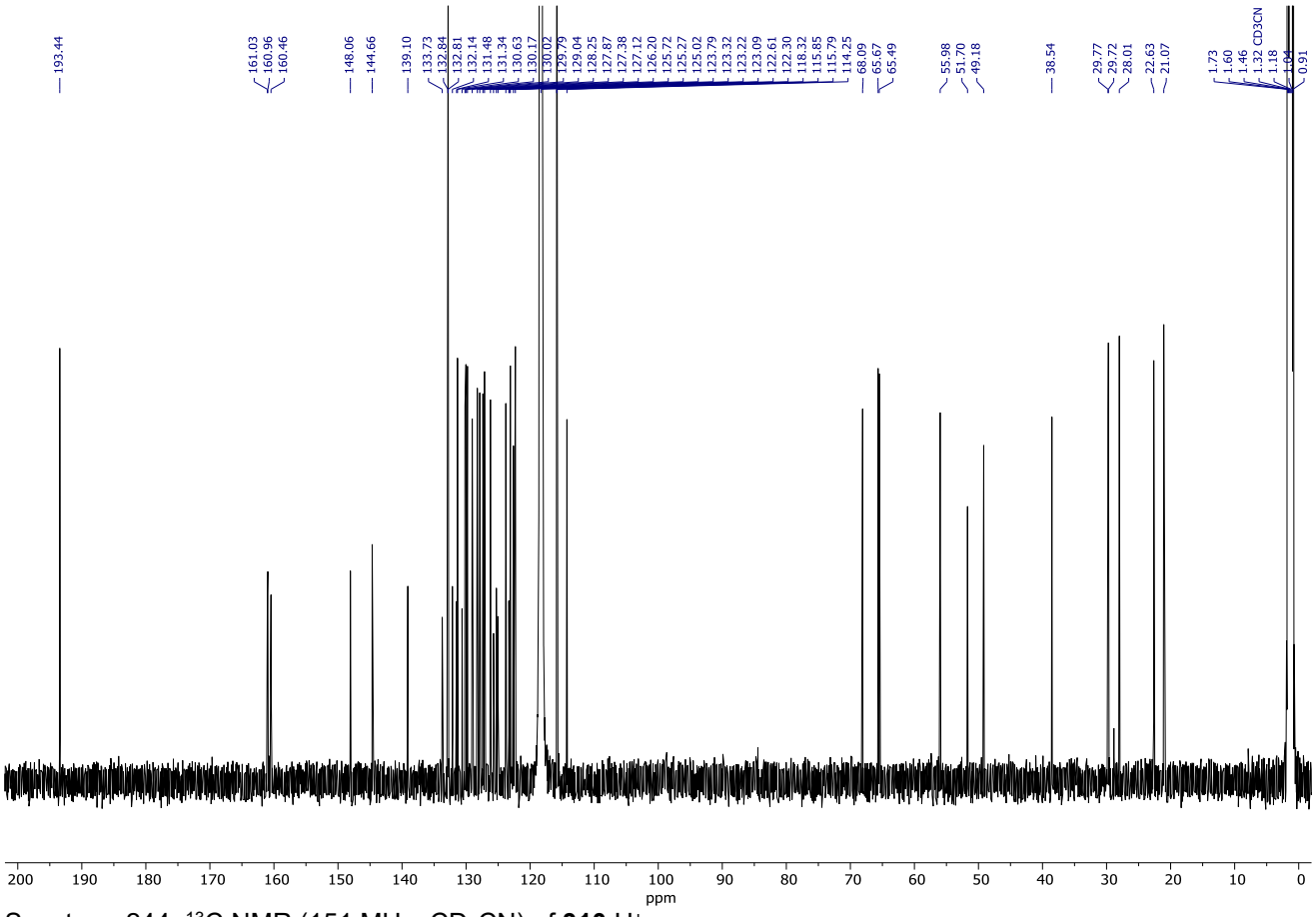

Spectrum 244. ^{13}C NMR (151 MHz, CD_3CN) of **310**·H^+.

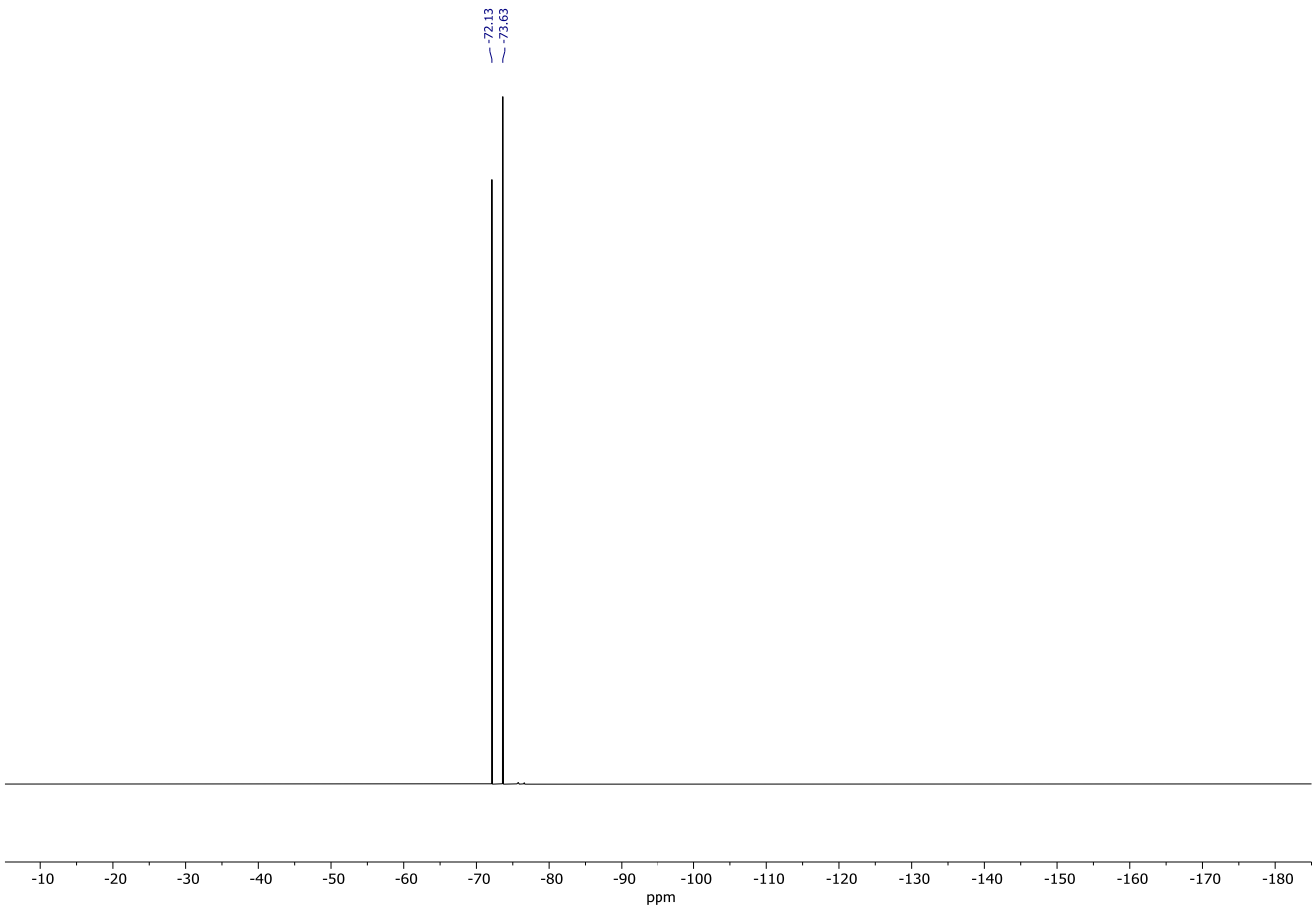

Spectrum 245. ^{19}F NMR (471 MHz, CD_3CN) of **310**·H^+.

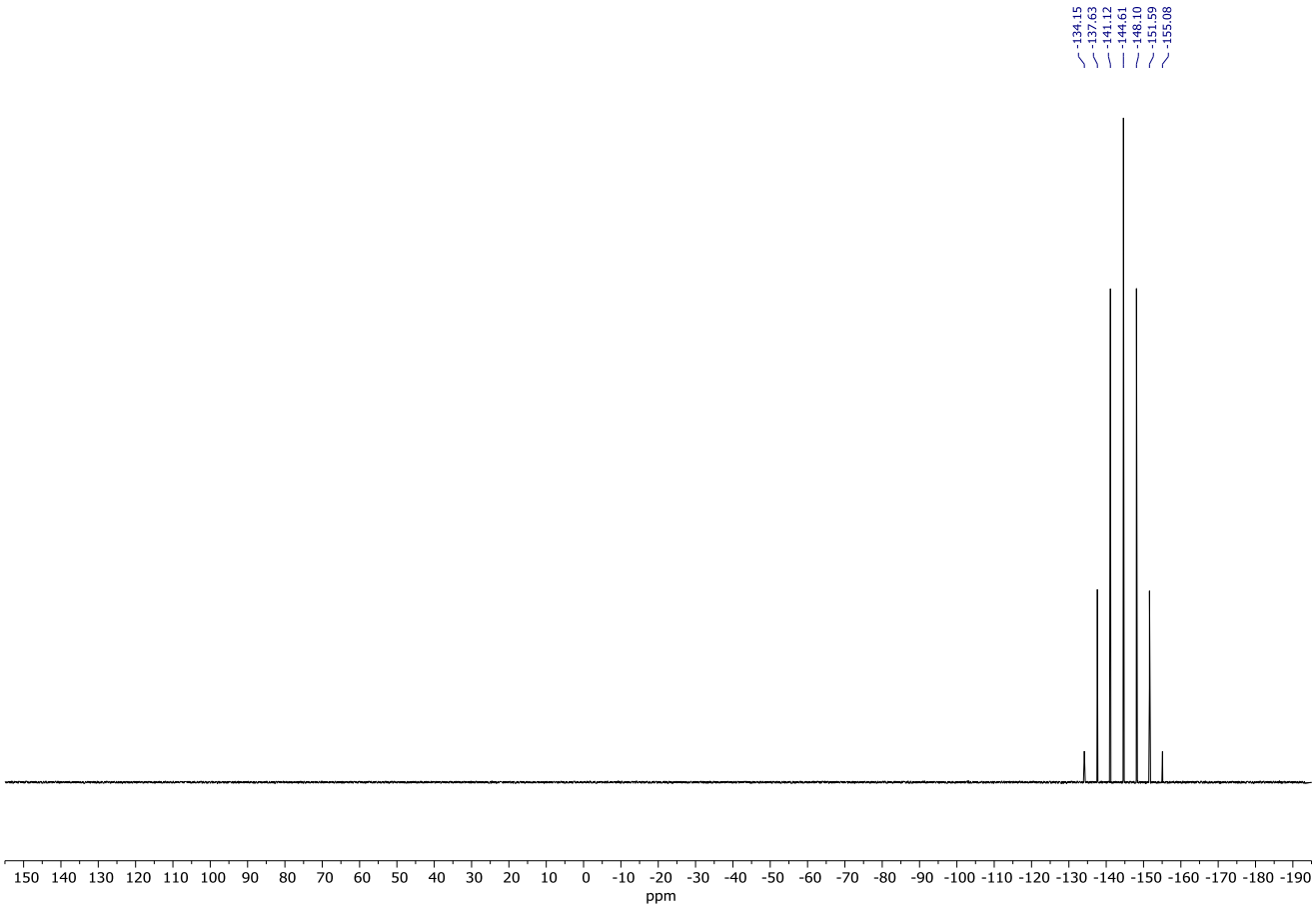

Spectrum 246. ^{31}P NMR (203 MHz, CD_3CN) of **310**·H^+.

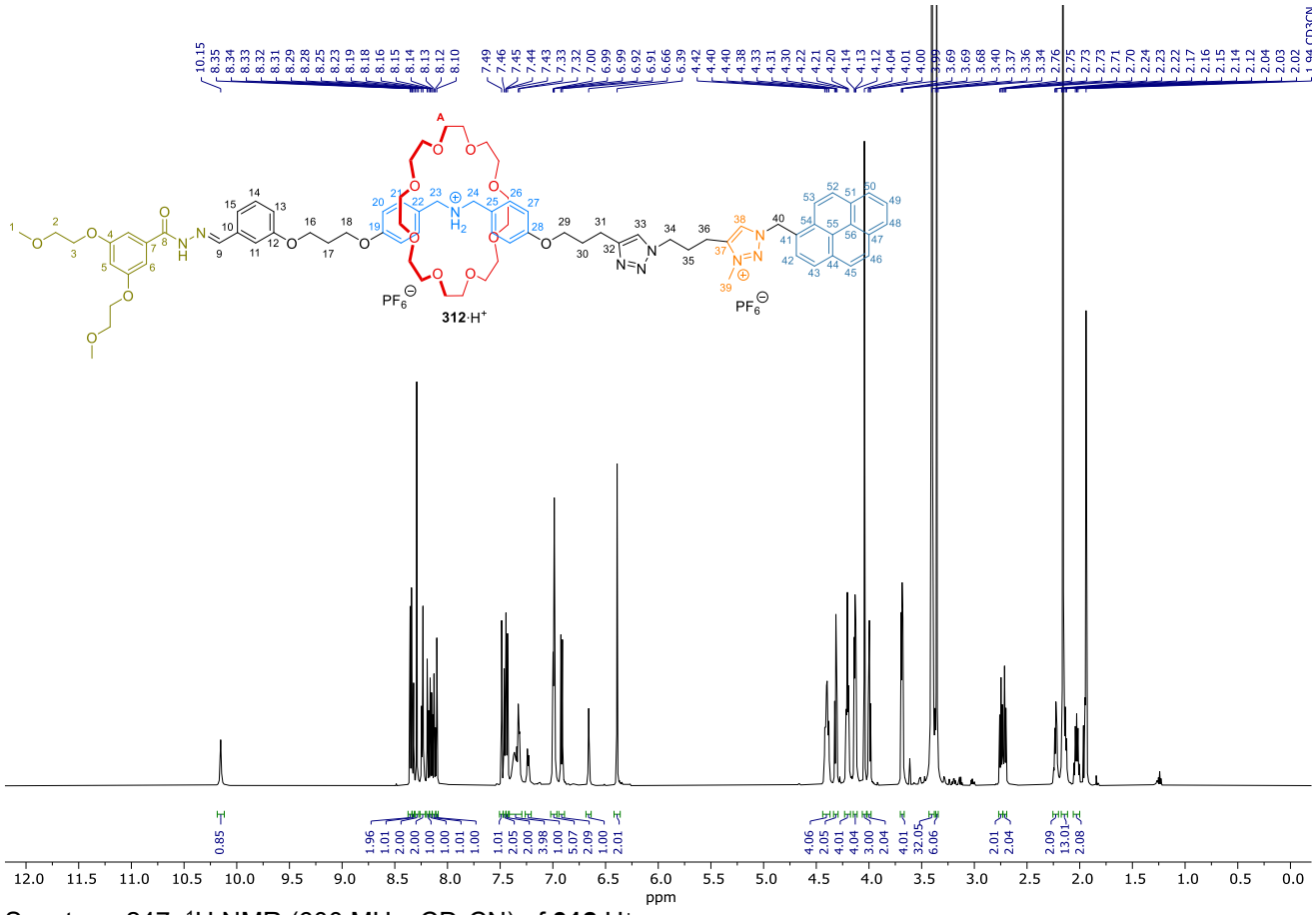

Spectrum 247. ^{1}H NMR (600 MHz, CD_3CN) of **312**·H^+.

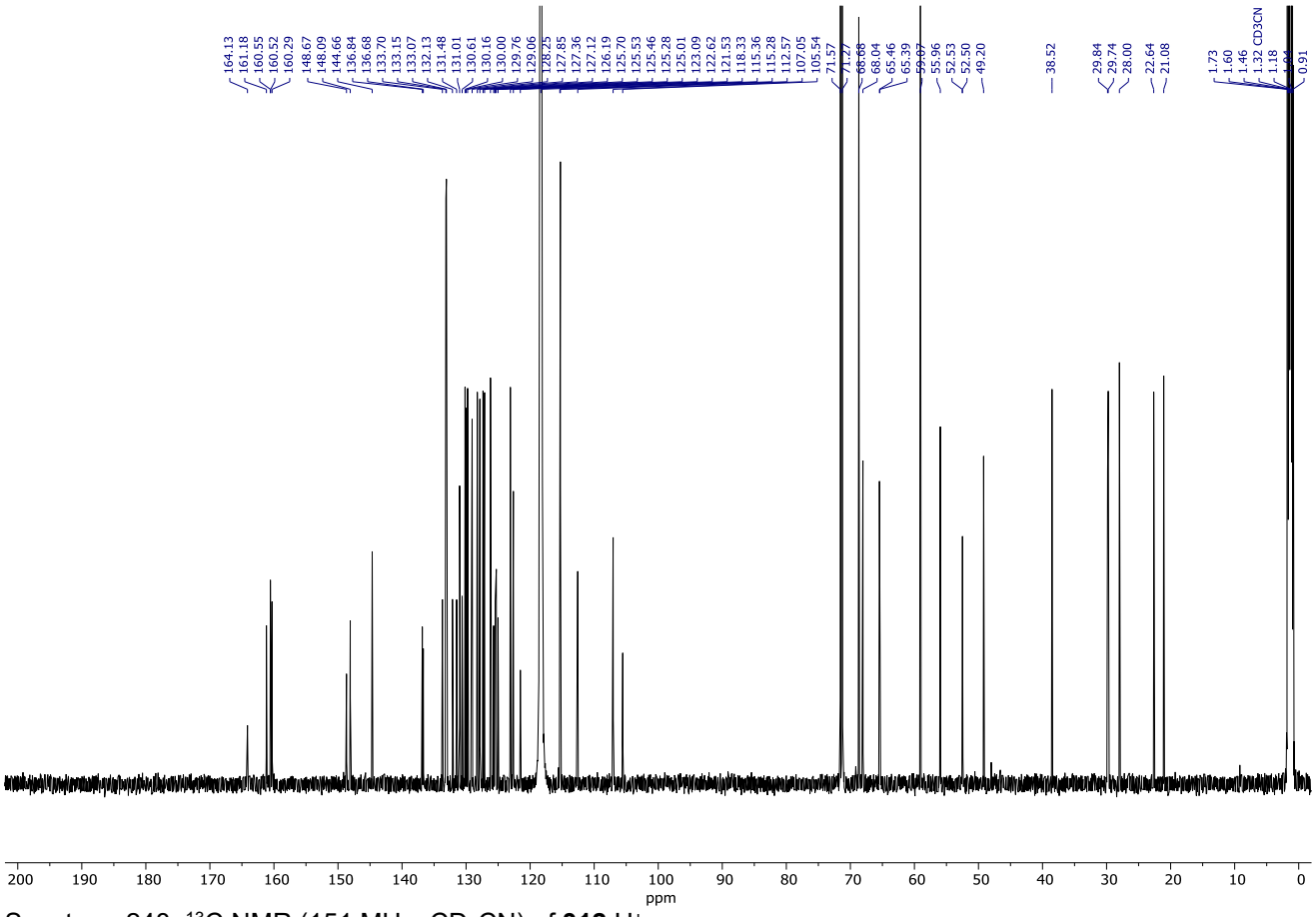

Spectrum 248. ^{13}C NMR (151 MHz, CD_3CN) of **312**·H^+.

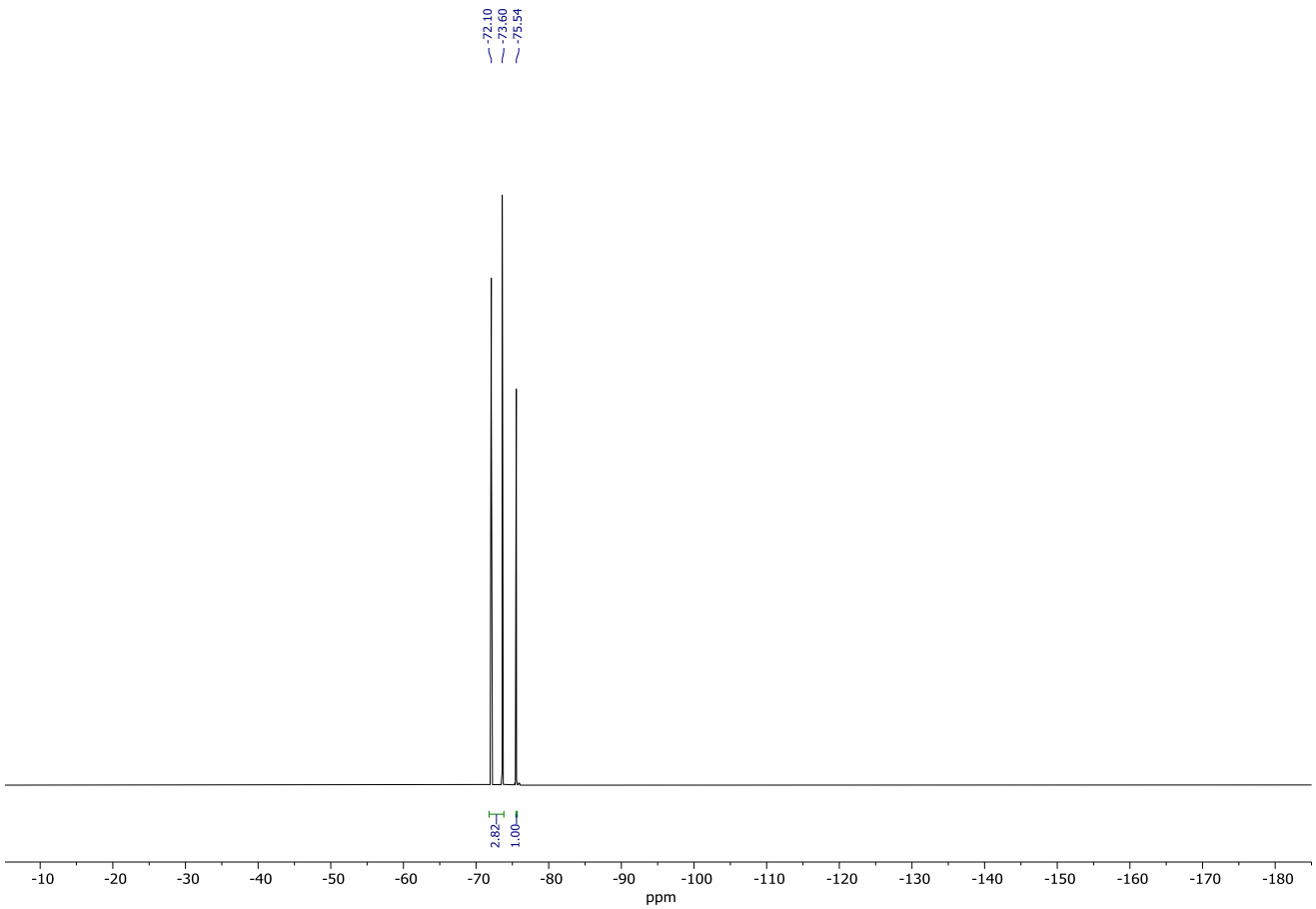

Spectrum 249. ^{19}F NMR (471 MHz, CD_3CN) of **312**·H^+.

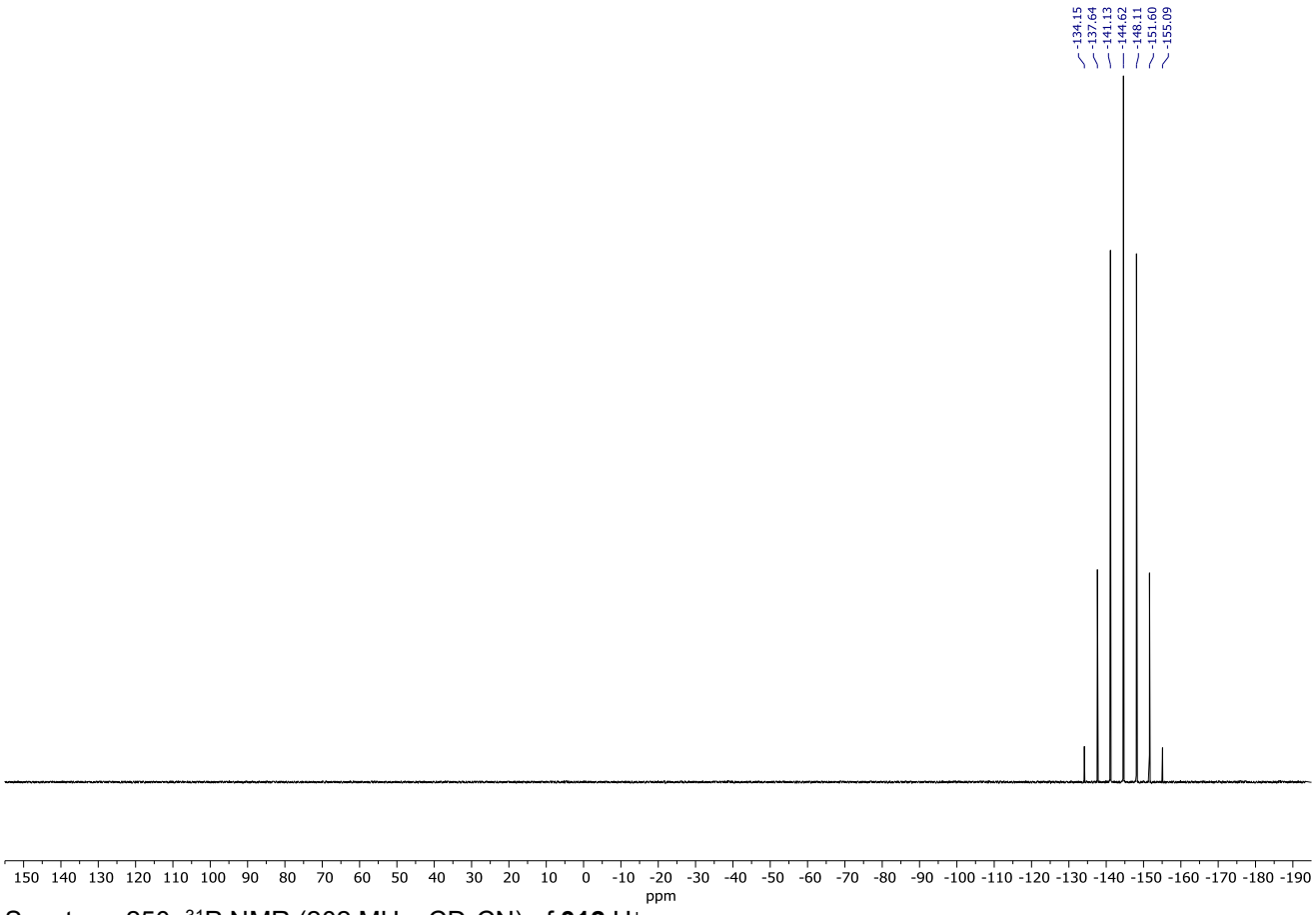

Spectrum 250. ^{31}P NMR (202 MHz, CD_3CN) of **312**·H^+.

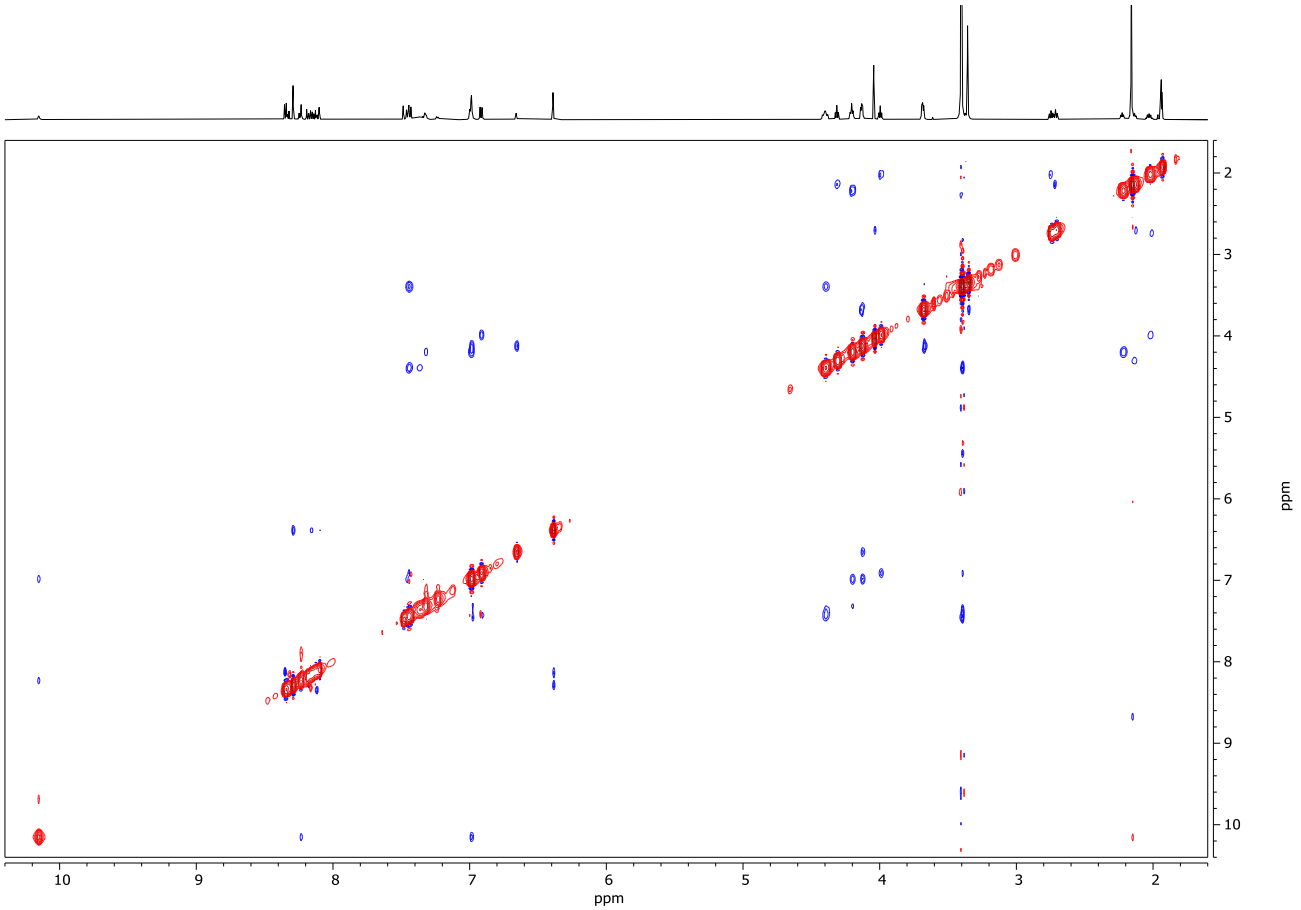

Spectrum 251. 2D NOESY (600 MHz, CD_3CN) of **312**·H^+. Data was recorded with 400 ms mixing time and a relaxation delay of 2.03 s. 2K data points were collected for 256 increments of 4 scans.

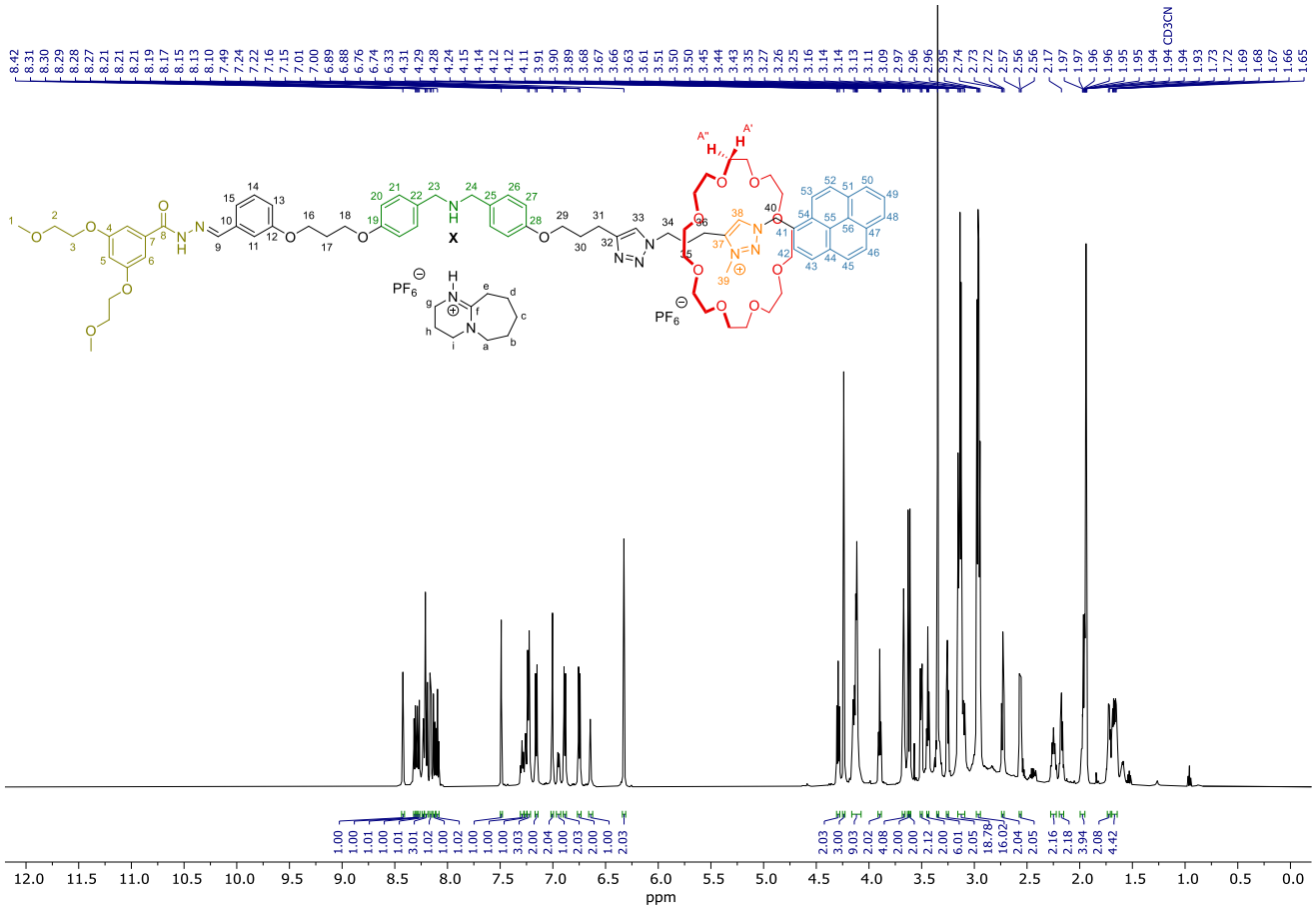

Spectrum 252. ^{1}H NMR (600 MHz, CD_3CN) of **312**.

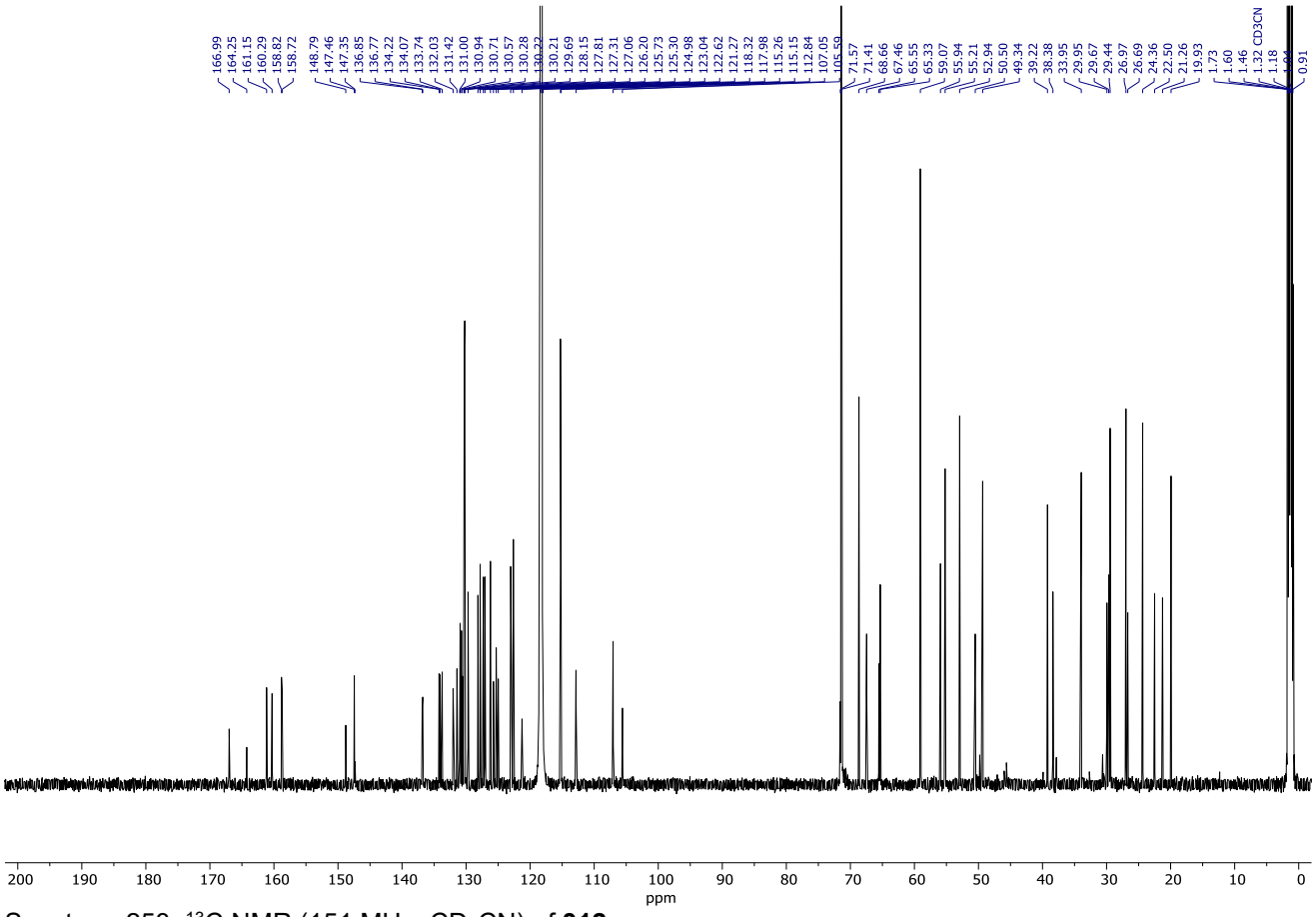

Spectrum 253. ^{13}C NMR (151 MHz, CD_3CN) of **312**.

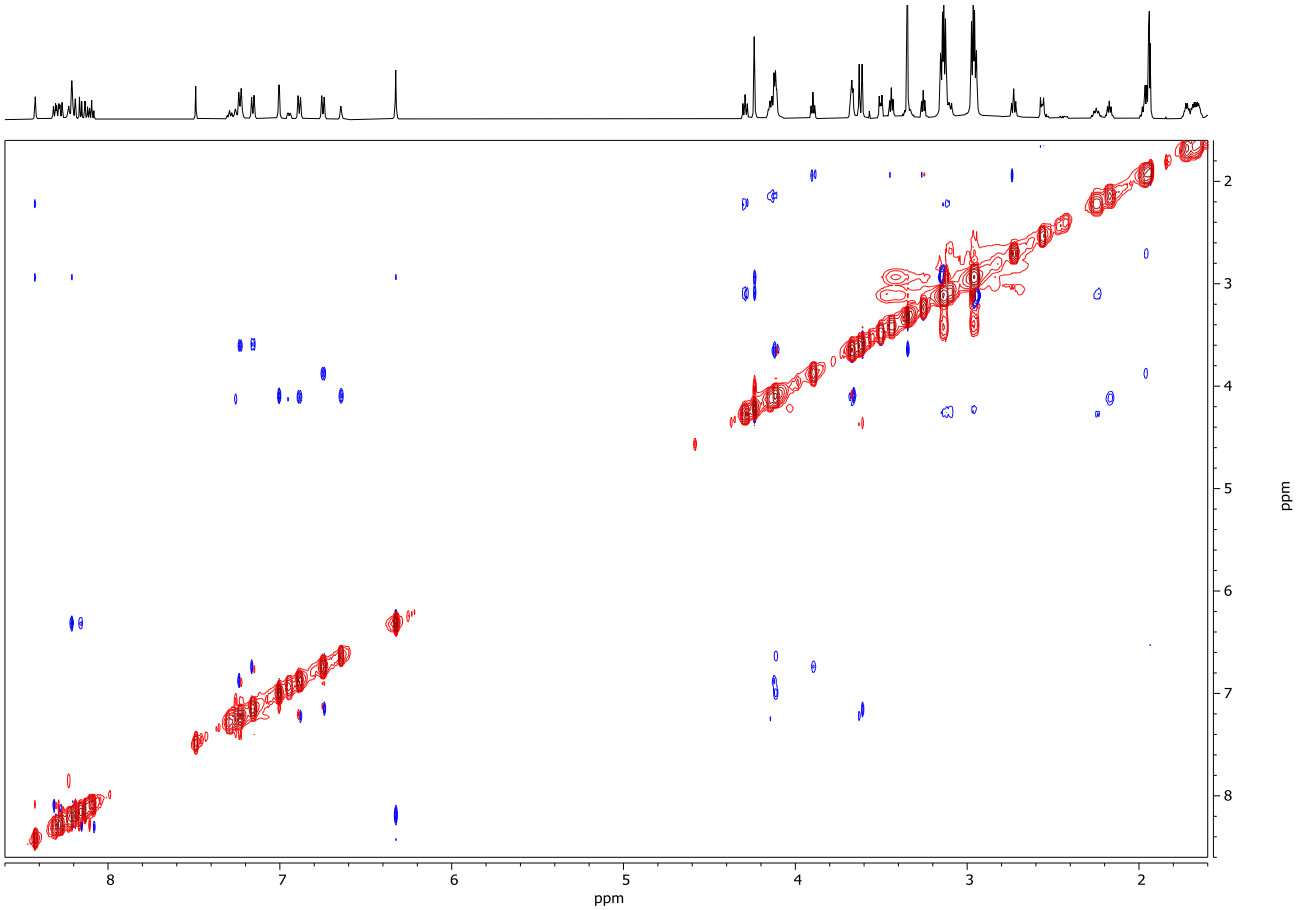

Spectrum 254. 2D NOESY (600 MHz, CD_3CN) of **312**. Data was recorded with a 400 ms mixing time and a relaxation delay of 2.02 s. 4K data points were collected for 256 increments of 4 scans.

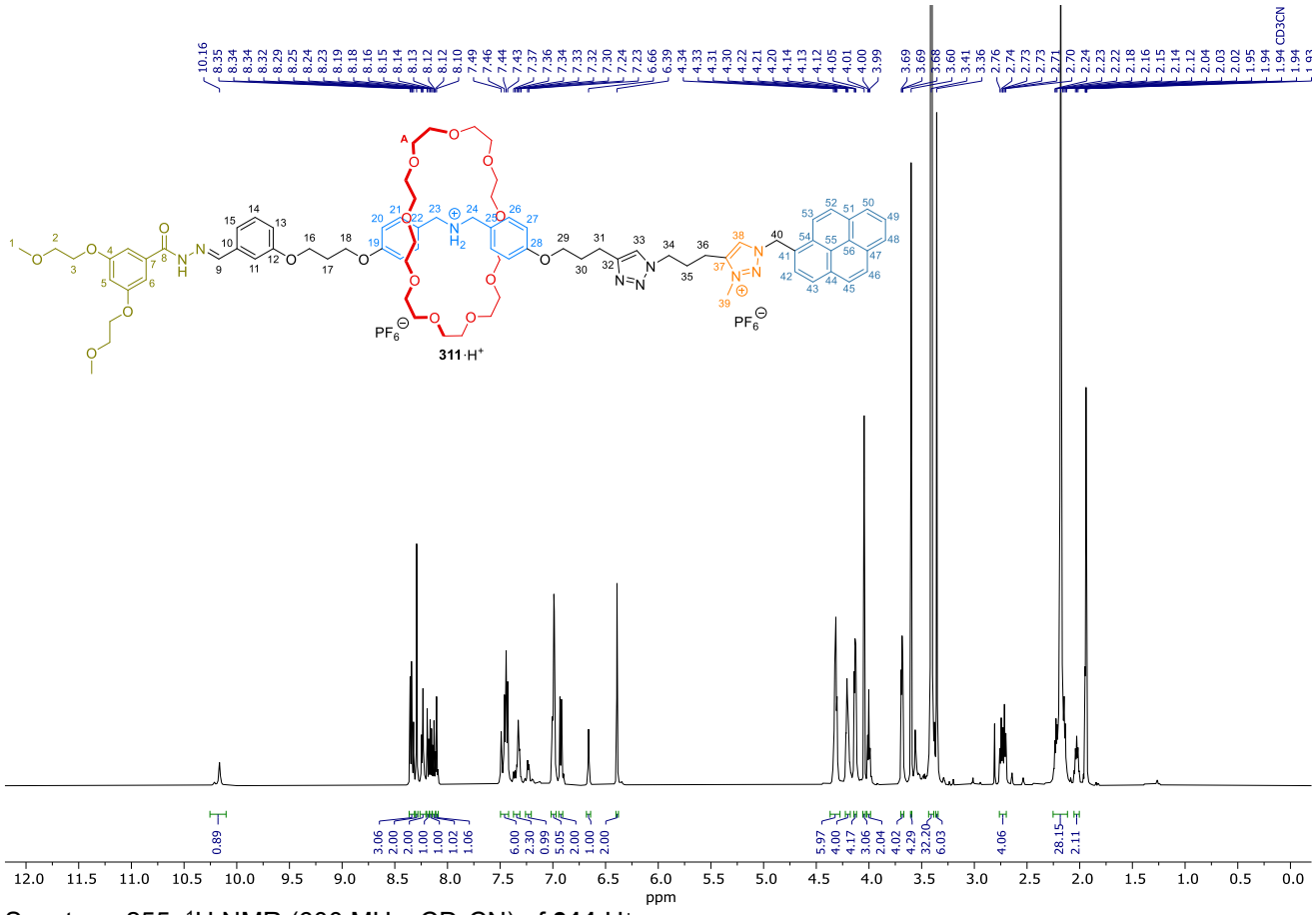

Spectrum 255. ^{1}H NMR (600 MHz, CD_3CN) of **311**·H^+.

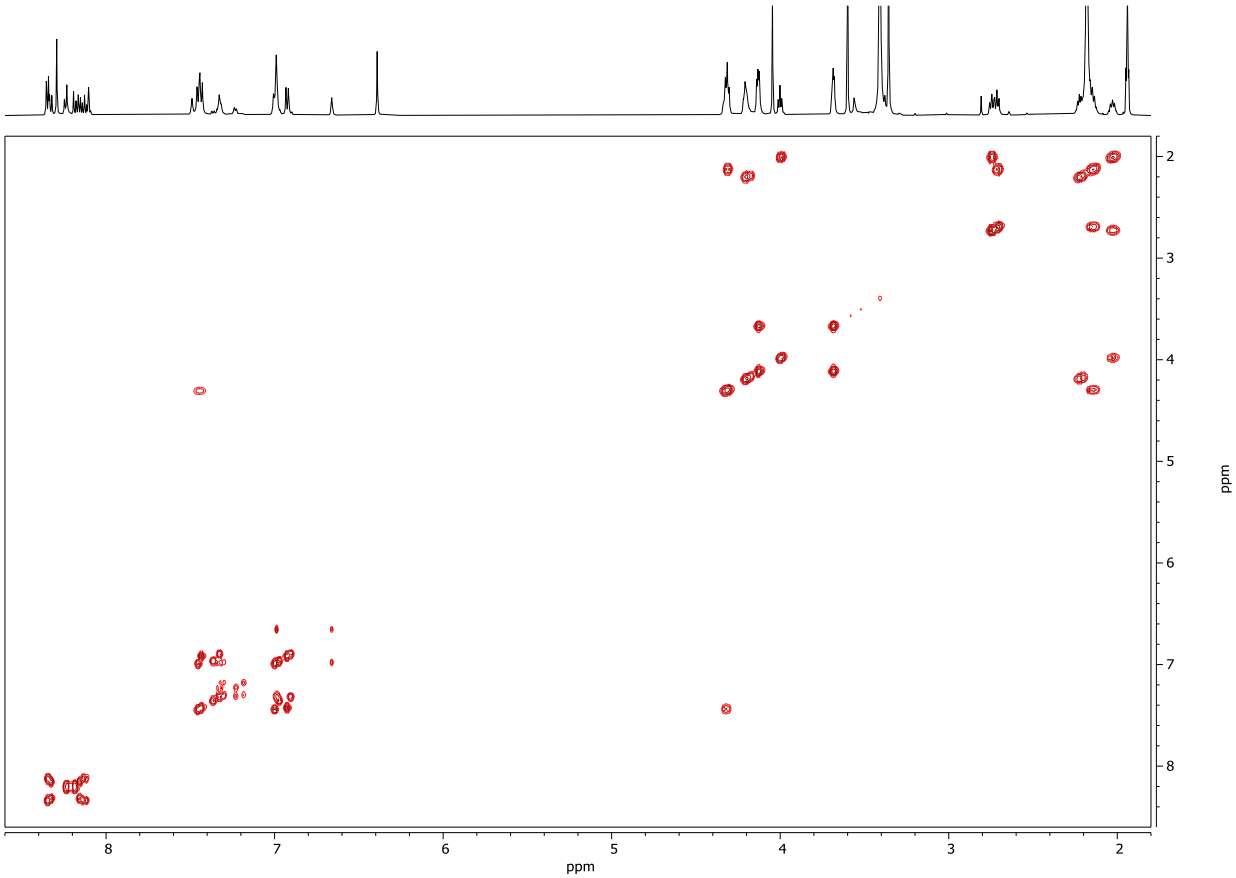

Spectrum 256. ^{1}H,^{1}H COSY-DQF (600 MHz, CD_3CN) of **311**·H^+. Data was recorded with a relaxation delay of 2.04 s. 4K data points were collected for 512 increments of 1 scan(s).

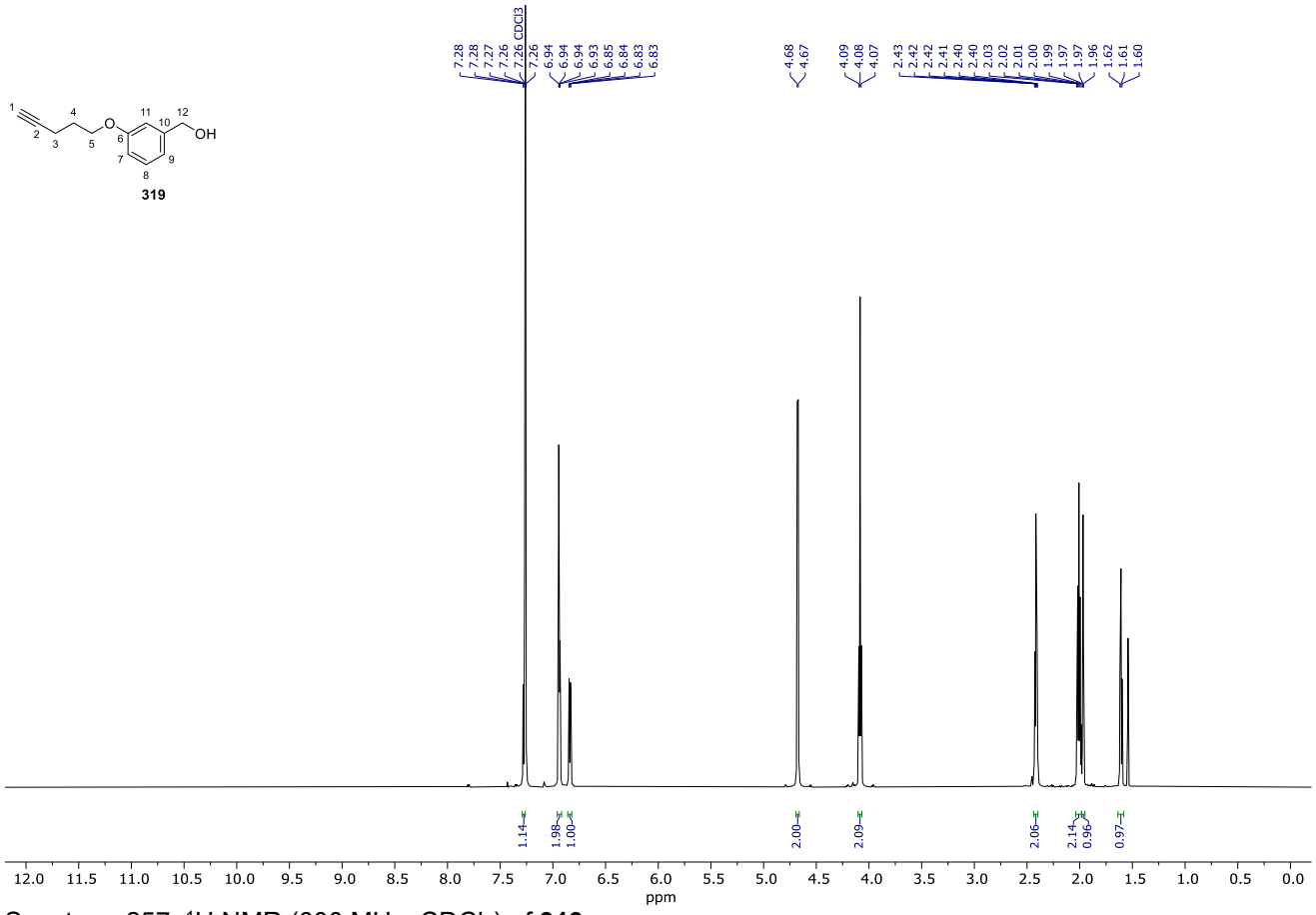

Spectrum 257. ^{1}H NMR (600 MHz, $CDCl_3$) of **319**.

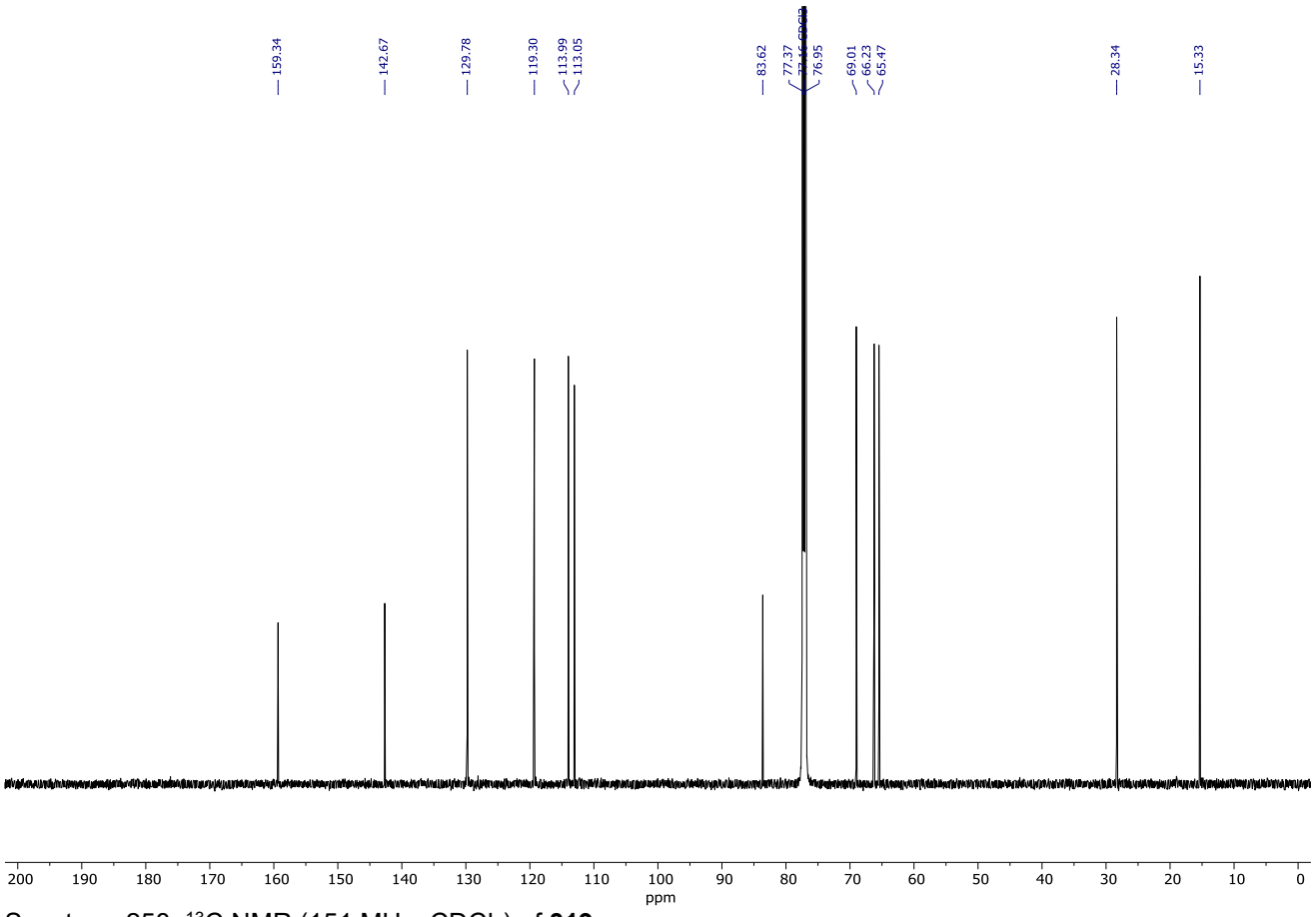

Spectrum 258. ^{13}C NMR (151 MHz, $CDCl_3$) of **319**.

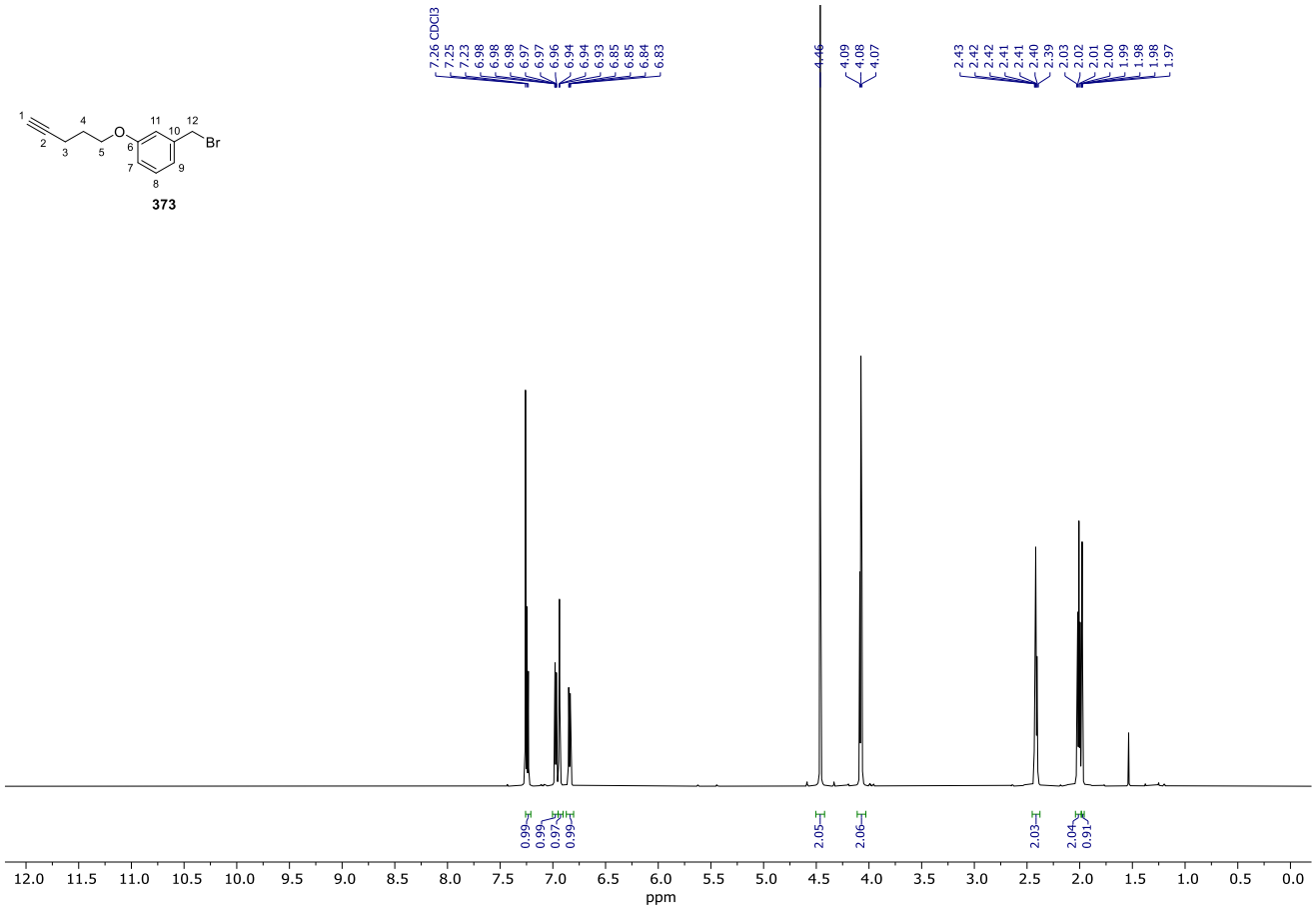

373

Spectrum 259. ^{1}H NMR (600 MHz, $CDCl_3$) of **373**.

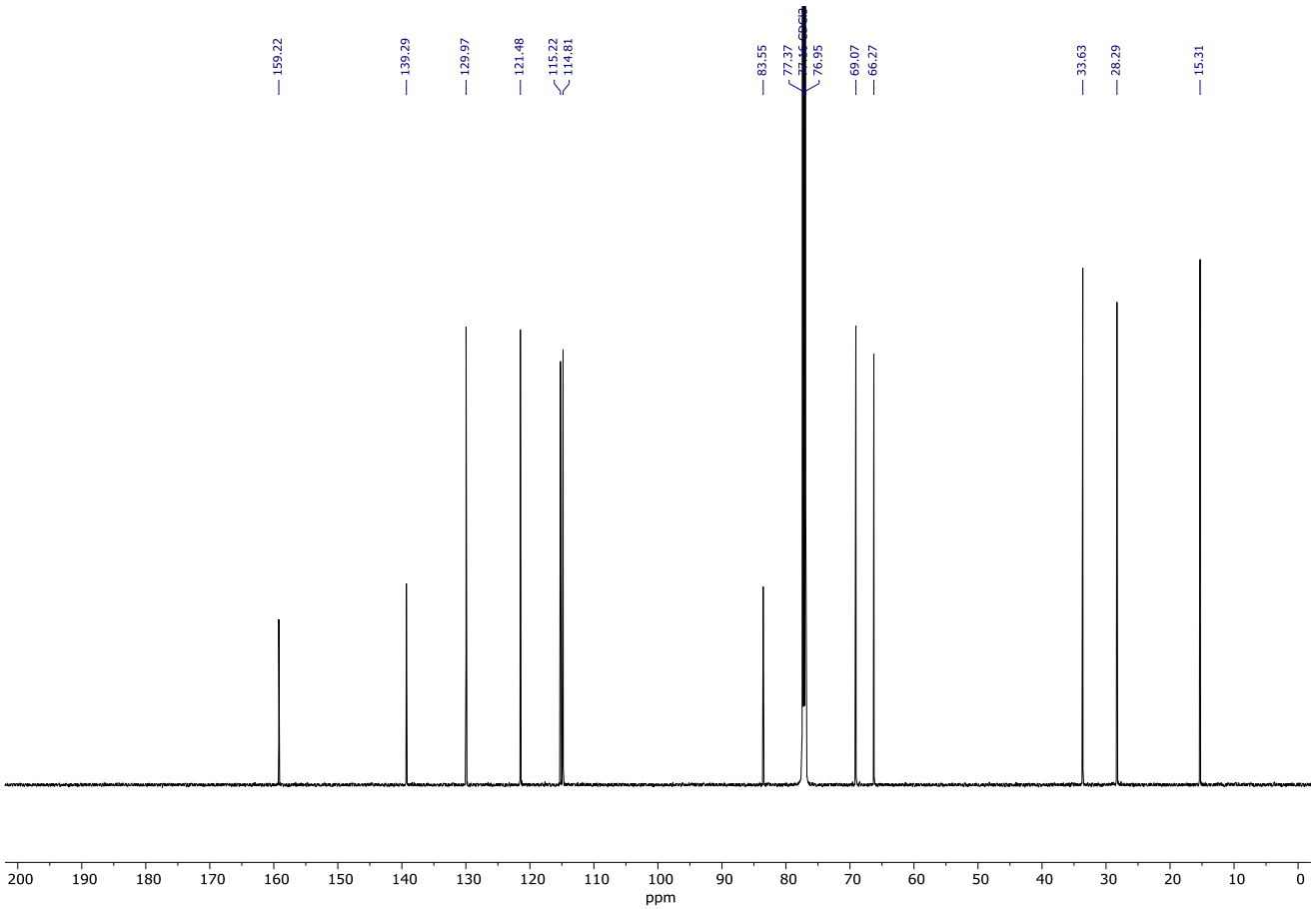

Spectrum 260. ^{13}C NMR (151 MHz, $CDCl_3$) of **373**.

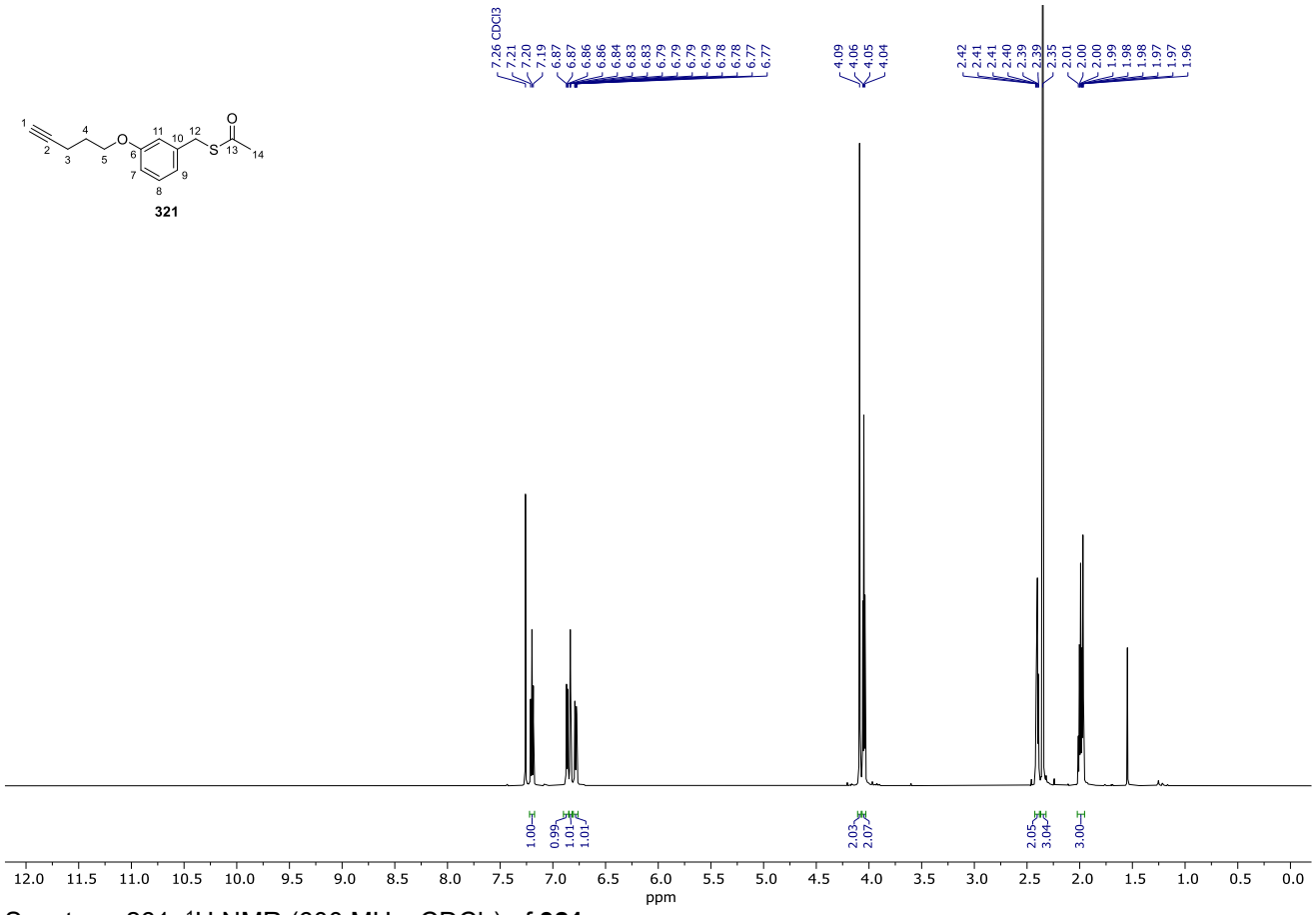

Spectrum 261. ^{1}H NMR (600 MHz, $CDCl_3$) of **321**.

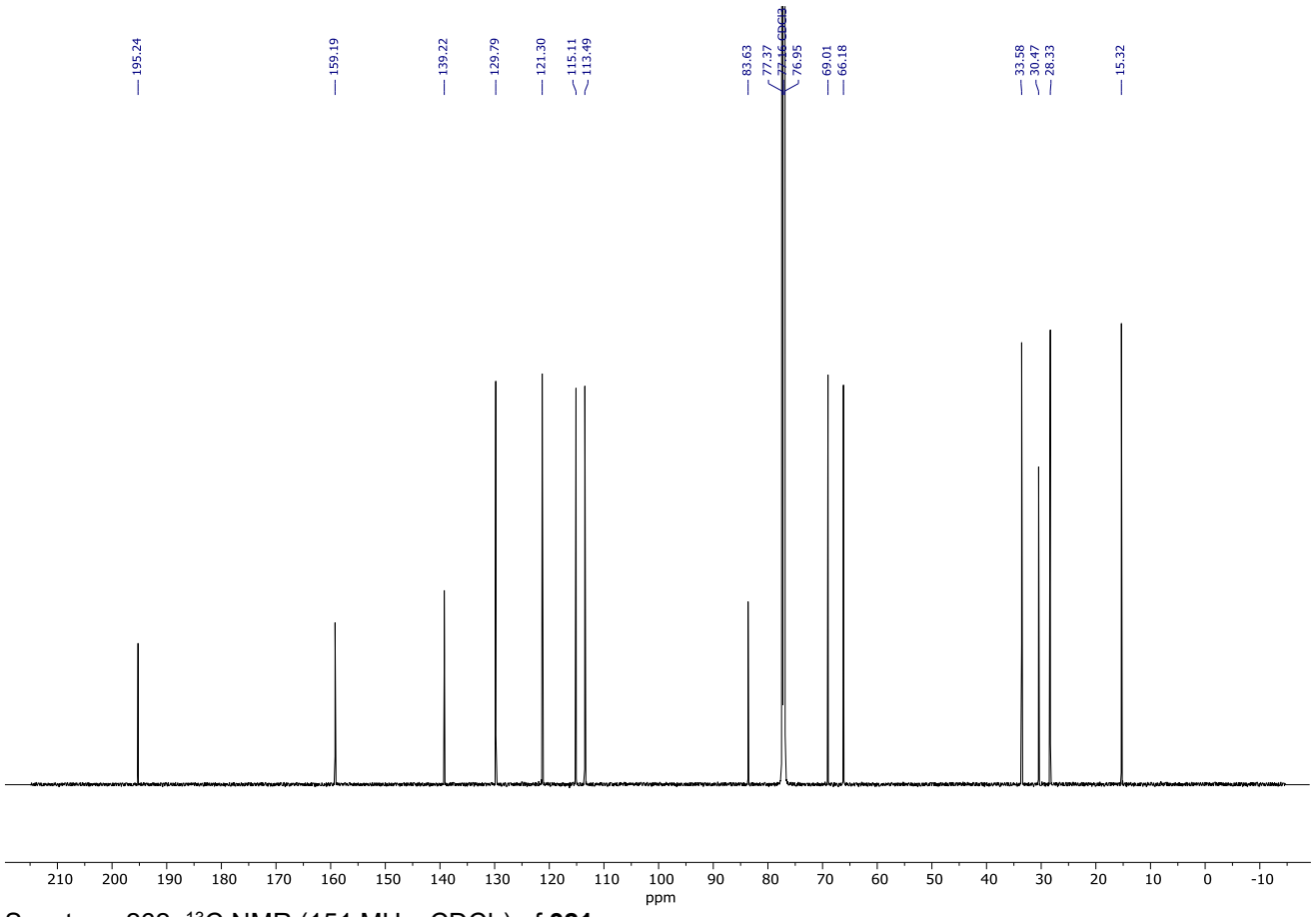

Spectrum 262. ^{13}C NMR (151 MHz, $CDCl_3$) of **321**.

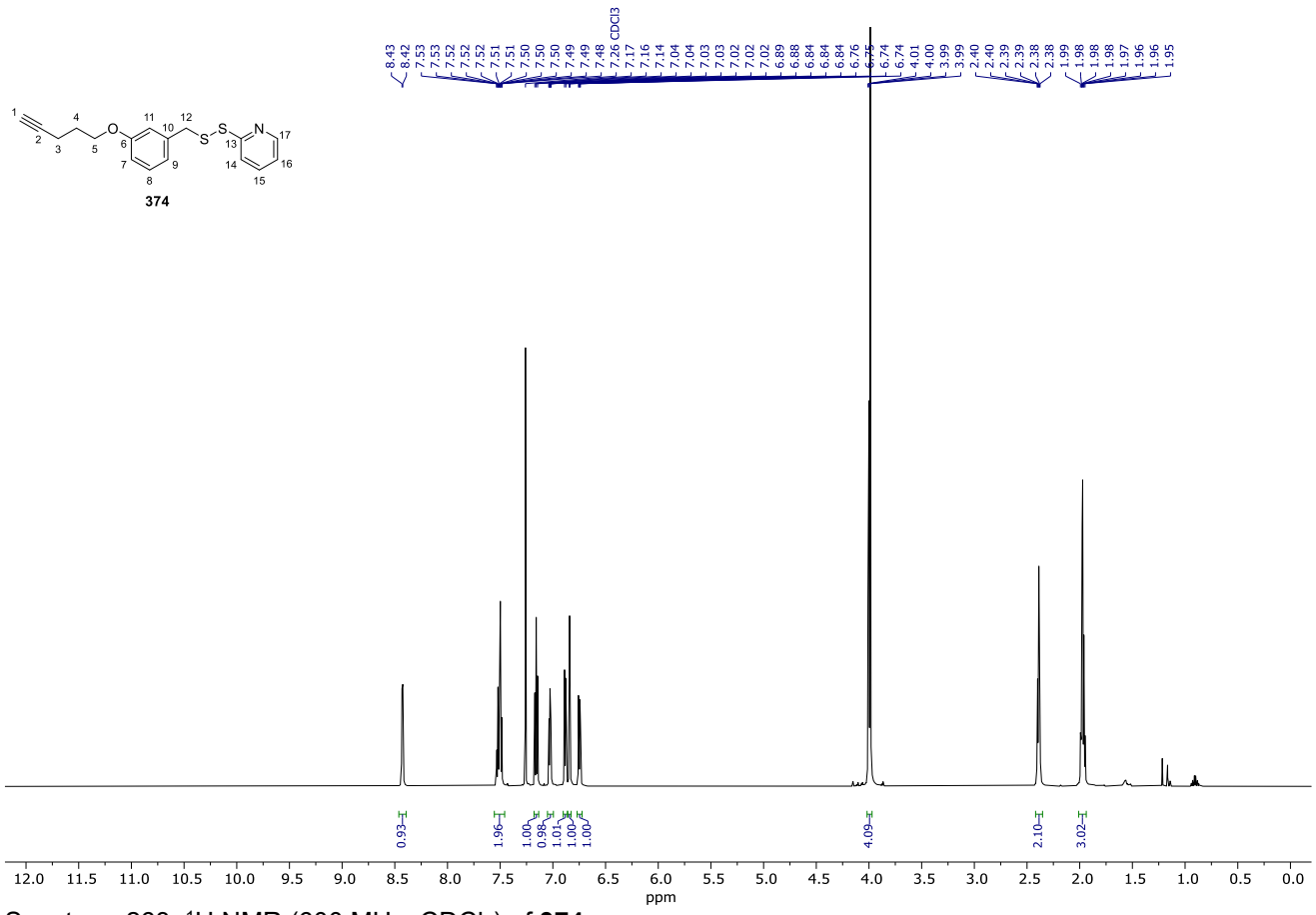

Spectrum 263. ^{1}H NMR (600 MHz, $CDCl_3$) of **374**.

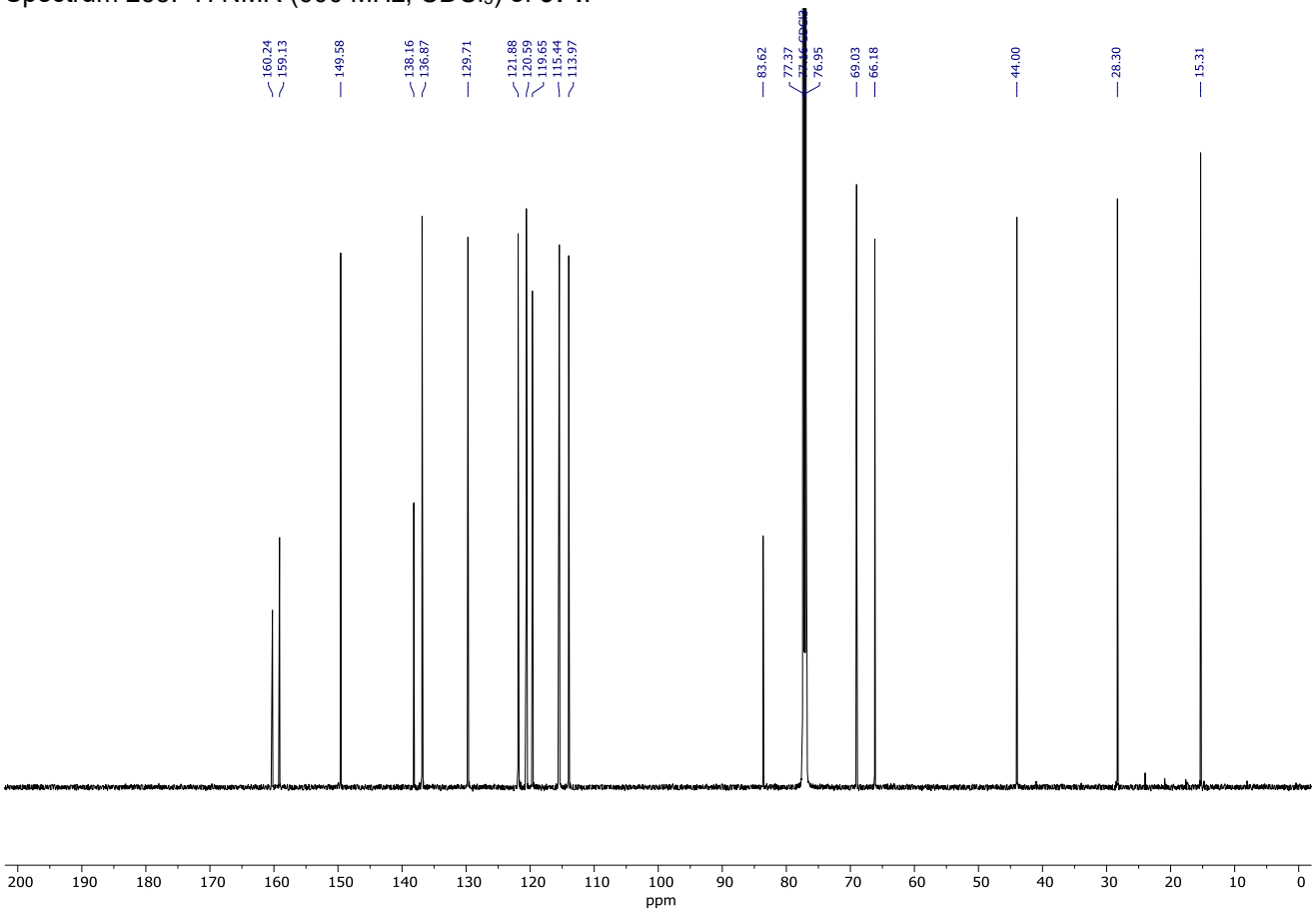

Spectrum 264. ^{13}C NMR (151 MHz, $CDCl_3$) of **374**.

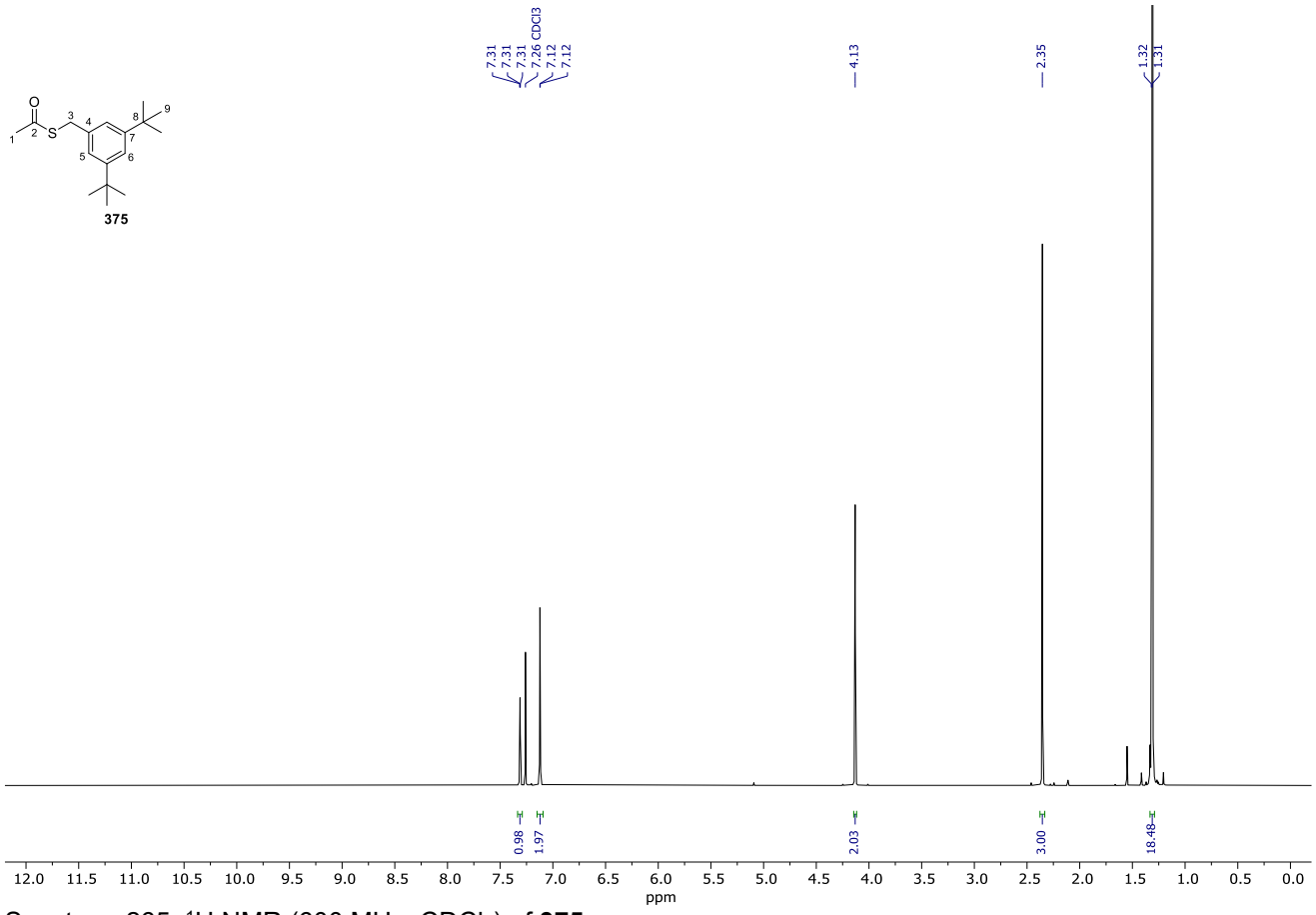

Spectrum 265. ^{1}H NMR (600 MHz, $CDCl_3$) of **375**.

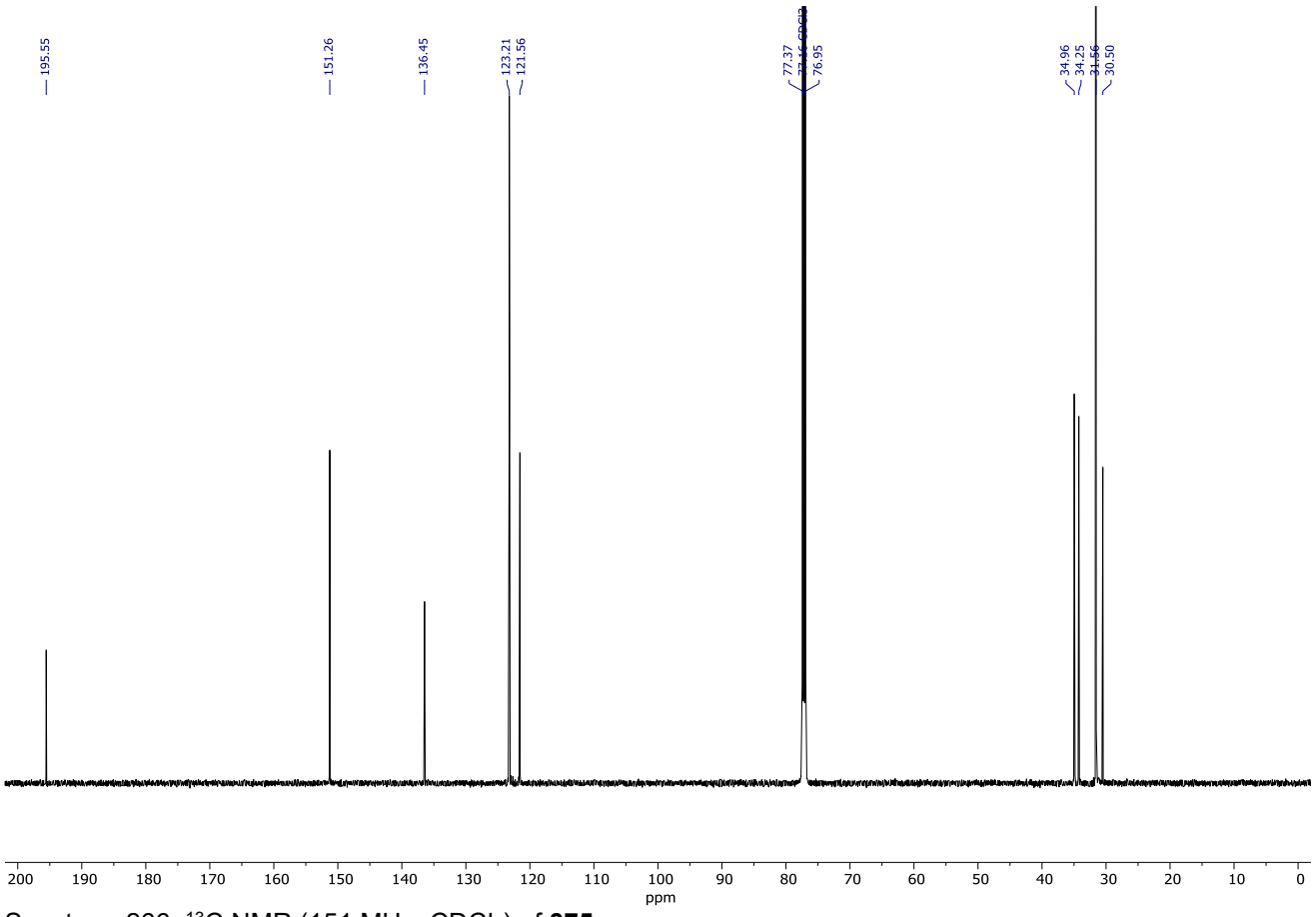

Spectrum 266. ^{13}C NMR (151 MHz, $CDCl_3$) of **375**.

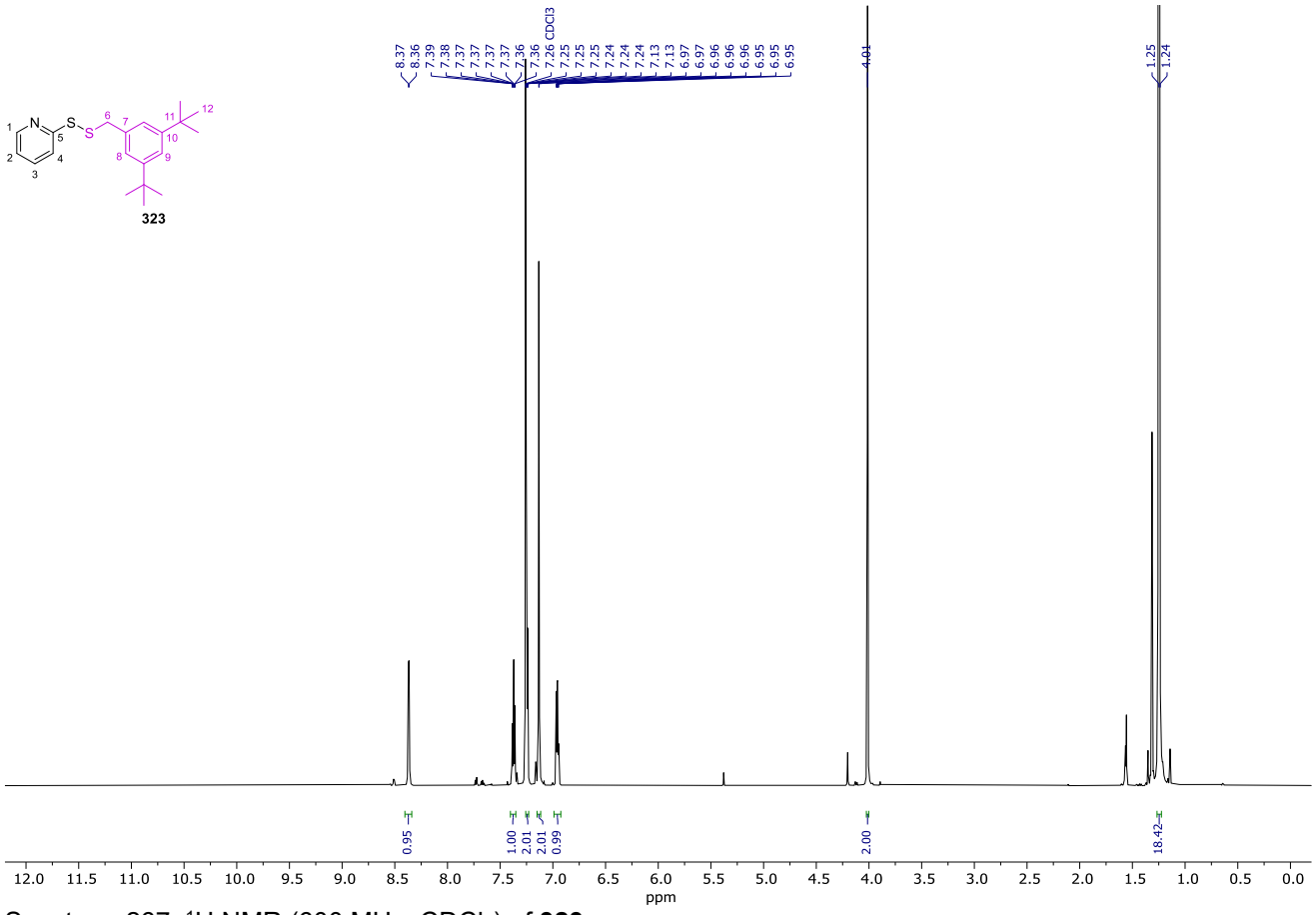

Spectrum 267. ^{1}H NMR (600 MHz, $CDCl_3$) of **323**.

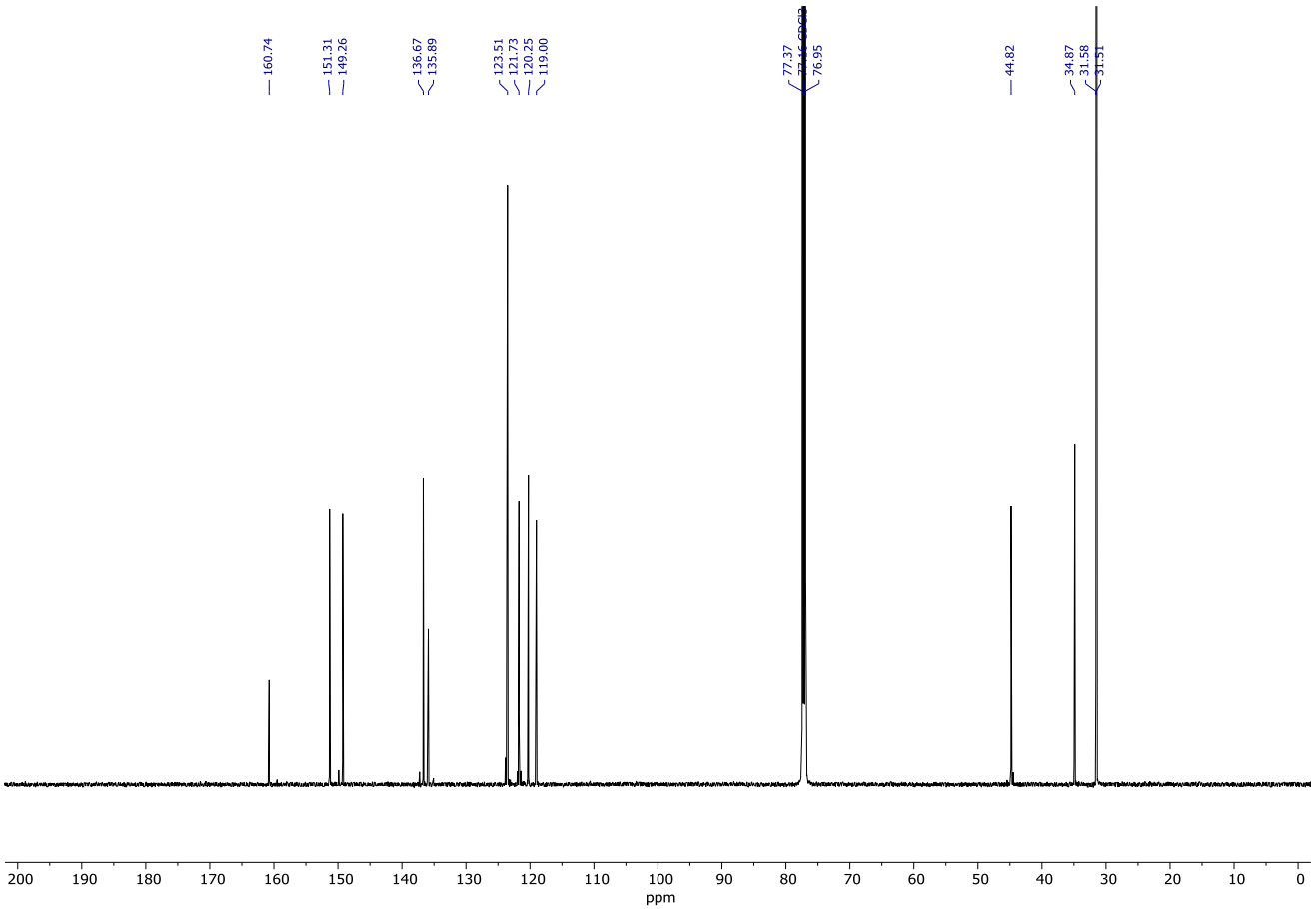

Spectrum 268. ^{13}C NMR (151 MHz, $CDCl_3$) of **323**.

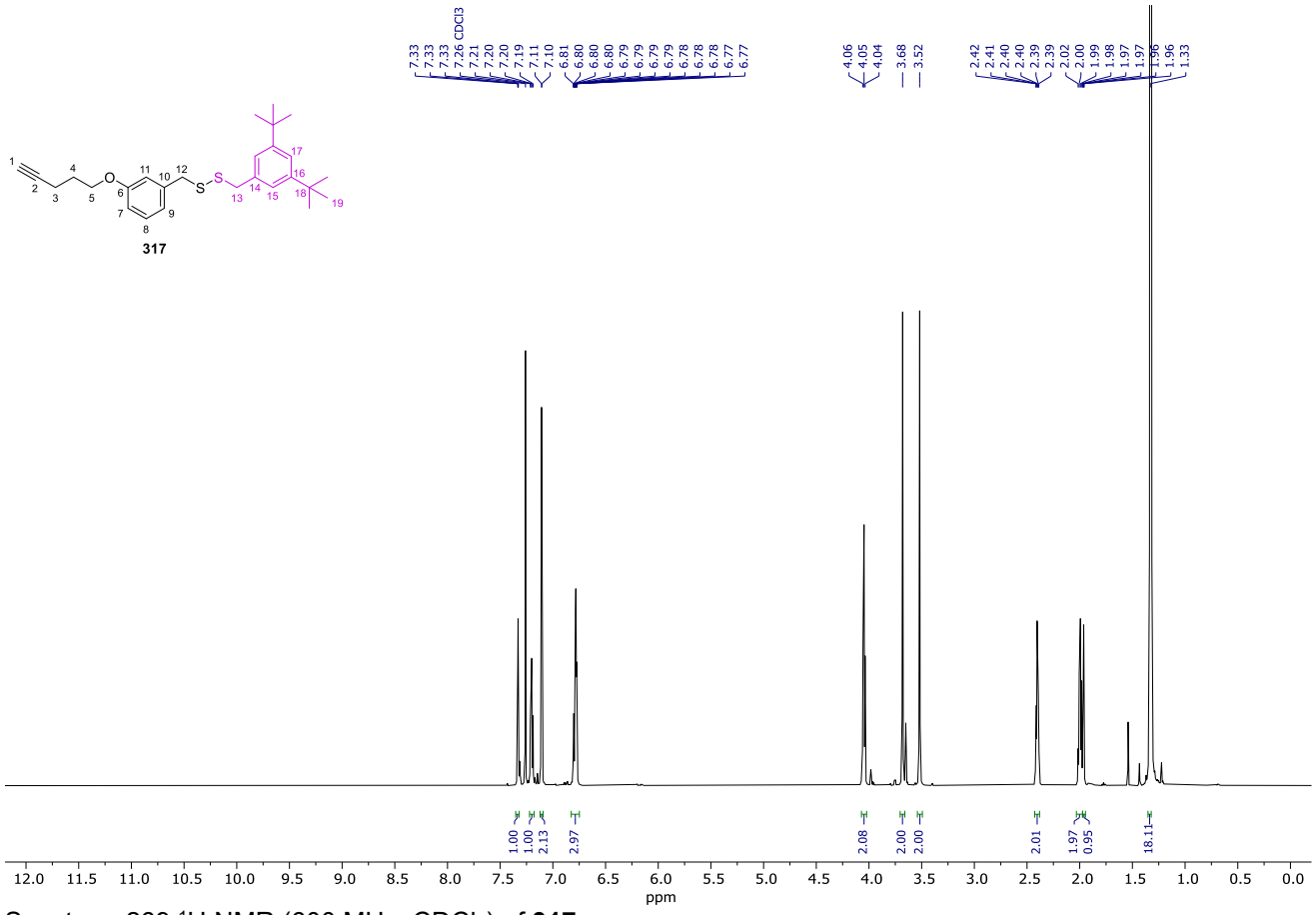

Spectrum 269.^{1}H NMR (600 MHz, $CDCl_3$) of **317**.

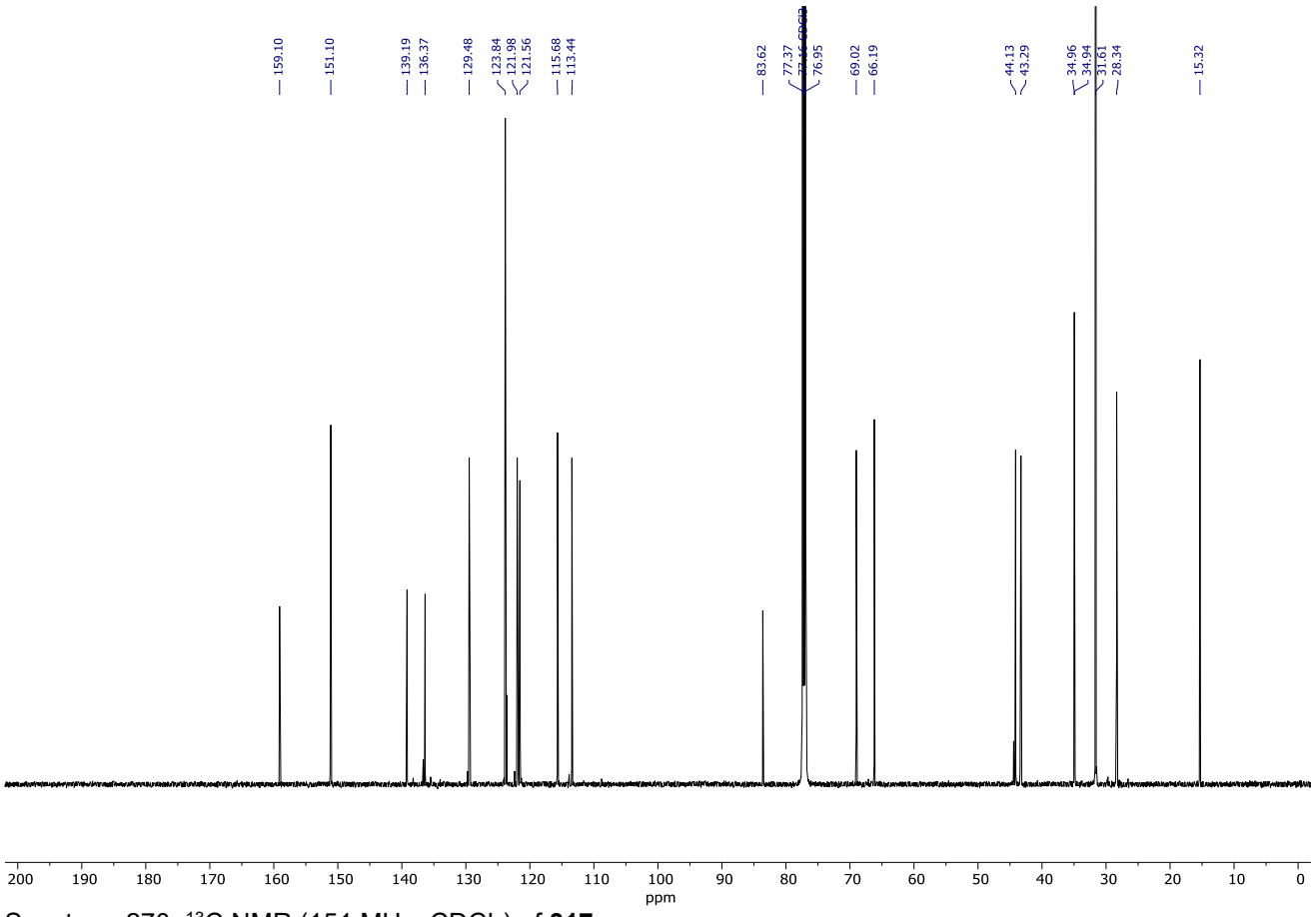

Spectrum 270. ^{13}C NMR (151 MHz, $CDCl_3$) of **317**.

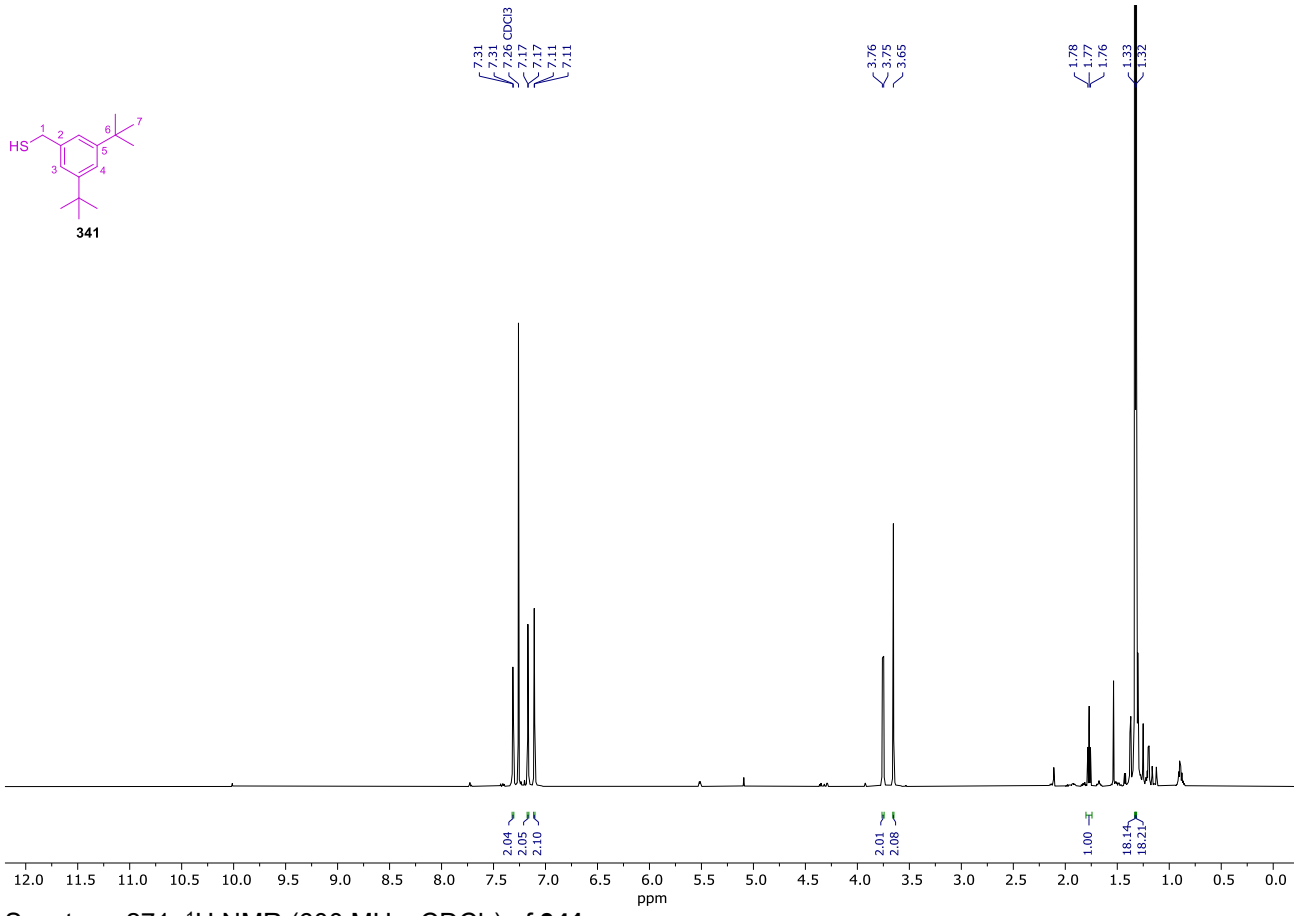

Spectrum 271. ^{1}H NMR (600 MHz, $CDCl_3$) of **341**.

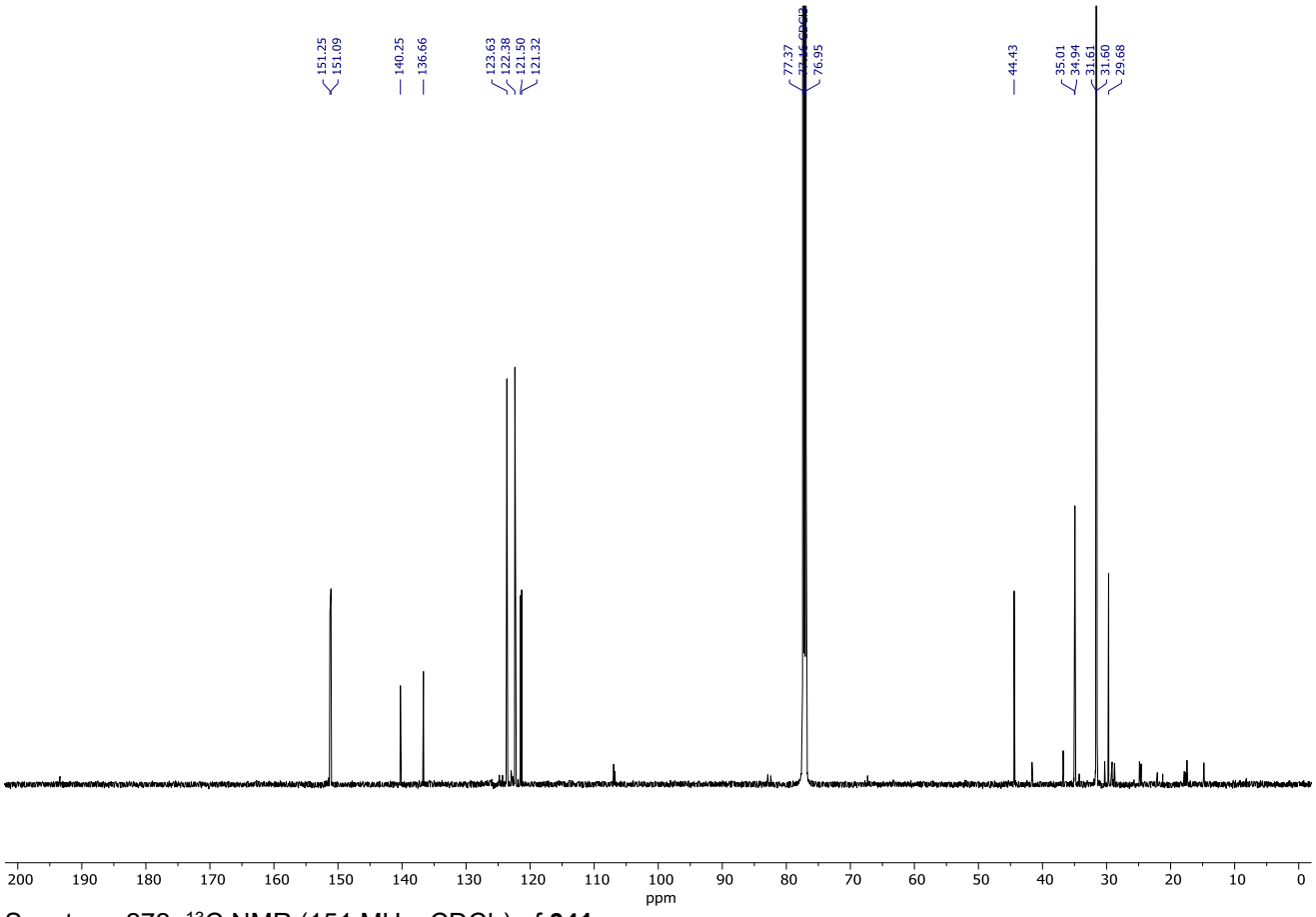

Spectrum 272. ^{13}C NMR (151 MHz, $CDCl_3$) of **341**.

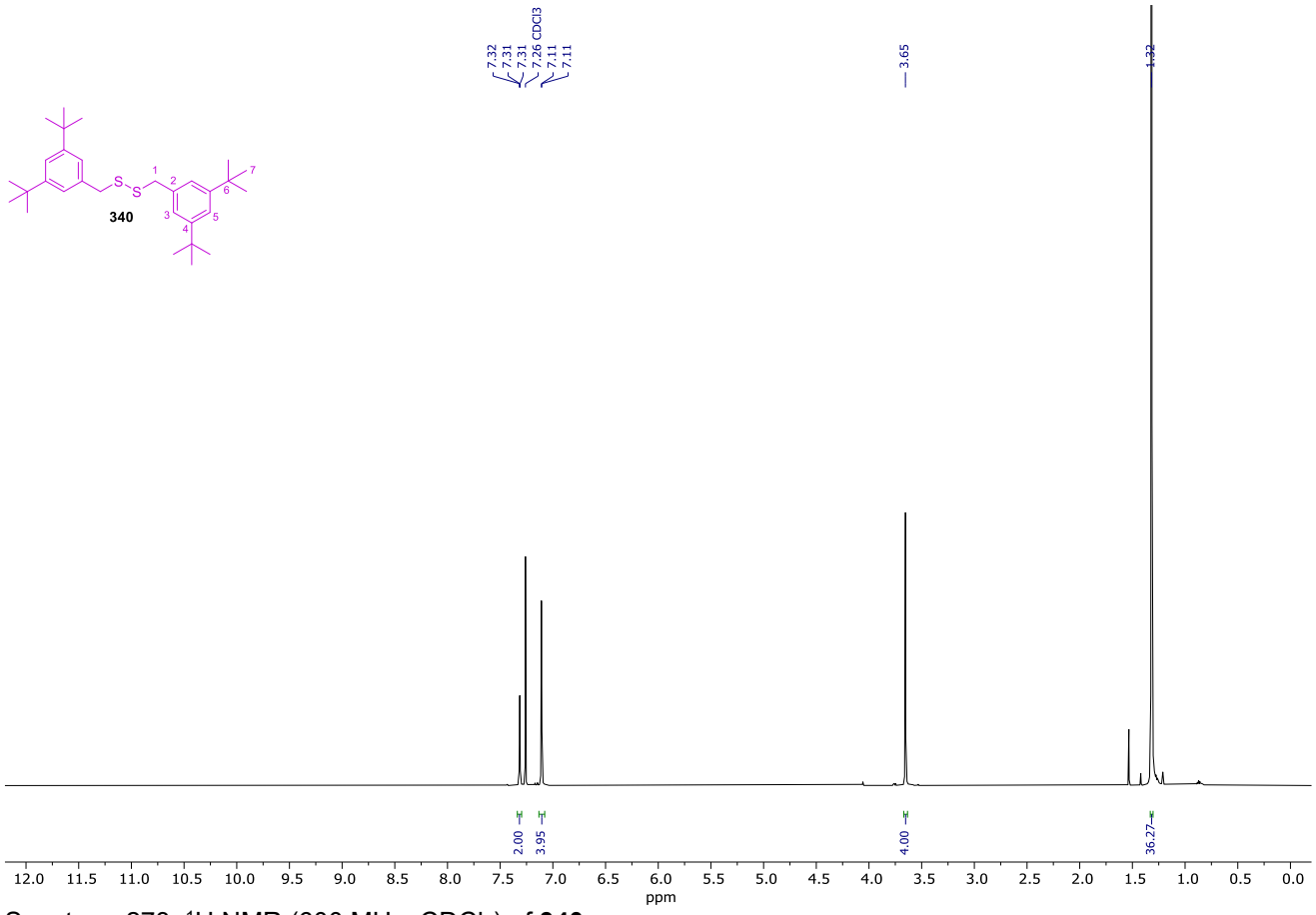

Spectrum 273. ^{1}H NMR (600 MHz, $CDCl_3$) of **340**.

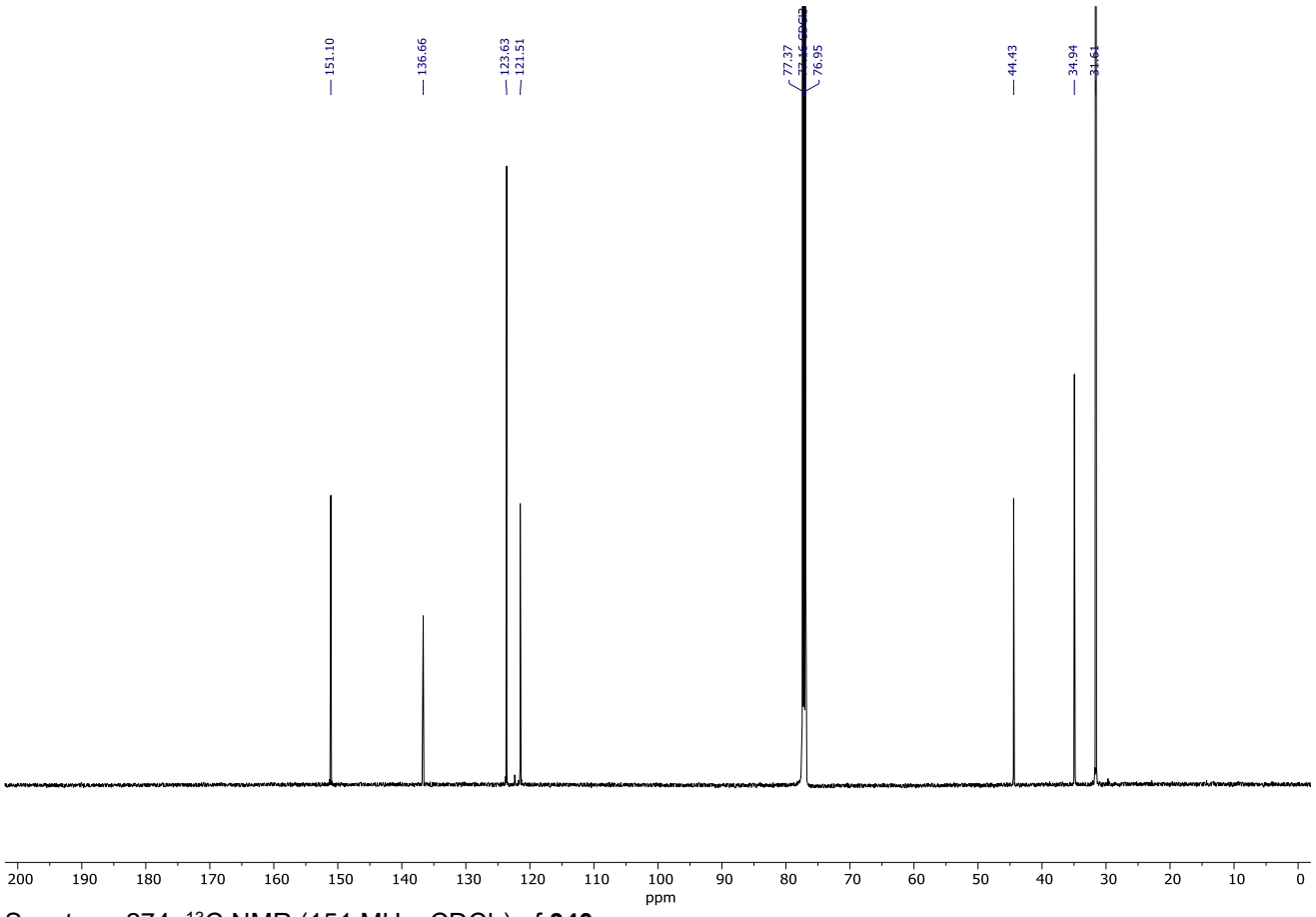

Spectrum 274. ^{13}C NMR (151 MHz, $CDCl_3$) of **340**.

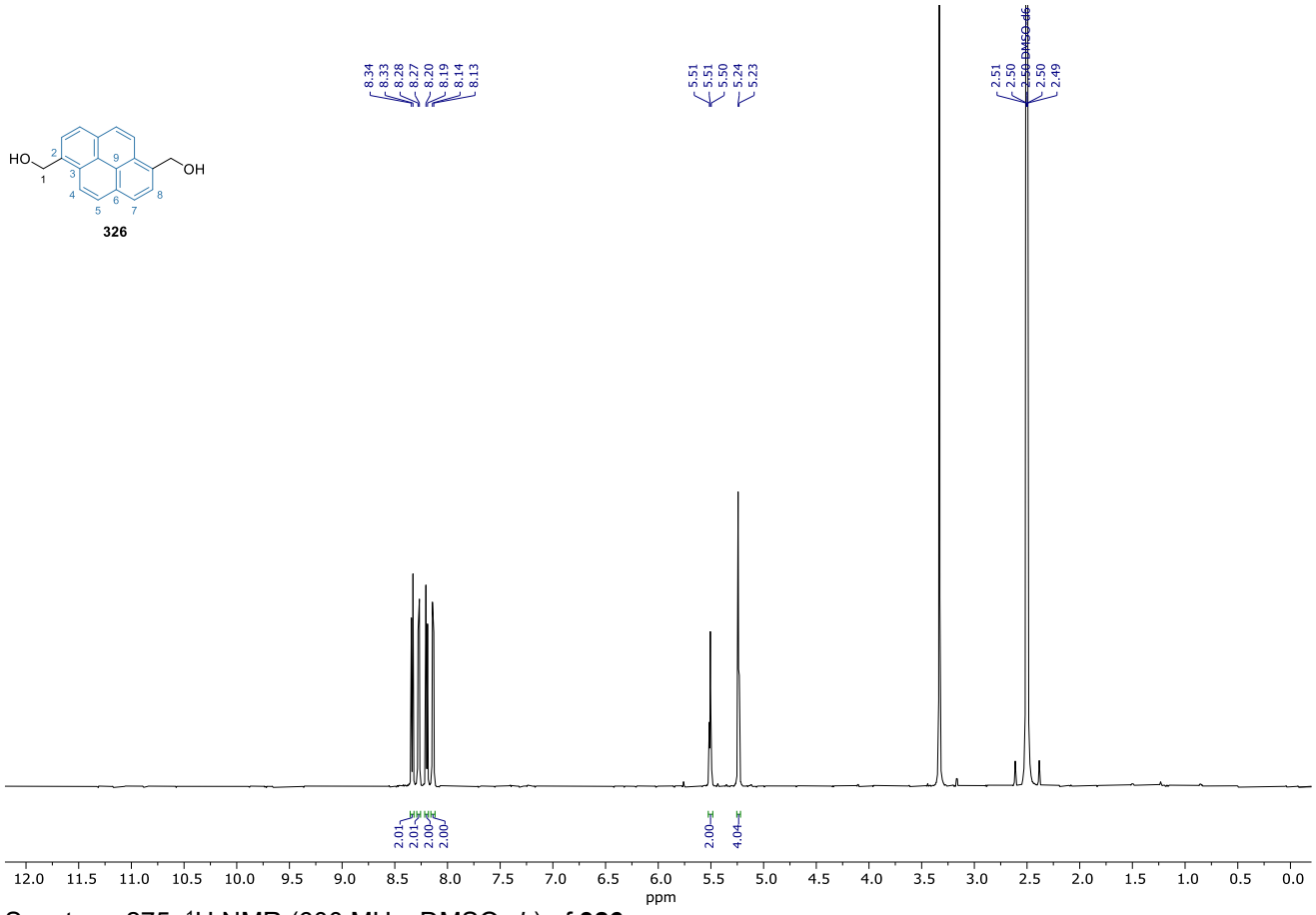

Spectrum 275. ^{1}H NMR (600 MHz, DMSO-d_6) of **326**.

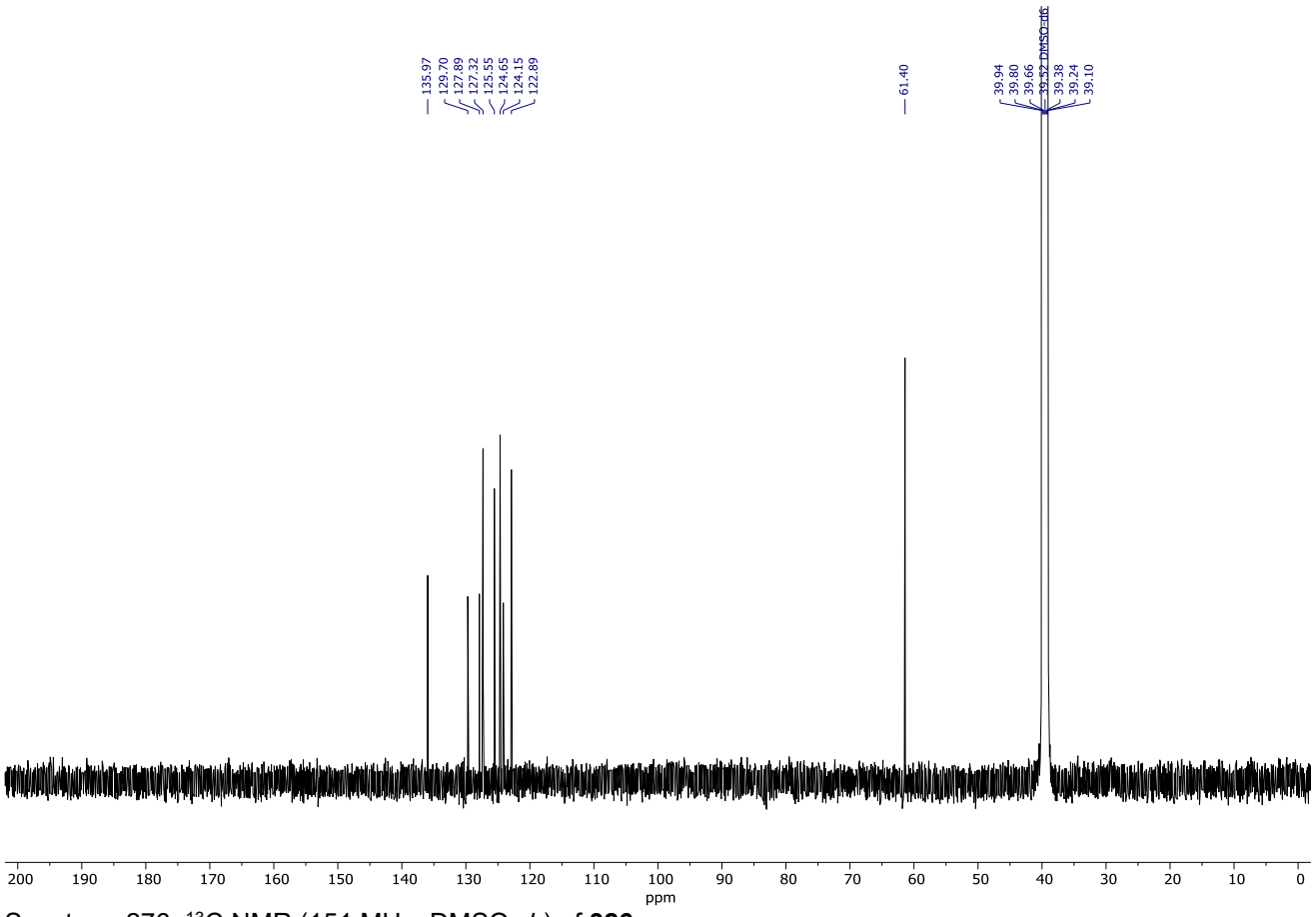

Spectrum 276. ^{13}C NMR (151 MHz, DMSO-d_6) of **326**.

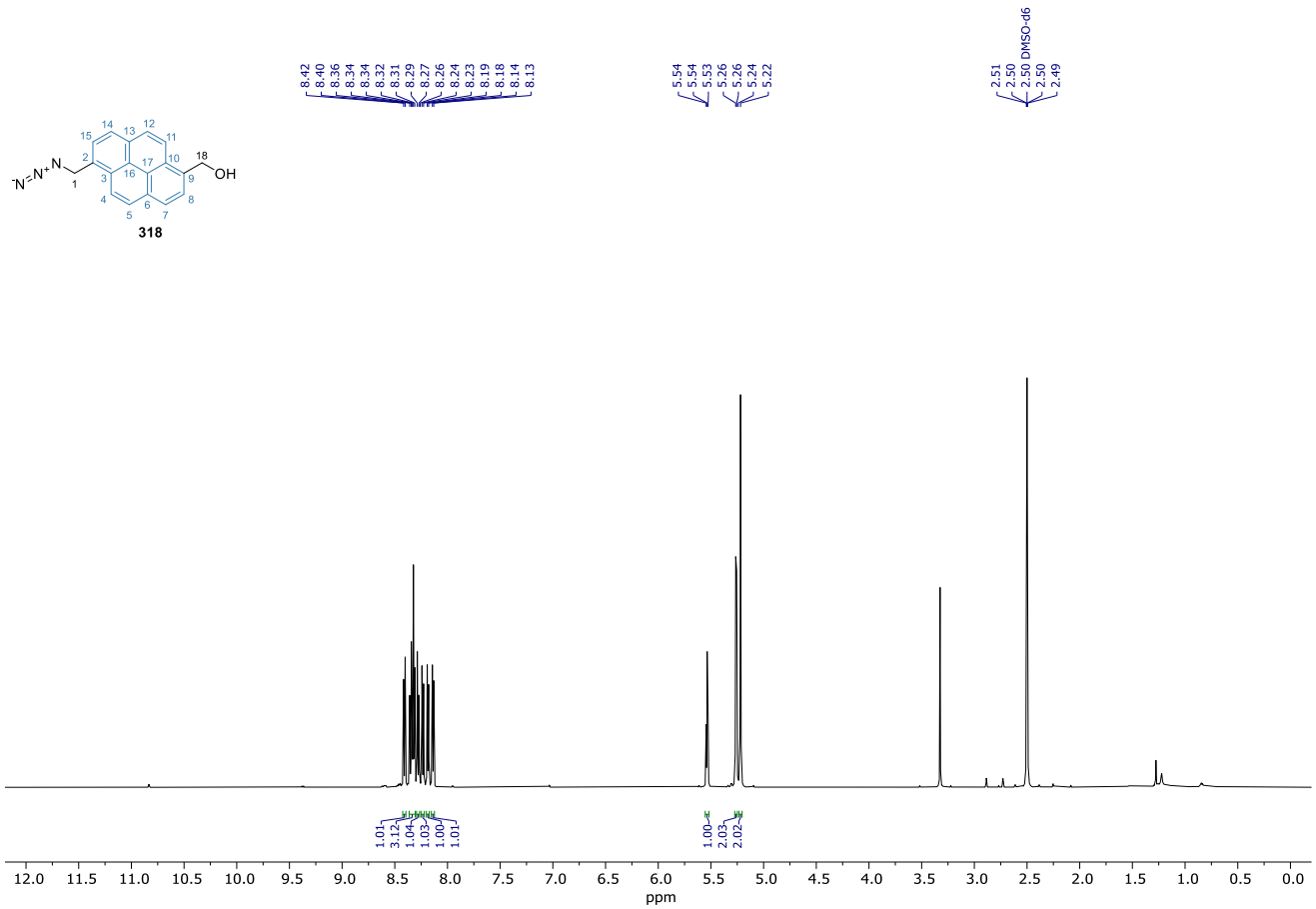

Spectrum 277. ^{1}H NMR (600 MHz, DMSO-d_6) of **318**.

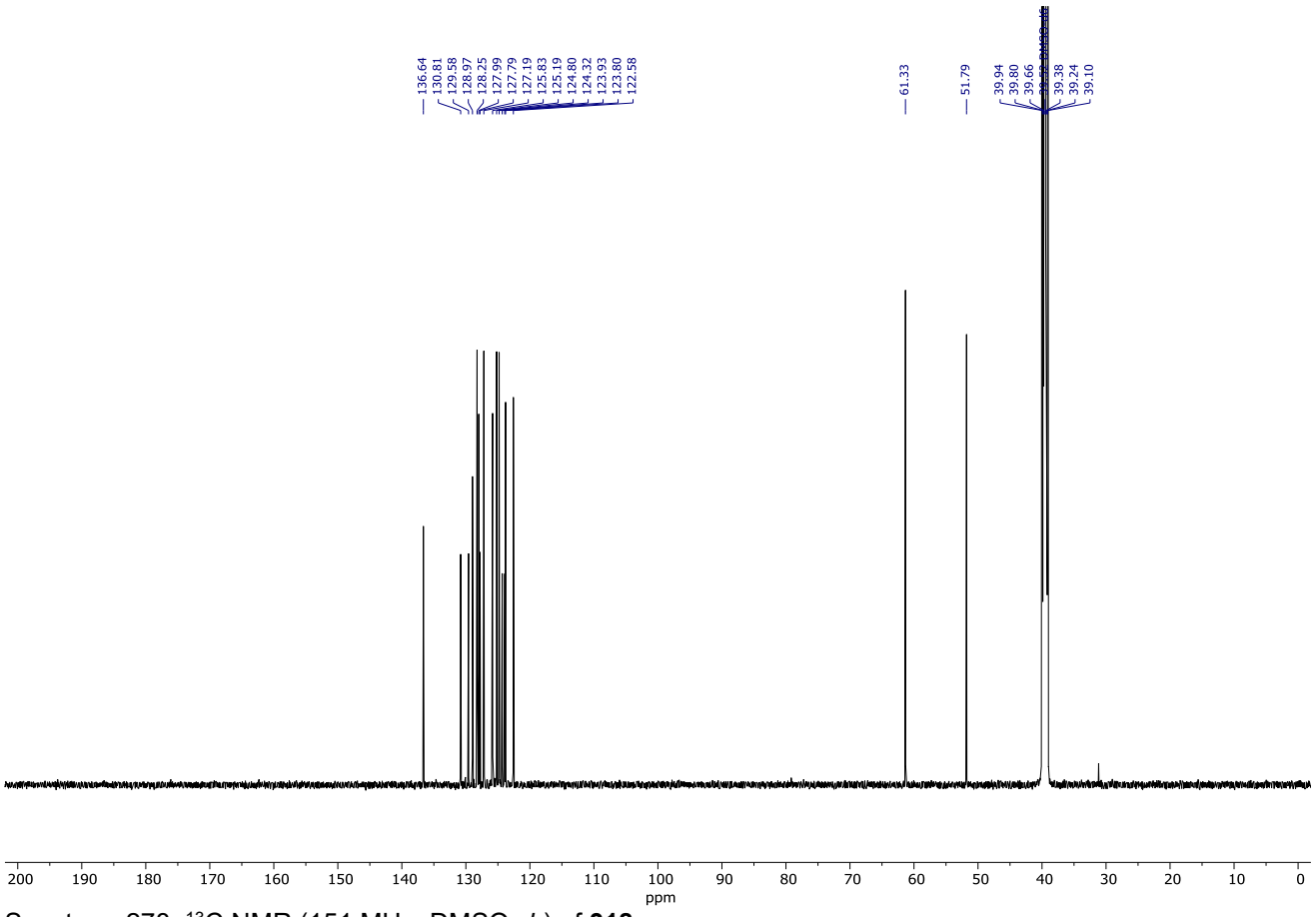

Spectrum 278. ^{13}C NMR (151 MHz, DMSO-d_6) of **318**.

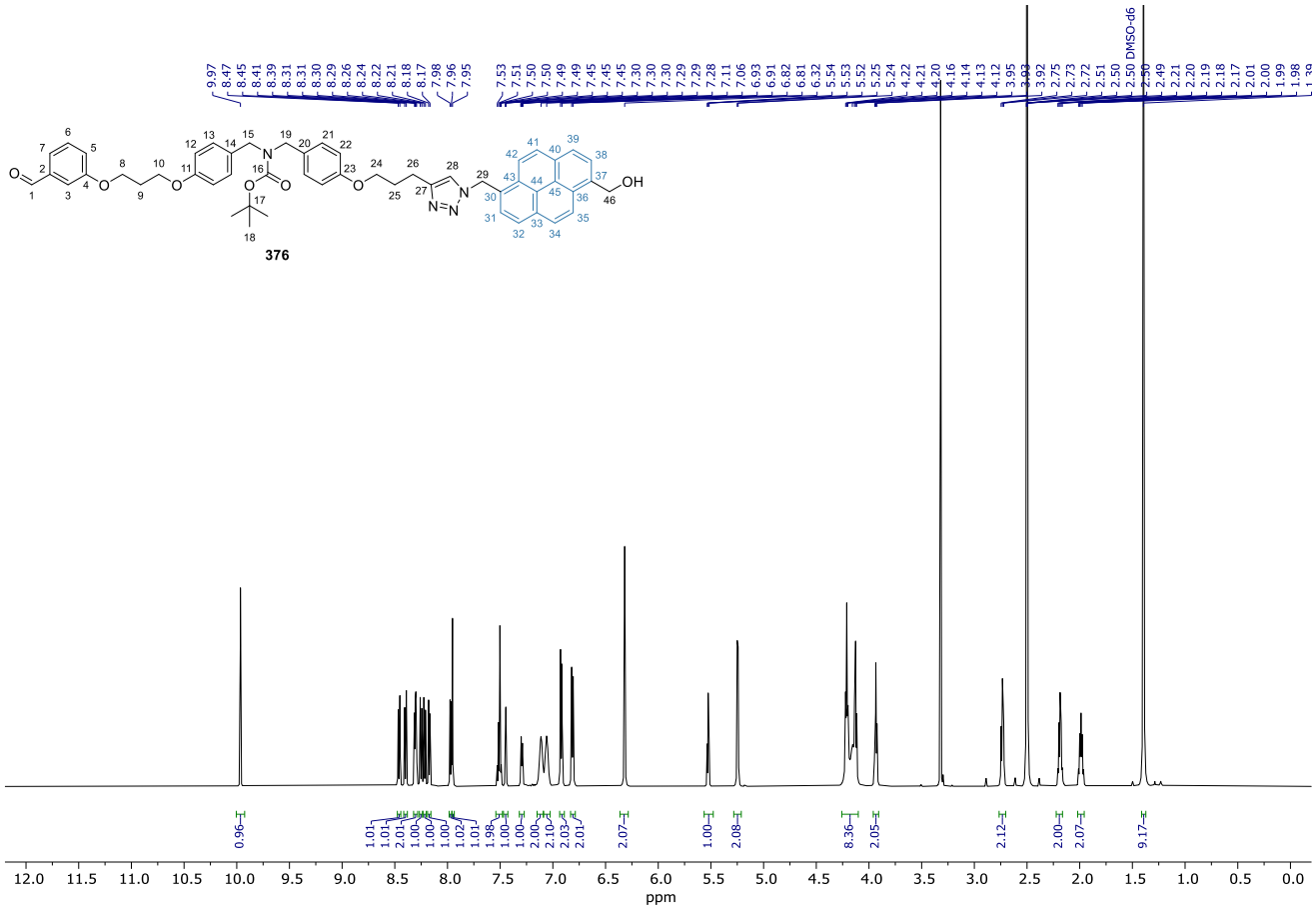

376

Spectrum 279. ^{1}H NMR (600 MHz, DMSO-d_6) of **376**.

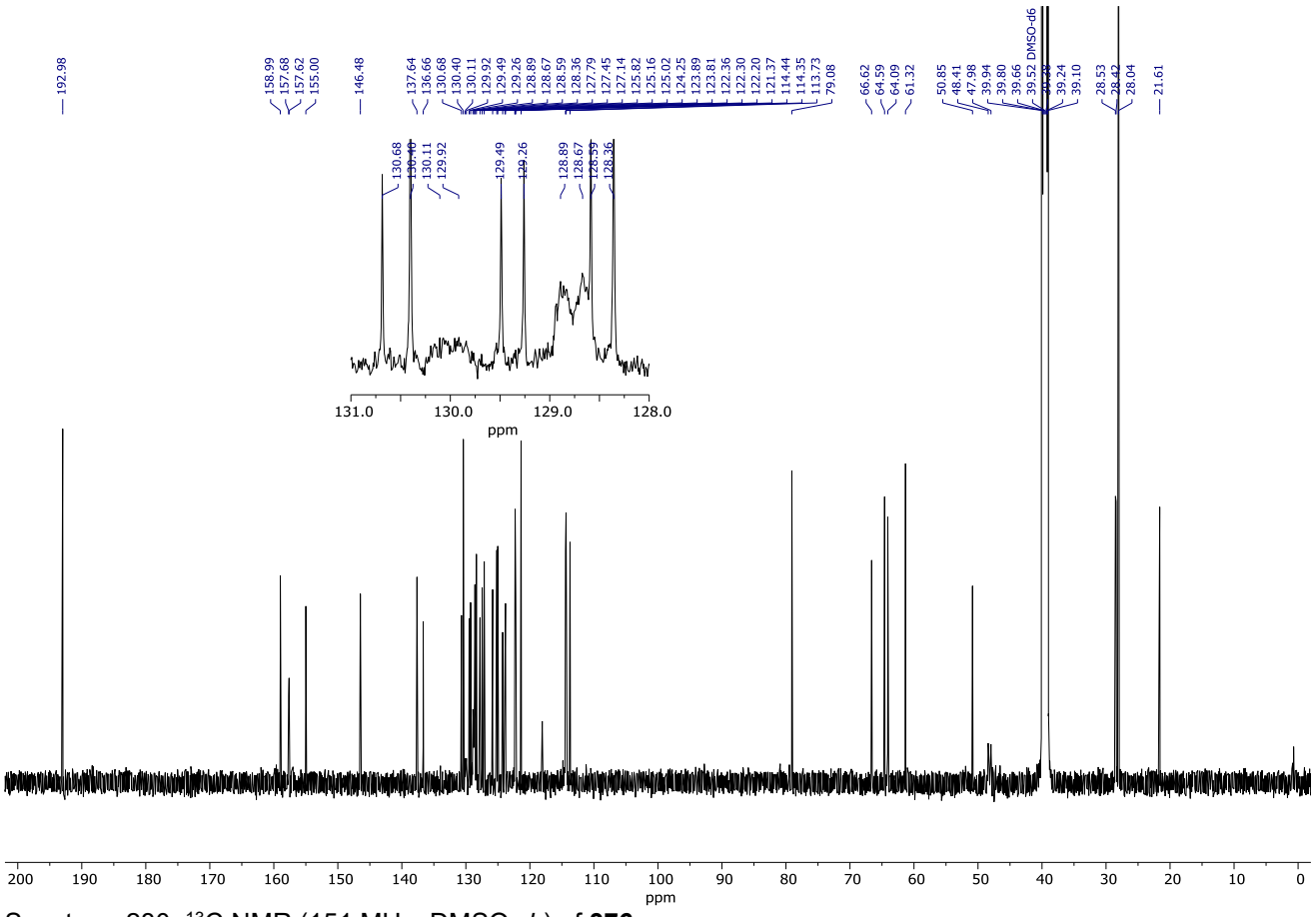

Spectrum 280. ^{13}C NMR (151 MHz, DMSO-d_6) of **376**.

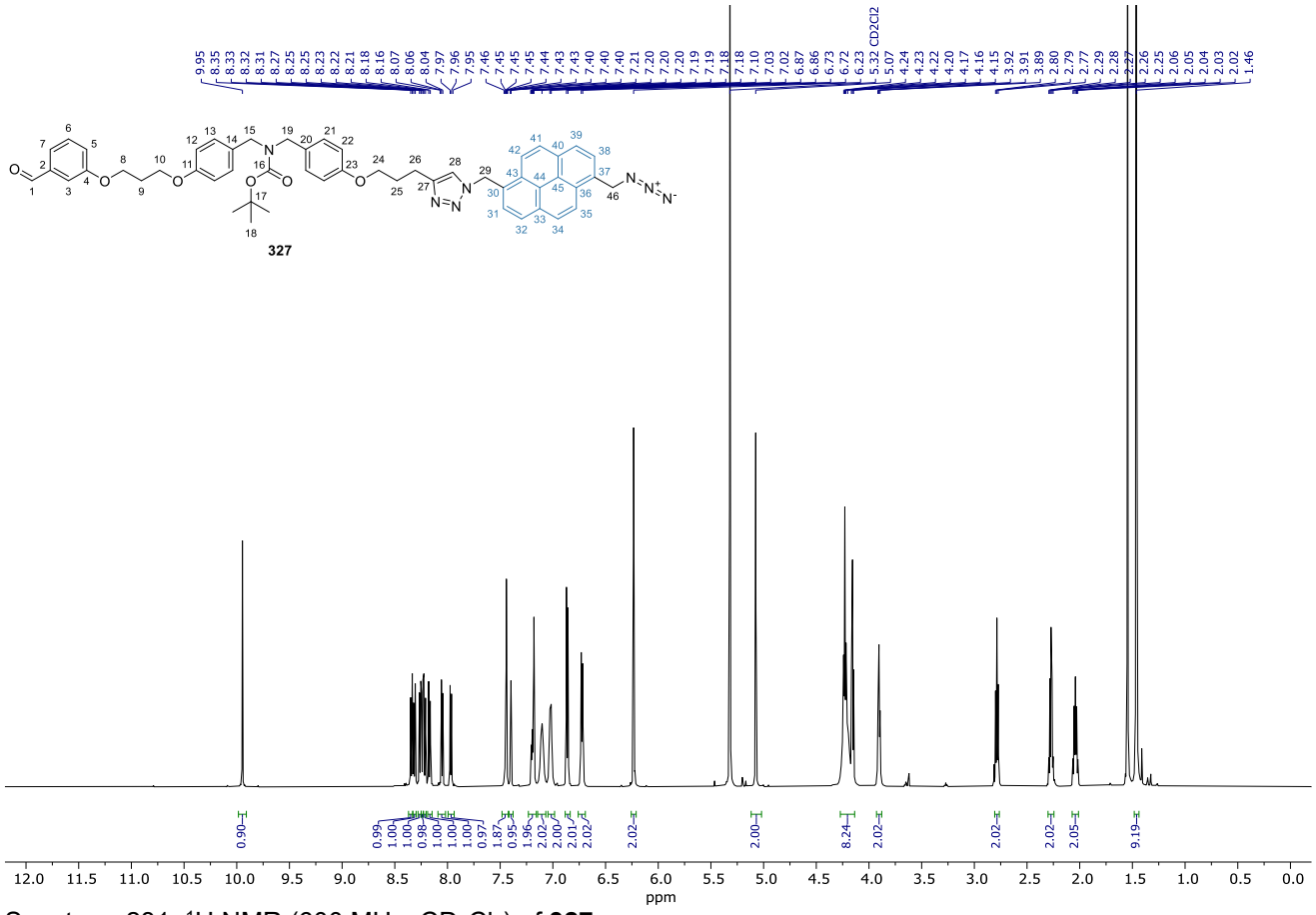

Spectrum 281. ^{1}H NMR (600 MHz, CD_2Cl_2) of **327**.

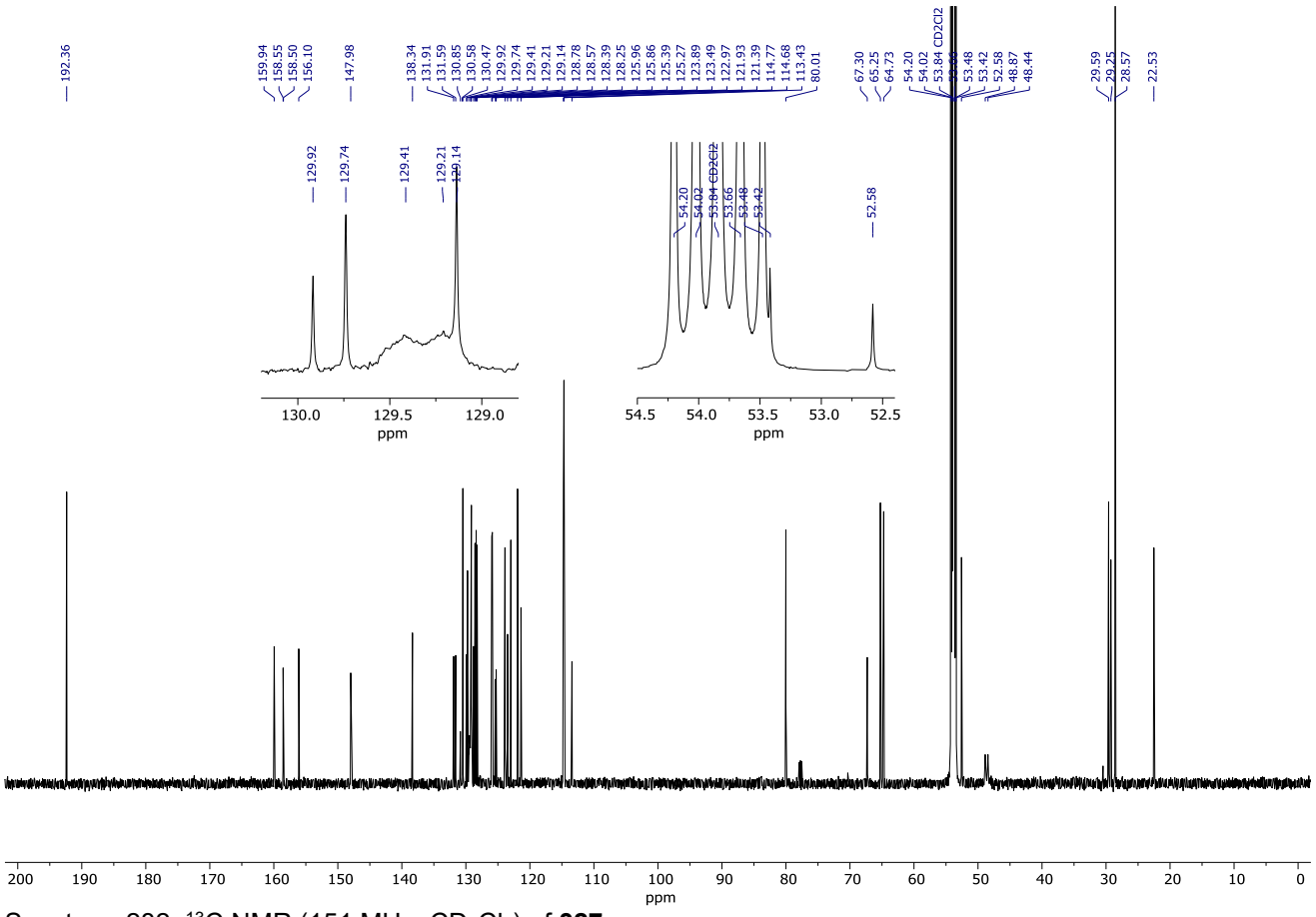

Spectrum 282. ^{13}C NMR (151 MHz, CD_2Cl_2) of **327**.

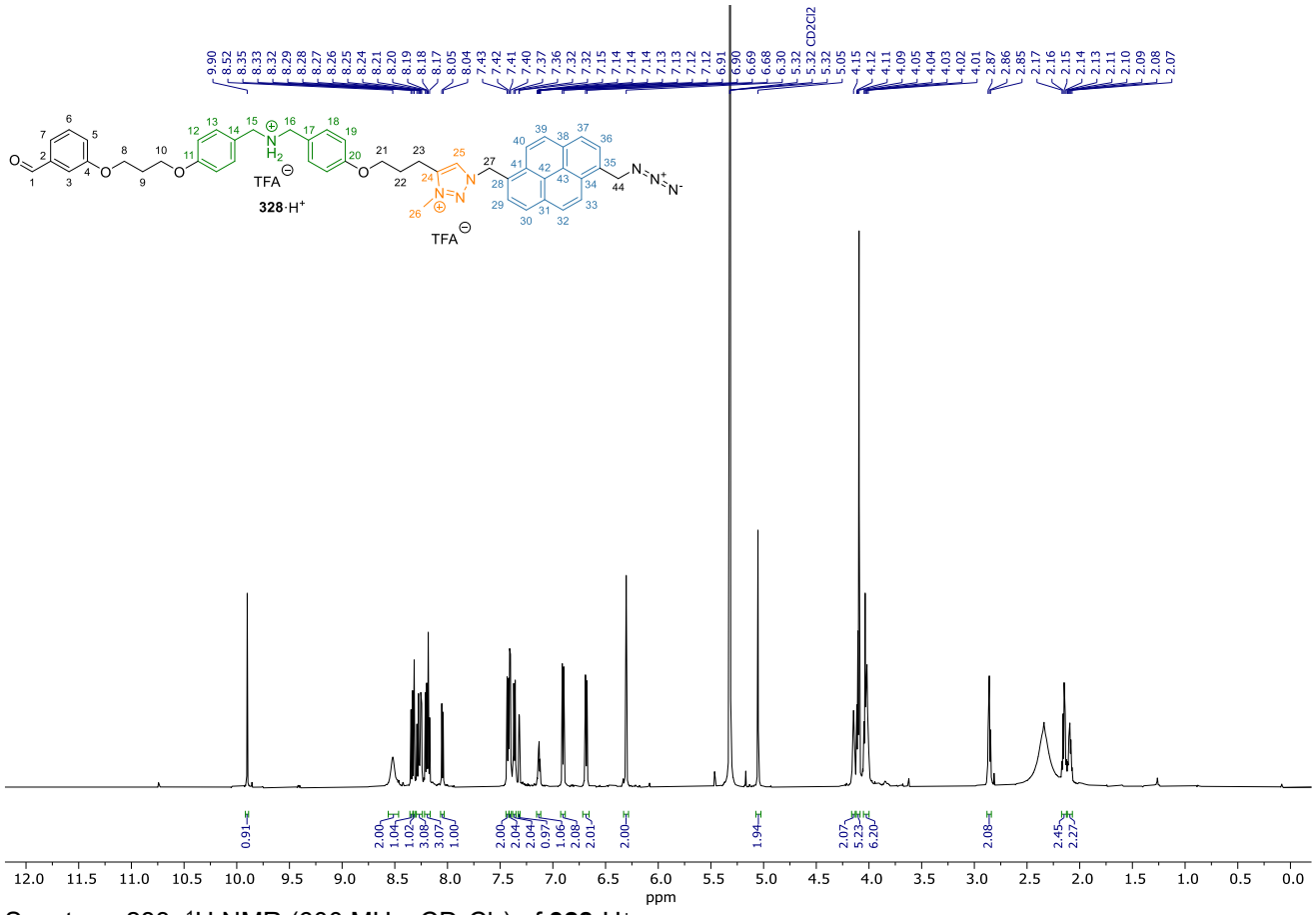

Spectrum 283. ^{1}H NMR (600 MHz, CD_2Cl_2) of **328**·H^+.

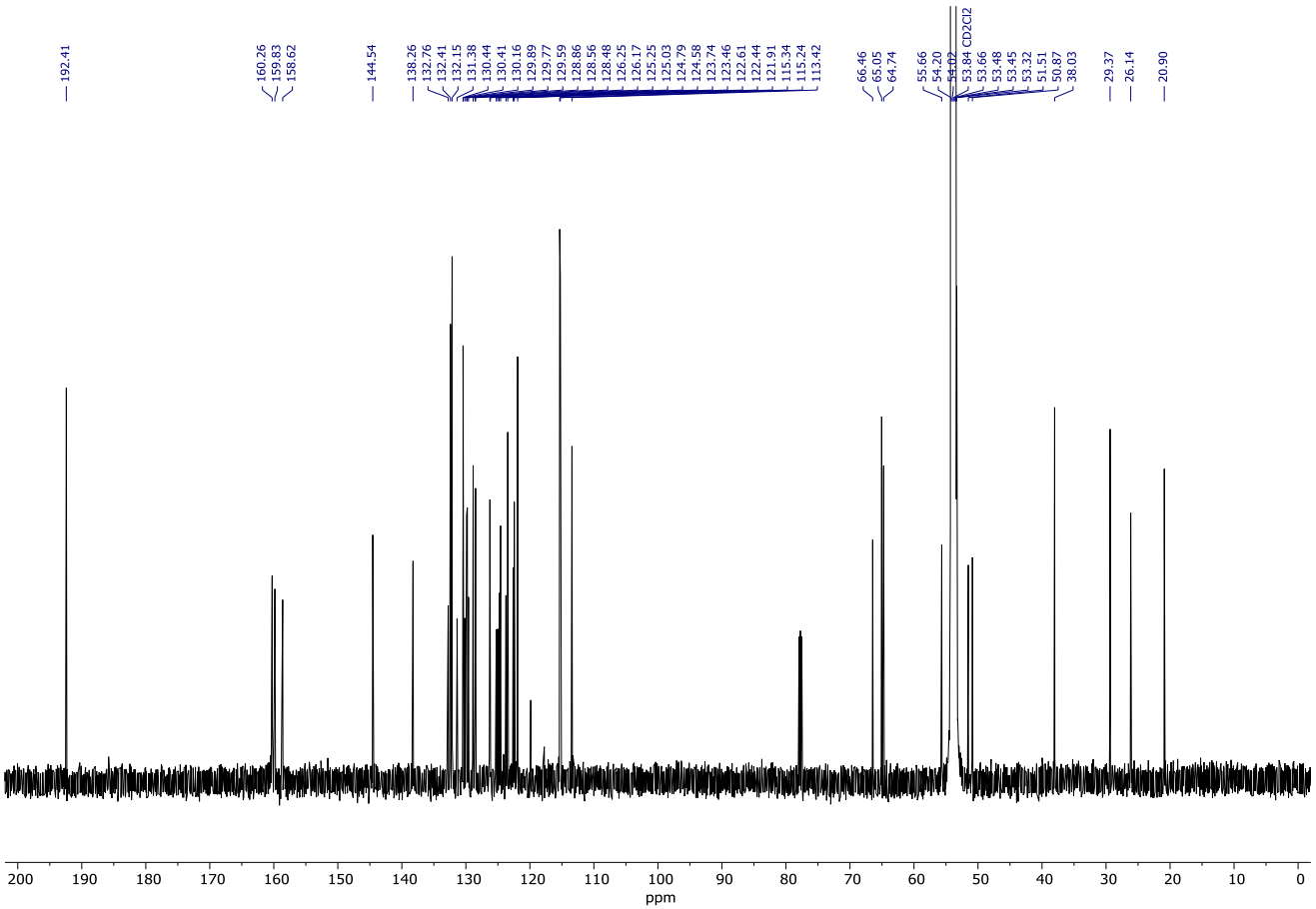

Spectrum 284. ^{13}C NMR (151 MHz, CD_2Cl_2) of **328**·H^+.

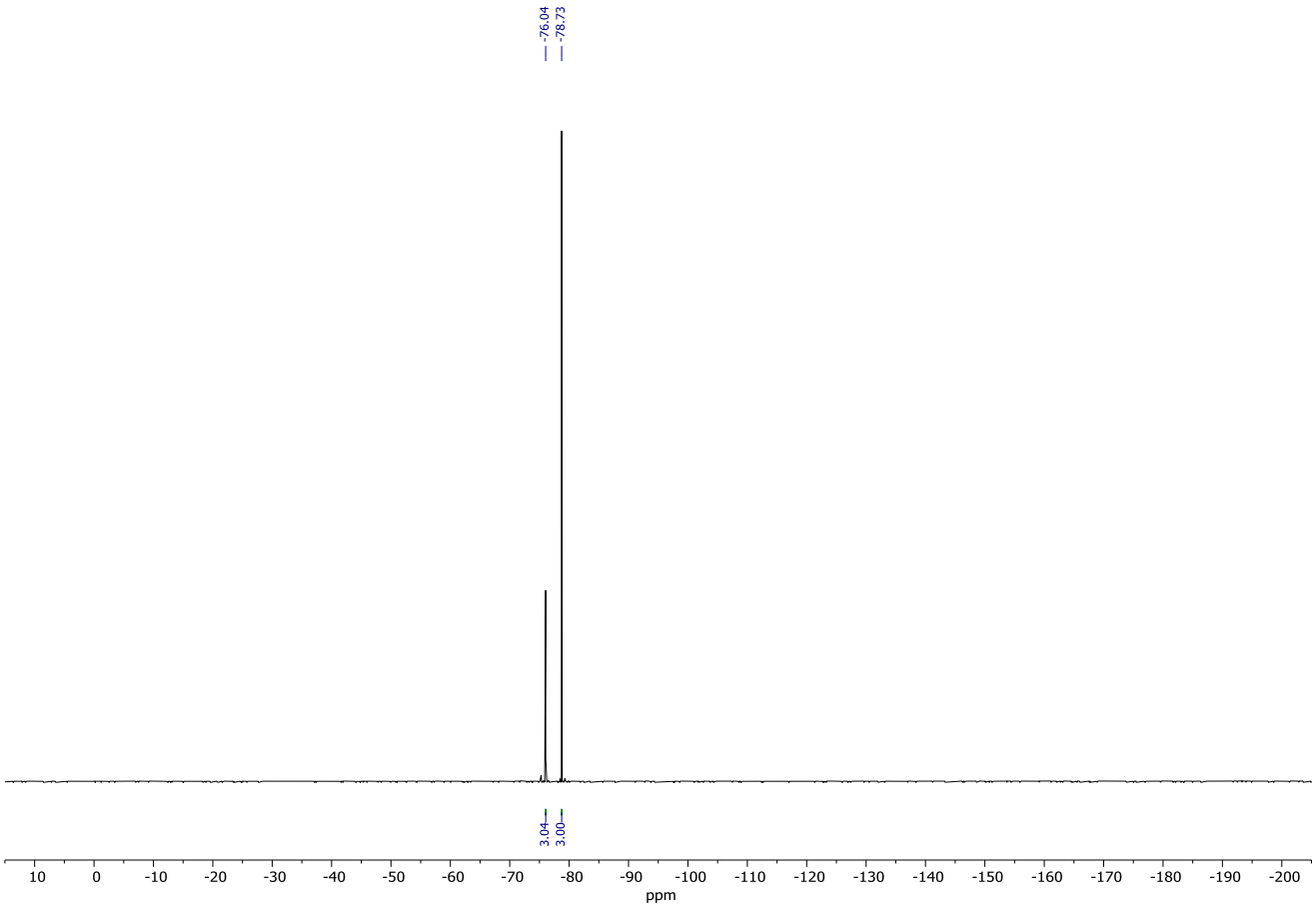

Spectrum 285. ^{19}F NMR (376 MHz, CD_2Cl_2) of **328**·H^+.

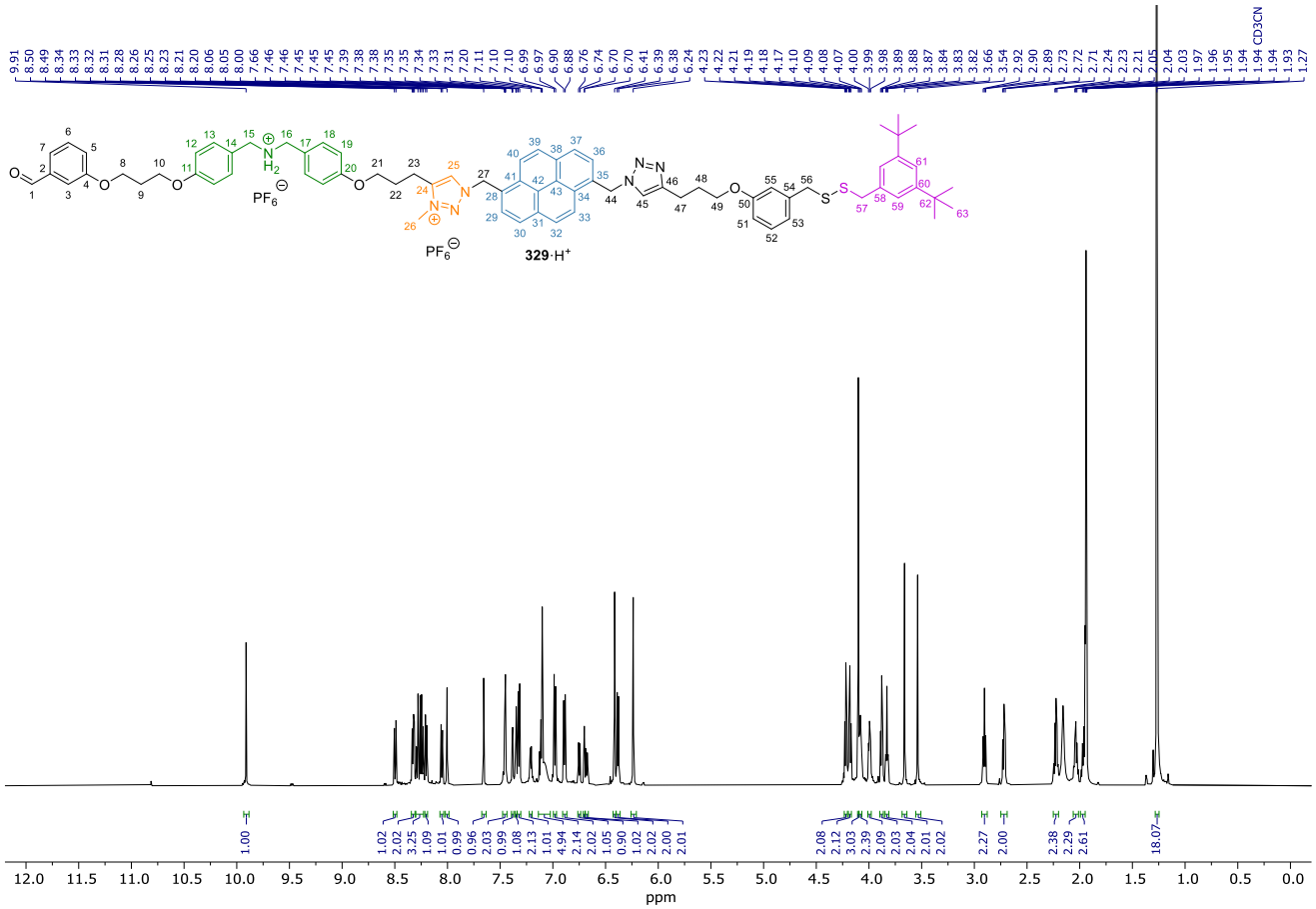

Spectrum 286. ^{1}H NMR (600 MHz, CD_3CN) of **329**·H^+.

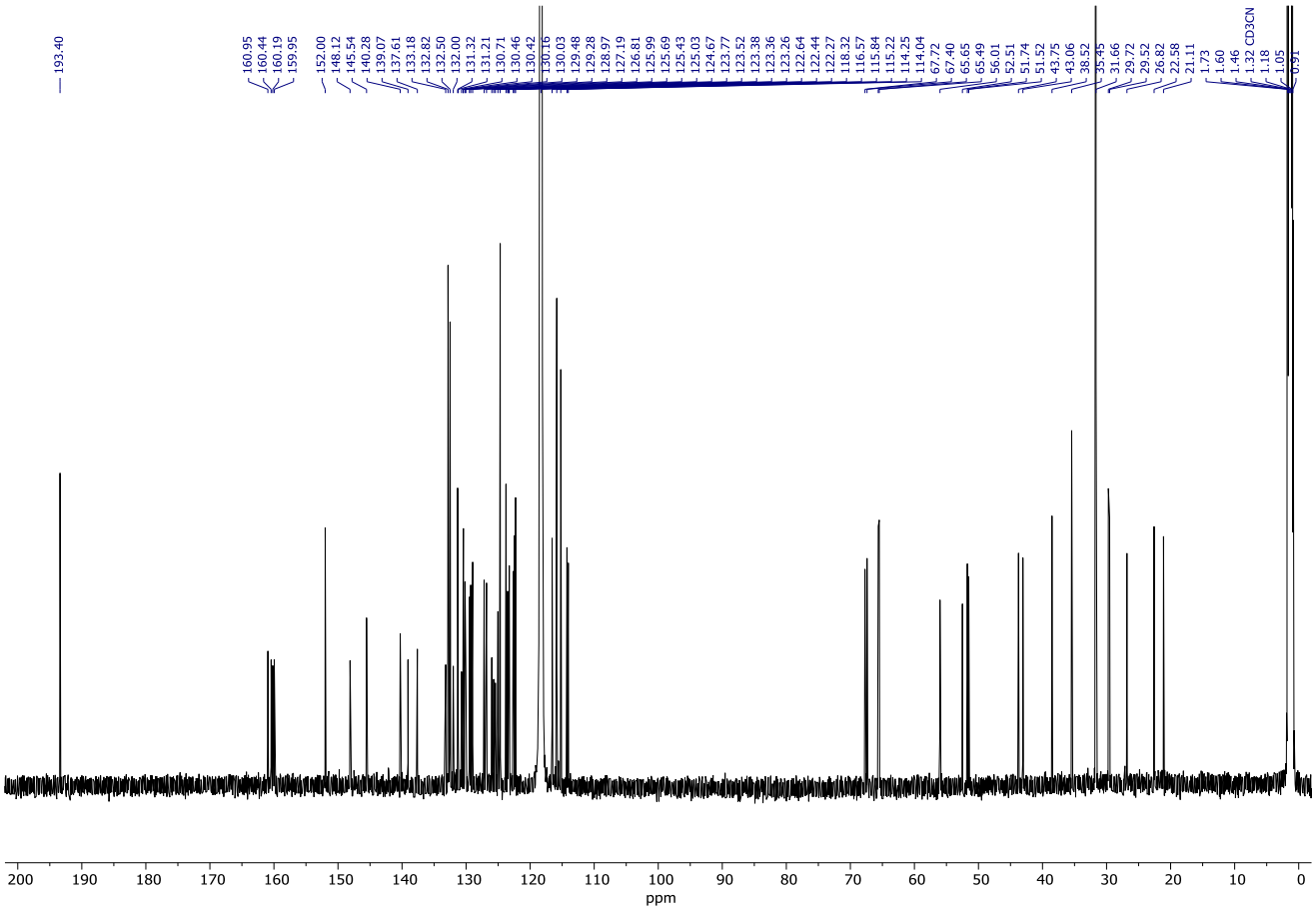

Spectrum 287. ^{13}C NMR (151 MHz, CD_3CN) of **329**·H^+.

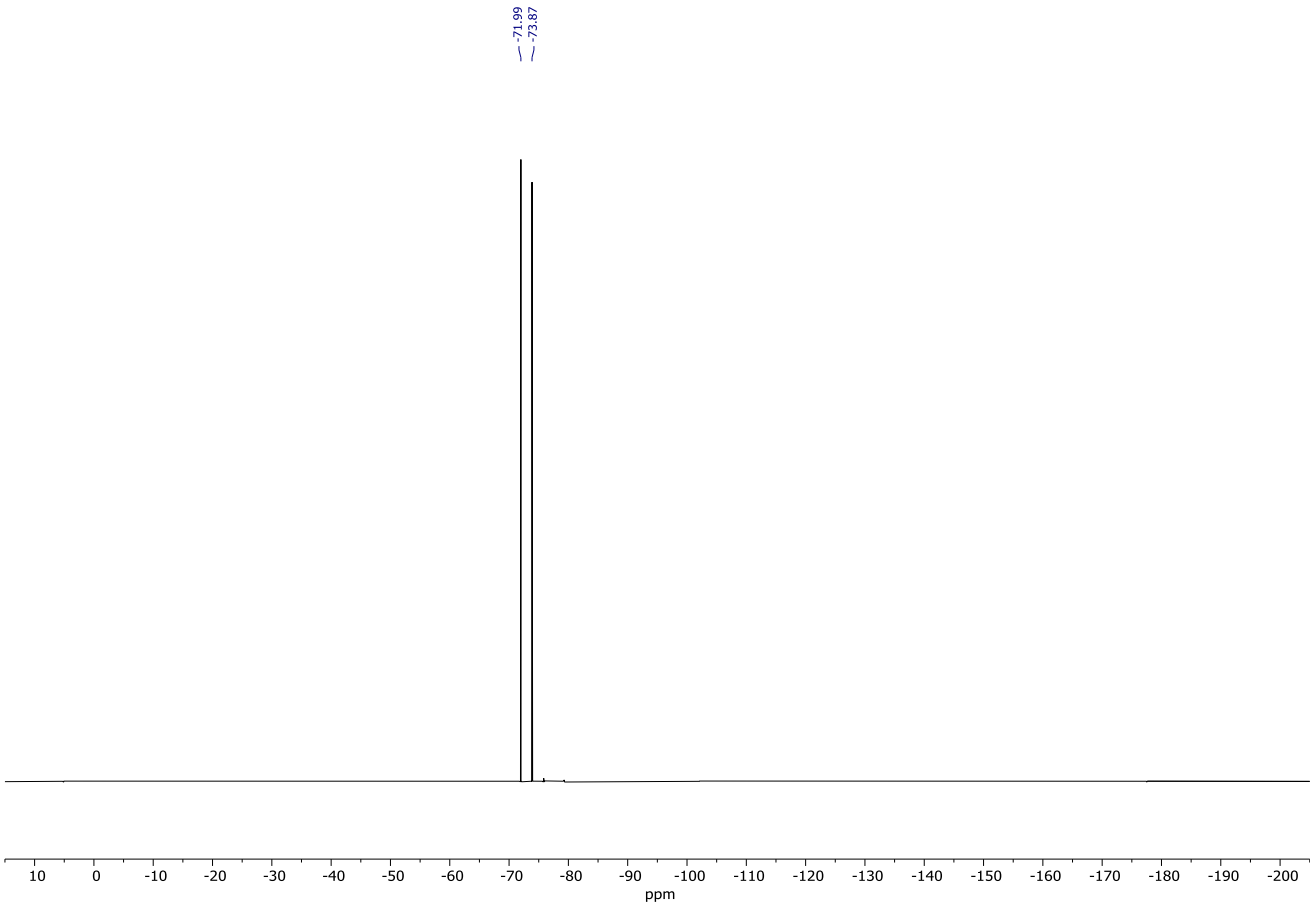

Spectrum 288. ^{19}F NMR (376 MHz, CD_3CN) of **329**·H^+.

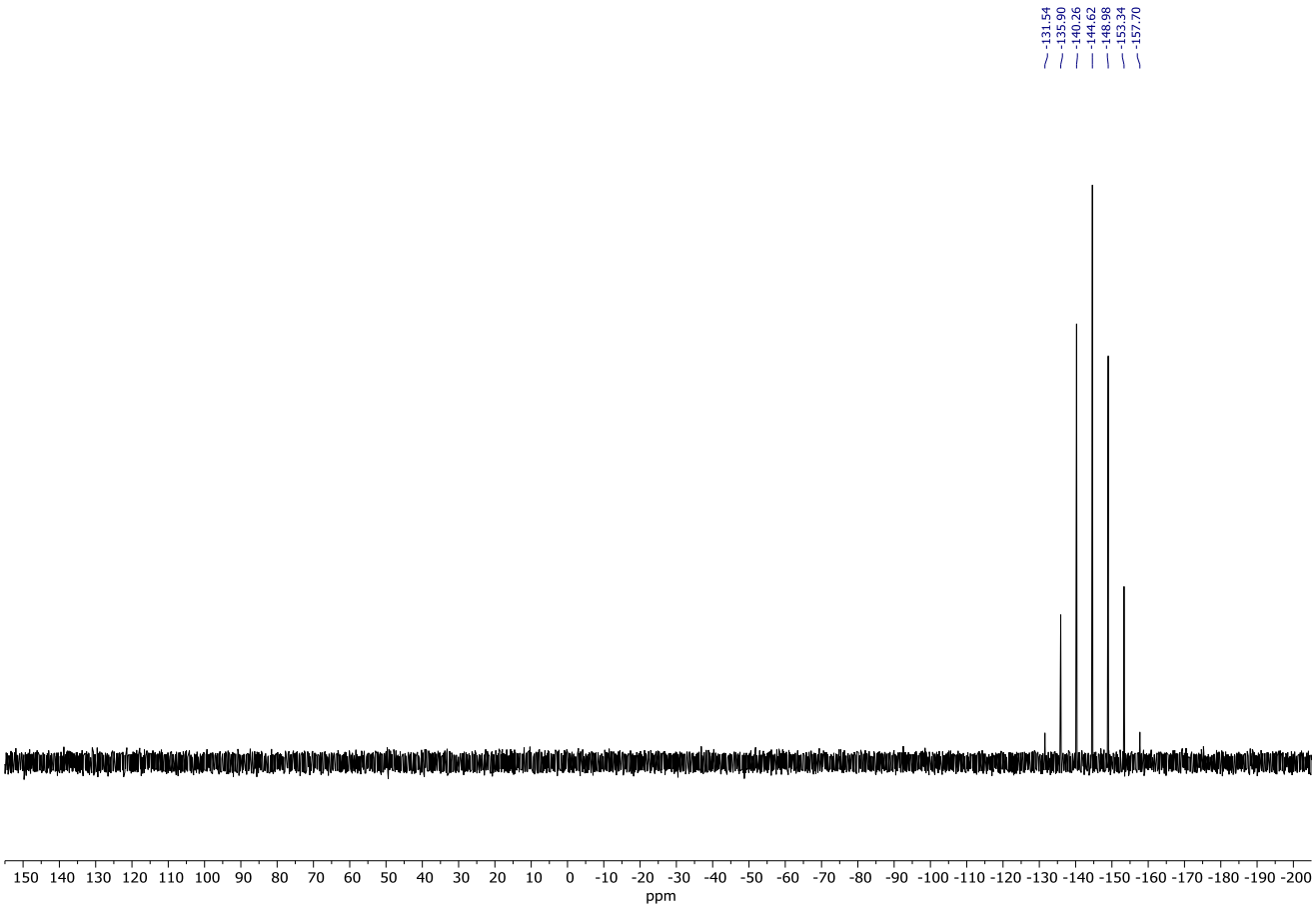

Spectrum 289. ^{31}P NMR (162 MHz, CD_3CN) of **329**·H^+.

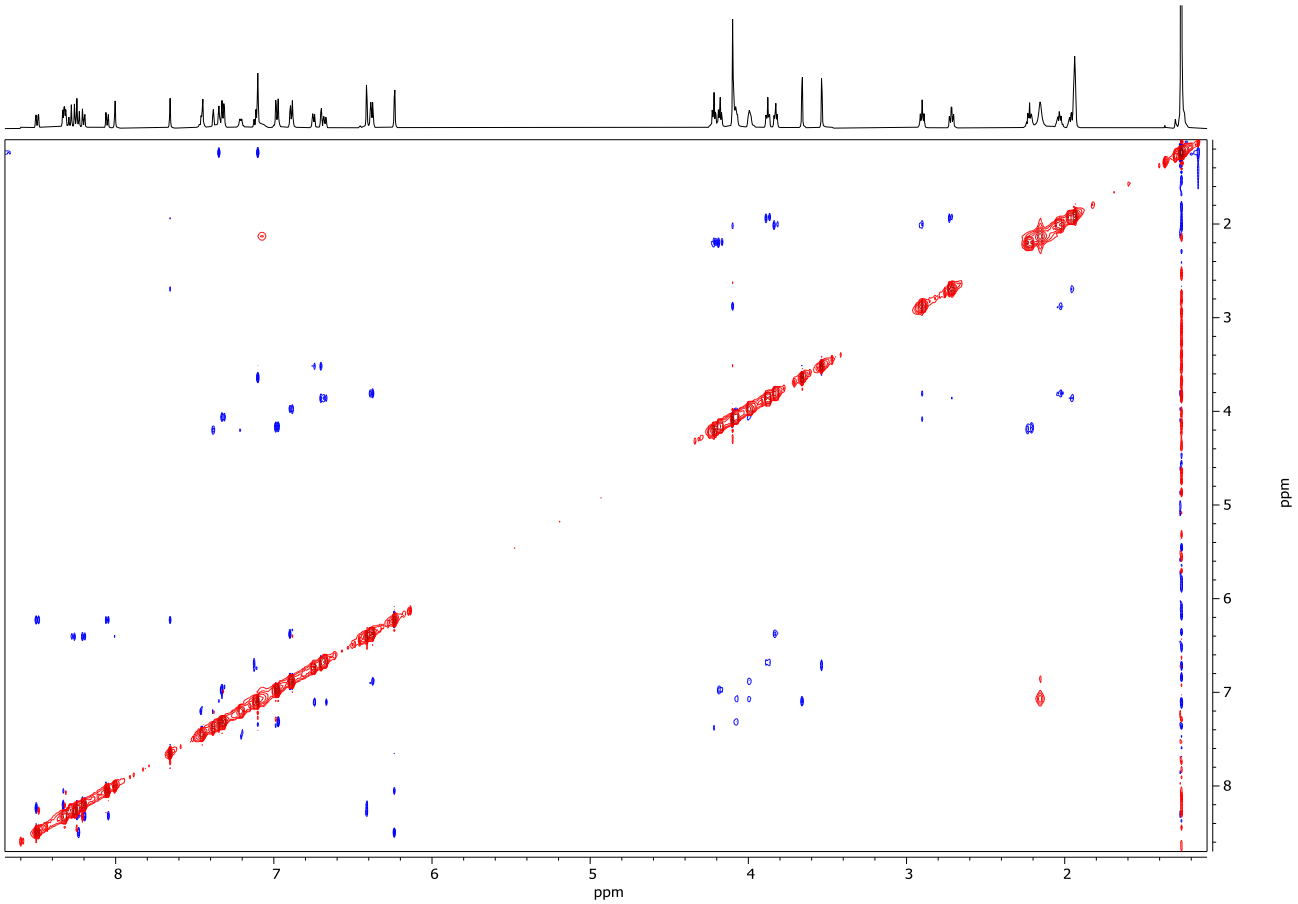

Spectrum 290. 2D NOESY (600 MHz, CD_3CN) of **329**·H^+. Data was recorded with 500 ms mixing time and a relaxation delay of 2.00 s. 4K data points were collected for 256 increments of 8 scans.

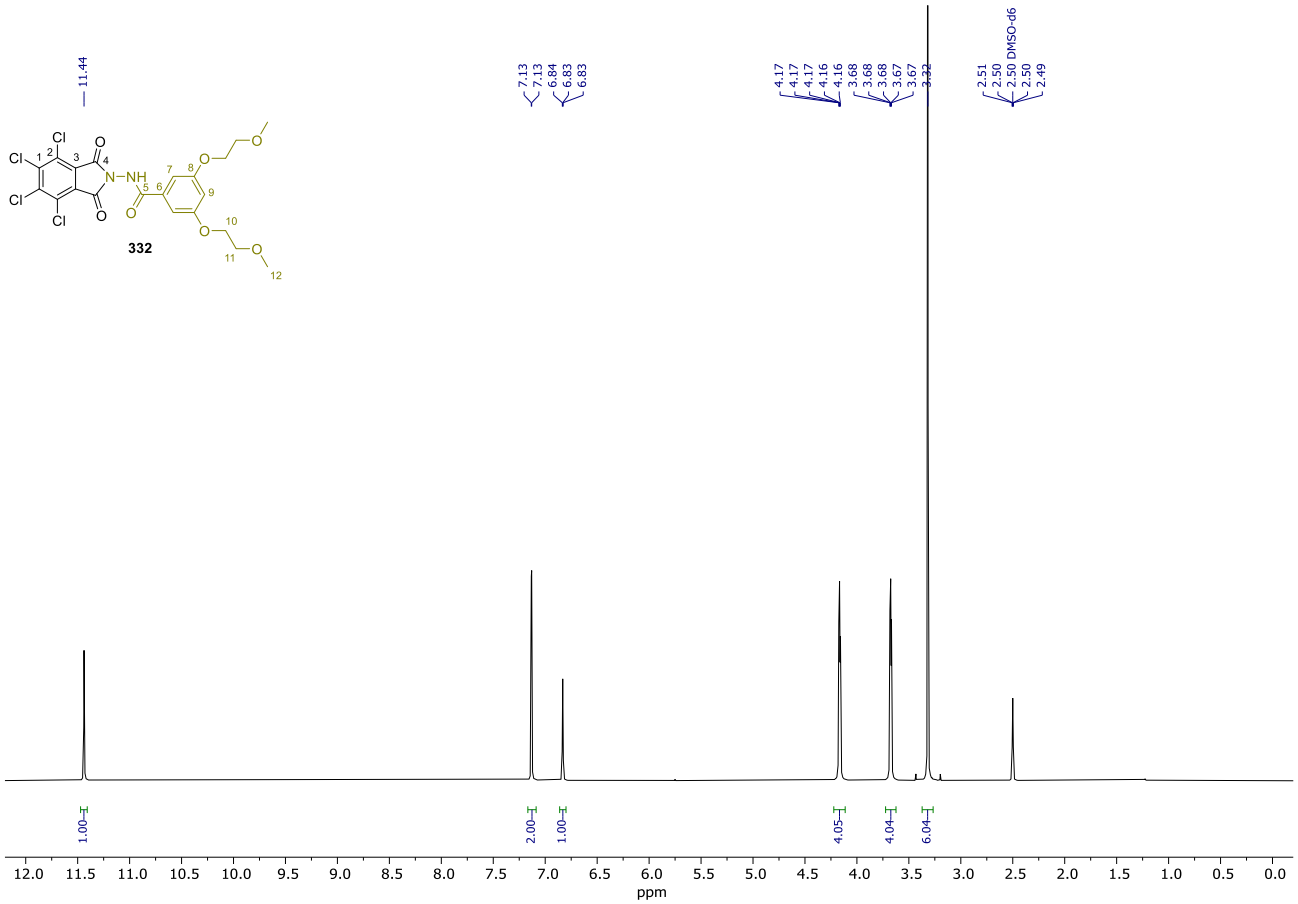

Spectrum 291. ^{1}H NMR (600 MHz, DMSO-d_6) of **332**.

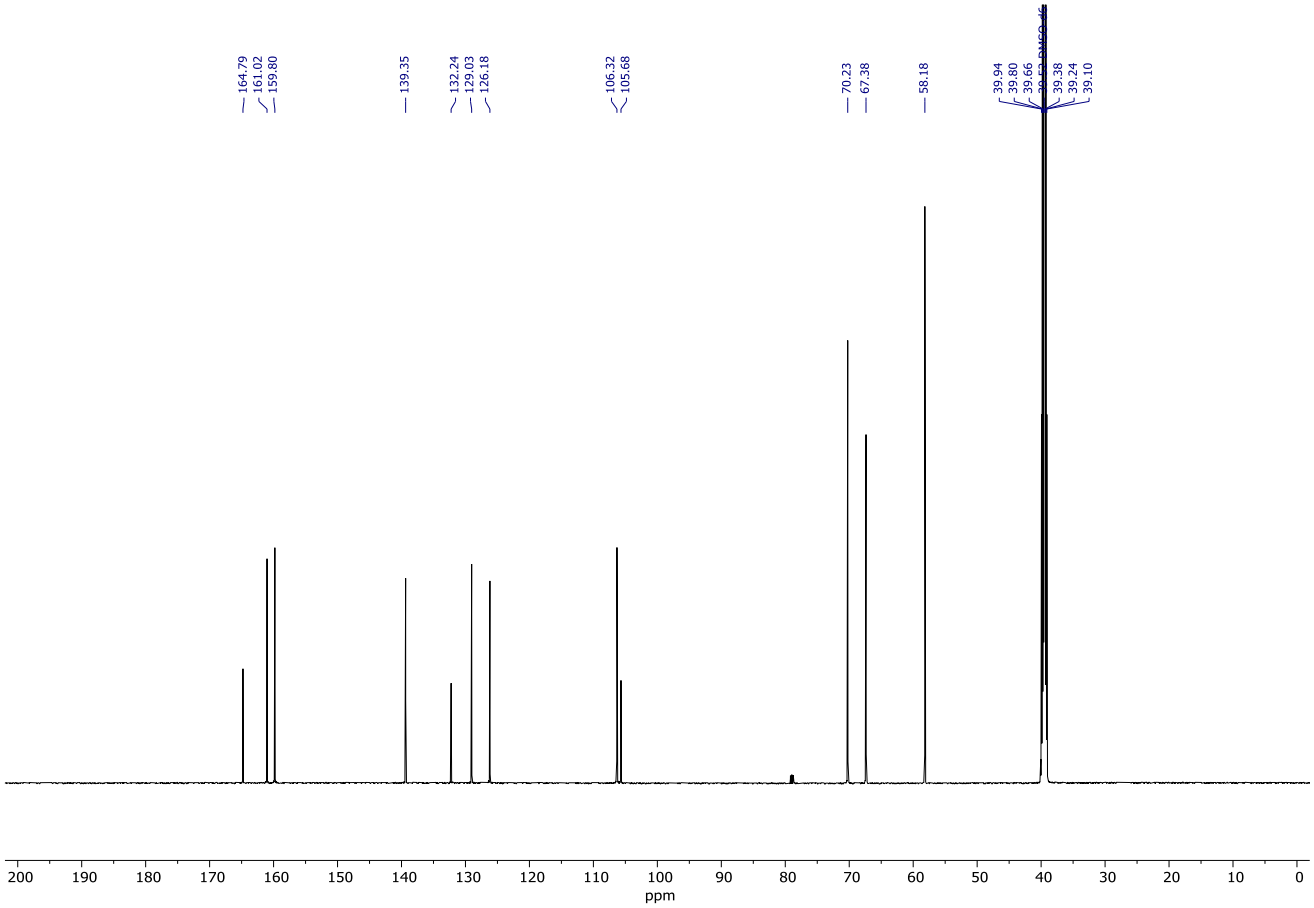

Spectrum 292. ^{13}C NMR (151 MHz, DMSO-d_6) of **332**.

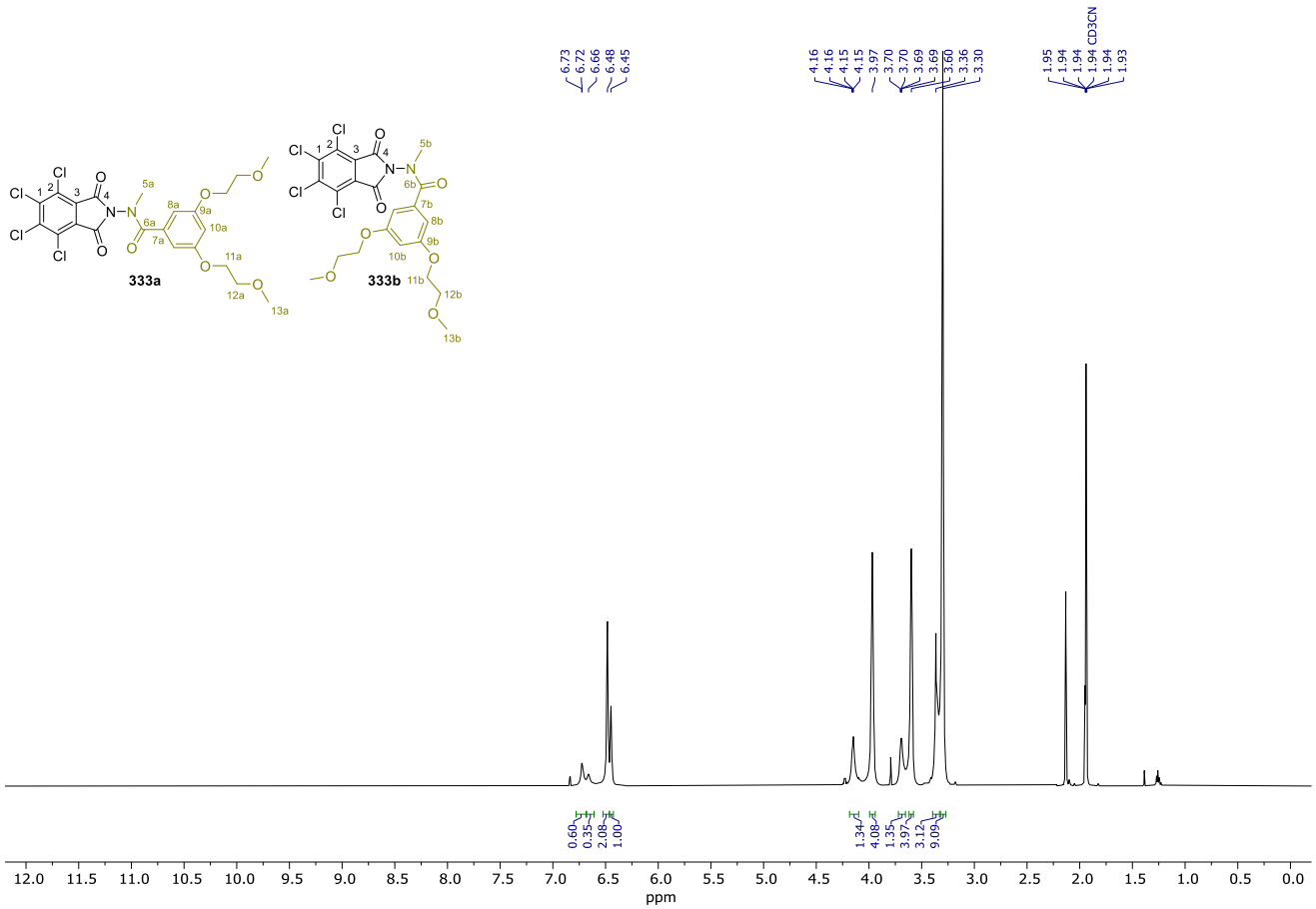

Spectrum 293. ^{1}H NMR (600 MHz, CD_3CN) of **333**.

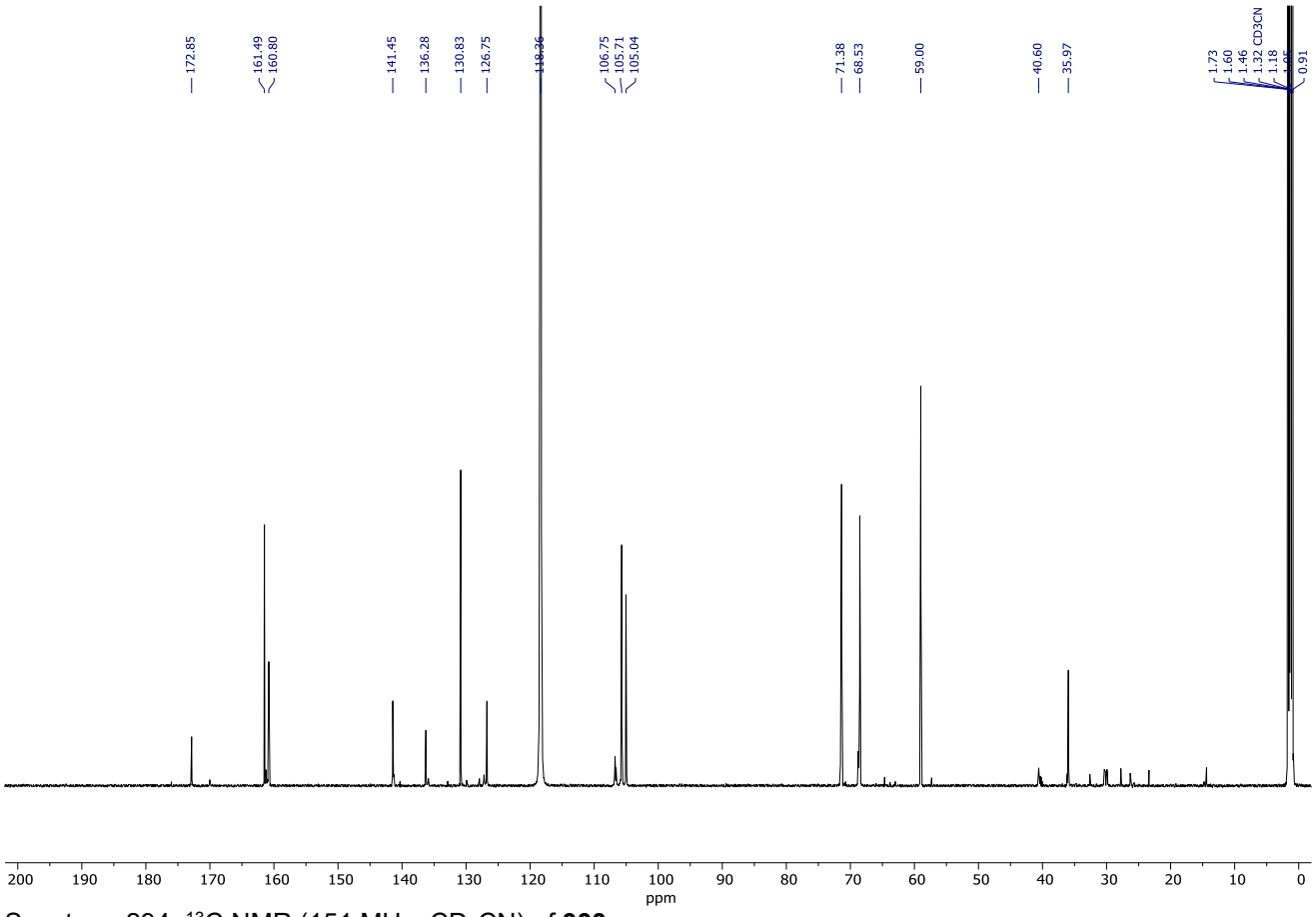

Spectrum 294. ^{13}C NMR (151 MHz, CD_3CN) of **333**.

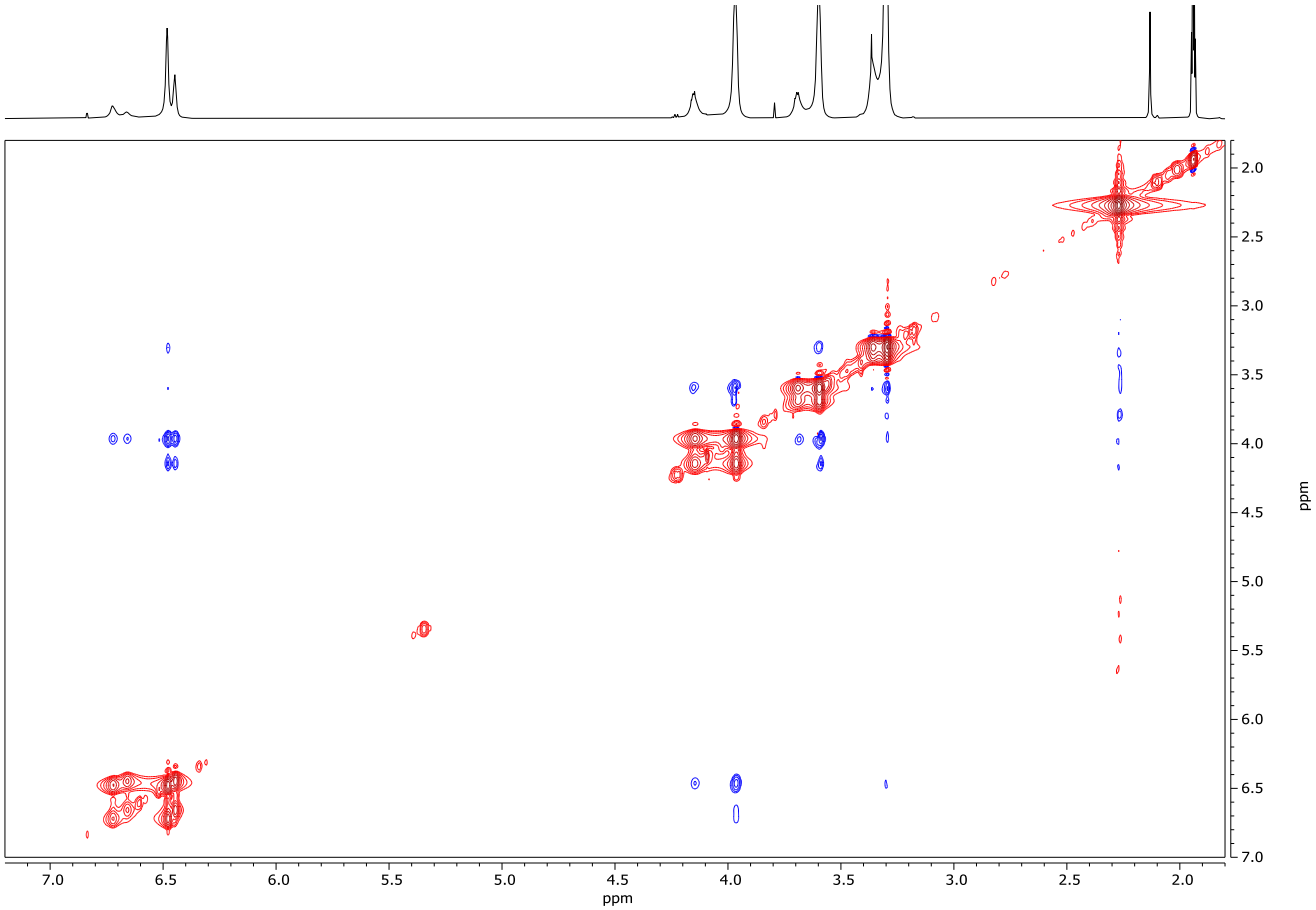

Spectrum 295. 2D NOESY (600 MHz, CD_3CN) of **333**. Data was recorded with a 400 ms mixing time and a relaxation delay of 1.96 s. 2K data points were collected for 256 increments of 4 scans.

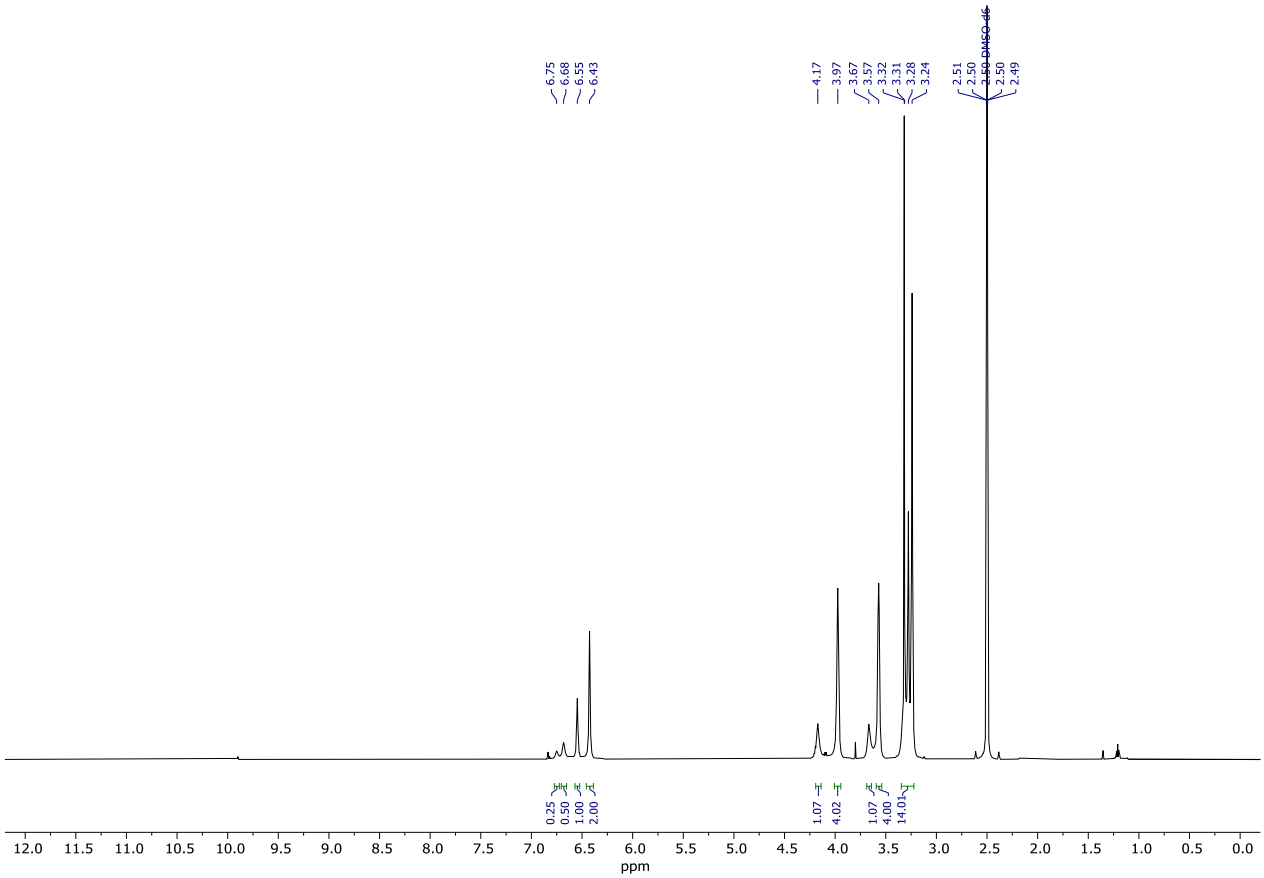

Spectrum 296. ^{1}H NMR (600 MHz, DMSO-d_6) of **333**.

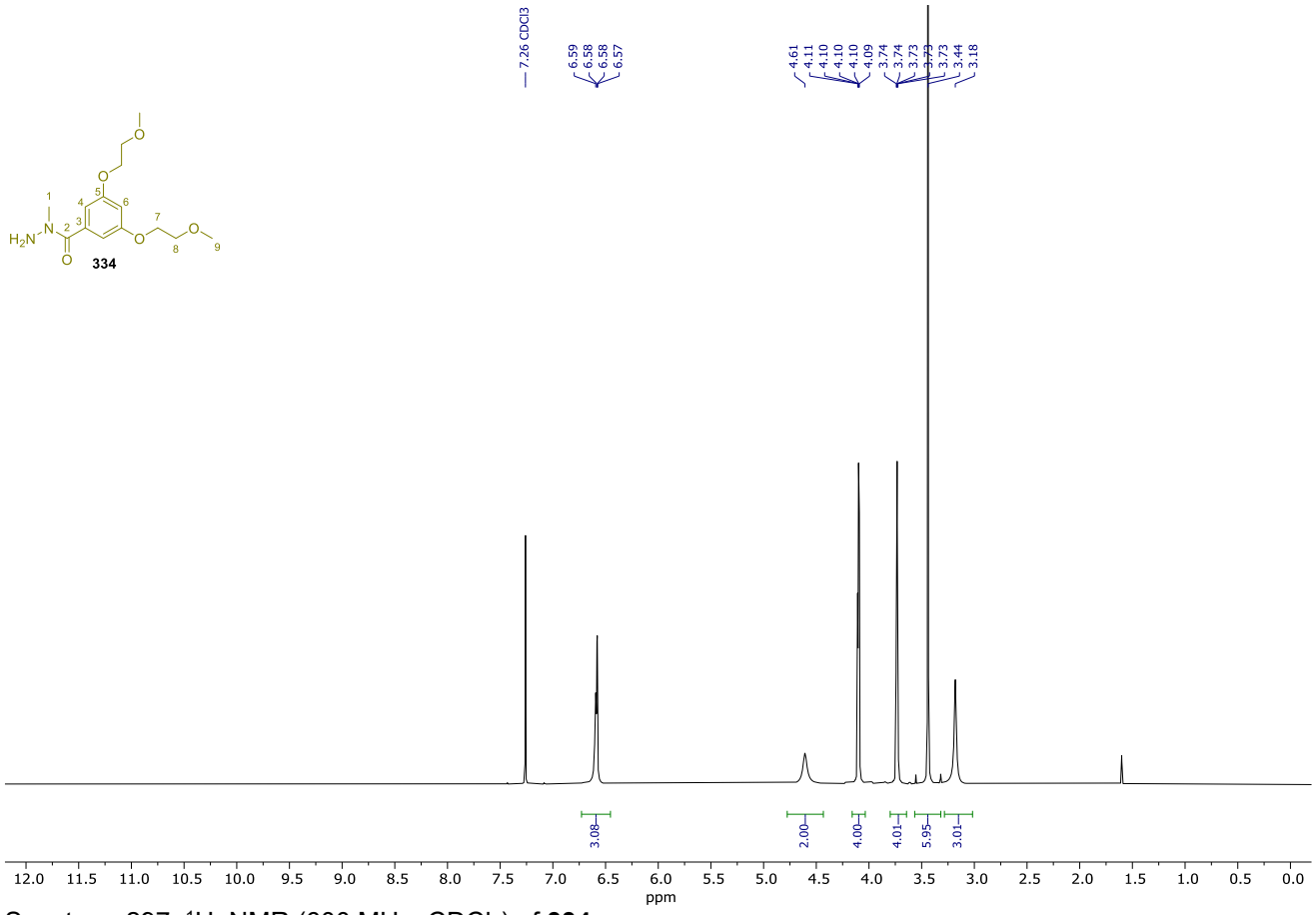

334

Spectrum 297. ^{1}H NMR (600 MHz, $CDCl_3$) of **334**.

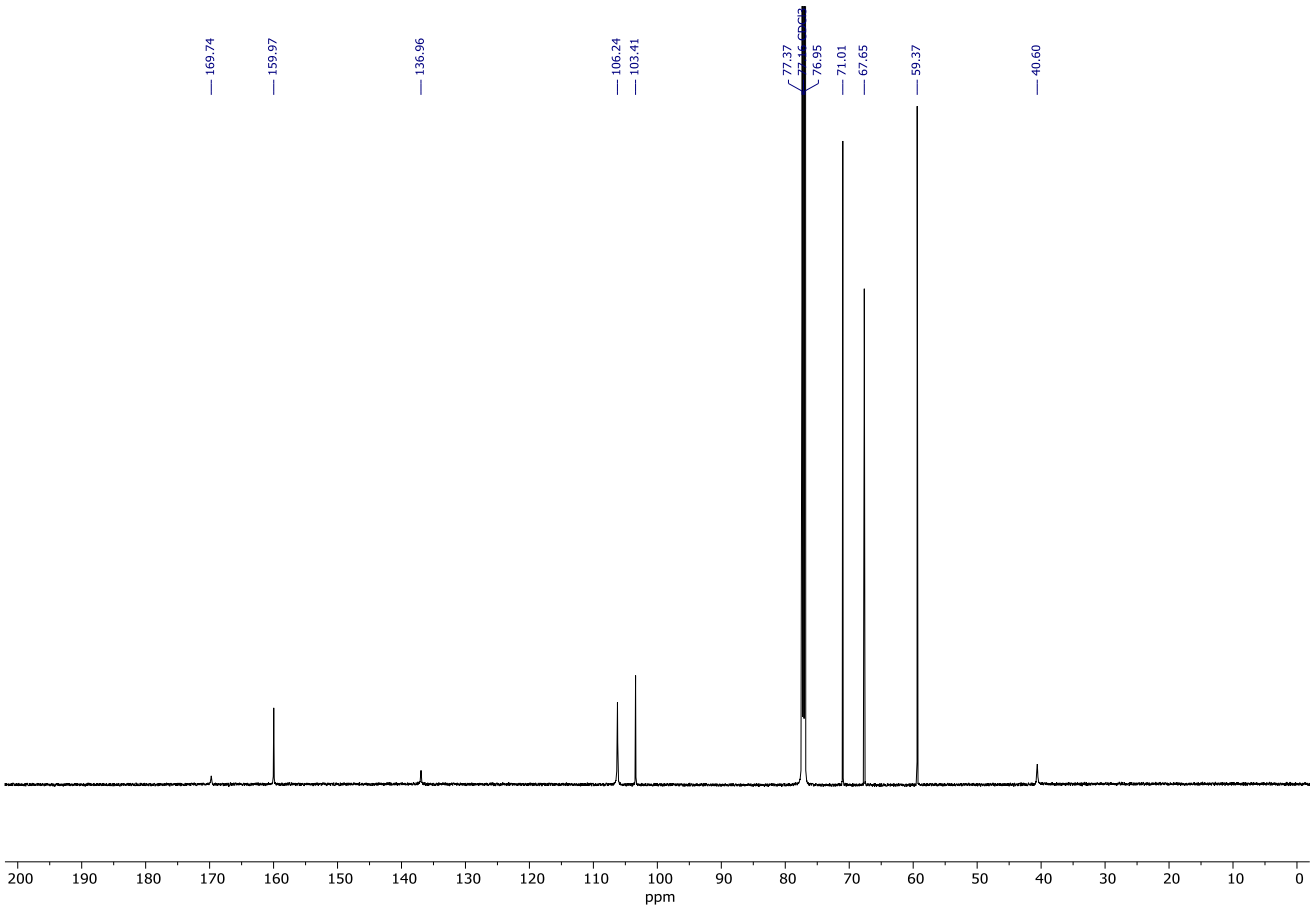

Spectrum 298. ^{13}C NMR (151 MHz, $CDCl_3$) of **334**.

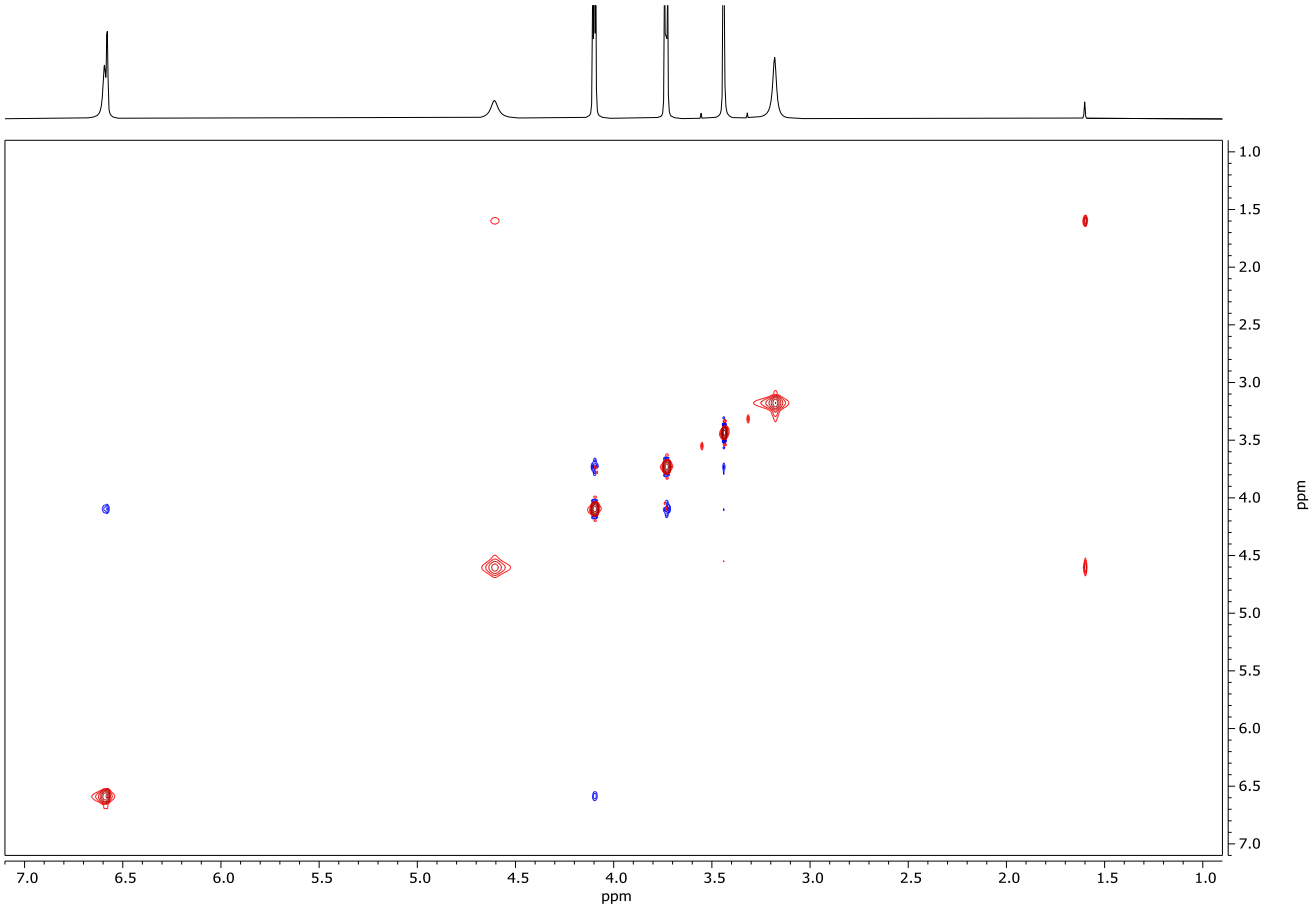

Spectrum 299. 2D NOESY (600 MHz, $CDCl_3$) of **334**. Data was recorded with a 400 ms mixing time and a relaxation delay of 1.94 s. 2K data points were collected for 256 increments of 4 scans.

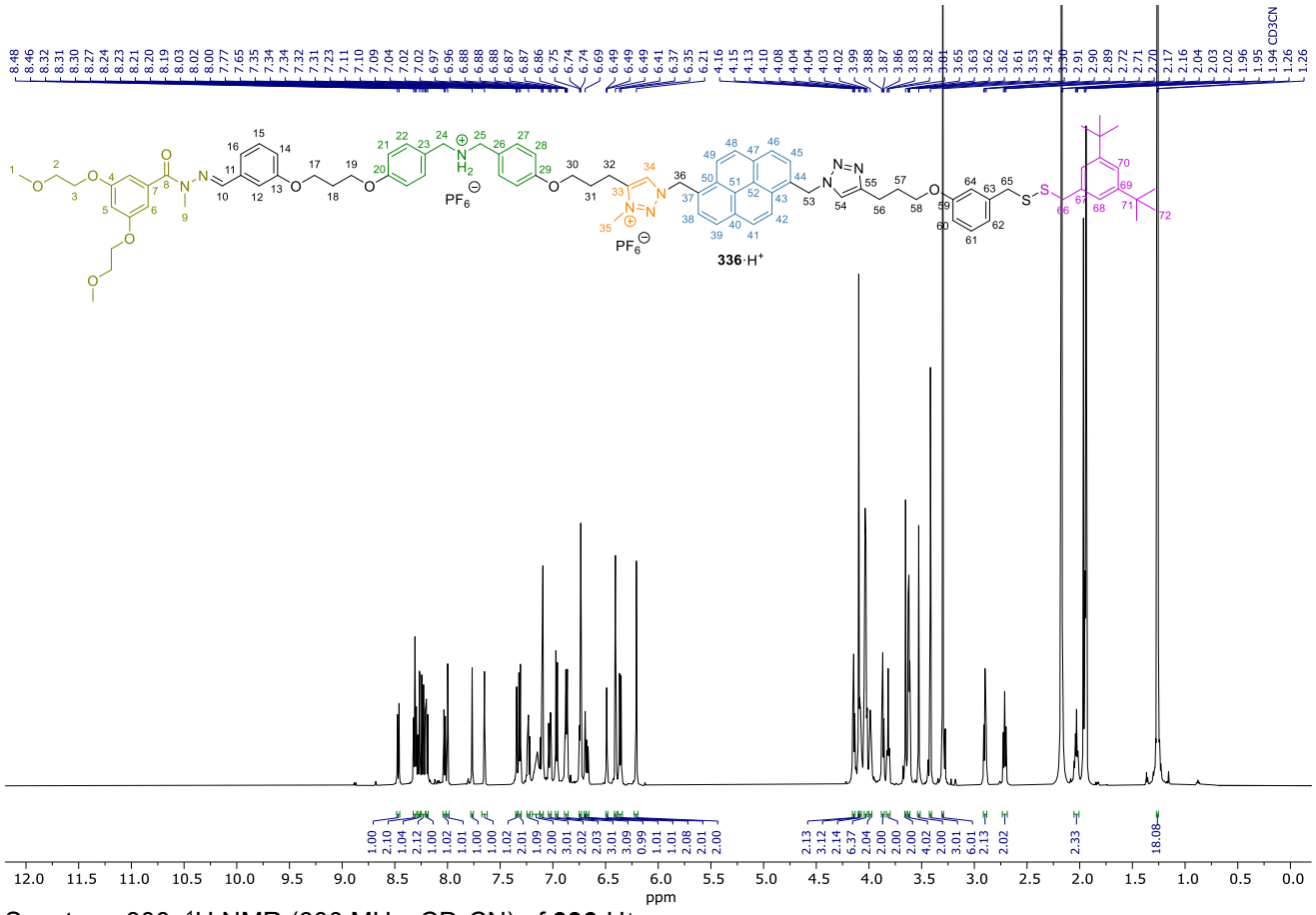

Spectrum 300. ^{1}H NMR (600 MHz, CD_3CN) of **336**·H^+.

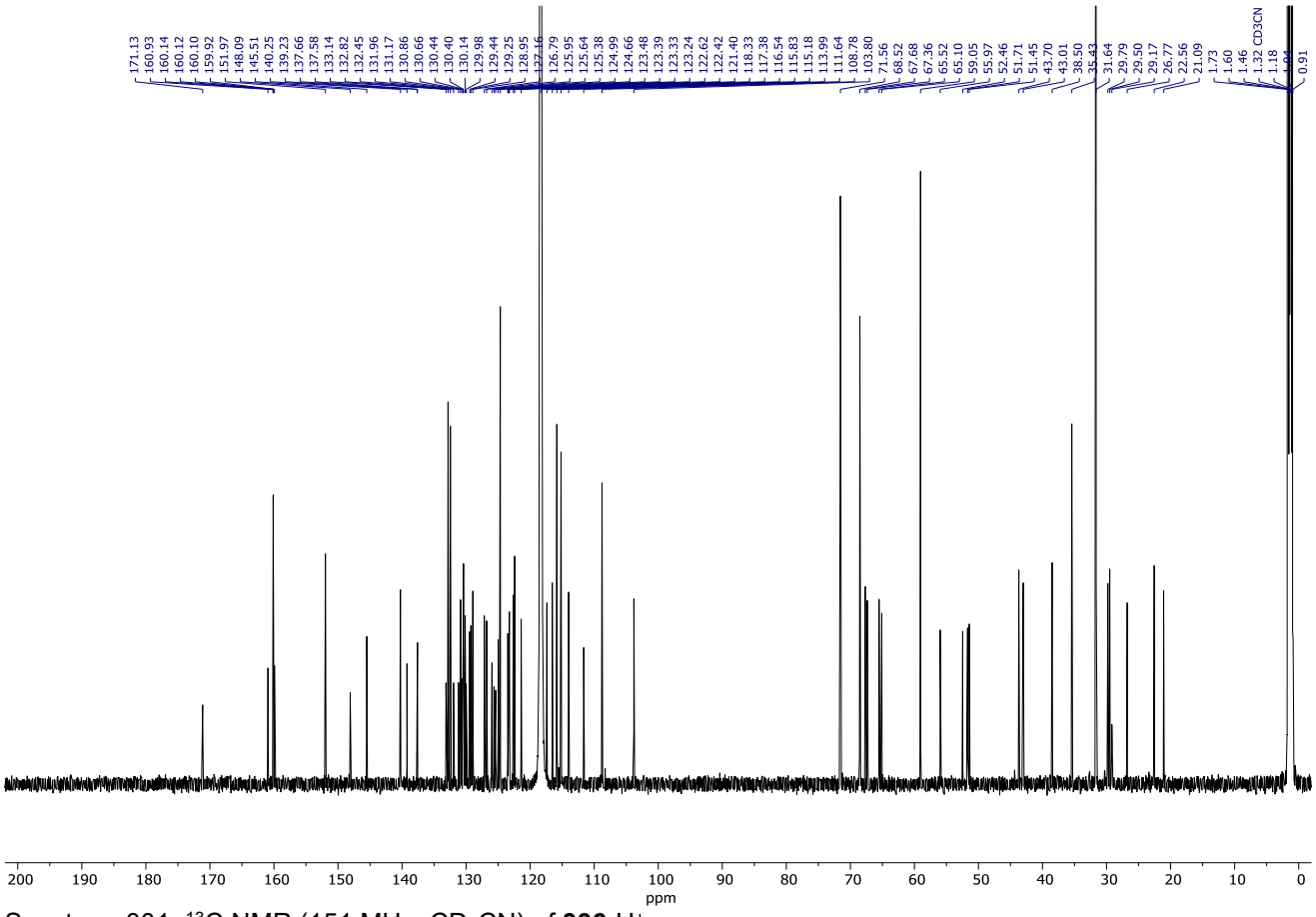

Spectrum 301. ^{13}C NMR (151 MHz, CD_3CN) of **336**·H^+.

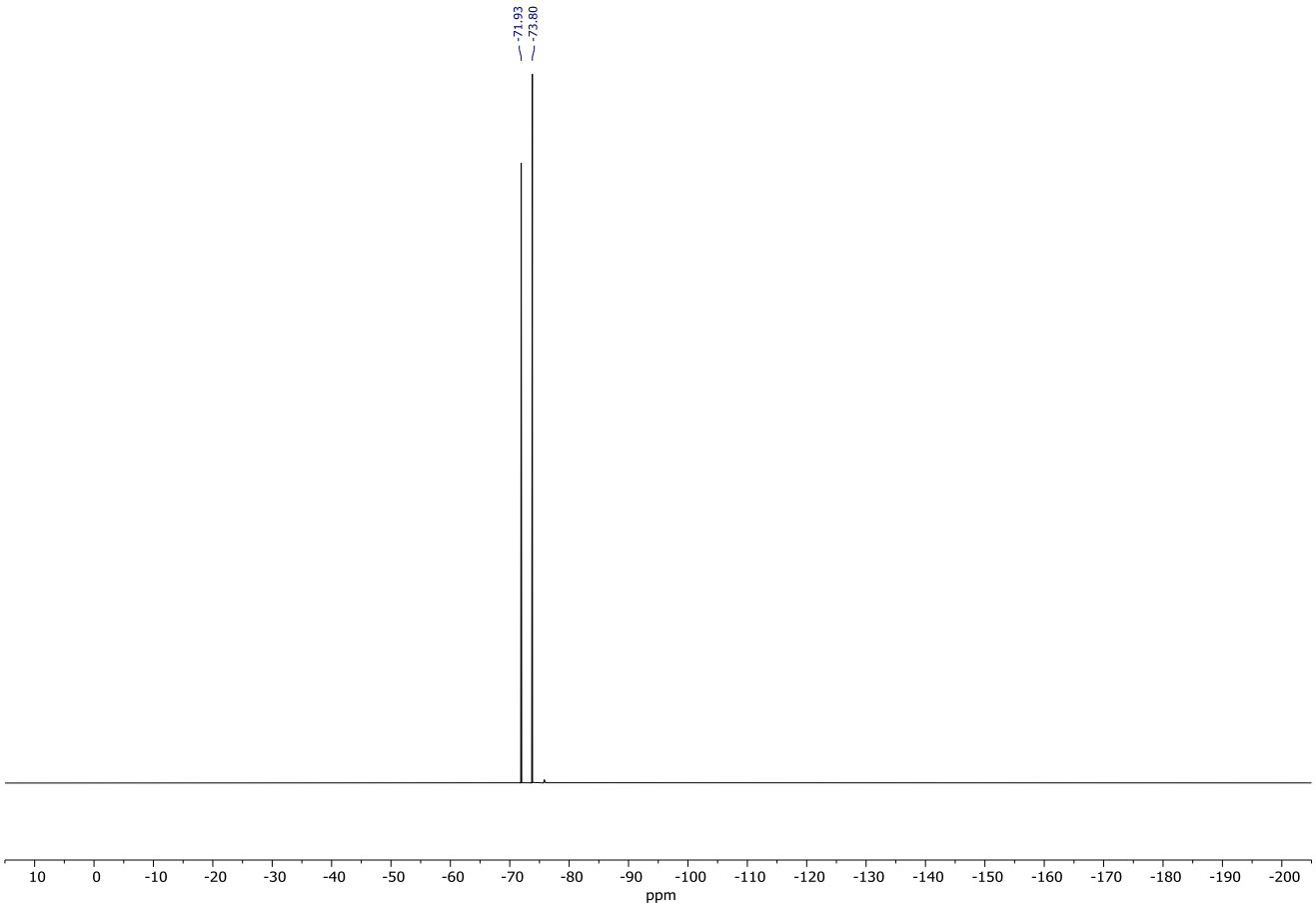

Spectrum 302. ^{19}F NMR (376 MHz, CD_3CN) of **336**·H^+.

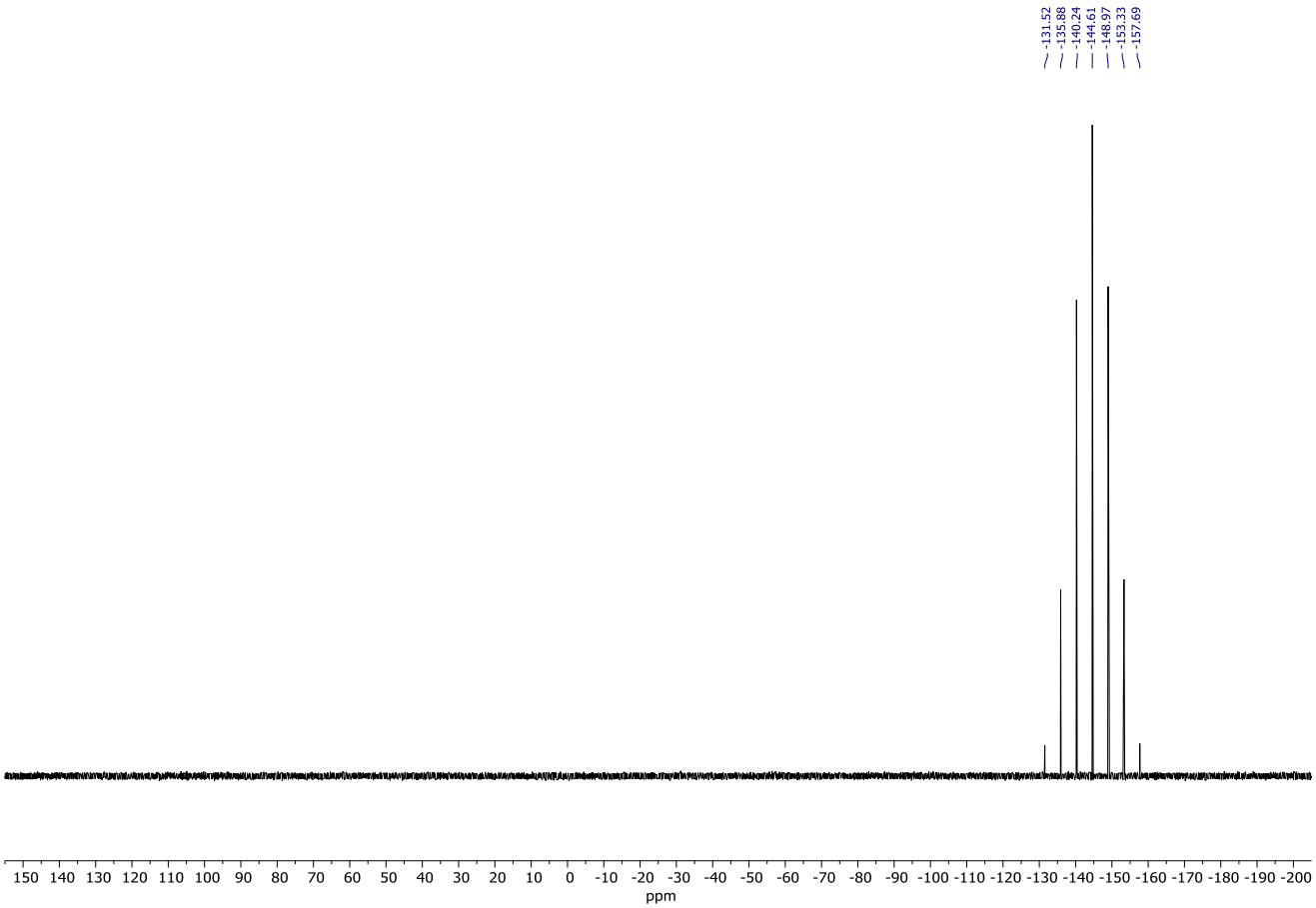

Spectrum 303. ^{31}P NMR (162 MHz, CD_3CN) of **336**·H^+.

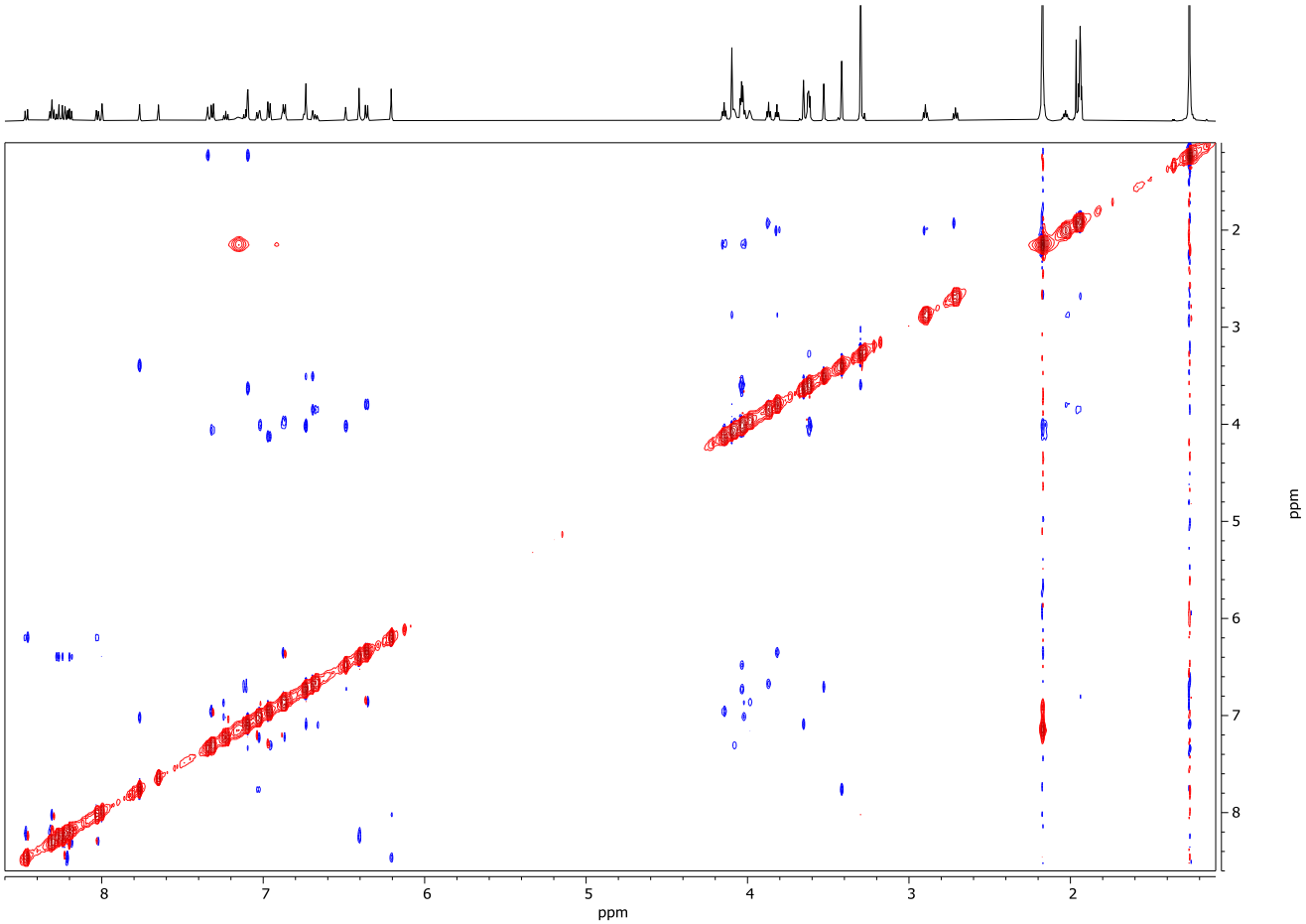

Spectrum 304. 2D NOESY (600 MHz, CD_3CN) of **336**·H^+. Data was recorded with 400 ms mixing time and a relaxation delay of 2.00 s. 4K data points were collected for 256 increments of 8 scans.

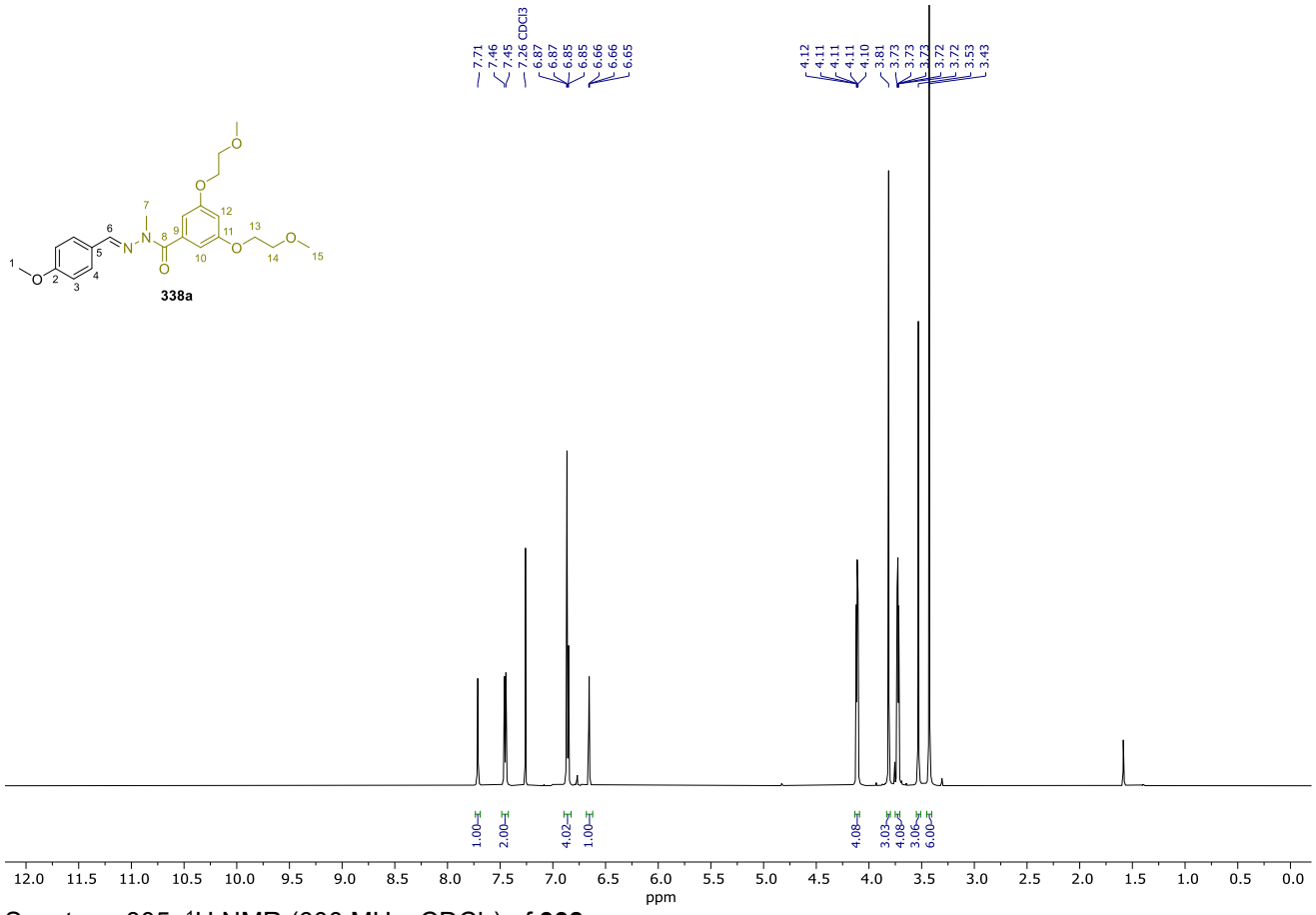

338a

Spectrum 305. ^{1}H NMR (600 MHz, $CDCl_3$) of **338a**.

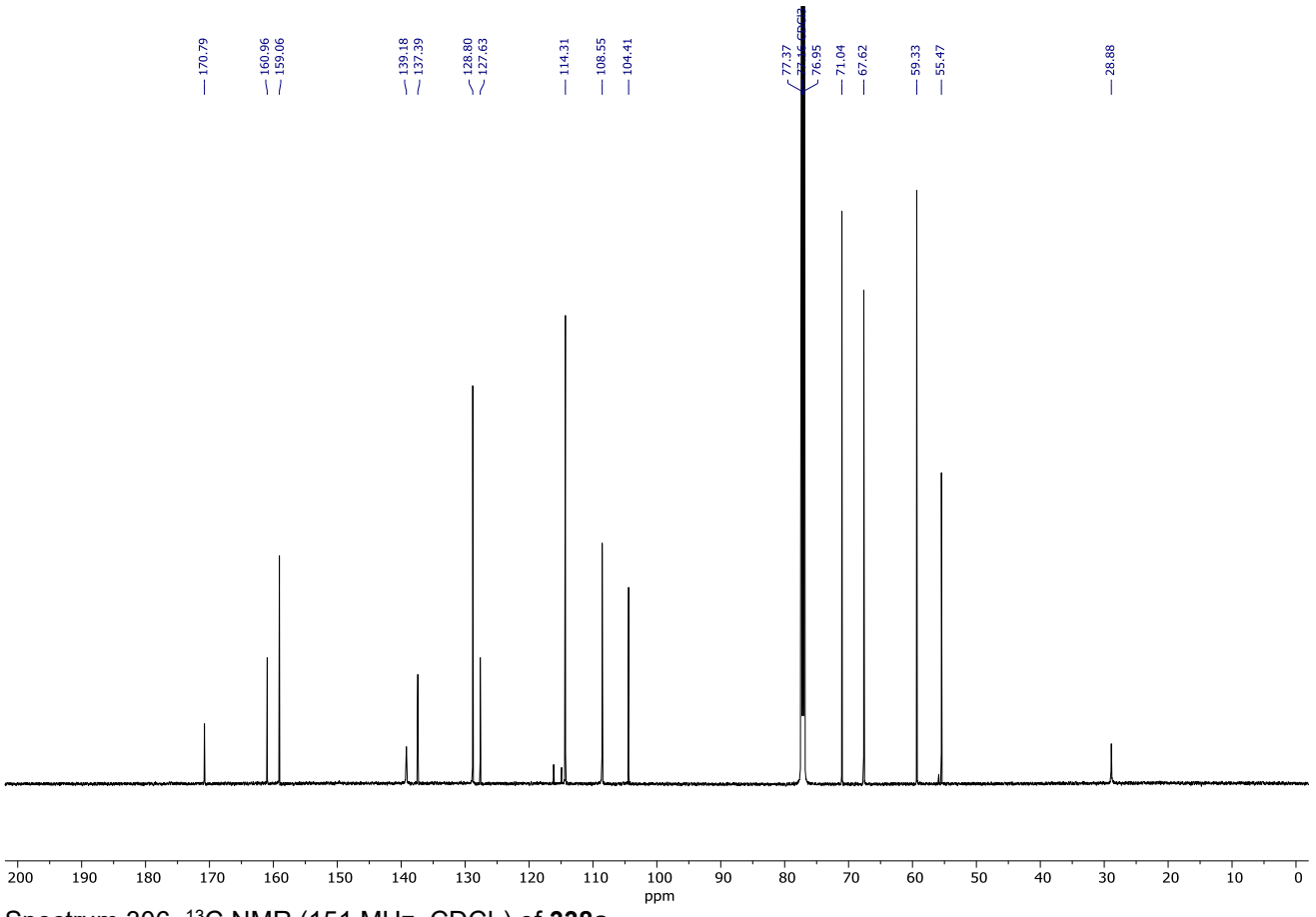

Spectrum 306. ^{13}C NMR (151 MHz, $CDCl_3$) of **338a**.

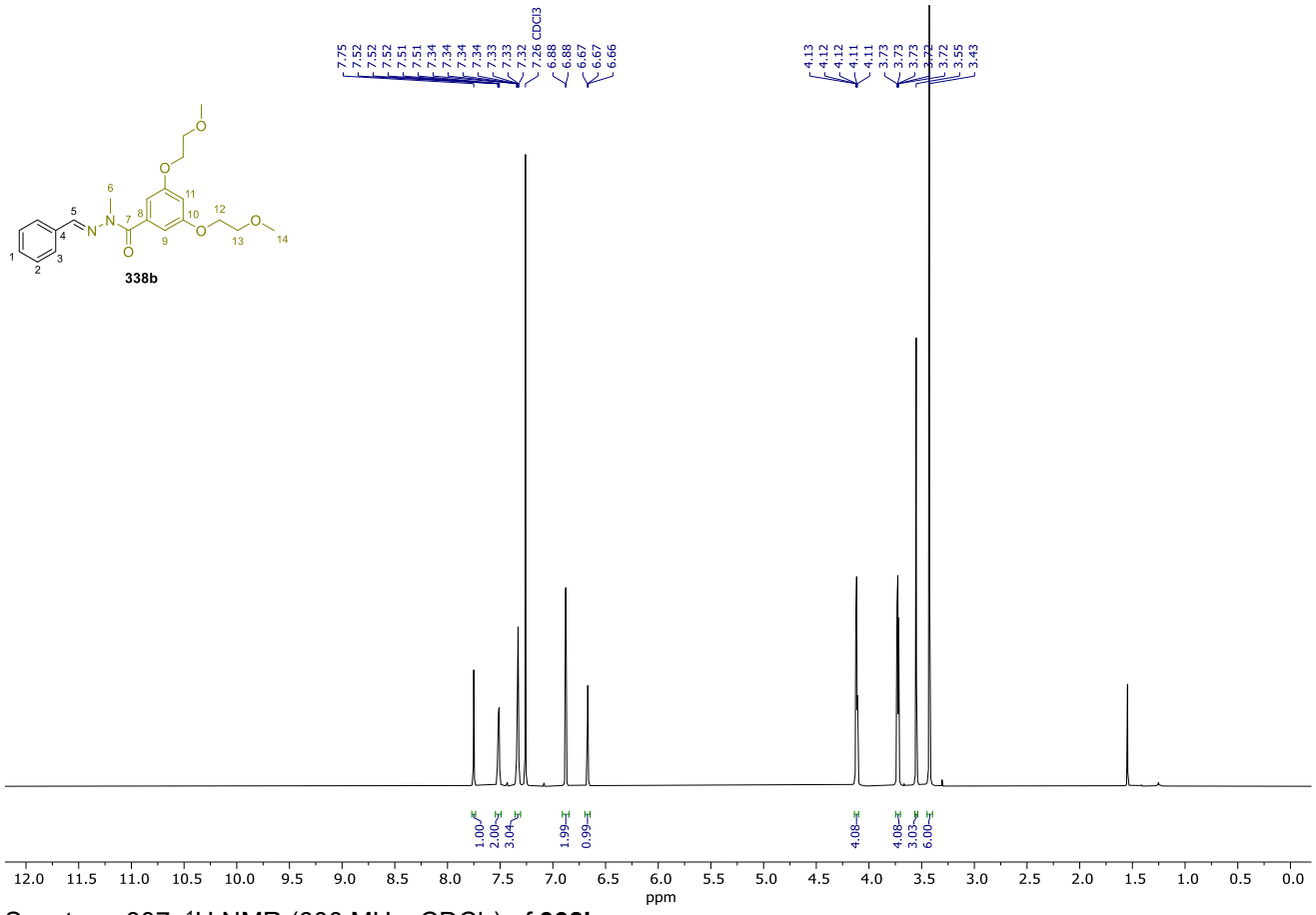

Spectrum 307. ^{1}H NMR (600 MHz, $CDCl_3$) of **338b**.

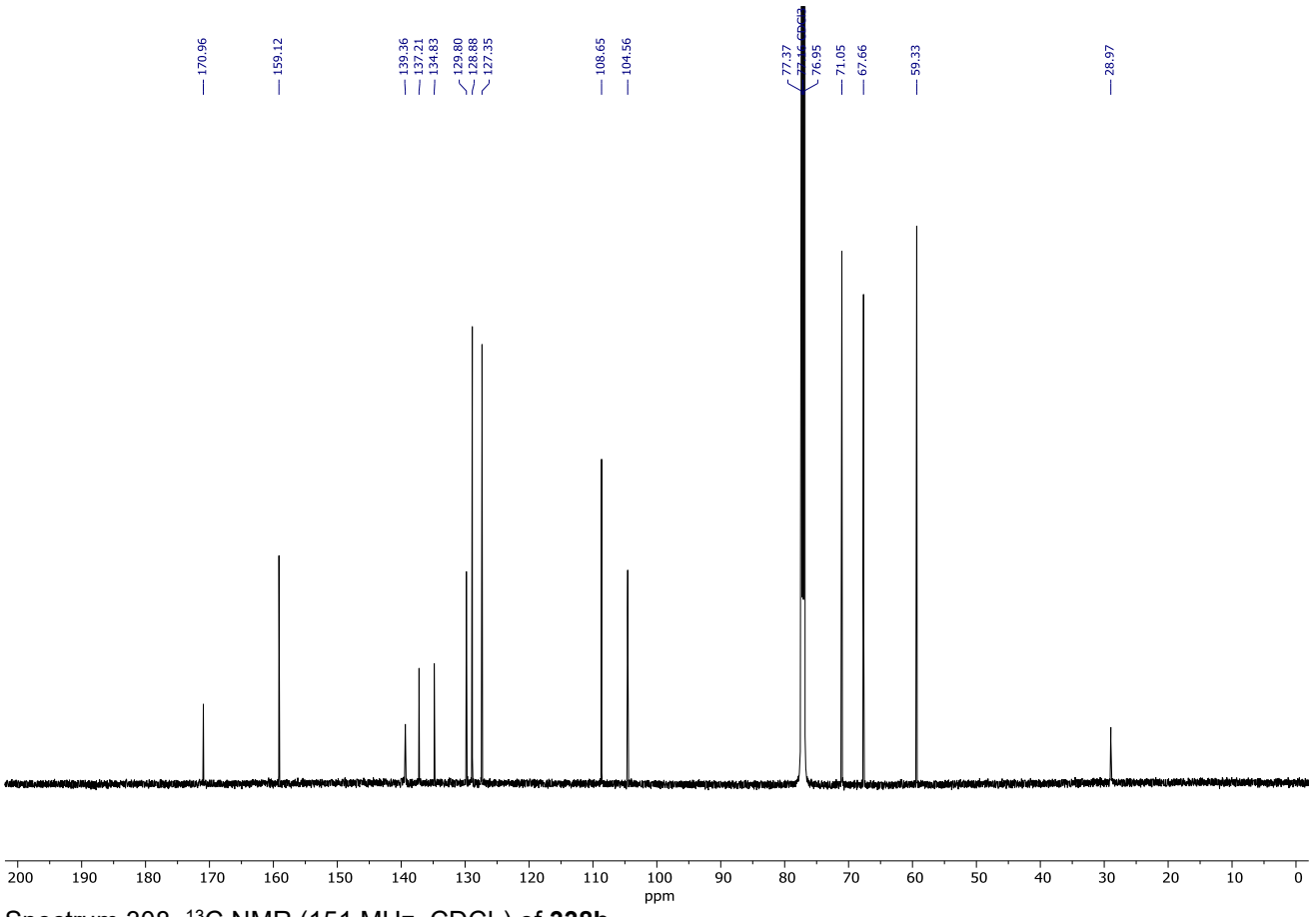

Spectrum 308. ^{13}C NMR (151 MHz, $CDCl_3$) of **338b**.

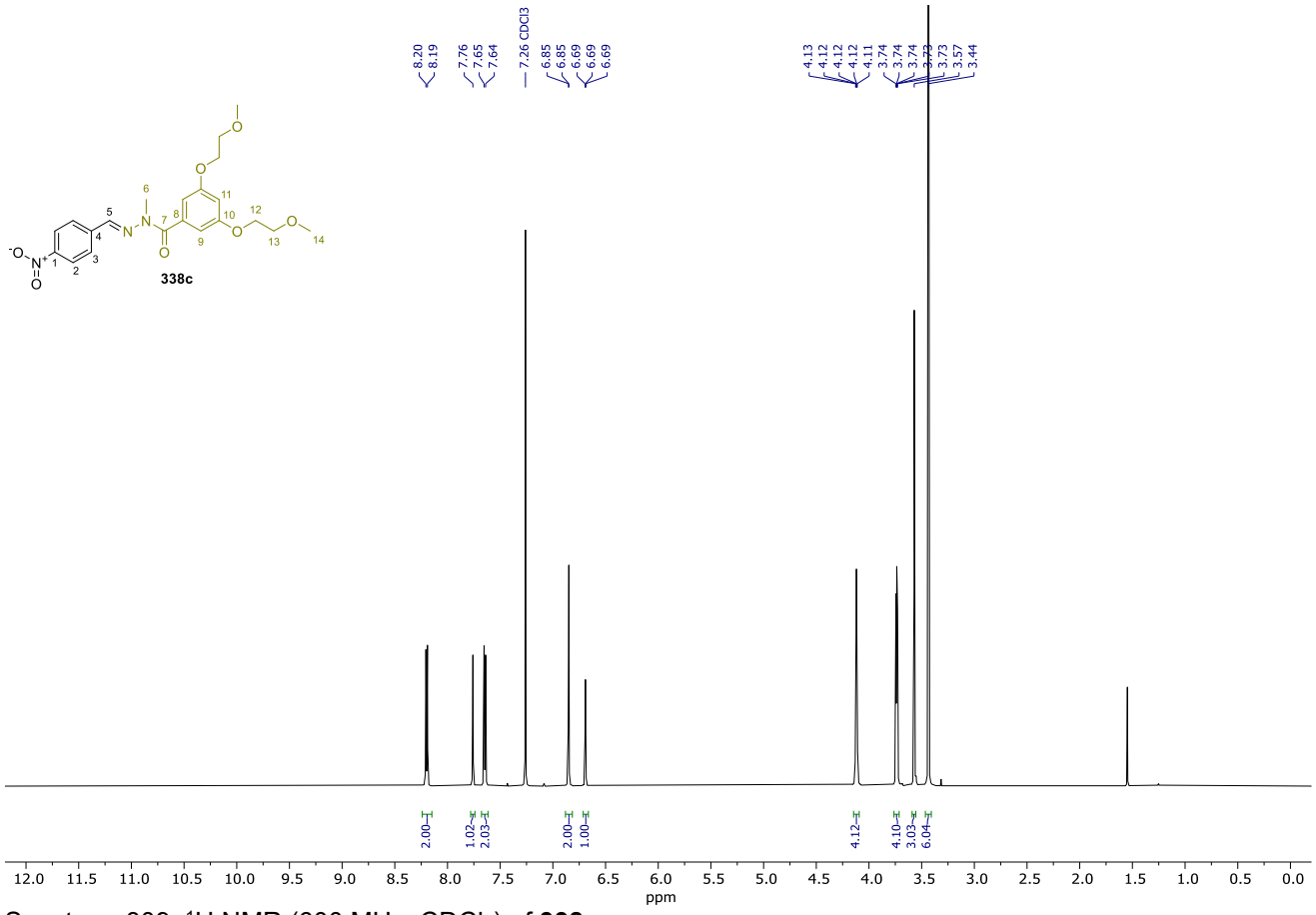

Spectrum 309. ^{1}H NMR (600 MHz, $CDCl_3$) of **338c**.

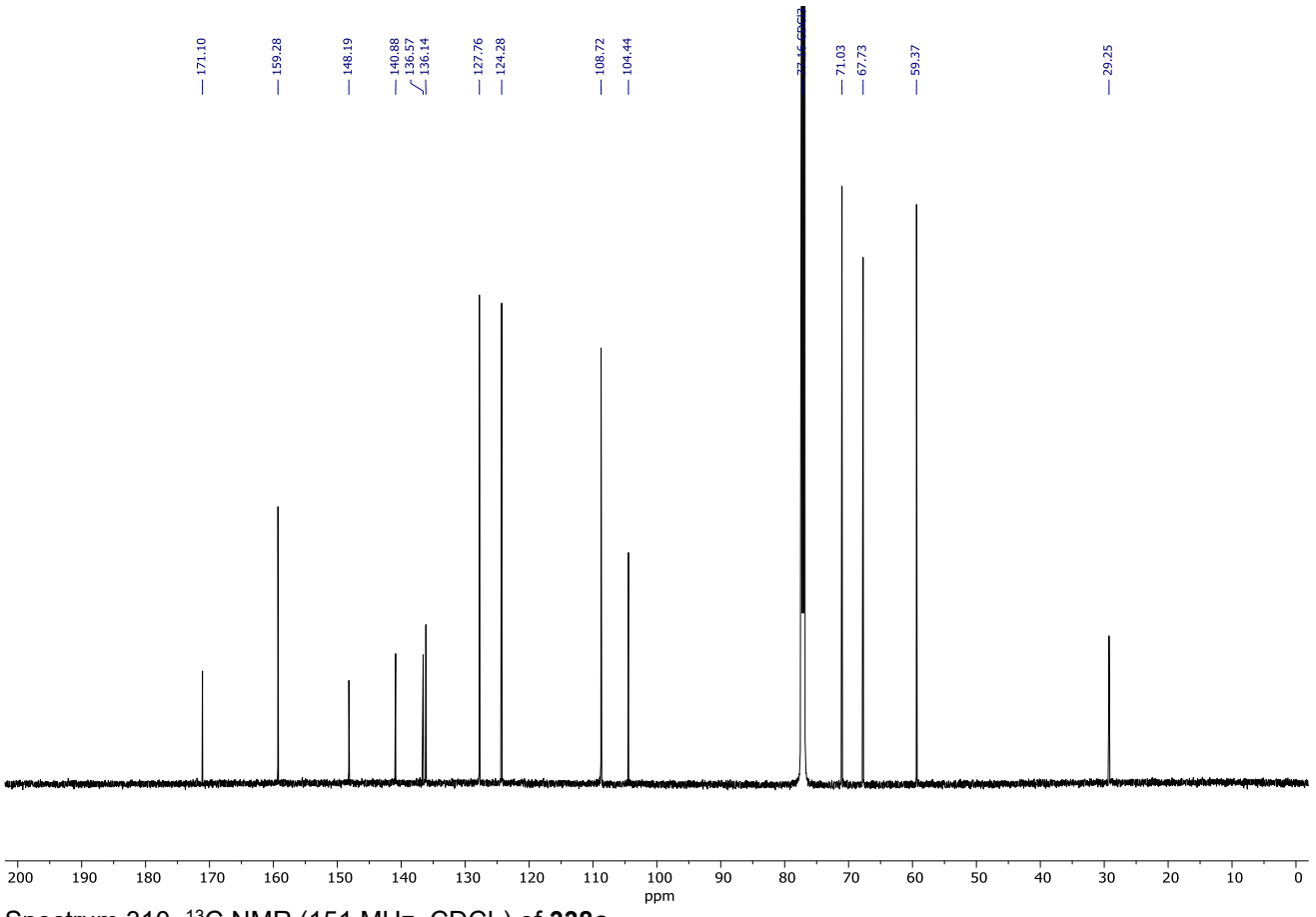

Spectrum 310. ^{13}C NMR (151 MHz, $CDCl_3$) of **338c**.

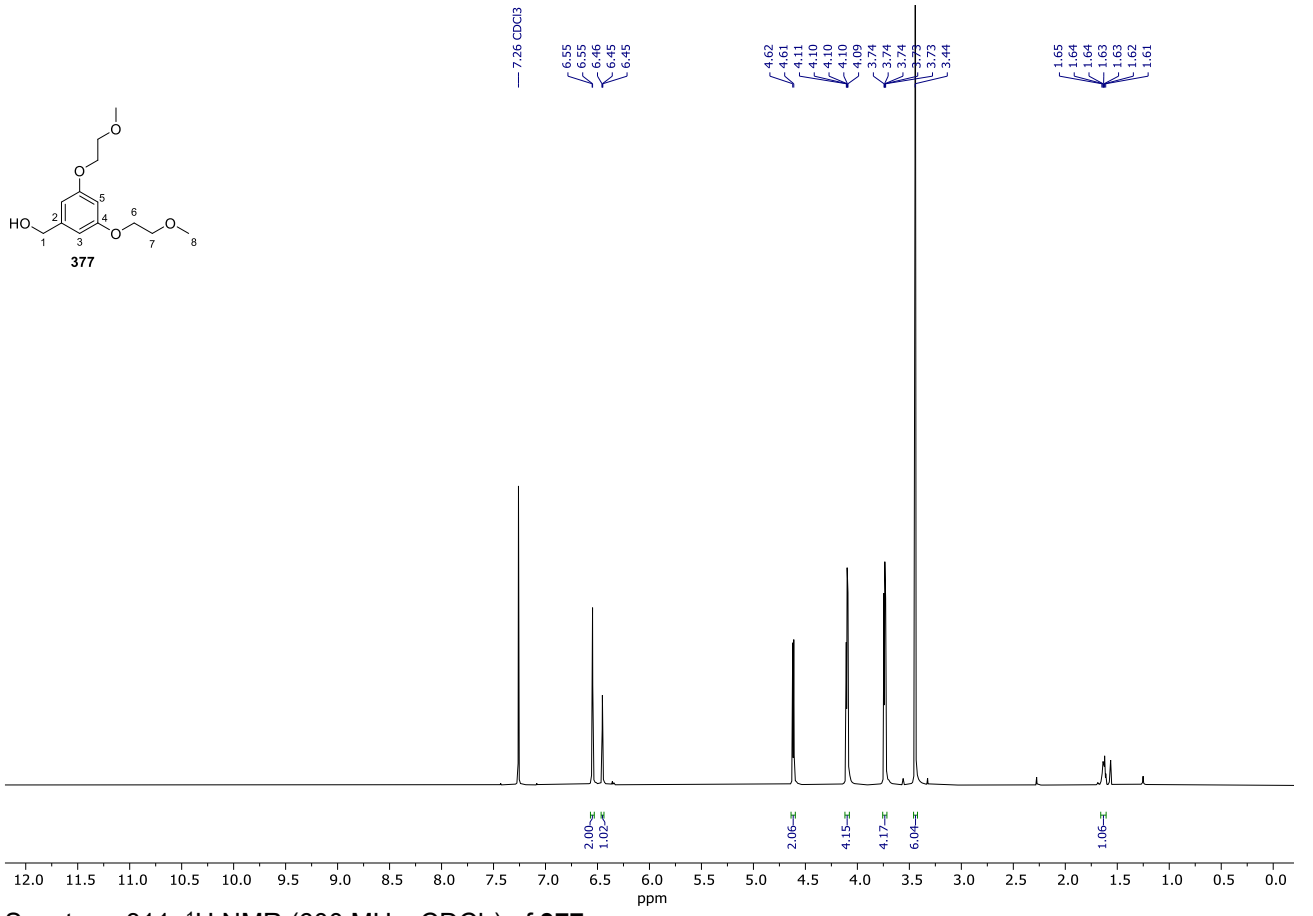

377

Spectrum 311. ^{1}H NMR (600 MHz, $CDCl_3$) of **377**.

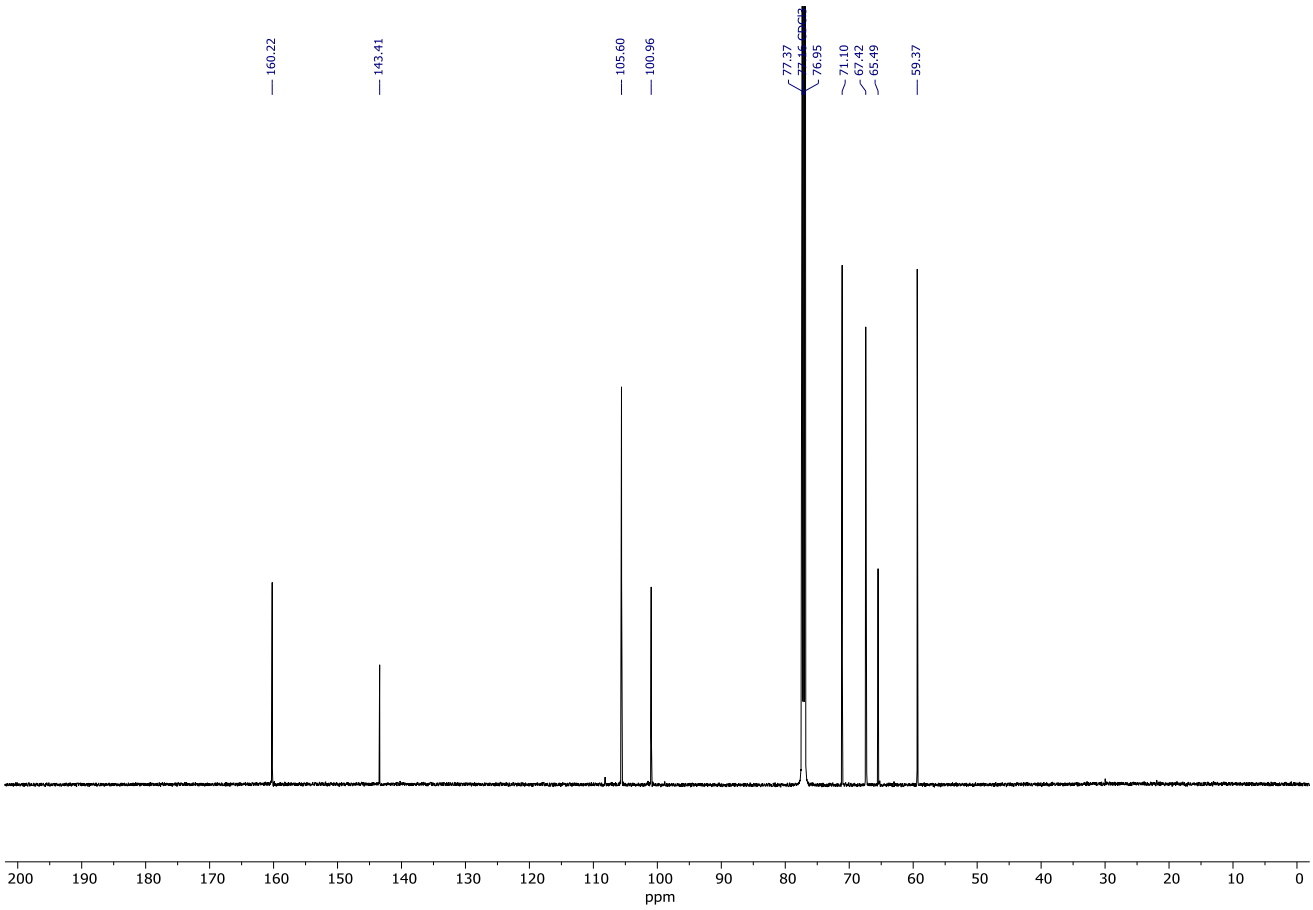

Spectrum 312. ^{13}C NMR (151 MHz, $CDCl_3$) of **377**.

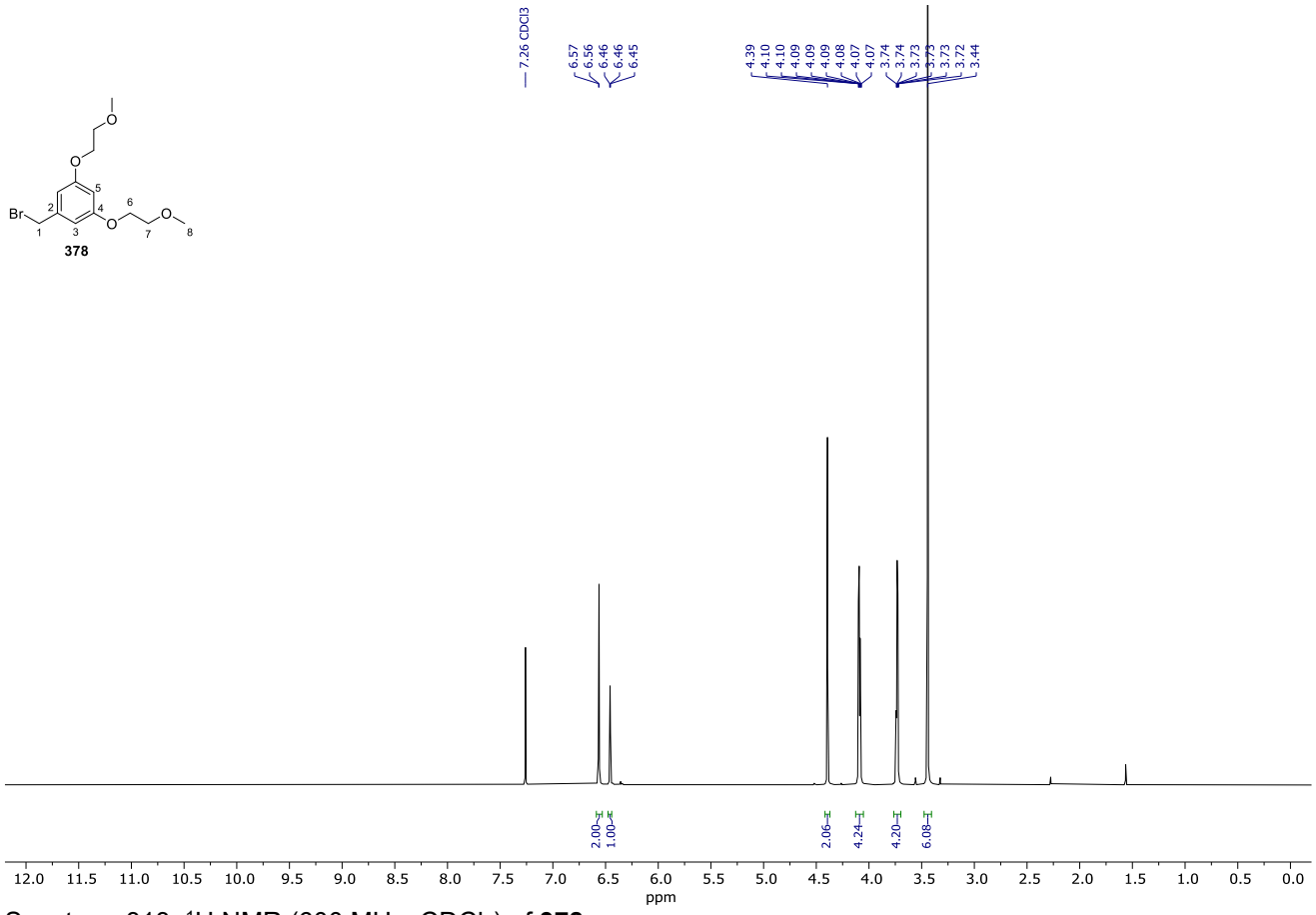

Spectrum 313. ^{1}H NMR (600 MHz, $CDCl_3$) of **378**.

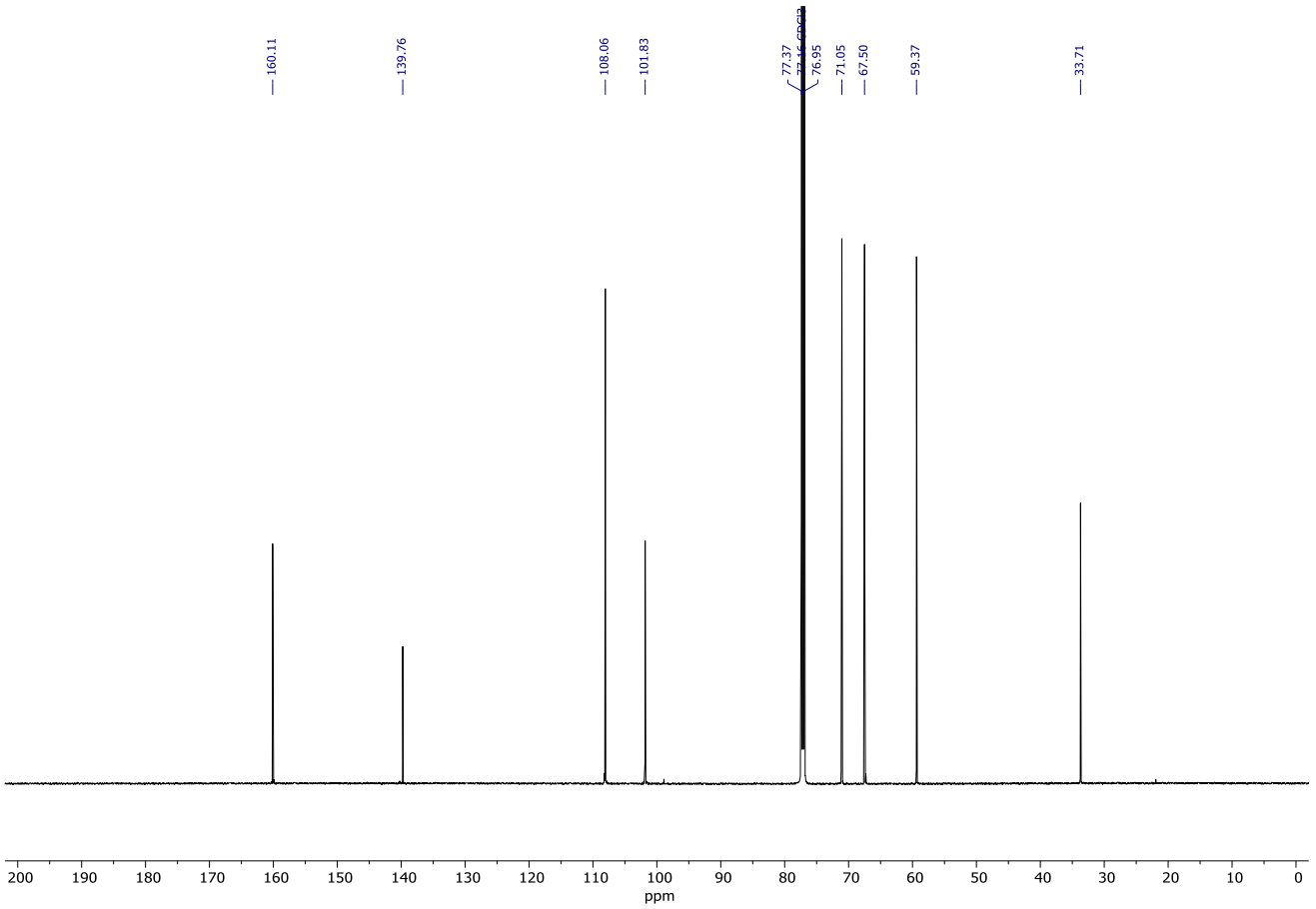

Spectrum 314. ^{13}C NMR (151 MHz, $CDCl_3$) of **378**.

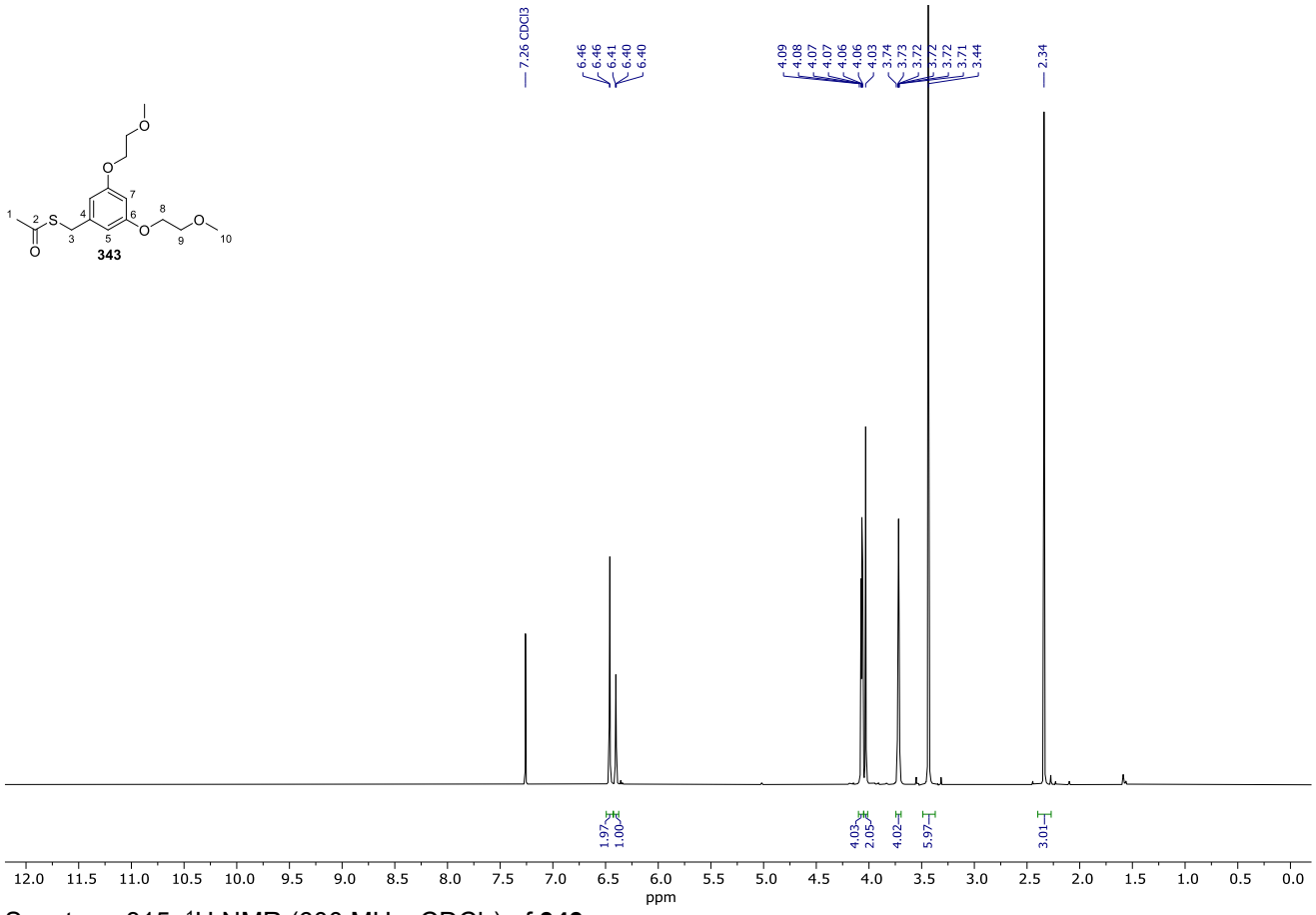

Spectrum 315. ^{1}H NMR (600 MHz, $CDCl_3$) of **343**.

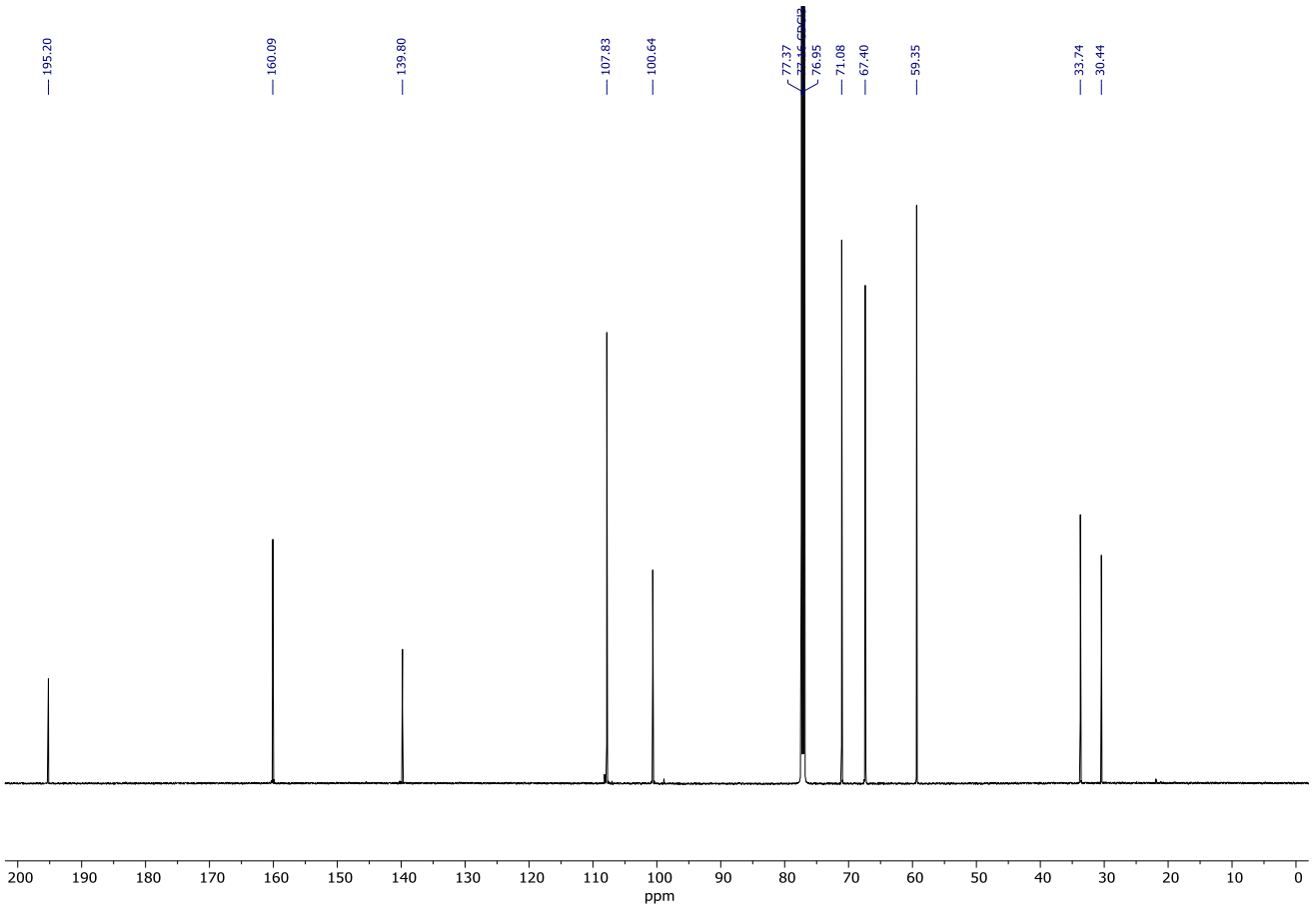

Spectrum 316. ^{13}C NMR (151 MHz, $CDCl_3$) of **343**.

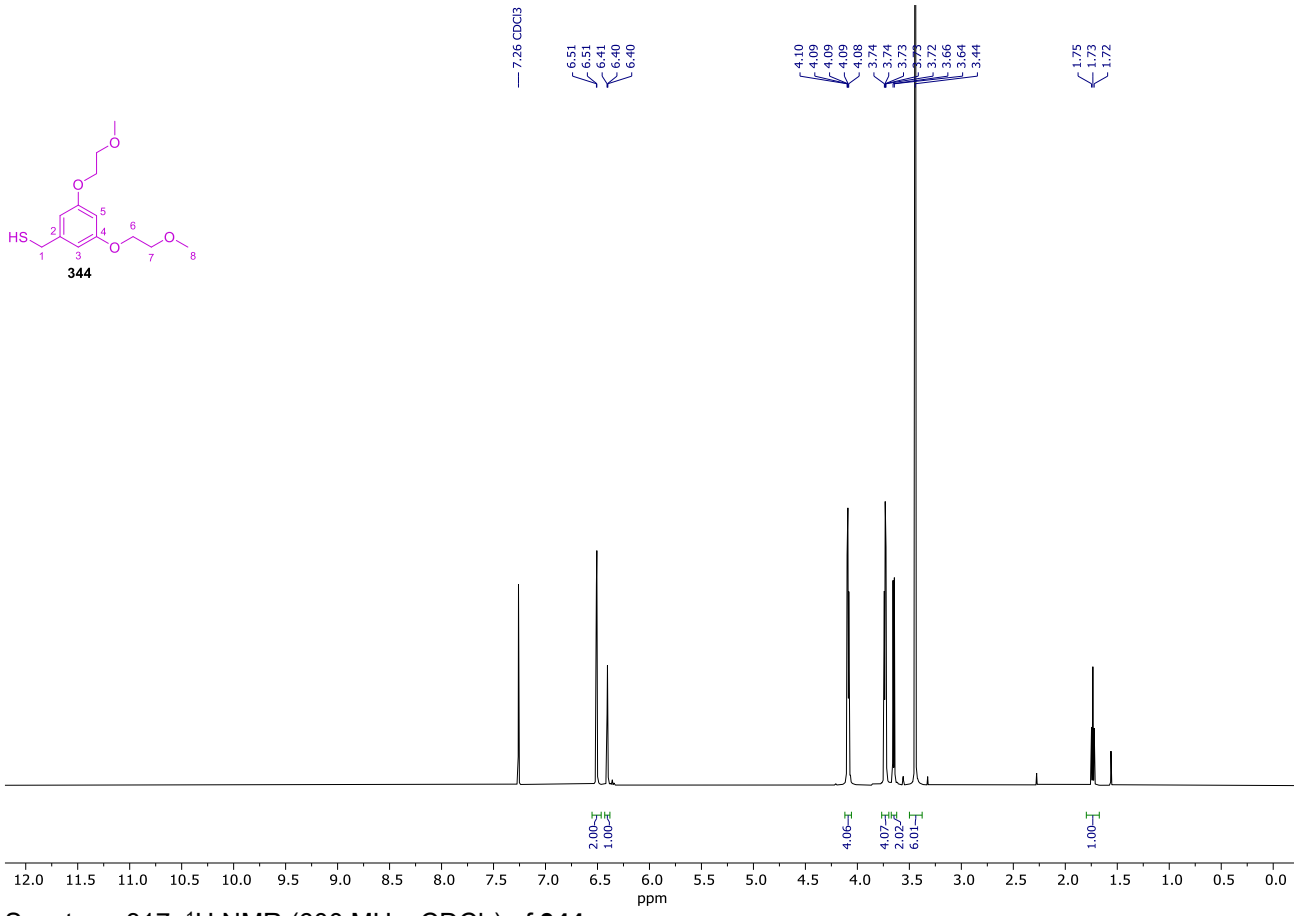

Spectrum 317. ^{1}H NMR (600 MHz, $CDCl_3$) of **344**.

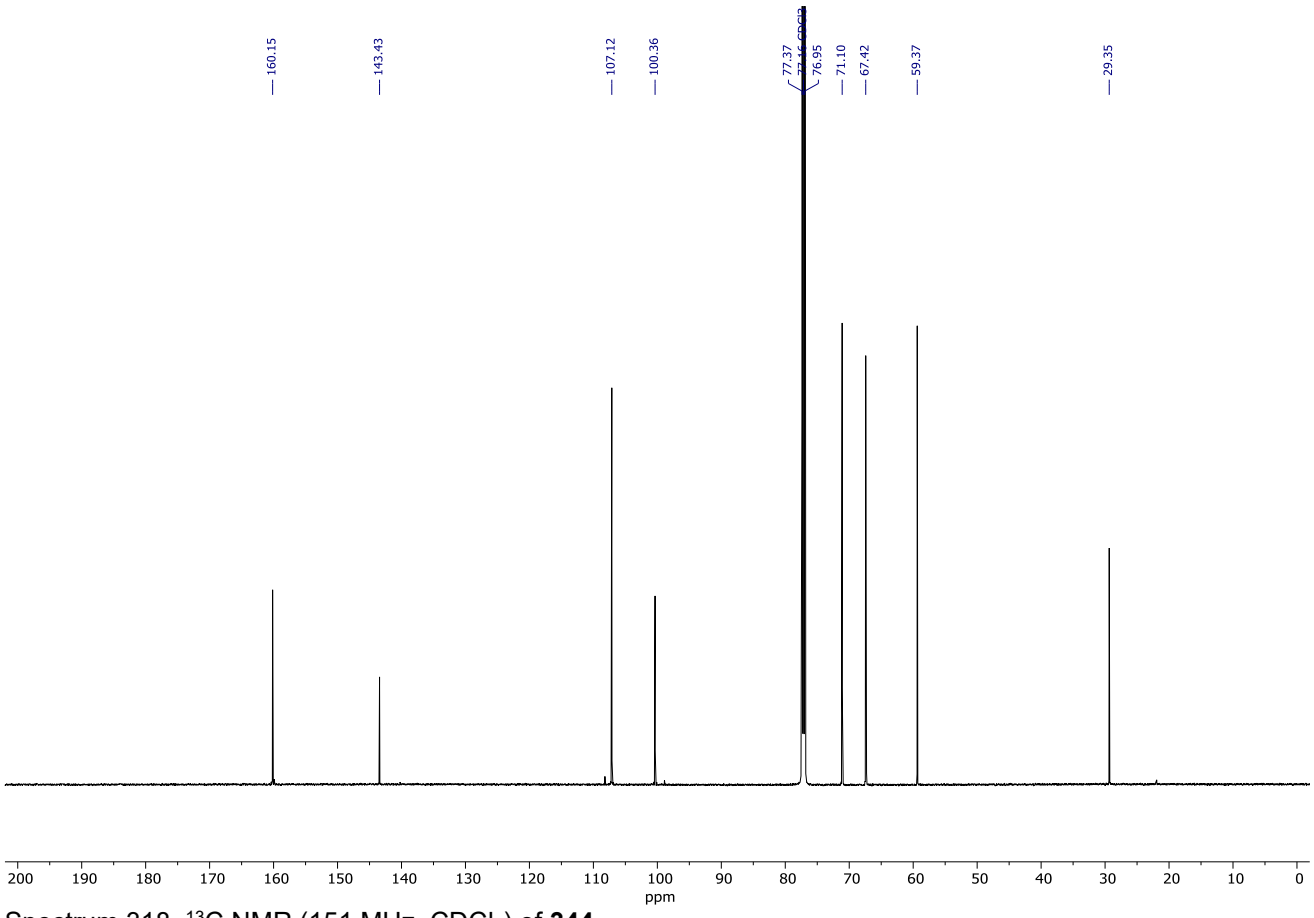

Spectrum 318. ^{13}C NMR (151 MHz, $CDCl_3$) of **344**.